NORTH ATLANTIC TREATY ORGANISATION

RESEARCH AND TECHNOLOGY ORGANISATION

BP 25, 7 RUE ANCELLE, F-92201 NEUILLY-SUR-SEINE CEDEX, FRANCE

RTO MEETING PROCEEDINGS 89

Reduction of Military Vehicle Acquisition Time and Cost through Advanced Modelling and Virtual Simulation

(La réduction des coûts et des délais d'acquisition des véhicules militaires par la modélisation avancée et la simulation de produit virtuel)

Papers presented at the RTO Applied Vehicle Technology Panel (AVT) Symposium held in Paris, France, 22-25 April 2002.

Published March 2003

Distribution and Availability on Back Cover

This page has been deliberately left blank

_____

Page intentionnellement blanche

NORTH ATLANTIC TREATY ORGANISATION

RESEARCH AND TECHNOLOGY ORGANISATION

BP 25, 7 RUE ANCELLE, F-92201 NEUILLY-SUR-SEINE CEDEX, FRANCE

RTO MEETING PROCEEDINGS 89

Reduction of Military Vehicle Acquisition Time and Cost through Advanced Modelling and Virtual Simulation

(La réduction des coûts et des délais d'acquisition des véhicules militaires par la modélisation avancée et la simulation de produit virtuel)

Papers presented at the RTO Applied Vehicle Technology Panel (AVT) Symposium held in Paris, France, 22-25 April 2002.

The Research and Technology Organisation (RTO) of NATO

RTO is the single focus in NATO for Defence Research and Technology activities. Its mission is to conduct and promote cooperative research and information exchange. The objective is to support the development and effective use of national defence research and technology and to meet the military needs of the Alliance, to maintain a technological lead, and to provide advice to NATO and national decision makers. The RTO performs its mission with the support of an extensive network of national experts. It also ensures effective coordination with other NATO bodies involved in R&T activities.

RTO reports both to the Military Committee of NATO and to the Conference of National Armament Directors. It comprises a Research and Technology Board (RTB) as the highest level of national representation and the Research and Technology Agency (RTA), a dedicated staff with its headquarters in Neuilly, near Paris, France. In order to facilitate contacts with the military users and other NATO activities, a small part of the RTA staff is located in NATO Headquarters in Brussels. The Brussels staff also coordinates RTO's cooperation with nations in Middle and Eastern Europe, to which RTO attaches particular importance especially as working together in the field of research is one of the more promising areas of initial cooperation.

The total spectrum of R&T activities is covered by the following 7 bodies:

- AVT   Applied Vehicle Technology Panel
- HFM   Human Factors and Medicine Panel
- IST   Information Systems Technology Panel
- NMSG   NATO Modelling and Simulation Group
- SAS   Studies, Analysis and Simulation Panel
- SCI   Systems Concepts and Integration Panel
- SET   Sensors and Electronics Technology Panel

These bodies are made up of national representatives as well as generally recognised 'world class' scientists. They also provide a communication link to military users and other NATO bodies. RTO's scientific and technological work is carried out by Technical Teams, created for specific activities and with a specific duration. Such Technical Teams can organise workshops, symposia, field trials, lecture series and training courses. An important function of these Technical Teams is to ensure the continuity of the expert networks.

RTO builds upon earlier cooperation in defence research and technology as set-up under the Advisory Group for Aerospace Research and Development (AGARD) and the Defence Research Group (DRG). AGARD and the DRG share common roots in that they were both established at the initiative of Dr Theodore von Kármán, a leading aerospace scientist, who early on recognised the importance of scientific support for the Allied Armed Forces. RTO is capitalising on these common roots in order to provide the Alliance and the NATO nations with a strong scientific and technological basis that will guarantee a solid base for the future.

Reduction of Military Vehicle Acquisition Time and Cost through Advanced Modelling and Virtual Simulation

(RTO MP-089 / AVT-090)

Executive Summary

The defense of NATO requires a new paradigm in the development and deployment of weapon systems. This paradigm is driven by the hard realities of diminishing defense budgets and the emerging threats of unconventional attacks typified by 11 September 2001. Design simulation tools and advanced modeling techniques and processes, coupled with a maturing set of virtual manufacturing tools, are now being applied to this development and deployment. Both military and commercial companies are rapidly lowering the cost and design cycle times of their products from both a design/development and recurring manufacturing perspective through this application. Applying these tools to the development of affordable weapon systems from concept to operation, as envisioned by both the RTO MSG and AVT Panels, is essential to achieving the cost and time reductions needed to meet the emerging threats that NATO faces. The multidisciplinary composition and applied vehicle technology focus of AVT provides an excellent framework for the further development, deployment and integration of this digital environment, which has tremendous potential to reduce cost and cycle time of weapon system development. AVT is performing a vital service to NATO by fostering this new paradigm of development based on electronic simulation by encouraging and enabling technical information exchange between the Nations.

The Applied Vehicle Technology Panel (AVT) of the Research and Technology Organization (RTO) of NATO conducted a highly successful Symposium on "Reduction of Military Vehicle Acquisition Time and Cost through Advanced Modeling and Virtual Product Simulation" on 22 through 25 April 2002. The objective of the symposium was to determine the state-of-the-art and future direction of virtual design, simulation, and manufacturing tools that dramatically reduce the cost and design cycle time to develop or upgrade NATO systems. The symposium included 62 presentations focused on recent and current research and developments in design, simulation, and virtual manufacturing tools. Modeling and simulation has been successfully applied to Design Synthesis, Qualification by Analysis, Manufacturing Simulation, Aerodynamics, Turbo-machinery, Hydrodynamics, Aero-elasticity, Flight Control, Mesh Generation & Adaptation, and Geometry Fidelity. Specialized topics related to computational fluid dynamics (CFD) were included in the symposium to address the persistence of cost overruns and schedule delays that occur with aerodynamic or hydrodynamic performance validation. This included specific examples of application of the technology to vehicle platforms, space systems, propulsion, power, and weapon systems by industry and government. Emerging simulation tools offer the promise of producing more accurate and powerful analyses from the perspectives of manufacturing, vehicle performance, support systems, and system operations. This will enable the industry to shift the emphasis on physical tests from a certification role, to a secondary and less costly role of benchmarking the computational tools needed to certify by analysis.

Three common themes permeated the symposium. First, that modeling and simulation have been applied to dramatically reduce the cost and cycle times associated with military acquisition. While a remarkable cross-section of the industry was presented, the symposium did not include as much simulation in virtual manufacturing, historically an area of significant AVT interest, as expected. Those papers that addressed the application of Virtual Reality to development and deployment (such as the CAVE system for US Army TACOM) demonstrated the tremendous integration potential of the technology to address historically subjective issues, such as ergonomics. Consistent application of these technologies to product development has resulted in reduced costs and cycle time with the

potential of achieving an overall 50% reduction. It is important to recognize that the most successful applications used Virtual Reality as the integration tool, both for the simulations and for the team. Second, that a number of new technologies, such as Knowledge-Based Engineering, are only just becoming available in the commercial marketplace and hold remarkable promise to enable further reductions in cost and cycle. Third, that while remarkable strides have been made in the application of modeling and simulation to replace physical testing, there is much work that remains to be done before widespread acceptance. The framework for this continued development would be much more powerful if it leverages both the existing successful examples and the new technologies mentioned herein.

A number of detailed recommendations were made to RTO as a part of the discussion at the end of the symposium and technical evaluation. These are discussed in depth in the full technical evaluation report.

La réduction des coûts et des délais d'acquisition des véhicules militaires par la modélisation avancée et la simulation de produit virtuel

(RTO MP-089 / AVT-090)

Synthèse

La défense des pays membres de l'OTAN rend nécessaire la définition d'un nouveau paradigme pour le développement et le déploiement des systèmes d'armes. Ce paradigme doit répondre à la dure réalité des budgets de défense en diminution et aux nouvelles menaces d'attaques peu conventionnelles mises en lumière par celle du 11 septembre 2001. Des outils de conception virtuels, des techniques et des processus de modélisation avancés, associés à des outils de fabrication virtuels en plein développement, sont actuellement appliqués à ce développement et à ce déploiement. Les compagnies militaires et civiles s'efforcent de réduire les coûts et les délais du cycle de conception de leurs produits, tant du point de vue de la conception/du développement que de celui de la fabrication en série, à l'aide de cette application. L'adaptation de ces outils au développement de systèmes d'armes abordables, telle qu'envisagée par les commissions MSG et AVT de la RTO, du stade de la conception jusqu'à l'exploitation, est indispensable pour atteindre les réductions de coûts et de délais demandées pour faire face aux menaces émergentes auxquelles l'OTAN se trouve confrontée. La composition pluridisciplinaire et l'importance accordée par AVT aux technologies appliquées aux véhicules, fournit un excellent cadre pour le développement, l'intégration et le déploiement plus poussés de cet environnement numérique, qui offre des possibilités extraordinaires de réduction des coûts et des délais de développement des systèmes d'armes. AVT rend un service essentiel à l'OTAN en encourageant le lancement de ce nouveau paradigme du développement basé sur la simulation électronique, par le biais de l'échange d'informations techniques entre les pays membres de l'organisation.

Du 22 au 25 avril 2002, la commission sur la technologie appliquée aux véhicules (AVT) de l'Organisation pour la recherche et la technologie de l'OTAN (RTO) a organisé un symposium très réussi sur le thème de « La réduction des coûts et des délais d'acquisition des véhicules militaires par le biais de la modélisation avancée et la simulation du produit virtuel ». L'objectif de ce symposium était de déterminer l'état actuel des connaissances et l'orientation future de la conception virtuelle, de la simulation, et des outils de fabrication susceptibles de réduire de façon considérable les coûts et les délais de conception, permettant de développer et de moderniser les systèmes de l'OTAN. Il a donné lieu à 62 communications sur les travaux de recherche et de développement actuels ou récents dans les domaines de la conception, la simulation et les outils de fabrication virtuels. La modélisation et la simulation ont été appliquées avec succès dans les domaines de la synthèse de la conception, la qualification par l'analyse, la simulation de la fabrication, l'aérodynamique, les turbomachines, l'hydrodynamique, l'aéroélasticité, le pilotage, la génération des maillages et l'adaptation, ainsi que la fidélité de la géométrie. Des questions spécialisées concernant l'aérodynamique numérique (CFD) ont été incluses afin d'examiner la persistance des dépassements de coûts et des retards dans les programmes qui se produisent dans le domaine de l'évaluation des performances aérodynamiques et hydrodynamiques. Ces questions comprenaient des exemples spécifiques d'applications technologiques aux véhicules, aux systèmes spatiaux, aux propulseurs, aux génératrices, et aux systèmes d'armes, réalisées par l'industrie et par les gouvernements. Les nouveaux outils de simulation promettent la réalisation d'analyses plus performantes et plus précises en ce qui concerne la fabrication, les performances, les systèmes de soutien et l'exploitation. De tels développements permettront aux industriels de changer la priorité qui était accordée aux essais physiques dans leur rôle de certification vers un rôle secondaire et moins coûteux qui sera l'identification des outils informatiques requis pour la certification par analyse.

Le symposium a été dominé par trois thèmes communs. Le premier a pour origine le constat que l'application de la modélisation et la simulation a eu pour effet de réduire considérablement les coûts et les délais associés à l'acquisition militaire. Bien que l'industrie ait été bien représentée, il y avait moins de contributions que prévu sur la simulation de la fabrication virtuelle, un domaine d'intérêt traditionnel pour AVT. Les communications concernant l'application de la réalité virtuelle au développement et au déploiement (comme le système CAVE du TACOM de l'US Army), ont démontré les possibilités d'intégration extraordinaires offertes par cette technologie pour la résolution de problèmes considérés jusqu'ici comme étant spécifiques à ce domaine, tels que l'ergonomie. L'application systématique de ces technologies au développement du produit a permis une réduction globale des coûts et les délais du cycle de fabrication, pouvant atteindre 50%. Il est important de savoir que les applications les plus réussies ont utilisé la réalité virtuelle en tant qu'outil d'intégration, tant pour les simulations que pour l'équipe. Le deuxième thème concerne un certain nombre de nouvelles technologies, telles que l'ingénierie basée sur la connaissance, qui viennent de paraître sur le marché et qui promettent des réductions de coûts et de délais encore plus remarquables. En troisième lieu, le symposium a conclu que bien que des progrès importants avaient été faits dans l'application de la modélisation et la simulation pour remplacer les essais physiques, il reste encore du chemin à faire avant que ces technologies ne soient généralement reconnues. Le développement futur devrait être basé sur les exemples existants et les nouvelles technologies mentionnées ci-dessus. Une importance particulière doit être accordée à la réalité virtuelle, et AVT devrait créer un groupe de travail sur l'application de cette technologie à la fabrication et aux mesures de soutien. Un certain nombre de recommandations plus détaillées ont été proposées à la RTO dans le cadre des discussions et des évaluations techniques qui ont clôturé le symposium. Ces recommandations sont détaillées dans le rapport d'évaluation technique.

De nombreuses recommandations détaillées ont été faites à la RTO pendant la discussion à la fin du symposium et de l'évaluation technique. Elles sont largement commentées dans le rapport d'évaluation technique.

Contents

---

† Paper not available.

A-II: TOOL INTEGRATION

A-III: QUALIFICATION BY ANALYSIS

Theme

The defence of NATO requires a new paradigm in the development and deployment of weapon systems. The development and integration of weapon systems modelling and simulation from concept to operation are essential to achieving the cost and time reductions needed to field new and improved weapon systems. Improved design simulation tools and advanced modelling methods, coupled with a maturing set of virtual manufacturing tools, are now being applied by air, land and sea vehicle companies to lower the cost and design cycle times of their products from both a design/development and recurring manufacturing perspective. The application of these advanced technologies across all aspects of the product development cycle can reduce these costs by as much as 50%. For example, the early identification and avoidance of problems currently downstream of the main design processes can dramatically reduce manufacturing costs, streamline manufacturing and assembly processes, increase supportability and maintainability, and avoid many operational problems that delay the time and cost effective deployment of modern weapon systems. AVT can perform a vital service in fostering this new paradigm because of its multidisciplinary composition and applied vehicle technology focus.

Part A of the Symposium emphasizes the use of advanced simulation to design, manufacture, and support new and existing NATO systems with reduced total cost and cycle time. This includes methods that allow us to reduce testing through the application of simulation, as well as methods that help us integrate toolsets together to produce an overarching concept-to-product simulation capability.

Part B of the Symposium is included to address the persistence of cost overruns and schedule delays that occur with aerodynamic or hydrodynamic performance validation. Emphasis is given to how CFD analysis and wind tunnel / hydrodynamic testing can be used together to most effectively reduce costs and developmental risk.

The Symposium will bring together specialists from Industry, Universities and Research Laboratories to review and report on the state-of-the-art in advanced modelling and virtual simulation. Keynote addresses will highlight the current use of tools and processes on military systems.

Thème

La défense des pays membres de l'OTAN rend nécessaire la définition d'un nouveau paradigme pour le développement et le déploiement des systèmes d'armes. Il est indispensable de développer et d'intégrer la modélisation et la simulation dans le cycle de fabrication des systèmes d'armes, de la conception jusqu'à l'exploitation, afin d'obtenir les diminutions de coûts et de délais qui permettront de mettre en service des systèmes d'armes nouveaux et améliorés. De nouveaux outils de simulation et des méthodes de modélisation avancées, associés à des outils de fabrication virtuelle de plus en plus performants, sont désormais mis en œuvre par les fabricants de véhicules aériens, terrestres et maritimes dans le but de réduire les coûts et les délais de conception de leurs produits tant du point de vue de leur conception/développement que de celui des cycles de fabrication. La mise en œuvre de ces technologies avancées pendant tout le cycle de développement du produit permettrait de réduire ces coûts jusqu'à 50%. Par exemple, l'identification rapide et l'évitement des problèmes actuellement rencontrés en aval des principaux processus de conception peuvent permettre de réduire les coûts de fabrication de façon considérable, de simplifier les processus de fabrication et de montage, d'améliorer la capacité de soutien et de maintenance, et d'éviter bon nombre des problèmes opérationnels qui entravent le déploiement rapide et rentable des systèmes d'armes modernes. AVT peut rendre un service essentiel en promouvant ce nouveau paradigme, en raison de sa composition pluridisciplinaire et de ses activités dans le domaine de la technologie appliquée aux véhicules.

La session A de ce symposium mettra en valeur l'utilisation de la simulation avancée qui permet de réduire coûts et délais lors de la conception, la fabrication et le soutien de systèmes OTAN nouveaux et existants. Elle traitera également des méthodes permettant de réduire le nombre d'essais par l'utilisation de la simulation, ainsi que des méthodes qui permettent de combiner des « boîtes à outils » pour réaliser une installation de simulation du type « du concept au produit ».

La session B examinera la persistance des dépassements de coûts et des retards dans les programmes lors de l'évaluation des performances aérodynamiques et hydrodynamiques. L'accent sera mis sur l'adéquation de l'association de l'analyse CFD et des essais en soufflerie ou hydrodynamiques pour la diminution des coûts et des risques de développement.

Le symposium rassemblera des spécialistes de l'industrie, des universités et des laboratoires de recherche, qui feront le point et rendront compte de l'état actuel des connaissances dans le domaine de la modélisation avancée et de la simulation virtuelle. Des discours d'ouverture mettront en lumière l'emploi actuel d'outils et de processus dans les systèmes militaires.

Publications of the RTO
Applied Vehicle Technology Panel

MEETING PROCEEDINGS (MP)

Reduction of Military Vehicle Acquisition Time and Cost through Advanced Modelling and Virtual Simulation
MP-089, March 2003

**Advanced Flow Management: Symposium Part A – Vortex Flows and High Angle of Attack for Military Vehicles /
Part B – Heat Transfer and Cooling in Propulsion and Power Systems**
MP-069(I), March 2003

Low Cost Composite Structures / Cost Effective Application of Titanium Alloys in Military Platforms
MP-069(II), March 2003

**Ageing Mechanisms and Control: Symposium Part A – Developments in Computational Aero- and Hydro-Acoustics /
Part B – Monitoring and Management of Gas Turbine Fleets for Extended Life and Reduced Costs**
MP-079(I), February 2003

Ageing Mechanisms and Control: Specialists' Meeting on Life Management Techniques for Ageing Air Vehicles
MP-079(II), February 2003

Unmanned Vehicles (UV) for Aerial, Ground and Naval Military Operations
MP-052, January 2002

**Active Control Technology for Enhanced Performance Operational Capabilities of Military Aircraft,
Land Vehicles and Sea Vehicles**
MP-051, June 2001

Design for Low Cost Operation and Support
MP-37, September 2000

Gas Turbine Operation and Technology for Land, Sea and Air Propulsion and Power Systems (Unclassified)
MP-34, September 2000

Aerodynamic Design and Optimization of Flight Vehicles in a Concurrent Multi-Disciplinary Environment
MP-35, June 2000

Structural Aspects of Flexible Aircraft Control
MP-36, May 2000

New Metallic Materials for the Structure of Aging Aircraft
MP-25, April 2000

Small Rocket Motors and Gas Generators for Land, Sea and Air Launched Weapons Systems
MP-23, April 2000

Application of Damage Tolerance Principles for Improved Airworthiness of Rotorcraft
MP-24, January 2000

Gas Turbine Engine Combustion, Emissions and Alternative Fuels
MP-14, June 1999

Fatigue in the Presence of Corrosion
MP-18, March 1999

Qualification of Life Extension Schemes for Engine Components
MP-17, March 1999

Fluid Dynamics Problems of Vehicles Operation Near or in the Air-Sea Interface
MP-15, February 1999

Design Principles and Methods for Aircraft Gas Turbine Engines
MP-8, February 1999

Airframe Inspection Reliability under Field/Depot Conditions
MP-10, November 1998

Intelligent Processing of High Performance Materials
MP-9, November 1998

EDUCATIONAL NOTES (EN)

Active Control of Engine Dynamics
EN-020, November 2002

Supercavitating Flows
EN-010, January 2002

Aging Aircraft Fleets: Structural and Other Subsystem Aspects
EN-015, March 2001

Aging Engines, Avionics, Subsystems and Helicopters
EN-14, October 2000

Measurement Techniques for High Enthalpy and Plasma Flows
EN-8, April 2000

Development and Operation of UAVs for Military and Civil Applications
EN-9, April 2000

Planar Optical Measurements Methods for Gas Turbine Engine Life
EN-6, September 1999

High Order Methods for Computational Physics, Published jointly with Springer-Verlag, Germany
EN-5, March 1999

Fluid Dynamics Research on Supersonic Aircraft
EN-4, November 1998

Integrated Multidisciplinary Design of High Pressure Multistage Compressor Systems
EN-1, September 1998

TECHNICAL REPORTS (TR)

Performance Prediction and Simulation of Gas Turbine Engine Operation
TR-044, April 2002

Evaluation of Methods for Solid Propellant Burning Rate Measurements
TR-043, February 2002

Design Loads for Future Aircraft
TR-045, February 2002

Ice Accretion Simulation Evaluation Test
TR-038, November 2001

NATO East-West Workshop on Magnetic Materials for Power Applications
TR-031, August 2001

Verification and Validation Data for Computational Unsteady Aerodynamics
TR-26, October 2000

Recommended Practices for Monitoring Gas Turbine Engine Life Consumption
TR-28, April 2000

A Feasibility Study of Collaborative Multi-facility Windtunnel Testing for CFD Validation
TR-27, December 1999

Programme Committee

CHAIRMAN
Mr. John Coyle
The Boeing Company, P.O. Box 516, Mail Stop S064-2809
Saint-Louis, Missouri 63166-0516, USA
email: john.m.coyle@boeing.com

CO-CHAIRMEN

Mr. Daniel Chaumette
Direction Technique Aéronef
Dassault Aviation
78 Quai Marcel Dassault
92214 Saint Cloud, France
email: daniel.chaumette@dassault-aviation.fr

Dr. Hany Moustapha
Pratt and Whitney Canada Corp.
1000 Marie Victorin (01RA4)
Longueuil, Quebec, Canada J4G 1A1
email: hany.moustapha@pwc.ca

MEMBERS

BELGIUM
Prof. C. Hirsch
Vrije Universiteit Brussel
Dienst Stromingsmechanica
Pleinlaan 2, B-1050 Brussels
email: hirsch@str10.vub.ac.be

GERMANY
Dr. Gerd Berchtold
EADS Germany
Military Aircraft, MT2
P.O. Box 801160
81663 Munich
email: gerd.berchtold@m.eads.net

ITALY
Prof. A. Salvetti
Universita Pisa (DIA)
via Diotisalvi 2
56126 Pisa
email: salvetti@ing.unipi.it

THE NETHERLANDS
Ir. H.H. Ottens
National Aerospace Laboratory-NLR
P.O. Box 153
8300 AD EMMERLOORD
email: ottens@nlr.nl

SPAIN
Dr. L.P. Ruiz Calavera
EADS CASA
Aerodynamics Department
Avenida John Lennon s/n
28906 Getafe, Madrid
email: luis.ruiz@casa.eads.net

TURKEY
Prof. Dr. C. Ciray
Middle East Technical University
Aeronautical Engineering Department
Inonu Bulvari, 06531 Ankara
email: cciray@rorqual.cc.metu.edu.tr

UNITED KINGDOM
Mr. M. Botley
MoD WSA
Marine Propulsion Systems IPT Leader
Cedar 2a, #3250
Abbey Wood, Bristol BS34 8JH
email: mpsipttl@wsa.dlo.mod.uk

Mr. C. Clarkson
BAE Systems
Warton Aerodrome (W392C), Warton
Near Preston, Lancs
email: chris.clarkson@bae.co.uk

Mr. K. Eaton
Alenia Marconi Systems Litd,
The Grove, Warren Lane, Stanmore
Middlesex HA7 4LY
em: kit.eaton@gecm.com

Mr. D. Rugg
Rolls-Royce plc.
Elton Road Laboratories
P.O. Box 31, Derby, DE24 8BJ
email: david.rugg@rolls-royce.com

UNITED STATES
Ms. M.A.R. Holly
BOEING
P.O. Box 516
M/C 064 2809
Saint Louis, Missouri, 63166
email: margaret.a.holly@boeing.com

Mr. D. Selegan
AFRL/VA,
2130 8th Street,
Wright Patterson Air Force Base
Ohio 45433-7542
email: david.selegan@wpafb.af.mil

Dr. J.C. Tromp
AFRL/VA,
2130 8th Street,
Wright Patterson Air Force Base
Ohio 45433-7542
email: jeffrey.tromp@wpafb.af.mil

Technical Evaluation and Report

Mrs. M.A.R. Holly
BOEING
P.O. Box 516
M/C 064 2809
Saint Louis, Missouri, 63166
United States

Dr. N. Sinha
Combustion Research
174 North Main Street
Building 3
Dublin PA 18917
United States

Prof. T. A. Weisshaar
Purdue University
School, Aeronautics &
Astronautics
1282 Grisson Hall
West Lafayette, IN 47907-1282
United States

Summary

The defense of NATO requires a new paradigm in the development and deployment of weapon systems. The development and integration of weapon systems modeling and simulation from concept to operation, as envisioned by both the RTO MSG and AVT Panels, are essential to achieving the cost and time reductions needed to field new and improved weapon systems. Improved design simulation tools and advanced modeling methods, coupled with a maturing set of virtual manufacturing tools, are now being applied by air, land and sea vehicle companies to lower the cost and design cycle times of their products from both a design/development and recurring manufacturing perspective. The application of these advanced technologies across all aspects of the product development cycle can reduce these costs by as much as 50%. AVT can perform a vital service in fostering this new paradigm because of its multidisciplinary composition and applied vehicle technology focus. It is important to NATO that the benefits from improved product simulation be realized in future systems.

The objective of the symposium was to determine the state-of-the-art and future direction of virtual design, simulation, and manufacturing tools that dramatically reduce the cost and design cycle time to develop or upgrade NATO systems. Sixty-two papers were presented which described state-of-the-art from nine member and PEP nations, a very thorough examination of current practices.

Introduction

The Applied Vehicle Technology Panel (AVT) of the Research and Technology Organization (RTO) of NATO organized an unclassified Symposium on "Reduction of Military Vehicle Acquisition Time and Cost through Advanced Modeling and Virtual Product Simulation." The objective of the symposium was to determine the state-of-the-art and future direction of virtual design, simulation, and manufacturing tools that dramatically reduce the cost and design cycle time to develop or upgrade NATO systems. This included vehicle platforms, space systems, propulsion, power, and weapon systems.

The symposium focused on recent and current research and developments in design, simulation, and virtual manufacturing tools. Specialized topics were specifically included in this symposium to address the persistence of cost overruns and schedule delays that occur with aerodynamic or hydrodynamic performance validation.

An expanded plenary session followed the opening ceremonies. The remainder of the symposium was structured in two parallel streams. The first stream "Design, Manufacturing, and Support Simulation" included the areas of Design Synthesis, Qualification by Analysis, and Manufacturing Simulation. Papers sought to contribute to our current understanding of

methods used to apply advanced simulation to design, manufacturing, and support of new and existing NATO systems. The second stream considered the "Optimum Blend of Numerical & Physical Fluid Experiments."   Papers sought to articulate our current understanding of the optimal blend of CFD analysis and wind tunnel / hydrodynamic testing to minimize costs and developmental risk.

Papers were presented as follows:
        Keynote Presentations - 6 presentations
        Part A
                Prototyping and Simulation - 11 papers
                Tool Integration - 8 papers
                Qualification by Analysis - 8 papers
                Design Synthesis - 14 papers
        Part B
                CFD Modeling of Non-Linear Phenomena - 5 papers
                CFD Validation Procedures and Error Evaluation - 4 papers
                Dynamically Coupled CFD - 6 papers
        Total Presentations - 62

This symposium presented a comprehensive view of the current applications of advanced modeling and simulation to achieve cycle and cost reductions in the acquisition of military vehicles.

Evaluation

In their book <u>Revolutionizing Product Development</u> [1] Wheelwright and Clark note that "Firms that get to market faster and more efficiently with products that are well-matched to the needs and expectations of target customers create significant competitive leverage. … The growing breadth and depth of technological and scientific knowledge has created new options for meeting the needs of an increasingly diverse and demanding market. The development of novel technologies and a new understanding of existing technologies increase the variety of possible solutions available to engineers and marketers… (f)urthermore, the new solutions are not only diverse, but also potentially transforming. New technologies in areas such as materials, electronics, and biology have the capacity to change fundamentally the character of a business and the nature of competition."

These remarks are particularly pertinent to the papers presented in the keynote presentations and in Part A of the symposium. These papers had a wide range of applications from space launch vehicles, aircraft, aircraft engines, naval weapons systems - from torpedoes to ships - and land vehicles. The primary focus was on the use of advanced simulation to design, manufacture, and support new and existing NATO systems with reduced total cost and cycle time.

In some cases (such as "Virtual Prototyping in Naval Ships" and "Simulation of Aircraft Deployment Support") shrinking budgets were cited as a driver for the application of modeling and simulation. Market share retention was cited in others ("The Digital Mock-Up as a Virtual Working Environment within the Development Process"). A number of significant issues raised during the keynote presentations were supported by the technical presentations of Part A.

---

[1] Steven C. Wheelwright, Kim B. Clark, *Revolutionizing Product Development – Quantum Leaps in Speed, Efficiency, and Quality*, The Free Press(A Division of Macmillan, Inc.), New York, 1992.

A most consistent issue related to the tools and the architecture. The available tools and processes are, at the present time, most mature in the area of structural geometry. However, this represents but a small portion of the total work that goes into any military product. Seminal work has been done in the application of modeling and simulation to other engineering disciplines ("Using Modeling and Simulation to Graphically Display the Interaction of the Fire and the Extinguishing Agent") and to manufacturing processes ("The Factory is Virtual….The Savings are Real"). Developers of tools and information technology (IT) architectures may not have a deep-seated understanding of all the information, processes, and the linkage among them - from all engineering disciplines, suppliers, procurement, manufacturing, training and support services - which must be managed if shared vision is to be achieved ("A Data-Centric Infrastructure for Multidisciplinary Analysis Integration and Management").

All Design Synthesis presentations observed that computer tool developers must understand the design process and the needs for information at each level as the design progresses if they are to be relevant. Inappropriate information or good information at the wrong time will have no effect on risk reduction, product quality or design cycle reduction. Total risk reduction, simply canceling the design project, is a response to too little information or too much data that creates more confusion than confidence. Some projects have been quite successful, despite the need for users to create custom work to address lack of commercially available integrated tools ("Virtual Development and Integration of Advanced Aerospace Systems: Alenia Aeronautics Experience").

In addition, varying degrees of maturity exist for acceptance and application of modeling and simulation. Again, the engineering community is where modeling and simulation have been most broadly applied, with structural geometry the area in which practices and acceptance are most mature, although progress has been made in other areas ("Demonstrating the Potential Use of Virtual Prototype Modelling Techniques for Future AFVs" and "Advanced Collaborative technologies to Support Systems Integration and Design").

The modeling and simulation technology solutions that have been brought to bear in the engineering community and those that have been brought to bear in the CAD/mfg/support solutions have not yet been fully integrated. Where solutions exist in these areas ("Simulation of Aircraft Deployment Support", "The Factory is Virtual…The Savings are Real", "Haptic Interfaces for Prototyping" and "Process Modelling of Fabrication of Critical Rotating Components for Gas Turbine Applications"), the tools and processes range from relatively straightforward and user-friendly to cumbersome with complex algorithms requiring highly specialized expertise. This means that industry and customers still bear the cost and cycle time penalty of waiting for translation of information among the various tools and that run take on the risk of not having consistent data in both types of systems. There is only downside risk in this situation. Engineering analysis and manufacturing analysis have only begun to be linked.

The issue of validating and verifying modeling and simulation as predictors of and replacements for testing was brought up multiple times ("Exemple d'utilisation des techniques d'optimisation en calcul des structures", "Multidisciplinary Simulation of Vehicle System Dynamics", "Virtual Testing with Validated Analysis Tools", "Affordable Evolution: The Engineering Change Proposal (ECP) 6038 F/A-18 Forward Fuselage Structural Certification", "Aircraft Structural Design Geared For High Reliance On Analysis for Acceptance", "Uncertainty Quantification in Airframe Design" and "Analytical Support in Aircraft Certification". In order to understand, manage, and reduce potential risk associated with the replacement of full-scale test articles, large amounts of historical data will be needed for

statistical analysis to correlate analytical predictions with actual test data to the desired confidence level. Governments' data rights in contracts may limit sharing of this data as well as the sharing of the best tools and techniques for modeling and simulation

The business jet and regional jet enterprises ("Challenges of Aircraft Design Integration") are particularly sensitive to schedule length so they have a demanding requirement for short product design cycles. Companies such as Bombardier, Embraer, Cessna, Raytheon and others in the business jet and regional jet market must produce new, high quality, products much like automobile manufacturers who introduce a stream of new models to satisfy the consumer. The Bombardier presentation was particularly focused on use of CFD to ensure that aircraft performance targets such as drag were met before the design project was launched.

Discussion time focused on how have advances in technology have and potential resulting organizational changes. The author's reply was that the main change was to optimize information exchange and flow. This was consistent with other observations during the meeting that the introduction of new information generated by computer codes required it to be timely and presented in appropriate fashion so that it could influence design decisions, not simply approve or re-work design decisions made much earlier.

A new torpedo with active ribs for acoustic noise suppression involves radical design where little database exists ("Undersea Weapon Design and Optimization".) The paper also used the results generated as input for CAIV (Cost as an independent variable) for risk management. This type of activity uses computer simulations to generate valuable information for new concepts with no existing database.

Efforts have been made to link or interface computer software to create a design process for reusable launch vehicles ("Collaborative Design Environment for Space Launch Vehicle Design and Optimization"). These efforts could create a "learning organization" to assess trades between technologies and also assess the impact of requirements on operational features of systems that require quick turnaround to fulfill mission requirements.

Simulation has been used to create understanding of the effects of decisions made by teams ("Modelling and Simulation in the Design Process of Armoured Vehicles".) The correlation between advanced modeling and actual test results can be quite good. Formal design methods to examine choices and their effect on the product effectiveness and quality have been applied ("A Preliminary Engine Design Process for an Affordable Capability".) This study used rapid data generation to provide better decisions and showed the need to incorporate formal methods to insert information into the design/development process.

Collaborative research to reduce development time, prioritize concepts, identify critical technologies and most importantly, define cost studied the application of a cost prediction tool ("Scenario-Based Affordability Assessment Tool"). The effort may lead to increased confidence levels and risk reduction in product development by developing computer simulations of the links between product features and cost.

The application of modeling and simulation to a variety of design challenges consistently demonstrated improvements in the quality of the design, the cycle time to produce the design, and/or the cost of producing the design. The challenge of inserting new technology into current or newly designed products ("Multi-scale Modeling & Simulation-Shortening Materials Transition from Processing to Product") is particularly important to the materials

community where the time from discovery to transition is measured in decades. An additional benefit is the creation of a learning organization that can identify new concepts.

Work applied to ship structures ("Impact Flows and Loads on Ship-Deck Structures" and "Optimal Shape Design of a Surface Combatant with Reduced Wave Pattern") demonstrated the capability of modeling and simulation to add information to the design process. In the latter case, genetic algorithms were used to identify surface features of ship's hulls to reduce drag. Turbomachinery design ("Preliminary Multi-disciplinary Optimisation in Turbomachinery Design") can particularly benefit from simulation of complex flow fields in compressors and turbines. An experiment in which accurate information generated by finite element models from NASTRAN was added to a team design exercise so that the design was improved and cycle time was shortened ("Improved Structural Design Using Evolutionary Finite Element Modeling").

Addition of external antennas so that they are effective while minimizing degradation of aerodynamic performance is another demonstration of the positive effects of modeling and simulation ("Reduction of Time and Costs for Antennas Integration Through Computational Electromagnetism").

Aeroelastic effects represent an expensive feature of the aircraft development process. An aeroelastic problem discovered during flight test can lead to costly changes in the production aircraft or lead to changes that so drastically reduce the performance that the aircraft project is abandoned. The CATIA-ELFINI computational code has been used to examine aeroelastic features of new designs to control risk and cost ("Current Developments in Computational Aeroelasticity at Dassault-Aviation for the design of Modern Military Aircraft and Business Aircraft"). This versatile tool is used to identify critical load cases and examine integration of non-linearities related to buffeting, free play and other effects that can limit the performance and life of vehicle structures. This type of analytical capability can identify critical tests and reduce the need for others. The result is a better design and reduced cost.

Part B of the Symposium focused on the persistence of cost overruns and schedule delays that occur with aerodynamic or hydrodynamic performance validation. Emphasis was given to how CFD analysis and wind tunnel/hydrodynamic testing can be used together to most effectively reduce costs and developmental risks. The15 papers presented covered a wide range of topics:
- Aerodynamics
    - -Aircraft
    - -Store Separation
    - -Helicopters
    - -Missiles
- Turbo-machinery
- Hydrodynamics
- Aero-elasticity
- Flight Control
- Mesh Generation & Adaptation, Geometry Fidelity

Overall, the papers presented reflected current state-of-the-art in tools and processes of CFD and a view of the future.

The presentations indicated the parallel computing architectures have become quite widespread. This is probably the single event that has had the most impact on CFD modeling and simulation. It appears that almost all CFD applications are now utilizing parallel platforms with a large variety of computing platforms represented. In addition, MPI

communication libraries have provided portability. The ready availability of large scale, massively parallel architectures is a very welcome development that puts tremendous computing power into the hands of design engineers. These tools reduce turnaround for CFD work performed by design engineers, thus reducing cycle and cost.

CFD is being integrated with a variety of multi-disciplinary design optimization techniques. There is clear evidence of the impact of CFD on the design process. Examples were given of such in the design of air vehicles, turbo-machinery, and hydrodynamics. In short, CFD applications have begun to migrate toward design support. In addition, CFD is being applied to problem solving in some non-traditional environments. Examples were presented of
      CFD application to MHD flowfield
      CFD coupling to CSD and aeroelasticity for flutter, LCO, etc.
      CFD coupling to ice formation in wings

Coupling to CSD lends itself to implementation on parallel platforms, permits analysis to move beyond the limits of aircraft components to a full aircraft. These presentations linked directly to the emphasis in the keynote presentations - that integration of the tools is key to achieving costs reductions. Coupling to ice formation allows the assessment of environmental impact on the aircraft and moves modeling and simulation into the realm of operation support analysis.

In addition, the use of unstructured mesh CFD is becoming increasingly common. The advantages of unstructured mesh are: facilitation of interface with CAD, CSD and other multi-disciplinary simulation tools; the development of a natural framework for mesh adaptation; and the facilitation of tool integration.

Given the remarkable advances in the application of CFD and modeling tools and techniques, challenges remain. CFD has not acquired any level of standardization. This means that there are multiple tools employed during design (structured and unstructured mesh), that there is no universal turbulence model (e.g. within 0, 1 and 2 equation models there is variability; there are non-linear extensions; unsteady flows require large eddy simulation). The breadth of physics encountered in CFD application and maturation is staggering. Lower order CFD methods will be useful in design and reduced order models have recently emerged. So while CFD has not yet attained the maturity of finite element modeling, the overall picture is very encouraging.

Observations

The keynote presentations focused on a high-level view of the application of modeling and simulation to military vehicles to reduce both the cost and cycle time of acquisition. Market and political factors are pressuring the military to reduce the costs and cycle of our products, a fact of contemporary business, placing strains on engineering resources, manufacturing resources, financial resources, and human resources.

The focus on decreasing the ratio of price for performance and the emergence of cost as the main parameter for entry into significant markets is a fact of business. All sectors (land, sea, air) have a similar focus and vision for the application of modeling and simulation and of its potential to reduce cycle time and cost in the acquisition of military vehicles. Both the military and contractors see the potential for modeling and simulation to anticipate and resolve issues in a virtual world that heretofore had been only done in the physical, where such issues would result in higher costs, longer cycle times, and significant revisions to products.

Moreover, the sectors consistently view modeling and simulation as a vehicle that enables, encourages, and energizes the application of multi-disciplined teams.

State-of-the-art tools (such as the U.S. Army CAVE system) allow groups of people to view the products both from a design perspective and an application perspective in a digital, three-dimensional environment. These systems allow businesses to actively collaborate real-time with suppliers, customers, and partners over the globe (as discussed by SAAB), working not just within teams, but also across teams. This brings all the people associated with the product, from technical engineer to the soldier, into the design process. It allows us (as shown by Dassault Aviation) to understand not just the individual area or technology for which each individual or small group may be responsible, but to understand the entire vehicle and how our customer will use it. It increases the power in the voice of those portions of the organization (such as manufacturing) that have heretofore lacked quantitative tools to support their positions and inputs to the design process. The vision, as expressed by Bombardier, is of a paperless aircraft that can be transported through the entire organization. BAe Systems vision takes this through the entire life cycle of the aircraft, from initial design stage through disposal.

Whether in structures or subsystems (as shown by the Air Force Research Laboratory), the key to reducing development costs is "…to avoid redesign by discovering and correcting problems at the earliest possible time in the … development process — preliminary and detailed design". Keynote presentations gave several examples of just how modeling and simulation work have already achieved significant cost and cycle reductions in land, sea, and air-based systems. In addition, presentations showed potential enhancements to the state-of-the art practices through the application of web-based technologies and with the integration of functional and geometric models (BAE Systems-Sea Systems).

In order to broaden the results achieved, the varying degrees of risk tolerance that currently exist among both users and customers must be addressed. Acceptance for the technical and programmatic changes that result from the application of modeling and simulation must be broad-based across industry, customers, and academia. Some communities continue to insist upon physical tests and hardware, having less than full confidence in the ability of the models and simulations to accurately reflect the product and its environment.

Linkage between modeling & simulation techniques and cost/cycle reduction has been demonstrated, achieving remarkable results in some areas. However, this linkage is not yet consistent across the industry nor has it been demonstrated for all aspects of the products (such as tailoring/minimization of test programs, subsystems-hydraulics, electrical). The industry is not yet able to directly and consistently link reductions in cost and cycle time for the development of military vehicles with the application of modeling and simulation techniques described during the conference.

There is broad, but not pervasive, recognition of need to move information up front - "frontloading" - to encourage early participation by downstream users of products and services in a multi-disciplinary team environment in which the team includes not only the various engineering disciplines, but manufacturing personnel, suppliers, partners, and customers. The challenges associated with cost models must, in addition, be recognized. These models and the associated processes suffer the same long cycle times and uncertainties in output of much of technical product modeling.

The papers presented in the Design Synthesis session show the fantastic progress that has been made in modeling and simulation, particularly in the structures and structural dynamics area. These tools allow design teams to consider in great depth many different design alternatives and to debate their merits using physics based data and personal experience. In some cases, there is no personal experience so the availability and accuracy of the physics based information is vital to low cost, low risk development in a reasonable time.

An efficient organization with experienced, knowledgeable designers and analysts, equipped with effective analytical tools, is essential to high quality product development. Between 1950 and 1990 two major efforts produced a revolution in aerospace design and development. The first was military competition between the NATO allies and the Soviet Union. The second was the introduction of commercial, high capacity transonic aircraft and turbo-jet/turbo-fan engines into the worldwide air transportation system.

These developments produced numerous innovative airplanes, ranging from Boeing 747's to high-speed jet fighters and bombers. These efforts also created trained designers at all levels. The time between initial design inception and final testing was relatively short, while funding for new projects reached extraordinarily high levels.

Many of the highly qualified people produced by this "golden age" have since retired or are on the verge of retirement. They have not always been replaced with people who have had wide design experience. The number of new and projected military and transport aircraft has declined drastically, while product requirements and complexity, together with the demands for reduced cost, reliability and fuel efficiency continue to increase. The challenge today is not just to do things faster, better with less cost, within an allotted time, but also to do it with fewer people with less experience than before and to provide experience and associated knowledge for younger engineers. This latter goal is often called "creating a learning organization" and has traditionally been accomplished by mentoring of the young and inexperienced by the older and more experienced.

High quality products require a wide variety of analytical methods ranging from simple first principles to sophisticated structural finite element methods and computational fluid dynamics codes. These products also require visual simulation - using tools such as CATIA - to foster integration of the diverse number of pieces that must be designed and assembled. Analytical and computational methods supported by the computer are essential so that design features can be selected, scrutinized for adequacy, and then changed when defects or performance limitations are discovered. As a result, there has been an explosion of software development at all levels of mathematical complexity.

Some sophisticated software tools have failed to have a large impact on either product cost reduction or quality. Part of this failure can be laid directly to the unwillingness or inability of the design and product development organization to use the new products or to evolve and change as much as analytical technology has changed. Additional blame must be placed at the feet of software tool developers who do not understand the needs of the design process or the business enterprise that surrounds the engineering design effort.

Effective product development must involve restructuring of the design and product development process to take advantage of the information produced by these tools. Gross points out that companies that have successfully re-engineered their business processes have adopted a "system oriented approach which focuses on the integration of all disciplines" and that their business processes are "re-engineered around a flow of information instead of a flow of tasks." This focus on information flow explains why some tools are regarded as useful

while others are not. Unless information is appropriate, meaningful and comprehendible, it will languish within the organization that generated it, having no impact on product development.

Steward ([2]) discusses the design of complex systems such as aerospace products and re-iterates the need for the timely generation and flow of information. Smith and Eppinger ([3]) stress the need for integration within complex processes, including when to connect and when to disconnect integrated processes so that concurrent design makes sense and is executable. This involves planning and controlling information flow.

All of the papers presented in this session can contribute to reduced cycle time, development of a learning organization, and improved product quality if they are integrated into an organization that uses the information generated in a timely effective manner. Educating the tool developer remains a primary need of effective organizations. Developing and understanding requirements for the system and laying out the path to an efficient product that can use new technology effectively remains an elusive goal. The rapid absorption of new technology developed by the Science and Technology (S&T) community also remains a challenge. Today there is an abundance or over-supply of technology when compared to the demand for systems.

In order to achieve cycle time and cost reductions that could result from the systematic application of CFD, the tools and processes need to be validated and verified. This is a critical issue that must be addressed even as focus of the technical community is directed toward efficient utilization and integration of the tool. There are three requirements to achieve the improvements in cycle time and cost which are clearly desired by the customer community:

1)   Standardization of CFD tools. This has not been achieved to date.
2)   Standardization of processes. This includes modeling practices and consistency across tool performance across design spaces. Currently CFE tools operate best within a narrow range of validity and cannot support design outside the validated parameter space. In addition, data interpretation is, at best, an inexact process.
3)   Validation and verification of the tool(s) and process(es). This will require collection and analysis of sufficient data to support statistical analysis with high reliability. Data from experiments (wind tunnel) as well as flight test will be required from a variety of vehicles and a variety of flight regimes to document the predictive power of CFD across the required parameter space and to enlarge the parameter space. Data need to be collected in a standardized, non-traditional way to include flowfield data in addition to current surface measurement techniques. This is particularly important in the areas of turbulence and transition.

In summary, while CFD has made tremendous progress towards supporting air vehicle design, much work remains to reach its full potential as an advanced modeling and simulation tool. For the near future, CFD must be complemented by experimental testing. This is a step that will contribute to the verification and validation effort discussed previously, increasing confidence in CFD techniques and tools.

---

[2] Steward, D.V., "The Design Structure System: A Method for Managing the Design of Complex Systems, IEEE Transactions, Engineering Management, EM-28, 3 (1981), pp. 71-74.
[3] Smith, R.P. Eppinger, S.D., "Identifying Controlling Features of Engineering Design Iteration," Management Science, Vol. 43, No. 3, March 1997, pp. 276-293.

Conclusions and Recommendations

Modeling and simulation allow the technical community to produce unprecedented amount of information at incredible speed. Integrated product teams can analyze alternatives and provide input to management decisions in time spans that are much shorter than ever. One of the impacts of this is that management decision-making must take place at increasing speed, lest the teams sit unproductive, awaiting a decision. This potential scenario means that the speed and accuracy of management decisions is an area for review and development.

While the symposium presented the significant progress which has been achieved in the areas of product modeling, CFD, and design synthesis, the absence of significant data on capabilities of modeling & simulation in manufacturing and support indicates an opportunity for further emphasis by RTO.

The verification and validation of modeling and simulation was discussed in Part A and Part B. The application of modeling and simulation to achieve the cycle time and cost reduction potential will require validation and verification of the tool(s) and process(es). This will require collection and analysis of sufficient data to support statistical analysis with high reliability. Data from experiments as well as laboratory, ground and flight test will be required from a variety of vehicles and a variety of flight regimes to document the predictive power of modeling and simulation.

Data need to be collected either in a standardized, non-traditional way or "normalized" to establish comparability. This is will allow statistical correlations to be established and quantify the degree to which modeling and simulation may replace all manner of "test" articles - for example, full scale structural test articles. In the case of application of modeling and simulation to manufacturing and support, data will also be needed to verify the predictive power of the models to anticipate issues and accurately represent conditions in the factory and in the field.

As much of the software used in these applications is commercial, software suppliers and developers may have collected much relevant data. Recognition of these correlations will enable substantial reductions in cycle time and cost by replacing "test" articles for these processes - for example, first article fabrication and inspection, first assembly build and inspection, maintenance demonstrations. RTO has the opportunity to set the standards for the minimum acceptable data set (i.e. correlation and confidence factor) for validation and verification of modeling and simulation tools and processes.

Acceptance of modeling and simulation as replacement for physical testing, whether for manufacturing processes or is not yet widespread. There are two apparent major influences in this scenario. The first is that the application of modeling and simulation has not yet been validated (per the previous discussion). The second is that stakeholders in physical testing may be uncomfortable. Overcoming both these factors in the part of both industry and government customers will require the encouragement of organizations like RTO to accept the data and achieve the cycle and cost reduction results associated. From a military planning perspective, this would dramatically improve the collective responsiveness to changes in the threat environment.

Modeling and simulation tools and techniques hold the promise to greatly enhance trade studies. These tools and techniques have to potential to provide much more information more quickly for each of the alternatives within a design space. The result would be a much thorough investigation of possibilities prior to making the commitment to a specific

configuration. With linkage of technical modeling and simulation activities to cost modeling for design space trades, both industry and customers would be able to more effectively achieve the objectives of any given program. Certainly, additional development work in the linkage of technical modeling and simulation activities with cost modeling tools will advance the state of this art and the state of the industry. RTO has the opportunity to provide the post-delivery life cycle portion of life cycle cost data for all the various deployment scenarios of member countries.

Current contracts address data rights in vastly different ways. These are, in many cases, not supportive of the sharing data and experiences in order to consolidate data. In order to achieve the most powerful potential applications of modeling and simulations (those which will replace full scale test articles and those which will integrate all the potential applications (manufacturing simulation, cost modeling, reliability based design), large amounts of data from multiple programs will need to be collected and analyzed. Contractors, agencies, and governments must support sharing of data, including contractual provisions which will encourage sharing for the greater gain. RTO could become the vehicle for facilitating this information sharing.

Investment in analysis techniques that relate engineering (technical analysis) and manufacturing analysis is an area of enormous importance. Fundamentals of material properties and manufacturing process characterization are best expressed in statistical terms. The relationship between technical requirements and the manufacturing capabilities are clearly enablers to enhanced affordability and to reliability based design. As one participant noted, "It may cost less to design what you can fabricate rather than try to fabricate …[parts] with no imperfections". RTO's support for these investments would emphasize the need to ensure that this potential is realized.

RTO has the opportunity to take an active role in the achievement of the full potential reduction of military vehicle acquisition time and cost through advanced modeling and virtual product simulation. Specifically, RTO has the opportunity to

- establish guidelines for acceptance of analysis in lieu of full-scale testing. This includes the amount and type of data to be analyzed and the confidence levels required by customers. It will also involve the sharing of technical information described earlier.
- further investigate reliability-based design and analysis. As a potential area to reduce cycle time and cost, this is the area with the most leverage. Products would be in service earlier, with fewer issues (resolved in the digital environment), at a lower cost, and life cycle cost (resulting from inspections and repairs) would be better managed.
- establish guidelines for multi-disciplined peer review of research projects. The symposium presented tremendous results from the application of multi-disciplined teams working within industry and with industry and government. However, the research projects presented still appear to be very discipline-oriented. Research traditions are of peer review, yet the results of multi-disciplined approaches are undeniably strong. Lack of explicit integration of research across disciplines to produce effective tools and processes will inhibit the maturation of modeling and simulation to achieve its full potential. RTO should establish guidelines for research review which include not only technical peers from the particular discipline but from other disciplines which will, upon application of the research, be impacted by the resulting tools and process(es).

- establish guidelines for code/tool/user validation/application which comply with ISO requirements. ISO certification has become fundamental to the military acquisition business. These standards represent common understanding and business standards across industries, companies, and countries. As modeling and simulation are more regularly applied, compliance with ISO standards will be more
- emphasize that improvements in the cost and cycle of our technical efforts should be accompanied by similar improvements in the associated business processes. Ideally, we will be able to link our cost modeling to our technical modeling in order to be able to trade cost as a parameter in the design process and have the same degree of confidence in the decision that we do in the technical decision.

Technical Evaluation – Part A

Discussor's Name: John Moon
Author's Name: Margaret Holly/Terry Weisshaar

Q: We need to do two things to go along with work developing reliability-based analysis
1) What are the actual benefits (cost/time)?
2) How do we certify and qualify the methods?

A: 1) Actual benefits will be a function of the particular platform to which the techniques are applied. In a typical military acquisition program, multiple test articles are built and testing prior to entering into production. For example, if a vehicle costs $20M, requires 18 months to built and three test articles are required, the savings become $60M and anywhere from 18-54 months for the total program. This gets products into the hands of customers earlier and potentially allows the customer to purchase more units.

2) Certification will require the collection and analysis of sufficient information to present a distribution of properties. The techniques applied will be very similar to those currently applied to subsystems to calculate parameters such as mean time between failures and mean time between unscheduled maintenance actions. These techniques are widely used in the electronics industry, in flight control systems, and in systems safety applications. It is their application to structural analysis and the using the analysis to replace test articles that is new.

Discussor's Name: John Coyle
Author's Name: Margaret Holly

Q: Analysis results need to reduce F/A-18 ECP6038 testing points out the potential that Reliability Based Design brings to the future. However, there is much effort required to bring this approach to maturity.

A: Absolutely. Bring reliability-based design to maturity will require sufficient amounts raw data in consistent formats to truly establish the population profiles on which this approach will be based. This can happen much more quickly if data can be shared across programs, across customers, across nations so that all will ultimately benefit.

Discussor's Name: Dr. Kam Ng, Office of Naval Research
Author's Name: T. Weisshaar

Q: Comments on Terry's remark on using modeling and simulation for transitioning products to customers.--Customers and end users still want to see testing and demonstrations before accepting the technology and products. Although they believe modeling and simulation, they consider it as a tool for product development. However, they do have interests for simulation-based acquisition for product planning, assessment and cost analysis

A: Modeling and simulation can only take us part of the way down the development path. The devil is definitely in the details – many of which depend on cost. However, we can often get a good handle on the performance of the device and its link to military missions, both current and new. A good example where simulation may prove helpful is the development of UAVs where the aircraft have new uses and new geometric forms. Our goal should be to speed up the virtual evolution of new concepts rather than costly trial and error.

Discussor's Name: David J. Moorhouse
Author's Name: T. Weisshaar

Q: I would like to refer to a comment made by Prof. Weisshaar about the use of reliability-based design. That has been commonplace in flight control systems design for many years. There is a prescribed probability of degradation due to FCS [Note: Terry, if you can define what this is, please educate me so it can be included in the final report. Thanks!] failures. The complete design is based on reliability predictions and probability. There may be lessons learned by exchanging information between completely different technical disciplines.

A: This is an excellent reminder that while structural design uses factors of safety to improve and address reliability, the flight controls people must also address reliability but without factors of safety since they make no sense in their work. This is a point that deserves serious consideration.

Discussor's name: Professor Ramana Grandhi, Wright State University, USA
Author's name: T. Weisshaar

Q: Comments for Professor Weisshaar (paraphrased). Wouldn't it be better to simply optimize the number of spars in the beginning instead of taking time to discuss this in a meeting? (The question referred to one of the activities for the design team that used finite element results as part of a design process).

A: Yes it would be better. However, when you go to a design team meeting for the first time you are uncertain of the "sticking points" of other group members. We did not find out that the number of spars was a serious point of contention until after the first meeting. This was one of the lessons learned from the project.

Discussor's name: Dr. Joseph Manter, Air Force Research Laboratory, USA
Author's name: T. Weisshaar

Q: Comments on Professor Weisshaar's paper. Do you think that your new design process will be used by your client on his next design project? Why?

A: Yes I do because key people in the design process embrace the concept. It allowed experts from various disciplines to ma ke appropriate design trades and then optimize the overall design. It also allowed the structural expert to optimize his design with a fuller understanding of the requirements and constraints not stated formally; for instance, there is a need for inspectability that cannot be expressed as part of a performance index to optimization.

Advances in Product Modelling and Simulation at Dassault Aviation

Lionel de la Sayette
Senior Vice President Research and Development
Dassault Aviation
78 quai Marcel Dassault
Cedex 300, F-92552 Saint Cloud
France

ABSTRACT

Aerospace industry has always been in the forefront in relying as much as possible on modelling and simulation to continuously increase global efficiency of product development and realization. A comprehensive combination of partial tests and simulation stands as a low-cost approach to limit the number of necessary prototypes to design, develop and qualify a new product.

For more than 30 years Dassault Aviation has invested large efforts in the field of product modelling and simulation, as it has always been considered as an essential asset in the sustained competitiveness of the company. The best known offspring of this policy is the CATIA software initially developed by Dassault Aviation for its own needs, and now a world standard marketed by Dassault Systèmes.

Another significant example of systematic resorting to simulation is given by the RAFALE program : the number of prototypes has been drastically reduced to only 4, for an airplane in 3 different versions and due to replace 7 existing different aircraft of French Forces.

Dassault Aviation field of activity includes both Military Air Sytems (manned aircraft and UAV) and Civil Aircraft (the FALCON line of business jets), and for both the company acts as an architect of complex systems and an aircraft designer.

The presentation will lay out what today's Dassault Aviation specific answers are in terms of processes and tools as well as the future challenges to be taken up considering future combat air systems.

Four main objectives drive the effort to improve the overall efficiency of every new product development :
  – Initialize the design from valid requirements.
  – Reduce time spent in each elementary task.
  – Parallelize as much as possible the workflow.
  – Set up dynamic risk management
Each one will fully benefit from Dassault's modelling expertise from preliminary upstream studies to comprehensive simulation of the whole life cycle costs.

The overall process developed today is a "multisimulation process" :
  – Multilevel : from the overall design to the detailed design
  – Multidisciplinary : integrated and based on the same reference
  – Multipartner/Multisite : developing global models including coherent and relevant models produced by partner companies.

Specific emphasis will be brought on associated scientific, information technology and management challenges. The key issues leading to efficient development of appropriate simulations in a cooperative environment will be discussed.

----

1. CONTEXT

The Dassault Aviation company field of activity covers both military and civil aircraft :

PRODUCTION AIRPLANES

M2000-D **M2000-9** **RAFALE M** **RAFALE B**

FALCON 50 EX **FALCON 2000 EX** **FALCON 900 EX**

CUSTOMERS BENEFIT FROM BEST PRICE / PERFORMANCE RATIO

– Military aircraft :

  – manned fighter, maritime patrol and trainer aircraft. Today the MIRAGE 2000 and RAFALE are in production in several versions, offering optimised solutions to specific requirements and a dramatic decrease in operating cost.

  – UAV : studies on UAV and UCAV are in progress, specifically directed to meet new emerging needs with a stealthy UAV demonstrator already flying.

– Civil Aircraft : the very successful line of Falcon business jets. Today several types are in production using improved methodologies from basic layout to 3D completion work. The brand new type, FALCON 7X, is developed taking into account major advances in cooperative design.

– Space : Dassault extends its expertise in reentry vehicle aerothermodynamics and is producing pyrotechnical systems for launchers and a wide range of customers.

The Dassault Company is acting both as an architect of complex systems and as an expert in the challenging field of aircraft design and development.

Since the sixties Dassault Aviation has devoted a considerable in-house effort in modelising the aircraft components and its physical behaviour ; the company has steadily considered as mandatory for its competitiveness to be able to use the best possible tools to fulfill two objectives :

– get the best product by way of a better optimization,

– reduce the development time and cost by streamlining the design to manufacturing process and by reducing the amount of required tests.

These efforts led to the development of very efficient codes for Aerodynamics, Structure design (CATIA and ELFINI), Flight controls and Performances, and more lately on Electromagnetic and Thermal signatures.

In parallel to these developments Dassault has also invested in Avionics - Flight Control Systems - Mission and Weapons Systems modelling, with simultaneous development of technologies, for example modular avionics, and methods, taking advantage of object oriented technologies.

SYSTEMS DEVELOPMENT : CONTINUOUS IMPROVEMENT

Two obviously successful examples of the results of this policy must be highlighted :

PRODUCT MODELLING AND SIMULATION
A LONG STANDING METHODOLOGY

OUTSTANDING SUCESS STORIES :

• **CATIA SOFTWARE FAMILY:**
  INITIALLY DEVELOPED IN HOUSE BY DASSAULT AVIATION
  NOW A WORLD REFERENCE PROSPERING UNDER
  DASSAULT SYSTEMES ' BANNER

• **DEVELOPMENT OF RAFALE :**
  INTENSIVE USE OF ADVANCED PRODUCT MODELLING AND SIMULATION
  A SUCCESSFUL DEVELOPMENT OF THREE DIFFERENT VERSIONS :

  C : Air, single seater
  B : Air, twin seater
  M : Carrier based, <u>single</u> seater } With only **4** prototypes

– The CATIA software : firstly developed in-house by Dassault Aviation in the late seventies for its own needs. This tool set has been then developed by Dassault Systèmes and became a world standard.

– Rafale Fighter : systematic use of advanced product modelling and simulation did allow to develop the aircraft with only 4 prototypes. Compared to other fighter programs facing cost overruns and delays, this has to be markedly pointed up for an aircraft with a fully integrated "omnirole mission system", developed in three versions : C = Air single seater, B = Air twin seater and the very demanding M = Naval single seater.

2. TODAY'S DASSAULT ANSWERS

In a customer driven market, customer needs are fast evolving and the improvements in product modelling and simulation must enable the timely and economic development of potential future products such as illustrated in this figure :

HOW CAN WE NOW AND TOMORROW ANSWER TO CUSTOMER'S NEW NEEDS

– Rafale mid life update

– UAVs and UCAVs

– Extended Falcon family

– Supersonic business jet

Four main objectives drive the effort to improve the overall efficiency of every new product development :

ACQUISITION TIME REDUCTION PRAGMATIC APPROACH

- START FROM VALID REQUIREMENTS , INCLUDING ECONOMICAL FEASIBILITY
- REDUCE DURATION OF ELEMENTARY TASKS :
- INTRODUCE STATE OF THE ART RULES INTO SPECIFIC DESIGN TOOLS FOR EACH DISCIPLINE
- PARALLELIZE AS MUCH AS POSSIBLE THE WORKFLOW, TAKING INTO ACCOUNT TRUSTABLE SIMULATIONS OR COHERENT CROSSCHECKS WITH PHYSICAL RESULTS
- SET UP DYNAMIC RISK MANAGEMENT USING "RED TEAMS" SKILLS AND TREATING DRIFTS AS SOON AS THEY OCCUR

➡ **REDUCE DRASTICALLY REWORK**

– Initialize design from valid requirements : this represents a major (and often underestimated) ingredient of a successful design. Product effective performance simulation is a way to let the customer test the use of a future system and better define its requirement, with an adequate balance between cost and performance.

An example is the technical-economical-operational simulation

START FROM VALID REQUIREMENTS : TECHNICAL-ECONOMICAL-OPERATIONAL SIMULATIONS
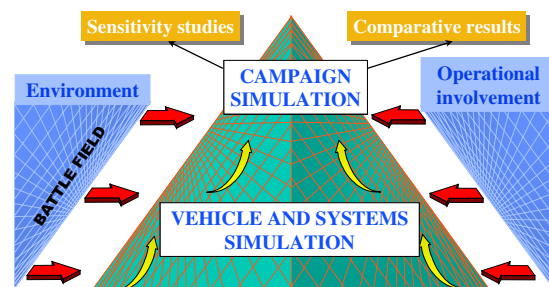
allowing to show the customer the global efficiency of the future product for differents uses and different design hypotheses.

– Reduce the duration of elementary tasks : a classical application of product modelling. This is being notably done introducing state of the art rules and automated checks into specific design tools needed by each discipline.

- Parallelize as much as possible the workflow : to reduce time to market, it is necessary to allow some overlapping between the different development phases without incurring excessive risk. This can only be done by using high quality simulations including maturity criteria.

- Set up dynamic risk management :

  - Using the experience and skills of "Red Teams" formed with senior managers.

  - Treating drifts, delays and discrepancies as soon as they occur

Today's improvements are focused on a "multisimulation" process :

  - Multilevel
  - Multidiciplinary
  - Multipartners/Multisites

- **Multilevel**

  The modelisation of the product is at different levels, for example for airframe in the following figure :

MULTILEVEL
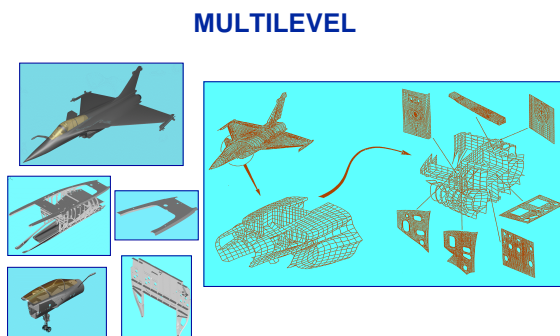
from complete airframe to detailed design of subcomponents and primary parts, keeping in memory associativity rules and parametric adjustments. It goes also from product design to manufacturing in a seamless process.

For mission systems (in this figure)

**MULTILEVEL BREAKDOWN
OF SYSTEMS REQUIREMENTS**

- TRACEABILITY
- FULL BENEFIT OF OBJECT ORIENTED TECHNOLOGY
- PROGRESSIVE VALIDATION PROCESS
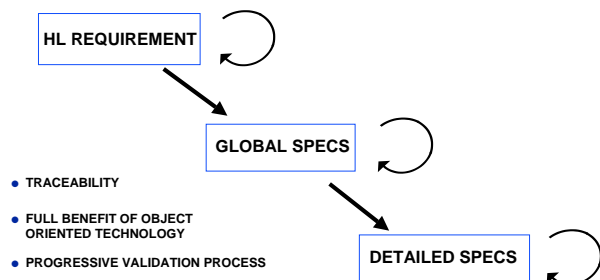
a proper breakdown of high level requirement to global specification and detailed specifications is necessary, enabling impact analysis of changes to the very end of elementary software components.

- **Multidisciplinary**

  Modelisation must integrate the models produced by the different technical disciplines, and this based on common product definition.

  Two significant examples of present results :

MULTIDISCIPLINARY : WEAPON INTEGRATION
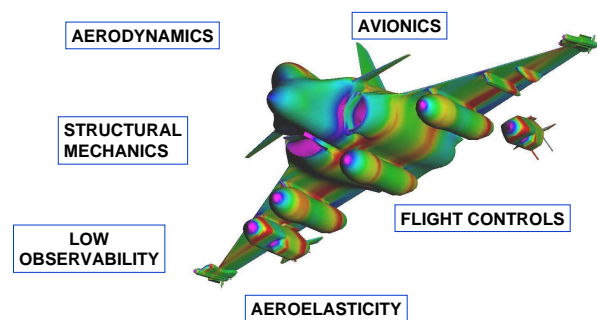
- One military : weapon integration : The figure above shows the launch of an Apache/Scalp cruise missile from a Rafale with three drop tanks. Weapons integration is a skilful combination of six disciplines : Aerodynamics, Structural mechanics, Low observability, Aeroelasticity, Flight controls and Avionics.

– Another example of multidisciplinary modelisation is a Falcon in manoeuver with a combination of structures, aerodynamics, flight mechanics and aeroelasticity.

MULTIDISCIPLINARY : FALCON IN MANOEUVER

AERODYNAMICS

STRUCTURE

FLIGHT MECHANICS
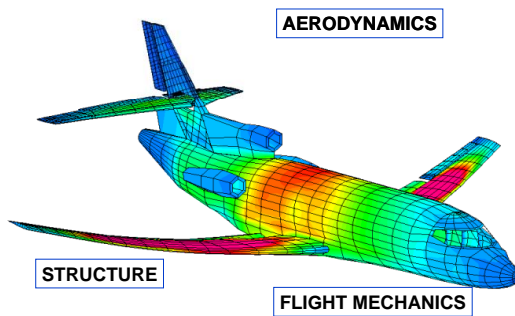
Two examples of current significant strides :

STIMULATING MULTIDISCIPLINARY CHALLENGE
DEVELOPMENT OF FUTURE RAFALE NAVY TWIN SEATER

RAFALE N

- **DIRECT TRANSPOSITION OF EXTERNAL STORES INTEGRATION**

- **INTENSIVE USE OF DYNAMIC SIMULATION AND SHOCK MODELLING ALLOW DIRECT TESTS ON CHARLES de GAULLE CARRIER WITH A PRODUCTION AIRCRAFT**

- **SUPPRESSION OF GROUND AND FLIGHT TEST ON DEDICATED CATAPULTING AND ARRESTING FACILITIES**

– The Rafale N : this new version of Rafale twin seater for the French Navy will be directly developed as a production aircraft. This is only possible by virtue of the quality of the modelisation, particularly the multidisciplinary modelisation of catapult launching and arrested landing.

– Cabin noise reduction :

MULTIDISCIPLINARY
NOISE REDUCTION IN A/C CABIN : A NEW DESIGN DRIVER

- **VIBRO-ACOUSTICS**

- **AERODYNAMICS**

- **STRUCTURAL PROPAGATIONS**

- **ADAPTED INSULATION MATERIALS**

➡ **FULL APPLICATION TO F7X PROGRAM**

A low noise level in cabins of business jets is a customer demand.
Traditionally this was done mostly experimentally by adding phonic insulations on existing airframe. That was both heavy and costly.
A new multidiciplinary design method allows introduction of noise level as a design driver in a new global optimization of structure and acoustic insulation.

Multipartner/Multisite

The aircraft being a global product and not the simple sum of independent subsystems, product modeling and simulation must allow to integrate in global models coherent and relevant models developed by partnering companies. Both to verify the behaviour of the subsystem in its environment, and to check overall behaviour of the complete system.

Two examples :

– Optimization of on board energy system. An example of multipartner studies is given in the next figure .

MULTIPARTNER : FRANCE-UK PARTNERSHIP OPTIMIZED ENERGY MANAGEMENT
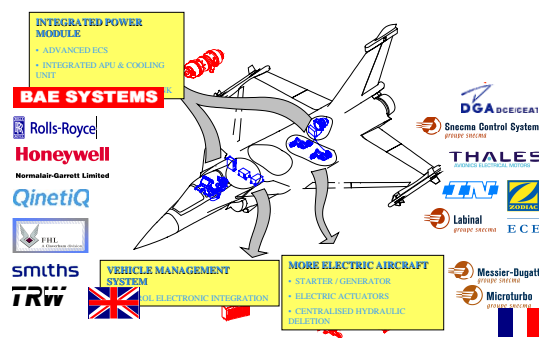
– This study is not only multipartner but also multiobjective as the results have to be applicable to different programs : existing combat A/C, UAV/UCAV and future European Combat Aircraft.

– Technical-operational simulation

MULTIPARTNER :
TECHNICAL-ECONOMICAL-OPERATIONAL SIMULATIONS
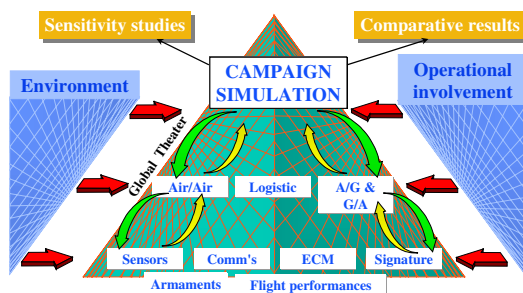
The combination of aircraft system models from different origins, environment model (theater) and operational involvement models permit very high level campaign simulation as well as more detailed simulation of operational phases (example Air to Air) and detailed modelization (for example for a sensor in its environment)

Today's developments including several companies in several countries force to rethink IT architecture and develop new systems enabling several actors, initially "physically" colocated for preliminary design phases, to work efficiently in their own sites "virtualy" colocated. Process commonality is also necessary to continue "concurrent engineering" between design offices as well as production teams in their plants. The need is there to insure a universal sharing of up to date data.

Development of the FALCON 7X

MULTIPARTNER :
F7X " IN CONTEXT AIRCRAFT DESIGN "
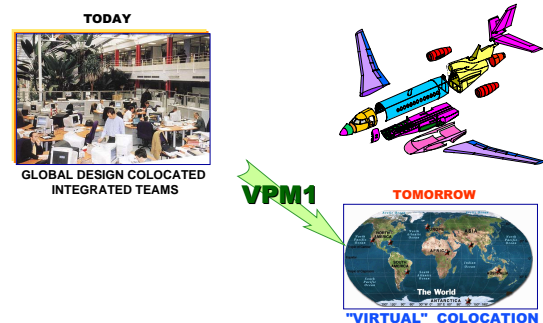
is at present being done by an integrated design team gathering in St Cloud representatives of 18 participating companies, then is to transition during this summer to "virtual" cooperative work, using latest technological development of VPM1 tools suite.

In the field of systems and software development, Dassault Aviation has also set up a wide range of "System and software workshops" for new developments of embedded systems : Flight Control System, Navigation and Weapon Systems, Utilities Systems.

Systematic use of object oriented technology among partnering companies allowed significant benefits and cost effectiveness derived from generic architecture and optimised commonality.

3 - TOMORROW CHALLENGES

To continue progression in the field of product modelling and simulation several challenges have to be considered :

- Scientific challenges,

- Information technology challenges,

- Management challenges, and pragmatic limits.

– **Scientific Challenges**

SCIENTIFIC CHALLENGES

- **Generalized automatic shape optimization**
- **Non-linear coupling**
  - ex.: transonic aeroelasticity
- **Distributed control**
- **Low-cost high-performance computing**
  - metacomputing
- **Formal verification of large finite state software modules**
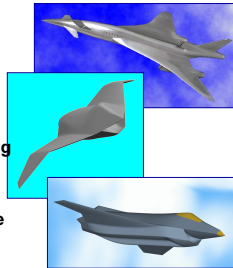
A number of subjects have still to be improved ; and will benefit from a coherent long-term investment plan :

- generalized automatic shape optimization,
- non linear coupling (a typical example is transonic aeroelasticity),
- distributed control,
- low-cost high performance computing,
- formal verification of large finite state software modules.

– **Information Technology Challenge**

IT CHALLENGES

- **OPEN ARCHITECTURES**
  TO TAKE FULL ADVANTAGE OF COTS PROGRESS AND EMERGING TECHNOLOGIES
  ⟹ **Avionics**
  ⟹ **Engineering and manufacturing frameworks**
- **TOOLS AND DATA PERENNITY**
  ALONG THE LIFE-CYCLE (30 TO 5O YEARS)
  ⟹ **Intensive data reuse**
  ⟹ **Seamless re-engineering process**
- **KNOWLEDGE MANAGEMENT**
  ⟹ **To cope with up to 20 years gaps between major programs**
 ⟹ **To capitalize safety critical information**

Three axes emerge :

- Open architectures to maximise use of COTS and be able to integrate new technologies
- Tests and data perennity

  As the life cycle of the product may be 30 to 50 years, it is mandatory to be able to migrate and reuse data with a limited effort.

  In the same vein, the company must be able to easily reengineer or modify parts of the product and replace without rupture engineering, manufacturing and support tools.

- Knowledge management

  There also the timespan between major programs must be considered with the problem of maintaining expertise of the design team ; a typical example is the capitalization of safety critical information for continuous improvement of crew and passenger safety.

– **Management challenge**

MANAGEMENT CHALLENGES
NEW DESIGN MANAGER'S COMPETENCIES

- **DEVELOPMENT OF FINAL PRODUCT'S VISION INCLUDING PERFORMANCES AND COSTS MODELLING : MAIN SYSTEM AND SUPPORT SYSTEM**
- **CREATE INTERDISCIPLINARY SYNERGIES TO TIME AND COST REDUCTION VIA GENERALIZATION OF CONCURRENT ENGINEERING**
- **ANALYSE MASTER AND IMPLEMENT COMPLEX PROCESSES : BE ABLE TO SPECIFY NEW INFORMATION SYSTEMS TAKING INTO ACCOUNT CLOSE PARTNERSHIP WITH OTHER COMPANIES**

To cope with the demands of the development of more and more complex and closely integrated products, managers with a new set of competences are needed.

They must be able to :

- Develop a final product's vision (performances and costs) both for the main system, and support system.
- Create interdisciplinary synergies to time and cost reduction via generalization of concurrent engineering ; these managers must especially have enough multidisciplinary knowledge to be able to remove "fences" between disciplines.
- Analyse, master and implement complex processes, and specify new information systems taking into

account close partnership with other companies.

- **Pragmatic limits**

MANAGEMENT CHALLENGES
COMMITTING TO BEST PRACTICES

- SET UP SIMULATIONS AND MODELLING SUPERVISION USING FORMALIZED AND STEADILY UPDATED PROCESSES

- INSIST ON ACCURACY AND RELIABILITY TO EVALUATE TECHNOLOGICAL RISKS ⟶ IDENTIFY MATURITY LEVEL

- CREATE A FULLY REUSABLE DATA BASE AND ASSOCIATED TOOL SET

- KEEP HIGH LEVEL SYNTHESIS REALLY ACTIVE , USING SIMPLIFIED MODELS

In addition to the limits resulting from constraints of the scientific tools, a more fondamental problem is the limitation of human understanding of the behaviour of a very complex system. It is still a dream to believe that a "true" and consequently detailed representation of highly integrated complex systems of systems can be understood and fully mastered by the engineering team. Tomorrow as yesterday, high level synthesis will still be carried out using also simplified behavioural models.

4 - CONCLUSION

Three factors can be summarized as key points to steadily improve design, manufacturing and support processes, permitting an effective enhancement of methologies and an advanced risk management of new projects :

1. Intensive use of technical-economical-operational simulation

2. Smooth communication and parallel teamwork

3. Implication of the customer from end to end, starting with preliminary specifications and including Life Cycle Cost.

_____

Paper Keynote #2

Discussor's name John Martin
Author L. de Jessey

Q: In my company we have a problem with level of detail between manufacturing detail and visualization detail, particularly for parts provided by third parties. Your presentation suggested that the digital mock-up is not complete until you have all data captured
How do you address the level of detail issue for a complete aircraft?

A: We have a common problem. For example, we buy engines for our aircraft so we can use a simple version of engine model in the mockup. Also our supplier information is often not of correct quality and we have a team to create suitable levels of model for our mock up from the design data

Collaborative Product Development Supported by Modelling and Simulation

Billy Fredriksson
Saab AB
Saab Aerospace
S-581 88 Linkoping
Sweden

billy.fredriksson@saab.se

Gunnar Holmberg
Saab AB
Saab Aerospace
S-581 88 Linkoping
Sweden

gunnar.holmberg@saab.se

Johan Lilliecreutz
Center for Market Analysis
Teknikringen 1E
S-583 30 Linkoping
Sweden

johan.lilliecreutz@cma.nu

Abstract

The development of aircraft involves many actors throughout the supply chain. The rationale for forming partnerships and selecting suppliers ranges from risk sharing, knowledge access to price and reliability of supply. The product, subject to many design drivers, uses a wide range of technologies in highly optimized conditions with ever-increasing cost pressure. The lifetime for technologies and subsystems, clockspeed, ranges over more than an order of magnitude between software functionality and airframe life while the functional integrity of the product has to remain throughout its life. This is implying a strong need for efficient collaboration throughout the supply chain supporting product integrity throughout its life.

The purpose of this paper is to show how modelling and simulation, M&S have been applied systematically as an enabler for Holistic Integrated Product Development at Saab. Early knowledge and understanding as well as ability to communicate through- out the supply chain play a critical role.

The findings are based on the research program LARP (initially Lean Aircraft Research Program) and the implementation experiences from Holistic Integrated Product Development at Saab. Studied cases include the auxiliary power unit development, a collaborative project with challenging integration both on functional and physical level. Results are demonstrating e.g. the importance of M&S for successful communication and coordination between integrator and supplier. The findings further high-lights the importance of creating value at early stages of product development, including New Business Models for Aerospace& Defense, Flexible Product Development and Supply Chain Innovation. All these subjects are studied in the current phase of LARP.

Background

Defence budgets have been subject to repeated cuts over a long time, forcing the governments and industries to act in order to ensure sufficient defence materiel supply as well as profitability for the industry. The self supply within single countries is reduced and international collaboration becomes a pre-requisite for the development of complex systems like aircraft. Drivers are both technology supply and competitiveness. This and other factors have led to a globalisation, where international companies, partnerships and supply chains are designed and created based on a rationale ranging from cost- and risk-sharing to knowledge access, technology supply and reliability of supply in general.

Possibilities in modelling and simulation, M&S, and information technology together with improved development practices support a move towards a focus on early stages of development, where much more effort is spent on initial studies before a program is started in order to reduce risk and the overall defence cost. This so called Simulation Based Acquisition, SBA <1>, is changing the business environment as the upfront investment is growing, while downstream programs could be expected to be in smaller series, less frequent and require more flexibility and adaptability.

Defence systems are used in an increasingly complex context. A growing flexibility in the type of operations is important where new types of interoperability is needed in order to be able to combine different defence

systems and achieve the increasing level of integration required to support the operation. Like most complex systems, the overall life cycle for defence systems is an order of magnitude longer than for some of the sub-systems it is composed of <2>. This implies that issues like obsolescence and changing requirements are driving a need for an easily upgradable system in order to ensure the required functionality and integrity of the system. Technologies and systems are growing in complexity and the investment for being able to introduce a new solution is growing.

From the above it is clear that the development of complex defence systems are facing several challenges. The context is ever changing, the product is growing in complexity, the cost pressure is increasing and the co-developing supply chain is becoming increasingly complex. In order to meet this situation, and to be able to continuously adapt, Saab has applied strategies such as Holistic Product Development <3> and Integrated Product Development <4>, IPD. We have been working together with universities in the Lean Aircraft Research Program, LARP <5> to support the reengineering of the industrial process. Some important aspects have been to support early knowledge, communication and teamwork through-out the supply chain. An important enabler to all these changes have shown to be M&S.

The purpose of this paper is to show how M&S have been applied systematically as an enabler for Holistic Integrated Product Development at Saab. Early knowledge and understanding as well as ability to communicate through- out the supply chain play a critical role.

LARP

LARP Overview

In many industries the leading prime contractors have now come to a point where they focus on their role as systems integrators. They are concentrating their design and production resources on core competencies and areas of strategic importance for the customers recognition of the brand image and identity of the product. Some of them will develop partnership relations with several competing manufacturers. In the most developed stage of partnership relations the supplier will be expected to act as if it was a subsidiary or division of the buying firm, i.e. almost back to vertical integration or hierarchies again after a wave of outsourcing. The systems integrators are developing new organizational patterns in order to reach the same or more efficient structures than if they would incorporate the most important suppliers.

The purpose and goal with LARP was *from a systems integrator perspective to develop models, methodologies and tools for efficient relationships between a systems integrator, customers and its major suppliers in the aerospace industry*. The empirical reality in LARP was two separate systems, APU (Auxiliary Power Unit) and GECU (General systems Electronic Control Unit), within the JAS 39 Gripen. The systems have been studied in depth since 1997 by a research group from Linköping university and the two graduates schools. IMIE (International Graduate School of Management and Industrial Engineering) is an alliance of thirteen divisions which represent a broad and interdisciplinary competence within management and industrial engineering. The other graduate school was ENDREA (The Swedish Engineering Design Research and Education Agenda) which focus is on developing, adapting and implementing theories and methods for managing and conducting world class product development in the manufacturing industry. Aerospace industry has been the industrial partner.

From a systems integrators (Saab Aerospace) view four research perspectives (subprojects) were highlighted; relations to the customer, relations to major suppliers, project management aspects and collaborative product development. The results from the studies have been presented in several academic thesis (PhD and Licentiate) and conference papers (see references) and in an edited book version <5>. The major conclusions from the four perspectives are summarized below.

Relation to the customer

An important aspect in the relation with the customer is marketing and related activities such as offset. Offset, an advanced form of counter trade is common in the international marketing of large infrastructure and defence systems. Offsets are activities that benefit the buying country for example in the form of local content, support of exports, subcontracts and technology transfer. Based on eight case studies of marketing of

large defence systems <6>, four models are developed to describe the offer, the seller, the buyer and the buyer-seller interaction. This sub-project is not further addressed in this paper.

Relations to major suppliers

These studies on relations to major suppliers <7,8> covered both existing relations and relations under transition due to changes in the systems integrators make or buy strategy, i.e transfer of an activity or outsourcing. They demonstrate the importance of differentiation in the supply base as well as the importance to continuously revisit the supply base strategy through- out the system life cycle.

The increased focus on lean production indicates a need for breaking each relation into bits and pieces, a strategy that influences both buyer and supplier. If there is a serious focus on lean supply and supply chain management, there also should be a focus on how to treat the supplier base. The lean supply strategy indicates that the entire supplier base should be treated similarly in order to obtain full efficiency. Characteristic of the lean supply relation is a clearer integration between buyers and suppliers, not necessarily meaning cross-ownership. The lean suppliers are early involved in product development and are expected, thereby, to participate actively in the buyer's development of new models.

When analysing the supplier base in the aerospace industry, we see a broad spectrum of system and technology levels - from the traditional sub-contractor of components to a sophisticated and closely integrated systems supplier. The hypothesis is that every supplier and relationship has different characteristics and therefore a different need for integration. Treating every relationship in the same way is not an efficient purchasing strategy. Lean production has in numerous studies been presented as "the way of the future" to handle increased competition. In a sense, *differentiation of existing supplier relations* could be a way to achieve efficiency.

Previous research on the phenomenon of outsourcing has mainly focused on strategic considerations. Nevertheless, the process of carrying out the transfer of an activity from being internally controlled to becoming externally managed may prove to be equally difficult because of interdependencies at the operational level. The most important existing outsourcing concepts were criticized for being based on an overly rational and static view of their core competence foundation, for failing to acknowledge the implications of strategic level versus operational level considerations, and for being overly deterministic.

An alternative outsourcing *process model* <8>, explicitly emphasizing the inter-linkage of make-buy decisions and transfer of control, transfer activities may lead to specific implicit make-buy decisions, i.e. that may not be perceived of as outright decisions. It was further argued that it is difficult to perceive of the final outcome of outsourcing when conceiving make-buy decisions, making it difficult to manage and control. Rather, a process of recurring sets of linked and dependent incremental make-buy decisions transfer activities to be managed in accordance with the outsourcing vision. Only a direction can be identified, whereas a clear goal cannot be defined beforehand, suggesting that continuous strategy adjustment and appraisal are necessary actions, was advanced as a potentially more accurate model of outsourcing.

Project Management

This sub- project <10,11> have studied how to manage complexity in projects initially from an intra-organisational and later from an inter-organisational perspective. It provides tools to analyze and design the organisation of projects such that team efficiency, concurrency and collaborative structure can be optimised from a communication perspective.

A collaboration is taking place on several levels (i.e. strategic, tactical and operational). This research is pointing at the importance of having these levels supported by relevant structural mechanisms and methods.

One of the key difficulties is to achieve a Work Breakdown Structure, WBS,   that is suitable for the actual collaboration scenario and product architecture. A methodology called Dependence Structure Matrix , DSM <9>, is introduced and applied to support this. DSM allows for analysis of the possible WBS solutions and architectural decompositions such that e.g. team tasks could be identified and communication need understood.

It has been shown that the method supports the design of the organisation, the identification of WBS:s that are more straight forward to assign to different teams, and that communication need will be better and earlier

understood. The work to establish the DSM- matrix should be participatory as it serves as a catalyst for the strategic dialogue between the parties and levels of collaboration.

<u>Collaborative Product Development</u>

Model based product development have been studied in a collaborative context <12>. These studies demonstrates the potential and maturity of functional modelling of specifications and analyses the need for a project web in collaborative product development.

A good quality, well understood specification is an instrumental prerequisite to efficient product development. The specification of complex systems have often suffered from the difficulty to express with sufficient precision and consistency its functional behaviour using natural language. This problem is accentuating in importance the more parties that are using the specification.

Here functional modelling have been applied as a specification tool and the intended behaviour of a number of systems have been modelled, both systems being developed in-house and by suppliers/ partners.

The research have shown that functional modelling is mature enough for systematic application. It has been shown that the use of a modelled specification generated a better specification than the textual one, as it detected inconsistencies at early stages. Further, in collaborative projects it has been shown that the common development of the model have accelerated the mutual understanding of the system and its behaviour in the total system.

In collaborative product development, large amounts of project information is exchanged which is not direct product documentation. In order to support this, attempts were made to implement a project web that could support the management of the development project <13>. As this was made in 1996-97 several difficulties appeared, among these immature internet technology and difficulty to guarantee security of information. A conclusion is that there is potential for a project web when IT- security can be achieved and approved.

Holistic and Integrated Product Development

The application of Holistic and Integrated Product Development, IPD, have been important approaches to improve performance and cost effectiveness for the development processes at Saab during recent years <3,4>. These provide a structured approach on how to improve the development capability, inspired by e.g. <14,15 >. The implementation of IPD has used an enabling approach with a starting point in maximising the individuals ability to contribute to and support a rapid convergence to feasible designs in a life cycle perspective.

"IPD is a structured way to maximise the contribution from people, processes and tools to achieve product optimality"

Where product optimality reflects the balance between cost and performance that best meets customer demands. In the design of this development process at Saab some aspects have been central:

- Provide easy access to information and knowledge
- Use M&S extensively to provide knowledge support to engineers in early development stages in order to allow for mature decisions as early as possible.
- Good and well understood specifications.
- Minimise the lead-time from decision to delivery.
- Support and simplify vertical and horizontal communication internally and externally.
- Provide ability for the engineers and experts to utilise their expertise in an efficient manner
- Promote Decision ability

The process is designed to easily and early bring in new expertise and easily start interaction with the purpose to achieve a possibility to dynamically allocate expertise into projects, e.g. customers, suppliers and shop-floor people and let them contribute to the product at early stages. This is more extensively reported in <3,4>.

 Development Rooms

The team members are working together and sharing information in order to agree on the best common design solutions covering all design drivers and constraints. In order to achieve this, the team uses computer based information and M&S. Current levels of technologies allows for the possibility to support interactivity to a large extent. Not only can models be selected and viewed within less than a minute in complex products, but changes can also be introduced in a meeting. Quick interference checks could be performed, linear analysis could be made, given limited mesh change needs and so on.

Based on the above, a development room has been designed, where two workstations and one PC provide computer power, two large screen projectors give the ability to view two of the three computers information simultaneously for the full team. The computers are normal installations on the network with ability to use any system and data available on the network given that the team have access authority. Following the success of this tool, a number of these rooms have been built.

This enables the team to work, in the room, viewing the design in its context e.g. from the CAD-system on one screen and discuss some type of issue or opportunity. On the other screen additional information available on the network can be viewed depending on the needs. Typical examples are bill of material, BOM, or other Product Data management Information, PDM, analysis, simulation or scheduling information. Changes can be introduced and to some extent analysed interactively.

Bringing the use of these development rooms into the team environment provided support for more dynamics in the meeting. The use of the tools, combined with the goal to improve the ability to reach joint decisions in the team, lead to the design of a methodology to take "action like" minutes from the meetings. A particular structure was formed, and tools were developed to support this. Initially the methodology was supported by standard "Office" software which was found not to be sufficiently efficient in a networked environment. To improve efficiency an early web-application was created.

This minutes application uses "screen grab" technology to allow users to pick any information from the computer screen and add it to the web minutes with texts, pictures, annotations as well as action items such as identification of responsible and date of completion during the meeting. An integrated archiving functionality is provided with the ability to follow design rationale from specification to released and verified product definitions. Several generations of the application have been developed and there is a continuous demand for more information to be handled within the application, e.g. scheduling. A current challenge is to identify support for easy search in the archive in order to promote reuse of earlier engineering solutions in new applications.

The Digital Mock Up, DMU, is the most frequently used model to discuss around in the rooms. The current technology implemented on the IPD-level includes exact solids CAD on workstations, high performance visualisation, simulation, analysis and retrieval tools and a model structure with one part instance in each model which allows a flexible and rapid build up of different context scenarios. The PDM support available in early stages of development is still limited. The weak area in the current solution is the somewhat cumbersome establishment of models for different product configurations. The requirements on the PDM-system to make progress in this area includes e.g. being able to master many concepts subject to intense change and provide good retrieval and analysis capabilities to compare the pro's and con's of the different concepts.
Furthermore, the manning of a team often consist of a core of people from the major disciplines, while they need to expand the team for particular tasks where additional expertise is needed, such as bringing in suppliers or customers. It is therefore important to provide good support, not only for the team to understand the product, but also to give them the ability to easily involve other people. The development rooms, the DMU and the visualisation tools are playing a significant role for this ability.

Analysis and Simulation

Analysis and simulation in a wide sense covers areas from system functional modelling, concepts, stressing and aerodynamics to assembly, shop floor simulation and maintenance and mission support. Many areas of

analysis have improved during the last decades where different performance aspects have become much more predictable.

The improved predictability has probably influenced the design decisions in the early stages of development such that it has been easier to justify a solution from a performance or functional point of view, rather than from a cost or manufacturability view.

Only in the last decade have areas such as assembly simulation and other manufacturing related simulations been able to contribute with sufficiently short response time to match performance simulations at early stages. This is a very fortunate development contributing to the balance in the team that has to be taken further, in order to meet the demand from the continuous movement towards more cost focused design criteria.

If the information provided fails to balance the level of consideration in the design criteria, which normally is the case, this need to be met through other efforts. One method utilised is the use of the different roles in the team, and try to strengthen the ability to influence decisions for people from disciplines having lower level of quality information available .

An example is that in early stages the manufacturing engineer could have difficulties in catching up with the consequences of design decisions. By making him/ her the one who runs the web based application for taking minutes from the meetings, he/ she can to some extent control the flow and have all possibility to influence the design from the very beginning.

Another issue in the same category is that different disciplines are progressing based on different information, which sometimes makes it difficult to maximise the profits from he concurrent development, e.g. the stress engineer is approaching the product in a different break-down approach than the systems installation engineer or the manufacturing engineer. Co-ordination is therefore needed during the evolution of the product in order to avoid decisions focusing on a limited set of design drivers due to the lack of certain types of information.

In general, models for analysis and simulation are considered as a part of a model concept where the models are established in early stages of design and maintained throughout the life cycle in order to remain as the main information carrier for the product aspect concerned. Early models are often mathematical simulations to be refined and correlated with experimental data or experience from application later on (e.g. ground vibration test for eigenfrequencies, manufacturing cost for costing or operational properties). The model concept serves as a strategy to make the best use of available information.

Supplier/ partner Integration

Since a high degree of the aircraft content is developed and supplied by other sources than the system integrator, it is important to achieve interaction mechanisms which supports co-ordination, where needed. Obviously this integration is dependent on how decomposable the work is. The first operational step is always to minimise the interaction needed between the parties. The next step is to identify which information is important to co-ordinate/ exchange and at what frequency it needs to be co-ordinated. At Saab we have basically worked with three levels of technology for integration

1: e-mail and file transfer
2: replication of data sets at a certain frequency
3: remote clients with shared databases

Sorting on these levels appear to be sufficient from an IT point of view. The difficulty is almost always to resolve security issues. The level of technology becomes a prerequisite for the type of methodology and tools that are needed to achieve a collaborative support. Often, a low technology level is driving increased complexity in the methodology in order to ensure e.g. configuration management. A practical level is normally level 2 where the selected DMU and analysis data are replicated at the supplier site with maximum delay of some hours. The same applies for the project web, as described above, as well as for planning information and so on. Information produced at the supplier site is released to the data storage at Saab.

The many supplier and partner relations that follows from the involvement in several aircraft projects with several partners drive the complexity of the company operations. In order to minimise this complexity and maintain the ability to optimise the performance of operations a strategy is used where clear interfaces are applied with limited impact on internal processes.

Concluding discussion

The situation of tomorrow for a systems integrator is characterized by aspects such as a wide range of integrated technology content with varying clockspeed, many design drivers, late definition of technologies and adaptability need. The systems integrators ability to handle intra and inter organizational relations, scalability, ability for growth and adaptability, knowledge management and shaping a value creation culture are of importance.

The application of lean principles to projects increases the ability to master lead time and cost. In order to have the right conditions for a lean project it is assumed that fundamental design decisions are taken at an early stage, ahead of the lean project. The arrival at this starting point, often referred to as having the architecture or layout of the product and its subsystem solutions and technologies ready for application, is not supported by the lean paradigm <16,17,18>. These aspects combined with the incentives to focus the effort at early stages according to SBA are all pointing towards the importance of the ability to make good design judgements at early stages. Furthermore, much of the innovation field has to be at initial stages as this is where the design freedom exists such that new values can be created with low cost and project implications, ahead of the lean projects having a starting point where many fundamental design decisions have been taken.

Constructive lean

The lean paradigm that focuses on up-front value creation through-out the supply chain or value network, we have chosen to label *constructive lean*. The challenge for constructive lean is to create the right environment for the whole supply chain at early stages to generate value and achieve the right conditions for a lean project. If this fails, there is a clear risk that only the traditional down-stream lean project remains. This could become a long term threat for the company as it only allows for current systems to generate profit by continuous cost and resource reduction, but does not stimulate the achievement of new competitive systems supporting the long term development of the company, a situation we label *anorectic lean*. The traditional lean project is still an important component of constructive lean, as the way to bring a new system to completion when it is through its architectural phase.

LARP Future Direction

The continuation of LARP is based on the constructive lean approach. The redirection of the Swedish defence into a Net Centric Warfare paradigm means e.g. that systems have to support a more flexible use and integration with other systems. Furthermore, the whole system of systems will be subject to continuous change, and all involved systems will need to adapt and be able to federate with a wide range of systems over time. The continued research will be focusing on the following four topics in order to further develop the constructive lean approach:

New Business Models

Current Defence acquisition strategies, e.g. Simulation Based Acquisition <1>, are moving in a direction where the effort both from the customer and from the integrator is increasing at early stages. This is changing the conditions for defence business. In this project possible business models are studied in order to identify models providing best incentives for all involved parties.

Flexible product development

The development and use of complex systems, e.g. defence systems, is subject to long life cycles with changing conditions implying that there is a need for flexibility in the system. The need for flexibility origins in areas such as new innovations, new requirements as well as obsolescence in high clock- speed sub-systems.

The strong connectivity between the development capability and the resulting system solution is stressing the need to have a development capability that is promoting these types of flexibilities. This research is focusing on how to create a framework for flexible product development.

Life cycle value

This project studies what the important aspects are in order to set up a development capability that supports life cycle value implementation in an optimal way. Case studies have been done together with Massachusettes Institute of Technology on several aircraft and a framework for life cycle management is proposed <19>. Studies will continue based on a wider industrial basis.

Supply chain innovation

The main driver in the area of *supply chain innovation* has its origins in the interaction between prime and SME. Here are some examples. First, development of more complex projects and systems, often fully integrated, stresses the importance of early access to technology and innovations. Second, the procurement strategy is focusing on a small supplier base with fewer and larger suppliers, which hinders the surveillance and acquisition of new technologies, often driven by SME:s. Third, the difference in size between prime and SME:s do not support effective risk and profit sharing and transferring of knowledge in early RTD phases of large projects. Important questions between systems integrators and the supply chain are; what are the incentives and initiatives? How is the interaction and interdependencies?

Collaborative Product Development

In the implementation of current development practices we have aimed at achieving a constructive lean ability which is enabling all involved parties to contribute at their best to the system solution in a life cycle perspective. In order to achieve this, team capabilities, collaboration and ability to achieve qualified design decisions early in the development cycle have been instrumental.

To improve the team capabilities we have built development rooms using M&S to support the team communication and allow for interaction with models during meetings. Intranet solutions have been used to help in decision making. The enabling approach which is focusing on providing value for end users at different levels such that a demand for the supporting methods and tools is important in order to achieve a wide implementation. The only obstacle to this approach found so far is when there is a long distance between people feeding an application with information and the people benefiting from the application.

The involvement of external parties in the team, co-located collaboration, have demonstrated the importance of models to support communication. As different organisations using different terminology, or even languages, it is necessary to provide the best support in order to reduce the risk for miss- understandings. M&S is reducing this risk both between organisations and within one organisation between e.g. design and manufacturing people. Functional modelling is contributing strongly to a better specification which is also better understood when developed together between e.g. integrator and supplier.

The integrated use of M&S through- out the supply chain, in distributed collaboration, implies a number of integration difficulties. Important is to maintain an internal process that is applicable to many projects and can be interfaced to other processes, such that the possibilities remain to upgrade and optimise the internal process without having to simultaneously propagate this change through the supply chain. This is supported by the LARP process for implementation of a collaboration. The results from the sub-projects Project Management and Collaborative Product Development have together with Saab experiences from collaborative projects applying IPD served as the basis for the LARP recommended process of implementing a collaborative development project. This process starts with the analysis of possibilities and constraints in the possible WBS and its distribution. Then DSM is applied in order to identify best possible WBS minimizing the communication need between enterprises. Following this IPD support is implemented in order to support the needed level of communication.

The early understanding of the consequences of early design decisions is key to the constructive lean environment. This understanding is a combination of experience from earlier projects, M&S as well as the teams ability to make the synthesis of the knowledge of its individual members. As M&S contains incomplete knowledge, it is important to use it together with other available information, such as experience and physical testing. The above described model concept which is combining the different sources of information throughout the life cycle provides a mechanism to federate information and also bring it into new projects to enable the use of earlier experience.

Conclusion

The business environment for complex defence systems is changing in a direction where early value creation and communication through- out the supply chain is playing an increasingly critical role. M&S is a key enabler for early value creation and communication through- out the supply chain in collaborative product development.

Abbreviations

IPD   Integrated Product Development
LARP   Lean Aircraft Research Program
M&S   Modelling and Simulation
RTD   Research and Technology Development
SBA   Simulation Based Acquisition
SME   Small to Medium size Enterprises

Referenses

<1>   Frost R, (1998), *Simulation Based Acquisition –An Ongoing Outlook-*, Simulation Interoperability Workshop, Fall 1998.

<2>   Fine, C (1998), *Clockspeed- Winning Industry Control in the Age of Temporary Advantage*, Perseus Books.

<3>   Fredriksson B., *Holistic Systems Engineering in Product Development*, Military Aircraft, 1995.

<4>   Holmberg, G., (2000), *Integrated Product Development - A key to Affordability*, ICAS 2000, Harrogate, UK

<5>   Lilliecreutz, J. & Holmberg, G., (eds.) (2000), *Constructive Lean - A Systems Integrators Perspective. The Relationships of Tomorrow Between Systems Integrators, Customers and Their Major Suppliers In the Aerospace Industry Findings from LARP part I*. Research Report from Linköping university and Saab AB Linköping, April, 2000.

<6>   Ahlström, M., (2000), "Offset Management for Large Systems - A Multibusiness Marketing Activity", Linköping Studies in Management and Economics, Dissertations, No. 46, Linköping university.

<7>   Lilliecreutz, J. & Ydreskog, L. (1999), Supplier Classification as an Enabler for a Differentiated Purchasing Strategy, Selected Conference Paper for publishing in International Journal of Purchasing and Supply Management – Special Edition and also in Global Purchasing & Supply Chain Management World Market Research Report.

<8>   Wasner, R. (1999) "The Outsourcing Process –Strategic and Operational Realities," Licentiate Thesis No. 163, Linköping university.

<9>   Eppinger, S.D. & Ulrich, K. T., (1995) Product Design and Development, McGraw-Hill Inc. New York.

<10>   Danilovic, M (2001), *Supplier Integration in Product Development*, The 10th International Annual IPSERA Conference 2001.

<11>   Danilovic, M (1999), *Loop – Leadership and Organization in Integrated Product Development,* PhD-Thesis, Linköping university.

<12>   Backlund, G., (2000), *Modeling Requirements in Systems Development - a Way to Manage Complexity*, Licentiate Thesis, Linköping university

<13>   Öhrwall Rönnbäck, A. (1999), *The Information Infrastructure in Collaborative Product Development*, Licentiate Thesis, Linköping university

<14>   Suh, N (1990), *The Principles of Design*, Oxford university Press.

<15>   Allen, T (1977), *Managing the Flow of Technology: Technology Transfer and the Dissemination of Technological Information Within the R&D Organization*, MIT Boston.

<16>   Womack, J; Jones, D; and Roos, D. (1990), *The Machine that Changed the World*, Rawson.

<17>   Womack, J; Jones, D; and Roos, D. (1996), *Lean Thinking*, Simon&Schuster

<18>   Murman E. M.; Walton, M; Rebentisch E (2000), *Challenges in the Better Faster Cheaper Era of Aeronautical Design, Engineering and Manufacturing*, ICAS 2000, Harrogate, UK. To appear in the Aeronautical Journal.

<19>   Hallander, I & Stanke, A (2001) *Lifecycle Value Framework for Tactical Aircraft Product Development*, INCOSE 2001, Sydney, Australia.

Paper Keynote #3
Discussor's name S. Woodford
Author Holmberg/Fredriksson

Q: In one of your diagrams, development and production costs increase significantly with time, but operation and support costs do not. Why is this?

A: SAAB has continually tried to minimize the support requirements for their aircraft. With Grippen, they support this aircraft with 1 technician and 2 conscripts from a Road_____. This gives autonomous operation and very low operation and support costs.

Advanced Modelling and Virtual Product Simulation in the Design and Build of Warships – A Practical View

Mr. John L Martin CEng. MRINA
Consultant Engineer
Future Engineering Methodology dept.
Building A45 (second Floor)
BAE SYSTEMS Marine
Barrow in Furness
Cumbria LA14 1AF, United Kingdom

Overview

In considering 'Reduction of Military Vehicle Acquisition Time and Cost through Advanced Modelling and Virtual Product Simulation' practical experience spanning five years of ship and submarine design and build was reviewed to seek quantification of the contribution made to cost reduction. It concluded that advanced modelling and virtual product simulation must be an integral part of the engineering processes to achieve an advantageous contribution to cost. This involves an effective design process and an efficient means of access to the appropriate product data supporting the geometric model/simulation technologies.

The application of Advanced Modelling and Virtual Product Simulation technologies is of limited value when used independently without the close association between the geometric models and the associated functional and physical data attributes which describe the requirement and design solution. This notion can also be illustrated in the traditional case of wood or scaled plastic physical mock-ups of ship or submarine layouts where modelled components were 'tagged' with a label description, or colour coded. i.e. orange to represent electrical routes, grey for HVAC and pre-defined colour codes for various pipe systems. Thus an advanced virtual model without any access to underlying data attributes is little more that a 'pretty picture'
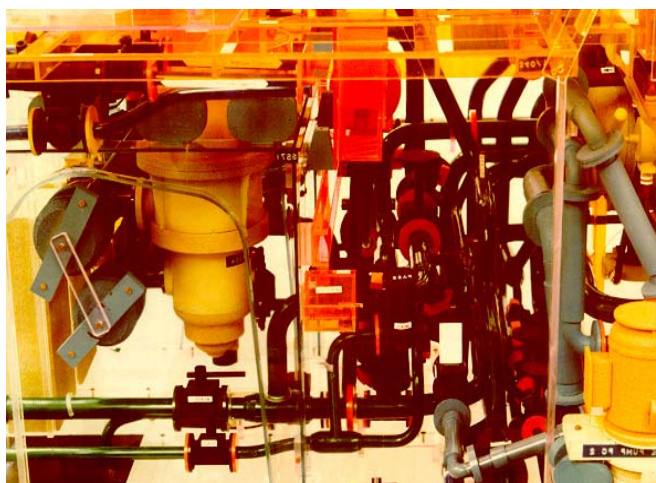
1/5th. Scale Plastic Model - Colour Coded and Labelled

The use of Advanced Modelling to capture design layout arrangements and Virtual Product Simulation to verify the design offer an opportunity to optimise cost effectiveness when they also offer access to the design specification data, contract standards, rules and conventions, and supplier/vendor equipment information. Only then can model content and simulation behaviour criteria be specified and used with confidence to confirm that the functionality and operability of the design and its component systems meets the stated requirement.

Although the quantification of the cost reduction of products due to the introduction of Advanced modelling and Virtual Product Simulation is difficult to resolve, it is perhaps significant to note that the company workforce was reduced from c15,000 staff (in 1990) to c5,000 (in 1995/6). Due to the benefits of introducing new processes and supporting technologies the workforce has remained at the lower figure during a very busy period of design and build contracts for three surface warship designs (LPH, LPD ,AO) and the Astute Class nuclear powered submarine.

Introduction

When asked to present this paper the brief was to describe a commercial example of how virtual design, simulation and manufacturing tools are currently applied in the development of specific total products in the maritime sector. The paper thus presents the advanced modelling and virtual product simulation environment and practices used within BAE SYSTEMS Sea Systems division. BAE SYSTEMS have considerable expertise across the company in all fields of advanced modelling and virtual product simulation and actively encourage the appropriate technologies to be adopted across multiple sites through centres of excellence whenever they may contribute to a high quality product at an efficient cost.

Advanced Modelling and Virtual Product Simulation are often discussed by companies as being worthy of investigation or evaluation review in line with keeping up to date with the 'latest' technologies in a design environment. Although these technologies have been around in a stable form for several years, they are rarely accepted as a desirable or essential ingredient in support of the day to day design process and still have a reputation as a yet to be proven state of the art concept. As a result, many companies tinker with the technologies in a limited way, often just to show they are up to date with the evolving systems, or to impress potential customers, and they fail to commit the technologies as a required element of the design process. This reduces or eliminates any potential advantages that can be achieved with a structured and serious application of the technologies.

The design or manufacturing process is the key to achieving optimum cost effectiveness. Suitable technologies and systems can then be selected and applied if and when they are necessary and sufficient to support the process. Without a process requirement or a clear specification of deliverables and objectives the introduction of Advanced Modelling and Virtual Product Simulation reduces to the classic situation of chasing technology and seeking a problem on which to apply the technology solution, often with expensive failure. Technology researchers and developers need to consider this situation and evolve the technologies to achieve optimum modelling or simulation functionality, whilst retaining a managed interface to associated product data attributes. The objective should be to introduce advanced modelling and virtual product simulation as an integral part of the day to day processes within a company. To achieve this the systems need to be simple to use by engineers without the need for continued specialist support.

This paper outlines the experience gained since the introduction of Advanced Modelling and continued studies in Virtual Product Simulation at a Shipyard.

Company Background in Advanced Modelling and Visualisation

In 1993 BAE SYSTEMS Sea Systems in conjunction with Virtual Presence (formally Advanced Robotic Research Ltd.) and 13 major UK companies carried out research to address the maturity of the evolving Virtual Reality technologies with the objective of assessing their suitability for engineering use. Following a comprehensive review and several pilot studies using submarine model data, it was concluded that the technology was suitable and a system was procured for implemented in August 1997 at the ship and submarine yard in Barrow in Furness, England. Advanced Modelling and Visualisation technologies have been applied to all of the ship and submarine design build contracts since 1997 and are an integral component

of the design process. Engineers have access to visualisation tools on their desktop computing workstations and a purpose built Virtual Reality Suite was created for use as a design review facility with a capacity of up to 30 review staff. (a typical formal design acceptance review for a ship or submarine compartment will be up to 25 people including project engineers, customer representatives and approval bodies such as Lloyds)
The visualisation facilities and their use at the Barrow shipyard have been described as 'world leading' due to their integration into the design and production processes and for their heavy use on a day to day basis by the project design build teams. Project teams have booked the review room facilities on a constant daily use during the past five years, indeed during peak periods the facilities were booked from 6-00am to 10-00pm when the project worked a daily two shift schedule.

The design review facility at the Barrow site has the following facilities:

- A rear projected flat screen stereo capable display c 2.7m * 2m
  - Note: the flat screen display was selected in preference to the trend of curved screen VR projection display facilities now accepted as the norm. A flat screen was considered superior for reviewing complex pipe and equipment layout in ship and submarine compartment arrangements.
- Seating for up to 30 staff with acceptable viewing from all seats
- A projection control system to enable projected images from a workstation, a personal computer (including laptop) the Virtual Reality processor, and video. A sound system in also linked to the controller and provision is made for a microphone for the speaker (if necessary)
- A Reality Engine SGI processor
- A headset immersion and tracking system with 3-D mouse

In a typical design review meeting, a laptop PC will be used to provide a presentation of the meeting agenda and specific details or issues on the topic to be reviewed. This is supported by images of the design presented on the virtual reality visualisation tools and by live access to the product model database through the workstation. This combination of device displays offers powerful and comprehensive access to the design geometric layout and the underlying specification data.

Design Review Facility

Visualisation Technologies and their Use or Intent

In order to produce effective and efficient products at optimum build and operational costs, engineering design processes are evolving to replace traditional 2-D orthogonal drawings with 3-D geometrical models. The multi-disciplined 3-D geometric models and their associated attribute data used in complex product designs such as ships and submarines contain a very large volume of information to describe the component parts of the product and their function and geometric relationship in the layout arrangement of the design.

Access and recovery of data and information from this product definition model is often difficult and inefficient. The introduction of advanced modelling and visualisation technologies ensures that the design can be visualised effectively to verify feasibility and to confirm that the customer requirement has been met. There are several visualisation scenarios in a design environment each addressing a particular aspect of the design process. The requirement is to have an efficient, effective and easy to use facility to display and manipulate high data volume complex 3-D models for comprehensive review at each scenario level.

Functionality available and used at the Barrow shipyard includes:

- Desktop Processor (Small screen)
  The desktop processor visualisation environment is used to allow the engineers to review a model of the product around a desk with one or two colleagues whilst carrying out design discussions and or resolving design issues or uncertainties. This is a day to day tool used by all of the detail design engineers and is available on the 650+ workstations attached to the engineering data network.
- Large screen Projection
  A large screen projection facility enables a team of staff to collectively review the design in a formal or informal meeting and to collectively discuss design problems or issues. The use of projection onto a large screen in a meeting room has proven to be very effective particularly with a considerable number of review engineers (25 or more). It is specifically used for design area layout review and verification meetings leading to customer acceptance and design approval.
- Stereo viewing
  The addition of stereo capable projection to the large screen viewing enhances the visualisation capability by giving a sense of depth to the image that is extremely useful when reviewing complex design areas. The stereo visualisation when used in conjunction with large screen projection is highly recommended for inclusion in design review visualisation environments.
- Headset immersion
  Headset immersion is a specialist tool with useful functionality once its limits of accuracy are known and understood. However, it is not a technology used daily in the design process. Design Engineers and the customer have requested the use of the headset to verify specific design concerns for current contracts, the headset was then used complimentary to the large screen projection facility in design review situations.
- Rendering
  Use of rendering, colour and material textures to enhance the visualisation model is a very useful function when assessing or developing ship layout design. Rendering has been used to add some 'realism' to the 3-D model when necessary to assess the effect or operability of design issues. Examples include the use of material rendering such as proposed console displays in operations rooms and stainless steel or patterned fabrics on compartment bulkheads in operational and domestic areas to assess colour balance, ergonomics and operational human factor comfort. Texture functionality is also used to visually present optional design solutions that may be assessed by users (the Royal Navy) and the customer (MOD) where the options can be reviewed for comparison and discussion.
- Conference viewing
  Conference viewing is the ability for two or more engineers in remote sites to communicate and concurrently review a design model whilst discussing the issues by phone or videoconference. This facility is often available with visualisation software products and has a high potential in the modern trend to design products across several sites and/or partner companies.
- Event Simulation
  Event based simulation involving the animation of geometric models is a feature of visualisation that is not readily accepted by design engineers. Occasionally, event simulation behaviours have been added to ship layout design models to illustrate particular aspects of geometry movement such as opening of doors or removal of equipment from a complex area. However, the applications to date have been of limited value. There is potential for event based simulation technology to be used in the design process if the input of the simulation behaviours can be in simple format (i.e. tabular) or can be imported from the result files from dedicated simulation tools.
- User Driven
  The success of acceptance of the visualisation technologies into the design process is a direct result of the 'user driven' philosophy in which the project design engineers are trained and sufficiently competent with the technologies to use them regularly without the need for specialist support. In addition, a simple and effective

means of input of design models into the visualisation system enables design review data to be prepared efficiently in minimum time for use in discussions or meetings.
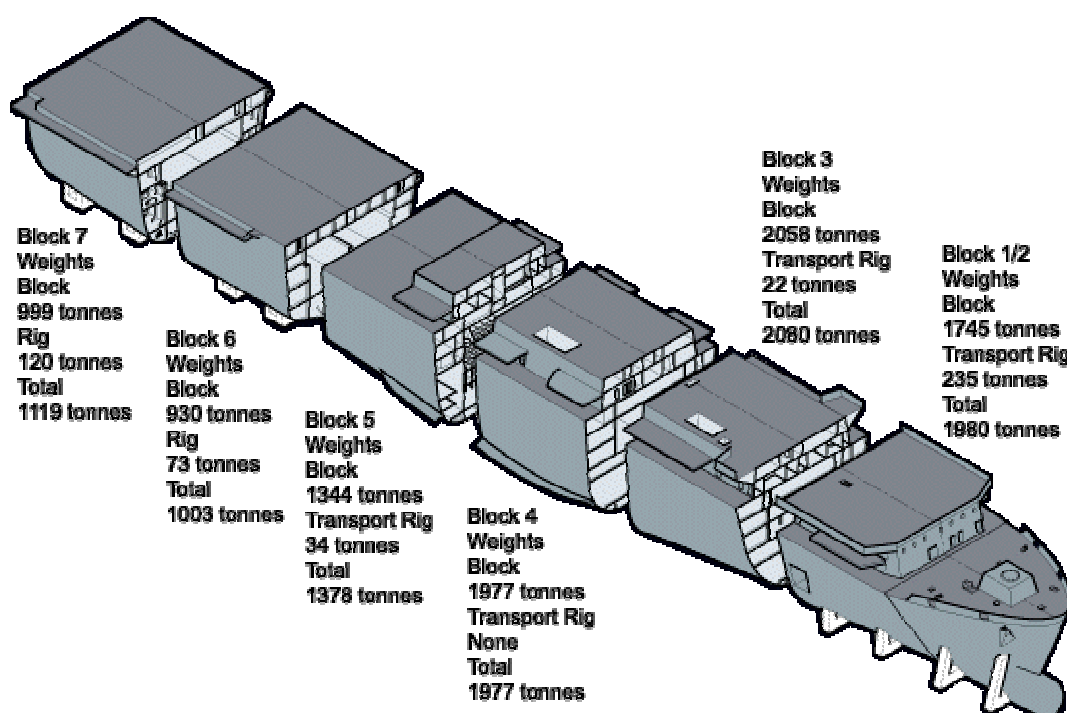
The design is developed using 3-D CAD models with an associated product database and the visualisation tools enable the engineers to retrieve the design layout geometry for any selected area of the vessel and prepare it for design review visualisation and discussion.

It is important to state that models are not created explicitly for visualisation. 3-D Models are created during the design process and then reviewed using visualisation tools. To create separate models for visualisation or virtual prototyping is an unacceptable concept in terms of cost, schedule, data integrity and design control.

Practical application of VR technologies

During 1995 a Business Improvement Project identified several areas to be addressed to improve the effectiveness of the company. They included a considerable change of culture in the existing working practices and design and build processes. In support of these new processes a number of systems were implemented to capture, control and manage product information. As a result, the LPD (Landing Platform Dock) surface warship contract was the first design build project to attempt a 100% digital definition and subsequently the first to use visualisation technologies for formal design acceptance by the customer. The significant changes in company practices and the introduction of advanced 3-D CAD modelling, product data management and visualisation technologies create the difficulty in quantifying the effects of the visualisation and virtual product model tools on the overall performance of the project.

The LPD ships had a build strategy based on seven large 'block' assemblies which were fabricated and outfit to an advanced state in the shipyard build hall and then moved across site to the launch slipways where they were connected to the adjacent blocks. This build strategy was supported by a design strategy that converted the functional design requirement into design areas matching the block breakdown. Design engineers together with production, procurement, logistics support, systems engineers, specialist professional and the customer formed teams for each design area. Advanced Modelling and Virtual Reality technologies were used extensively for formal and informal design reviews on a daily basis as the project design evolved.

Block 7
Weights
Block
999 tonnes
Rig
120 tonnes
Total
1119 tonnes

Block 6
Weights
Block
930 tonnes
Rig
73 tonnes
Total
1003 tonnes

Block 5
Weights
Block
1344 tonnes
Transport Rig
34 tonnes
Total
1378 tonnes

Block 4
Weights
Block
1977 tonnes
Transport Rig
None
Total
1977 tonnes

Block 3
Weights
Block
2058 tonnes
Transport Rig
22 tonnes
Total
2080 tonnes

Block 1/2
Weights
Block
1745 tonnes
Transport Rig
235 tonnes
Total
1980 tonnes

LPD Block Breakdown

The design layout is modelled in 3-D geometry based on a product structure tree that can be used to selectively view a section or the entire area as necessary for the design or review. The design is developed

with consideration from all aspects of the business and advanced modelling technologies enable the review teams to assess and influence the design throughout its evolution. In particular, the production engineering aspects of design are considered to optimise the use of equipment modules, identify when to outfit items for cost effectiveness and develop an installation plan to suit the build strategy.

The production planning activities carried out during the design process enable the design and production requirements to be merged to achieve cost effectiveness and efficiency. Any design issues or identified production problems are resolved using visualisation of the model and simple simulation of equipment movement, access for the workforce and manipulation of required tools etc is assessed.
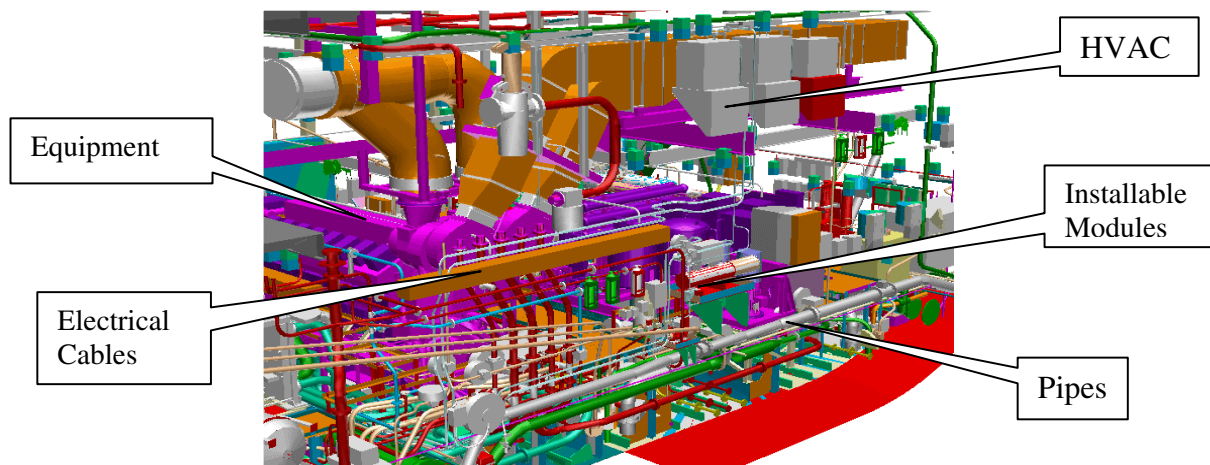
Typical 3-D Geometry Model

This facility was extensively used in the LPD project for the first time with variable levels of success. In shipbuilding, a critical consideration of the build and outfit process is the necessity to ensure that all major items are installed in the structure assembly prior to it being 'closed' by installation of the bulkheads and deckhead. i.e. Major equipment must be installed on the ship prior to the compartment boundaries being sealed, otherwise large holes need to be cut in the structure to ship these components causing potential structural weakness of the vessel. The models and associated data enabled these issues to be resolved successfully.

The following sequence of images illustrate the build process, which had a considerable contribution from the use of the modelling reviews which ensured the build sequence was optimised for the block build philosophy.


Block Build – All major equipment fitted

Full block build with advanced stages of outfit

The Build Blocks and their fabricated sub-units are a large complex and heavy assemblies which require production engineering effort in the provision of temporary supports, jigs and rigs for the build and movement of the blocks. This is particularly relevant for the extreme forward and aft blocks that often have narrow structures at the base and overhanging steelwork towards the top of the block. This together with the weight and centre of gravity considerations involves the design and build of suitable transportation rigs that enable the block to be moved safely without restricting the access required to line up the block with its adjacent block in the build hall or at the berth. Advanced modelling can help visualise these issues and solutions.

Block movement from Build Hall to Berth
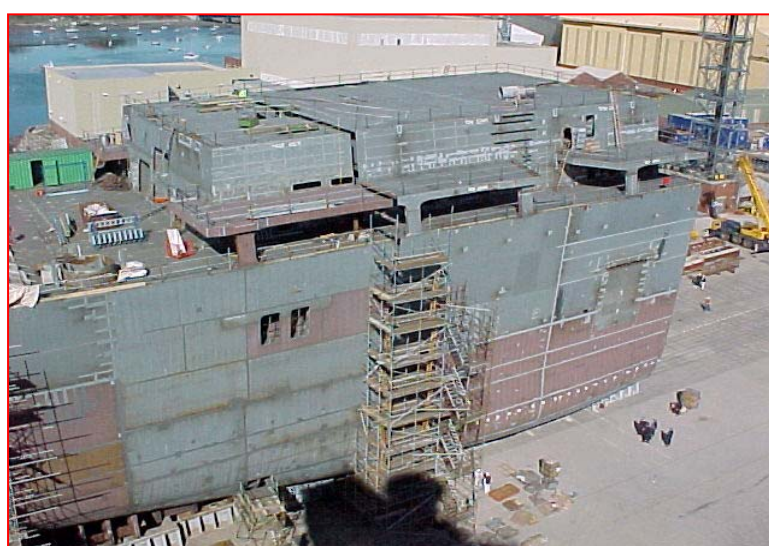
Block matched to adjacent one on berth

The second surface ship contract, involving two Auxiliary Oil Tankers, also used the developing processes and the systems applied to the LPD and the visualisation and virtual prototyping tools for internal and external design reviews.

The Astute class project is the first submarine design to use the technologies. Submarine design in the past has been supported by physical prototypes of either a full size wood mock-up or a scaled plastic model, both of which are expensive to produce in time and cost and which have an considerable effect on project schedule. The scaled prototype physical model was a representation of the design layout with sufficient accuracy for direct extraction of production details. (to feed Numerical Control Machine tools for pipe bending, for example). Elimination of the physical prototype will result in considerable cost, time and schedule saving. The Astute project has declared that advanced modelling and virtual prototype technologies will replace the physical model.

Concept Design Studies

The concept design phase of a project is such that 80% of the costs of the design are committed at this stage in the process.

In addition to the current design build projects, Advanced Modelling and Virtual Product simulation tools are used in concept design studies for future ships. The use of a product structure tree enables a design to be developed with several options included and a selection of options chosen as one possible design solution. Alternative design options can be selected and reviewed as necessary to assess the strengths and weaknesses of each configuration. If all of the selected design options are then analysed using simulation studies, a optimum design can be identified from the feasable alternatives.

Advanced Modelling and Virtual Prototype Simulation are particularly useful at the concept design stage and several studies have been carried out in conjunction with the MOD and industrial partners in the effectiveness of aircraft carrier flight deck layout and its relationship with aircraft operations. These studies involved use of flight simulators to control the behaviour of the aircraft and ship sea state simulators to control the behaviour of the ship in varying conditions. Pilot opinions were sought for the layout of the flight deck for manoeuvring, take-off and landing. The operation of the aircraft was directed by voice (telephone) contact between the pilot and a 'shipboard' flight controller, who gave permissions for taxiing, take-off landing etc as per normal aircraft carrier routine at sea.

Aircraft Flight Simulation with Aircraft Carrier Model

A secondary simulation study included analysis of aircraft manoeuvring by ship crew using hangar and flight deck towing equipment, verification of the refuelling facilities and assessment of the weapons handling and aircraft preparation activities. These studies used a mix of kinematics simulation and human factor manikin simulation.
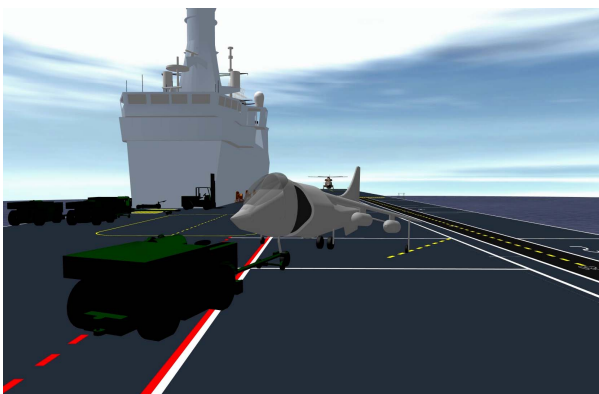
Tow-truck Simulation Model

Actual Tow-truck

When combined, these simulation studies offer a comprehensive understanding of the aircraft to ship interface critical to the design of a carrier, and is being done twelve years before the ship is due to be delivered. The ability to assess the relationship between a developing aircraft design and a ship concept design enables the critical issues to be resolved at this early stage and will lead to reduced long term cost.

Human Factors - Manikin Simulation.

Human Factor issues are evolving as critical requirements in design contracts. However, the technologies available in support of human factor design studies are limited, complex to use, and often involve data conversion processes often causing data inaccuracies. The requirement for human factor studies has been addressed at the Barrow shipyard in several alternatives. Simple manikin representations of typical human forms in fixed positions such as standing, sitting, crouching etc. are used to indicate a sense of scale in the 3-D models of ship compartments and give an early indication of design feasibility. More advanced manikin representations are used to assess operational positions in the design or the ability to construct parts of the ship or submarine that may be difficult due to access problems, density of surrounding components or services, or the need to carry or otherwise ship specialist tools. Both of the above technologies are used regularly by the design teams.

Additional studies have been made on the use of mathematically accurate manikin systems to evaluate their functionality and usefulness as aids in the design process. For example, a recent study involved the evaluation of two maintenance activities on the LPD project. The objective was to understand the feasibility of manikin simulation tools as an in-service support training aid. The study involved the change of oil filters for the ship diesel engines, and the more complex task of removal of a cylinder head from the engine. To carry out the studies, the 3-D models for the design were modified to include the internal component parts used in the maintenance task as these items are not normally modelled for design layout with experienced Human Factor engineers from NNC (formally a company subsidiary) carrying out the simulation. The study involved the manikin locating tools and spares, approaching the work and carrying out a known sequence of operations for the task. The study was to show access to the work, handling of tools and equipment and the process for the task. Unexpectedly the study identified design issues affecting the maintainability of the ship including the lack of secure dry storage for tools and replaceable items such as nuts, washers, spacers etc. and the difficulties of access to the rear of the cylinder head due to lack of suitable step or platform. The simple study thus illustrated that the technology potential when used in consideration of design for maintainability.

Manikin Study – Design For Maintenance

Measure of Success

One measure of the success of the application of the advanced modelling and virtual product simulation implementation at the Barrow shipyard is the decision by the design projects to build similar facilities to overcome the high demand. Three other facilities are thus in the process of being procured for project use. An alternative measure of success is the effect of advanced modelling and virtual product simulation in the consideration of design options in the concept and early stages of design. Issues that were often debated and

discussed using traditional design methodologies are often now readily accepted from the initial model visualisation and the design engineers spend their time more productively discussing new issues or proposals rather than verifying the 'old' issues.

The introduction of the technologies to the concept design stage of the design process has been successful in defining feasible solutions quickly and ensuring that the customer and users can understand the design concept. Discussions and concerns are considered against optional solutions, and each is assessed against outline requirements even at this early stage.

On all current projects the use of advanced modelling and virtual product simulation technologies has enabled the design teams to regularly assess and discuss the design layout and operability through informal and formal reviews. A key factor in this success is the philosophy of a user driven facility that can be used at any time by the project teams without the need for specialist support. This has been achieved by incorporation of an integral data conversion tool, technologies which are easy to use and operate, and integration of the visualisation facilities as one of the processors on the engineering network giving efficient access to files and models.

As stated earlier, the quantification of the effect on cost reduction directly attributed to the modelling and simulation technologies cannot easily be extracted from the general contribution made by improved design processes and the supporting systems. However, if the application of the technologies was shown to have a negative effect on the design, manufacturing, schedule or cost of the projects, they would not have continued to use the review facilities each day over the past five years.

The use of Advanced Modelling and Virtual product simulation has resulted in customer agreement to formally approve and sign-off the design via visualisation reviews of the models. This is a considerable success and partially due to the customer access and involvement with the models throughout and design process, acceptance meetings are now more productive as most key issues have been resolved prior to the review.

The illustration and verification of build strategies has also been successfully addressed using the technologies with resulting build sequences being developed and design areas selected to suit build requirements improving efficiency in the manufacturing process.

The studies into simulation based design have also been a success and have proven the concept and usefulness of this technology.

A final consideration in the successful application of advanced modelling and virtual product simulation is to use the technologies as a key element of the design process. It is not acceptable for a design to be developed using 2-D drawings or other technologies and then recaptured using advanced modelling. This creates rework, leads to data errors, affects the control of the design, and brings doubts into the quality, maturity and integrity of the resultant model.

Major Issues

Contrary to the success of the application of Advanced Modelling the following issues must still to be addressed:

- Geometric data is not sufficient to define a product, improved access is required from the geometry to the underlying specification, functional and component data.
- Database contents, data quality, data search and retrieval technologies are critical in the quest to reduce costs and are constantly being reviewed based on experience from the projects
- Geometry models must be controlled at component level for optimum management of the design options, use in simulation tools, and application throughout the scope of the life cycle.

Improvements

In applying the technologies, the successes outlined above have been realised on real, complex, high volume design projects. However, there is considerable scope for improvement in the use of the technologies including further development of user awareness of the functionality available to enhance the work already being done, improved access for the models to the underlying data attributes and information, and development of modelling strategies to suit simulation based design.

Simulation although often used in design analysis is still not strongly associated with advanced modelling visualisation and needs to be progressively introduced into the process following the results of the studies.

Introducing Advanced Modelling and Virtual Product Simulation technologies as an integral component of the design lifecycle management process is also being undertaken to help resolve some of the outstanding issues identified when analysing the lessons learnt from the design build projects.

Summary

The application of Advanced Modelling and Virtual Product Simulation at the Barrow shipyard has been a considerable success, with the design review and virtual reality visualisation facilities used constantly since their introduction in 1997. Advanced modelling is a day to day technology used by all design and detail engineers involved in the design process. The design review facility for large numbers of staff to collectively review the design layout models has a success measured by its constant demand by the projects, and the decision for new projects to build similar facilities. The technologies have been applied as a real and useful design tool on all projects since 1997, including concept designs and future projects bid preparations.
The requirement for improved access to underlying database information from the models is an issue that is being addressed to improve the use of the technologies.
Simple simulation such as animation of the geometric models and use of simple manikins is used regularly by the projects, however the development of a strategy for the implementation of further simulation applications is proposed following the success of the trial studies.
As a practical example of commercial use of Advanced Modelling and Virtual Product Simulation, the BAE SYSTEMS Sea Systems implementation illustrated above has shown that the technologies can be used effectively and efficiently, and can become an integral part of the design life cycle.

Conclusion

The requirement for the Reduction of Military Vehicle Time and Cost through Advanced Modelling and Virtual Product Simulation is an objective that is difficult to achieve on its own without improvement of design processes, lifecycle management, and well structured product databases with effective data access. However, Advanced Modelling and Virtual Product Simulation can offer a significant contribution to the optimisation of design solutions. In particular, use of the technologies in the concept and early stages of design, will influence costs considerably.

Paper Keynote #4
Discussor's name J. Coyle
Author John Martin

Q: Are you using the visualization data for delivery of information to the factory?

A: Production is very heavily involved in the development process and uses the data directly

This page has been deliberately left blank

_____

Page intentionnellement blanche

Reducing Military Aircraft Engine Development
Cost through Modeling and Simulation

Charles A. Skira
U. S. Air Force
AFRL/PRTA
1950 Fifth Street
WPAFB, OH 43433-7251, USA

Introduction

By the year 2010, more than half of the Air Force fighter fleet will consist of existing F-15's, F-16's and F-117A's -- well beyond their original expected service life. Nonetheless, the need exists to replace our most aged fleets of aircraft despite the uncertainty of future defense budgets.   Cost may be the determing factor that shapes the look of our military's future force structure. The goal of today's military acquisition reform process is to meet user system and service operational requirements while focusing on minimizing costs associated with life cycle cost. The term cost as an independent variable (CAIV) has been given to this process in which consideration is given, up front and early, to minimizing acquisition and deployment costs, maintenance strategy, reliability, maintainability and availability. Acquisition costs include both the development process and system production.

One factor that inhibits the introduction of new weapons systems into our future force structure is the exorbitant cost of developing new systems. Although the development cost for a new system is but a small fraction of the total systems life cycle cost, it is arguably the most significant element. Development cost is the first cost incurred for a new system and, in an era of tightening budgets, it tends to dominate all other system factors, including the performance and capability improvements offered by a new system. Also, there are fewer practical methods available to adjust the development cost without impacting the ultimate system configuration. Once a system enters the production or operational deployment phase, there are many means available to bring costs in line with budgets, such as reducing the number of total system buys, stretching out the production phase, or reducing the number of flying hours in peacetime operations.

In the past thirty years, weapon systems development costs have been steadily increasing with each succeeding system costing more than the last one. In fact, the cost of developing a new weapons system may become a factor in deciding whether a new system is procured or not. Clearly, there is a need to reduce the cost of developing new military systems. Besides the obvious benefit of saving real dollars at the most critical point in a weapon system's life cycle, lowering development costs could help tip the scales in favor of developing a new system as opposed to modifying an existing system. Studies have shown that a new system usually offers significant capability and performance benefits, as well as cost benefits, over those of a derivative weapons system[1]. Reducing the cost of developing new weapons systems also can mean that more systems could be developed within a constrained budget, a situation that is most favorable to sustaining our industrial base. A new weapon system, rather than a derivative or modification also offers the best opportunity for technology advancement and for technology transition into the hands of the nation's warfighter.

The Engine Development Process

The acquisition reform process has been an ongoing Department of Defense (DoD) activity since the early 1960's. A formal description of the way the DoD procures new systems is called the Defense Systems Acquisition Management Process and it is shown in figure 1. The acquisition management process is characterized by four major program milestones and phases. A new weapons system procurement officially begins with the establishment of a systems program office, or SPO. This occurs once approval is granted to conduct concept studies to define a weapon system that meets a required mission need. After conceptual studies are conducted, the next major milestone is the approval to proceed to the program definition and risk reduction phase. This phase was formerly known as concept demonstration and validation, or dem/val, for short. The purpose of this phase is to identify major system alternatives, identify technical risk and economic uncertainty, and to prove, through demonstration, that the associated technologies and processes are understood and are attainable.

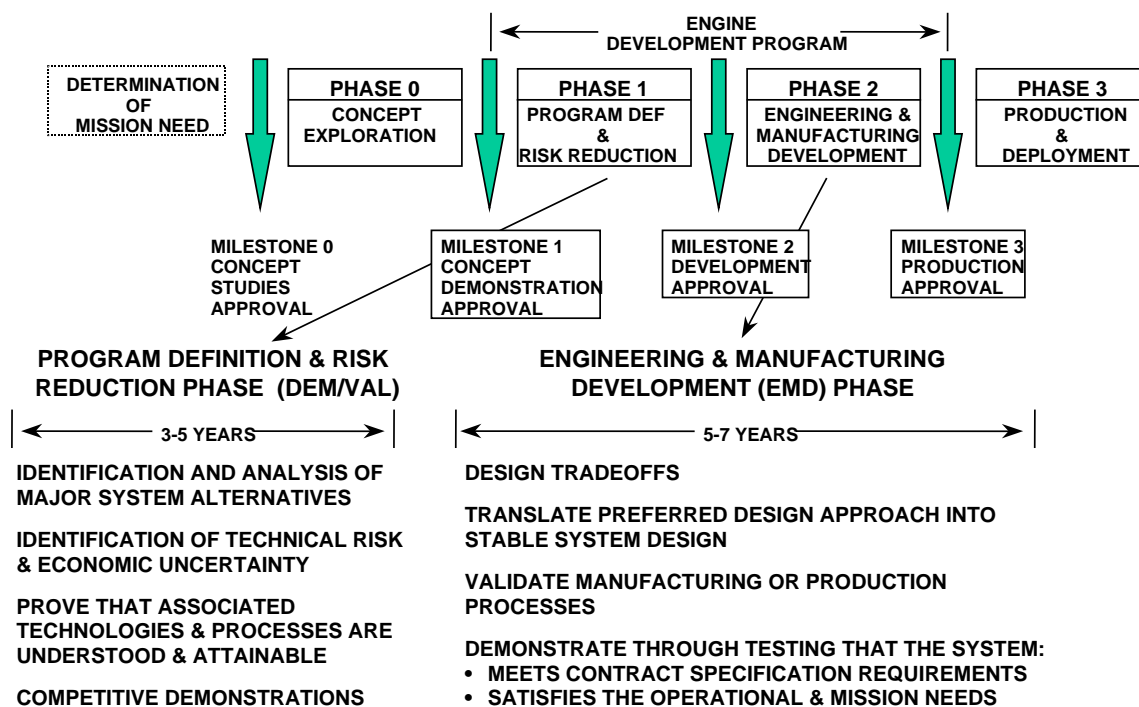_DEFENSE SYSTEMS ACQUISITION MANAGEMENT PROCESS_

Figure 1. Definition Of Engine Development Program

Once this effort is completed, approval would be granted to move into the next phase of the acquisition process: the engineering and manufacturing development (EMD) phase. In the EMD phase, design tradeoffs are completed and a final design is chosen. After that, two significant activities take place concurrently. The first is to validate the manufacturing processes that will be employed during the production and deployment phase. The second is to demonstrate through testing that the system meets the contract specification requirements and satisfies the operational and mission needs. After the EMD phase, approval would be sought to enter the final program phase, the production and deployment phase. The accepted definition of a development program is defined as the Program Definition and Risk Reduction and EMD phases of the acquisition management process and it is the definition used in this paper. The general acquisition management process shown in figure 1 applies to any military systems procurement. In figure 1, the length of the Program Definition and Risk Reduction and EMD phases shown are typical of those for a new military gas turbine engine development program. For an aircraft or other major subsystem, those times will be different.

Historical Perspective

Figure 2 represents a historical snapshot of military gas turbine engine development programs for fighter aircraft over the past thirty years. An analysis of this historical information yielded some interesting insights into the major program activities and cost drivers that characterize and define an engine development program. First of all, it is apparent that no two engine development programs in recent history are exactly alike. In general, the length of each succeeding engine development program has increased, however, the number of test engines and test hours has decreased. It should be noted that the Navy's F414 engine is considered to be a low risk derivative of the F404 engine, despite the fact that the F414 is about 25% larger than the F404. Since the F414 is a derivative engine, it follows that the length of the program would be shorter. In figure 2, there are two entries for the F119 engine development program. The actual F119 development program was modified shortly after it began to include a prototype demonstration, which occurred between the Dem/Val and EMD phases of the program. The principal purpose of the prototype demonstration was to support the aircraft flight test evaluations of the YF-22 and YF-23 prototype aircraft. The addition of the prototype demonstration added additional time and cost to the original F119 engine development program. During the time period shown in figure 2, a major change in engine development philosophy occurred and what is not readily apparent from figure 2 is how this military engine development cycle has evolved. In the days of the F100, an engine development program concluded with a 150-hour military qualification test (MQT). After that, the engines were produced and put in the field. Any problems that were encountered in the field were addressed during what was known as a component improvement program or CIP. By contrast, the F119 must demonstrate failure free operation within an expected service life of about 5,000 hours in the EMD portion of the development program. Figure 3 shows a comparison of the development program requirements for the F100-100, the F100-220, and the F119-100 engines. The requirements have increased tremendously over this relatively short time period[2]. Over the years there has been an increased emphasis on increasing engine reliability and durability, and the benefits are obvious. Today's engines are better in every aspect of performance and durability than their predecessors. Also, emphasis on reducing radar and infrared signature, and multi-axis thrust vectoring exhaust nozzles have introduced additional elements of cost. These are some of the factors that have driven the cost of developing a new engine upwards.
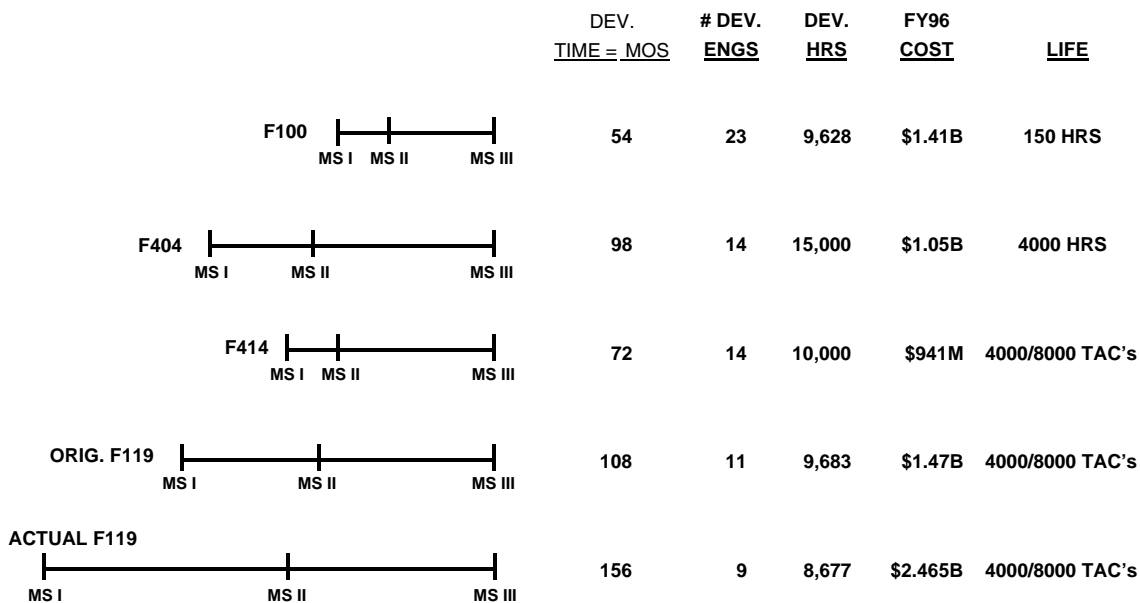
	DEV. TIME = MOS	# DEV. ENGS	DEV. HRS	FY96 COST	LIFE
F100 (MS I, MS II, MS III)	54	23	9,628	$1.41B	150 HRS
F404 (MS I, MS II, MS III)	98	14	15,000	$1.05B	4000 HRS
F414 (MS I, MS II, MS III)	72	14	10,000	$941M	4000/8000 TAC's
ORIG. F119 (MS I, MS II, MS III)	108	11	9,683	$1.47B	4000/8000 TAC's
ACTUAL F119 (MS I, MS II, MS III)	156	9	8,677	$2.465B	4000/8000 TAC's

Figure 2. Historical Summary of Military Gas Turbine Engine Development Programs

F100-100 (CIRCA 1970)	F100-220 (CIRCA 1980)	F119-100 (CIRCA 1990)
• PERFORMANCE FOCUS • MINIMAL ANALYTICAL UNDERPINNING • ITERATIVE TAAF APPROACH (Test, Analyze and Fix) • LIMITED INSTRUMENTED TESTING • NON-REPRESENTATIVE ENDURANCE TESTING (QT) • INSUFFICIENT ANALYTICAL & EMPIRICAL TOOL SET • LITTLE ATTENTION TO LIFE MANAGEMENT	• BALANCED FOCUS BETWEEN PERF. & DURABILITY • MATERIAL CHARACTERIZATION • INCREASED EMPHASIS ON ANALYSIS • ATTENTION TO ACTUAL ENVIRONMENT/USAGE • REPRESENTATIVE ENDURANCE TESTING (AMT) • DAMAGE TOLERANCE DESIGN APPROACH FOR SAFETY CRITICAL COMPONENTS • FULL LIFE TESTING OF MAJOR STRUCTURAL COMPONENTS	• APPLICATION TO ALL SUBSYSTEMS/COMPONENTS • EXPANSION OF PROCESS TO ALL FUNCTIONAL DISCIPLINES (PERF, OPER, ETC) • EXTENSIVE ANALYTICAL RIGOR IN DESIGN • COMPREHENSIVE ENVIRONMENT/RESPONSE CHARACTERIZATION • PROOF/MARGIN TESTING • DAMAGE TOLERANCE EXTENDED TO MISSION CRITICAL COMPONENTS • EXTENSIVE COMPONENT, SUBSYSTEM, & SYSTEM LEVEL "SMART" TESTING • PROCESS DEVELOPMENT & MATURATION IN EMD

Figure 3. Evolution of the engine development process

Notional Engine Development Program

In spite of the fact that the engine development process has changed significantly over the recent past, an average, or notional, engine development program can be defined, by taking a weighted average of the F100, the F404, the F414 and the originally proposed F119 engine development programs. The notional development program is a ten year, $1.5B effort, involving the fabrication and assembly of 14 test engines, 9 flight test engines and includes over 11,000 hours of engine test. The culmination of this effort is a fully qualified gas turbine engine ready for production. Despite some significant differences in program development cost over the time period depicted in figure 2, the cost distribution among the major tasks of each engine development program has remained relatively constant. This cost breakout and the schedule for the notional engine development program is shown in figure 4.

Based on the notional engine development program costs shown in figure 4, it is apparent that in order to make any significant reductions in engine development cost it will be necessary to attack the largest cost contributors. Those are the cost of engine hardware (tooling, fabrication and assembly) and the cost of engine testing. Clearly, both of these factors are not independent, as the number of test articles is a direct function of the type and number of test hours required in the program. The objective of an engine development program is to demonstrate through test, including flight test, that an engine meets the contract specification requirements and satisfies the operational and mission needs for which it was intended. There are practical limits, in terms of time and cost, on how well a test program can actually emulate operational conditions. An inverse relationship between the amount of engine testing and the level of risk associated with meeting the contract specifications has long been recognized. Obviously, there are trade-offs to be made, but there has historically been, a justifiable reluctance to make any compromises when fielding a system for fear of not meeting the intended operational and mission needs.
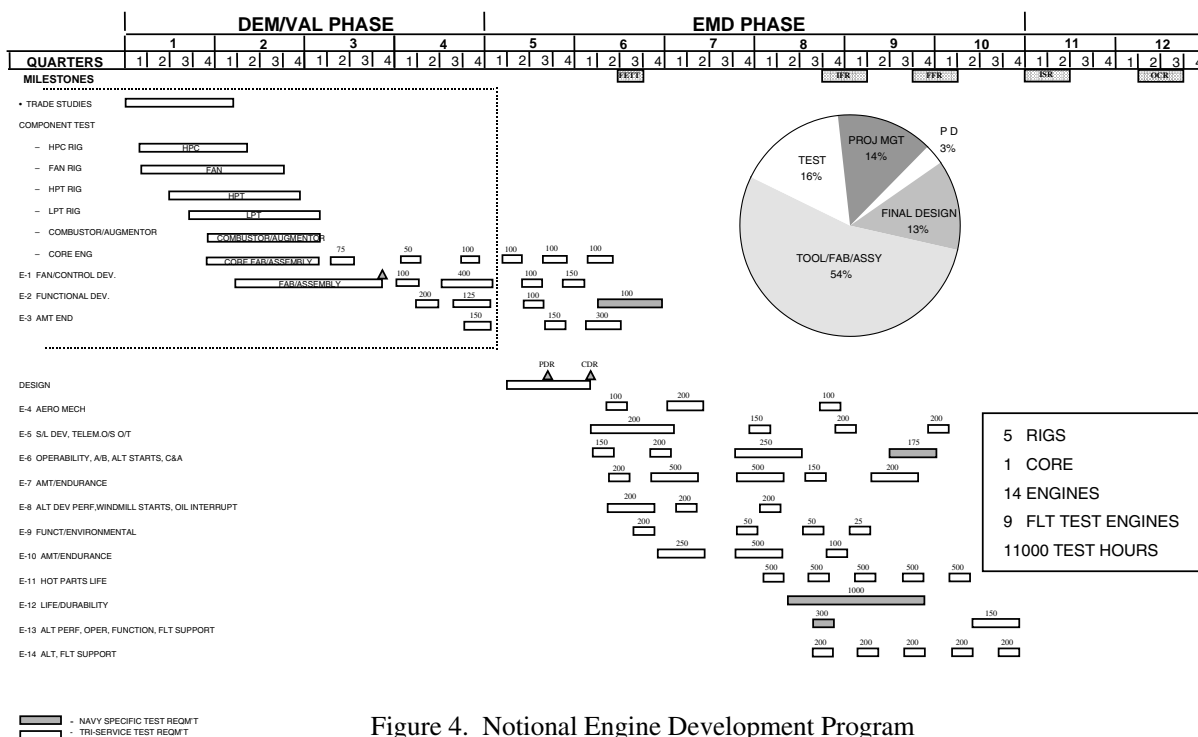
Figure 4. Notional Engine Development Program

The Key to Reducing Costs

The objective of any realistic cost reduction effort would be to reduce the amount of engine testing, and thereby the number of test engines necessary for an engine development program, without adding any undo risk to the overall program. All new engines under development will experience problems along the way. Serious problems that arise during the test portion of the development program that which require a major engine or component redesign to resolve are going to be very costly to correct. The kind of serious problems that would require such an action would be ones that cause the engine to fall far short of meeting operational needs or impact flight safety.

One vital key to reducing the cost of an engine development program is to identify and correct problems as early as possible in the program[3]. Obviously, the earliest time to do that is during the design process when engine hardware, the costliest element of an engine development program, is yet to be made. The key, then, to reducing engine development cost is to develop better simulation and design tools that accurately predict the physical phenomena occurring within the engine. With better design tools, the engine's performance, operability, life, structural integrity and durability can be estimated with greater precision. If the estimation accuracy can be raised high enough, dedicated engine testing to verify these metrics can be significantly reduced. This reduction in test hours means that fewer test engines will be required, thus resulting in further cost reductions. Having better design tools will also impact the other elements of an engine development program, namely the design activity and program management.

The benefits of advanced, computer-aided design methods have been documented throughout the technical literature. The most notable and dramatic example to date may be Boeing's experience using the Dassault/IBM CATIA (Computer Aided Three-Dimensional Interactive Application) design software during the development of the Boeing 777 aircraft[4]. The commercial development of computer aided design, engineering and manufacturing (CAD, CAE and CAM) software has become an emerging growth industry worldwide and it's development continues to evolve dramatically. Figure 5 shows the historical evolution of CAD/CAM/CAE software in terms of its analytical capability and also attempts to predict the type of computer aided design tools that might be available in the future.
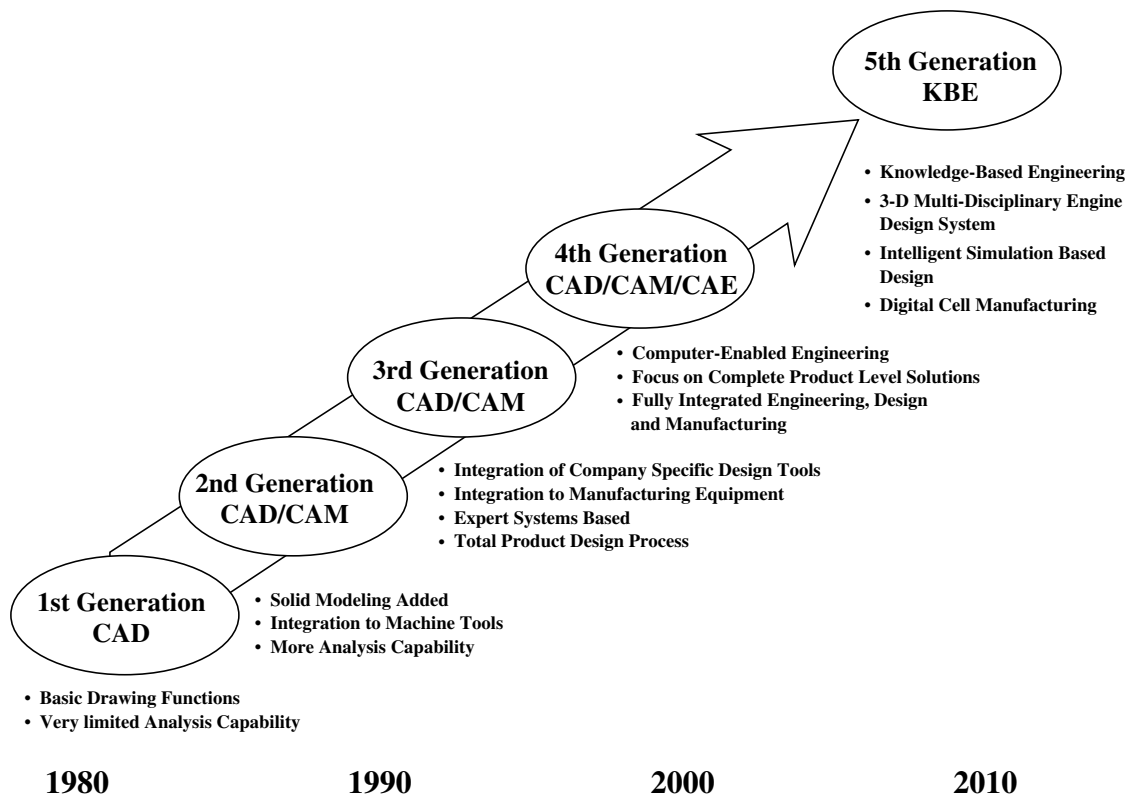
5th Generation
KBE

- Knowledge-Based Engineering
- 3-D Multi-Disciplinary Engine Design System
- Intelligent Simulation Based Design
- Digital Cell Manufacturing

4th Generation
CAD/CAM/CAE

- Computer-Enabled Engineering
- Focus on Complete Product Level Solutions
- Fully Integrated Engineering, Design and Manufacturing

3rd Generation
CAD/CAM

- Integration of Company Specific Design Tools
- Integration to Manufacturing Equipment
- Expert Systems Based
- Total Product Design Process

2nd Generation
CAD/CAM

- Solid Modeling Added
- Integration to Machine Tools
- More Analysis Capability

1st Generation
CAD

- Basic Drawing Functions
- Very limited Analysis Capability

1980   **1990**   **2000**   **2010**

Figure 5. The Evolution of Computer Aided Design, Manufacturing and Engineering Systems

The evolution of computer aided design software has followed the explosive development of microprocessor technology. Early CAD systems were limited to basic 2D drawing capability. As CAD systems evolved, the integration with numerically controlled machine tools soon followed, and the era of computer aided manufacturing emerged. As the evolution continued, more and more analytical capability was added. Today, detailed two-dimensional aerodynamic, thermodynamic and structural analysis and design software packages are routinely available to design engineers.

In order to have a major impact on engine development cost, the predictive accuracy of advanced simulation and design tools will have to improve significantly. The required accuracy of such a design system is shown in Table 1. To illustrate the level of improvement required, an estimate of the accuracy of today's current predictive capability is also shown in Table 1.

PHYSICAL PHENOMENA	TODAY'S ACCURACY	REQUIRED ACCURACY
Performance (Steady State & Transient)	+/- 2.0 %	+/- 0.5 %
Operability	+/- 20.0 %	+/- 2.0 %
Aerothermodynamic	+/- 3.0 %	+/- 1.0 %
3D Structural	+/- 5.0 %	+/- 2.0 %
HCF/Fracture Mechanics	+/- 20.0 %	+/- 10.0 %
Performance Integrated with Control	+/- 2.0 %	+/- 0.5 %
Life - LCF	+/- 25.0 %	+/- 5.0 %
- HCF	+/- 100.0 %	+/- 20.0 %
- Oxidation Resistance	+/- 10.0 %	+/- 5.0 %
- Stress Rupture	+/- 10.0 %	+/- 5.0 %
Material Properties	+/- 10.0 %	+/- 5.0 %

Table 1. Modeling and Simulation Accuracy

To meet the improved accuracy goals, future, automated design software tools should focus on the development of highly accurate, three-dimensional, multi-disciplinary engine design systems. Multi disciplinary, in this context, means the ability to include aerodynamic, thermodynamic, structural and secondary flow together within the same design package.

The term being applied to this future capability is Knowledge Based Engineering and it implies a higher level of capability and interaction. These systems would incorporate years of design experience, lessons learned and knowledge in a rules-based design system, so that moderately experienced engineers could use them with confidence.

This comprehensive interaction during design is depicted in Figure 6 and it shows that the 3D multidisciplinary design system is at the heart of the overall process. The mission parameters and engine cycle requirements become the principal input to the design system. The principal output is a solid geometry master model of the engine configuration that meets all of the desired performance and life requirements. The solid geometry master model, in the form of an electronic computer file, will interface with and facilitate the manufacturing process, including tooling design and fabrication, the engine assembly and functionality, and the oversight and management of the program.
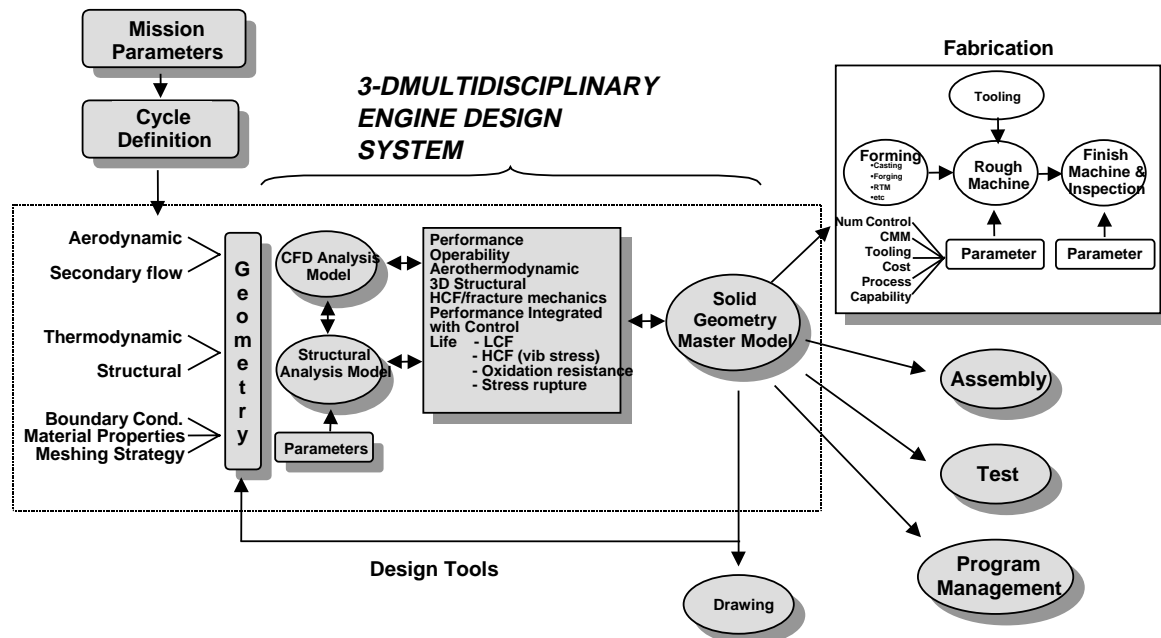
Figure 6. The Role of Design System in the Engine Development Process

The Reduced Cost Engine Development Program

What would be the impact of this improved modeling and prediction capability on the cost of an engine development program? First of all, the new design tools would shorten considerably the amount of time to arrive at a final engine design and greatly improve the design itself.

Historically, about 3 major redesigns would occur during an engine development program just to correct design deficiencies uncovered during the test phases of the program. It is anticipated that no major engine redesigns would be necessary with the advent of these new design tools. Secondly, these design models would permit the establishment and use of a "virtual engine test cell" whereby the engine's performance and operability characteristics could be verified and validated via simulation prior to actual hardware testing. This would lead to a reduction in the amount of actual engine testing required, and, in turn, would lead to a reduction in the number of engines needed in the development program. All aspects of an engine development program would be impacted, including program management. The following section describes

in detail the cost analysis that was done to determine the impact of advanced design and simulation tools on a new engine development program.

In order to determine the impact of a "virtual test cell" on the amount of engine testing required in an engine development program, it is prudent to first examine the purpose of an engine test program. Generally, the requirements fall into two broad categories: verifying engine performance and ensuring safety of flight. A typical set of engine test requirements for an engine development program is shown below in Table 2.

- Fan/Compressor Aeromechanical Performance
- C&A Environmental
- Altitude Performance
- Augmentor Development
- Low Pressure Aeromechanical Performance
- Envelope Exploration
- Stall Margin/Operability
- Inlet/Engine Compatibility
- Control Optimization
- Pressure/Thermal Surveys
- Heat Rejection
- Oil & Electrical Interrupt
- Overspeed & Overtemperature
- Accelerated Mission Test
- Ingestion: Water/Ice/Birds
- Vibration/Critical Speeds
- Blade Out/Containment
- Windmill/Altitude Start

Table 2. Typical Engine Test Requirements

Table 2 illustrates just how broad the scope of the overall test activity is. Simulated engine testing would greatly impact some of the test requirements in table 2 and have little or no impact on others. For example, it would be relatively easy to verify aerodynamic performance with simulation, but quite hard, if not impossible, to verify blade-out containment with simulation. The type of test hour reductions that may be realizable with advanced design and simulation tools is shown in Table 3.

This represents an overall reduction in total engine test time of about 30 percent. Accordingly, the number of engine hardware sets required to support the engine test program would drop from 14 to 9.

Test Activity	Notional	Proposed
Aero/Mechanical	775	400
Functional/Environmental	675	500
AMT/Endurance	3225	2875
Operability (SL)	750	450
(Alt)	2595	1325
Hot Part Life/Durability	3000	2000
Total Test Hours	11020	7550

Table 3. Test Hour Reduction Potential

Secondary cost benefits would also be realizable.   As indicated in figure 6, the output of the 3D multidisciplinary design system is a solid geometry master model. This master model would become an integral part of a seamless set of software modules that would interface with all other aspects of the program

operation, from human resources, contracting, finance, manufacturing and planning. The term enterprise resource planning, or ERP, has recently been coined to describe the aerospace and defense companies efforts to reengineer and computerize all aspects of their operations as a means of reducing cycle times and costs [5].

The solid geometry master model would become a data input data to computer aided manufacturing software tools to design the tooling fixtures, casting molds and forging dies with greater precision. First-time quality will be greatly improved, reducing rework on manufactured parts by 50%. The electronic data files describing the solid geometry master model would provide an accurate and seamless interface among the designers, manufacturing and outside vendors and suppliers, ensuring and enabling integrated product development (IPD). Form, fit and function could be accomplished electronically, eliminating the need for mock-ups and reducing the cost and time associated with assembly.

The ability to instantaneously transfer data electronically, and to conduct paperless design and test reviews will impact the number of support staff and the number of programmatic meetings. Once again, the key enabler to reducing program management costs is the existence of the 3-D, solid geometry master model that is created by the advanced design system. Technical and programmatic performance can be tracked daily with a system that is accessible, flexible and easy to understand. Table 4 describes the groundrules and assumptions that were used in the cost analysis.

Development Activity	Notional	Proposed
Tooling Cost	$ 90 M	$ 45 M
Fab & Assembly/Engine	$ 45 M	$ 30 M
Rig: Fab/Assembly/Test		
- Fan/Comp, C&A	$ 10 M	$ 7 M
- Comb/HPT/LPT	$ 4 M	$ 2.8 M
- Aug/Noz/Mech Sys	$ 2 M	$ 1.4 M
Ave Test Cost/Hour	$ 18.5 K	$ 20 K
- Sea Level	$ 15 K	$ 18 K
- Altitude	$ 25 K	$ 30 K
- AMT/Endurance	$ 10 K	$ 10 K
- Specialized	$ 60 K	$ 60 K
Ave # of Design Iterations	~ 3	~ 1.2

- All Costs based on FY 90 $'s
- No flight test activity in DEM/VAL
- No significant program redirection & sufficient funds
  are available to maintain the program schedule

Table 4. Groundrules and Assumptions

A 50% reduction in tooling cost was assumed due to the impact of automated tooling design based on the solid geometry master model and a reduction in the number of design iterations needed to achieve a final product definition. A 33% reduction in the average engine cost in the development program was assumed due to the reduction in the number of engines required, the anticipated reduction in required rework, the improved quality, the reduction in manufacturing lead times, and improvements in assembly [6].

Similarly, the cost of fabricating, assembling and testing rig hardware would be reduced by about 30%. In the analysis of rig costs it was observed that the rig costs varied by component. Fan, compressor and controls and accessory rig tests cost on the order of $10 M apiece; combustor and high and low pressure turbine rig tests cost about $4 M; and augmentor, exhaust nozzle, and mechanical systems cost on the order of $2 M each. There were exceptions to this rule. The F119 engine is a two-spool, counter-rotating engine with a 2D, thrust vectoring exhaust nozzle. Both the nozzle rig, which used sub-scale hardware which helped defer some of the cost, and the counter-rotating bearing rig were more expensive. In evaluating rig costs, a factor that should be considered is the level of technology involved in the new engine design. This will often times dictate whether a rig test is needed or not.

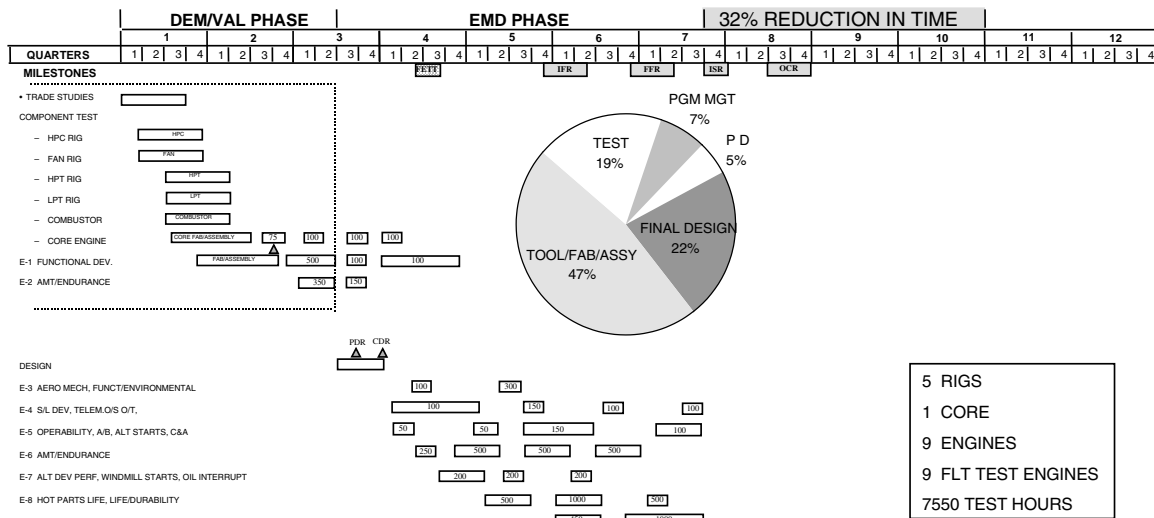DEM/VAL PHASE | EMD PHASE | 32% REDUCTION IN TIME

Figure 7. Proposed Reduced Cost Engine Development Program

One more thought concerning rig hardware and tests is offered. Some engine manufacturers have discussed eliminating rig tests because their design systems are so good. In the author's opinion, that would not be a wise thing to do. While eliminating rig tests sounds impressive, it violates one of the axioms surrounding the reduction of engine development cost. That is that cost is dependent on when problems are discovered and corrected. Rig tests represent a small fraction of a total engine development program's cost, more importantly, they offer the first opportunity to verify a design through actual hardware tests, and for this fact alone, they are a bargain.

Full-scale hardware tests were assumed to increase in cost by about 20%. This is to account for an anticipated increased level of post-test analysis featuring the improved simulation tools and an increase in the amount of on-engine instrumentation to support that analysis. This increased cost per test hour will be more than offset by a reduction in the number of test hours required.   Like rig tests, full-scale engine test costs vary by the type and nature of the test. The costs shown in Table 4 include all costs associated with an engine test, including engineering support and facilities. Specialized tests, such as FOD tests, blade out containment, cold soak starting, etc. are very expensive due mainly to the unique test facilities required and possible hardware losses. Fortunately the total test time for these types of tests is relatively low.

The groundrules and assumptions depicted in Table 4 were factored into the framework of the notional engine development program shown in Figure 4 to arrive at an estimate of the cost reduction potential due to improved design tools.   Table 5 shows a cost comparison between the notional baseline engine development program and the proposed, lower cost program that takes full advantage of the improved design tools and simulation potential capability previously described. The numbers in parenthesis shown in Table 5, indicate the cost distribution by development activity on a percentage basis for the notional program and for the proposed program.

Development Activity	Notional	Proposed
Preliminary Design	$ 46 M (3%)	$ 37 M (5%)
Final Design	$ 198 M (13%)	$ 160 M (22%)
Tooling/Fab/Assembly		
Rig	$ 30 M (2%)	$ 22 M (3%)
Core/Engine	$ 481 M (32%)	$ 164 M (22%)
Flt Test Engines	$ 310 M (21%)	$ 156 M (21%)
Test		
Rig	$ 16 M (1%)	$ 16 M (2%)
Core/Engine	$ 202 M (14%)	$ 126 M (17%)
Project Mgt/Other	$ 213 M (14%)	$ 52 M (8%)
Total	$ 1496 M	$ 733 M

Table 5. Development Cost Comparison

These percentages are interesting in that they could indicate a shift in the development program philosophy in favor of increased emphasis on the upfront design activity. From a cost viewpoint, savings on the order of 50% are potentially realizable for a new engine development program.

The cost distribution and a program schedule for the proposed reduced cost engine development program are shown in Figure 7. With the advanced design tools and simulation capability, a 32% reduction in program length is possible. This represents a reduction in program length of 39 months. The number of test hours is reduced by over 30% and the test costs can be reduced by about 35%.

The largest area of cost reduction potential lies in the cost of hardware. Specifically, this includes the cost of tooling, fabrication and assembly of rig test hardware, engine test hardware and the engine hardware needed to support a flight test program. The number of flight test engines was fixed at 9 for both the notional and proposed development programs in this analysis. Moreover, the number of engines directly involved in the development activity falls by over 36%, while the total hardware costs fall by nearly 60%. There are three principal factors contributing to this dramatic reduction in hardware cost. The largest contributor is due to the reduction in the number of major engine redesigns, followed by the reduction in the number of engines required and, finally, the reduction in tooling costs.

In the proposed program, program management costs are reduced by 70% compared to the notional engine program. These projected savings are due to the overall reduction in the length of the program, the reduction in engine hardware, and in test hours. Another factor that will contribute to the reduction in program management costs is the anticipated impact of enterprise resource planning tools which will permit effortless, daily tracking of the program's cost, schedule and technical progress interactively with very few support personnel.

Summary

The engine is one of the few subsystems that have a positive impact on an aircraft weapons system. For a given mission requirement, using a high thrust to weight ratio engine translates into a smaller, lighter and less costly aircraft. In spite of these obvious benefits, the cost of developing a new high performance military aircraft engine is becoming prohibitively more and more expensive, as the requirements for each new engine seems to be increasing without bound. Clearly, there is a need to reduce the cost of future military engine development programs without compromising the basic program requirement to demonstrate that an engine satisfies all of the operational and mission needs for which it was designed.

An analysis of the engine development process indicates that significant cost reduction potential is possible if improved computer-aided design tools and simulation techniques can be developed. The predictive accuracy of these advanced software tools has been defined. With these improvements, the design effort can be shortened considerably and the number actual engine test hours would be significantly reduced. This would lead to a dramatic reduction in the number of test engines required to conduct an engine development program. Subsequently, the length of the development program may be reduced by a third. All of these factors contribute to the potential cost reduction of an engine development program that is on the order of 50%.

References

1. Skira, Charles A., Reducing the Cost of Advanced Technology Engines, AIAA 97-3156, 33rd Joint Propulsion Conference, Seattle, WA

2. May, R. J. and Smith, Maj. M. F., Development Concept for Advanced Fighter Engines, 83-1298, 19th Joint Propulsion Conference, Seattle, WA

3. Alley, William R., and Stetson, Harold D., A Monte Carlo Simulation of the Engine Development Process, AIAA 83-1230, 19th Joint Propulsion Conference, Seattle, WA

4. "Concurrent Engineering in the Aircraft Industry", *Aerospace Engineering*, Vol. 17, No 9, Sep 97, pp. 15-19

5. "Aerospace Invests Billions in ERP Software, Processes", *Aviation Week & Space Technology*, January 25, 1999, pp. 68-70

6. Bokulich, Frank, "CAD Software Integration", *Aerospace Engineering*, March 1999, pp. 17-25

Paper Keynote #5
Discussor's name R. McClelland
Author Skira

Q: 1. Is there any hope of reduction of air flight safety test hardware?
    2. Are there any actual development programs underway using this vision?

A: 1. No-difficult problem
    2. No-not yet

Prototypage virtuel pour les programmes navals

(Virtual Prototyping in Naval Ships)

Mona Khoury
DGA
Centre Technique des Systèmes Navals
BP 28
83800 Toulon Naval
France

Résumé

Dans ce papier est présentée une méthodologie, basée sur le prototypage virtuel, actuellement en cours de mise au point en France, pour optimiser les coûts et délais d'un programme naval.

L'idée principale est de fédérer les données industrielles de conception et les outils de simulation dans une architecture logicielle unique de façon à faciliter l'accès aux résultats de simulation à l'ensemble des participants d'un programme naval, et surtout à l'équipe de Direction du Programme.

Les différents aspects de cette méthodologie sont décrits et des exemples des premiers résultats sont donnés.

Introduction

Avec la réduction des budgets de défense dans la plupart des pays occidentaux, la maîtrise des coûts et délais dans le cadre d'un programme naval est devenue un enjeu vital.

Par ailleurs l'accroissement des capacités informatiques a favorisé le développement d'outils de simulation très complexes et très complets.

La conjonction de ces deux paramètres – réduction budgétaire et développement de l'informatique – a naturellement conduit à envisager l'usage de la simulation de façon systématique tout au long d'un programme naval comme un élément essentiel pour en réduire les aléas techniques et donc les coûts et délais.

Le développement de la méthodologie baptisée « prototypage virtuel » par la DGA en France s'inscrit dans ce contexte. Dans ce papier, cette méthodologie est décrite en détails et les premiers exemples d'application sont donnés.

Abréviations

DGA : Délégation Générale de l'Armement
DP :   Direction de Programme
DCE : Direction des Centres d'Expertises et d'Essais
CTSN :Centre Technique des Systèmes Navals

Le contexte :

On se place ici dans le cadre d'un programme naval qui a des contraintes financières et calendaires bien précises. La Direction de Programme a en charge :
-    l'écriture des spécifications du système recherché à partir de l'expression du besoin opérationnel
-    la passation du contrat correspondant avec un industriel
-    l'évaluation des fournitures de l'industriel

Pour ce dernier point, le DP fait appel à des experts étatiques. En France, c'est la DCE, une des directions de la DGA, qui joue ce rôle. Pour réaliser leurs tâches d'évaluation, les experts étatiques s'appuient sur un certain nombre d'outils qui sont essentiellement des essais et des simulations.

Le prototypage virtuel consiste à développer une méthodologie centrée sur l'utilisation des moyens de simulation. A ce titre il s'inscrit dans le cadre plus large de « l'acquisition fondée sur la simulation » (simulation based acquisition).

Description de la méthodologie

1. Identification des simulations

La première étape pour utiliser la simulation dans le cadre d'un programme naval est l'identification des outils de simulation nécessaires. Ceci nécessite qu'en amont au programme, dès la phase de préparation, un important effort soit fait du côté des experts étatiques pour identifier les outils de simulation à utiliser pour les travaux d'évaluation et les données nécessaires (avec leur format) pour alimenter ces outils. Ceci doit bien sûr se faire en cohérence avec les exigences de la Direction de Programme. En face de chaque exigence, de chaque fonction spécifiée, il faut se poser la question de l'évaluation. Suivant le cas, la réponse à cette question peut être multiple :
- l'évaluation se fait au moyen d'un essai, une simulation n'est pas ou difficilement envisageable
- l'évaluation peut se faire par simulation mais le temps nécessaire à la mise au point de l'outil de simulation et à sa validation n'est pas compatible du programme
- l'évaluation peut se faire avec un outil de simulation existant ou dont le développement et la validation sont compatibles des contraintes calendaires du programme

Dans ce dernier cas seulement, on considère avoir identifié un outil de simulation à utiliser dans le cadre du programme. Il faut encore s'assurer que cet outil a été validé et que son domaine de validité est connu avec précision. Ce dernier point est essentiel pour que le DP puisse se fier en toute sécurité aux résultats des simulations. Toute la crédibilité de la démarche est basée sur la rigueur apportée aux aspects validation des simulations.

2. Accès aux données

L'un des problèmes majeurs que l'on rencontre lorsque l'on veut utiliser des simulations dans le cadre d'un programme naval à des fins d'évaluation est l'obtention des données. En effet l'expert côté étatique doit disposer des données industrielles de conception qui servent de données d'entrée aux simulations. Or il rencontre souvent des difficultés pour obtenir ces données :
- l'industriel ne veut pas les fournir par souci de propriété intellectuelle
- la fourniture de ces données a un coût
- même quand des données sont disponibles il est parfois difficile de s'assurer qu'elles sont à jour

Ces problèmes vont induire des retards dans la fourniture des résultats et des doutes sur la crédibilité des simulations. Ces difficultés vont donc freiner le Directeur de Programme dans l'utilisation de la simulation et l'empêcher de l'utiliser de façon systématique.

La solution à adopter est la suivante : il faut dès le début d'un programme définir les données nécessaires et leur format et exiger contractuellement de l'industriel la fourniture de ces données et leur mise à jour régulière.

3. Fédération des données :

L'étape suivante est la mise en place d'une structure informatique, que l'on peut qualifier de structure d'accueil des données. C'est l'industriel qui alimente cette structure au profit des différents experts simulation et du prototype virtuel. Cette structure permet :
- de centraliser les données : ceci facilite à la fois l'accès et la mise à jour des données au fur et à mesure de l'avancement du programme.
- d'extraire facilement, au bon format, les données nécessaires à un outil de simulation donné

Cette structure informatique a donc les interfaces suivantes :
- interface avec les données de conception (fichiers CAO et données techniques)
- interfaces avec les différents outils de simulation identifiés : il y aura autant d'interfaces spécifiques que d'outils choisis

Cette structure est organisée de telle façon que l'on puisse garder en mémoire les différentes versions des données. Cela permet de faciliter la comparaison entre différentes solutions et de mieux évaluer la progression du programme.

4. Fédération des résultats

Avec les 3 étapes décrites ci-dessus on a optimisé la mise en œuvre des simulations. Il s'agit dans cette étape, d'une certaine façon, d'optimiser l'utilisation des résultats. Les résultats d'une simulation sont en général assez complexes. La plupart des outils de simulation destinés à évaluer une fourniture industrielle sont des outils d'experts dont l'interprétation des résultats n'est pas toujours facile. Le but de cette étape est double. Il s'agit de :

- rendre accessible aux différents acteurs d'une équipe de programme l'ensemble des résultats de simulation significatifs. En effet, jusqu'à aujourd'hui, le DP a accès aux résultats de simulation au travers des rapports d'experts et au cours de réunions organisées avec chaque expert du domaine qui présente ses résultats sous forme de courbes ou graphes plus ou moins aisément compréhensibles par un non-spécialiste. Ceci veut dire, qu'en dehors de quelques cas bien spécifiques, le DP se penche très peu sur les résultats de simulation quand il se pose une question. Le fait de disposer au sein de l'équipe de programme d'un outil informatique présentant de façon conviviale tous les résultats significatifs de simulation disponibles à un instant donné, avec un certain degré d'interactivité, devrait largement inciter le DP à faire appel plus systématiquement aux simulations.

- faciliter le dialogue des différents acteurs entre eux

- faciliter le couplage des simulations entre elles, par exemple on peut envisager le scénario suivant : attaque d'un missile (mise en œuvre outil de simulation guerre électronique) – impact (mise en œuvre outil de simulation vulnérabilité) – incendie (mise en œuvre simulation propagation incendie – modèle facteurs humains) – lutte contre les sinistres (mise en œuvre modèle d'organisation de lutte contre les sinistres). On peut ainsi jouer des scénarios opérationnels très complets mettant en œuvre un grand nombre d'outils différents de simulation.

La solution adoptée par le Centre Technique des Systèmes Navals de la DCE, en accord avec le Service des Programmes Navals, est de fédérer l'ensemble des résultats de simulation au sein d'un prototype virtuel de navire, d'où le nom de prototypage virtuel donné au processus décrit ici. L'obtention du prototype virtuel et son utilisation dans le programme constituent l'étape ultime du processus.

Le prototype virtuel ainsi conçu comprendra donc les interfaces suivantes :

- interface avec la structure de fédération des données pour récupérer les fichiers CAO qui permettent la mise au point des « objets bateau »
- interfaces avec les différents outils de simulation pour intégration de leurs résultats dans le prototype virtuel. Il existe autant d'interfaces que d'outils de simulation.

L'ensemble du processus – fédération des données / fédération des résultats - peut être représenté par le schéma suivant :

```
┌─────────────────────────────┐                    ┌─────────────────────────────┐
│   DONNEES INDUSTRIELLES      │                    │   OUTILS DE SIMULATION      │
│                             │                    │                             │
│       Fichiers CAO          │                    │       Tenue à la mer        │
│                             │       ┌────┐        │       Vulnérabilité         │
│   Données de conception     │──────→│ T2 │───────→│        Signatures           │
│ (ex. masse, énergie, ...)   │       └────┘        │        Manutention          │
│                             │                    │        Maintenance          │
│                             │                    │          Etc …              │
└──────────────┬──────────────┘                    └──────────────┬──────────────┘
               │                                                   │
            ┌────┐        ┌──────────────────────────┐         ┌────┐
            │ T1 │───────→│    PROTOTYPE VIRTUEL      │←────────│ T3 │
            └────┘        └──────────────────────────┘         └────┘
```
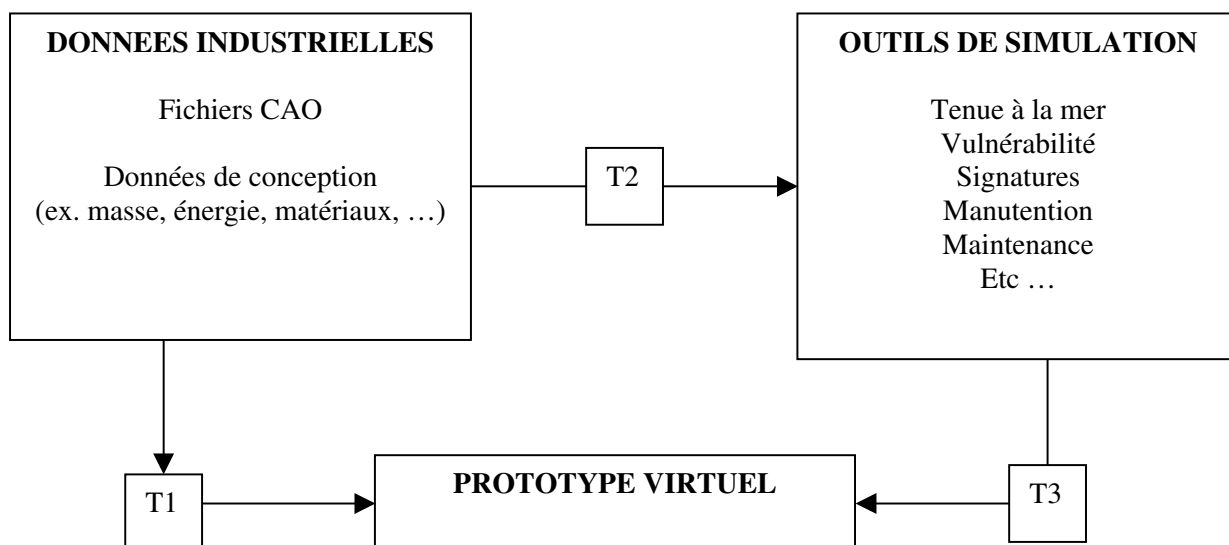
5. Outils utilisés

Pour bâtir ce PV on utilise les outils informatiques suivants :
-   des stations de travail de type SGI, à hautes performances graphiques
-   un logiciel « modeleur » qui permet la récupération des données CAO et leur traitement pour maîtriser le niveau de détail et conserver au prototype virtuel son utilisation « temps réel »
-   un logiciel de réalité virtuelle permettant l'intégration des différents résultats de simulation et l'animation du navire virtuel en temps réel, avec le comportement déduit des simulations.

Notons que la présentation des résultats de simulation sous cette forme vient compléter le travail des experts et non pas le remplacer, à charge pour les experts d'identifier les cas significatifs qui doivent être intégrés au prototype virtuel. Notons également que, pour certains domaines techniques, le prototype virtuel comprend un accès à une visualisation plus classique des résultats de simulation, sous forme de graphiques ou de courbes.

6. Mise à disposition du Prototype Virtuel

Le prototype virtuel ainsi réalisé est mis à la disposition de l'équipe intégrée de programme à travers un réseau informatique sécurisé. Cette équipe comprend les membres de la Direction de Programme mais aussi des opérationnels et des industriels. Le prototype virtuel leur permet différents types d'analyse :

-   évaluation des performances : tenue à la mer, vulnérabilité, signatures, …
-   validation de procédures : manutention d'armes, ravitaillement à la mer, …
-   immersion virtuelle : surtout pour les aspects Facteurs Humains : accessibilité, maintenabilité, …

Une interface spécifique est réalisée pour permettre un accès facile au type d'analyse envisagée et aux différents domaines techniques et fonctions représentés.

Ce prototype peut être utilisé :

-   ponctuellement, pour examiner de plus près tel ou tel aspect
-   lors des revues de projets : comparaison avec les versions précédentes, mise en œuvre de scénarios opérationnels, …
-   lorsque deux solutions de conception sont envisageables, comme aide à la décision

Pour la Direction de Programme, le prototype virtuel est essentiellement un outil d'évaluation, ce qui est son but initial.

Pour les opérationnels, il permet de se rendre compte de la façon dont leur besoin opérationnel sera rempli, mais aussi de disposer de l'information nécessaire, sous une forme aisément compréhensible, quand des choix sont nécessaires, pour des raisons de coût par exemple.

Pour les industriels il est un outil d'aide à la conception important.

Pour tous il est un outil de dialogue.

Premiers résultats

Les premiers résultats présentés ici concernent la partie interface outils de simulation – prototype. Une maquette de prototype virtuel, fondée sur la frégate La Fayette, a été réalisée avec intégration des simulations suivantes :

- tenue à la mer, avec et sans avarie, manoeuvrabilité : prise en compte d'une déformation de la houle autour du navire et intégration de fichiers résultats du code FREDYN utilisé par le Bassin d'Essais des Carènes de la DCE. Cette partie constitue la brique de base du prototype virtuel puisque nombre de simulations se font à partir du navire en mouvement.

- opérations hélicoptère : intégration de fichiers résultats du code IDYNA du Centre Technique des Systèmes navals, ce code permet de simuler le comportement d'un hélicoptère à l'appontage et lors des manœuvres sur le pont (calcul des mouvements de l'hélicoptère et des efforts sur les trains d'atterrissage, les amortisseurs et aux différents points de liaison entre l'hélicoptère et le pont).

- Vulnérabilité, propagation incendie : intégration de fichiers résultats du code de vulnérabilité MINERVE développé par le Groupe d'Etudes et de Recherches en Balistique, Armes et Munitions. Ce code permet de visualiser l'impact d'une agression (extérieure ou intérieure, comme l'explosion d'une munition en soute) : effet du souffle, propagation des éclats. On peut visualiser les locaux et équipements touchés et voir ainsi la dégradation fonctionnelle résultante. Ce code peut être couplé au code de propagation incendie LUCIFER mis en œuvre au Centre Technique des Systèmes Navals. On peut associer ensuite les aspects lutte contre les sinistres avec mise en œuvre des moyens automatiques et organisation humaine.

Les outils mentionnés ci-dessus sont les moyens de simulation identifiés comme outils d'évaluation dans les domaines techniques cités. Les travaux sur cette maquette se poursuivent actuellement avec les aspects signature et s'orientent également vers une intégration des aspects système de combat.

Par ailleurs, l'aménagement intérieur étant représenté, il est facile d'examiner les aspects facteurs humains :
- ergonomie
- accessibilité
- maintenabilité

Certaines applications ont également été effectuées dans le cadre du programme HORIZON.

Conclusion

La méthodologie prototypage virtuel présentée ici s'inscrit entièrement dans la politique de simulation pour l'acquisition. Elle vise :
- à optimiser l'usage des simulations pour que les programmes retirent les bénéfices des développements importants menés dans le domaine de la simulation, ces dernières années.
- à exploiter les avantages des techniques de réalité virtuelle en prenant en compte les aspects facteurs humains (accessibilité, ergonomie, maintenabilité, validation de procédures, …) dans leur ensemble à un stade très précoce du programme.

Un investissement de départ est certes nécessaire : il faut prévoir contractuellement la fourniture des données industrielles et un équipement informatique minimal au niveau de la Direction de Programme. Cependant le gain attendu au niveau de la maîtrise technique du Programme, et donc en terme de coûts et délais, compensera largement cet effort.

Paper #1
Discussor's name F. Kafyeke
Author Khoury

Q: What software do you use to extract 3D CAD data and convert it to numerical data usable for engineering analysis?

A: We do not use an off-the-shelf commercial code for this. We use software specifically developed for the purpose by contractors.

Page intentionnellement blanche

_____

This page has been deliberately left blank

The Digital Mock-up as a Virtual Working Environment within the Development Process

Steffen Kaun
European Aeronautic Defence and Space Company
Military Aircraft
81663 Munich, Germany

Steffen.Kaun@m.eads.net

0. Abstract

The need for a reduction of engineering time and cost during the last years made an optimisation of the development processes inevitable. In order to defend their market shares, all companies were forced to employ more efficient development methodologies and to bring all their software tools up to date. As a result the CAD world for new projects has essentially changed from the 2D to 3D world. However, from an early stage it became evident that 3D modelling alone was not sufficient to achieve the required benefits. It was realised that only with a sensible administration and steering of all the new 3D data can the advantages of a virtual working environment be fully utilised.
The realisation of a Digital Mock-up (DMU) requires design methodologies and processes adopted to the companies needs that will ensure that all data is up to date and of good quality.

This presentation will discuss the realisation of a virtual working environment in military aircraft development. The DMU world with CATIA, 4D-Navigator and VPM at EADS Military Aircraft in Ottobrunn, Germany is described exemplary.
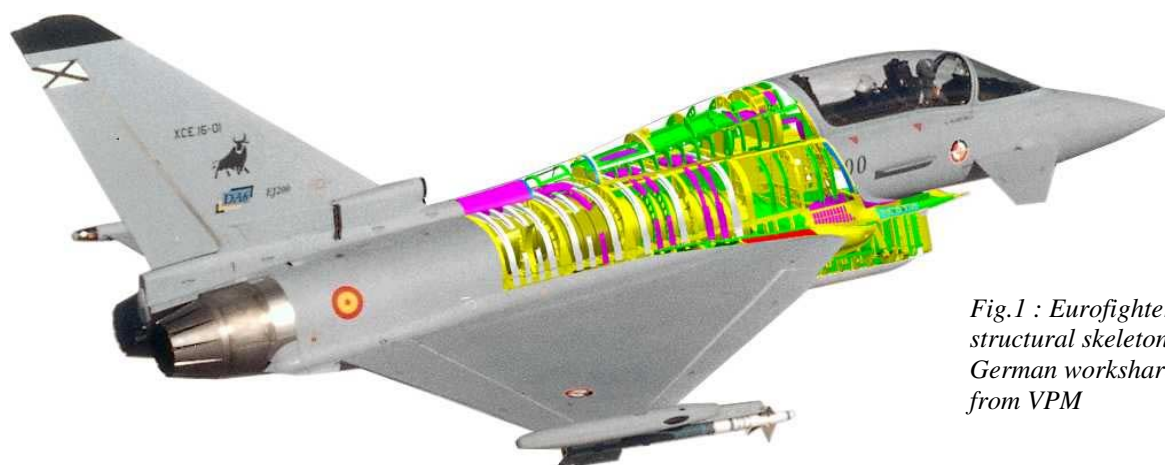
Fig.1 : Eurofighter with the structural skeleton of the German workshare loaded from VPM

1. The Design Environment in the Past

All the military aircraft projects during the last years like Tornado, Phantom, MIG29 used a drawing based design methodology in which drawing trees, bill of materials and effectivity sheets together created a configured product structure.
It was the task of the designer to prepare the required design context. By doing this he had to contact all the affected system developers (fuel, hydraulics, electrics, environment control, ...) and the personnel from the airframe design. Very often the responsible person was on a business trip, on holiday or just out for lunch. So a long time was needed just to collect the required information. And in the end the designer was not sure if he had not forgotten some important details.
Clearance checks were performed either on the drawing sheet with the help of a lot of additional views or in a hardware mock-up. Installation and deinstallation investigations also needed a hardware mock-up. But in those wooden or metal mock-ups only one variant was shown.

Also with the old tools it was possible to develop good aircraft, but the effort needed to do all the design work was labour intensive. A realistic parallel design of structure and all systems was not possible or at least combined with a lot of difficulties.

2. The Digital Mock-up (DMU)

<u>Necessity</u>

The commission to develop a new series production fighter aircraft a few years ago forced all the concerned engineering departments in Europe to deliver product data under extreme cost and time pressure.
This was not possible any more with the "old" design methodologies and tools (like 2D CAD systems) as used in the past.

A requirement existed to develop a complex product with:

- a high packing density
- whose single components can only originate in their environment
- all within a tight timeframe
- requiring concurrent development of all systems
- an increasing amount of variants (making "real-life" mock-ups unachievable)
- an ability to integrate existing processes and tools.

These points led the CAD and PDM departments to find a specific DMU solution that utilises existing design methodologies along with developing software that is adopted to the companies every single need.

At EADS Military Aircraft therefore a DMU working environment was created with CATIA V4, 4D-Navigator and a customised EnoviaVPM.

Requirements

In each international military aircraft project tools and processes have to be found or developed that are able

- To handle around 15000 parts (without standard parts) in the workshare of one participating partner company
- To handle around 50000 parts (without standard parts) in the whole aircraft
- To manage up to 200000 CAD models
- To cover the versioning process
- To navigate in the product structure
- To deal with a vast number of variants
- To provide all the analyses for an integrated design
- To integrate both original and reduced geometry
- To enable a new form of data exchange for geometry, product structure and positioning data with development partners and suppliers because the old way of exchanging microfiches is not able to cover all the necessary information.

Certainly all provided data must be reliable and up to date. Incomplete or obsolete information more often leads to non-acceptance of the new system.
Also the performance of the system must be agreeable by all users concerned. Loading of CAD data from the DMU for example should not take much longer than reading filebased models.

Definition

All requirements can only be met by a definition of the Digital Mock-up as follows:

The Digital Mock-up is a complete virtual product environment for the whole process of 3-dimensional development and maintenance of a complex product including configuration and change management.

All design work has to be done within the DMU world. The designer must fully embrace this new technology, entering the DMU environment first thing in the morning, thus carrying out all design tasks in it throughout the entire day.
All the investigations that are done in a separate environment or on a single sheet of paper disappear sooner or later and are not usable for others.
On the other hand care has to be taken that the designers do not feel intimidated or controlled by the system. They should not lose their freedom to be creative.

Prerequisites in the Design Process

The purchase of a new software on its own is definitely insufficient to form a Digital Mock-up. Some prerequisites in the design process must be fulfilled, like

- Part based methodology of working
- Modelling according to the rule "one part – one CAD model"
- The master of the geometry is the 3D model

- Definition of modelling rules, that have to be followed strictly
- High level detail modelling needed
- All the drawings (if needed at all) have to be derived from the 3D models (see fig.2).
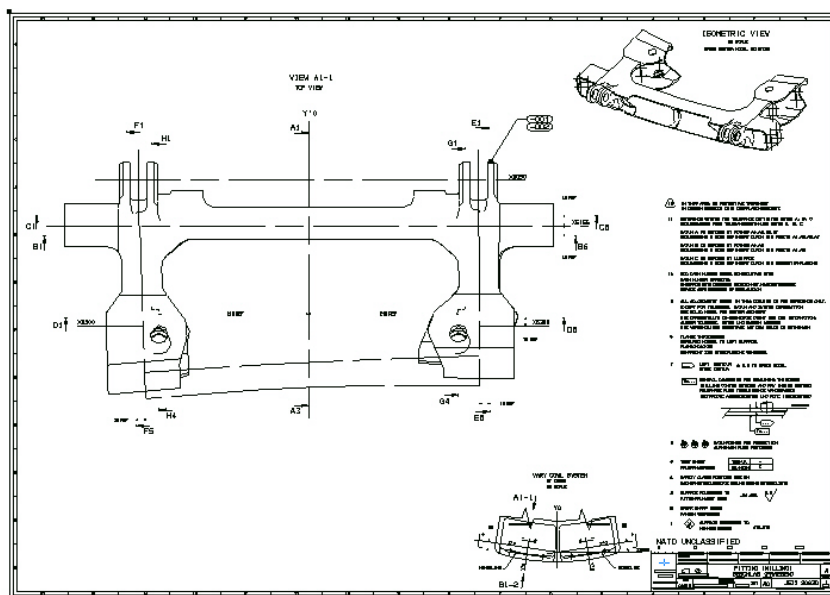
Fig.2: Master 3D model with derived drawing
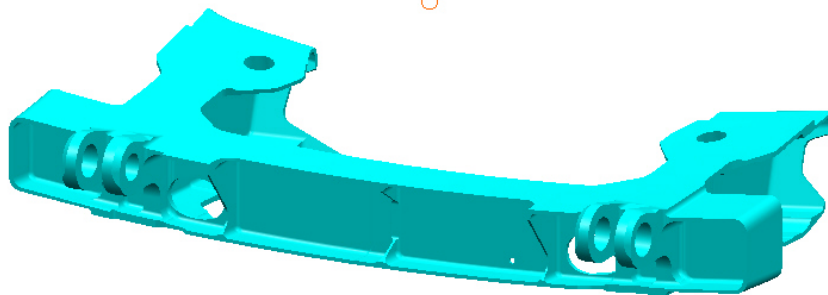
Without the fulfilment of these prerequisites it is not possible to obtain all the advantages out of the new data management systems and the new 3D CAD tools.

3. The New Design Process

The understanding of the Digital Mock-up described above leads to a DMU working process that starts with the concept and definition phase, which covers pre and detailed design as well as supporting all development departments during modification phases.

With the introduction of this new working environment the working process of all concerned departments changes basically. Part based data management is mandatory. Parallel development of all the systems and the airframe requires the readiness of every single developer to provide data to all colleagues even before completion of their task.
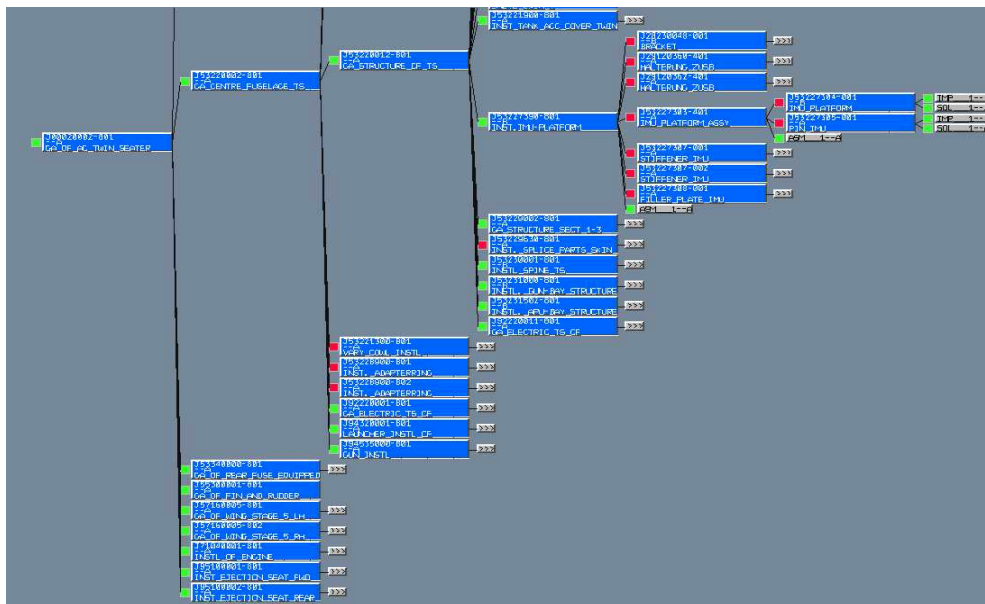
Fig. 3: Product structure in VPM

The DMU working process is implemented very early in the project phase, primarily creating a 'rough product structure'. This is followed by defining the main components and relating them to each other (see fig.3). Step by step the first 3D-CAD models are attached to the product structure, resulting in the growth of the Digital Mock-up (see fig.4).
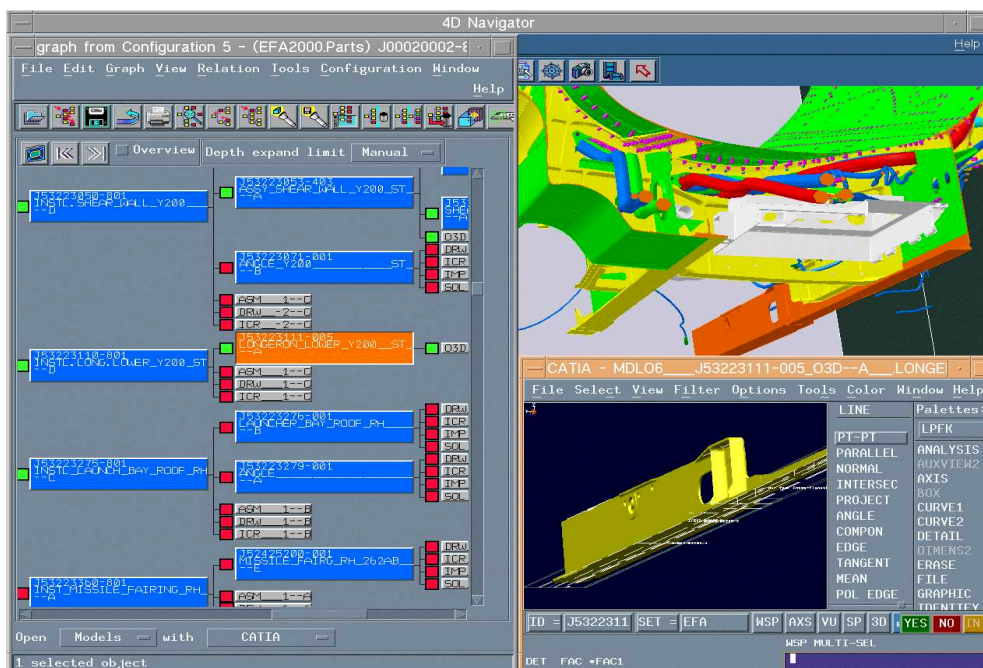
Fig. 4: Product structure linked with 3D–geometry , EnoviaVPM, 4D-Navigator, CATIA V4

The release status of parts and models must be clearly visible for all DMU users. This information is essential for all departments that work with the provided geometry to evaluate the possibility and probability of changes.

The management of aircraft variants and effectivities is also absolutely necessary (see fig.5). As every military aircraft is somehow unique a detailed view on every single aircraft must be possible. This can only be achieved with a sensible effectivity control module.

As modifications on in-service aircraft are carried out for single aircraft, national fleets or special serial numbers the designers must be able to filter the needed product structure for the selected configuration.
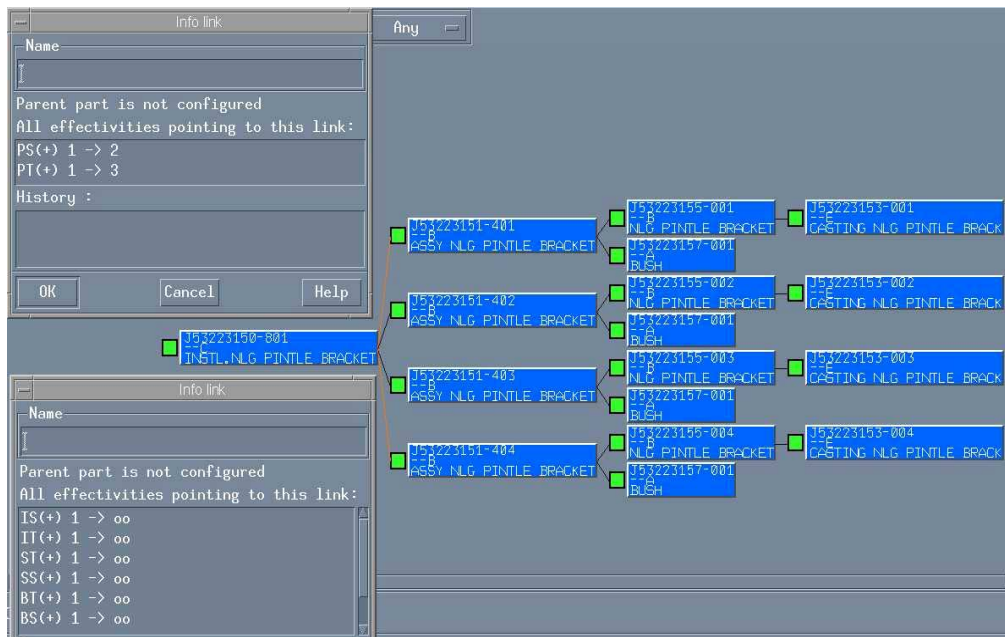
Fig. 5: Product structure links with effectivities only for selected aircraft

The daily work in a virtual environment now makes it possible to identify problem areas right from the beginning when modelling parts. Solutions can be found long before the first activities of manufacturing have begun:

Volume and neighbourhood queries enable design in context and parallel development. Time intensive manual searches for the design environment are therefore eliminated.

Let's take a designer of the hydraulic system for example. A frequent job is to create a hydraulic pipe from point A to point B. Therefore he needs to know all the surrounding geometry like fuel pipes, equipment, electrical cables, structure etc. As all those parts belong to different systems they are all shown in different branches of the product structure and on different installation drawings. Without the help of the data management system it is nearly impossible to find all the necessary geometry.

Therefore the system must enable queries that search for all parts in a selected aircraft zone and/or in the neighbourhood of a selected item.
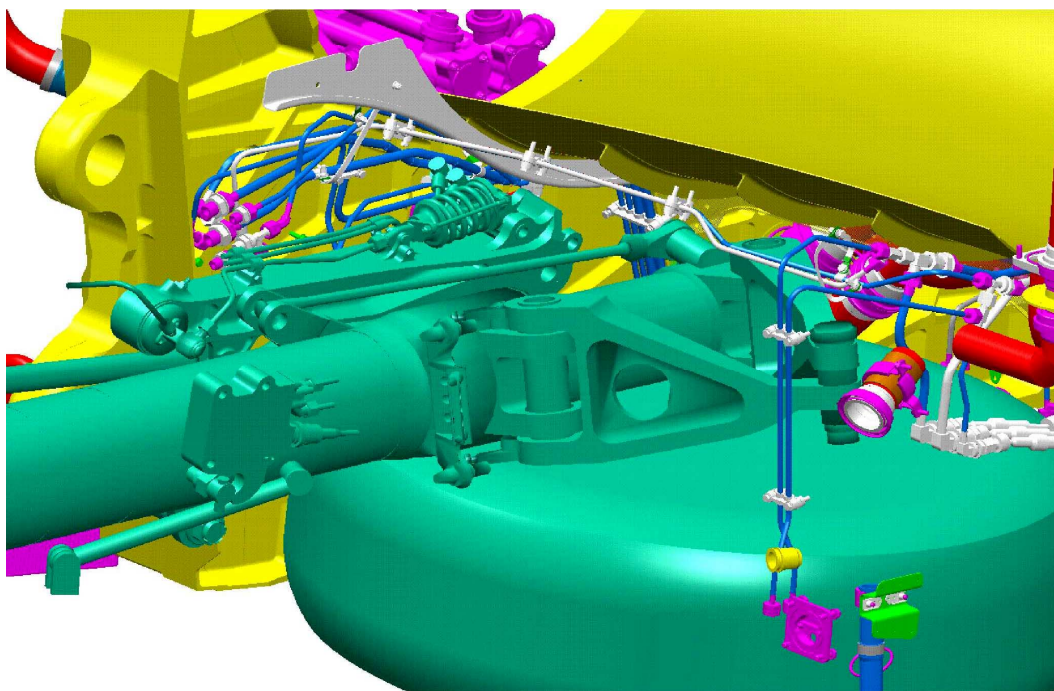
Fig. 6: Result of neighbourhood query (box defining a hydraulic pipe)

The result of this neighbourhood query can be loaded into a visualisation tool like 4D-Navigator (see fig. 6), the important parts can be selected, loaded into the 3D-CAD tool and used as passive models during design of the part "under construction".

Again with the help of the visualisation tool, collision checks between one or several selected parts and all the surrounding items can be performed.
Therefore interdisciplinary collision analysis early on in the design phase will reduce the amount of occurring problems during manufacturing and assembly. (see fig. 7)
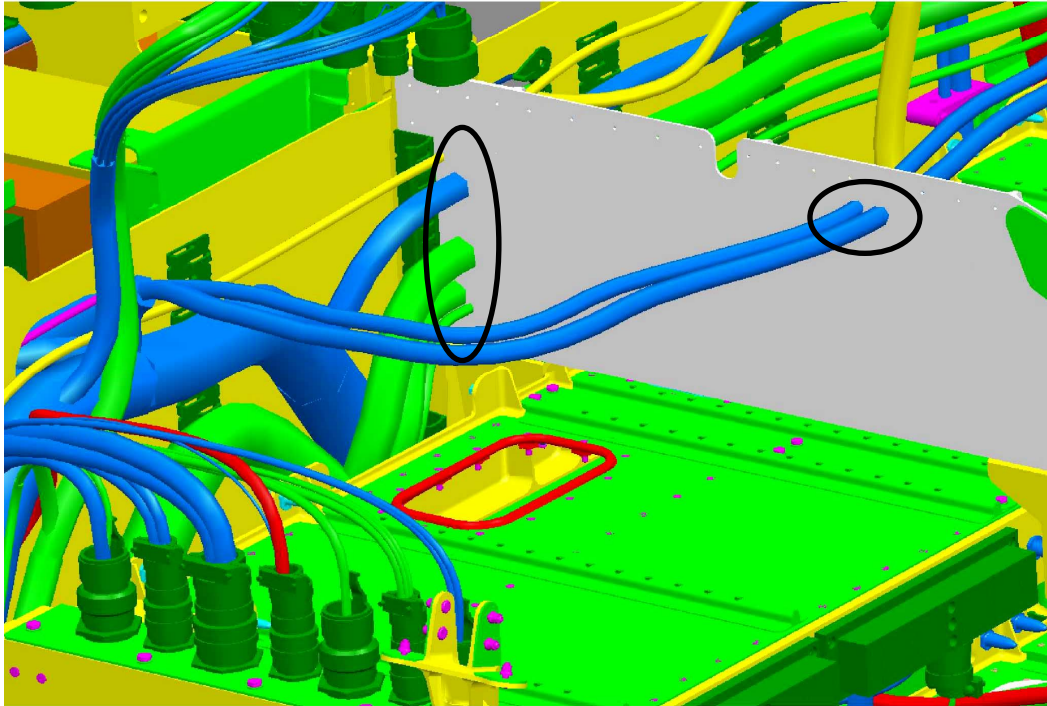
Fig. 7: Result of interdisciplinary collision analysis: Problems found in an early stage of the design phase enable a solution before the first part is manufactured

Possible installation and de-installation investigations are invaluable for future maintainability and reparability purposes.
Certainly, virtual installations are not so easy to perform as "real-life" installations on a hardware mock-up. But in the DMU environment these checks can be done on any configuration and with parts that do not yet exist as hardware. (see fig. 8)

Fig. 8: Disassembly Analysis

Design conferences aided by the virtual environment enable quick solution of problems within the development team. It is no longer required to meet all the affected departments all the time for problem solving at the aircraft assembly line. This is very helpful especially when the design departments are located far away from manufacturing. (see fig. 9)

Fig. 9: Design conference supported by the virtual environment

4. Introduction of a DMU Process

Occurring Problems during introduction

The introduction of a new working methodology, coupled with the introduction of 'State of the Art' software, like any new technology comes with a lot of inherit problems initially, such as:

⇨ Change over to a complete 3D design process initially causes additional work in the design office as much more data has to be fed into the system
⇨ The implementation of a new system for an existing project causes problems during the transition period:
  ⇨ Because the quality of the old data is insufficient
  ⇨ Existing processes have to be changed without delaying the project
  ⇨ A tight timeframe for the current project leads to a minimum acceptance of failure on the side of the user
⇨ Personnel will require extensive training in order to fully utilise the new system, some more than others!
⇨ Insufficient software maturity and documentation make the required modifications in the new systems even more complicated
⇨ There are only a few software specialists available on the market

The Implementation at EADS Military Aircraft

EADS Military Aircraft, faced with the problems described above, searched for the optimum solution. A direct result of this was the foundation of a small team to act as a service provider for the project as a whole, at the beginning. This team consisted of well accepted colleagues from various departments, who were responsible for introducing the new process in small steps. Lessons have been learned from the past that with a process covering multiple interfaces confusion is caused by its introduction in one step, therefore new functionalities were only invented after all existing features had been accepted by the users. Step by step the team was supported by "superusers" from all departments concerned.

The availability of continuous system support during the initial phase and the attempt to clarify the concepts with various demonstrations, ultimately led to a widespread overall acceptance of the new system and the new working processes by the users.

The Benefits

The benefits achieved by the introduction of a data management tool in context with a 3D-CAD system and a visualisation software can be realised in different areas of the process chain:

Reduction of iteration loops by a better first design

Increase of product quality, as the system promotes a 'Get it Right First Time' philosophy, thus avoiding unnecessary changes or repairs before delivery

Improvement of the product by greater consideration given to aspects of maintainability and reparability

Faster Design due to much more efficient search mechanisms

Avoidance of mechanical mock-ups

Omission of extensive support for departments outside the design office (e.g. product support, assembly).

Potential for distributed development in an international partnership

Open Problems

Unfortunately no available PDM system on the market is able to meet all the requirements of paragraph 2. Some tools have their strength in the management of different kinds of product structures, some in the handling of geometry, others in configuration control. Even with extensive customising it is not possible to satisfy all the company's needs with one software. This leads very often to a coexistence of several systems with the distinct disadvantage of data duplication.

Another topic under discussion is the exchange of data with partners or suppliers. Most PDM systems offer STEP interfaces that are theoretically able to transfer all the necessary information from one PDM system to another. Some attempts were already successful. But in general those STEP processors need a lot of customising. Especially in the data exchange between two big companies with a lot of different tools, data structures and data items it is hard to find a common basis. Other difficulties appear in the data exchange with suppliers that have no data management system at all. A preferable online data access seems also to be complicated as CAD data due to it's large size, needs a lot of time to be transferred. Also security problems delay the realisation of data sharing.

5. Summary

Summing up it can be said that in future the Digital Mock-up will be the backbone of all activities in the development process of all complex products.

However the purchase of new software on its own is not sufficient to change the working process. An over all cultural change throughout the organisation is needed to support the technology and new processes. This coupled with detailed know-how of all tools available (including existing processes) will assure the overall success of the implementation. Only with this background can a virtual working environment be created and the enormous possibilities that are on offer by the new tools be fully exploited.

Paper #2
Discussor's name Bochenek
Author Kaun

Q: You mentioned that one of the major issues preventing full use of digital design is the "security" need and requirements. How is EADS handling this?

A: Security is a big issue and currently not resolved
Looking at encryption devices and direct network connection with partners

Discussor's name F. Kafyeke
Author Kaun

Q: What is the CAD software you use for the digital mockup?

A: CATIA v4

Simulation of Aircraft Deployment Support

Laurent Bazin de Jessey, Gilles Debache
Dassault Aviation
Military Customer Support Division
78, Quai Marcel Dassault
Cedex 300 92552 St Cloud Cedex
France

Tel.: 33 1 47 11 63 23
Fax.: 33 1 47 11 54 74
Email: laurent.de-jessey@dassault-aviation.fr

Abstract

Dassault Aviation uses different software tools as decision-support system for several goals in the logistics support simulation area. A great number of such tools are based on complex mathematical methods that nevertheless required simplification assumptions for the simulated model. They are often irrelevant for logistics network with very erratic behaviors (small fleets for example) where the "steady state" approach is not usable. During the last years software providers have disseminated cheap tools based on Monte Carlo approach which allow to perform, in a very short time, a great number of types of simulation related to Operations Research. "Simulation of Aircraft Deployment Support" (SADS) was developed by the Military Customer Support Division of Dassault Aviation to perform simulations for logistics deployment and support analysis of aircraft sustainment. The SADS tool includes animated visualizations, and is based on the common used ARENA$^{©}$ software (Systems Modeling Corporation) dedicated to modelling and simulation.

1.   A new approach for Simulation of Aircraft fleets support

1.1   The background

The "full support" approach which is more and more common in the sustainment of military aircraft area, requires a very accurate attention about the commitments to level of services (like availability of fleets or mission success rate).

Regarding these constraints, different types of simulation (like cost or support and warehouse networks) are very useful for the following tasks, to make cost effective and relevant proposals for future contracts :

- Integrated Logistics Support approach for design of the aircraft and support concept (warehouses network and relevant logistics facilities associated with reliability and maintainability studies).
- Dissemination of the Initial Provisioning Lists for the calculation of the initial logistics resources.
- Supply and support Chain Management for the management of the logistics resources (replenishment of consumables and repair of parts, inventory management) facing a moving context (like new operational needs or raise of the maintenance costs of geriatric aircraft).

1.2   Features of some existing support modelling tools for behaviour simulation

A great number of "in house" software tools dedicated to these needs were disseminated this last decade. They use analytical algorithms based essentially on classical mathematics tools like the "Poisson law" methods for the calculation of level of stocks (theory of replenishment with constant failure rate) and the "Markov Chain" methods when some parameters, as the lead times or times to repair for example, aren't constant.

Based on average values and on simplification assumptions, their main advantage is their capacity to solve the equations describing the model and so to find automatically optimized solutions for several given criteria (like ownership cost or commitment to a given level of service).

For instance, the Initial Provisioning List process for large fleets can often take advantage of thorough but rapid calculations done by such tools. They are based on simplifications and average values of parameters without prohibitive impact regarding the required accuracy of the results.

1.3   The limits of analytical tools as help decision systems

But after Initial Provisioning, for the Supply and Support Chain Management (SCM) during the life of the fleets, the strategic forecasts and fleets average parameters are, most often, extremely poor predictors of operational tempo and of the repair/replenishment demand, particularly at the aircraft level (organizational or intermediate level). Additionally, the users and the manufacturers highlight the lack of systematic feedback about the existing fleets support. Often, very few historical data are available about operational readiness, cost of ownership, efficiency of the repair chain, adequacy of quantities of spares parts or health monitoring of reparable items.

So, the classic analytical methods, based on average values and standard deviations of common probabilistic functions, aren't always relevant for this kind of need. And the current modelling tools based on resolution of probabilistic equations aren't efficient for unsteady scenario and process. Indeed, these mathematical models impose prohibitive simplifications in order to be solvable. And there are numerous examples where these assumptions have severe impacts on the level of confidence of the results, like small fleets (less than 10 aircraft), logistics footprint for deployment, erratic operational mission schedules and sudden change of the required availability. Consequently it is very hard, with the existing tools mentioned above, to perform short-term evaluations of the responsiveness of the support system in a very erratic context.

Regarding the maintenance cost of these tools, an other fact must be underlined : when the user needs to implement some changes in the input characteristics of the logistics network, the complexity of these algorithms requires too often unaffordable evolutions. Indeed, they can be performed virtually only by the rare specialists who own the knowledge about this proprietary tools.

1.4   A new generation of simulation tools based on random replications

Nowadays, a new generation of standard software for simulations and animated visualizations are proposed for process with deterministic or random behaviours.

These software are based on Monte Carlo replication method. They offer ergonomic and graphical interfaces which allow to model rapidly, in a realistic way, very complex systems with reusable templates. Consequently, they are easy to use by non-dedicated persons reluctant to complex algorithms implementations. These efforts are very gratifying because you can run immediately animated simulations which show, in an interactive way, the behaviour of the described system whatever the level of its complexity (logistics network facilities, number of random input parameters). In spite of their inability to perform automatic optimizations ("What if ?" approach), they can be considered nevertheless as the "best of breed" to demonstrate the capabilities of complex and random workflow organizations.

These software are often used by manufacturers to model human resources in production facilities or materials needs in workshop.
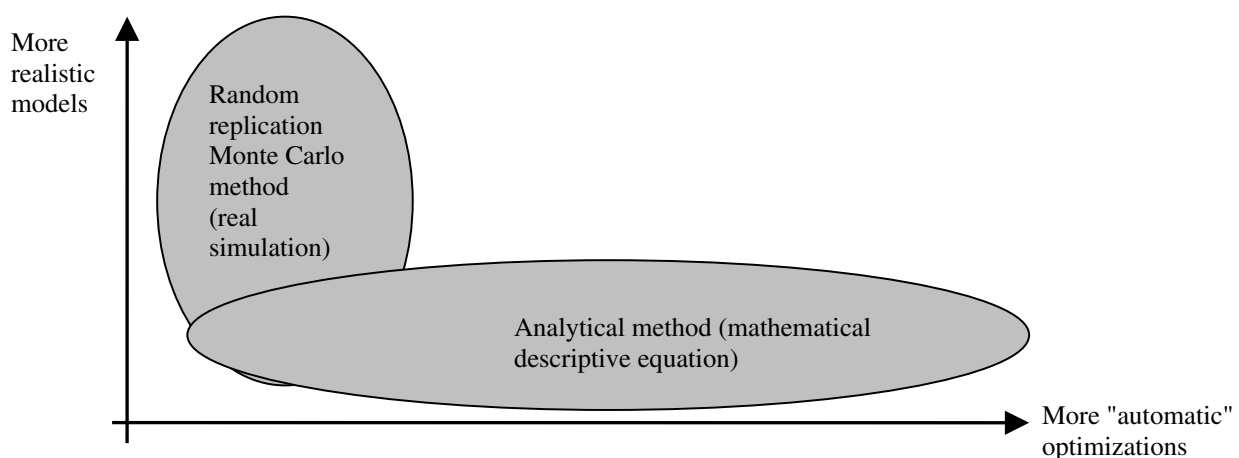
Dassault Aviation uses such software tools, based on random simulation, by different ways in response to its specific requirements for logistics and support activities. As mentioned above, the aim is to fulfil numerous needs where the "steady state" approach is not necessarily relevant. One of these tools, named "Simulation of Aircraft Deployment Support", is specifically dedicated to model aircraft deployment support.

2. What is SADS ?

2.1 Main features

SADS (Simulation of Aircraft Deployment Support) is a software developed "in house" by the Military Customer Support Division of Dassault Aviation. It is based on ARENA$^{©}$ software tool for animated simulations (based on Monte Carlo method and visualizations of deterministic or random process). It is operated on a common PC.

2.2 Goals

SADS is dedicated to operational help-decision for deployment of aircraft (fleet size, logistics footprint, supply chain network) with model of the random behaviour of aircraft subsystems and of logistics networks and maintenance organizations (with their human resources).

SADS is particularly relevant to complex logistics and maintenance models where hazard is very present and where erratic behaviours are relatively unpredictable. It is particularly relevant to studies for full "contractor assisted support" proposals. So, SADS can be used for a large number of matters like the following : level of repair analysis (to influence aircraft system design), calculations for support system design (initial provisioning), business model evaluation (life cycle cost), determination of the best ways for risk mitigation (lead time coverage, safety level for a given no stock-out probability), comparisons of the supportability of different types of aircraft, evaluation of the availability of aircraft depending on deployed logistics footprint during isolated deployments, measurement of the performances of different supply and repair chain organizations regarding expected service level (missions success rate).

2.3 Limitations and best uses

The simulation with SADS isn't relevant to optimize automatically a support system (the best solutions must be found manually), or to calculate directly optimum solutions (example : to calculate the more cost effective level of repair and support network in accordance to a given operational requirement). But SADS is relevant to size accurately a given logistics support network which was initially roughly calculated by analytic methods, and to make comprehensive and very realistic validations. This approach is detailed in the following figure.
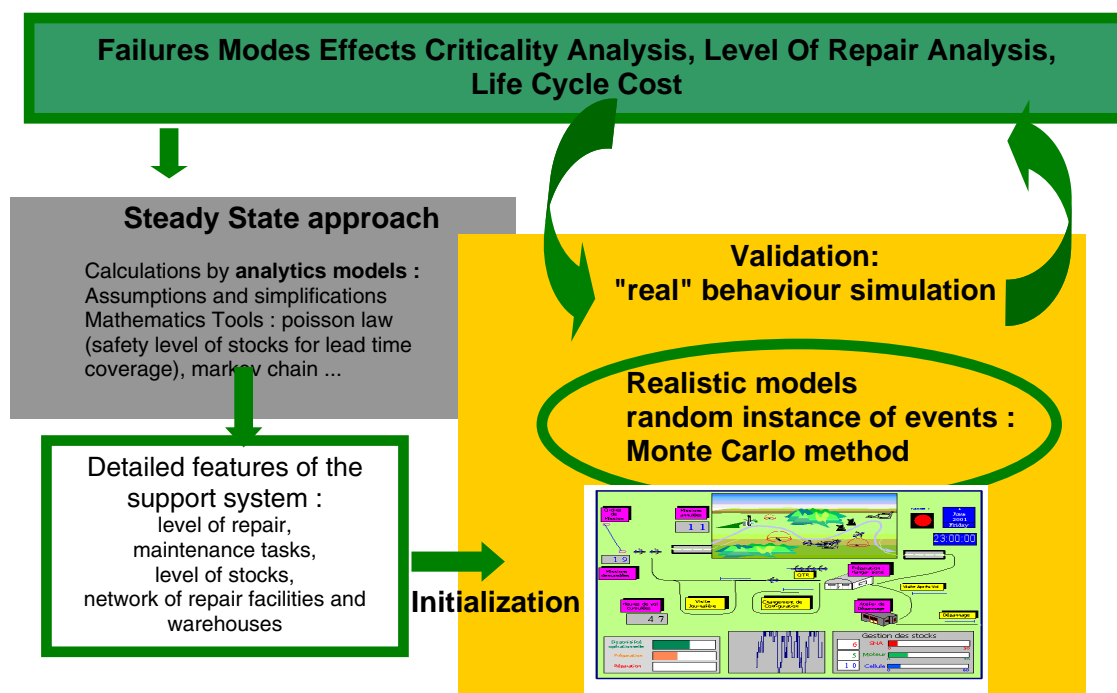
3.   Detailed presentation

3.1   Main parameters
The main input parameters of the model are the following :

- Size of the fleet (the number of initial available aircraft can be defined).

- Description of the operational context : mission schedule, patrol size, duration of flights.

- Type of aircraft (different types of aircraft can be defined) : breakdown of the aircraft (description of aircraft elements or subsystems by LRUs (Line Replaceable Unit) characterized by MTBF, parameters for flight servicing and visits (human resources and time required).

- Maintenance tasks to replace failed LRUs (time to restore).

- Maintenance capacities (human resources) : preparation, flight servicing, visit and maintenance of aircraft (visit before flight, visit after flight, daily visit, change of configuration, OTR (operational turn around) air-air or air-ground at the organizational level), repair of LRUs at intermediate level by exchange of Shop Replaceable Assemblies.

- Logistics network and available resources (intermediate level warehouse, maintenance depot level activities) : repairability of LRUs, consummations of SRAs (Shop Replaceable Assemblies), replenishment of spare parts (flow and throughput times of spares replenishment from the depot level to the aircraft).

3.2   Global view of the model
A graphical view of the model is provided in the following figures.

ORGANIZATIONAL LEVEL :
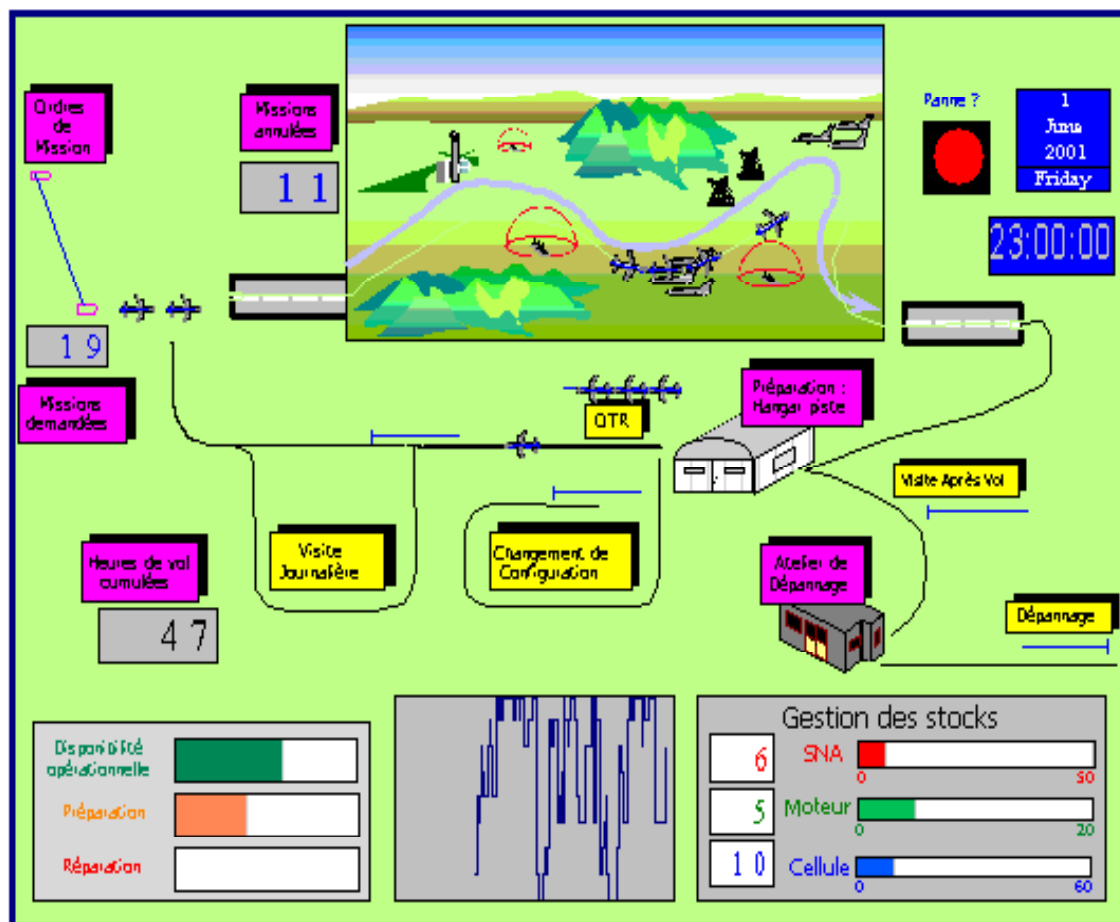
INTERMEDIATE AND DEPOT LEVEL :
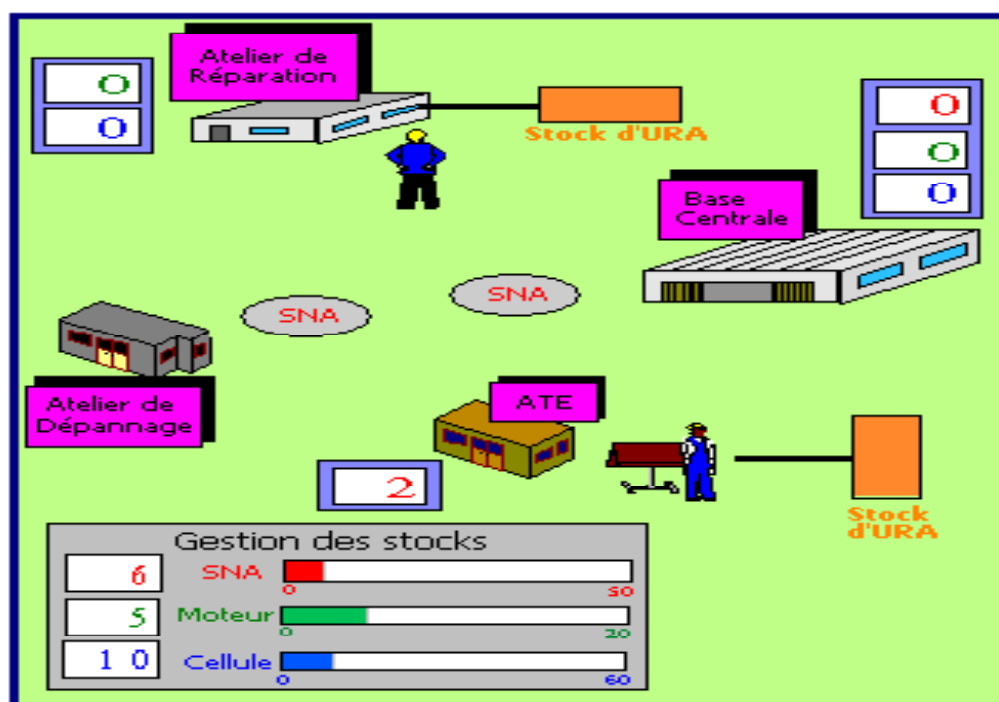
3.3   Used scenario and detailed parameters

Note that every value of the following parameters can be easily changed, depending on the needs of the users.

- Aircraft description :

For the aircraft, three subsystems (considered as LRUs) are defined for this simplified use of SADS aimed at showing the different operational behaviours (engine, WDNS[1], aircraft systems).

- For each LRU the following elements are described :

Maintainability : Time to restore (lognormal distribution law with shape parameters "Mu" and "Sigma" based on extractions of Logistics Support Analysis Record), with a complementary parameter "exchange time" for the engine only.
Number of required mechanists for the maintenance tasks.
Reliability (Time between failures : exponential distribution with shape parameter "lambda" as the constant rate of failure).

---

[1] weapons delivery and navigation systems.

- Example of input Data for each aircraft :

Cumulative distribution of "Time to Restore" (time in minutes) :

Cumulative distribution of Time to Repair
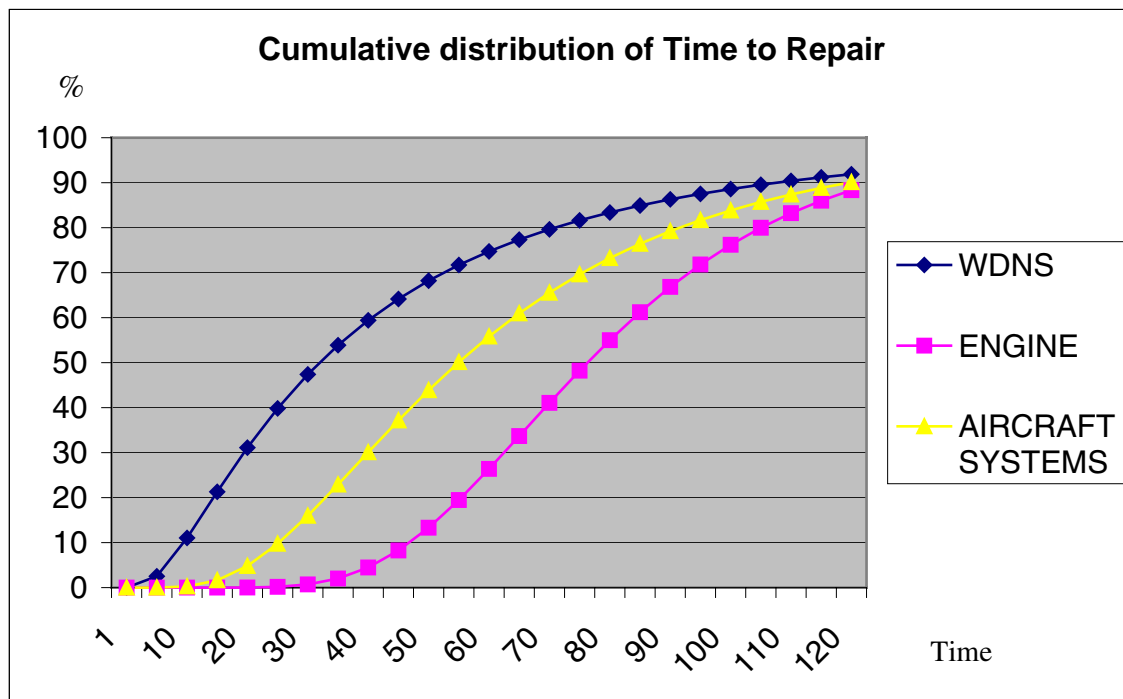
MTBF (flight hours) :

WDNS   9
Engine   50
Aircraft Systems   11

Human resources :

	Duration (minutes)	Number
Visit before flight	15	2
Daily visit	45	2
Visit after flight	15	1
Air-air Turnaround	23	6
Air-ground Turnaround	45	6
Change of configuration	45	3
Engine exchange time	45	4
LRU exchange		3

- Operational needs :
Every day, missions are generated responding to a defined schedule (15 missions per day, one mission every 1.5 hours). Each mission is characterized by the required number of aircraft (random distribution between 2 and 4) and its duration (2 hours).
If the number of available aircraft is insufficient, the mission is canceled ; the number of canceled missions is recorded.

- At the organizational level :
The preparation tasks of aircraft are characterized by the type of visit and flight servicing on aircraft (visit before flight, visit after flight, daily visit, change of configuration, operational turnaround); the need of OTR

and change of configuration is determined randomly (with a fixed average rate) for every aircraft after every flight.

For maintenance works, the failures of LRUs during flight are randomly generated depending on the probabilistic law of failure of each type of LRU. Note that for the flight hours count, in case of failure of one LRU, the time duration of flight is the time preceeding the failure. For the required human resources (mechanists), time and human resources are required depending, for each task, on the type of LRU as mentioned for the aircraft parameters. Note that, for the engine, if the time to change the engine is smaller than the time to restore randomly determined, the time to repair the aircraft is the time to change the engine. The number of mechanists who are available for all this tasks, can be defined as an input parameter.

- At the intermediate level

The activity of aircraft generates needs for "ready for issue" LRUs, so the intermediate level activities are modelled with several representative parameters. The number of spare parts available in warehouse for aircraft is tracked, the warehouse is replenished by the repair workshop. For the maintenance tasks dedicated to the repair of parts and the replenishment of warehouses, a repairability rate is defined for each LRU; so a certain quantity of LRUs isn't repaired at the intermediate level and is directly sent to the depot level. The time to repair at the intermediate level is determined randomly with the probabilistic laws depending on each type of LRU. Two workshops with limited human resources and waiting queue are defined, "Automatic Test Equipment" for WDNS, and Repair workshop for engine or aircraft systems. Elimination rate is not yet incorporated in the model.

Workshop	LRU	repairability rate	Time to repair (random triangular law, shape parameters in hours)	human resources required for repair of one URL
ATE	WDNS	80%	18, 24, 30	2 mechanists during 4,8 hours
Repair	Engine	20%	18, 24, 30	4 mechanists during 20 hours
Repair	Aircraft systems	20%	18, 24, 30	4 mechanists during 8 hours

- At the depot level :

The activities of depot are described by transportation times, repair times and replenishment of intermediate level warehouses. The global Turn Around Time is determined by a random triangular law with the following shape parameters : 144, 168, 192 (in hours).

3.4 Demonstration : output parameters and metrics of the behaviour of the system

The metrics used to evaluate the behaviour of the system (efficiency, proportion of busy technicians, level of service, operational efficiency…) can be freely implemented in an large number of different ways. Indeed, every entity of the model can be measured, and the relevant data can be captured and recorded during each simulation. All sorts of charts and figures can be produced easily, with standard interfaces, to calculate and show all sorts of synthetic parameters.

But the first way to verify the behaviour or the efficiency of the system is to look directly at the simulation ; this is particularly relevant for very erratic contexts.

As an example see the impact on availability of insufficient number of spares in stocks :
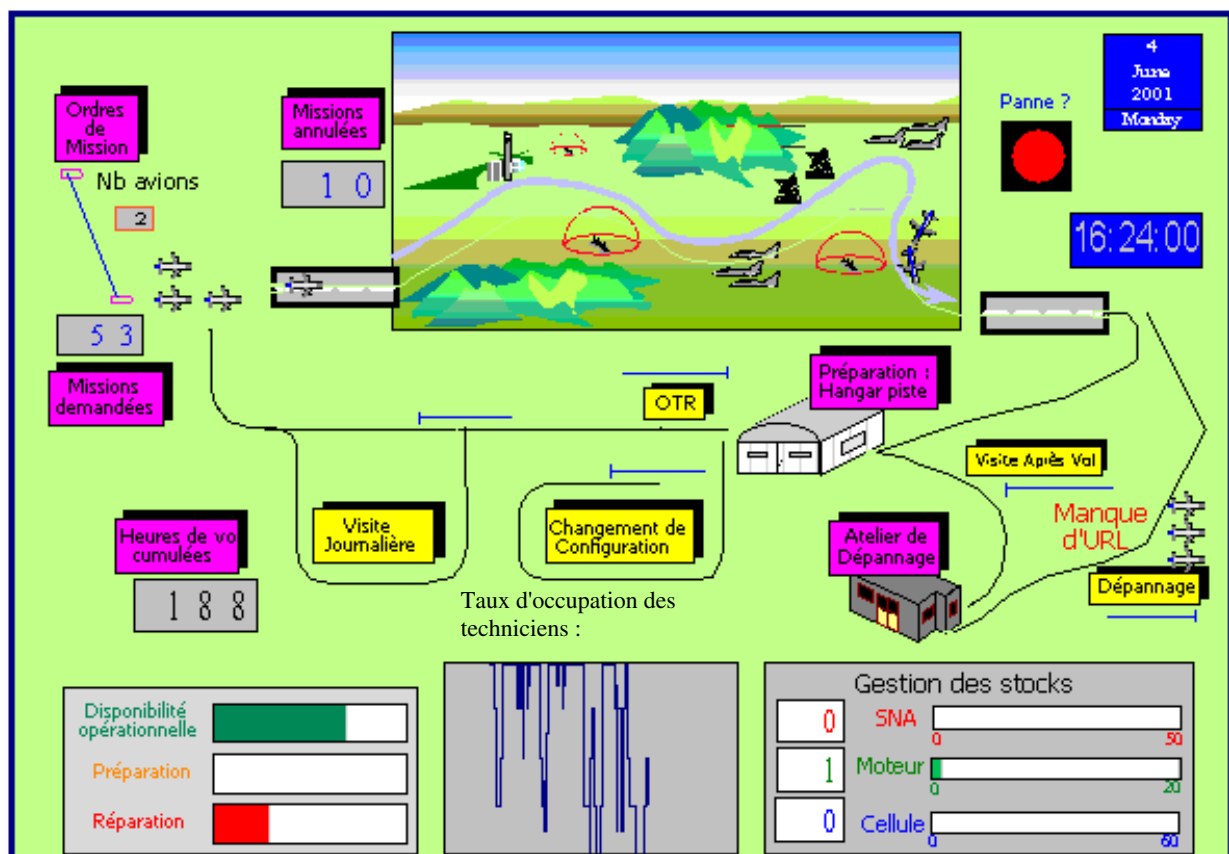
Depending on the chosen output parameters, several instances of use can be performed as the evaluation of a given sustainment network (obtained level of service), the evaluation of the required size of a fleet for a determined mission schedule regarding logistics means or to tighten the space of multi dimensional feasible region (size of fleet, human resources, stocks) for a given rate of missions success. An other way of using SADS is to compare different types of aircraft, regarding the availability of their LRUs and their Time to Repair for a given logistics capability.

To illustrate the features mentioned above, the following scenario is provided about the optimization of logistics resources for a given operational need. The objective is to minimize level of stocks without impact on the rate of non aborted mission. To meet this requirement several simulations are run (the assumptions for each parameters are those which were mentioned above)

- First Simulation :

	Initial number of LRU
WDNS	25
Engine	15
Aircraft Systems	30

The results are :

	Number of used LRU
WDNS	107
Engine	34
Aircraft Systems	96

Rate of non aborted mission   : 81,76 %
Cumulative total of hours of flight   :1862,30
Average number of available aircraft :6,50 sur 10

Evolution of quantities of spares parts in warehouse
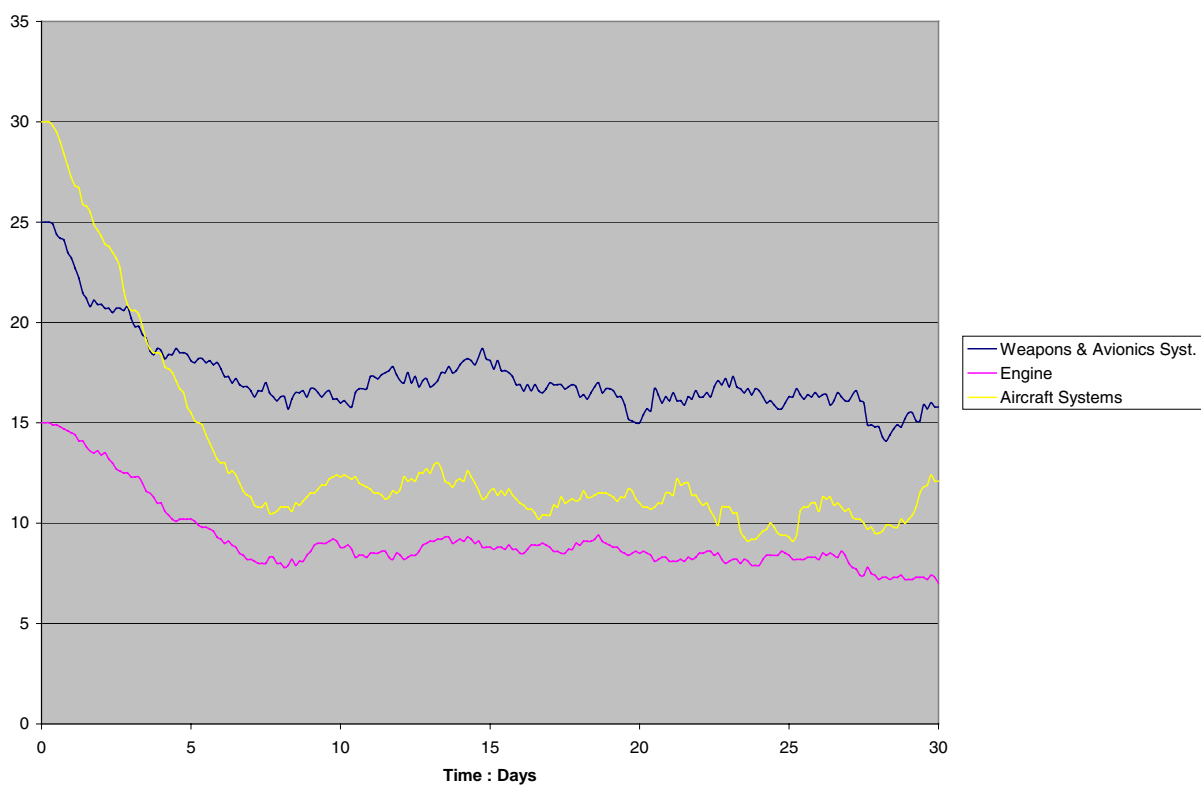
- Second simulation :

	Initial number of LRU
WDNS	15
Engine	15
Aircraft Systems	25

The results are :

	Number of used LRU
WDNS	106
Engine	33
Aircraft Systems	101

Rate of non aborted mission : 80,69 %
Cumulative total of hours of flight : 1822,00
Average number of available aircraft : 6,50 sur 10

Evolution of quantities of spares parts in warehouse
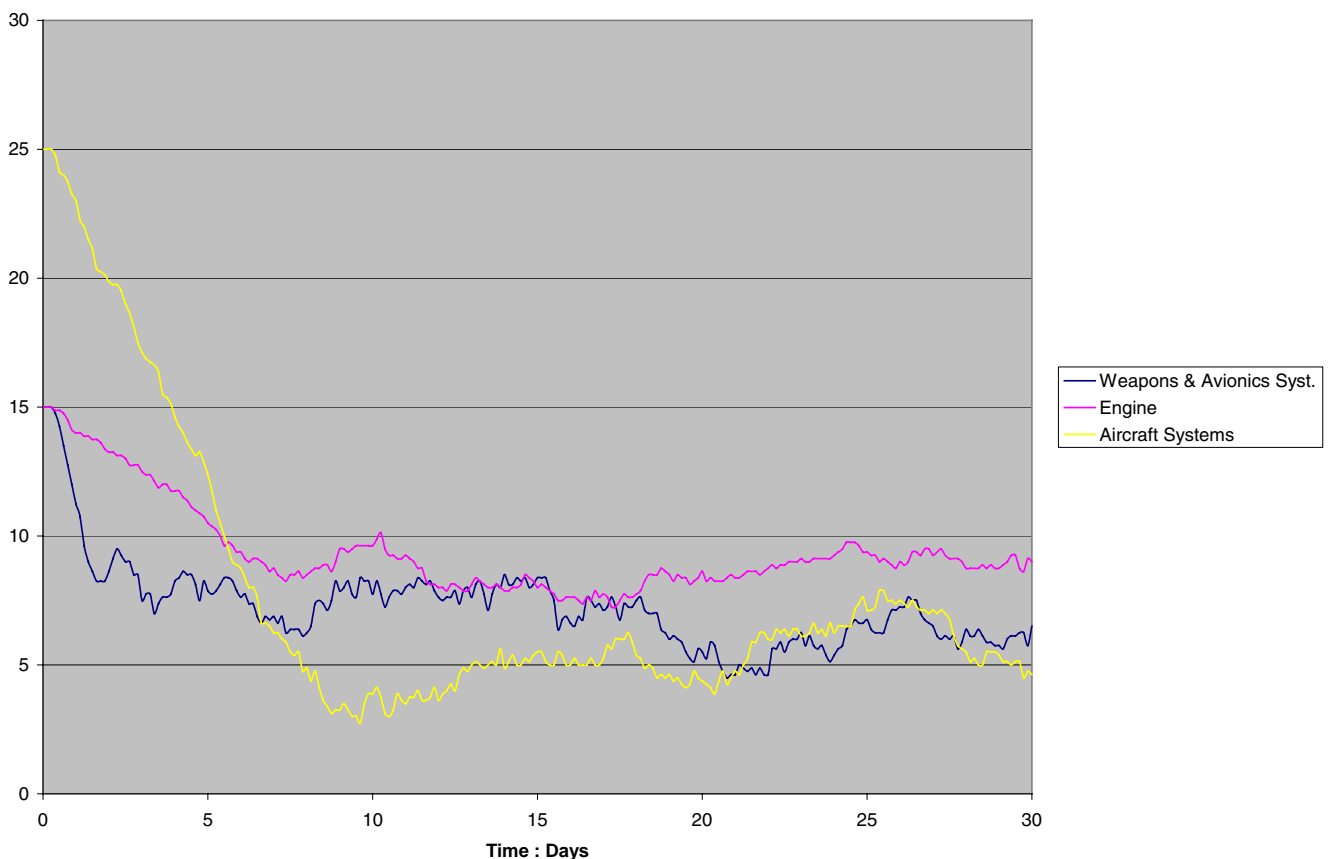
So we have demonstrated that a significant reduction of initial quantities of spares parts has no real impact on the availability of aircraft and missions success rate.

3.5 Convergence criteria and validation of the models

The first step in order to validate the model is to determine convergence criteria. Indeed, the results obtained by Monte Carlo simulations must be associated with the required confidence level. The confidence interval must be measured with representative metrics (one or several discriminating output parameters). The confidence interval of the results for an output parameter is linked with the number of random input parameters, the probabilistic distribution of each input parameter and the number of replications which were

run for the simulation. The required confidence interval must be compliant with the number of replications which can be performed in accordance with the available hardware capacities (time of computation). For example, with 6 Random input parameters for this model (3 probabilistic laws "Times To Repair" and 3 probabilistic laws "Time Between Failures") we have chosen the number of non aborted missions (15 missions are generated every days) and the number of failures per WDNS URL as output parameters ; simulated duration for each replication is 3 days. So, the following confidence intervals[2] (half width at 95 %) were obtained :

10 replications :	**Half width**	Average	Maximum	Minimum
Number of canceled missions	**1.25**	2.80	7.00	1.00
Number of WDNS failures	**2.15**	10.20	15.00	7.00

50 replications	**Half width**	Average	Maximum	Minimum
Number of canceled missions	**0.49**	3.32	8.00	0.00
Number of WDNS failures	**0.99**	11.2400	22.0000	5.0000

100 replications	**Half width**	Average	Maximum	Minimum
Number of canceled missions	**0.28**	3.34	8.00	0.00
Number of WDNS failures	**0.63**	11.45	22.00	5.00

With these examples we verify how the confidence interval narrows when the number of replications increases.

Then, the validation of the model can be ended by the following methods :
- compare the reactivity of the SADS simulation system responding to the change of the values of discriminating input parameters,
- compare the results with other tools (like analytical algorithms).

3.6   Main advantages in comparison with other types of legacy systems

As mentioned above, the main advantages of such common-used information technology (ARENA$^{©}$ and Monte Carlo Simulation Method) are the possibility to build by an interactive and graphical way complex models of logistics and maintenance networks. So you can show the realistic behaviour (with all required details) of the system through animations (function of the time) with the ability to perform accurate real life age tracking of the described system (the convergence criteria are easy to determine).

Additionally, in spite of this ease of use, you have the free choice of probabilistic distribution functions (for instance whatever their complexity and their features) relevant to the real behaviour of the operational systems without simplification constraints.

Note that the ownership costs (license for ARENA$^{©}$) are compensated by the "light" maintenance (open source, no proprietary contract) of the model.

4.   Conclusion

As said above the model is always scalable, so the following enhancements are scheduled to propose a more comprehensive model : detailed age track parameters of aircraft activities (number of landing,…) for scheduled maintenance on LRUs, different or random features of missions regarding the tracking of aging parameters, multiple LRUs, simulation of forecasting tools and adaptation of the reactivity of the supply or repair chain (show the added value of pro active support chain).

It is important to note that each user, with a minimum knowledge of the ARENA$^{©}$ tool, is able to complement the model so as to make it relevant to his particular needs. Generally, the goal is to enhance the realism of input parameters (more realistic probabilistic distribution law, deterministic parameters change by random data) regarding the modeled context, to complete the core model (functional workflow and logistics network), and, finally, to add output metrics. But currently, SADS is well suited to accurate comparisons between different types of aircraft programs, particularly for isolated deployments.

---

[2] This value is interpreted by saying "in 95% of repeated trials, the sample mean would be reported as within the interval sample mean ± half width".

Additionally, the Military Customer Support Division may extend the use of SADS. The objective is to demonstrate and calculate the added value of an adaptable logistics loop (priority, Turn Around Time) which should be able to adapt his reactivity and his responsiveness in front of, for example, sudden changes of the customers operational needs or increase of unscheduled maintenance tasks. The aim is to give help decision data to build a collaborative logistics approach between Dassault Aviation and his customers so as to bridge the void between planning and execution.

As a final conclusion we could underline that, in comparison with the classical approach based on analytical algorithms which are useful for a large number of needs (see PRICE HL$^{©}$ or CESAR$^{©}$ [3] for initial conception's stages or long-term ownership's cost optimisation), the approach based on Monte Carlo random trials is relevant to short term "dynamic behavior" only but it does it very well. So, software as SADS, could be used in a very efficient way for the Air Forces or Naval Air Forces as help decision tool.

---

[3] Software tool of the "Direction Générale de l'Armement" (French Ministery of Defense) used at Dassault Aviation.

Using Modeling and Simulation to Graphically Display the Interaction of the Fire and the Extinguishing Agent

Robert G. Washburn
US Army TACOM
AMSTA-TR-D/233
Warren, MI 48397-5000, USA

and

Dr. Neal E. Blackwell
US Army CECOM RD&E Center
10125 Gratriot Rd., Suite 100
AMSEL-RD-C2-AP-EE-E
Fort Belvoir, VA 22060-5816, USA

The U.S. Army Tank Automotive Research, Development, and Engineering Center (TARDEC) uses state-of-the-art modeling and simulation techniques as an integral part of its Simulation and Modeling for Acquisition, Requirement, and Training (SMART) effort. This paper will address how we applied these powerful tools to accurately depict how Halon-alternative agents react in a military vehicle.

Armored vehicle technology has an order of precedence that must be taken into account in today's vehicle designs, they are to not be: detected, acquired, hit, penetrated, or most importantly, killed. If munitions do make it to penetration, then, in order to protect soldiers from fires inside vehicle compartments, an extinguishing system must be used. Today's modern armored vehicles are equipped with high-speed fire sensors that can, within milliseconds, trigger the valves on the pressurized fire suppression bottles to quickly extinguish a potentially deadly fire.

The most popular and effective suppression gas has been Halon 1301. However, research has shown that Halon 1301 is an Ozone Depleting Chemical (ODC). In a search for environmentally friendly Halon-alternatives many variables must be manipulated such as bottle pressure, nozzle placement, nozzle design, distribution manifolds, shape of interior space, and exposure time to toxic gases in order to make the replacement agent as effective and safe as Halon 1301.

An armored vehicle that is penetrated has very little time to keep the fire from expanding. The fire needs to be suppressed as soon as possible. An adequate time to suppress the fire is approximately 0.2 seconds, which can be accomplished if nozzles are placed optimally. This short time is necessary to maintain safe concentrations of gaseous agent and toxic gases. It is the job of today's modeling and simulation software to help the system designer efficiently place the fire suppressant agent nozzles.

It was determined that an innovative approach needed to be taken in order to investigate this problem. As such, subject matter experts from the Communication Electronics Command (CECOM) and TARDEC were formed. TARDEC brought to the table its extensive program experience in developing and using Halon alternatives. Programs that accumulated a great deal of

test data and experience in the performance, characteristics, and behavior of various agents, as well as toxicology concerns. CECOM's expertise is in fire suppression modeling. The team determined that the approach they would use to investigate this problem would be to leverage TARDEC's earlier work, and use the numerical techniques used in the model to spin-off of the electronics cooling modeling that CECOM was conducting. The team felt that the use of today's state-of-the-art visualization tools would facilitate understanding and solving the problem. It was determined that the CAVE Automated Virtual Environment (CAVE) hardware and software was best suited to make this happen effectively and efficiently. The team decided to perform four different configurations of nozzle placement, and then a 3D visualization result of the Halon Alternative agents would be experienced in the CAVE's virtual environment. It was determined that FM-200 would be the extinguishing agent with which these experiments would be conducted[1].
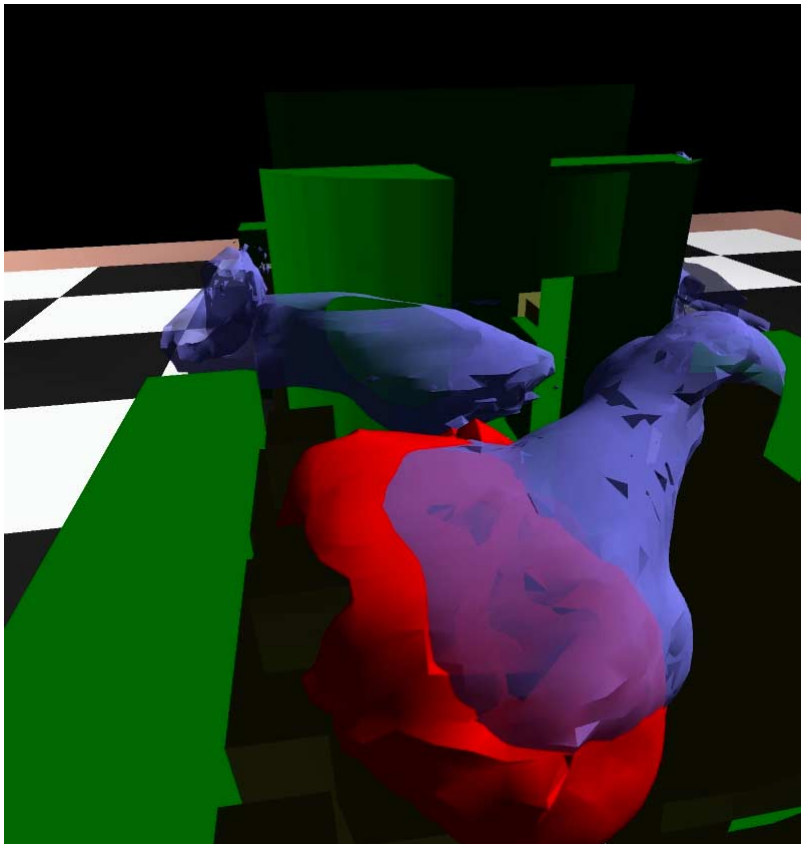
Figure 1: Interaction of Flame with Extinguishing Agent

The original output was generated using the TASCFLOW computational fluid dynamics code licensed by AEA Technology. It is a structured, multi-block code that was initially tailored to predict combustion in gas turbine engine combustors, where a spray of jet fuel (or JP8 in the M1 turbine engine) is ignited in the combustion chamber for gas turbine engines. Enhancements specific to the Army's needs had to be included. The fire suppression component was another module that had to be coded. CECOM led this effort.

---

[1] FM-200 is also known as HFC-227ea or heptafluoropropane, while its full chemical designation is 1,1,1,2,3,3,3-heptafluoropropane.

Three years ago (when this data was processed) 200,000 grids took a week of processing with a 500 MHz Alpha CPU. Now a 660,000-grid solution can be solved in 3 days on a high end PC. CPU-intense analysis of the fire is necessary due to the large number of 3-D coordinates that must be processed; those of the fire from ignition to extinguishment and those of the extinguishing agent from the nozzle until dissipation. For example, the two sections of the fire-extinguishing agent in figure 1 are comprised of over 17,500 nodes. We proposed a method of taking many consecutive time-step "snapshots" from beginning to end in order to present this data graphically by showing the vehicle system, the soldiers, the flame, and the extinguishing agent in separate colors to make it easy to analyze the interaction of the flame and the extinguishing agent throughout the simulation (shown in Figure 1; red is flame, blue is the extinguishing agent) by using a Virtual Reality Modeling Language (VRML) output to translate into our CAVE. VRML was chosen since it was determined to be the easiest modeling standard to translate the TASCFLOW "spreadsheet data" into usable graphics data. Tcl scripting language was used extensively in order to remove things like the texture information inherent in the VRML frames, but not used in our CAVE-formatted files.

The CAVE is a multi-person, room-sized, high-resolution, surround-sound, projection-based virtual reality (VR) system. The CAVE was designed from the beginning to be a useful tool for scientific visualization; the goal was to help scientists achieve discoveries faster, while matching the resolution, color and flicker-free qualities of high-end workstations. The illusion of immersion is created by projecting 3D computer graphics into a 2.5 meter cube composed of display screens that surround the viewer on the left, right, front, and bottom (see Figure 2). It is coupled with head and hand tracking systems to produce the correct stereo perspective and to isolate the position and orientation of a 3D input device. A sound system provides audio feedback. The viewer explores the virtual world by moving around inside the cube and grabbing objects with a three-button, wand-like device. Unlike users of the video-arcade type of VR system, CAVE dwellers do not wear helmets to experience VR. Instead, they put on lightweight stereo glasses and walk around inside the CAVE as they interact with virtual objects. Multiple viewers often share virtual experiences and easily carry on discussions inside the CAVE, enabling researchers to exchange discoveries and ideas. One user is the active viewer, controlling the stereo projection reference point, while the rest of the users are passive viewers.
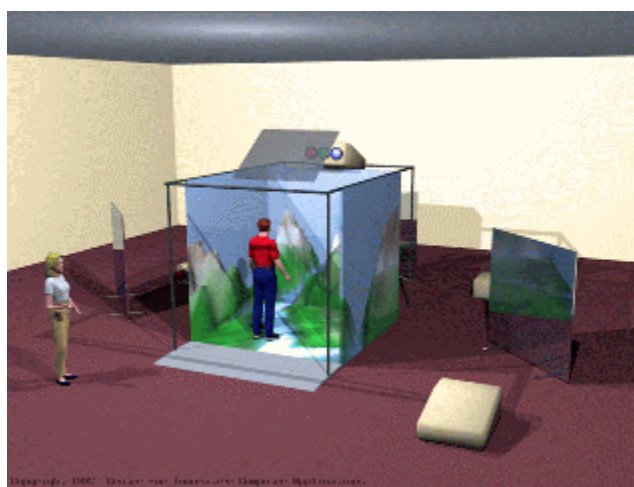
Figure 2: a CAVE[2]

---

[2] Figure 2 illustrates a generic CAVE, courtesy of the CAVERNUS Image Gallery, which can be found at: http://archive.ncsa.uiuc.edu/VR/cavernus/GALLERY/Gallery.html

The observer can walk anywhere in this cube and with the 3-dimensional mouse "walk" around the complete model, in our case a tank that was over 6m long. This gave the engineers and users a better understanding of how the extinguishing system reacted with the four suppression system configurations tested. For example, while watching the "playback" of the second configuration it was at first considered a success since no flame affected the soldiers in the rear section of the vehicle. But as one "walked" into the driver's section it was noticed that the bulk of the fire was pushed into this compartment; this configuration was quickly eliminated.

Figure 3 shows the actual CAVE used at TARDEC. A Silicon Graphics Onyx-2 workstation powers it. It has eight 300 MHz R12000 MIPS processors. One processor each is devoted to each view; front, left, right, and floor. The remaining four handle (in parallel) the remaining duties such as serial data; head and mouse tracking and button input instructions. In this CAVE a user has the ability to stand within the virtual flame and suppressing agent to further analyze the interaction of these two. This simulation is only capable while immersed in the CAVE's virtual world. With a press of the virtual mouse button the observer could then control the rate at which the simulation plays out; from a single stop action frame to a continuous "real-time" rate (or any speed between) in order to study the interactions. An obvious use of this immersion is that one could put themselves in any of the seated positions and "see" the fire as the soldier would see it. The tools that were developed during this experiment will be used on current and future combat vehicle studies of fire extinguishing systems.
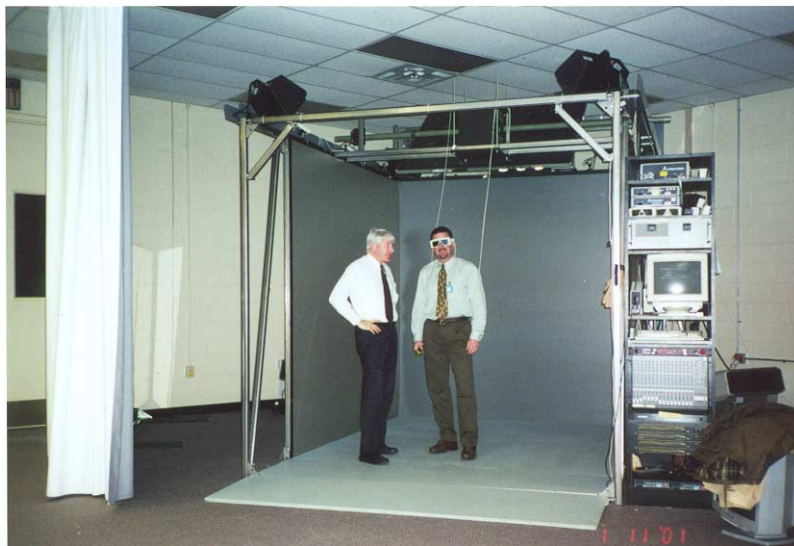
Figure 3: Dr. Blackwell and a user in the TARDEC CAVE

The Department of Defense has mandated that the replacement agent must: 1) be as effective as Halon 1301, 2) minimize space claim growth, 3) maximize use of existing hardware, 4) prevent second degree burns, 5) allow crewman to stay in the vehicle, and 5) be retrofittable. By using modeling and simulation software the engineer can more readily eliminate designs that do not meet the mandated requirements, while iteratively improving and optimizing the system to benefit the Army and most importantly, the soldier.

Paper #4
Discussor's name R. McClelland
Author Blackwell/Bochenek

Q: How effective would the display technology be in 2D in a commercial facility?

A: You of course lose the 3D, but you retain the ability to move around in the 3D CAD model. That is still a big improvement over Power Point.

This page has been deliberately left blank

———————————

Page intentionnellement blanche

The Factory is Virtual ……The Savings are Real

Robert G. Brown
CEO Advisor
DELMIA Corp.
5500 New King Street
Troy, MI 48098, USA

John M. Caddick
Sr. Manager - Virtual Manufacturing
Space and Communications Division
The Boeing Company
Mail Stop H013-A312
5301 Bolsa Ave
Huntington Beach, CA 92647, USA

Introduction

Modeling and simulation of manufacturability and supportability have been used to different degrees in the JSF, AAAV, DD-21, Future Frigate, Virginia Class Submarine, and many lifecycle extension programs. The use of digital manufacturing tools has resulted in innovative manufacturing techniques to significantly reduce tooling cost and to create modular build and test methodologies. Supportability studies have impacted designs to reduce lifecycle costs by reducing manning levels, by eliminating the need for special tooling and by avoiding un-maintainable conditions. The number of physical product prototypes and tooling mock-ups has been reduced by proving out tooling and processes in the 3D digital environment. Based on the learning curves experienced in the digital manufacturing environment, initial physical prototype builds have been completed with significantly fewer labor hours than have historically been required, and without the delays and costs associated with missing un-buildable conditions before the physical build. Reductions in non-conformances during the initial build versus previous programs have exceeded 90 percent. The modeling and simulation efforts of the IPT during the design and engineering, manufacturing and development phases are now being used for generating electronic 3D work instructions and serve as the build-to authority for the shop floor. The same models and similar processes can be utilized for service and maintenance processes.

The "next step" is to integrate the pre-planning and process planning activities as the front end of the contiguous digital workflow, and utilize the modeling and simulation solutions for the 'process verification' step. The capture in a digital format and reuse of the corporate manufacturing knowledge base is now practical. A product, process and manufacturing resource (PPR) database maintains the relationships between each process activity and the product data and resource data required to accomplish that activity. It must handle the variants possible including the differences for each tail number or hull number. Effectivity must be managed for not only product data, but also process and resource data. Interfaces with existing legacy CAD, PDM, manufacturing execution and MRP/ERP systems must be established within each corporate IT environment. The capability and benefits that have been achieved in the automotive industry with a common, shared PPR database for conceptualizing, designing, planning, validating, optimizing and executing a lean production

system are well documented. Early adopters within the defense industries are now applying these lessons learned in their operations.

Innovation Focus Moves to Manufacturing & Life Cycle Support

Most major industries have moved to 3D CAD for product design and have realized the savings in this portion of the product realization cycle.
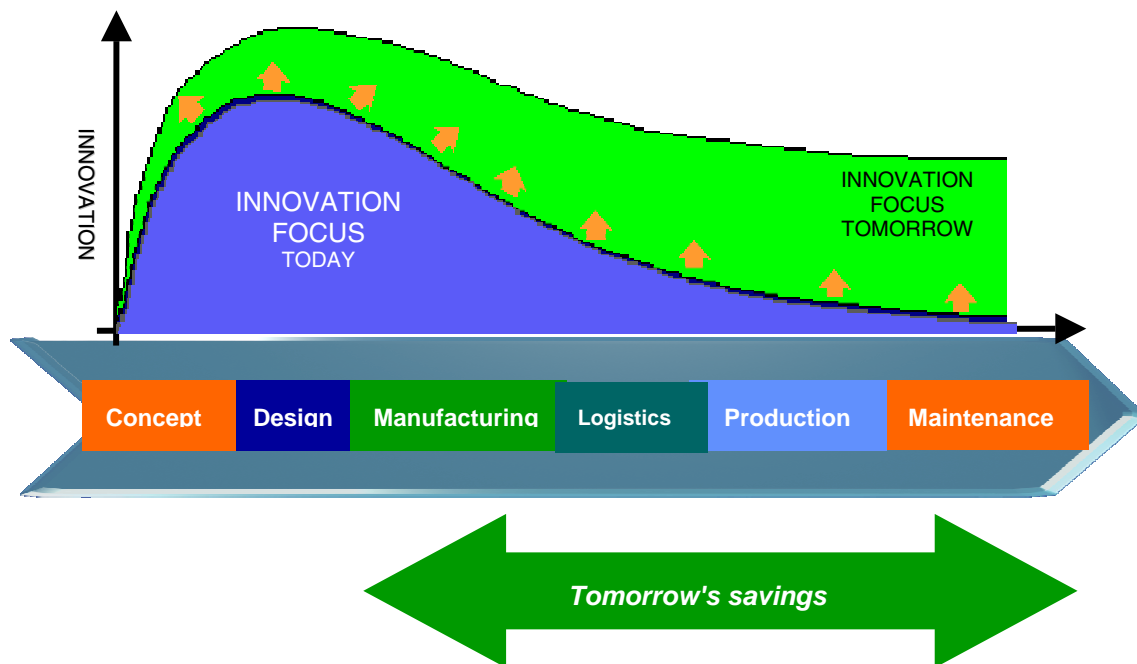
They are now beginning to leverage this investment in 3D CAD downstream in planning, validating and executing their manufacturing plan for these new products. The ability to perform thousands of iterations of different manufacturing and maintenance concepts in the digital environment without the cost and time delays associated with physical mockups has enabled manufacturers to realize the benefits from:

- Design for fabrication
- Design for assembly
- Design for maintainability
- Factory layout and flow simulation
- Innovative product designs and manufacturing processes
- Re-engineering the processes and flow for lean manufacturing
- The generation of simulation based, 3D work instructions / training

The Digital Factory

The Digital Factory environment uses the input from the CAD and PDM systems on *What to produce,* or the Engineering Bill of Materials and uses digital models of the manufacturing resources such as labor, tools, fixtures, plant layout which is the *With what to produce* so that the planners and manufacturing engineers can design the most efficient production system, and determine *How to produce*.
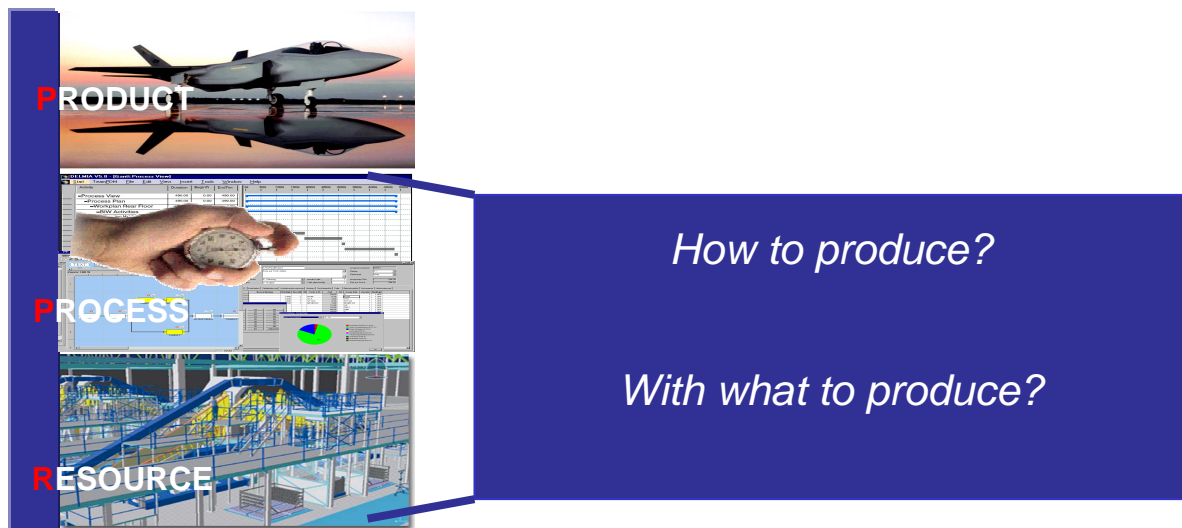
The Digital Factory provides the collaborative environment for the Integrated Product Teams to concurrently develop the product designs, manufacturing tooling and processes, as well as, maintenance tooling and processes. This parallel development of product and process decreases the product development cycle and the ability to work with digital mockups of the product and tooling enables the process engineers to begin at the conceptual phases and constantly refine their processes as the designs mature. By proving out their tooling concepts and manufacturing processes in the digital environment they prevent costly engineering change orders caused by un-buildable conditions during the product launch. Using the 3D simulations developed during the process validation efforts to create 3D work instructions to the shop floor greatly enhances the communication of the design intent of the manufacturing engineer to the mechanics, and minimizes their learning curve.

The Shared Product, Process and Resource database.

Up to 60 percent of the historical effort of using modeling and simulation in manufacturing has been gathering the *correct* information to use in the models. Now that the Product, Process and Resource (PPR) database is inter-connected to the enterprise's PDM and CAD data, this problem is minimized for the product and tooling data. Only recently has the capability existed to maintain a process centric database that maintains the linkages for each process activity, and the product data the goes into and out of that process step, as well as, the manufacturing resources that are required by the process activity. This database also maintains the manufacturing related attributes associated with the product, process and resources and a library of best practices. Then the initial conceptual process plan can be developed well before any CAD data is available, reusing best practices wherever possible. This conceptual plan can be linked to existing manufacturing resources. Then when the CAD

data for the product is available a 3D verification of the manufacturing concept in the context of the manufacturing resources and product design can be completed quickly and accurately.

From Concept Design Through Production Ramp Up

As the product, tooling and process designs mature they can be validated against the constraints and the manufacturing cycle times and costs accurately determined. Ergonomic simulations will verify that the tasks can be accomplished safely and within the time desired. Tooling concepts are evaluated and optimized. The plant layout and material flow evolves from the manufacturing concepts and can be extracted from the PPR database to conduct trade studies of alternative manufacturing concepts, plant layouts, production rates and manning levels. Once the production system is finalized, these models can be used to document and publish 3D work instructions to the mechanics on the shop floor and in the field for maintenance activities.

Boeing has realized significant saving from Digital Manufacturing

Boeing's Commercial, Space, and Military/Defense business units are using DELMIA virtual manufacturing, digital pre-assembly and discrete event simulation tools, to significantly lower production cost and cycle-time on a number of existing, as well as, new products/programs. Critical to successfully supporting these product/programs is the ability to identify potential production problems and design deficiencies during the product development stage prior to final design commitment. Also critical is the ability to accurately assess tooling, support equipment and factory requirements early on. Boeing utilizes the digital manufacturing tools to provide an effective means of improving Boeings product development, production, and factory change over processes.

Assembly Simulation

Assembly simulation has been used on many aircraft and aerospace programs such as the space shuttle, UCAV and the F/A-18EFF pictured above. Significant benefits have been realized in the areas of:

- Validating Design/Assembly Integrity Prior to Commitment
- Validating Operation Sequences & Tooling Concepts
- Identifying Assembly Anomalies
- Driving & Validating Design Release Schedule
- Enabling Optimization of Assembly Processes
- Reducing Downstream Production Planning (Assembly)
- Creating Consistent Virtual/Simulation Based Work Instructions
- Capturing Best Assembly Practices

Savings in assembly hours in the range of 40-60% have been realized across multiple programs. Cost avoidance due to interferences eliminated, ergonomic problems and incorrect assembly sequences have resulted in 20-55% savings over historical performances.

Resource Planning and Flow Simulation
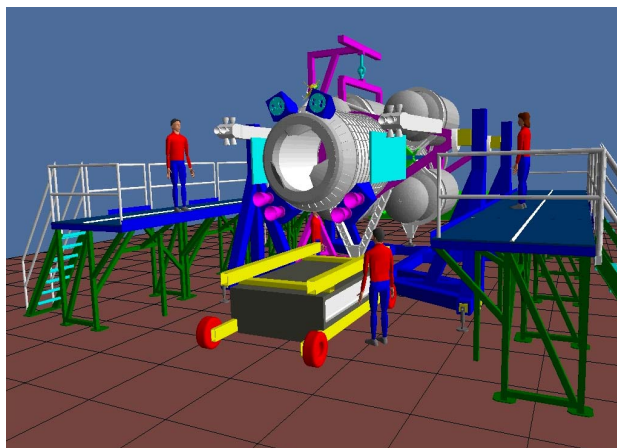
The planning and simulation of factory operations for military, commercial and space programs has provided the capability to develop and prove out lean manufacturing operations first in the digital environment, before committing time and money to the physical manufacturing facilities. These same simulations have been used to generate 3D work instructions for the mechanics on the shop floor. Some of the benefits realized include:

- Production Drawing Changes   40%   Reduction
- Tooling Design & Fabrication   50%   Reduction
- Planning Hours (assembly)   25%   Reduction
- Assembly Hours & Cycle time   30%   Reduction
- Technician Errors/Reworks   50%   Reduction
- Planning Errors/Reworks   50%   Reduction
- Technician Preparation   15%   Reduction

Ergonomic Analysis
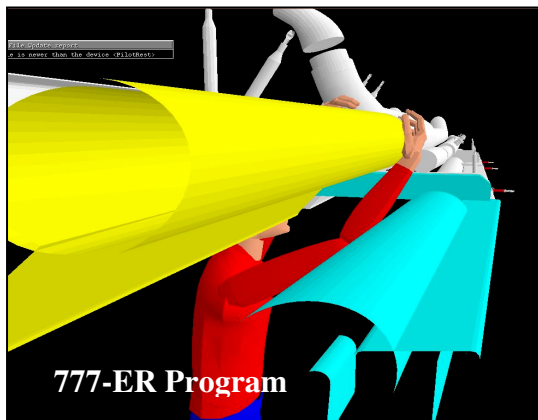
Ergonomic Analysis has been applied to numerous commercial, military and space related manufacturing and maintenance tasks. They have dealt with accessibility problems, serviceability with the required tools, human factors and employee safety. Some of the benefits derived from these studies include:

- Identifying Hazardous Operations (Hardware / Personnel)
- Validating Serviceability/Operations
- Ensuring Accessibility During Assembly / Test / Operation / Maintenance
- Highlighting Potential Tooling and Equipment Requirements

Lockheed Martin - "The factory you see may be virtual, but the time and money savings are real."

This simulation is for the removal of the engine on the prototype JSF aircraft. Lockheed Martin made extensive use of manufacturing and maintenance simulations during the development of their contract winning design. This simulation was also used to brief the crew that installed the engine into the aircraft. The first actual installation was done in three hours, which is very quick, and the crew credited the simulation for part of their thorough preparation. Since simulation enabled the team to consider maintenance issues very early in

the design cycle, there were numerous instances where the maintainability studies influenced the design of the aircraft.

Simulation was also used for program a large Gantry Automated Drilling System for drilling and milling the wing carry-through section. Because the wing carry-through section is the aircraft's biggest and most critical structural component, the simulation show an entire section of the factory including all the material handling that would be required. Through the use of simulation they were able to develop a process that reduced the task from four persons for three days, to three people for 30 minutes.

General Dynamics Electric Boat – "Manufacturing Efficiencies Previously Achieved on the Third Ship Set are now Realized on the first Ship Set"

Starting with the DARPA funded Simulation Based Design project during the second half of the 1990s, General Dynamics Electric Boat has adopted a Design / Build philosophy that is heavily dependent on 3D, physics based simulation. Using assembly planning and simulation to create innovative manufacturing practices they feel that the can reduce the Design / Build time from 14 years to 7 years. They expect that the revised manufacturing processes will reduce the cost of the submarine by approximately 30 percent. One of the savings is a 50 percent reduction in change orders since they have already proven out the fabrication and assembly processes in the digital environment. This will also enable them to have the manufacturing efficiencies previously achieved on the third ship set on the first ship set.

Conclusion

A great deal has been accomplished through the heretofore, intermittent use of manufacturing modeling and simulation. Because of the cost involved in gathering and verifying the data to be used in the simulations, and the lack of 3D data in some industries, it has not yet become the way of doing business every day for most defense manufacturers. As the industry moves to 3D design and the digital manufacturing solutions become easier to integrate into the knowledge management and IT environments, the productivity of the users increases dramatically. The ability today to share a common database of product, process and resource data across the enterprise significantly increases the productivity of the manufacturing engineers. The future savings from the virtual factory will provide the competitive edge in the aerospace and defense marketplace.

Paper #6
Discussor's name G. M. Appleyard
Author J. M. Caddick, R. G. Brown

Q: 1) Are the quoted manufacturing cost/time savings achieved with the same manufacturing/assembly techniques/concepts?
2) Please can you comment on any synergies you perceive between advanced manufacturing/assembly techniques/concepts and Virtual Manufacturing simulation?

A: 1) Basic methods used are the same. However, simulation enables significant benefits by providing assembly sequencing and optimization.
2) DFA (design for assembly) techniques are validated through simulation, thus tools complement one another.

Discussor's name S. Kaun
Author J. M. Caddick, R. G. Brown

Q: Are there any interfaces available to transfer the geometrical data from the various PDM systems to the DELMIA tools? Did any difficulties appear when transferring the geometry from UNIX to the NT world?

A: A standard interface to the ENOVIA VPM exists. Customer interfaces to Metaphase and iMAN have been developed. Since every PDM installation is unique, some customization is required. All DELMIA applications run on NT and can access the CAD data from UNIX based CAD systems.

Discussor's name M. Bergamasco
Author J. M. Caddick, R. G. Brown

Q: For assembly testing and/or ergonomics studies, does you company use specific man-machine interfaces such as haptic interfaces?

A: Drivers exist for data gloves, pinch gloves, and major magnetic motion sensor systems. Users can use the available tool kit to develop their own drivers for haptic devices.

Virtual Development and Integration of Advanced Aerospace Systems: Alenia Aeronautics Experience

Marco Delpiano, Marco Fabbri, Claudia Garda, Elena Valfrè
Alenia Aeronautica S.p.A.
Corso Marche, 41
10146 Torino, Italy

mdelpiano@aeronautica.alenia.it, mfabbri@aeronautica.alenia.it
cgarda@aeronautica.alenia.it, evalfre@aeronautica.alenia.it

1. Introduction

The Italian Aerospace Industry has been involved, over the last few years, in a significant evolution which applies both to design and production processes and to international co-operation with a consequent improvement of its product and services requiring new professional roles and skill.

In fact, the development of an aeronautical project is based on a specific approach in the technique-scientific disciplines management: the Concurrent Engineering. According to this methodology, the product is developed with a multidisciplinary and integrated framework, having as objective the optimization of the whole aircraft system. A number of examples demonstrates that this approach allowed to reach dramatic results in reduction of development time and cost.

Practical experience of Concurrent Engineering can be combined with up-to-date Information Technology to exploit the capability for enhanced design and manufacturing processes. In fact, the management of advanced project requires an integrated process management with the necessity of defining specific methods and tools that allow to verify in advance all possible problems of the product in particular with virtual product management (Digital Mock-Up) and with the integrated product data management (Product Data Management, Enterprise Resource Management).

Moreover, this process has to be managed in a "Synthetic Environment" that is a combination or "federation" between a number of models, simulations and real equipment, possibly including human operators in the loop, into a common representation of the world. Using state-of-the-art networking technology, this environment is used to provide consistency and concurrency across previously isolated processes. The use of such networked systems, either within a single company or among partner companies, is also an effective mean of developing co-operative effort within teams, especially where a Concurrent Engineering approach is adopted.

Alenia Aeronautica has gained a solid and consolidated experience in this field within a number of past and ongoing programs. This paper will describe this experience, and will tackle the methods which are used and planned to be used, so to cross-transfer the above experience to other military as well as civilian programs.

This document is organised as follows: a brief description of the Concurrent Engineering concept as used for developing aeronautical programmes is provided first. An illustration of tools presently used to implement the above concept is next, along with examples of its application with respect to some ongoing programmes. Synthetic Environment development is then introduced; current activities taking place at the Flight Simulation Department aimed at developing a kernel simulation Synthetic Environment are described. Finally the path for joint Concurrent Engineering and Synthetic Environment development is explored. Three noteworthy but more general projects in line with this vision are the participation in European funded projects on Concurrent Engineering, Distributed and Integrated Configuration Management Process and Synthetic Environment.

2. Concurrent Engineering

The Concurrent Engineering (CE) is a systematic approach for the integrated definition of the product with all manufacturing related processes. This approach requires to take into account of all elements of the Product Life Cycle since the beginning of the project, i.e. from the concept to the disposal.

In the aeronautical product development this means:

- to organise the development of the Product/Process in an integrated and simultaneous way in order to reduce time and minimise the changes verifying the feasibility of functionality/components before the first release;

- to satisfy the qualitative requirements of the final product and to reduce Costs in the In Service Phase;

- to guarantee the respect of activity schedule.

The CE requires the involvement of Pre-Design, all Design Disciplines, Production, Procurement, Product Support, Quality and Planning/Control, allowing each member of a specific Function to develop his activities taking into account in each project phase all elements of the Product Life Cycle.

The 3 key elements of Concurrent Engineering are:

- Organisation

- Methods

- Tools

2.1 Organisation

Organizational aspects are strictly related to the CE approach: a key factor of CE is the Design Built Team.

A Design Built Team (DBT) is an integrated, multifunctional and sometimes also multipartner team defined in a different composition in relation to a specific phase of the program that is transversal to the hierarchical organisation structure and that exists only for the time required to the achievement of specific objectives.

The DBT's are essential for the process, allowing inter-functional communication and the inclusion in the project of all disciplines requirements before the product release. DBT's Inter-functionality and multi-disciplinarity guarantee that each Function has a global visibility of all activities performed in the different Phases/Sub-phases of the Process.

Moreover, the Integrated Schedule defined in co-operation by different Functions and the Continuous Information Sharing allows to reduce errors, changes and repairs, increasing the Productivity.

2.2 Methods

Methods are standards, rules and recommended practices (applicable at international, government and company level) which have to be followed for appropriate work of the CE.

The "Best Practices" of CE are based on the implementation of an Integrated Process Management that allows to manage activities not only as a specific aspect of a discipline (figure 1) but also with transversal and multidisciplinary process (figure 2) allowing a better and integrated vision of the product.
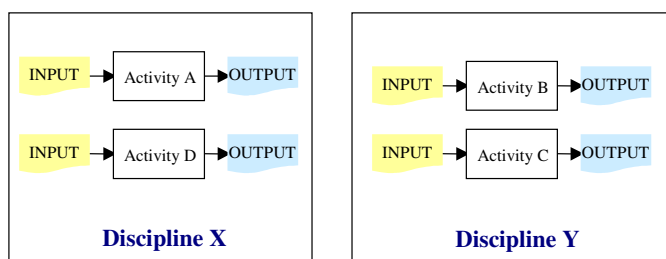
Fig. 1 – Process Management by discipline   Fig. 2 – Integrated Process Management
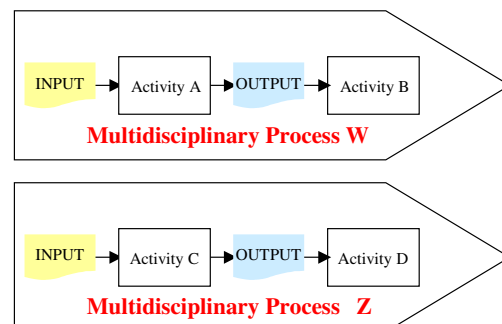
2.3 Tools

Information Technology covers a key role in the support of the Concurrent Engineering approach. The tools that are supporting the digital and sharing of integrated data within a multifunctional, multidisciplinary and multipartner approach are based on Computer Aided Application (CAE, CAD, CAM and DMU), Product Data Management (PDM) application, Communication tools, Network, Synthetic Environment, etc..

In this paper we will concentrate in describing tools related to DMU, PDM and Synthetic Environment area.

3. Alenia experience in Virtual Product Management

3.1 PDM and DMU Introduction

PDM is a tool which assures the integration of the information defined by different Functions and controls the information evolution along the product lifecycle.

One of the most important PDM tasks is to handle the Product Structure by means of a full Configuration Management. In other words, it assures the management of all product configurations, in several views (as required, as designed, as planned, as built, etc.), and the distribution of information to other applications.
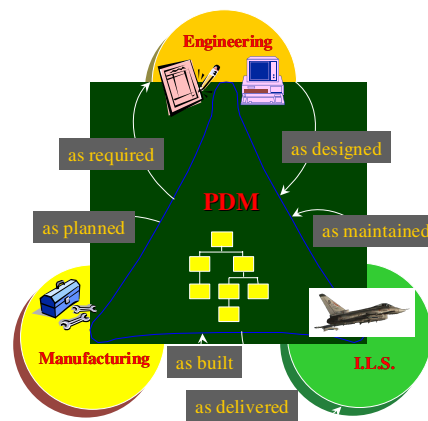
Fig. 3 – PDM for Product Configuration Management

The user access to applications and data is done through PDM. The database shared among applications is made-up with product and processes data. In other words PDM enables data access and data sharing in different departments and sites.

With PDM it is possible to manage the correct configuration of the product, as for physical, electrical and software items, together with standard parts and equipment.

The main features of PDM, as described in the following chapters, are:

- Multiple View Management

- Change Process Management

- Advanced Information Management

- Multi-site PDM Implementation

- Configured Digital Mock-Up

- Visualisation

- Technical Publication and Training

The adopted Alenia PDM tool is ENOVIA Product Manager Version 3.4 (PM) marketed and customised for Alenia by IBM. The CAD/CAM tool adopted for Eurofighter Typhoon and A380 programs is CATIA Version 4.2.2.1 which numbers among its packages the CATIA Data - Product Manager Integration (CDP).

CATIA is a Dassault Systèmes product, marketed by IBM. The Visualiser used in our Company to allow the access to CAD data also to the users simply equipped with a PC is the VisMockUp tool, Version 3.1, of UGS-EAI. This tool was customised by EAI to interface it with PM by means of an interface named "PM Agent".

One of the main added value of Alenia PDM implementation is the connection with CAD world, that is the Configured Digital Mock-Up, so that it is possible to retrieve and visualise the Digital Mock-Up of the requested configuration. The views covered by actual PDM are just the as designed and the as planned; in addition there are some information about the as built view. The use of the tool has been extended to all Alenia sites in 2001.

The first PDM project has been implemented for the Eurofighter Typhoon Project. The implementation of PDM for the new program A380 has been based on the complete reuse of Eurofighter Typhoon PDM innovative functionality and architecture with some customisation needed in order to be compliant with the civil aircraft process and the Airbus France requirements.

In this paper, we will describe the Alenia state of art/experience mainly focussing on Engineering activities.

3.2 Multiple View Management

In Alenia PDM system, in the product structure are managed different kinds of Part Numbers (P/Ns):

- Detail: a part which can not be split in other finished Parts, with its own CAD model, with additional information, such as materials codes and protective treatments, for the production.

- Assembly: a collection of parts forming a self-contained, independently mounted unit. Finished and storable Part composed by two or more Parts (Details or other Assemblies), with its own CAD model.

- Installation: a part composed by two or more parts (Details, Assemblies or other Installations), which can be realised only during the manufacturing of an higher level Assembly, with its own CAD model.

- Standard parts: parts, with or without CAD models, bought by the company from a supplier.

The designed parts pass through a process of validation with a formal signature and with a workflow that involves different departments in the company, not only in Engineering, so that all the information linked to a part are validated.

The two views of the product structure, Engineering (as-designed) and Manufacturing (as-planned) are both contained in the Alenia PDM system and are strictly connected. In particular the Manufacturing Bill of Material (BoM) is obtained from the Engineering one through the "Accept" process.

When designers have finished their activities on a set of Part Numbers organized in a single Engineering Release Authority (ERA), this Engineering structure is released (through a validation workflow managed by the system) and becomes available for Manufacturing acceptance. The acceptance of the ERA by Manufacturing users makes the new Engineering Structure integrated in the already created Manufacturing BoM, saving the pre-existent Manufacturing data and indicating if some specific actions are needed to guarantee structure coherency.

In the Manufacturing View are made all the Manufacturing activities in order to consolidate the Manufacturing BoM: creation of only Manufacturing Part Number, insert of data and documents, restructuring actions, etc.. When the structure is ready it is made effective and sent to the Material Resources Planning tool.

3.3 Change process management

In the Alenia PDM system, the Change Process is managed with a specific workflow. The change of different Part Numbers is managed with a change document that is called Request For Alteration (RFA), when the request is originated by Engineering, and Manufacturing Change Alteration (MCA), when the request is originated by the Manufacturing. These documents are managed through PDM, along all their lifecycle, their different status and their different issues.

Moreover, with the Alenia Change Process workflow (figure 4) it is managed the information concerning the point in the production phase in which the change has to be verified and embodied, and the indication of the correct embodiment.
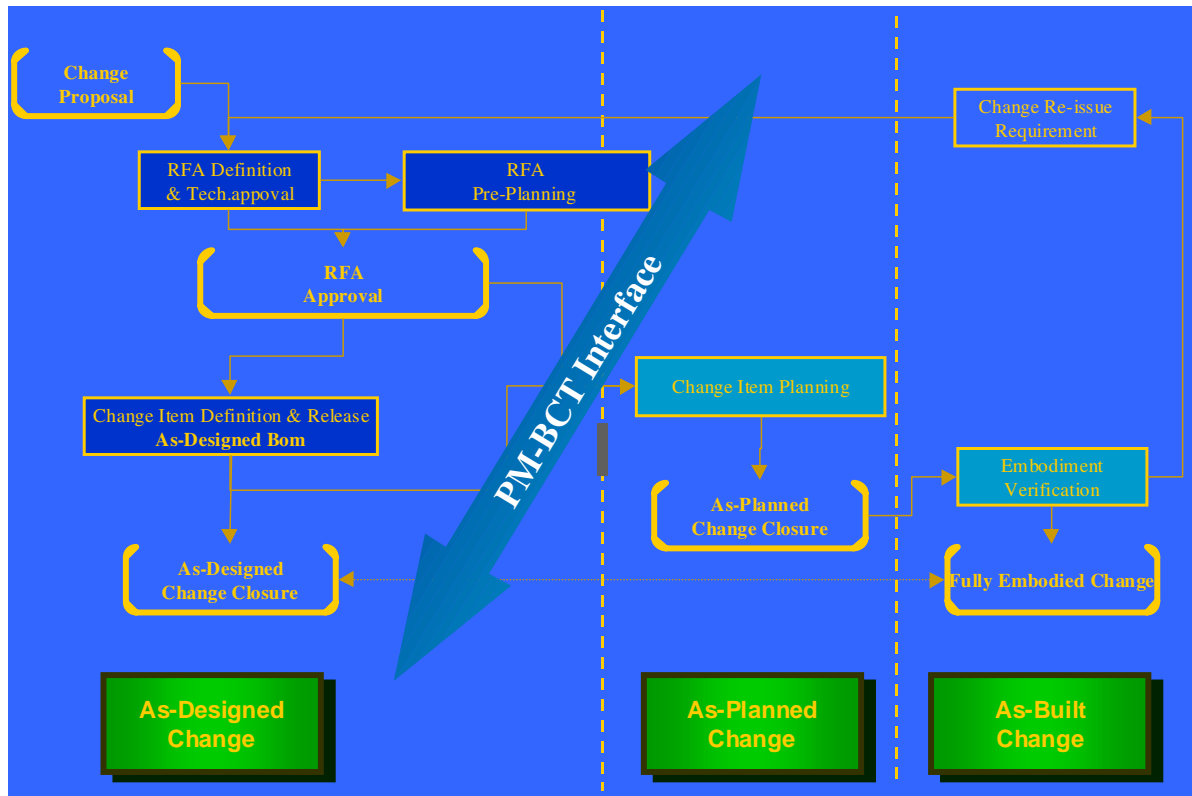
Figure 4 – Change Process Workflow

3.4 Advanced Information Management

PDM tools, and specifically the workflow functionality, can be used not only for releasing data, but also for Advanced Information Management.

Alenia PDM system has the capability to manage all information that is partially released during the product lifecycle and before the final part release. Not only the information related to an item have to be managed in an advanced way, but also the links between the items, so generating a preliminary Product Structure.

Two concepts have to be used in this approach:

- Maturity Stages
- Advance Information Release.

3.4.1   Maturity Stages

Maturity Stages represent the different levels of completeness related to the information (geometrical and non geometrical) which defines a part. The Maturity Stages have to be defined for each specific technology and incrementally. Therefore the usage of Maturity Stages enables an integrated schedule of the activities to be performed by the different company departments (Engineering, Manufacturing, Procurement, Quality, etc.) without waiting the final drawing/model release.

Each time a new issue for a specific maturity stage or a new maturity stage is reached, the new set of information automatically supersede the older and all the relevant company departments are notified with the change.

Inside Engineering departments, the Maturity Stages represent a tool which can be used in order to:

- monitor the progress of the Product Development process;
- improve visibility about the completeness reached by design information within the other company departments.

Inside Manufacturing Engineering, the Maturity Stages represent a way to operate in Concurrent Engineering and a tool by means of which it becomes possible to verify the level of completeness of the project evolution accordingly to the integrated schedule agreed inside Design Built Teams.

3.4.2 Advance Release Information

To complement Maturity Stages, another concept has to be used which defines advance but official release of information from Engineering towards Manufacturing departments.

Advance Release Information are themselves referred to a part being defined accordingly to its technological class as well as to their different usage in downstream processes (figure 6).

Three main kind of manufacturing activities can be defined which can/must start before the final official part release, those being:

- material purchase/supply
- tooling design
- Numerical Control part program design

The relationship between Maturity Stages and Advance Release Information can be summarized in the two following points:

- a minimum Maturity Stage exists which enables an Advance Information Release; this stage can vary with the part technological class and with the type of release
- the content of the package of information being released in advance can be equal to the minimum Maturity Stage content, a subset of it or a superset of it.

Managing advance information doesn't mean that data can be modified without any control. Anyway, procedures used for Advance Information Release as well as for their modifications have to be somewhat simplified compared to the final release ones.

Advance Information Releases are negotiated between Engineering and Manufacturing and result inside the Design Built Team schedule.

Fig. 6 – Advanced Release Information

3.5 Multi-site PDM Implementation

Alenia Aeronautica is a Company organised on different sites often working on the same programs. This implies that the same information must be visualised and used in parallel by various users belonging to different sites in a distributed environment.

To obtain this result a Wide Area Network (WAN) was implemented in the past years (figure 7). Nevertheless this situations can represent a tremendous problem if the data to be shared comprise thousands of CAD models with an average size of 1.5 Mb, because this means an unbearable effort for the WAN and a tremendous slowness for the users.

Figure 7 - Alenia Multi-Site PDM Implementation

The solution adopted, defined as "CAD data replication on remote sites", is based on the following.

- Metadata (Part Numbers, material codes, model names, etc..) are stored on a unique master site (Torino for Eurofighter Typhoon program, Pomigliano for A380 program) and accessed by the users at each site directly via WAN

- The CAD models are replicated on three sites (Torino, Pomigliano and Foggia), accessed by the users on the site nearest to them, avoiding unnecessary traffic on the WAN and limiting it to the Local Area Network (LAN)

- The alignment between the three sites is asynchronous and is realised during the night by means of a replication regarding the CAD models created/updated during the day.

3.6 Configured Digital Mock-Up

The use of Digital Mock-Up (DMU) in Alenia as a basic tool for aeronautic design began in the middle of the '80's, evolving and growing in terms of quality and quantity in line with the CAD systems and with IT capabilities. Therefore we moved from the part modeling initially using wire-frame methodology, then using wire-frame/surfaces or, as alternative, faceted solids, until to arrive to the exact solids. In parallel we passed from partial DMU's dedicated only to some critical zones under a system/installation point of view, then to DMU's simulating big aircraft components (e.g. an engine nacelle, a fuselage segment or a pylon) till to

reach the modeling of each single aircraft component, from the screw to the landing gear, generating in such a way a completely virtual aircraft.

For first and second generation DMU's we worked on some tens or, in the most complex situation, on a hundred of big CAD models which acted each one as a collector of the most considerable parts under a space allocation point of view for a certain aircraft zone or for a specific sub-group, disregarding not dimensionally significant parts. The preparation and the updating of the above models was entrusted to a Mock-Up "administrator" and only a small group of people was able to assemble them correctly for visualizing a certain aircraft configuration (i.e. the models valid only for Twin-seat or Single-seat).

However the above methodology is not applicable anymore in programs like Eurofighter Typhoon or A380, whether because the number of models to be handled would become in thousands, or because the number of DMU "clients" in the Company would increase exponentially, being no more limited to Design and Manufacturing Engineering, but extending to a lot of downstream departments, from the personnel dedicated to manuals preparation up to shop floor people.

The common requirement for all these new users is to access to DMU data without deep CAD knowledge and with the certainty of visualizing always the correct data for the required configuration.

Therefore, it appears the demand of a "configured" DMU that should permit the access to the models no longer as simple models but as virtual representations of physical parts, using as a key the relationships among the Part Numbers stored and configured in a product structure managed by means of a PDM. In the same database the PDM handles also the CAD models, viewed as Part Number reference documents, and, when existing, the part positioning in the space (figure 8).

To make use of a PDM system for managing the product data involves in any case the adoption of precise rules for data generation and administration, to be able to fully exploit its capabilities.

To cover the above requirement, since 1996 has been run in the Eurofighter consortium the DPA (Digital Product Assembly) Project, that is an initiative of the four EPC's (Eurofighter Partner Companies) applicable to the various phases of the program (development, production, product support), which embodies the usage of common CAD tools (CATIA, L-Cable) and selected applications as well as common standards and procedures to ensure data usability throughout the consortium.

The goal is to supply the basis to operate in true Concurrent Engineering, facilitating the information exchange among the EPC's and a simultaneous/controlled access to the product data.
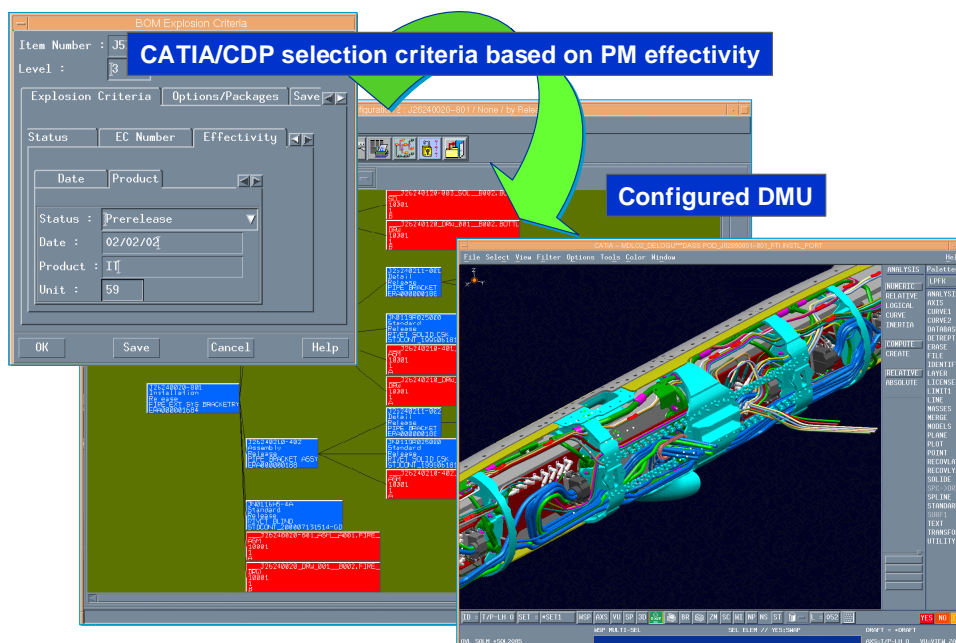
Fig. 8 – Example of access to the Configured DMU

With regard to DMU, the DPA key rule for the correct management of design data is "One part, one model, one drawing", which means that each Part Number has its dedicated 3D solid model, that the 2D model relevant to the drawing is separated from the solid model, and that, however, possible other models, when necessary, are represented in a dedicated file. Therefore it is possible to access to single models or, in case of 3D solids, to groups of tens or hundreds at once, taking into account also the relevant positions in terms of roto-translations previously stored.

The access to the CATIA models occurs starting from a graph in a bi-directional relationship with the models themselves. In other words it is possible to select a leaf representing a model on the graph and highlight on the CATIA window the corresponding solid or, on the contrary, by selecting a solid, to visualise which is the corresponding leaf on the graph.

3.7 Visualisation

The access to CAD data and to the Configured DMU by means of CDP/CATIA, even if it is precise and reliable, shows two limitations:

- the first is that most of the company users only need to consult the CAD data and do not have to contribute to their generation; consequently it is not convenient to train very many users in the CAD utilization for consultation purposes (buying also the necessary CAD licenses);

- the second is that it implies the availability of a quite expensive hardware as a Workstation, which is also not very much diffused in the company.

The introduction of the Visualiser just permits to eliminate the above limitations, satisfying the demand of those users which require a simple usage tool, a tool that works on an hardware universally diffused like Personal Computers.

The technology the Visualiser is based on is called "tessellation", that permits to reduce the weight of CAD data up to a magnitude factor, eliminating the CAD model of that information which are useful during the generation and modification phases but useless for consultation (for example the solid tree) and accepting an exact solid simplification; in effect the exact solid is treated as a faceted solid with an acceptable error margin (e.g. 0.2 mm). Through the tessellation the solid models are duplicated in "tessellated" format, while the 2D models are duplicated in CGM format (or other formats, for example the TIF one).

The Alenia selected tool, VisMockUp (or VisView, its "light" version), was interfaced with the PM/CDP world by means of a software written ad hoc nominated "PM Agent" (figure 9).
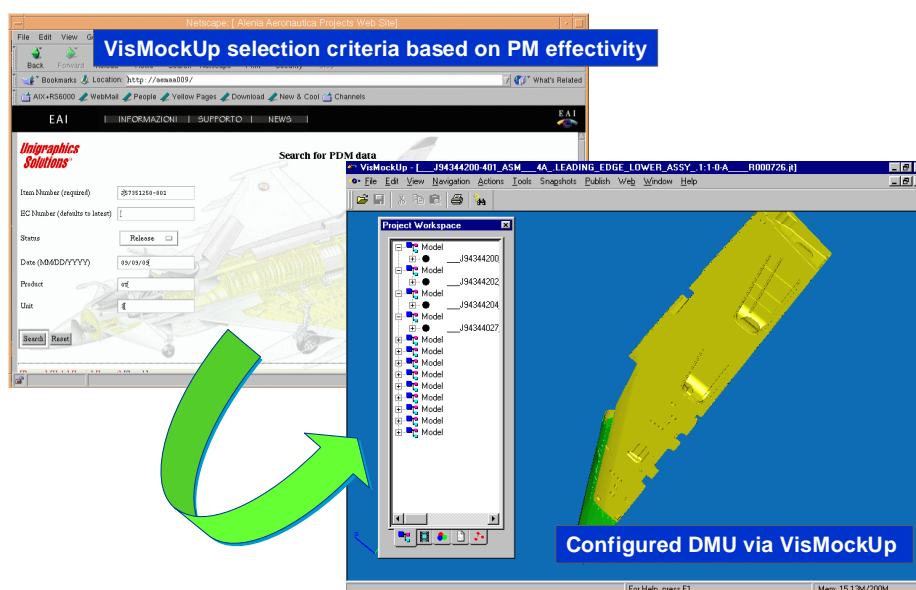
Fig. 9 – Integration between PDM and Visualiser

The CAD models generated during the day are tessellated night time maintaining an unambiguous/bi-directional relation between the tessellated data and the metadata related to the original models. In such a way, the day after all company users can access to the CAD data using a browser on PC, following essentially two methods:

- access to data of a single 3D or 2D model, with possibility of superimposing some models of the same type;

- access to relevant data for an assembly at whatever level of the product structure, with methods that are analogous to the CDP ones (but in this situation, the only accessible data are the 3D tessellated models).

With the second technique, it is really given to the user the possibility of manipulate a Configured DMU through VisMockUp also on PC.

3.8 Technical Publication and Training

Technical Publication and Training people are an "historical" customer of Product Structure and Configuration Management data, including all related attributes (e.g. material codes). Also in the past, starting from these data together with the traditional paper drawings, they were able to prepare documentation like Part Catalogues, Repair Manuals, Maintenance Manuals etc..

The most important added values given by Alenia PDM/CDP/Visualiser environment are the following:

- a unique and integrated environment for BoM and related attributes, Configuration Management information, Configured DMU and 2D Drawing Models;

- the possibility to use the Configured DMU directly to generate the pictures necessary for generate thousands of illustrations avoiding the old problem of moving from an "orthogonal projections" representation to an "isometric view" representation;

- the opportunity to generate short films to be used for training purposes.

4. Alenia Experience in Flight Simulation and Synthetic Environment

The history of flight simulation at Alenia Aeronautica dates back to 1961. A number of development and production standard flight simulators has been developed in-house since then, closely following technological advances in the field of computation, visual systems, and man-machine interfaces that have taken place since that time. From the first analogue calculators to state-of-the-art super-computers, things have changed quite dramatically and an ever increasing realism has been brought to more and more affordable systems.

The concept of Synthetic Environment (SE) was born from the consideration that the real time networking of several and different simulation systems enables the construction of an operational environment within which the variety, complexity, realism and inter-dependence of the external world are recreated, with an accuracy strictly derived by the simulation resources used.

One can generally refers to SE as an integrated simulation system consisting of the ensemble of live human operators, real systems and virtual models. Its goal is usually a real-time, distributed and interactive simulation exercise.

The availability of a SE offers several advantages: optimization of design, development, acquisition of weapon system processes; greater training effectiveness; greater mission rehearsal realism; lesser environmental impact during development and training.

4.1 Flight simulation facilities

Four flight simulators are available at Alenia Aeronautica in Torino: Eurofighter Typhoon in two versions, development and production standard, Alenia-Aermacchi-Embraer AM-X ground attack, and Alenia-LM Aero C-27J Spartan tactical transport aircraft.

The C-27J Simulator (figure 10) is presently used to support the development activities and flight testing of this evolution of the G-222 aircraft, and has also been conceived for training aircrew of the customers' Air Forces.

The AM-X simulator (figure 11) is the most senior within the department and has been used for training of more than a hundred Italian and Brazilian Air Force pilots, between 1989 and 1993.

Figure 10 – C27-J Flight Simulator

Figure 11 – AM-X Flight Simulator

The two Eurofighter Typhoon simulators (figures 12 and 13) are very tightly interdependent, since they have been devised as a twin dome facility able to provide air-to-air combat training capability. Most of the hardware components within the twin dome are linked by a high-speed optical link, a Versatile Module Equipment based reflective memory. While virtually all components of the production simulator are part of the loop, some important elements of the Development simulator remain on the local Ethernet. This is due to the incremental upgrade of existing simulators, but is not a hindrance to the efficient mutual exchange of status and position data provided by the optical link between the two simulators.

Figure 12 – Eurofughter development simulator

Figure 13 – Eurofighter production simulator

This type of link remains, in our opinion, a very efficient and cost-effective method to share information and memory segments at a local level. A similar architecture is also deployed in another optical loop, connecting the various elements of the C-27J simulator. By including in this loop the host computer for the older AM-X simulator, a direct exchange of status and position data between the two is possible. This second loop does enable formation flights, being connected to the twin dome reflective memory loop via high speed Ethernet link.

4.2 Simulation Synthetic Environment

A first-level SE is being set up within the Flight Simulation Center, formed by all available flight simulators (Eurofighter Typhoon development and production, C-27J, AM-X) in association with a virtual operational environment populated by a proprietary tactical scenario and several support tools. As more elements become available, they can be added to the SE.
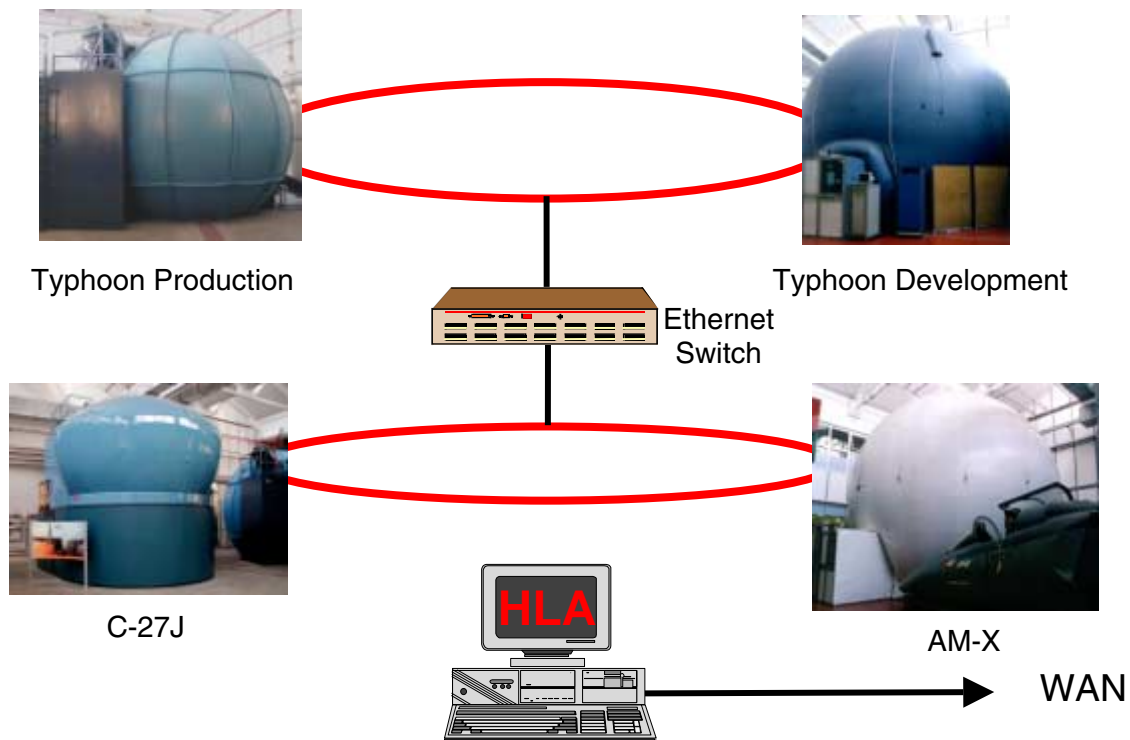
Figure 14 – Simulation Synthetic Environment diagram

With the importance of simulator networking in mind, High Level Architecture (HLA) technology is being gradually introduced by first linking all local resources among them (figure 14). A gradual extension of the network to external resources was subsequently started, and further projects involving international extensions are presently in their evaluation phases.

This activity consists in linking available simulators in real time, so that each simulator is aware of the others and can engage in joint operations with various degrees of interoperability.

Most flight simulators are legacy, i.e. have been designed for stand-alone operation with the main purpose of support, development and design activities. Typical SE applications require a substantial level of interoperability; as a consequence, a considerable amount of optimization and integration is needed.

The HLA is arguably the preferred methodology and software architecture used for such links today. Originated in 1995 by the Defense Modeling and Simulation Office (DMSO), a US Department of Defense Agency offering both the software and some minimal documentation free of charge, the HLA was created first as a fully functional version and disseminated as quickly as possible among the widest user-base possible.

On September 20th, 2000, the HLA has been voted on and instituted as IEEE 1516 standard, with specific purposes of promoting resource reuse and interoperability.

Alenia Aeronautica is presently evaluating HLA infrastructure as a tool to extend the local SE to one which includes distributed simulations.

With this respect, a dedicated machine is going to be included, which will be dedicated to HLA software. It will run the Run Time Infrastructure (RTI), the basic infrastructure allowing to implement the HLA standard, and it will host the HLA application responsible for representing the federate constituted by all entities connected by the ring. Its tasks will include publishing status data to the outside, subscribing to services available outside of the department, and providing a software layer to use for external interaction, according to the specifications of HLA.

It is worth to note that these iterative development steps for introducing HLA imply a number of challenges.

- Different data structure addressed by HLA (Object Oriented) and legacy simulations (structured programming).

- Need of expertise in both legacy systems architecture and new technologies/paradigms with a proper "system oriented" view.

Additionally, at the present stage of development, the use of DMSO-provided software might imply complications in that it has been developed with the aim of providing the users community with a workable, non-optimized mean to implement HLA. Therefore RTI performances have to be optimized towards each specific federation, either by trials or with automatic tools.

5. Towards a company-wide Synthetic Environment

The Distributed Environment described above is the kernel of a company-wide initiative encompassing tighter co-operation bonds between all departments in charge of the product design, i.e. weapon system design. The objective is the exploitation of a company Synthetic Environment intended as a pool of models, simulations, real equipment, with human actors in the loop, operating into a common virtual representation of the world. In this respect the SE should act as a common framework for providing consistency and concurrency to groups of previously detached processes. This environment would enable the visualization of complex military systems behavior (also considering changes to the systems or to their operating environment), and provides powerful means of communication between and within teams, therefore attaining the scope of Concurrent Engineering.

5.1 Development concept

The vision that would serve as a reference to develop the above concept comprises three main outposts that are also the key factor of Concurrent Engineering (figure 15).

- Organization: this area comprises organizational matters, functions and roles definition.

- Methods: standards, rules and recommended practices (applicable at international, government and company level) which has to be followed for appropriate work of the SE.

- Tools: Information Technology to support the activities as identified in the Organization area.
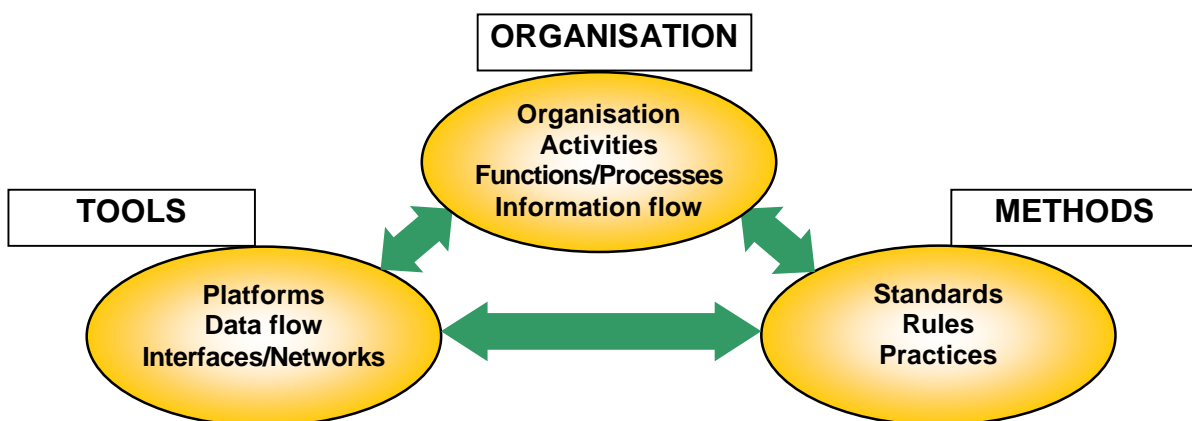
Fig. 15 - Concurrent Engineering and Synthetic Environment outposts

The introduction of the above architecture would imply a number of advantages.

- Improvement of the product quality and in-service support.

- Overall reduction of product lifecycle costs.

- Enhancement of the production process in terms of interfaces both inside the company and with Suppliers and Customers.

On the other hand, some issues could weaken or slow down the development of the above structure. One significant issue is cost: as a matter of fact, setting up of the above organization requires massive investments in terms of infrastructures, systems and human resources, in order to adapt according to program rules and industrial consortium rules, if any. This in turn has a significant impact on tools to be used and which shall allow proper data manipulation, tailoring and exchange. It is therefore evident that the introduction of a company SE requires balanced evaluation and an iterative development.

5.2 What next? First step: Functional Product Structure

Even if Concurrent Engineering, Virtual Product Management, Simulation and Synthetic Environment are good basis to move towards a Company-wide Synthetic Environment, the final result can be achieved only through a gradual approach, removing one obstacle at once.

Following the above philosophy, one of the possible improvements in the Virtual Product Management could be obtained in the information readability. In other words, using the Configured DMU and the Visualizer we have now a powerful and easy-to-use tool to navigate the Product Structure (PS) with its related data. The problem is that PS links are given following a Design/Manufacturing point of view that does not normally coincides with a functional point of view. For example, a fuel bracket riveted to a fuselage frame, in the As Designed/As Planned PS is linked to a structural installation regardless of the logical link between the bracket and the fuel pipe it constrains.

On the other hand, at the moment documents managed by our PDM are mainly related to the existing Part Numbers, therefore all the Engineering documents related to Aircraft Systems and Sub-systems which are not directly grouped under a part number, even if they could be managed inside the PDM as simple document objects, are not manageable in a complex and navigable structure. This means a limited readability of the system engineering data for non-specialist users and for the Customer.

The solution to the two above issues is the usage of a Functional PS (sometimes named as System Product Structure) which is defined as follows.

"Product Structure constructed using functional criteria for the classification and grouping of parts, to obtain a hierarchy of systems and subsystems, i.e. systems elements grouped by system functions (landing gear, controls, propulsion, radar, hydraulic, fuel, etc.), structural components grouped by structural function (i.e. fuselage, wings, horizontal tail), etc.. This Product Structure contains all the links with the related documentation."

Following this approach, documents like 3D models, drawing models, change records, etc. are managed in the Physical PS, while software and equipment specifications, qualification documents etc. are managed in the Functional PS. Zone collectors represent sub-system parts in a particular volume of the aircraft. Also the readability for Integrated Logistic Support customer is dramatically enhanced (figure 16).
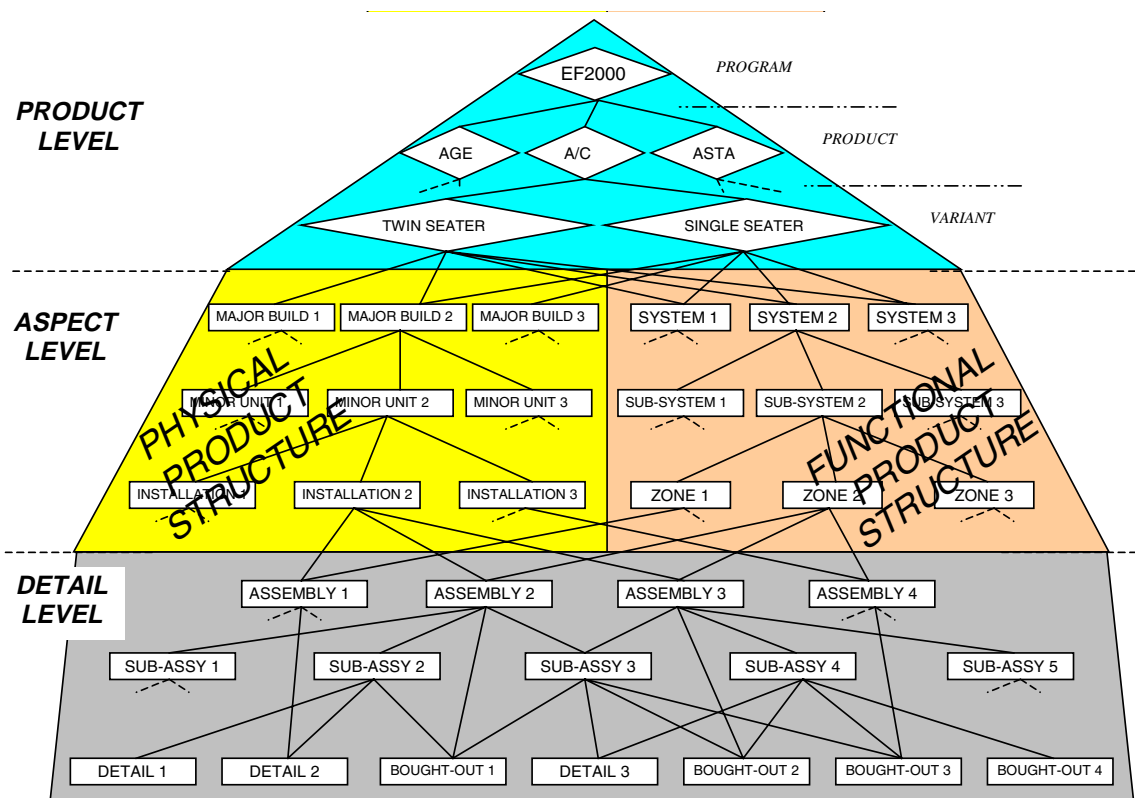
Figure 16 - Multiple Product Structure

The functional PS is therefore the natural framework through which SE resources can be integrated into the design process. At this level, entire functional structures within the project database can be accessed and visualized within the SE, which in turn can provide a physical model describing the behavior of the system or subsystem at study. Such a model will then be placed into the highly representative environment made available by virtual resources, and thereby tested under various evaluation criteria. This includes testing in specific atmospheric conditions, geographical configurations, or operational settings.

Man-in-the-loop mock-up validation is also an interesting possibility, given the real-time characteristics of most synthetic environments. If networked, this possibility is open also to remote users, with immense procurement/marketing advantages.

The advantages of the above solution are obvious, but unfortunately we have to take into account also the negative implications, i.e. the cost for creating and maintaining a conceptually new PS, the training for additional write access users and, in case of a program like Eurofighter Typhoon, which is already in an advanced phase, the additional cost for the data entry necessary to recover and reorganize the existing documents.

5.3 Research activities

While considering the above obstacles, evaluation of proper ways to further develop the vision is carried out through a number of activities, namely the European funded project ENHANCE, DIECoM and the WEAG Research and Technology Project 11.13.

- ENHANCE (Enhanced Aeronautical Concurrent Engineering) is a wide scope 3-year duration research project supported by the European Commission which started in February 1999 within the activities of the 4th Research Framework Programme. The main objectives of the project are: reduce the time-to-market, reduce the development cost and reduce the data management, conversion and transmission cost of European Aeronautical product development. Main focus of the project is on product engineering and design in an extended enterprise concept but there is activity devoted to product support, certification, contracts and multi-site team-working. Results include common processes, methods and tools to be used and exploited not only by the project partners themselves but also by the Supply Chain to improve

Concurrent Engineering practice for all levels of the Aeronautical Supply Chain. These take the form of 'Demonstrators' that show how these common processes, methods and tools meet their respective target requirements in terms of time, cost and quality.

- DIECoM (Distributed and Integrated Environment for Configuration Management) is a 2-year duration research project funded by the European Commission which started in September 2001 within the activities of the 5th Research Framework Programme. The main objectives of the project are:

  − to improve European Aerospace and Automotive industries capabilities in the Product and its associated customers' services Configuration Management;

  − to define an integrated process (procedures and rules) for Product Data Management (PDM), Software Configuration Management (SCM) and Electrical Data Management (EDM);

  − to validate the integrated process with two Pilot Demonstrators based on Commercial On The Shelf Information Technology tools. These demonstrators will be implemented with Enovia V5 and Websphere technologies respectively Dassault Systèmes and IBM products.

- RTP11.13 "Realizing the Potential of Networked Simulation in Europe" is a Western European Armament Group-funded project developed within Common European Priority Area 11 (CEPA) "Defense Modeling & Simulation Technologies". The project, which refers to the European Cooperation for the Long-term In Defense (EUCLID) framework and involves 22 companies from 13 European nations, started in November 2000 and has a duration of 36 months. The main goal of the program is to overcome the obstacles that prevent SE from being exploited in Europe, by developing a process and an integrated set of prototype tools intended to reduce the cost and time-scale needed to specify, create and utilize Synthetic Environments for collective training, defense planning, and system acquisition. In order to achieve this goal, a number of objectives have to be met, and in particular, it is necessary:

  − to determine and mitigate obstacles which prevent networked simulations from being exploited in Europe;

  − to provide processes and tools which will reduce the lifecycle of Synthetic Environment generation, execution and evaluation;

  − to set-up a European repository of simulation assets.

The experience described in the previous paragraph aims therefore at providing the basic technical infrastructure, while the above projects will serve to provide basic, international common-ground to implement Organization, Methods and Tools areas.

6 List of Acronyms

BoM	Bill of Material
CAD	Computer Assisted Design
CAE	Computer Assisted Engineering
CAM	Computer Assisted Manufacturing
CDP	CATIA Data - Product Manager Integration
CE	Concurrent Engineering
DBT	Design Built Team
DMSO	Defence Modelling and Simulation Office
DMU	Digital Mock-Up
DPA	Digital Product Assembly
EF	Eurofighter
EPC	Eurofighter Partner Companies
ERA	Engineering Release Authority

EUCLID	European Cooperation for the Long-term In Defence
HLA	High Level Architecture
IEEE	Institute of Electrical and Electronic Engineers
IT	Information Technology
LAN	Local Area Network
MCA	Manufacturing Change Alteration
MRP	Material Resources Planning
PDM	Product Data Management
PM	Product Manager
PN	Part Numbers
PS	Product Structure
RFA	Request For Alteration
RTI	Run Time Infrastructure
RTP	Research and Technology Project
SE	Synthetic Environment
VME	Versatile Module Equipment
WAN	Wide Area Network

Paper #7
Discussor's name F. Kafyeke
Author M. Fabbri

Q: You have outlined many tools that help improve the design to manufacturing process. Do you have any tools that help simulations of technical characteristics of the design (structural or aerodynamic analysis)?

A: Simulations are performed very early on various components of the designed product to make sure that they satisfy customer requirements [versus specific package tool identified].

Demonstrating the Potential Use of Virtual Prototype Modelling Techniques for Future AFVs

Dr M.A. French
Land Systems
Building 124
DERA, Chertsey
Chobham Lane
Chertsey, Surrey KT16 0EE

United Kingdom

M.J. Lewis
QinetiQ
A7-R2008 Ively Road
Farnborough, Hampshire GU14 OLX
United Kingdom

Abstract/Executive Summary

The need to provide light weight armoured fighting vehicle (AFV) structures while maintaining or increasing the survivability of these structures has increased the need to develop new materials and design processes. One way to address this requirement is to use composite materials to increase the structural and ballistic efficiency of the hull. Composite materials offer a number of advantages including weight reduction by the elimination of the spall liner and integral stealth protection leading to signature reductions. QinetiQ in partnership with Vickers Defence Systems, have produced a full-sized composite demonstrator AFV called the Advanced Composite Armoured Vehicle Platform (ACAVP).

To obtain the maximum benefit from new materials new modelling techniques are being developed by QinetiQ. These techniques will increase the accuracy of the structural analysis used in the design of future AFV structures and also provided additional information to assist in the design and integration of sub components which include the main armament and vehicle suspension systems. The developed modelling techniques have also been applied to gun systems and a range of vehicle components. In effect a virtual prototyping tool has been developed.

This paper provides a description of the ACAVP demonstrator, which was subsequently used as the test bed vehicle to validate the virtual prototype modelling. The paper describes the testing procedure and compares the results generated from the vehicle and those produced by the model. It is shown that good agreement can be achieved between the model and test vehicle.

Introduction

The need to provide light weight armoured fighting vehicle (AFV) structures while maintaining or increasing the survivability of these structures has increased the need to develop new materials and design processes. One way to address this requirement is to use composite materials to increase the structural and ballistic efficiency of the hull. Composite materials offer a number of advantages including weight reduction by the elimination of the spall liner and integral stealth protection leading to signature reductions. QinetiQ in partnership with Vickers Defence Systems, have produced a full-sized composite demonstrator AFV called the Advanced Composite Armoured Vehicle Platform (ACAVP).

To obtain the maximum benefit from new materials new modelling techniques are being developed by QinetiQ. These techniques will increase the accuracy of the structural analysis used in the design of future AFV structures and also provided additional information to assist in the design and integration of sub components which include the main armament and vehicle suspension systems. The developed modelling techniques have also been applied to gun systems and a range of vehicle components. In effect a virtual prototyping tool has been developed.

This paper provides a description of the ACAVP demonstrator, which was subsequently used as the test bed vehicle to validate the virtual prototype modelling. The paper describes the testing procedure and compares the results generated from the vehicle and those produced by the model. It is shown that good agreement can be achieved between the model and test vehicle.

Advantages of Composite Materials

The advantages offered by composite materials over metallic materials are now quite well known in terms of their mechanical properties when measure on a weight for weight basis (Table 1). It is worth reiterating that the main driver for the utilisation of composite materials in military vehicles is the ability of composite materials to reduce vehicle hull and armour weights. One way that this can be achieved is by the elimination of parasitic mass in the form of a separate spall liner, from a composite vehicle. This is achieved by the composite hull acting both as a spall liner material and as a structural material capable of carrying all the operational loads associated with the vehicle. However, a major design problem preventing composite materials from significantly reducing hull weight is the opposing needs to provide the vehicle with both ballistic protection and mechanical structural performance. The level of ballistic protection provided normally correlates to the weight of the vehicle's hull and armour. Consequently, reducing hull weight can lead to a reduction in ballistic protection, unless the weight reduction is put back as additional armour mass.

Other advantages of composites : GRP composite is a poor transmitter of sound, its damping capacity being attributed to the fibre matrix interface. A reduction in radiated noise leads to lower crew fatigue [1], and a lower acoustic signature for the vehicle. Further work is required in this area before the full advantage offered by composites can be quantitatively assessed, and this is a subject that is being actively tackled by the modelling being conducted at Chertsey and will be described later in this paper. A summary of the additional advantages of composite materials compared to traditional materials used for AFVs are:

- increased ballistic protection against small arms;
- reduced behind armour damage;
- reduced parts count.

As discussed above, the use of composite materials in military vehicles is not new to the British army, since it already operates the CAV 100 and the Bv206 vehicles. However, in both these vehicles a metal chassis carries the structural loads from the running gear, whereas in the case of ACAVP the composite hull carries all these loads.

ACAVP Demonstrator Design

Vehicle description: The ACAVP demonstrator is based on a future scout reconnaissance vehicle with a battle weight in the range of 18 - 25 tonnes (figure 1). The engine is situated at the rear of the vehicle, which, together with radar absorbing materials and IR paints, reduces the vehicle's signature. The vehicle has mobility at least equal to Warrior IFV and the hull has been designed to allow for transportation in a Hercules aircraft. The demonstrator is designed to accommodate a mission module in the centre of the vehicle and two men sitting abreast at the front. The vehicle has demonstrated complete electro-magnetic compatibility including radio and EMI features.

Metal appliqué armour appropriate to meet typical light armoured vehicle ballistic threat requirements has been designed together with the required armour fixings The ability to rapidly deploy an AFV has been addressed in the ACAVP vehicle by using the armour in combination with the composite hull. The appliqué does not form part of the vehicle's load bearing structure and can be easily removed to allow the vehicle to attain the weight limit imposed by the load carrying capacity of a C130 aircraft.

Vehicle design: Solid modelling design tools were used extensively throughout the development of the demonstrator vehicle providing an efficient means of managing changes in geometry and vehicle configuration. Finite element analysis techniques were used to evaluate the performance of alternative structural concepts and materials with geometry from the solid models being used directly in the creation of finite element models resulting in close integration between the design and analysis tasks.

Three primary requirements were responsible for determining the design of the vehicle hull structure, ballistic performance, mechanical properties, and manufacturing process. The hull is required to perform as a ballistically efficient component in the overall armour system, any compromise to the efficiency of the system at the threat levels seen by the vehicle would have had a dramatic impact on vehicle weight. The structure must have sufficient strength and stiffness to carry all automotive loads in both armoured and un-armoured conditions. The design must also take full consideration of the strengths and

weaknesses of composite materials unique material properties and the range of available manufacturing processes.

The primary hull structure consists of two large e-glass/epoxy composite mouldings joined around the lateral line of the vehicle. The upper moulding forms the roof, glacis, upper sides and rear of the hull. The roof is one of only three areas of the vehicle not covered by metal appliqué in the fully armoured configuration and is designed to defeat artillery fragments. Two layers of specialised materials are incorporated in to the material lay-up of the upper moulding. Under the outer surface there is a layer of radar absorbent material to reduce the vehicles signature, while under the inner surface there is a layer of EMC shielding to protect the vehicles radios and other vulnerable equipment. The glacis plate at the front of the vehicle is inclined at an angle of 60 degrees to take full advantage of the increased ballistic performance offered by plates at obliquity. The side plates and rear are inclined at 5 degrees to minimise the vehicles radar signature.

Internal bulkheads are used to isolate the crew from the noise and fumes of the powerpack and compensate for the reduction in vehicle stiffness caused by the large appetures in the roof.. Stiffness was a major consideration in the vehicles development as the composite materials considered for the hull generally had very low stiffness compared to traditional materials such as steel or aluminium. The composite hull of the demonstrator vehicle provides the same vehicle stiffness as Warrior. Two large composite transverse bulkheads are positioned in front of the engine bay and behind the crew compartment, in addition to increasing the stiffness of the vehicle these also help support the weight of the turret on the roof. Longitudinal bulkheads run down the length of the vehicle closing of the sponson area. Standard Warrior running gear was used for the demonstrator vehicle as it was readily available and has proven reliability. The standard equipment was originally designed to interface with the vertical lower sidewalls of an aluminium hull so was not suited to attachment directly onto a composite hull. The demonstrator vehicle employs interface plates to provide a suitable mounting surface for the equipment and transfer load the composite hull. The standard Warrior suspension units employ torsion bars, which traverse the entire width of the vehicle. These torsion bars are protected by composite torsion bar covers, which also help react the bending loads induced at the suspension attachments.

The lower moulding forms the floor, lower sidewall, rear, and toeplate. The composite floor offers broadly equivalent mine protection to existing in service vehicles, with extra protection provided in the crew compartment by a secondary floor. The lower sidewall includes a draft angle of to aid extraction from the mould during the manufacturing process and forms part of a spaced armour system which employs the skirt plate as its outer element. The obliquity of the toeplate is limited by practical considerations such as space required for the driver and ability of the hull to support the idlers during severe load conditions such as terrain impacts. The design of each area of the vehicle structure is a balance between a number of different, often conflicting requirements.

Analysis Design Tools – Virtual prototype modelling

Structural design of ACAVP: An extensive programme of component and material testing supported the structural analysis of the demonstrator hull. Material tests were carried out at the end of each development phase of the manufacturing process to ensure the properties used in the finite element models were as close a s possible to those of the final hull. Testing of larger components such as sections of the composite hull and hull joint were undertaken as soon as they became available.

The highest risk to the accuracy of the structural analysis results was the absence of reliable load data defining the worst conditions the vehicle structure would be likely to see in service. Loads used in the analysis were derived from standard conditions used in the development of Warrior. Measured trials data and results of ride models suggested that these conditions were over conservative although experience also shows that the maximum loads experienced by a vehicle is also dependant on the skill and motivation of the driver and crew.

Traditionally the absence of accurate load data has not been a problem in AFV design as the hulls consisted of thick steel or aluminium armour plates whose thickness was driven by ballistic rather than structural requirements. However, the constant development of the weapons used to attack AFV's has led to the situation where sophisticated new armour system are required if the weight of modern vehicles is to be maintained at a practical level. These armour systems employ a combination of different materials

and air gaps to achieve mass efficiencies of two to three times traditional armour systems. The drawback of using these systems is that many of the elements of the system do not lend themselves to performing the role of vehicle structure.

Glass and carbon composites take advantage of the fact that most of these systems employ a spall liner backing to catch fragments and prevent them entering the vehicle, composite materials have been proven to be the most weight efficient materials for performing this role. Increasing the thickness of this spall liner to the point where it can be used as an effective structure provides the opportunity of integrating highly efficient armour systems with vehicle structure for future AFV's. The key to designing these systems is minimising the deviation away from the optimum ballistic configuration which requires that the areal density of the composite hull structure be kept as close as possible to that of the spall liner in the optimum system. To do this effectively it has been necessary to develop a range of modelling techniques capable of accurately predicting the loads on each element of the running gear during simulated worst case operational conditions. These techniques have now been developed to include representation of the structural flexibility of the hull, which provides the opportunity of using tem to predict vibration and provide data for studies into vehicle noise.

Virtual prototype modelling: The techniques developed extend the capabilities of ADAMS mechanical system simulation software produced by MDI which is widely used by the automotive and aerospace industries to model complex systems. The development and analysis of system models, often referred to as virtual prototyping, offers many benefits to the designers and sponsors of new systems. They increase understanding of the physics of the mechanical system leading to more efficient lighter systems, and help the designer to make critical design decisions earlier in development. As the project progresses the simulations become more refined leading to greater accuracy and reducing the need for expensive testing by getting the design right first time.

The techniques developed for the analysis of tracked vehicles consist of two modules. A pre-processing module which automates creation of the complex models, assembling the many components of the system, and creating the constraints and forces which define the interaction of components with each other and the environment. And an analysis module which supports the ADAMS solver in performing the simulation, providing specialised functions for complex conditions such as interaction of the track with the sprocket or the terrain.

The track system is modelled in detail with the mass and inertia of each individual track link and definition of connections and impacts with other track system components represented. The non-linear characteristics of a number of different suspension units including Warrior and Challenger 2 have been defined and successfully simulated in the many models created to date.

Simulation of tracked vehicle systems undertaking extreme manoeuvres in truly three-dimensional environments has now been conducted. The simulations provide detailed information on almost any aspect of the system including position, velocity and acceleration of each component or the time history of the forces at connections and points of impact between components. The force information generated can be used to undertake detailed finite element analysis of components or aid our understanding of mechanisms such as the variation in track tension at different positions around the track.

It is also possible to simulate the behaviour of subsystems such as the gun control system of a main battle tank as it interact with the vehicle. This is achieved by attaching a subsystem model to the vehicle model and solving the model concurrently with a control package such as Matlab. Virtual prototyping offers to opportunity of investigating the performance of new equipment such as weapon systems and identifying any potential problems such as levels of recoil force transmitted to the hull at the design phase.

These techniques have now been successfully validated using data obtained from physical testing of the demonstrator vehicle. Peak loads at the wheel stations were found to be within 10% of measured values for a wide variety of different operational conditions. Figure 3 shows the predicted loads on each wheelstation as the model traverses a gap at 10 kph. A comparison between predicted and measured at the front wheel station is presented in figure 4.

Confidence in the accuracy of predicted values is very dependent on the type of simulation being conducted and the quality of the data used to define the systems components and their behaviour. Work undertaken on light artillery guns has shown that errors of less than 5% are achievable if extensive trials data is available and the behaviour of individual subsystems is validated through testing.

A new facility in the ADAMS software now makes it possible to use a finite element model of the hull structure to produce a flexbody representation of the vehicle structure in the ADAMS simulation that deforms and vibrates in a similar fashion to the physical hull structure. Work on the validation of the vibration predicted by models employing flexbody hulls is continuing. Modal testing of the demonstrator hull shows good agreement with results of the finite element and flexbody models.

Current research is focussing on the detailed characterisation of the parameters that define the interaction of the components in the running gear and their influence on the overal vehicle characteristics. A longer term aim is to evaluate the use of the flexible hull to characterise vibration input into the hull at each source such as suspension and powerpack and feed this information into specialised software for predicting internal and external noise. Noise is a major problem in military vehicles both in terms of the effect it has the crew and from a vehicle signature perspective.

Summary

In view of the findings of the ACAVP programme to date, it is possible to state that composite materials can offer a weight saving over conventional vehicles for future armoured fighting vehicles. Further reductions in weight could be achieved by the use of carbon fibre composite materials and by the ability to accurately model and predict the loading regimes encountered by AFVs.

The ability to model the structure of tracked AFV concepts and in service vehicles has been demonstrated. The successful testing of the produced models compared to the ACAVP vehicle has demonstrated the applicability of using these techniques. The successful modelling of gun systems has also increased confidence in their accuracy. These modelling tools have the potential to lead to increased accuracy in the design load cases for future AFVs leading to optimised structural designs and reductions in vehicle weight. The ability to model the flexibility of the hull and attached components will allow the AFV designers to identify vibration problems at a much earlier stage in the design process. This will help to prevent vibration related crew problems from occurring in the finished vehicle and should increase the performance of subsystems influenced by hull vibration.

Future

The future design of armoured fighting vehicles is difficult to predict but there is a strong desire to reverse the ever increasing weight of AFVs, though predictions of a twenty tonne vehicle operating in the same role as a conventional sixty tonne MBT will be difficult to achieve. Any approach that reduces vehicle weight is obviously of great interest. Composite materials can help to reduce weight but composites are not the answer to every question posed by the already diverse and ever increasing requirements predicted by military doctrine. Composite material solutions must be combined with synergistic vehicle designs and the tools to accurately design the vehicles to meet the anticipated performance characteristics and associated loading regimes. Modelling tools to predict structural loading in vehicles have been developed and studies to identify vibration are on going. The studies have also demostrated that the loads generated by gun systems can also be accurately modelled. By combining theses techniques and investigating the potential to identifying noise both within the vehicle and external to the vehicle would complete the toolset required for a truly virtual vehicle. This is the ultimate aim of the current study.

Acknowledgements

References

1.   R M Ogorkiewicz, "Armoured vehicles of composite materials", International Defense Review, 1989, Vol.22/7.

2.   Janes Defence Weekly 17 June 1995, pp31-32.

3.   A Vasudev & M J Mehlman, "A comparative study of the ballistic performance of glass reinforced plastic materials", SAMPE Quarterly, Vol.18, No.4, July 1987, pp 43-48.

4.   T P Stuart & I G Crouch, "Ballistic performance of resin transfer moulded GFRP panels with integral and machined metallic fixings", DRA Report Unpublished.

5.   F Macianica, "Ballistic technology of lightweight armour", AMMRC, 1981.

6.   M A French "Advanced Composite Armoured Vehicle Platform (ACAVP)",Lightweight Armour Systems Symposium: RMCS, Shrivenham, June 1995

7.   M J Lewis "ACAVP Structural analysis -Final design phase", DERA Report August 1997

Table 1 : Properties of engineering materials at 20°C					
Material	**Density**	**Tensile Strength**		**Young's Modulus**	
	kg/m^3 (ρ)	Absolute MPa (σ_t)	Specific (σ_t/ρ) MPa/(kg/m^3)	Absolute GPa (E)	Specific (E/ρ) MPa/(kg/m^3)
Steel RHA	7850	775	0.10	210	26.8
Aluminium 7017	2750	425	0.15	70	25.5
Titanium (6Al-4V)	4400	800	0.18	110	25
GRP Vf 0.55 Quasi-isotropic (0/-45/90/+45)	1902	300	0.16	22	11.6
CRP Vf 0.55 Quasi-isotropic (0/-45/90/+45)	1520	350	0.23	42	27.6

Vf = the volume fraction of fibres in the composite material. (The numbers in brackets indicate the principal fibre angles)

Figure 1   ACAVP Demonstrator Vehicle
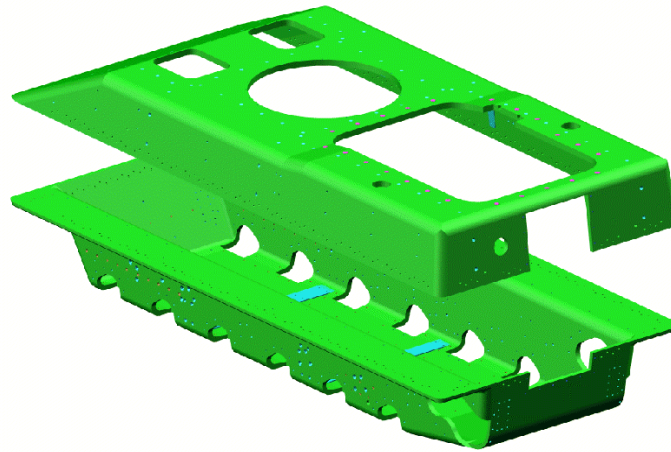
Figure 2   ACAVP Demonstrator Mouldings
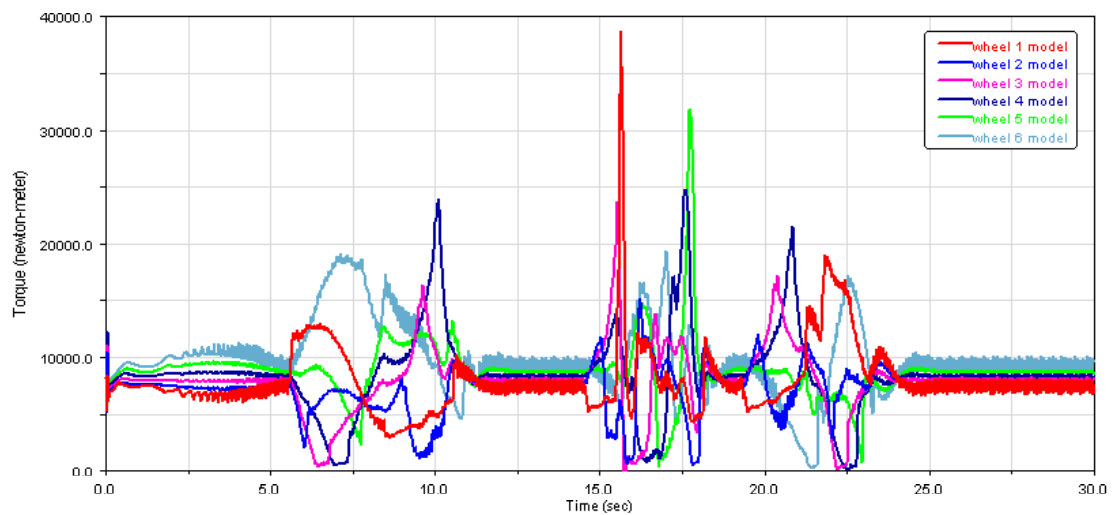
Figure 3 Predicted suspension torque over obstacle
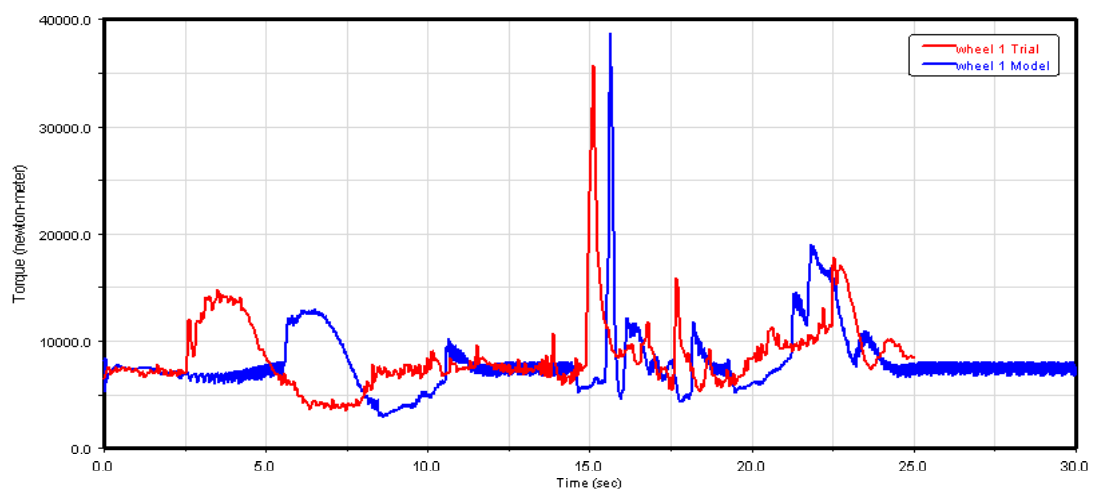
Figure 4 Predicted versus measured torque at front wheel station

Advanced Collaborative Environments Supporting Systems Integration and Design

Grace M. Bochenek, Ph.D. and Kenneth J. Ciarelli
U.S. Army Tank Automotive and Armaments Command (TACOM)
Tank-Automotive Research, Development, and Engineering Center (TARDEC)
6501 E. 11 Mile Road
AMSTA-TR-N (MS 289)
Warren, Michigan 48397-5000, USA

INTRODUCTION

Engineers at the U.S. Army Tank-Automotive Research, Development, and Engineering Center (TARDEC), in cooperation with its commercial and government partners, are combining emerging computer technologies with simulation within distributed multi-functional teams to create robust, collaborative lifecycle processes for Army materiel. As part of a continuous improvement strategy of its simulation-based development and support processes, TARDEC launched an initiative called Advanced Collaborative Environments (ACE) to better link the people and information involved in Army processes. They established new processes supported by collaboration technologies that when employed, help accelerate system acquisition.

The primary objective of this collaborative environment effort is to empower each stakeholder in a system's lifecycle with timely, relevant information in "views" that are understandable and easily accessible. ACE-enabled collaboration permits multi-functional integrated concept/product teams to simultaneously enter a virtual product design world, and jointly evaluate design issues, ideas and parameters, each from their own experience, perspective, and functional responsibility. To accomplish these objectives, TARDEC has invested in two key technologies, web-based information technology (WebIT), and immersive virtual environments (VE), that when coupled together, are catalysts for change.

These tools and organizational capabilities can be applied in any Program Management (PM) office, whether the product under development is a concept or a fielded system. These tools are independently accessible from a personal computer, or on a portable laptop, using WebIT, and/or in a common, shared virtual environment, where an entire evaluation team can come together to exchange ideas.

This paper will demonstrate the importance of collaboration within today's global business environment; will explain the advanced collaborative environment tool set TARDEC developed and assembled (WebIT and Immersive VE); will outline the benefits of their employment, and their use to support issue identification and resolution. Further, we will highlight our experiences, provide insight gained from real applications to the Army's Brigade Combat Team program, and show effects on the Army acquisition process, and identify future directions.

NEW SYSTEM DEVELOPMENT METHODS SUPPORTING VIRTUAL INTEGRATION

Traditional methods of system design and acquisition have often been described as serial and linear. They have also been characterized as a sequence of "throw it over the wall" processes where functional groups make contributions sometimes independent of other internal and external

groups. The problem grows exponentially as a system progresses from one phase or milestone to the next. At the onset of a new milestone, one often experiences an entire change of people, information, and models used for design and analysis. As a result, critical decisions, which can significantly impact overall system design and development, are frequently made without regard to the effect on or consequences to other functional elements, and are made without the knowledge gained in previous phases.

The need to overcome some of the limitations of traditional system acquisition practices is required to meet the challenges of today's dynamic military environment. The Department of Defense has begun a strategic technology and innovation management initiative called "simulation-based acquisition"-- an integrative process designed to promote the rapid and economical development of quality products through the use of computer-based simulation. Implementation objectives of this initiative are to encourage and support iterative, cross-functional team collaboration and early user evaluations. The objectives of this simulation-supported approach are to substantially reduce product design cost, risk, and initial development time while improving the quality and utility of military transportation, weapon, and support systems.

Today, timely system acquisition success relies on the ability of cross-functional teams to share product design information, make informative decisions, and minimize system cycle time. Within this type of environment, it is necessary for individuals to share information and collaborate in the decision making process. This collaboration requires the exchange of information for purposes such as notification and clarification, and the processing of information for monitoring, negotiating, and decision making (Dhar & Olson, 1989).

Cooperation in the early phases of a system's lifecycle ensures that everyone impacted by the design has early access to product specification and relevant information, and has the ability to influence the final configuration, identifying and preventing future problems. Tools that support cross-functional team interactivity provide individual team members with accessibility to information regarding system design versions, soldier operational requirements, system models, and simulation/analytical data. These collaboration support tools also provide team members with the ability to collectively discuss system issues, formulate decisions, and respond to changes. To improve the probability of system success, these tools should allow teams to interact and make decisions from multiple perspectives in a shared information space using accurate information. The immersive virtual environments described in this paper represent one form of collaboration tool that is growing in functionality and use throughout the systems development community.

COLLABORATION TECHNOLOGIES

Many underlying technologies (e.g., modeling and simulation, network computing) form the basis of simulation-based acquisition practices. Two key technologies which compose TACOM-TARDEC's Advanced Collaborative Environments (ACE) initiative to better link the people and information involved in Army processes are: (1) web-based information technology (WebIT), and (2) immersive virtual environments (VE).

Web-based IT makes distributed information accessible in various useable forms and provides automated tools to assist in its processing. The immersive VE improves communication between process participants by providing natural shared views of system information that was previously only available to specialists. Both facilitate the vital collaboration needed in re-engineered life cycle processes.

Web based Information Technology (WebIT)

Key to improving acquisition processes is the ability to connect people and information in a timely and flexible manner. To address this requirement, TARDEC has chosen to use a Web IT framework developed by Parametric Technology Corp. (PTC), called Windchill™. It provides a web-based enterprise information management system with integrated tools to support automated workflow. Unlike existing point solutions that focus on a single department or product, such as data management or PDM, Windchill addresses product and process life cycle management across the extended enterprise.

Windchill leverages the Web's unique decentralized distribution model to "virtually" connect together many autonomous information systems, allowing them to behave as a unified whole. It utilizes existing web environments, leveraging existing investments.

Several automakers are investing in Web-IT and are investigating methods to integrate them into their processes to streamline their development efforts. For example, FastCar, a Daimler Chrysler initiative, links the flow of information from at least six of its major information systems that traditionally have not been able to seamlessly communicate. Focusing on linking finance, engineering, and purchasing, the initiative provides the organization real-time information and decision making. They recognize that designers go through hundreds of variations, and WebIT helps other groups understand what is changing in real-time. Daimler Chrysler refers to this as the "Single Point of Truth," or a unified model, so everyone can see and react. For example, a stamping engineer can watch what's happening to a design so he can make sure the company's stamping plants can actually make the body a designer creates.

One of the unique features of TARDEC's web-based environment is the desktop visualization utility. Windchill offers data visualization through its ProductViewTM component, providing full-featured viewing capabilities for parts, assemblies and drawings. ProductView lets you view data and perform other tasks without requiring access to the application that originally produced the data. Figure 1 shows a soldier accessing virtual models from his desktop. Individuals can use this tool to find data, view it, mark it up for comment and collaboration, analyze it, and take measurements. Some of the features include: (Parametric Technology, 1999)

- data access for all users in a company to any product data
- view 3-D geometric models of complex products
- view shaded, wire frame, transparent, meshed or sectioned models with accuracy
- zoom, pan, rotate, fly through, and explode components of 3-D models
- create animation sequences and enable collision detection
- measure distances including 2-point distance, point-to-axis, point-to-curve, length, diameter, and radius
- view a single geometric model of a large, complex product, even if components were created using different CAD systems
- mark up and analyze any data with dimensions, notes, and sections, and share with others for design reviews and collaboration.

Figure 1 Accessing Product Data from the Laptop

Immersive Virtual Environments

Immersive VE technology (often-called virtual reality or VR) is a suite of 3-D graphics-based visualization software and devices, allowing multiple individuals to concurrently view a virtual system or product model while maintaining natural, human communication. These virtual systems operate within a computer-generated environment with real-time user interaction.

These technologies involve stimulating the human senses of sight, sound, and touch, making users believe they are interacting with real vehicle systems, when in actuality, they are only interacting with computer-generated replicas.

Using VE systems, a team can visualize and interact with a full system, assemblies, sub-assemblies, or components in 3-D -- a concept often called virtual prototyping (VP). Several different but related definitions for this concept exist. Some define VP as a computer-based simulation of systems and subsystems that facilitates immersion and navigation with a degree of functional realism comparable to a physical prototype (Garcia, Gocke, and Johnson, 1994). Others define VP as a mechanism for visualization and testing of computer-aided design models on a computer before they are physically created (Lee, 1995), while others simply define VP as an electronic prototype (Dai & Goebel, 1994).

From these definitions, it can be seen that VP is a simulation-based process that can be used to support the development and acquisition of new products, which is why this technology is of importance to the U.S. Army and other development organizations.

TARDEC has chosen to invest in two relatively new immersive projection technologies--the CAVE^{TM} and PowerWall^{TM} VE systems. These environments allow multiple individuals to concurrently view a virtual system or product model while simultaneously maintaining natural, human communication. As a result, TARDEC researchers and system developers are using this advanced high-end visualization technology to develop future military vehicle systems and to support their long-term use.

The Army has begun to establish methods and processes for the routine use of these immersive projection-based tools in future military procurements. The essence of this strategy is that all phases of system development, acquisition, and support ("womb to tomb") would be accomplished using computer simulation models and VEs.

CAVE^{TM} System Description

The CAVE™system is a multi-person, 10x10x10ft3 room-sized, high-resolution 3-D video and audio environment. The CAVE™ system uses three rear-projected screenwalls, a floor that serves as a screen, our Mylar mirrors, and four Electrochrome Marquee© projectors (Model 9500/P43). Also required are Liquid Crystal Display (LCD) stereoscopic shutter glasses (one set for each user), infrared (IR) emitters (needed for stereoscopic glass shuttering), and an Ascension Flock of Birds© electro-magnetic position sensing system (to detect X, Y, and Z coordinates and orientations of head and hand controller positions). The heart of the system is a high-end capacity Silicon Graphics Inc. Infinite Reality© computer (containing four advanced graphics processors). Also, included with this computer system are four raster manager boards, 128 Mbytes of texture memory, eight 195Mhz Model R10000 processors (used to create 1280x1024 pixel resolution stereo images on each of the four projection screens), and a hand controller (wand). Figure 2 is a picture of the layout of TARDEC's CAVE system showing the four projectors and mirror systems and their orientations. Additional devices integrated into the CAVE™ system are a 3-D sound system and force feedback haptic devices, which provide users with the sense of spatial sound and touch.

As an example, the immersive nature of CAVE technology has been used to support interior system design and ergonomic evaluations. A primary focus for organizations like John Deere, Caterpillar, NASA, the U.S. Air Force, and the U.S. Army TARDEC, has been the application of CAVE technology to support user evaluations of virtual crewstation and operator interaction in these compartments. Other useful applications include visualization and interactive interrogation of volumetric varying data as experienced in the oil industry, molecular modeling, and computational fluid dynamics.

PowerWall^{TM} System Description

Similar to the CAVE system, the PowerWall is a multi-person high-resolution 3-D video and audio environment. This large-scale visualization environment is ideal for group presentations and collaborative design reviews. The TARDEC PowerWall system (Figure 3) uses two rear-projected Electrochrome Marquee© edge-blended projectors that are used to create a high-resolution seamless image. The two-projector system can produce a 2304 x 1024 resolution image. The system is a 14x10 ft rigid flat vertical surface. Models or environments are displayed from the floor to the ceiling.

As in the CAVE, stereoscopic shutter glasses and IR emitters are used to create the 3-D stereoscopic visualization. Most PowerWall systems do not use any position and orientation tracking systems. The lack of head and hand tracking leaves more processing power for improved resolution and minimal system latency. However, in contrast to the CAVE, the PowerWall system does not provide users with a full sense of immersion.

Most applications of Powerwall technology are full 1:1 scale reviews of system or subsystem exteriors. The automotive industry uses Powerwall technology to support interactive digital styling reviews (Celsnek, 1989), virtual showroom reviews (Smith & Leigh, 2000), and aerodynamic flow simulations (Stewart & Buttolo, 1999).

Figure 2 Soldiers Evaluating Virtual Systems in TARDEC's CAVE System

Figure 3 Exterior Full Scale Vehicle View Using TARDEC's PowerWall System

BENEFITS OF EMPLOYING COLLABORATION TECHNOLOGIES

When employed, the U. S. Army TARDEC's collaboration technologies allow cross-functional teams to assemble and solve problems while discussing requirements and design characteristics with the assistance of web-based and high-end computer hardware and software support. This capability provides a common focal point necessary, according to some researchers, for multidisciplinary (managerial, technical, marketing, and manufacturing) groups to resolve issues by sharpening their viewpoints in support of collaborative system evaluation (Barkan & Iansiti, 1993; Horton & Radcliff, 1995).

Both the web-based and immersive virtual environment systems offer the potential for true team interaction. They provide multiple individuals within a work environment to simultaneously view a virtual product or system model. All team members can either simultaneously or independently enter a virtual product design world, and evaluate system issues, ideas, parameters, and performance--each from their own experience, perspective, viewpoint, and functional responsibility. This unique multi-functional virtual system development environment allows all members to become active participants in the development effort, sharing ideas early, recognizing functional dependencies, resolving issues jointly, and making more informed decisions. The design has higher quality and utility because everyone from user to engineer provides meaningful input from the start. Everyone is involved in the process; therefore, everyone has ownership of the outcome. Ultimately you lower system development risk because fewer hidden issues will surface, directly impacting time to field and overall cost. TARDEC's experience having organizations use collaboration technologies and processes verifies these communication benefits and are described later in this paper.

Some of the benefits of employing an Advanced Collaborative Environment approach are:
- Everyone involved in the design and development starts on the same page and stays on the same page from project inception to completion.
- Consensus can be reached because participants can "see" what the vehicle (or other equipment) will look like and what it will do. Throughout the process, there is an interactive on-demand exchange of information, knowledge and experience.
- When used early in the process, changes will have the least impact on cost and schedule, and the highest impact on performance.
- The ACE facilitates working design reviews. Changes can be proposed and made while the project team is looking at the same virtual models, and before bending metal.

- Empowers the warfighters to take a direct, active role in fielding a quality system, thereby maximizing operational effectiveness.
- Expensive waiting for information and delays are virtually eliminated.

TARDEC APPLICATION EXPERIENCE

At TARDEC, earlier application of immersive VE technologies have been applied to conceptual design, product improvements of fielded systems, and most recently, to the U. S. Army's Brigade Combat Team (BCT) program. Over the past year, we have coupled these high-end visualization methods with our WebIT tools to promote even greater access of participants to system designs. The BCT program managers have used ACE-enabled collaboration to facilitate and improve communication between the Program Management Office, soldier user community, safety experts, testers and contractors. From the outset, the TARDEC ACE Group has supported the program's various integrated product teams. This section summarizes TARDEC's experiences to date.

Each of the applications involved placing soldiers, engineers, testers, and/or project managers into a common environment with a virtual representation of a vehicle system, sometimes in its operational environment. Rather than the traditional review process using briefing charts and text descriptions, these participants accessed designs from their desktop, or they were immersed inside the design alternatives and observed the functional behaviors of the systems. The improved communication facilitated by the collaboration technologies significantly reduced the time to reach a common understanding of the proposed alternatives, as well as the time to come to a consensus on many of the evaluation results.

Concept Design Reviews -- soldiers and engineers evaluating and deciding together

Some of the first applications of CAVE technology at TARDEC were its use in exploration and design review of vehicle concepts. The technology supported the Future Infantry Vehicle, Future Scout and Cavalry System, and Mobile Surgical Unit programs.

Future Infantry Vehicle (FIV) Concept Evaluations TARDEC engineers and Combat Developers from the U.S. Army's Infantry Center utilized the CAVE system to support design evaluations of the FIV vehicle concepts and to review user requirements. Prior to using the CAVE, concept development involved frequent site visits to exchange two-dimensional drawings of CAD models contained in briefing charts and text descriptions of requirements. These visits often stretched over many months. During each visit, while reviewing the questions/issues from the last visit, it was clear to the participants that neither group had a common understanding of the previously proposed concept features. Presentation of the FIV concept designs in the CAVE permitted soldiers and engineers to stand next to, inside of, and on top of the virtual vehicles and examine/discuss the various components that surrounded them (Figure 4). Many of the conclusions, which were mutually agreed to in the CAVE, would not have been found until the construction of an expensive hardware mockup.

The immersive tools supported tradeoffs between technical vehicle design and soldier operational requirements. Some of the specific issues the FIV concept review addressed with the CAVE included the following. The space claims for the squad size, which the user desired, looked acceptable on paper but after getting inside the vehicle, it was obvious to all participants that the soldiers were too cramped. Either the vehicle size constraints had to change or the squad size had to change. The location and remote operation characteristics (e.g., field of view) of a small turreted weapon at the rear of the vehicle were agreed to. The layout of stowed equipment was a common discussion topic. The selection of several technologies -- because of their effect on space claims -- was easily justified inside the virtual vehicle.

Without exception, participants thought the FIV CAVE design reviews shortened the process in determining the most promising concept solutions. These are quotes from some of the participants.

"For a year the combat developers and TARDEC engineers have been going back and forth trying to down select from five or six concept designs to a more manageable figure of three. After you guys put these designs in the CAVE, we very quickly (within weeks) had a better understanding, looking at the requirements versus the design options, allowed us to better understand tradeoffs that we would have to make." (Infantry Liaison Officer at TARDEC).

"Now that we have the designs in the CAVE for our collaborative work with TARDEC, we must now add optional movement within short scenarios. Seeing a draft requirement function within an operational environment is much better than a large chart presentation. I want one of these at Fort Benning." (Director, Combat Development Office, Infantry Center, Fort Benning).

"By reviewing the designs in the CAVE with the engineers, discussing characteristics of the sub components allowed me to very quickly compare my requirements to the concept design capability. I am interacting with design, engineers and staff simultaneously. Things become more informal and we quickly get down to business in our tradeoff analysis." (Combat Developer, Fort Benning).

Future Scout and Cavalry System (FSCS) The FSCS program is a joint U.S-U.K. effort with two international teams of contractors developing scout vehicle prototypes. To accelerate the effort, the program began with delivery of the Army's in-house developed FSCS concept vehicle designs. It was important for all participants to clearly understand the concept vehicles already considered and the rationale behind them. The CAVE was used to present the initial designs to the two program offices, the contractor teams, and the two sets of user representatives. Future virtual design reviews using the CAVE of in-process contractor team designs are planned.

For this CAVE application, some functionality in terms of subsystem motion and 3-D sound was added to the geometric models. The functional simulation was used to help describe the operational characteristics of the extensive suite of sensors and a novel elevating mast that supported a sensor pod. Multiple versions of the chassis (e.g., tracked and wheeled) and multiple versions of the weapon system were presented (Figure 5). All were configured in the CAVE to be easily switched interactively so the full spectrum of alternatives was presented and dialog about trade studies supported.

Figure 4 Soldier in Virtual FIV

Figure 5 Two FSCS Vehicle Concepts and C130 Aircraft

In this application, the TARDEC concept engineers matched the support of the other participants because the CAVE reduced the level of effort needed to explain many of the new vehicle technologies, which had been rather difficult during concept development reviews. These are quotes from some of the participants.

"Letting the soldiers see the mast operate and then go up to the top of the mast and actually see what the sensor sees, makes my job of explaining the design and getting their buy-in a lot easier." (TARDEC Concept Team Leader).

"Can the corner of the driver seat be removed so I can see the driver's hands? How long would it take to make that change?" (Noncommissioned officer, Fort. Knox, U.S. Army).

"I can see where the gear is stowed but can I pull the duffel bags and other equipment out of the hatch using the CAVE so that I can assess this design in operation?" (Soldier, U.K. Army).
"What do we have to do to use this technology to conduct our own design reviews during development and for formal reviews?" (Project Manager from one of the FSCS Contractor Teams).

Product Improvement Reviews – program managers and engineers finding the best solutions for field issues

Some recent applications of CAVE technology at TARDEC have involved the evaluation of alternative solutions to fielded system upgrades. The technology supported the Family of Medium Tactical Vehicles (FMTV) program.

Family of Medium Tactical Vehicles (FMTV) In support of TARDEC's ongoing engineering efforts to the Program Manager (PM), FMTV, the CAVE was used to conduct the evaluation of vehicle system upgrades by PM engineers, the PM, and TARDEC design engineers. A specific case involved the assessment of several new tailgate configurations that incorporated an integral ladder. Some of the proposed alternatives that included mechanisms for automatic deployment would have been difficult to describe using only 2-D drawings.

These are quotes from some of the participants.

"It gives us the opportunity to visualize functionality of concepts when reviewing Engineering change proposals." (Chief Engineer, PM FMTV).

"It allows the engineers to see potential interference/integration problems and how items interact together." (FMTV engineer).

"We looked at 5 or 6 solid models of tailgate alternatives in the CAVE. In one review we picked two alternatives that we are now developing detailed prototype drawings for fabrication of hardware to get to the field for evaluation. " (FMTV engineer).

"I would like to defer to my lead engineer's comments but yes, seeing the designs and their movements helped speed up the decision making process. " (PM, FMTV).

Impacting Real Army Programs – Program management office uses collaboration to support integrated product teams and system familiarization

Brigade Combat Team (BCT) The BCT Program involves the development of ten vehicle variants, with the first system being delivery 18 months after contract award. A condensed schedule and minimal or incomplete physical prototypes means soldiers would not have access or

exposure to the system until it rolled out of the factory. Therefore, the ACE strategy is key to meeting the BCT's aggressive schedule. Using collaboration tools, soldiers have become familiar with the designs and are an integral part of the design process. For the past nine months, using ACE tools, the BCT Management Office uncovered a variety of issues for each BCT vehicle configuration, including hard to detect integration issues, safety, and operator-specific issues. They have set a standard for future simulation-based acquisitions -- using ACE, they familiarized key distributed stakeholders with virtual designs, they resolved integration issues early, brainstormed potential configurations, and extended the capability to hundreds of people at their desktops.

System familiarization. In the past design reviews were conducted using traditional 2-D multimedia packages like Microsoft PowerPoint. These methods were the only means of communicating system designs to the Army warfighter. These 2-D representations provided limited understanding of the system and its functionality. Normally one had to wait until a physical prototype was delivered to have real access to the system. Today we don't rely on formal, paper-based reviews. We can use these collaboration technologies to foster real interaction with real contractor designs and have meaningful discussions. For example, vehicle integrated product teams using TARDEC's immersive CAVE system were able to see, crawl around, and begin to understand the operation of a Norway-built remote weapon station four months before the prototype was delivered or before the prime contractor completed the subsystem integration). Soldiers were able to become familiar with the design and were able to begin developing operational instructions and plans for its use.

ACE improves overall system understanding. Adding system or subsystem behaviors to the virtual models makes it clear to all how a system works, functions, and operates. We can show animated sequences of events like the tasks involved in breaking down the remote weapons station for C130 aircraft transportability, or the cycling of a round with an autoloader. Contractors participating in the session easily answer soldier questions like, "Once we remove the six bolts where do we store them?" Since models are 1:1 scale, soldiers can stand in the commander's station and check fields of view for out-of- hatch operation, scan placement of the commander's displays, or evaluate the placement of stowage items. This interactive method of communication forms consensus sooner, which differentiates between concerns users can accept within program constraints and budget.

Resolving Integration Issues. ACE technology helps identify integration problems up-front, eliminating as many problems as possible, thereby reducing risk because fewer hidden issues exist. During a recent virtual design review, the lead engineer from General Dynamics Land Systems, responsible for overall system integration of the Mobile Gun System variant, discovered an orientation problem with the manual elevation and transverse handles of the gun system, and an inaccurate wind sensor placement. These were quickly identified and resolved. Integration problems like these would have been discovered much later in the process, where fixes are more expensive.

Brainstorming Alternatives. ACE supports early brainstorming of potential alternatives. Ideas can be mocked up virtually, reviewed by the team -- allowing many design alternatives to be explored. For example, the Product Manager for the Mobile Gun System was able to brainstorm possible designs for operational doors that house the automatic rounds for the mobile gun system, a real safety concern (Figure 6). The warfighter, product manager, safety, expert and prime contractor were able to discuss possible options in the virtual environment and jointly make a decision on the best design that addresses both performance and operational needs.

Access from the Desktop. Using TARDEC's web-based system, anyone within an organization can access distributed data, search and find information, respond to tasks more quickly, and most

importantly, everyone in the process has the same valuable information at their fingertips. From the desktop, anyone can access the same design data that is used in the high-end VE simulations. Directly from e-mail, someone can easily access the same BCT variant models; they can rotate and view them from any perspective. The WebIT technologies allow participants to examine the issues, make accurate measurements, mark up the design, add comments to help facilitate solutions to problems and make individual inputs part of the entire organization's collaborative environment so that all the parties in the collaboration share the same information.
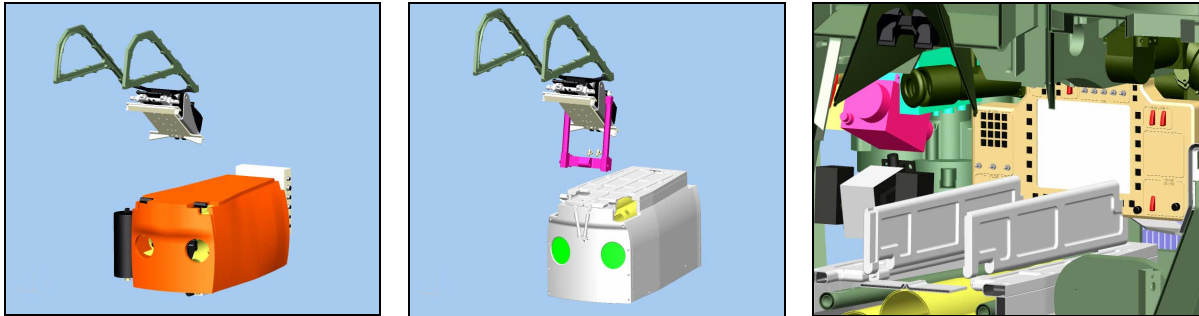
Figure 6 Brainstorming Autoloader Configurations

FUTURE VISION AND SUMMARY REMARKS

Our current global environment is confounded with complexities associated with linking distributed data, distributed information, distributed tools, and distributed human expertise. In some respects it can be considered the "Acquisition Battlefield" of today. Gaining efficiency within this type of distributed environment is the challenge. It is becoming increasingly more important for all stakeholders in ann Army system's acquisition to have visibility into the same information so that they can share a common understanding of the information and the issues, and are thus able to make more knowledgeable decisions in concert with all those involved. An acquisition strategy that focuses on collaboration promotes early and frequent involvement from all participants. Changes made to a design can be quickly assessed, and its impact to various aspects of a program to include cost, training, to logistics can be evaluated in real-time.

The U.S. Army TARDEC has chosen to establish an Advanced Collaborative Environments program and to invest in web-based information technology and new VE technology--the CAVE and PowerWall systems. Over the past two years, TARDEC established a functional immersive virtual simulation-based environment, and more recently, coupled it with information management tools to facilitate a truly integrated business environment. The ACE strategy has been applied to several real Army vehicle programs, involving real Army soldiers to resolve real Army challenges. This capability promotes the assembly of cross-functional teams to identify and resolve potential system problems early in the system development/upgrade process, where the cost of changes is reduced. Importantly, this technology allows multiple individuals to have access to early system designs and information so that all the voices of a system integration and design effort are heard. This technology supports the U.S. Army's need to significantly improve present acquisition activities and to move into a simulation-based acquisition era. However, some challenges still exist. Cultural acceptance in system processes and developing capable and trained technical people to implement these concepts still remains.

REFERENCES

Barkan P. and Iansiti M. (1993). Prototyping: A tool for rapid learning in product development, <u>Concurrent Engineering: Research and Applications</u>, vol. 1, pp. 125-134.

Celusnak, T. R. (1998) Virtual Reality in Automotive Design: Putting the "Reality" into VR. <u>In proceedings Virtual Design for Manufacturing Conference</u>, Detroit, Michigan, SAE.

Dai, F. and Goebel, M., (1994) Virtual prototyping--an approach using VR techniques, <u>Computers in Engineering</u>, vol. 1, pp. 311-316, ASME.

Dhar V. and Olson M. H. (1989). Assumptions underlying systems that support work group collaboration. In <u>Technical Support for Work Group Collaboration</u>, M. H. Olson, Ed*.,* pp. 167-182, New Jersey: Lawrence Erlbaum Associates.

Garcia, A. B., Gocke, Jr. R. P., and Johnson Jr., N. P. (1994). <u>Virtual Prototyping Concept to Production</u>, Fort Belvoir, VA: Defense System Management College Press.

Horton, G. I. and Radcliff, D. F. (1995). Nature of rapid proof-of-concept prototyping." <u>Journal of Engineering Design</u>, vol. 6, no. 1, pp. 3-16.

Lee, G. (1995). Virtual prototyping on personal computers. <u>Mechanical Engineering</u>, vol. 117, no. 7, pp. 70-73.

Parametric Technology (1999) ProductView Online Help

Smith, R. C., Pawlicki, R.R., Leigh, J., and Brown, D.A. (2000). Collaborative VisualEyes. <u>In Proceedings International Projection Technology Workshop</u>, Ames, Iowa.

Stewart, P. and Buttolo, P. (1999). Putting People Power Into Virtual Reality. <u>Mechanical Engineering Design</u> pp. 18-22

Paper #9
Discussor's name R. McClelland
Author G. Bochenek

Q: 1) What is the cost to set up a CAVE?
   2) Will it come down?

A: 1) $700,000-800,000 US plus the cost of the computer
   2) Yes. In the future, PC's will replace the high cost computers and the cost of the projectors will come down.

A Data-Centric Infrastructure for Multidisciplinary Analysis Integration and Management

Jean-Yves Trépanier   François Guibault   Benoît Ozell
CERCA (Centre de Recherche en Calcul Appliqué)
5160 Boul. Décarie, Suite 400
Montréal, Québec, Canada, H3X2H9

email: firstname.lastname@cerca.umontreal.ca

Abstract

This paper presents the overall architecture of the VADOR application framework. The purpose of the VADOR framework is to enable the seamless integration of commercial and in-house analysis applications in a heterogeneous, distributed computing environment, to allow the deployment of automatic design optimisation algorithms and to provide a comprehensive data-management infrastructure for design and analysis data. The emerging database will then provide the basis of a future knowledge-based engineering system and will allow IT links with other IT systems in the enterprise. A multi-tiered client-server architecture has been devised, which comprises a client GUI for interactive data definition and execution launching, separate data and execution servers, and autonomous remotely executable application wrappers.

1.0 Introduction

Computational-based design, including computational fluid dynamics (CFD) and computational structural dynamics (CSD), to name a few, are key technologies in the aerospace industry and are now part of the daily work of engineers. However, such a highly complex computational-based design environment, composed of a mix of commercial and "in house" programs tailored to the specific requirements of the design and analysis tasks, the application of multidisciplinary analysis and optimisation (MDO) practices faces a number of significant challenges, including integration, collaboration and data sharing and management. In this context, there is a need for a software infrastructure which will integrate heterogeneous applications, enable data sharing and collaboration, and insure proper data management.

In addition to these requirements for MDO applicability, there is currently a broad effort in organisations to leverage information technologies in order to enhance the access to information at all levels in the enterprise. Large companies are deploying ERP and PDM systems to better organise their information. At the technical engineering level, information is often residing in the engineers' experience and a system which could capture this information could be of a great benefit for the engineering departments as well as for the enterprise.

These two needs are at the heart of the VADOR (Virtual Airplane Design Optimisation framewoRk) project, and the specific objectives of the project are:

- To develop a state-of-the-art software framework capable of supporting an MDO paradigm in a collaborative design environment.
- To develop a comprehensive data-management infrastructure allowing to closely follow the design data used and shared by the design team and which will provide the basis of future knowledge-based engineering systems and IT links with other IT systems in the enterprise.

2.0 Framework Design and Architecture

The VADOR framework is an object-oriented infrastructure which manages files, groups of files, programs and processes and maintain a database which stores the links between these basic objects. The next section presents the main characteristics of the framework.

2.1 Data files

Objects called *DataComponent*, or *DC* encapsulate the data files in the framework. An *AtomicDC* encapsulates one data file of a given type. The description of more complex groups of files is performed by allowing user-defined hierarchical composition of *DataComponents*. The definition of *Composite DataComponent*, or *CDC*, contains a list of *AtomicDC* types or *CompositeDC* types. *DC*'s and *CDC*'s encapsulate the file references (URL) and a large set of attributes required for data management which are all stored in a relational database.

2.2 Programs and processes

VADOR provides a model for the encapsulation of the programs and processes used to create the data and provide mechanisms to logically link data and processes at an abstract level. A program, which can be any piece of software requiring some data files as input and producing some data files as output, is encapsulated in an object called *AtomicStrategyComponent* A process, which is an assembly of programs to be executed in a controlled sequence of operations, is encapsulated in a *CompositeStrategyComponent*. Programs and processes are fundamentally defined in relation with the type of *DC* that they produce and the type of *DC* they require as inputs.

2.3 Distributed Architecture

The distributed architecture of the VADOR system is illustrated on Figure 1. The main elements of the system are: the Graphical User Interface (GUI), the Librarian Server, the Executive Server, the CPU Servers and the Database Management System (DBMS).
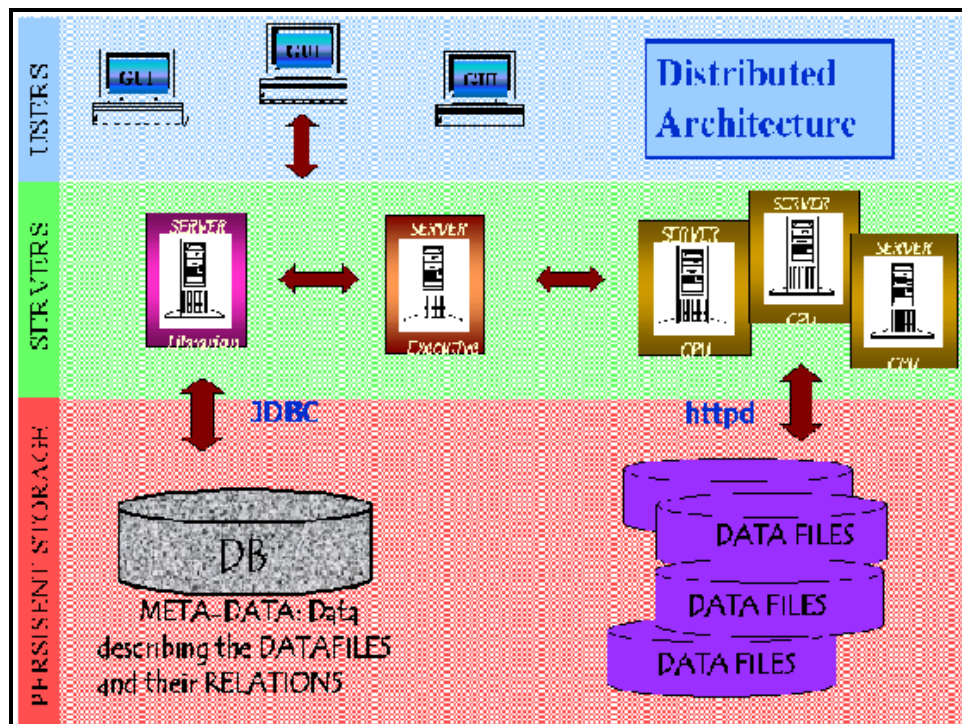
Figure 1 The distributed architecture of the VADOR system

2.4 Graphical User Interface

The VADOR GUI, shown in Figure 2, is a Java program running on the user's machine which provides an interface between engineers and the VADOR services. VADOR provides two main classes of services: the first class of services concerns the data and process definition and the tools registration. This is performed via four different tools called **BUILDERS**. The second class of services include data management services, automatic execution of processes and data inspection tools. These two classes of services are described below.
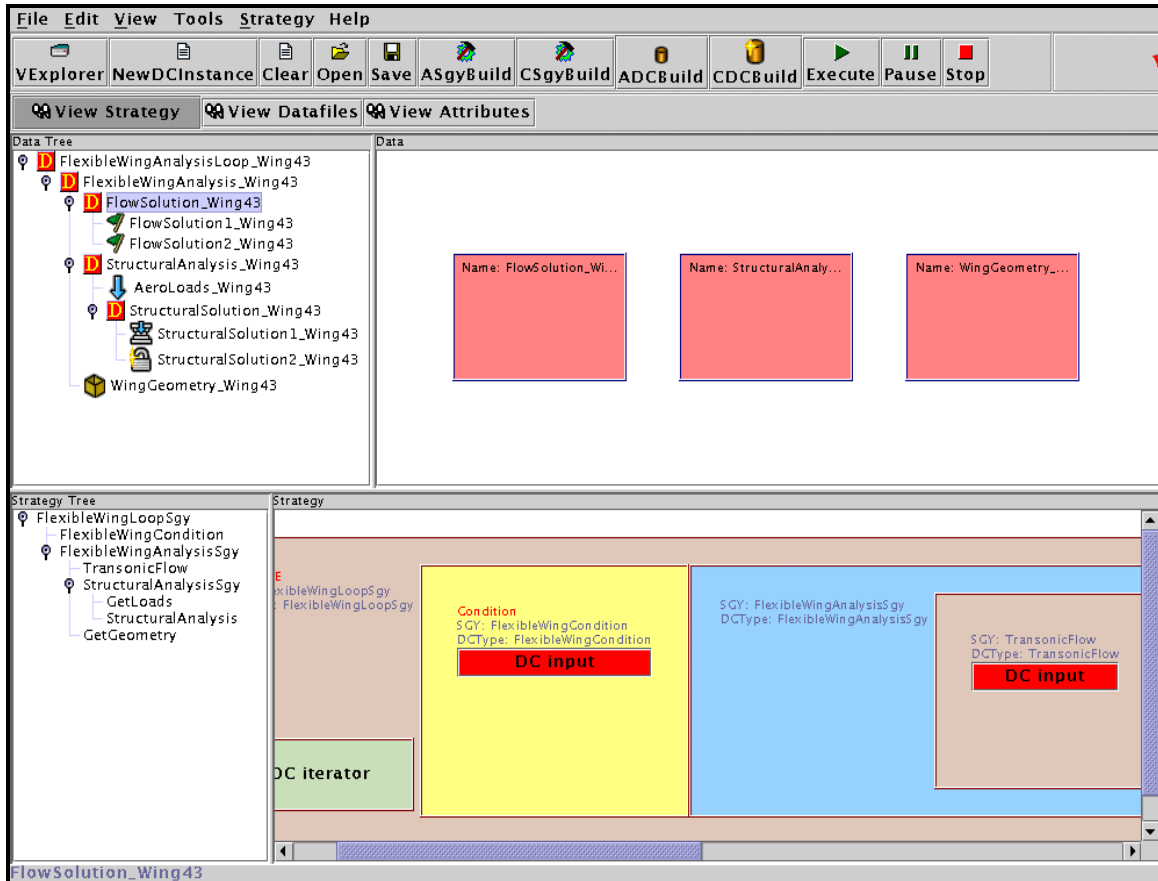
Figure 2 The VADOR Graphical User Interface

2.4.1 Builders tools for data and process definition

The GUI provides tools to define *DataComponents* type and to define *StrategyComponents*. The tool used to define an *AtomicDataComponent* type, called the AtomicDCBuilder, is illustrated on figure 4. A different dialog box, called the CompositeDCBuilder, illustrated on figure 5, is used to construct a hierarchical composition of data into a tree structure. The tool used to encapsulate programs into *AtomicStrategyComponents* is called the AtomicStrategyBuilder and is shown on figure 3. A separate window, called the Composite Strategy Builder is used to describe processes including loops and if constructs. A view of the Composite StrategyBuilder is given on figure 6. On this figure, a strategy consisting of three sequential programs is modelled, each program having its own inputs and producing an element of a hierarchical *DataComponent* shown in a tree view on the left. The complete strategy is producing a *Composite DC*.
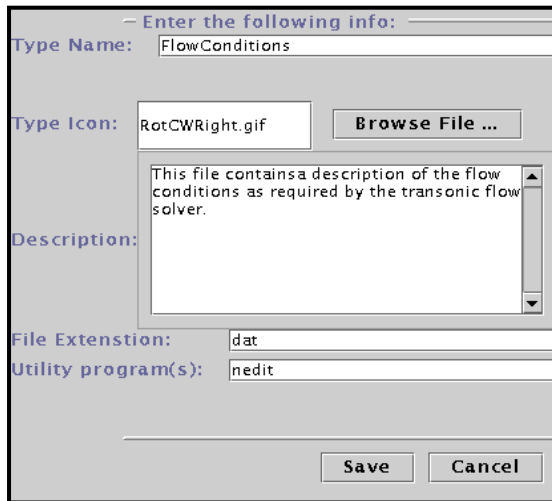
Figure 3 The Atomic Data Component Builder   **Figure 4 The Atomic Strategy Builder**
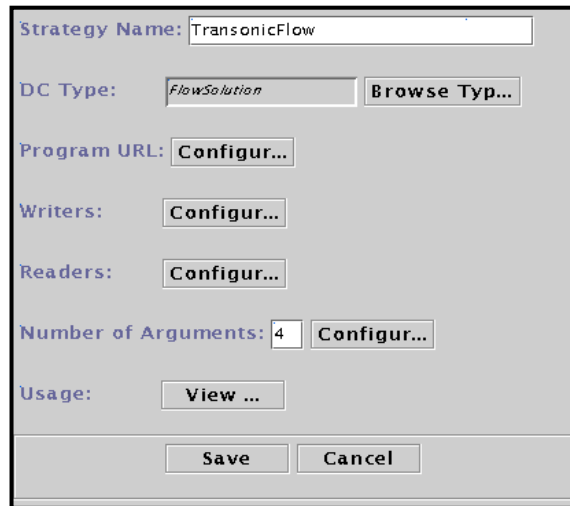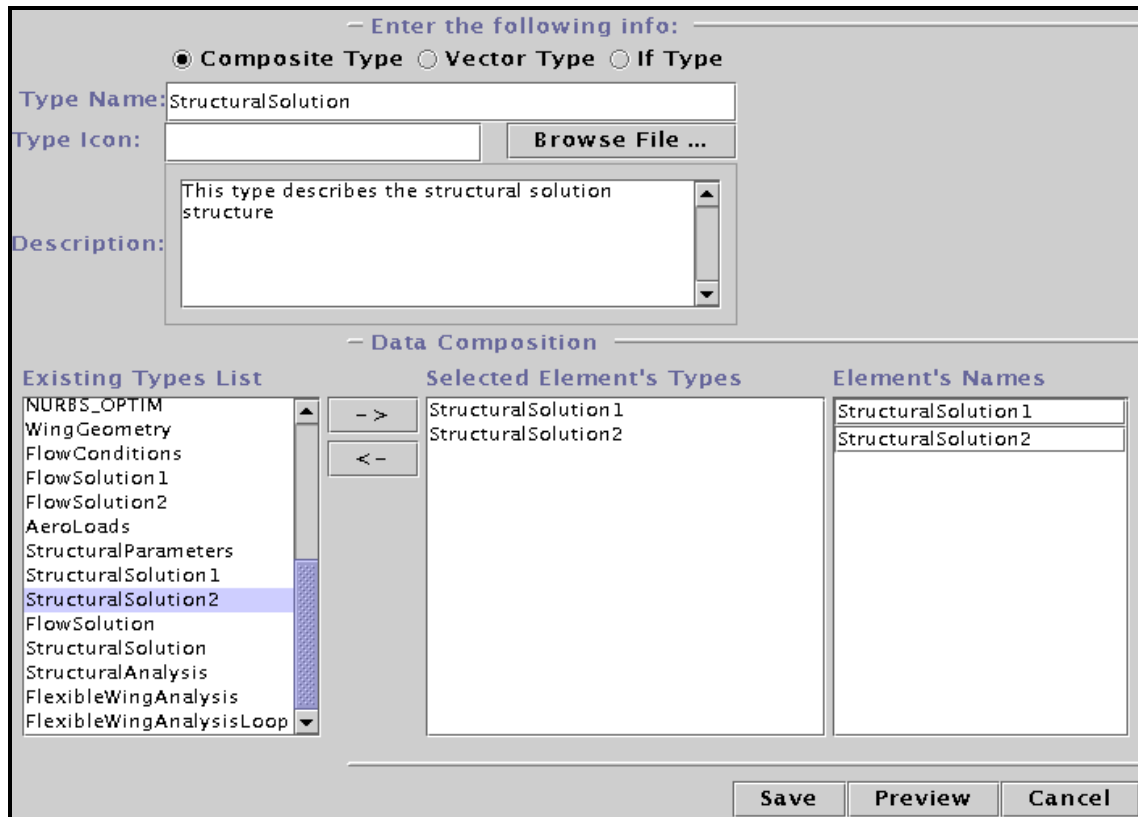
Figure 5 The Composite Data Component Builder Dialog Box

2.4.2 Data Management, Automatic Execution and Inspection Services

The data management services provided by VADOR includes a data classification layer and an automatic naming scheme for *DataComponents* and data files created under the system. A view of the VadorExplorer, the GUI window giving access to the classification layer, is shown on the figure below.

Using the information encapsulated in the ***DataComponent*** attributes, VADOR allows users to trace the upstream history of a given piece of data including the creator of the data, the programs used to create the data and the input data used. Users can also be informed on the downstream influence of a given piece of data by asking which data has been produced using a given piece of data as input. These services results in a comprehensive documentation about data dependencies and data influences.

Design and analysis work is performed in the system by first selecting the type of data to create in a user-defined list and then by selecting a strategy to create the data. Only the strategies which have been defined in the definition phase for the type of data to be created will be presented to the user. Once the data type and strategies are known, the system will generate a new instance of data, pointing to empty data files, and will ask the user to complete the definition of input data files to the programs. Again, files will be requested for various types, as described in the integration phase. After the selection of input files, the process is ready for execution and the user can select machines where the programs are to be executed and launch the execution. The control will then be passed to the executive server until the process execution terminates.
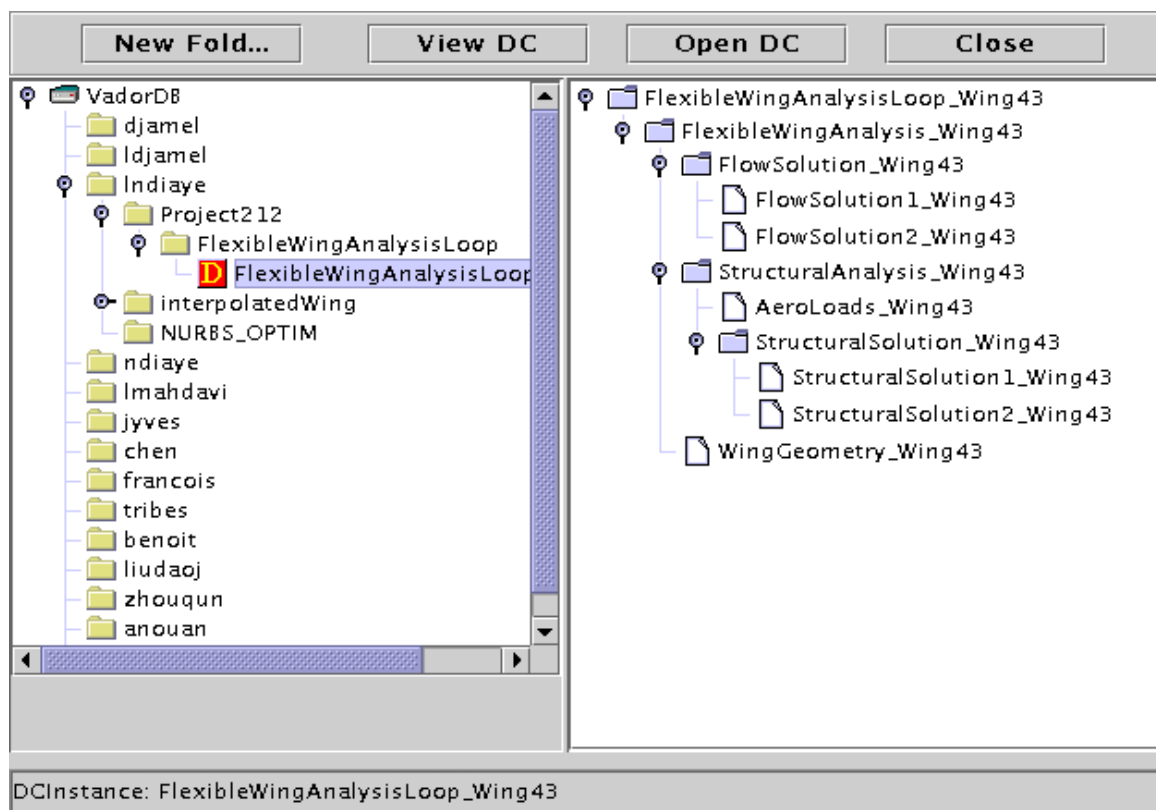
Referring to Figure 2, the upper half of the main window provides a graphical representation of a ***DataComponent***, where a tree representation is used to display on the left the composition of a hierarchic ***DataComponent***. The leaves of the tree represent the actual data files and their type can be easily identified by the corresponding icon. Individual rectangles shown in the right window identify individual ***DataComponent***, enabling selection and queries to be made on their contents. Utility programs, defined in the DCBuilder tool, can be invoked from the menu or the mouse in order to edit or visualise the contents of the encapsulated data files.

The lower half of the main window provides a graphical representation of the ***StrategyComponent***, where a tree representation is used to display the composition of a hierarchic ***StrategyComponent***. The complete ***StrategyComponent*** is graphically represented by recursively including ***StrategyComponent*** within each other.

2.5 Librarian Server

The Librarian Server is the central Component server in the VADOR system. The Librarian is providing services for the handling and archival of Components. The Librarian stores permanently the components in a relational database using the JDBC driver. Details about the organisation of the database are given below.
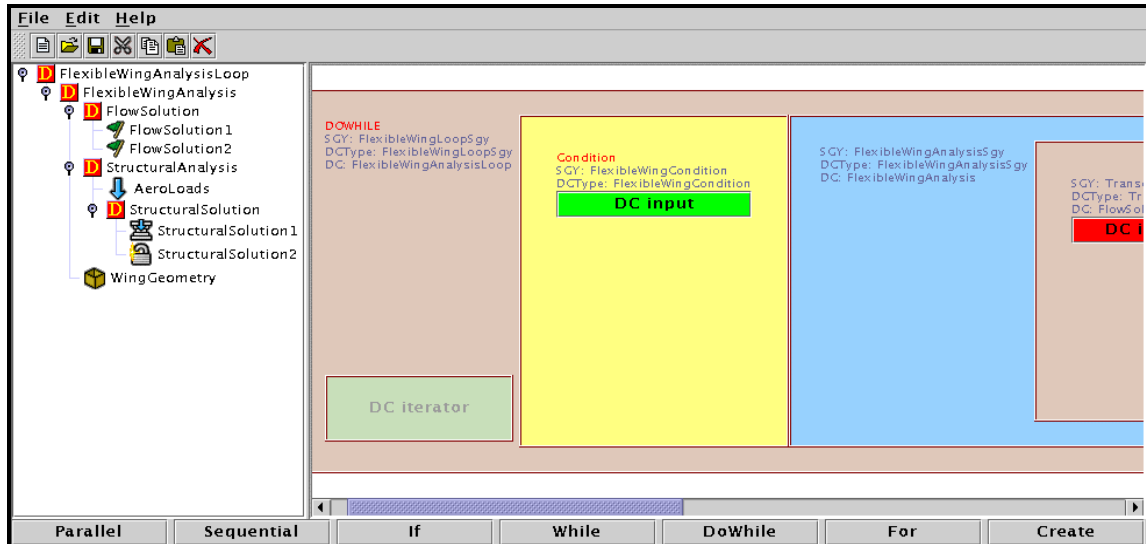
Figure 6 A view of the Composite Strategy Builder used to define processes

2.6 Executive Server

The Executive is a Java server program that manages the execution of *StrategyComponents* to create *DataComponents* on a distributed network of heterogeneous computers. It answers the needs of process automation in an heterogeneous distributed environment. The Executive is a multithreaded server capable of handling multiple tasks. The Executive interacts with the Librarian to retrieve *DataComponents* to be created and to update the database contents after execution. The Executive usually receives simple requests from the GUI to create *DataComponents* and it communicates with the Librarian to retrieve the *DataComponent* object. It traverse the Strategy Tree to generate the data creation sequence and it communicates with the CPU Servers on different hosts to run the analysis programs. During the execution process, it notifies the Librarian server after execution of each program in order to update the status of the components in the database.

2.7 CPU Servers

CPU servers, also called wrappers, are Java server programs waiting for requests on machines where analysis programs are to be run. The CPU servers wraps any scripts or executable programs on specific machines. The CPU Servers have the responsibility to run analysis programs with a list of I/O files and flags transmitted by the Executive Server. The result of the execution of the programs are the creation of the data files encapsulated in the *DataComponents*. The CPU Servers also have the responsibility to get the input files required for the execution and put the output files to required locations after execution. File transfers are performed under the control of the CPU Servers using standard web servers for downloading and uploading files. The analysis programs are usually executable legacy programs to be executed on a specific machine, or a few machines, on the network. Note that the execution time required to run these programs can vary from a few milliseconds to many days, depending on the specific engineering analysis to perform.

3.0 Process example

A process in the VADOR framework is a controlled sequence of program execution which is used to produce complex data. Processes are encapsulated in Composite *StrategyComponents* objects which are defined by the users using standard elements of structured procedural programming languages: sequential blocks, parallel blocks, if constructs and controlled loops. The figure shows a typical process which will be used to illustrate the definition of a Composite *StrategyComponent* used to create a Composite *DataComponent.* In the figure, parallelepipeds indicate files and rectangles indicate programs.

First, we need to define the data produced by the process. This is done by defining the Atomic DC types A, B, C, D, E, F, G, H. We also need to define a composite data type C-PLUS-D to encapsulate the output of the program P1. Considering the fact that the A and B types are not part of the process but are rather inputs to the process, we need to define a composite DC type C-TO-H containing one C-PLUS-D, and one E,F,G and H respectively to encapsulate the output of the complete process. The composite DC type C-TO-H will encapsulate 6 data files.

The process is modelled as a sequential process composed of three blocks. In the first block of the sequence, the program P1 produces a C-PLUS-D type DC using an A type DC and a B type DC as input. In the second block of the sequence, the programs P2 and P3 are executed in parallel, the P2 program producing an E type DC using a C type DC as input and the program P3 produces an F type DC using a D type DC as input. The third and last block of the sequence contains an if construct with its associated True and False branches. The test uses input data contained in either or both the E and F DC types to branch. In the FALSE branch, the P4 program produces a G type DC using a E and a F type DC as input while in the TRUE branch, the P5 program produces a H type DC using the same input. It is clear that at the end of the process, either the G or the H type DC will be pointing to a non-existing data file.
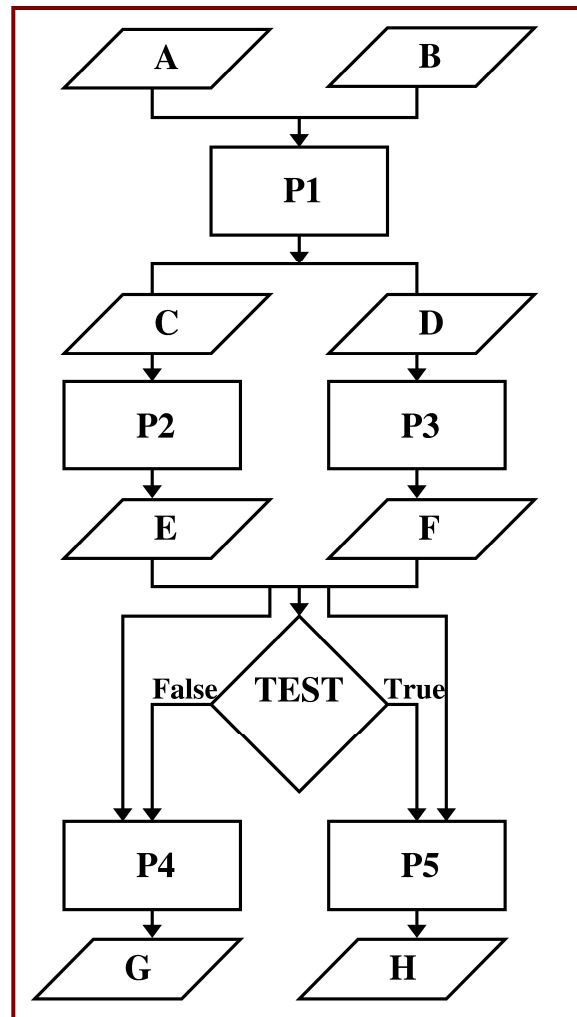
Note that there is clear separation in the system between the sequence of execution and the dependencies. For example, the system allows one to describe a process which will use as input a file which will be produced later in the process. This provides flexibility in the description of complex process. However, at execution time, the process may not be able to execute and appropriate messages will be generated.

4.0 Relational Database

VADOR make use of a standard Database Management System (DBMS) to store and access information describing the various Components. The DBMS currently used by the framework is the MySQL DBMS, a publicly available system which stores information using a relational model using the standard SQL language for database queries. A view of the various tables and their relations is

reproduced using the UML representation on figure 7. It is important to emphasise that the present data model separates the engineering data usually contained in data files, from descriptive information. Only the descriptive information, or metadata, is stored in the relational database. The users' data files (potentially large files) will usually reside where they have been created by the application programs.

Devising a schema for a relational data model is not a simple task and the tables contents and their relations as currently described in figure 4 are the results of a few iterations and will probably require adjustments in the future. The final schema, or data model, will be one of the main results of the VADOR project since it defines the core of the system on which everything else is built. It also defines the information that the system will be able to provide to other IT systems through appropriate APIs.

4.1 Data and Process Definition Tables

Referring to figure 4, the first table, called the DCDefinition Table stores the definition of Atomic and Composite DataComponents Types. When the DC type is Composite, the elements of the composition are listed in the Table DCElements. The DCDefinition table identifies each type of data in the VADOR system by a unique typeID, known as the Primary Key (PK) of the table and associates with this typeID a typeName, a typeIcon, an IsAtomic field and a Description field. The typeName is given by the user and is required to be unique. The typeIcon refers to an icon file managed by the system which will be used by the GUI to provide visual recognition of the *DataComponents* based on their type, as shown in figure 2. The IsAtomic field allows to distinguish between Atomic and Composite DC types. The Description field is a string given by the user at the moment of the type definition which will be later accessible through the GUI for information on types. Composite DC are defined in the table DCElements. Every element appearing in a composite DC type has a unique dcElementID, has a dcElementName, has a ChildID, has a counter and has a typeID. The typeName should be chosen carefully to match engineering practices and an Icon should be designed for visual support.

Programs and processes are defined in the table named StrategyDefinition. A relation is present between the StrategyDefinition Table and the DcDefinition Table, indicating explicitly the DC Type that the strategy can create. A Composite StrategyComponent is described by its elements stored in the StrategyElements Table.

The above described four table are the core of the data and process definition in the VADOR framework. Note that users will not in general need to deal with the database tables but only with the GUI presented previously.

4.2 MetaData Tables

The central table for metadata storage and management is the DcInst table which stores instances of *DataComponents*. DC Instances encapsulate single data file or groups of data files and attach to these files metadata information. The table has two fundamental links with the Definition tables. First, the DcInst table has a relation with the DcDefinition table in order to uniquely define the type of data described by the instance. Second, the DcInst table stores the strategy used to create the data through a relation with the StrategyDefinition table. The DcInst table contains general descriptive information about the instance required for data management. For a composite DC type, the elements instances of the composition are listed in the DcElementsInst table.

The DcInst table also has numerous relations with various tables in order to provide additional information and control on the data. Relations with the DcAccess table enable a flexible control on access permission to the data on a user base. Relations with the ExternalInputDcInst table allow to uniquely identify the data used as input to processes and thus provide comprehensive forward and backward dependencies capabilities. The ExecutionInfo table will store information about the execution statistics and will enable future deployment of load balancing capabilities. Relations with

the DcFolder enables the efficient classification of the data based on user's defined projects through the VADOR Explorer.

5.0 Conclusion and prospective

The object-oriented methodology has been used in the development of a data-centric framework. The implementation is done using the JAVA computer language. Collaboration and data-sharing are enabled through the usage of the concept of Components and through data standardisation. Two kinds of components have been defined: DataComponents and StrategyComponents. DataComponents encapsulate the design-and-analysis data while StrategyComponents encapsulate the design-and-analysis workflow. In order to provide data management capabilities, the components have a set of attributes, including the owner, access permission, history, comments, status and more. In order to promote standardisation, user defined data types are introduced, which are then used for validation and documentation. DataComponents and StrategyComponents are hierarchically arranged, i.e. they may contain other components, giving the capability to describe the most complex problems. The leaves of this composition are called the atomic components. The atomic DataComponents encapsulate exactly one data file, while the atomic StrategyComponents encapsulate one program or script.

The VADOR system results from the assembly of distributed servers, allowing scalability in a multiple users environment. The Librarian server provides access and storage services for DataComponents and StrategyComponents. The Executive server controls the execution of sequences of analysis programs. The CPU servers, or wrappers, run analysis programs. File transfers are performed via standard Web file servers. A relational database stores data references and attributes as well as data creation strategies. VADOR uses standard SQL databases for portability.

The current version of the VADOR framework is a flexible and configurable software, adaptable to the needs of every engineer. It is capable of representing information, including data and methods, uniformly from the enterprise work flow charts to the detailed engineering tasks. It allows process execution automation on a distributed network and enables sharing of data and methods while providing critical information to all users on the location and owner of data and methods, the methods used to produce the data and the status of data and tasks. The integration of data and processes into the framework enforces documentation of data formats and methods, and as a result promotes standardisation.

The VADOR team is currently implementing various additional services in the framework, including a load monitor and balancing facility, a data register where users can indicate their interests on specific events related to data or strategies, and the generic implementation of optimisation strategies. Future directions include a comprehensive support of generic design strategies, including formal decomposition methodologies for MDO problem formulation and optimisation. Efforts will also be deployed to define and use standard data descriptions for seamless data exchange between heterogeneous applications.
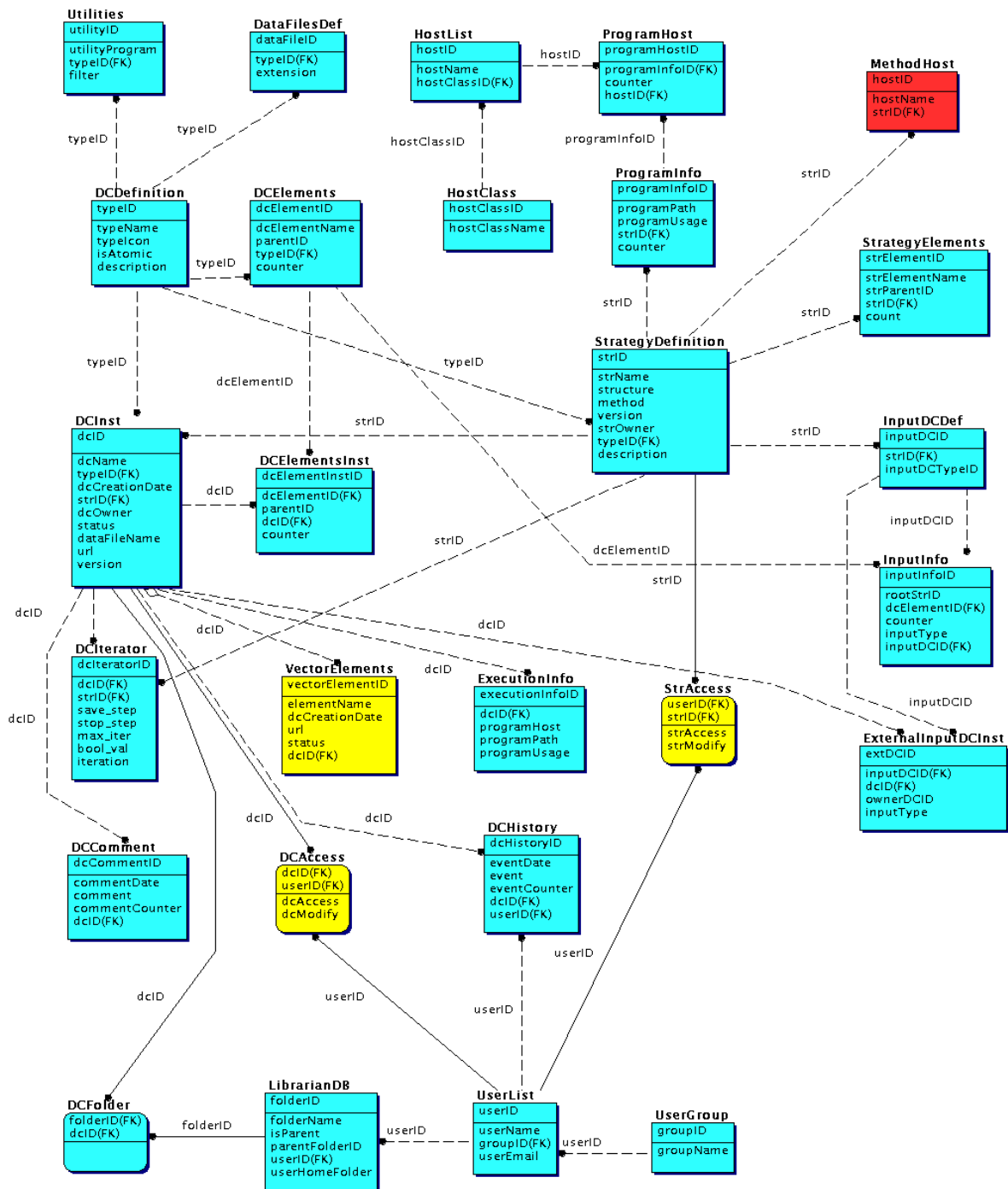
Figure 7 Relational Database Tables and relations

Paper #10
Discussor's name M. Stevenson
Author J. Y. Trepanier

Q: 1) How is geometry handled in the system?
    2) How do you handle computational requirements vs. database complexity?

A: 1) The system is managing files. Geometry files, such as CATIA files, can be referenced by the system as external input files. Then, specialized translation programs are used to extract data from CAD files and produce the files required for analysis work. In some cases, the process of preparation of input files for analysis from the CAD files is manual.
2) The system will store computational requirements for each task performed under the control of the system based on information gathered during execution. This information will constitute a rich database enabling the correlation of computational requirements with data and process attributes. This will then be used to estimate CPU requirements for a given task and to feed a load balancing facility.

This page has been deliberately left blank

———————————

Page intentionnellement blanche

Process Modelling of the Fabrication of Critical Rotating Components for Gas Turbine Applications

R.C. Reed
Department of Materials Science and Metallurgy
University of Cambridge
Cambridge CB2 3QZ, UK

P.D. Lee and M. McLean
Department of Materials
Imperial College of Science, Technology & Medicine
London SW7 2BP, UK

Abstract

The fabrication of rotating components for a gas turbine engine requires a number of different manufacturing processes: casting, thermal-mechanical shaping (from ingot or powder), heat-treatment, machining and joining. Numerical algorithms and advanced computer hardware/software are being used increasingly to simulate these manufacturing processes and the materials behaviour resulting from them that controls the service performance. The purpose of this paper is to provide the reader with a flavour of the range of research that is being carried out, the benefits that it confers and its current limitations. Finally, some challenges for the future are identified.

1. Introduction

The fabrication of critical rotating components for the hot sections of gas turbine engines, from premium grades of nickel-base superalloys that have been designed specifically for their excellent mechanical behaviour at elevated temperatures, requires a number of different manufacturing processes. These include melting and investment casting, thermal-mechanical working (including forging and rolling), heat treatment, machining and welding (see Fig. 1). The manufacturing stream is complex and normally involves a number of specialist suppliers. Among the characteristics of the manufacturing cycle are: (i) the period required for processing and hence delivery can take many months and involve international transport between various stages, (ii) these delays tie up capital with obvious costs which can be exacerbated by material losses, (iii) the complexity of the manufacturing process can lead to fragmentation and loss of data certifying the quality of material and its susceptibility to performance-limiting defects, and (iv) there is a barrier to responding quickly to changes in specification and the requirements of the end-users, i.e. the gas turbine manufacturers.

Computer modelling is currently being used for the simulation of different stages of the manufacturing process in an effort to deal with these difficulties. In fact the accuracy, speed and sophistication of the computation are improving to such an extent that very significant benefits are now being derived. In the present paper, a number of case studies will be presented which are representative of the UK's state-of-the-art in this field, termed *process modelling*. In the past decade or so, progress has been made at coupling treatments of the *macroscopic* characteristics of the processes to the response of the material on the *microstructural* scale. This is an important stage in relating the process to eventual service
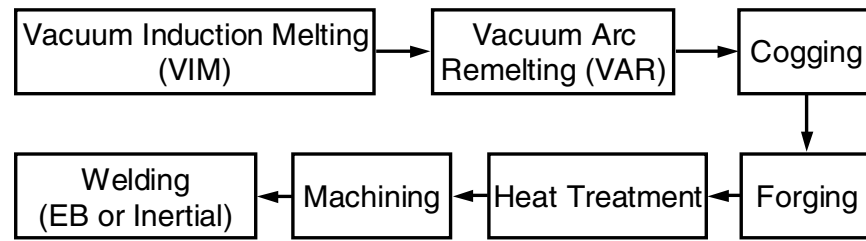
Fig. 1. The manufacturing processes used for the fabrication of turbine discs arrangements.

performance. An important characteristic of the UK process modelling has been extensive collaboration with the gas turbine manufacturers and materials suppliers, who have provided access to manufacturing facilities on the factory floor; these have been instrumented for targeted trials designed to test and calibrate the models. In the final part of the paper some challenges for the future are identified.

2. Background

In order to appreciate the value of process modelling in this context, it is helpful to consider some of the processes in a little detail. Consider first a 'secondary' melting process such as vacuum arc remelting (VAR). Its main purposes are to improve the chemical homogeneity of the ingot by eliminating the gross segregation, which is inherited from 'primary' vacuum induction melting (VIM), and to produce a sound defect-free ingot for subsequent thermal-mechanical processing. The aim of the modeller will be to help the manufacturing engineer to achieve this homogeneity and material soundness by control of the process variables under his control. In practice, the modeller will make predictions of: (i) the location of the fusion boundary, and any alteration to its location due to changes in processing conditions, (ii) the fraction of the billet that is not subject to steady-state or stationary conditions, (iii) the typical average microstructure that results from the process and (iv) the likely occurrence and stability of defects such as *white spot* or *freckles*, which occur when pieces of the electrode remain unmelted after entering the molten pool or there are convectional instabilities in the melt. Computer modelling represents a very powerful tool for the analysis of these effects.

The use of process modelling for the simulation of the subsequent thermal-mechanical shaping processes can also be contemplated. A typical VAR ingot needs to be worked repeatedly in a 'cogging' press in order to refine the as-cast grain structure through repeated sequences of recrystallisation and deformation, which have the further effect of reducing microsegregation. An accurate treatment of these phenomena is the challenge to the modeller. Predictions of the rate of recrystallisation are potentially valuable, so that excessive cost is not incurred due to unnecessary stages in the process. Closed-die forging operations are also amenable to modelling; predictions which might be required include the manner in which the die cavity is filled, so that the deformation sequences can be designed in an optimal fashion, and so that the susceptibility to forging defects can be assessed. Finally, an elastic-plastic analysis of the heat treatment of the blank turbine disc forging is necessary, since residual stresses result from the significant thermal stresses which originate from the quenching operation. These must be known so that any subsequent machining sequences can be chosen appropriately.

Finally, there are examples of assembly processes such as joining, which are highly amenable to modelling and simulation. Consider for example the high-pressure (HP) compressor sections of the aeroengine, which are now often manufactured from superalloys, since the operating conditions are beyond the temperature capability of titanium alloys. The assemblies require joining, often by electron beam welding. Process simulations are useful

for the prediction of weld-induced distortions which can sometimes be so large that they exceed the pre-defined tolerances, leading to excessive non-conformance and scrap. Higher strength superalloys are joined by inertia welding, and here significant advantages have been gained through the use of modelling for the optimisation of tooling and jigging arrangements.

In the past, there has been a tendency to treat each stage of the process cycle in isolation. However, the major challenge now facing researchers and industry is to address the complete manufacturing chain to produce compatible and interacting models that can optimise the production of critical components, both in terms of quality and cost. To this end, a multi-institutional initiative is under way in the UK, within the EPSRC's *Materials Processing for Engineering Applications (MAPEA)* initiative, to develop and validate models for turbine disc manufacture. The aim is to track the structure, including possible defects, from the initial cast ingot to the final product in order to minimise unnecessary scrap in late stage of the manufacture.

3. Process Modelling of Manufacturing Processes

It is beyond the scope of this paper to give a rigorous analysis of all of the various approaches to process modelling. Rather, we give some examples of recent developments and of work in progress to illustrate the progress that is being made.

3.1 Solidification Processing

Nickel-base alloys are often produced by a combination of primary and secondary remelting processes followed by thermal mechanical processing or an investment casting operation to produce varying complexity of rotating parts. Control of structure and avoidance of defects in both process routes requires a detailed understanding of the solidification processes. Modelling of these processes can help predict both the average structure, the deviation about this average, and can give insight into the conditions causing defects (both intrinsic and extrinsic) which often limit the performance of the material in service.

VACUUM ARC REMELTING

VAR is one of the principal secondary-melting technologies used to produce nickel-base superalloys for the manufacture of turbine-discs in aero-engines. It operates on either a *Vacuum Induction Melted* (VIM) ingot or VIM barstock that has been *Electro Slag Refined* (ESR) to remove unwanted inclusions. VAR is used to produce a sound ingot that is free of macroscopic segregation and has a relatively fine and homogeneous grain structure. An arc is struck between the starting ingot (VAR or VAR/ESR) and a water-cooled crucible; the ingot progressively melts and drips into the crucible where it solidifies in a controlled manner. The intense heat in the arc and melt pool helps to further reduce the number of inclusions. However, a number of types of defect that can be generated in the VAR process and be carried through to later process stages. These include *inclusions* that originate from ceramics used in VIM processing, *white spot* that is associated with fall-in from the electrode or alloy skull (illustrated schematically in Fig. 2) and *freckles* that are localised macrosegregate caused by convection instabilities. A numerical model is being developed to simulate the VAR process that allows the process control parameters and alloy properties to be related to the formation of a range of microstructural features and defects. This will help enable the processing conditions for new alloys to be optimised with a minimum of time-consuming trial and error experimentation.

A multiscale model was developed to simulate the VAR process, with different spatial and temporal modelling scales being used depending on the problem being addressed. The fluid flow and heat transport in the melt pool and mushy zone of ingot are described by the incompressible form of the Navier-Stokes equations and the accompanying energy and electromagnetic conservation equations. These equations are solved simultaneously using an in-house transient finite volume model with a moving mesh.

Fig. 2. Schematic of the potential origins of white spots in VAR.

This allows the influence of even small process perturbations to be studied at almost any stage of the process. Fig. 3a shows the predicted flow field for one set of conditions, whilst Fig. 4a shows both the flow and thermal fields near the melt pool when the ingot has reached half its final length for typical conditions. Validation of the model is ongoing against instrumented trials on both laboratory scale and using an industrial VAR furnace.

One important application of the model has been the prediction of inclusion survival. Fig. 2 schematically illustrates the most common sources of intrinsic and extrinsic inclusions, including: various types of *white spot* (a zone lean in niobium), splash, and the extrinsic defects such as tungsten carbide and steel shot. White spot can arise from dendrites in the shrinkage pipe of the VIM electrode or from the first solid fraction that forms as the shelf or skull in contact with the water-cooled mould falling through the molten pool and being entrapped in the mushy zone before completely melting. If the solid debris is melted or dissolved in the VAR molten pool then it is likely to be innocuous. If it falls to the bottom of the pool and is incorporated in the semi-solid region, it can either survive as a foreign inclusion or as a white spot compositional heterogeneity.

Fig. 3. (a) Simulated fall-in trajectories for three initial spherical particles sizes. (b) Process map illustrating the remaining volume percentage of a dendrite-cluster as a function of drop height H, shaded area is white spot free.

The consequences of various types of solid-matter falling into the VAR melt pool have been considered. Simulations of particle cluster trajectory, temperature distributions and dissolution were performed for alloy and process parameters relevant to industrial VAR processing of INCONEL 718 (Fig. 3a).[1, 2] Operational safety windows for the avoidance of white spot were plotted as a function of the cluster size and composition for each variable. The drop height, composition and the initial particle temperature all had a significant influence on the potential for white spot formation. However, the operational safety window was most sensitive to the composition and drop height. Process maps were produced to indicate the potential for white spot formation as a function of the principal process variables and particle characteristics. Fig. 3b shows the importance of the drop height of dendrite fall-in on the dissolution rate. Such maps offer the potential to tailor the process conditions to specific alloys in order to avoid the formation of detrimental white spot.

The model was also used to determine which types of extraneous particles, such as steel shot, tungsten carbide tool tips, etc, have the potential to pass through the molten pool without completely remelting, producing an inclusion in the final ingot.[2] Steel shot particles were found to present little risk of forming inclusions in the VAR process. The similar densities of steel and superalloy lead to long residence times in the melt; a melting time of 1.5 seconds for the largest particle considered indicates that a steel shot particle will not be able to reach the mushy zone before dissolving. Tungsten carbide particles, however, have little buoyancy in the superalloy melt and rapidly drop to the semi-solid region, presenting a high risk of forming detrimental inclusions. This model was used to reduce VAR costs by determining when shot peening was not required between melts.

The thermal and fluid flow conditions in the melt have a profound effect on the microstructures produced in the solid ingot; this in turn determines the subsequent behaviour during forging and in service. One objective of the multiscale models has been to predict the development of grain structure throughout the entire processing chain, including VAR processing. The thermal profiles as a function of time generated by the macromodel were passed to a mesoscale model to predict the different microstructural features. This mesomodel is a cellular automata (CA) model, that tracks not only the average grain sizes and their distributions, but also their morphology and texture indicating; for example, the conditions leading to a transition from columnar to equiaxed grain growth. The predicted grain structure is compared to the experimentally observed structure in Fig. 4. The model also predicts how strong of a perturbation in processing conditions is required to produce areas of discontinuous grain morphology (and hence how tightly the process must be controlled). One such discontinuity is termed a *tree ring* structure, and has been linked to the onset of freckle. Tree rings are zones of fine equiaxed grains interrupting the continuity of the columnar grain structure that predominates over the outer half of VAR ingots. The model also predicts these discontinuities, as shown by the highlighted squares in Fig. 4b&c. The duration and magnitude of perturbations required to form heterogeneities in the grain structure was systematically investigated, allowing process windows to be determined for the prevention of these defects.[3]

In summary, the combination of experiments at the industrial and laboratory scale and the development of a multi-scale model have provided detailed insight into the VAR process. This potentially provides a process optimisation tool that can reduce the expensive and time-consuming commissioning of VAR processing of new alloys. By linking mesoscopic models to the continuum VAR model, key features that limit the final performance can be predicted, including grain development (such as tree-rings) and the dissolution/melting of exogenous particles in the melt pool. This has allowed the production of process maps that link the occurrence of tree-rings and white spot to the major process variables. Application of these maps to prevent defects has a massive financial impact, especially for defects that may not be detected until further downstream in the process.
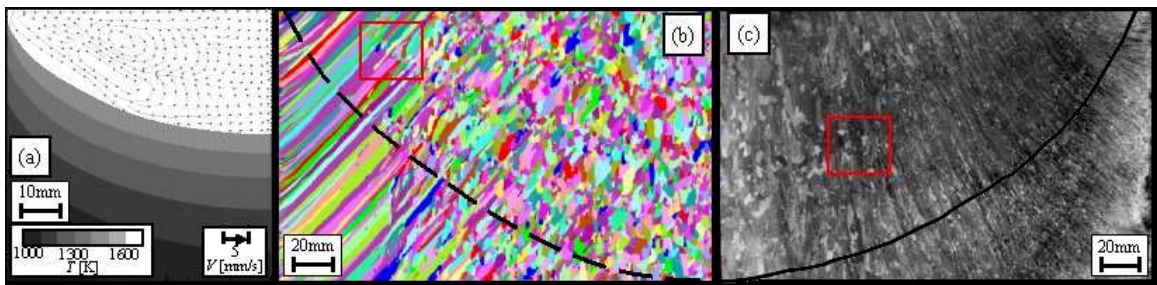
Fig. 4. (a) Macromodel predicted temperatures and fluid flow near the melt pool. Comparison of (b) multiscale model predicted and (c) experimentally observed (optical macrograph) grain structure. The melt pool shape is shown as a black line, predicted by the macromodel in (b) and calculated from the tree rings in (c).
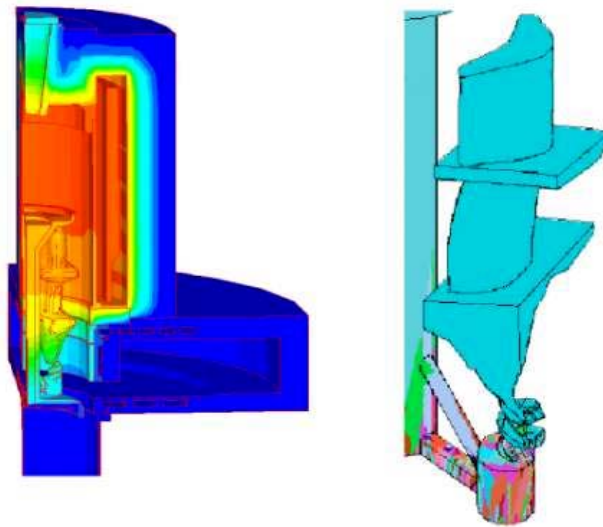
Fig. 5. Process model of the investment casting of high pressure turbine blading. (a) Thermal model. (b) Predicted grain structure.

3.2 Investment Casting

Process simulations of the investment casting of directionally solidified and single crystal turbine blade aerofoils are now also possible[4], as indicated in Fig. 5. Heat transfer during solidification of shaped castings in furnaces with complex baffle-geometry can be calculated using appropriate radiation factors to allow the shape of the mushy zone, the temperature gradients and the rate of solidification to be estimated with some precision. The heat transfer analyses have been coupled with grain structure calculations based upon the cellular automata technique, such that stochastic calculations of grain density can be made. The analyses are suitable for the evaluation of novel designs of grain selector, and also the evaluation of the susceptibility to stray grain formation around re-entrant features such as shrouds. These kinds of computational tools have been used to identify the optimal processing conditions required for the production of new types of turbine blade, with significant savings in costs and time via reductions in the number of design/make iterations. In a typical foundry, the probability of any given casting being defective is significant; modelling represents a powerful tool for dealing with this situation. Indeed, it is claimed by one industrial concern with which the authors have worked that costs running into many millions of pounds have been saved.
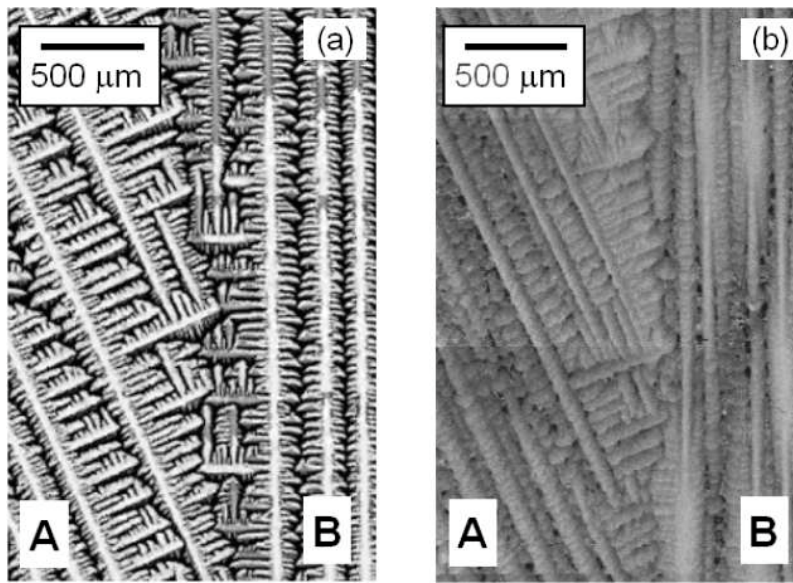
Fig. 6 (a) Predicted and (b) experimental results (after ref. 2) of competitive growth for two diverging grains, A and B, with misorientations of 25° and 1°, respectively.

The effectiveness of numerical models requires that they incorporate an appropriate knowledge of the physics controlling the process under consideration. The characteristic range of orientations produced and the propensity to stray grain formation in single crystal castings varies very significantly between alloys with small compositional differences. The modelling techniques are now being extended to include full tracking of the solute profiles at the micron scale and simulation of the dendritic morphologies. This allows the competition between dendrites growing at an arbitrary angle of misorientation to be simulated. Due to the increase in tip undercooling, for constrained growth in a constant thermal gradient, dendrites with a preferred growth direction will grow faster than those that are misoriented, with the preferred orientations overgrowing misoriented ones. This effect was shown experimentally by Wagner *et al.*[5] for two bicrystals crystals of CMSX4 superalloy grown with different misorientations, one with converging and the other with diverging dendrites. The experimental conditions of Wagner *et al.*[5] were simulated using a cellular automata-finite difference (CA-FD) model two grains of 1° and 25° misorientation grown in divergent directions (see Fig. 6(a)). The highly misoriented grain must form ternary dendrite arms to maintain its growth in the direction of the gradient, showing excellent qualitative agreement to the experiments of Wagner *et al* (Fig. 6(b)). The challenge is to understand why alloys with marginal differences in chemistry behave so differently and to define the process conditions required for optimum single crystal processing.

3.3 Simulation of Thermal-Mechanical Working and Heat Treatment

During the manufacture of high integrity superalloy disc components for gas turbines, the forgemaster carries out a series of forging operations to shape a pre-forged billet to within as near the required component shape as possible, in order to minimise costs associated with machining and excessive waste of material. Most usually, stringent limits will be placed on the grain size induced by processing; this is to ensure adequate mechanical properties and a capability for non-destructive testing (NDT). In practice, successful processing requires the optimum amount of deformation to be imposed at the correct temperature within the right time-scale. The relationships between the processing parameters, the flow-field and the metallurgical structure are time dependent and strongly temperature dependent. Historically, great reliance has been placed on the skill and experience of the forgemaster to determine optimum processing conditions.

Nowadays, finite-element (FEM) based models are being used routinely to enable forging procedures to be designed and analysed before resorting to trials on the factory floor, see Fig. 7. However, before the simulations can be made, it is necessary to quantify the rheological behaviour of the material using laboratory-scale compression tests and to carry out data reduction to determine the appropriate mechanical and structural constitutive equations, which are usually viscoplastic in nature.[6] Within the computer these manifest themselves as datasets which are read by the software and materials subroutines which estimate the evolution of metallurgical structure, i.e. the fraction of grains recrystallised, grain size.[7] In practice, the simulations prove very useful for (i) estimating whether the load capacity of the press is likely to be exceeded, usually at the latter stages of processing (ii) the evolution of the temperature field, which is influenced by the balance of heat lost by convection to the surroundings, lost by conduction through the dies and created by adiabatic heating (iii) the rheological flow, and related defects such as cold shuts and (iv) determining whether excessive grain growth occurs due to the solvus temperature being exceeded, most commonly due to a large contribution from adiabatic heating. The computations represent a rational way of choosing the die geometries and forging sequences, which is of course the primary role of the forgemaster.

Fig. 7 Closed die forging of INCONEL718 turbine disc. (a) Etched forging illustrating dead zone. (b) Predicted extent of recrystallisation and corresponding flow lines.

After processing, the forgings are subjected to heat treatment followed by a series of machining operations. A number of advantages are conferred by carrying out a thermal elastic-plastic process simulation[8] of this stage of processing, see Fig. 8. These relate to the estimation of the residual stress field, which arises due to the differential thermal contraction of the metal upon cooling, such that the local yield stress is exceeded. Quantification of the stress field allows the subsequent sequence of machining operations to be chosen optimally; problems can otherwise occur due to the relaxation of the stresses as machining proceeds, since

Fig. 8 Predicted radial component of residual stress in an IN718 V2500 aero-engine disc, quenched in oil from 980°C. Cross-section through an axisymmetric finite element mesh of the disc with its axis vertical and centre of symmetry at x=0mm. Regions of high tensile and compressive stress (yellow and blue, respectively), approaching the assumed room temperature yield stress of 300MPa, are clearly visible.

movement of the metal can mean that tolerances can be exceeded. In practice, an accurate estimate of the residual stress field requires an accurate knowledge of the heat transfer between metal and quenching medium; thus heat transfer coefficients must be well characterised. The calculations[8] indicate the plasticity occurs first on the outside surfaces, such that the regions near the free surfaces end up in compression; balancing tensile stresses exist away from the peripheral regions. The stresses are large, and usually a significant fraction of the uniaxial yield stress; the hydrostatic component of the stress field is large too. Recently, we have used neutron diffractometry to confirm the size and extent of the stress field, and so far, the simulations are consistent with the experimental information which has been acquired.

3.4 Simulation of Joining Processes

Joining processes are used widely in the fabrication of turbine engines, particularly for compressor and combustor sections. Often high integrity processes such as electron beam welding (EBW) are employed. The components being assembled are a very long way down the manufacturing stream, so that their value to the turbine manufacturer at this stage is considerable. Thus techniques which help to minimise scrap and non-conformance, e.g. computer modelling and simulation, tend to have great emphasis placed on them. Fortunately, much progress with regard to the analysis of welded structures has been made in recent years. The aim here is to understand and predict the macroscopic transient fields of temperature, displacement, strain and stress, by employing the equations of continuum mechanics. The research[e.g. 9, 10] has reached the point where it is possible to make useful predictions of residual stresses, distortion, cracking and buckling phenomena - the most critical issues from an industrial viewpoint.

The first step is to solve some form of the energy equation, usually with the finite element method; this is because the thermal strain computed from the heat transfer analysis can be considered to provide the driving force for weld-induced distortions. Care must be taken when deciding how to model the heat source, since the physical effects occurring in the molten zone, particularly for processes such as electron beam welding, are not well understood and are subject to debate; thus a balance must be struck between the desire to appeal to all the physical phenomena at play and the practical need to keep the computational cost to within reasonable limits, whilst keeping in mind the numerical answers which need to be generated. The second part of the analysis involves carrying out thermal stress analysis which typically involves large strains and large rotations. The most popular constitutive equation has been elastic-plastic, i.e. creep is not usually accounted for. The basic equations are the conservation of linear momentum, angular momentum, the constitutive equation and the compatibility equation. The chief difficulty arises almost entirely in decomposing the deformation into a translation, rotation and stretch on the one hand and then decomposing the deformation into contributions due to elasticity, plasticity and thermal expansion on the other.

Fig. 9 illustrates a practical example which relates to the electron beam welding of the high pressure compressor assembly of a modern civil aeroengine.[11] This consists of a number of discs which are joined by a weld of length greater than a metre, with secondary (cosmetic) passes added for the purpose of removing weld bead undercut which would otherwise affect the fatigue properties. As a consequence of welding, large residual stresses are set up and these can be estimated for the as-welded state and with an appropriate creep model, after stress-relief heat treatment. The analysis confirms that it is the hoop component of the stress field which is the most significant; thus the weld acts in the same manner as a tourniquet.[11] The transverse (axial) component is smaller, but it is this which is responsible for increasing the separation between the machined disc bores, in
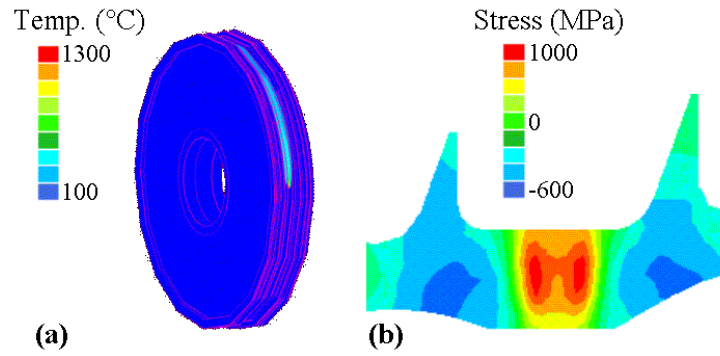
Fig. 9 (a) Predicted thermal field during EB welding of a superalloy compressor assembly. (b) Corresponding residual hoop stress (MPa) after welding.
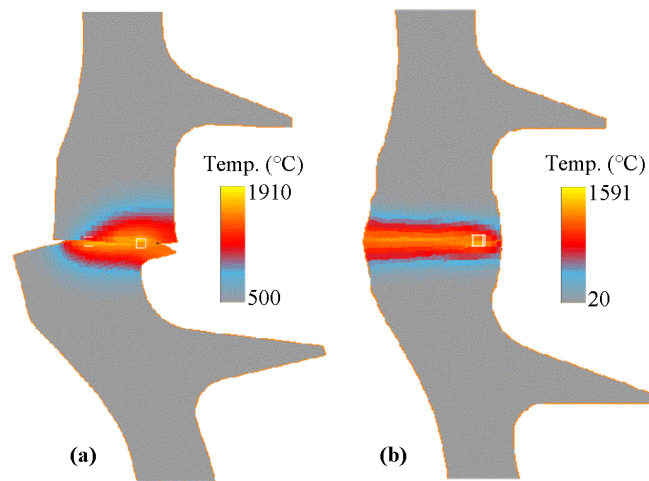
Fig. 10 Simulation of inertia welding of superalloy compressor assembly. (a) Initial jigging arrangement. (b) Modified jigging.
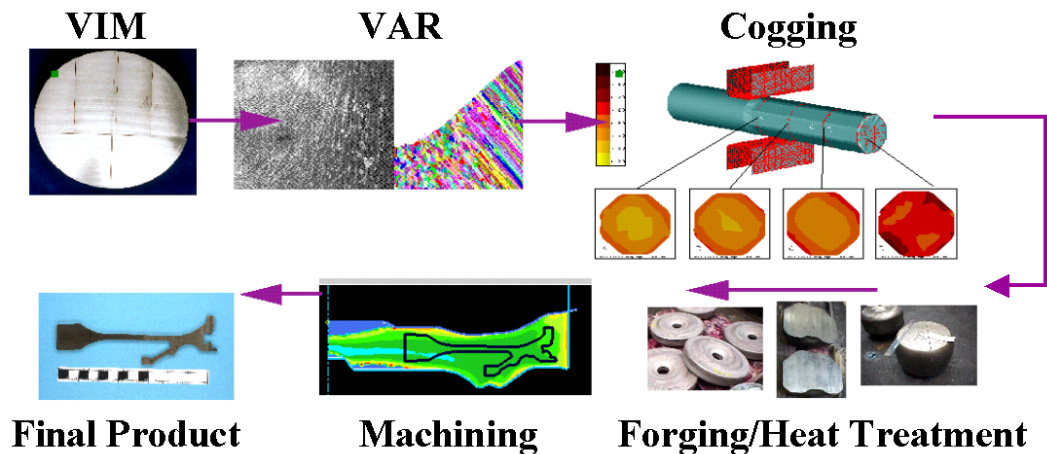
Fig. 11 Digital model of supply chain.

such a manner that the assembly ceases to be exactly radially symmetric; the situation worsens when cosmetic passes are added. The results from these calculations have been compared with measurements made on real assemblies, using needle-probe metrology and neutron diffractometry.[12] These comparisons have convinced us of the power of computer modelling for the anticipation of residual stresses and distortions in welded assemblies such as this. These also provide guidance for the remedial action that needs to be taken when problems arise.

A final example relates to the simulation of the inertia welding of compressor assemblies, see Fig. 10.[13] The temperature capability required of superalloys for hot-end compressor applications is now such that new disc alloys such as RR1000 are being contemplated. Unfortunately, conventional joining processes such as EBW cannot be used since the higher alloying content renders them prone to solidification cracking. Instead, inertia welding must be used. One half of the assembly is accelerated to a significant rotational speed before placing it against the other half, with the aid of an axial load; the heat generated is sufficient to cause a bond without significant melting at the bond. Our calculations indicate that the extent of the bond-line mismatch depends heavily upon the manner in which the two halves of the assembly are held in place during welding; this is consistent with experience.[13] Since the capital cost associated with the jigging arrangement is considerable and it takes up to six months to have it fabricated and delivered, computational modelling has a role to play in the development and application of this joining technology.

4. Summary and Conclusions

In this paper, we have discussed the application of process modelling to support the fabrication of the critical rotating components required for the gas turbine engine. A number of examples have been given. In this field, one aims to build mathematical models of the phenomena occurring during the manufacturing processes. Macroscopic phenomena such as heat flow and continuum mechanics should be included; however, it is becoming increasingly possible to include simulations of microstructure evolution using sophisticated metallurgical models. The emphasis should always be to include as much as possible of the underlying theory, without making the simulations unwieldy, intractable or lengthy. Usually it is necessary to avoid losing sight of the reasons for pursuing a modelling approach.

The major advantages of a building a process model include

- considerable predictive capability, provided that the modelling is sufficiently accurate;

- the provision of an ability to study the effects of changes in the process variables (such as withdrawal rate, geometry, quench rate, welding speed) without resorting to experimental trials;

- the possibility of optimising the processing route in order to reduce and even eliminate manufacturing waste;

- during component prototyping, a potential reduction in the number of design/make iterations which prove necessary; and

- the instilling of greater confidence in a process derived from a better understanding of the physical principles at play.

Future challenges relate to the incorporation of better metallurgical models for microstructure evolution, e.g. solidification, grain growth and texture, which will enable an improved coupling of phenomena occurring on the macro- and micro- scales. Furthermore, more development needs to be carried out to link together the models of the different processes (e.g. casting, forging, heat treatment, welding); this will facilitate the storing of information that characterises the risk of defects being present. We envisage a digital model

of the supply chain, see Fig. 11, which allows the appropriate information to be stored, operated upon, and retrieved at various points along the manufacturing route.

Acknowledgements

References

1. Zhang, W., Lee, P. D. and McLean, M., *Metall. Mater. Trans. B,* 2002-accepted for publication.

2. Zhang, W., Lee, P. D. and McLean, M., Intermetallics and Superalloys: EUROMAT 99 - Volume 10, D. G. Morris, S. Naka, P. Caron, Eds. (Wiley-Vch, 2000), 123.

3. Xu, X., Zhang, W., Lee, P. D., McLean, M., Ward, R. M. and Jacobs, M. H., Proceedings of Mod. Castings, Welding Adv. Solid. Processes-IX, P. R. Sahm, P. N. Hansen, J. G. Conley, Eds., Aachen, Germany (SHAKER, 2000), 574.

4. Carter, P., Cox, D. C., Gandin, C. A. and Reed, R. C., *Materials Science and Engineering A,* 2000, **280**, 233.

5. Wagner, A., D'Souza, N., Shollock, B. A. and McLean, M., Proc. Int. Sym. on Liq. Metal Proc. & Casting, A. Mitchell, J. Van Den Avyle, Eds., Santa Fe, New Mexico, Sept. 23-26 (AVS, N.Y., N.Y., 2001), 301.

6. Roberts, S. M., Walsh, S. A., Lewis, J. P., Evans, R. W. and Reed, R. C., *Materials Science and Engineering,* 2002 accepted for publication.

7. Dandre, C. A., Roberts, S. M., Evans, R. W. and Reed, R. C., *Mater. Sci. Technol.,* 2000, **16**, 14.

8. Rist, M. A. and Reed, R. C., unpublished work, (University of Cambridge, 2002).

9. Dye, D., Hunziker, O., Roberts, S. M. and Reed, R. C., *Metall. Mater. Trans. A-Phys. Metall. Mater. Sci.,* 2001, **32**, 1713.

10. Dye, D., Hunziker, O. and Reed, R. C., *Acta Mater.,* 2001, **49**, 683.

11. Stone, H. J., Roberts, S. M. and Reed, R. C., *Metall. Mater. Trans. A-Phys. Metall. Mater. Sci.,* 2000, **31**, 2261.

12. Stone, H. J., PhD Thesis, University of Cambridge (1999).

13. Roberts, S. M. and Reed, R. C., unpublished work, (University of Cambridge, 2002).

Paper #11
Discussor' name: Prof. Xiao Guo
Author Trepanier
Q: How are the periods between processes simulated, since the microstructure can change during this time as well as during each processing operation?

A: Most of the changes in the microstructure between process steps occurs with relatively slow kinetics and over large scales, and hence relatively coarse meshes and long timesteps can be used, reducing the computational cost of simulating these transitional periods between the main processing operations.

Discussor's name: Prof. Glyn Davies
Author Trepanier

Q: "You showed some excellent examples of multiscale models for the predictions of properties in metallic systems; is there any similar work on polymer composites?"

A: "I am not aware of any groups simulating the complete manufacturing chain for polymer composites, but individual groups are applying multiscale modeling separately to each step in the processing chain, such as the recent work on the multiscale simulation of Resin Transfer Moulding at Imperial College. This work does need to be brought together and extended to the prediction of properties."

This page has been deliberately left blank

———————————

Page intentionnellement blanche

Haptic Interfaces for Virtual Prototyping

M. Bergamasco, A. Frisoli
PERCRO Scuola Superiore S.Anna
P.zza Martiri della Liberta, 33
56127 Pisa, Italy

A. Gucciardino
Italian M.O.D.
Land Armaments Directorate
via Marsala 104
00185 Rome, Italy

S. Scattareggia Marchese
via Panoramica 340
98168 Messina, Italy

Abstract

This paper analyzes the general requirements of Haptic Interfaces (HIs) for Virtual Prototyping operations. In particular two different paradigms of interaction with virtual objects are presented, respectively based on an anthropomorphic and a desktop Haptic Interface. The main aspects of mechanical and control system design of HIs and force rendering in Virtual Environments are discussed too. The experimental results of the simulations conducted with a force feedback arm exoskeleton are presented, pointing out the current limits of the existing devices and outlining the future developments.

1   Introduction

Virtual prototyping technologies can reduce the time and costs necessary to develop and construct new products and bridge the disciplinary and distance gaps among different collaborators working on the same project [3].
Virtual Prototyping is based on the simulation in a realistic three-dimensional Virtual Environment of the functionality expected from the new product. Before the real construction of the first prototype, it enables designers to evaluate the fulfillment of ergonomics, engineering and design requirements, and the feasibility/adequacy of the product to the foreseen usage [2]. One of the key issues in Virtual Prototyping applications is the capability provided to the operator of interacting in an efficient and sensorially sufficient way with the virtual model of the object.

The sense of touch appears to be fundamental to assess the properties of the prototype of a complex system, such as a vehicle. Although CAD systems are becoming widespread, there is still some important information that a CAD program alone cannot supply. The designer cannot see from the CAD how the operator will fit into cab or assess how the controls will feel during operation. During the development of new vehicles the designer must still wait until a mock-up or a prototype is built to find out how the controls feel and whether or not they are easy to use [1]. Vehicle simulators immersed in Virtual Environments [6][4] (see Figure 1), where either the

contact or the inertial forces are replicated to the operator, have been successfully employed for the evaluation of ergonomics aspects in the cockpit.

Figure 1 The MORIS motion simulator realized by PERCRO

During the design process of military vehicles, inertial motion simulators could be employed for assessing the injury potential to the truck or tank occupants, in case of explosion of anti-vehicular mines. The explosion of anti-vehicular mines represents one of the most common battlefields threats, which can cause serious injuries to the occupants, particularly to the cervical spine and legs. Possible solutions for reducing the injury potential are currently under study.

One possible solution is the equipment of vehicles with mechanically damped seats, capable of suppressing the huge vibrations induced by mine explosion. According to this approach, mechanical dampers can be employed for connecting the seat to the vehicle frame.

Inertial simulators represent a potential mean for testing and improving the design of seats with mechanical dampers. A parallel manipulator, e.g. the one shown in Figure 1, can be used to simulate the high accelerations produced by the blast pressure consequent to the explosion of 3-4 kg TNT mine. The prototype of the seat can be placed on the upper platform of the simulator, either with a dummy or a human person seated on it. Experiments may be conducted on dummies by reproducing acceleration fields of the same magnitude of real ones. Moreover

reduced acceleration fields can be replicated on human operators seated on the experimental mock-up, in order to carry out a medical assessment of the system, by evaluating the injury potential to the human body. The results of the medical protocol conducted on the human body can be extrapolated, in terms of induced injury, to the case of higher acceleration vector fields.

Conceptually the rendering to the human operator of the sensation of a physical interaction with a virtual environment can be achieved by utilizing appropriate interfaces capable of generating adequate sensory stimuli to the operator. Such interfaces, called Haptic Interfaces (HIs), are force feedback devices that can exert a controlled force on the operator's limb as if he was touching a real object.
HIs can greatly enhance the realism and the sensation of immersion perceived by the operator in the Virtual Environment, while using CAD tools for the design/assessment of new products.

The most important characteristics that an HI must fulfill are high backdrivability, low inertia (related with the transparency during the motion of the device), absence of mechanical plays, mechanical stiffness greater than 5 N/mm, isotropic force response in the workspace (necessary to avoid vibrations and penetration into virtual objects). The low-level control system needs to run with a frequency up to 1KHz and to maintain the coherence with the graphics representation of the simulation.

HIs, can be usefully employed for the simulation of virtual assembly and maintenance procedures, with the aim of studying the feasibility of some particular mounting operations in mechanical assemblies and verifying the level of operator's tiredness induced by the task.
In particular in order to evaluate the execution of such procedures in complex mechanical assemblies, it is necessary to use HIs with a workspace close to the real one of the human arm and with multiple contact points on the operator's arm. Force feedback anthropomorphic arm exoskeletons, which can be worn by the operator in a natural way with a reduced encumbrance, are the ideal candidate solutions for the simulation of such complex tasks.

The possibility of exerting contact forces on different points of the operator's arm allows assessing the feasibility of mounting procedures in huge assemblies. For instance it would be possible to evaluate the reachability of a screwed hole in a motor housing by the operator's arm holding a wrench and to find the interference with other parts along the wrench path.

This paper describes two different Haptic Interface systems, which can be employed for the execution of operations of virtual prototyping. The underlying issues related both to the control and the design of such systems are also presented.

2   Characteristics of Haptic Interface systems

Some basic features of Haptic Interface systems can play a relevant role in the execution of Virtual Prototyping operations:

- Number of Points of contact: Haptic Interfaces providing multiple point of contact allow an enrichment of the experience in the virtual environment. Both the time necessary to identify the shape of an object in a virtual environment and the adopted exploratory procedure are directly correlated to this number [10]. Exoskeletons systems generally allow replicating

multiple points of contact. In Virtual Prototyping applications this provides the possibility of simulating operations such as assembling and maintenance, by taking into account also the encumbrance of the operator's arm during the execution of operations.

- Grounded vs. Portable Haptic Interfaces. Portable Haptic Interfaces allow the operator to perform a free motion and to touch virtual objects within a large workspace. Grounded Haptic Interfaces have the main advantage of being generally characterized by a reduced encumbrance, which allows to locate them on a desktop, while, as a drawback, the reachable workspace is reduced.

- Capability of replicating torques: Capability of replicating torques is important when operations of assembling have to be replicated. Typically in the case of inserting a peg in the hole, the reaction torques generated by the misalignment of hole/peg axes provide the indication of correct fitting to the operator.

- Mechanical properties of Haptic Interfaces: Haptic Interfaces are traditionally designed according to the following general guidelines: low moving masses and inertia, low friction, high back-drivability, adoption of smooth, low play transmission systems, high structural stiffness, high force and position bandwidth. The fulfillment of such requirements is generally achieved by the adoption of tendon transmissions for remote actuation together with grounding of motors.

3   The arm force exoskeleton

The PERCRO arm force exoskeleton [7] (see Figure 2) is a 7 degrees of freedom (DOF) HI, tendon actuated with DC brushed motors. The system can be configured with 5 DOF only, with a handle or a glove fixed to its last link. The kinematics of the first 5 DOF of the system is shown in Figure 3.

The exoskeleton is equipped with optical encoders at each joint and three force sensors, based on a strain gauge architecture that can measure the torque on the last three joints of the system.

Figure 2 The arm force feedback exoskeleton
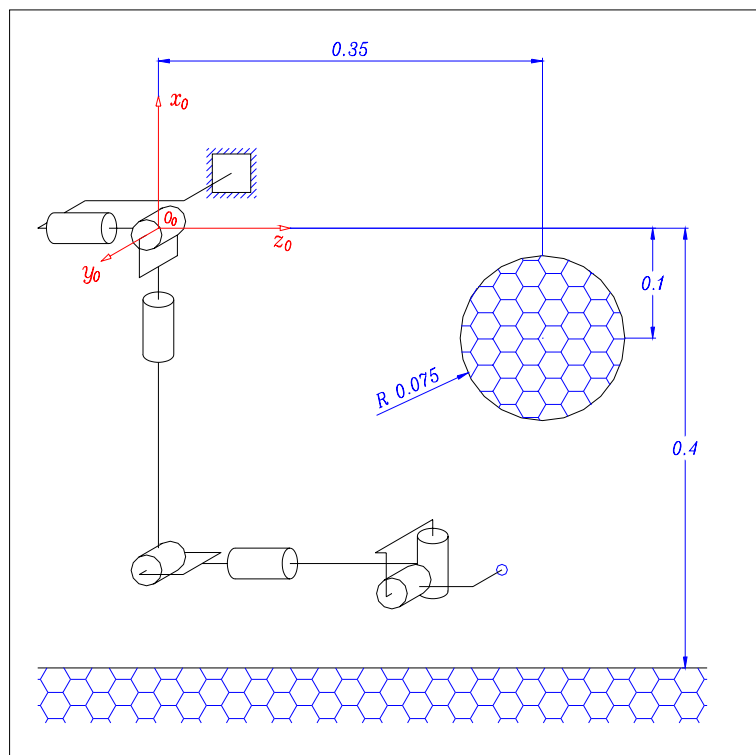
Figure 3 The virtual environment and the Arm-Exoskeleton worn by the operator in the 5DOF set-up
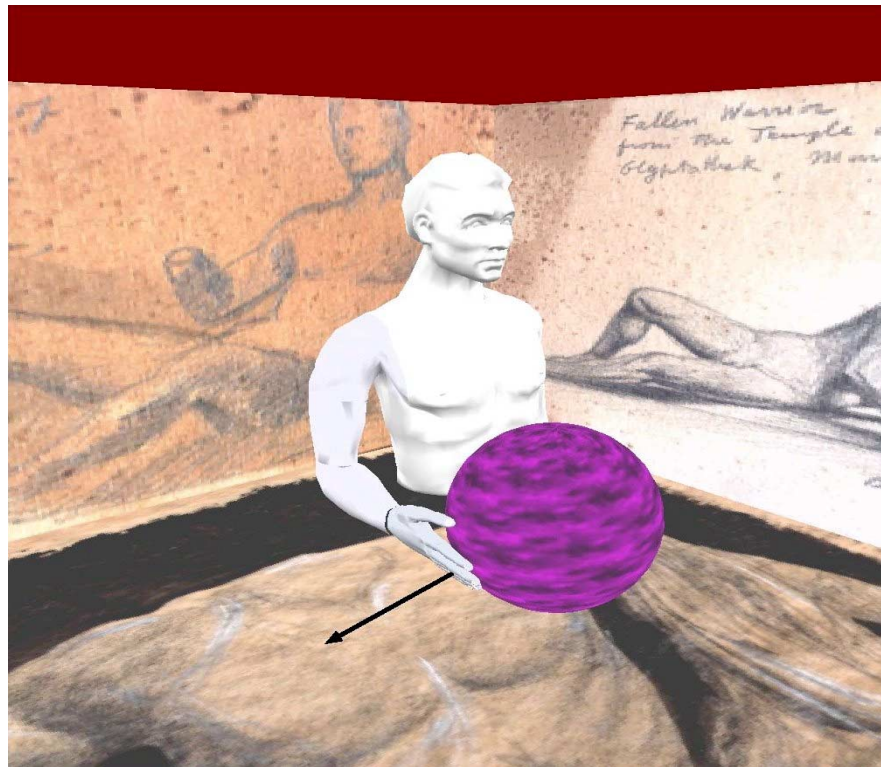
Figure 4 Representation of the contact in the Virtual Environment

In the following the results of some haptic experiments that have been conducted on the arm exoskeleton are presented.

In the Virtual Environment a full-body avatar of the operator is represented as it is shown in Figure 4, while the contact forces are displayed as solid arrows. The operator can observe the movements of his arm on a wide screen, on which all the computer generated Virtual Environment is projected. Several objects with different geometrical shapes have been represented, such as a sphere, a wall, a cube and polyhedral objects, according to the scheme illustrated in Figure 3. The operator can move freely his arm in the space, without feeling the weight of the exoskeleton, since gravity and friction forces are compensated by the action of motors.

A measure of forces and displacements of the contact point during the simulation allows to assess the performance of the system, i.e. the capability of providing the correct perception of the contact to the user.
When the hand enters in contact with an object, forces are generated against the operator's hand in order to impede it to penetrate in the object.
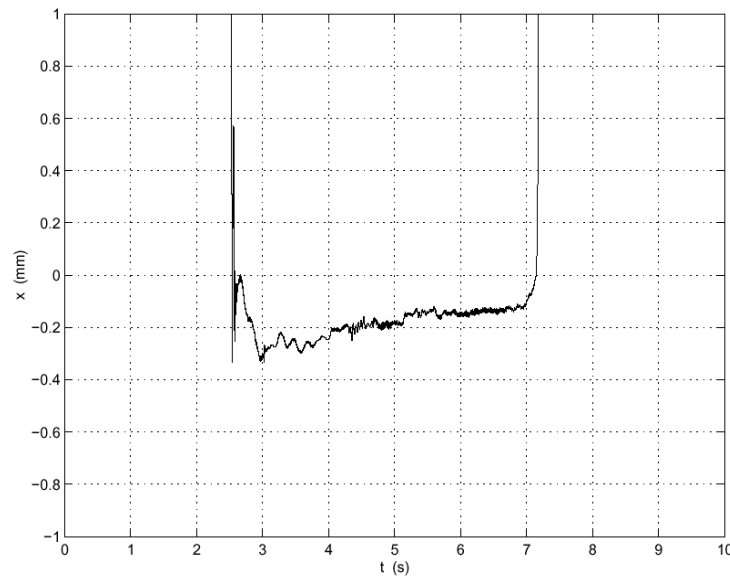
Figure 5 Plot of position vs. time during the simulation of the contact with a virtual wall at x=-0.2 mm
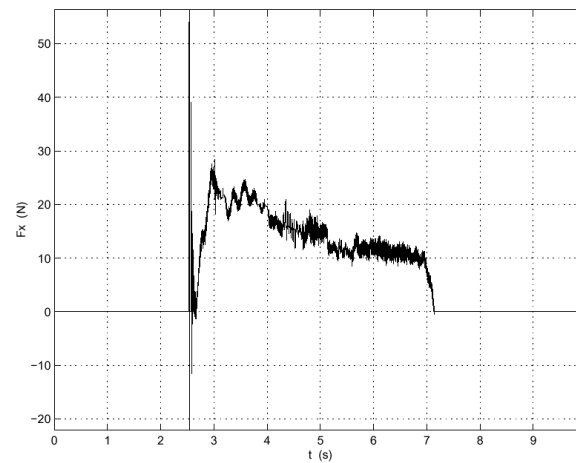
Figure 6 Plot of force vs. time during the simulation of the contact with a virtual wall at x=-0.2 mm

Figure 5 and Figure 6 respectively show experimentally measured position and force during the contact between the operator's hand and a virtual wall. The haptic cues are displayed to the operator by simulating virtual mechanical impedance at the contact point. The calibration studies of the controller have permitted to set up the optimum value of the impedance, in order to avoid the onset of vibrations or the sensation of a very soft surface. As it can be observed in the plots, after a transient peak due to the collision with the surface, the reaction force reaches a stable value of about 15 N.

The optimum parameters of the simulated mechanical impedance that determine the best performance during the contact have been estimated as a mechanical stiffness of 80 N/mm and a viscous damping of 0.3 N/(s·mm).

Anthropomorphic force-feedback exoskeletons can be suitably employed in Virtual Prototyping applications, where a full immersion of the operator can be realized by wearing such devices in a natural and comfortable way.

In order to extend the capability of PERCRO arm exoskeleton system, a portable device for the hand has been recently designed at PERCRO for the force-feedback on user's fingertips during grasping.
Such a device will be worn by user's forearm and integrated with the arm exoskeleton on its terminal link that will support its weight. While the micro-system will allow enhancing the stiffness and the perceived inertia of the systems where a manipulation task is performed with the fingers, the macro system will allow reaching a greater workspace with the hand.
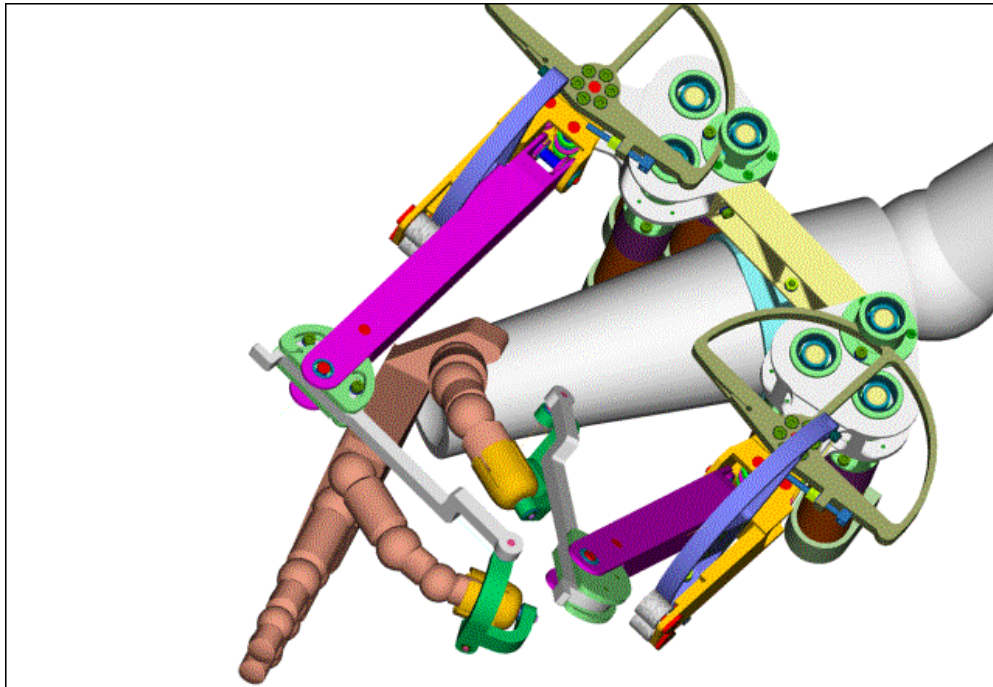
Figure 7 The pinching haptic interface

Such a system will allow the simulation of grasping and moving objects in the space, with the correct feeling of interaction forces/torques generated by the contact with other objects.

4   The Desktop Haptic Interface system

Another paradigm of interaction with a virtual environment can be realized with desktop HIs.
HIs with reduced number of degree of freedom can be employed for the three-dimensional exploration and navigation in the Virtual Environment enriched with the sensation of contact with the virtual objects. Low DOF HIs represent an alternative choice, when it is not requested to

sense the posture of the entire human arm and the nature of the performed task can be carried out with a single contact point.

An example of such a device is the desktop two Haptic Interface system realized at PERCRO, shown in Figure 8. Such a 2 DOF HI [5] is actuated by a novel transmission system, which allows increasing the isotropic behavior of the system force response. The HI can exert forces up to 10 N in its plane. Although the system possesses a plane geometry, it can be used for rendering 3-dimensional shapes too, by exploiting vector fields of lateral forces: a force resistant to the motion of the operator's hand and lying in the plane of motion is perceived as a positive slope, while a force pushing along the motion direction as a negative slope. This effect has been exploited in numerous investigations [11] to display virtual features, such as holes or bumps. The main advantage of a desktop device is the reduced cost with respect to higher DOF HIs.

Figure 8 The desktop 2 DOF HI

The system is controlled in real-time through a control system based on two main treads running with different clocks, according to the architecture shown in Figure 9. Two different nodes manage the execution of the two threads. The Haptic Module is executed on a DSpace Control Board, while the Graphics Module is executed on a Pentium III 1GHz equipped with NVidia GetForce3 Graphics Card.
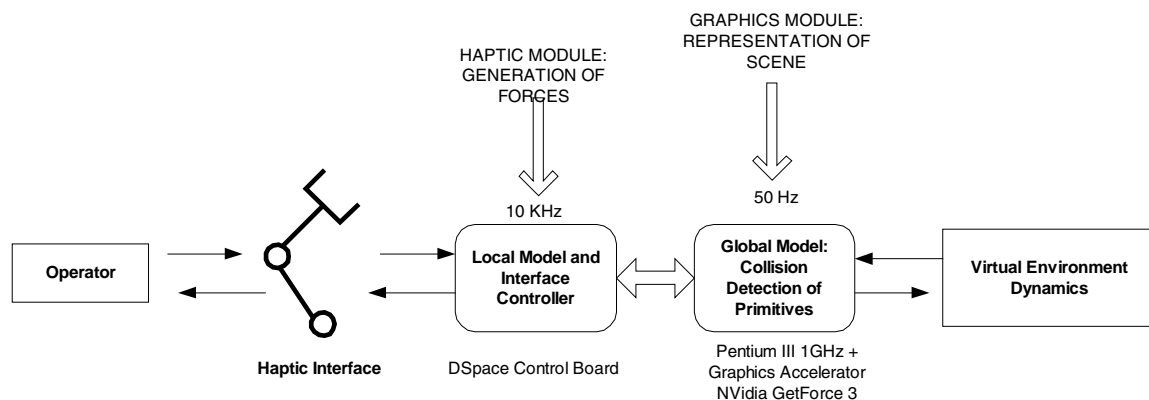
Figure 9 Block representation of system architecture

The thread that manages the graphic representation of the overall virtual environment is executed at each 30 msec and, detects primitives that are in contact each other in the Virtual Environments by means of a collision detection algorithm.

In the case of the planar kinematics, it has been adopted a collision detection algorithm based on the generation of Voronoi diagrams and distance fields of colliding primitives using graphics hardware. Such an algorithm, developed for Computer Graphics purpose only [8], has been integrated with a hierarchical collision detection algorithm and adapted in order to fulfill the requirements of force feedback generation.

Figure 10 shows the concept underlying the collision detection algorithm in a simple case of contact between a point and a circle, represented by means of polygonal representation. When the point is closed to the circle, Voronoi diagrams are computed in a square area surrounding the point. Such an area is divided in sub-areas with different colors, each different color identifying the polygon edge that is closest to the point.
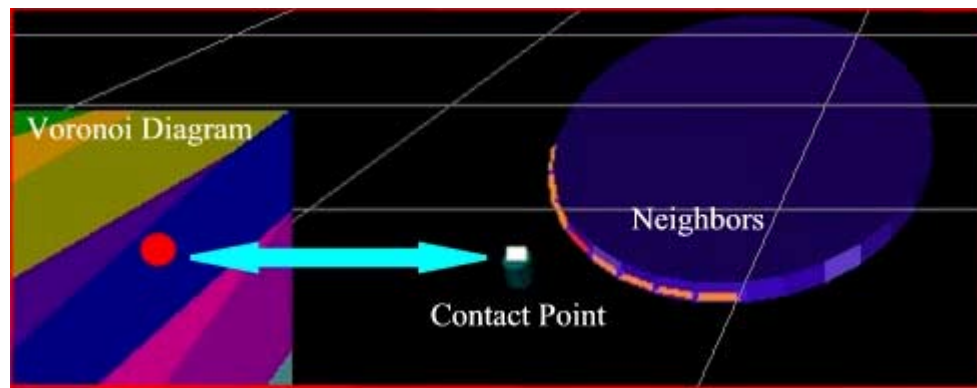
Figure 10 Example of Voronoi Diagram associated to the contact of point with a circle

On the basis of the contact primitives, a local model of the virtual environment is extracted by selecting neighbors of the primitives that are in proximity of the contact point. Such local model is then sent to the Haptic Module, which generates the force feedback at a refresh rate of 10 KHz. The Haptic Module is based on a Fast Collision Algorithms incorporating a God-Object for the computation of forces, according to [9].

Figures 10,11,12 show a sequence of different frames of a virtual simulation of insertion of peg in the hole. When the peg is pushed against a boundary of the yellow housing, a reaction force is computed in real time, which avoids the penetration of the two bodies.

The peg in the hole represents a paradigm of assembling operations. In such a case the contact forces allow to feel whether the correct relative position of the two bodies has been addressed for the insertion task.
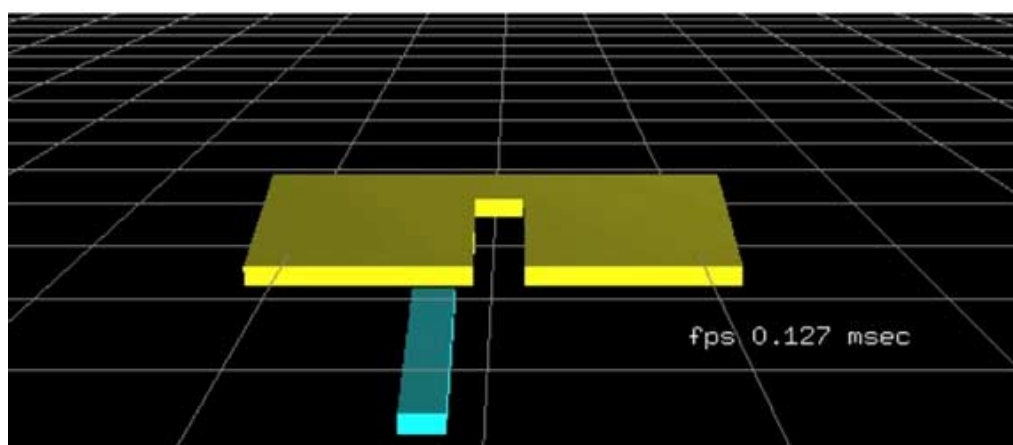
Figure 11 Peg in the Hole task: non colliding objects
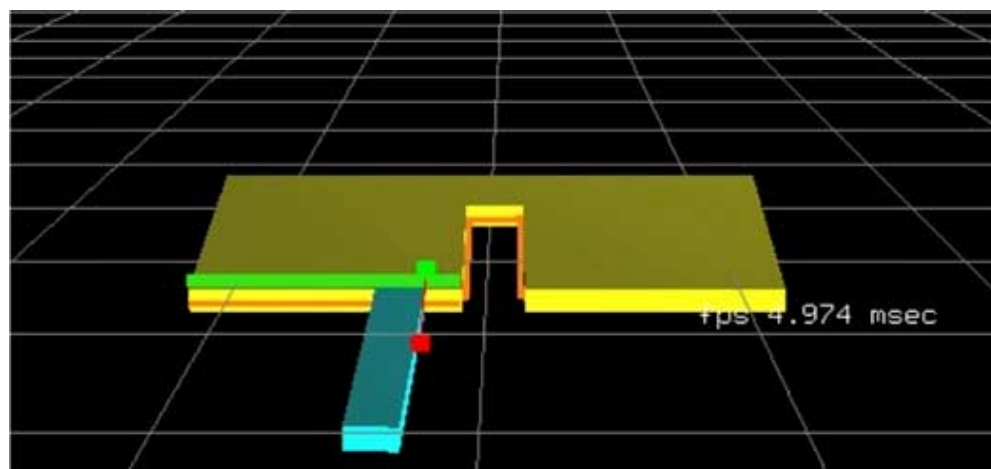
Figure 12 Peg in the Hole Task: The peg is colliding with an edge of the yellow housing
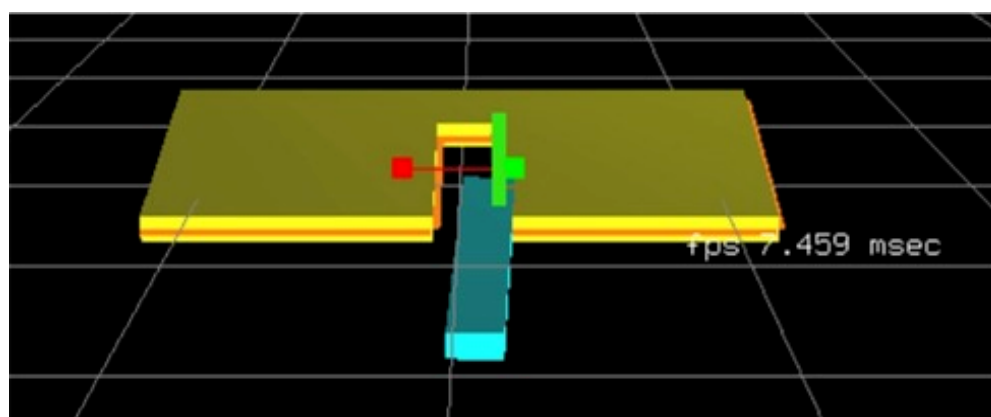
Figure 13 Peg in the Hole task: The peg is colliding with an edge inside the hole

5   Conclusions

Haptic Interface systems present a great potential for applications in virtual prototyping. Although multi-degree of freedom systems are preferable for complexity of tasks that can be simulated, low degree of freedom haptic interfaces could constitute a valid alternative, in term of cost and encumbrance of device.

During the design phase of military vehicles, inertial motion simulators can be suitable employed for the assessment of protection/safety adds-on, e.g mechanically damped seats for the reduction of potential injury to the occupants, both from a technical and medical perspective.

Beyond the assessment of occupant safety in case of mine detonation under armoured vehicles, another issue worth of investigation is the assessment of the stress conditions, which a pilot of fighting aircraft is subjected to during flight. As a concluding remark, the usage of HIs is a meaningful tool for the design of military vehicles that allows great economy of time and money, especially when it is requested to assess the relation between human and machine under extreme conditions of work.

Reference

[1]   Niesen MR, Luecke GR, *Virtual Dynamic Prototyping for Operator Interface Design* Proc, of IEEE RO-MAN99, Pisa-Italy.

[2]   Yoshikawa T, Yoshimoto K, *Haptic Simulation of assembly operation in Virtual Environment,* Proc. of ASME IMECE 2000, Symposium on Haptic Interfaces and Teleoperation, Orlando FL-US.

[3]   Lu SC-Y, Shpitalni M, Gadh Rajit, *Virtual and Augmented Reality Technologies for Product Realization,* Annals of the CIRP Vol. 48/2/1999.

[4]   Frisoli A, Avizzano CA, Bergamasco M, Data S, Santi C, "Dynamic modeling of primary commands for a car simulator", IEEE 2001 IEEE/ASME International Conference on Advanced Intelligent Mechatronics (AIM '01) 8–12 July 2001 Como, Italy.

[5]   G.M.Prisco, A.Frisoli, F.Salsedo, M.Bergamasco,"A novel tendon driven 5-bar linkage with large isotropic workspace", Proc. of ASME (American Society of Mechanical Engineers) IMECE99, International Mechanical Engineering Congress and Exposition (http://www.eng2.uconn.edu/alarm/imece99), Nashville (TN-USA).

[6]   D Ferrazzin, F Salsedo, A Frisoli, M Bergamasco, "Strategy Manager Implementation in a Motion Based Two-Wheeled Vehicle Simulator", 32nd ISATA, International Synposium of Automative Technology and Automation, Vienna-Austria.

[7]   Bergamasco M, *Force replication to the Human Operator: The Development of Arm and Hand exoskeletons as Haptic Interfaces,* Proc. of 7th International Symposium of Robotic Research 1995, Springer Verlag.

[8]   Hoff KE, Culver T, Keyser J, Lin M, Manosha D, *Fast Computation of Generalized Voronoi Diagrams Using graphics hardware,* SIGGRAPH '99

[9]   Craig Zilles and Ken Salisbury, *A Constraint-based God-object Method For Haptic Display*, IROS '95.

[10]   G Jansson, *Basis Issues concerning visually impaired people's use of haptic displays*, Proceedings 2000 Intl COnf Disability, Virtual Reality \& Assoc. Tech.

[11]   J. M. Weisenberger, M. J. Krier, M. A. Rinker ,*"Judging the Orientation of Sinusoidal and Square-Wave Virtual Gratings Presented via 2-DOF and 3-DOF Haptic Interfaces,"* Vol. 1, No. 4, March, 28, 2000

Exemples d'utilisation des techniques d'optimisation
en calcul de structures de réacteurs

Christian Paleczny et David Monteiro-Fernandes
Snecma Moteurs
Centre de Villaroche
77550 Moissy Cramayel
France

Introduction

Le contexte général de la compétition sur le marché militaire de l'aéronautique oblige les différents acteurs à réduire leurs coûts et à augmenter les performances de leurs produits. Cela implique un effort dans tous les domaines qui doit se traduire notamment par la réduction des cycles de développement, la diminution du nombre d'essais et la réduction du coût de fabrication.

Dans cette optique, les outils de simulation sont devenus indispensables pour prédire le comportement des pièces. Cela a permis de diminuer le nombre d'essais de manière significative, tout en concevant des pièces de plus en plus performantes et fiables.

L'évolution importante des capacités des ordinateurs permet désormais d'envisager des analyses de plus en plus complexes et de plus en plus nombreuses en phase de conception. Cela permet également de diminuer encore plus les risques technologiques.

Le dimensionnement mécanique des pièces et des structures pèse pour une lourde part dans ces coûts de développements. C'est le dimensionnement mécanique qui garantit l'intégrité physique du moteur.
A ce titre, les concepteurs sont tenus à une grande rigueur dans le travail effectué et au respect des procédures qualité. L'optimisation, c'est-à-dire l'atteinte d'un objectif donné (un niveau de contrainte, une fréquence) tout en respectant un certain nombre de critères (variation de forme, durée de vie, …) est un domaine qui prend une importance croissante dans tous les bureaux d'études aéronautiques.

En optimisation de structures, nous distinguons différentes catégories :

- ❑ optimisation à base de connaissances (avant-projets)
- ❑ optimisation topologique (forme non définie par une CAO)
- ❑ optimisation de dimensionnement (épaisseurs de coques, caractéristiques matériau)
- ❑ optimisation géométrique (architecture figée)

A la différence du secteur automobile et des avionneurs, la plupart des composants des réacteurs nécessitent une optimisation géométrique dès le début de la phase de conception. L'optimisation géométrique est une catégorie assez complexe car sa mise en œuvre nécessite, dans un bureau d'études, le couplage automatique d'un logiciel de CAO paramétrée, d'un logiciel de maillages, d'un solveur élément finis et d'un logiciel d'optimisation. Certains logiciels intègrent toutes ces fonctionnalités de façon « transparente » et ont donc des performances très intéressantes. Néanmoins, ils ont des limites que les modélisations des composants des réacteurs atteignent de façon très fréquente.

C'est pourquoi, ces dernières années, se sont développés des logiciels d'optimisation ouverts permettant de gérer tout type de modélisation. Ces logiciels apportent des possibilités de couplage avec des logiciels de CAO, des solveurs éléments finis ou des logiciels développés en interne.

Après un bref chapitre détaillant les principales étapes permettant de bâtir un problème d'optimisation, cet article présentera quelques exemples d'utilisation de ces logiciels dans un contexte de bureau d'études mécaniques.

Processus d'optimisation

Le dimensionnement classique dans un bureau d'études repose encore souvent sur une approche essais-erreurs. C'est à dire, pour réaliser un composant, le concepteur doit:

□ réaliser un modèle CAO initial à partir d'un cahier des charges, de son expérience et de l'environnement général où se situe sa pièce
□ réaliser ensuite des modélisations (statique, dynamique, etc) permettant de vérifier les critères de dimensionnement
□ itérer en modifiant sa conception de manière à respecter son cahier des charges

Le principe de base des logiciels d'optimisation est de pouvoir reproduire de façon automatique ce qu'un concepteur réalisait auparavant manuellement, en y ajoutant de nombreuses plus-values:

□ possibilité de balayer un espace de conception plus large
□ calculs automatiques
□ possibilités de réaliser des plans d'expériences et de créer ainsi des fonctions d'approximation
□ atteinte d'optimum grâce à des algorithmes de plus en plus performants

Pour le concepteur, les étapes-clefs en optimisation de forme sont donc:
□ la réalisation du modèle de CAO paramétrée
□ la détermination des analyses à effectuer (statique, dynamique, non linéaire, etc)
□ la réalisation d'un modèle paramétré éléments finis et associé à la géométrie
□ la définition des critères de dimensionnement associés à la pièces (contraintes maxi, plage de fréquence interdite, masse, déplacement maxi, etc)
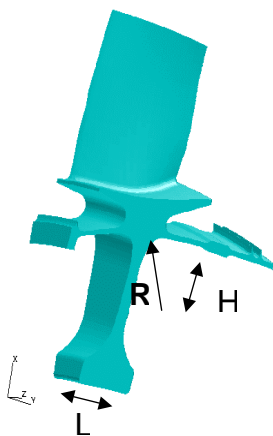
Figure 1 – Modèle CAO paramétré   *Figure 2 – Maillage paramétré*   *Figure 3 - Résultats*
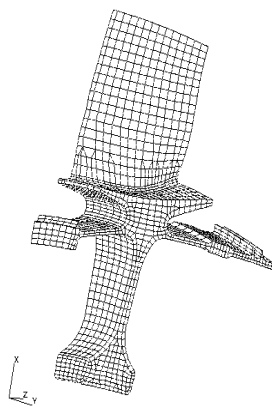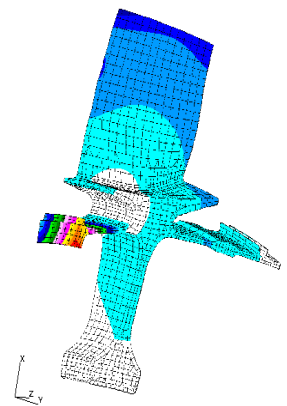
Le logiciel d'optimisation va être chargé de reconnaître et de gérer ces modèles (Eléments Finis, CAO, etc), de permettre à l'utilisateur d'identifier les paramètres sensibles, de piloter automatiquement le processus complet de calcul et de traiter les résultats en fonction des paramètres.

Le plan d'expériences se contentera de permettre la création de fonction d'approximation des fonctions (mais possibilités d'erreurs importante entre la fonction estimée et les points réels), tandis que l'optimisation directe utilisera les valeurs réelles des fonctions et en général les sensibilités (influence des paramètres sur les fonctions = dérivée des fonctions par rapport aux paramètres) pour atteindre des valeurs optimales.
D'autres utilisations sont possibles : analyses probabilistes ou de Monte-Carlo, recalage de modèles (calculs-essais), etc.

Sans entrer dans les détails techniques (notion de perturbateur de maillage, gestion du calcul d'erreur, etc), dans le cadre de l'optimisation de structures, le logiciel d'optimisation va effectuer en batch le processus itératif suivant :
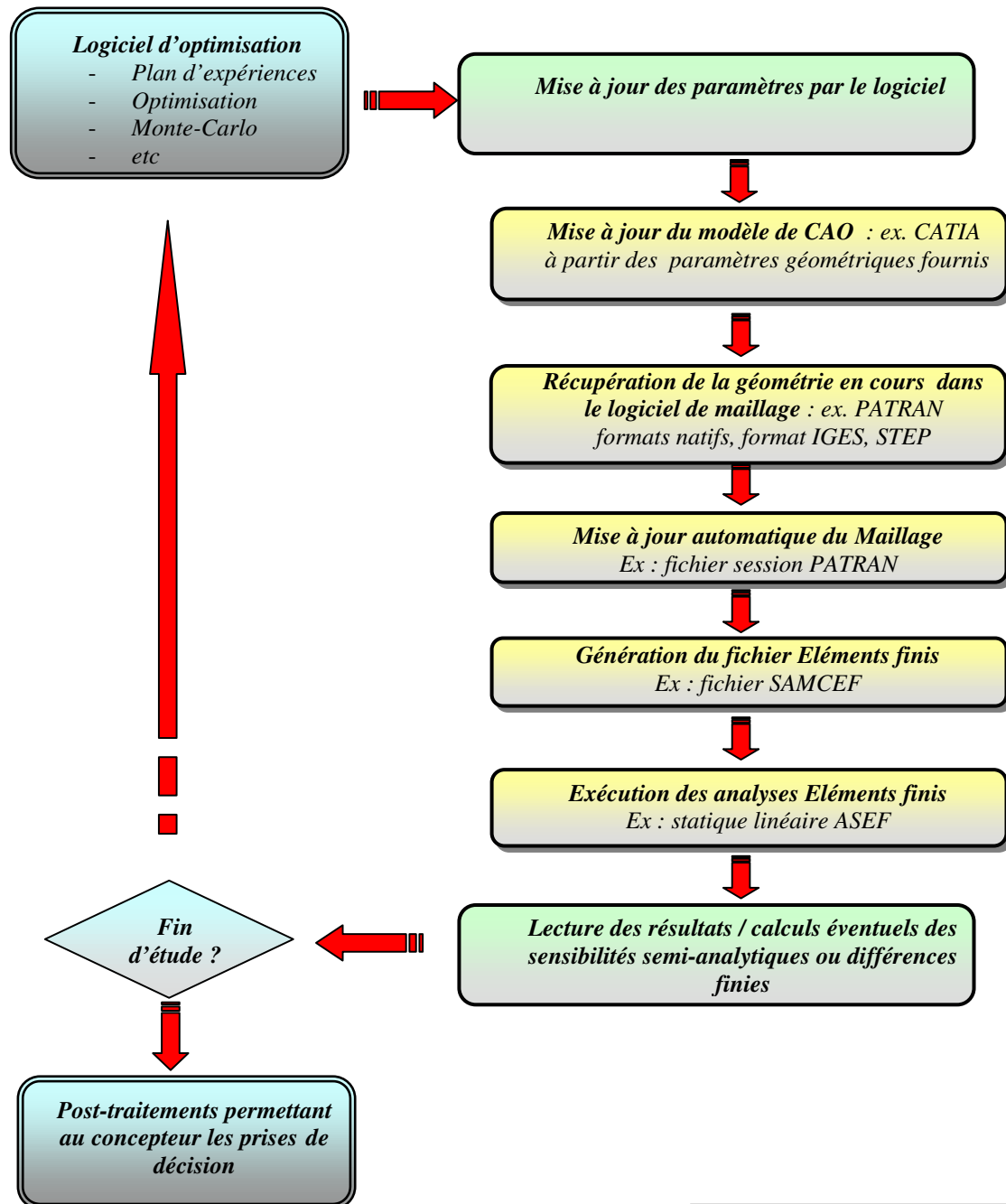
Ce processus se représente en général sous forme de schéma intégrant chacun des modules et des actions à exécuter.
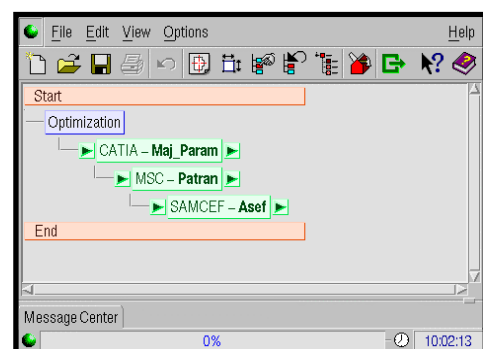
Optimisation d'un disque à l'éclatement

Le premier exemple illustre un cas que les logiciels d'optimisation de base ne savent pas traiter, car il nécessite d'utiliser un code de mécanique non linéaire et porte sur un critère (rupture de pièce) rarement implémenté. L'exemple a servi dans le passé à valider l'utilisation de plan d'expériences et d'études d'optimisation au sein du bureau d'études.

La pièce concernée est un disque de réacteur. Le rôle essentiel des disques est la rétention des aubes de compresseur ou de turbine et le maintien des jeux en bout d'aube. Ce sont des pièces tournantes « à défaillance catastrophique » pour l'avion. Le dimensionnement de ces disques requiert donc le respect des règles imposées par les autorités certifiantes et le respect d'un ensemble de critères issu du savoir-faire de Snecma Moteurs.
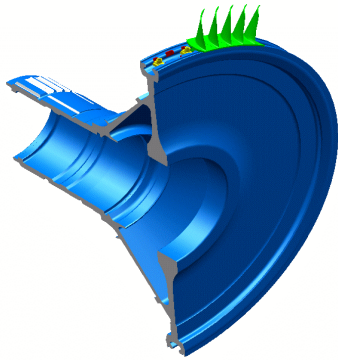
Figure 4 – modèle de disque   *Figure 5 – détermination de la vitesse d'éclatement*
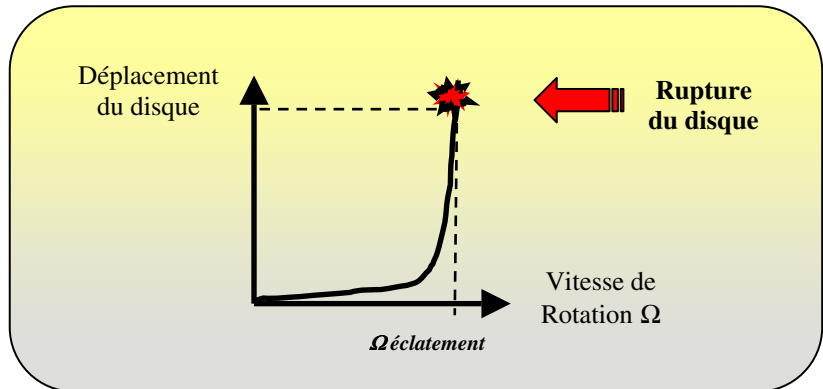
L'expérience a montré que les disques éclatent dès que l'on dépasse une vitesse de rotation critique, à cause de l'augmentation rapide des charges centrifuges. Cette vitesse d'éclatement peut être obtenue par essai, par formules analytiques ou estimée par des modèles éléments finis. A titre d'information, le modèle numérique que l'on réalise utilise des lois de comportement matériaux non linéaires ainsi que des hypothèses de grands déplacements.

L'étude d'optimisation consiste à minimiser la masse du disque tout en respectant une vitesse de rupture supérieure à une limite imposée (ex : 1600 rad/s). Pour cette étude, nous avons modélisé un disque simple et décidé de sélectionner trois paramètres qui influent sur la rupture : l'épaisseur de la toile du disque E1, la hauteur L3 et la largeur L2 d'alésage. Le modèle réalisé est un modèle 2D. L'aube est modélisée par un ensemble de masses ponctuelles situées au niveau de la jante.
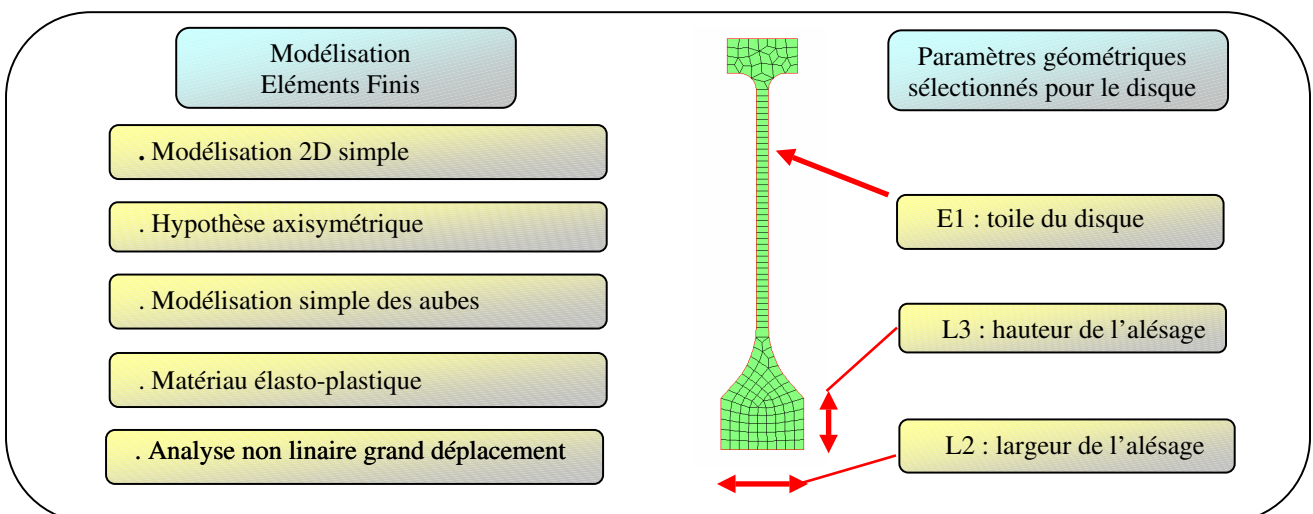
Figure 6 – paramétrage et maillage du disque

Le problème d'optimisation que l'on se propose d'étudier est donc :
- ❑ minimiser la masse du disque,
- ❑ vérifier que la vitesse d'éclatement de la pièce est supérieure à la vitesse limite.

Afin d'explorer l'espace de conception et d'étudier le comportement des fonctions, une étude paramétrique a été menée. Cette étude permet de déterminer l'évolution de la vitesse d'éclatement et de la masse en fonction des paramètres. Cette étude permet aussi de trouver une position approchée de l'optimum et de valider l'optimum trouvé par la méthode directe.

Un exemple d'application numérique est donné ci-après. L'espace de conception est défini par les plages de variation des paramètres suivantes:

2*E1 : *4.4 à 6 mm par pas de 0.4 mm (5 valeurs),*
2*L2 : *30 à 40 mm par pas de 2.5 mm (5 valeurs),*
L3 : *15 à 20 mm par pas de 1.25 mm (5 valeurs).*
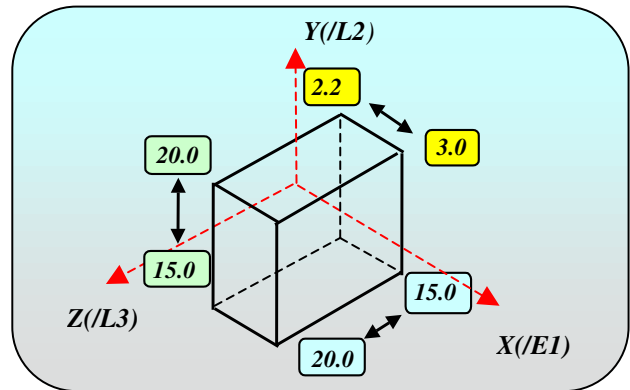
Toutes les combinaisons des paramètres ont été étudiées, soit 125 calculs non linéaires dans un domaine de conception cohérent avec l'objectif. Une fois ces calculs obtenus, nous avons créé une surface de réponse, nous pouvons donc avoir une représentation de l'évolution des critères dimensionnants en fonction des paramètres géométriques.

La même étude a été ensuite lancée en vue d'une optimisation directe en utilisant un algorithme classique (linéarisation convexe). Le logiciel a convergé en une dizaine d'itération vers un point optimum très proche de ce que l'on trouve en analysant les résultats du plan d'expériences.

Zone où se situe le minimum de la masse dans l'étude d'optimisation

Zone du minimum de la masse trouvé à partir de l'étude paramétrique
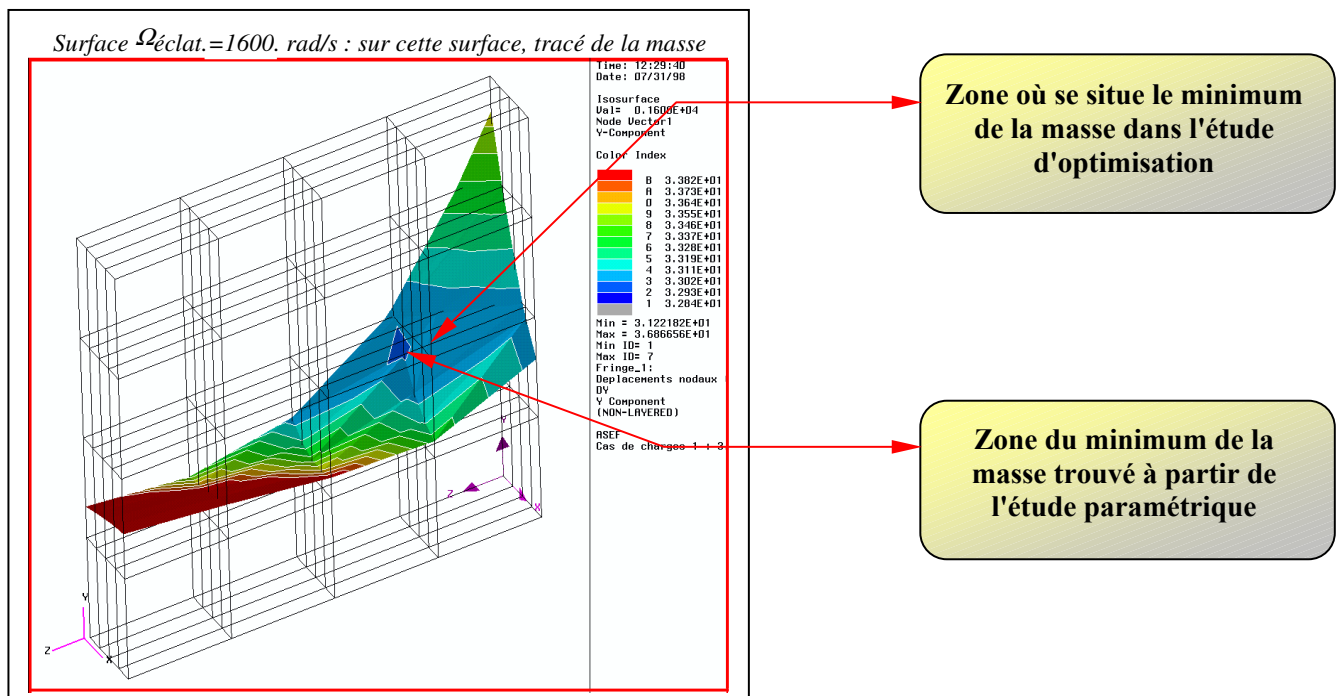
Figure 8 – Surface de réponse et optimum direct

Optimisation de brides festonnées

Un réacteur est constitué de nombreuses brides de liaison. Elles sont présentes aussi bien sur des pièces en rotation que sur des carters structuraux.

L'opération de festonnage des brides permet de gagner de la masse, ainsi que de diminuer les niveaux de contrainte au fond des trous de vis (contrainte générée par le flux des contraintes tangentielles). Le bon dimensionnement de la géométrie des festons permet d'absorber une partie de ces contraintes.

L'étude que nous présentons a permis :
- ❑ de valider la chaîne complète d'optimisation intégrant le logiciel de CAO (CATIA), le logiciel de maillage (PATRAN) et le solveur éléments finis (SAMCEF)
- ❑ de mieux appréhender la problématique « qualité de maillage » et « optimisation », lorsque l'on ne dispose pas de techniques de « perturbateur de maillage » (re-localisation automatique des nœuds du maillage en fonction des variations de géométrie), ni de calculs de sensibilités semi-analytiques.

Le modèle de bride paramétrée est décrit dans les figures suivantes. En utilisant les symétries, on ne se préoccupe que d'une demi-période circulaire de cette bride.
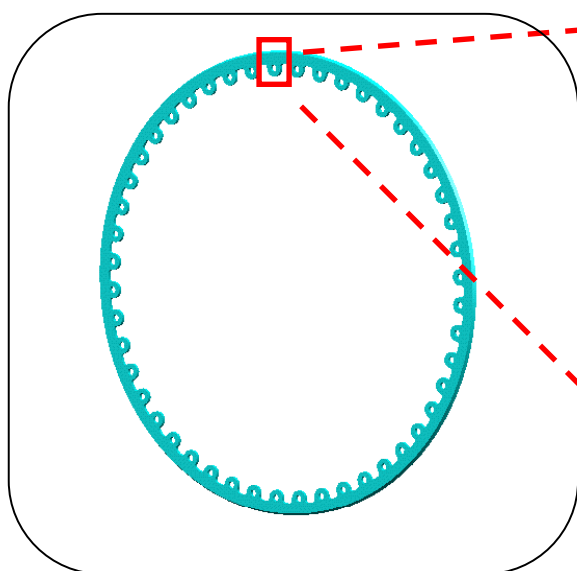
Figure 9 – Bride complète
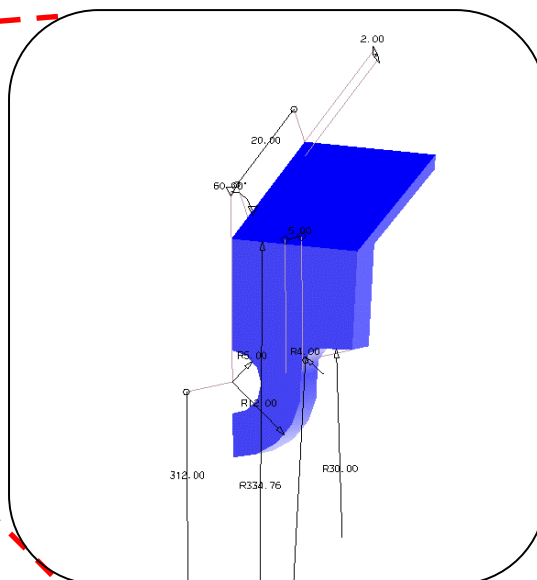
Figure 10 – Modèle CATIA & Paramètres

Cet exemple permet de montrer les différences de résultats à travers différentes stratégies de maillage et donc d'illustrer l'impact sur une éventuelle optimisation de la bride. En effet, l'optimisation nécessite le calcul des sensibilités qui, dans ce cas, sont calculées par différences finies.

Trois stratégies sont étudiées :

- ❑ un maillage libre (figure 11),
- ❑ un maillage réglé (figure 12),
- ❑ un maillage hybride (figure 13).
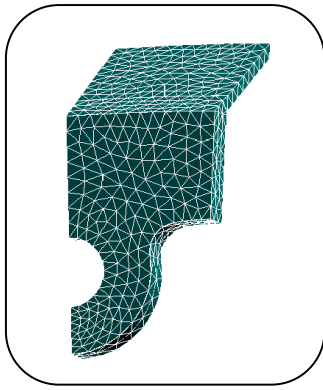
Figure 11 – Maillage libre
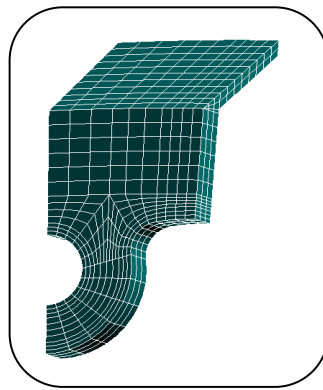
Figure 12 maillage réglé
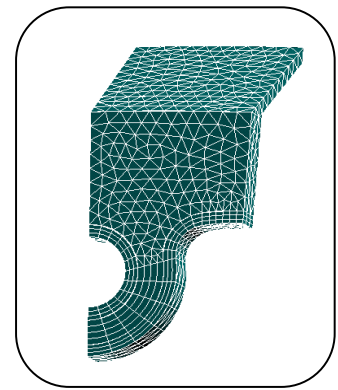
Figure 13 maillage hybride

Modélisation Eléments Finis

. Visualisation des contraintes de Von Mises aux bords de la bride
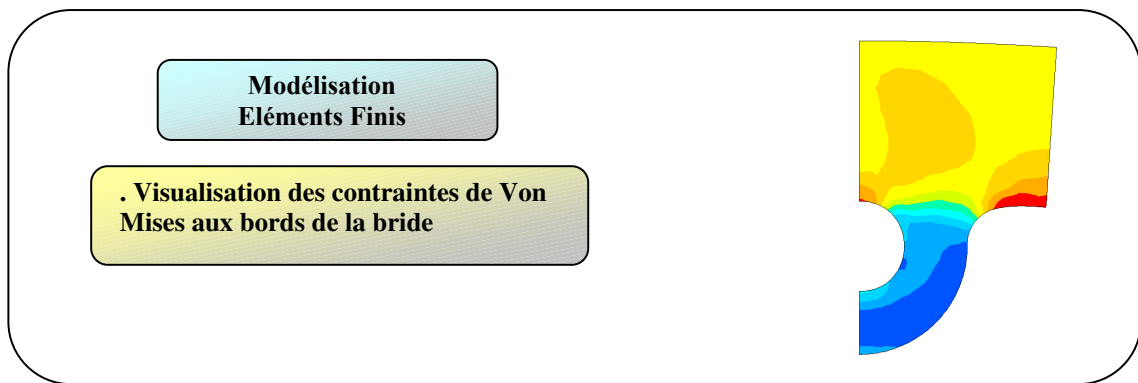
Figure 14 Visualisation des contraintes dans la bride

La figure suivante montre l'évolution de la contrainte de Von Mises maximale atteinte en fond de trou, en fonction du rayon de fond de feston.
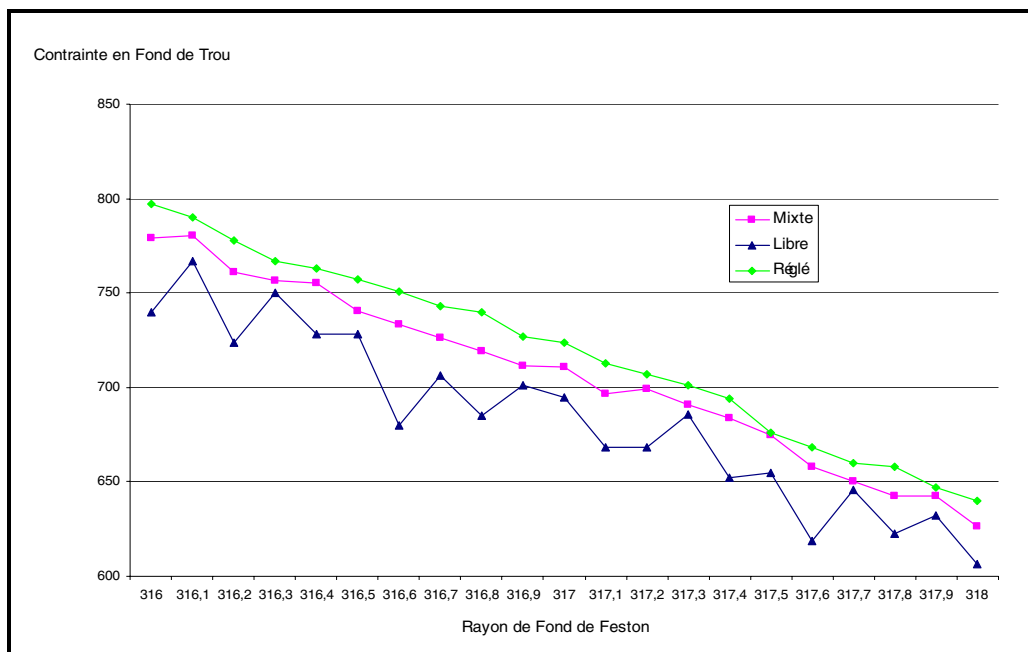
Figure 15 Evolution des contraintes maxi en fonction du rayon de feston

Ces courbes permettent de constater que les résultats obtenus sont très sensibles au type de maillage employé.

Le niveau moyen de la contrainte est différent pour chacune des courbes. Cela s'explique par le fait que les mailles sont de tailles différentes suivant le type de maillage. Les pentes sont aussi très différentes. Cette différence s'explique par la variation de l'élément le plus contraint. Cette variation est d'autant plus grande que l'on utilise un maillage libre.

Cette étude montre qu'en l'absence de perturbateur de maillage une optimisation ne peut être réalisée sur un maillage libre. En effet, les sensibilités sont fausses et empêchent les algorithmes d'optimisation de converger.

Cependant la complexité des pièces étudiées rend parfois délicat la réalisation d'un maillage réglé. Combinant les avantages de l'une et de l'autre, la stratégie de « maillages hybrides » est un bon compromis pour être appliquée dans une chaîne d'optimisation.

Conclusion

Les deux exemples proposés illustrent qu'en quelques années les techniques d'optimisation ont évolué de façon importante et permettent désormais de traiter des problèmes d'optimisation de forme de plus en plus complexes. Ainsi, il est possible d'utiliser tous les types d'analyse mécanique et également de coupler les logiciels de CAO, les logiciels de maillage et les solveurs éléments finis.

Néanmoins, ces exemples illustrent également certains dangers dans l'utilisation des logiciels sans réellement en maîtriser tous les aspects (calcul des sensibilités erroné par une qualité de maillage insuffisante, absence de pertubateur de maillage, fonctions en « escalier » non continues et conduisant à des sensibilités nulles, problèmes des minima locaux, problèmes multi-objectifs, approximation insuffisante des surfaces de réponse, etc).

Nous avons noté d'autres freins d'utilisation de l'optimisation qui sont liés, non pas à l'optimisation en elle-même, mais à la difficulté de réalisation des modèles paramétrés (CAO ou maillage automatique complètement associé à la CAO) et à la difficulté de poser correctement un problème d'optimisation.

Nous travaillons pour lever ces quelques imperfections et il nous apparaît également nécessaire de former et d'aider les ingénieurs d'un bureau d'études afin qu'ils acquièrent « un niveau de culture en optimisation » .

Pour conclure, nous sommes convaincus que la facilité d'utilisation des futurs logiciels de CAO paramétrés comme CATIA v5 et l'intégration de la plupart des logiciels de maillage dans ces environnements vont permettre de multiplier de façon importante les études d'optimisation et de rendre plus industrielles les études multi-disciplinaires.

Paper #13
Discussor's name: Kirit Patel
Author's name: Mr. Girard

Q: In your pre-optimization process, you spent some time in the design of the disc you showed. How much improvement in design time has resulted from your new optimization method?

A: The optimization techniques allow us to explore a much larger space in the design area for the same amount of time as traditional techniques. Consequently, the main improvement is not in design time, but in quality of the final design. This results in direct reduction of time and cost in the global design process: it helps to reach the 'Best Design at first time' and reduce non-quality & re-design, therefore reducing cost and delays on a program

Integrated Design and Analysis of an Aircraft Fuel System

R.M. Tookey, M.G. Spicer and D.J. Diston
BAE SYSTEMS
Warton Aerodrome
Preston, Lancashire, PR4 1AX
United Kingdom

Summary

Using an aircraft fuel tank as an industrial case-study, the paper describes some recent research developments at BAE SYSTEMS that allow the airframe and systems life-cycles to become better aligned. In particular, the paper demonstrates that the design and analysis of the fuel system can be integrated with the airframe structure. This will reduce qualification times in the future and enable Simulation Based Acquisition (SBA), that is, the procurement of aircraft based on synthetic results rather than physical testing.

Introduction

The current generation of military aircraft requires a prolonged and costly activity to develop and qualify the fuel system. This involves a combination of performance analysis, fuel rig and flight test programmes, culminating in system qualification. There is a requirement therefore:

- to improve the qualification process by complementing the physical testing with fully-integrated analysis and simulation capabilities within a Synthetic Environment (SE);
- to reduce the need for physical testing by taking into account the real world functional and operational characteristics of the fuel system within the SE;
- to lever the optimum trade-off, i.e. enabling Multi-Disciplinary Optimisation (MDO), during the early development phases of the aircraft life-cycles;
- to calibrate the synthetic fuel system with actual fuel rig and flight test results.

These requirements can be satisfied by integrating the physical and functional design of the fuel system, thereby aligning the airframe and systems life-cycles. If successful, then this becomes an enabler for SBA.

The qualification includes gauging analysis of tank contents, one-dimensional network analysis for pressure, flow and thermal distributions, as well as the selective use of Computational Fluid Dynamics (CFD) for three-dimensional flow analysis. Each of these analyses is currently performed separately and the results are summarised in a form suitable for simulation of the overall fuel system. This is used as a means of demonstrating system capability and predicting performance. Subject to appropriate validation, operational scenarios can be investigated in detail on an engineering workstation. This reduces the uncertainty in design and the amount of (expensive) system testing.

The Flight Control System (FCS) requires the continuous estimation of fuel mass and centre of gravity (CG). These can be derived from the mass and CG of individual fuel cells for any combination of aircraft pitch and roll angles. For a specific cell, this is constructed as a relationship between the volume of fuel and the height of the equilibrium-free fuel surface, as illustrated in Figure 1. Currently, CATIA V4 solids representing the fuel in each cell are first constructed. An in-house software application then repeatedly splits each fuel cell solid with gauging planes which take into account the aircraft pitch and roll angles and percentage divisions along the length of the gauge probe. The application analyses the remaining fuel solids for their volumes and CGs and produces text file output. This is applied to each gauge probe and typically considers 55 combinations of pitch and roll angles and 21 equally-spaced percentage lengths, i.e. a total of 1155 solid split operations and analysis interrogations. Inevitably, this analysis provides no information beyond the physical

extremes of the gauge probe. A fuel cell can fill above 100% of the wetted probe length, in which case, the excess fuel is ungauged. In addition, it can drain below 0%, in which case, all the fuel is ungauged. Note that, although undesirable, this is not a restriction of the functionality in CATIA V4.
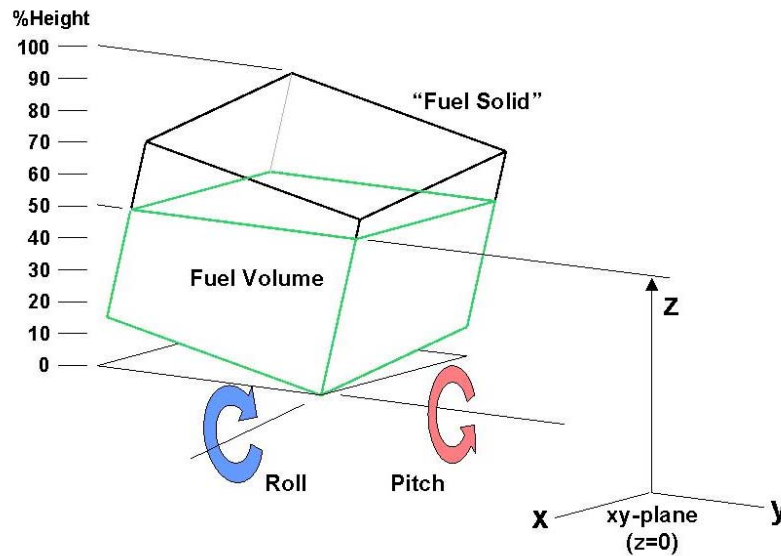
FIGURE 1. Gauging parameters

The paper first reviews the current process at BAE SYSTEMS for designing and analysing an aircraft fuel system using the case-study illustrated in Figure 2, i.e. the wing nacelle tank for Nimrod. The construction of an integrated assembly of solid models, i.e. a Digital Mock-Up (DMU), representing the airframe structure and fuel system is then described. This is followed by the development of a software application for remote modification and analysis of the constructed model. In particular, the application automates the gauging analysis and produces percentage cell volume and CG output in the required format for simulation. The general structure of this simulation is described and sample results presented.

FIGURE 2. Fuel tank case-study

The research developments described in this paper have been achieved using recent advances in computing technology, such as CATIA V5 from Dassault Systèmes and its associated Application Programming Interface (API). The challenge for BAE SYSTEMS now is to develop the corresponding integrated processes to support this technology and to establish a SE that can provide credible qualification evidence.

Review of current process

During conceptual design, the initial external shape of the aircraft is first specified by a set of oversize surfaces. A key diagram then specifies the internal structural layout. Although it can be a set of 2D drawings containing reference lines and curves, the key diagram is usually a Computer-Aided Design (CAD) model containing reference planes and surfaces: the planes correspond to the neutral axes of the spars, ribs, frames and floors. At this stage of the design process, the parts are represented by oversize surfaces constructed on the reference planes and then trimmed back to the external surfaces. From this information, simple solids representing the fuel cells can be constructed by first assembling adjacent faces into volumes and then closing them. Figure 3(a) illustrates the conceptual model of the wing nacelle tank containing a single surface representing the external shape of the nacelle and three solids representing the fuel cells within the tank.

The fuel cells are initially gauged over their extreme dimensions using a virtual gauge probe. This involves constructing a geometric line representing the probe and a series of gauging planes at particular aircraft pitch and roll angles. These planes are then positioned at percentage lengths along each probe to represent the fuel surface. The fuel cell solids are split with these gauging planes and the resulting solids representing the fuel are analysed for their volumes (as a percentage of the total cell volume), CGs and heights from the *xy* plane. This helps the fuel engineers to provide first estimates of the fuel mass and CG, which then impacts on aircraft performance, controllability and structural layout. In addition, the initial fuel system can be designed, i.e. pumps, pipes and gauge probes can be positioned and frame cut-outs can be located and sized. The part designers build this information into the assembly of models, i.e. the DMU.

The definition of the airframe and fuel system matures during preliminary design. Internal surfaces are designed, possibly allowing for the complex architecture of Carbon-Fibre Composite (CFC) skins, and the key diagram is finalised. The parts are now represented by simple solids, which possibly contain large cut-outs but do not yet contain pockets and fillets. Complex fuel solids are constructed by subtracting the assembly of structural parts, e.g. skins, spars, ribs, frames and floors, and systems parts, e.g. pumps, pipes and gauge probes. For performance reasons, however, simple skin solids with constant thicknesses are used instead of the complex ones with architectured internal surfaces. Note that these simple skin solids have larger volumes than the corresponding complex ones since they include the volume of the numerous stringers that strengthen the skin and will eventually be included within the DMU during detailed design. Figure 3(b) illustrates the preliminary model of the wing nacelle tank containing a single external surface, three fuel solids and multiple solids representing the structural and systems parts.

(a)   (b)
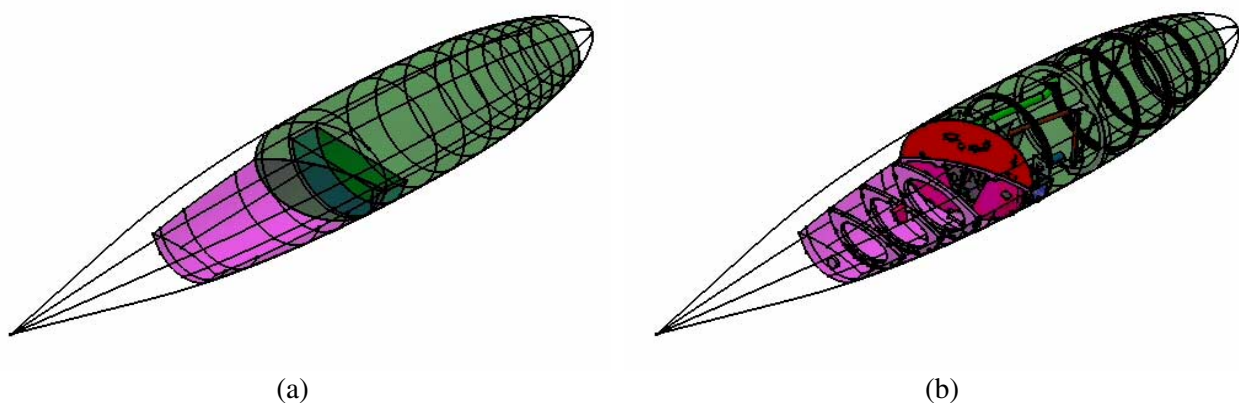
FIGURE 3. (a) Simple and (b) complex fuel solids for the wing nacelle tank

This time the fuel cells are gauged using physical gauge probes, rather than virtual ones, i.e. they are represented by cylinders of fixed diameter and length. Based on the gauging analysis, the fuel engineer modifies the probe positions in order to minimise the amount of ungauged and unusable fuel. Fuel is ungauged if the fuel surface is outside the length spanned by the probe electrodes, although the term usually implies that the surface is below the probe. Fuel is unusable if the fuel surface is below the level at which the pumps can operate wet. One solution is to use lightweight inserts to occupy the dead space, which is satisfactory provided

the dead space is not too large. In addition, the complex fuel solids can be exported to third party tools, such as FLUENT, for detailed three-dimensional CFD flow analysis.

The part solids are fully detailed during detailed design, i.e. all cut-outs, pockets, fillets and stringers are explicitly modelled. However, the complex fuel solids are not modified to reflect this additional detail in the DMU. Instead, the existing values of the volumes and CGs are calibrated using proportionate scaling. The scaled values are used to populate look-up tables embedded within the airborne software. Fuel contents and CG can then be calculated using the current aircraft pitch and roll angles (determined from inertial data) and percentage probe lengths (determined from the wetted probe points). This determines the range of a particular mission and imposes restrictions to the flight envelope if the overall aircraft's controllable CG range is exceeded.

Finally, physical tests are performed to verify the synthetic results and calibrate the estimated volumes and CGs from the preliminary solids. The goal is to reduce costs and lead times by minimising the dependence on physical test rigs. This implies the need to host the bulk of the fuel system design and analysis within a SE. It is clear from the above review that the systems life-cycle is dependent on the airframe life-cycle, which traditionally means that the two are sequential. The next two sections will describe some research developments that make the two life-cycles more concurrent. This could either reduce the lead times for the same output quality, or improve the output quality for the same lead times through more design iterations.

Model construction

This section describes the construction of the CAD model using CATIA V5. This will be compatible with the application for gauging analysis described in the next section. Recall that parametrised and associative solids are constructed representing the fuel in each cell. The individual fuel cell solids are first assembled together to form a simple fuel solid. An assembly of solids representing the airframe structure and fuel system is then subtracted from this to leave a complex fuel solid. A single parametrised gauging plane is now constructed corresponding to specific aircraft pitch and roll angles and percentage lengths along a gauge probe. This splits the complex fuel solid to leave a solid representing the corresponding fuel in the cell. Figure 4 illustrates one of the fuel solids using aircraft pitch and roll angles of 0° and a percentage length of 100% along a physical gauge probe, whose axis is shown as a line. It is clear that there is a significant amount of ungauged fuel, with the actual gauging limited to approximately 97% of the total cell volume. This suggests the probe position could be improved.

All of the driving (input) and driven (output) parameters are constructed individually and linked to geometry. Driving parameters include the cell and probe for analysis, aircraft pitch and roll angles, and percentage probe length; driven parameters include the percentage cell volume, CG and height from the *xy* plane. The model contains two types of probe. The first is virtual and gauges over the extremes of the tank, while the second is physical and corresponds to a standard part of fixed diameter and length. The physical probes are initially positioned vertically within the DMU on specified bottom points and then the fuel engineer pitches and rolls them into appropriate positions. Therefore, the model contains additional driving parameters corresponding to the probe bottom points and probe pitch and roll angles, and additional driven parameters corresponding to the (offset) distances of the probe end points from the inside of the tank and the probe top points. Alternatively, the top point $\mathbf{r}_t$ could be calculated from the bottom point $\mathbf{r}_b$ for each probe using

$$\mathbf{r}_t = \mathbf{r}_b + l \begin{pmatrix} 1 & 0 & 0 \\ 0 & \cos\phi & -\sin\phi \\ 0 & \sin\phi & \cos\phi \end{pmatrix} \begin{pmatrix} \cos\theta & 0 & \sin\theta \\ 0 & 1 & 0 \\ -\sin\theta & 0 & \cos\theta \end{pmatrix} \begin{pmatrix} 0 \\ 0 \\ 1 \end{pmatrix} = \mathbf{r}_b + l \begin{pmatrix} \sin\theta \\ -\cos\theta\sin\phi \\ \cos\theta\cos\phi \end{pmatrix},$$

where l, θ and ϕ correspond to the probe length, the pitch angle and the roll angle respectively. Note that, by convention, the pitch rotation matrix is always applied before the roll rotation matrix when manipulating an aircraft part within the DMU. However, for gauging purposes, the CAD model orients the fuel surface and not the fuel solids, which means the roll rotation matrix must be applied before the pitch rotation matrix.
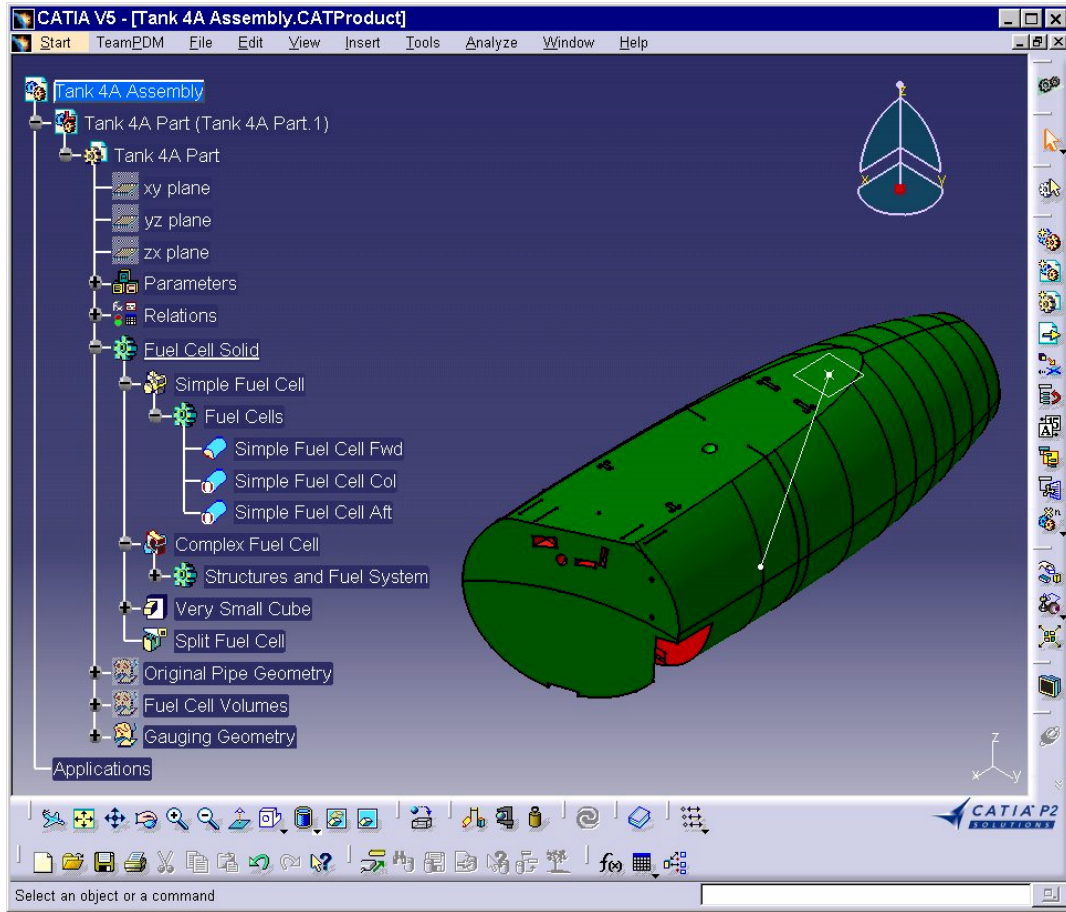
FIGURE 4. Graphical window for a fuel cell gauged by a physical probe

Rules are used to ensure the CAD model, i.e. the fuel solid, is correctly constructed using the input parameters specified by the fuel engineer. The rule for constructing the fuel solid activates and de-activates the Boolean operations used to assemble the individual fuel cell solids. The de-activated operations for constructing one of the fuel cells are visible in the graphical window (Figure 4). Since the probes have been constructed using geometric lines and not Boolean operations, then the rule for constructing the probe uses a weighted average of all (virtual and physical) gauge probe end points, i.e.

$$\mathbf{r}_b = w^v \mathbf{r}_b^v + w^{p1} \mathbf{r}_b^{p1} + w^{p2} \mathbf{r}_b^{p2} + ... + w^{pn} \mathbf{r}_b^{pn}$$

and

$$\mathbf{r}_t = w^v \mathbf{r}_t^v + w^{p1} \mathbf{r}_t^{p1} + w^{p2} \mathbf{r}_t^{p2} + ... + w^{pn} \mathbf{r}_b^{pn} ,$$

where $\mathbf{r}^v$, $\mathbf{r}^{pi}$ and w correspond to the virtual probe, the ith physical probe and the weights respectively.

Figures 5, 6 and 7 illustrate the effects of gauging a fuel cell using the virtual (extreme) and physical gauge probes at various aircraft pitch angles. A fixed aircraft roll angle of 0° and percentage probe length of 25% is assumed. Figure 5 illustrates that the analyses can provide similar results when the lengths of the virtual and physical probes are the same. However, the analyses can provide significantly different results when this is not the case (cf. Figure 6) due to the virtual probe being variable, i.e. dependent on the aircraft's attitude, while the physical probe is fixed. This is further exacerbated during inverted flight, e.g. for a combat aircraft. Consider when the fuel surface corresponds to 25% of the probe length, then the CAD model should suggest that the fuel occupies approximately 75% of the cell volume. This is true for the physical gauge probes, but not for the virtual one. The correct fuel solid can be constructed using another rule, which recognises the inverted flight condition and positions the gauging plane accordingly, i.e. at the same percentage but measured

from the other end of the virtual probe (cf. Figure 7). Note that identical simulation data can be determined using either gauging strategy by considering the height of the fuel surface from the *xy* plane.
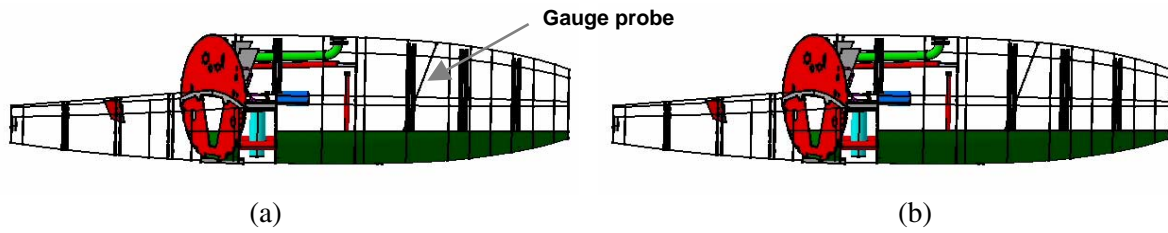
FIGURE 5. Gauging of a fuel cell using (a) virtual and (b) physical probes at an aircraft pitch angle of 0°
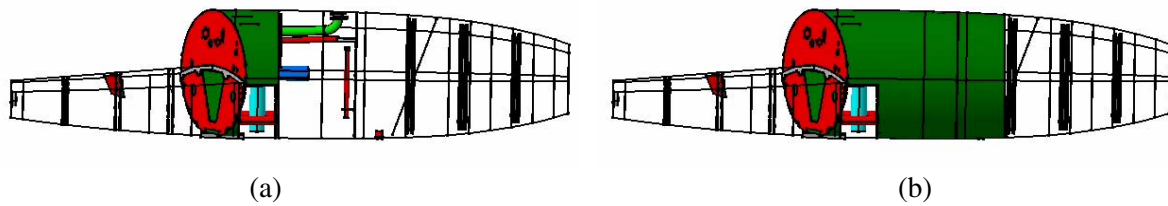
FIGURE 6. Gauging of a fuel cell using (a) virtual and (b) physical probes at an aircraft pitch angle of 90°
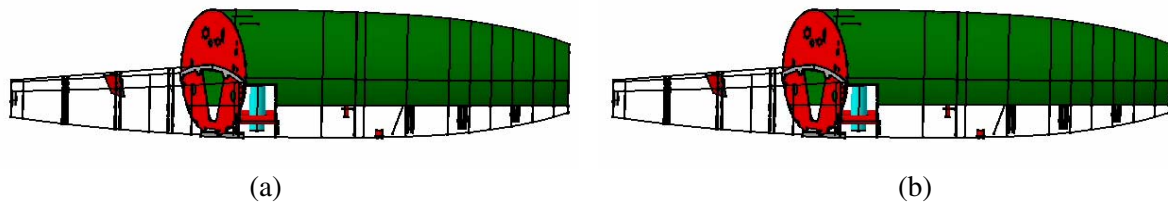
FIGURE 7. Gauging of a fuel cell using (a) virtual and (b) physical probes at an aircraft pitch angle of 180°

Since the assembly of models is parametric and associative, then all solids can be modified and automatically updated by the modelling system. In addition, external and internal surfaces can be replaced and the reference planes defining the key diagram can be re-positioned. Having constructed the fuel solid, corresponding to the fuel engineer's specifications, then it can be analysed for its percentage cell volume, CG and height from the *xy* plane. Recall that the gauging analysis typically considers 1155 solid split operations and analysis interrogations for each probe in each cell. Clearly, this is a time-consuming and labour-intensive process if performed interactively by the fuel engineer.

Application development

This section describes the development of an application using the CATIA V5 API that allows the fuel engineer to perform side-studies on the fuel system and automate the gauging analysis on the CAD model. Through its user interface, the developed application will access the CAD model remotely and produce a C header file (.h) in the required format for simulation, together with a Microsoft Excel spreadsheet (.xls) and text file (.txt).

Initially, the fuel engineer starts CATIA V5 from the application and selects either the local or a remote server containing the CAD software and licences. This creates a process on the selected machine where the analysis is to be performed. A model is then selected in which one or more fuel cells reside and opened in the CAD window (Figure 4). The specification tree is reproduced within the application window so that the fuel engineer can specify any driving (input) parameters that were built into the CAD model by the part designer and select the fuel cell for analysis. The fuel engineer can then force the CAD model to update the geometry and any driven (output) parameters. Note that the fuel engineer cannot save these modifications against the model: he is only able to perform a side-study and would have to submit a traditional Engineering Change

Request (ECR) form to the part designer. Figures 8(a) and (b) display the application's specification windows for a fuel cell analysed with virtual and physical gauge probes respectively. Note that the application displays the probe end points and the (offset) distances from these points to the inside of the tank. Figure 8(a) corresponds to conceptual design, where the distances are zero and a percentage probe length of 100% corresponds to a percentage cell volume of 100%, i.e. all of the fuel is gauged. Figure 8(b) corresponds to detailed design, where the distances are positive and a percentage probe length of 100% corresponds to a percentage cell volume of approximately 97%, i.e. some of the fuel is ungauged.

(a)   (b)
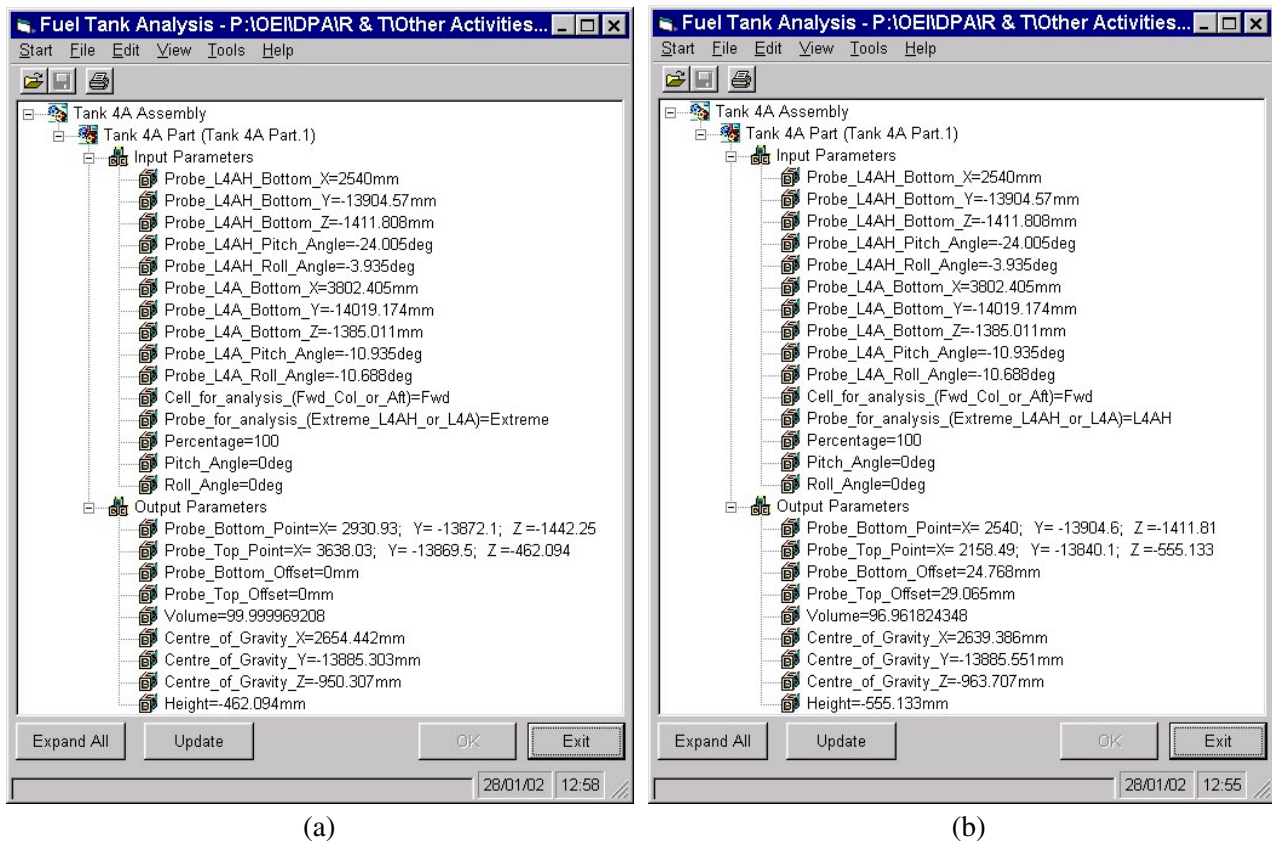
FIGURE 8. Specification window for a fuel cell gauged by (a) virtual and (b) physical probes

The default analysis considers single aircraft pitch and roll angles of 0°. The fuel engineer can either modify these individual values, specify a range of equally-spaced values, or specify a set of distinct values. By default, for each combination of aircraft pitch and roll angles, 5 equally-spaced planar splits are made between percentage probe lengths of 0% and 100%. Again, the fuel engineer can either modify the number of equally-spaced values or specify a set of distinct values. Alternatively, the fuel engineer has the option of opening a text file which specifies the CAD model to be analysed and the gauging parameters, i.e. the aircraft pitch and roll angles and percentage probe lengths. The fuel engineer can choose to de-select the CG calculation which significantly improves the performance of the analysis interrogations.

Four types of output are available. Figure 9 illustrates the application's graphical output using 3 aircraft pitch angles, 3 aircraft roll angles and 11 percentage lengths along a physical gauge probe. The graph displays polylines of percentage cell volume plotted against percentage probe length for particular combinations of aircraft pitch and roll angles, together with individual analysis points. The fuel engineer has the option of saving the gauging results to either a text file (.txt), a Microsoft Excel spreadsheet (.xls) or a C header file (.h) in the required format for simulation. The graph displays that the fuel occupies approximately 97% of the total cell volume when the wetted point is 100% along the probe length and the aircraft pitch and roll angles are 0°. Similarly, there is ungauged fuel for many other combinations of gauging parameters.
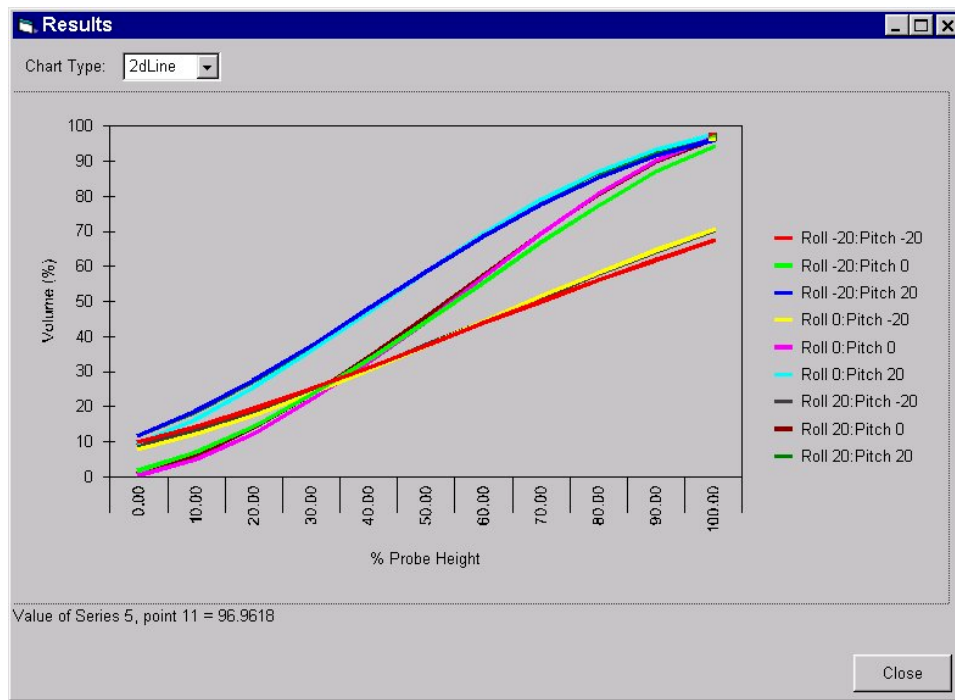
FIGURE 9. Graphical window for a fuel cell gauged by a physical probe

Use of application within fuel system simulation

A significant use within the systems life-cycle is the provision of high quality data for fuel simulation. In order to represent the internal distribution and dispersal of fuel between cells, it is necessary to accurately represent the relationship between fuel height and volume in all cells. This has to be updated dynamically as fuel enters and leaves a cell. The rate of fuel transfer between cells is a function of the height difference across inter-cell frames and the shape and position of frame cut-outs. Early in the systems life-cycle, it may be sufficient to approximate an inter-cell transfer by a semi-permeable surface which offers a notionally uniform restriction to fluid flow. Later, it will be necessary to investigate detailed flow phenomena in areas where problems have been found, such as unacceptably slow transfer, puddles of unusable fuel and sloshing of large fuel masses.

The simplest functional model for representing inter-cell flows is a network model, comprising nodes and connections. In a classical nodal network, these concepts are applied to pipes, pumps and valves. The nodes act as small accumulators for the fluid in the pipes and, given the bulk modulus of the fluid, they provide a calculation of pipe pressure. The problem for fuel simulation is that the working fluid is assumed to be incompressible and so the bulk modulus has to be relaxed in order to facilitate a computationally efficient process. This is reasonable for bulk transfers, but may be unreasonable for the investigation of specific phenomena such as water hammer.

Fluid nodes, as used in fuel tank simulations, contain height-volume information that is driven by the mass and heat content of each cell at each simulation step. Mass and heat content determine fuel temperature and density, which are both assumed to be homogeneous properties of a cell. Thus volume is calculated and converted into a height, using data similar to that presented in Figure 9. This height information is then transmitted to interface components, e.g. faces and pumps. Note that a face is a generic term for an aircraft structure that permits flow. Pumps inlets and pipe inlets/outlets are described functionally between interface co-ordinates for the flow paths together with flow control relationships, i.e. pump curves and valve curves. The co-ordinate geometry is critical to what happens at the tank boundaries since the submergence of interfaces determines pressure at those interfaces. The component geometry is important in establishing exact fuel volumes for the FCS, but approximate volumes, such as space envelopes, suffice for simulation.

A typical architecture for fuel simulation is shown in Figure 10. It is a bond graph representation of the wing nacelle tank used in the case-study showing 3 fuel cells, 2 inter-cell faces and 3 interfaces between the fuel cells and pipes. A bond graph is a conceptual notation for defining energy flow around a system. Bonds are shown as "harpoons" pointing in the assumed direction of energy flow. Two complementary variables are defined for each bond, in this case pressure and flow, the product of which is power. These models are inherently power-conserving and internally consistent. In addition, they are quick to construct and suited to network modelling.
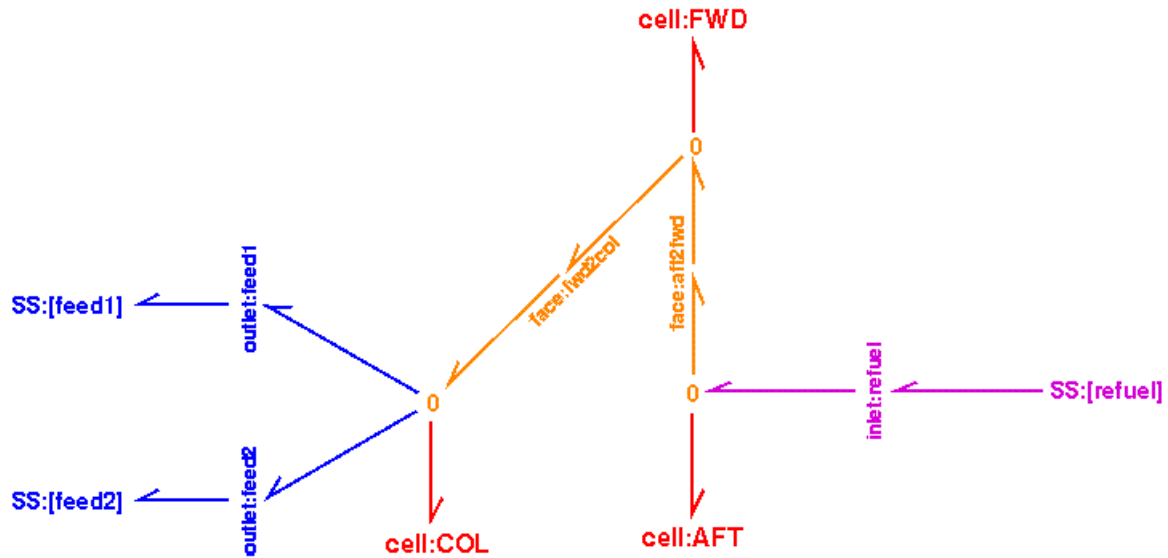
FIGURE 10. Bond graph representation for the wing nacelle tank

Bond graph tools translate diagrams (plus component specifications) into sets of equations that can be solved and compiled into simulation code. The substantial benefit of an integrated approach to airframe and systems modelling is that network models of this type can now be readily applied to systems that have a large amount of geometrical data associated with them. The application described in this paper makes this data available in a form suitable for direct inclusion in large simulations within the traditional burden of manual preparation.

The end result of this type of work is to be able to predict fuel performance over time. Sample results from a refuel simulation are shown in Figure 11, giving the change in cell mass and height over about half an hour as part of a complete aircraft refuelling exercise. These results are indicative of the general behaviour of fuel in tanks. However, the value of an integrated approach is clear. It shows the fuel engineer how the fuel system works under operational conditions and shows the part designer how the airframe needs to be configured in order to be able to move fuel around.
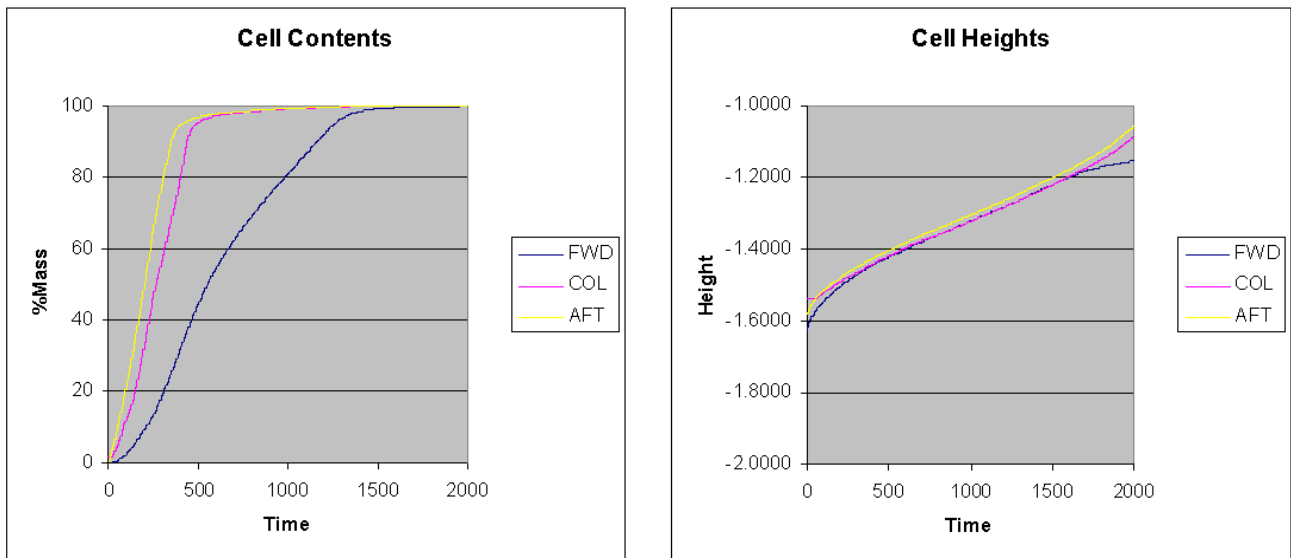
FIGURE 11. Sample results from refuel simulation

Having achieved this link between airframe and systems, immediate possibilities exist for visualising the simulation. These are based on fuel solids within the CAD model accessing the same height-volume data that was exported for simulation. This would provide feedback from the system design process to the airframe design process and, in addition, offer a route into SE presentation (through movie clips and possibly interactive graphics). The value of this capability is potentially enormous, enabling fuel engineers and part designers to view and manipulate their product in advance of it actually being built.

Conclusion

The paper has successfully demonstrated that the design and analysis of the fuel system can be integrated with the airframe structure. This integration will clearly reduce qualification times and enable Simulation Based Acquisition. The key developments of the proposed integrated process over the current one include:

- the construction of a single parametrised gauging plane, rather than multiple isolated ones;
- extreme gauging analysis using a percentage of the overall cell volume, together with the physical probe length;
- formatted output for the simulation, i.e. a C header file (.h), together with Microsoft Excel spreadsheet (.xls) and text file (.txt) output.

The main benefit is that the application is run independently of CATIA V5 as a remote process. This allows the fuel engineer to perform "what if …?" and "how to …?" side-studies without committing any design changes to the solid models and the manufactured parts. In addition, the dependence of the fuel engineers on specialist CAD knowledge and modelling skills has been removed. However, effective communications are required between the part designers and fuel engineers to establish the correct CAD models and manage the change process.

The process is limited in that without visual feedback, the fuel engineer cannot determine whether the solid models have updated correctly, i.e. without introducing clashes between the different parts within the DMU. Furthermore, parts cannot be inserted or removed from the model: they can only be modified. However, with careful specification of the fuel system, the fuel engineer should only need to introduce minor modifications and thus the visual feedback may be unnecessary. When these limitations have been addressed and a new integrated process has been implemented within a production environment, then clearly the airframe and systems life-cycles will become better aligned. It is worth noting that similar integrated processes could be applied to the design and analysis of other aircraft systems for power and thermal management.

Bibliography

Cook, M.V. [1997], *Flight Dynamics Principles*, Arnold.

Fielding, J.P. [1999], *Introduction to Aircraft Design*, Cambridge University Press.

Karnopp, D.S., Margolis, D.L. & Rosenberg, R.C. [1990], *System Dynamics: A Unified Approach*, John Wiley.

Moir, I. & Seabridge, A.G. [1992], *Aircraft Systems*, Longman Scientific & Technical.

Paper #14
Discussor's Name: Kirit Pael
Author's Name: Dr. Richard Tookey

Q: This analysis technique is being demonstrated in a design mode. Can this be applied in the manufacturing definition process?

A: The technique of accessing a CATIA v5 assembly using a VB application can be applied to component parts (in design mode), as well as tooling parts (in manufacturing mode), provided the part designer has constructed a parametric and associative CATIA v5 assembly and has exposed the relevant (input and output) parameters for the VB application.

This page has been deliberately left blank

Page intentionnellement blanche

An Integrated Optimization System for Turbomachinery Blade Shape Design

Dr. S. Pierret
Numeca International s.a.
Avenue Franklin Roosevelt 5
1050 Brussels, Belgium
pierret@numeca.be

Prof. Ch. Hirsch
Vrije Universiteit Brussel
Dept. Fluid Mechanics, Pleinlaan 2
1050 Brussels, Belgium

Abstract

This paper presents a new integrated methodology for the optimisation of turbomachinery blade shapes coupling a user interface, a blade geometry generator to an automatic CFD solution process and an optimisation algorithm.

The methodology relies on the interaction between a genetic algorithm, a database and user generated objective functions and constraints. The latter includes aerodynamic, geometrical and structural constraint functions, while future developments will extend these to aero-acoustic optimisation objectives.

Several examples, covering gas turbine configurations are presented.

1. Introduction

Designing turbomachinery blades is a complex task involving many different objectives and constraints coming from various disciplines. In order to help the designer in this complex task, various complex codes are now available to define complex blade geometries (CAD system), compute the flow field inside the blade channel (CFD codes) and the mechanical stresses inside the blade metal (structural codes). Although the CFD software are getting more accurate, fast and user-friendly they do not provide algorithms able to automatically optimize the performance of a geometry. As a consequence, blade designers often start from an existing geometry and try to adapt and improve it based on a trial and error procedure. In this procedure, the designer modifies the blade manually based on his own experience and computes the flow field on the modified blade. However, the very short design time schedule, often imposed by the market, do not allow the designers to test many modifications and therefore can not take full advantage of the huge potential and huge amount of information provided by the CAD, CFD and structural codes.

Further improvement of this design cycle is probably one of the main challenges of the next decade in the turbomachinery community. Major improvements are expected in terms of reduced design time, reduced engineering time, better optimum and increased design complexity. This challenge can only be tackled by selecting and further developing general and efficient design algorithms integrated into a software dedicated to this specific design task.

Today, several other design methods are available such as gradient methods based on finite difference [1] or more recently based on the sensitivity and the adjoint equation [2], genetic algorithm [3], simulated annealing, response surface methods, inverse design [4] or expert systems [5].

Generally speaking it is hard, if not impossible, to state the superiority of one method over the others for every type of design problems. All these methods have advantages and disadvantages and are therefore limited to some class of problems and cannot cover the whole field of design problems.

An ideal design method should satisfy a number of criteria :

- Generality of the formulation : ability to treat various kind of design or optimization problems (aerodynamic, structural, ...) and various ways to evaluate the system performance (computer codes, experiments, correlations, ...),

- Multi-objective : ability to treat simultaneously various objectives from different fields,

- Reduced computational resources : ability to use a reduced number of calls to expensive computer codes,

- Robust and automatic : ability to avoid local minimum and to run without any human intervention and expertize during the design cycle,

The solution to the definition of an ideal design method seems to combine the advantages of many design techniques into a single design method. A design method has been developed that is based on the concept of function approximation and that combines other very popular techniques such as artificial neural networks, genetic algorithm, database and CFD analysis tools [6], [7].

A completely new commercial package (FINE^{TM}/Design3D) has been developed at NUMECA International that offers more flexibility, improved performance, graphical-user interface (GUI) and full automatization of the design cycle. This new software incorporates various very popular and efficient techniques such as artificial neural networks, genetic algorithms, databases and CFD analysis tools.

FINE^{TM}/Design3D offers a fully automatic coupling to the NUMECA fast and high fidelity CFD simulator FINE^{TM}/Turbo that contains a mesh generator IGG^{TM}/Autogrid, a flow solver EuranusTurbo and a post processor CFView^{TM}. EURANUS [8] is a finite volume discretization code based on explicit time marching algorithms. The explicit Runge-Kutta time stepping procedure is used to advance the solution to steady state. A centered space discretization is applied and scalar local time stepping is used to advance the solution in time. Acceleration techniques such as implicit residual smoothing and multigrid are used systematically.

2. FINE^{TM}/Design3D

2.1 General Principle of the Design Method

The basic idea of the present method, of which a flow chart is shown in Figure 1, is to accelerate the design of new blades using the knowledge acquired during previous designs of similar blades.

The core of the design system is a database containing the results of all Navier-Stokes computations performed during the previous and present design processes. The database contains three kinds of data :

- The fluid properties and flow-field boundary conditions used by the Navier-Stokes solver which are the inlet flow angle, the pressure ratio, the Reynolds number, the ratio of specific heats.

- The parameters defining the geometry

- The aerodynamic performance characterized by the aerodynamic efficiency, the outlet flow angle and the isentropic Mach number distribution on the blade surface.
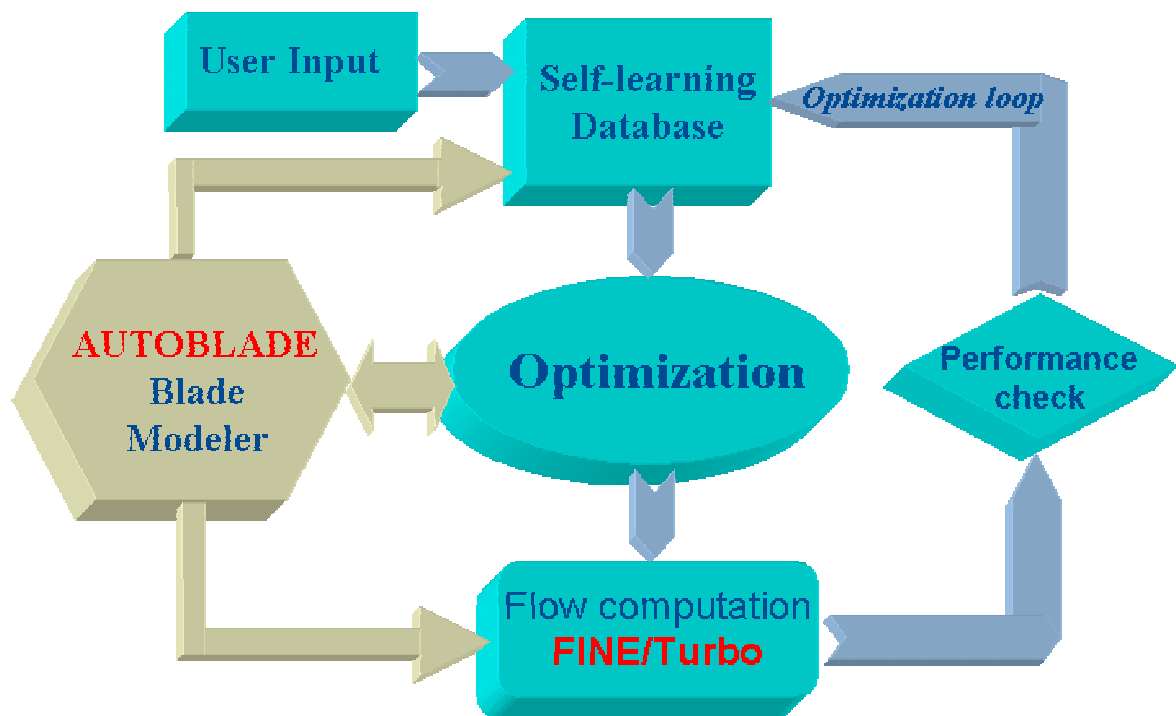
Figure 1 : Blade Design Algorithm

The blade design algorithm encompasses five components :

- The design starts with the aerodynamic, geometrical and mechanical requirements imposed by the user, namely : the inlet and outlet flow angles, the ratio of the outlet static pressure over the inlet total pressure, the Reynolds number, the blade cross-section area, the moments of inertia (Imin and Imax), the leading and trailing edge radius, and various other mechanical and geometrical constraints.

- The second step is the construction of the approximate relation between the parametric geometry and aerodynamic boundary conditions on one side, and the aerodynamic performance on the other side. An artificial neural network contains free parameters that have to be adapted in order to fit the database samples. The fitting or identification process is done by back-propagation of the errors and in the context of neural networks, is called "learning process". After the mapping of the database samples, the neural network is able to generalize; meaning that it can predict the aerodynamic performance of blade geometries under given flow-field boundary conditions that are not inside the database.

- The aim of the third step is to find a new optimized geometry that will be analyzed by the flow solver. This is realized using an optimization procedure such as: a genetic algorithm (GA) or simulated annealing (SA); the aerodynamic performance being evaluated by means of the trained neural network. The global blade performance is evaluated through an objective function, which translates all the user-imposed constraints into a single number.The result of this optimization is a point in the design space which is expected to be the optimum of the real problem.

- In the fourth step, the new geometry provided by the optimization is evaluated by means of the flow solver and this new sample is added to the database.

- Finally, the performance is compared to the imposed one. If the target performance has not been achieved, another design iteration is started, and the same process is repeated until the optimum blade is obtained.

A new design iteration always starts with the neural network learning. As the design proceeds, the database grows, leading to improvements of the approximate relation and therefore to a better localization of the real optimum.

2.2. The Parameteric Blade Modeler (AutoBlade)

The geometry parametrization is a critical element in the success of any shape optimization method. Ideally, the parametrization of the geometry should be able to generate a large variety of physically realistic shapes with as few design variables as possible.

AutoBlade[TM] is a geometry modeler developed and tuned for turbomachinery applications. Turbomachinery designers are accustomed to work with two-dimensional sections that are then stacked to the three-dimensional blade geometry. AutoBlade[TM] offers two design modes for the two dimensional blade sections. The first one constructs the blade by independent suction and pressure sides. The second mode first defines a camber line and adds a symmetric thickness to obtain the suction and the pressure sides. The blade edges can be rounded or blunt. Splitter blades are also supported allowing various definitions of splitter blades. The tangential lean and meriodional sweep of the 2D sections stacking can be controlled independently using various types of curves and parameters.

AutoBlade[TM] provides several methods to construct the endwalls : Bézier curves, C or B-spline curves with an arbitrary number of control points.

AutoBlade[TM] also offers the possibility to analyze the 3D blade shape. It can compute various quantities:

- Blade angle/curvature/thickness distributions,
- Channel width distribution,
- Throat area and location in 2D/3D,
- LE/TE wedge angles,
- Unguided turning,
- Maximum thickness and location,
- 2D section area, moment of inertia, torsional inertia,

AutoBlade[TM] is integrated into the NUMECA FINE environment and offers a simple, interactive, user-friendly and multi-windows graphical user-interface.

AutoBlade[TM] is able to treat various types of turbomachinery blades such as : centrifugal/axial compressors and turbines, pumps, fans, return channels, blowers, inducers, ... Figures 2 to 5 represents some examples of blade geometries obtained with AutoBlade[TM].
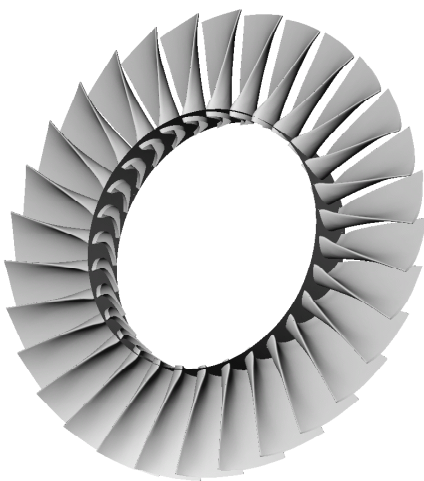
Figure 2 : axial turbine with a highly twisted blade   Figure 3 : centrifugal compressor with splitter blades
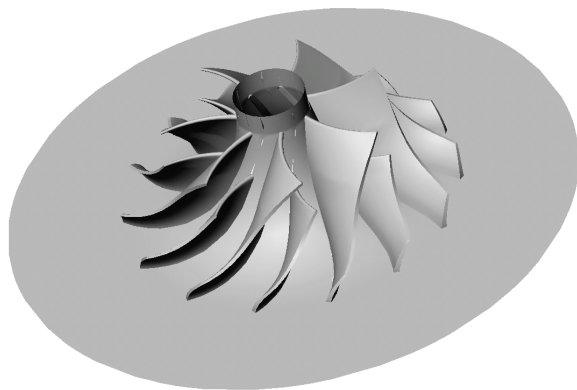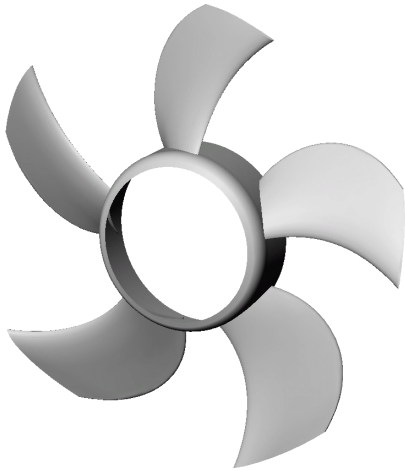
Figure 4 : fan with a significant tangential lean and meridional sweep
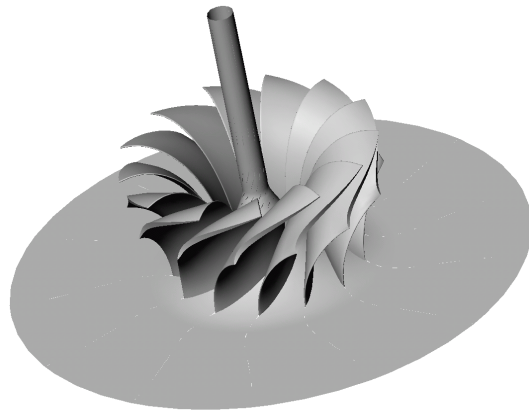
Figure 5 : hydraulic Francis turbine

2.3 The approximate model

The basic principle of the method is to build an approximate model of the original analysis problem (the three-dimensional Navier-Stokes equations). This approximate model can then be used inside an optimization loop instead of the original model. In this way the performance evaluation by the approximate model is not costly and the number of performance evaluations performed by the approximate model for the optimization is no longer critical.

Among the large number of possible techniques able to construct the approximate model, artificial neural network (ANN) has been selected. Although the initial motivation for developing ANN was to develop computer models that could imitate certain brain functions, ANN can also be thought of as a powerful interpolator. Artificial neural networks are non-linear models that can be trained to map functions with multiple inputs and outputs. The recent increase in neural network research results from the observation that neural networks have powerful mapping and pattern recognition capabilities, surpassing those of other techniques in many applications (both in accuracy and/or in computational speed).

Typical applications of neural nets are speech recognition, handwritten character recognition, image compression, noise filtering, nuclear power-plant control, automobile auto-pilot and medical diagnosis. However, this list is far from complete, and new applications seem to appear every day.

2.4 The optimization algorithms

The goal of the optimization is to find the minimum of the objective function using the simplified analysis model. Here, an essential issue is the robustness of the numerical optimization algorithm.

The choice of the optimization algorithm is mainly based on the following two considerations :

- Many local optima may exist in the design space and therefore a global optimization technique is required.

- The evaluation of the blade performance using the approximate model is very fast (a few ms). Consequently, the number of required function evaluations is now of far less importance than if a detailed Navier-Stokes computation was needed at each step.

Based on the first consideration, the straightforward application of numerical optimization techniques that rely on derivatives are questionable because they are only local optimization techniques. On the contrary, stochastic techniques such as the genetic algorithm (GA) or simulated annealing (SA) are global optimization techniques that do not get stuck in local minimum and therefore offer an alternative to conventional gradient methods for optimization problems where the function evaluation is very fast.

Genetic algorithms were designed by Holland in the 70s, and improved and made well known by Goldberg. A genetic algorithm is summarized as follows (Figure 6). An initial population is generated by randomly selecting individuals in the whole design space. Then, pairs of individuals are selected from this population

based on their objective function values. The performance of an individual is measured by its fitness. Then, each pair of individuals undergoes a reproduction mechanism to generate a new population in such a way that fitter individuals will spread their genes with higher probability. The children replace their parents. As this proceeds, inferior traits in the pool die out due to lack of reproduction. At the same time, strong traits tend to combine with other strong traits to produce children who perform better.
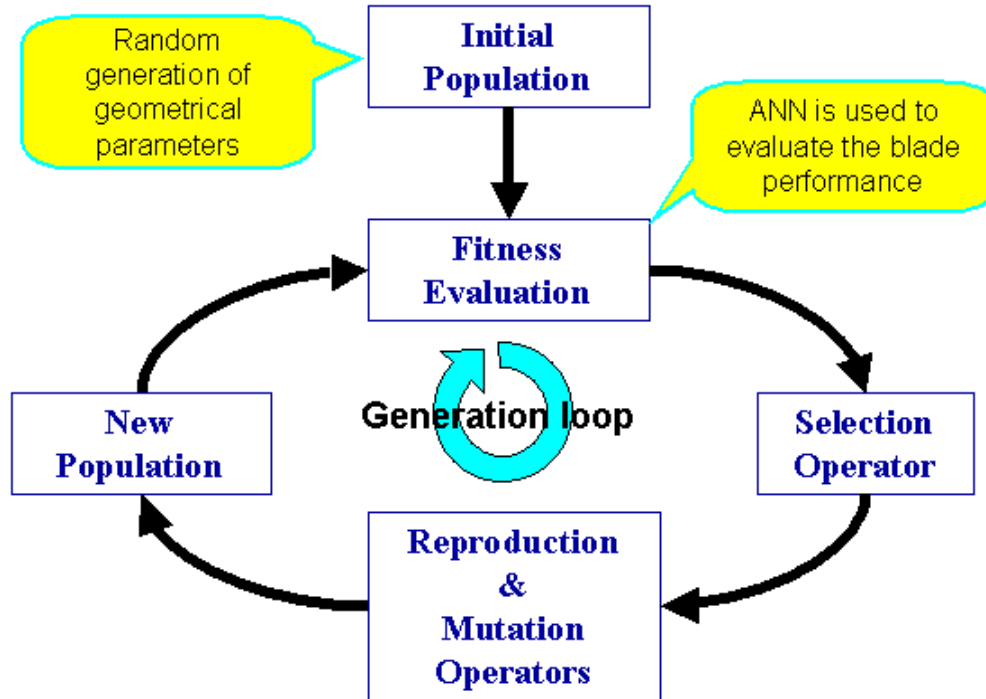
Figure 6 : Genetic Algorithm

2.5 The objective function

Among the design objectives of the detailed aerodynamic shape optimization, efficiency is only one of the many considerations. A good design must also satisfy the mechanical and manufacturing constraints as well as the aerodynamic constraints (turning, separation safety margin and good off-design performance).

The problem we are faced with is the minimization of an objective function (loss coefficient) in function of several variables (the geometrical parameters) subject to several constraints (mechanical, manufacturing and aerodynamic constraints), the objective function, and the constraints being non-linear. The general approach to this problem is to transform the original constrained minimization problem into an unconstrained one by converting the constraints into penalty terms that are increasing when violating the constraints. A pseudo-objective function is then created by summing up all the penalty terms and the original objective

3. Optimization Results

This section presents two optimization results obtained with FINE^{TM}/Design3D.

3.1 Design of an axial turbine blade

Secondary flows are known to have a more significant impact on turbine than on compressor blades due to the higher turning angle. The purpose of this optimization case study is to demonstrate that FINE/Design3D is able to automatically optimize the stacking lean of a turbine blade in order to maximize the aerodynamic efficiency. In this case a high-pressure turbine nozzle is considered. The incoming flow enters axially and the outlet flow angle is –71 deg. Realistic total pressure and total temperature profiles are used at the inlet.

The tangential lean and meridional sweep of the blade stacking laws are defined by 3 parameters each. The goal of this optimization is to improve the aerodynamic efficiency while keeping the shape of the 2D sections unchanged.

Figure 7 shows the convergence history of the design process. The efficiency has been improved from 97.6% (radial stacking) to 98.0 % after only two optimization cycles (2 CFD computations).
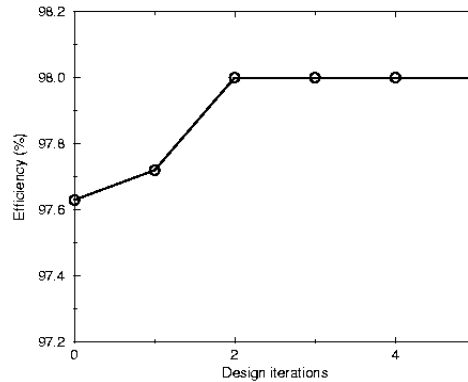
Figure 7 : Convergence history of the turbine stacking optimization.
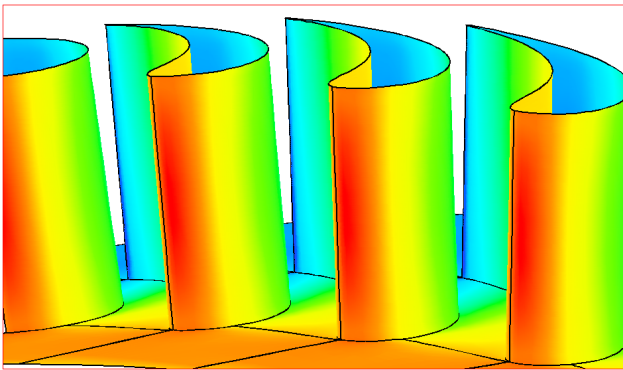
Figure 8 : Initial radially stacked blade (static pressure contours)
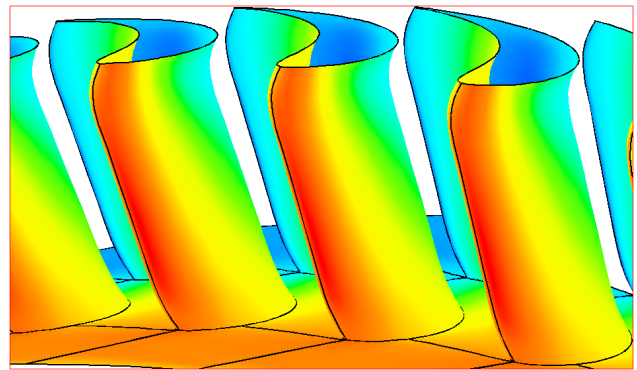
Figure 9 : Optimized blade geometry (static pressure contours).

Figures 8 and 9 show the initial and final blade geometries. The final blade shape has a large lean near the end walls, which is in agreement with the secondary flow reduction guidelines found in the littérature.

3.2 Design of a transonic axial compressor blade

Shock waves in turbomachinery are known to have a large impact on the overall loss coefficient as well as on the boundary layer stability. The purpose of this optimization case study is to demonstrate that FINE/Design3D is able to automatically optimize the blade shape of a transonic compressor rotor blade in order to maximize the aerodynamic efficiency by reducing the shock intensity. Another critical aspect of this type of rotor blade is to ensure good mechanical properties. This is performed by imposing strong mechanical constraints during the optimization.

The well-known NASA rotor37 compressor blade is considered in this study. The most critical section for the shock point of view (the tip section) is modified during the optimization. The inlet flow angles and inlet total conditions are imposed as well as the static pressure at the outlet. The objective is to maximize the efficiency. Constraints are imposed on the outlet flows angles, the cross section area of the 2D sections and the momentum of inertia of the 2D cross sections.
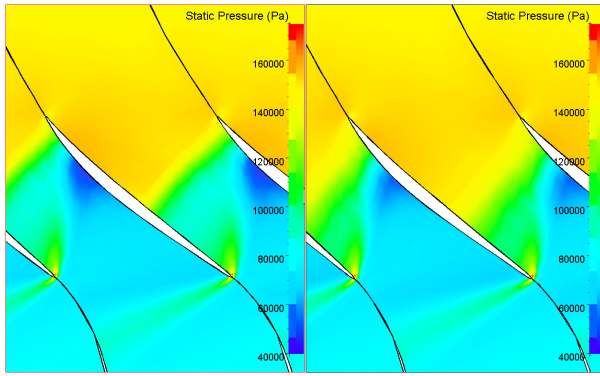
Figure 10: Pressure distribution around the blades for the original (left) and the optimized (right) geometry.
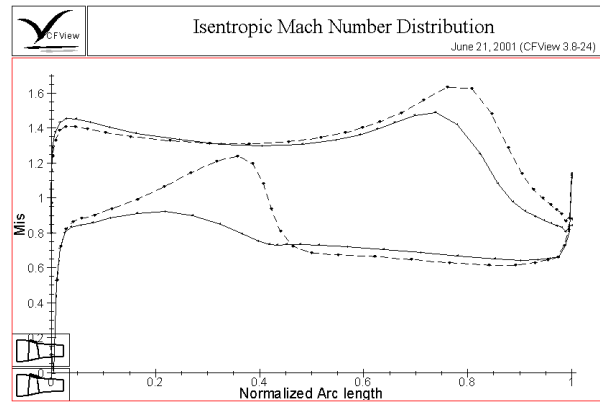
Figure 11 : pressure distribution along the blade wall for the original (dashed) and the optimized (solid) blade geometry.

The efficiency has been improved from 84.8% to 85.7% after only three optimization cycles. Most of this efficiency improvement is obtained from the reduced shock wave intensity impinging on the suction side (Figure 10). One can notice on the blade wall pressure distributions presented in Figure 11 that the intensity of the shock has been significantly decreased.

The final outlet flow angle at the tip is very close to the imposed one (0.6 deg difference). Finally, all the mechanical constraints are respected within 5 % of the original geometry.

4. Conclusions.

This paper presents a new design environment for turbomachinery blade design (FINE^{TM}/Design3D), based on the concept of function approximation, artificial neural network, genetic algorithm and CFD computations.

Application of this new environment to the design of typical turbomachinery blades has shown the effectiveness of the method in designing new and efficient turbomachinery blades with only a very limited number of calls to the CFD analysis code while satisfying mechanical and geometrical comstraints.

5. Bibliography

[1] G N. Vanderplaats, "Numerical optimization techniques for engineering design", McGraw-Hill, 1984

[2] A. Jameson, "Aerodynamic design via control theory", Journal of scientific computing, pages 233-260, 1988

[3] D E. Goldberg, "Genetic Algorithm". Addison Wesley 1994.

[4] A Demeulenaere, "Conception et Développement d'une Méthode Inverse pour la Génération d'Aubes de Turbomachines", PhD thesis, von Karman Institute and Université de Liège, 1997

[5] S S. Tong and B A. Gregory, "Turbine preliminary design using artificial intelligence and numerical optimization techniques", Journal of Turbomachinery, pages 1-7, January 1992.

[6] S. Pierret, "Designing Turbomachinery Blades by Means of the Function Approximation Concept based on Artificial Neural Network, Genetic Algorithm, and the Navier-Stokes Equations", PhD thesis, von Karman Institute and Faculté Polythenique de Mons, 1999.

[7] S. Pierret, A. Demeulenaere, B. Gouverneur, Ch. Hirsch, "Designing Turbomachinery Blades with the Function Approximation Concept and the Navier-Stokes Equations", 8th AIAA/NASA/USAF/ISSMO Symposium on MDO, Sep6-Sep8, 2000,Long Beach, CA.

[8] N. Hakimi, S. Pierret, C. Hirsch, "Presentation and application of a new extended K-e Model with wall functions", ECOMAS 2000, Barcelona.

Multi-Disciplinary Simulation of Vehicle System Dynamics

W.R. Krüger, O. Vaculin, W. Kortüm
DLR - German Aerospace Center
Institute for Aeroelastity
D - 82234 Wessling
Germany

Wolf.Krueger@DLR.de
Ondrej.Vaculin@DLR.de
Willi.Kortuem@DLR.de

Summary

Modeling and computer simulation play an important role in all engineering disciplines. As specialized simulation tools have become very sophisticated and, at the same time, the simulation of complex systems and phenomena showed the limits of mono-disciplinary approaches, multi-disciplinary simulation has gained wide acceptance.

For the coupling of different simulation tools interfaces are necessary, including both aspects of physics and numerics as well as of software engineering. This paper tries to give a general classification of interfaces between simulation tools. Following, the multibody simulation approach is presented. With a great number of interfaces to other engineering disciplines like FEA, CAD, CFD, and control design engineering, multibody simulation programs are true multidisciplinary tools which can be used from the pre-design phase to trouble shooting on a production vehicle. As an example, the MBS tool SIMPACK and its integration in the concurrent engineering loop will be presented along with two applications from automotive and aerospace design.

1   Multi-Disciplinary Simulation

Vehicles, i.e. ground vehicles (cars, trucks, trains) as well as air, space and water vehicles, today are complex systems. Requirements of shorter development times, greater safety, longer life time, greater comfort and lower costs have made computer based simulation a necessary tool of the development process. As manufacturers as well as civil and military customers try to incorporate multidisciplinary design methods in the conceptual design phase, a systematic approach needs to be introduced.

Modeling and computer simulation have become tools in all engineering disciplines. Two modeling philosophies for multidisciplinary simulation exist, Fig. 1:

- In one approach, all model components are implemented in a single modeling or simulation tool, using common libraries or a common modeling language, and creating a single model comprising elements of all involved disciplines.
- In a second approach the coupling of specialized tools by the means of interfaces is performed. This is especially suited for systems where sub-models already exist in specialized tools and where those models are too large and complex to be transferred into a single simulation tool.

This paper will deal only with the second approach, i.e. with the coupling of tools via interfaces.
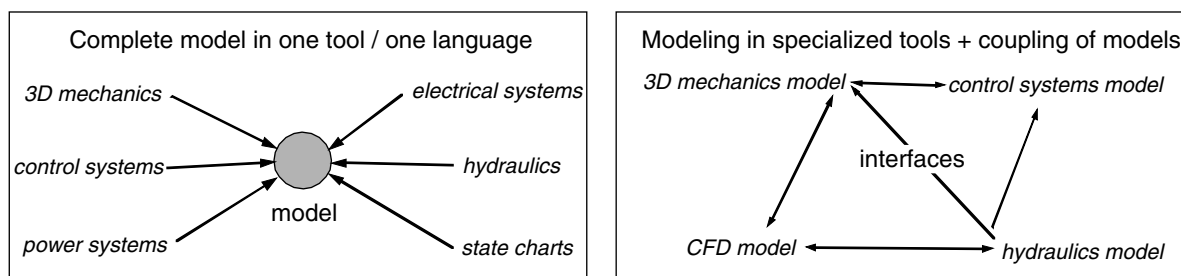
Figure 1: Approaches to multidisciplinary simulation

The most widely used computer aided engineering (CAE) tools are computer aided design (CAD), finite element analysis (FEA), control design (often called CACE - Computer Aided Control Engineering), and computational fluid dynamics (CFD). A mediating role between these disciplines is taken by the multibody simulation (MBS) approach. It aims at the simulation of the total vehicle dynamics and offers a good compromise between "fast", "robust", and "exact" simulation [1].

The models used in the engineering fields differ considerably depending on application and the complexity of the task. As an example, in "classical" flight mechanics the aircraft was often represented as a point mass (the coupling of flight mechanical and structural oscillations, of course, today demands a more detailed modeling). Contrary to that, the methods of the finite element analysis and computational fluid dynamics decompose structure and surface of the aircraft in millions of small computational units, a development that has been made possible by the powerful improvement of computer hardware and software in the last decades. In addition, modern CAD programs allow the design of a virtual prototype before a single component is in production. However, this large versatility of models requires an enormous, sometimes redundant modeling effort, and makes it difficult to exchange the obtained results.

Cheap, small and powerful electronics and actuator technology enabled the development of mechanical devices closely interacting with control facilities. For such "mechatronic" systems, an integrated design of mechanical structures and control is indispensable. Multibody simulation is well suited for this procedure and is therefore an important tool in the concurrent engineering process. Multibody simulation allows model simulation and analysis using the know-how of all engineering disciplines mentioned above. To be able to perform these tasks, the program needs intelligent bi-directional interfaces to tools of neighboring disciplines like CAD, FEA, and CACE which allow a continuous comprehensive data exchange. Multibody simulation is suitable both for the pre-design and for the analysis of existing systems, and can be applied for stability and comfort analysis, aircraft response on certain maneuvers, for ground and gust loads, and for life-time prediction. A further advantage for the design process is the possibility to perform parameter studies on a complex simulation model and to optimize free parameters ("design-by-simulation"). Finally, an MBS program is used to calculate system response in a large number of critical operational cases automatically which is of advantage for certification cases. A multibody simulation tool which fulfills these requirements is an essential part of the integrated design process.

2   Interfaces for Coupled Simulation

2.1   Classification of Interfaces

Simulation tools have usually been designed as stand-alone applications in a prescribed work flow. Any two tools rarely use the same native model description or data structure. Interfaces provide a means of communication between two or more coupled applications.

Interfaces are implemented in a variety of ways, and several possibilities for the classification of interfaces exist. When looking at interfaces it is important not only to take into consideration the implementation issues but also their mathematical and physical background. The classifications presented in the following section are therefore based on functionality and work flow, mathematical and physical properties, and software and hardware implementation aspects. It should be noted that a classification cannot always be unambiguous. Other aspects as those mentioned exist, and interfaces can belong to different categories at the same time.

2.2   Functionality / Work Flow

Uni-Directional vs. Bi-Directional Interfaces

Interfaces can be categorized in terms of work flow aspects. Here, a distinction can be made between uni-directional and bi-directional interfaces, Fig. 2. An uni-directional interface is needed if one program is used as a pre-processor for a second program. Typical examples are grid generators for finite element analyses. Bi-directional interfaces handle the flow of information between two running simulations. Typical examples are co-simulation interfaces.
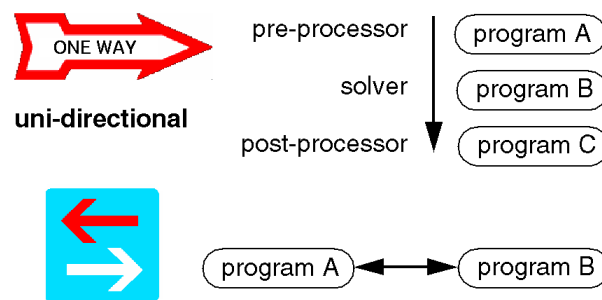
Figure 2: Uni-directional and bi-directional interfaces

2.3 Mathematical / Physical Aspects

Model Description

Depending on application and software, simulation models are described in various ways. For the classification of interfaces it is helpful to distinguish between different model descriptions.

First, simulation models are often described in *application specific parameters*, Fig. 3a. In this case, only the class of a model element, often represented by a number, and values for pre-defined variables are given in an input file. An example is the input file of the MBS code SIMPACK (see Sec. 3) where a certain library element, e.g. a joint type or a force element type is described by its number, and for each element a different set of input values are pre-defined. Other simulation codes, e.g. FEA codes, use the same principle to describe models.

Such a description has the advantage that parameter-based input files are relatively short and of low complexity. However, the parameters in such input files do not give a lot of information about the underlying physical element definition. Interfaces are often based on such native model descriptions, and especially in the case of commercial packages changing the input file is often the simplest way to access these programs in an automated way.

In a second class of models, the so-called *descriptive models,* Fig. 3b, the physical properties of the systems as well as the parameters are defined. This includes particularly models described by differential equations where a solution in time space can only be obtained by the use of an additional solver. In the general case those models can be a function of an arbitrary number of parameters; a special case often used for model exchange are state-space matrices, i.e. linear time independent models. The solvers used for generating solutions for descriptive models depend strongly on the form and numerical properties of the systems.

A third class of models is formed by the so-called *operational models*, Fig. 3c. The output of an operational model is directly the requested response, e.g. in time space. Thus, operational models can either be differential equations with a solver or analytical models where a response can be calculated directly from the input. An operational model can be a 'black box', meaning that the actual model properties are hidden from the user and only well-defined responses on single inputs are given. Therefore operational models are common for interfaces, especially for co-simulation purposes, see Fig. 3.
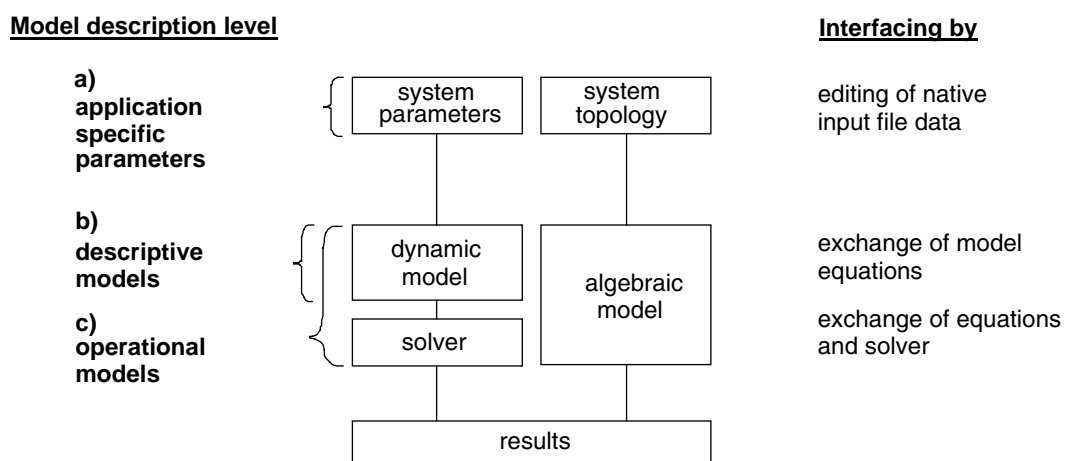
Figure 3: Levels of model description (acc. to [2], modified)

Numerical Integration

Another classification of interfaces is based on their numerical integration schemes. The numerical integration of the coupled system can be performed in one tool by a common numerical integrator; this method is often called *tight* or *close coupling*, Fig. 4a. In this case, the sub-models have to be connected into one complete model and all the states of that model have to be accessible by the numerical integrator. Furthermore, the integrator must be able to handle all types of model behavior and equations used by the included models. The performance of the numeric integration of the coupled system should remain acceptable. Performance and numerical stability can have limits if the numerical properties or the dimensions of the sub-models differ widely.

The numeric integration can also be distributed. In this case the coupled tools use each their own solvers and only inputs and outputs are exchanged, most often at pre-defined communication time points, thus using explicit overall time integration methods. This scheme is often called *weak* or *loose coupling*, Fig. 4b. The states of one sub-model are hidden from the integrators of the other model the disciplines, hence the common name *co-simulation*, the calculation performance can be increased. However, the communication intervals have to be chosen carefully for reasons of performance and stability. Furthermore, it can be shown that some systems, e.g. with closed kinematic loops, do not converge at all with an explicit loose coupling scheme [3].

It should be noted here that both close coupling and loose coupling can be achieved independently from the selected implementation method. However, in practical applications the word co-simulation is often used exclusively for loose coupling in combination with a multi-process or IPC solution. In the following, the term co-simulation will be used as a synonym for loose coupling in general.

| a) close coupling | b) loose coupling |
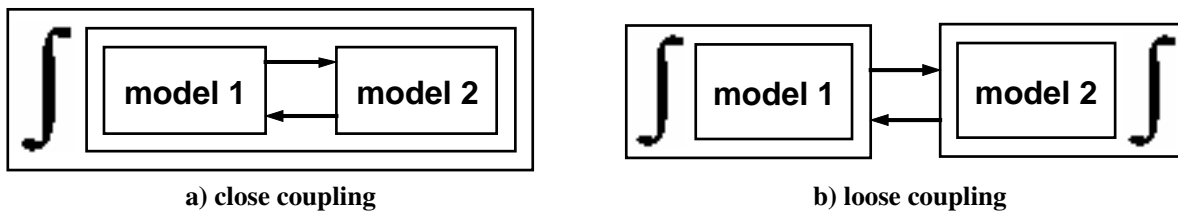
Figure 4: Numerical integration for close and loose coupling

Model Size Adaption

Often models of different complexity are coupled. Differences are either the model size, e.g. the number of degrees of freedom, or in the type of system description. Many physical problems can be described, e.g., dimensionless, in one, two, or three dimensions. If models of different complexity are coupled, solutions have to be found to either reduce the complexity of a sub-model to that of the main model or to interpolate between the sub-models. An example for model reduction are the use of modal representation of flexible bodies or the mathematical model reduction techniques used in control design; an example for the need of interpolation is the simultaneous use of 1D, 2D and 3D models in a turbine simulation.

2.4 Software / Hardware and Implementation Issues

Programming

From the programming implementation point of view the interface can be realized as a *single process* or a *multi-process solution*. This classification is independent of the selected numerical integration aspect. Single processes can be obtained on the source code level or on the object code level. In the first case, source code is transferred and all sub-models or programs are compiled and linked into a single executable. This solution makes the interface platform independent.

On the other hand it is possible to interchange pre-compiled objects and link them into a common executable. This can only be done, however, if all code modules have been compiled for the same platform and operating system. In a multi-process solution all models are simulated in their own executables.

Data Transfer

In a coupled simulation data has to be transferred between the sub-models. Data transfer can be performed inside a code by defined parameter lists of subroutine calls or between codes by file transfer,

inter process communication, or a mixture of both. The choice between the methods depends on the amount of information exchanged, performance, and the simulation environment available.

File interfaces are often used if models are results of pre-processors, have to be portable across platforms, and if a large amount of data has to be transferred between simulations. They are exported from one program and imported by the partner program. Inter process communication (IPC) can be chosen if the processes run in parallel, the amount of data is not too large, and the processes can be connected by a network.

Inter process communication in itself is a large field, and the selection of soft- and hardware is based on the requirements. Communication can be achieved by using directly basic functionalities of operating systems as shared memory or sockets, or by using more comprehensive commercial or public-domain packages which supply communication libraries as PVM, MPI, or CORBA.

When large amounts of data have to be exchanged, e.g. in a coupled simulation of CFD and FEA programs, often file interfaces and IPC are used in parallel. Communication routines are used to schedule the process, but the bulk of the data describing a model is exchanged by files.

Platform Dependence

The coupling of simulations can be realized either on a single CPU *single platform, single node*, several computers of the same type (e.g. clusters) or on different nodes of the same computer *single platform, multi-node*, or on different computers of different types and/or operating systems *multi-node*. All these variations require different solutions for simulation interfaces.

Evidently, a single process solution (see above) as a rule runs on a single node. [1] However, a multi-process solution can, and often will, also be limited to a single node. For this limitation there are a number of advantages. First, often the coupling effort is smaller for non-distributed calculations, because all developments can be made in the same environment, network problems are avoided, and some types of coupling methods (e.g. shared memory) are only accessible this way. Additionally, only one implementation of coupling software is necessary. However, all codes have to be available for the same platform, and questions of available computer memory and computational power for the coupled simulation have to be taken into consideration.

Multi-node solutions of single processor types address this problem by multiplying the power of the hardware while using the same working environment for all nodes. In addition to a single-node solution a scheduling scheme to distribute work load on the nodes is necessary. A multi-node solution is used when many parallel computations of similar structure are required, e.g. in multi-block CFD analyses and in simulations for optimization.

In many cases programs are specialized for different environment, e.g. MBS programs for workstations and CFD programs for high-performance computers. In other cases, programs might be limited to special computers for reasons of (non-)portability or licensing. In these cases, a multi-platform solution has to be achieved. Interfacing routines have to be available for all included platforms, different scheduling systems, e.g. cuing vs. have to be integrated

For complex work flows comprising several programs on distributed networks a number of specialized coupling libraries (e.g. CORBA) and work flow managers, addressing the questions mentioned above, have been developed.

3   MBS as a Basic Element of Interdisciplinary System Dynamics Analysis

3.1   Multibody Systems

Originally, MBS software was designed for the analysis of purely mechanical rigid body systems, sometimes added by force laws from other fields such as hydraulics or electronics, mostly included as source code. Since rigid body MBS is not relying on the exact structure and geometry of its components its main applications were principle dynamic investigations in the early development phase of a project. Today the request for the features of MBS-software, in particular for vehicle system dynamics, is much more demanding. Modern MBS software packages enable interdisciplinary modeling and analysis, either by own enhancements of the MBS functionality or via interfaces to other CAE tools. As a rule, the individual extensions of MBS programs are well adopted to the needs of MBS computation but limited in their facilities and performance. Interfaces to other CAE software on the other hand not only

---

[1]   Depending on the structure of the program scheduling algorithms might be able to distribute work load even of single process simulations to different nodes of a computer.

offer the entire possibilities and functionality of proven software tools but widely reduce the modeling effort as most of these models already exist anyhow, e.g. for CAD drawings or FEA stress analysis, and only need the appropriate conversion.

3.2   SIMPACK

The MBS program package SIMPACK, [4], has been developed at DLR (German Aerospace Center) as a tool for the simulation of complex dynamic systems in aerospace, transportation (vehicle) systems and robotics applications. Consequent upgrading has matured SIMPACK from a typical MBS-code for analysis of specified systems into a mechatronic simulation and design tool. The basis of SIMPACK are its multibody formalisms, i.e. the algorithms which automatically generate the equations of motion. In SIMPACK CPU-time-saving *O(N)*-algorithms (the number of operations grows only linearly with the number of the degrees-of-freedom) are establishing the equations of motion in explicit or in residual form. The equations of motion of the MBS are set up in the form of ordinary differential equations (ODE) or - particularly in the case of closed-loops - optionally in differential-algebraic form (DAE). Adequate solvers, i.e. numerical integration algorithms, were incorporated or developed, some of them in close correlation with formulating the equations of motion. Beyond the "normal" solvers for time-integration (i.e. the narrow sense of simulation) a variety of special numerical analysis methods, in particular for linear system analysis (linearization, eigenvalues, root locii, frequency response, stochastic analysis in time- and frequency-domain) were modified for their special use in vehicle dynamics and integrated. Moreover, computational procedures for stationary solutions (equilibria, nominal forces) respectively for kinematic analysis were developed and implemented.

SIMPACK has developed and is maintaining bi-directional interfaces to a variety of CAE program packages, Fig. 5. The most important interfaces are presented in the following sections - including elastic bodies from FEA, defining controllers in a CACE environment and improving the dynamics with a multi-objective optimization tool, importing CAD data and coupling of rigid and elastic multibody systems to aerodynamics and CFD calculations.
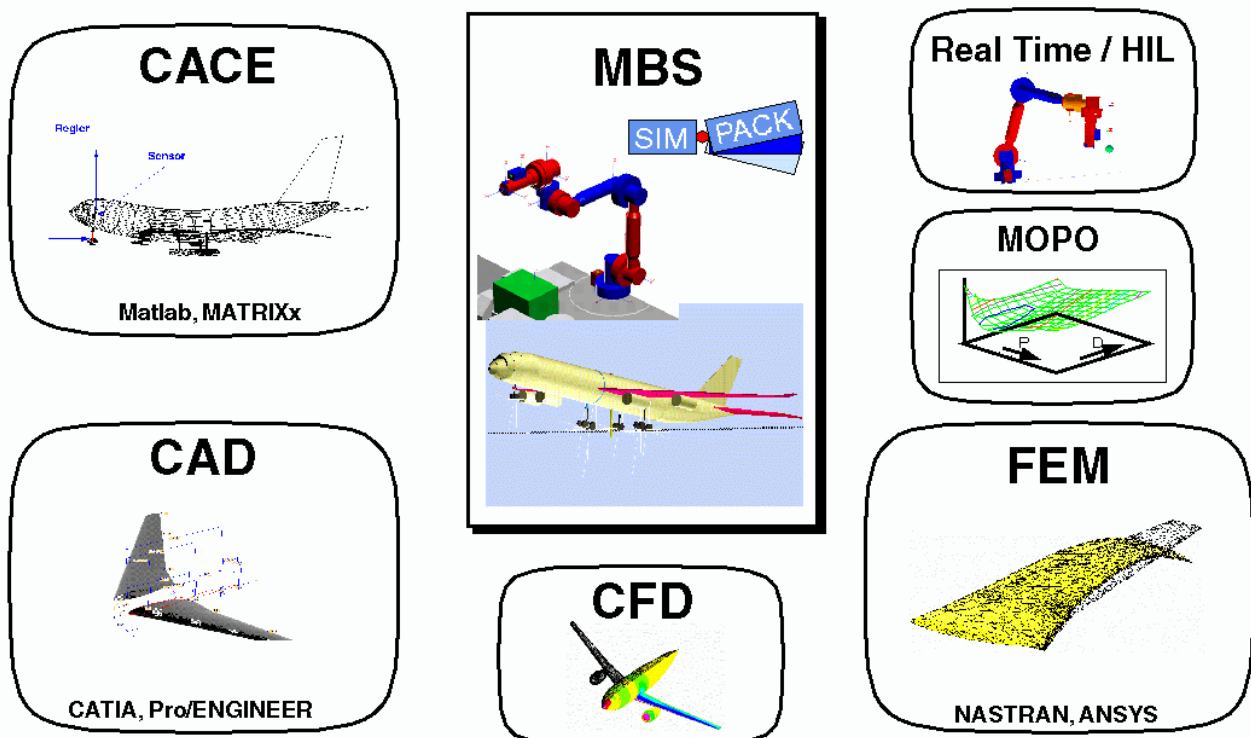
Figure 5: Multibody simulation in the integrated design environment

3.3   Modeling of Elastic Bodies for MBS Analysis

The representation of elastic bodies deriving from FEA modeling in MBS simulation requires adequate pre-processing efforts. A simple transfer of data between FEA and MBS, e.g. for co-simulation, will

result in unacceptable calculation times. In SIMPACK, the pre-processor FEMBS (from FEA to MBS) converts FEA analysis results to an adequate elastic MBS body, Fig. 6.
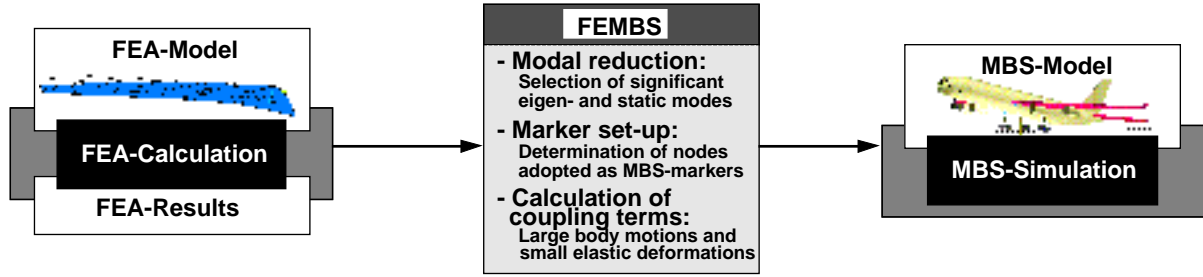
Figure 6: From FEA to MBS: defining elastic bodies in MBS

The spacial motion of an elastic body is divided into a global motion, characterized by the movements of the body reference frame, and its elastic deformation which is expressed by the displacements of all (infinite) body points in relation to the body reference frame, Fig. 7.
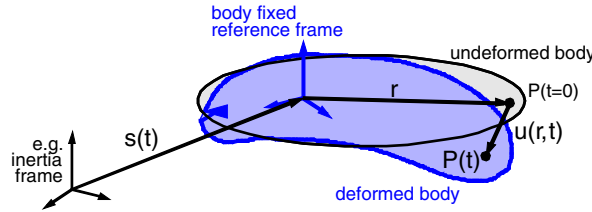
Figure 7: Separation of global motion and deformation

The global motion equals the rigid body motion of a classical rigid MBS body. The location and time dependent body deformation vector $u(r,t)$ is split by a separation function often referred to as "RITZ approach" into a location dependent displacement matrix $\Phi(r)$ and the corresponding time dependent elastic states $q(t)$:

$$u(r, t) = \Phi(r)q(t)$$

The displacement matrix consists of mode shapes of eigenvalue and static load analyses. The eigen- and staticmodes as well as the stiffness matrix are computed in FEA; additionally, geometric stiffening effects, e.g. due to centrifugal forces, can be included. FEMBS enables the user to select only those modes which are necessary to represent the body flexibility for the individual load case. With these data, the equations of motion of the multibody system can be extended:

$$M(\mathbf{q})\begin{bmatrix}\ddot{s}_t \\ \ddot{s}_r \\ \ddot{q}\end{bmatrix} + k(\dot{s}, \mathbf{q}, \dot{\mathbf{q}}) + \begin{bmatrix}0 \\ 0 \\ \mathbf{Kq}\end{bmatrix} = h(s, \mathbf{q}, \dots),$$

where s denotes the "rigid" MBS states (translational and rotational), k gyroscopic terms, h external forces and K the stiffness matrix. The mass matrix M is enlarged:

$$M = \begin{bmatrix} mE & m\tilde{c}^T(\mathbf{q}) & \mathbf{C_t^T}(\mathbf{q}) \\ \dots & I(\mathbf{q}) & \mathbf{C_r^T}(\mathbf{q}) \\ \dots & \dots & \mathbf{M_e} \end{bmatrix}.$$

The body mass matrix mE remains unchanged while the inertia matrix I and the STEINER terms mc^T are now dependent from the deformation. The additional "elastic terms" are volume integrals of matrices deriving from M, K, Φ and are approximated by TAYLOR expansions.

This so-called "close" coupling of FEA and MBS enables the user to calculate the elastic deformation of flexible bodies fast, in good accuracy and in a form which harmonizes with SIMPACK's MBS-optimized numerical integrators. For a more detailed explanation we refer to [1], [5].

3.4 Control System Design and Analysis

A number of interfaces between SIMPACK and Computer Aided Control Engineering (CACE) software, most notably to MATLAB and MATRIXx, are well established [6].

MATLAB and MATRIXx are tools for control design and system analysis which form a design chain with their block-oriented simulation environments MATLAB-Simulink and MATRIXx-SystemBuild and the code generation tools Real-Time Workshop (MATLAB) and AutoCode (MATRIXx). The packages are similar in structure and complexity which is no coincidence since both programs evolved from the same roots, the original Matlab by Little and Moler (cf. [7]). The tools offer analysis methods in the time and the frequency domain as well as many basic control design functions. They offer different interfaces for model import and export; the interfaces between SIMPACK and MATLAB or MATRIXx are called SIMAT and SIMAX, respectively.

Model Transfer from SIMPACK to CACE

Linear System Interface
SIMPACK models can be linearized and exported in the form of linear system matrices in a MATLAB / MATRIXx-readable format. The model is represented in the following form:

$$\dot{x} = Ax + Bu$$
$$y = Cx + Du$$

where x can consist of rigid-body motion states, states of elastic bodies (in modal formulation, see Sec. 3.3), and states of force elements; the input u can be any kind of excitation, prescribed motion or external force. The models can be the basis for linear system analysis and for control design in MATLAB / MATRIXx. Inside Simulink or SystemBuild the model can be used directly in a state-space block. The interface allows a very fast model export, is platform independent and universal. Restrictions are, as the name suggests, the limitation to linearized models and the one-way data transfer of the MBS environment to the CACE program. The Linear System Interface is an example of a uni-directional interface for close coupling of the systems.

Symbolic Code Interface
Models with non-negligible nonlinear effects can also be exported from SIMPACK in a platform independent way in the form of so-called Symbolic Code. While generally the Symbolic Code is capable of exporting any kind of mechanical system, only models described by ordinary differential equations (ODEs) can be used by the SIMAX Symbolic Code Interface. Here, the model has the following form:

$$\dot{x} = f(x, u, t)$$
$$y = f(x, u, t)$$

SIMPACK generates model dependent, portable FORTRAN code which can be connected to Simulink as an S-function or to SystemBuild as a UserCode Block. With a suitable converter the symbolic code can also be transferred into C to be used in a Hardware-in-the-Loop environment. However, the code is model dependent, i.e. if the multibody system is modified, the FORTRAN code must be generated, compiled, and linked again. Furthermore, no re-transfer of simulation results into SIMPACK is possible. The Symbolic Code Interface, too, a uni-directional interface for close coupling of the systems.

Communication between SIMPACK and CACE

Function Call Interface
The maximum communication between SIMPACK and the CACE tool can be reached by the use of the Function Call Interface which allows to include SIMPACK in MATLAB or MATRIXx in its full functionality. As a bi-directional interface, it also works using the S-function / UserCode Block, forming one simulation module from MATLAB / MATRIXx and SIMPACK routines. The numerical integration is performed in the CACE tool which calls SIMPACK subroutines for the right-hand-side of the equations of motion (close coupling). The interface is restricted to models which can be described by ordinary differential equations. While in MATLAB / MATRIXx only the elements selected for the y-vector as defined in that equation are visible, all the results of the simulation, including the graphical animation of the multibody system, can afterwards be plotted and animated in SIMPACK. It has to be noted, however, that for the Function Call Interface both the CACE tool and SIMPACK have to be available on the same platform since a common executable is formed. Furthermore, for large systems, the integration might become slow when compared to a simulation purely inside SIMPACK because the MATLAB and MATRIXx integrators are not optimized for the solution of mechanical models.

Co-Simulation Interface
If SIMPACK and MATLAB or MATRIXx are available on different platforms, a combined simulation can be performed using co-simulation via inter-process communication (IPC). In that case, each package forms its own executable which communicate by the means of sockets, i.e. a network link providing a two-way communication channel between processes, either user-programmed or based on commercial or public-domain IPC libraries. Data exchange is performed in discrete time steps. Since all MBS model components are solved inside SIMPACK, taking advantage of the optimized integrators, no restrictions to modeling apply. The interface is capable of using models in the differential algebraic equation formulation (DAE):

$$0 = f(\dot{x}, x, u)$$
$$y = f(\dot{x}, x, u)$$

where x includes rigid body states, elastic body states, force element states, holonomic constraints and other algebraic equations to determine additional auxiliary conditions (e.g. for the on-line determination of accelerations and of friction forces). As in the Function Call Interface all simulation results are available for post-processing in both MATLAB / MATRIXx and SIMPACK. Restrictions are a longer simulation time since due to sequential ("step-by-step") co-simulation stability can often only be reached by very small communication intervals.

Transfer of Systems from CACE to SIMPACK

All the interfaces described above can be used to make an MBS model available for control design tools. However, once a control structure is established, it is essential that the complete model can be simulated in the MBS environment for evaluation and optimization purposes. For this reason, two ways have been developed to export a defined control loop from the CACE tool to SIMPACK.

Inverse Symbolic Code Interface
After a control design concept is set up in Simulink / SystemBuild, any chosen parameters can be defined as free parameters and the control structure can be exported. For this kind of model export, MATLAB offers the Real-Time Workshop, MATRIXx the module "AutoCode" which generate portable C code from block diagram models. The code can be used as a user-defined control force element and connected to the multibody simulation via the SIMPACK programmable interface (see Sec. 3.8). However, the Real-Time Workshop and AutoCode are separately licensed which can lead to considerable additional costs.

MBS Syntax Interface
Sometimes not all elements defined in the block diagrams can be exported as source code. Furthermore, sometimes the result of a MATLAB or MATRIXx calculation is only a gain matrix for which the code export would be too cumbersome. In this case it is possible to save the results of the control design in the syntax of single SIMPACK force elements. An element thus defined is then placed in the data base from which the simulation model is assembled, a process which has been automated by the development of special MATLAB and MATRIXx script files.

3.5   Parameter Variation and Multi-objective Optimization (MOPS)
In its analysis toolbox, SIMPACK offers an automized parameter variation which is used to get an overview over system performance as a function of parameter changes. The user defined set of "free" parameters may include mechanical values or force law coefficients as well as control parameters.
The free parameter set cannot only be investigated for its sensitivities: the optimal system configuration can be found with SIMPACK's multi-objective optimization tool MOPS (Multi-Objective Parameter Synthesis), [8]. MOPS is an independent optimization tool whose complete functionality can be operated with the SIMPACK GUI (graphical user interface). The simulation evaluated within the optimization loop can include static, linear and nonlinear simulations of multiple MBS-models, characterized by the same free parameters (Multi Model Optimization). A data handling module is added for structured control of the interactive optimization design process, where design parameters, model and simulation scenarios are varied, starting out from the first optimization test to the final optimal system.

The free system-parameters p_i varied within their given limits until an "optimal compromise" is found. In doing so the criteria $c_i(p)$ (performance indices) are weighted by user-defined factors d_i and the optimization strategy tries to minimize $c_i(p)/d_i$ working always at the (present) $\max_i(c_i(p)/d_i)$, i.e.

$$\alpha^* = \min_p \; \max_i \left(\frac{c_i(p)}{d_i} \right)$$

with α^* denoting the maximum preference function. The optimum is always a point (depending on d_i) on the PARETO-optimal boundary, [9].

3.6 CAD-Interface

Computer Aided Design (CAD) systems are a central part of the design process. Modern CAD systems allow the definition of 3D models from single parts to complex virtual prototypes. The dynamic analysis of such a system can be done either by including a dynamic solver in the CAD program or by importing CAD data in an MBS program. Both ways have been implemented in SIMPACK. Models from CATIA, Pro/ENGINEER and I-DEAS can be imported in SIMPACK, i.e. the geometric and mass properties as well as the 3D visualization are taken from the original CAD model. SIMPACK can also be completely included as a module in Pro/ENGINEER where all the functionalities are available in the CAD environment and a consistent data handling between CAD and dynamic simulation is achieved.

3.7 CFD-Interface

Aerodynamic forces on rigid bodies can be included in the MBS calculation by simple force elements, e.g. using standard methods of aerodynamic derivatives. Distributed aerodynamic forces on elastic bodies can be included as close coupling, i.e. by introduction of the aeroelastic equations in the MBS model, or by loose coupling, i.e. co-simulation between the MBS code and a computational fluid dynamics (CFD) code.

The *close coupling* enhances the non-linear equation of motion of the hybrid multibody system by "aerodynamic terms", which are computed in a pre-processing step to the multibody simulation. The approach allows to consider the effects of time-dependent, distributed airloads on the flexible aircraft structure without affecting the simulation efficiency. The pre-processing software tool AeroFEMBS uses standard codes, e.g. three-dimensional potential flow methods, to analyze the aerodynamic loading of the aircraft in high-lift configuration and prepares the corresponding aerodynamics input file for the multibody simulation. Thus, AeroFEMBS allows to include realistic aerodynamic effects into multibody simulation, including distributed airloads on elastic lifting bodies, effects of elastic body deformation on the aerodynamic load distribution, consideration of control surface deflections, velocity-dependent unsteady airloads resulting from elastic deformation and ground effects [10].

For the loose coupling a co-simulation between SIMPACK and a CFD code is established. In general, the MBS representation of the elastic structures and the CFD representation of the surface use different grids. Main points of interest are therefore the data transfer between the codes and the interpolation between the different grids. In recent applications the MPI-based coupling library MpCCI (Mesh-based parallel Code Coupling Interface, [11]) has been used both for data transfer and for grid interpolation [12].

3.8 Programming Interface

A much-used interface for the development of user-defined modules and coupling of external code is the so-called User-Force-Element, a programming interface which allows the introduction of FORTRAN and C elements into the SIMPACK simulation. Various sub-systems can be included, among others controllers (as done in the case of the SIMAT "Inverse Symbolic Code" interface), actuators, tyre models, hydraulic elements. The CFD coupling with MpCCI has also been established by using the programming interface.

3.9 Co-Simulation Interface

In addition to the programming interface SIMPACK offers a standard, open IPC co-simulation interface. The co-simulation is the basis for one of the SIMAT and SIMAX interfaces, another established link exists to the hydraulic simulation tool AMEsim. However, any code which meets the data definition for the interface can be coupled, using either built-in communication libraries or those supplied by the user.

4   Application Examples

4.1   Control Design and Optimization: Semi-Active Truck Suspension for Reduction of Ground Loads

Road Friendly Suspension Design

The following example presents the use of the interface between SIMPACK and MATLAB for the design of semi-active suspensions of trucks in order to fulfil the conflicting demands of road friendliness and comfort. The spatial decomposition approach is used to design the suspension structure. The contribution of the semi-active suspension is verified by experiments including cornering and braking with a complex truck simulation model.

The maintenance of the road networks becomes a very expensive task for road repair authorities. Furthermore, damaged roads cause additional deterioration of the vehicles and also of the road. Controlled automotive suspensions, in particular active and semi-active damping, have been studied for a long time particularly with the comfort objectives. The influence of semi-active suspensions to the decrease of road loads has been already proven by many simulation and field experiments, [13].

The vehicle generated road damage is caused by static and dynamic forces between road and tyre, [14]. Estimations indicate that a fully loaded truck deteriorates a road in the order of magnitude of 10^4 times more compared to the passage of a passenger car. Since presently only the static values of the road-tyre forces are regulated by national and international standards, further investigations must be focused to the reduction of the dynamic forces. The dynamic loads can be reduced by proper suspension design, but passive design has been almost driven to its limits.

The increasing demands on suspensions together with relatively cheap and powerful electronics and actuator technology enable a wide investigation of mechatronic suspensions, active or semi-active, with suitable, road friendly oriented, control laws.

Truck Simulation Model

The simulation model of a heavy duty platform truck is used in this study. The vehicle is designed for long-distance transport on hard-surface roads.

The model is equipped with a steerable front axle and a steering mechanism including a simple driver model. Furthermore, the vehicle brakes as well as a drive train with a velocity controller are implemented. The cabin is fully suspended.

The vehicle model has two basic versions, *passive* and *controllable*. The controllable version is equipped with semi-active dampers Mannesmann Sachs CDC N 50/55 on the axles and semi-active dampers in the cabin suspension. The total mass of the model is 16 tons. The MBS model of the truck consists of 41 bodies and has 64 states in the passive version. 36 outputs are defined for control and evaluation purposes.

For the design of the controller the SIMAT co-simulation interface is used. The SIMPACK solver numerically integrates the mechanical part of the model while the control part is integrated in the MATLAB/Simulink environment. The co-simulation sampling frequency is set to 200 Hz. This approach enables to apply models with closed kinematic loops. Fig. 8 is a 3D representation of the SIMPACK model.
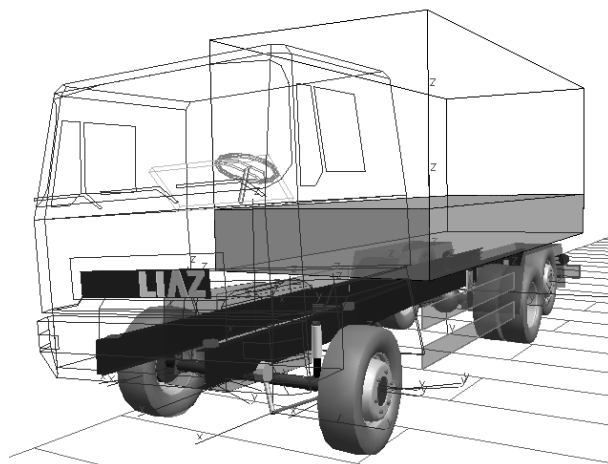
Figure 8: Truck Model

Semi-active Suspension Controller Design

The spatial decomposition approach resolves the contradictory demands on the controller by the *structure of the system*, thus this method can be also called more generally *spatial distribution of control tasks*. The controlled system is divided into two or more subsystems with different objectives for each control. Each system is then optimized using less conflicting criteria or even only one criterion for one specific task. Certainly, such decomposition is not possible to be applied to all dynamic systems.

The suspension systems of a heavy duty vehicle consist of independent suspensions, such as axle suspensions, which are mounted between the vehicle axles and the frame, and suspensions of the vehicle cabin, which support the cabin on the frame. The vehicle in Fig. 8 has four independent suspension systems: (i) front axle suspension, (ii) rear axle suspension, (iii) cabin suspension, and (iv) seat suspension. The strategy is to optimize the axle suspensions exclusively for the objective of road friendliness (minimization of road-tire force fluctuation) and the cabin and seat suspension for the ride comfort.

The controller parameters have been designed by simulation with a Multilevel Coordinate Search global optimization algorithm. The controller parameters are optimized subsequently. The axle controllers are optimized in the first sub-process and then the axle controller parameters are fixed and the comfort controllers are optimized. The semi-active dampers are controlled by well established control laws. The axle suspensions, which are designed as road-friendly oriented, are controlled by the extended ground hook concept. The comfort oriented cabin suspensions are controlled by the skyhook law. The strategy of the controllers and of the optimization is described in detail in [16].

The optimization of the axle suspension for minimization of road-tire force fluctuation can result in an increase of vertical acceleration of the heavy duty vehicle. However, while there are some limits for acceleration transferred to the vehicle cargo, those limits are expected to be fulfilled. A resulting deterioration of the comfort for the driver is solved by optimizing the cabin suspension and the suspension of the seat.

The spatial decomposition method can be applied to active, semi-active and passive suspension systems. Nevertheless, controllable suspension systems can profit from the decomposition significantly more.

Simulation Results

The simulation scenario consists of an S-shaped track with a curve radius of 120 m. The vehicle is excited before the curve entrance by a deterministic ramp. The ramp is 0.08 m high and 5.8 m long, ascent and descent lengths are 2.5 m. The vehicle intensively brakes between 3.5 s and 7.5 s from a speed of 22 m/s down to 4 m/s. The total simulation time is 12 seconds and the initial vehicle velocity is set to 80 km/h.

The simulation results for the truck equipped with a passive suspension compared to the semi-active system are presented in Fig. 9. The peaks at time 0.5 s are caused by the ramp.

Fig. 9a presents the vertical acceleration of the driver. The comfort increase is very significant in this case. The passive suspension of the cabin is relatively soft and moreover the vehicle frame, which is the base for the cabin suspension is better suspended.

The road-tyre forces are presented for the outer right tires of the rear axle in Fig. 9b. The influence of braking is visible at the time 4 s. A reduction of road-tire forces is observable.
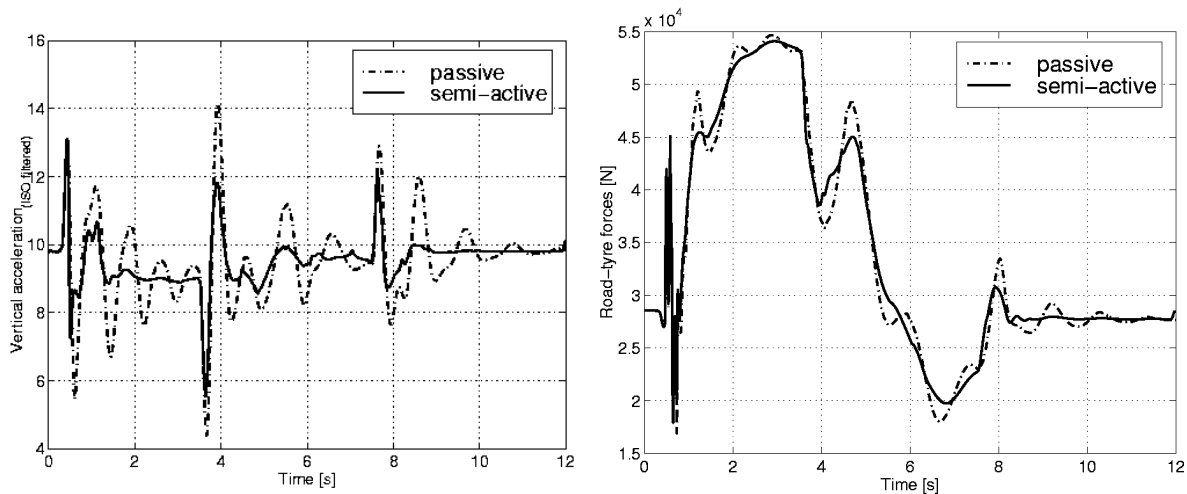
Figure 9: Cabin acceleration and road tire forces of truck

The simulation results indicate that the vehicle equipped with a semi-active suspension designed with the spatial decomposition control profits from a decrease of vertical acceleration and vertical road-tire forces. Generally, the simulation experiments have proved the potential of improvement of road friendliness by semi-active damping for vehicle maneuvers.

4.2 Interaction of Aircraft and Landing Gear

Conventional Design Process

A landing gear of a large transport aircraft has to accomplish a variety of functions. Among others, it has to:

- dissipate the energy of the vertical velocity at touch-down,
- suspend bumps from uneven runways/taxiways and provide a satisfying rolling comfort.

Modern transport aircraft are complex constructions. Their development requires a high level of special knowledge and experience on a multitude of disciplines. Therefore, many aircraft manufacturers confide a specialist with design and fabrication of the landing gear. As a rule, a basic design data set is defined at an early development stage containing, for example, mass and geometry data, configuration, specifications and operating envelopes. Provided with these basic data, the landing gear manufacturer designs a landing gear appropriate for the defined aircraft. Parallel to the work on the landing gear, the "airframer" develops and manufactures the airframe according to the ground load cases set up in cooperation of both partners. The limited knowledge about the partner's part often leeds to calculation and certification cases where simple models represent the other component, e.g. the "drop-test"-model with an equivalent single mass representing the airframe for the design of the landing gear shock absorber. This parallel strategy has the advantage that the development process can rely on fixed data; iteration loops caused by alterations of the basic design data due to optimization results of the partner are avoided.

On the other hand, the dynamic behavior of the combined system which is, in case of high structural flexibility, decisively influenced by dynamical interactions cannot be evaluated. A simple example shall illustrate this effect [17]: A large transport aircraft is rolling, at high velocity, over two sinusoidal bumps of a height of 3.8cm (1.5in), 21m (70ft) apart, Fig. 10. If this case is calculated with a conventional rigid airframe model, we receive a result for the applied vertical acceleration in the cockpit of 0.2g, Fig. 10, curve 1. Including the elasticity of the airframe, the maximum acceleration of the cockpit triples because of resonance phenomena, Fig. 10, curve 2.
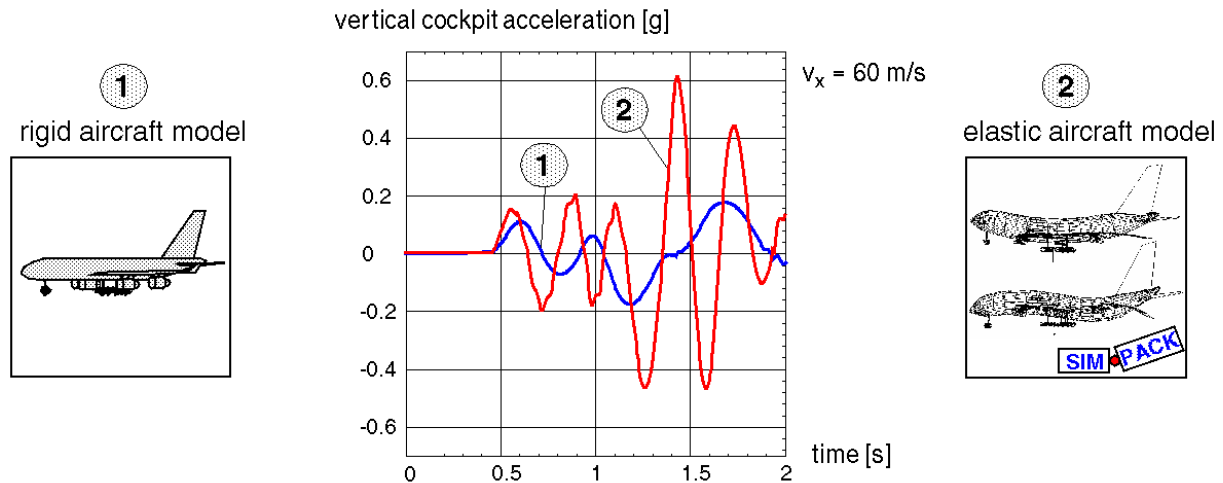
Figure 10: Comparison Between Rigid and Elastic Modeling

Integrated design

The later problematic interaction effects between airframe and landing gear are detected, the smaller is the available design freedom for alternative solutions - with progressively climbing costs. Preventive efforts should therefore take effect as early as possible to implement necessary adoptions to the design quickly, efficiently and without loss of performance.

Consideration of component interactions due to structural elasticities influences the entire design process. Neither airframer nor landing gear manufacturer can rely on a fixed set of basic design data; the level of detail of the basic design data set necessary to assess the most important influences on the system dynamics enforce the inclusion of data which are subject to permanent changes during the development process. This requires alterations on the level of design strategy, e.g distribution of responsibility or data handling, as well as modifications of the computational methods.

Compared to the conventional design strategy where the manufacturers develop their product in a widely independent development process, Fig. 11, left, the so-called "Integrated Design" strategy leads to a close cooperation [18]. The final solution matures out of the development and optimization process of both manufacturers, Fig. 11, right. Unfavorable lay-outs are detected early and can be corrected with comparatively small effort.

Basis for such a coupled design process is an aircraft/landing gear model comprising data from both the airframer and the landing gear manufacturer.
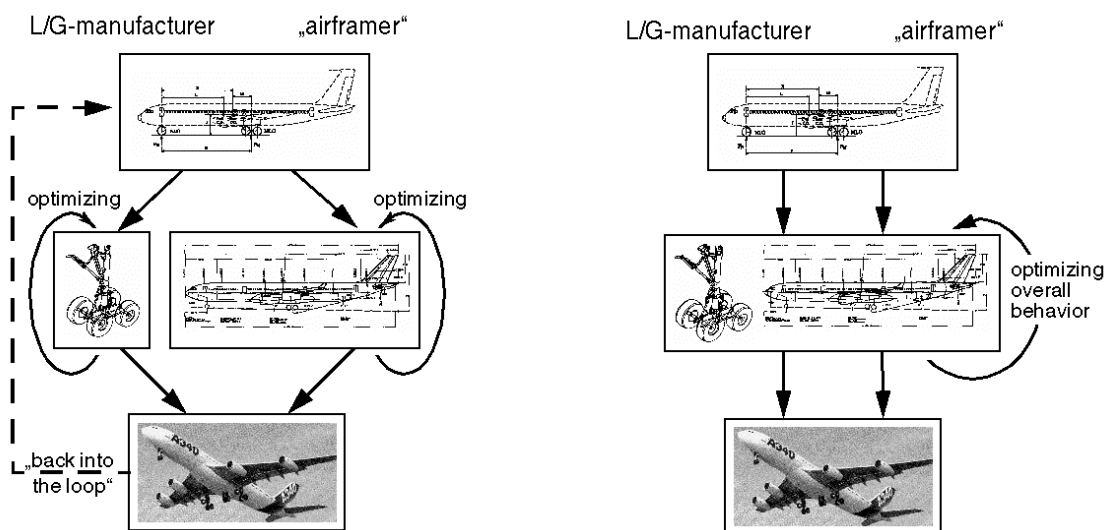
Figure 11: Conventional and Integrated Design Process

Fig. 12 shows an example of such an integrated model for dynamic analysis of airframe / landing gear interaction. A multibody simulation model is assembled, using the interfaces described in Sec. 3. The data comes from a number of different sources – for the airframe, usually a FEA model exists; CAD

models are used to build the simulation model of the landing gears; measurement data enters the simulation for the modeling of the runway and the tires; controllers are imported as code from a control design tool; finally, force laws describing the dynamic behavior of the shock absorbers are programmed and introduced via the programming interface. Simulation runs cover the whole operational envelope on the ground, i.e. touch-down, taxiing, cornering, push-back, and take-off. After the evaluation the results are passed back to the relevant disciplines, most notably forces for stress calculation and certification purposes. Such an integrated design has been performed in the German Flexible Aircraft project [17].
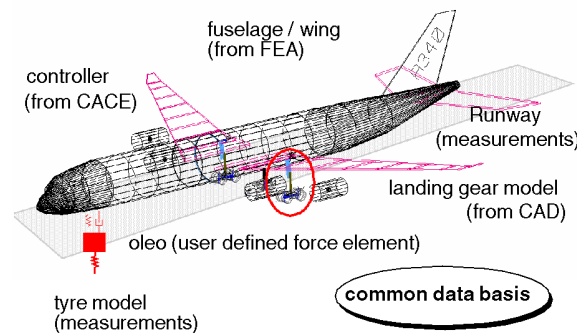
Figure 12: Multidisciplinary simulation model of transport aircraft

5   Summary and Outlook

Numerical simulation is an invaluable tool for the integration of system components. It allows the user to analyze his system up to any chosen degree of complexity, to determine physical variables at any given point of the system, to change design parameters and perform numerical optimizations, and, by doing so, to keep the costs of the vehicle design down.

While the simulation tools have become very sophisticated in their own domains, the simulation of complex systems calls for multidisciplinary simulation. This can be achieved by the coupling of the existing codes. For this purpose, interfaces between the codes have to be developed. These interfaces have to take into consideration the nature of the description of the physical model, numerical properties of the respective simulation methods, and software and hardware implementation issues.

Multibody system analysis is a powerful tool for multidisciplinary analysis of mechanical and mechatronic systems. For the efficient employment of an MBS analysis, a multitude of engineering disciplines have to be considered in the simulation. Combinations of different CAE (computer aided engineering) tools, like MBS, CAD, FEA, and CACE, allow the computation and evaluation of a complex system with the desired accuracy and in affordable computation times. MBS as the analysis tool of the overall system behavior can form the center element of this multidisciplinary design environment.

6   Bibliography

[1]   W. Rulka. Effiziente Simulation der Dynamik mechatronischer Systeme für industrielle Anwendungen. Dissertation an der TU Wien. DLR IB 532-01-06. Oberpfaffenhofen, Germany, 2001.

[2]   A. Veitl, T. Gordon, A. van de Sand, M. Howell, M. Valasek, O. Vaculin, P. Steinbauer. Methodologies for Coupling Simulation Models and Codes in Mechatronic System Analysis and Design. Veitl, A.; Gordon, T. In: The Dynamics of Vehicles on Roads and Tracks; Supplement to Vehicle System Dynamics, Vol. 33, pp 231-243, 2000.

[3]   R. Kübler, W. Schiehlen. Vehicle Modular Simulation in System Dynamics. In: International Conference on Multi-Body Dynamics - New Techniques and Applications, IMechE Conference Transactions 1998-13.

[4]   W. Kortüm, W. Rulka, M. Spieck: Simulation of Mechatronic Vehicles with SIMPACK. MOSIS 97, Ostrava, Czech Republic, 1997.

[5]   O. Wallrapp. Standardization of Flexible Body Modeling in Multibody System Codes. Part I: Definition of Standard Input Data. Mech. Struc. & Mach., 22(3), 1994, pp. 283 - 304.

[6] O. Vaculin, W.R. Krüger, M. Spieck. Coupling of Multibody and Control Simulation Tools for the Design of Mechatronic Systems. Proceedings of ASME 2001 International Design Engineering Technical Conferences, 9-12. Sept. 2001, Pittsburgh, PA, USA.

[7] W. Kortüm, P. Lugner. Systemdynamik und Regelung von Fahrzeugen. Springer Verlag Berlin, Heidelberg, New-York 1994.

[8] G. Grübel, H.-D. Joos. "Multi-Objective Parameter Synthesis (MOPS)", in: Magni, J.-F., Bennani, S., Terlouw, J. (editors): "Robust Flight Control - A Design Challenge", Lecture Notes in Control and Information Sciences 224, Springer Verlag London Limited, 1997.

[9] H. Wentscher. Design and Analysis of Semi-Active Landing Gears for Transportation Aircraft. DLR-Forschungsbericht 96-11, Köln, 1996.

[10] M. Spieck, W.R. Krüger. Aerodynamic Forces on Elastic Bodies in Multibody Systems. Proceedings of USACM, Sixth U.S. National Congress on Computational Mechanics. August 1-3 2001, Dearborn, Michigan.

[11] R. Ahrem, P. Post, K. Wolf: A Communication Library to Couple Simulation Codes on Distributed Systems for Multi-Physics Computations. In: Proc. of ParCo99 Conference, Imperial College Press, 1999.

[12] W.R. Krüger, R. Heinrich. Strömungs-Struktur-Kopplung von Mehrkörpersimulation und CFD. Proc. of Deutscher Luft- und Raumfahrtkongress 2001, Hamburg, Deutsche Gesellschaft für Luft- und Raumfahrt, 2001.

[13] K. Yi, J.K. Hedrick. Active and Semi-Active Heavy Truck Suspensions to Reduce Pavement Damage. SAE Technical Paper Series, no. 892486, 1989.

[14] D. Cebon. Vehicle Generated Road Damage: A Review. Vehicle System Dynamics, 18, 1989, pp. 107 - 150.

[15] W. Huyer, A. Neumaier. Global optimization by multilevel coordinate search. Journal of Global Optimization, 14, 1999, pp. 331-355.

[16] O. Vaculin, M. Valasek, W. Kortüm. Multi-Objective Semi-Active Truck Suspension by Spatial Decomposition. 17th IAVSD Symposium on Dynamics of Vehicles on Roads and Tracks. Lyngby, DK, 2001. tbp in 2002.

[17] W.R. Krüger, M. Spieck. Interdisciplinary Landing Gear Lay-Out for Large Transport Aircraft. Proceedings of the AIAA/USAF/NASA/ISSMO Symposium on Multidisciplinary Analysis and Optimization (AIAA-98-4964), St. Louis, 1998

[18] W.R. Krüger. Integrated Design Process for the Development of Semi-Active Landing Gears for Transport Aircraft. DLR-Forschungsbericht 2001-27, Köln, 2001.

An Object Oriented Extensible Architecture for Affordable Aerospace Propulsion Systems

Gregory J. Follen
Computing & Interdisciplinary Systems Office
NASA Glenn Research Center
21000 Brookpark Rd., M.S. 142-5
Cleveland, Ohio 44135, USA

gfollen@grc.nasa.gov

Summary
Driven by a need to explore and develop propulsion systems that exceeded current computing capabilities, NASA Glenn embarked on a novel strategy leading to the development of an architecture that enables propulsion simulations never thought possible before. Full engine 3 Dimensional Computational Fluid Dynamic propulsion system simulations were deemed impossible due to the impracticality of the hardware and software computing systems required. However, with a software paradigm shift and an embracing of parallel and distributed processing, an architecture was designed to meet the needs of future propulsion system modeling. The author suggests that the architecture designed at the NASA Glenn Research Center for propulsion system modeling has potential for impacting the direction of development of affordable weapons systems currently under consideration by the Applied Vehicle Technology Panel (AVT).

This paper discusses the salient features of the NPSS Architecture including its interface layer, object layer, implementation for accessing legacy codes, numerical zooming infrastructure and its computing layer. The computing layer focuses on the use and deployment of these propulsion simulations on parallel and distributed computing platforms which has been the focus of NASA Ames. Additional features of the object oriented architecture that support Multi-Disciplinary (MD) Coupling, computer aided design (CAD) access and MD coupling objects will be discussed. Included will be a discussion of the successes, challenges and benefits of implementing this architecture.

Numerical Propulsion System Simulation

Today, propulsion engineers use what are called preliminary and conceptual design codes to numerically create and analyze commercial, military and rocket propulsion systems. Most of these computer codes were written in the 60's and 70's and many, if not all, are written in FORTRAN. For some time now, analyzing and building propulsion systems has been prohibitively expensive due largely to the iterative nature of designing, analyzing and testing of hardware before a final configuration is achieved. In order to reduce cost, risk, time to market, expand capability, assure accuracy to mission requirements and increase confidence in designs, innovative ways have to be found to numerically create propulsion systems that bring the design closer to the final configuration before hardware is ever built and tested.

The NASA Glenn led Numerical Propulsion System Simulation (NPSS) is a project funded by and partnered with NASA Ames targeted at impacting this need. NPSS set out to advance the

state of the art in propulsion modeling as well as create a common architecture to numerically model propulsion systems. NASA Ames embarked on developing the parallel and distributed computing platforms needed by such simulations.

The current state of the art in propulsion modeling centers on the use of 0 Dimensional preliminary and conceptual design methodology. However, NPSS wanted to look beyond the current ways propulsion systems were designed and created. NPSS dreamed of a system that allowed an engineer the flexibility to numerically assemble an engine using 3-Dimensional components or any combination of 0,1,2,3 Dimensional component codes. The "plug-n-play" or "substitute at will" concept captures the essence of this goal. Figure 1 embodies this concept.
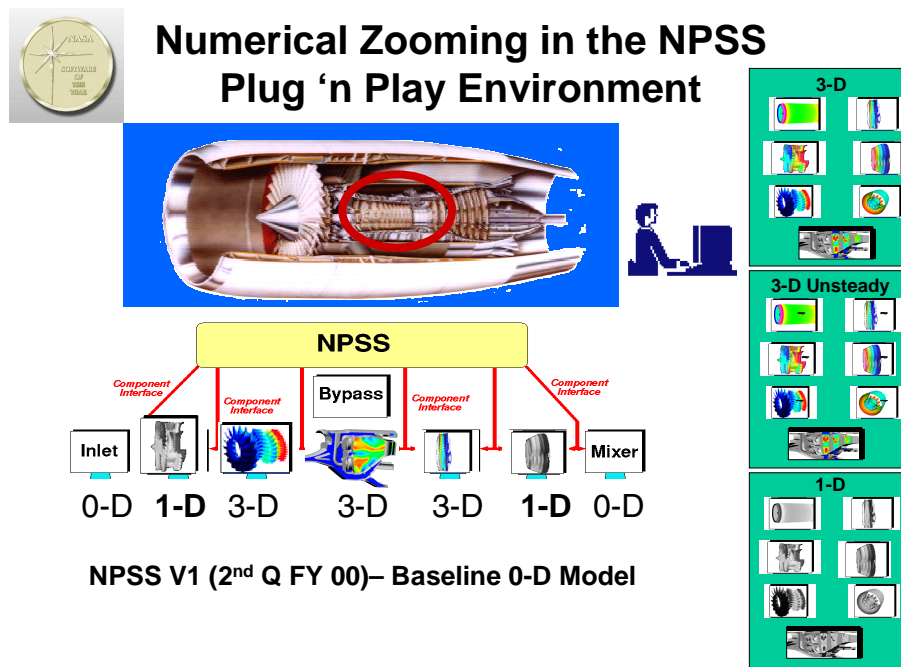
Figure 1.

With this in mind, an object-oriented architecture was designed and laid out to fulfill this vision. The NPSS object-oriented architecture allows an engineer to numerically assemble a propulsion system comprised of differing dimensionality component codes (Numerical Zooming), different disciplines (MD coupling), all irrespective of the computing platforms these codes execute on while producing results on cost effective computing platforms overnight. The first deliverable within the NPSS Architecture is NPSS V1.0. Although V1.0 preserves the traditional preliminary and conceptual design methodology for designing engines that is the state of the art today, it was created to move the state of the art in propulsion system modeling into the future. As such, NPSS V1.0 is an object oriented preliminary and conceptual design code used by aerospace engineers to predict and analyze the aero-thermodynamic behavior of commercial jet aircraft, military, and rocket engines. However, it is more than this, as it has designed into it the infrastructure supporting Numerical Zooming to higher dimension codes and coupling to differing discipline analysis. As the state of the art in propulsion modeling moves into the future away from a strict adherence to 0 Dimensional analysis towards a mixture of 0,1,2,3 Dimensional codes, the same NPSS' architecture exists to support this maturity in modeling.

The NPSS architecture is pictorially represented by figure 2. The architecture is open and extensible. To this end, the architecture exploits the capabilities of object-oriented programming (inheritance, polymorphism, and encapsulation) as well as modern object-oriented concepts including frameworks, component objects, and distributed object standards.
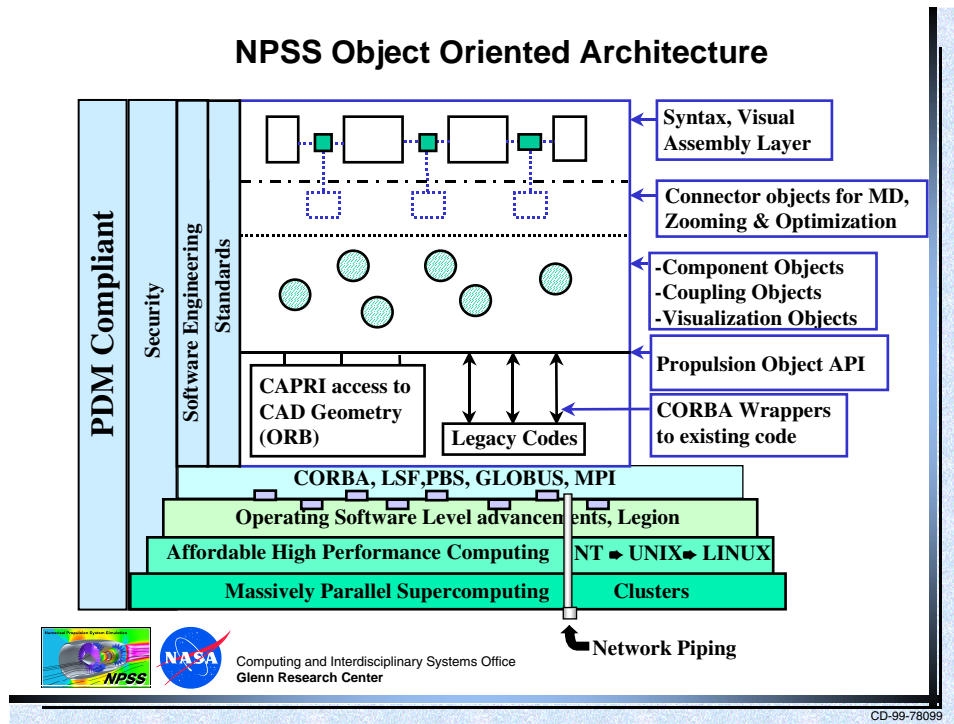
Figure 2.

Design Philosophy

The NPSS Architecture was designed following a hybrid object oriented design philosophy. The early work by I. Jacobson and G. Booch were followed where appropriate and extended by experiences known within the NASA culture. An overall philosophy for NPSS was to view the architecture from a leap-frogging approach, purchase from the commercial sector what you could, minimize commercial licensing and build from scratch that what you must. Whatever benefited the project from new and innovative hardware or software was to be incorporated into the architecture as quickly as possible without a huge development effort and without disturbing the quality and stability of the current system. To make the advances in propulsion design, time could not be wasted on re-checking answers, re-writing code and re-designing entire sections of the architecture. This was the fundamental reason the object-oriented paradigm was chosen. Beliefs then, and proven now, demonstrate that the object oriented design methodology was correct.

NPSS Architecture

Referring to figure 2. above, there are fundamentally three main areas of the architecture. These are: the Interface Layer, Object Layer and the Computing Layer. Within the Interface Layer, a command and a visual interface exist. The Object Layer contains the fundamental engineering specifics for propulsion systems and the appropriate support objects needed by propulsion systems such as access to geometry and legacy FORTRAN codes used by many, if not all, propulsion companies. Last but not least, the Computing Layer exists on which to deploy

propulsion system simulations. This last layer, Computing, is and has been the most dynamic over the last ten years and continues to change about every 18-24 months.

Interface Layer
From the beginning of the architectures' development, the priorities were to get the engineering and physics right and then add a visual interface later. Given this, the main interface to NPSS has been a command line. However, do not assume that this is a simplistic interface to NPSS. On the contrary, the command line and its suite of syntax are quite elegant, mature and sophisticated.   Two versions of the command interface exist:

> Batch: npss [-*options*]file1 *file2 . . .*
> Interactive: npss [-i][-*trace*][-*options*]file1 *file2 . . .*

Contained within the file1 is the actual NPSS syntax that defines the propulsion system to be designed and analyzed. The language used here is C++ like but not pure C++. Early exposure to pure C++ as the syntax changed the direction to create a C++ like syntax. This change allowed an easier and early adoption of NPSS. While most engineers wanted a FORTRAN language, many of the concepts envisioned fell victim to FORTRAN's language syntax. The syntax itself has many features of a programming language and indeed, a feature we've added is an NPSS syntax to C++ converter. This feature allows code first developed with the syntax to be later compiled as part of an executable library available for later use. A sample of the syntax looks like the following.

```
Model BWB {
        Element FlightConditions AMB0 {. . .}
        Element Inlet Inlet {. . .}
        Element Fan Fan{…}
        Element Compressor Compressor{..}
        Element Combustor Combustor{…}
        Element Turbine Turbine {…}
        Element Nozzle Nozzle(…}
        linkPorts ("FlightConditions.Outlet", "INLET.F1_I", "FL0",……);
}
```

The syntax has programming constructs such as: The ability to declare new variables that are combinations of other variables, comments, If-then-else, do while's, arithmetic functions: *, /, +, -, exponentiation, logicals, >, <, =,...., etc.

Recently, a visual front end to NPSS has been under development. The visual front end communicates with the NPSS system through the command interface as just described. An early view of this interface is included as shown in figure 3.   Visually speaking, NPSS provides the ability to assemble and connect a propulsion system together and then execute this simulation as well as store or archive it as necessary. It is the author's belief that in order to maintain flexibility, maturity of NPSS and advancement to its capabilities, a visual interface and a command interface must always exist separately. Once the visual interface becomes part of a code, a violation to the integrity of the original intent of the code has occurred and can never be recovered. Even as future interfaces emerge such as voice activation, screen sensing and even optical movement or heads up displays, in order to break off the current visual interface and make use of the futuristic interfaces, a command interface will need to exist.
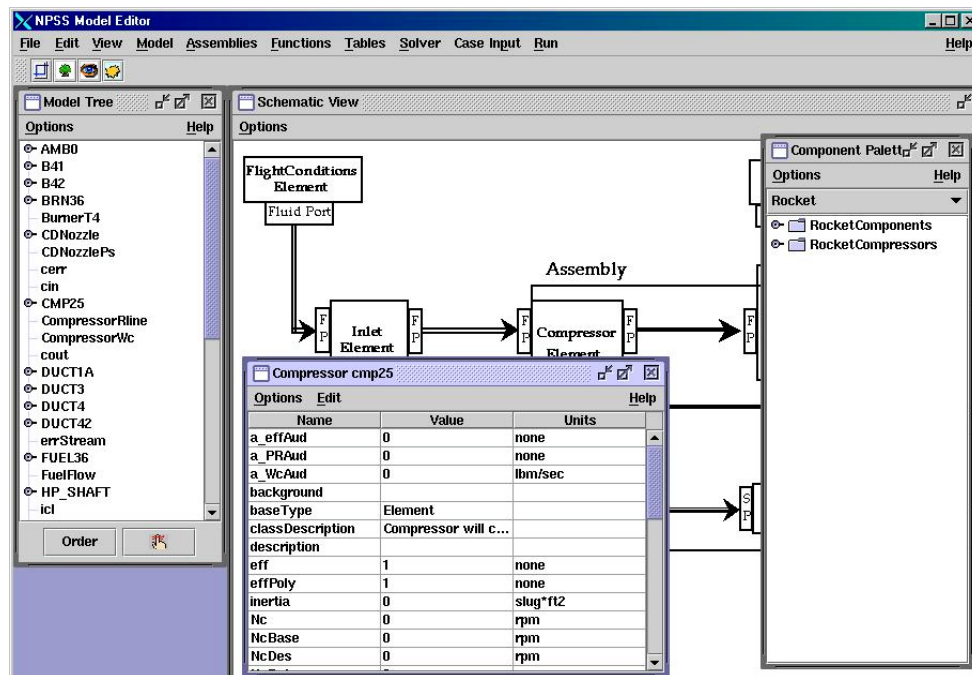
Figure 3.

Object Layer

The development of the object layer has garnered the most attention and development. This is where all the propulsion objects exist both for airbreathing and rocket engines. Additionally, this is where all the infrastructure objects are for moving information from one element to another, for accessing object codes (FORTRAN, C, C++,…) through CORBA on other machines and other address spaces. The numerical zooming, code coupling and security infrastructure also exists here as well.

Propulsion and Rocket Objects

NASA Glenn has populated this layer with airbreathing, rocket and to a lesser extent ground based power objects. What is marquee about this architecture is that the infrastructure contained within the NPSS syntax is the same for airbreathing, rocket and ground based power objects. While the NASA Glenn led team came together to define what a common set of airbreathing, rocket and ground based power objects are and defined their numeric behavior, this does not mean that the objects' behavior and characteristics cannot be changed on demand. On the contrary, the ability to change or extend the objects behavior is central to the use of the object-oriented paradigm. The objects provided can be used as they are or can be changed based upon appropriate need. Additionally, the developer is assured that the object has been tested and proven to be accurate. So, any abnormal behavior is due solely to the new features just introduced by the developer. The basic objects used within the NPSS Architecture for 0 Dimensional and 1 Dimensional analysis are:

•Elements
    –Primary building blocks connected together via Ports
    –Perform high-level calculations
•Subelements
    –Interchangeable secondary building blocks that plug into Elements or other Subelements
    –Perform detailed calculations

•Flow Stations
> –Responsible for thermodynamic and continuity calculations
> –Access the thermodynamic packages

•Ports
> –Used to connect Elements together
> –Five types (Mechanical, Fluid, Fuel, Thermal, Data)
> –Directional in nature (i.e., outputs connect to inputs)

•Tables
> –Organized set of numbers that relate n-dimensional inputs to one or more outputs
> –Support linear and second or third order LaGrange interpolation
> –Support fixed value end-points or extrapolation (linear/2nd/3rd order LaGrange)
> –May be used at any location a function is called and vice-versa

Of particular note, in this object definition, is that there isn't a reference to anything related to propulsion. The NPSS Architecture's object structure, as defined, has allowed its general usage amongst airbreathing, rocket, fuel cell and ground based power propulsion by the writing of the appropriate functional objects. The author believes there are more applications to come.

Zooming, Code Coupling

In order to recover the wealth of investment in current FORTRAN, C, or other codes, NPSS has adopted and developed a Common Object Request Broker Architecture (CORBA) interface to make it appear as though these codes are actually C++ objects within the architecture. While NPSS cannot gain complete control over these codes, it does provide three common procedures for integration. These procedures are currently GET a variable, SET a variable, and EXECUTE and are available no matter what the particular focus of the code you are accessing or in NPSS terms "zooming" to. The zooming infrastructure has been successfully demonstrated between an NPSS turbofan model and a 1 Dimensional high-pressure compressor code as pictorially represented by figure 4. A similar zooming accomplishment has also been completed between an NPSS Expander Cycle Engine model and a 1 Dimensional Pump code called PUMPA.
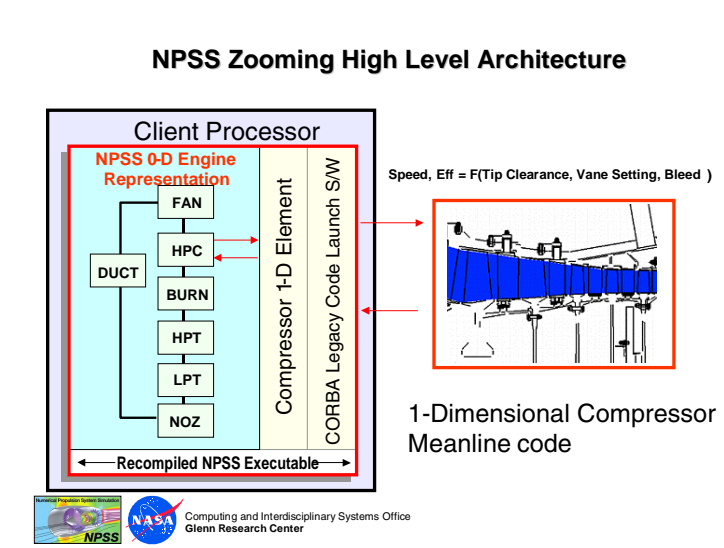
Figure 4.

Distributed, Parallel Computing
The basic internal communication scheme used by the NPSS Architecture for moving data across address spaces and separate machines is through its CORBA interface. This is a point-to-point concept of distributed computing and coupling of codes. Leveraging CORBA and its associated Security (CORBASec) software has proven quite useful. From a parallel processing sense, the NPSS Architecture has adopted the NASA Ames' Grid Computing software called GLOBUS. The GLOBUS software can be thought of as a scheduler of schedulers since it is 'aware' of scheduling software such as Load Sharing Facility (LSF,Platform Computing), Portable Batch System (PBS,NASA Ames), Load Leveler (IBM). The NPSS Architecture makes an assumption that any 3 Dimensional Computational Fluid Dynamics (CFD) code, structures codes that will be integrated into an NPSS Simulation, already uses one of the above schedulers as well as a particular message-passing library such as Parallel Virtual Machine (PVM), Message Passing Interface (MPI) or some derivative of these.   For NPSS' needs, the Grid Computing software GLOBUS, needed to be aware of CORBA based simulations in the same way that it is aware of LSF, or PVM based simulations. The NPSS team has developed a CORBA interface to the GLOBUS services to support the NPSS Architecture. NPSS' goal has been to deploy complex propulsion simulations that can be solved in an overnight timeframe in less than fifteen hours on cost effective computing platforms. The corresponding Architecture goal is to deploy these subject simulations on any computing cluster with minimal to no changes to the codes.

Coupling of Codes & Geometry Application Program Interface (API)
In developing the appropriate objects to support code coupling both from a single discipline and multi-discipline perspective, a prototyping activity was set forth through a contract. The contract specified to prototype the needed objects to couple a 3 Dimensional structures code with a 3 Dimensional fluids code and thereby provide guidance to a design that would encompass most of the objects needed to support coupling of these codes.   Once the NPSS project understood what made sense to do, the team could then begin the formal development of the C++ objects and make this part of the NPSS Architecture.   While this work is continuing, current objects include: single precision variable object, structured grid object, structured interface object, meta variable object, FORTRAN character object, FORTRAN callable API, and a CORBA Object called ForeignElement.

The NPSS Architecture needed a common geometry API that interfaced to the current suite of commercial CAD vendors. It was already known that differing 3 Dimensional codes acquired their respective geometry in different ways which introduced the potential for errors in the analysis as the geometry was not interpreted the same way by all authors of codes. To address this issue, an activity was started with Massachusettes Institute of Technology (MIT) to create a common interface for reading geometry from Unigraphics, ProE, CATIA as these represented the most common CAD systems within the propulsion community NPSS worked with.   The result of this work is a library/API called CAPRI. If the code developer adopts the CAPRI API then geometry from UG, ProE, CATIA and other CAD systems can be read directly. Work is ongoing to implement the Write function. No status is provided here on the Write function.

Computing Layer
The High Performance Computing and Communication Program that funded NPSS had as one of its goals the development of massively parallel computers with high speed networks. Knowing this and realizing that early computing platforms of this type would be volitale, the NPSS Arhitecture was designed to 'leap-frog' this computing technology with no or minimal penalty to

the NPSS applications. Where it was necessary for an application to port to an architecture, NPSS intended to use CORBA to reach that application. The developers of the NPSS Architecture wanted minimal proprietary computing presence so as to be able to jump from one parallel or distributed computing platform as needed. The thought of porting codes to particular architectures and then port them again all the while re-validating these codes was to be avoided.

NASA Glenn's participation in the development of parallel computers and networks focused on cost effective clusters. Originally, a thirty-two node cluster of IBM 560's with multiple networks was assembled from commercially available UNIX machines. These systems were ugraded to IBM 590's but never grew beyond the original 32 nodes. Following this cluster came a 128 node Pentium PC cluster comprised of 64 dual processor Pentium 400 Mhz systems running LINUX. Both these systems were batch oriented with the resources controlled by Platform Computing's Load Sharing Facility (LSF). A partnership arose between NASA Glenn, Platform Computing and a commerical propulsion company to support parallel applications within LSF and to develop a multi-cluster capability. Both these features exist within LSF today. Currently, the NPSS project is moving to adopt the GLOBUS software that can co-exist with LSF and has support for scheduling applications built on differing batch schedulers such as the Portable Batch Scheduler (PBS).

Software Engineering Principles
NPSS made an assumption that in order to see its Architecture and code used within the US Industry, adherence to an identifiable and recognizable software development process was mandatory. Even within a research center, software engineering principles have a place. In many research efforts, software engineering practices are a 'post development' activity. Many developers always seem to have time to go back and fix what they didn't have time to design for or around from the beginning. This was not the case with NPSS. From the start, software development plans, configuration management plans, and verification and validation plans and design plans were developed and used. At a minimum, any software development effort should have configuration management and some form of verification and validation at the subsystem and full system level. Without these phases, research codes never become anything but single user research codes. Any development effort sponsored by the AVT should include a presence of software engineering practices as appropriate for this community.

Along with a sophisticated yet manageable software development process, NPSS adopted an incremental release process by which bug fixes and urgently needed enhancements found their way into smaller or incremental releases rather than waiting for full releases of the software. Regression testing and documentation are still maintained within this incremental release process and in fact are more manageable.

Benefits to Date of NPSS
Early indicators on the benefits of using NPSS reveal a 55% reduction in the time to perform engine system simulation throughout the product life cycle. Additionally, expectations include a 50% improvement in business processes with partners and customers.
From zooming, a reduction factor of 10 was achieved by using the NPSS architecture to integrate high-fidelity compressor code into a system model. What normally took two days was achieved in two hours making a simulation do able whereas before it was possible but not practical.

Summary & Appropriateness to AVT
The words used in the theme of this AVT meeting are very similar to the words used in the goals and approach in the development of NPSS. The AVT theme states, "The defense of NATO requires a new paradigm in the development and deployment…", " essential to achieving the cost and time reductions needed to field new and improved…". NPSS' goal is to reduce time and cost in development of new propulsion systems while increasing confidence and reducing risk in achieving a final design. The NPSS Architecture emerged to impact airbreathing propulsion in the ways mentioned above. However, soon after its first incremental release, NPSS' potential use to impact space propulsion and ground based power also was realized. The NPSS architecture was re-used to model rockets, ground based power systems and even fuel cells by populating only its object layer with the behavior needed for space propulsion, ground based power and fuel cells. The remaining architecture was reused. The process by which NPSS was built is noteworthy. Designing a system that combines a production phase with prototyping and deployed on an incremental release schedule, provides for early access to fixes and new features that ultimately lead to the stated goals of reducing risk and reducing the time to final design. It is the opinion of the author that similar gains to AVT are available in building Affordable Weapons systems for NATO as are now being realized within NPSS' propulsion and power community.

Acknowledgement

References

1. Lytle, J. K., Follen, G. J., Naiman, C. G., Evans, A. L., Owen, A. K., Veres, J. P., and Lopez, I., Numerical Propulsion System Simulation (NPSS), 2000 Industry Review, NASA Glenn Research Center, October 2000.
2. Townsend, S.E., Using External Codes With NPSS, NASA Glenn Research Center, October 2000.
3. Sang, J., Follen, G. J., Kim, C., and Lopez, I., Townsend, S. E., Enhancing the Remote Variable Operations in NPSS/CCDK, NASA Glenn Research Center, October 2000.
4. Lytle, J. K., Follen, G. J., Naiman, C. G., Evans, A. L., Veres, J. P., and ET. AL., 1999 Numerical Propulsion System Simulation Industry Review, NASA/TR 209795, NASA Glenn Research Center, October 6, 1999.
5. Lytle, J. K., Numerical Propulsion System Simulation: An Overview, CAS 2000 Workshop/The Ames Research Center, February 15- 17, 2000.
6. Claus, R., Follen, G. J., Haimes, R., and Jones, W., CAPRI - Computational Analysis Programming Interface/ A CAD infra-structure for Aerospace Analysis and Design Simulations, NASA HPCC/CAS Workshop/NASA Ames Research Center, February 15, 2000 - February 17, 2000.
7. Follen, G. J., and auBuchon, M., Numerical Zooming Between the NPSS Version 1 and a 1-Dimensional Meanline Design Analysis Code, AIAA 99-SL-217/USA-35, September 5, 1999 - September 10, 1999; 14th International Symposium on Airbreathing Engines (XIV ISABE), Florence, Italy.
8. Hall, E. J., Modular Multi-Fidelity Simulation Methodology for Multiple Spool Turbofan Engines, NASA HPCC/CAS Workshop/NASA Ames Research Center, February 15, 2000 - February 17, 2000.

9. Sang, J., Kim, C., and Lopez, I., Developing CORBA-Based Distributed Scientific Applications From Legacy Fortran Programs, NASA/TM 209950, CAS Workshop/NASA Ames Research Center,, February 15, 2000 - August 1, 2000.

10. Lopez, I., Follen, G. J., Gutierrez, R., Foster, I., Ginsburg, B., and ET. AL., NPSS on NASA's IPG: Using CORBA and GLOBUS to Coordinate Multidisciplinary Aeroscience Applications, NASA/TM 209956, CAS Workshop/NASA Ames Research Center, February 15, 2000 – February 17, 2000.

11. Townsend, S.E., Coupling ADPAC to NPSS for an EEE Simulation, NASA Glenn Research Center, October 1999.

12. Reed, J. A., and Afjeh, A. A., Computational Simulation of Gas Turbines: Part I, II - Extensible Domain Framework, ASME, International Gas Turbine & Aeroengine Congress & Exhibition, Indianapolis, Indiana, June 7, 1999 - June 10, 1999.

13. Evans, A. L., Naiman, C. G., Lopez, I., and Follen, G. J., Numerical Propulsion System Simulation's National Cycle Program, 34th AIAA/ASME/SAE/ASEE; Joint Propulsion Conference & Exhibit, Cleveland, OH, July 13, 1998 - July 15, 1998.

14. Hall, E. J., Delaney, R. A., Lynn, S. R., and Veres, J. P., Energy Efficient Engine Low Pressure Subsystem Aerodynamic Analysis, NASA CR-206597, 34th Annual AIAA/ASME/SAE/ASEE Joint Propulsion Conference & Exhibit, July 13, 1998 - July 15, 1998, Cleveland, Ohio, AIAA 98-3119.

15. Haimes, R., CAPRI - Computational Analysis Programming Interface, 6th Int'l Conference on Numerical Grid Generation, University of Greenwich; Greenwich, UK, July 6, 1998 - July 9, 1998.

16. Lytle, J. K., The Numerical Propulsion System Simulation: A Multidisciplinary Design System for Aerospace Vehicles, NASA/TM-1999-209194, September 5, 1999 - September 10, 1999, 14th International Symposium on Air Breathing Engines sponsored by the International Society for Air Breathing Engines, Florence, Italy.

17. Foster,I., Tuecke, S., Kesselman, C., et al, www.globus.org

Impact of System-Level Engineering Approaches on the Airframe Development Cycle Via Integration of KBE with CAD Modeling and PDM

Frederick Emch
Technical Group Leader
Electronic Data Systems
13690 Riverport Drive, MC 215
Maryland Heights, MO 63043, USA

Executive Summary

Airframe companies have performed numerous studies over the years that conclude the overwhelming percentage of cost to manufacture a new aircraft, is set during the development phase. The majority of this development cost is set during conceptual and preliminary design, typically occurring at the aircraft OEM. If these costs are to be dramatically reduced, the development process must include the expertise of the entire extended enterprise as early as possible in the development cycle. Technology exists today that allows this extended team to collaborate in the design decision-making process. Suppliers, partners, and customers can participate by concurrently performing their own initial development activities, while the OEM team performs their preliminary design work. On the technology side, one of the keys is the integration of state-of-the-art CAD, KBE, and PDM tools such as EDS' Unigraphics™, Unigraphics/Knowledge Fusion™, and I-man™. The challenge is developing processes that use these tools to allow the entire extended team to work concurrently, using a common database, to quickly iterate the design to meet aggressive performance and cost reduction goals.

A new System Engineering approach, made possible through an EDS tool called Unigraphics/WAVE™, enables true concurrent engineering throughout the extended enterprise. At the same time that detail design aspects are being worked, the global, or system-level trade studies can progress. When global changes are finalized, all work progressing within the extended enterprise is updated, rather than lost. This includes work started by partners and suppliers. Through this approach, great strides can be accomplished in the reduction of design cycle time because all work is done in parallel rather than in series. In addition, everyone in the extended enterprise is always working with the same controlled data, which is accomplished through the I-man PDM system.

Performing trades studies and what-if studies using this new process is very rapid, which results in many more product iterations in a reduced development cycle. Also, aggressive performance and cost goals can be met. Even though these system engineering tools and processes are not forms of analysis per se, they greatly aid in the incorporation of mature and late-stage analysis results. For instance, strength analysis can progress late into the design cycle, and still be incorporated into the design because the team's work will be automatically updated. These late results are sometimes not incorporated in the more traditional design process due to schedule concerns, and this can result in increased vehicle weight.

Knowledge-Based Engineering (KBE) enables a richer and more robust design database by including the rationale behind why certain alternatives were chosen for the final product configuration. To decrease the

design cycle time, KBE automates many repetitive tasks. External databases and spreadsheets can also be tied into the KBE process. KBE also enables consistency of engineering data and the enterprise-wide reuse of that data.

The EDS tool Unigraphics/Knowledge Fusion, a merging of KBE and CAD, enables product and process to exist in the one system. With Unigraphics/Knowledge Fusion, a KBE language (Intent!) has been deeply embedded into a high-end product development system (Unigraphics). Intent! is an industry-proven language from Heide Corporation. Many companies have been using Intent! for years to provide KBE benefits to their engineering processes. One of the biggest benefits of this deep embedding is that the output from the KBE system does not have to be translated to a CAD system. With Unigraphics/Knowledge Fusion, the KBE and CAD are one system. The benefits of this merging to the development process include the creation of customized and proprietary applications or "wizards" that guide the user through the automated facility. The KBE data is stored in the I-man PDM system for easy retrieval and use by the extended enterprise. Cycle time is shortened by design reuse and a consistency of process is achieved.

Abstract

A classic airframe development problem is the disconnect between initial layouts/trade studies of structural arrangements and the detail designs that emanate from these layouts. Hence, the process of communicating design change has been time consuming, inefficient, and prone to errors.

This paper describes new methods now available that enable the linkage between system-level layouts and the digital master models. Knowledge-Based Engineering (KBE) tools can now be directly linked to preliminary CAD models to refine concepts. Product Data Management (PDM) manages both the KBE and CAD data. As system-level definition and knowledge evolve, changes are automatically propagated down the hierarchy of airframe definition. The result: cycle time reduction and achievement of aggressive performance targets.

Challenges of the Airframe Design Cycle

To address the challenges of reducing design cycle time and cost in the design engineering process, we must look not only at the technology used, but also at the processes themselves. Due to the complexity of the airframe, it must be broken down into subsystems, which can be designed independently within the context and requirements of the overall aircraft - one example being the wing torque box. This subsystem can be designed in relative isolation, but must adhere to the design requirements of the overall wing subsystem. Subsequently, the wing must adhere to the requirements of the total aircraft system to accomplish design requirements such as performance and cost. A major problem exists in that much of this high-level design intent resides only in the minds of the engineers. One of the challenges is how this design intent can be captured and reused to produce superior designs.

The traditional engineering process is drawing-based, either by manual means or electronically through the use of CAD. Looking at the technology side, parametric design is a production-proven capability in most high-end CAD systems today. This capability allows for definition of hundreds to thousands of

design variables within a detail part. Any of these variables can be modified, with the part being automatically updated. However, one of the limitations of parametrics is the relative inability to handle topological changes. To exacerbate the problem, some CAD systems require the user to parameterize everything in the geometric model. These parametrically driven detail parts, often in the thousands, make up the subsystems that define the aircraft. Another challenge to the design process, is whether engineers can grasp how these parts will behave as a result of high-level design changes.

System Engineering Approach

These challenges necessitate a new approach to the engineering process that takes advantage of the power of parametrics, and captures design intent and allows engineers to exercise a system engineering methodology. Much of the traditional design approach focuses on the parametrics of the detail parts. This is very much a "bottom-up" approach in that the low-level requirements combine to form the overall design. The reason the new approach is called "System Engineering" is that the requirements of the overall aircraft system drive the design in a "top-down" fashion.
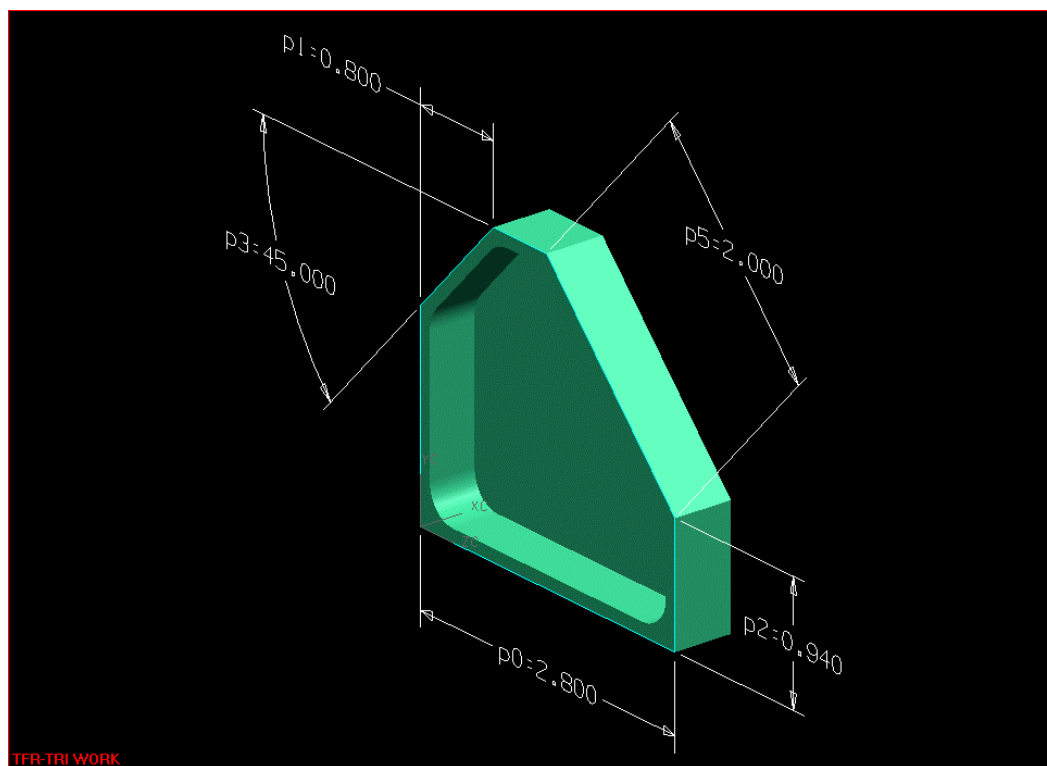
Figure 1

Example of parametrics in a detail part

Parametric design, allows for every design detail to be defined in terms of a parameter. These parameters can be edited at a later time, with the part adjusting automatically to that edit. Figure 1 illustrates these detail part parameters. This technology has been a huge boost to productivity, especially in aerospace. Structural parts are analyzed for strength requirements and the number of analysis/design update

iterations is often quite large. Even though parametric modeling is not an analysis tool by itself, it enables many more analysis/design update iterations to occur in a shortened development period. This allows for earlier incorporation of analysis results, which in turn provides the attainment of aggressive performance goals. The biggest benefit to detail part parametrics is the ability to incorporate mature analysis results late in the part release cycle. In more traditional processes, a design change due to mature analysis results may not be incorporated due to schedule constraints. This often results in the part weighing more than it needs to, with overall subsystem or vehicle weight targets not being achieved. With parametrics, the ability to incorporate last-minute analysis results is very achievable, with the design remaining on schedule.

The challenge posed by parametrics is that even in small parts, the number of parameters can be in the hundreds or even thousands. This can be overwhelming for the engineer attempting to analyze how system-level design changes will affect the thousands of detail parts and the thousands of parameters in each part. In addition to the complexity of the numbers of parameters, another challenge is understanding how the model was constructed in order to effectively make changes. The manner in which the parametrics are applied to a part can be different with every engineer. This can especially be a problem for an engineer looking at a model that they did not construct. Adding part-to-part relationships to the mix, results in a "parametric spaghetti", in which it is difficult, or nearly impossible, to know what a change to one area of the design will have on other areas. Figure 2 illustrates many of the interpart relationships, which can be present in a product assembly. This issue calls for a systematic approach to the construction of parametric models and assemblies.
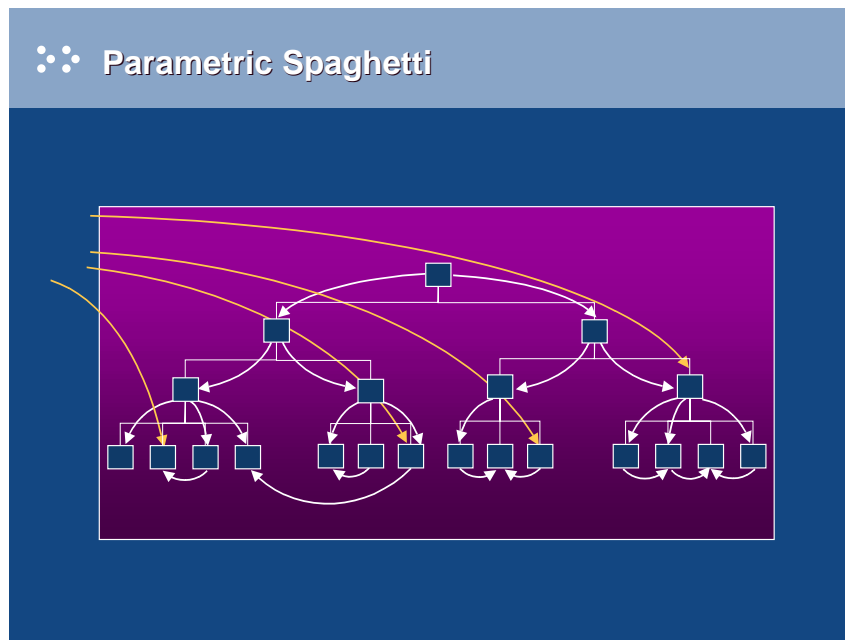
Figure 2

The complexity of interpart relationships

Top-Down design methodology is another key component in this new approach. Whereas a focus on the parametrics of the detail parts tends to lead to a Bottom-Up method, a focus on the overall aircraft requirements and subsequent subsystems tends to drive a Top-Down method. Top-Down is now possible

due to advances in the technology that create a systematic approach to building such a structure, and also provides the ability to control the change propagation at every step in the process.

The system engineering approach is the merging of the Top-Down design methodology with the power of parametrics. The advantage to the design process is the ability to greatly shorten development cycles while attaining aggressive performance goals. The Unigraphics CAD system offers this system engineering approach and is named Unigraphics/WAVE.

To start the new process, one needs to identify the major subsystems that make up the entire product. In the case of an aircraft, the major subsystems include the fuselage, wing, and empennage. These major subsystems can then be further broken down into components of greater detail and function. The entire structure forms an aircraft hierarchy of product requirements and functionality. The concept here is that there are "global" requirements and relationships that tend to drive "local" requirements and relationships (such as those contained with subsystems and subsequent details). The segregation of these global and local relationships is the key to the process. In the well-defined structure of product requirements, only those relationships that pertain to that particular level need to be defined. The upper level relationships need to control only the relationships of those levels directly beneath. This is the mechanism that limits the number of parameters required at each level, thus greatly reducing the complexity at any level.

An example of this hierarchy is the aircraft level and the immediate sublevels of fuselage, wing, and empennage. In the aircraft level, one needs to define only the parameters that control the interfaces between the major subsystems as well as any global requirements, such as the optimal Center of Gravity (CG) for the aircraft. The requirements for the wing and the key design parameters for wing design need to be defined only at the wing level. The parameters that define interfaces to the fuselage, or the design of a leading edge machining, would be defined in lower levels.
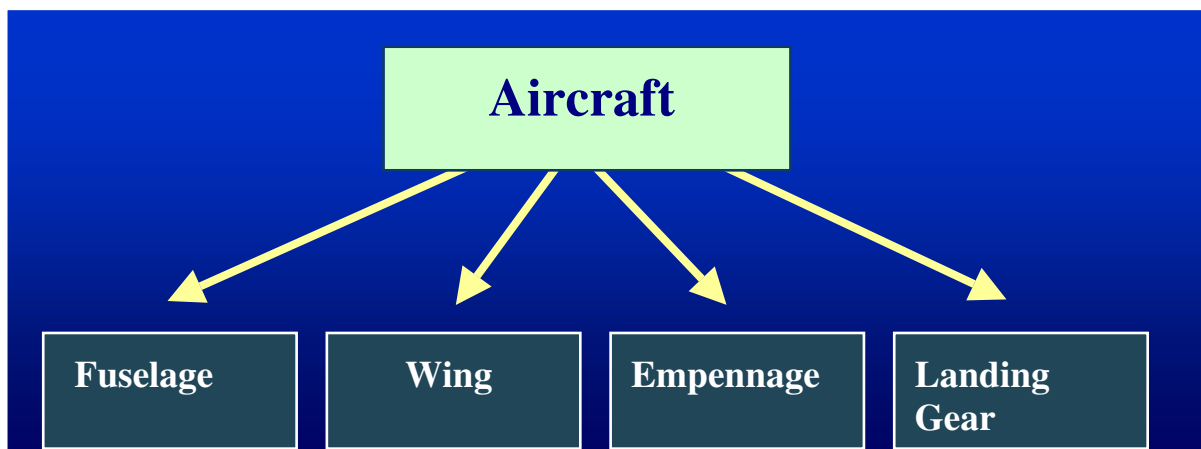
Figure 3

The control structure

The Unigraphics/WAVE Control Structure is the key to controlling the massive quantities of parameters generated in parametric design. For example, at the wing level, a very small number of key parameters drive the total wing design. Often, 20 to 40 key parameters in an upper level, are able to establish control

of the thousands of detail design parameters that make up the entire subassembly hierarchy. Another function of the Control Structure is the definition of interfaces between subsystems and between major elements within the subsystems themselves. The Control Structure assumes the role of system-to-system negotiator when conflicts arise regarding the interfaces. Again, the Control Structure approach captures, electronically, what used to be a manual process of design team communication that may not have occurred.

The Unigraphics/WAVE Control Structure offers a rich set of capabilities to do "what-if" trade studies at a high level. At the wing level, one could study high-level changes to wing plan form shape, including changes to the moldline. Because of the isolation between "global" and "local" relationships, the extensive detail design work progresses unaffected by these trade studies, until that time as the studies have produced a new set of design criteria to be propagated down the design hierarchy (Top-Down design). This approach offers a hard link between high-level layouts, and the master digital models that emanate from those layouts. The traditional approach handles this communication in a manual fashion that is often very ineffective.

The critical element that enables this new process to work, is the ability to finely control change propagation throughout the process. The timing of when and where Top-Down changes are propagated throughout the product structure is tightly controlled. In the above example, the wing plan form and moldline shape are being manipulated in a series of design trade studies. This could potentially cause hundreds or thousands of detail parts to need updating. The person iterating the wing design can isolate these high-level changes from the rest of the team, which produces two major advantages: 1) the rest of the design team keeps working, concurrently, in an uninterrupted fashion, and 2) the person doing the design trades can limit the parametric updates to his set of key parameters. By limiting the set of parameters to a small number, one is able to iterate through a much larger number of trades versus the time it would take to update the entire team through every trade cycle. The fact that the entire team is able to work concurrently, both the high-level aspects in conjunction with the more detailed work, results in shorter overall design cycle times and increases the team's chances of achieving challenging performance goals.

Product Data Management also plays a crucial role in the process. The entire Unigraphics/WAVE Control Structure as well as the complete assembly hierarchy, is contained in, and controlled by the EDS PDM system named I-man. Product structure in Unigraphics and in I-man is always kept up-to-date and synchronized. In fact, for a team member, partner, or supplier to view the hierarchical structure, they do not have to be in Unigraphics – this can take place in I-man.

Knowledge-Based Engineering

Many companies today employ a Knowledge-Based Engineering (KBE) system to:

- Decrease cycle automating repetitive design tasks.

- Capture and re-distribute critical company knowledge typically residing only in the minds of engineers, designers, and manufacturing personnel

- Ensure engineering rules and best practices are adhered to from design all the way through manufacturing.

- Protect loss of enterprise expertise due to employee turnover.

- Store knowledge in a format that is reusable and easily transportable by the design team.

Fundamentally, the key is re-use – the recycling of company knowledge and best practices that exist in several forms and that are present in every phase of the product life cycle. The various forms of knowledge are many: CAD datasets, CAM datasets, analysis data, text documents, company manuals, spreadsheets, databases, and rules of thumb. Engineers spend huge amounts of time simply searching for the information they need. An important question is the accuracy and relevancy of the data they do find – is the information current, is it the right information for the particular application at hand?

Clearly, a tool that addresses many of these information-type questions is Product Data Management. Robust and mature PDM tools, such as the EDS I-man product, enable the engineer to search for data and know that the data is current and applicable to the task at hand. I-man is capable of managing the many varied forms of data in the enterprise and to manage the life cycle of that data including engineering release. A key is capturing all the above company knowledge and best practices electronically, and making it available to the enterprise under PDM control. When all stages of a product's life cycle has immediate access to this data, cycle time and cost can be reduced significantly.

The Merging of KBE and CAD

Traditional KBE systems tend to be programming tools and are not very graphically oriented. This is typically where CAD systems shine. Designers enjoy the graphical interaction and ease of use of CAD. Creating, editing, and managing parametric features is also a strength of CAD, while being a weakness on the KBE side. Conversely, CAD systems do not handle non-geometric attributes exceptionally well. Non-geometric attributes are handled robustly with KBE. With CAD, you really are seeing the "end result" of an engineering process with limited description of the rationale and history of trade studies that went into that configuration. KBE on the other hand, is geared toward defining and recording processes as well as describing the rationale. CAD can vary a set of features already present in an efficient manner, but KBE is very robust at executing just the unique set of features needed for a set of specified design requirements. Most KBE systems recognize when whole sets of features need to be swapped for other features due to different requirements.

Until recently, the benefits of KBE have been isolated from the CAD environment. With the EDS tool called Unigraphics/Knowledge Fusion, the benefits of a fully merged CAD/KBE capability are now realized. With this merging, a Knowledge-Based Engineering language (Intent!) has been deeply embedded into a high-end product development system (Unigraphics). Intent! is an industry-proven KBE language from Heide Corporation. Many companies have been using Intent! for years to provide KBE benefits to their engineering processes. The term "embedded" needs to be emphasized, as apposed to "integrated" or "loosely associated". One of the biggest benefits of this deep embedding is that the output from the KBE system does not have to be translated to a CAD system. With Unigraphics/Knowledge Fusion, the KBE and CAD are one system.

Aircraft Floor Beam Example
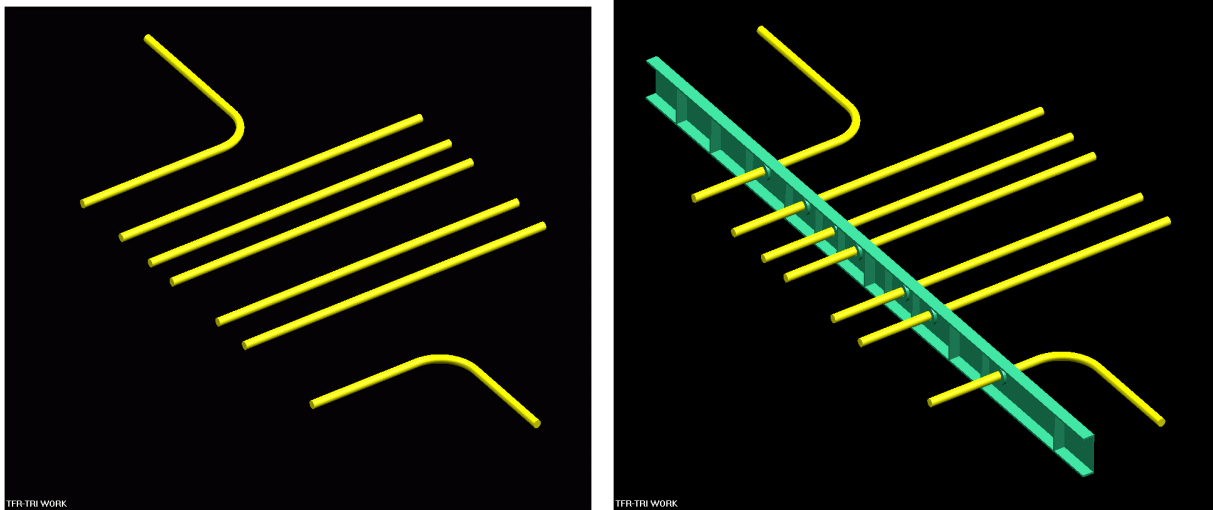
Figure 4

Automatic generation of an aircraft floor beam using a Knowledge Fusion program

Figure 4 shows a part called up from PDM which contains system routings in the under-floor area. Using a Unigraphics/Knowledge Fusion program, a floor beam is generated at the station 0 location. This example demonstrates several advantages of the process:

- A generative approach. A complete floor beam design was created in CAD using a textual KBE program.

- The resulting CAD geometry did not have to be translated from KBE to CAD.

- The resulting geometry in CAD is completely parametric. In Unigraphics, the geometry is comprised of features, which are fully editable at a later time.

- The program was called from the PDM database. In PDM, a library exists of available programs. A particular program can be found using a query on the database.

- The new floor beam is saved in the I-man PDM database. The new Item in the database can be found by queries and contains not just the geometry, but also the KBE rules that govern its construction, and later editing.

- Using I-man, if changes are later made to the program, the user can find out which parts and assemblies have made use of that program and would potentially be affected.
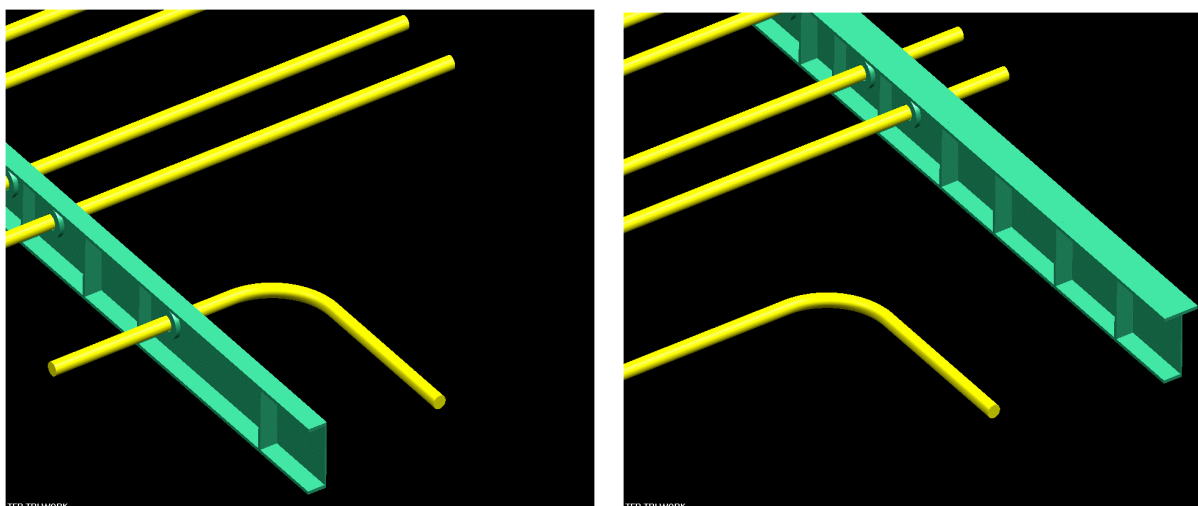
Figure 5

Edits to an existing model that uses a Unigraphics/Knowledge Fusion program

Figure 5 shows the result of editing the previously created model. The station parameter has been edited from 0 to 50, and the non-geometric parameter of "aircraft type" has been changed from "passenger" to "cargo". This editing demonstrates these advantages:

- The geometric and non-geometric rules that govern the creation and subsequent editing of floor beam parameters, are now stored in the Unigraphics part. These KBE rules become an integral part of a CAD file, which can be edited by the user at a later time.

- Editing of geometry parameters in Unigraphics automatically updates the Unigraphics/Knowledge Fusion rules (which now reside in the CAD file). This demonstrates 2-way associativity - KBE updates CAD, and changes to CAD update the KBE rule base.

- A capability of the floor beam program is to create a set of pad-ups around a system penetration, as well as a through hole, and a support stiffener. A separate program was written that creates this specific set of features. This technique highlights the modular nature of Unigraphics/Knowledge Fusion in that a program can consist of calls to other pre-existing programs. This cuts down on time to create automation programs.

- Figure 5 shows, that at station 0, a set of pad-ups exist for the near system run, but does not exist at the station 50 location since a penetration for the system is no longer required. A look at the feature list in Unigraphics shows that those pad-up features no longer exist in the model. This is a differentiator with pure parametrics. Only those features that are **required** are built in the CAD model.

- We also see from Figure 5, that an additional vertical stiffener has been added to break up the long distance between stiffeners. This could be the result of an analysis routine that calculates minimum distance between stiffeners based on loading, gauges, etc. This analysis routine could be either built into the program or an external program that Unigraphics/Knowledge Fusion communicates with.

- Finally, we see that at station 50, we have also toggled the non-geometric attribute "aircraft type" from a "passenger" to "cargo". Because of higher loading conditions, the basic beam shape has changed from a "C" section to a more capable "J" section.

Aircraft Stringer Example

The following example takes Unigraphics/Knowledge Fusion one-step further to develop a custom application or "wizard" dialog to perform a specific design task. In this case, a wizard dialog has been created for designers and engineers to quickly create aircraft stringers.

The creation of the custom dialog or "wizard" is an easy process. The user is prompted along the creation process by a series of dialogs that guide the connection of the Unigraphics/Knowledge Fusion program to the wizard. An "Instructions" button can be added to the wizard that takes the user to documentation. In this case, the instructions created are a series of web pages that offer step-by-step instructions, including images, on how to create stringers using the facility. Figure 6 shows the initial web page presented to the user showing the hyper links to other pages.

Figure 6

Web-based instructions for using stringer wizard

Figure 7 shows the before and after screen shots of using the Stringer Wizard. The before shot shows a portion of the "given" geometry which is the aircraft loft IML (inner moldline) surface. These items are picked from the screen using the applicable buttons on the wizard. The stringer type chosen for this example is a "Z" section. The material chosen was 6061-T6 Aluminum. The stringer plane orientation selected was normal to the moldline surface.

A crucial benefit of wizard creation is the incorporation of proprietary techniques and standards that are unique to the company. In this way, the most valuable aspects of a companies' intellectual resources and methods, can be used over and over again in a controlled fashion, to uphold standards and improve design quality.
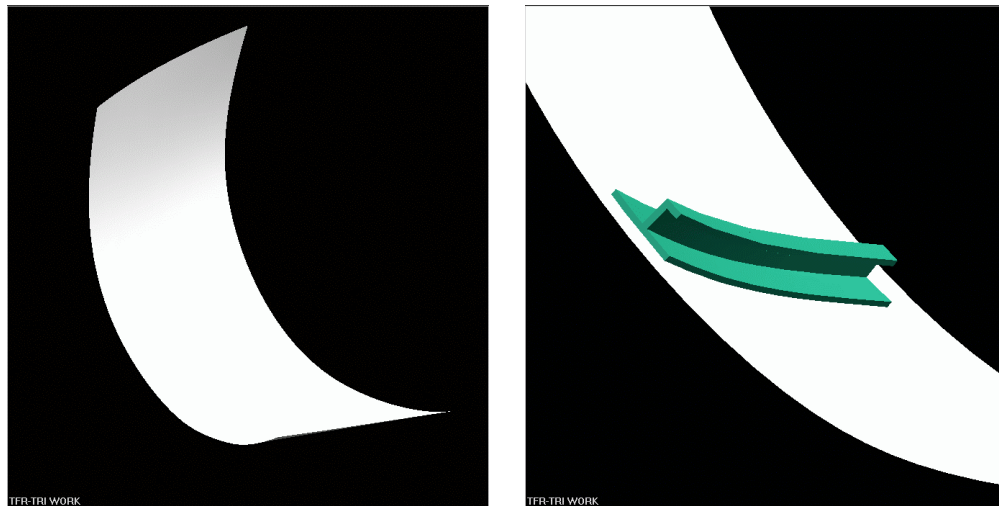
Figure 7

Before and after part creation using the stringer wizard

The Merging of Technologies and Processes

Another capability of Unigraphics/Knowledge Fusion is being able to query external databases and return values. An example of this was the wing, where the system engineering approach to design was used. KBE can add another capability to the approach previously outlined. If there was a database that contained aerodynamic test data, that database could be queried and return values that could help drive the Control Structure of the wing. Once the new values are back in the Control Structure, the hierarchy updates according to the rules already existing in the structure. The update process is governed by controls that have already been put into place. This ensures that the "what-if" process a rapid one. New configurations can be saved as design revisions in the PDM database and serve as a design history. This is an example of the marrying of a number of technologies: KBE (Unigraphics/Knowledge Fusion), the system engineering Control Structure approach (Unigraphics/WAVE), communication with external databases, parametric design, and PDM (EDS I-man).

Real-time cost analysis of design alternatives and trade studies is also possible using this merging of technologies. The governing formulae that determine product cost can be hard coded into a Knowledge Fusion program. These cost formulae are tied to the actual geometry in CAD parts and also tied to external databases that contain large quantities of cost-related data. Some examples of cost data include:

- In the CAD file, the length of welds between parts or the amount of material removed for a machining.

- In an external database, tables that would list the cost per inch of weld given the type or form of material.

As different design alternatives, such as material choices or product shape and size, are examined, the cost of that alternative is returned in real time. This feedback can dramatically lower total product cost by providing the capability to arrive at cost-effective design decisions quite early in the development process while still achieving the design goals.

Conclusion

The majority of the cost of developing a new aircraft is set during conceptual and preliminary design, typically occurring at the aircraft OEM. If these costs are to be dramatically reduced, the development process must include the expertise of the entire extended enterprise as early as possible in the development cycle. Technology exists today that allows this extended team to collaborate in the design decision-making process and remain associative at all levels in the process. Suppliers, partners, and customers can participate by performing their own initial development activities, while the OEM team concurrently performs their preliminary design work. If the OEM makes a major change, all team members are kept up-to-date. On the technology side, one of the keys is the integration of state-of-the-art CAD, KBE, and PDM tools. These tools allow the entire extended team to work concurrently, using a common database, to quickly iterate the design to meet aggressive performance and cost reduction goals. Aircraft design organizations have demonstrated the savings of these tools and processes in demanding production environments.

A new System Engineering approach (Unigraphics/WAVE) enables true concurrent engineering throughout the extended enterprise. At the same time the detail design aspects are being worked, the global, or system-level, trade studies can also progress. When global changes are finalized, all work progressing within the extended enterprise is updated, rather than lost. Through this approach, great strides can be accomplished in the reduction of design cycle time because all work is done in parallel rather than in series. Everyone in the extended enterprise is always working with the same controlled data, which is accomplished through Product Data Management (I-man).

Knowledge-Based Engineering (KBE) enables a richer and more robust design database by including the rationale behind why certain alternatives were chosen for the final product configuration. To decrease the design cycle time, KBE automates many repetitive tasks. External databases and spreadsheets can also be tied into the KBE process. KBE enables the capture and re-distribution of critical company knowledge that typically resides only in the minds of engineers, designers, and manufacturing personnel. KBE also enables consistency of engineering data and the enterprise-wide reuse of that data. A merging of KBE and CAD called Unigraphics/Knowledge Fusion enables product and process to exist in one system. Benefits to the development process of this merging include the creation of customized and proprietary applications or "wizards" that guide the user through a particular design task. The result is not only a significant reduction in cycle time and cost, but also a great improvement in engineering and final product quality.

References

[1] "UG/WAVE Product Portfolio Engineering," Unigraphics Solutions, 1998.

[2] "Product and Process Knowledge in one System," Unigraphics Solutions, 2000.

Virtual Testing with Validated Analysis Tools

Craig Collier
Collier Research Corporation
2 Eaton St. Suite 504
Hampton, Virginia 23669 / USA
craig.collier@hypersizer.com

Duane Veley
AFRL/VASD, Building 45
2130 Eighth Street, Suite 1
Wright-Patterson AFB, OH 45433-7542 / USA

Steve Owens
Lockheed Martin Aeronautics-Fort Worth
JSF Airframe SEIT / Certification/Development Test
Lockheed Blvd – MZ 6502
Fort Worth, Texas 76108 / USA

Abstract

Collier Research Corporation is working with Lockheed Martin Aeronautics (LM Aero) under United States Air Force Research Lab (AFRL) funding to develop a "certification-by-analysis" process to reduce unexpected failures during experimental testing that will, in turn, accelerate Air Force structural certification. The goal is early identification and avoidance of conceptual and preliminary design problems on new and sustaining aircraft programs using a "design-by-analysis" process that includes the commercial structural sizing software called HyperSizer®.

1. Introduction

Aerospace structures are certified with a combination of tests and analyses. Traditionally, and in the foreseeable future, tests serve two primary purposes:

- For certifying a specific hardware architecture that can support its identified worst case design-to loads
- For certifying the analysis methods and tools, which are then used to certify the untested load cases

Unlike unique hardware architectures, analysis tools benefit from a history of testing in that all previous test correlations can and should collectively contribute to increased confidence of their use. Analysis tools have and will continue to play an essential role in structural certification. This paper suggests a way to improve reliability of analysis tools so that eventually the aerospace industry will be able to reduce specific architecture testing which accounts for 25–30% of product costs.

This paper is not focused on the evaluation of analysis methods, but rather on how to increase confidence in the predictions made with any given analysis method and the software that implements it. Described is an *analysis building-block* approach for *verification and validation* (V&V), which parallels conventional building-block testing processes. A building block analysis verification process is a systematic way to validate specific analysis method cases, verify implementation in the software tool, calibrate prediction to test data, and establish failure data scatter as PDF's (probability density functions) from tests for probabilistic analyses.

Also described is a process for gaining more benefit from analysis tools by automating their use in conceptual and preliminary design phases. This aspect of minimizing design cycle time is most important since it accounts for 40–50% of product development costs. The objective is to deploy analysis tools as soon as reasonable in the design phase to make the biggest impact on the design progression. Referred to as design-by-analysis, this process provides beneficial early identification and avoidance of conceptual and preliminary design problems that could become extremely expensive to remedy in the final design cycle. In this way, *Virtual testing* is continuous throughout the design progression, and confidence is maintained in being able to successfully certify structure at time of testing - with no unpleasant surprises.

Connection to HyperSizer

It is necessary to include a background description in this paper of the HyperSizer analysis tool to be able define how it can contribute to the certification by analysis process. HyperSizer [1] provides aerospace industry accepted standard engineering analysis methods, physics based solutions, empirical data, and plug-in capability for industry and government specialty analysis codes. These analysis methods are automated with their I/O seamlessly integrated (thereby reducing human error), linked with leading FEA packages and FEM modelers, and deployed in a modern Windows product where data integrity is maintained with an internal database management system. The software is also provided as an object model that can be customized and integrated into customer's structural analysis software. HyperSizer was originally developed as a research code at NASA Langley Research Center. Since 1996, it has been commercially developed and supported by Collier Research. An important aspect toward validation is HyperSizer's data entry safeguard for unforeseen use by a non-developer. That is a relatively experienced engineer in the subject field, who is not the tool developer, can reliably obtain with the tool the correct result. In addition to analysis, HyperSizer performs automated structural sizing to find the lightest combination of design concept, material, and cross sectional dimensions for specific vehicle architectures. Referred to as robust sizing, the goal is to identify designs that are more likely to prove successful at time of test certification.

Content of this paper starts with a background into current practices for structural certification, and proceeds with the scope of our current research, an identification of the problems and solutions pursued, a connection to HyperSizer structural sizing and finite element analysis (FEA) software, and then ends by illustrating these structural certification software processes in a cause and effect diagram.

2. Background on Structural Certification

The term, "certification" is essentially an endorsement or sanctioning of the entire air vehicle design and analysis process by the customer. Typically, structural design and development of an aircraft proceeds through a "building block" series of analyses and tests beginning with:

- specifications for materials, quality assurance, and manufacturing processes
- definition of fundamental material physical and mechanical allowable properties
- understanding of often complex physics via element tests
- confirmation of failure modes via subcomponent tests
- prediction of built-up full-scale component level tests
- verification of global response predictions via full-scale airframe ground and flight tests

These tests and supporting analyses form the basis for certification of the structural integrity of the airframe. Currently, most of these varied tests are used to validate analysis predictions, or in some cases to provide the sole means of certification by test. Confidence and risk reduction are key attributes of the process that are achieved through structural testing following a deterministic approach.

"Certification" of an air vehicle is achieved with acceptance by the certifying agency of results from ground and flight-testing coupled with successful correlation to predicted structural behavior. The certifying agency works with the manufacturer to tailor the structural integrity plan. The manufacturer and the certifying agency agree on all of the structural materials and associated manufacturing processes, as well as the verification methodology used to demonstrate compliance with the design requirements. The word "certification" indicates that someone has issued a certificate, a written testimony to the truth of any fact. For a new aircraft, the word certification is an appropriate term since the authorities issue an airworthiness certificate. However, certification can also be described as a process of risk management. In environments such as that of the US Air Force, which acts as both a customer and a certifying agency, the certification agency acts throughout the entire process of developing the air vehicle, from defining the requirements to designing and developing the system to insuring that everything is in place and the personnel are trained for the operational environment. It is this process of risk management that undergirds the certification by analysis program.

3. Scope of Research/Approach

Analyses for structural certification determine that a structure is capable of supporting all required loadings. This is accomplished with two primary data: applied loadings and allowable loadings. An allowable loading is due to a combination of the material's strength and the response of the structural design based on details such as panel concept, shape, size, etc. Reliability of a structure is defined as the probability that the allowable load is greater than the applied load [2,3]. Potential failure occurs when the curve tails overlap, as indicated in the middle of Figure 1.
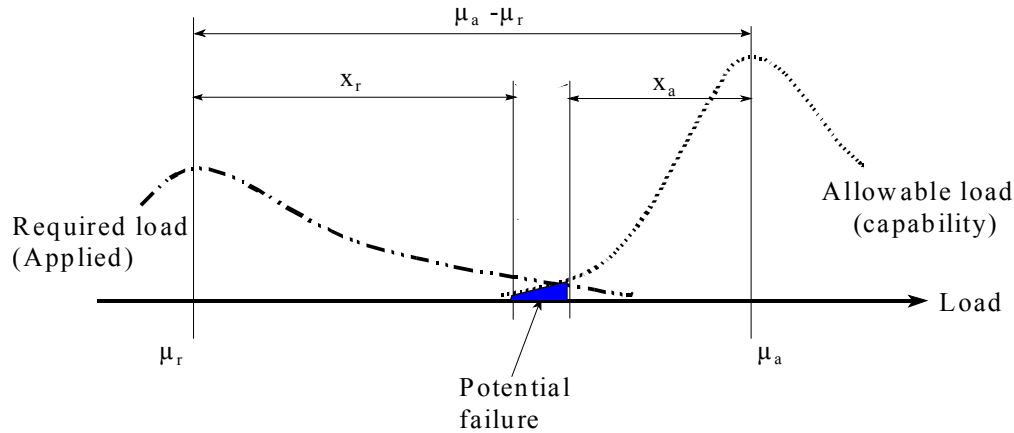
Figure 1. Reliability of a structure is defined as the probability that the allowable load is greater than the required load, or alternatively as R=1-PF.

In Figure 1, the required load is that resulting from applied external loads such as aerodynamic pressure. The allowable load is the load carrying capability of the structure. External flight loads are resolved into internal loads using FEA such as MSC/NASTRAN, and allowable loads are computed with analysis methods that predict failure modes such as HyperSizer.

Allowable Load

The emphasis of our research is on the allowable load distribution, indicated as the curve on the right hand side of Figure 1, which portrays how a structure of the same shape, size, and material will exhibit a range of allowable load capability. That is, seemingly identical test articles will not fail at a one given load, but instead fail within a range of loads due to natural data scatter/stochastic response. Figure 2 illustrates this as a histogram of occurrences, with the highest frequency of failure centered around the mean value, and the range quantified as a statistical deviation, σ. From a design and certification perspective, the material allowables, manufacturing tolerances, uncertainties in boundary conditions, and analysis inaccuracies all come into play.
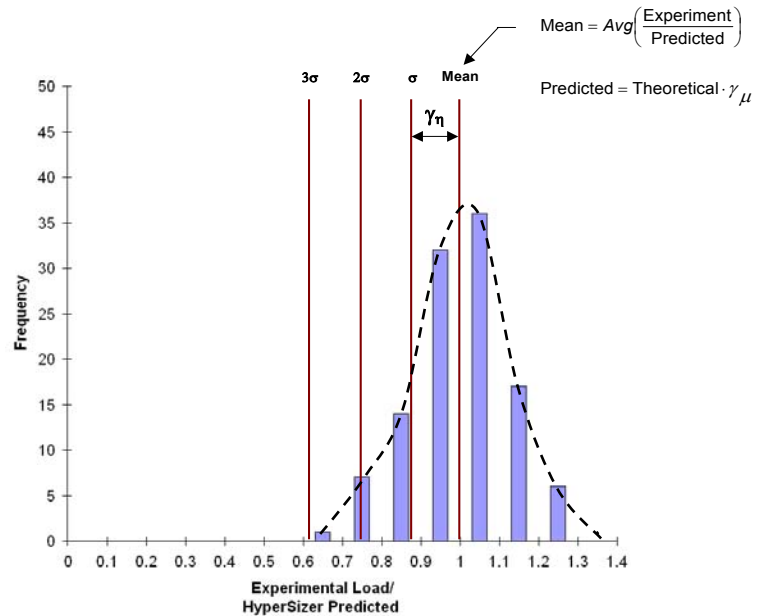
Figure 2. The frequency of failure from test data, illustrated as a histogram with the statistical distribution (dotted curve) used to quantify load carrying confidence.

4. Problems Identified and Solutions Pursued

After being fabricated and assembled following a tightly controlled manufacturing process, what appear to be identical aircraft structures will have different load carrying capabilities. These differences can be dramatic in some cases, and slight in others. The issues are not unique to aerospace. Other industries such as automotive, shipbuilding, and civil construction all struggle with the same issues. In short, industries that produce many copies of a particular design, such as the automotive industry, can afford many full scale tests of their product and reduce their conservatism in safety factors. Industries such as civil construction that make one-of-a-kind designs (think of the golden gate bridge) cannot economically perform full scale tests, and thus have to rely completely on analysis, usually with very conservative safety factors. The aerospace industry, being performance driven and extremely weight sensitive, cannot afford highly conservative safety factors, nor afford to perform multiple full-scale aircraft failure tests. As a result, a one shot, full-scale static strength test is usually performed.

Manufacturing full scale hardware is invaluable for proving out fabrication and assembly techniques. Full scale tests are invaluable for quantifying service fatigue and for calibrating strain gage readings to the internal load paths predicted with the "loads FEM". Full-scale ground tests also demonstrate that hundreds of predicted flight loads can be sustained with an additional 1.5 factor of safety. However, full-scale airframes are not usually tested to failure, and if they are, the test only tells us the critical failure mode and location for that one selected worst case load. There are thousands of loading conditions the airframe must survive, and even though hundreds are tested, there are untested loads that will control the design and sizing of at least some parts of the airframe. As a consequence, "too much credence is given to deterministic tests" [4], and aerospace design will continually be dependent upon analysis for structural certification.

Certification by analysis must start with an analysis building block approach. As such, it is necessary for the suite of analysis methods and tools to demonstrate an ability to accurately predict a series of smaller and well-defined problems that collectively make up the larger problem that has many response interactions and boundary condition uncertainties. We refer to this as a building-block analysis tool validation and verification. The premise is if a suite of analysis tools can predict each block of the building-block process, then, taking into account boundary condition interaction, they together will be capable of simulating the entire part. And since element and subcomponent tests are much less expensive than full-scale components to test, many more of them can be economically tested to obtain statistically significant data, and more importantly, as the name implies, their test results and corresponding analysis methods can be reused as building blocks for other structural designs. To meet a level of robustness reusability requires the analysis building block approach will address precision, reliability, and accuracy of Figure 3, with probability density function (PDF) signatures.

PDF Signatures Described

The differences in load carrying strength in seemingly identical structures may be partially attributed to manufacturing anomalies. In the case of curved panel buckling, which is particularly susceptible to imperfections and historically has proven to occur at loads substantially below theoretical predictions, *manufacturing signatures* [5] have been proposed to account for the amount of imperfections expected for a given manufacturing process. The manufacturing signature would be a measure of the imperfection for use in the analysis and thus allow a reduced buckling knockdown factor [6].

Precision	Reliability	Accuracy
(Provided by high fidelity analysis)	(provided by probabilistic methods)	(provided by test calibration)
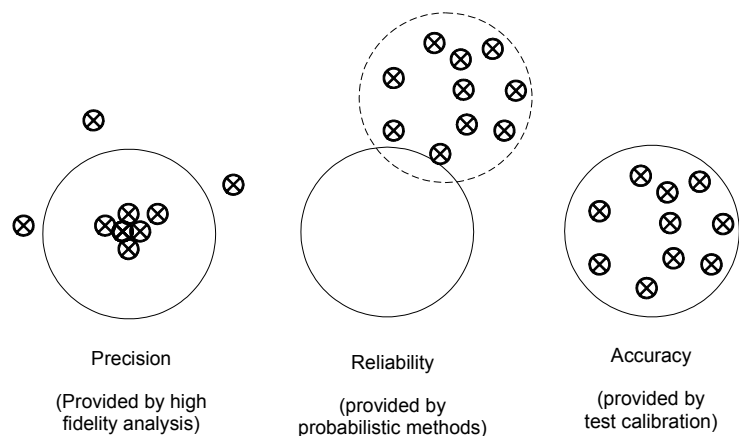
Figure 3. High fidelity analyses provide precision, defined as an ability to hit a bull's eye but not ensuring that all results fall within the target. Probabilistic methods reliably bring the scatter into the circle, and calibration is required to accurately hit the target.

It seems conceivable to categorize the types of structures and loadings that will have responses fall within tight bands of results, and those that have a large amount of scatter in their behavior. These response PDF distributions can be categorized into what we call ***PDF signatures***. By definition, PDF signatures are unique, repeatable, and, as demonstrated next, crucial for reliability based structural certification.

PDF Signature Example

Figure 4a shows normalized PDFs for four separate kinds of tests to ultimate failure: 1) 32 steel beer cans compression tested in 1987 and reported in [7], 2) 14 aluminum diet Pepsi cans compression tested in 2001, 3) 74 composite curved laminates compression tested in 1973, and 4 composite beams flexural strength tested in 1998. Note the very close match in PDF curves for the two metallic can buckling tests, indicating the same PDF signature. The curved laminate test is slightly more stochastic than the metallic cylinder test, and both PDF signatures are drastically different than the composite beam bending strength PDF.

Figure 4b illustrates how two different PDF signatures indicate the amount of additional safety factor required to meet prescribed structural integrity reliability. In the case of cylindrical buckling (flatter PDF) requires a substantial buckling knockdown factor of (0.7/1.95 = 0.375) [6,7] for a deterministic analysis that then would include an additional 1.5 ultimate load factor. In contrast, beam strength analyses (narrow PDF) are not typically knocked down, but if they were in this case it would be by the ratio of (0.911/1.17 = .78) to achieve the same safety as a 0.375. cylindrical buckling knockdown.

Figure 4c represents a typical PDF signature derived from test data that can be used for accurate prediction of mean (μ) failure load, and choosing the level of risk. This is accomplished with two factors. The first factor, γ_{μ}, is used to calibrate theoretical solutions to typical measured test values. The calibration is usually a reduction of the theoretical as indicated by the arrow moving to the left. The second factor, coefficient of experimental failure load variation, γ_{η}, is a measure of the statistical deviation. Once the predicted mean buckling load is obtained (the dashed line), the user

Figure 4a, 4b, and 4c. PDF plots normalized to (failure load/μ), where μ is the mean failure load.

Reliability	K
90%	1.41
99%	2.512
84.13%	1
99.86%	3

may scale the level of reliability using any K value, some of which are shown in the table. Thus, a specific PDF signature for a given structure and loading type permits more reliable prediction of both expected failure load and allowable load.

5. Connection to HyperSizer Structural Sizing Software

Currently, HyperSizer is used by the aerospace community for product development (PD). This is due to its ability to perform rapid structural analysis and design sizing that includes many failure analyses for all load conditions at all areas of an airframe. We are moving beyond the conceptual and preliminary design phases, to mature HyperSizer's usability for final design. HyperSizer contributes in several ways to the certification by analysis initiative. Many analyses required for airframe certification are included in its controlled software environment, which in itself is a framework for plugging-in user defined validated analysis codes. As an automated sizing tool, it will soon be able to produce robust designs using the PDF signatures as described in the previous section. As an example, the typical building block honeycomb failure analyses shown in Figure 5, are intended to be defined with PDF signatures and made an integral part of HyperSizer's reliability based analysis and design sizing.

Failure analyses

HyperSizer provides many different types of strength and stability analyses, such as beam and panel buckling, cross section local buckling and crippling, local post-buckling, frequency, deformation, stiffness, and material strength based on detailed stresses and strains throughout a built-up shape on a ply-by-ply basis. Some of HyperSizer analysis methods are physics based, and others come from time honored and accepted standard engineering practices and empirical data. HyperSizer's purpose is to automate all of these approved methods for reliable and consistent use by the stress engineer. In short, our intent is to "validate the method's physics - verify the method's software implementation – calibrate the methods accuracy – and assure the method's correct engineering use."

Failure Analyses Delivered with HyperSizer
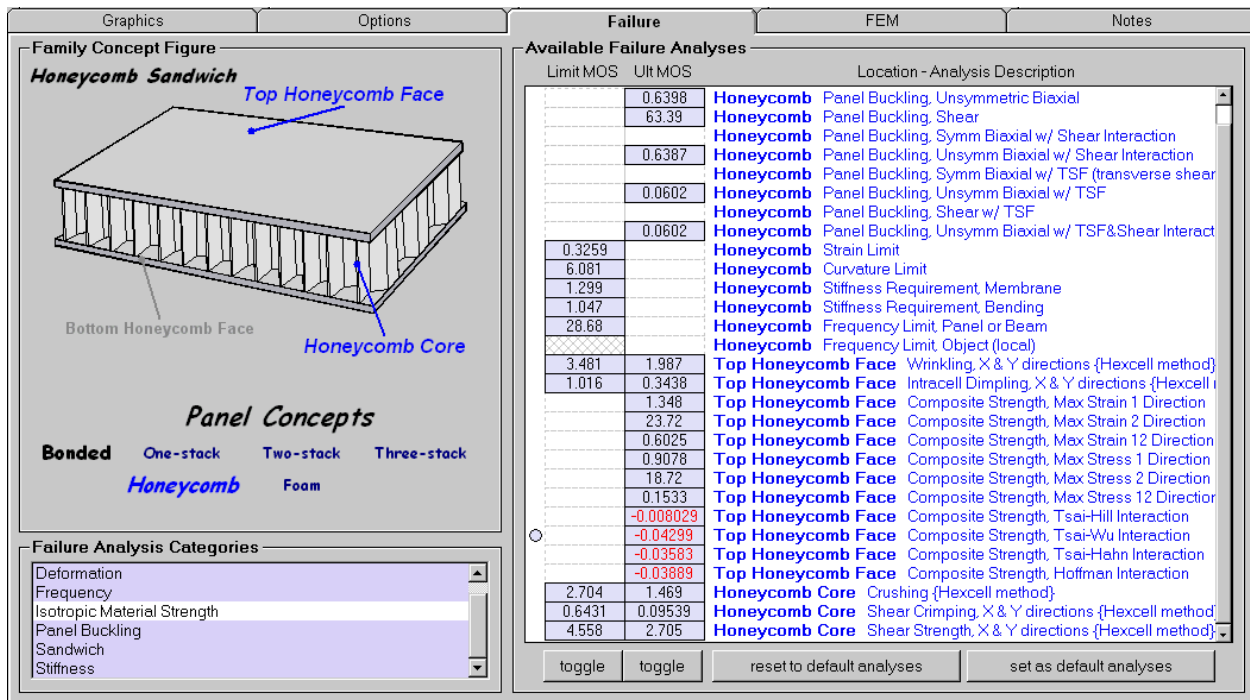
Figure 5. A HyperSizer screen shot of the failure mode margin-of-safety GUI for a honeycomb sandwich panel. Each failure analysis is summarized with a margin-of-safety (MoS) for limit and ultimate loads.

Customer Failure Analysis Plug-ins

Each aerospace company usually has analysis methods and associated programs to solve problems in their own unique way. For this reason, there is a capability for the users of these companies to integrate their proprietary and legacy codes into HyperSizer.

HyperSizer provides an engineering environment where user developed or company proprietary analyses codes can be "plugged-in." This Input/Output integration provides more reliability by reducing possible human error for legacy analysis programs that typically require tedious manual data input. The programs can be written in either Fortran, C, or C++ languages. Legacy codes are invaluable for providing certification-by-analysis because of their validation and verification (V&V) history. Therefore the purpose is to connect in an automated fashion the legacy codes into the data flow stream of other tools and processes, Figure 6.
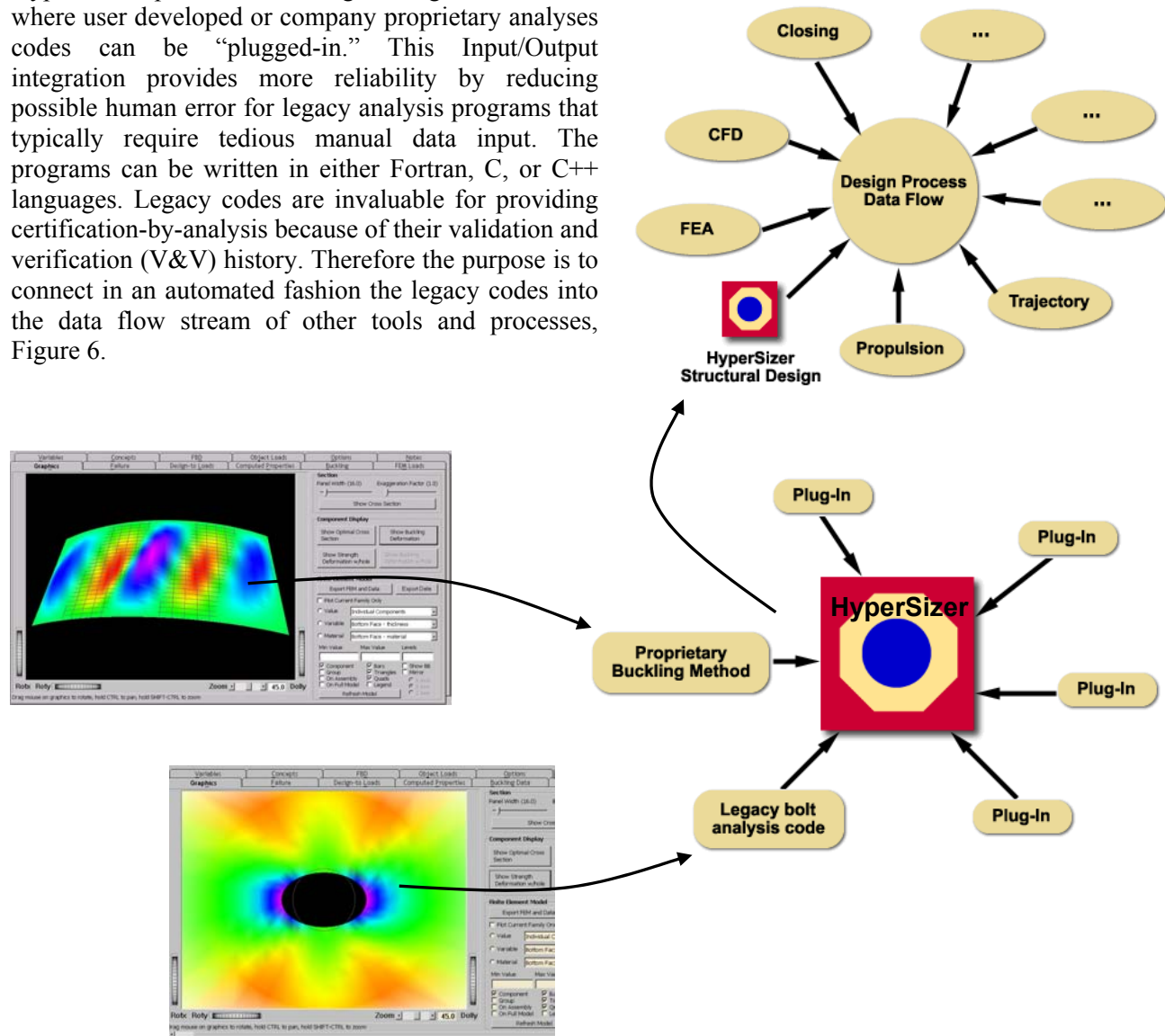
Figure 6.   In the illustration, two legacy programs are plugged into the HyperSizer structural analysis and sizing optimization software. The first program is a much used Raleigh Ritz analysis for buckling. The second program is the BJSFM composite unloaded and bolt loaded hole laminate analysis. All of the data associated to these types of programs, including the HyperSizer generated graphical images shown, are completely integrated within the structural analysis and sizing optimization process. This structural analysis and sizing framework along with plug-ins can then be made part of a larger design system by use of its open and flexible object model. This level of tool I/O automation greatly reduces potential human error.

Sizing Optimization

Making available analysis tools in an automated sizing process to be used during conceptual and preliminary design phases provides a design-by-analysis capability for increased structural reliability. HyperSizer can concurrently optimize panel and beam concepts, material selection, cross sectional dimensions, and layups. In doing so, it can handle complete vehicle systems modeled with many FEM grids and elements and ensure that optimum designs pass all available structural integrity analyses. Its results include accurate weight predictions and multiple equivalent weight designs for manufacturing trades. The design-by-analysis capability is able to find the best combination of all:

- **Panel/beam concepts-** optimum concept found from a library of commonly used designs: Z shape, mechanically fastened panel vs. blade shaped, integrally machined stiffened panel
- **Design dimensions and thicknesses-** facesheet, flange, and web sheet thicknesses and widths, heights, stiffener spacings
- **Material selection-** All isotropic metallic, orthotropic composite, foams, and honeycomb cores are available as candidates
- **Layups-** Thousands of pre-defined or user-defined layups are available as candidates for any panel or beam segment
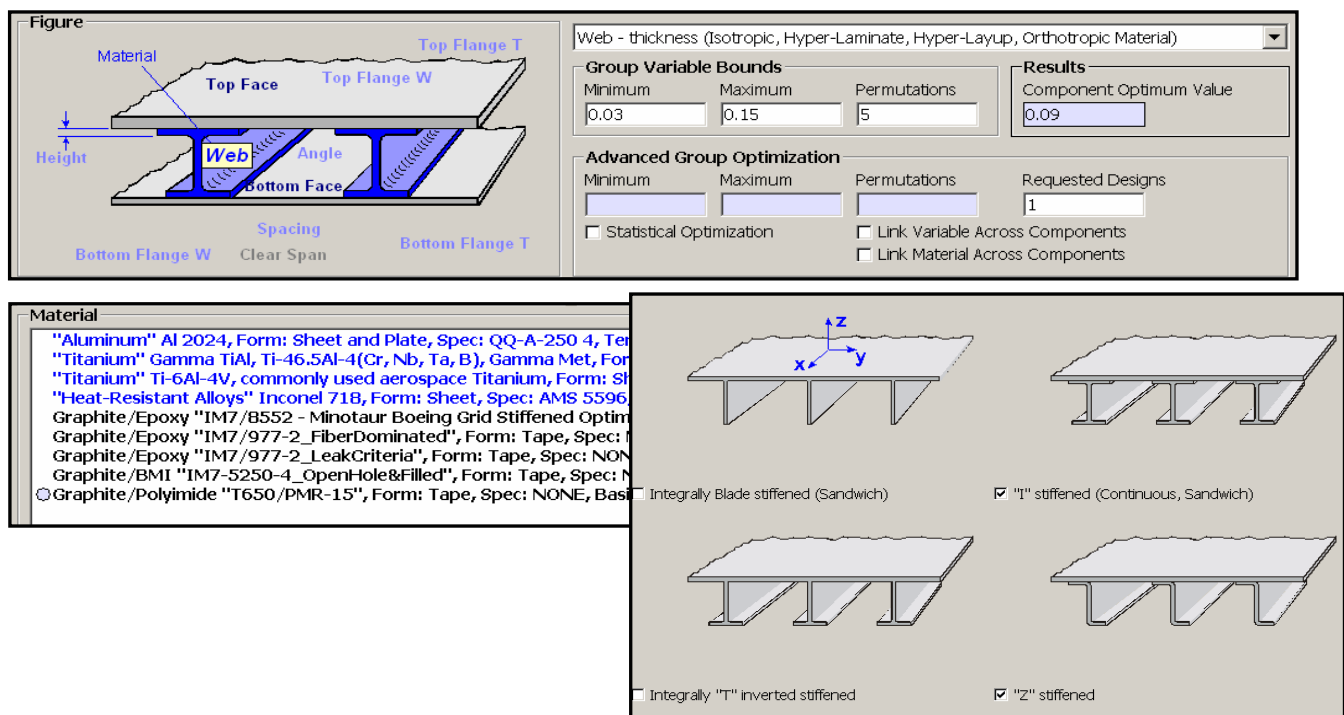
Figure 7. Illustrated is the process of directly sizing the design by permutation of all continuous and discrete variables. This is accomplished by specifying each variable's minimum and maximum bounds, and its number of permutations. Then for variables that have material associated to them, such as the stiffener web, many different composite and metallic materials can be assigned to the variable. Finally, different types of concepts can be explored such as I, T, blade, and Z stiffened shapes.

6. Connection to Finite Element Analysis Software

As indicated with the left curve of Figure 1, applied external loads are mapped onto the FEM and resolved into computed *internal* loads (load paths) of the airframe. HyperSizer reads the FEA computed internal loads and updates the FEM materials properties with new design sizing data. HyperSizer post-processes the computed FEA element forces by applying statistical analyses to each individual loading component (Nx, Ny, Nxy, Mx, My, Mxy, Qx, and Qy) and to each individual load case. This process resolves inconsistency in determining proper design-to loads.
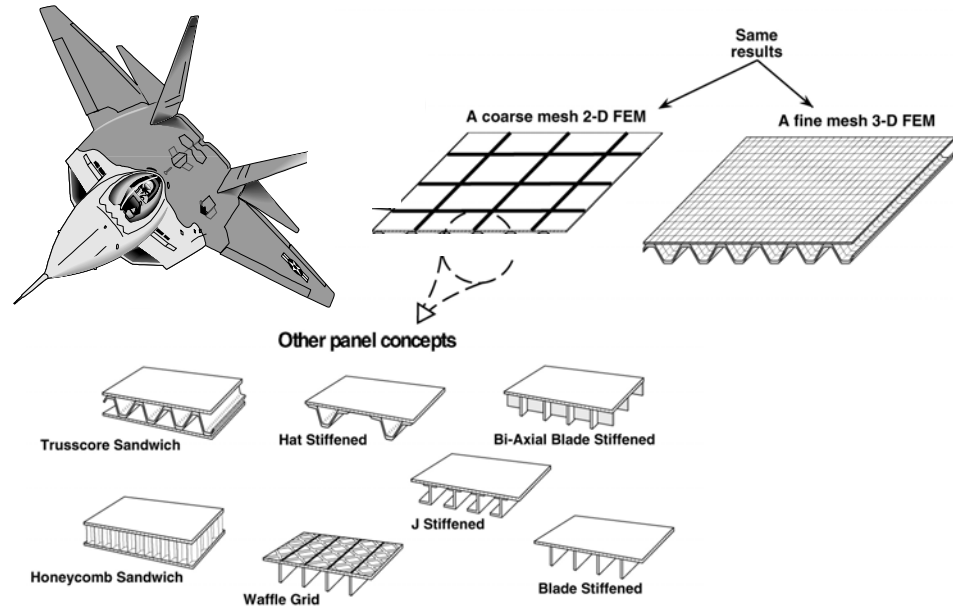
Figure 8. HyperSizer's approach is to generate FEM properties for shell finite elements using a planar, 2-D coarse mesh, permitting the FEA solver to compute internal loads accurately as accomplished with finely meshed 3-D discrete models. This allows the design-by-analysis process to determine the best panel design for all vehicle locations, using the same loads model mesh.

The entire process, as depicted in Figure 9, is being implemented by Collier Research using HyperSizer®, FEA such as NASTRAN™ for *global* loads models, StressCheck™ for *local* models, and other discipline tools. Lockheed Martin Aeronautics will apply this integrated process and tools to on-going new designs and redesigns of military aircraft.
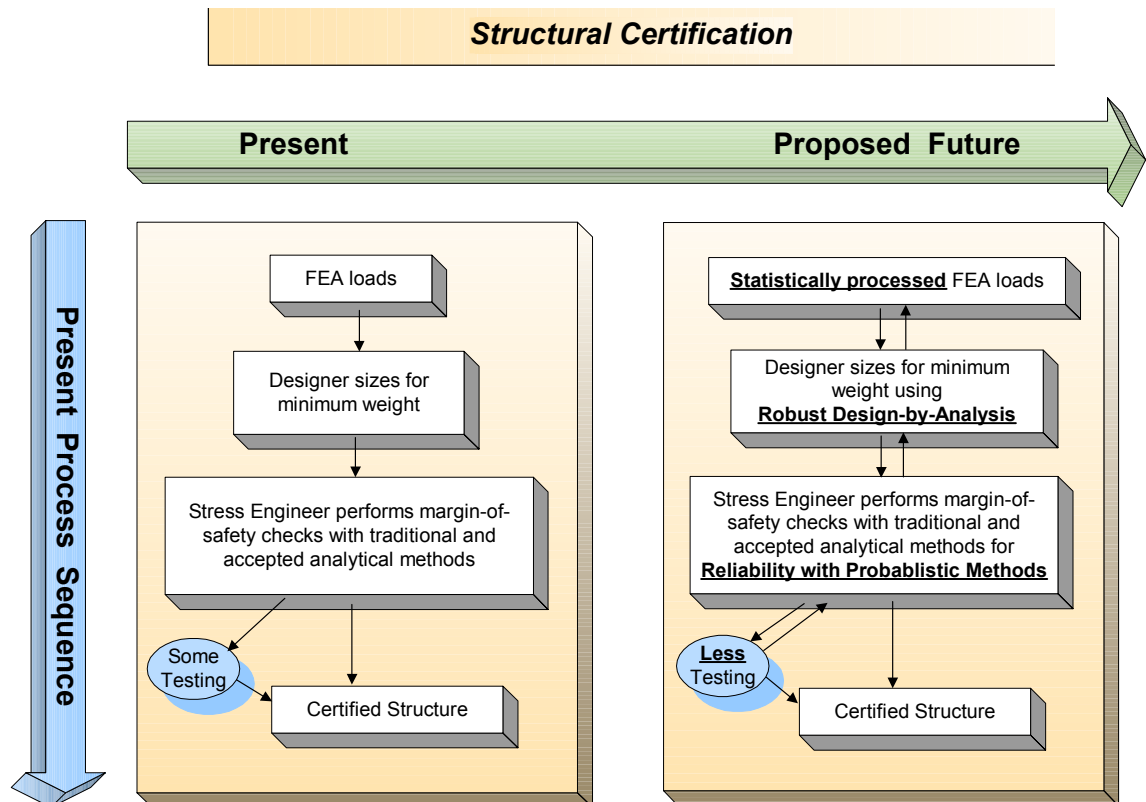
Figure 9. The overall process for structural certification by analysis. The present process shown in the left box is one-way and loosely connected. Proposed on the right side is a two-way, highly integrated process with tight I/O communication.

7. Cause and Effect of the Proposed Software Process
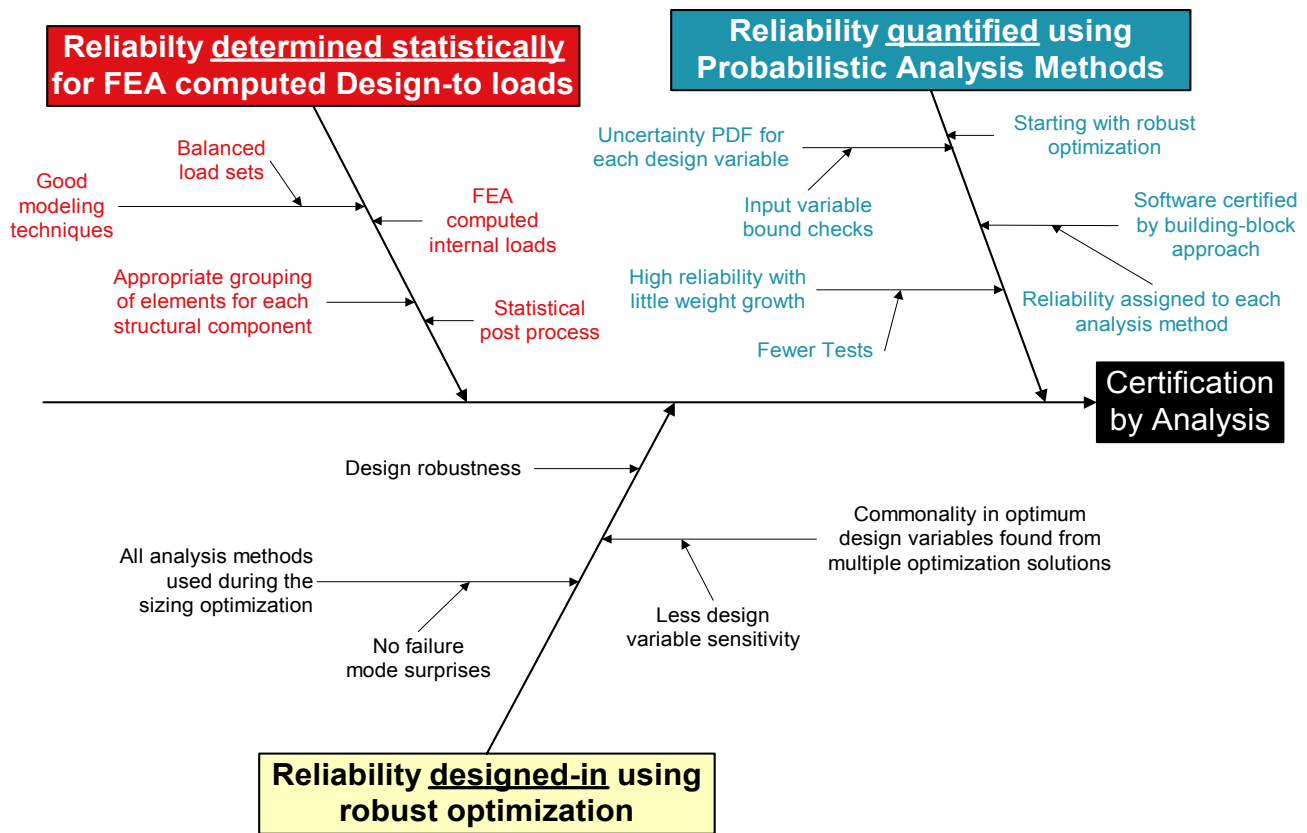
Figure 10. Cause and effect of proposed process. An important concept of this process is that certification-by-analysis starts with design-by-analysis.

To quantify and capture each of these individual processes, I/O data must be consistently passed to each level of analysis and design. This consistent and reduced human error process is part of the roadmap and is envisioned to be implemented by Collier Research and demonstrated by Lockheed Martin on their on-going projects. A key objective is achieving a building block validation and verification (V&V) documented process. Without such documentation the product customer will not have the basis available for certifying the methods used.

Reliability Determined Statistically for FEA Computed Design-To Loads

Red items in figure 10 cover the generation of FEA computed internal loads. Good modeling techniques include proper mesh density, correctly defined material axes and element normals, and beam element orientation vectors. Balanced load cases ensure that the summation of external loads such as flight pressures and control surface forces are in equilibrium with inertia loads caused from the time dependent mass (fuel burn) and trajectory event acceleration. Once this level of model check-out has been achieved, the resulting FEA computed internal loads (running loads) are fairly reliable. However, before using these loads for sizing and analysis, a grouping of elements that define manufacturable parts of the structure must be defined. These groupings of elements are referred to in HyperSizer as structural components. It is important that structural components are modeled with a fine enough mesh to capture the load gradient. One of the strong points of HyperSizer is that it is capable of quite accurately representing the stiffened shape of a panel with a planar and coarsely meshed set of shell finite elements, see figure 8. In addition to the definition of structural components, HyperSizer also post-processes the computed FEA element forces by applying statistical analyses to each individual loading component. This process has been included to overcome the ***uncertainty*** used by industry stress analysts in determining the proper design-to loads.

HyperSizer provides a more reliable way to establish the proper magnitude of forces, and attempts to account for possible FEA solution non-convergence due to a lack of mesh refinement.

Reliability designed-in using robust optimization

Yellow items in figure 10 cover sizing optimization of the structure. A primary concept of this proposed process is to use nearly all of the available analyses during sizing optimization so that no new failure mode surprises will occur when going to the final analysis step. Another primary concept for achieving a reliable and robust optimization is that design variable sensitivities are minimized and a commonality in optimum design variables is found from multiple optimized solutions. HyperSizer accomplishes this by performing a statistical optimization on the found optimum designs. Since multiple, equally performing optimum designs are found, if one particular design is later discovered to have difficulty in certification, alternate fall back designs are readily available and can easily be substituted. The ultimate objective is to find a robust design to manufacture and certify.

Reliability Quantified Using Probabilistic Methods

Blue items in figure 10 cover the final analysis and margin-of-safety reporting. The bulk of our research is intended to focus on this aspect of the process. Starting with a robust optimum design, the objective is to define the uncertainty PDF for each variable input. For design dimensions, this would include manufacturing tolerances. Once a robust optimum design is found, then high reliability can be quantified with little weight growth using the V&V analysis methods together with probabilistic methods (PM). Various PMs would be implemented including perhaps full Monte Carlo simulations of rapid analyses.

To address human error, checks would be applied to each input value that would define an envelope of applicable lower and upper bounds for given analysis methods. Such checks would also catch and filter out inappropriate variable combinations generated by the automated optimization process.

Key to quantifying overall structural reliability is to assign a reliability factor to each analysis method and to each potential failure mode that accounts for natural scatter in physical response. Knowing which analysis methods and corresponding tests have tight bounds on data scatter is necessary for quantifying joint probability of failure caused by failures of independent design details. A side benefit of implementing PM is that unknown physics have a less detrimental impact on reliability.

8. Conclusion

Certification tests for aircraft structures are necessary to ensure load carrying capability and performance of each component. However, hardware testing is costly and unpredicted failures can delay product development. In current certification procedures, a limited number of tests are performed, especially at full-scale. The solution is to augment experimental testing with automated analysis with PDF signatures for the goal of increasing structural reliability. This process is called "certification-by-analysis." Collier Research is working with Lockheed Martin Aeronautics to develop a certification-by-analysis process using finite element analysis (FEA) and the commercial aerospace structural analysis software HyperSizer.

A key aspect to this effort is attempting structural certification by analysis for a specific architecture by fully leveraging commonality in building blocks. That is to take into account appropriate existing building block test data via PDF signatures for more reliable analyses. The rapid and more reliable analyses form the basis for a design-by-analysis process to be used during conceptual and preliminary design. This will enable a higher probability of successful certification. This motivation is depicted in Figure 11.
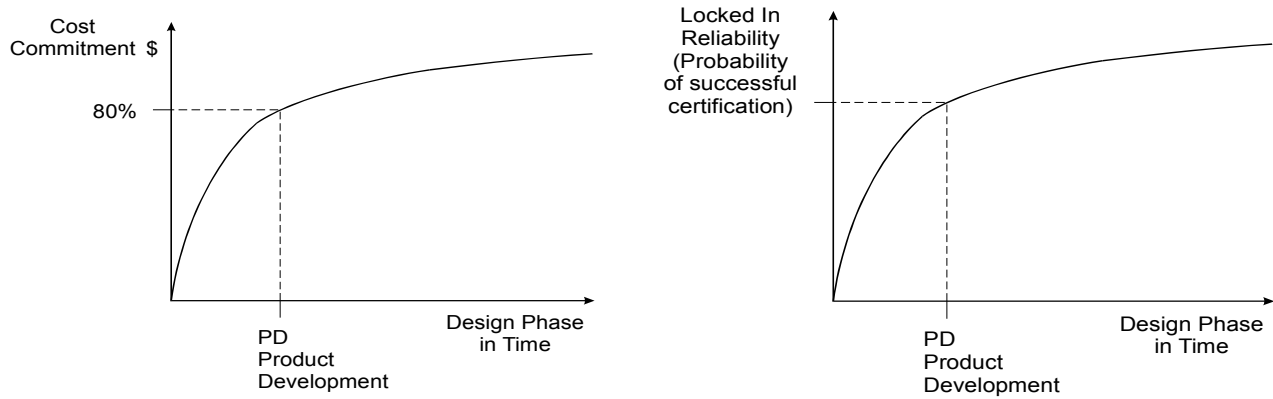
Figure 11. The left chart is often used to depict that a development project's cost commitment occurs early in the design phase. The right chart depicts that a locked in reliability (probability of successful certification) is also locked in during the early phase of product development. This gives rise to the need in designing-in reliability early in the conceptual and preliminary phases of a design.

9. References

1. http://hypersizer.com/, product web site

2. NASA TP-1998-207194, M.H. Rheinfurth and L.W. Howell "Probability and Statistics in Aerospace Engineering" March 1998

3. MIL HDBK 17e, Standardization of Engineering Data Methodologies for Composite Materials", 1996.

4. Veley, Duane, Chris Pettit and Richard Holzwarth, "Increased Reliance on Analysis for Certification of Aircraft Structures," Proceedings of the International Conference on Structural Safety and Reliability (ICOSSAR), June 2001. Presented at the April 2001 AVT-092 meeting

5. Hilburger, M.W. and Starnes, J.H., Jr. "Effects of Imperfections on the Buckling Response of Compression-Loaded Composite Shells", International Journal of Non-linear Mechanics, No. 37 (2002) pp. 623-643.

6. NASA SP-8007, Buckling of Thin-Walled Circular Cylinders, NASA Space Vehicle Design Criteria

7. Johann Arbocz, James Starnes, and Michael Nemeth, "On the Accuracy of Probabilistic Buckling Load Predictions" AIAA-2001-1236

Trademarks

HyperSizer® is a registered trademark of Collier Research Corporation

NASTRAN® is a registered trademark of NASA

MSC/NASTRAN™ is an enhanced proprietary product of the MacNeal-Schwendler Corporation.

StressCheck™ is a trademark of ESRD

AFFORDABLE EVOLUTION:
ENGINEERING CHANGE PROPOSAL (ECP) 6038
F/A-18E/F FORWARD FUSELAGE STRUCTURAL CERTIFICATION

Mr. Mark K. Holly, The Boeing Company, St. Louis, MO, USA

Abstract

The F/A-18E/F is getting an improved forward fuselage which can be built at a substantially lower cost while accommodating a new Active Electronically Scanned Array (AESA) radar. Structural design and certification costs have been mitigated by simulation and analysis. These efforts launched early in the program established confidence that some requirements, traditionally demonstrated by test, could instead be satisfied with high fidelity modeling and simulation.

Structural recertification costs have created a barrier to change in the past. At the same time, aircraft programs face pressure to improve performance, accommodate new avionics and equipment, expand payloads, correct defects and improve affordability. Engineering Change Proposal (ECP) 6038 authorizes a change to the F/A-18E/F Forward Fuselage. Early high fidelity analysis and simulations built upon the large foundation of data gathered during the Engineering and Manufacturing Demonstration (EMD) phase of the F/A-18E/F program provided the confidence that design goals could be met and that testing could be minimized.

The excellent matching of EMD test data was not only a major accomplishment of the ECP 6038 team. It also establishes a concept of modularization in that a relatively large component of the aircraft has undergone a significant design

change without affecting the rest of the air vehicle. This has far reaching implications toward future change strategies.

Introduction

The F/A-18E/F Program has demonstrated excellent program performance over the last decade. Incorporating a larger wing plan form with thirty three percent more fuel and two more wing pylons results in twenty eight percent more payload. The E/F has been on schedule, on cost and performing to plan.

At its beginning an Active Electronically Scanned Array (AESA) radar was envisioned in the E/F's future. The airframe was designed to accommodate the weight of such a component. Engineers even tried to anticipate how they might integrate the future radar with its neighboring structure. As AESA has come to fruition its fiber optics, cooling lines, wire, and conduit could still just fit in the space provided some years back. However, future growth was very constrained. Figure 1 represents the forward fuselage systems with none of the structure represented.
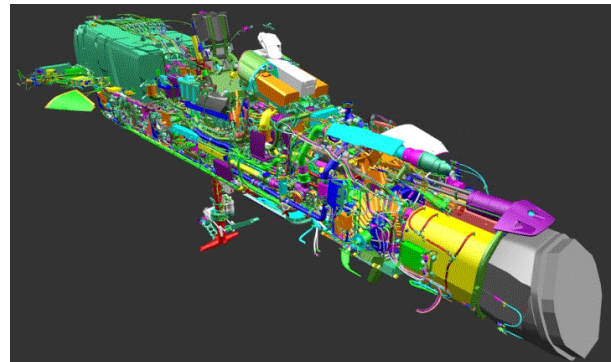
Figure 1. Forward Fuselage Systems With AESA

A critical eye was cast upon the existing forward fuselage structure. This component of the F/A-18E/F airframe retained much similarity to it's A/B/C/D ancestors. An integrated team of designers, structural analysts, dynamicists, manufacturing engineers, airframe mechanics,

systems installers, test engineers and cost analysts studied the forward fuselage for ninety days in February to May of 1999. They concluded a different design could be built for less recurring cost and systems routing could be enhanced. ECP 6038 implements the conclusions of this study.

The ECP 6038 Configuration

The ECP 6038 configuration replaces the extensive use of sheet metal and smaller machinings with composite moldline skins, highly unitized machinings and a large aluminum sand casting in the in-flight refueling probe area. The part count reduction is evident by the comparison of Figures 2 and 3.
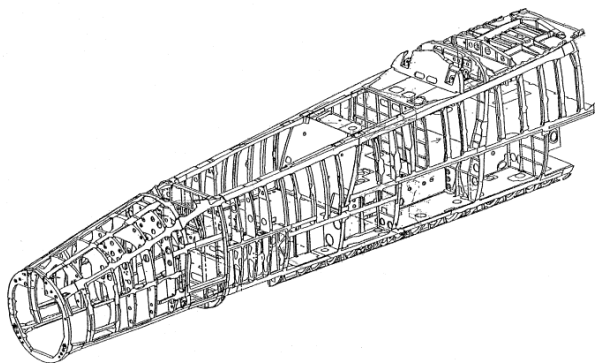
Figure 2. Original F/A-18E/F Forward Fuselage Substructure
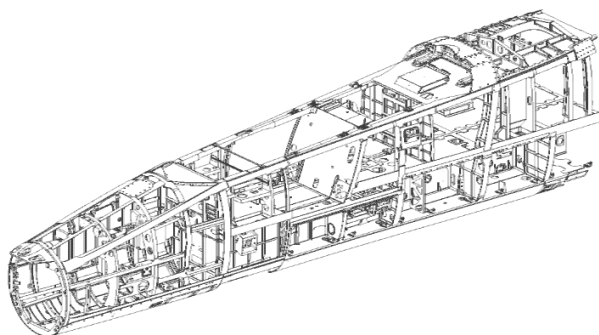
Figure 3. ECP 6038 Forward Fuselage Substructure

In addition to the obvious part count reduction, the assembly of these parts is further simplified by coordination of part features so that the need for assembly tooling has been dramatically reduced along with the part count. These structural modifications to the forward fuselage improve the affordability of the F/A-18E/F forward fuselage

while integrating equipment and providing additional system routing paths for future growth.

The scope of ECP 6038 completely redesigns the forward fuselage from Y128.5 at the radome to Y383 at a manufacturing splice. Major forward and aft running members were retained from the original structure preserving the load paths of the previous design. Although extensively changed this configuration maintains commonality with the original configuration at the outer moldline, pilot's eye, inflight refueling receptacle, gun, nose landing gear, canopy, and the aft manufacturing splice. These areas are shown in Figure 4.

The new ECP 6038 configuration has achieved forty percent fewer parts, fifty one percent fewer fasteners, and twenty six percent fewer standard assembly hours. The first article to be built, designated FT76 and serving as the full scale structural test article, demonstrated eighty four percent fewer defects than airframes (E20 to E25) constructed of the original configuration. In full rate production the assembly cycle time is expected to shrink by thirty one percent.
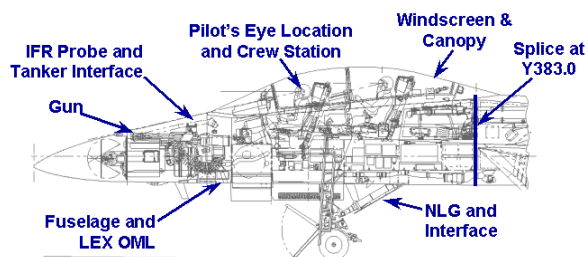
Figure 4. F/A-18F ECP 6038 Design Constraints

The Structural Certification Challenge

The F/A-18E/F ECP 6038 Forward Fuselage implements a redesign of the structure for maximum affordability and systems growth. It maintains the overall structural load paths of the existing E/F forward fuselage but minimizes part count through unitization. This strategy preserves the applicability of what has been learned in the Engineering and Manufacturing Development (EMD) phase of the program. The legacy static, dynamic and flight test data including the associated lessons learned have been comprehensively applied during the synthesis of the ECP 6038 configuration. Testing has been minimized and test assets are being reused where possible.

As previously mentioned, the new fuselage preserves the load paths of the original design. This was a critical strategy. To preserve the assumption that the external loads and some internal loads of the forward fuselage did not change, it was important to control the dynamic characteristics of the airframe and some local interface stiffness. These would be continuously monitored throughout the synthesis and maturation of the design.

External Loads - Flight maneuver loads associated with multiple store releases were one type of loading which could affect the forward fuselage. However, the most important loads where associated with catapult and arrested landings. Global bending stiffness and local nose landing gear backup stiffness of the fuselage are important to these types of loading.

The shock loads at the terminal phase of a catapult were particular concern. This event induces high accelerations on the locally mounted equipment and the forward fuel tank. Increases in the severity of this phenomenon could affect equipment qualification loads. The tank would undergo extensive unitization and the design team needed to pay attention to this event in the tank design.

Aero-elastic Stability – Although flutter is not usually particularly sensitive to forward fuselage dynamics, the F/A-18 has a quite long and narrow forward fuselage configuration. In the early A/B/C/D models the wing Leading Edge Extension (LEX) had only a couple of discrete structural connections to the fuselage. In these models, forward fuselage lateral bending stiffness played an important role in some of the flutter mechanisms.

The E/F configuration has a much larger LEX which is continuously attached to the side of the fuselage. Therefore lateral fuselage bending is not as predominant in the flutter mechanisms as with the earlier models. Still the ECP 6038 team needed to assure that this characteristic was preserved.

Aeroservoelastic (ASE) Stability – The first vertical bending frequency of the fuselage affects the longitudinal stability of the flight control system. If this frequency changed by much, new software and new validation tests may be required.

Y383 Manufacturing Splice Loads – Containing the extent of the redesigned areas was a major concern of this program. The rest of the airframe was already certified. Change beyond the manufacturing splice would clearly begin increasing the nonrecurring implementation costs. Therefore it the splice had to remain the same both physically and with respect to loading distributions.

Other Components – The canopy, windscreen, nose landing gear system, and gun were not to change. The stiffness at the interfaces with these items had to be controlled so that interface loads to which these items were qualified would remain the same.

Weight Neutrality – The forward fuselage changes were to be weight neutral in there impact upon the airplane. As previously stated, the beginning of the E/F program the added weight of an AESA radar was included in the design. Performance and loads calculations included this affect and weight and balance was preserved in the existing aircraft thru ballast in the nose. The new fuselage was not to impact the combined structure/ballast weight.

Three Lifetimes – The only exception to weight neutrality was an allocation to design the new airframe to three lifetimes (Eighteen thousand hours of spectrum fatigue). The airframe is intended to have a six thousand hour life. Normally the fatigue test is intended to demonstrate twice the design life to account for normal variation in material properties and variations in the severity of fleet usage.

The rational behind the three lifetime requirement was the desire to make the airframe as robust as possible. The EMD fatigue test has already extended its required twelve thousand hour demonstration toward a goal of three lifetimes. If three lifetimes were used as a goal for the ECP 6038 design, it increases probability of achieving its required minimum the two lifetimes and holds the possibility of extending the life by analysis of the test results.

Simulation Addresses Early Risks

The F/A-18E/F is in production. If introduction of the new fuselage were delayed until all the risks could all be mitigated with testing, the benefits would be moot. So there was a practical reason for minimizing test requirements aside from their nonrecurring costs. A strategy of combining

simulation, testing and reusing existing test assets was explored. What requirements could substantially be satisfied by analysis alone and what requirements absolutely required test verification?

An Underappreciated Asset - The biggest asset the ECP 6038 customer/contractor team had was the wealth of data that had been collected during EMD. There was static, fatigue and dynamic strain gage, deflection gage and accelerometer data for thousands of ground and flight test points. Plus there was the knowledge within the team composted of F-18 veterans combined with state of the art developers of what had worked and what did not.

The concerns over external loads, flutter, ASE and component interface loads all revolve around stiffness. Stiffness could be determined by finite element modeling. In the last decade, computing capability had increased by orders of magnitude. Therefore very comprehensive models could be built.

One major confidence building measure was to build a completely new finite element model (FEM) of the EMD forward fuselage as depicted in Figure 5. The new FEM was then rigorously correlated with the test data acquired during the static, fatigue and ground vibration testing. The FEM of the new ECP 6038 configuration would incorporate anything learned in this process. With these two models there was a consistent way to evaluate the relative differences between both configurations.
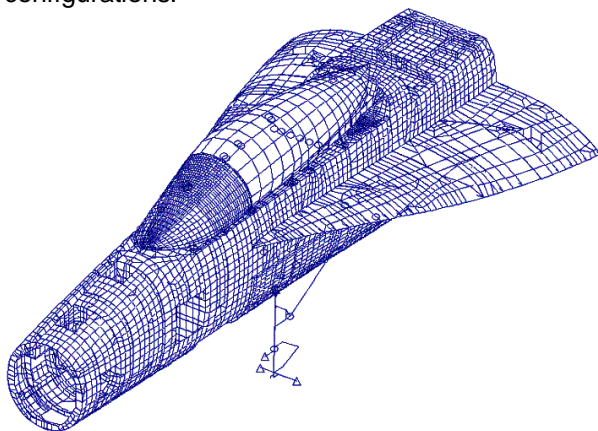
Figure 5. A New EMD Finite Element Model

What constitutes good correlation? That was not a straight forward question. In the static tests, ultimate load was only reached once. That really could not be considered a statically significant sample. The fatigue tests provided a better sample size with strain surveys being repeated throughout the test. This not only provided an average response. It also provided a standard deviation. Variation was something that had not really been considered until the team started asking how to implement the process. The standard deviation provided an estimate of systematic variation in the tests. Something for which the FEM could not be held responsible.

Figure 6. EMD Full-Scale Airframe Test

Although an individual hydraulic cylinder might have very little individual variation, when combined with the one hundred and eighty one other load controllers in the full-scale fatigue test as shown in Figure 6, greater variation is bound to occur.

This study of the fatigue test strain survey results for seventy five gages and thirteen conditions showed the strain gage standard deviation to be about 7.6% for measurands placed near the major members during the repeated strain surveys conducted every one thousand spectrum flight hours. For secondary members the variations were higher although stress levels were lower.

Manufacturing variation could introduce additional variation in a new test article which should be considered in predicting responses. Taking this variation into account, all the strain gages associated with the significant load paths in the EMD FEM matched the test data. The model deflections were indistinguishable from the test article as well. Similar to the terminology used in manufacturing to describe a design that accounts for manufacturing process variations, ECP 6038 refers to the FEM as being correlated within the process capability of the test data.

Although the forward fuselage had relatively few problems during the EMD test program, those anomolies that did occur were studied during the strain correlation work. These results suggest that every part of the vehicle that has a remote chance of picking up load by straining sympathetically with the structure should be represented in the FEM even though past practices tended to discount "nonstructural" parts.

Interface Loads at Y383- A detailed comparison of the validated EMD finite element model with the model of the new structure showed a good match of the interface loads for the critical design conditions. The major members matched within 5% with no attempt to tune the results. As the model matured, the differences between the models narrowed to about 2.5%, well within the scatter of the test data. For all intents and purposes the interface loads were deemed "no change" with respect to the rest of the vehicle.

Any risks could now really be considered to be contained within the redesigned area. Since the static test article, dubbed ST 50, was still available (Figure 6) with its complicated test set up in place, the costs of a fatigue and static test of the forward fuselage were relatively small considered the risk reduction it could provide. Although for new structure and the analysis capability available today one might argue foregoing a test was a legitimate possibility, in this case it was decided to test the new design using the old test set up to mitigate the cost. Fatigue first, after which the static ultimate tests would be conducted of a new forward fuselage on the reused aft section of static test article.

Global Dynamic Response - With a correlated static representation of the structure, the dynamic response was contemplated next. Although the thicker composite outer moldline skins make the forward fuselage slightly stiffer than the EMD configuration, it was important to assure the global mode shapes are essentially the same to prevent gross changes in the flutter mechanisms of the vehicle. A slight frequency increase was expected.

Should the stiffness increase pose a problem, ways of stiffening the skins were contemplated that would lessen the fuselage impact. But these approaches would cost more. Continuing with the stiffer fuselage and evaluating the ramifications in pursuit of cost savings was the course followed. The detailed finite element models were used to

support the analytical estimation of global air vehicle natural frequencies. Compatible with the detail included in the FEMs for structural analysis, the mass properties were distributed to these models in a very detailed fashion. The detailed models were excercised dynamically along with less detailed beam-rod dynamic FEMs to evaluate the responses of the new configuration.
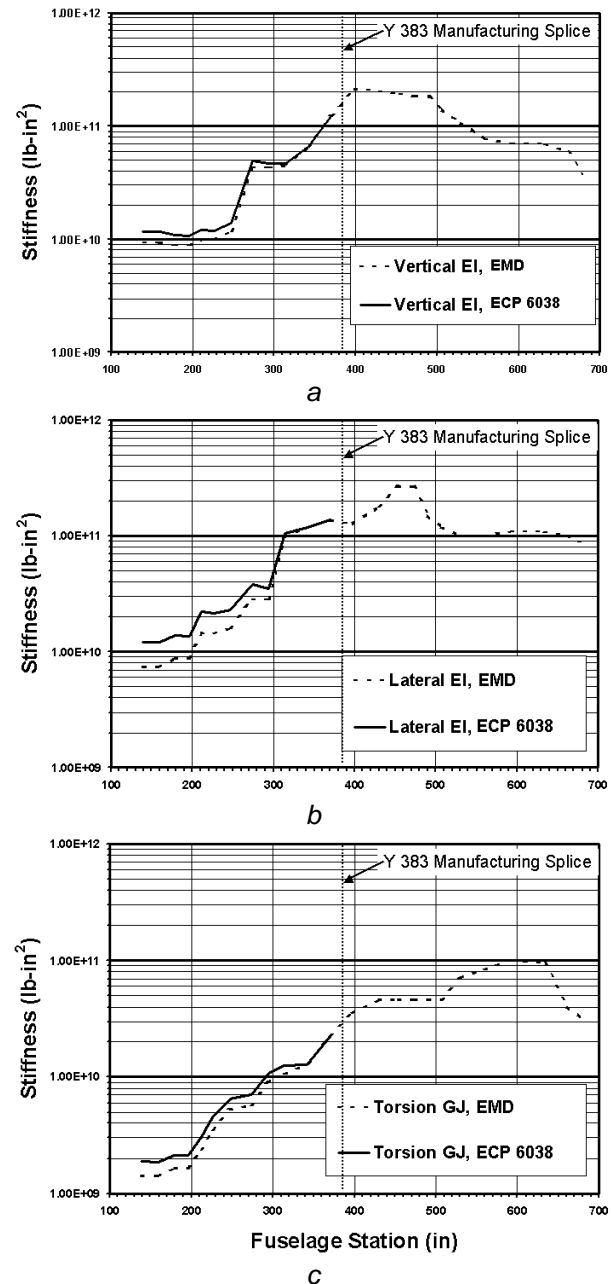
Figure 7. Half Fuselage Vertical, Lateral and Torsional Stiffness Comparisons

Within two months of the program kickoff the first estimates of frequency differences between the

EMD and ECP 6038 configurations were being determined and preliminary impacts on flutter, ASE and store release loads were being assessed. Even with stiffness differences well in excess of these initial estimates, run as hypothetical worst case scenarios, the affect was benign. Figure 7 compares the vertical, lateral and torsional stiffness differences the EMD and ECP 6038 configurations.

	Min.	Max.	Avg.
F1VB	2.5	6.6	3.4
F2VB	2.1	5.4	2.4
F1LB	1.3	10.4	6.4
F2LB	3.7	11.8	7.8
F1T	1.4	13.4	5.6

Table 1. Percent Change In Air Vehicle Frequencies

With the stiffness increases determined they were subsequently used to determine natural frequency changes and finally the impact of these changes on flutter mechanisms and speeds. Table 1. shows the change in frequencies over a variety of internal fuel and store configurations. The first vertical bending frequency increase ranges between a 2.5% to 6.6% increase.

For most the flutter mechanisms these stiffness changes increased the flutter speeds. One clean wing mechanism dropped by 0.1% and one of eighteen critical stores carriage configurations lost 2%. These were considered acceptable. Structural modal Interaction (SMI) with the flight control system was not considered a barrier to proceeding either.

To confirm the performance of the new design an E-model aircraft with be ground vibration tested on three clean wing fuel states and two store configurations. An F-model clean wing will also be tested. An SMI test will be performed on an E-model aircraft. Far short of a comprehensive flight test program

Catapult Shock Response – The structure and the systems contained in the forward fuselage undergo large short duration accelerations during

catapults and arrested landings. As illustrated by the load versus time history curve of catapult tow force in Figure 8, the force undergoes a moderately rapid rise to about 250,000 pounds at the beginning. It sustains this loading for a period of time. Then it abruptly drops to nothing when the shuttle of the catapult hits the water break, launching the aircraft.
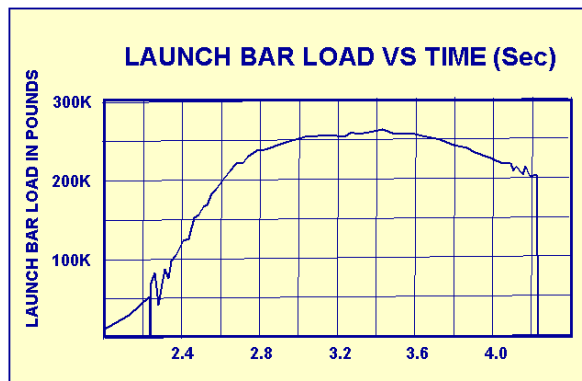
Figure 8. Catapult Force Versus Time

The abrupt event at the end of the stroke causes locally measured vertical accelerations of as high as 40g in local portions of the forward fuselage. The new design could not be permitted to increase the severe environment associated with this event. Much of the equipment in fuselage was qualified to this specific environment and a fuel tank is located in the area most subjected to the large vertical acceleration.

The structural response during the beginning of the catapult stroke is a direct result of the load applied with a small dynamic oscillation superposed. During the relatively flat plateau, the airframe stabilizes with a deflected shape similar to that pictured in Figure 9, an exaggerated representation of the finite element model under catapult loads.
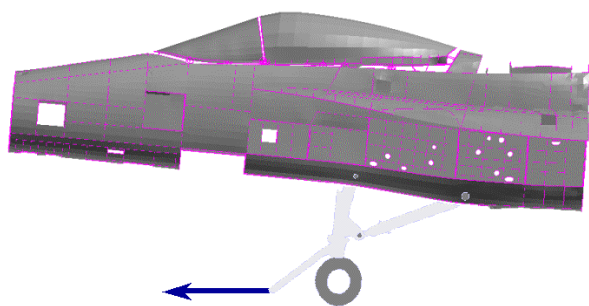
Figure 8. Catapult Distorted Forward Fuselage

The deflected shape of the structure clearly shows how the drag brace of the nose landing gear pulls forward and downward on the local structure. This strain energy is abruptly released at the end of the event. The high local distortion near the back of the drag brace results in a large vertical acceleration of the equipment bay and fuel tank directly above the drag brace.

The fuel tank was one of the areas of particular concern because of the configuration change to the floor of the tank turning it from a ninety piece combination of sheet metal and machinings into two highly integrated machinings buried in the heart of the assembly. The design team had to confident that they understood the fuel to structure interaction during this highly dynamic event to avoid future problems.

To fully understand the response a nonlinear transient simulation of the tank during the vertical acceleration was performed with fuel to structure interaction. This model is depicted in Figure 9.
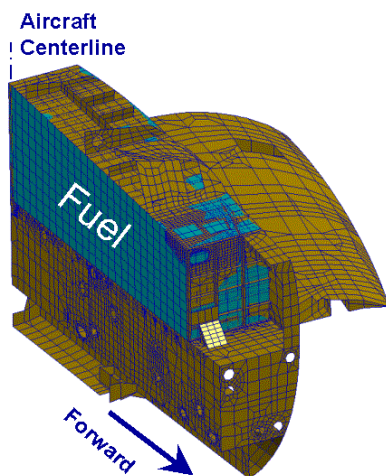
Figure 9. Fuel-Structure Interaction Model

The previously measured time histories from EMD flight test similar to the one shown in Figure 10. were applied to the model of the fuel tank. It was important capture the response time history as well as the peak stress levels to determine the allowable fatigue stresses for this part of the structure. This transient response was combined with the other flight and ground loads to create a composite loading spectrum representing a comprehensive set of loading events on the floor for design and also to assure repairability.
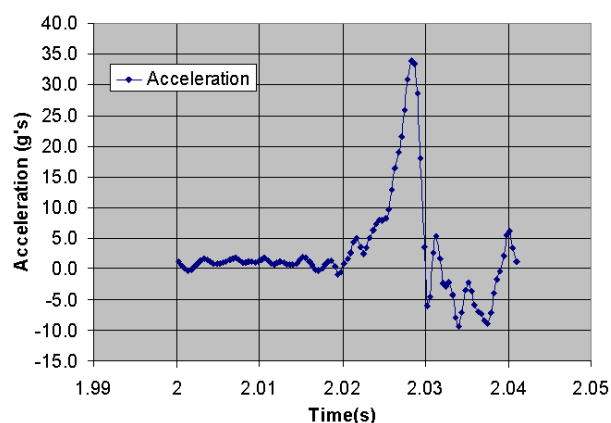
Figure 10. Structure Acceleration Time History

With the successful characterization of the this loading event it was not felt necessary to provide additional testing of the structure through some sort of component testing. Instead, the first airframe would be measured with a small number of accelerometers and strain gages during a full scale series of catapults to confirm the conclusions of the simulations.

Test Requirements Summary

Considering the scope of the ECP 6038 forward fuselage change, early analysis and simulations have built confidence in the understanding if the new design to keep the magnitude of the required physical test demonstrations austere. A fatigue test to two lifetimes and static test will be run on the same airframe reusing the aft section of the EMD static test article.

Because of the large panel sizes of the composite skins, an acoustic demonstration panel will be tested. Acoustic measurements will also be conducted on the ground during a gunfire test and for about four flights with about forty measurands.

Full scale ground vibration and structural mode interaction tests will be conducted to validate the flutter and control systems evaluations performed to date.

Finally the structural response of the forward fuselage will be measured during catapults and arrested landings to assure the responses match the detailed simulations run on the full cell and on other pieces of equipment.

Conclusions

Today's computing environment has provided the ECP 6038 program with alternatives to physical tests with modeling practices validated with previous similar experience. The vast test data available from the F/A-18E/F EMD Program provided a basis to validate modeling practices providing these analysis alternatives. The customer/design team could then contemplate what alternatives could satisfy some requirements traditionally done by physical demonstrations.

The EMD model validation effort built confidence that the scope of the change was limited to the forward fuselage requiring no effort beyond the manufacturing splice.

The global stiffness changes were determined to be benign with respect to flutter and the flight control system. This avoided the requirement for an extensively outfitted aircraft to perform flutter clearance and control law validation flying.

Finally the local simulations of transient response provided confidence that the structure would behave like its predecessor on a smaller scale avoiding equipment and systems re-qualification.

The ECP 6038 forward fuselage effort is proving that large changes to existing systems can be made affordably and that modularity concepts in new systems are viable.

Paper #24
Discussor's Name: Jacub Kacekowski
Author's Name: Mark K. Holly

Q: How do you perform static tests, especially with mixed structures?

A: Mixed composite/metallic structure present a certification challenge. It is uneconomical to perform tests at temperature plus it requires an extremely long time to saturate a structure with moisture to represent the environment properly.   Therefore, even in the most test intensive of programs, it is usually necessary to rely on analysis to combine and evaluate the full-scale results, correcting for thermal and environmental factors. The environmental effects should be determined by coupons and thermal stresses would be determined by finite element modeling.

The full-scale article, if taken to failure, would help to determine the magnitude and mode of failure, then analytical corrections would be applied. If the mode of failure was precipitated by buckling, the analysis becomes nonlinear and complex.

In the end it is nearly impossible to certify a structure solely by testing.

This page has been deliberately left blank

———————

Page intentionnellement blanche

Aircraft Structural Design Geared for
High Reliance on Analysis for Acceptance

K. Griffin, D. Wieland
Structural Engineering Department
Southwest Research Institute
P. O. Drawer 28510
San Antonio, TX 78228-0510, USA

A. West, H. Smith, M. Holly
The Boeing Company
P. O. Box 516, M/C S064-2809
St. Louis, MO 63156-0516, USA

H. Millwater
University of Texas at San Antonio
Department of Mechanical Engineering
6900 North Loop 1604 West
San Antonio, TX 78249-0670, USA

R. Holzwarth
Air Force Research Laboratory
Air Vehicles Directorate
Structures Division (AFRL/VAS)
2130 Eighth Street, Suite 1
Wright-Patterson AFB, OH 45433-7542, USA

Abstract

The results of an initial study of key structural areas for the design of a state-of-the-art composite fighter wing are used to highlight the fundamental changes that can be expected when aircraft acceptance considers analyses as a prime tool for demonstrating that the structure is safe for flight. For analyses to become the primary basis for accepting an aircraft structural design, a high level of confidence must be developed for the analysis methods used. The strategy investigated here is to maximize this confidence level in the use of probabilistic aircraft structural design methods rather than conventional deterministic methods. In a recent advanced lightweight aircraft structure development program, an advanced design of composite materials was created, using the latest deterministic design and manufacturing features. This composite fighter design effort provides a good benchmark for exploring the potential differences in design and testing that can be expected if probabilistic design methods are used to establish high confidence in design analysis. This present study chose two key aspects of the wing on which to investigate these differences. First examined is a local model of the cobonded joint attaching the wing box cover to the wing spars. For the second, the post-buckled design of the wing box cover is examined while subjected to the most severe maneuver load case.

Introduction

A significant level of interest has developed in recent years in the possibility of developing analysis capabilities with sufficient fidelity that they could be evolved into the primary source of information leading to the qualification or certification of a new aircraft structure for flight. In this design and acceptance environment, structural testing would evolve to a role of assuring correct analytical evaluations, rather than providing final clearance for flight using the traditional full-scale structural article limit load/ultimate load testing approach, especially of large final articles.

In this environment, testing would evolve into a new role of developing a sufficient database to model the way structure could vary over a production run. Testing would be used to fine-tune the analysis methods and models. These analyses would then provide the final check for clearance of a new design. The key to success is developing various procedures to raise analysis precision to this level. This effort explores the use of probabilistic methods in aircraft structural design to achieve the needed analysis precision. Examination is made of how test programs supporting the analyses would be restructured and, hopefully, reduced in cost when restructured to support analyses-based clearances.

Use of probabilistic methods in design has long been considered an intriguing way of introducing the unavoidable uncertainties in the characterizations of all our physical descriptors of aircraft structure. They allow the characterization of the uncertainties in modeling, materials, structural geometry, loads, etc. in the analyses such that the uncertainty of the analyses can be observed and addressed. The primary technical drawback to the use of probabilistic methods, for a long time, was the Monte Carlo methods traditionally used for calculating the probabilities of occurrences.

By their very nature, aircraft structures must have very low probabilities of failure in order to be acceptable for flight. Thus, the use of traditional Monte Carlo methods demanded a large number of analysis evaluations corresponding to all the variations needed for the design variables. Many evaluations were needed to generate enough failure cases to adequately define the "tail" of the probability of failure curve where acceptable values of aircraft structural failures reside. This would now be further aggravated by the large increases expected in analysis model complexity such as structural finite element analysis (FEA) models as the fidelity is increased to meet the objective of analysis carrying the burden of clearance for flight.

Developments in probabilistic methods have changed the analytical environment needed to calculate probabilities of failure of very reliable structure such as that found on aircraft. These methods, outlined in this paper, have the ability to project functional representations of the probability of failure with few analytical evaluations, as compared to that required by the older Monte Carlo methods. These methods, as shown in this paper, make the concept of characterizing structural failure in terms of probability of failure a practical reality.

The New Design Process

As the concept of probabilistic methods-based design is now computationally practical, the whole structural design process can be reconsidered. One outcome, examined here, is the restructure of the design process around assessment of structural viability, by reducing the analytical projection of failure probability to an acceptably low value. The traditional test program to support design acceptance can now be changed. Rather than demonstrate structural adequacy by overloading single test articles with test programs using excessive loads, the tests can be geared to develop adequate understanding of the variations in the design variables and quality of the analytical modeling. Using that understanding, a probability of failure can be designed into the structure that can account for both modeling errors and design variable errors. Use of this concept is examined by applying probabilistic design methods to the key design variables of an example wing.

To understand how the structural design process may be restructured, a design research program led by Southwest Research Institute, Structural Engineering Department, with Boeing - Military Aircraft and Missile Systems, was executed to examine, using a state-of-the-art wing design as a benchmark for comparison, how restructuring can be formulated. This paper documents some of the observations and findings of that program, and some of the implications they offer in moving the burden of structural acceptability to analyses. The aircraft structure used was a composite wing designed under an advanced aircraft structures development program, whose purpose was to identify structural design concepts and manufacturing processes that could lead to more unitized design, and assess their payoffs in application. This structure was deemed a good candidate because it represents the state-of-the-art in aircraft design, has high quality state-of-the-art computational models available, and has available key experimental component test data.

The reformulation of structural design into a form geared for high reliance on analyses uses probabilistic methods as its basic building block for characterizing the acceptability of the analyses. Testing supports the development of the probability of failure calculations. The design process then becomes an evolution of details and basic models into analytical models of increasing detail and sophistication, with each level of model evolution building on the previous level.

Two levels of design detail in wing structure were investigated. First studied was the local behavior of a cobonded joint representing an attachment concept that could be used between substructure and wing skins of modern composite wings. This represents an early level of detail that defines the basic elements of an overall

wing design. This was followed by a probabilistic design study of the wing box skin while carrying, in a post-buckled mode, a high g airload case that was pivotal in the advanced structures development wing skin design. This represents the higher levels of assembly and complete design analyses that would ultimately describe the probability of failure for the aircraft structure.

Investigations into Analyses of Structural Details

To illustrate how structural design can rely heavily on elemental analyses bolstered by support testing as the basic building blocks for acceptance of structural concepts, a cobonded joint was analyzed as one of the basic building blocks of the new wing structural design later used in this investigation. The cobonded joint is representative of the structure that connects the lower wing skin to the spar, as shown in Figure 1. This cobonded joint was chosen as a basic design element because it is a key structural link for many areas of the wing structural box used in modern composite wing design. It also had failure test data available, although limited, from the advanced structures development effort that provided the baseline for this program. This failure test data represents the kind of support testing that should be typical of this new probabilistic approach in design.

In current practice, structural certification of this kind of attachment area requires multiple test elements representing the significant details of the joint. Deterministic design allowables for these joints would be determined semi-empirically, using a combination of joint test data and analysis. This traditional approach requires significant amounts of time and resources. Also, the tests could require as much as a year and a half to complete, due to tooling and environmental conditioning requirements. In addition, if the design changes, the tests have to be redone, since the test articles have to reflect the final joint geometry. The probabilistic analyses of this effort demonstrate that a new approach is available. This approach allows safe prediction of the structural performance of these types of structural elements from basic data sets. In addition, since these sets are basic in most composite wing designs, they can be used without retest, as the design evolves. That is, the variability in performance of basic structural elements due to the combined variations of material properties, manufacturing processes, and environmental effects are analytically predictable based on experimental building blocks of the basic elements. This permits the testing of classes of elements to be considerably reduced or eliminated, the cycle time to be cut by 50 - 70% for future programs, and the avoidance of many retests as the geometry changes.

RTM Carbon/Glass Hybrid Spars
Cobonded To Fibersteered Lower
Wing Skin

- RTM Composites
- Fiber Placed/Steered
- FM300 Adhesive
- HIP'd Titanium Castings
- Aluminum Sheet Metal
- Titanium Machining
- HSM Aluminum
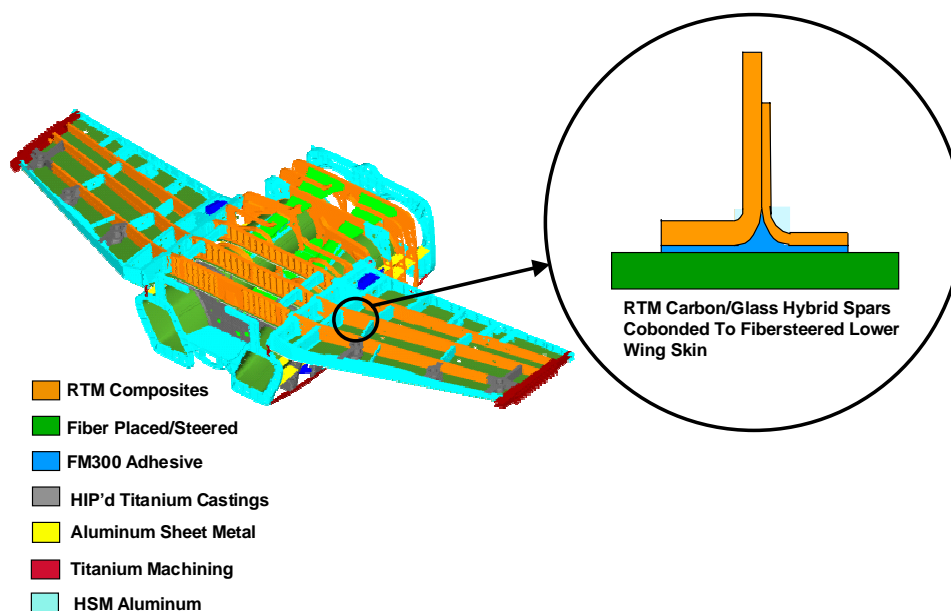
Figure 1 Wing and Cobonded Joint Structure

Boeing has performed destructive testing on joint specimens at cold, room, and elevated temperatures. Three replicate test structures were used at each temperature. The test procedure consisted of clamping the left and right edges of the flanges, and applying a pull-off load (P) until failure, see Figure 2. The value of the pull-off load was recorded.
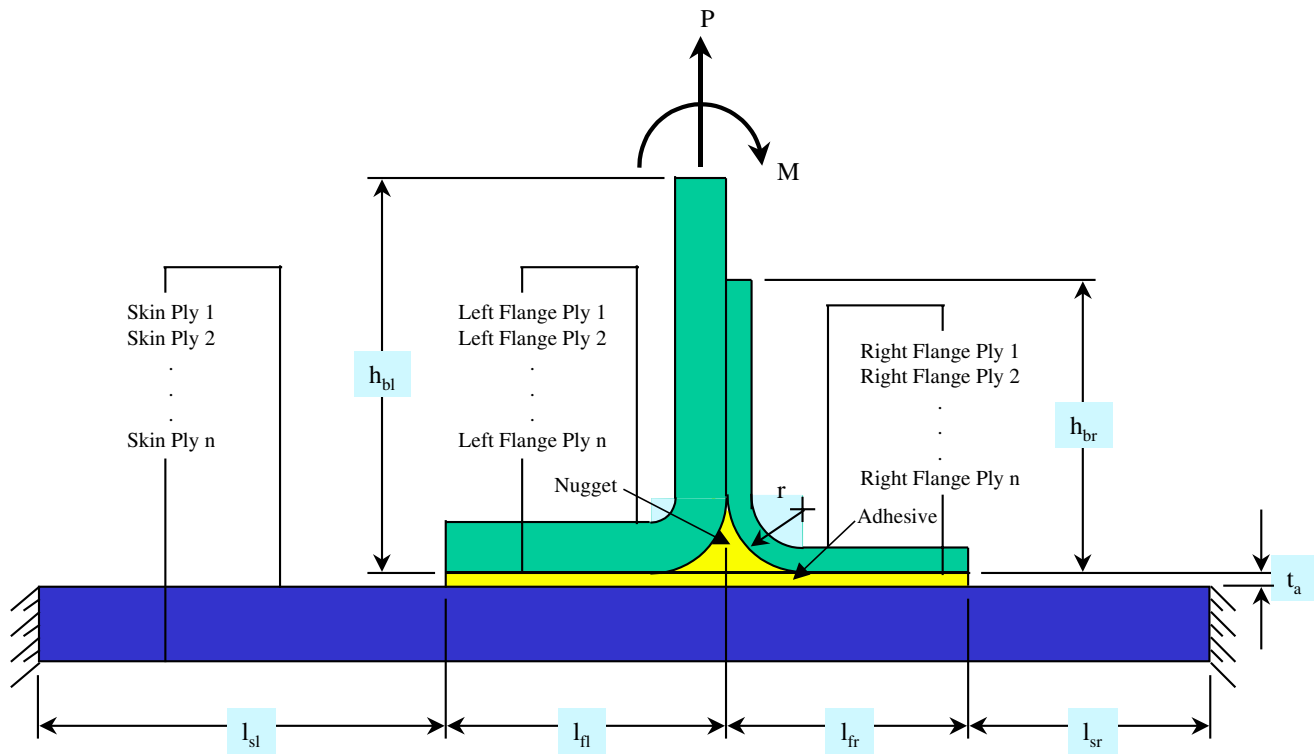
Figure 2 Schematic of Cobonded Joint Blade Model

The probability distribution function of the pull-off load was computed, using the Southwest Research Institute NESSUS™ probabilistic analysis software in conjunction with the THELMA nonlinear finite element software and the BLADEM preprocessor to THELMA. NESSUS™ is a general-purpose probabilistic analysis software that contains a library of statistical distributions, a selection of probabilistic analysis methods, and facilities for interfacing with deterministic mechanics programs.[1] THELMA is a nonlinear finite element analysis program specialized for generalized plane strain analysis of composite structures.[2] BLADEM is a preprocessor for THELMA that is specialized for composite joints such as that shown in Figure 2.[3] THELMA and BLADEM are proprietary Boeing codes.

The probabilistic model consists of 20 independent random variables, shown in Table 1. Dependent random variables are derived from the independent random variables. The dependent random variables are: for the Tape (E3, G23, G31, Nu31), and for the Cloth (E3, G23, G31, Nu31, Nu23). The coefficient of variation (COV) equals the standard deviation divided by the mean value. Material property data are available at cold, room, and elevated test temperatures. The data indicates that a truncated normal distribution is a good model.

Table 1 Independent Random Variables for Cobonded Joint Test Structure (75°F)

Composite Tape	COV (%)	Distribution*
Modulus of Elasticity (E1)	3.2	TNORM
Modulus of Elasticity (E2)	2.0	TNORM
Shear Modulus (G12)	5.0	TNORM
Poisson's Ratio (Nu12)	11.9	TNORM
Ply Thickness	10.0	TNORM
Interlaminar Tensile Strength (S3)	7.8	TNORM
Interlaminar Shear Strength (T)	8.7	TNORM
Composite Cloth		
Modulus of Elasticity (E1)	6.9	TNORM
Modulus of Elasticity (E2)	5.0	TNORM
Shear Modulus (G12)	5.4	TNORM
Poisson's Ratio (Nu12)	41.5	LOGNORMAL
Thickness	1.5	TNORM
Interlaminar Tensile Strength (S3)	4.6	TNORM
Interlaminar Shear Strength (T)	8.4	TNORM
Adhesive		
Initial Shear Modulus (G)	12.8	TNORM
Tau Ultimate (τult)	9.1	TNORM
Gamma Ultimate (Γult)	22.9	TNORM
Nugget Radius (NR)	3.0	TNORM
Ply Thickness	10.0	TNORM
Interlaminar Shear Strength (T)	3.8	TNORM

*TNORM = truncated normal (at $\pm\,3\sigma$)

Failure is predicted computationally when the failure index exceeds 1.0. The failure index is defined as

$$FI = \sqrt{\left(\frac{\sigma_3}{S_3}\right)^2 + \frac{\left(\tau_{31}^2\right) + \left(\tau_{23}^2\right)}{T^2}} \qquad (1)$$

where

σ_3 = tensile stress,

τ_{31} & τ_{23} = shear stresses,

S_3 = Interlaminar tensile strength (composites),

  Flatwise Tensile strength (adhesives),

T = Interlaminar shear strength (composites),

  Shear strength (adhesives).

The 1, 2, and 3 subscripts represent the axes of the plies. The first, 1, represents the local x direction. The second, 2, represents the local y direction, and the third, 3, represents the local z direction. In the case of the composite plies, fibers run in the 1-2 plane. The third direction, 3, is perpendicular to this plane.

The failure index is a random variable. The probability of failure of the structure is the probability of the failure index being greater than 1.0. The distribution of the pull-off load at failure was determined computationally, and compared with experimental results. This is a basic change in the way the failure is viewed, with respect to more conventional design practices. In conventional design, factors of safety on applied loads and reduced property allowables for structural material strengths are built into all aspects of the structural calculations. These tend to mask or sidestep the uncertainties included in the various contributors to the failure calculations. Unfortunately, in conventional margins of safety calculations, all insight is lost into how the actual failure numbers should vary over a production population. Typically, the lack of insight demands that the full-scale articles must be subjected to extensive testing, with extra load built in to account for the accumulated uncertainties. Conversely, probabilistic methods-based design is geared to study the uncertainties, starting at the basic levels such as this bonded joint, as illustrated by the following evaluation.

Failure in the joint can be caused by failure in any of the locations: skin, left or right flanges, nugget, or the adhesive. The results indicate that failure of the joint at 75 degrees is governed by failure in the flange. The nugget does have a small contribution to the system probability of failure, but was not included here. The probability results are shown in Table 2 below, and the probability density function is shown in Figure 3.

Table 2 Probablity Results for Cobonded Joint Test Structure

Load	Pf
300	0.0002
325	0.006
350	0.079
360	0.119
372	0.238
385	0.348
400	0.559
405	0.587
410	0.607
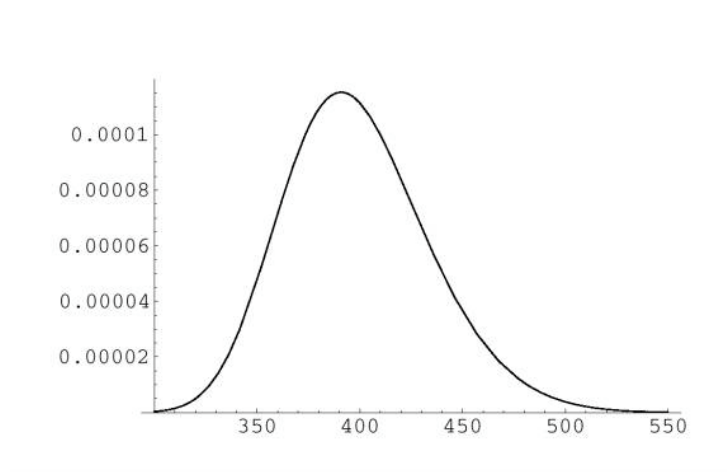
Figure 3 Probability Density Function of Pull-Off Load

Table 3 shows the comparison between the predicted (computational) and experimental results for the failure load. The results indicate the predicted spread in the failure load is much larger than that obtained by test. The most likely reason for this is the scatter used for the random variables during the computations is much larger than that experienced by the test articles. This highlights a fundamental difference that testing support for probabilistic methods-based design should demand.

Table 3 Comparison of Computational and Experimental Results

	Experimental*	Computational
COV (%)	2.15	8.02

*Based on three test results

The test articles are manufactured as a single structure, from a single batch of adhesive, tape, and cloth, then sectioned into three test articles, whereas the scatter used for the random variables is obtained from material, over several years. The scatter is unknown for a single batch of the materials tested. It is comforting, however, that scatter from the computational results is of the same magnitude, and larger than the test results. A smaller scatter would indicate a problem with either the computational model or the random variable inputs.

One important conclusion is that one should obtain statistics for the variables of the test articles in order to calibrate computational and experimental results. In addition, some processes of building-block test programs might be displaced by probabilistic analysis, thereby reducing test complexity and cycle time. This can result in significant savings of cost and time, during the development process.

The sensitivity factors, in terms of the change in probability with respect to a change in the mean or standard deviation of the random variables, are given in Table 4 below. Insight into these sensitivities is one of the major benefits of design procedures based on probabilistic methods. These sensitivities are by-products of the processes of building the functional-based probability density functions, but provide major insight into the robustness and weaknesses of the design process, at each level of progression towards the full structure analysis.

The sensitivities are normalized and given in percent. The results indicate the tape thickness, nugget radius, cloth tensile, and cloth shear strengths are important variables, with tape thickness being the most dominant. The nugget radius is a manufacturing issue, and the others are material performance issues. The large values of the important sensitivities, such as tape thickness, indicate which design variables are most influential in preventing failure of the structure being developed.

Table 4 Sensitivity Results for Cobonded Joint Test Structure*

Random Variable	dprob/dmean (Normalized %)	dprob/dstdev (Normalized %)
Cloth E1	1.0	0.1
Cloth E2	0.2	0
Cloth G12	0	0
Cloth Nu12	0	0
Cloth Thick	3.1	0
Tape E1	2.1	0
Tape E2	0.1	0
Tape G12	0.4	0
Tape NU12	0	0
Tape Thick	**50.7**	**55.6**
Adhesive Goct	1.5	1.5
Adhesive Tau-ult	0	0
Adhesive Gam-ult	0	0
Adhesive Thickness	0	0
Nugget Radius	**26.4**	**5.9**
Cloth Interlaminar Tensile Strength	**7.7**	**14.2**
Cloth Interlaminar Shear Strength	**6.9**	**22.6**
Tape Interlaminar Tensile Strength	0	0
Tape Interlaminar Shear Strength	0	0
Adhesive Shear Strength	0	0

* Corresponding to a load of 300 lbs./in.

Development of Analyses of Assemblies and Complete Structure

Analyses of the collection of basic elements of the structure that form the models for the large assemblies, and ultimately the complete aircraft structure, will ultimately provide the basis for accepting the structure is safe for flight. While some larger article testing will be desired, the costs of these articles will make untenable the testing of a population of them necessary to experimentally define their probability of failure. Thus, when the design reaches the level of complexity of this class of analyses, the basic probabilistic characterization of their structural capability will rely on the roll-up or buildup of probabilities of the smaller elements, as just examined. The following represents the large model probabilistic design evaluations that are expected at the culmination of structural design, wherein the acceptance for flight is primarily based on analyses that have good smaller element testing.

The wing structure to be considered, from which the basic blade joint structural element of the previous section was derived, is that shown in Figure 1. Specifically, the following analysis focuses on the wing structural box covers, or wing skins, and their performance when subjected to a defining load condition that puts this skin in a highly compressive stress state. This is a lightweight composite wing structure with syncore sandwich stiffened wing skins, and was chosen for analysis due to its criticality in flight performance, flight safety, and cost. The analysis focused on the cobonded joint, which attaches the wing box lower cover to the wing spars. Variations in material properties were explored to assess the reliability of the wing at the critical wing-spar interface, and to determine the important material inputs.

The specific design case is the highest down-bending limit load case, and was chosen since it gave the greatest deflection of the wing for all of the down-bending cases. The lower wing skin is the principle structure to be examined because skins and flanges were bonded together on the lower wing skin; the upper surface of the wing skin was bolted to the substructure.

The finite element model of the wing skin is shown in Figure 4, and the deformed model is shown in Figure 5. The fuselage and the outer wing were not included in the model, but were simulated using interface loads applied to the inner wing model using the freebody option in PATRAN. The removal of elements saved on computation time for results not needed in those areas.
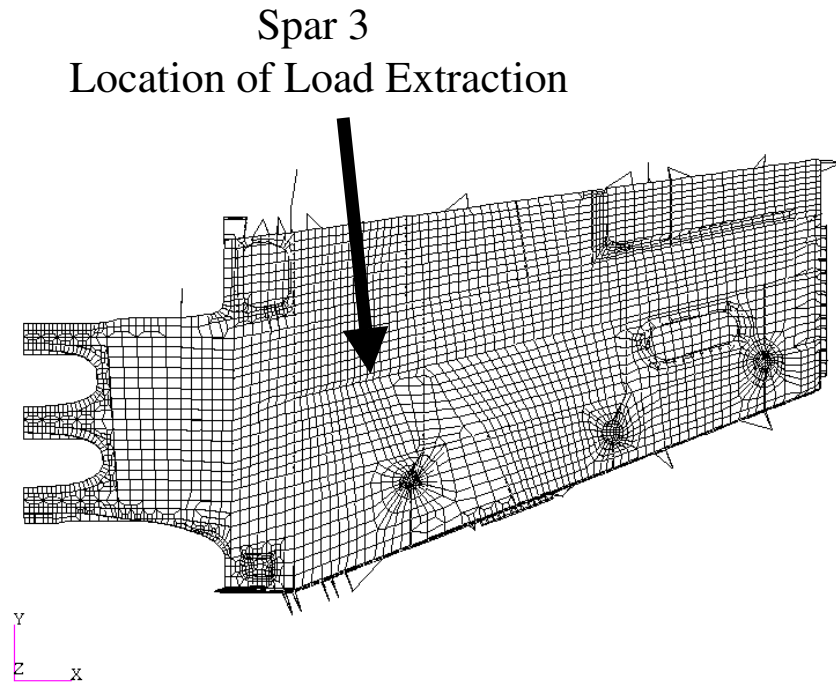
Figure 4 NASTRAN Wing Model
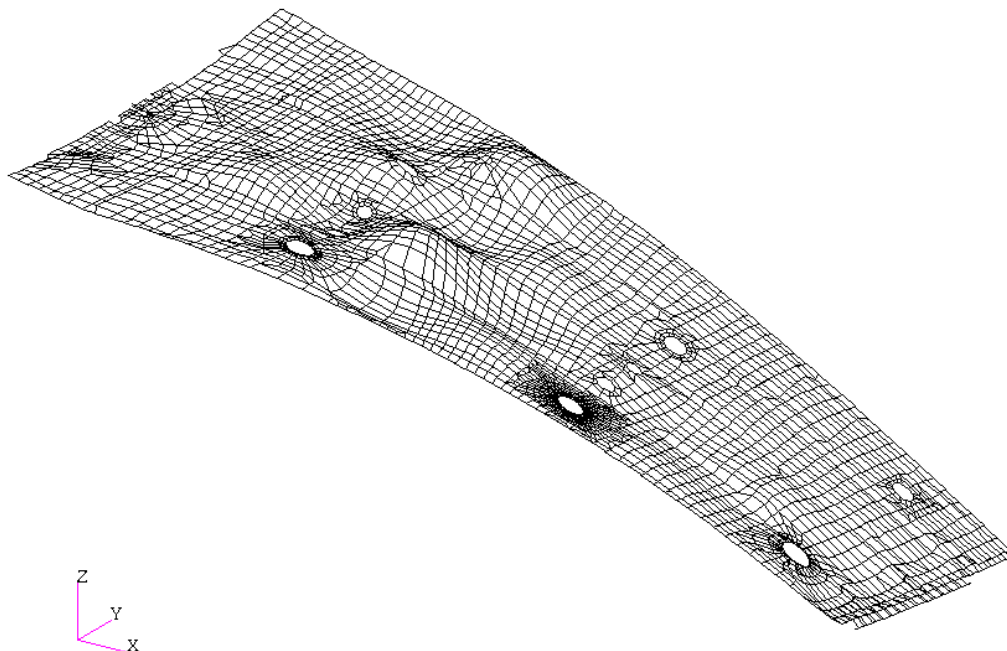
Figure 5 Deformation Plot of Wing Model at Ten Times Actual Deflection

The critical areas of the lower wing consisted of laminated composite material. Each of these laminates had multiple plies varying in orientation. However, the lay-up orientations were not varied for this probabilistic analysis; only variations in material properties were considered.

A structural analysis model has been developed that couples a global post-buckled wing analysis with a local blade analysis. This represents the high degree of complexity that is needed in the large-model probabilistic evaluations for failure. NASTRAN is used for the wing analysis, and BLADEM/THELMA is used for the local blade analysis.

A sequence of steps in the analysis procedure is shown in Table 5 below, and summarized in Figure 6. The steps are repeated each time NESSUS™ requires a deterministic solution. In Figure 6, bdf refers to NASTRAN bulk data file and op2 refers to the NASTRAN output 2 file. FREEBODY.EXE is a code developed by Boeing that converts NASTRAN freebody output loads into BLADEM/THELMA loads. Failure is predicted computationally when the failure index exceeds 1.0, as shown in equation 1.

Table 5 Wing-Blade Analysis Procedure

1) Run NESSUS to generate input files for the wing NASTRAN model and the BLADEM model.
2) Run PATRAN to generate detailed input file for NASTRAN. This inputs the correct material properties for the composite tape and cloth into the database.
3) Run a geometric non-linear NASTRAN analysis to generate stresses, strains, and deformations of the wing structure.
4) Run PATRAN to extract displacements from the large-scale wing model and place the displacements on the small section of the wing model that encompasses the blade region.
5) Run NASTRAN on this small model to obtain freebody forces, using a geometrically linear run (freebody forces are not available in non-linear NASTRAN models).
6) Run PATRAN to extract the results from NASTRAN.
7) Run FREEBODY.EXE to convert the NASTRAN output loads to BLADEM/THELMA loads.
8) Run the BLADEM/THELMA Model to solve for stresses/strains on a fine-meshed detailed model of the blade.
9) Read the BLADEM/THELMA results back into NESSUS, and compute the failure index. Exclude regions near the boundaries of the blade to avoid boundary condition effects.
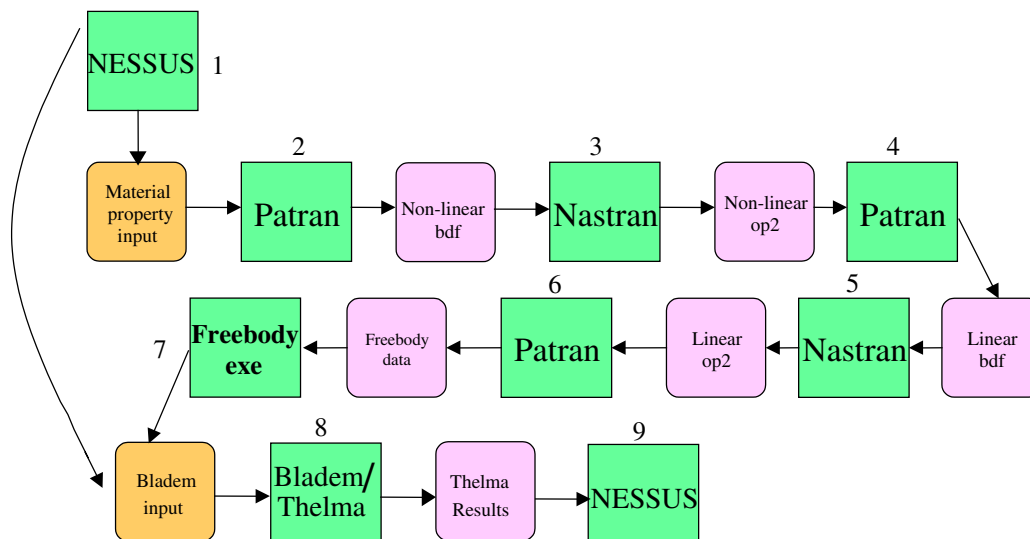
Figure 6 Wing-Blade Analysis Procedure

The random variables considered in this analysis are shown in Table 6. There are 18 independent random variables. Values are for 75 degrees Fahrenheit. Variables in italics are dependent variables.

Two different composite tapes were used. Tape 1, designated "Tape" in Table 6, was used only in the skins. Tape 2 was used to calculate properties in the cloth flange plies.

Table 6 Random Variables for Wing-Blade Analysis

#	Mat'l	Variable	COV (%)	Distribution*
1	Tape	Modulus of elasticity - E1 (tension & compression)	1.3	TNORM
2	Tape	Modulus of elasticity - E2 (tension & compression)	4.5	TNORM
	Tape	*Modulus of elasticity - E3 (= E2)*		
3	Tape	Shear modulus - G12 (tension & compression)	2.7	TNORM
	Tape	*Shear modulus - G23 (tension & compression) = E2/(2*(1+Nu23))*		
	Tape	*Shear modulus – G13 (tension & compression) = G12 = G31*		
4	Tape	Poisson's ratio – Nu12	5.1	TNORM
	Tape	*Poisson's ratio – Nu23 = 0.3*		
	Tape	*Poisson's ratio – Nu31 (=E2*Nu12/E1)*		
5	Cloth	Modulus of elasticity - E1	5.8	TNORM
6	Cloth	Modulus of elasticity - E2	6.2	TNORM
7	Cloth	Modulus of elasticity - E3	6.2	TNORM
8	Cloth	Shear modulus - G12	1.8	TNORM
9	Cloth	Shear modulus - G23	2.2	TNORM
	Cloth	*Shear modulus - G31 (=G23)*		
10	Cloth	Poisson's ratio – Nu12	62.5	LOGNORMAL
11	Cloth	Poisson's ratio – Nu23	7.3	TNORM
12	Tape 2	Modulus of elasticity - E1 (Cloth Nu31 = E3*Nu23/E1 Tape 2)	2.7	TNORM
13	Adhesive	Modulus of elasticity – E	9.1	TNORM
14	Adhesive	Shear modulus – G	9.1	TNORM
15	Tape	Interlaminar Tensile Strength	6.1	TNORM
16	Tape	Interlaminar Shear Strength	4.7	TNORM
17	Cloth	Interlaminar Tensile Strength	6.9	TNORM
18	Cloth	Interlaminar Shear Strength	8.2	TNORM

*TNORM = truncated normal (at $\pm 3\sigma$)

The structural deformation of the blade using the nominal (mean) values for the random variables is discussed in this section. The deformed structure of the local blade model is shown in Figure 7.

Figure 7 Deformed Blade Structure

A stress plot of the critical sigma 3 tensile stress component and the high stressed region is shown in Figure 8.
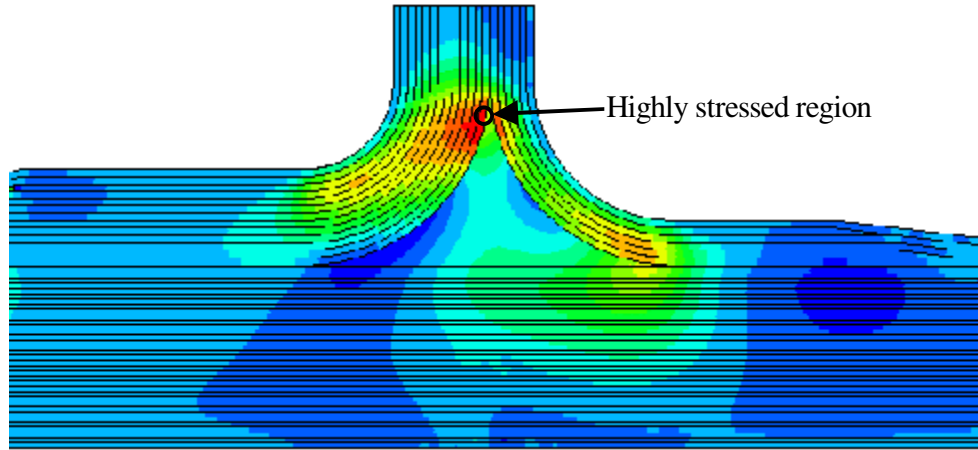
Figure 8 Sigma 3 Blade Results

Probability of failure calculations were performed for the major structural components of the blade (nugget, adhesive, skin plies, left and right flange plies). Table 7 below summarizes the results. The largest probability of failure is in the first ply of the left flange, at the high stressed region shown in Figure 8. This probability is denoted Ω. The probabilities of failure in the other locations of the blade are shown relative to Ω.

Table 7 Probability of Failure Results for Blade Locations

Blade Region	Probability of Failure Relative to Ω
Adhesive	0.0
Nugget	0.0
Skin Plies (1-35)	0.0
Left Flange	
Ply 1	1.0 (Ω)
Ply 2	0.53
Ply 3	0.32
Ply 4	0.22
Ply 5	0.08
Ply 6	0.05
Right Flange	
Ply 1	0.07
Ply 2	1.7E-4

A by-product of the probabilistic algorithm used to determine the probability of failure is deterministic sensitivity results. NESSUS^{TM} computes a first order Taylor series expansion of the Failure Index, with respect to the random variables, e.g.,

$$FI \cong a_0 + \sum_{i=1}^{N} a_i X_i^* \qquad (2)$$

where a_0 and a_i are the coefficients determined from the analysis, and X_i^* are the random variables values about which the Taylor series is computed. In effect, the Taylor series coefficients are the deterministic sensitivity factors, e.g., $a_i = \left.\dfrac{\partial FI}{\partial X_i}\right|_{X_i^*}$.

The relative importance of each random variable can be determined from the equation

$$\gamma_i = \frac{a_i X_i^*}{\displaystyle\sum_{j=1}^{N} a_j X_j^*}, \tag{3}$$

then normalized such that the largest value of γ_i equals one. The values indicate the relative change in FI due to a change in random variable i. The normalized sensitivities are shown in Table 8.

Table 8 Deterministic Sensitivities

Random Variable	Normalized Sensitivity	ΔFI/ΔRV
Tape E1	0.09	-0.08
Tape E2	0.03	-0.03
Tape G12	0.11	-0.11
Tape Nu12	0.05	-0.05
Cloth E1	0.18	-0.18
Cloth E2	**-0.49**	**0.47**
Cloth E3	-0.11	0.11
Cloth G12	-0.02	0.02
Cloth G23	-0.22	0.21
Cloth Nu12	0.00	0.00
Cloth Nu23	-0.01	0.01
Cloth Nu31	0.00	0.00
Adhesive E	0.00	0.00
Adhesive G	-0.07	0.07
Interlaminar Tape Tensile Strength	0.00	0.00
Interlaminar Tape Shear Strength	0.00	0.00
Interlaminar Cloth Tensile Strength	**1.00**	**-0.97**
Interlaminar Cloth Shear Strength	0.00	0.00

Another sensitivity study is to assess the percent change in FI, given a percent change in each random variable, for example, 1%. That is, compute

$$\frac{\Delta FI}{\Delta X_i} * (1\% X_i). \tag{4}$$

The third column of Table 9 gives the results, which indicate that a 1% change in the cloth tensile strength yields approximately a 1% drop in FI. The negative sign on the cloth tensile strength indicates that an increase in its value yields a decrease in FI. The sensitivities clearly show the cloth interlaminar tensile strength is the dominant variable, with the Cloth E2 variable also important, followed by the Cloth G23 variable.

Probabilistic sensitivities consider both the deterministic sensitivities and the scatter of the random variable. These results can be used to determine the expected changes in the probability of failure, due to modifications in the mean value or standard deviation of the random variables. The results shown in Table 9 are similar to the deterministic sensitivities, and clearly indicate the Failure Index is most sensitive to the mean value and standard deviation of the cloth tensile strength, and somewhat sensitive to the Cloth E2 variable.

Table 9 Probabilistic Sensitivity Factors for Left Flange 1st Ply

Random Variable	d prob/ d mean	Normalized (%)	d prob/ d stddev	Normalized (%)
Tape E1	-1.77E-08	1	-3.35E-10	0
Tape E2	-1.21E-07	0	-2.07E-09	0
Tape G12	-7.47E-07	1	-1.17E-08	0
Tape Nu12	-7.52E-01	0	-1.13E-02	0
Cloth E1	-1.02E-07	2	-3.76E-09	0
Cloth E2	**2.76E-07**	**17**	**-2.85E-08**	**5**
Cloth E3	4.13E-07	1	-6.47E-09	0
Cloth G12	1.23E-07	0	-2.89E-09	0
Cloth G23	1.50E-06	4	-2.96E-08	0
Cloth Nu12	2.97E-01	0	-1.05E-01	0
Cloth Nu23	2.45E-01	0	-4.70E-03	0
Cloth Nu31	-9.37E-10	0	-1.55E-10	0
Adhesive E	1.46E-07	0	-6.36E-09	0
Adhesive G	6.21E-06	0	-1.56E-07	0
Interlaminar Tape Tensile Strength	2.21E-12	0	-1.64E-06	0
Interlaminar Tape Shear Strength	9.96E-14	0	-1.12E-07	0
Interlaminar Cloth Tensile Strength	**-8.15E-04**	**74**	**-1.88E-04**	**95**
Interlaminar Cloth Shear Strength	-2.17E-07	0	-8.77E-08	0

One can assess the reduction in the probability of failure as the failure index is modified and, also, how much must one decrease the failure index to lower the probability of failure to a target value. A study was performed, using the solutions of the left flange first ply. The study assumes the sensitivity of the failure index to the random variables remains constant, but the constant term, i.e., a_0 is reduced. This approach is easy to do, and does not require any additional finite element solutions.

The results are shown in Table 10, again relative to a probability of failure Ω. The results indicate that a 20% reduction in the failure index leads to a reduction in the failure probability of 300 times. Using this information, the designer can determine appropriate deterministically-based design targets of the failure index.

Table 10 Probability of Failure as a Function of the Failure Index

FI	Probability of Failure Relative to Ω
1.0	1.0 (Ω)
0.95	0.57
0.9	0.22
0.85	0.05
0.8	3.3E-3
0.7	1.7E-6

A system reliability analysis, considering failure in all locations and plies of the blade, was completed. In other words, the probability of failure of the blade is defined as failure of any location of the blade. The locations considered were adhesive, nugget, left flange, skin, and right flange. Failure in all plies was considered.

The system reliability is determined mathematically as

$$
\begin{aligned}
P[blade] &= P[\text{failure in any region}] = \\
&P[F_{nugget} \cup F_{adhesive} \cup F_{SkinPly1} \cdots \cup F_{SkinPlyN} \cup \\
&F_{LeftFlangePly1} \cdots \cup F_{LeftFlangePlyN} \cup \\
&F_{RightFlangePly1} \cdots \cup F_{RightFlangePlyN}]
\end{aligned}
\tag{5}
$$

where the symbol $\cup$ denotes a "union" of events.

The system reliability methodology used makes no assumptions regarding the independence or correlation of the failure locations. The analysis uses Monte Carlo or Importance Sampling, using the approximate limit state derived during the component probability calculations.

The results indicate that the failure modes are fully correlated. That is, failure will always occur first in the left flange 1st ply, for any realization of random variables. For example, there are no situations where failure will occur in the second ply of the left flange without already having failed in the first ply of the left flange. Therefore, the probability of failure of the blade *is* the probability of failure of the left flange 1st ply.

The probability of failure results of the blade, i.e., Ω, was larger than desired. As such, a redesign of the wing-blade was undertaken. A series of modifications to the design was carried out. The quality of the redesign was estimated deterministically by examining the computed failure index, using nominal values of the random variables. After a good candidate was discovered from these deterministic analyses, a probabilistic analysis was run to assess the probability of failure.

Three modifications were found that significantly reduced the failure index, two involved a geometric quantity, and one involved a material property. The modifications were to eliminate one ply layer from the right flange, to increase the nugget radius, and to reduce the Young's modulus of the cloth in the 2 direction, i.e., the E2 variable. The random variable statistics for E2 were modified such that the mean value was one-half its previous value, and the COV was unchanged. The importance of the magnitude in nugget radius can be seen in the sensitivities shown in Table 4.

The softening of the spar, by reducing E2 of the cloth, reduced the loads and moments in the wing. This, in turn, lowered the failure index. The knowledge that a significant reduction in the failure index could be

obtained by modifying E2 of the cloth and changing the nugget radius was discovered by evaluating the probabilistic sensitivity factors, i.e., Table 9 and Table 4. This information would not be straightforward to determine, without the sensitivity analyses. It may not be possible to implement this solution in an actual aircraft, as softening the spar may have adverse effects on wing stiffness and aeroelastic performance. Nevertheless, the design trade identifies a simple approach to significantly increasing safety for such a wing. Informed managers, aware of the consequences, can make the appropriate decision.

The distribution of the failure index for the redesign is shown in Figure 9. The mean failure index equals 0.6835, the standard deviation equals 0.049, and the probability of failure is less than 10^{-30}. Thus, the probability of failure of the wing blade was reduced many orders of magnitude, to approximately zero.
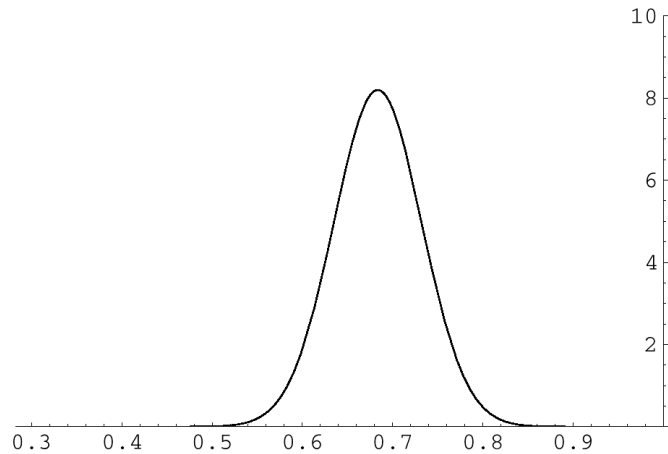
Figure 9 Probability Density Function of the Failure Index after Redesign

Observations for Reliance on Analyses for Acceptance

The details of key elements of a state-of-the-art composite wing airframe were used to identify and explore issues arising from an approach relying primarily on analysis for acceptance of airframe structure. A centerpiece of the analysis process, identified as needed for this reliance, is the application of probabilistic methods to the design and analysis process. The approach used was to develop high confidence in analysis of small pieces of the problem, and then building a large and complex analysis from these building blocks. In this, the approach taken is similar to the iterative design/test approach currently in common use. This roll-up of complexity allowed the uncertainties of the large analysis to be developed from those developed in the smaller and simpler analyses. The performance of the post-buckled wing box cover relied on a local model of the cobonded joint modeling the attachment of the wing box cover to the wing spars. The failure margin of the cobonded joint, whether it is thought of in terms of reliability or margin of safety, was critical to the structural safety of the wing. In this way, the buildup from simple analysis models to the final complex models needed for design acceptance was represented.

The analysis of the cobonded joint test article revealed a coefficient of variation of the pull-off load several times larger than that computed from three test results. The larger scatter predicted is most likely due to the fact that the scatter used for the material properties in the analysis was larger than the scatter found among the three test articles. This is because the test articles are manufactured as one structure, from one batch of materials, then sectioned. The material properties used in the analysis, however, were based on statistics of material properties collected over several years. This study reinforced the fact that realistic statistics of the random variables representing their variations expected over the production runs of the full structure be used in the test articles and in the probabilistic analysis, in order to accurately correlate calculations with tests.

This is significant because it indicates that using traditional element tests may not give a reliable prediction of the production population. Traditionally, strong measures are taken to assure maximum uniformity in the test articles. If one relies solely on pull-off tests from the same batch of material, then the actual population may have a larger scatter, making the results unconservative. Therefore, the use of probabilistic methods can anticipate variabilities for joints when it is not affordable to run the number of tests necessary to characterize all the effects of independent parameters that enter into this analysis. Thus, even in the small element stages of analysis buildup, the use of realistic design variable variations in a vigorous probabilistic design process should produce basic analyses that are equal to but likely better than what limited testing can suggest.

The probabilistic analyses of the structure described in this effort demonstrate that a new approach is available, one that allows safe prediction of the structural performance of these types of structural elements from basic data sets that can be used without retest, as the design evolves. That is, the variability in performance of basic structural elements due to the combined variations of material properties, manufacturing processes, and environmental effects are analytically predictable, based on experimental building blocks of the basic elements. This permits the testing of classes of elements to be considerably reduced or eliminated, and some retests that arise from geometry, manufacturing process, or material change may be eliminated. Cycle time for future programs is likely to be reduced by a substantial amount. An additional benefit could be a more effective design, as detail improvements thought of after initial testing may be more effectively implemented. This same benefit may eventually apply to the introduction of design changes in production or service.

A global-local probabilistic analysis of the wing-blade structure was performed to quantify the probability of failure, and to identify the random variables to modify that would most cost-effectively achieve a safer structure. Based on these findings, a redesign was carried out. In this case, two geometric and one material property change were sufficient to reduce the probability of failure by many orders of magnitude, such that the probability of failure of the redesigned structure is, basically, zero. Recognize that this design guidance provided a better design than could have been achieved by attempting to guide the redesign by limited testing.

For the larger analysis model of the wing, observations can be taken that reflect how complete structure would be treated. Traditional methods of acceptance rely on scaled-up loading of single test articles, to determine if the structure is adequate for its expected use. Variations and unexpected loadings are accounted for in the up-scaling of the loading. If probability of failure (POF) methods are used for acceptance, typically the analyses are used to project POF values, and the testing establishes the adequacy of the analyses. These are fundamentally different programs, with different conclusions to be drawn.

If POF analysis methods are used for acceptance, the degree of change in the way aircraft structure would be developed cannot be underestimated. The conclusions, in general, focus on the fundamental change in philosophy that every design variable must be represented by a distribution, rather than a single value. All the methods, then, must account for this. Note that the fundamental response analyses do not change. Force will always be equal to mass times acceleration; force will always equal to stiffness times deflection. However, over the production run of an aircraft structure, its stiffness will vary some, and the forces applied to it will vary some. Thus, its deflections will vary some. These variations cannot be captured by traditional test methods for acceptance, and cannot be exploited for improved overall design performance.

Design acceptability is measured by an acceptable probability of performance. POF approaches require probabilistic design methods to be useful analytical tools. It appears there are cost and schedule benefits from probabilistic design, when it is evaluated with the entire program taken as a whole. The ability to eliminate some testing, avoid some retesting, and define design refinements, using the sensitivity analyses, should make the probabilistic design approach less expensive and faster in the long run, and provide the high confidence analysis needed for structural acceptance.

Testing plays a different role with this approach. Testing provides distributions in how the design variables may vary, but the real change is that hardware testing is aimed more at refining the analyses than certifying the structure is safe. Safety evaluations through POF define structural safety. This fundamental change is the

largest and most pervasive change in the structural design process, and dictates much of the following observations.

While the same analysis models used in deterministic approaches are also used with probabilistic design approaches, the analysis steps in probabilistic design are much more demanding than before. Where, before, the response of a configuration was calculated to determine if selected values of the design variables provided adequate strength, in probabilistic design there are ranges and distributions of these variables. This means that in the simplest deterministic approaches, a multitude of response evaluations are required based on the important combinations of the design variables. Fortunately, the probabilistic analysis tools have evolved to a degree where the multiplicity of these evaluations is minimized. Still, there are many more evaluations with probabilistic methods.

The probabilistic analysis process demands more skills than the traditional deterministic approaches of the design engineer. Higher resolution response analyses are used earlier in the design cycle, often requiring insight into such subjects as nonlinear, temperature dependant procedures. The nonlinear buckling response example of the wing may be more typical than past experience would suggest. In fact, this investigation suggests that a good team for design would consist of engineers familiar with best modeling schemes to produce high quality idealizations. They would complement more traditional structural engineers, who have great insight into structural solutions for new aircraft configurations. Added to these engineers would be engineers who have a focus on the basic mechanics of probabilistic analyses, models, and statistics. Each of these members brings needed depth to the design process that may not have been needed before.

While identifying the problem areas and extremely sensitive design variables may be easier with probabilistic methods, the selection of the corrective or improving modification may rely on traditional approaches. These would likely be evaluated using deterministic methods to define the selection of a nominal value for the modified design value that needed changing. In this effort, for example, the selection of general direction of change in the design variables identified by sensitivities was first examined with deterministic dry runs. Once the correct direction is identified, these new values can be examined to determine if they are successful, using the probabilistic methods.

The large amount of data required to perform these response evaluations, and the equally large volume of results, highlight the data management challenges associated with probabilistic methods. Where once there existed single assumed values for the design variables, now there are many. Where once there existed a single response prediction, now there are many. This is further complicated by the fact that in building from simple models/analyses to complex ones, it is important to assure the correct distributions are passed on to the next level of analysis complexity. This suggests that some of the deterministic procedure-based structural optimization codes may still be useful in identifying design solutions for problems identified with probabilistic methods.

More detailed information is needed for the design process, and this information is needed earlier in the process. Material value distributions are needed at the outset. Geometry variations are needed before any geometry variations can be measured. While this implies that more is then known about the design, it occurs at a time when little can be known in some area because it is just being conceived. Thus, reliance on design information databases that document past histories in the distributions of materials and geometries become crucial. However, this means someone must be willing to invest in gathering and storing this information after the design is set and has been sold. It is important that the integrity of the data be ensured, as is the case in present deterministic analysis approaches. More use of online database management systems that can be used to better ensure data integrity and consistency is certainly in order.

There are long-term implications built into this data. Changes or improvements in manufacturing processes or material capabilities must be addressed with reanalysis of the probabilistic results, since assumed improvements in any single factor may not always combine in a beneficial way. It also means that testing must include the realistic changes that should be expected over a long production run with different suppliers

of the materials and process hardware. This was illustrated with the results of the local blade stiffener calculations. The analysis of the cobonded joint test article revealed a coefficient of variation of the pull-off load several times larger than that computed from three test results. The predicted larger scatter is due to several differences between the model and the way the test specimens were manufactured. The test articles were manufactured as one structure, from one batch of materials, and then sectioned into three specimens. As a result, the test did not reflect the full variability of the material properties that would be seen between different batches of material, nor did it reflect the differences in geometry that would be present between different manufacturing runs.

Early design insight is greater and more complete with the probabilistic approach. The sensitivity analyses available with probabilistic analyses are of great value in many ways. They can tell you what variables are important, which ones must be held to close tolerances, where detailed testing is needed, and can suggest which variables can greatly improve the performance of the structure with little or non-obvious changes. The insight to soften the E2 values of the composite cloth in the blade is a prime example of the latter. Without the insight of the sensitivity studies available in the new method, this design solution most likely would not have been examined.

There appears to be the opportunity to tailor the POF of all the components of a structure to provide a better risk balance and, thus, remove unnecessary overdesign. Since the building-block approach forms up the POF of each component from those elements it is made of, probabilistic design offers the ability to tailor these building blocks so that all contribute equally to the overall POF. It also allows the designer to better identify the crucial elements needing design attention.

With greater specificity in the way a structure fails, by knowing the probability of each failure mode, the designer can work toward supplying more graceful failure modes for the structure. This "leak before massive rupture" structural response can be most useful in saving aircraft from sudden catastrophic failure modes that provide little warning or opportunity to safely return.

The testing approach outlined here in support of probabilistic design is changed, fundamentally, from traditional approaches. More details are needed early, but testing done on other programs using similar materials and fabrication methods can provide much of that. The detail of the measurements taken for a range of loads is much greater than the traditional method of determining rupture loads. Subcritical strain and deflection data are key to fine-tuning analysis models. The probabilistic analyses allow safe prediction of the structural performance of these types of structural elements from basic data sets that can be used without retest, as the design evolves. That is, the variability in performance of basic structural elements due to the combined variations of material properties, manufacturing processes, and environmental effects are analytically predictable, based on experimental building blocks of the basic elements.

References

1. NESSUS 2.4 Users Manual, Southwest Research Institute, San Antonio, TX, 1999.
2. THELMA Users Manual, Thermal-Elastic Analysis of Structures in Generalized Plane Strain with Non-Linear Materials, Version 7, Boeing - Military Aircraft and Missile Systems, St. Louis, MO, 1998.
3. BLADEM Users Manual, Blade Analysis Model, Version 3, Boeing - Military Aircraft and Missile Systems, St. Louis, MO, 1999.

This page has been deliberately left blank

Page intentionnellement blanche

Uncertainty Quantification in Airframe Design

Ramana V. Grandhi
Distinguished Professor
209 Russ Engineering Center
Department of Mechanical and Materials Engineering
Wright State University
Dayton, OH 45435, USA

rgrandhi@cs.wright.edu

Abstract

Multiple configurations in various stages of aircraft design have to be experimentally tested and validated to study the performance of various systems subjected to non-deterministic design parameters. These tests are expensive and time consuming, increasing the acquisition cost and time for military aircraft/equipment. Therefore, analytical certification aims at reducing/eliminating the expensive prototype testing during these intermediate design stages by propagating the input variance through the design. Analytical certification involves modeling the variance/uncertainties in the design parameters and estimating the variance in the component/system performance.

Based on the nature and extent of uncertainty existing in an engineering system, different approaches can be used for uncertainty propagation. If the uncertainty of the system is due to imprecise information and lack of statistical data, the Possibilistic theory can be used. During preliminary design, uncertainties need to be accounted for and due to lack of sufficient information assigning a probability distribution may not be possible. Moreover, the flight conditions (loads, control surface settings, etc.) during a mission could take values within certain bounds, which do not follow any particular pattern. The uncertain information in these cases is available as intervals with lower and upper limits. In this case, the fuzzy arithmetic based method is suitable to estimate the possibility of failure. The use of surrogate models to improve the efficiency of prediction is presented in this paper. Various numerical examples are presented to demonstrate the applicability of the method to practical problems.

Introduction

Aerospace structural design involves analyzing various disciplines like structures, controls, aerodynamics, aeroelasticity, electromagnetics, etc. The design process requires integration of multiple disciplines to model the actual behavior of the system. This complex design process usually becomes challenging with the presence of uncertainties in material properties, loads, boundary conditions, geometric properties, manufacturing processes, environment, and mathematical models. Incorporation of these uncertainties into the design enables the prediction of the aircraft performance variation in the presence of uncertainties and more importantly their sensitivity for targeted testing and quality control.

The traditional way to propagate the uncertainty is to use safety factors in the design, which essentially ignores the source of a given uncertainty. This safety factor approach produces designs that satisfy all the requirements but not optimum for the given conditions. Moreover, the safety factor based approach is suitable and applicable for situations where the new design is a derivative of an existing design. It becomes impractical and expensive to apply the safety factor based design to new systems because this procedure requires extensive testing to assign a safety factor that produces a conservative design.

As the complexity of the multifunctional structure increases, the cost of manufacturing the prototype to validate the designs and determine the level of safety would increase alarmingly. Thus, the need for analytical certification of components is compelling. Uncertainty quantification techniques are tools that aid in analytical certification. Uncertainty quantification and their effects are not unique. They depend on the amount of data engineers incorporate about a particular event or variable. Depending on the

information available, the designer has to choose the quantification technique that would propagate the uncertainties through the system. Depending on the nature of information available, various techniques are appropriate for propagating the uncertainty through the system integration and design process.

In engineering design, the designers often have to deal with uncertainties in structural loads, material properties, initial conditions, control system settings, etc. The uncertainty can be classified as random and non-random. The random uncertainty can be dealt with by using the existing probabilistic methods and the safety of the design can be quantified [1-6]. In situations where the information required for assigning the probability distribution to a variable is not available, the non-randomness comes into picture. The impreciseness of the parameter is available as a bound. Various interval analysis techniques are available to deal with variables that have bounds. However, these techniques provide one bound for the response compared to the fuzzy approach that provides the bounds on the response at various confidence intervals. From the literature available on fuzzy arithmetic approach, fuzzy set models, which require little data, appear to be well suited to deal with design under uncertainty when little is known about the uncertainty.

Interval data might be available from the sparse output of instrument measurements; the mean of a normal distribution could be available from many experts; parameters of another distribution fit with high precision from a large collection of measured point data; and finally, the mean of another distribution may only be presumed to lie within an interval. Also, in real situations, the uncertainty in a given input parameter might be independently estimated from several completely different sources and thus have completely different mathematical representations.

Fuzzy theory provides a means by which incomplete or subjective information can be represented in an analytical form. This kind of uncertainty can arise during design and manufacture, where a geometric parameter, x can be subjected to tolerances as $x \pm \Delta x$. Moreover, no additional information is available to assign a probability distribution within the interval. Then the parameter can be treated as a fuzzy number. The main advantage of the fuzzy theory is that it can accommodate the confidence levels of variables and as the design progresses, the design need not be reevaluated to obtain the new bounds on the response due to change in confidence levels of the design parameters. These bounds will be available for any confidence level from 0 to 1, once the design is analyzed using the fuzzy theory. The technique used to construct the fuzzy number for the uncertain variable is discussed in the later section.

In 1965 [7] Zadeh provided the first tools, i.e. fuzzy sets, specially devised for dealing with vagueness. Since then various researchers have advanced the subject and its recent applications are in areas like artificial intelligence, image processing, speech recognition, biological and medical sciences, decision theory, economics, geography, sociology, psychology, linguistics and semiotics. Literature has shown that it is indeed a useful tool to quantify the impreciseness and vagueness present in real-life problems. Most of the engineering applications have been in controls, decision-making and optimization. Kaufmann and Gupta in Ref [8] reviewed the area of fuzzy arithmetic. Buckley and Qu [9], Sanchez [10], and Zhao and Govind [11] investigated the mathematics of fuzzy equations and their solutions. These solution methods are applicable to problems with explicit response functions and inapplicable when the response is implicit. Vallipapan and Pham [12] introduced the use of fuzzy information in the finite element analysis of geotechnical engineering application. In their work, the authors used fuzzy sets in the finite element formulation to model the elastic soil medium. They introduced the lower and upper fuzzy bounds values for the input parameters at a particular membership level, or α cut, and solved the resulting deterministic model.

Fuzzy finite element analysis can be broadly classified into two categories, namely, explicit and implicit techniques. In explicit techniques, the solution of the response is explicitly obtained by operations on an α level representation. The advantage of this method is that the interval equations as a function of α are solved only once and the bounds on the response at any α level are readily available. However, this method has its practical problems including the possibility of obtaining unbounded, unrealistic and non-unique solutions to the response bounds. Moreover, these methods are still being developed and they have not been well tested since they do not use the legacy finite element software.

The second category is the implicit formulation where all the binary combinations of the extreme values of the fuzzy variables at a particular α level are explored and the bounds of the response are obtained. At each combination of the variables, one finite element simulation is required and the

computational effort involved is exponentially related to the number of variables. The implicit methods result in exact bounds (provided there is no maxima or minima within the bound) at a considerable cost.

Braibant et al [13] presented non-deterministic possibilistic approaches for structural analysis and optimization. If the system is fuzzy, it is possible to establish a connection between the interval method and the fuzzy analysis by using the concept of membership level or α-cuts. α is actually the level of satisfaction, which changes from 0 to 1. At the level of satisfaction α, the variation domain of the variable x is given by the interval [ι_α , $\overline{\iota_\alpha}$]. By representing the design parameters using α-cuts approach, all the interval expressions involved in the analysis can be evaluated at different fuzzy levels or α values. In practice, the fuzzy response of a structure is computed in three steps. First, the fuzzy members describing the parameter uncertainties are sampled for different degrees of membership in which each parameter is given an interval. This is what is called "fuzzification". Second, the finite element equilibrium equations are solved at each level, leading to the corresponding variation intervals of the structural responses. Finally, putting the intervals together for each structural response, the interval related to different degrees of membership allows the fuzzy response to be built. Difficulty arises when solving the discretized interval equilibrium equations.

In order to improve the efficiency of the above solution algorithms involving fuzzy data, the Hansen Algorithm [14], Neumann Approximate Vertex Solution and Vertex Solution [15] were introduced in Ref. [13]. The Vertex Solution is considered as the most robust but the computation cost could be prohibitive when the number of uncertain parameters is very large. The Hansen Algorithm is one of the most popular explicit direct algorithms and the iterative algorithms of the Gauss-Seidel or Jacobi family have to be used as a basis to solve the interval linear equation system. For the Hansen Algorithm, two modifications were introduced to limit the occurrence of unbounded solutions in the basic algorithm. These methods are applicable for implicit problems whose response behaves in a linear fashion. However, in most engineering problems, the response is highly nonlinear and a linear approximation at the central values could lead to erroneous results. For the Neumann Approximate Vertex Solution, the linear approximation is used for the stiffness matrix and the load vector with respect to uncertain parameters. The number of numerical simulations for Neumann is $2n$, where n is the number of uncertain variables. However, the "Vertex Solution" requires 2^n number of simulations. The cost involved in vertex method is exponential and it is not a viable solution to large-scale engineering problems.

Akpan [17] et.al presented response surface based fuzzy analysis. In their work, they have constructed a second-order response surface model and used this response surface to evaluate the function value in the vertex method. This method is applicable to problems with a limited number of uncertain variables since the cost of building the response surface increases with the number of uncertain variables. Moreover, the vertex method fails to capture the accurate bound when the function has maxima or minima within the range of the input parameters.

The above-mentioned difficulties in dealing with the fuzzy based analysis of structural systems are dealt with in the current study. In this current study, fuzzy set theory is applied to quantify the non-random uncertainties. The ability to efficiently handle large-scale implicit problems with high degree of accuracy is a salient feature of this method. The imprecision or fuzziness in the response of interest is calculated by using the Zadeh's extension principle. The computational implementation of the extension principle on implicit functions like a Finite Element Analysis (FEA) model or the Computational Fluid Dynamics (CFD) model is performed with the use of high quality function approximations. These function approximations reduce the cost involved in actual function value evaluations. Examples are provided to demonstrate the solution procedure and the applicability of the method.

Using the definition of the fuzzy number, the available uncertain information can be used to construct the fuzzy number. The present method is used to model the uncertainty when the available information about the uncertain variable is limited. The following section discusses the technique used to model the fuzzy number using the available information.

Triangular Membership Function

In structural engineering it is often possible to acquire knowledge about various parameters in the form of low, probable and high values. Based on this information, the membership functions can be constructed. Following the concepts of fuzzy set theory the parameters are modeled as fuzzy numbers,

where the information is imprecise due to vagueness. In this work we have adopted the suggestion found in Ref [12] to define a linear membership function.

The two extreme left and right fuzzy members L' and H' respectively, at $\mu(x) = 0$ are defined as

$$L' = \begin{cases} P - 2(P - L), & P \geq 2(P - L) \\ 0, & P \leq 2(P - L) \end{cases} \tag{5}$$

$$H' = P + 2(H - P) \tag{6}$$

where L, P, and H are the expert's estimates of low, probable and high values, respectively.

The following triangular membership function is obtained:

$$\mu(x) = \begin{cases} 0 & x \leq L' \\ \dfrac{x - L'}{P - L'} & L' \leq x \leq P \\ \dfrac{H' - x}{H' - P} & P \leq x \leq H' \\ 0 & x \geq H' \end{cases} \tag{7}$$

Several different shapes of membership can be used for different types of imprecision. This methodology permits the solution of problems involving imprecisely defined geometry, external loads, initial conditions, etc.

Multi-Point Approximation

The approximation technique used in this paper is the Multi-Point Approximation (MPA) technique. The multi-point approximation can be regarded as the connection of many local approximations. With function and sensitivity information of limit-state already available at a series of points, one local approximation is built at each point. All local approximations are then integrated into a multi-point approximation by the use of a weighting function. The MPA can be written using the following general formulation:

$$\tilde{F}(X) = \sum_{k=1}^{K} W_k(X)\tilde{F}_k(X) \tag{8}$$

where k is the number of local approximations, $\tilde{F}_k(X)$ is a two-point local approximation and W_k is a weighting function that adjusts the contribution of $\tilde{F}_k(X)$ to $\tilde{F}(X)$ in Eq. 8. The evaluation of this weighting function involves the selection of a blending function and a power index "m". The procedural details for evaluating the weighting function are discussed in Ref.18.

The weighting function is given by the equation

$$W_k(\mathbf{X}) = \frac{\phi_k(\mathbf{X})}{\sum_{j=1}^{K} \phi_j(\mathbf{X})} \tag{9}$$

where $\phi_k(X)$ is the blending function. The blending function used in this paper is given by:

$$\phi_k(\mathbf{X}) = \frac{1}{h_k} \tag{10}$$

This blending function combines the local approximations into one MPA and controls how fast the MPA adapts to the local approximation at a particular design point. The local approximations considered in this paper are TANA2 and they are of the type,

$$\tilde{F}(X) = F(X_2) + \sum_{i=1}^{n} \frac{\partial F(X_2)}{\partial x_i} \frac{x_{i,2}^{1-p_i}}{p_i} (x_i^{p_i} - x_{i,2}^{p_i}) + \frac{1}{2} \varepsilon \sum_{i=1}^{n} (x_i^{p_i} - x_{i,2}^{p_i})^2 \tag{11}$$

where X_2 is the expansion point for the approximation. X_1 and X_2 are two design vectors at which the function and gradient information of F(X) are used to build TANA2 model. This equation is a second-order Taylor series expansion in terms of the intervening variables $y_i (y_i = x_i^{p_i})$, in which the Hessian matrix has only diagonal elements of the same value ε. Therefore, this approximation does not need the calculation of the second-order derivatives.

The construction of MPA requires sampling (D-Optimal design) in the entire domain represented by the uncertain variables. Design of experiments technique is used to efficiently select the data points required for the construction of MPA.

These types of designs are always an option regardless of the type of model the experimenter wishes to fit (for example, first order, first order plus some interactions, full quadratic, cubic, etc.) or the objective specified for the experiment (for example, screening, response surface, etc.). Given the total number of treatment runs for an experiment and a specified model, the computer algorithm chooses the optimal set of design runs from a *candidate set* of possible design treatment runs. This candidate set of treatment runs usually consists of all possible combinations of various factor levels that one wishes to use in the experiment.

Uncertainty Quantification Method

The problem dealt with here is the estimation of the membership function of the response subject to uncertain input parameters. The uncertainty is non-random and it is defined using the fuzzy set theory. The estimation of the fuzzy membership function for the implicit response requires the use of interval analysis at each α level. The interval analysis techniques available in the literature as discussed earlier use linear approximation at the central values or evaluate the function at all the vertices formed by the lower and upper limits of the uncertain variables. These methods require a significant number of function evaluations and sometimes fail to capture the bounds of response for non-monotonic response functions. Therefore, a method using the nonlinear function approximations to reduce the computational effort involved in the analysis is presented. The UQ method has two main tasks: (1) Fuzzification; and (2) Computation of fuzzy response based on extension principle. These are discussed below:

Fuzzification

A fuzzy set is an imprecisely defined set without a crisp boundary and it provides a gradual transition from 'belonging' to 'not belonging' to the set. The process of quantifying a fuzzy variable is known as fuzzification. When the input parameters are uncertain then they have to be fuzzified. This is done by constructing a membership function (possibility distribution) for the variable. In the present work, convex normal triangular membership functions are used to characterize the fuzzy input variables.

Fuzzy Membership Function Estimation

In order to employ the extension principle, the membership function of the response is obtained from the surrogate model of the response, using multi-point approximations. Then this approximation is used along with the numerical estimation method for estimating the membership function of the response.

The following are the main steps involved in the approximation of the response

1. Use design of experiments to obtain the location of design points that are used to approximate the response

2. Perform actual analysis and obtain the function value and gradients of the response at the above selected design points
3. Construct TANA2 at the design points and blend them into a single approximation using the Multi-Point Approximation (MPA) techniques
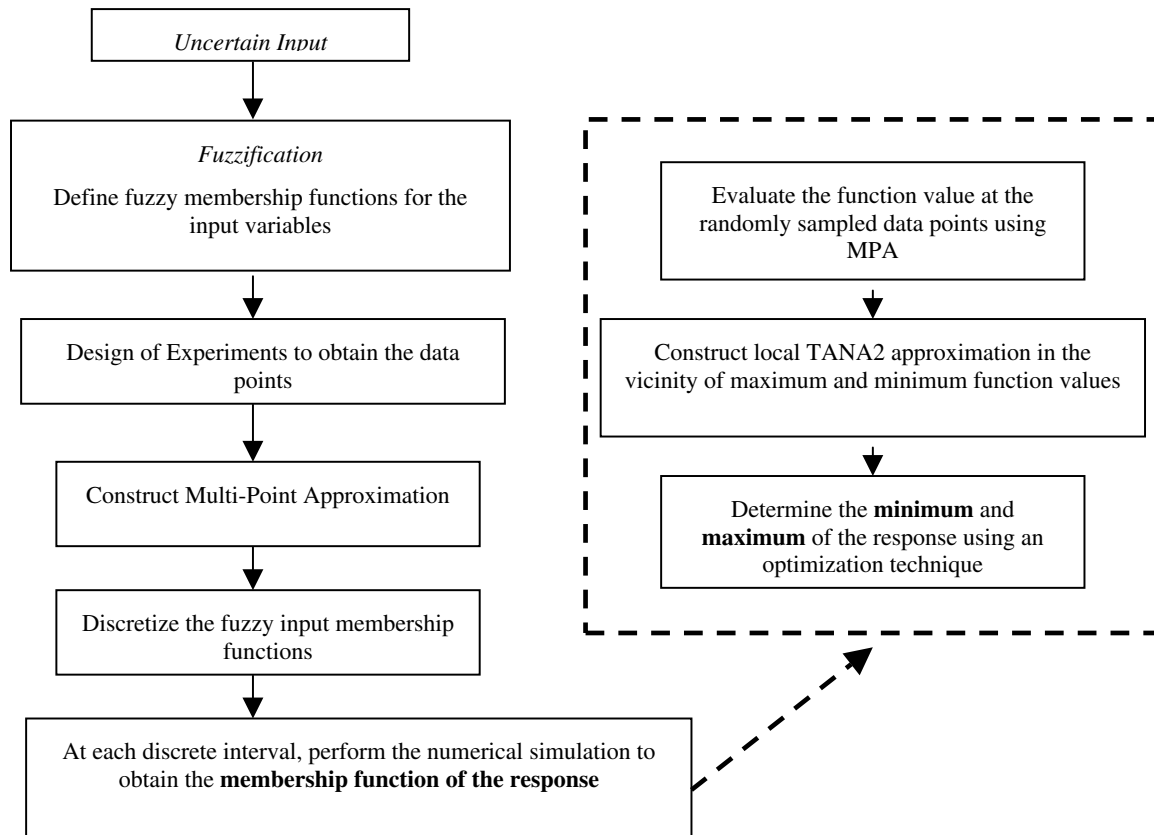
Figure 1 Possibilistic Structural Analysis Algorithm

      Once the fuzzy input variables and the approximate response function are available, the vertex method can be used on the approximate response function to obtain the bounds on the response. However, the vertex method is computationally expensive and does not produce accurate results when the response is non-monotonic. Therefore, a more robust method to accurately estimate the bounds of the response at different possibility levels is presented in this work.

The following are the steps involved in estimation of the bounds on the response:

1. Discretize the membership function of the input parameters at various α cuts (possibility levels). At each of these discretized level the maximum and minimum of the response are calculated to construct the membership function of the response.
2. Evaluate the approximate function value at randomly sampled data points for each discretized α level. The data point that results in a minimum function value is used as a starting point of the optimization process. The data points are selected by using uniform distribution for sampling. This assumption of uniform distribution does not affect the final result because it is used only to sample the data. Use of a different distribution would assume bias towards a certain region in the entire design space and would result in erroneous results.
3. Use TANA2 approximation during the search process to reduce the computational cost. The TANA2 approximation is constructed using new data points in the vicinity of the data point determined in step 2.
4. Repeat step 2 to obtain a maximum value of the response by constructing new TANA2 approximation.

      Once the minimum and maximum values of the function are obtained, the membership function of the response can be determined. Using this membership function the possibility of failure for the structure can be determined using the possibility theory. Figure 1is a pictorial representation of the UQ method. The

process in the dotted lines, in figure 1 is the numerical technique used to determine the membership function of the response.

Flexible Wing Example

Figure 2 shows the structural model of the flexible wing whose membership function for the frequency response is considered. The structure represents a fighter wing model with all the dynamic characteristics. There are 118 nodes in the wing section, 12 nodes in fuselage part and one reference node. The connection of the wing to the fuselage is modeled using simple beam elements. The upper and lower skins are modeled using quadrilateral and triangle membrane elements. The rib and spar webs are represented by shear panel elements, while the rib and spar caps are represented by rod elements. The vertical stiffness is supported by rod elements.

The wing structure is composed of 562 elements, which are classified as skins, ribs, spars, rib caps, spar caps, and posts. The weight of the whole fuselage is 16,000 lb and due to symmetry, each wing carries 8,000 lb. In addition to the load, 1,600 lb of nonstructural mass is distributed among the free nodes. First natural frequency of the structure is considered as the response in this example. The structure is analyzed using the finite element software ASTROS [20].

The response function considered in this example is as shown below:

$$G(X) = \frac{(2\,\pi\,f)^2}{\lambda_1} - 1$$

where f is the lower limit on the fundamental frequency that is 3.0 Hz. and λ_1 is the fundamental eigenvalue. The vector X represents all the uncertain variables defined as triangular membership functions. Table 1 shows the lower and upper limits of the uncertain variables along with the central value used to construct the triangular membership functions.

The uncertain variables are obtained by using physical linking of the design parameters in order to reduce the size of the 562 element problem. Physical linking facilitates the reduction of number of uncertain variables, so that manufacturing and assembly issues are represented in modeling. At the same time, the computational schemes can be applied to practical large-scale problems. Upper wing skin is modeled to have the chord wise element thickness as uncertain variable. This linking results in seven uncertain variables for the upper skin since there are seven rib sections excluding the root. The lower skin properties are matched to the properties of the upper skin. The upper and lower spar caps are assigned one uncertain variable. The leading edge spar web is assigned one uncertain variable and the upper and lower spar caps are assigned one variable. Seven variables are used to model the spars. There are seven rib sections that are assigned one uncertain variable each. The upper and lower rib caps are modeled as one variable. The smart actuators are modeled as one variable and the vertical stiffeners are modeled as another variable.

The values of the uncertain variables are taken from an optimization study. The optimization study was performed using the weight of the structure as the cost function and this is minimized subject to a frequency constraint. A lower limit of 3 Hz was used as a constraint on fundamental frequency. The structure was optimized with this frequency constraint and the final design is selected as the central design. The initial weight of the structure was 13,000 lb. and the final design had a weight of 9833 lb. Figure 3 shows the iteration history for the above optimization problem. Once the central design is selected, uncertainty is modeled as deviation from the central design. This type of modeling would be suitable when dealing with designs that have tolerance information.

D-optimal design technique was used to select 512 data points to construct MPA for the response function. Local TANA2 approximations were constructed using the data points and these were blended using a blending function to obtain one MPA. Once the approximation is constructed random sampling is performed in the uncertain space and the maximum and minimum for the function are determined. These maximum and minimum points are perturbed and new simulation is performed at the perturbed data points. This additional information is used in constructing a new TANA2 approximation that is used to determine the lower and upper limit of the response.
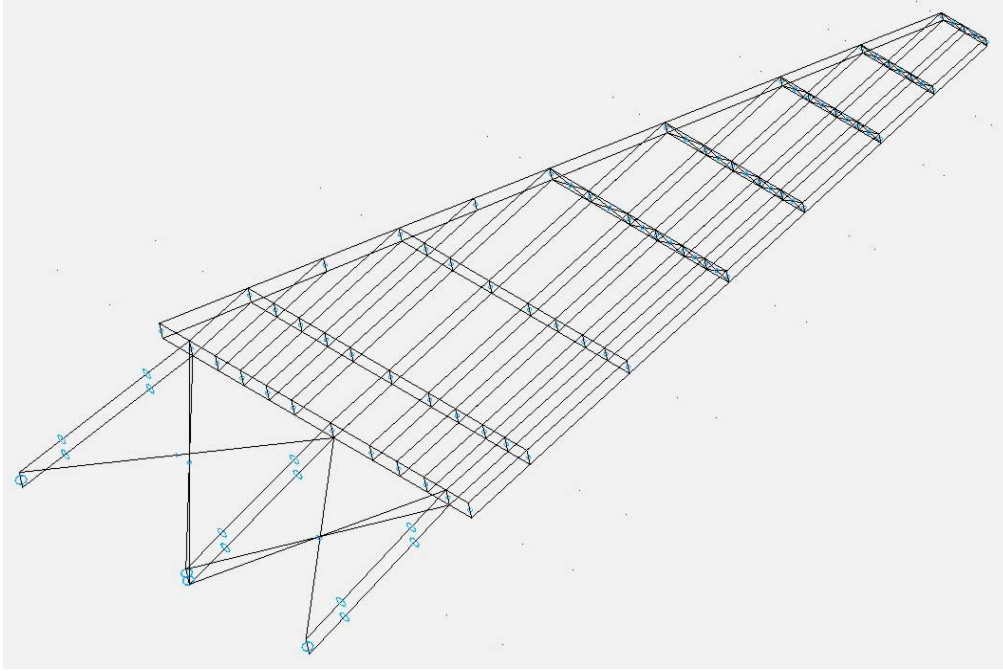
Figure 2. Flexible wing structural model

At every data point, the function value and gradients are estimated using ASTROS. The gradients are available analytical at every data point. A total of 572 simulations were performed to obtain the membership function of the response. Each of these simulations is a computationally expensive finite element analysis. Among these, 512 simulations are performed at each of the data points from the D-optimal design, 40 simulations were required to construct the TANA2 approximation, used in optimization to find the maximum and minimum. Finally 20 simulations were performed to obtain the actual function value at the optimum points for minimum and maximum values.
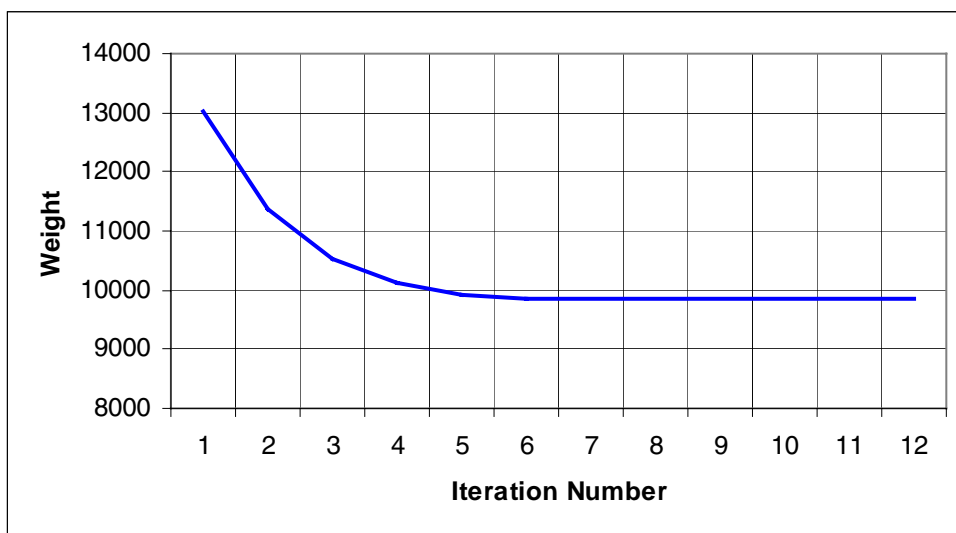
Figure 3: Iteration History

These lower and upper limits are obtained at each of the possibility levels to produce the membership function of the response as shown in Figure 4. The membership function determines the bounds on the response at various confidence levels. For example, the response value would be equal to –

0.00153 if the structural parameters were deterministic and assumed the central value. However, the uncertainty in the input data would result in the bounded response depending on the bounds of input parameters.

The possibility of failure is equal to the maximum value of the confidence level in the range of response values considered. For example, from the plot of the membership function of frequency, the possibility of failure that the frequency would be less than -0.1 is 47%. This is obtained by considering the interval from –0.1 to the lower limit when the confidence level is 0 and taking the value of the maximum confidence level for all those values. The possibilistic analysis method is an efficient technique to estimate the possibility of failure of the response. The efficiency of the method is achieved by using the high fidelity surrogate models for the response.

Uncertain Variable	Lower Limit (in.)	Central Value (in.)	Upper Limit (in.)
1	0.10	0.130	0.15
2	0.06	0.080	0.10
3	0.05	0.070	0.09
4	0.04	0.056	0.08
5	0.02	0.036	0.05
6	0.01	0.020	0.03
7	0.01	0.020	0.03
8	0.01	0.020	0.03
9	0.01	0.020	0.03
10	0.01	0.020	0.03
11	0.01	0.020	0.03
12	0.01	0.020	0.03
13	0.01	0.020	0.03
14	0.01	0.020	0.03
15	0.02	0.026	0.031
16	0.01	0.015	0.02
17	0.03	0.040	0.05
18	0.01	0.020	0.03
19	0.01	0.020	0.03
20	0.01	0.020	0.03
21	0.01	0.020	0.03
22	0.01	0.020	0.03
23	0.02	0.030	0.04
24	0.02	0.030	0.04
25	0.035	0.045	0.055
26	0.01	0.020	0.03
27	0.01	0.020	0.03

Table 1: Bounds on the Uncertain Structural Parameters

A value of possibility equal to zero means that there is no possibility and a value of one indicates maximum possibility. The above membership function describes the relationship between the possibility level and frequency. The membership function can give information about the possibility for a range of frequencies. In this technique, the structure can be designed to operate in the range of response values that satisfy certain confidence level requirements.

Therefore, when designing a structure such as this fighter wing, the designer must decide what level of confidence has to be achieved for the design. Once that confidence level is decided, the problem boils down to controlling the various uncertain parameters in order to obtain a required membership function. These uncertain parameters can be controlled by posing this as an optimization problem where the objective could be minimization of weight of the structure and the constraint is that the possibility of a particular value (say frequency less than a certain limiting value) is less than a predetermined level of confidence. This optimization task would produce a design whose frequency is within the acceptable range at a particular level of confidence and also the structure would have least weight.
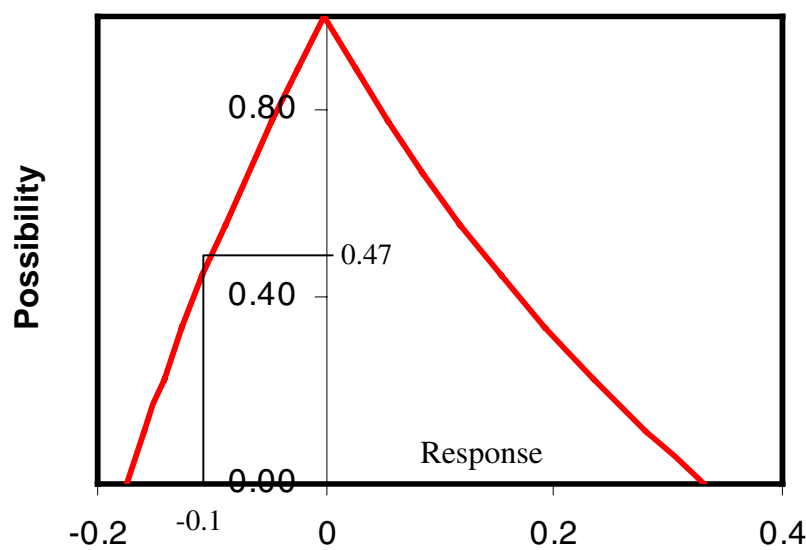
Figure 4: Bounds on Frequency Response

Summary

The uncertainty quantification method presented in this paper aims at reducing or even eliminating the testing on prototypes during the intermediate stages. These methods can be used to determine the variance in the response analytically and the design can be updated according to this information. This reduces the cost and time for military vehicle acquisition considerably. Moreover, these methods can also be used to develop a targeted testing procedure for the final design prototypes thereby, reducing the number of actual tests.

In this paper a methodology for dealing with vague information is presented. In the presence of vague information, usual practice is to assign some distribution information that closely matches the available information. However, this practice would introduce more uncertainty into the system and the results obtained can be orders of magnitude away from the actual failure probability.

Therefore, the presented method uses the available information without assuming any additional information and predicts the possibility distribution for the response. This possibilistic analysis is useful in the preliminary design stage where very less data is available for the design parameters. The efficiency of the UQ method is evident when dealing with the implicit response functions that require expensive FEA

simulations to obtain the function values. Therefore, the use of function approximations is emphasized to reduce the computational cost involved in the analysis procedure.

In possibility analysis a membership function has to be assigned for the uncertain variable. This membership function can be constructed when the intervals information at various confidence levels is known. However, this information is usually unavailable, therefore, a distribution is assumed that best represents the available data. In this paper, a triangular membership function is assigned to the uncertain variables because it is assumed that the data is dispersed around a central design. The membership function of the response depends on the assumption of a distribution for the individual uncertain variables. Therefore, assumption of an invalid distribution would produce results that do not represent the actual problem. However, the values of the response at zero percent confidence are not dependent on any kind of distribution information. Therefore, when there is absolutely no information about the uncertain variables the analysis is performed at zero percent confidence.

The possibilistic analysis method discussed here would estimate the bounds on the response subject to uncertain intervals. These bounds give an insight into the problem and they can be used to design structures that are less sensitive to the uncertainties in the input parameters. These bounds can be used in an analysis procedure that adjusts the bounds of input parameters to determine a configuration of these parameters that would result in the narrowest bound on the response. Moreover, the worst-case bounds on the response can be forced to fall in the safe operating zone to obtain a highly reliable component or system. These design configurations produce structures that are robust and perform safely in an uncertain operating environment.

Acknowledgements

References

1.   Penmetsa, R. C., and Grandhi, R. V., "Efficient Estimation of Structural Reliability for Problems with Uncertain Intervals," *Accepted for Publication in International Journal of Computers and Structures*, November 2001

2.   Penmetsa, R. C., and Grandhi, R. V., "Structural System Reliability Quantification using Multi-Point Approximations," *Accepted for Publication in AIAA Journal*, March 2002.

3.   Penmetsa R. C., and Grandhi R. V., "Structural Failure Probability Prediction Using Fast Fourier Transformations for High Accuracy," Journal of Finite Elements in Analysis and Design (to appear), 2002.

4.   Cia, G.Q. and Elishakoff, I., "Refined Second-Order Reliability Analysis," *Structural Safety*, 1994, 14(4), pp. 267-276.

5.   Yu, X., Choi, K. K., and Chang, K. H., "Mixed Design Approach for Probabilistic Structural Durability," *Structural Optimization*, Vol. 14 (2-3), 1997, pp. 81-90.

6.   Bucher, C. G., and Bourgund, U., "A Fast Efficient Response Surface Approach for Structural Reliability Problems," *Structural Safety*, No.7, 1990, pp.57-66.

7.   Zadeh, L., "Fuzzy Sets," *Information and Control*, Vol. 8, 1965, pp. 338-353

8.   Kaufmann, A., and Gupta, M., Introduction to Fuzzy Arithmetic, Van Nostrand Reinhold Company, New York, 1985

9.   Buckley, J. J. and Qu, Y., "Solving Systems of Linear Fuzzy Equations," *Fuzzy Sets and Systems*, Vol. 43, 1991, pp.33-43

10.   Sanchez, E., "Solution of Fuzzy Equations with Extended Operations," *Fuzzy Sets and Systems*, Vol. 12, 1984, pp.237-248

11.   Zhao, R., and Govind, R., "Solutions of Algebraic Equations Involving Generalized Fuzzy Numbers," *Information Sciences*, Vol. 56, 1991, pp.199-243

12.   Vallipapan, S., and Pham, T. D., "Fuzzy Finite Element Analysis of a Foundation on an Elastic Soil Medium," *International Journal for Numerical and Analytical Methods in Geomechanics*, Vol.17, No.11, Nov. 1993, pp.771-789

13.   Briabant, V., Oudshoorn, A., Boyer, C., and Delcroix, F., "Nondeterministic Possibilistic Approaches for Structural Analysis and Optimal Design," *AIAA Journal*, Vol.37, No.10, October 1999, pp. 1298-1303

14.   Hansen, E. R., Global Optimization using Interval Analysis, Pure and Applied Mathematics Series, Marcel Dekker, New York, 1992

15.   Dong, W. M., and Wong, F. S., "Fuzzy Weighted Averages and Implementation of the Extension Principle", *Fuzzy Sets and Systems*, Vol. 21, 1987, pp.183-199

16.   Lallemand, B., Plessis, G., Tison, T., and Level, P., "Neumann Expansion for Fuzzy Finite Element Analysis," *Engineering Computations*, Vol. 16, N0. 5, 1999, pp.572-583

17.   Akpan, U. O., Koko, T. S., and Orisamolu, I. R., "Response Surface Based Fuzzy Analysis of Structural Analysis of Structural Systems," *Proceedings of 41st AIAA/ ASME/ ASCE/ AHS/ ASC Structures, Structural Dynamics and Materials Conference*, Atlanta, GA, April-2000, AIAA-2000-1634

18.   Xu, S., and Grandhi, R. V., "Multi-Point Approximation Development: Thermal Structural Optimization Case Study," *International Journal for Numerical Methods in Engineering*, Vol.48, No. 1, 2000, pp.1151-1164

19.   Rao, S. S., and Weintraub, P. N., "Modeling and Analysis of Fuzzy Systems using Finite Element Method," *Proceedings of 41st AIAA/ ASME/ ASCE/ AHS/ ASC Structures, Structural Dynamics and Materials Conference*, Atlanta, GA, April-2000, AIAA-2000-1633

20.   Neill, D. J., Herendeen, D. L., and Hoesly, R. L., ASTROS User's Manual, Vol 1, WL-TR-93-3025, 1993

Paper #26

Discussor's Name: Steve Whittle
Author's Name: Ramana Grandhi

Q: Your presentation concentrated on how input uncertainty propagates through models to produce levels of uncertainty in the output properties. Equally important are levels of uncertainty in the model itself. Have you considered/completed model dependability analysis in you research?

A: Uncertainties in simulations come from many sources such as input parameters, finite element models, type of elements, numerical analyses selected, nonlinear solution techniques chosen, initial conditions, assumptions in solvers, and soon. This presentation concentrated on input parameters and we are in preliminary stages of research in model uncertainty and including them. The key factor is how to characterize model uncertainties and then choosing a proper method for propagation in simulation.

Analytical Support in Aircraft Certification

Jakub Kaczkowski
Wojciech Potkanski
Institute of Aviation
Al. Krakowska 110/114
02-256 Warsaw
Poland

1   Abstract

The high cost of designing a new airplane enforced engineers to look for new cheaper methods. One method for the cost reduction is wide use of computer simulations in designing and certification process. From many different methods of analysis, FEM appears to be the best, but in spite of all improvements, present level of fidelity is still too low to completely eliminate experiments in the designing process. This explains why Building Block Approach is still the main method for designing, but certification process, which is only verification one, is more suitable for use computer methods only. Results of static tests and FEM analysis for two airplanes designed in the Institute of Aviation will be shown in this presentation. To allow for comprehensive insight of the problem of fidelity of analysis, two different airplanes were selected. First one is the metal jet trainer I-22 Iryda designed according to the AP970 regulations and the second one - four places all-composite aircraft designed and certified according to the FAR.23 regulations.

2   Iryda I-22 and PZL I-23 Manager Aircraft

The I-22 and I-23 Manager aircraft are the newest products of the, operating for the last 70 years in Warsaw, Institute of Aviation (ILot). Founded in 1926, the Aviation Institute initially concentrated on testing and issuing certificate of airworthiness. After the WW2, it has broadened its scope of activity onto the design of flying apparatus of sorts. The successful designs of the first Polish, Gil (1946), and Zuk (1959) helicopters, were created here. A few training-fighter jets were designed as well, one of which, namely TS-11 Iskra won a set of world records to its name. A reconnaissance airship, and the line of rescue hovercraft vessel designs, were also successfully undertaken. The mentioned above training-fighter jets, were equipped with the series of the jet engines designed by the Institute, of which the most noteable are the SO3 and K16.

Fig. 1 Last M96 version of training - fighter jet I-22 Iryda

Fig. 2 Personal & Business aircraft PZL I-23

Herein the latest version of the I-22 Iryda aircraft is presented. This is a highly maneuverable development version, where, in comparison to the previous one, the new wing with the Fowler flaps and LERX slots has been introduced, as well as the fin lengths increased, in order to provide additional stability at large angle of attack. The I-23 Manager is a single jet engine, low-wing monoplane provided with the classical tail units and tri retractable landing gear. The airframe structure is almost exclusively composites. Thanks to that and a thorough aerodynamics the 1200 km extreme range of the plane has been reached.

3 Design computations

The Institute of Aviation (ILot) customarily applies the three stage computational process, wherein increasing accuracy models are analyzed, for the designs of military and transport aircrafts.

First stage of analysis - choice of load cases for strength calculations.

The MEWA system worked out by the ILot is utilized at this stage. The idea of this being to use the superimposing of simple structural and aerodynamic models.
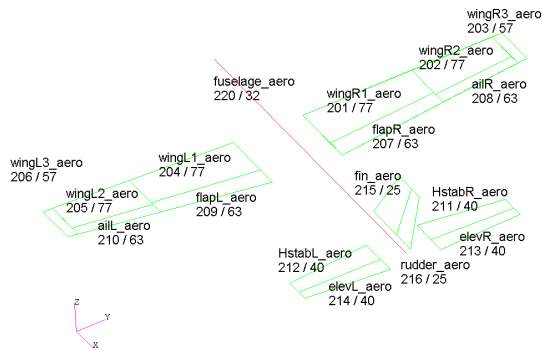
Fig. 3 PZL I-23 aerodynamic loads model   **PZL I-23 structural loads model**
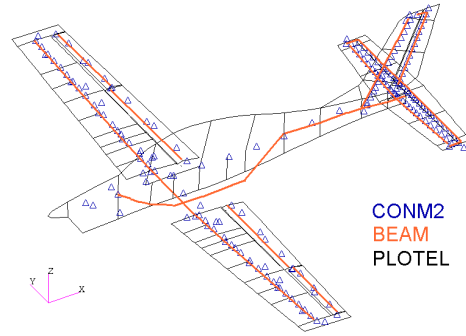
The modified Multhopp's method is applied to determining aerodynamic loads. It yields very good results to the wings of moderate to high aspect ratio. The modification of the classical Multhopp's method entails complementing the Multhopp method by the calculations of the potential flow over once bent thin plate, so that the characteristics of the pitching moment, determined in aerodynamic tunnel, can be achieved.

The load, defined in such a manner, is later applied to the simplified by beams, model of the plane's structure. The resulting from the above distributions of moments and forces in the beams allows selecting critical load cases, dedicated for further analysis. Around a thousand different load cases are analyzed. For instance, for the PZL I-23 aircraft 14 mass variations were considered. This permitted to separate a certain group of load cases for further more detail strength calculations. In the concrete case of PZL I-23 aircraft 67 load cases were chosen for further computations.

Second stage computing model - general strength analysis

In this phase the Finite Element Method is usually used for analyzing of an aircraft as a whole or any of its main systems. To permit these models to be effectively utilized they have to be small. The upper limit of the FEM models built in the last decade of twentieth century, in ILot did nor exceed 20 thousands elements. At present, thanks to the technical progress, the models can go up to 200 thousand elements. The twenty thousands number limit caused the global models to have low mesh density, roughly from 1 to 6 elements per one skin panel. The adopted accuracy, not permitting for in depth modeling of a plane detail, was not a problem, because adopted models served solely for determining the distribution of internal forces in members. It was so, because only in the third stage, the detail local analyzing of strength was performed.
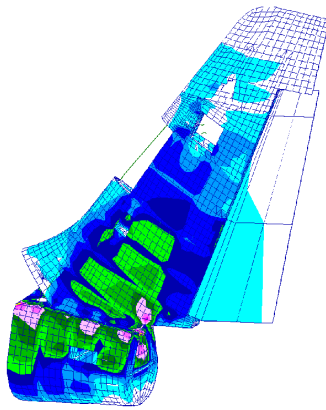
Fig. 4 Global FEM model of the I-22 aircraft vertical tail
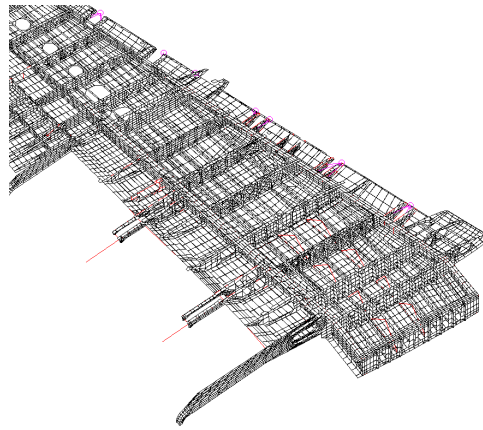
Fig. 5 Global FEM model of the wing, without the top skin, of the I-22 Iryda aircraft

Third stage computing model - local strength analysis

The internal loads determined in the previous stage serve now for the purpose of the strength analyzing of particular aircraft structural elements. Various calculating methods are applied at this stage - the mix of FEM and analytical methods, depending on the degree of complexity of the real object.
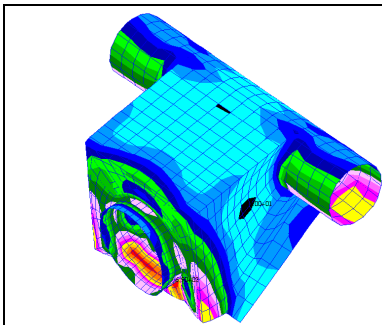
Fig. 6 PZL I-23 aircraft engine shock absorber seat.	PZL I-23 aircraft wing's flap fitting	I-22 aircraft flight controls component
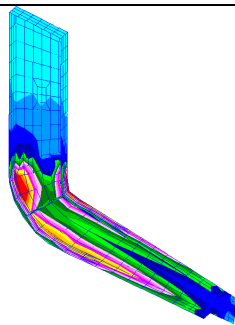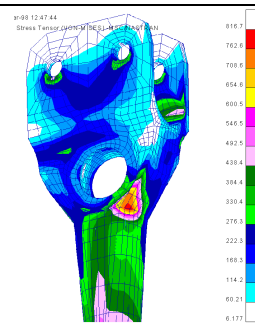
Because the PZL I-23 has been classed as the tourist aircraft, in order to save costs of designing process, some simplifying approach was adopted in combining the two and three stages. In so doing a global computational model of increased accuracy was arrived at.
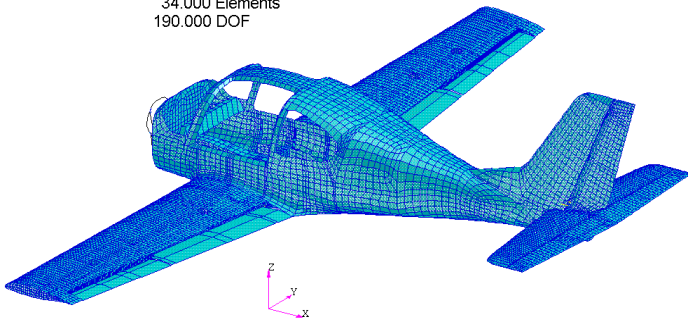
Fig. 7 PZL I-23 aircraft Global FEM model.

Size of the model rendered it impractical for calculations. It was therefore divided into separate models

1) Fuselage with engine frame
2) Wing
3) Horizontal Tail
4) Rudder
5) Flaps
6) Ailerons

A choice of models is presented below
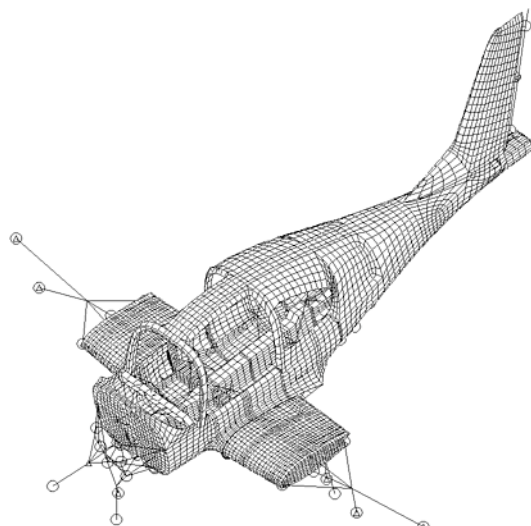
Fig. 8 Fuselage model of PZL I-23 aircraft
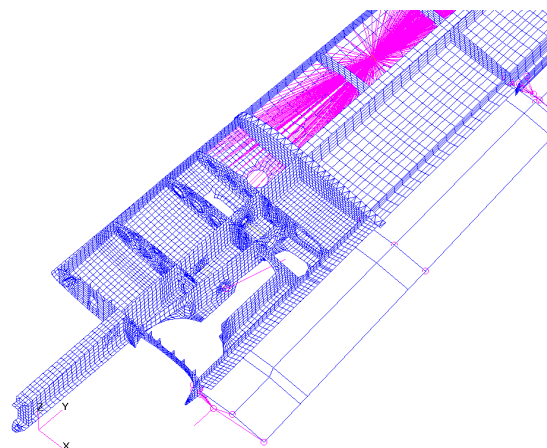
Wing model of PZL I-23 aircraft (view after top skin removal)

Strength calculations were performed using system MSC.Nastran in the case of PZL I-23 aircraft linear calculations were predominantly performed: linear static and linear buckling. In the case of metal made I-22 Iryda, non-linear calculations in full range of both geometry and material were performed.

The fact that the calculations for the PZL I-23 aircraft were limited to the linear bracket only, stems from the properties of composites are linear and for this type of structure one resigns off the structure work, once the stability has been lost.

The program RCS, devised by the ILot, permits to analyze vast number of load cases thanks to "the automatic charging the model with load cases". For example, in the computations of the PZL I-23 aircraft, in total 67 cases of loading were taken into account. The fuselage was computed for 25 load cases, and the wing for 32 cases, engine frame for 13, horizontal tail for 6, rudder for 3, and the flaps for 2 loading cases.

In cases of laminated and composites structures to assess the strength the First Ply Failure hypothesis was applied. The strength of each ply was adjudicated by means of Tsai-Hill hypothesis. The allowable level of stress were determined as a result of material tests. On the PZL I-23 aircraft joits were predominantly glued and then screwed together to ensure the correct pressure in assembling. While assessing strength, the calculated intensities of the shear and normal forces in the joint were compared with the forces determined in the materials tests. A novelty being that in the calculations normal forces were allowed for, and not only shear forces.
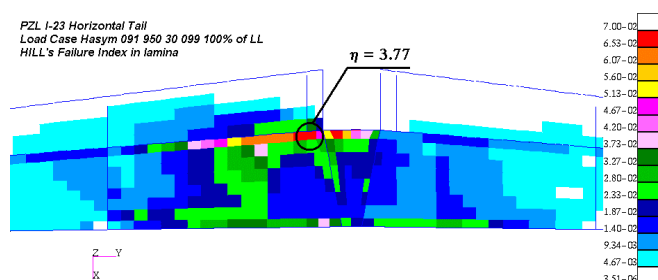
Fig. 9 Distribution of failure indexes in bottom skin of the horizontal tail of PZL I-23 aircraft
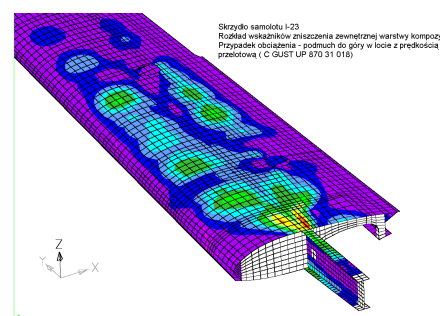
Distribution of failure indexes the wing skin of PZL I-23 aircraft

The metal structure strength was analyzed by checking the magnitude of von Mises stresses, found in the way of non-linear computations, with allowance for plasticity phenomenon.
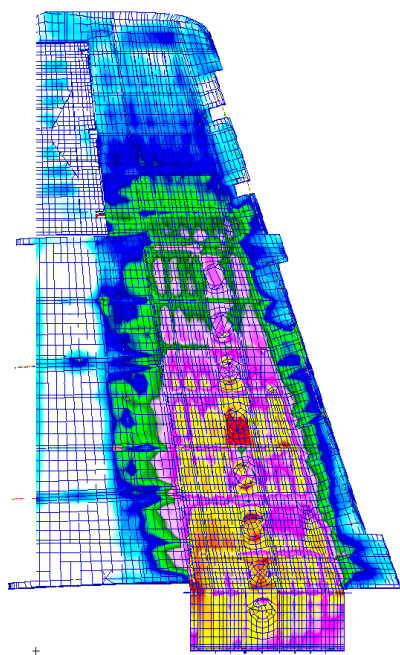
Fig. 10 Distribution of von Mises stress in wing of I-22 Iryda aircraft; load case – point D of the maneuvering envelope.
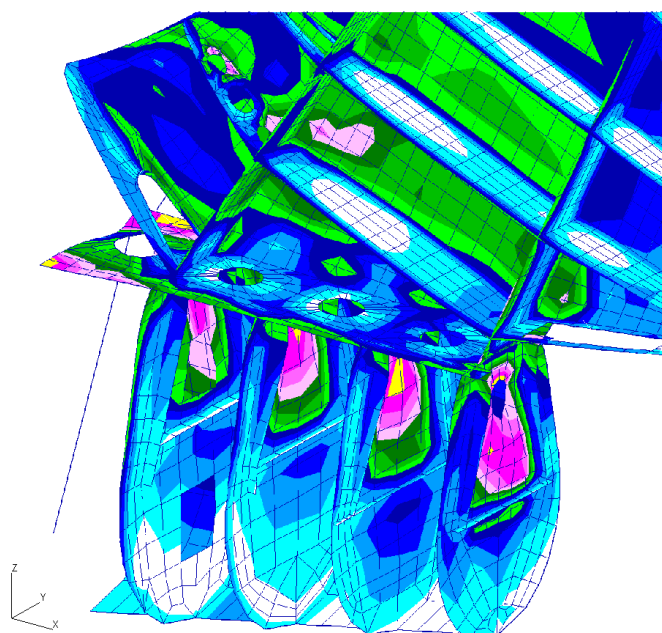
Distribution of von Mises stress in the junction of vertical tail with the bodywork of I-22 aircraft.

The performed computations not only allowed to design the structure, but to substantially decrease the number of load cases to conduct, during the static tests. Utilization of computer methods in aircraft design process, allows considering the influence of those cases on the design in question, which are not yet required by the regulations and standards in force. In the design of the structure of PZL I-23 aircraft, the results of the dynamic simulation of the whole vessel hitting the ground were taken into account, although the amendment 42 of FAR23 regulations, calls only for the dynamic check of the pilot - pilot's seat system.
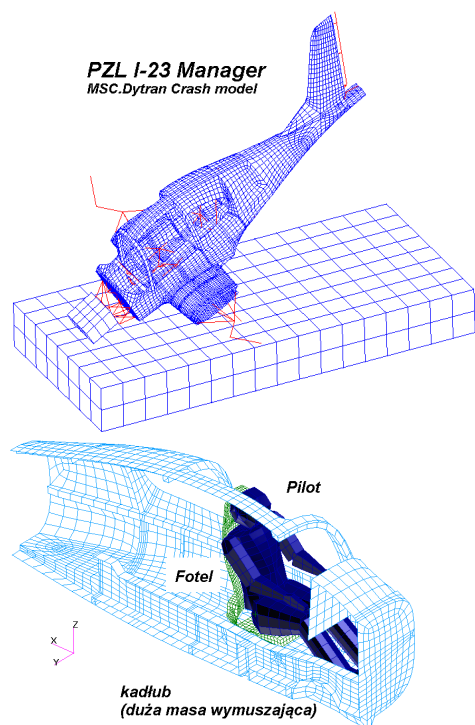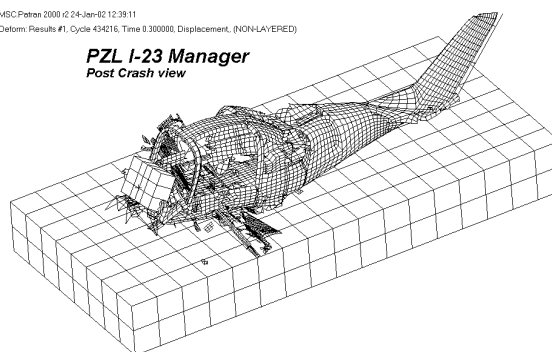
Fig. 11 Crash analysis of the PZL I-23 aircraft

Analysis performed on two levels, global i.e. by analyzing mode of aircraft destruction, and local, by analyzing pilot's reaction in the crash
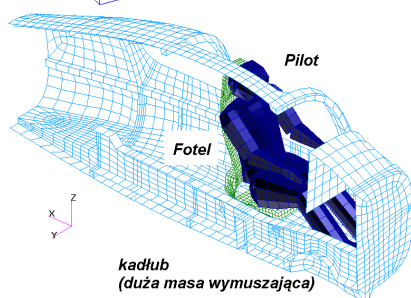
4 Certification Process

For brevity sake, and also because the Iryda I-22 plane having been a military product, undergoes the different cycle of qualifying tests, we will here concentrate in some detail on the certification process of the composite aircraft PZL I-23 only. Because of the materials used in its construction, the PZL I-23 is not a typical aircraft, and for that reason the certification process must not completely resign from static tests. The FAR 23.307 regulation allows to apply - in the proving process of aircraft structures - analytical methods, provided that experience has already proved, these methods. In the case of PZL I-23 aircraft the computations performed allowed only to substantially reduce the number of load cases called for in the static trials.

Tab 1 Summary of strength tests of the PZL I-23 aircraft

No	Element investigated	Critical load case	Notes
1	Horizontal Tail	A Man Upd 950 30 091 Hasym091 950 30 099P	FAR 23.423(a), - A sudden deflection of the elevator controls
2	Pilot's seat	ELDC – 3 cases C GUST UP 630 15 018 Crash Test – 2 cases.	Emergency landing condition Positive Gust load FAR 23.333(c) Emergency landing dynamic condition – FAR 23.562 (b)
3	Aircraft controls	41 load cases	Lage number due to the lack of analysis
4	Wing flap	FL H GUST	A head-on Gust FAR 23.345 (c) (1)
5	Aileron	C AIL 950 30 052	Sudden aileron deflection - FAR 23.349 (b)(d)
6	Rudder	AV MAN 950 30 058 Mod	A Sudden rudder deflection FAR 23.441(a)(1)
7	Engine frame	9 load cases	
8	Fuselage	AV MAN 950 30 058 Mod A MAN UPd 950 30 091 Hasym009 825 21 078 L A 1150 Mod LL2P25 1117 28 103 ELC Complete turnover	Sudden rudder deflection. FAR 23.441(a)(1) Sudden elevator deflection FAR 23.423(a) Point A of the man. envelope. FAR23.333 (b) Level Landing - FAR 23. 479(a)(2)(ii) Complete turnover - FAR 23.561 (d) (2)
9	Wing	A 1150 Mod SL 950 30 109 LL2P25 1117 28 103	Point A of the man. envelope. FAR23.333 (b) Level Landing - FAR 23. 479(a)(2)(ii)
10	Landing gears	LL2P25 1117 28 103 SL 950 30 109 Dynamic testing	Level Landing - FAR 23. 479(a)(2)(ii)
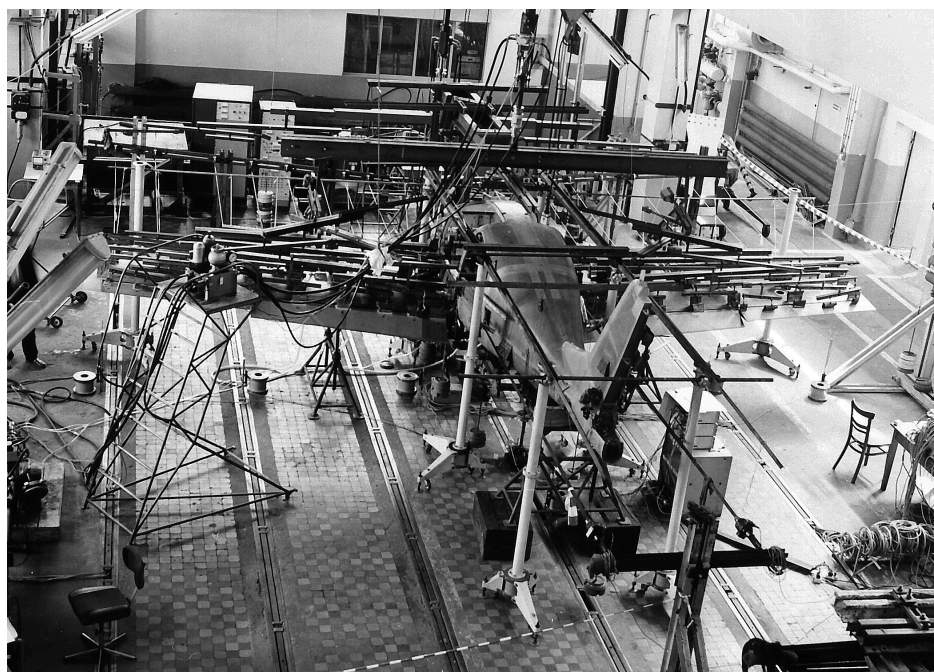
Fig. 12 PZL I-23 aircraft in the course of static tests – load case A 1150 Mod.

Depending on needs the testing were carried under two types of climatic conditions:
- room conditions (temp apprx 18 deg C, RH normal)
- hot conditions (temp apprx 55 deg C, RH elevated)

Due to the fact that PZL I-23 aircraft has been made of composites, two additional ultimate load factors were allowed.

υdm allowing for random distribution of material properties, and equal:

υ_{dm} 1.19   For manually saturated elements. Determined on the ground of strength variability coefficient, in bending test of W-3 helicopter rotor blade coupons (WSK Swidnik)

1.10   For elements made by vacuum forming of prepregs in autoclave. Determined on the grounds of the manufacturer, CIBA, delivered data.

υdk - allowing for strength drop due to temperature and humidity

υdk = 1.18   For the whole structure, both for elements made of glass fabrics delivered by Interglass (fuselage) and for delivered by CIBA prepregs (wing). The coefficient value was determined no strength of the tests of material samples, conducted in ILot. The drop in value of dynamic shear modulus was taken as a criterion.

Furthermore the special coefficients given by FAR 23.619 and FAR 23.785 remain in force. Finally the following magnitudes for the ultimate load coefficient were taken:

Tab. 2 Coefficients of ultimate loads required

	Test conditions	
Element investigated	Room temperature	temp. 55deg C
Metal elements: engine frame, ribs, landing gears	1.5	1.5
Metallic seat fittings	2.0	2.0
Metal fittings (isolated tests)	1.725	1.725
Composite elements made by hand resin saturation: fuselage, empennage, seats	2.11 (1.5 * 1.19 * 1.18)	1.78 (1.5 * 1.19)
Composite elements made from prepregs in autoclave: wing, ailerons, flaps	1.95 (1.5 * 1.1 * 1.18)	1.65 (1.5 * 1.1)

As can be seen from the table, the two different values for ultimate load coefficients for the metal and composite components, render the static testing complicated. Subject to need this problem was handled in different manner:

- by using metal substitute elements in static testing conducted with the load exceeding 150% of limit load,
- over sizing fittings, so that they could take increased load.
- conducting static test up to the load level corresponding to the load capacity of metal component. The strength of a composite construction, for the missing load level was proven by calculations. The models take for such calculations were scaled from the results of static tests.

5 Verification of calculations

Majority of the static tests were simulated in calculations; in this way the information on the accuracy of calculations was gained. In course of the static tests the following were analyzed:

- strains in extreme layers of laminate and metal skin in the places where stresses concentration was expected
- inner forces in components eg: the engine frame rods, components of control system
- reaction forces in joining nods, eg: wing-fuselage fitting
- structural displacements
- The beginning of instability were monitored

Due to space limitations only few chosen case with the closest to experimental results will be presented.

verification of strains in extreme layers of laminates

the measurements of the strains in the frame #1, performed during testing of the engine frame and the fuselage nose will serve as one verification example.
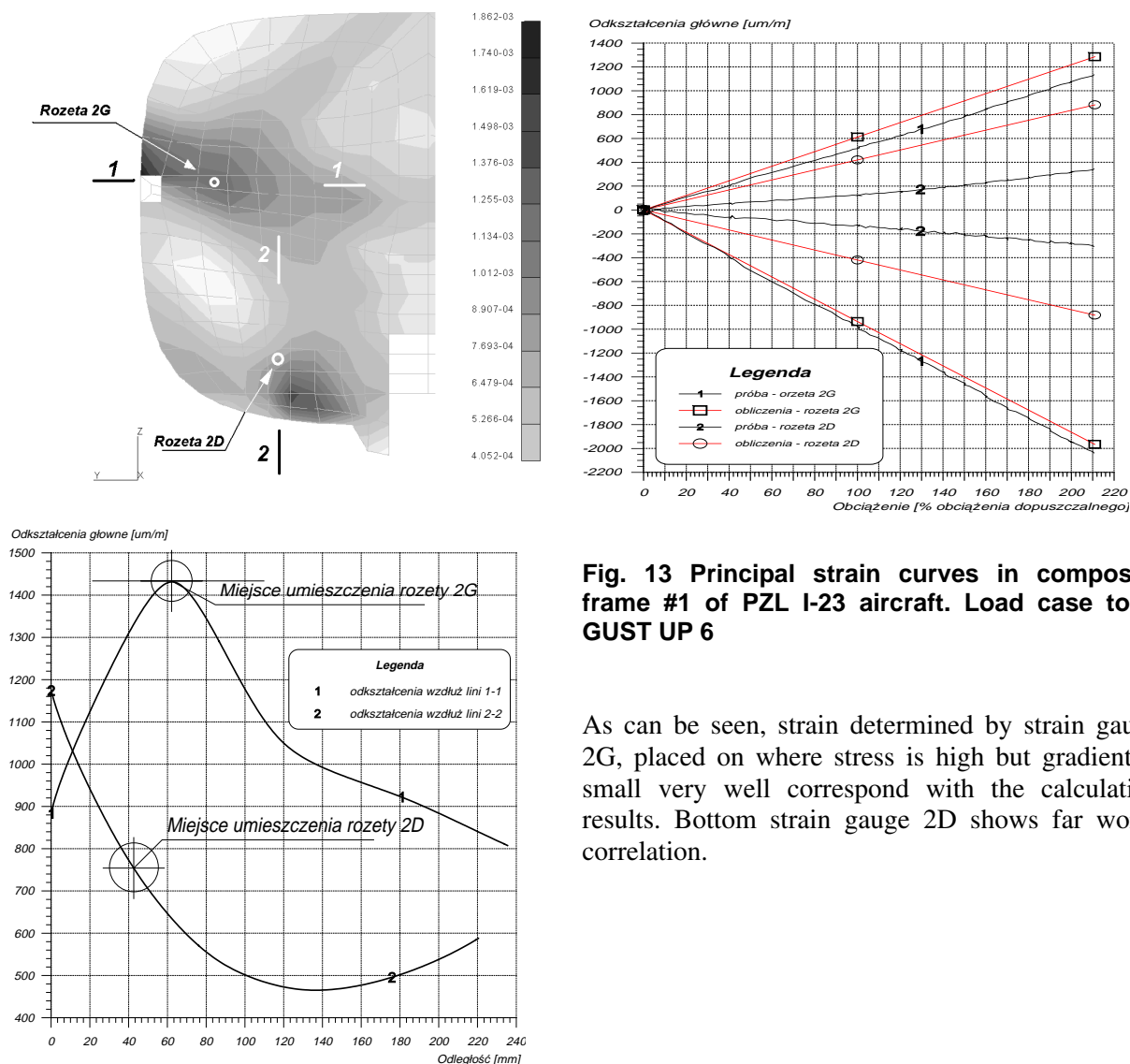
Fig. 13 Principal strain curves in composite frame #1 of PZL I-23 aircraft. Load case to C GUST UP 6

As can be seen, strain determined by strain gauge 2G, placed on where stress is high but gradient is small very well correspond with the calculation results. Bottom strain gauge 2D shows far worse correlation.

Verification of strains in metal skin

Rozeta 4/1D

Rozeta 4/6D

Rozeta 4/8D
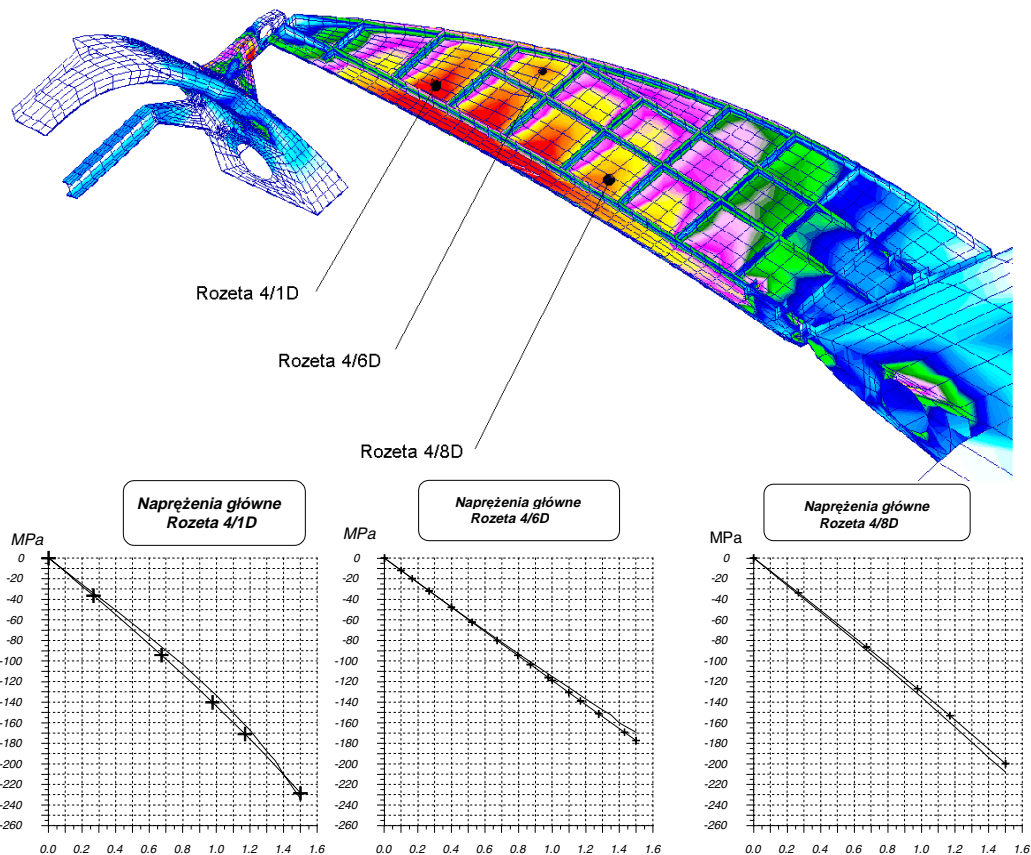
Fig. 14 Comparison of calculated results (+ denoted lines), with measured values during static testing, (smooth lines), in the wing strake (LERX slot) of the Iryda I-22 aircraft. The model for calculations was presented with the top skin "taken off", hence presenting the internal structure.

The comparison performed allowed to determine the calculation error, found from the formula:

$$\Delta = \frac{test\_results - calculated\_results}{test\_results} \cdot 100\%$$

Tab 3. Verification of calculation summary

No	Criterion	Error
1	Strains in the laminate	62 %
2	Strains in the metal skin	56 %
3	Internal forces in components	24 %
4	Reaction forces in connections	15 %
5	Deformation	23 %

The tests conducted allow to draw following conclusions:

1) The presented global models of metal and composite aircrafts do not differ much in the quality of obtained results. The errors in determined internal force and deformation and stresses and strains are similar.

2) The origin of relatively large, 60% error is simple. In static tests one searches for places of highest stress, and to this purpose strain gauges are glued in places of parameters discontinuity or disproportion, like small holes, rigidity changes etc. the global models by their very nature do not allow for them, allowing

for presenting the overall work of structure. If gauges were glued in regular areas then the results would remind those for internal forces.

3) The plastic properties of metal structures, which composites lack, decide that the stress determination does not pose bigger problem in strength calculation of metal structures. The influence of plasticity is best shown while contemplating a simple tension of a notched plate. Otherwise regular stress distribution changes its character near the hole. In some areas the stresses increase and in other decrease. The ratio of the maxim undisturbed stress to disturbed is called stress concentration factor. Its value depends not only on the sample's geometry but also from the stress (strain) magnitude.
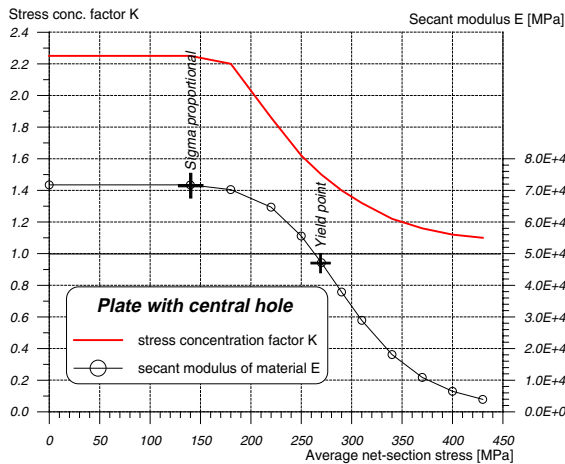
The graph presents that stress concentration factor decreases as yield stresses increases. On reaching ultimate tensile stress level the notch influence is negligible - the factor is close to 1.0

The presence of this phenomenon compensates inaccuracies of models used to assess the strength of metallic constructions. In case of composites their characteristics is linear. Stress concentration near notch exists in the whole regime of structure working, demanding detail, local models, similar to those used in fatigue calculations. Optionally, additional safety factors should be used in calculations.

Fig. 15 Stress concentration factor

6 Conclusions

The works conducted in ILot allow for following conclusions:

1) The state-of-the-art computational techniques do not yield the sufficient accuracy of results, so that the static tests could be abandoned.

2) In spite of relatively large stress determining errors static tests of metal structures generally run without major surprises, contrary to composite structures. The forgiving lack of failure in metal structures, in spite of not accounting for most of stress concentrations, is largely due to the plasticity phenomenon, absent in composites.

3) The application of additional safety coefficients for composite structures renders static testing complicated and more expensive. To avoid over sizing of metal components, computational proving of their strength sufficiency is necessary.

4) Necessity to use very particular computational models for composite structures, requires creating additional management systems for local models, so that very complex strength calculations might be more effective

5) Because still insufficiently developed theory of laminated materials, it seems mandatory to apply for the calculations additional safety factors, thus wasting possible mass benefits.

Analytical Qualification of Composite Structures

G.A.O. Davies, D. Hitchings
Department of Aeronautics, Imperial College
South Kensington
London SW7 2BY
United Kingdom

Abstract

The feasibility of replacing substructure and component testing by analytical "virtual testing" is addressed here for composite structures. The special difficulties in estimating the failure loads of composite structures are described, especially when initiation starts from a local stress concentration. Damage may initiate and then propagate, but final failure can occur at a load significantly higher than that for initiation. The separate modes of in-plane (fibre-dominated) and delamination (matrix dominated) are shown to need different strength and fracture strategies. Several examples are chosen of realistic structures, ranging from notches through to stiffened compression panels, starting with the easiest (in-plane dominated) and finishing with the most difficult mixed in-plane and debonding case.

1. INTRODUCTION

The need to replace expensive structural testing by theoretical simulation is no longer a contentious issue. It is accepted. In fact it was first explored in 1990 by an AGARD workshop "Analytical Qualification of Aircraft Structures" [Ref 1]. Amongst its conclusions twelve years ago was that "composite structures are more sensitive to secondary effects than metallic structures and, as a result, require more detailed local analysis than is used for metallic structures to model critical failure mechanisms and predict failure reliably". However no one doubts that full-scale static and fatigue tests will always be obligatory for both civil and military aircraft. The use of real or virtual testing for substructures and components is a choice that can be left to the designers and manufacturers who need to save resources and time-to-market, but also need to ensure that the full scale test will confirm the design safety factors. Why then are we certain that full scale tests will always be obligatory, when modern finite element software can quite quickly create models starting from the digital pre-assembly? (or electronic mock-up) One reason is the uncertainty in predicting the fatigue life of safety-critical metallic primary structures. A FE model may miss out highly local stress concentrations which initiate cracks and which can then become unstable. This is one reason why full scale tests are not insisted by the airworthiness authorities for later versions of aircraft which may be "stretched" significantly from the original prototype. At least the stress concentrations will be the same even if the loading may be different.

Composite structures are even less likely to escape full scale tests for a reason similar to the above. Laminated high performance composite structures are ultra sensitive to local stress concentrations which give rise to 3-D stress fields having components in the "through-thickness" direction: the Achilles heel of composites structures. The sensitivity to local stress concentrations has led to excessive caution in defining the reliable stresses and strains. For example the design allowable compressive strain is often taken as 0.3% to 0.4% whereas a coupon test should survive at least twice these figures. Ironically the superior fatigue performance of composite structures may be due more to these conservative safety factors than to the durability of the basic material.

How then has industry managed to design reasonably safe and light composite structures? Basically the usual FE analysis is reliable enough to deliver local stresses/forces/moments in a global solution. However if there is any doubt about stress concentrations somewhere, a very local experimental test will be designed, such as a stiffener pull-off in a compression panel as illustrated in Figure 1. The loads causing failure will then be compared to the theoretical internal loads in the global FE solution.There are countless examples of detail and component tests being used as part of the design process for a new aircraft. It is the purpose of this paper to examine the capability of theoretical and software tools in evaluating the allowable loads in a local model, and so avoid the expensive testing of many such generic features.

One issue to be considered is whether the local allowable loads are valid anyway. The initiation of failure may lower the local stiffness so that the interface loads are themselves lowered. Thus can we ignore the coupling between the local and global structures? We will show that the use of local loads, not changing, is closer to the truth than using interface displacements, i.e. the surrounding structure has a very large reservoir of strain energy. Of course the initiation of failure in brittle composite structures may be unstable anyway and no local redistribution will save it. We will show that damage propagation away from the local stress concentration may be either unstable and rapid, or stable and then arresting, depending on the nature of the surrounding structure.

It should be mentioned that this local/global approach for composite structures is already being marketed by at least three commercial code developers.

- Alpha Star Corporation (GENOA) use strategies developed at NASA Ames.
- MERL use strategies developed at NASA Langley.
- ESI (PAM series)

Anecdotal evidence from industry is that these codes have limitations, and require considerable skill to use, that is the failure simulation is far from being an automatic routine. We will look at the problems of simulating failure and suggest the way forward.

2. FAILURE MECHANISMS

Restricting ourselves to laminated structures we have to differentiate between in-plane fibre-dominated failure and out-of-plane matrix-dominated (delamination or debonding). In-plane failures due to stress concentrations are not strictly amenable to fracture mechanics since in tension no sharp cracks develop: there is much blunting of a potential crack front with matrix cracking delamination and fibre bridging. In fact, unlike metals, a sharper crack front can develop under compression and the use of energy release rate criteria has been successful in estimating the compressive failure load in plates with circular holes [Ref 2]. In the absence of sharp cracks it is feasible to use a strength criteria, based on laminate stresses or strains. It is not the purpose of this paper to discuss the many empirical failure criteria, usually a polynomial in the various stress components for a uni-directional laminar. We assume that some criteria can be applied to a single ply in a laminated stack, and as the load is increased some first ply failure occurs at which the local stiffness in (say) a finite element, is put to zero or reduced to a negligible value. The load is then increased further and the pattern repeated so the damage propagates through the thickness and away from the source until eventual failure. The damage propagation is analogous to plasticity and limit loads in metallic structures. This approach has been successfully demonstrated for simple coupon tests [Ref 3] and we here show how it works for realistic structures.

The other failure mode is delamination and this is much more difficult to simulate in realistic structures. It does mean coping with a sharp crack and singularity, so strength criteria will not work. Fracture mechanics in some form has to be used, and the most direct way is to evaluate the strain energy release rate (SERR) by opening a crack or closing it, and comparing

with a known critical value determined by test. The main problem here is that the delamination crack front has to be moved and monitored. This is computationally expensive and the FE mesh size may have to be fine to evaluate the SERR accurately and capture the shape of the crack front as the applied load is increased. An alternative strategy is the use of interface elements, which may be dimensionless with zero thickness but whose force/displacement law captures the physics of crack propagation. We have used the model shown in Figure 2 for a crack of unit length. The slope of the rise could be a measure of say resin stiffness, and the strength a measure of allowable stress in tension (mode 1) or shear (mode 2). We have used a linear decay over the so called "process zone" but the important feature is that the area enclosed is equal to the critical SERR G_{IC} or G_{IIC}. The big advantage of interface elements is that no "flaw" is needed to start propagation, and no crack front is needed to monitor. The user of course has to insert complete areas of interface elements where delamination or debonding is thought likely.

Whether the failure is in-plane or delamination we recognise that the material is softening with a global stiffness change that may be negative-definite. This always causes numerical problems. It can even happen elastically in the case of compression panels taken beyond initial buckling when a mode change occurs. The structure may snap-through or even snap-back. We have therefore adopted the technique of simulating all failure events as dynamic, and using explicit integration. For static problems, even non-linear, it can be expensive to load incrementally and solve the dynamic response at each increment. It is therefore necessary to use fictitious mass and damping so that the static solution is reached as quickly as possible, thus a critically damping behaviour is aimed for. Consider the equations of motion for the displacement vector **r.**

$$\mathbf{Mr''\ +\ Cr'\ +Kr\ =0}$$

We choose proportional damping $\mathbf{C} = \alpha\,\mathbf{M} + \beta\,\mathbf{K},$ but it is impossible to choose the two parameters α and β to achieve critical damping over the full range of eigenfrequencies for large M and K. One strategy which works well is to put $\mathbf{M} = \mathbf{K}$. All undamped eigenvalues are then unity and critical damping can be achieved. However an even simpler strategy is to put $\mathbf{M} = \mathbf{0}$ and $\mathbf{C} = \mathbf{K}$. The single eigenvalue is now real and negative and we and if we have not achieved convergence in (say) 20 iterations, the step size is doubled.

Some examples of failure simulation are now illustrated, starting with the easiest pure in-plane fibre-dominated failures and proceeding through to the most difficult debonding in compression panels.

3. STRESS CONCENTRATIONS DUE TO CIRCULAR HOLES

This example is taken from a research program undertaken by a UK Industry/MoD Consortium, and aimed at evaluating the best criteria for predicting failure in carbon fibre panels with various sizes of circular holes and subjected to a biaxial stress field. It was known that strength would decrease with hole size, but, unlike brittle metals, linear elastic fracture mechanics will not work. We show here results for a biaxial field of equal tension (in the "x" direction) and compression (in the "y" direction). Attempts to explain failure using the local stress field and various "failure" stress criteria were not very successful as Figure 3 indicates, the experimental values being roughly twice those of the popular "point stress" criteria. The notched plates were surrounded by a reinforced structure leading to the load input points, details of which are actually confidential. However the net result was that damage initiation at the hole edge did not propagate in an unstable fashion, but the surrounding reinforcements

acted as effective crack inhibitors until final failure occurred at a later loading stage. The explicit degradation algorithm shows in Figure 4 the first loss of stiffness occurring at a load of 100kN, and eventually leading to total failure at a load of 138kN. (The small residual stiffness above this loading is due to assuming any ply stiffness retains 10% of its elastic value after failure, and is a device simply to avoid expensive convergent times.) The plots of damage in Figure 5 show an initial propagation along the x axis due to the lower compressive strength of the material but eventually the damage extends over the whole plate. (The patchy displays are due to the plotting routine!). Figure 6 summarises the effect of hole size and the agreement between test and prediction is satisfying. Delamination was not modelled in this exercise, although it does occur at the hole boundary, but it did not lead to buckling and propagation. The next example is also uninfluenced by delamination.

4.   COMPRESSION AFTER IMPACT (CAI) STRENGTH OF SANDWICH PANELS

This example is a sandwich panel having carbon fibre skins and an aluminium alloy honeycomb core. This ductile core is a very good energy absorber of low velocity impact. The CAI behaviour depends on whether the skin is stiff enough, and the core interface weak, so that the skin recovers as shown in Figure 7 leaving an invisible void which makes the panel vulnerable. Compression loading can cause the unsupported skin to buckle which will then propagate in a mode 1 fashion. However if a strong core can hold the indentation, then applied compression will cause the indentation to push further into the core and increase the local bending strains. A point will eventually be reached when these strains reach the allowable strength values and the indentation will propagate rapidly as a narrow band right across the panel. Delamination plays no role in this history, and, to simulate the rapid propagation across the entire panel, we found it necessary to combine the local and global behaviour from the very start, simply using a refined mesh in the region of the impactor. Traditional Mindlin plate elements were used for the skins but individual plies were degraded by 90% when the Chang-Chang failure criteria was exceeded. The core was idealised as a homogenous elastoplastic medium with properties in compression, tension and shear found from experimental tests. The explicit routine was used to simulate the impact event and create damage and residual deformations, and then the same routine was used for the CAI strength simulation.

Figure 8 shows the force histories for an impact of 120J energy, confirming the validity of the model. The residual indentation was also predicted well. The model was then subjected to incremental compressive loading and at a value of 480kN the damage and deformation propagated suddenly in a narrow band right across the panel as shown in Figure 9. The predicted fibre damage map in Figure 10 shows this band on the damaged side which then lead to the panel pivoting across this "hinge" and starting to cause failure in the other skin. This damage band can be compared with the experimental C-scan in Figure 11 which shows the signal from the crushed core. The failure of 480kN compares with the test value of 505kN; and a value of 770kN for the undamaged panel.

5.   COMPRESSION AFTER IMPACT STRENGTH OF CURVED PANELS

We now proceed to a problem where delamination cannot be ignored. If flat plates are subjected to low velocity impact it can be shown that the internal delamination is driven primarily by the magnitude of the impact force [Ref 4] which is greater the stiffer the plate. On the other hand fibre damage is driven mostly by the bending strains which will be large if the plate is very flexible. It has been common to assume that delamination does not affect the flexural stiffness much so that the impact force can be predicted allowing only for loss of stiffness due to fibre failure. Figure 12 shows how necessary it is to include this flexural stiffness degradation. However if a curved shell is impacted it will have a significantly higher stiffness and therefore impact forces, so it was necessary to see if delamination should be

included in the impact simulation, and also whether both flexural degradation and delamination should be included in the CAI simulation. The rigs chosen (Figure 13) were modifications to the standard Boeing impact and CAI test rigs. It was found that, for a thin 2mm curved panel, an impact of only 1.86J energy produced 900mm^2 delamination. (900mm^2 is a circle of diameter 340mm or 17 times the plate thickness). This compares with an area of only 300mm^2 for a flat plate subjected to a much larger 7J energy impact. The importance of recognising the loss of stiffness due to delamination was quickly established. In Figure 14 the force histories for 1.86J impact on the curved panels, are shown for the test results and the FE predictions. By modelling both fibre damage and delamination the maximum force of 1200N and the half-period of 3ms was captured well. However by ignoring delamination the stiffer structure has a half-period of only 2ms and the maximum force rises to 1800N.

Having created the internal damage by the FE code FE77, it is then possible to load in compression the damaged structure once more. It should be mentioned that it is important to start applying loading to the damaged but static structure, and it was found necessary to increase the artificial damping once the impact mass had left the structure, to avoid a long computational time for the free vibrations to disappear. Figure 15 shows the FE model and the history of displacements as the compressive load is applied. The load is expressed as a multiple of the initial buckling load. The displacements shown are those of the two surfaces of the shell at the impacted point. They show clearly how these surfaces, even separated by a central delamination, stay together and do not "open up" as is often assumed for flat plates. This is characteristic of cylindrical shells which always buckle "inwards" to decrease the local curvature, and the FE predictions mimicked the tests exactly. As the load is applied there is an outward displacement due to Poisson effect but at 0.6 of the buckling load there is a snap-through in stages into the post-buckled region and then a "snap-back" at a load factor of 1.3. This corresponds to a mode change as indicated in the figure, and confirms the utility of using a dynamic explicit strategy.

Simulation condition		Failure Load kN
Eigenvalue Initial buckling	No delamination	208.2
	Delaminated	158.2
Incremental compressive loading	Impact damaged, no delamination	186.9
	Delaminated	124.5
	With fibre degradation	65.4

Table 1. Failure loads for curved panel, 2mm thick.

One of the advantages of a numerical model is that the separate effects of the various failure mechanisms can be assessed as indicated in Table 1. The first eigenvalue gave the buckling of the perfect panel as 208.2kN. If the central delamination is included the increased flexibility reduces this to 158.2kN. Simulating the CAI loading of the impact damaged panel shows a failure load of 186.9Kn, but by including the delamination this is reduced to 124.5kN. Now when the panel is loaded, due to the damage producing an eccentricity, there is further local bending and fibre failure before panel failure at a load of 65.4kN. The only omission in

the simulation was propagation of the delamination front during loading, and this is currently being worked upon.The experimental failure load was 51kN. This is a fairly massive reduction from the undamaged failure load.

6.   FAILURE OF COMPRESSION PANELS DUE TO STIFFENER DEBONDING

The success in modelling the previous example was somewhat fortuitous since the delamination propagation was clearly unstable under compression loading. This may not always happen, so we have looked at the pros and cons of evaluating SERR directly or by using interface elements, especially for geometrically complex configurations. The example quoted here is that of a post-buckled compression panel with "J" stiffeners. It was decided to use the global/local approach, i.e. use a fairly crude FE model to buckle the panel and then find local internal forces and moments to be applied to a 2-D plane strain section at either the nodal lines or the buckled crests of the panel. Figure 16 shows that the twisting moments for example peak at the node lines whilst the bending moments and axial forces peak at the buckled crests as shown more clearly in Figure 17 where the compressive stresses have been shed to the stiffeners as the panel buckles. These local membrane forces were then applied to the very fine mesh section shown in Figure 18 to see if failure could be predicted. This particular stiffener design had used tapered flanges to eliminate the through-thickness shear stresses at the flange edge, and which would cause failure at the node lines. Failure this time originated in the base "noodle". The SERR was found directly by using virtual crack extension at selected points. In this case we had been able to take a test panel and section it after failure showing that the stiffener debonding had started in the triangular noodle region at the base of the stiffener. We have therefore evaluated the SERR along the experimentally observed line shown in the figure and using forces/moments at the applied load which caused failure in the test. In this case no coupling between the global and the local displacements was allowed. The SERR increases dramatically as the crack opens, reaching the critical values of G_{IC} in 5mm.

Thereafter the value for soft loading (load control) soars to more than 1250J/m^2 whilst the hard loading (displacement control) peaks at 700J/m^2 which is still three times the critical value. The soft loading does decrease the SERR after the peak but never becomes lower than the critical value even when the debond is complete. The other curves in the figure shown were to investigate the effect of using a high or low value of filler in the noodle insert. It turned out not to be a sensitive parameter but the shape of the noodle is much more influential, showing that a precisely machined insert is necessary.

The mesh used in this local model is probably much finer than needed, but we wished to see how high the tensile (mode I) stresses were at the flange/noodle interface. They turned out to be 40Mpa maximum in the region of the crack starter. This is lower than the expected resin strength of 50-55Mpa. This is one disadvantage of the direct method used in a true fracture mechanics strategy, i.e. how do we start the crack. We should also admit that the selection of the virtual crack zone is a non-trivial exercise, certainly it is difficult to make it an automatic procedure based solely on local stress concentrations. We therefore advocate the use of interface elements, which have the initiation routine embedded in them, but with a word of caution in conclusion

In any structure where a localised zone undergoes softening, the usual implicit algorithms may not converge, even when the "arc-length" method is used. To illustrate this we show the very simple double cantilever beam test specimen loaded to precipitate a mode 1 unstable fracture. If the chosen FE mesh is too coarse then an element sitting astride the loading/unloading ridge of Figure 1 may have two Gauss points, one on the stiffening side and the other on the softening side. It is possible for the structure to temporarily unload back towards the origin before returning to the current branch as shown in Figure 19. The only way to avoid this is to use a fine mesh so that more than two Gauss points are situated in the process

zone. This is a high price to pay for the implicit strategy which needs to satisfy equilibrium at every load increment. We would therefore advocate the robust explicit method which does not need to satisfy equilibrium at every stage. This research is ongoing.

7.   CONCLUSIONS

- In-plane failure (strength criterion) and out-of-plane failure
  (delamination) need to be treated differently (but simultaneously
   if necessary.)
- Both forms may initiate and then propagate before structural failure, so any initiation stress
   or initiation fracture criterion will be conservative.
- Failure routines and location of sources will need to be virtually automatic to be accepted
   as a design tool.
- Explicit solvers and interface elements lend themselves
   naturally to automation.
- Virtual testing of components and substructures needs to establish credibility, or at the
   very least pin-point essential tests

8.   ACKNOWLEDGEMENTS

9.   REFERENCES

1. AGARD Report 772. "Analytical qualification of aircraft structures.". *70th meeting of S & M panel*. Sorrento. April 1990.

2. Soutis C, Curtis P T, and Fleck N A. "Compressive failure of notched carbon fibre composites.". *Proc. Roy. Soc. London. Series A*. **440.** 1993. Pp 241-256.

3. Gotsis P K, Chamis C C, Minnetyan. " Prediction of composite laminate fracture." *Composite Science and Technology*. **58.** No. 7.1998. Pp1137-1149
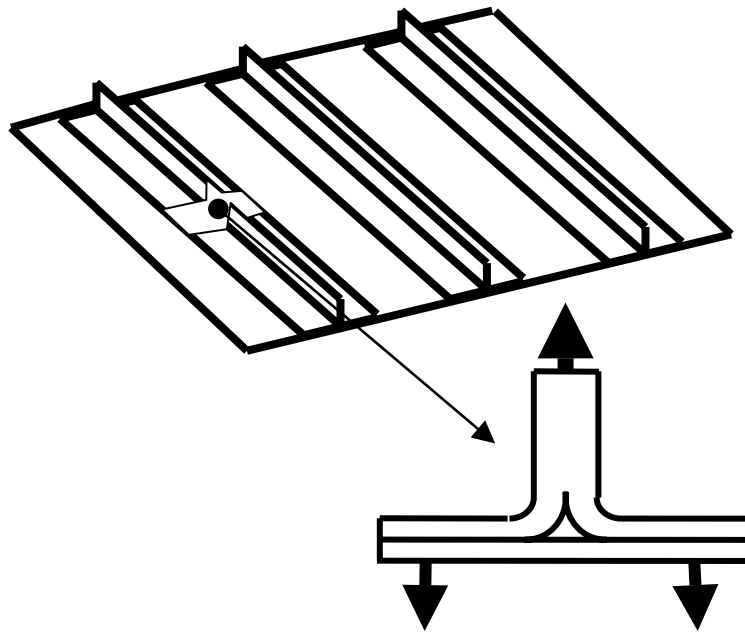
Fig.1. Global and local strategy
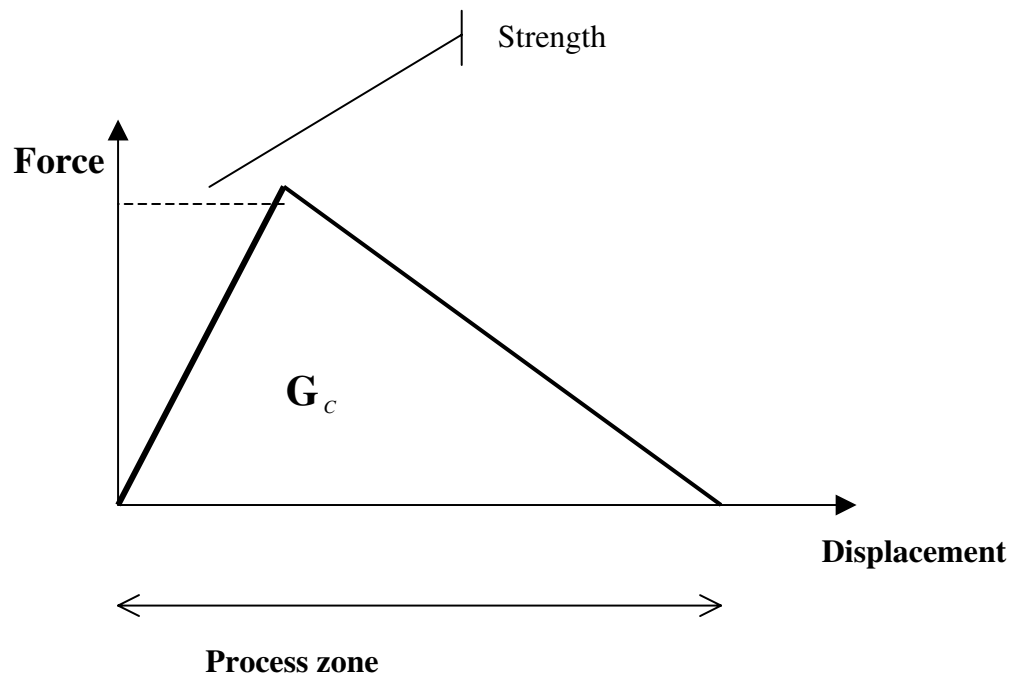
Fig. 2.   Force/displacement law for interface element
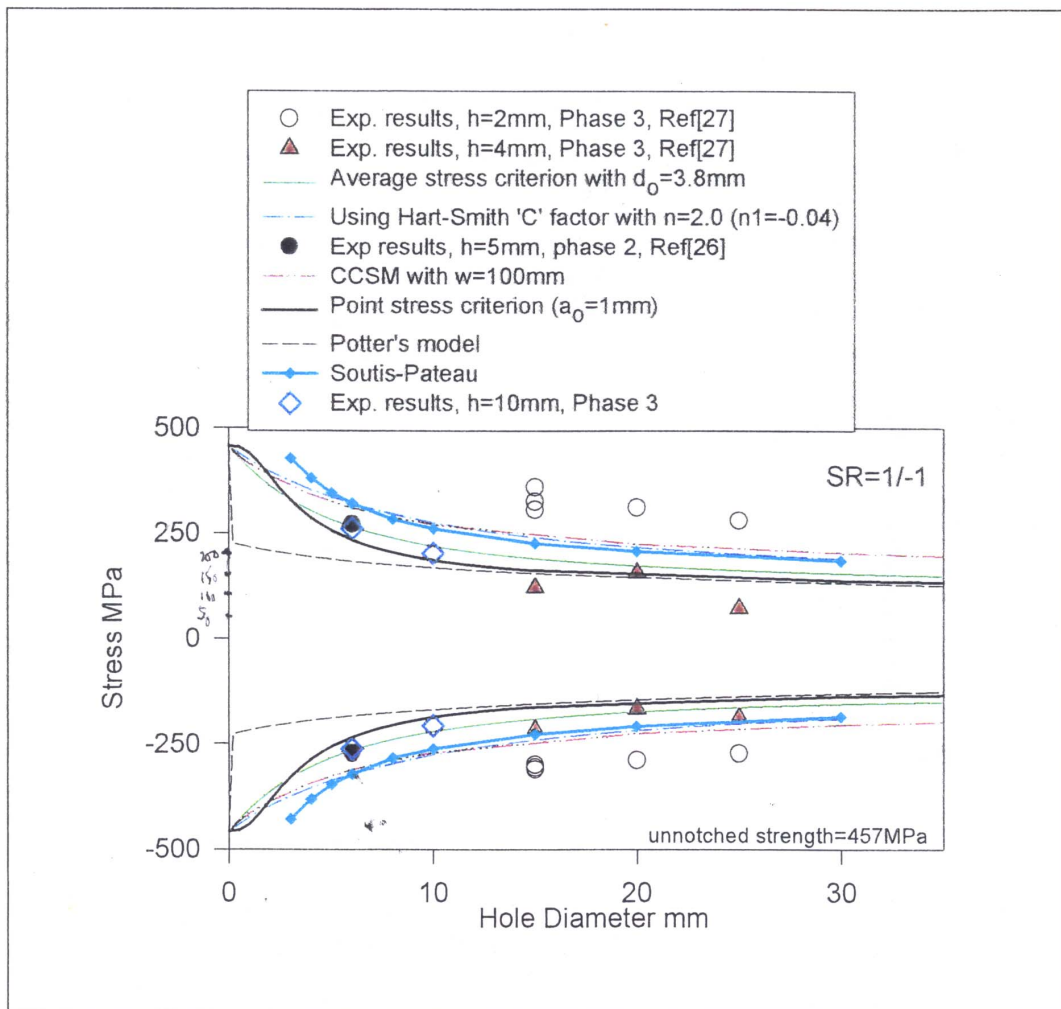
Fig. 3. Various common theoretical predictors for strength of notched composites with increasing hole size
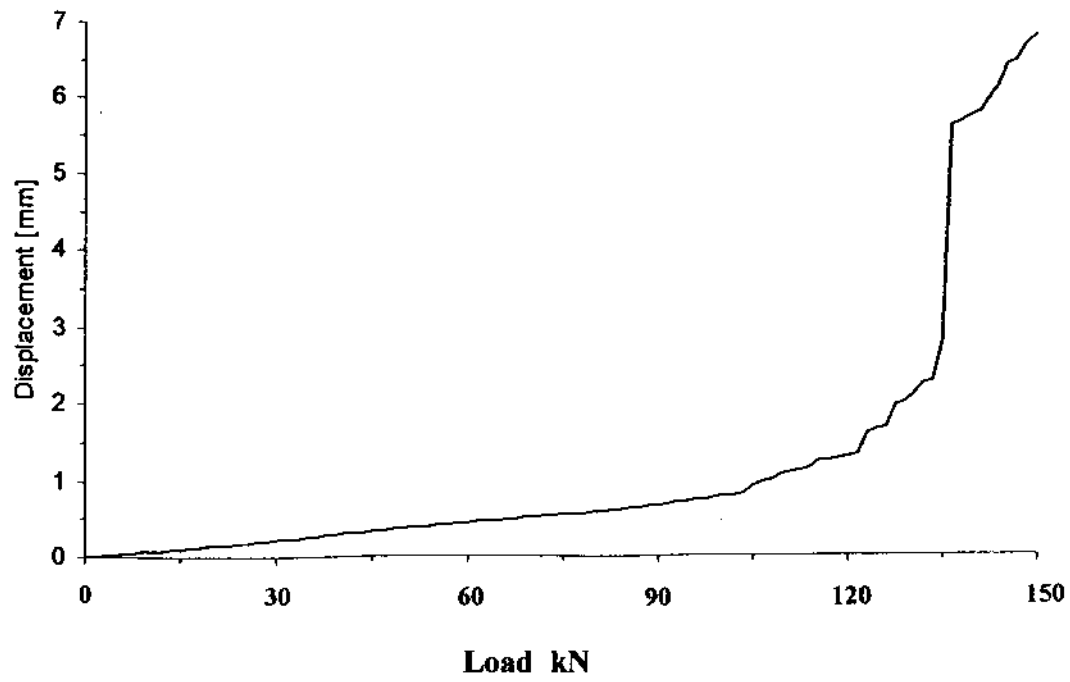
Fig. 4. Load against displacement for structure with circular hole.
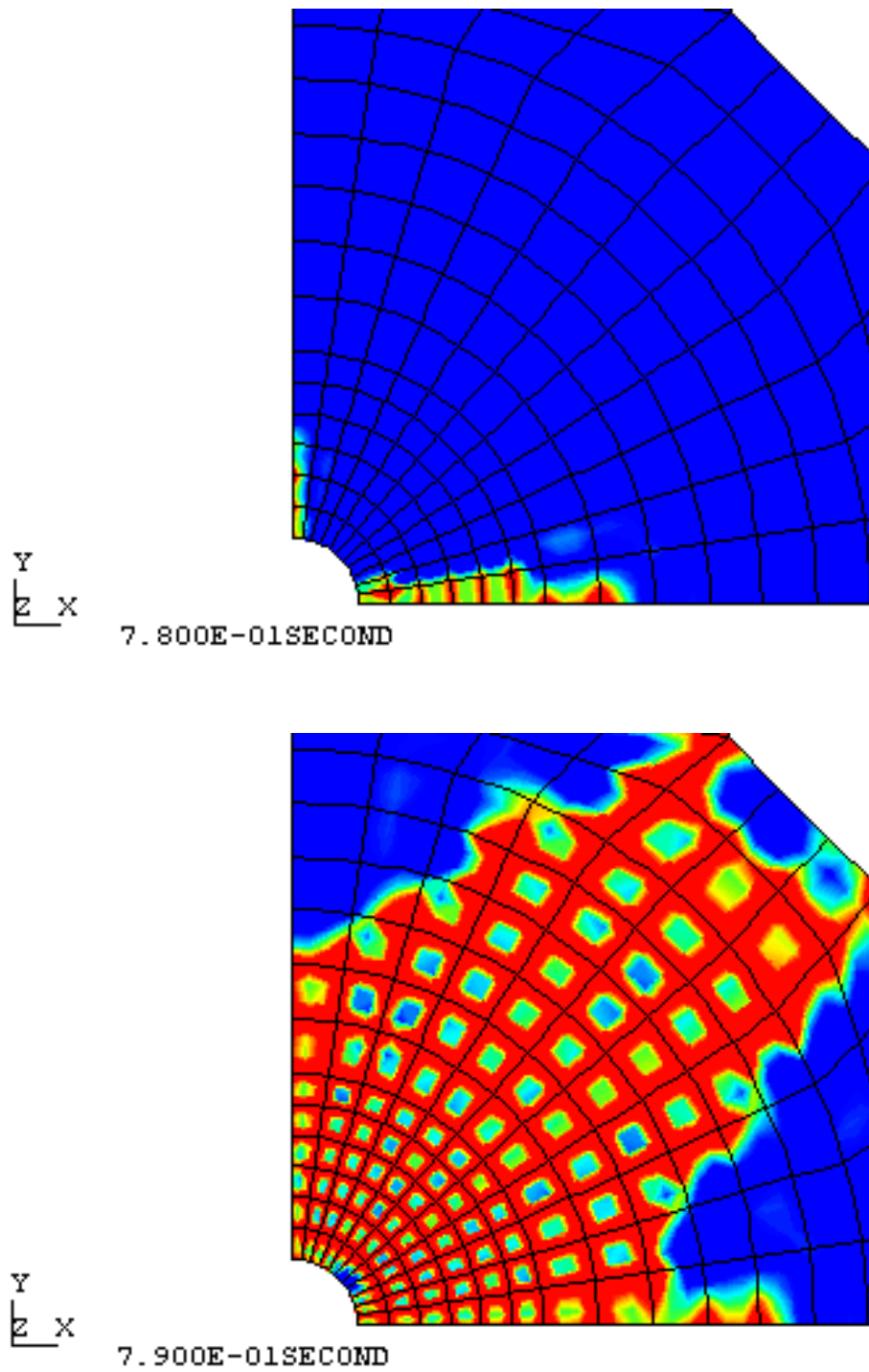
Fig. 5. A 1/4 of plate with circular hole subjected to bi-axial stress field.
In-plane damage maps at initiation and at final failure

2 mm laminate thickness
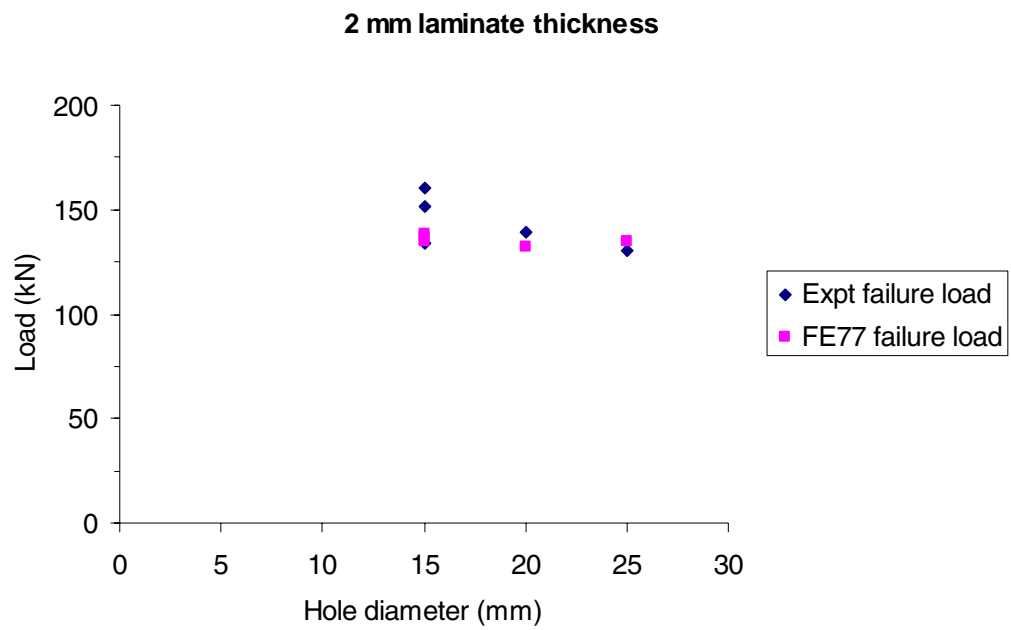
Fig. 6. Effect of notch size on strength of structure with circular holes.

Fig. 7(a)   Permanent skin indentation
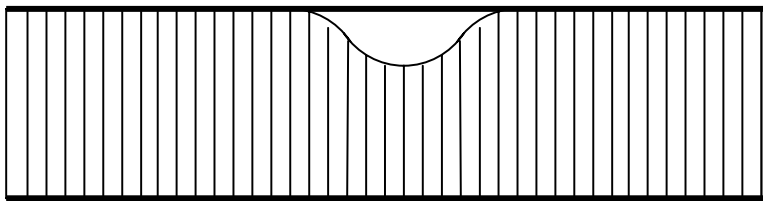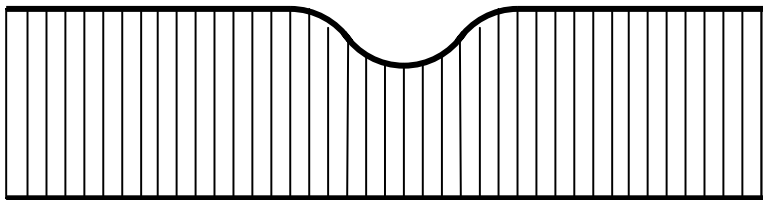
Fig.   7(b)   Skin recovers

Fig. 7.   Possible results of impact on sandwich structure with ductile core
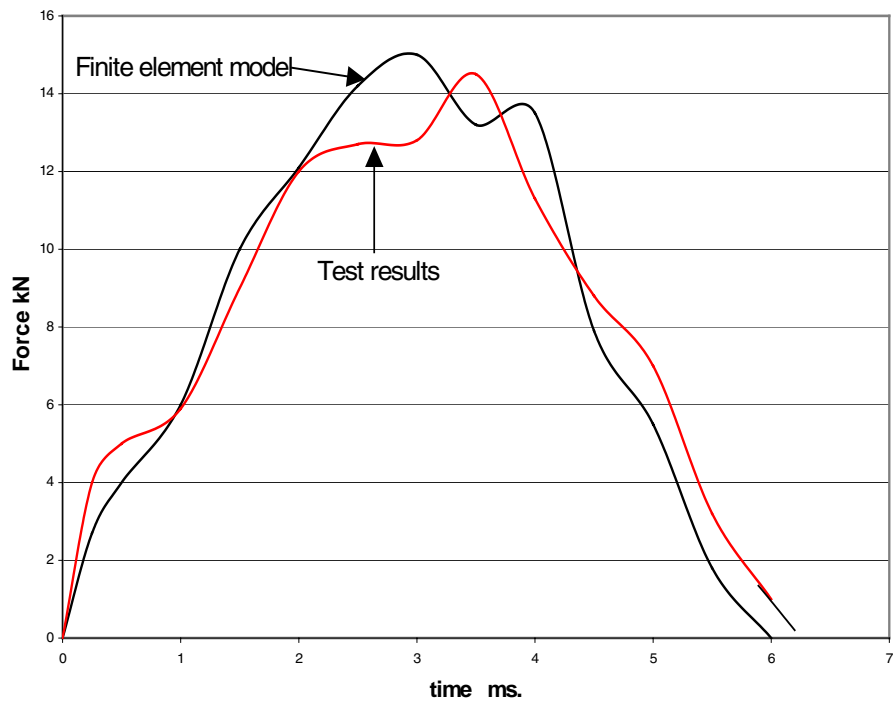
Fig. 8. Sandwich panel: impact force histories

Fig. 9.   Section through F.E.-predicted displacement right across panel.
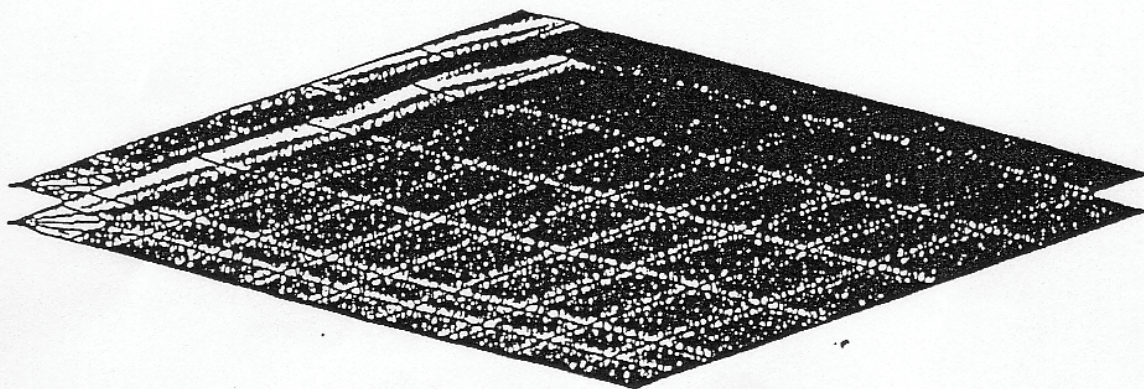
(lower skin shown is impacted front-face.)

Fig. 10. F.E.-predicted fibre damage at panel failure.
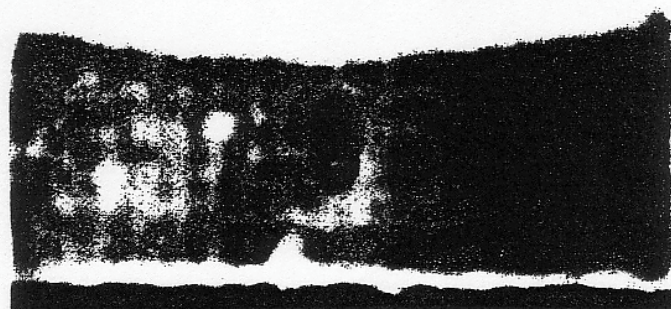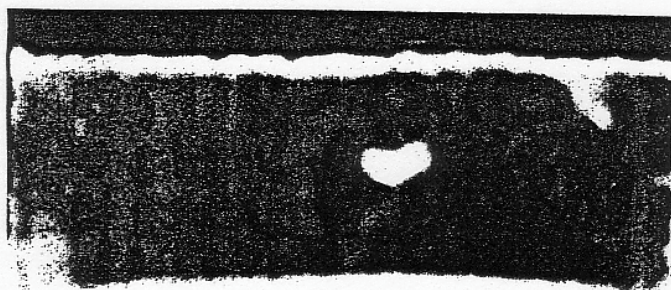
Fig. 11.   C-scan revealing extent of crushed aluminium honeycomb core.
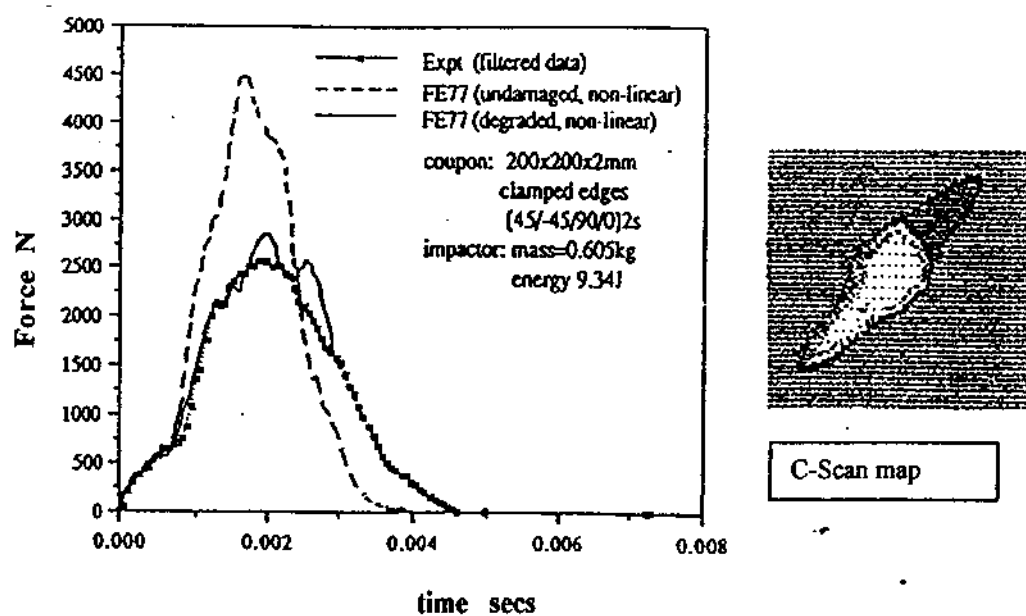
Fig. 12. Impact force history with significant fibre damage and splitting / delamination on back face.
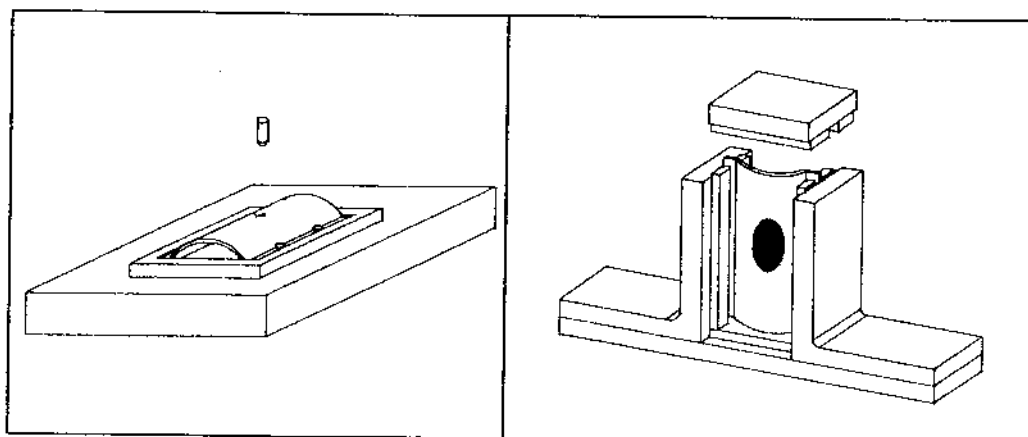
Fig. 13. Impact and C A I rigs for curved panels.

Impacted cylinder force histories
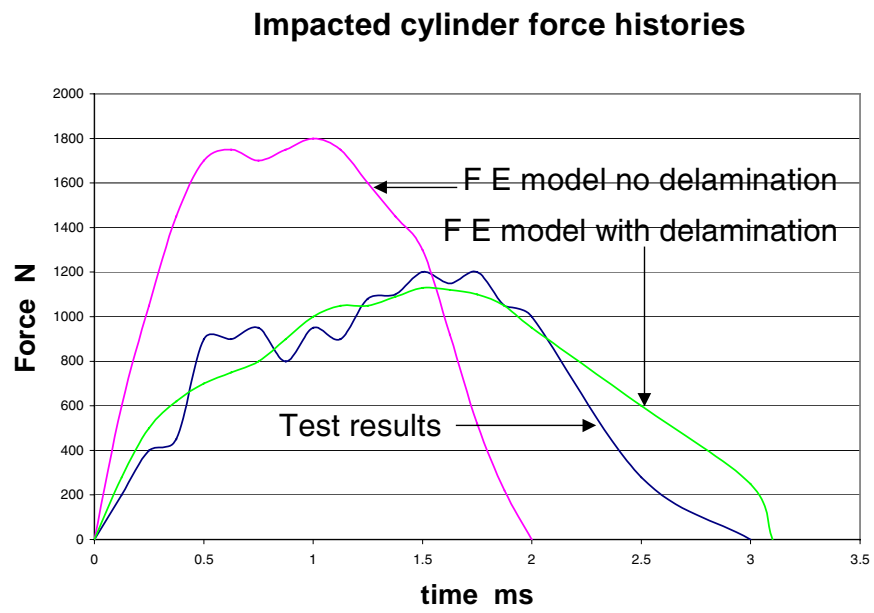
Fig. 14. Force history for curved panel with and without delamination
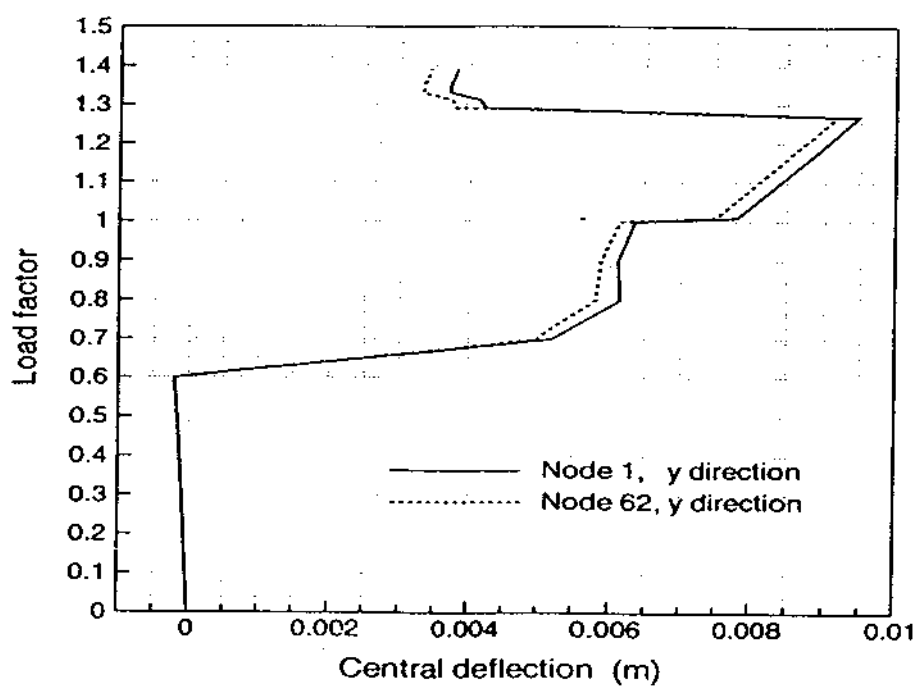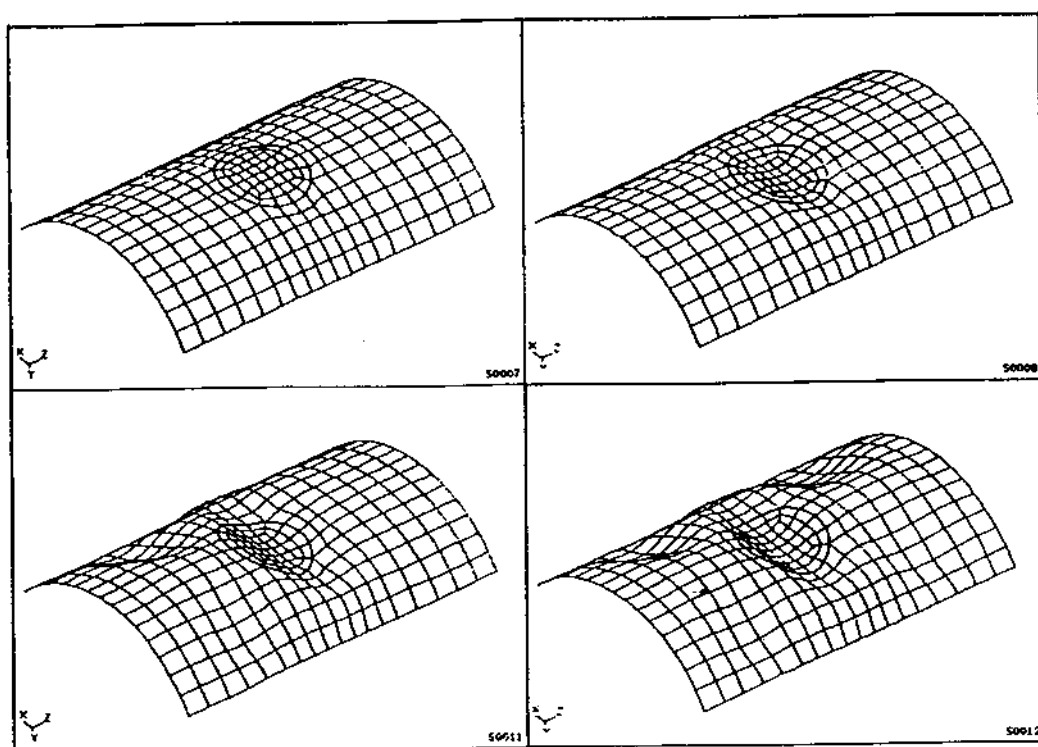
Fig. 15. F.E. model during C A I loading.
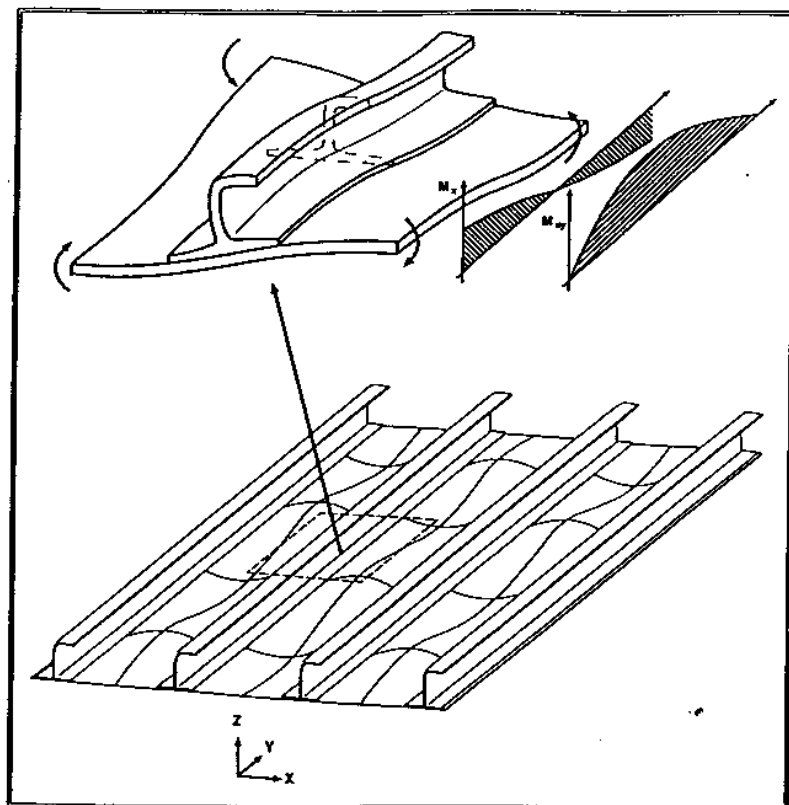
Fig. 16. Variation of bending and twisting moments along a post-buckled compression panel.
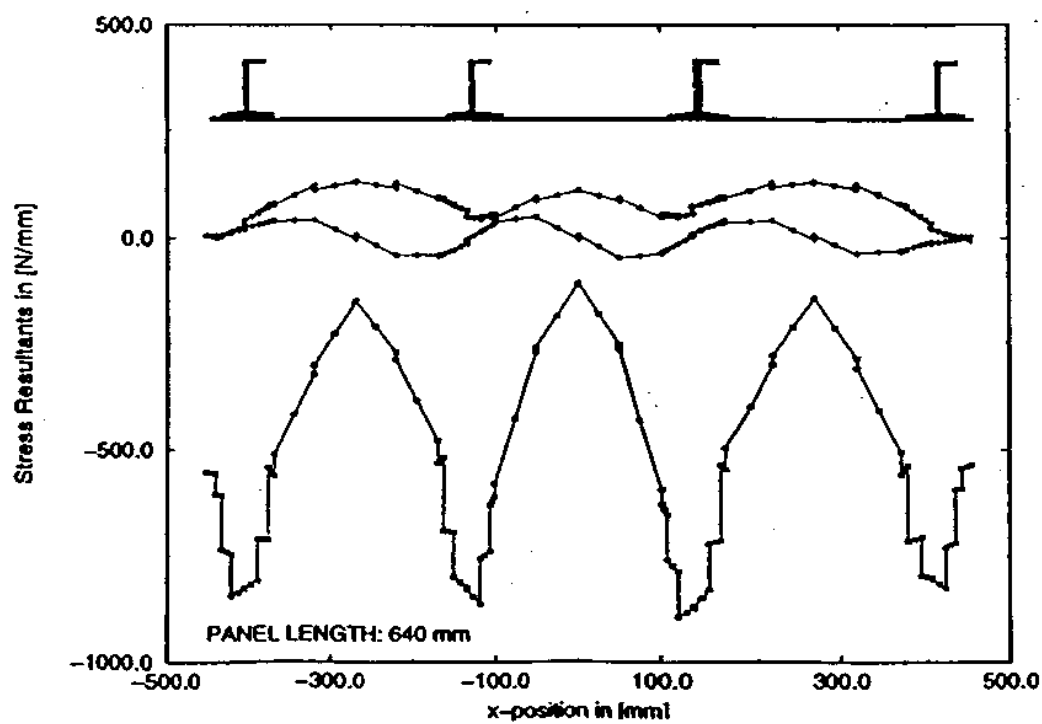
Fig. 17. Membrane compressive and shear stress resultants across buckled crest of stiffened panel.
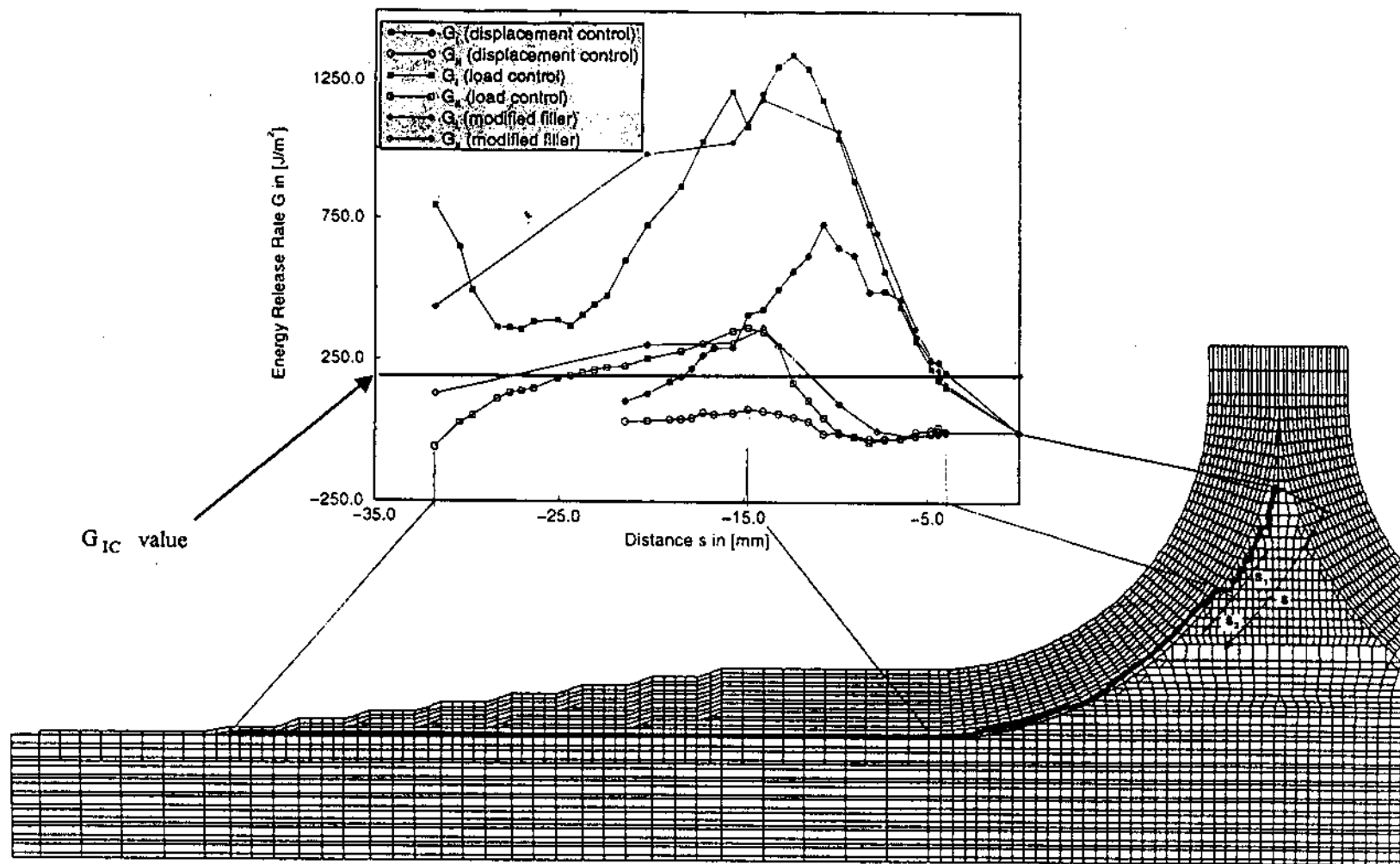
Fig. 18. F.E. model of (noodle) detail at base of stiffener.

This page has been deliberately left blank

_____

Page intentionnellement blanche

Using High-Fidelity Analysis Methods and Experimental Results to Account for the Effects of Imperfections on the Buckling Response of Composite Shell Structures

James H. Starnes, Jr. and Mark W. Hilburger
NASA Langley Research Center
Hampton, VA 23681-2199, USA

ABSTRACT

The results of an experimental and analytical study of the effects of initial imperfections on the buckling response of unstiffened thin-walled compression-loaded graphite-epoxy cylindrical shells are presented. The analytical results include the effects of traditional and nontraditional initial imperfections and uncertainties in the values of selected shell parameters on the buckling loads of the shells. The nonlinear structural analysis results correlate very well with the experimental results. The high-fidelity nonlinear analysis procedure used to generate the analytical results can also be used to form the basis of a new shell design procedure that could reduce the traditional dependence on empirical results in the shell design process.

KEYWORDS: high-fidelity nonlinear structural analysis, composite shells, shell stability, initial imperfections

INTRODUCTION

With the increasing need to produce lighter-weight aerospace structures, advanced composite materials are being used in new structural designs to reduce structural weight. One of the contributors to the high cost of developing new designs for aerospace structures made of composite materials is the cost of developing material properties and structural design allowable values. To reduce this cost, improved design methods appropriate for advanced composite materials are needed. The present paper describes a verified high-fidelity nonlinear structural analysis procedure that has the potential for reducing the traditional dependence on empirical results in the structural design process for composite structures. Reducing the traditional dependence on empirical results in the design process means that the more than ten thousand structural-design-allowable-value tests that are commonly conducted today could be reduced to, say, several hundred carefully selected tests needed to verify the design at various dimensional levels (e.g., coupons, structural details, panels, etc.). A reduction in the number of tests needed to support the current empirically based structural design process should reduce some of the costs associated with developing a new structural design.

Today, designers often use a design-level analysis procedure with empirical data to develop new structural designs for strength and buckling critical structures. The traditional approach to designing thin-walled buckling-resistant isotropic shell structures is to predict the buckling load of the shell with a deterministic linear bifurcation buckling analysis that is usually based on nominal structural dimensions and material properties of an idealized, geometrically perfect shell. The results of this analysis are then reduced by an empirical "knockdown" factor (e.g., Ref. 1) to account for the difference between the predicted buckling load and the actual buckling load of the shell determined from tests. The knockdown factor used in the design of buckling-resistant shells is often based on the

"Lower Bound" design recommendations reported in such sources as Reference 1. This design philosophy can potentially result in overly conservative designs for these structures. While it is generally recognized that initial geometric shell-wall imperfections are a major contributor to the discrepancy between predicted and experimentally measured shell buckling loads (e.g., Ref. 2), the traditional sources of design knockdown factors do not include data or information related to the sensitivity of the buckling loads to initial imperfections, or information for composite shell structures. Recent studies (e.g., Refs. 3-4) have shown that traditional geometric shell-wall imperfections, and other nontraditional forms of imperfections or variations in geometric and material parameters, loading conditions, and boundary conditions can significantly affect the buckling load of compression-loaded composite shell structures. The effects of these traditional and nontraditional classes of initial imperfections on composite shell buckling are generally not well understood by structural designers. Modern high-fidelity nonlinear analysis procedures (e.g., Ref. 5) offer the opportunity to improve some of the engineering approximations that are used in the shell design process, and to provide insight into the effects of traditional and nontraditional imperfections on the buckling response of composite shell structures.

The present paper describes a high-fidelity nonlinear structural analysis procedure that can be used for the design of buckling-resistant composite shell structures. The results of an experimental and analytical study of the effects of initial imperfections on the buckling response of graphite-epoxy cylindrical shells are presented. The results identify the effects of traditional initial geometric shell-wall imperfections and several relatively unknown and nontraditional imperfections, such as shell-end geometric imperfections, shell-wall thickness variations, variations in loads applied to the ends of the shells, and variations in the boundary conditions, on the buckling loads of these shells. The effects of manufacturing anomalies caused by small gaps between adjacent pieces of graphite-epoxy tape in a shell-wall layer or ply of graphite-epoxy material are also discussed. The high-fidelity nonlinear shell analysis procedure accurately accounts for the effects of these traditional and nontraditional imperfections on the shell buckling loads. The analysis results are compared with the experimental results, and this comparison suggests that the analysis procedure can be used for determining accurate, high-fidelity design knockdown factors for predicting shell buckling loads in the design process. This analysis procedure can be used to form the basis for a shell design approach that should make it possible to reduce the need for empirical knockdown factors currently used in design, and to reduce the cost of developing buckling-resistant shell designs. Once this high-fidelity analysis-based design procedure is established for bucking-critical composite shell structures, it could be generalized to form the basis of an analysis-based design procedure for other composite structural design applications.

TEST SPECIMENS, IMPERFECTION MEASUREMENTS, AND TESTS

Test Specimens

The specimens tested in this study were fabricated from 12-in.-wide, 0.005-in.-thick AS4/3502 graphite-epoxy preimpregnated unidirectional tape material made by Hercules, Inc. The nominal unidirectional lamina properties of a typical 0.005-in.-thick ply with a fiber volume fraction of 0.62 are: longitudinal compression modulus $E_1 = 18.5$ Msi, transverse modulus $E_2 = 1.64$ Msi, in-plane shear modulus $G_{12} = 0.87$ Msi, and major Poisson's ratio $\nu_{12} = 0.30$. The material was laid up on a 15.75-in.-diameter mandrel and cured in an autoclave to form six shells with different shell-wall laminates. These shells include 8- and 16-ply shells with either $[45/0_2]_s$, $[45/90_2]_s$, $[45/0/90]_s$, $[45/0_2]_{2s}$, $[45/90_2]_{2s}$, or $[45/0/90]_{2s}$ laminates. The resulting shells are referred to herein as shells or specimens C1 through C6, respectively. These specimens had a nominal length of 16.0 in. and a nominal radius of 8.0 in. The 8- and 16-ply specimens had nominal shell-wall thicknesses of 0.04 in. and 0.08 in., and shell-radius-to-thickness

ratios of 200 and 100, respectively. Both ends of the specimens were potted in an aluminum-filled epoxy material to prevent the ends of the specimens from failing prematurely. The potting material extended approximately 1.0 inch along the length of the specimens at each end resulting in an exposed length that was approximately 14.0 in. long. The ends of the specimens were machined flat and parallel to facilitate proper load introduction during the tests. A photograph of a typical specimen and the specimen coordinate system used to represent the corresponding geometry is shown in Fig.1. The shell length, test-section length, radius, and thickness are designated as L, L_T, R and t, respectively.

Imperfection Measurements

Three-dimensional surveys of the inner and outer shell-wall surfaces of the specimens were made prior to testing the specimens to determine their initial geometric shell-wall imperfection shapes and shell-wall thickness distributions. Measurements were taken over a uniform grid with increments of 0.125 in. in the axial direction and 0.139 in. (approximately 1° of arc) in the circumferential direction over the exposed surfaces of the specimens. The inner surface measurement was used to determine the initial geometric shell-wall imperfection shape of a specimen, and the difference between the outer and inner surface measurements was used to determine the shell-wall thickness distribution. A contour plot of the nondimensionalized initial geometric shell-wall mid-surface imperfections for specimen C3 is shown in Fig. 2. The measured shell-wall imperfection w_o is nondimensionalized by the average measured shell-wall thickness $t_{ave} = 0.0381$ inches. These results indicate that the initial geometric shell-wall imperfection is periodic in the circumferential direction and has slight variations in the axial direction. The amplitude of the imperfection varies from $+1.341 t_{ave}$ to $-1.535 t_{ave}$. A contour plot of the nondimensionalized shell-wall thickness variation for specimen C3 is shown in Fig. 3, where the measured thickness values t_o are nondimensionalized by the average measured shell-wall thickness t_{ave}. These results indicate that the shell-wall thickness, and hence the laminate stiffnesses, varies significantly over a short distance. The thickness varies from 0.928 to $1.321 t_{ave}$. Most of the thickness variation is due to local variations in the resin content of the laminate associated with the fabrication process. However, the darker angular pattern in Fig. 3 is due to small gaps between adjacent pieces of graphite-epoxy tape in some of the laminate plies that were generated during the lay-up and curing processes. Such a region is referred to herein as a lamina ply-gap or a ply-gap. These locally thin shell-wall regions have a significant shell-wall mid-surface eccentricity, and have reduced stiffnesses relative to the rest of the shell wall. Lamina ply-gaps with gap widths as large as 0.15 in. have been observed in some of the specimens. The lighter angular patterns in Fig. 3 are caused by locally thickened regions of the outermost plies of the laminate that develop during the curing process to form outer shell-wall surface ridges. Typical magnified cross-sectional views illustrating the microstructure of typical ply-gaps and outer surface ridges in a laminated shell wall are presented in Ref. 3.

Measurements of the specimen top and bottom loading surfaces were made every degree around the circumference of the specimens to determine the variation in the shell-end or loading-surface geometry. Typical top and bottom shell-end geometry variations are shown in Fig. 4 for specimen C3 and are denoted by $\delta_{top}(\theta)$ and $\delta_{bot}(\theta)$, respectively. The maximum amplitude of this shell-end variation is approximately 0.0015 in., or approximately 0.01% of the specimen length.

Test Apparatus and Tests

The specimens were instrumented with electrical resistance strain gages, and direct-current differential transducers (DCDT's) were used to measure displacements. Three non-collinear DCDT's were positioned at three corners of the upper loading platen

of the test machine and used to measure the end-shortening displacement Δ and the rotations ϕ_y and ϕ_z of the loading platen as illustrated in Fig. 1. The specimens were loaded in compression with a 300,000-lb hydraulic universal-testing machine by applying an end-shortening displacement to the shell ends. The upper loading platen was aligned with the loading surface of the specimen as well as possible before the test by adjusting leveling bolts in the corners of the upper loading platen until strains measured by selected strain gages indicated a uniform axial strain distribution in the shell wall. The shadow moiré interferometry technique was used to observe the shell-wall radial (perpendicular to the shell outer surface) deformation patterns. All data were recorded with a data acquisition system, and the moiré patterns were recorded photographically and on videotape. The specimens were loaded until buckling or failure of the shells occurred.

FINITE-ELEMENT MODELS AND ANALYSES

Nonlinear Analysis Procedure

The shells considered in this study were analyzed with the STAGS (STructural Analysis of General Shells) nonlinear shell analysis code.[5] STAGS is a finite-element code developed for the nonlinear static and dynamic analysis of general shells, and includes the effects of geometric and material nonlinearities in the analysis. The code uses both the modified and full Newton methods for its nonlinear solution algorithms, and accounts for large rotations in a shell by using a co-rotational algorithm at the element level. A pseudo arc-length path-following method is used to continue a solution past the limit points of a nonlinear response. The transient analysis option in STAGS uses proportional structural damping and an implicit numerical time-integration method.

The responses of the shells were determined using the following analysis procedure. The prebuckling responses were determined using the geometrically nonlinear quasi-static analysis capability in STAGS. The pseudo arc-length path-following method was used to compute the initial shell response until just before buckling occurred. The unstable buckling response of the shell was predicted using the nonlinear transient analysis option of the code. The transient analysis was initiated from an unstable equilibrium state close to the limit point by incrementing the end displacement by a small amount. The transient analysis was continued until the kinetic energy in the shell had dissipated, which indicated that the transient response had attenuated. Once the transient analysis had attenuated to a near-steady-state solution, the load relaxation option of the code was used to establish a static equilibrium state. Conventional linear bifurcation buckling analysis results were also determined with STAGS for comparison with the nonlinear response results.

Finite-Element Models

A typical finite-element model of a specimen is illustrated in Fig. 1. The STAGS 410 quadrilateral element was used in the models. The elements of the finite-element mesh are approximately 0.2-in. by 0.2-in. square. Each element has four integration points, which are distributed in such a way as to provide a modeling resolution of approximately 0.1-in. by 0.1-in square. This integration-point spacing is on the order of the measurement-point spacing used when measuring the initial geometric imperfections of the specimens. This highly refined mesh is necessary to model rapidly varying geometric and material parameters such as nonuniform shell-wall thicknesses and lamina stiffness properties.

Geometrically perfect and imperfect shells were analyzed in the present study. Nominal shell geometry, laminate thickness, lamina mechanical properties, and boundary conditions were used to model the geometrically perfect shells. The nominal boundary conditions consist of setting the circumferential and normal displacements v and w

equal to zero in the 1.0-in.-long potted boundary illustrated in Fig. 1, setting $u(L/2, \theta) = 0$, and applying a uniform end-shortening $u(-L/2, \theta) = \Delta$. The geometrically perfect finite-element models were modified to include the effects of the measured shell imperfections in order to model the geometrically imperfect shells. These modeling modifications include the effects of the measured initial geometric shell-wall imperfections, shell-wall thickness variations, local shell-wall lamina ply-gaps, thickness-adjusted lamina properties, boundary stiffness conditions, shell-end geometric imperfections, and nonuniform end loads.

The initial geometric shell-wall imperfection $w_o(x,\theta)$ is included in the finite-element models by introducing an initial normal perturbation to each node of the mesh by using a user-written subroutine with STAGS for that purpose. A linear interpolation algorithm was used to calculate the value of the imperfection for the coordinates of each finite-element node based on the measured shell-wall data. The shell-wall thickness, mid-surface eccentricity, and lamina material properties are adjusted at each integration point of each element in the finite-element models. The shell-wall eccentricity is calculated relative to the average shell-wall mid-surface. The lamina properties are adjusted by using the rule of mixtures. In the rule-of-mixtures calculations, it is assumed that any variation in the lamina ply thickness from the nominal thickness is due to a variation in resin volume only, and that the fiber volume remains constant for each ply. Details of modeling the ply-gap regions and results from a numerical parametric study of the effects of ply gaps on the buckling loads of these composite shells are given in Ref. 3.

To provide a better simulation of the elastic boundary constraints provided by the potting material at the ends of the specimens, effective axial and radial potting-support stiffnesses were determined for each shell specimen using a two-dimensional generalized plane-strain finite-element analysis of the potting-material–shell-wall detail. The predicted results indicate that the effective axial potted-shell stiffness range from 1.1 to 2.4 times the nominal shell-wall stiffness and the nominal effective radial potting-support stiffness was predicted to be approximately equal to 1.0E5 lbf/in. In the present study the nominal effective axial potted-shell stiffnesses are equal to 1.2, 2.0, 1.3, 1.1, 1.4, and 1.2 times the nominal shell-wall stiffness of shells C1 through C6, respectively. The predicted results also indicate that the increase in the effective axial potted-shell stiffness is inversely proportional to the nominal shell wall stiffness. Details on the boundary stiffness analyses and effects of the boundary stiffness on the response of the shells are given in Refs. 3-4.

Nonuniform specimen end loading is due to initial specimen-end or loading-surface imperfections and to upper loading-platen rotations that are measured during the experiment. First, the measured upper and lower specimen-end imperfections $\delta_{top}(\theta)$ and $\delta_{bot}(\theta)$ were included in the finite-element model by introducing an initial in-plane axial perturbation to the nodes at the loaded ends of the shell. Then, the compression load was applied to the shell in two parts. The nonuniform specimen-end imperfections, $-\delta_{top}(\theta)$ and $-\delta_{bot}(\theta)$, were applied as displacements to the upper and lower ends of the shell, respectively, at the beginning of the analysis to simulate a full contact condition between the shell ends and the loading platens. Then, the experimentally measured end-shortening displacement Δ and upper loading-platen rotations ϕ_y and ϕ_z were applied to the upper shell end while holding the lower shell end fixed as illustrated in Fig. 1.

Failure Analyses

A conventional Tsai-Wu tensor failure criterion was used to predict material failure in the shells. Two additional failure criteria were used and include a delamination failure criterion and an in-plane failure criterion. The transverse shear stresses were assumed to be distributed parabolically through the shell-wall thickness. The material allowable values used in the criteria are: longitudinal strength = 124.0 ksi, transverse

strength = 8.4 ksi, and shear strength = 11.6 ksi. When either failure criterion is equal to or greater than one, the material is assumed to have failed. Each stress component of the failure criteria is examined to determine the mode of failure. The failure criteria were used to indicate the possibility of material failure and to establish failure trends associated with the composite shells.

PARAMETER UNCERTAINTY CHARACTERIZATION

Several shell parameter values have a significant amount of uncertainty, and an attempt to characterize the effects of these uncertainties was made. The shell parameters with uncertainties considered include uncertainties in geometric imperfection measurements, lamina fiber volume fraction, fiber and matrix properties, applied end-load distribution, and boundary condition stiffnesses.

Imperfection measurement uncertainty is due to the accuracy tolerance of the coordinate measurement device used to measure the shell-wall geometry and end-surface imperfection, and this tolerance is equal to ± 0.0006 in. This tolerance corresponds to less than 0.01% uncertainty in the shell-wall imperfection measurement (e.g., Fig. 2). The measurement tolerance corresponds to a ±3.0% uncertainty in the thickness measurement (e.g., Fig. 3), and approximately ±6% uncertainty in the shell-end imperfection measurement (e.g., Fig. 4). The uncertainty in fiber and matrix properties and fiber volume fraction was based on published data contained in Volume 2 of the MIL 17 Handbook for composite materials and from the material manufacturer. The nominal fiber and matrix properties can vary ±5% and the nominal fiber volume fraction can vary ±3%. The nominal fiber properties used in the present study are: longitudinal modulus = 31.19 Msi, transverse modulus = 3.49 Msi, shear modulus of 1.81 Msi, and Poisson's ratio = 0.27. The nominal matrix properties used are: Young's modulus = 0.53 Msi, shear modulus = 0.22 Msi, and Poisson's ratio = 0.35. The nominal fiber volume fraction is equal to 0.62.

The applied load distribution uncertainty is due to the shell end-surface imperfection uncertainty and the uncertainty in the orientation of the loading platen with respect to specimen shell-ends while the load is being applied during the test. Applied load distribution uncertainties are characterized indirectly by comparing the measured and predicted axial strains at selected points near the shell top and bottom loading surfaces. A correction to the applied displacement distribution was determined from the differences in the measured and predicted strains as follows. A user-written program external to the STAGS code was used to analyze the differences in the measured and predicted strains for a specified applied load value. This program used an iterative predictor-corrector method to determine a correction to the applied shell-end displacements. A new finite-element analysis was conducted with this displacement correction included in the model. This process was repeated iteratively until the difference in the predicted and measured strains reached a predetermined tolerance. A typical predicted displacement correction is presented in Ref. 3 and the amplitude of the displacement correction is on the order of ±0.0005 in.

Boundary condition stiffness uncertainty is due to uncertainties in the potting material stiffness and in the integrity of the bond between the potting material and the shell wall. Visual inspection of the specimens before and after testing indicated that the potting material has a tendency to separate from the shell wall. This boundary condition stiffness uncertainty was not rigorously characterized. However, results from several numerical experiments indicate that variations in the boundary stiffness can have a significant effect on the displacement and strains near the shell ends, and can affect the character of the collapse response of the shells, e.g., Ref. 4. Therefore, it was arbitrarily assumed that the effective axial and radial boundary stiffnesses could vary ±10%.

RESULTS AND DISCUSSION

Analytically predicted and experimentally measured results for the six graphite-epoxy shells considered in this study are presented in this section. The predicted results were obtained from finite-element models of geometrically perfect shells and shells that include initial geometric shell-wall imperfections, shell-wall thickness variations and thickness-adjusted lamina properties, local shell-wall lamina ply-gaps, boundary support conditions, and nonuniform loading effects. In addition, uncertainties in geometric and material properties, loading distribution, and boundary stiffnesses were included in the analyses. These results are presented to illustrate the overall behavior of compression-loaded graphite-epoxy shells and the effects of imperfections and parameter uncertainties on their response. First, results illustrating a typical nonlinear response of the quasi-isotropic 8-ply shell are presented. Then, comparisons between selected analytically predicted results and experimentally measured results for the 8-ply and 16-ply shells are presented. The results include predicted and measured load–end-shortening response curves, predicted prebuckling, buckling and postbuckling deformation response patterns, and predicted material failures.

Typical Nonlinear Response of an Imperfect Compression-loaded Cylindrical Shell

Results from a nonlinear analysis of the imperfect 8-ply $[45/0/90]_s$ shell C3 are presented in this section. The nonlinear analysis results are from a shell model that includes the effects of the measured initial shell-wall geometric and thickness imperfections, thickness-adjusted material properties, measured loading variations, and elastic radial support conditions. The predicted load-shortening response of shell C3 is shown in Fig. 5a. The axial load P and end-shortening Δ are normalized with respect to the linear bifurcation buckling load of the geometrically perfect nominal shell, $P_{bif} = 42.59$ kips, and the nominal shell-wall thickness, $t = 0.04$ in, respectively. The load–end-shortening curve indicates a linear prebuckling response. General instability occurs at a normalized axial load of $P/P_{bif} = 0.977$, marked by the letter A. The general instability response is followed by a sudden reduction in the axial load supported by the shell and is associated with the transient collapse response of the shell. The corresponding load-time history of the transient collapse response is shown in Fig. 5b. The load-time history curve has a sudden reduction in axial load until the collapse response attenuates and the axial load achieves a steady-state value. The kinetic energy in the shell obtains a maximum value during the transient collapse response, dissipates over time, and the shell reaches a stable postbuckling equilibrium state after approximately 0.007-0.008 seconds. The effective axial stiffness of the specimen is reduced in the postbuckling load range as indicated by the reduction in the slope of the load-shortening response curve.

The transient deformation responses for selected time steps during the transient collapse response of shell C3, indicated by the letters A through F in Figs. 5a and 5b, are presented in Fig. 6a through 6f, respectively. Just before buckling occurs, the shell wall deformations are characterized by several localized ellipse-like buckles as indicated in Fig. 6a. The localization in the deformation pattern is caused by the combination of a local geometric shell-wall imperfection that is in the form of a significant variation in the shell-wall mid-surface geometry, and the intersection of a helical ply-gap and a circumferentially aligned ply-gap in the shell at $x/L_T = 0.25$ and $\theta = 210°$. The localized deformations occur in regions with destabilizing compressive axial and circumferential stresses. After approximately 0.0012 seconds have elapsed in the transient response, a single ellipse-like buckle has grown in amplitude and couples with the destabilizing stresses in the shell wall to cause the general instability and collapse of the shell. The magnitude of the shell-wall radial displacement varies between ±0.5 times the shell-wall thickness. After additional time has elapsed, additional local buckles have formed around the circumference and along the length of the shell as indicated in Fig. 6c, and the normalized axial load has decreased from 0.974 to 0.759. The magnitude of the shell-

wall radial displacement varies between +2 to -4 times the shell-wall thickness. As the buckling process continues, the normalized axial load has decreased further to 0.554, and the deformation pattern in the shell wall continues to evolve and additional ellipse-like buckles have formed around the circumference of the shell as indicated in Fig. 6d. In addition, some of the buckles in the shell begin to coalesce into larger diamond-shaped buckles. The magnitude of the shell-wall radial displacement varies between +3 to -7 times the shell-wall thickness. After approximately 0.01 seconds have elapsed, the kinetic energy in the shell has dissipated to a negligible level indicating that the transient response has attenuated, and the shell has deformed into the stable postbuckling mode-shape indicated in Fig. 6e. As loading continues, the diamond-shaped buckles increase in size and the magnitude of the radial deformations of the buckles and the outer-surface ridges increase to between +4 and -9 times the shell-wall thickness as shown in Fig. 6f.

Predicted and Measured Response Comparisons

Selected results from nonlinear analyses of the six composite shells are compared to the experimentally measured results in this section. The nonlinear analysis results are for shell models that include the effects of the measured initial geometric and thickness imperfections, thickness-adjusted material property variations, measured loading variations, elastic radial support conditions, and selected specimen parameter uncertainties. The specimen parameter uncertainties considered include uncertainties in the imperfection measurement accuracy, fiber and matrix properties, fiber volume fraction, applied load, and boundary stiffness. Upper and lower response bounds were determined based upon the results of a traditional combinatorial analysis of the effects of the selected parameter uncertainties. Predicted and measured load–end-shortening response curves are presented in this section.

Eight-ply shells.- Three sets of analytically predicted and experimentally measured load–end-shortening response curves for the 8-ply shells C1, C2, and C3 are shown in Fig. 7. The axial load P is normalized by EA, where E is the effective axial stiffness of the shell and A is the nominal shell cross-sectional area. The end-shortening Δ is normalized by the nominal shell length $L = 16.0$ in. The solid and dashed lines in the figure represent experimentally measured and analytically predicted results, respectively. Each shell has two predicted response curves representing predicted upper and lower bounds to the response based on specimen parameter uncertainties, and the regions between the response bounds are shaded for clarity. The measured buckling load of each shell is marked by a filled circle and the ultimate failure load of each shell is marked with an X. In addition, each shell has one or more analytically predicted failure boundaries represented by the dark gray solid lines in the figure. Each failure boundary is labeled with the number 1, 2, or 3, which denote matrix failure initiation, fiber failure initiation, and delamination failure initiation, respectively. The measured results indicate that the prebuckling responses are linear up to the general instability load. General instability occurs at normalized loads of $P/EA = 0.00122$, 0.0044, and 0.0022 for specimens C1, C2, and C3, respectively, and are 7.8, 13.7, and 17.6% lower than the predicted linear bifurcation buckling loads for the corresponding geometrically perfect, nominal shells, respectively. The general instability loads are followed by a sudden reduction in the axial load supported by the specimens, which is associated with the unstable transient collapse response of the specimens. During collapse, the specimens buckled into the classical diamond-shaped general instability mode-shape, and the collapse response was accompanied by an audible snapping sound. In addition, no significant visible failures were observed in the specimens as a result of the collapse response. The specimens achieved a stable postbuckling equilibrium state and had additional load carrying capacity in the postbuckling load range. Additional audible popping sounds were heard during the loading of the specimens in the postbuckling load range, which suggests that a progressive accumulation of material failures is occurring in the specimens. The accumulation of material failures continued until the ultimate failure

of the specimens occurred. The results in Fig. 7 indicate that, for the most part, the measured responses fall within the analytically predicted response bounds. In particular, the results indicate that the measured response curves tend to correlate with the mid-point between the upper and lower predicted response bounds. The predicted results indicate that, in most cases, material failure in the specimens is likely to occur at load levels near the general instability load and in the postbuckling load range. More specifically, matrix compression failure is predicted to occur in specimens C2 and C3 near the general instability point, followed by fiber compression failures and delamination type failures in the postbuckling load range. In contrast, the analytically results predict that matrix and fiber compression failures occur in specimen C1 in the postbuckling load range. These failure predictions correlate well with the failure trends observed in the tests. Predicted initial post-collapse radial displacement contours and the corresponding observed moiré fringe patterns for these specimens were observed to correlate well, as shown in Ref. 4.

Sixteen-ply shells.- Analytically predicted and experimentally measured load–end-shortening response curves for the 16-ply shells C4 through C6 are shown in Fig. 8. The axial load P is normalized by EA, where E is the effective axial stiffness of the shell and A is the nominal shell cross-sectional area. The end-shortening Δ is normalized by the nominal shell length L = 16.0 in. The solid and dashed lines in the figure represent experimentally measured and analytically predicted results, respectively. Each shell has two predicted response curves representing predicted upper and lower bounds to the response based on specimen parameter uncertainties, and the regions between the response bounds are shaded for clarity. The measured buckling load of each shell is marked by a filled circle and the ultimate failure load of each shell is marked with an X. In addition, each shell has one or more analytically predicted failure boundaries represented by the dark gray solid lines in the figure. Each failure boundary is labeled with the number 1, 2, or 3, which represent matrix failure initiation, fiber failure initiation, and delamination failure initiation, respectively. The measured results indicate that the initial load-shortening responses are, for the most part, linear up to the limit-point load for each specimen as indicated in the figure. However, the load-shortening responses for specimens C5 and C6 have a slight nonlinear behavior at end-shortening values greater than $\Delta/L = 0.004$. General instability occurs at normalized loads of $P/EA = 0.0027$, and 0.0049 for specimens C4, and C6, respectively, and are 16.8, and 18.4% lower than the predicted linear bifurcation buckling loads for the corresponding geometrically perfect, nominal shells, respectively. The results show that the general instability loads of specimens C4 and C6 coincide with the ultimate failure loads of the specimens, and these specimens do not have postbuckling load carrying capacity. More specifically, experimental results indicated that, upon collapse, specimens C4 and C6 have a significant amount of material failure including fiber and matrix compression failures and delamination failures, which caused the ultimate failure of the specimens. The predicted results indicate that, in most cases, the initiation of material failure is likely to occur during the initial portion of the transient collapse response as shown in Fig. 8, and these results explain the observed failure trends in specimens C4 and C6. In contrast, specimen C5 does not have a general instability load, rather, this specimen fails completely at a load of $P/EA = 0.0062$, which is 43.9% lower than the predicted linear bifurcation buckling load for the corresponding geometrically perfect, nominal shell. The overall failure of this specimen is characterized by a significant amount of delamination failures and fiber and matrix compression failures around the entire circumference of the shell. Post-test inspection indicated that the overall failure of the shell might have been initiated by a material failure near an axially aligned ply-gap in the shell wall. Predicted initial post-collapse radial displacement contours and the corresponding observed moiré fringe patterns for specimen C4 were observed to correlate well. Similar results were obtained for specimen C6 and indicate similar failure trends.

CONCLUDING REMARKS

The results of an experimental and analytical study of the effects of imperfections on the nonlinear response and buckling loads of unstiffened thin-walled compression-loaded graphite-epoxy cylindrical shells are presented. Numerical results for the nonlinear prebuckling, transient buckling, and postbuckling response of shells with measured imperfections are presented. The numerical results include the effects of traditional initial geometric shell-wall mid-surface imperfections and the effects of other nontraditional imperfections. These nontraditional imperfections include shell-wall thickness variations, material property variations, shell-end geometric imperfections, local shell-wall ply-gaps associated with the fabrication process, variations in loads applied to the end of the shell, and elastic boundary support conditions. In addition, upper and lower bounds to the nonlinear response of the shells are presented, which were determined from a combinatorial analysis of the effects of uncertainties in the values of several shell parameters. The uncertainties considered in the present study include uncertainties in the geometric imperfection measurements, lamina fiber volume fraction, lamina fiber and matrix properties, boundary condition stiffnesses, and applied load distribution. A high-fidelity nonlinear shell analysis procedure has been used to predict the nonlinear response and failure of the shells, and the analysis procedure accurately accounts for the effects of these traditional and nontraditional imperfections and parameter uncertainties on the nonlinear response and failure of the shells. The analysis results generally correlate well with the experimental results indicating that it is possible to predict accurately the complex nonlinear response and buckling loads for compression-loaded composite shell structures.

The numerical results indicate that the effects of the traditional and nontraditional imperfections, and uncertainties in the values of selected parameters considered in this study can be important for predicting the buckling loads of composite shells since they can significantly affect the nonlinear response and buckling loads of the shells. The results indicate that, for the most part, the measured response of the shells falls mid-way between the predicted upper and lower bounds to the response that are associated with the uncertainties or variations in the shell parameters considered in the study. These results indicate that the nonlinear analysis procedure used in this study can be used to determine accurate, high-fidelity design knockdown factors and response bounds that can be used for predicting composite shell buckling and failure loads in the design process. The traditional and nontraditional imperfections considered in this study could be used to formulate the basis for a generalized imperfection signature of a composite shell that includes the effects of variations or uncertainties in the shell-geometry, fabrication-process, load-distribution and boundary stiffness parameters. The high-fidelity nonlinear analysis procedure used in this study can be used to form the basis for a shell analysis and design approach that includes this generalized imperfection signature and addresses some of the critical shell-buckling design criteria and design considerations for composite shell structures. This high-fidelity nonlinear analysis procedure could be used in the shell design process without resorting to the traditional empirical shell design approach that can affect the cost of developing new composite shell designs.

REFERENCES

1. Anon., Buckling of Thin-Walled Circular Cylinders. NASA Space Vehicle Design Criteria, NASA SP-8007, September 1965.

2. Koiter, W. T., "On the Stability of Elastic Equilibrium," (in Dutch), H. J. Paris, Amsterdam, Holland, 1945; translation available as AFFDL-TR-70-25, February 1970, Wright-Patterson Air Force Base.

3. Hilburger, M. W., and Starnes, J. H., Jr., "High-fidelity Analysis of Compression-loaded Composite Shells," Proceedings of the 42nd AIAA/ASME/ASCE/AHS/ASC Structures, Structural Dynamics, and Materials Conference, Seattle, WA, 2001. AIAA Paper No. 2001-1394, April 2001.

4. Hilburger, M. W., and Starnes, J. H., Jr., "Effects of Imperfections on the Buckling Response of Compression-Loaded Composite Shells." *International Journal of Non-Linear Mechanics*, Vol. 37, 2000, pp. 623-643.

5. Rankin, C. C., Brogan, F. A., Loden, W. A., and Cabiness, H. D., "STAGS Users Manual, Version 3.0," Lockheed Martin Missiles & Space Co., Inc., Advanced Technology Center, Palo Alto, CA, Report LMSC P032594, 1999.
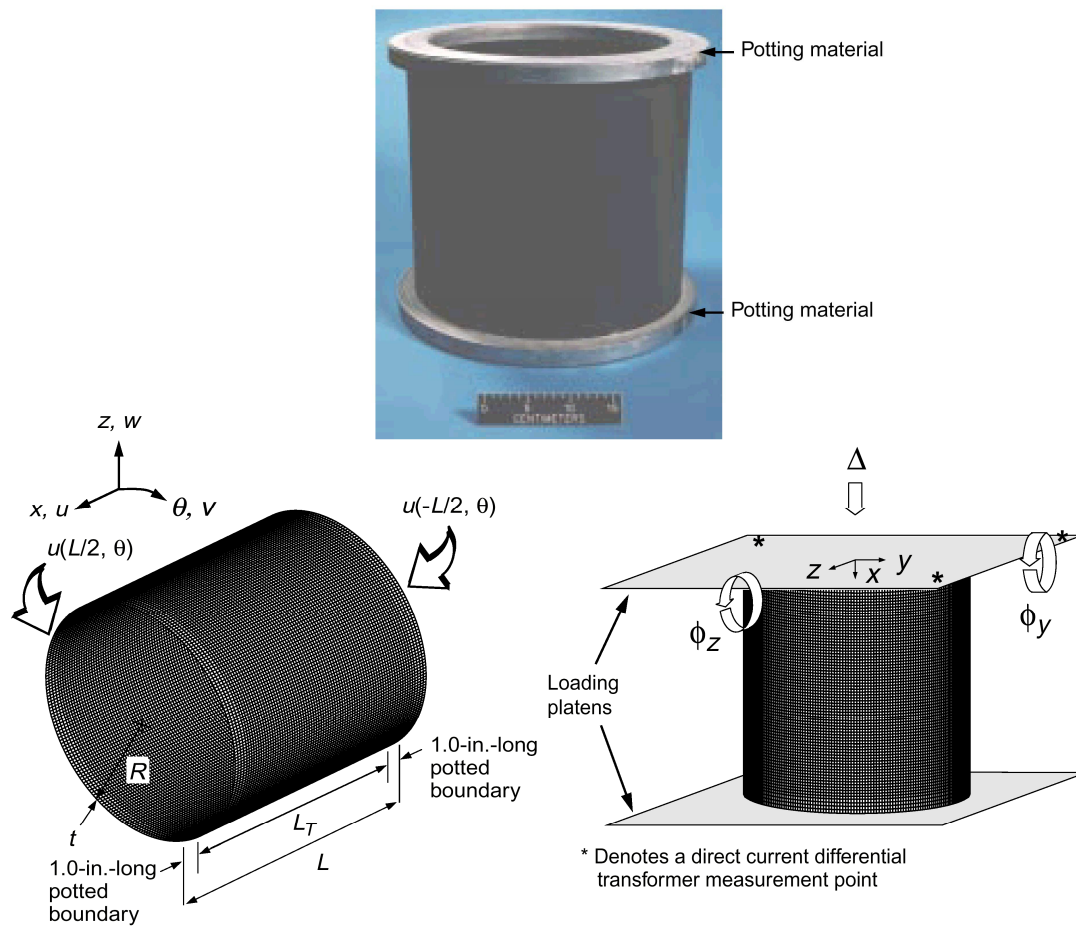
Fig. 1 Typical specimen, finite-element model geometry and loading conditions.
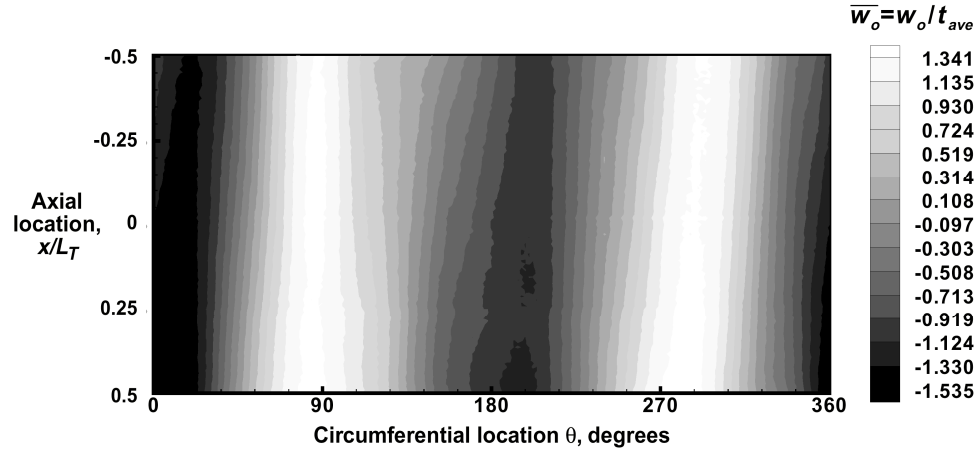
Fig. 2 Typical measured inner-surface imperfection shape for shell specimen C3.
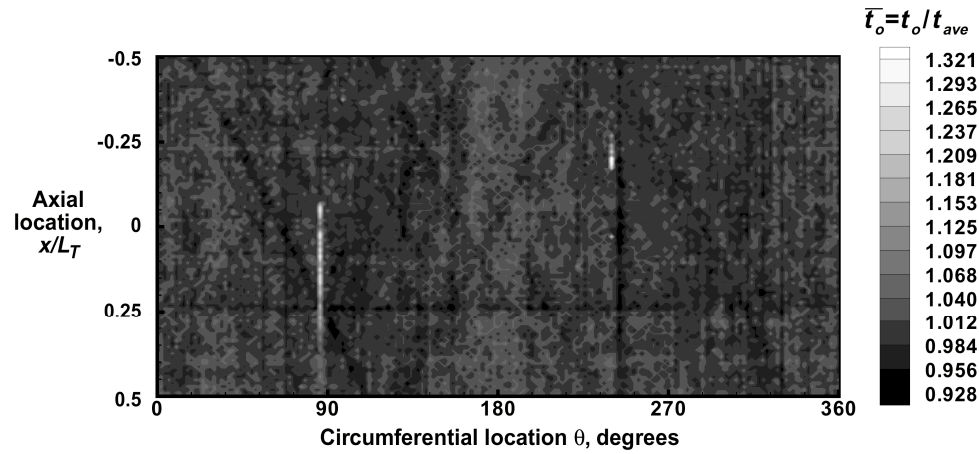
Fig. 3 Typical measured wall thickness variation for a shell specimen C3.
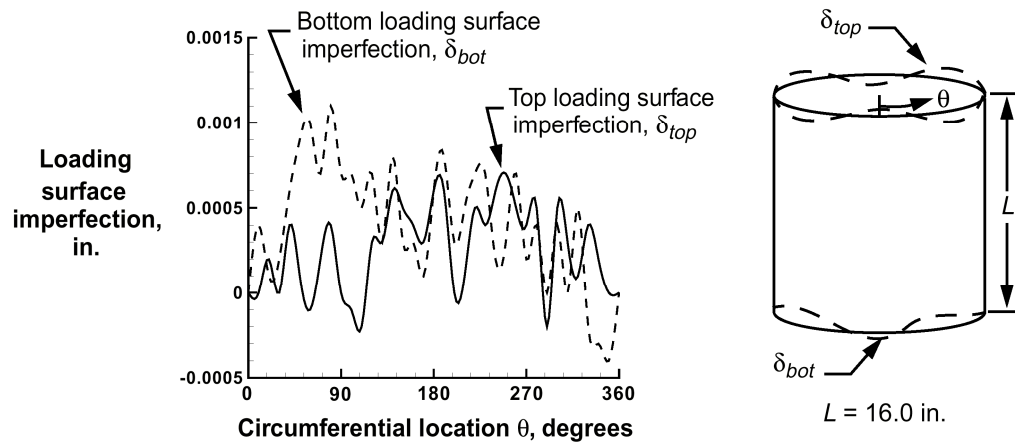
Fig. 4 Typical measured shell-end or loading-surface imperfections for a shell specimen C3.

a) Normalized load–end-shortening response curve   b) Normalized load-time history during collapse
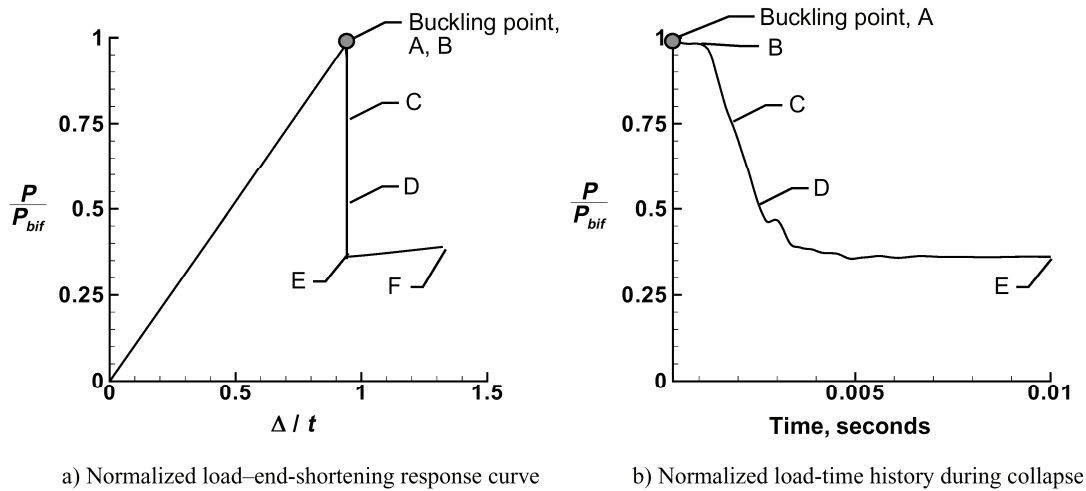
Fig. 5 Analytically predicted nonlinear response of an imperfect, compression-loaded, quasi-isotropic shell C3.

a) Prebuckling deformations
Time = 0.0 seconds
$\Delta/t = 0.93$
$P / P_{bif} = 0.977$

b) Initial buckling deformations
Time = 0.0012 seconds
$\Delta/t = 0.94$
$P / P_{bif} = 0.974$

c) Transient buckling deformations
Time = 0.0019 seconds
$\Delta/t = 0.94$
$P / P_{bif} = 0.759$

d) Transient buckling deformations
Time = 0.0024 seconds
$\Delta/t = 0.94$
$P / P_{bif} = 0.554$

e) Initial post-buckling deformations
Time = 0.01 seconds
$\Delta/t = 0.94$
$P / P_{bif} = 0.364$

f) Post-buckling deformations
$\Delta/t = 1.3$
$P / P_{bif} = 0.390$
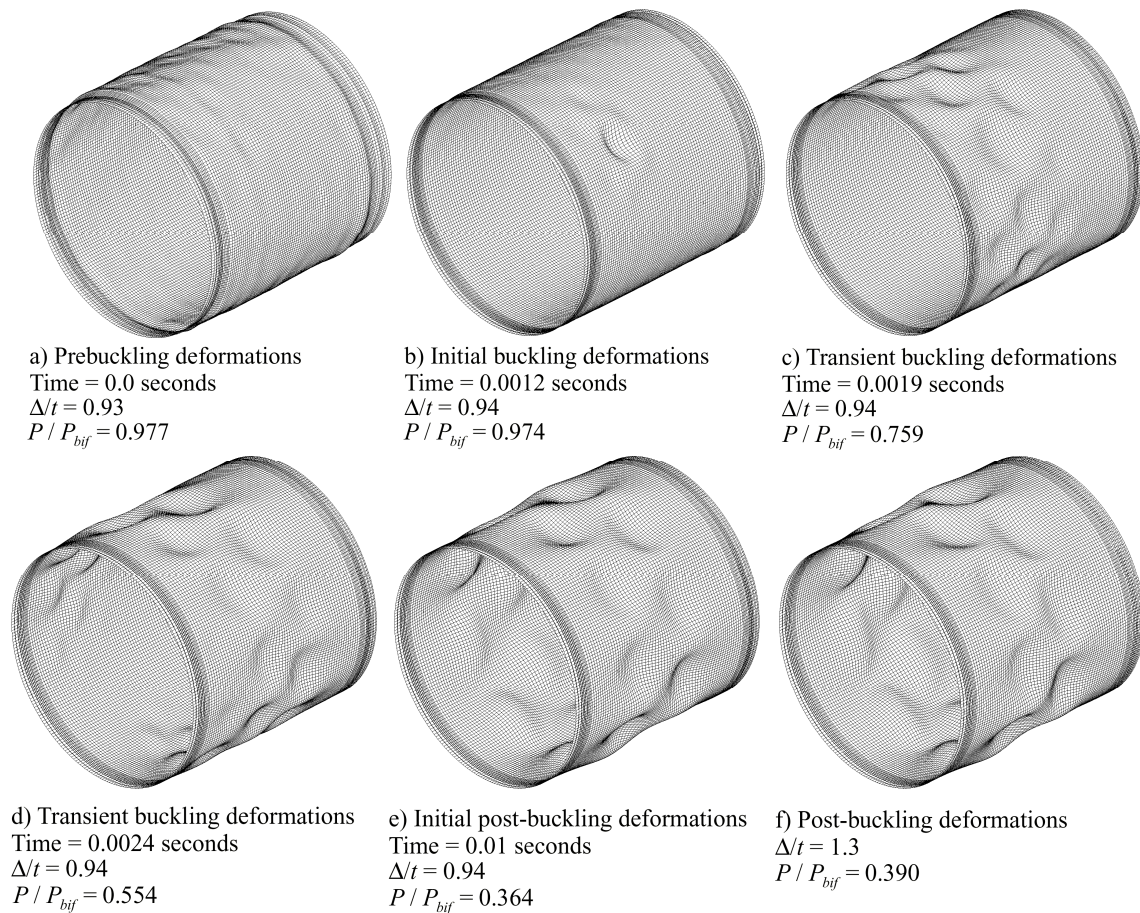
Fig. 6 Analytically predicted prebuckling, buckling, and postbuckling response of an imperfect, compression-loaded, quasi-isotropic shell C3.
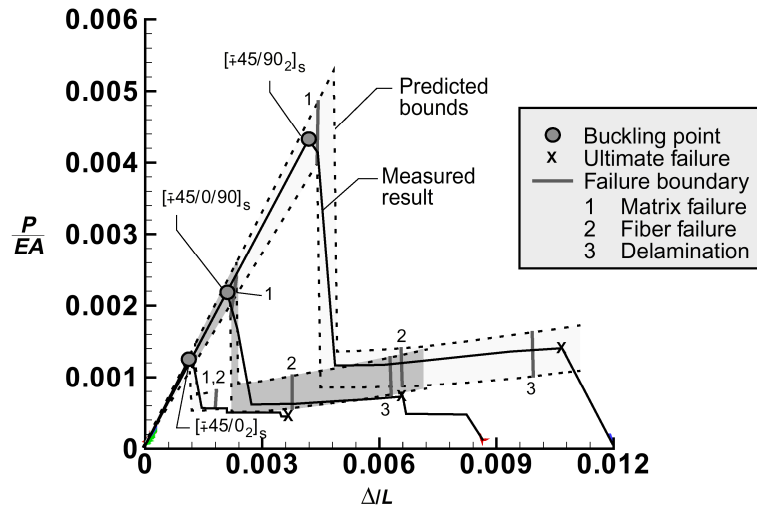
Fig. 7 Analytically predicted and experimentally measured load–end-shortening response curves for 8-ply compression-loaded shells; predicted results represent response bounds.
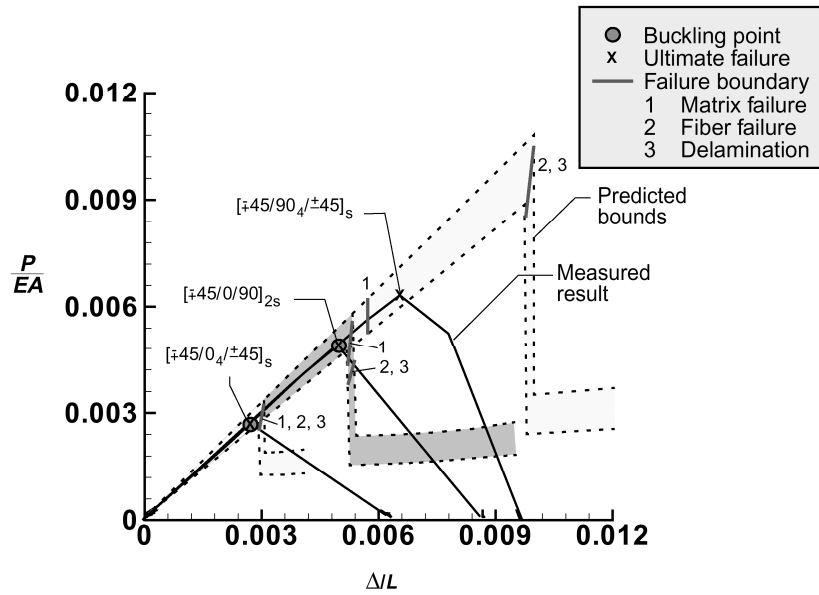
Fig. 8 Analytically predicted and experimentally measured load–end-shortening response curves for 16-ply compression-loaded shells; predicted results represent response bounds.

A New On-Board Gauge Calibration Process
for Aircraft Engine Testing

Jean-Pierre Lombard, Eric Seinturier, Marc Berthillier
SNECMA Moteurs
Centre de Villaroche
F-77550 Moissy Cramayel
France

1   ABSTRACT

A new procedure for calibrating on-board gauges on the blade assemblies of turbomachines is proposed in this paper. The calibration of an engine gauge, determined *a priori* during a component dynamic test, makes it possible to establish the levels of dynamic stress on the entire instrumented airfoil (based on the readings output by the gauge during the engine test). The method proposed is based on the use of holographic dynamic measurements enabling the qualification of a finite element model in relation to the component test. The calibration relations are then determined based on the qualified model. The procedure proposed enables an increase in the reliability of the calibration relations by making it possible to take into account in the model the real conditions of the engine test (thermal, centrifugal and aerodynamic loads, and the shapes of dynamic modes of the complete blade assembly). Similarly, it enables a drastic reduction in the costs relating to the component tests required to establish these relations.

2   INTRODUCTION

The procedures for designing blade assemblies for turbo engines use different types of analysis, in particular to guarantee the safety of the engine. With regard to dynamic considerations, these analyses are based both on the results of tests and on the results of calculations. Whatever the design approach, the certification authorities require engine tests in order to qualify the machine before use.

Qualification tests consist in measuring the levels of dynamic stress during operation of every flight envelope, in particular for all rotating parts. To do so, strain gauges are installed on the stators or rotor wheels of the qualification engine. These on-board gauges are called engine gauges. Based on the measurements made during operation, the dynamic stress status is determined for the entire blade assembly based on **calibration factors,** i.e. the **relations governing the transfer of strain or stress between engine gauges and the gauges distributed over the airfoil**. These relations are established during component dynamic tests carried out beforehand. After the qualification test (during operation), the maximum stress on the airfoil (deduced from the engine gauges using the calibration factors) is then compared with the admissible dynamic stress determined by numerical means: the real dynamic margin is then estimated.

This procedure for determining the real dynamic margin requires data on:
• the static stress field obtained by finite element calculation,
• the distribution of dynamic stress per mode, obtained by component testing or by finite element calculation,
• the measurements concerning dynamic engine stress during operation output by the engine gauge.

The engine qualification test is carried out at the end of the design cycle. At this point in time, if the dynamic margins are insufficient, re-design is required as well as a new qualification test, thereby increasing the cost of design of the engine.

The quality with which calibration factors are evaluated is thus vital. This implies expensive, in-depth component dynamic testing. In this paper we propose to reduce the time and the costs involved in determining these calibration factors, and to increase the precision and the frequency band of validity, by using dynamic field measurements of holographic type **[SMI.99]** and results obtained by finite element calculation.

3   DESIGN CRITERIA OF BLADE ASSEMBLY FOR HIGH CYCLE FATIGUE : BASIC PRINCIPLES

Here we briefly review a few basic concepts to make it easier to understand our paper.

Consider a blade of a rotor wheel in a fluid flow, with steady and unsteady components (whose angular frequency is similar to that of the fundamental mode of vibration of the blade), rotating at a given speed.
The steady component is due to the difference in the downstream and upstream pressures of the wheel in question. The unsteady component is mainly related to the wake of the stator wheel located upstream of the rotor wheel in question, as well as to the other obstacles in the aerodynamic flow, upstream and downstream of the wheel in question.
For a given temperature, the blade is therefore subject to a static load caused, on the one hand, by the centrifugal force resulting from the rotation of the wheel around the axis of the engine, and on the other hand, by the steady component of the aerodynamic pressure. The unsteady component of the aerodynamic pressure generates a purely dynamic load on the airfoil (see Figure 1).
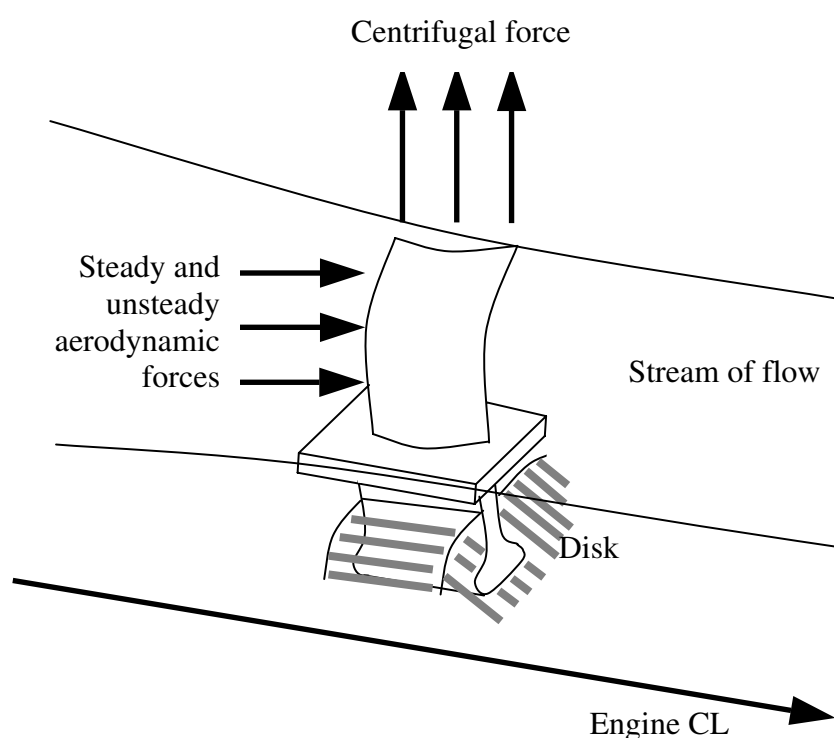
Figure 1: Loads applied to a blade rotating in a fluid flow

The blade is designed for high cycle fatigue such that it has an infinitely long service life. This means that the level of stress obtained on any point of the blade under the combined static and dynamic load does not exceed the fatigue limit criteria **[LEM.96]**. The fatigue limit is experimentally obtained by dynamic tests on a test piece with a static preload. The fatigue limit stress pairs are sought for various static/dynamic load ratios (Woehler curves). Based on these limit values, a Goodman diagram is established for a given number of cycles (a cycle corresponding to a period of the dynamic load) and defines the area of the admissible static and dynamic stress pairs corresponding to an infinite service life (Figure 2).
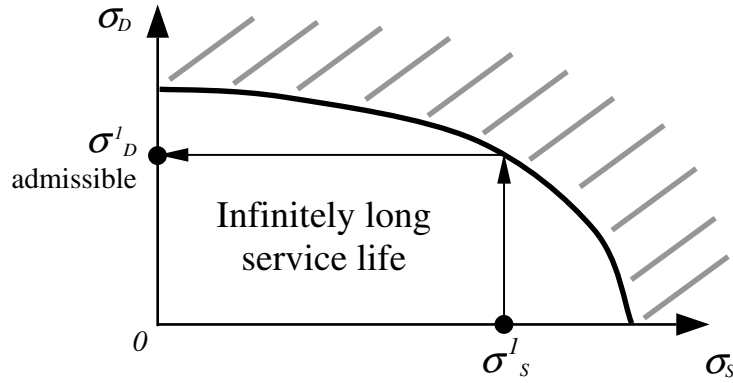
Figure 2: Goodman diagram

The Goodman curve makes it possible to relate an admissible dynamic stress $\sigma^1{}_D$ to a given static stress $\sigma^1{}_S$. In the dimensioning phase, the static stress factors are correctly evaluated by finite element calculation, since the related load is correctly characterised. On the other hand, characterising the dynamic stress generated by the unsteady aerodynamic pressure is a more delicate matter. This is because parameters are involved that are difficult to evaluate, such as the characterisation of the unsteady pressure fields caused by the different obstacles upstream and downstream of the wheel in question, as well as their periodicity, mechanical and aerodynamic damping, and the shape of the high-level modes of vibration. This is why these dynamic stress factors must be measured during the qualification test. These measurements are the subject of a special procedure described in the following paragraph.

4   CURRENT CALIBRATION PROCEDURE FOR ENGINE GAUGES

Consider a blade of a given stator or rotor wheel. In the case of blades formed by sectors for certain stator wheels and of blisks, the calibration principle is similar. The calibration phase for engine gauges is carried out on the basis of component dynamic tests. This operation breaks down into two types of tests: stress distribution measurement and calibration tests of the engine gauges.

In the 2 types of tests, the airfoil to be characterised (rotor or stator wheel) is fastened into position with a test jaw (which in turn is fastened onto a test bench). The jaw is designed in order to reproduce as faithfully as possible the boundary conditions during operation. The blade is instrumented with strain gauges (see Figure 3). The excitation applied is of scanned sine-wave type, obtained by means of an electrodynamic vibrating table, an electrodynamic shaker, a piezoelectric shaker, or a siren type shaker (a jet of pulsed air). For each resonance frequency, the signals output by the strain gauges are processed using a spectrum analyser.

4.1   Stress distribution measurement

This measurement is carried out on a single reference blade, for which the measurements are designed to precisely define the stress distribution on the blade for each excited mode of vibration. Although only carried out once, this test is extremely expensive because of the high density of gauges used. The instrumentation of the airfoil can comprise more than a hundred strain gauges: some are located in the middle of the airfoil (low-frequency modes) while most are located along the edges where strains mainly appear on high-frequency modes (see Figure 3). This measurement makes it possible to determine for each mode a strain transfer relation between the instrumented points (and directions). This relation is defined based on the strains d_{jv}

observed at point j on mode v. These values are combined in the strain transfer matrix D defined by expression (1).

$$D = \begin{bmatrix} d_{11} & d_{12} & \cdots & d_{1v} & \cdots \\ d_{21} & d_{22} & \cdots & d_{2v} & \\ \vdots & \vdots & \ddots & \vdots & \\ d_{j1} & d_{j2} & \cdots & d_{jv} & \\ \vdots & & & & \ddots \end{bmatrix} \tag{1}$$

This strain transfer matrix can be normalised in relation to one of the instrumented points and forms the transfer matrix $\overline{D}^{\,j}$, normalised in relation to point j, defined by expression (2).

$$\overline{D}^{\,j} = \begin{bmatrix} \overline{D}_1^{\,j} & \overline{D}_2^{\,j} & \cdots & \overline{D}_v^{\,j} & \cdots \end{bmatrix} = \begin{bmatrix} d_{11}/d_{j1} & d_{12}/d_{j2} & \cdots & d_{1v}/d_{jv} & \cdots \\ d_{21}/d_{j1} & d_{22}/d_{j2} & \cdots & d_{2v}/d_{jv} & \\ \vdots & \vdots & \ddots & \vdots & \\ 1 & 1 & \cdots & 1 & \\ \vdots & & & & \ddots \end{bmatrix} \tag{2}$$

This transfer relation, characterised by matrix $\overline{D}^{\,j}$ enables the expansion of the strain values for each point instrumented during the distribution test, based on the value of strain at point j, at right angles with an engine gauge or a reference gauge for example.
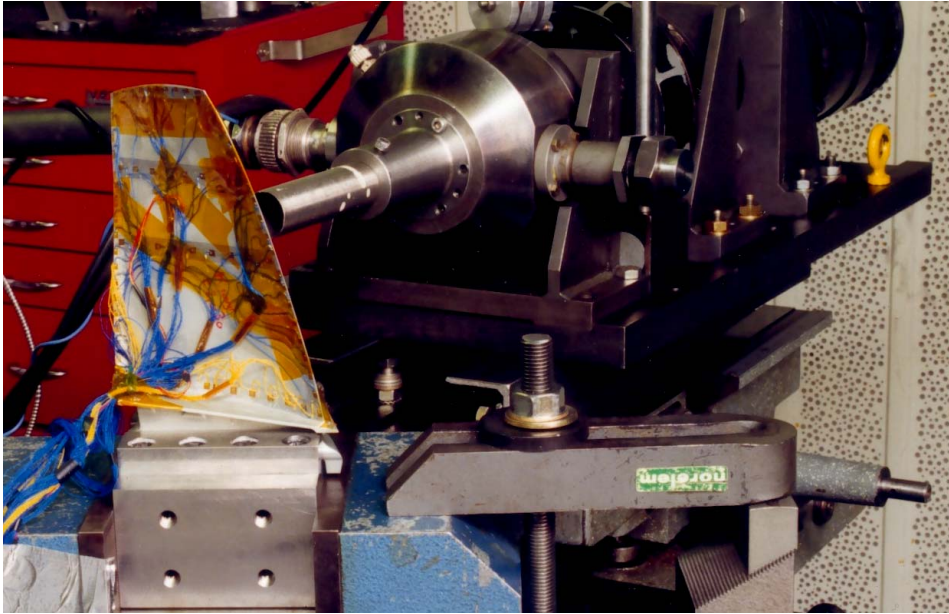
Figure 3: Measurement of stress distribution by strain measurement
on a HP compressor blade - excitation by a jet of pulsed air

4.2 Calibration of engine gauges

This test is carried out for each airfoil instrumented with engine gauges. The instrumentation for these component tests can be limited to a few engine gauges and a dozen reference gauges. All these gauges (engine and reference gauges) are placed in positions chosen from among those used when stress distribution is precisely measured. This calibration test is necessary because engine gauges are subject to a special

instrumentation procedure. Engine gauges must be capable of meeting criteria of thermal resistance and static load resistance of the levels caused by the rotation of the wheel. To do so, they are fastened onto the airfoil and protected by a bonding agent. Because of the fastening method and the position of the gauges, this type of instrumentation requires on-site calibration. Calibration is carried out in relation to reference gauges with a known level of sensitivity. The calibration relation is defined between the engine gauge (measurement of strain d^{jm}) and a reference gauge (measurement of strain d^{jr}) using the calibration coefficient α :

$$d^{jr} = \alpha \cdot d^{jm} \tag{3}$$

4.3   Calibration factors

Calibration factors are established, based on distribution factors (defined by relation (2)) and the calibration values for the engine gauges (relation (3)). In this way, for a mode ν of angular frequency ω_ν, the dynamic strain values $d(\omega_\nu)$ are deduced for the airfoil (where are located the gauges instrumented during the distribution test), based on the value measured on the engine gauge $d^{jm}(\omega_\nu)$, by means of relation (4):

$$d(\omega_\nu) = \begin{bmatrix} d_1(\omega_\nu) \\ d_2(\omega_\nu) \\ \vdots \\ d_{jr}(\omega_\nu) \\ \vdots \end{bmatrix} = \overline{D}_\nu^{jr} \cdot d^{jr}(\omega_\nu) = \overline{D}_\nu^{jr} \cdot \alpha_\nu \cdot d^{jm}(\omega_\nu) \tag{4}$$

The calibration procedure is performed for all the blades instrumented with engine gauges and for the blade that was used to measure the distribution of dynamic stress. After this procedure, the blades are installed on the qualification engine. Based on the calibration factors (i.e. the calibration coefficients for the engine gauges as well as the strain transfer relations) and on the static stress calculated by the finite element method, the allowable dynamic stress (scope limit) is determined for each mode of vibration and for each engine gauge. During the engine qualification test, the levels measured by the engine gauges are monitored to guarantee the integrity of the structure. These dynamic levels are then analysed and the safety margins are deduced for all the instrumented wheels. The engine is qualified if these safety margins are large enough. If not, a new design is required for the components in question.

5   PROPOSED CALIBRATION PROCEDURE

The calibration phase comprises two types of component tests: measurement of stress distribution (an expensive test requiring a high level of instrumentation) and calibration tests of the engine gauges. In this paper, we propose to use holographic measurements of field type (Figure 4) in order to qualify the finite element model. This qualification of the FE model is based on a quantitative comparison of the modal displacement fields both measured and calculated. The qualified model is then used to determine the stress distribution in the airfoil.

Holographic measurement techniques are frequently used in industry and are the subject of research work dedicated to improving identification and correlation procedures **[FOL.00] [HUM.99] [LEP.01]**. The technique for acquiring dynamic data by this means of measurement is based on the principle of holographic interferometry. The surface to be measured is illuminated by means of a continuous or pulsed wave laser. The acquisition of optical data is obtained by a CCD video camera (Figure 4). A hologram of the structure is obtained by interference between the reflected laser beam and a reference laser beam. Based on the interference of two holograms of the structure at 2 different instants in time, the requisite displacement data can be obtained.
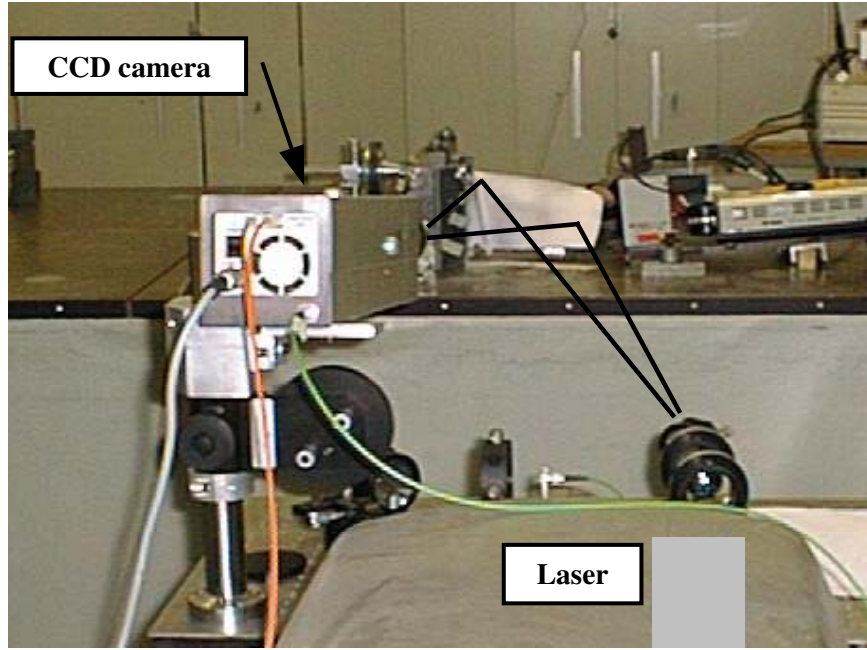
Figure 4: Dynamic measurement by laser holography

This new procedure has a number of advantages:
- The behaviour of the blade is not modified by the instrumentation since measurement is made by optical readings.
- Since stress distribution is obtained by finite element calculation, maximum modal stress can be obtained and the effects of steady centrifugal, thermal and aerodynamic loads can be precisely taken into account in dynamic stress transfer relations, at the operating level of the engine in question, as well as the shape of the normal mode with nodal diameters appropriate to the excitation.
- A component dynamic test of quantitative holography type is relatively inexpensive in relation to a stress distribution test, since the blade is not subject to lengthy, pains-taking instrumentation.

5.1 Mathematical model hypotheses

In general, blade assemblies are structures with little damping (damping is limited to around 1% at most). For this reason, within the framework of a component test under periodic excitation, it is legitimate to consider only the contribution of the excited mode in the dynamic response of the blade near the resonance frequency. Given the hypothesis of a material with linear behaviour and small displacements, the dynamic equilibrium equation for the blade formulated for the sinusoidal excitation of angular frequency ω results in relation (5) :

$$\left[K + j\omega B - \omega^2 M\right] y(\omega) = f(\omega) \tag{5}$$

where *K, B,* and *M* are respectively the stiffness, damping and mass matrices for the structure, and $y(\omega)$ and $f(\omega)$ are the vectors of harmonic displacement response and harmonic force applied to the structure.

After conventional breakdown of the harmonic response of the structure on a truncated basis of *m* fundamental modes of vibration for the conservative system (relation (6)), the dynamic equilibrium of the structure is governed by relation (7):

$$y(\omega) = Y_m\, c(\omega) \tag{6}$$

$$\left[\Lambda_m + j\omega\,\beta_m - \omega^2 I_m\right] c(\omega) = Y_m^T f(\omega) \tag{7}$$

in which Λ_m, Y_m are respectively the spectral and modal matrices of the m first fundamental modes of vibration of the conservative system, normalised per unit of generalised mass, $c(\omega)$ is the vector of the generalised co-ordinates and β_m the generalised damping matrix.

Based on the hypothesis that the only contribution is that of the excited mode ν (characterised by its angular frequency ω_ν and its eigenvector y_ν), the harmonic response of the structure near resonance angular frequency ω_ν is given by relation (8):

$$y(\omega) = \frac{y_\nu y_\nu^T f(\omega)}{\omega_\nu^2 - \omega^2 + j\omega\,\beta_\nu} \tag{8}$$

where $\beta_\nu = 2\,a_\nu\,\omega_\nu$ is the generalised damping of mode ν and a_ν the reduced damping coefficient.

At resonance angular frequency ($\omega = \omega_\nu$), the harmonic response during displacement of the structure is defined by relation (9):

$$y(\omega_\nu) = \frac{y_\nu y_\nu^T f(\omega_\nu)}{j\omega_\nu\,\beta_\nu} \tag{9}$$

The dynamic stress field σ is deduced from the dynamic displacement field y of the structure by means of a relation of linear dependence. At angular frequency ω_ν, it is defined by relation (10):

$$\sigma(\omega_\nu) = D\,\varepsilon(\omega_\nu) = D\,B\,y(\omega_\nu) \tag{10}$$

where D is the elasticity matrix of material, B is the derived matrix of the shape functions, and $\varepsilon(\omega_\nu)$ the dynamic strain field at angular frequency ω_ν.

6   RESULTS OF CORRELATION BETWEEN CALCULATION AND TEST

In order to illustrate the interest of the proposed procedure, two results of correlation calculations/tests are presented for an HP compressor blade (not illustrated in this paper). First of all, we compare the modal stress fields calculated and measured by strain measurement. Secondly, we compare the modal displacements calculated by finite elements and measured by holography. It should be noted that the blades are of the same type. The same finite element model is used in both cases for numerical prediction. Only the boundary conditions are different.

6.1   Correlation criteria

Two comparison criteria are used here in order to compare the calculation results with the results of tests at the instrumented points (in the direction of measurement). One criterion is based on the relative error E_f committed when predicting eigenfrequencies, and a second criterion quantifies the colinearity (or similitude of shape) of the vectors measured and calculated (MAC criterion). Matching between the predicted and observed modes is evaluated by this shape criterion.

- Relative error on frequency E_f

$$E_f = \frac{\left| f_{cal} - f_{mes} \right|}{f_{mes}} \tag{11}$$

where f_{mes} (f_{cal}) is the measured (calculated) eigenfrequency.

- Modal assurance criterion (or matching) on displacement MAC_y, on stress MAC_σ :

$$MAC_y = \frac{\left(y_{cal}^T \cdot y_{mes}\right)^2}{\left\|y_{cal}\right\|^2 \left\|y_{mes}\right\|^2}, \quad MAC_\sigma = \frac{\left(\sigma_{cal}^T \cdot \sigma_{mes}\right)^2}{\left\|\sigma_{cal}\right\|^2 \left\|\sigma_{mes}\right\|^2} \tag{12}$$

where y_{mes} (y_{cal}) and σ_{mes} (σ_{cal}) are the measured (calculated) displacement and stress eigenvectors.

Remark: the value of the MAC criterion is 1 for two colinear vectors, 0 for two orthogonal vectors.

6.2   Strain measurement

Dynamic strain distribution is measured using single-direction strain gauges distributed over the entire airfoil. The excitation of the airfoil is of siren type in the low frequency band and of piezo-electric type in the medium frequency band. 25 modes were measured. The amplitude and the phase of strain were read for each gauge and each mode of resonance.

The result of matching the measured modes and calculated modes, obtained by the criterion MAC_σ, is presented in Figure 5 for the 13 first modes. Only 47 gauge values were used in estimating this criterion. The relative error on the corresponding eigenfrequencies is illustrated in Figure 6.
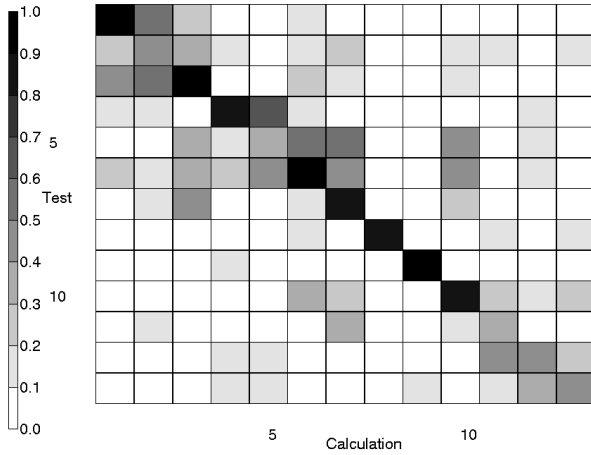
Figure 5: Matching matrix (MAC_σ)
between measured modes and calculated modes
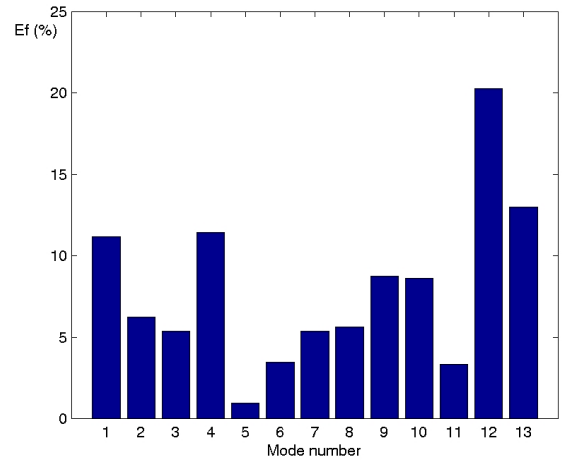
Figure 6: Relative error (%) in frequency (E_f)
between matched measured and calculated modes

As can be seen in Figure 5, 8 modes are matched with significant MAC_σ values, higher than 0.7. Mode nos. 2 and 5 (corresponding to the first twists of the blade) were not correctly observed by the measuring gauges selected. The relative errors in eigenfrequency obtained with the matched modes are around 12% at the most. The stress modeshapes calculated and measured are presented in Figure 7 for mode no.10. For guidance, gauges 1 to 47 describe the contour of the blade.
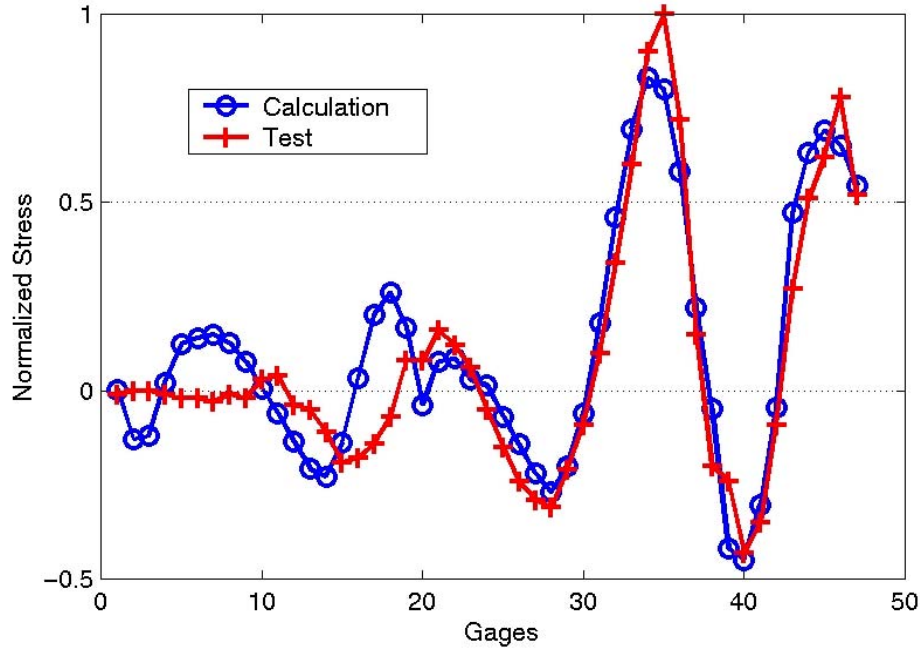
Figure 7: Stress modeshapes calculated and measured for mode no.10

The matching criterion value for mode no.10 is 0.86.

6.3   Holographic measurement

Holographic measurements enable the characterisation of 26 fundamental modes of vibration. Excitation is of piezo-electric type. Holographic images comprise 250,000 measurement points (or pixels). After identification of the geometric transformation between the measurement locator and the calculation locator, the adaptation between measured and calculated data is carried out by projecting the measurement values onto the corresponding partition of the finite element meshing. This operation implies reducing the number of data measured to the number of nodes in the model, i.e. between a hundred and a few thousand nodes. This adaptation operation uses a procedure of geometric smoothing, in which a measured displacement projected onto a node in the mesh is obtained by a combination of the values of the pixels in the vicinity of the node in question.

The entire adaptation procedure for the measurement and calculation data, as well as the calculation of the correlation criteria, are performed using an in-house Snecma Moteurs operational tool.

The result of the matching between measured and calculated modes, obtained using the MAC_y criterion, is presented in Figure 8 for the 26 modes measured. The matching criterion is calculated for all the nodes of the mesh of the airfoil corresponding to the surface measured. The relative error on the corresponding eigenfrequencies is illustrated in Figure 9.
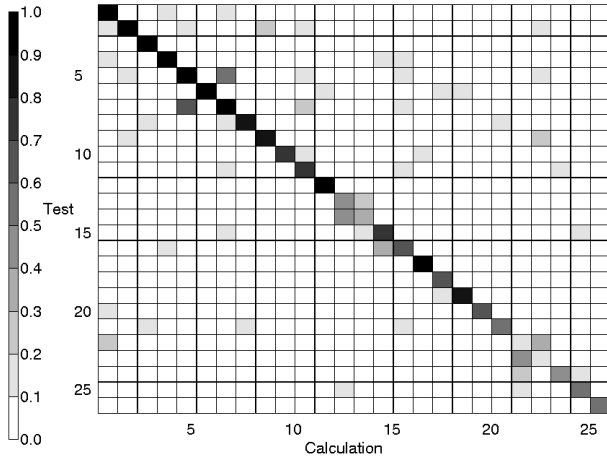
Figure 8: Matching matrix (MAC_y)
for measured and calculated modes
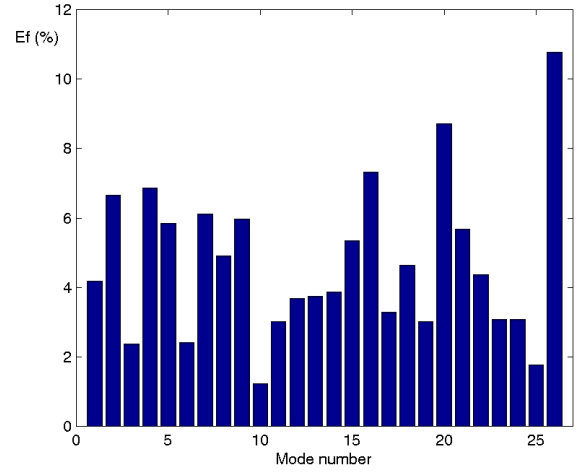
Figure 9: Relative error (%) in frequency (E_f)
between matched measured and calculated modes

Examination of the modal assurance criterion indicates that the correlation between the calculated and measured modes is excellent. 17 modes are matched with a MAC_y value higher than 0.7. Given the number of nodes on which the criterion is evaluated, these results reflect the aptitude of the mathematical model to correctly represent the shapes identified by measurement.

Only two measured modes have a MAC_y value of less than 0.5, i.e. measured mode nos.14 and 22. The relative errors in eigenfrequency obtained on the matched modes are around 11% at the most.

For guidance, Figures 10 and 11 show the measured displacement fields on the airfoil (projected onto the nodes of the mesh) and calculated in relation to mode no.20.
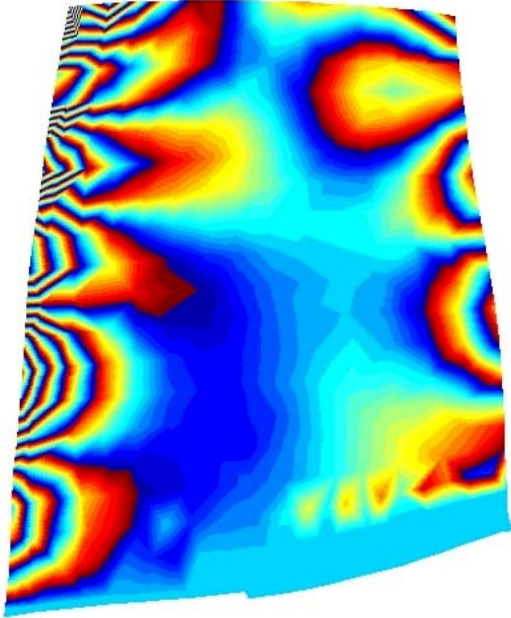
Figure 10: Measured displacement field
of mode no.20, projected onto the nodes of the model
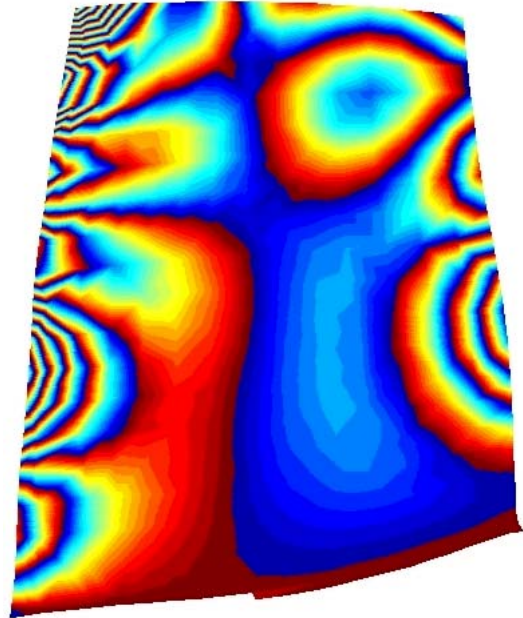
Figure 11: Calculated displacement field
of mode no.20

The corresponding MAC_y value is 0.83.

7   CONCLUSIONS

Comparison between the model and stress distribution tests based on strain measurement enables the correct correlation of 8 modes of vibration. For uncorrelated measured modes, it is difficult to relate the modes output by calculation with any certainty.

The comparison between the model and holographic measurements makes it possible to correctly correlate all the modes. The wealth of information available via dynamic field measurements (in this case measurement by holographic interferometry) enables non-conflicting matching between model measurement and prediction.

The difficulty in correlating modes 10 to 25 observed in the stress distribution test by strain measurement is due to several factors:

- Modification of the characteristics of the structure: a gauge bonded onto the structure and its connector technology introduce local disturbances of stiffness, mass and damping that are not taken into account in the mathematical model. This structural modification, which is proportional to the density of instrumentation, has no effect on the first global modes but has a considerable impact on the eigen-shape of the high-level modes of vibration.
- Dispersion in gauge sensitivity (dispersion due to instrumentation, and to sensitivity tolerances).
- Errors in adaptation between measured and calculated values: calculated stress values are sensitive to the size of the elements. A variation in the position between a gauge and the element of the corresponding mesh introduces an additional error, in particular in areas of the airfoil with high stress gradients.

Optical measurement by holography enables the characterisation of modal displacement fields without disturbing the structure and provides a dense quantity of data, of much greater wealth than that produced by calculation. Using this information requires an adaptation procedure in order to condense measurements onto the nodes of the model. This special operation has proved to be extremely robust.

The results presented clearly show the advantage in using optical field measurements, which, because of the quality and wealth of the data output, enable clear, non-conflicting matching between measured and calculated modes of vibration.

The use of a qualified model for component tests based on optical measurements makes it possible to take engine operating conditions into account in estimating modal stress factors, i.e. the influence of thermal, centrifugal, and steady aerodynamic loads. Similarly, these stress factors can be calculated in the case of normal modes with nodal diameters (which can be excited by the identified harmonics of the engine speed), which is difficult to reproduce in a component test. Access to the maximum modal stress is another advantage of the calibration method using a model validated by component tests. This is because in the case of strain measurement, the maximum stress measured is determined only at instrumented points.

The procedure proposed to estimate the distribution of dynamic stress is based on the qualification of a finite element model by correlation with holographic interferometry measurements, which increases the reliability of the calibration factors of the engine gauges. In addition, the costs incurred and the time spent in the component tests related to this procedure are considerably reduced compared with a conventional procedure based on strain measurement.

This approach of calibration methodology contributes to improve the quality of prediction of dynamic behaviour, particularly the fatigue life prediction of highly loaded components, and therefore to increase the safety of flights.

8   REFERENCES

[FOL.00]   FOLTETE E., RAYNAUD J-L., « *Caractérisation dynamique quantitative d'une structure mécanique par interférométrie speckle électronique en vue du recalage de modèle* », Colloque Méthodes et Techniques Optiques pour l'Industrie, Biarritz, 21-24 Novembre 2000.

[HUM.99]   HUMBERT L., « *Recalage des modèles éléments finis à partir de mesures vibratoires* », Thèse de Doctorat de l'Ecole Centrale de Lyon, N° 99-42, 1999.

[LEM.96]　　LEMAITRE J., CHABOCHE J.-L., « *Mécanique des matériaux solides* », 2ème édition, Ed. Dunod, 1996, pp. 364-367.

[LEP.01]　　LEPAGE A., LINET V., PIRANDA J., FOLTETE E., « *High spatial resolution vibration analysis using hybrid method : accelerometers - double pulse ESPI* », FRINGE 2001- The 4th International Workshop on Automatic Processing of Fringe Patterns, Brême, 17-19 Septembre 2001, pp. 451-458.

[SMI.90]　　SMIGIELSKI P., « *Holographie industrielle* », Teknea, 1990.

Bird Impact Analysis on a Bladed Disk

D. Chevrolet, S. Audic, J. Bonini
SNECMA MOTEURS
Site de Villaroche
77550 Moissy Cramayel
France

E-mail : david.chevrolet@snecma.fr

ABSTRACT

A Smooth Particle Hydrodynamics (SPH) method has been developed to provide a transient structural analysis of fan blades during bird strikes [1], [3]
The bird is modeled by a set of lagrangian particles and a specific state of equation evaluates the pressure in the projectile. The SPH method has been coupled with the Finite Elements method by a contact algorithm and implemented in the fast dynamic code EUROPLEXUS [2], [4].

Unlike the classical Lagrangian formulations, this model avoids the severe distortions of projectile mesh during impact phase. An uniform bird slicing by the rotating blades is not assumed prior to the calculation. The method has been applied to compute the response and the residual deformations of a bladed disk.

1. INTRODUCTION

Bird strike in a turbofan engine is a phenomenon which can occur at each flight's stage and principally during take off and landing. These impacts generate severe loads on the fan stage and sometimes the strains undergone by the structure can lead to failure.

Prior to the final certification test, some expensive spin tests are usually performed to validate the initial design choices. A failure during a bird ingestion will be very expensive because of the necessary re-design of the blade (costs, delays). To reduce the number of these tests and to avoid any delay during the certification tests the manufacturers perform analyses with non-linear transient structural codes.
The task lies then in the development of a convenient and suitable industrial strategy to demonstrate the reliability of a Finite Element (FE) modelling to predict the impact loads and damage.
The classical Finite Elements method do not allow to treat completely this problem. The Lagrangian formulation is too tricky to handle for the bird because of large deformations. The coupled Euler-Lagrange method creates a significant numerical dissipation despite difficult remeshing in the case of rotating structures. Moreover, CPU time widely increases for these last calculations because a large area has to be meshed to anticipate fluid deformations and blades rotation. So, all these methods present major drawbacks to model bird the slicing by a rotating structure.

To avoid all this problems, SNECMA calculates bird strike with a SPH method. This formulation has been implemented in the fast dynamic analysis code EUROPLEXUS developed jointly by the French "Commissariat à l'Energie Atomique" and by the JRC of the European Community at ISPRA.

2. THE SPH METHOD

The SPH [5] method has been defined by astrophysicists during the 70's. But at the beginning of the 90's, some mechanical scientists have adapted this method to treat impact at very high velocities [6], [7], [8].
The SPH method is well-suited to simulate problems that present mesh distortions and large displacements.

2.1. Mathematical principles

The discrete field f, scalar or not, defined in a domain Ω can be approached and regularised by a field family $\langle f \rangle_h$, defined by :

$$\langle f \rangle_h = \int_\Omega f(y) \cdot W(x - y, h) \cdot dy \qquad (1)$$

with W Kernel or weight function

        h smoothing parameter which determine the volume Ω_i around x where W takes its greatest values. This parameter h defines the regularity of $\langle f \rangle_h$

The field f can be the velocity, the density, the pressure …

The volume Ω_i is smaller than the domain Ω and the kernel W generally verify the following properties :

1. $W(x - y, h) > 0$ in Ω_i with $\Omega_i \subset \Omega$

2. $W(x - y, h) = 0$ $\forall y \notin \Omega_i$

3. $\int_\Omega W(x - y, h) \cdot dy = 1$ (consistent condition)

4. $W(s, h)$ is monotonous and decreases with $s = \|x - y\|$

5. $W(s, h) \to \delta(s)$ with $h \to 0$ where $\delta(s)$ is the Dirac distribution

The most common kernels W are the Gauss, cubic or quadratic fonctions.

If the values of the field f are known for a finite number N of points x_i, the integral (1) can be approximated by a directe sum :

$$\langle f \rangle_h (\underline{x}) \cong \sum_{i=1}^{N} m_i \cdot \frac{f(\underline{x}_i)}{\rho(\underline{x}_i)} \cdot W(\underline{x} - \underline{x}_i, h) \qquad (2)$$

The mass m_i is associated to the particles $\underline{x}_i$ and the ratio $\dfrac{m_i}{\rho(\underline{x}_i)}$ represents the volume of the domain Ω_i connected to x_i.

The equation (2) looks like form functions in the finite element formulation.

The approximation of the field f can be easily applied to the fundamental equations of Mechanics. At the node number k :

▪ continuity equation :

$$\frac{d\rho(\underline{x}_k, t)}{dt} = \rho(\underline{x}_k, t) \cdot \sum_{i=1}^{N} \frac{m_i}{\rho(\underline{x}_i, t)} \cdot (v(\underline{x}_k, t) - v(\underline{x}_i, t)) \cdot \nabla_k W(|\underline{x}_k - \underline{x}_i|, h) \qquad (3)$$

▪ momentum equation :

$$\frac{d\langle \underline{v} \rangle(\underline{x}_k, t)}{dt} = -\sum_{i=1}^{N} m_i \cdot \left[\frac{\langle p \rangle(\underline{x}_i, t)}{\langle \rho \rangle^2 (\underline{x}_i, t)} + \frac{\langle p \rangle(\underline{x}_k, t)}{\langle \rho \rangle^2 (\underline{x}_k, t)} + \pi_{ij} \right] \cdot \nabla_k W(|\underline{x}_k - \underline{x}_i|, h) \qquad (4)$$

The pressure P is given by a state equation $\langle p \rangle(\underline{x}_i, t) = p(\langle \rho(\underline{x}_i, t) \rangle$ and π_{ij} is an artificial viscosity proposed by Monaghan and Gingold [9].

Two general remarks can be add to the presentation of the SPH method :

▪ The continuity equation avoids the boundary effects because the density evolves only when the distances between particles change.

▪ Corrections have to be introduced in this formulation to take into account the space and the time variations of the smoothing length. The time variations of h are described by the law of Benz [10] :

$$\frac{dh(\underline{x}_i, t)}{dt} = -\frac{1}{3} \cdot h(\underline{x}_i, t) \cdot \sum_{j=1}^{N} \frac{m_j}{\rho(\underline{x}_j, t)} \cdot (v(\underline{x}_i, t) - v(\underline{x}_j, t)) \cdot \nabla_k W(|\underline{x}_i - \underline{x}_j|, h) \qquad (5)$$

The space variations of h are obtained by the scatter approximation : $h(x,y) = \dfrac{h(x)+h(y)}{2}$.

This relation should be reintroduced in all the previous mechanical equations.

2.2. Application of the SPH method to the bird strike

The projectile is modeled by a set of Lagrangian particles arranged in a compact hexagonal system. Each particles is initially connected to twelve other particles but the connectivity is time dependant.
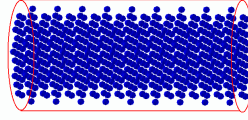
Figure 1 : projectile mesh

The mass of each particle is concentrated at the centre of the outer sphere. The bird material model is based on the studies of J. Willbeck [10]. He has developed a synthetic bird model which is composed of commercial gelatin and 10% of phenolic micro-balloons.
The state equation is based on the pressure-density relationship of each constituent. But to improve the calculation, this law distinguishes a shock and a reduction in pressure. This model gives very accurate loading including the Hugoniot peak and the stagnation pressure.

The SPH method used the cubic kernel with compact support [1], [11] :

$$W(r,h) = \frac{1}{\pi h^3} \begin{cases} \dfrac{3}{2} \cdot \left[\dfrac{2}{3} - \left(\dfrac{r}{h}\right)^2 + \dfrac{1}{2} \cdot \left(\dfrac{r}{h}\right)^3 \right] & 0 \le \dfrac{r}{h} \le 1 \\[4mm] \dfrac{1}{4} \cdot \left(2 - \dfrac{r}{h}\right)^3 & 1 \le \dfrac{r}{h} \le 2 \\[4mm] 0 & \dfrac{r}{h} \ge 2 \end{cases} \qquad (6)$$

The contact algorithm realize the coupling between SPH and the classical Finite Elements Methods. This interaction is treated as the shock of two spheres : one is a particle (bird) and the other is a factitious node representing the nodes of an element (blade).
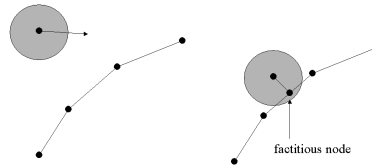
Figure 2 : contact detection

The global momentum is conserved in the normal direction whereas possible friction forces are not taken into account in the tangent direction [12] :

$$m_e \tilde{\underline{v}}_e + m_d \tilde{\underline{v}}_d = m_e \underline{v}_e + m_d \underline{v}_d \quad (7)$$

e   particle
d   defending node
tilde stands for 'before impact'

The bird presents an hydrodynamics behaviour during impact, so the normal velocities after the shock are chosen equal (shock without rebound) :

$$\underline{v}_e = \underline{v}_d \quad (8)$$

These equations (7), (8) allow to calculate the velocity and the acceleration of the bird particles. This method gives accurate results only if the diameter of the particles and the size of the elements are equivalent.

3. INDUSTRIAL APPLICATION

Bird strikes are today currently simulated on civil fan using SPH method. The results for all kinds of blades (wide chord solid blades, hollow fan blades, shrouded blades …) are very close to experimental data [2],[4],[12].
This method has been applied to anticipate the mechanical behaviour of blades under different impact conditions than fan blades : the blades dimension and the rotation speed are different from fan civil applications. The nominal rotation speed is around 13.600 rpm and the seagull is fired with an axial velocity of 197 m/s.

To limit CPU time, only the impacted part of the rotor is represented. Each blade is meshed with shell elements and the disk with brick elements. The structural mesh approximately includes 33.000 degrees of freedom (cf. figure 3).

To compute accurately the bird slicing, the blades must be in motion in the global frame. A procedure was defined to describe the rotation of the impacted structure. This procedure follows three steps :
- calculation of the centrifugal stresses
- determination of the bird slicing
- deceleration of the rotor.

The first step is essential because the dynamic behaviour of the blades are widely influenced by this additional strength.
The boundary conditions must take into account the cyclic symmetry of the disk to model the effect of the rotor which is not meshed. The centrifugal forces are determined in the rotating frame. They are applied on every node and tend to expand the structure in the radial direction. Thus, it is necessary to impose the displacement continuity for each node of the lateral disk faces located at the same radial position (9).

$$v_{r1} = v_{r2}$$
$$v_{\theta 1} = v_{\theta 2} \qquad (9)$$

v_r radial velocity

v_θ tangential velocity

(The mark 1 refers to one face and the mark 2 to the other face)

The calculation is conducted until the stresses are stabilised (the structure is damped on the first bending mode of a blade).
The bird impact appends on the global frame to represent correctly the slicing and the centrifugal stresses of the deformed structure. Numerically, the rotation is introduced by prescribed displacement on the nodes located on the lateral disk faces. The initial velocities is automatically determined by the code from the radial position of each node and from the rotation speed of the rotor.

The objective of this simulation is to anticipate the mechanical behaviour of the blades, so the outer shape of the projectile does not represent a real geometry of bird but a right circular cylinder (cf. figure 1).

The material behaviour of the blades is described by a dynamic elastic-plastic law. Contact conditions are imposed between each blade and the bird but also between blades to avoid penetrations under high bending moments.

The results are presented on a sector of three blades (figure 3-4). Snecma does not have test data to validate the computations, but the first results seem to predict realistic behaviour of blades. The deformation under impact is more severe than impact on a civil engine. During the bird slice, larger deflections occurred at the leading edge. The bird slice cut by each airfoil is not regular (even if the bird density is constant) because blades and projectile interact (figure 4).

No active element failure criteria is implemented in the code. The predicted maximum dynamic strain and its location indicate the possible cracking and material loss. The value of this criteria is determined with experimental data.

This simulation provide useful data to validate the design and the load definitions under impact. The global response of the structure under impact depends on the initial geometry and the simulation determines the mode which is excited (torsion or bending). For example, a torsional deflection can lead to peak strain response at the airfoil root region and failure.

Furthermore, the predicted response allow to validate the engine design. The computation provide information about the possible contact between the impacted blades and :

- the fan casing (radial deflection – figure 5)
- the following blades (tangential deflection – figure 6)
- the other compressor stage (axial deflection – figure 7)

4. CONCLUSIONS

The bird slicing is especially well-predicted without any assumption. The results confirm the major interest of the SPH method.

The calculations were not validated by experimental data but the global and local deformations seem to be well predicted : the blades interact with the bird and the results are coherent with the higher speed impact in such conditions.

The SPH method has demonstrated its ability to be used as an efficient analytical tool for predicting impact loads and damages due to bird ingestion. Since the analysis does not require important computer resource and CPU time, it can be used during the conception iterations and the qualification tests are performed on the final optimised geometry. The computations contribute to improve the quality of prediction of the dynamic behaviour of the blades under impact and therefore to increase the safety of flights.

ACKNOWLEDGEMENTS

REFRENCES

[1]   A. Letellier. Contribution à la modélisation d'oiseaux sur les aubes des réacteurs. PhD, Université d'Evry 1996

[2]   A. Letellier, M. Berthillier, H. Bung and P. Galon. Bird impact on fan blade analysis using SPH method coupled with finite elements. Symposium on structures under extreme loading conditions. Orlando, 1997

[3]   A. Legay, D. Leray. PLEXUS, introduction de la viscosité SPH. Rapport CEA, SEMT/DYN/RT/98.040/A, 1998

[4]   P. Vignolles, P.X. Bussonet and J. Talbotec. Conception des aubes fan soumises à l'impact d'oiseaux. AGARD CP 1995

[5]   W. Benz. Numerical modelling of non-linear stellar pulsation : problems and prospects. Kluwer Academic, Boston, MA, 269-288, 1990

[6]   G.R. Johnson, R. Stryk. Dynamic three dimensional computations for solids with variable nodal connectivity. Int J for Num Methods (28),1989

[7]   G.R. Johnson, E. Peteren, R. Strik. Incorporation of an SPH option into the EPIC code for a wide range of high velocity impact computations. Int J of Impact Engineering (14), 1993

[8]   S.W. Attaway, M.W. Heinstein and J.W. Swegle. Coupling of smooth particle hydrodynamics with the finite element method. Nuclear Engineering and design (150), 199-205, 1994

[9]   J.J. Monaghan, R.A. Gingold. Smoothed particle hydrodynamics : theory and applications to non-spherical stars, Montly Notices of the Royal Astronomical Society (181), 1997

[10]   W. Benz. Smooth Particle Hydrodynamics : a review. Harvard-Smithsoniam Center for Astrophysics, 1989

[11]   J. Wilbeck. Impact behaviour of low strength projectiles. Technical Report 77-134, Air Force Material Laboratory, Wrigth-Patterson Air Force Base, Ohio 45433, 1978

[12]   J. Bonini, H. Bung. Structural Impact-Friction modelling in Explicit finite element code with the Lagrange Multiplier, 14th Conference on Structural Mechanics in Reactor Technology, vol. 6, 37-44, 1997.
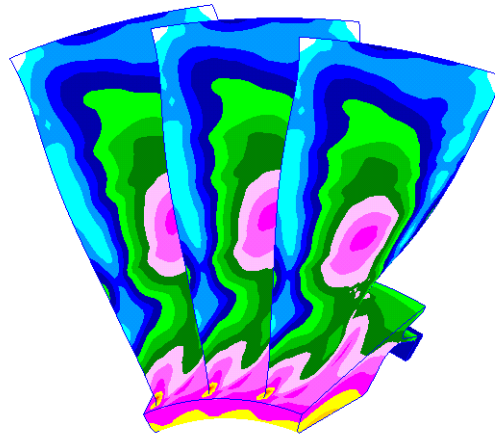
Figure 3: Pre-stresses field in the bladed disk
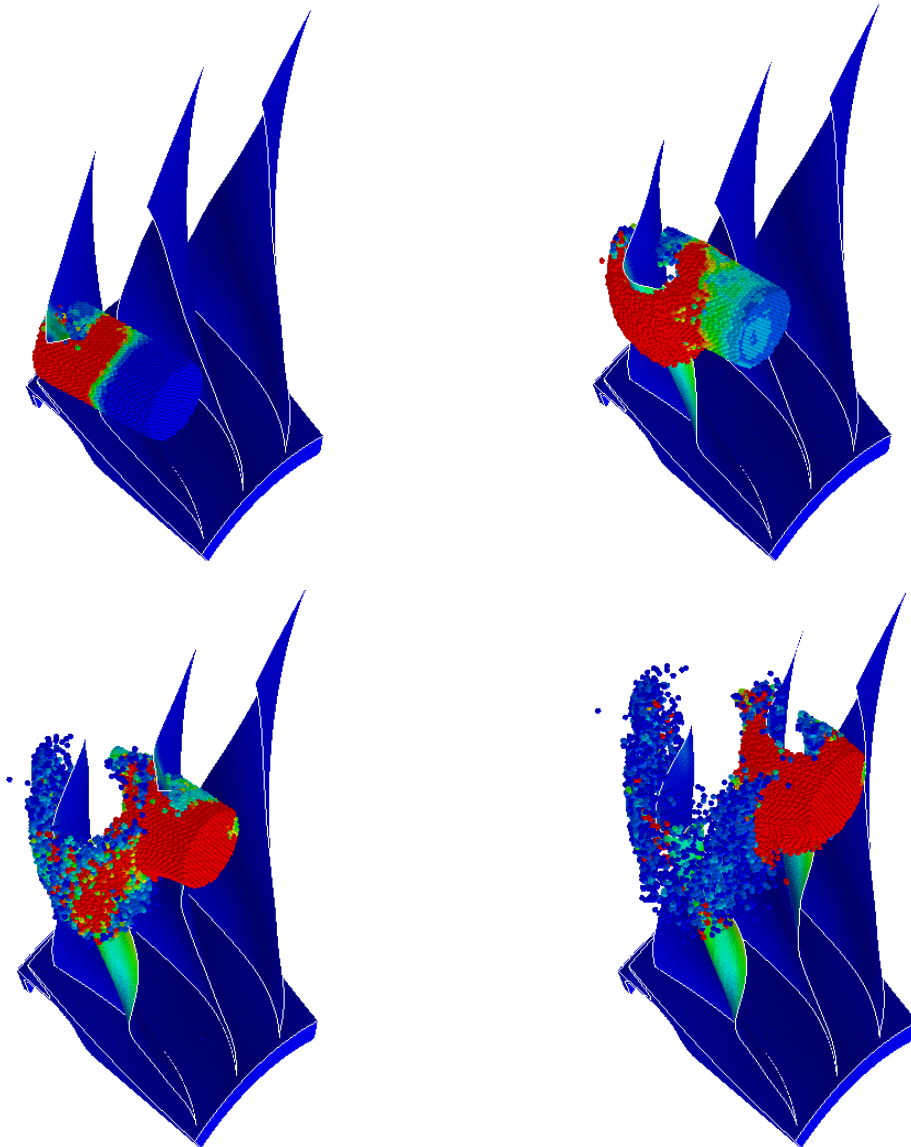
Figure 4 : bird slicing
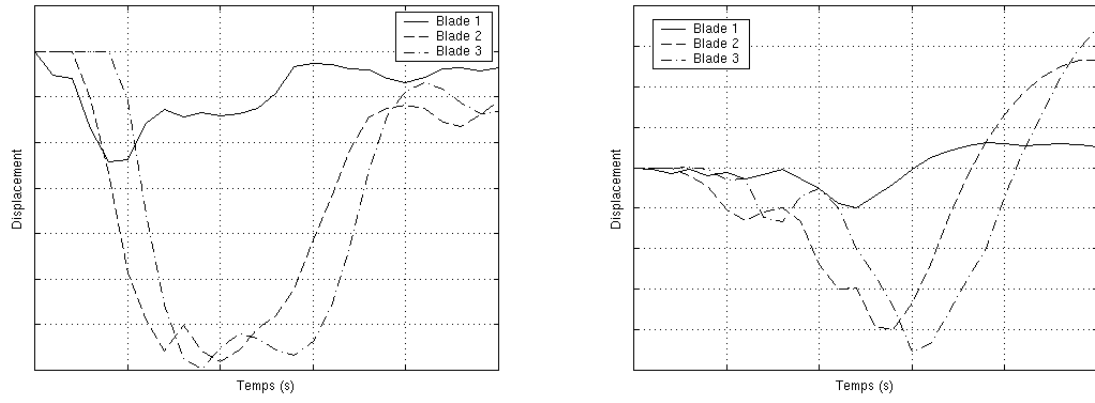
Figure 5: Blade tip leading and trailing edge radial deflection
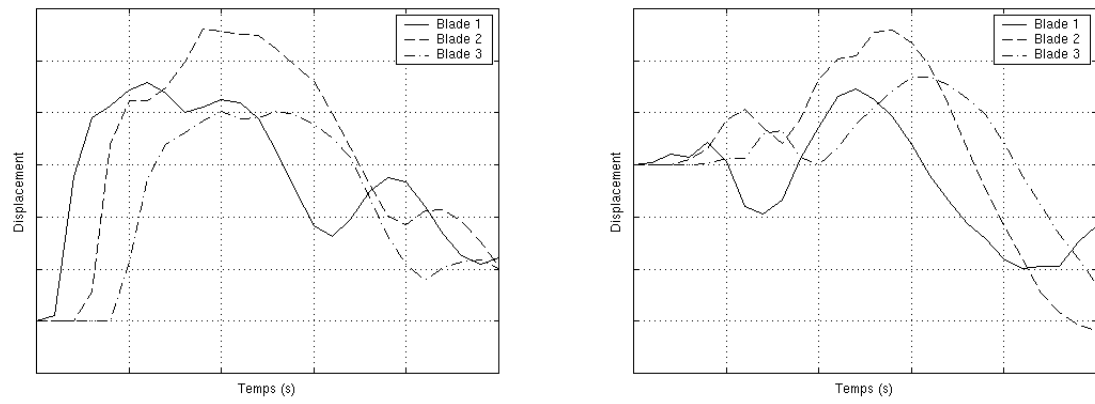
Figure 6: Blade tip leading and trailing edge tangential deflection
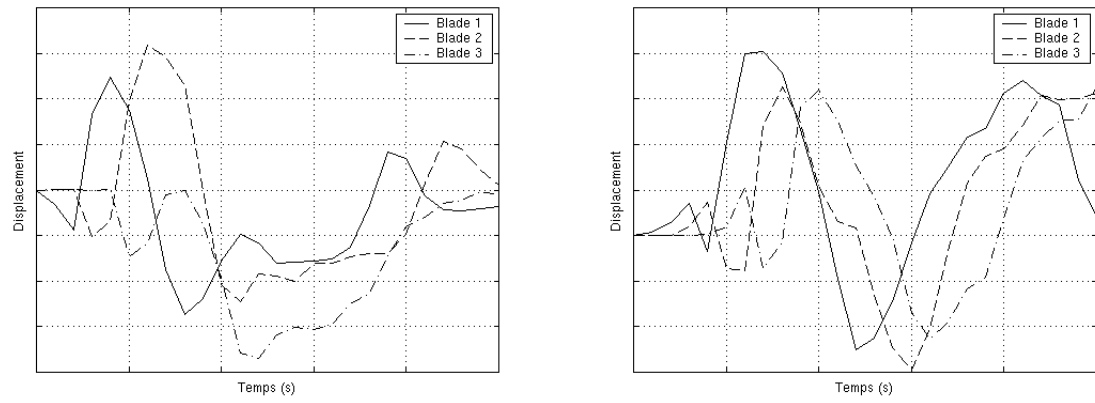
Figure 7: Blade tip leading and trailing edge axial deflection

Paper #31
Discussor's Name: Azzeddine Soulaimani
Author's Name: D. Chevrolet

Q: How do you apply the solid boundary conditions for the SPH method?

A: We are simply using conservation of the momentum at the boundary.

Use of RANS Calculations in the Design of a Submarine Sail

Joseph J. Gorski and Roderick M. Coleman
NSWC, Carderock
9500 MacArthur Boulevard
West Bethesda, MD 20817-5700, USA

Abstract

The application of a Reynolds Averaged Navier-Stokes (RANS) code in the design of an "Advanced Sail" for a submarine is discussed. To validate the code on similar sail shapes calculations are compared with experimentally obtained data at 1/35 scale from a wind tunnel and 1/17 scale from a water channel. This data comparison includes flow visualization, axial velocity and surface pressures. The agreement demonstrates that RANS codes can be used to provide the significant hydrodynamics associated with these sail shapes. To improve the design several modifications to a sail are evaluated using the RANS code. Based on the predicted secondary flow downstream of the sail as well as the drag a new design is chosen, without having to build and test the inferior shapes, reducing time and cost for the program. This improved sail was then built at 1/4 scale and demonstrated on the U.S. Navy's Large Scale Vehicle.

Introduction

The U. S. Navy is investigating the benefits of an "Advanced Sail" for improved effectiveness in littoral regions while minimizing the impact on performing traditional missions. The canopy-like shapes, Fig. 1, provide a significant increase in payload over conventional sails. The increased volume, on the order of a factor of four over conventional airfoil shaped sails, can be used for special operating forces stowage, high data rate antennae, countermeasures, littoral warfare missiles, and other payload systems while maintaining all current systems and capabilities, Dozier et al [1]. To minimize impact the Advanced Sail designs cannot significantly add to the drag of the submarine or degrade the flow into the propeller over conventional designs, despite the increased size.
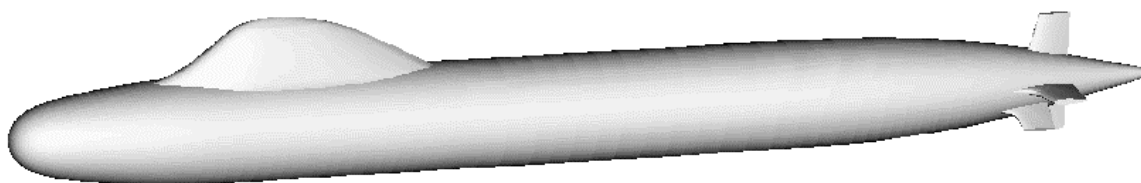
Fig. 1 Submarine configured with an Advanced Sail.

Submarines are basically axisymmetric bodies with appendages to offer a minimum of resistance so that the vehicles can be economically powered and move efficiently through the water. Appendages provide an opportunity for wakes and vortices to be generated which can impact drag and quiet operation of a submarine, which are critical in its design. Any protrusions from the surface will tend to increase the drag, due to pressure gradients, increased wetted surface area, and energy spent in vortex generation. Vortices typically consist of necklace vortices from hull/appendage junctions, tip vortices from the appendages, and vortices generated directly from the hull due to angles of attack. The vortical flow generated from the hull and appendages can also significantly influence the maneuvering characteristics of a submarine. Spatial flow

distortions into the propeller created by upstream wakes, vortices or flow separations can contribute to noise generation as well as propeller vibration.   The largest appendage on any submarine is usually the sail and consequently its drag and wake are important considerations in a design. Increasing its size by a factor of four over conventional sails, while minimizing impact on drag or propeller inflow, requires streamlined shapes due to the much larger wetted surface area. Additionally, longitudinal vortices are created downstream of canopy sails, such as these, even with their streamlined shapes, Gorski [2]. To minimize these secondary flows, as well as the drag, created by these large sails requires a large amount of building and testing of models or computations of candidate shapes for evaluation.

To reduce schedule and cost the Advanced Sail program has relied heavily on computational fluid dynamics (CFD) tools to help in the hydrodynamic evaluation of the sail shapes. The main hydrodynamic considerations for the Advanced Sail shapes are minimizing drag and secondary flow created by them. Because of the viscous nature of these areas inviscid calculations are of limited value and Reynolds Averaged Navier-Stokes (RANS) codes have been the focus of the computational effort. Perhaps the first fully appended submarine RANS calculation was done by Gorski et al [3] for the SUBOFF configuration, which was extensively measured [4] to provide a data-base to test CFD methods. At the time of the SUBOFF program it was shown that RANS calculations could predict the pressures quite well and some of the mean flow, but generally under predicted the strength of necklace vortices. Since that time there have been considerable efforts directed at submarine RANS calculations, Gorski [2]. Modern RANS codes take advantage of the large parallel computers and provide calculations on much finer grids than at the time of SUBOFF. This allows for better flow predictions, in a timely manner, and RANS codes are accurate enough and have matured to a point where they can be used for submarine design [5].

In general a new paradigm for surface ship and submarine design is evolving which uses a mix of experiments and computations. The days of the old series tests, where systematic variations of a hull form are built and tested experimentally, are fading due to time and cost considerations and since computations are an attractive alternative. In particular, viscous calculations are becoming faster and more affordable as gridding improves and computers get more powerful.   However, confidence needs to be built up in the predictions. Despite the successes of RANS predicting drag and detailed flow into the propeller may still be an issue, depending on how much detail is needed.   Consequently, model tests are often done to provide conventional data for hull form evaluation as well as validation data for the computations.   The current program involves experiments on a variety of sail shapes including: 1/35 scale models in a wind tunnel, 1/17 scale models in a water channel, and a 1/4 scale demonstration. The experiments can often run through a variety of speeds and operating conditions once a model is built for shape evaluations. The computations provide a fast means to evaluate shape alternatives for sail redesign.   Thus, less model construction and testing is required of shapes that can be rejected based on the computations. As more confidence is gained in the computations it may be possible to reduce model construction and testing to the final shape or shapes. The current paper demonstrates how the RANS calculations compared with some of the experimental data as well as how RANS computations are used in the redesign process for the Advanced Sail.

CFD Process

It should be pointed out that to perform good flow calculations is not simply a matter of turning on a particular piece of software, particularly for complicated geometries or flows. The computations, with either RANS or potential flow solvers, involve a process not completely unlike that of doing a model experiment. A test of whether a particular code can predict certain measured physics is dependent on all pieces of this process. An idea of what this process is like is shown in Fig. 2. The validation of the calculation against experimental data depends on all of the steps in the process. A problem with any one of them can lead to differences in the computed and measured data.

Prerequisite to generating computational grids is the satisfactory specification of the actual geometry. Details, such as ensuring there are no gaps in the geometry and trimming surfaces, must be taken care of before the geometry can be used easily with grid generation software. For the actual definition of the geometry, a single B-spline surface for each component is preferred. B-splines can model the most complex

shapes and provide smooth, continuous definition with well-behaved intersections. In the IGES format, they can be transferred between most CAD and grid generation software packages.
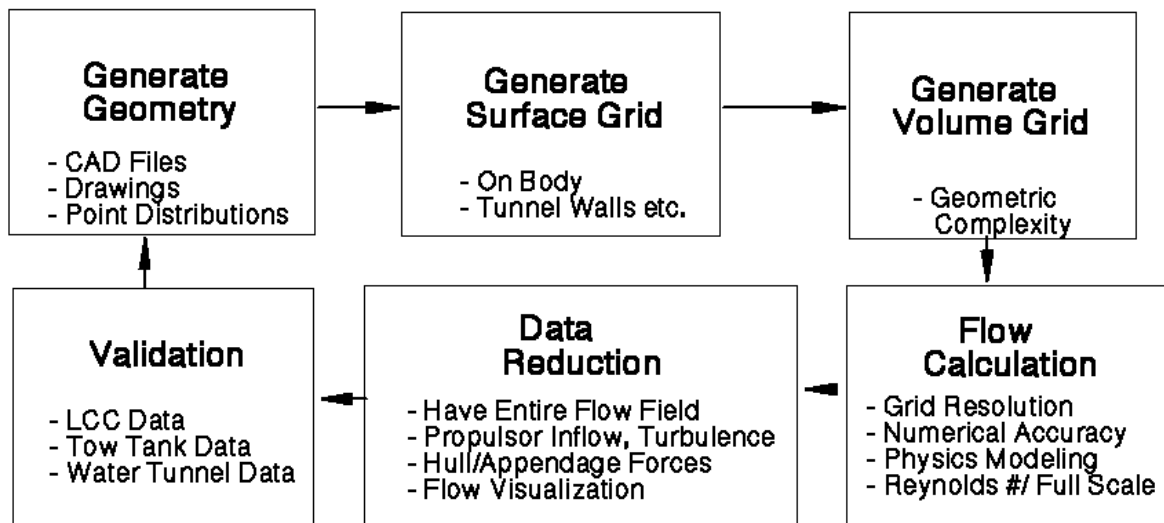
Fig. 2 CFD Process

When generating the computational grid, a surface grid must first be generated on the body and all surrounding boundaries where boundary conditions are imposed. This surface grid breaks up the smooth B-spline surface into discrete points and one must make sure the grid conforms to the actual geometry. Additionally, these surface grids must be clustered in areas of high geometry gradients or where the flow is expected to change rapidly to help provide accurate predictions.   It is very important in shaping or sculpting a geometry that enough attention to detail is done so that changes in the actual geometry are properly represented in the discretized geometry. A volume grid is next generated providing discrete points in the entire flow domain where the Navier-Stokes equations are solved. A computed solution can only be as good as the grid on which it is computed. If there are high gradients in the flow, such as in boundary layers, wakes and vortices, it is necessary to have enough grid points in these areas to resolve them. If enough grid points are not present the computation will diffuse these high gradients. Once a flow feature is diffused in this, or any other way, its impact and interaction on the surrounding and downstream flow cannot be predicted accurately. For viscous calculations, and drag comparisons in particular (Gorski [6]) attention must be paid to these details to insure one is predicting flow differences due to actual geometry changes and not differences due to computational changes. In practice it is sometimes difficult to achieve good grid quality, a sensible amount of time spent, and a practical grid size all at the same time. For the current computations which consist of the sail and bare hull approximately 1.2 million points are used for half the body with port/starboard symmetry assumed. With these streamlined sails, it is possible to have the grid conform to the overall surface much like a bump as shown in Fig. 3. Here 191 points are along the length of the body, 65 extend outward away from the hull and 97 wrap around it with some clustering toward the top for better sail wake definition. In the design cycle a new grid could often be generated in a few hours to days depending on the extent of the modifications.

Obviously flow solutions also depend on the RANS code used.   In the current effort the incompressible Reynolds Averaged Navier-Stokes equations are solved using the Mississippi State University code UNCLE [7,8]. The equations are solved using the pseudo-compressibility approach of Chorin[9] where an artificial time term is added to the continuity equation and all of the equations are marched in this artificial time to convergence.   Only steady state computations are performed for this effort.   For the present calculations a third-order upwind biased discretization, based on the MUSCL approach of Van Leer et al [10], is used for the convective terms. The equations are solved implicitly using a discretized Newton-relaxation method[11] with multigrid techniques implemented for faster convergence[12]. An important factor in being able to compute and evaluate the hull modifications and operating conditions of interest is the implementation of a parallel version of the UNCLE code[13]. The code uses MPI for message passing due to its portability.

To run in parallel the computational grid is decomposed into various blocks, which are sent to different processors. Load balancing is obtained by making the blocks as equally sized as possible. For the present calculations 18 processors are used which allowed for new solutions in a few days depending on computer load. More details of the solver can be found in the various references provided.
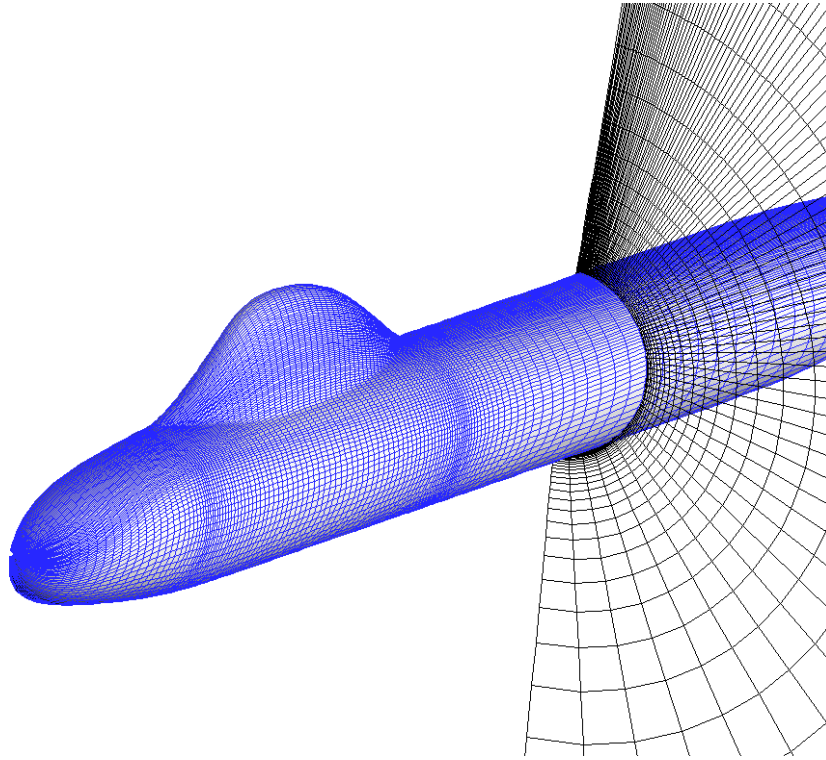
Fig. 3 Computational grid on the surface and at a single axial plane.

Another issue affecting accuracy is the turbulence modeling used. Two-equation models have become the standard for practical applications. In the current study both a k - ε and q - ω model are used. The k - ε model is that developed by Liou and Shih [14] which is a variant of the model developed by Shih and Lumley [15]. The variation from the original model is the inclusion of a variable Cμ based on the mean strain rate. This is a low Reynolds k - ε model in the sense that the equations are solved right to the wall without the use of wall functions for the mean flow. The q-ω model used is that developed by Coakley [16]. With this two-equation model, q, which is the square root of kinetic energy, is solved for rather than kinetic energy. Also, rather than solving for the rate of dissipation of turbulent kinetic energy, ε, here the specific dissipation rate of kinetic energy, ω, is solved for. The two dissipations are related through the relation ω = ε/k. One advantage of the ω formulation is that it replaces the ε²/k source term of the ε equation, which is problematic near walls and other locations where kinetic energy approaches zero, with a better behaved term which adds to stability of the solution. The q-ω equations are also solved directly to the wall with q and the normal derivative of ω both set to zero. For solving directly to the wall it is generally preferable to have the first point off of the wall well within the viscous sub-layer and a value of y^+ around 1 is used here. Going to higher Reynolds numbers requires the relative distance of the first point off of the wall to become smaller.

Validation Effort

The computed solutions cover the entire flow field, whereas experimental data is available only at specific locations. Consequently, computations can provide much information not available in an experiment. To gain confidence in the calculations, particularly when doing unconventional hull forms, it is desirable to have some experimental data to validate the computations. For the Advanced Sail effort extensive

measurements have been obtained, both for design evaluation and code validation efforts. Models of several sails at 1/35 scale were tested in the Subsonic Wind Tunnel at the Naval Surface Warfare Center, Carderock Division (NSWCCD). Measurements consisted of forces and moments, surface pressures, wake surveys and flow visualization. This provided some data for code validation as well as information to help down select to two sail shapes. Models for these two candidate shapes were built, at 1/17-scale, and tested in the Navy's Large Cavitation Channel (LCC) in Memphis, TN. Measurements consisted of wake surveys and pressure measurements. To some extent this involved the traditional build and test philosophy of old although computations were used extensively to down select to the shapes tested in the wind tunnel from a large group of candidate sail shapes. However, the calculations were further used to refine the selected sail shape to a final design, which will be discussed in the redesign effort. RANS calculations have been performed on several of the wind tunnel tested models, but only the two sails also tested in the LCC are shown here.

The first sail shown here is the canopy shape of Fig. 1. Computed surface streamlines over the sail are shown in Fig. 4 and those on the hull around the sail in Fig. 5. Also shown are oil paint dot flow visualizations from the wind tunnel test, which the computations agree well with. The flow goes smoothly over and around the streamlined sail without any necklace vortex being formed. However, as discussed by Gorski [2], longitudinal vortices are still formed downstream of the sail as seen in Fig. 6, which shows secondary flow streamlines at two locations downstream of the sail. This pressure driven secondary flow, also referred to as secondary flow due to curvature, is a result of the flow turning around the sail. Transverse vorticity is generated in the hull boundary layer as the boundary layer on the hull approaches the sail. As the flow streamlines curve around the sail a longitudinal component of vorticity develops which flows downstream around the sail producing a pair of vortices similar to the necklace vortex of a wing/body junction. Although no necklace vortex is formed the large turning of the flow around the sail can lead to strong secondary flows. Enhancing this pressure driven secondary flow is flow down the back of the sail which has a component inward which impinges on the hull and can produce vortical flow of the same sense as that generated from turning around the sail. A similar effect was documented by Walter and Patel [17] for a surface mounted ellipsoid which had a very weak necklace vortex, but a strong spanwise component of flow from the tip inward to the wall at the trailing edge of the ellipsoid creating longitudinal vortices similar to a necklace vortex. This overall secondary flow causes the streamlines behind the sail to move outward away from the centerline, Fig. 5. Laser Doppler Velocimetry (LDV) measurements were obtained in the LCC at various axial locations. Shown in Fig. 7 is the measured axial velocity at X/L = 0.825 as compared to the calculations with both turbulence models. There is a significant bulge in the axial velocity due to the longitudinal vortices, which convect high velocity flow in toward the hull along the centerline and low velocity boundary layer flow away from the hull outboard from the centerline. The k - ε prediction has smoothed out the bulge considerably where as the q - ω model predicts it nicely. To insure this is a turbulence modeling issue a finer grid was also run with 129 points wrapping around ½ the body and more clustering toward the centerline, but the finer grid provided little difference in the predicted flow field. This shows the k - ε model is damping out the vortex too much, which is not unusual for the k - ε model in general, Gorski [18]. Computed and measure surface pressures on the sail are shown in Fig. 8.
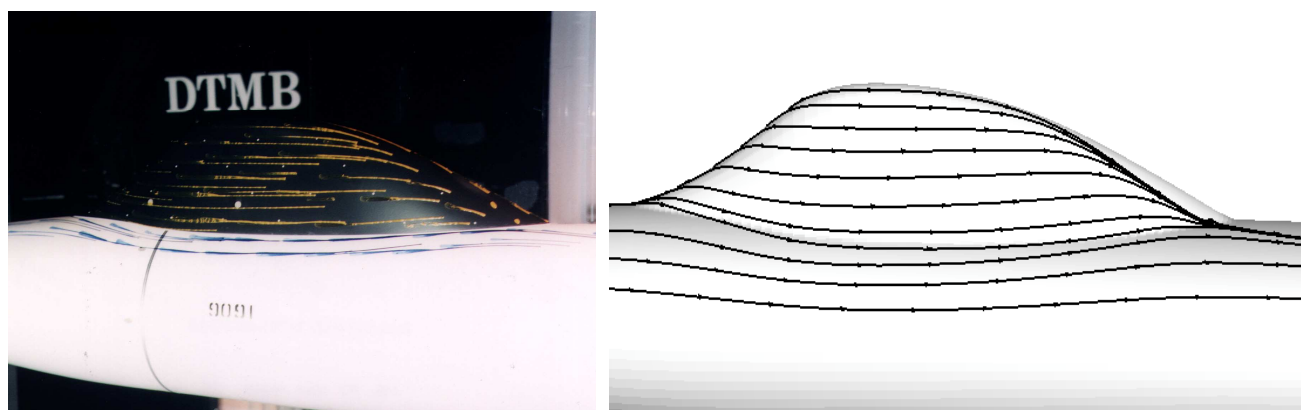
Fig. 4 Wind tunnel oil flow traces and computed surface streamlines for canopy sail.
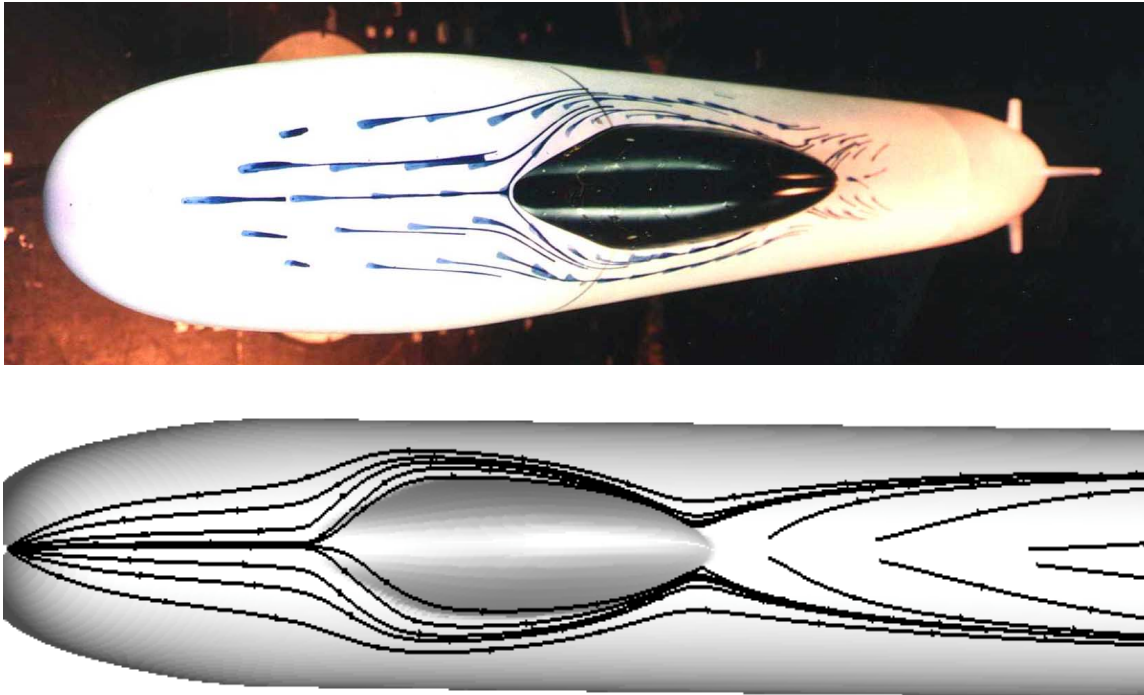
Fig. 5 Wind tunnel oil flow traces and computed surface streamlines around the canopy sail.
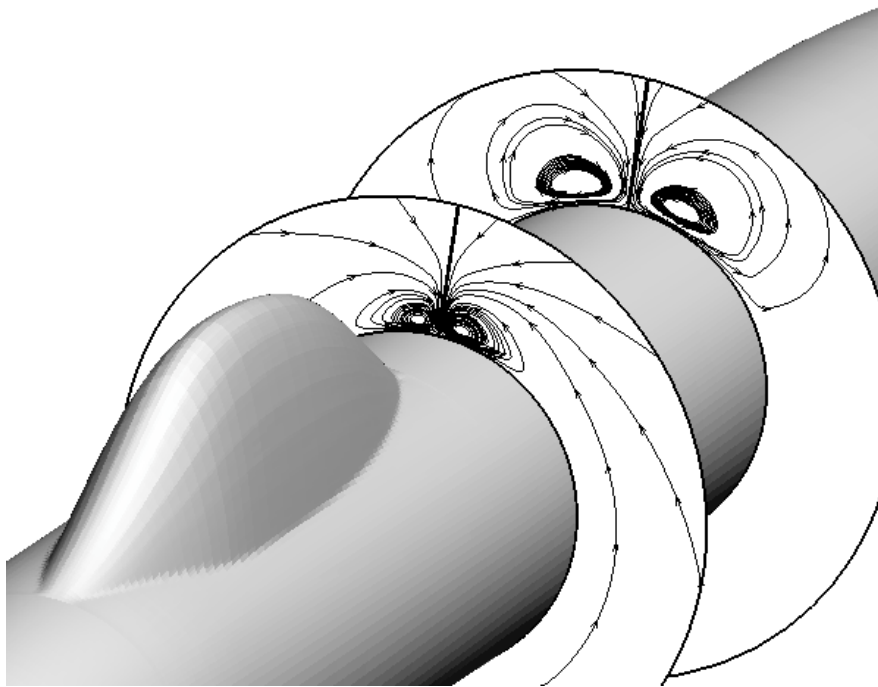
Fig. 6 Secondary flow streamlines downstream of the sail.
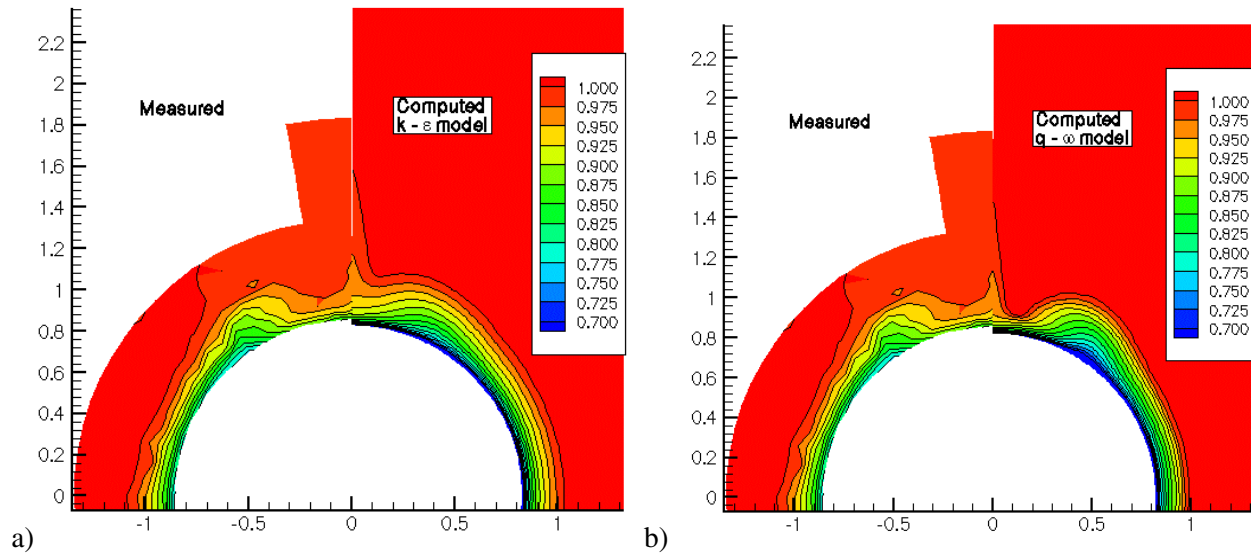
Fig. 7 Comparison of measured and computed axial velocity at X/L = 0.825 a) k-ε model b) q-ω model.
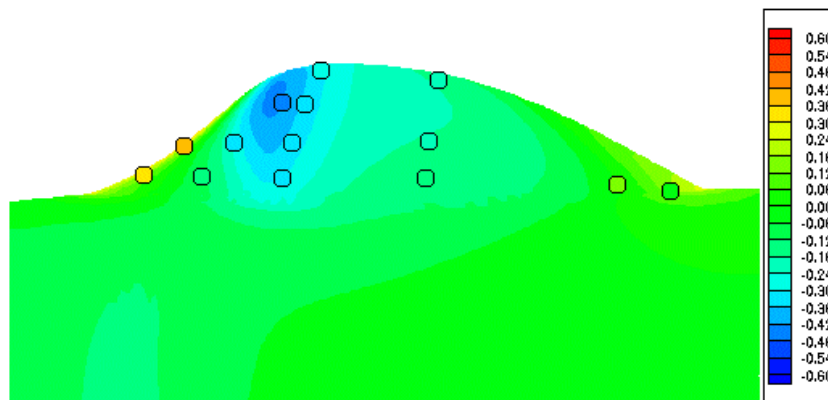
Fig. 8 Cp on the sail as compared with LCC measured values.

A second shape tested in the LCC is considerably different than the first.   The height of this second shape rises more quickly than the first, but still has a large fillet at the leading edge. It is rounded over the top and has a rather blunt trailing edge, which probably is what leads to greater drag for this configuration than the first. The flow goes smoothly around the sail with a downward component over the back end of the sail. The blunt trailing edge leads to a separation at the back end as shown in Fig. 9 for both the computation and wind tunnel flow visualization using a liquid crystal coating, which reacts to changes in shear in the boundary layer. Shown in Fig. 10 are streamlines on the hull around the sail. Again no traditional necklace vortex is generated, but there is significant flow turning.   Streamlines behind the sail again have an outward component due to the secondary flow created by this sail.   Comparisons of the computed axial velocity with that measured in the LCC are shown in Fig. 11. The bulge out of the flow from the hull is weaker than seen for the first sail due to a weaker vortex generated around the sail. This vortex bulge is considerably outboard from the centerline also.   With this weaker vortex the k-ε model does a good job of predicting the flow, better than it did for the first sail. The q-ω model again produces a stronger vortex than the k-ε model, but again is in reasonable agreement with the data.
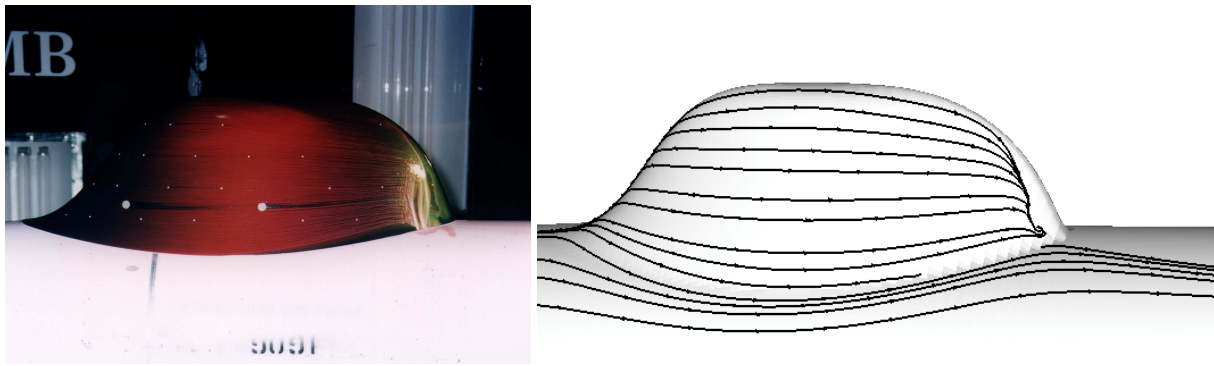
Fig. 9 Surface streamlines on the 2nd sail shape.
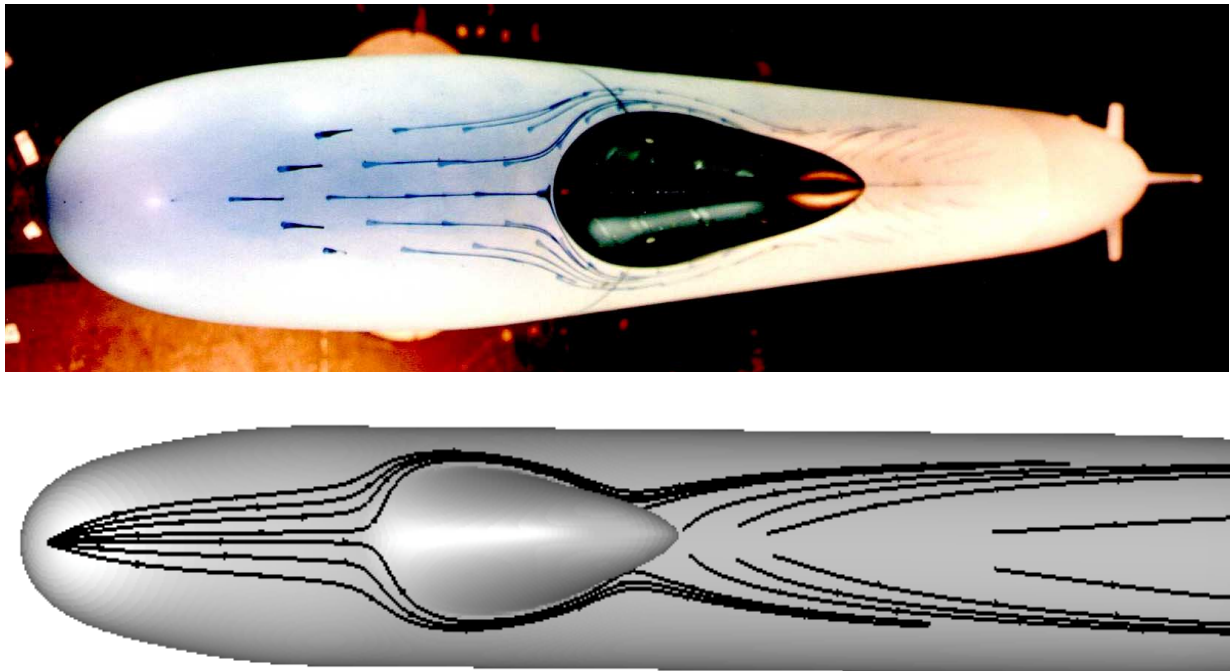
Fig. 10 Hull streamlines around the second sail.
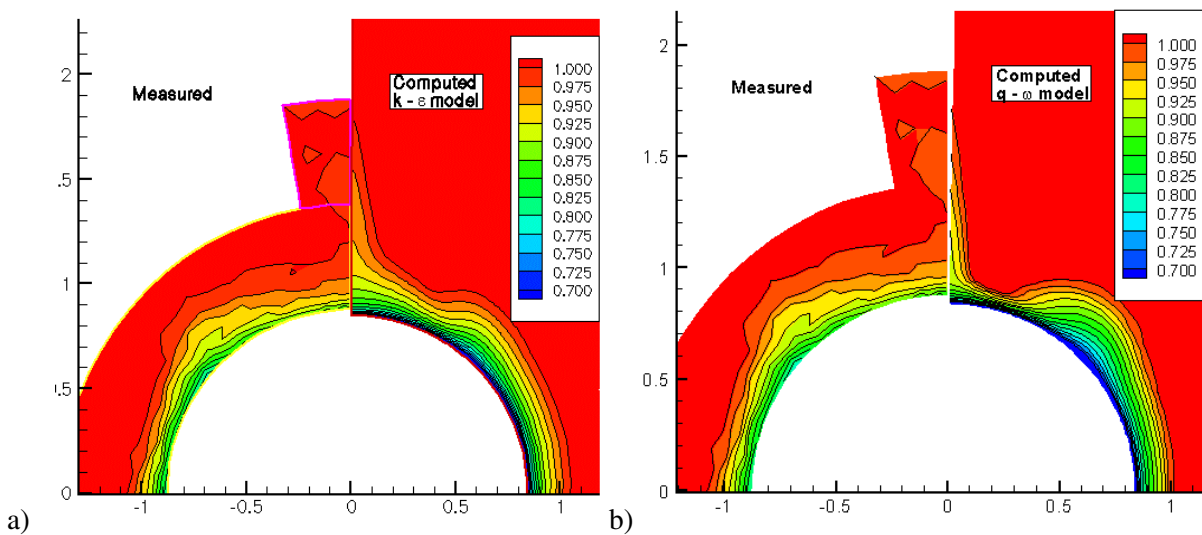
Fig. 11 Computed and measured axial velocity contours at X/L = 0.825; a) k-ε model; b) q-ω model.

Redesign Effort

　　The above computations demonstrate that RANS calculations can predict the significant flow features due to these sail shapes as well as differences between them. Additionally, the computations are able to predict the relative difference in drag between the two shapes. The second sail creates more drag than the first sail, possibly due to the blunter stern and leading edge. The first sail has more internal volume, but produces stronger secondary flow, which will convect downstream into the propeller. To try to combine some of the benefits of both a redesign effort is pursued to see if the shape can be improved. The first sail is chosen as the starting point due to its greater volume and less drag. To minimize changes to the sail only the back end is changed in effect retaining the drag reducing properties of the first sail. Also, it is believed that the blunter stern of the second sail helps reduce the strength of the secondary flow. Three different modifications are shown here. These changes involve increasing the trailing edge steepness of the spine. Efforts are also made to maintain the same length so as not to lose internal volume. A side view of these three shapes is shown in Fig. 12 and referred to as Mod-A, Mod-B, and Mod-C. Surface streamlines for the three shapes as well as axial velocity contours as compared to the original sail are shown in Fig. 13. Mod-A is the smallest change and provides a small knuckle at the back end. This knuckle creates a blunter trailing edge to the sail which leads to a slight flow separation there with a 0.8% increase in drag over the original sail. However, this small change produces a significantly weaker vortex as evidenced by the much smoother axial velocity contours. This smoother flow entering the propeller is very desirable. Mod-B is a very blunt stern with significant flow separation at the stern, which increases the drag 3.2% over the original sail and leads to an even stronger vortex than the original sail. Obviously, this very blunt stern does not work with the streamlined shape of this sail. Mod-C has a higher profile than the other modifications with some bluntness toward the back end. This sail shape also reduces the secondary flow over the original shape and provides an axial velocity field similar to Mod-A. It larger size leads to a 1.2% drag increase over the original sail. This effort has demonstrated two alternatives to the original sail shape, which provide significantly smoother flow into the propeller with a modest drag penalty. Subsequently, Mod-A was chosen, based largely on these computations, and efforts proceeded to build and test a 1/20 scale model at the LCC. This new sail, designated AS98, was then built and tested on the Large Scale Vehicle (1/4 scale) at the NSWCCD Acoustic Research Detachment in Bayview Idaho, Fig. 14.
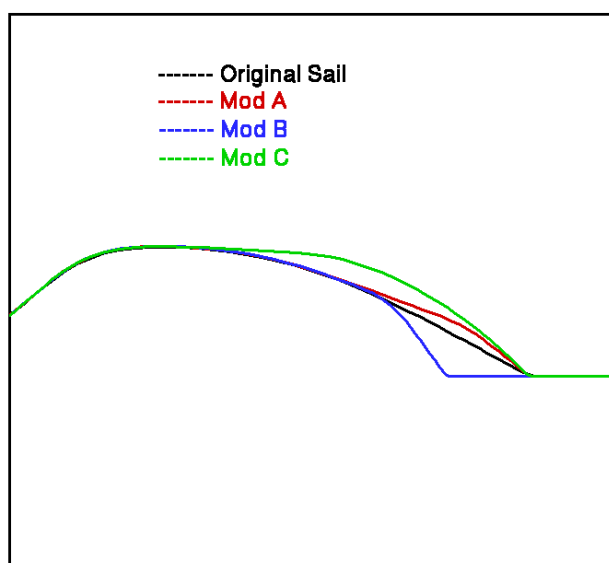
Fig. 12 Side view of modified sail shapes.
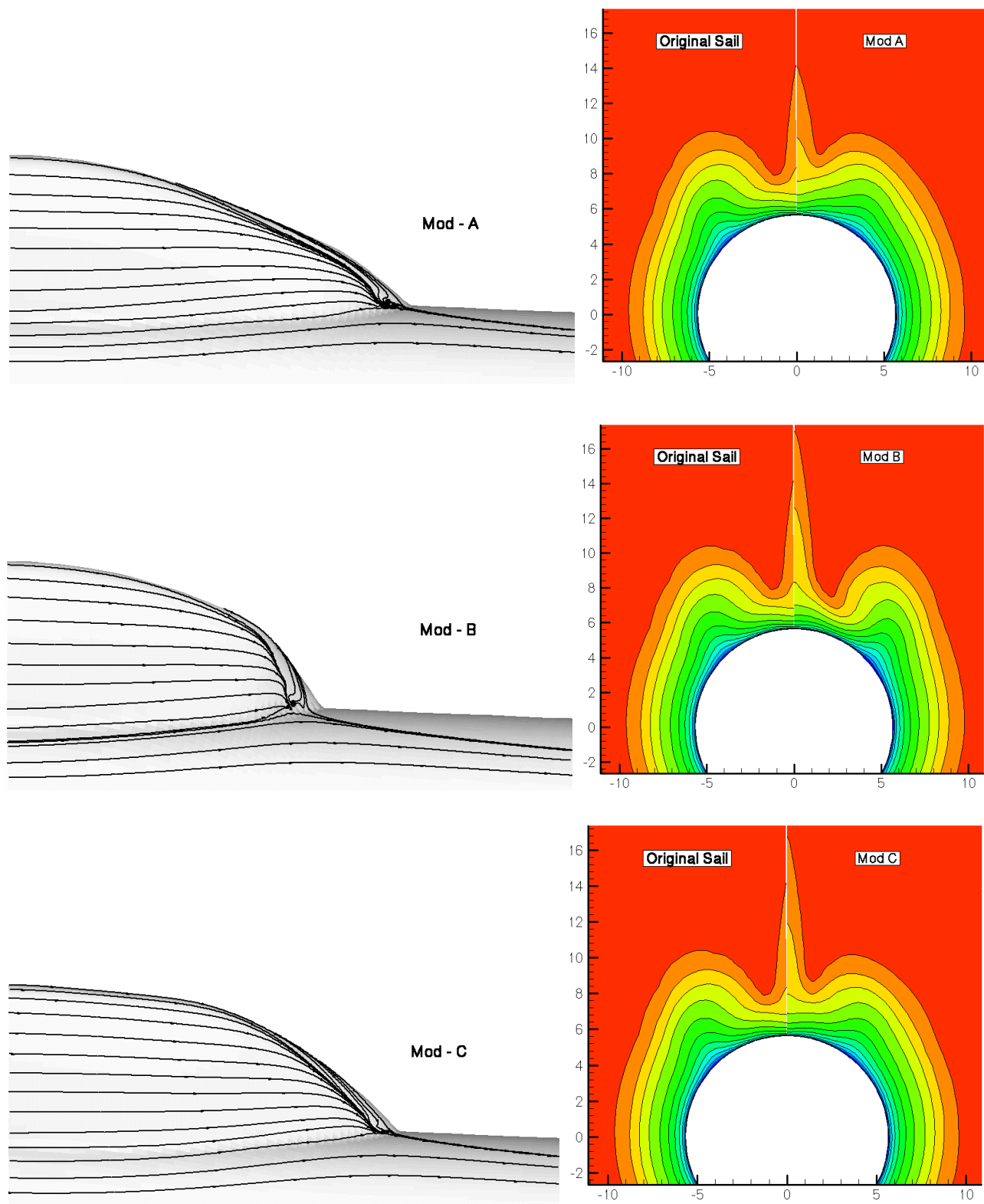
Fig. 13 Surface streamlines and axial velocity contours for the redesigned sail shapes.

Fig. 14 Advanced Sail installed on the Large Scale Vehicle, from Dozier et al [1].

Summary

Over the last decade there has been increased emphasis on the use of computational tools to evaluate submarine flows and guide their design. In particular, with the advent of parallel computational capabilities, viscous RANS simulations have seen a larger role in predicting these flow fields. The shift to a more computational based design and analysis approach leads to the possibility of better designs in a shorter amount of time. Such computations allow for the rank ordering of designs as well as providing the entire flow field, which can lead to better understanding of the flow physics. The current effort demonstrates the use of a RANS code in the design of an "Advanced Sail" for a submarine. The code is validated on similar sail shapes by comparing with experimentally obtained data from a wind tunnel and a water channel. This data comparison includes flow visualization, axial velocity and surface pressures. The agreement demonstrates that RANS codes can be used to provide the significant hydrodynamics associated with these sail shapes. Modifications to a sail are evaluated computationally providing drag differences as well as the secondary flow downstream of the sail. This allowed for the development of an improved shape, which was subsequently built and tested at 1/4 scale with plans for future implementation on the Virginia Class of submarines. Such computations provide a cost effective way to evaluate various shapes, that may improve a design, without having to build and test them. In this way computations will eventually reduce many design oriented tests, such as the series tests of old, which will be replaced with more comprehensive tests of the final design to fully evaluate and understand it.

Acknowledgment

References

[1] Dozier, D., Stout, M., and Zoccola, M., "Advanced Sail Development," *Wavelengths, An Employee Digest of Events and Information*, Carderock Division, Naval Surface Warfare Center, pp. 15 – 17, June, 2001.

[2] Gorski, J. J., "Marine Vortices and Their Computation," *Proc. NATO RTO Applied Vehicle Technology Panel Symposium on Advanced Flow Management*, Loen, Norway, May, 2001.

[3] Gorski, J. J., Coleman, R. M., and Haussling, H. J., "Computation of Incompressible Flow Around the DARPA SUBOFF Bodies," David Taylor Research Center Report, DTRC – 90/016, 1990.

[4] Liu, H-L. and Huang, T. T., "Summary of DARPA Suboff Experimental Program Data," NSWC Report, CRDKNSWC/HD – 1298 – 11, 1998.

[5] Atkins, D. J., "The Application of Computational Fluid Dynamics to the Hydrodynamic Design of Submarines," *Proc. Warship '99, Naval Submarines 6*, London, 1999.

[6] Gorski, J. J. "Drag Calculations of Unappended Bodies of Revolution," CRDKNSWC/HD-1362-07, May 1998.

[7] Taylor, L. K. and D. L. Whitfield, "Unsteady Three-Dimensional Incompressible Euler and Navier-Stokes Solver for Stationary and Dynamic Grids," AIAA Paper No. 91-1650, June 1991.

[8] Taylor, L. K., A. Arabshahi, and D. L. Whitfield, "Unsteady Three-Dimensional Incompressible Navier-Stokes Computations for a Prolate Spheroid Undergoing Time-Dependent Maneuvers," AIAA Paper No. 95-0313, Jan. 1995.

[9] Chorin, A. J., "A Numerical Method for Solving Incompressible Viscous Flow Problems," *Journal of Computational Physics*, Vol. 2, pp. 12-26, 1967.

[10] Van Leer, B., J. L. Thomas, P. L. Roe, and R. W. Newsome, "A Comparison of Numerical Flux Formulas for the Euler and Navier-Stokes Equations," AIAA Paper No. 87-1104-CP, June 1987.

[11] Whitfield, D. L. and L. K. Taylor, "Discretized Newton-Relaxation Solution of High Resolution Flux-Difference Split Schemes," AIAA Paper No. 91-1539, June 1991.

[12] Sheng, C., L. Taylor, and D. Whitfield, "Multiblock Multigrid Solution of Three-Dimensional Incompressible Turbulent Flows About Appended Submarine Configurations," AIAA Paper No. 95-0203, Jan. 1995.

[13] Taylor, L., K., et al., "Large-Scale Simulations for Maneuvering Submarines and Propulsors," AIAA Paper No. 98-2930, 1998.

[14] Liou, W. and T-H. Shih, "Transonic Turbulent Flow Predictions With New Two-Equation Turbulence Models," NASA Contractor Report 198444, Jan. 1996.

[15] Shih, T-H. and J. L. Lumley, "Kolmogorov Behavior of Near-Wall Turbulence and its Application in Turbulence Modeling," Comp. Fluid Dyn., Vol. 1, pp. 43 - 56, 1993.

[16] Coakley, T. J., "Turbulence Methods for the Compressible Navier-Stokes Equations,''AIAA Paper No. 83-1693, 1983.

[17] Walter, J. A. and V. C. Patel, "Measurements in Three-Dimensional Wake of a Surface-Mounted Winglike Symmetrical Ellipsoid," *Exp. Thermal Fluid Science*, Vol. 13, pp. 266 – 291, 1996.

[18] Gorski, J. J., "Present State of Numerical Ship Hydrodynamics and Validation Experiments," *Proc. OMAE'01, 20th Int. Conf. Offshore Mech. Arctic Eng.*, Rio de Janeiro, Brazil, OMAE01/OFT – 1350, June, 2001.

Paper #33
Discussor's name M. Bernard
Author J. J. Gorski

Q: Is it possible to take into account the free surface in your RANS calculations around submarines (sometimes, submarines are near the free surface, even if they are totally submerged)?

A: We are doing both linearized and non-linear free surface calculations with this same code for surface ships.

Discussor's name K. Orlik-Rukemann
Author J. J. Gorski

Q: 1. Are your calculations mainly applicable to the static case?
    2. Are maneuvering dynamics of submarines of much interest?

A: 1. Yes, static only
    2. Yes, it may be, especially for extreme cases.

This page has been deliberately left blank

_____

Page intentionnellement blanche

Simulation of Surface Ship Dynamics Using Unsteady RANS Codes

Ki-Han Kim
Office of Naval Research, Code 333
Arlington, VA 22217
USA

(kimk@onr.navy.mil)

Abstract

This paper presents progress in a three-year Challenge Project, begun in 2001 and led by the Office of Naval Research (ONR), with the objective of demonstrating a capability to simulate time-dependent six-degree-of-freedom (6-DOF) motions of ships in waves and the associated near-field flow using unsteady Reynolds-Averaged Navier-Stokes (RANS) codes. Challenge Projects are sponsored by the U.S. Department of Defense's (DoD) High Performance Computing Modernization Program (HPCMP) Office. Two unsteady RANS codes are used in a progression of building-block simulations at both model and full scale and for practical configurations including detailed resolution of propulsors and appendages. The RANS codes are UNCLE, developed at the Mississippi State University (MSU), and CFDSHIP-IOWA, developed at the University of Iowa. The team members for this project are K.-H. Kim (ONR, team leader), R. Miller and J. Gorski (Naval Surface Warfare Center, Carderock Division), R. Wilson and F. Stern (University of Iowa), L. Taylor (MSU), and M. Hyman (Naval Surface Warfare Center, Coastal Systems Station). Computations are presented for increasingly complex bodies. Bilge-keel forces on a three-dimensional rolling cylinder were accurately predicted. Detailed flow and force characteristics were calculated for an unappended naval combatant hull in prescribed pitch and heave. Initial calculations for a fully appended combatant hull gave good qualitative predictions for surface pressure and free-surface elevation. Calculations for a rudder-induced turn led to evaluation of improved methods for representing a free surface.

Introduction

The traditional U.S. naval ship design methodology of repeatedly building and testing various hullforms for surface combatants is rapidly being changed by successful implementation of advanced computational tools and by availability of massive computational resources primarily through U.S. DoD HPCMP. Future surface ship designs will undoubtedly rely more heavily on computations than in the past. The new process will enable a variety of design decisions and trade-offs based on computations. Furthermore, naval ships of the future will be radically different from those currently in the fleet, in order to meet emerging requirements and to accommodate emerging technologies such as electric drive as the main propulsion system. A preceding Challenge Project (1996-2000) entitled "Time-Domain Computational Ship Hydrodynamics" [1], and the more recent "ONR Surface Combatant Accelerated Hydrodynamics S&T Initiative" (1999-2000), made a significant contribution to establishing this new surface ship design paradigm.

The current Challenge Project begun in 2001 is focusing on demonstrating the capability of simulating 6-DOF maneuvering and seakeeping of full-scale ships using unsteady RANS codes. The first year's efforts were summarized in [2]. The technical challenge is to predict the high-Reynolds number turbulent flows to adequately simulate the interaction of large-scale waves and motions of the ship with small-scale turbulence

and associated forces and moments. One of the major stumbling blocks has been an inadequate capability for computing the nonlinear turbulent free-surface flow about a hull. A major first step was made under the previous Challenge Project where state-of-the-art unsteady RANS methods were used to simulate flow characteristics around an unappended U.S. Navy combatant, DDG-51 hull in regular head waves. Those accomplishments paved the way for prediction of 6-DOF motions of a fully appended ship in a seaway. In this current Challenge Project, two unsteady RANS methods will be applied to simulate time-dependent 6-DOF motions of surface ship in waves, with particular emphasis on roll motion. The two RANS codes to be used are UNCLE, developed at the Computational Simulation and Design Center (SimCenter), Mississippi State University and CFDSHIP-IOWA, developed at the Iowa Institute of Hydraulic Research, University of Iowa.

This effort will perform increasingly demanding simulations of propelled surface ship motion, progressing from model to full scale. The ship hullform chosen for the computations is a conventional transom-stern U.S. Navy destroyer (DDG-51) and its scale model (1/24.8-scale Model 5415), including propeller shafts, support struts, rudders and rotating propellers. A tiered approach is being pursued in which high-fidelity calculations are performed on simpler geometries, for comparisons with experimental data at model scale, in conjunction with highly sophisticated complete-geometry simulations up to full scale.

In this paper, computational results are presented that include prediction of roll motion of a simple three-dimensional cylinder with bilge keels; comparison of the predictions with experimental measurements in a circulating water channel; computations of coupled pitch and heave motions of Mode 5415; and computations of flow around fully appended Model 5415 in straight-ahead motion and rudder-induced maneuver in the horizontal plane.

Future computations will demonstrate the capability to simulate 6-DOF ship motions, maneuvers, and near-field wake, including propeller and viscous effects. The predictions will be one of the first-ever such calculations, which include detailed modeling of the viscous effects on complex interaction of pitch, heave, and roll motions. The product of this research will provide a simulation-based design environment for Navy surface ship hull design, including surface-combatant and other future hullforms.

The study seeks to develop a validated predictive capability for the influence of viscous effects on ship motion for use in conjunction with existing design tools, and to perform large-scale detailed predictions for selected cases identified as critical or of high importance in the design-iteration process. It will introduce the most advanced tools into acquisition and fleet applications. In particular, scalable parallel computing is greatly advancing the complexity of problems for which analysis and design based on large-scale complex flow simulations are becoming feasible.

Computational Tools

The SimCenter at Mississippi State University has developed scalable flow simulation software for both multiblock *structured* grids having arbitrary block connectivity [3] and for multi-element *unstructured* grids [4], known as UNCLE and U^{2}NCLE, respectively. The current parallel algorithm in UNCLE and U^{2}NCLE combines multiple-iteration implicit schemes, characteristic-based finite-volume spatial approximations, and numerical flux linearizations with Block-Jacobi Gauss-Seidel relaxation for the innermost iteration to provide scalable concurrency [5]. Nonlinear free surface [6], general grid motion [7] and moving control surface [8] capabilities have also been incorporated into this algorithm. All tetrahedral and multi-element meshes have been generated with an advancing normal methodology for the boundary layer elements, and with an advancing front/local reconnection (AFLR) methodology for the isotropic elements as given in [9]. This procedure allows generation of high-quality unstructured grids suitable for simulation of high Reynolds number viscous flows with sublayer resolution. All geometry preparation and surface grid generation is performed using SolidMesh [10] with AFLR surface grid generation [11].

The University of Iowa has developed an unsteady RANS code, CFDSHIP-IOWA, for general ship hydrodynamic problems, including resistance, motion, and propulsor. It is a general-purpose parallel code that solves the unsteady RANS equations in either time-accurate or steady-flow mode [12]. The code is written in Fortran 90/95 and has been designed with a modular open-source architecture that supports model

development from outside users without detailed knowledge of data structure and procedures for processor communication required for parallel computing. Version 3.03 is based on a structured multiblock grid approach utilizing higher-order finite difference discretization with collocated flow variables and a pressure-implicit splitting of operators (PISO) algorithm for velocity-pressure coupling. The free surface is modeled using a free-surface tracking algorithm where a two-dimensional kinematic free-surface boundary condition is solved for the wave elevation and the computational grid is dynamically conformed to the hull and predicted free surface at each time step. The surface-tracking approach becomes problematic for free-surface flows with large wave steepness and/or large differences between the unconformed and conformed grid. Such problems could potentially arise for simulation of ships with moderate to large motions. In an effort to increase robustness for such simulations, a fixed-grid approach based on the level-set technique has recently been implemented and tested for simulation of steady free-surface flow around the Wigley and Series 60 ship geometries.

The CFDSHIP-IOWA data structure allows the code to be compiled and executed on either serial or parallel platforms and provides a high level of portability. Large-scale parallel computing is achieved using a multi-level approach where the Message Passing Interface (MPI) is used to distribute computational blocks onto separate processors in coarse-grain mode and OpenMP is used for fine grain loop-level parallelism. This algorithm permits load balancing by allocating threads based on relative block size. The code was extended to allow prescribed and predicted 6-DOF ship motions with incident waves. Chimera overset gridding capability was added recently. This new capability was successfully implemented in the code using Pegasus 5.1 software - developed at NASA Ames through the DoD HPCMO Common High Performance Computing Software Initiative (CHSSI) program - as a pre-processor which automatically creates hole boundaries from boundary condition data and interpolation coefficients for setting boundary values at overlapping block interfaces. The new capabilities will enhance the robustness, fidelity, and efficiency of the current structured-grid approach for applications with fully-appended surface ship configurations with motions.

Viscous Roll Motion of a 3-D Cylinder with Bilge Keels

Roll motion limits ship operability, affects crew performance and ship habitability, and affects dynamic stability and ship capsize. Viscous roll-damping prediction is one of the critical but difficult parts of the motion prediction process. Consequently, current ship-motion prediction methods, mostly potential-flow methods, account for roll effects based on empirical databases obtained primarily from model-scale tests [13]. An initial focus of this project is computation of roll motions for validation of the codes. Using two simple three-dimensional cylinders with bilge keels undergoing a forced roll motion, the accuracy of RANS codes is being determined by comparing the predictions with experimental data for the flow field around the bilge keel and the resulting forces.

The roll motion of a ship is largely influenced by viscous effects. Bilge keels significantly increase the damping of roll motions as well as generate a lift force if any forward motion of the ship is present. Predicting roll effects analytically has been difficult because of the significant viscous effects, even with bilge keels present. As demonstrated by Sarpkaya and O'Keefe [14] bilge-keel damping is a result of the vortices shed from the edge of the keel; damping coefficients from flat plate tests in a free stream are not necessarily accurate for wall-bounded bilge keels. Consequently, roll effects have largely been included in flow predictions empirically, requiring numerous model-scale tests to define coefficients that describe the roll motion. Model-scale coefficients do not necessarily relate well to full-scale behavior due to the differences in Reynolds number. Few viscous computations of roll motions have been reported in the recent past. Yeung, et al. [15] recently presented two-dimensional computational results. The current effort simulates roll motions of a 3-D cylinder with bilge keels. These calculations will provide an indication of the accuracy that can be obtained with RANS codes for predicting viscous roll damping. Such predictions are vital to accurately predicting the seakeeping and maneuvering characteristics of surface ships.

Experiments were recently carried out in the Circulating Water Channel at NSWC, Carderock Division using 3-D cylinders with bilge keels (see Figure 1). That water channel has a 6.7 m (22 ft)-wide and 9.1 m (30 ft)-long square test section with a free surface. Four cylinder/bilge keel configurations were tested, including a

19-inch diameter cylinder with 1 and 2 inch-wide bilge keels and a 35 inch-diameter cylinder with 2 and 4 inch-wide bilge keels. Measurements were made with the models fully and partially submerged in calm water and circulating water simulating forward speed. The cylinders were 13 feet long with an elliptical nose; forces were measured over a 2-foot section of the keels as roll motions were imposed at different frequencies and amplitudes. Forces and pressures were measured on the cylinder. The vortical flow field, including the vortices shedding from the bilge keels, was measured using a Particle Image Velocimetry (PIV) system attached to the rolling cylinder.

Computations were made using the structured UNCLE code. The roll cycle was divided into 360 time steps. Six subiterations per time step were used in most of the calculations. The calculations were performed using 84 processors on Maui's IBM-SP3 computer. The solution for 10 cycles of roll motion took approximately 24 hours with 6 subiterations per time step. Forces on the bilge keels and pressures on the cylinder were computed at every time step. Velocity and vorticity at selected axial locations were also computed at each time step. A fully 3-D structured computational domain consisting of 3 million grid points was created using GRIDGEN, with y+ of 1 for the point closest to the wall. The computational domain extended one body length forward and to the sides, and two body lengths downstream of the body. It was divided into 84 equally sized (33x33x33) blocks for parallel processing.

Initial computations were made for the partially submerged cylinder (35-inch diameter with 2-inch wide bilge keel) undergoing a prescribed roll motion in a steady onset flow at 2 knots, assuming a pure sinusoidal roll motion. The computations were made with a zero Froude number approximation for the free-surface boundary condition using the assumed sinusoidal roll angle as input. Figure 2 shows the computed axial velocity contours. Growth of contours due to convected and locally created vorticity can be seen along the bilge keels. Figure 3 compares the forces on the bilge keel as a function of time. The agreement is qualitatively good. The measured force showed large fluctuations during one cycle of motion. Detailed examination of the measured roll motion revealed that the motion was not smooth and sinusoidal, but fluctuating due to a non-smooth rolling motion of the body caused by the chain drive mechanism that rotates the cylinder.

New computations were subsequently made using the actual, non-smooth angular velocity as input to the RANS solver to account for the actual cylinder motion. Figures 4 and 5 show the comparison of the predicted and measured forces on the bilge keel, with and without forward speed, respectively. The computations are in excellent agreement with the measurements. The computations were able to capture the measured force fluctuations caused by non-smooth angular velocity of the cylinder.

Pitch and Heave Motions of Unappended Model 5415

The problem of prediction of unsteady surface ship hydrodynamics with general 6-DOF motions and incident waves is being investigated using a building block approach in which simulations with either horizontal or vertical plane motions are performed separately before more-complex coupled motions are investigated. Simulations performed in the first year (2001) of the project employed Model 5415 undergoing horizontal plane motions with uniform forward speed and prescribed sinusoidal roll motion [2]. The results showed that the rolling motion resulted in unsteady asymmetric axial velocity contours and a serpentine motion of the vortices emanating from the sonar dome.

Recently, vertical-plane motions were investigated for Model 5415 with combined pitch and heave motions using the CFDSHIP-IOWA code. The simulations were performed for the unappended Model 5415 with double-body geometry at Re=12x10^6. A 16-block structured grid system with 894,504 total grid points was utilized for the simulation that required 16 processors and 525 total CPU hours on the SGI Origin 3000 at Army Research Laboratory in Aberdeen, Maryland. Figure 6 shows the time history of the prescribed heave distance and pitch angle normalized by maximum heave amplitude A_H=0.01L and pitch angle A_P=5 degrees, respectively. Time t is non-dimensionalized with a time scale T defined by T=L/U where L and U are the ship length and forward speed, respectively. The period of the prescribed sinusoidal motions was specified as 0.5T. The prescribed motions modeled a surface ship that is free to pitch and heave while encountering incident head waves. A converged steady-state solution for Model 5415 with uniform forward speed restrained from motions

was used as an initial condition for the unsteady simulation. During the first period and a half ($0 < t/T < 0.75$), the amplitudes of the sinusoidal pitch and heave motions were gradually increased to their maximum values. The resulting solution underwent a transient response for the first two periods after which the transient died out and a periodic response was achieved for $t > T$. Results are shown for one typical period of the periodic response, $1 < t/T < 1.5$.

Figure 7 shows a time sequence of axial velocity contours at every quarter period. For $t=1.125T$ (Figure 7a), the ship was pitching counterclockwise (bow up) at zero pitch angle, so that the boundary layer thickness was reduced along the afterbody while flow separates under the sonar dome due to its upward vertical motion. One-half period later at $t=1.375T$ (Figure 7c), the ship was pitching clockwise (bow down) at zero pitch angle, resulting in a dramatic thickening of the boundary layer and the initial development of a pair of outboard rotating vortices along the afterbody. The downward vertical motion of the bow resulted in the formation of a wake above the sonar dome. At $t=1.5T$ (Figure 7d), the ship reached maximum negative pitch angle and the upward vertical motion of the stern resulted in strengthening of the afterbody vortices.

The time history of the total axial force (C_T) and pitch moment (M_T) is shown in Figure 8 along with frictional (F) and pressure (P) contributions. The response of the axial force was mainly second-harmonic, while that of the pitch moment was purely first-harmonic.

Maneuvering Simulation of Fully Appended Model 5415

Computations of the nonlinear turbulent free-surface flow about a ship hull, particularly at full scale, are extremely demanding. Small-scale appendages and other geometric details such as control surfaces, rotating propulsors, propeller shafts, struts and bilge keels are important for roll-damping predictions. As complexity increases, it gets increasingly difficult to generate good structured grids, and unstructured grids become more attractive. For the present computations using the unstructured U^{2}NCLE code, the geometry of the fully appended Model 5415 was discretized with a high-resolution multi-element unstructured grid, with viscous sublayer resolution on all components. Extensive experimental data for the unappended Model 5415 has been reported [16], and recently experimental data was presented for a rather complete configuration, including rudders, propeller shafts, support struts, and propellers [17].

A free-surface capability was demonstrated during the first year of this Challenge Project [2]. First-ever nonlinear free-surface simulations with a surface-tracking approach for fully appended Model 5415 with rudders, propeller shafts, support struts and rotating propellers were performed at model-scale Reynolds number for steady ahead motion in calm water using the unstructured U^{2}NCLE code. The unstructured mesh used consisted of over 5.7 million nodes, with over 7.7 million prisms and 9.6 million tetrahedra. The flow conditions were $Re = 12.02 \times 10^6$ and $Fr = 0.28$, an especially difficult condition due to the partially wetted transom stern. The propeller rotation was outboard over the top at 436 RPM. The surface-pressure distribution and the free-surface elevation are shown in Figure 9. The surface pressures indicate the complexity of the flow field, and the expected trends are apparent on the struts, shafts, rudders, and hull. In addition, the effect of the propeller wash on the rudders is apparent from the rather strong low-pressure region on the outboard side of the rudder and a relatively benign pressure distribution on the inboard side. Comparison of experimental [16] and computational results for the free-surface elevation immediately aft of the stern is also shown in Figure 9. Qualitative agreement with the experimental data is good overall, including the maximum free-surface elevation. It should be noted that the computed results are shown at a particular instant of time and the experiments showed the flow in this region to be quite unsteady. The solution for this full-configuration Model 5415 was run with 1440 time steps per propeller revolution. Each propeller revolution required 48 hours on 75 IBM-SP3/512Mb processors (3600 processor hours).

A maneuver was initiated by a rudder deflection for the same configuration and grid, initially with zero Froude number, i.e. a rigid free-surface condition. That essentially reduced the simulation to a 3-DOF maneuver. Using the solution in Figure 9 as an initial condition, a maneuver was initiated by rotating the rudders, leading edge to port, at a rate of approximately 11 degrees per second. Surface-pressure distribution as well as axial velocity distribution in the cutting planes are shown in Figure 10 for the initial stages of this

maneuver. The rudders had deflected approximately 6 degrees at that point and the asymmetry in the pressure distributions on the port and starboard rudders is evident. Axial velocity is displayed on a vertical cutting plane through the center of the propeller shaft in the upper left-hand corner of this figure. Axial velocity is also shown on a horizontal cutting plane through the propellers and rudders in the lower right-hand corner of Figure 10. The asymmetry in the axial velocity contours due to the movement of the rudders is clearly shown.

A rudder-induced maneuvering simulation with a non-rigid free-surface condition encountered difficulties associated with free-surface robustness. Improvements in the free-surface robustness are currently being pursued in two ways. One entails modifications to the free-surface fitting (or tracking/conforming) approach used in Figure 9, and the other is a surface-capturing approach in which the free surface is not fit, but is captured within a region of thickness of a few grid points. These two approaches have now been demonstrated and validated for a Wigley hull in straight-ahead motion, as shown in Figure 11. The predicted free-surface elevations along the hull using the surface-tracking and -capturing methods are compared with the experimental data. The agreement is good. This surface-capturing technique appears very promising in terms of robustness. Using this technique, the flow around the unappended Model 5415 in ahead motion was also computed and is shown in Figure 12. Figure 13 compares the wave elevation along the Model 5415 hull for different methods. The surface-capturing technique performs as well as the previous surface-tracking technique. Improvement and validation of a robust free-surface-capturing technique is currently being done for the maneuvering simulations. Future simulations will be undertaken for maneuvering with the nonlinear free-surface capturing technique.

Summary and Future Efforts

Computations are presented for increasingly complex bodies. Bilge-keel forces on a three-dimensional rolling cylinder were accurately predicted. Detailed flow and force characteristics were calculated for an unappended naval combatant hull in prescribed pitch and heave motions. Initial calculations for a fully appended combatant hull gave good qualitative predictions for surface pressure and free-surface elevation. Calculations for a rudder-induced turn led to evaluation of improved methods for representing a free surface. A surface-capturing technique appears very promising in terms of robustness.

A rudder-induced maneuver with the surface-capturing method will be computed for the fully appended Model 5415. Integration of the computed viscous stresses and pressure distribution on this configuration will provide the hydrodynamic forces and moments acting on the ship. Integration of the 6-DOF equations using these forces and moments will yield the time evolution of the ship's velocity and rotation rate. The sensitivity of the computed trajectory with respect to the free surface will also be examined by comparing this maneuvering solution to the one obtained at Fr=0.

Future efforts will also include unsteady simulations of Model 5415 in incident waves with both forced and free roll motions. Initial free roll simulations will include prediction of roll decay after the model is released from some initial angular displacement at t=0 and will allow for comparison with experimental measurements to be performed at University of Iowa. Planned simulations for Model 5415 with forced and free roll motions will be considerably more complex and computationally demanding.

Acknowledgement

References

1. Rood, E. P., "Computational Ship Hydrodynamics for Revolutionary Naval Combatants," *Proceedings, DoD High Performance Computing Modernization Program Users Group Conference*, Albuquerque, NM (Jun 2000).

2. Kim, K.-H., "Unsteady RANS Simulation for Surface Ship Dynamics," *Proceedings, DoD High Performance Computing Modernization Program Users Group Conference,* Biloxi, MS (Jun 2001).

3. Pankajakshan, R., Taylor, L.K., Sheng, C., Jiang, M., Briley, W.R., and Whitfield, D.L., "Parallel Efficiency in Implicit Multiblock, Multigrid Simulations, with Application To Submarine Maneuvering," *AIAA Paper 2001-1093*, 39th Aerospace Sciences Meeting, Reno, NV (Jan 2001).

4. Hyams, D.G., Sreenivas, K., Sheng, C., Briley, W.R., Marcum, D.L., and Whitfield, D.L., "An Investigation of Parallel Implicit Solution Algorithms for Incompressible Flows on Multielement Unstructured Topologies," *AIAA Paper 2000-0271*, 38th Aerospace Sciences Meeting, Reno, NV (Jan 2000).

5. Hyams, D.G., Sreenivas, K., Sheng, C., Nichols, S., Taylor, L., Briley, W.R., Marcum, D.L., and Whitfield, D.L., "An Unstructured Multielement Solution Algorithm for Complex Geometry Hydrodynamic Simulations," *Proceedings, 23rd Symposium on Naval Hydrodynamics*, Val de Reuil, France (Sep 2000).

6. Burg, C.O.E, Sreenivas, K., Hyams, D.G., and Mitchell, B., "Unstructured Nonlinear Free Surface Simulations for the Fully-Appended DTMB Model 5415 Series Hull Including Rotating Propellers," To be presented at the 24th ONR Symposium on Naval Hydrodynamics, Kyushu, Japan (Jul 2002).

7. Jayaraman, B. and Marcum, D.L., "A General Procedure for Dynamic Unstructured Grids," 7th International Conference on Numerical Grid Generation in Computational Field Simulations, Whistler, Canada (Sep 2000).

8. Pankajakshan, R., Taylor, L.K., Jiang, M., Remotigue, M.G., Briley, W.R., and Whitfield, D.L., "Parallel Simulations for Control-Surface Induced Submarine Maneuvers," *AIAA Paper 2000-0962*, 38th Aerospace Sciences Meeting, Reno, NV (Jan 2000).

9. Marcum, D.L., and Gaither, J. A., "Mixed Element Type Unstructured Grid Generation for Viscous Flow Applications," *AIAA Paper 1999-3252*, 14th AIAA CFD Conference, Norfolk, VA (Jun 1999).

10. Gaither, J. A., "*A Solid Modeling Topology Data Structure for General Grid Generation,*" Master's Thesis, Mississippi State University (1997).

11. Marcum, D.L, "Unstructured Grid Generation Components for Complete Systems," 5th International Conference on Numerical Grid Generation in Computational Field Simulations, Starkville, MS (Apr 1996).

12. Paterson, E.G., R. Wilson, and F. Stern, "General Purpose Parallel Unsteady RANS for Ship Hydrodynamics," *Computers and Fluids* (Jun 2000).

13. Himeno, Y., "Prediction of Ship Roll Damping - State of the Art," Report No. 239, U. of Michigan (1981).

14. Sarpkaya, T. and O'Keefe, J. L., "Oscillating Flow About Two and Three-Dimensional Bilge Keels," *J. Offshore Mech. Arctic Eng.*, Vol. 118, pp. 1 – 6 (1996).

15. Yeung, R. W., Roddier, D., Alessandrini, B., Gentaz, L., and Liao, S.-W., "On Roll Hydrodynamics of Cylinders Fitted with Bilge Keels," *Proceedings, 23rd Symposium on Naval Hydrodynamics*, Val de Reuil, France (Sep 2000).

16. Ratcliffe, T.J, and Lindenmuth, W.T., "Kelvin Wake Measurements Obtained on Five Surface Ship Models," DTRC Report 89/038 (Jan 1990).

17. Ratcliffe, T.J, "An Experimental and Computational Study of the Effects of Propulsion on the Free-Surface Flow Astern of Model 5414," *Proceedings, 23rd Symposium on Naval Hydrodynamics*, Val de Reuil, France (Sep 2000).
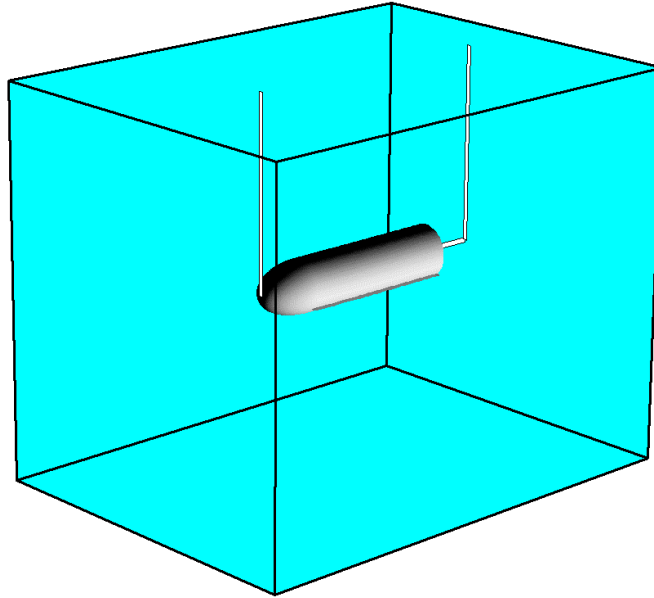
Figure 1. Experimental Setup for Roll Experiments in the Circulating Water Channel
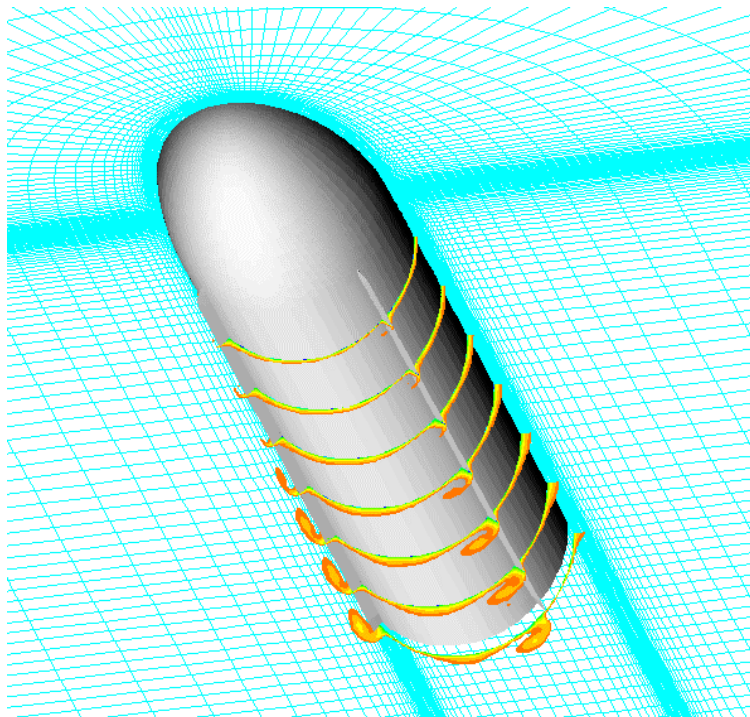
Figure 2. Axial Velocity Contours – Partially Submerged Cylinder (D=35 in.)
(f = 0.32 Hz, Amp = 15 deg, Fwd Speed = 2.0 knots)
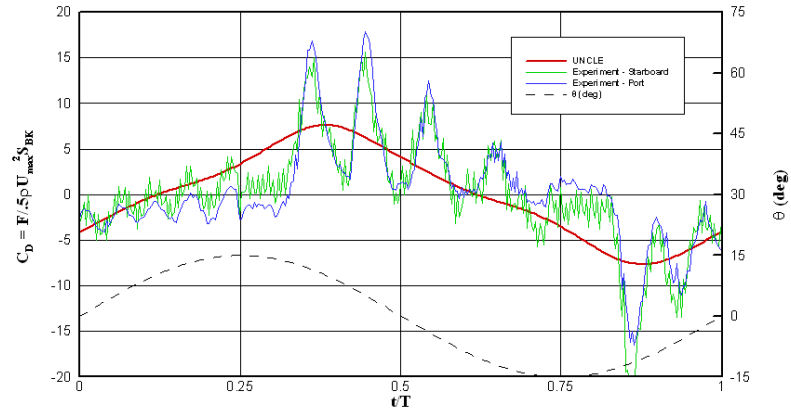
Figure 3. Force on Bilge Keel - Submerged Body (f = 0.32 Hz, Amp = 15 deg, Fwd Speed = 0 knots)
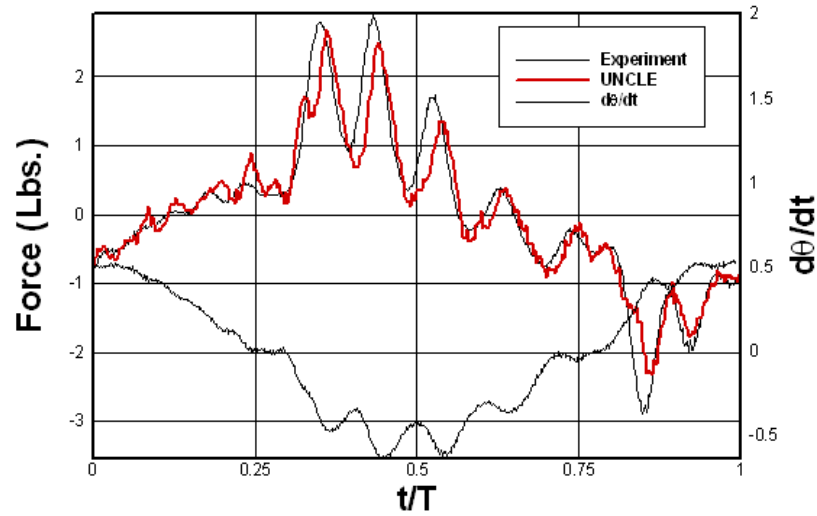
Figure 4. Force on Bilge Keel - Submerged Body (f = 0.32 Hz, Amp = 15 deg, Fwd Speed = 0 knots)
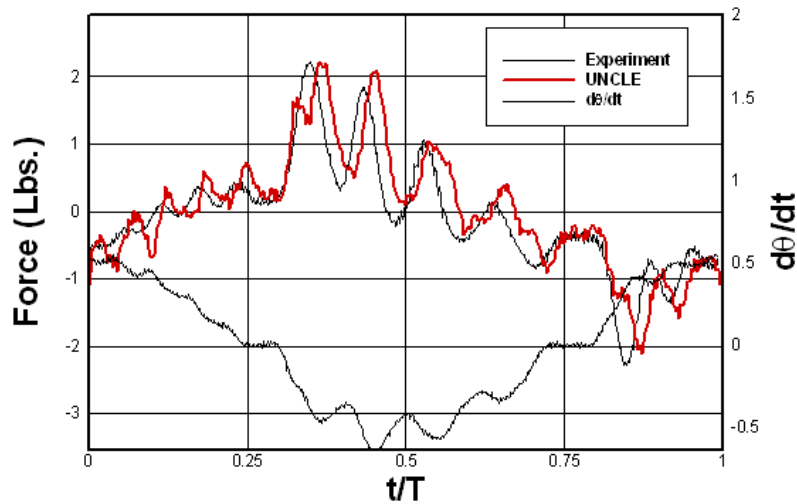
Figure 5. Force on Bilge Keel - Submerged Body (f = 0.32 Hz, Amp = 15 deg, Fwd Speed = 2 knots)
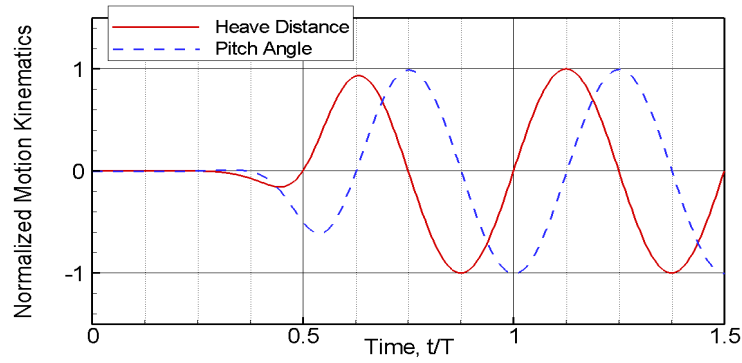
Figure 6. Time History of Pitch and Heave Motions for Unsteady RANS Simulation of Model 5415 using CFDSHIP-IOWA
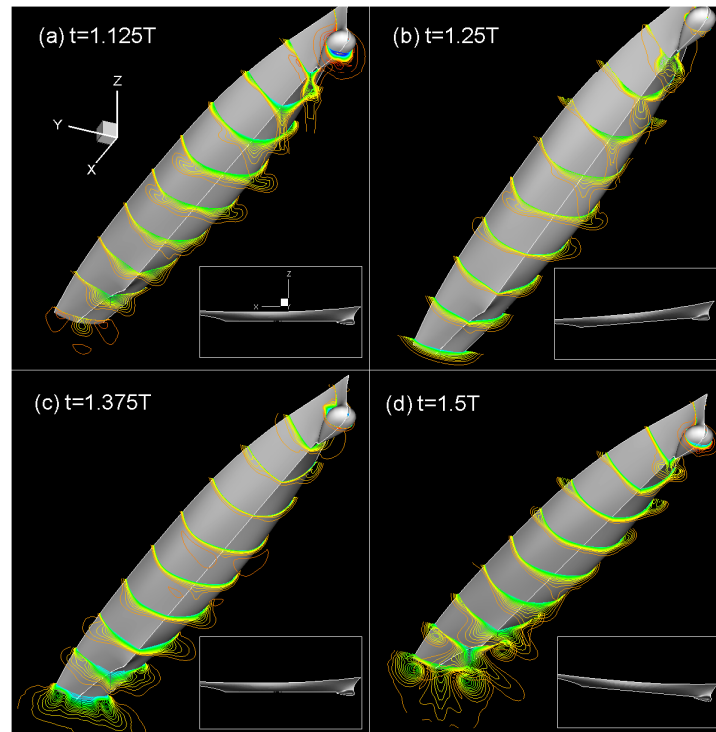
Figure 7. Time Sequence of Axial Velocity Contours for One Period of Prescribed Pitch and Heave Motion from Unsteady RANS Simulation of Model 5415 Using CFDSHIP-IOWA
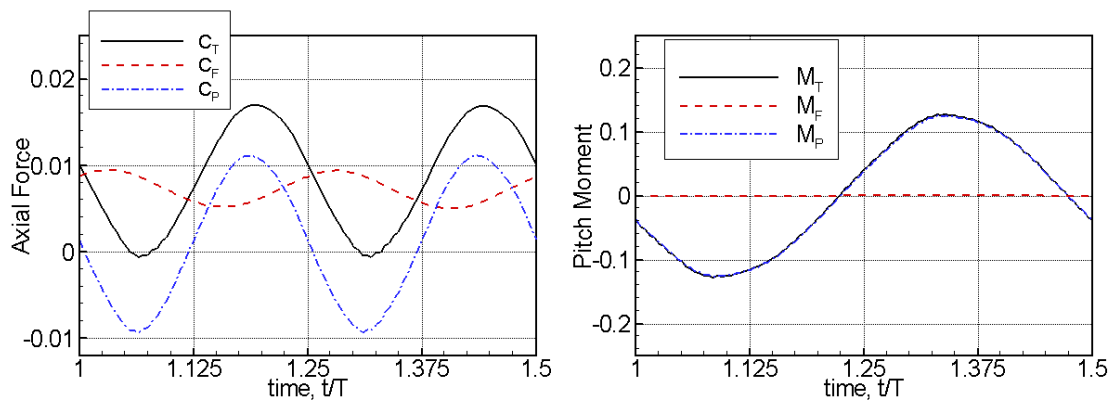
Figure 8. Time History of Axial Force and Pitch Moment of Model 5415 with Prescribed Pitch and Heave Motions from Unsteady RANS Simulation Using CFDSHIP-IOWA
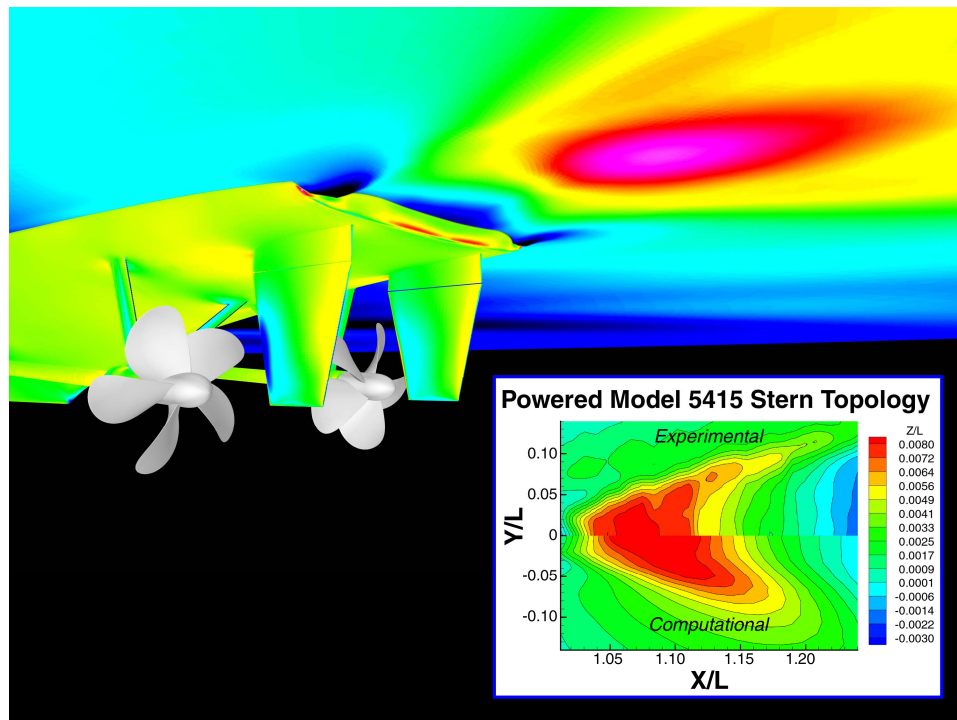
Figure 9. Nonlinear Free Surface Simulation for a Fully Appended Model 5415 Using U^{2}NCLE
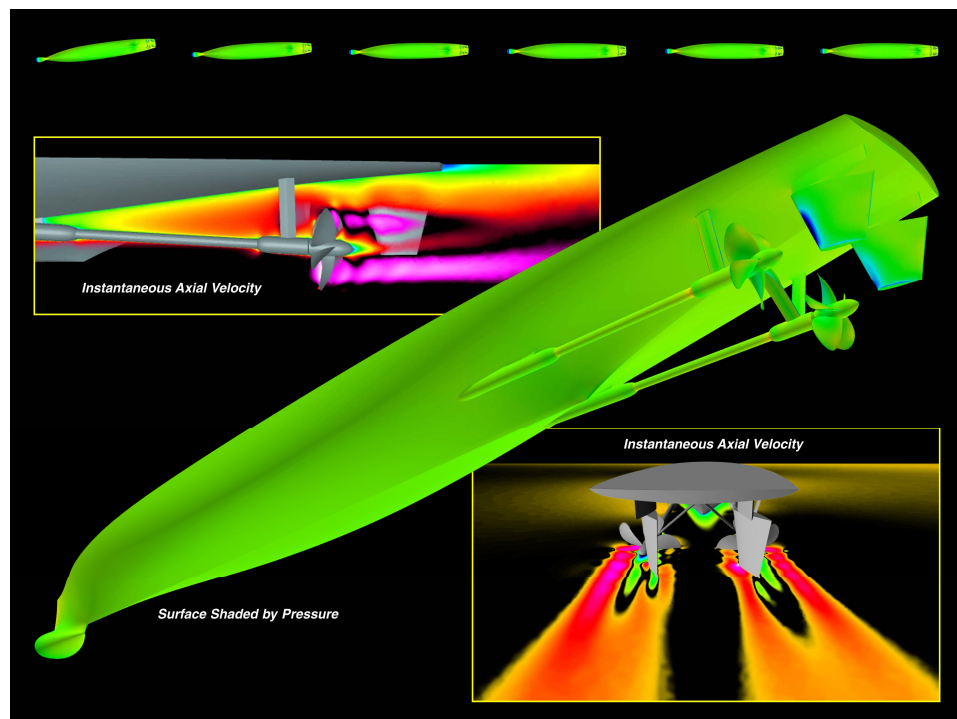
Figure 10. Rudder-Induced Propelled Turning Maneuver with Rigid Free-Surface Condition Using U^{2}NCLE
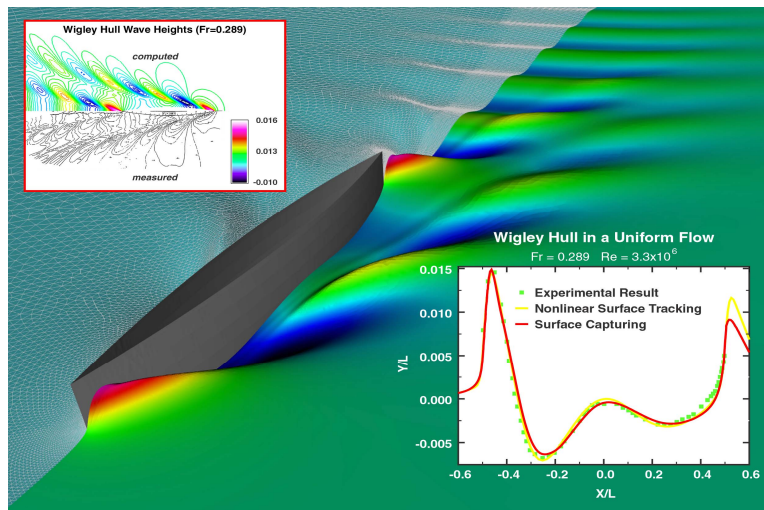
Figure 11. Wave Elevation Using Surface Fitting and Capturing Approaches (Wigley Hull) Using U^{2}NCLE
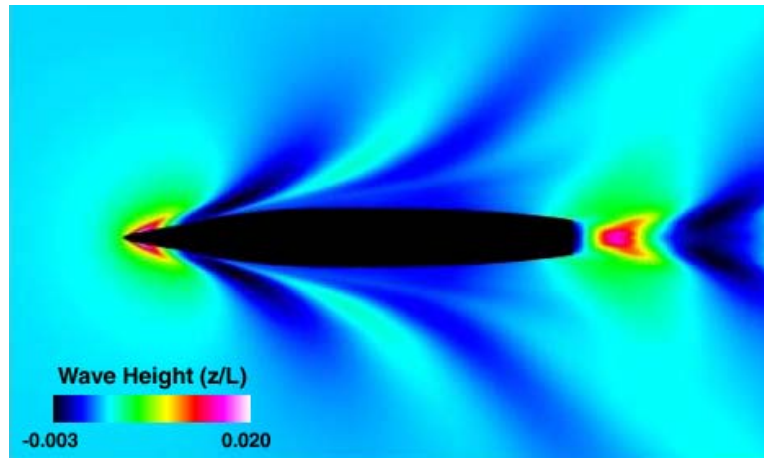
Figure 12. Free-Surface Contours using the Surface Capturing Approach on Model 5415
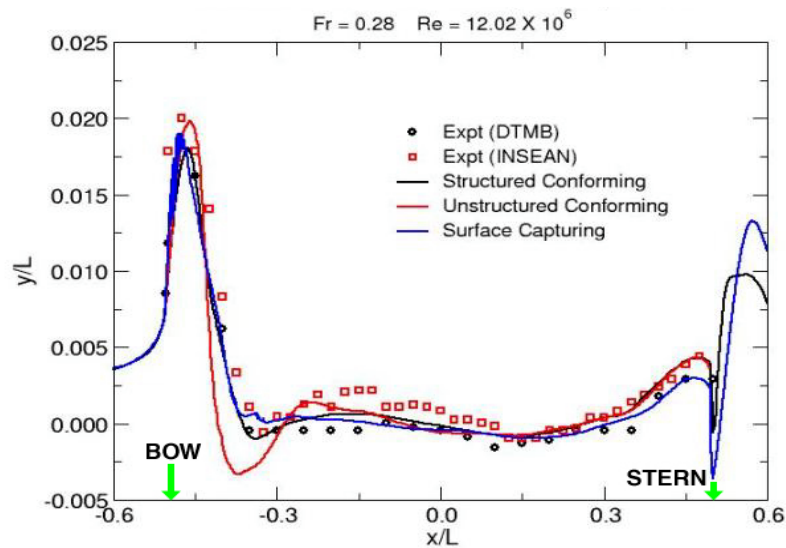
Figure 13. Comparison of Free Surface Elevation on Model 5415 Using U^{2}NCLE

Paper #35
Discussor's name Dr. B. Oskam
Author Dr. K. H. Kim

Q: Your simulation of the fully appended model 5415 is based on the unsteady Reynolds-averaged Navier-Stokes equations with 7 revolutions per second of the propeller. How do you separate the propeller-induced unsteadiness (7 revolutions per second) from the turbulence unsteadiness in, say, the hull boundary layer?

A: Code is based on assumption that the two time scales are sufficiently different.

This page has been deliberately left blank

_____

Page intentionnellement blanche

A numerical study of breaking waves

R. Muscari, A. Di Mascio

INSEAN – Via di Vallerano, 139 – 00128 Roma – Italy

e-mail: muscari@insean.it

1 Summary

The focus of the present work is on the numerical simulation of steady flows with spilling breaking waves. In particular, the breaker is modeled through a hydrostatic pressure and a shear stress exerted on the free–surface. Many elements of the exposed model are derived by Cointe and Tulin's theory of steady breaker. The model has been implemented in a RANSE code in a simple but effective way through a modification in the free–surface boundary conditions. At present, the resulting code is valid for two–dimensional flows, and has been accordingly tested against the experimental data obtained by Duncan for the flow generated by a hydrofoil towed under the free–surface at different velocities and depths.

2 Introduction

Breaking waves are often encountered when dealing with ship flows. The appearance of a breaker on the bow wave is generally associated to a strong dumping of the following wave train and to the inception of a turbulent shear flow just under the free–surface. These effects have been experimentally studied by several authors (Dong et al., 1997; Roth et al., 1999), but despite the important changes that a breaking wave induces on the flow around the hull, the presence of a breaker is often overlooked in numerical codes.

This is due to some major difficulties: the choice of a criterion for the onset of breaking, the detection of the points where breaking take place, the calculation of its strength from the wave geometry and/or from the flow variables, the effects on the underlying flow, the description of the turbulent wake that follows the breaker below the free–surface, and so on.

The study of a two–dimensional flow such that described in (Duncan, 1981, 1983), and sketched in figure 2, greatly simplifies the problem, from both the experimental and the numerical point of view. A two–dimensional hydrofoil moving at speed U under the free–surface is considered. Depending on the speed and the depth of the foil, the resulting wave–train can feature an almost steady breaker on the forward face of the leading wave. This experimental set–up has been studied by Cointe and Tulin (1994), who provide useful hints for the calculation of the breaker geometry and the modelization of its influence on the wave–train. The breaker is seen as an eddy riding on the forward face of the breaking wave, exerting 'suitable' pressure and friction on the wave–breaker dividing streamline. To our purposes this theory has an attractive aspect, i.e. it yields some boundary conditions to model the breaker which are simple but effective and readily applicable.

The implementation of Cointe and Tulin's ideas in an existing RANSE code (described in Di Mascio et al. (1998, 2001)) required some further work. The main distinguishing features of the proposed model with respect to Cointe and Tulin's (1994) is the way in which the geometry of the breaking region is related to the wave height. Moreover, the breaking region is not modeled as a sharp triangle,

but rather as a smoothed geometrical shape in order to mitigate the abrupt transition in the free–surface dynamic boundary conditions and, hence, to enhance convergence to steady state. Finally, we implement the dissipative effects of the breaker through a boundary conditions on the velocity field along the wave–breaker dividing streamline. In particular, we set the normal derivative of the tangential velocity, on the basis of local equilibrium considerations and classical solutions of the mixing layer.

In order to validate the algorithm, we performed a simulation of Duncan's experiment and the results, together with some implementation details, are described in the following.

3   A breaking model for steady viscous flow simulations

According to Cointe and Tulin's theory, the breaker is imagined as an almost stagnant eddy lying on the forward face of the leading wave. Consequently, it exerts on the underlying flow both a pressure, due to its weight, and a shear stress, that keeps the breaker in its position withstanding the gravity force.

From a numerical point of view, this means that we can simulate the presence of the breaker through a slight modification of the boundary conditions and, in particular, by adding a suitable hydrostatic pressure and a shear stress on the breaker–wave dividing streamline.
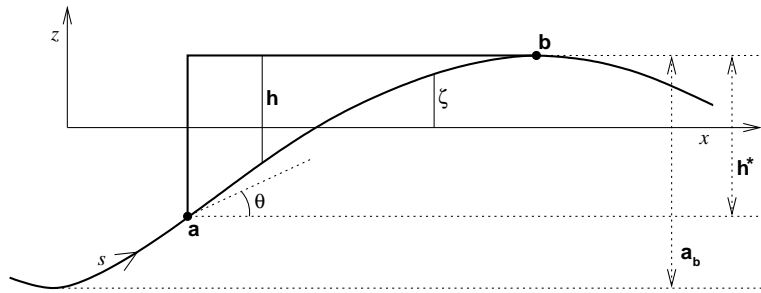
Figure 1: Geometry of the breaking wave.

Referring to figure 1, the model is turned on when $a_b > 0.69 \, \mathsf{Fr}^2$ (Tulin and Cointe, 1986), where a_b is the crest–trough distance of the first wave and Fr the Froude number.

Once the model is activated, we first detect the location of the crest (i.e., the top of the breaker) and the trough of the leading wave. Then, the breaker height is computed from

$$h^* = 0.64 \, a_b \tag{1}$$

in accordance with experimental findings by Duncan (1981). This expression was preferred to the one found in (Cointe and Tulin, 1994)

$$h^* = \frac{\mathsf{Fr}^2}{2} - \zeta_b \tag{2}$$

because the latter holds only once the flow has attained its steady state, but it is not useful within the iterative algorithm to reach the steady state itself.

On all points of the free–surface between x_{toe} and x_{top}, the pressure is enforced to be

$$p(x) = \frac{\zeta(x) + \rho_b \, h(x)}{\mathsf{Fr}^2} \tag{3}$$

where $h(x)$ is the top–flat function, smoothed in order to improve convergence, and ρ_b is the density of the breaker, which we assume, as in the Cointe and Tulin's model, equal to 0.6. For the velocity we assign the normal derivative of the tangential velocity:

$$\frac{\partial q^t}{\partial n} = \delta \, \frac{1 - \chi}{1 + \gamma \, \chi} \qquad \text{with} \qquad \chi = \frac{x - x_a}{x_b - x_a} \tag{4}$$

which resembles the solution of the Tollmien mixing layer in the nearby of the toe.

4 Discussion

We have applied the model to the simulation of the wavy flow past a submerged profile, in the same conditions as the experiments reported in (Duncan, 1981, 1983) and illustrated in fig. 2. A `NACA 0012` profile, whose chord is `20.3 cm`, is towed in a tank at a speed of 0.8 `m/s`, with an angle of attack of 5°. As in the towing tank experiments, the depth is varied by changing the water level, whereas the profile is kept fixed with respect to the bottom. For the sake of brevity, we consider here only the immersion d=`18.5 cm`, which is the first depth considered by Duncan for which breaking spontaneously occurs, and still is not so strong to spoil completely the following wave train.
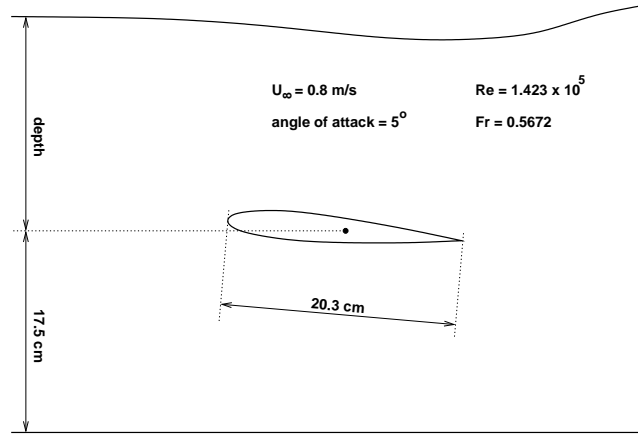
Figure 2: Experimental setup

We use a multi-grid approach with the finest grid consisting of about 60,000 cells, and each coarser grid obtained by halving the finer one.

The L_2-norm of residuals and non-dimensional resistance histories for the simulation without breaking model (fig. 3a) are good for the coarser grids but on the finest one the residuals oscillate around a small but constant value. In fact, the physical solution features a breaker, whereas the first wave of the wave–train in the simulation is too step and its shape is simply due to the fact that the code cannot cope with multivalued surface height (fig. 3b).

Using the breaking model dramatically improves the solution in terms of both convergence (fig. 4a) and wave pattern (fig. 4b, with error bars for the numerical data calculated as suggested in (ITTC Quality Manual, 2001; Roache, 1997)). Although the first wave height is not well captured, the following train shows a very good accordance with experiments in both height and phase.

The major difference with respect to the experimental results is located on the first trough, which is not as deep as in the measurements by Duncan. This same problem is shared by other Navier–Stokes
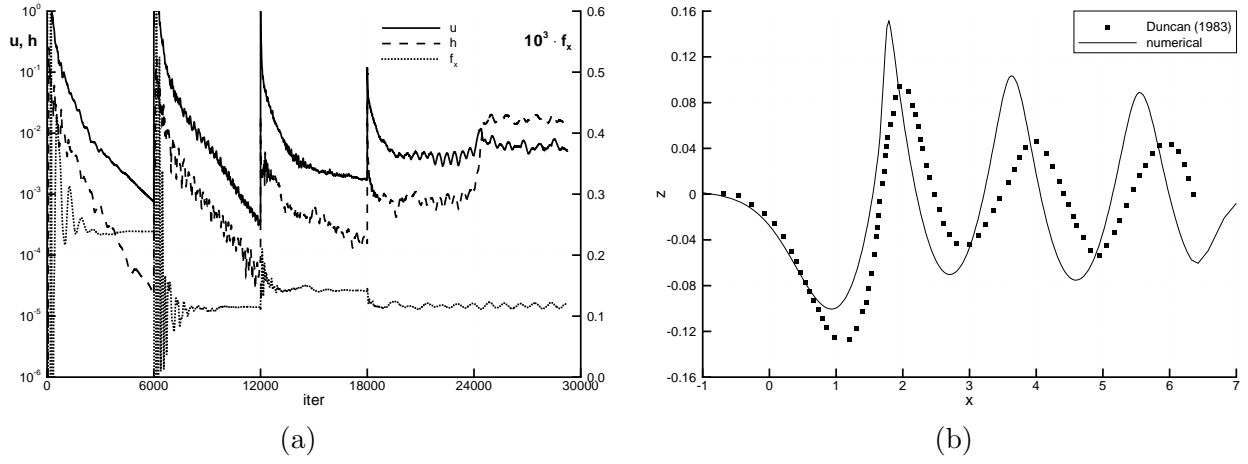
Figure 3: No breaking model; (a) residuals and resistance histories, (b) computed wave pattern vs. experiments.
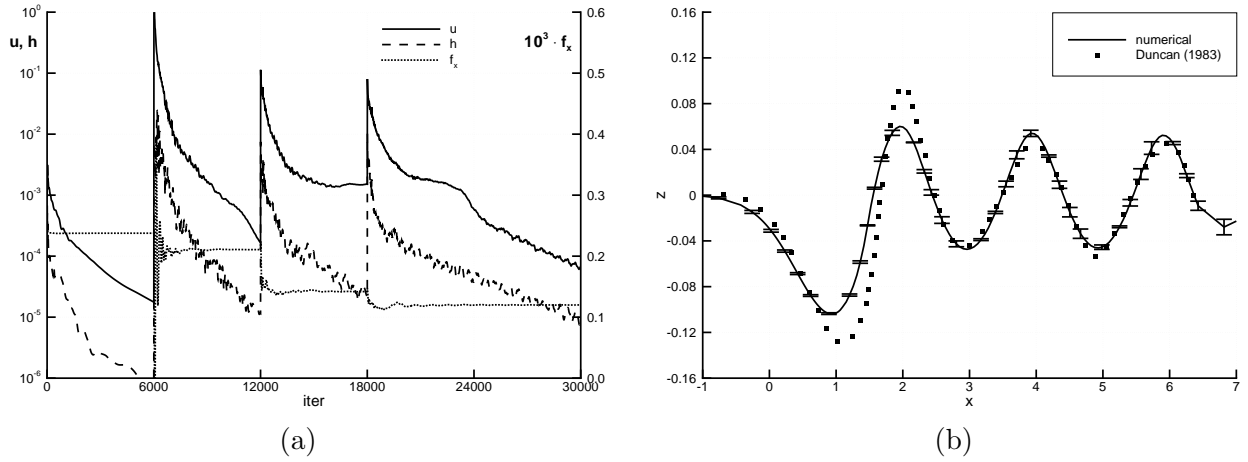
Figure 4: Simulation with breaking model; (a) residuals and resistance histories, (b) computed wave pattern vs. experiments.

simulations, especially at relatively low Reynolds' numbers (Mori and Shin, 1988; Hino, 1997; Rhee and Stern, 2001).

In fig. 5 the velocity profile is shown near the free–surface under the second trough after the breaker. Duncan's results are shown both with symbols corresponding to actual measurements and with the fitting curve computed in (Duncan, 1983). Numerical results mirror the expected trend, that is the profile for a Stokes' wave, up to the wake of the breaker. The velocity values out of the wake are slightly overpredicted, within 1% from the experiments, whereas the wake thickness is underestimated, as can be evinced from the experiments which are, in this respect, rather spread.

Finally, we have verified that the height of the breaker computed through eq. (1) is in accordance with that yielded by eq. (2). The two values, $h^*_{(1)} \simeq 0.105$ and $h^*_{(2)} \simeq 0.101$, are in very good agreement, thus validating the use of eq. (1) within the iterative algorithm.
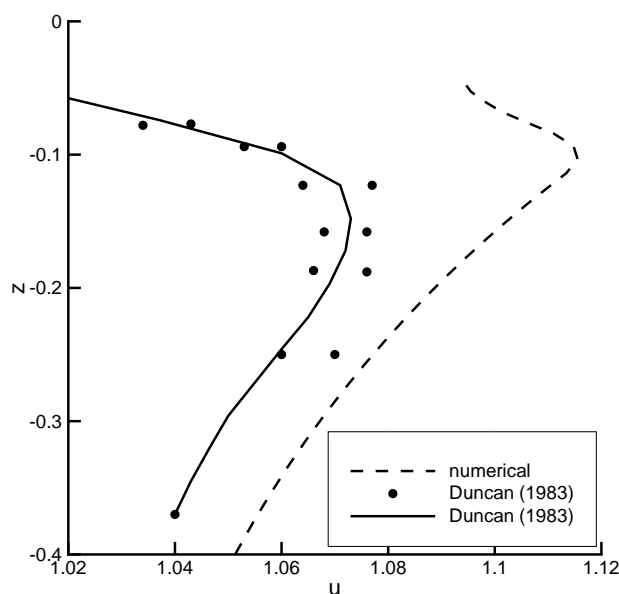
Figure 5: Velocity profile under the second trough after the breaker.

5 Conclusions

A numerical model for steady spilling breakers simulation with RANSE codes has been proposed. The basic ideas for the model are derived from Cointe and Tulin's theory. Nevertheless, important changes were found to be necessary in order to get a stable iterative algorithm when coupling the model with a steady state computation of wavy flow with breaking waves.

Even if the underlying theory is somewhat over–simplified with respect to the physics of the problem (see Lin and Rockwell (1995) for a more accurate description of a two–dimensional flow in presence of breaking) the model can be implemented straightforwardly and yields excellent results for the test case considered.

The proposed model will be generalized and extended to three–dimensional flows past ship hulls in a future work.

References

Cointe, R. and Tulin, M. P. (1994). A theory of steady breakers. *J. Fluid Mech.*, 276:1.

Di Mascio, A., Broglia, R., and Favini, B. (1998). Numerical simulation of free-surface viscous flow by eno-type schemes. In *3rd Int. Conf. on Hydrod.*, Seul, Korea.

Di Mascio, A., Broglia, R., and Favini, B. (2001). *A second order Godunov–type scheme for naval hydrodynamics*, pages 253–261. Kluwer Academic/Plenum Publishers.

Dong, R. R., Katz, J., and Huang, T. T. (1997). On the structure of bow waves on a ship model. *J. Fluid Mech.*, 347:77–115.

Duncan, J. H. (1981). An experimental investigation of breaking waves produced by a towed hydrofoil. *Proc. R. Soc. Lond. A*, 377:331.

Duncan, J. H. (1983). The breaking and non-breaking wave resistance of a two-dimensional hydrofoil. *J. Fluid Mech.*, 126:507.

Hino, T. (1997). An unstructured grid method for incompressible viscous flows with a free–surface. In *35th aerospace sciences meeting & exhibit*. AIAA-97-0862.

ITTC Quality Manual (2001). Resistance Committee of 23th ITTC.

Lin, J. C. and Rockwell, D. (1995). Evolution of a quasi–steady breaking wave. *J. Fluid Mech.*, 302:29–44.

Mori, K. H. and Shin, M. S. (1988). Sub–breaking wave: its characteristics, appearing condition and numerical simulation. In *Proc. 17th Symp. on Naval Hydrodynamics*, The Hague, The Netherlands.

Rhee, S. H. and Stern, F. (2001). Private communication.

Roache, P. J. (1997). Quantification of uncertainty in computational fluid dynamics. *Ann. Rev. Fluid Mech.*, 29:123.

Roth, G. I., Mascenik, D. T., and Katz, J. (1999). Measurements of the flow structure and turbulence within a ship bow wave. *Physics of Fluids*, 11(11):3512.

Tulin, M. P. and Cointe, R. (1986). A theory of steady breakers. In *Proc. 16th Symp. Naval Hydro-dynamics*, Washington D.C. National Academy Press.

Unsteady Flow Simulation: A Numerical Challenge

Francesco Martelli, Elisabetta Belardini, Paolo Adami
Energetics Department Sergio Stecco
University of Florence
via S. Marta, 3
Florence-50139
Italy

ABSTRACT

The prediction of unsteady flow field in turbine blades as well as in the turbomachinery stages is now an affordable item, and is required by the reduced margin for increasing efficiency, stability and life of propulsion components. The numerical tools are now capable to run within reasonable time 3D unsteady calculation for full stage, and the new techniques on the computation and parallel computer allow the improvements of results in terms of cost and accuracy. Despite these advantages many questions remain open and the physical modelling joint with the numerical improvements is still a challenge if it has to produce usable results, compared with the experiments. On the other side the huge amount of data extracted from experiments require care and skinless to become useful tools for design. The two activities interact and support each other in the attempt to improve design quality. Aim of this paper is the report on some experience and the attempt to give some answer on that challenge, presenting results of a recent activity on modelling side compared with experiments as well. A full-3D unstructured solver based on an upwind TVD finite volume scheme has been developed and applied to the simulation of an unsteady turbine stage. The development of the numerical strategy is discussed with particular concern on the validation of the unsteady model through a comparison against experiments, NISRE approach and a 3D steady stage computation. The present work considers the application of the fully unstructured hybrid solver for internal viscous flows, as well. The multiblock version of the solver developed for turbine is considered, because of the highly improved performance as compared to the single domain version of the code. Moreover, the high numerical costs involved in 3D unsteady computations required the development of a new parallel single program multiple-data version of the numerical solver. The results compare favourably with a set of time averaged and unsteady experimental data available for the turbine stage under investigation, which is representative of a wide class of aero-engines.

Nomenclature

f,g,h	Convective fluxes	*Greek symbols*		
f	Frequency	ρ	Density	
J	Implicit residual Jacobian	τ	numerical time	
Q	Conserved variables vector	ω	Rotational speed	
p	Static pressure	*Subsripts*		
$P0,T0$	Total pressure and temperature	*1,2,3*	NGV inlet, interstage and rotor outlet planes	
R	Residual vector			
S	Source term residual	*Acronymous*		
t	Physical time	*GMRES*	Generalised Minimal Residual Method	
V	Element *volume*			
s	Curvilinear abscissa	*ILU*	Incomplete LU factorisation	
W	Mass flow rate	*NISRE*	Not Isoentropic Simple Radial Equilibrium	
x,y,z	Space coordinate			
W	Mass flow rate	*PE*	Processing Element of a Parallel Architecture	

1. INTRODUCTION

Computational Fluid Dynamics (CFD) has become an effective tool in the analysis of complex flows and the design of more efficient machinery components, thanks to its versatility in the investigation of different working conditions and to the capability in analysing overall and detailed information about the flow. The simulation of a transonic turbine stage requires both efficiency and accuracy in order to forecast the stage performances and the realistic representation of the unsteady stator/rotor interaction. In this regard many applications of structured codes for 3D turbine investigations have been reported in literature.

A basic assessment considering the research activity and the main impact of unsteadiness phenomena is given by Sharma et al., (1992). Among all the approaches proposed some authors use implicit ADI factorisation schemes for the simulation of quasi-3D stator-rotor interaction, while others apply an explicit multi-grid technique. Both the unsteady approaches are based on a dual-time stepping extension of the basic time marching procedure developed for steady state computations. Giles, (1990) describes a similar numerical scheme with the application of a different approach for a generic not even stator-rotor blade count ratio. A recent work of Dorney *et al.* (1997), compares accuracy and efficiency of different predicting models with increasing complexity, ranging from fully unsteady simulations to loosely coupled methods, for stage performances prediction. Other computational studies for turbine row interaction have been carried out by several authors among which Haa et al. (1993), Gallus et al. (1994), Dawes (1994), He (1996) and Walraevens *et al.* (1998). More recently von Hoyningen-Huene and Jung, (2000) have reported the application and comparison of different unsteady approaches for structured grids. The comparison considers an explicit method, a time consistent multi-grid and a dual-time step with multi-grid on structured grids.

A common drawback of all the structured approaches is the crude way required to improve accuracy in confined region of rapid gradient which also implies a costly grid refinement in a large, and not necessary, portion of the flow domain. A more sensible approach would instead refine the mesh locally only in regions where a sharp variation of the solution is expected. The first examples of unstructured codes for compressible simulations come from the external aerodynamics while more recently viscous extensions have been reported by Kwon and Hah, (1995) and Mavriplis, (1995). The more rational mesh refinement and the higher geometrical flexibility are the most attractive aspects of the unstructured approaches, allowing complex configurations to be represented and easily handled by the solution algorithm.

The main drawback is, undeniably, the high CPU and memory demand, which can rapidly waste the advantages offered by the increased geometrical flexibility. In this regard very few general applications have been documented in literature on the use of unstructured solvers for unsteady stator rotor interaction. An example is reported by Sayma *et al.* (2000), using semi-structured grids with a dual time step approach. A different strategy is proposed by Rai (1989) aiming to improve the geometrical flexibility through the use of patched structured grids.

The present work considers the application of a fully unstructured hybrid solver (HybFlow, Adami *et al.* 1998) for internal viscous flows. The multiblock version of the solver developed for turbine rows (Adami et al., 2000) is considered, because of the highly improved performance as compared to the single domain version of the code. Moreover, the high numerical costs involved in 3D unsteady computations required the development of a new parallel single program multiple-data version of the numerical solver. This improved version of HybFlow is applied to the simulation of the BRITE HP turbine stage experimentally tested in the compression tube facility CT3 of the Von Karman Institute (Dénos *et al.* 1999, 2000).

2. THE GOVERNING EQUATIONS

The basic numerical scheme of HybFlow code solves the compressible Navier-Stokes equations cast in strong conservative form (Adami, 1998). For the simulation of the flow field conditions inside turbine rotor rows, the conventional condensed formalism has been adopted:

$$\frac{\partial Q}{\partial t} + \frac{\partial f}{\partial x} + \frac{\partial g}{\partial y} + \frac{\partial h}{\partial z} = S \tag{1}$$

The governing equations have been extended to cope with a moving frame of reference rotating together with the rotor row. The same formalism of governing equations can be retained for both the fixed and the rotating frame adding the centrifugal and Coriolis terms in S, provided that, when applied to the rotor row, the velocity vector and all total quantities are referred to the relative frame (Belardini *et. al* 2000). The perfect gas state equation is finally used for the closure of the mathematical model.

3. THE NUMERICAL METHOD

The spatial discretization

The solver HybFlow is specialised for the computation of internal compressible/incompressible flows with and without chemical reactions. A brief description of the basic numerical scheme follows, while more details can be found in Adami *et al.* 1998, Adami *et al.* 2000, Belardini *et. al.* 2000. The spatial discretization is based on a finite volume approach for hybrid unstructured grids. Roe's approximate method is used for the upwind scheme. A linear reconstruction of the solution inside the elements provides a second order discretisation, and monotonicity is ensured through the TVD slope limiter proposed by Barth, (1991).

Two possible time accurate discretization are available:

◊ The explicit approach; the time accurate solution is computed using a five-step multi-stage Runge-Kutta scheme, with the classical scheme.

◊ The implicit dual-time stepping discretization;

The dual-time stepping approach adds an extra numerical time derivative to the physical unsteady equation (1):

$$\frac{\partial Q}{\partial \tau} + \left[\frac{\partial Q}{\partial t} + R(Q) - S(Q) \right] = 0 \tag{2}$$

The physical time derivative can be expressed using a second order back-ward finite difference:

$$\left. \frac{\Delta Q}{\Delta t} \right|_{phys}^{(k)} = \frac{3Q^{(k)} - 4Q^n + Q^{n-1}}{2\Delta t}$$

A classical time marching approach is then recovered to drive to convergence the numerical unsteady term. The time marching procedure is based on the approximate implicit Newton method for systems of non-linear equations. The physical time derivative is discretized with second order backward approximation and, collecting together the terms of the implicit Jacobian matrix, the classical formalism of the implicit method is recovered as follows:

$$\left\{ \frac{I}{\Delta \tau} + J^*(Q^{(k)}) \right\} \Delta Q^{(k)} = R^* \left(Q^{(k)} \right)$$

where

$$J^*\left(Q^{(k)}\right) = \frac{\partial}{\partial Q}\left[\left.\frac{\Delta Q}{\Delta t}\right|_{phys}^{(k)} + R(Q^{(k)}) - S(Q^{(k)})\right]$$

$$R^*\left(Q^{(k)}\right) = -\left[\left.\frac{\Delta Q}{\Delta t}\right|_{phys}^{(k)} + R\left(Q^{(k)}\right) - S\left(Q^{(k)}\right)\right]$$

(3)

When the selected convergence criterion is satisfied $\Delta Q^{(k)} \approx 0$ and the physical solution at time level $n+1$ is updated: $Q^{n+1} = Q^{(k)}$

Stability of the numerical algorithm is provided by the time-marching relaxation term appearing in the implicit operator and resulting from the numerical time derivative $I/\Delta\tau$. The matrix of the implicit method is computed numerically by finite differences expressions of the residual vector *R* with respect to the solution (see Adami, 1998), while the contribution from the source terms is computed through analytical derivatives of *S*. The linear system stemming from equation (3) is solved at each integration step by the same iterative method GMRES (Saad, 1994) used for the steady state simulations. The efficient convergence of the linear solution requires preconditioning. The preconditioning matrix is computed performing an incomplete ILU(0) factorisation of the implicit matrix (Saad, 1994). It is worthwhile remembering that the whole procedure GMRES-ILU(0) makes use of a condensed storage format which accounts for matrices with non-zero elements only.

As proved in Fig. 1-a the implicit dual time stepping strategy shows an effective behavior in terms of robustness and stability. In fact the numerical time marching converges to the unsteady physical solution within 10 numerical sub-iterations with about 3 orders reduction of the initial residuals.

4. THE PARALLEL MULTI-BLOCK APPROACH FOR STAGE COMPUTATIONS

The multi-block and parallel strategy

Although basic solver provides an accurate description of internal flows at different Mach numbers, when dealing with complex geometry the simulation can require high CPU time and memory storage. A significant memory saving and reduction of the overall CPU cost has been obtained by means of different numerical tools. Firstly a multi-block strategy implementation allowed a significant reduction of memory usage, thanks to the reduced dimensions of the linear system matrix during the implicit marching of the solution. The multiblock approach had a positive effect on computing time also. In spite of the loss in robustness of the solver due to the additional new internal explicit boundaries created, the overall computational cost is considerably reduced.

Besides the domain decomposition technique represented an essential step, in view of the implementation of the code on parallel architectures. The parallel version of the code is based on the standard MPI message passing libraries to ensure high portability. The neighbouring elements residing on the local memory of different CPUs require the explicit activation of a communication procedure among processors to satisfy the physical flow continuity. The increase in the number of processors leads to a considerable decrease of computational costs. Nevertheless, communications amongst different processors represent a computational overhead, which can grow rapidly with the number of processors involved if the computational activity is incorrectly shared.

The present parallel approach distributes individual portions of the overall grid among different CPUs (data partitioning). In this case all processors perform the same set of operations solving the flow field inside the sub-domains assigned to each CPU: the distribution strategy, aimed to guarantee almost the same number of elements inside each block and a quite uniform distribution of blocks to different Pes, thus allowing a global load balancing.

In this regard the histogram of Figure 1 reports the early time profiling of the parallel solver (percentage of the different computational activities with respect to the total CPU time), during the solution of a test case. The test run on 16 processors on CINECA Origin 3800, a shared memory multiprocessor system based on Processing Elements (PEs) R12000 running at 400 MHz. Although physically distributed, the memory can be logically shared by the hardware able to address a unified global space.

In the porting of scalar solvers to parallel architectures a crucial feature in the estimation of code performance is the communication cost which is strictly related to the structure of the code and the algorithm. Usually for an implicit solver the system matrix storage and inversion require around $75 \div 80\%$ of the total computational time. During this time the algorithm does not require inter-processor communications.

Early analysis of the scalar solver performance showed that, despite the use of efficient numerical strategies and of a compact storage method (Adami *et al.*, 1998), the implicit system required about 88% of the code memory demand. Overall, the time spent for residuals assembly and system matrix inversion was more than 90% of the total elapsed time. A more recent profiling of the parallel solver shows that matrix inversion is still the most time consuming activity requiring about 65% of the global CPU time, followed by communications (15%), flux assembly and I/O management. The distribution of these percentages is obviously dependent from the particular processor but the maximum difference remained below 3% demonstrating an acceptable load repartition. In view of these features of the solver all the optimisation strategies performed on the parallel code were mainly focused on the reduction of system inversion CPU time and communication strategy Among these the use of the most advanced compilers options (such as the better exploitation of pipeline mechanism, fast improved math libraries and the optimisation of the cache use) brought a 16% global CPU time reduction on numerical experiments performed in simpler configurations. Beside the Fortran routines managing the message passage MPI standard where implemented with the introduction of Fortran 90 dynamic allocation to reduce the dimension of the data packages to be sent or received during communications. This allowed another 3% CPU time reduction on a local 4 CPUs workstation. A different storage of system matrix lead to a limitation of global primary 'cache miss' and thus a further 6% reduction of the global CPU time.
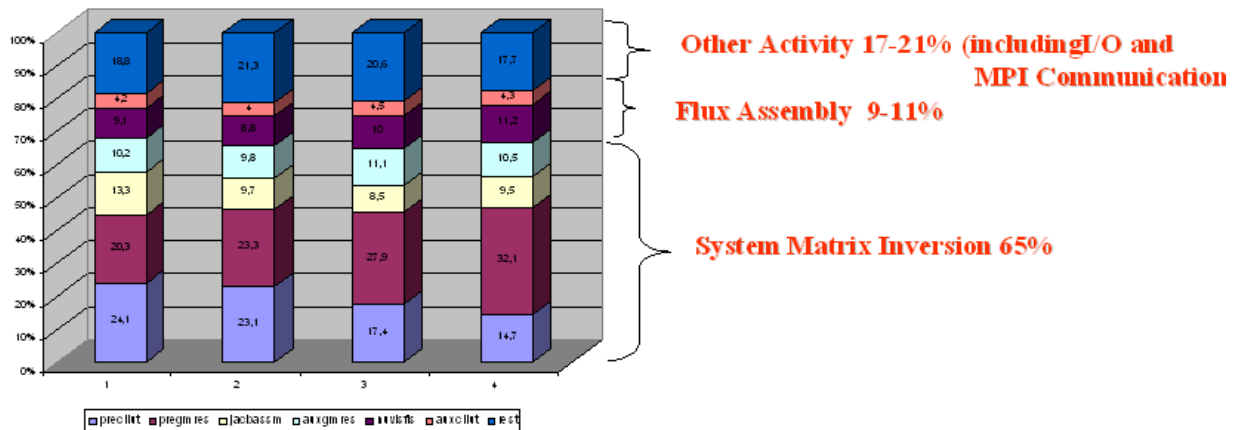
Figure 1 Time Profiling of the Solver on 16 CPU

To face the greater and greater dimensions of the flow problems and the management and storage of the amount of the data involved, attention can not be focused only on the optimisation of the flow solver itself but should take into account even all the routines of the so called pre and post-processing phases which had to be revised and improved. In this respect Figure 2 reports the main phases of a multi stage CFD computation which starts from the solid modelling and grid generation of the single stator and rotor rows using commercial software (Centaur[TM]). The complete grid geometry of the stage is then assembled in a unique domain which is divided in smaller blocks trough a fully automatic domain decomposition technique (see Fig. 2). Finally the multiblock domain is distributed amongst the different processors and the processing of the data for unsteady

computation is performed (*Parallel and unsteady treatment* in Fig. 2). At this point the inlet data set is ready for the CFD simulation which will produced the basic flow features at various time steps of the simulation. Finally the data produced will be processed and synthesised to produce variables easy to be understood and interpreted to capture the basic flow physics of the problem such as time averaged pressure on the blade surface, unsteady pressure fluctuation in some interesting points or for the comparison with experimental data, pitch -wise time averages for secondary flow description and movies. With simpler flow configurations the pre and post processing phases where not critical but with the increasing of the problems dimension all these routines had to be revised and improved. In fact with increasing grid dimensions the CFD solver is surprisingly not the crucial phase of the whole approach while the most memory demanding step is the domain decomposition and the most CPU intensive step is the computing of unsteady information for the sliding mesh nterface (see next paragraph). The reason for this behaviour can be explained remembering that with increasing grid dimensions a larger CPU's cluster may be used to tackle the computational cost increase during the CFD application having a fully parallel structure. Conversely the same does not hold for the pre and post processing routines which naturally retain a scalar character required to manage the whole physical domain.

This problems has been presently reduced, keeping the same structure of the pre processing routines, with a proper use of the memory space through the Fortran 90 standard which allows a flexible dynamic memory allocation and de-allocation of unused matrices. With regard to the unsteady treatment the main problem was represented by the length of the interpolation searching techniques which required more than 48 hours to complete the final set up of the data for the unsteady simulation of the viscous grid made of 1.8M elements. In this case a more efficient searching strategy for the interpolation technique and a rationale use of the I/O management have been introduced to obtain a significant reduction of total required time (about ten times).
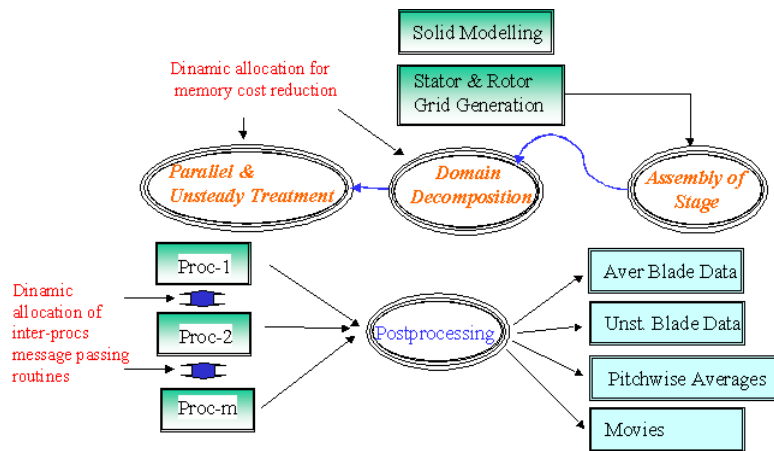
Figure 2: Pre and Post ProcessingTreatment

Boundary Conditions Sliding Interface

Inlet conditions are given at the stator inlet plane using the nominal total pressure and total temperature profiles as also the inlet flow angle. In the exit plane, hub static pressure is imposed and the radial equilibrium equation is applied to evaluate the static pressure distribution assuming an axially developed flow field. Solid surfaces are assumed to be adiabatic with zero normal mass and momentum fluxes. Periodicity is ensured with an exact point to point correspondence between elements belonging to the periodic boundaries. On the rotor stator interface a local interpolation has been developed to account for the relative rows movement and for the change of reference frame.
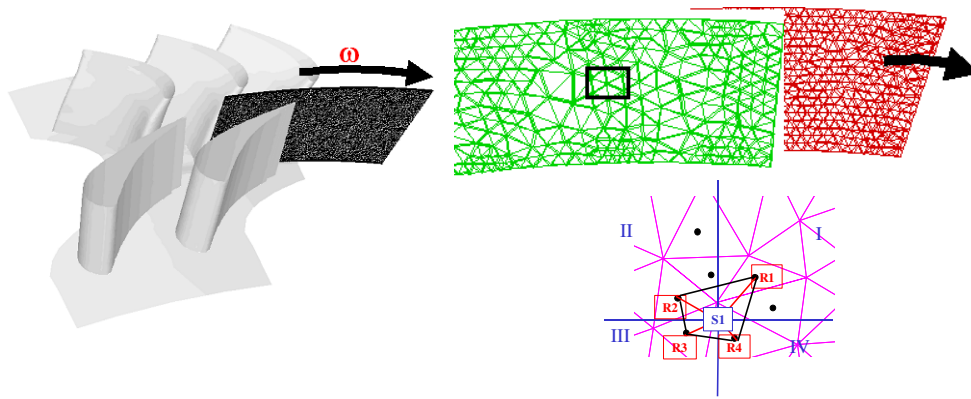
Figure 3: Interpolation Strategy in Sliding Interface

The grid close to the rotor-stator boundary is fully three-dimensional and unstructured to allow simple and efficient grid generation in the inter-stage gap. Thus, elements with triangular and quadrilateral faces from both stator and rotor grids need to be interfaced at varying angular positions (Figure 3). In such situations, the map of neighbouring elements and the definition of a simple matching strategy for the two rows poses serious difficulties, also because of the continuous displacement of the two moving blades during the unsteady computation. This geometrical problem has been overcome by the implementation of a crude, but general interpolation scheme between the two rows, as summarised in Figure 3. The interpolation strategy guarantees the continuity of static variables (density, pressure and temperature), while velocity components are discontinuous, according to the relationships between absolute and relative frames. Although the present method is not strictly conservative, the computations revealed that the mass imbalance is always well below 1%. A substantial reduction in the computing time to complete the full unsteady simulation (made up of several periodic revolutions), can be obtained with the storage of all information pertaining to the sliding interface interpolation in a look-up table accompanying the grid file. In this way the parameters for corresponding time periodic positions can be computed once for all time steps, avoiding time-consuming recalculations.

Grid Sequencing Strategy

In a CFD simulation usually an initial guess solution is used to start the computation. This rough solution is updated till the solver reaches the final exact numerical solution of the physical problem. When a complex domain and different physical aspects are involved, such as coolant injection mixed with the coupling of rotating and stationary parts, rarely this initial guess solution can be chosen close to the real one and thus stability problems may arise while several time steps can be required before the final convergence is obtained.

The number of this numerical steps has been strongly reduced, mainly in the viscous computation, using the grid sequencing strategy. The basic idea beyond this method is the creation and use of a family of grids with progressively increasing element number. An unsteady unviscous computation can be performed on the coarser grid to capture the fundamental flow physics or the basic frequency spectrum of the unsteady pressure fluctuations which are both almost independent from viscous phenomena. In the present application the coarse unviscid grid is made up of 360000 elements, of which 24000 on blade surface and 5700 on the sliding surface dividing the NGV from the rotor rows.
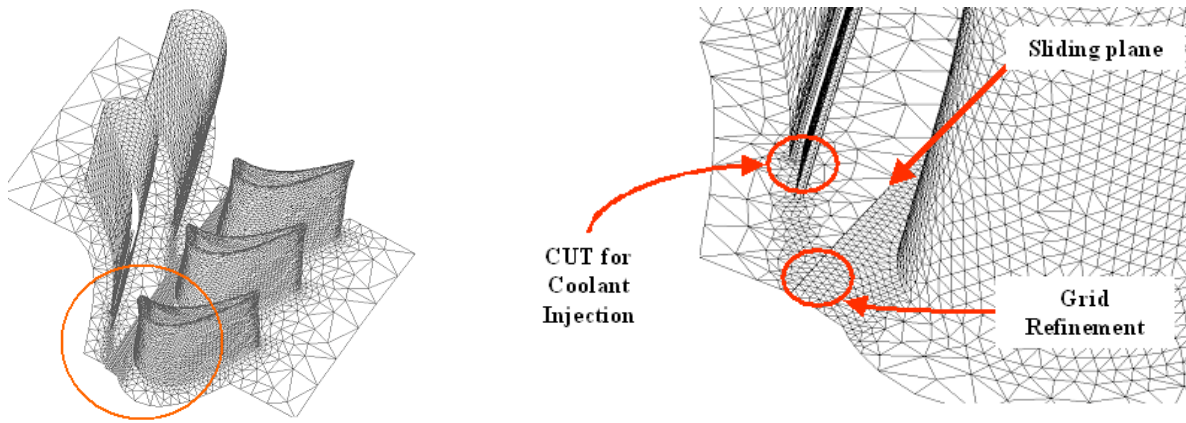
Figure 4.   Coarse Grid for Unviscid Computations

(b) X= 60 mm   **(c) X= 80 mm**
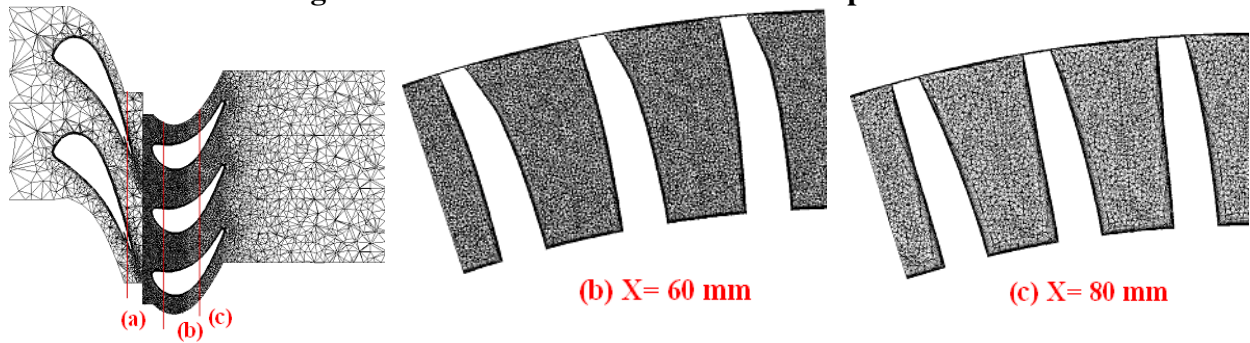
Figure 5: Refined Grid for Viscous Computations

The final converged numerical solution for unviscid simulation still requires a large number of steps but the CPU time is reduced in view of the smaller dimensions of the grid. Once the solution is obtained on the coarse grid a viscous and turbulent computations can be carried out on the second refined grid (Figure 4a) to capture the effect boundary layers development on the performance and efficiency of the stage. The initial guess solution can be represented by the unviscid solution obtained on the coarse grid which can be transferred to the refined simulation through an automatic grid adaptation technique. A general unstructured 3D routine has been ad hoc developed to interpolate the solution from the coarse to the second refined grid which is reported in Figure 4. A further refinement step has then performed using a third viscous grid shown in Figure 5. Grid refinement is evident in the radial section at midspan (Figure 5) where 10 prismatic layers have been introduced all around the NGV and rotor blade surfaces to capture the basic features of the boundary layer. Node elements have been also added in the rotor vane passage flow and mainly in the coolant injection area (slide (a) in figure 5) of the NGV which is thought to be responsible, together with the shock detaching from the TE of the stator blade, for the unsteady pressure fluctuations measured on the rotor blade. A strong grid refinement is also applied all over the pitch-wise direction ahead the rotor blade (slide (b)) in order to accurately capture the effect of the NGV wake for all relative positions of the two rows. Numerical computations performed demonstrated that this refinement requires a soft smoothing toward the trailing edge of the rotor to avoid the effect of the grid sensitivity of the solution on the different sizes of neighbouring cells which can strongly affect the accuracy/stability of the flow solution. Despite the refinement the global grid has a still feasible number of elements (1.8 Ml elements, 41000 on solid surfaces and 20000 on the sliding plane) owing to the high flexibility of the unstructured approach.

5.   APPLICATION TO THE 3D VKI ANNULAR STAGE

Stage description

The present investigation is carried out on the first stage of the HP turbine with prismatic stators and fully three-dimensional rotor selected in the frame of the TATEF project. The project is devoted to gain a better understanding of the stator-rotor interaction phenomena for transonic annular

cascades. A brief description of the cascade is presented here, while more details about the experimental test rig and the data can be found in Denos et al. 1999.

A detailed measurement campaign provides data in several different operating conditions. In the present work nominal unsteady flow field conditions will be analysed. The main mid-span parameters of the test case at the nominal pressure ratio and for the nominal reference Reynolds Number ($\approx 10^6$) are:

Mis(exit NGV)=1.08, M(exit rotor)=0.42.

Cooling air injection is provided in the experimental configuration at the nozzle trailing edge through a pressure side cut of the blade..

Numerical simulation

The 3D unstructured grid topology used to perform the in viscid numerical simulation is shown in figure 4. Applying a slight stretching (about 0.8%) to the rotor vane geometry, an exact pitch ratio is obtained using 2 stator blades and 3 rotor blades. This modification to the geometry was positively tested by Michelassi et al. (1999).

The unviscid and viscous (first refinement) computations have been performed using the parallel version of the code on a cluster of four DEC ALPHA-XP1000-666 Mhz workstations. The coarse unviscid grid has been divided using 24 blocks equally distributed amongst the 4 CPUs with a memory request of the implicit procedure of 55 Mb.

The unsteady periodic solution has been reached starting from the rest condition and keeping the rotor blades fixed. The starting static pressure distribution has been established using a linear law between the inlet prescribed total pressure and the outlet measured static pressure. During the computation the rotating speed of the blades is gradually increased until the nominal velocity of 6500 RPM is reached in a physical period (three rotor passages). The physical time step is computed by dividing the natural periodic angle in a suitable number of steps able to guarantee both stability of the numerical procedure and an acceptable time resolution of the unsteady frequencies. The physical time, required to complete an entire period of the whole domain, can be easily computed from the ratio $\alpha/\omega = 2.88 * 10^{-4}$ s where ω is the rotational speed and α is the periodic angle (16.744 Deg). The nominal total quantities are used as boundary conditions at the NGV inlet assuming flat profiles for both T0 and P0. For the coolant jet, inlet conditions are set in order to match a global mass flow rate as observed in the experimental tests. At the outlet of the stage the integral value of the nominal experimental outlet static pressure is imposed.

In this regard one hundred steps per subdivision for the periodic pitch seemed enough to guarantee the accuracy of the unsteady solution and to capture the first main frequencies of the unsteady flow. The numerical time marching convergence of each unsteady physical solution can be achieved within 10 numerical sub-iterations with a reduction of the initial residuals larger than 4 orders of magnitude. The unsteady flow field converges to a pattern periodic in time after five complete passages of 2 stators and 3 rotors vanes. The viscous solution has been obtained starting from the solution obtained from the in viscid computation using the grid sequencing strategies and the ad hoc interpolation technique previously mentioned.

The computations have been performed with the same solver but using 16 processors on CINECA Origin 3800. The grid has been divided in about 400 blocks distributed amongst the 16 processing elements and two hundred steps have been chosen to complete the periodic passage. The number of sub iteration is 10 while the unsteady flow field converged to a new periodic pattern in time after 3 complete passages.

Results and discussion
<u>Inviscid results</u>

Once the periodic solution is achieved for the unsteady numerical computation, an overall mass error less than 1% has been observed from the stage inlet and outlet sections.

Hub and tip static pressure profiles are measured in the test rig at a station placed 0.035 axial chords downstream the nozzle trailing edge, using both Kulite transducers and static pressure taps

(Denos *et al.*, 1999). The instantaneous numerical pressure profiles have been time averaged both at hub and tip and compared against measurements in Figure 6 for a NGV blade pitch.

a) hub wall   b) tip wall
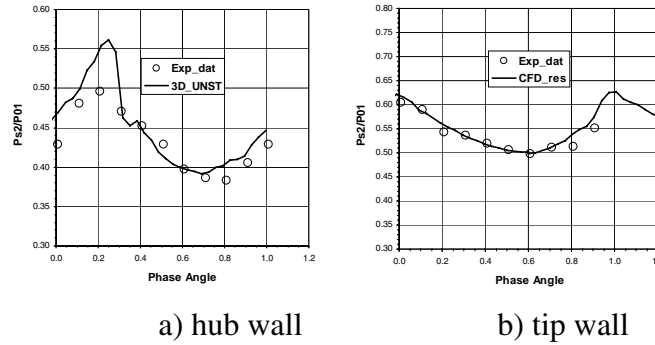
Figure 6: hub and tip time-averaged pressure profiles
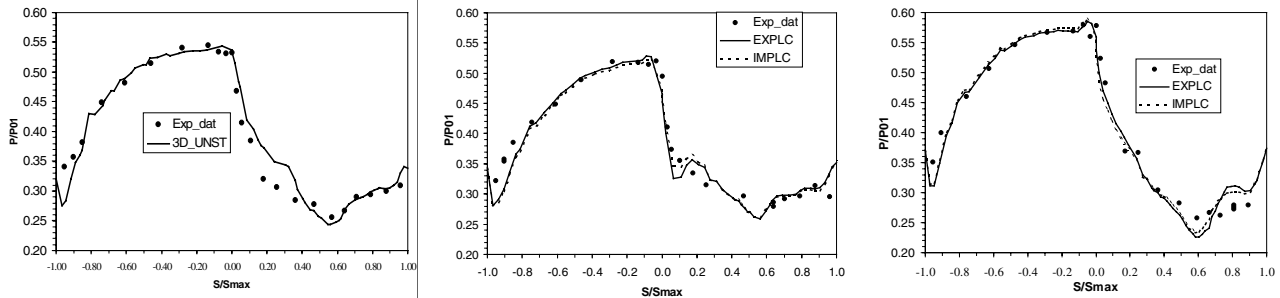
a) Averaged rotor pressure - 50% span   b) Averaged rotor pressure - 15% span   c) Averaged rotor pressure - 85% span

Figure 7: Time averaged Pressure Profiles

Moving from 0 to 1 along the abscissa, the measuring points move from the pressure side towards the suction side of the nozzle blade. Fig. 6 indicates a quite correct estimate of the average inter-stage working pressure in the numerical simulation. The steep pressure rise observed for the phase value around 0.2 can be explained by the over estimation of vane trailing shock intensity in the numerical computation caused by the absence in the calculation of viscous effects. This behaviour is more pronounced near the hub surface where the inviscid assumption is expected to give a less accurate prediction in view of the more relevant role played by the boundary layer thickness on the lower wall contouring. The time-averaged pressure profiles on the rotor blade are reported in Figure 7, for three radial sections at 50%, 15% and 85% of the blade span. In these figures static pressure over stage inlet total pressure is plotted against curvilinear abscissa on the rotor surface (positive/negative values indicate respectively locations on the suction/pressure side).

The agreement with experiments is satisfactory on the pressure side, while on the suction side and close to s/smax=0.2, the flow acceleration is slightly under predicted. This might indicate either a three-dimensional effect or a slight underestimation of the incidence (see Michelassi et al. 1999, 2001). The pressure rise and the shock location is correctly captured for s/smax=0.6.

At the 15% section close to the hub the computed pressure profile agrees closely with the experiments except for s/smax=0.1 on the suction side. In this location it is argued that the strong shock detaching from the stator trailing edge interacts with the rotor blades suction side giving the observed pressure rise on the rotor surface.

The instantaneous views of wall pressure patterns, indicate that the flow on the LE of the suction side may periodically undergo a strong acceleration, followed by a recompression shock in correspondence of some relative positions. For other phase angles, the flow pattern is quite different, and the same acceleration/compression pattern is not detected. A similar pattern can be detected close to tip, although slightly smeared with respect to the 15% section. This effect is responsible for the steep pressure rise shown by the hub averaged pressure comparison of Figure 7.

The near tip region pressure field of figure 7 reveals a stronger acceleration of the flow on the suction side close to the rotor trailing edge (s/smax=0.6). This over expansion is followed,

downstream the minimum value, by the pressure rise typical of a recompression shock, which is more pronounced than in the experiments.

The absence of smoothing effect of the fluid viscosity on the pressure rise in a shock wave seems to be partially responsible for the overestimation of pressure unsteadiness. Moreover, the flow pattern at 85% span, close to the trailing edge is affected by the tip clearance, as indicated by the stage simulations by Michelassi et al. (2001). As a consequence a significant mass can flow from pressure to suction side, thereby decreasing the blade load and, ultimately, increasing the minimum pressure level on the suction side TE.

Figure 8 reports the pitch-wise unsteady averaged quantities obtained with the inviscid simulations. The axial flow angle distribution at the rotor blade exit is compared with both experimental data and the results obtained from a NISRE computation (from Dènos et al. 1999) in which losses are evenly distributed along the rotor span. The agreement between the NISRE approach and the unsteady averaged profiles is good. This is not surprising since both approaches do not predict any sort of secondary flow. Actually the waving shape of the measured exit flow angle is due to the combined effect of various secondary effects, mainly the presence of the blade passage vortex and tip-hub horse shoe vortices.

Figure 8a also shows that the secondary flows penetrate quite close to the rotor mid-span, as proved by the deviation from the nominal exit flow angle (12-deg at mid-span). Figure 8b compares the experimental time and pitch-wise-averaged total temperature distribution with the unsteady numerical results. For radial position above 0.4 the total temperature profile is followed closely, but the absence of secondary effects in the calculations provokes a nearly constant total temperaure distribution which is far from experiments close to the root portion of the blade. On account of what seen for the exit flow angle, this disagreement is not surprising. Still the unsteady simulations demonstrate that the mid-span value of the total pressure is remarkably well reproduced, thereby proving the existence of a nearly two-dimensional flow portion around the rotor blade. The agreement with the NISRE calculations are good, although both are not able to reproduce the correct total temperature profile which, as seen for the exit flow angle, is strongly affected by secondary flows which, while governing the exit flow angle, can alter the local extraction of energy. Globally the integral value of the inviscid total temperatures is in good agreement with the experimental data and NISRE estimate, allowing a reasonable forecast of energy exchanges. Near hub, where secondary flows and wall boundary layers are well developed, the accuracy of the unsteady computation is similar to that obtained with the NISRE approach.

a) Averaged Alfa Flow angle   b) Averaged Total Temperature   c) Averaged Total Pressure
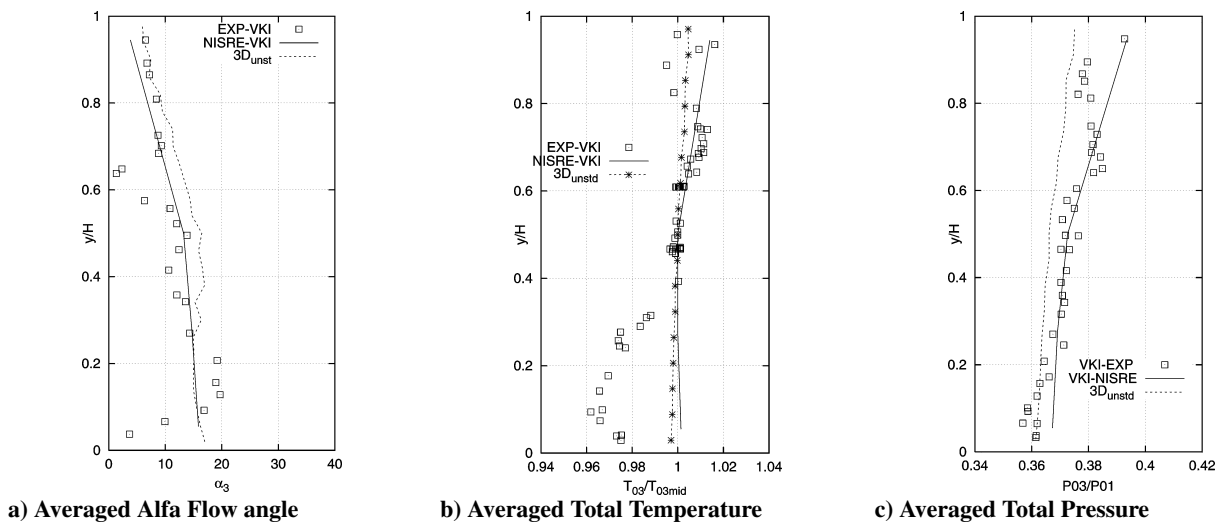
Figure 8: Pitch-wise Averaged Quantities

The total pressure profiles shown in figure 8c allow the same conclusions to be drawn. The time averaged values stemming from the unsteady inviscid calculations follow the experimental results with better accuracy, especially in the lower part of the blade in spite of some inaccuracies connected to the inviscid approximation. The capability of the unsteady approach to model the time

dependent flow should be checked by the analysis of the frequency spectrum. Instantaneous pressure has been monitored for several representative points located along rotor and stator blade surface (Denos et. al., 1999, Figure 18-a).

| a) Rotor Gauge Position | b) Rotor LE gauge 4 | c) Rotor TE gauge 12 |

Figure 9: Frequency Spectrum
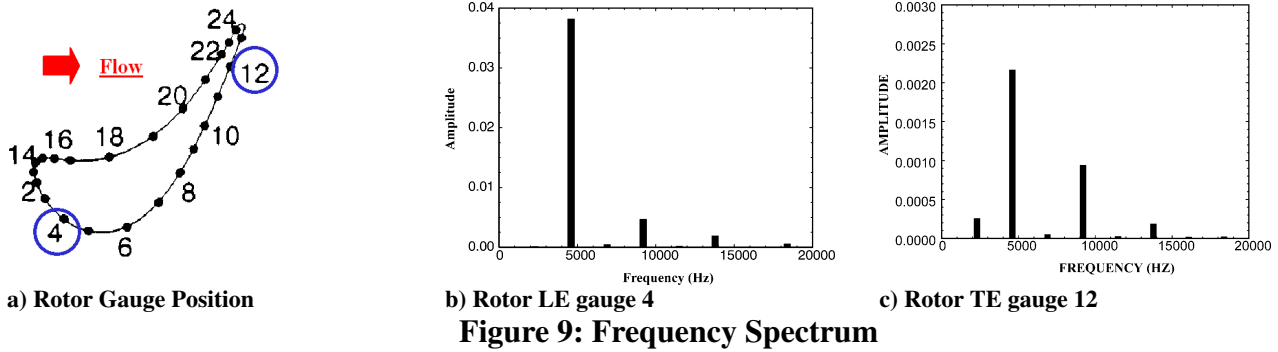
The frequency analysis for two points located near LE and TE of rotor blade on suction surface are reported in Figure 9. For both gauges the main harmonic observed is the stator blades passing frequency. These basic frequencies of the spectrum (figures 18-b and 18-c) can be computed from the speed rotation (6500 RPM) and the blade count ratio (2:3) leading to a main peaks at f=4.66 kHz and the corresponding multiples (9.32 kHz, 13.98 kHz …). The remarkable amplitude of the first harmonic at LE is due both to the not uniform exit flow field from the stator blades (mainly due to the presence of vane TE shock impinging on the rotor) and to the small gap existing between the stator TE and the rotor LE. The amplitude of the pressure discontinuity varies considerably depending on the location on the rotor blade. The maximum amplitude is at gauge 4 because directly heat by the shock wave. Flowing toward the TE, the pressure fluctuations are strongly reduced (two orders) by the action of the vane acceleration effect, as can be observed in figure 9-c.

Figure 10: Unsteady Pressure Fluctuations
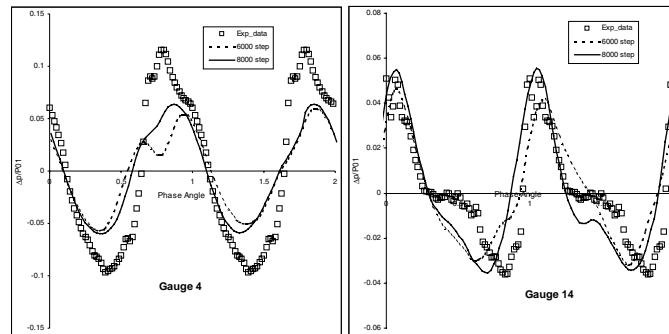
Figure 10 shows the unsteady pressure fluctuations $\Delta p/P01 = (p - p_{averaged})/P01$ for two rotor blade locations at mid-span. The two selected points lay on the suction side at approximately 20% axial chord (again point 4 in Figure 9) and on the leading edge (point 14). On the axis the phase spans from 0 to 2 while a complete periodic passage is completed (e.g. 2 NGV vanes and 3 rotor blades). The experimental data have been described by Dènos et al., 2000, who proposed a detailed interpretation of the flow in the stator/rotor gap. In the experiments pressure traces on gauge 4 clearly indicate high amplitude fluctuations in the rotor LE region, related to the passage of the vane TE fish tale shock (periodically oscillating around the axial direction from about +20° to –20°). In the same Figure two time-accurate computations, are compared with the experimental unsteady profile, obtained doubling the number of time steps during the unsteady simulation and the accuracy seems to improve with the increasing time resolution. The basic feature of the instantaneous signal are reproduced by the numerical results even if peak amplitudes of pressure fluctuations are under predicted mainly at gauge 4. Anyway in this point the under estimation behaves coherently with the pressure disagreement already observed at the same station in the averaged profiles of Figures 7. Moreover, in this location the stator wake hits the rotor blade almost tangentially (Michelassi et al.,

1999). This could provoke a complex interaction between the rotor boundary layer and the stator wake, which is clearly governed by viscous effects.

<u>Viscous results</u>

The time-averaged static pressure profiles on the rotor blade are reported in Figure 11 against curvilinear abscissa, for the same radial sections of Figure 7. The agreement with experiments at 50% span on pressure side confirms the in-viscid results. On the suction side the under prediction of flow acceleration is still present confirming the slight underestimation of the incidence but the pressure distribution of the experimental results near the shock location is more accurately followed.
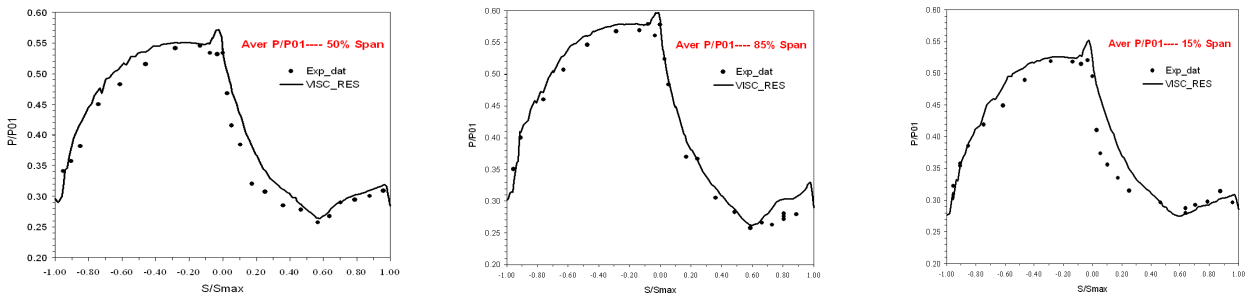
a) Averaged rotor pressure - 50% span   b) Averaged rotor pressure - 15% span   c) Averaged rotor pressure - 85% span
Figure 11: Time averaged Pressure Profiles

As expected in the viscous computation the up-down shape shown in the in viscid assumption disappeared due to the presence of smoothing effect of the fluid viscosity on the level of acceleration and recompression in correspondence of some relative positions of the two rows. Also the strong acceleration of the flow on the suction side close to the rotor trailing edge at tip and hub disappeared (Figures 11a and 11b), according to the more accurate physical assumption and the agreement with experimental results is improved.

Phenomena such secondary flow development inside the stator blade and their evolution in the rotor blade, depending on the relative blade position between rotor and stator and the blade wakes development have a deep impact on loss profile and distribution and thus on the whole turbomachine performances.

The viscous approximation can provide an useful tool for the basic understanding of such phenomena. In this regard in Figure 11.b the entropy contours at the stator exit are shown in axial plane 1, situated at 10 % of the axial chord downstream the stator TE. The stator wake is well outlined by the high loss region in the middle of the area.

As can be noticed the mid-span flow is essentially 2D, most of the loss being confined in the blade wake. Near hub and tip other high loss areas (1) can be underlined due to the development of wall boundary layers in the stator channel. The extension and thickness is small in comparison to the radial and pitchwise extension of the blade, limiting their influence in the regions very close to solid surfaces. As expected the boundary layer growth doesn't seem to affect the core of the flow, which remains almost undisturbed.

b) Entropy Contours – Plane 1

c) Entropy Contours – Plane 2

d) Entropy Contours – Plane 3

e) Entropy Contours – Midspan

f) Entropy Contours – ½Period
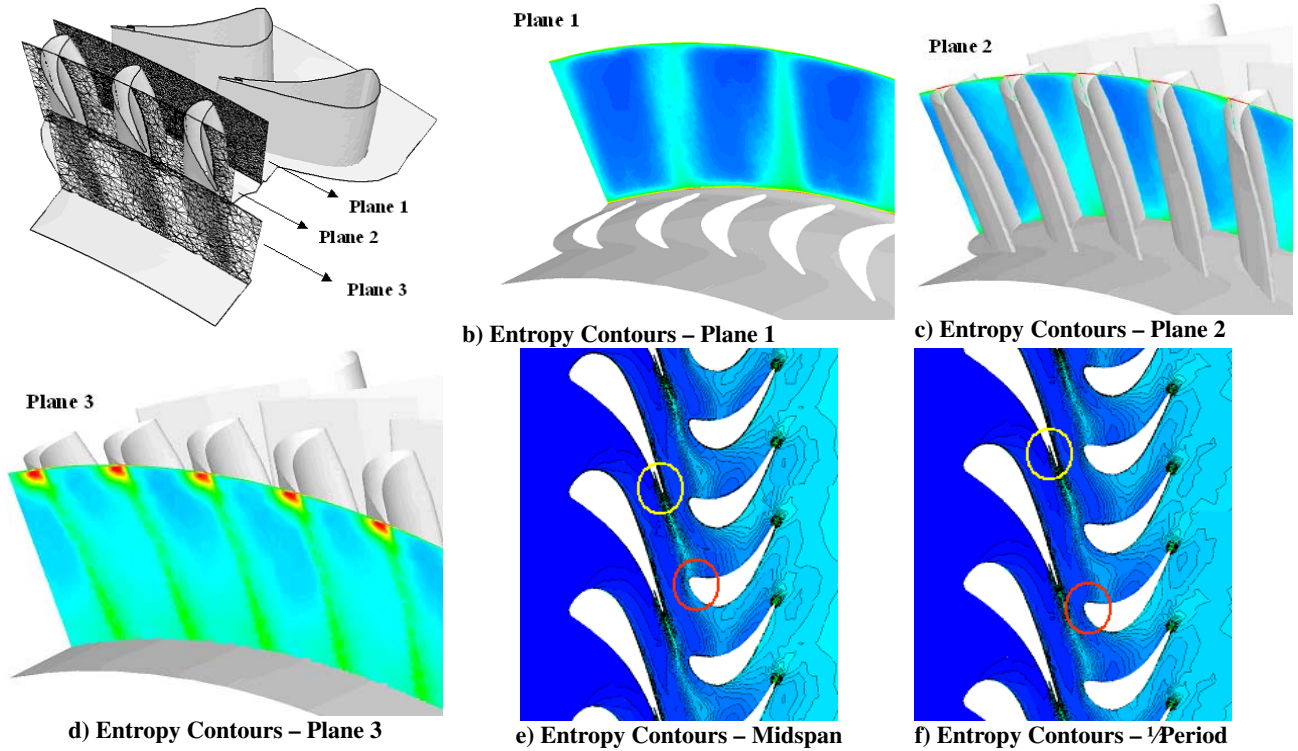
Figure 12: Entropy Contours

In Figure 12 e the entropy contours at 50% span are shown and the TE wakes can be clearly identified. These contours confirm that the entropy production in the NGV is essentially provoked by the SS boundary layer that grows until the final part of the blade, detaches in correspondence of the stator TE region, diffuses and finally impinges on the rotor blade. On the pressure side the boundary layer is almost invisible till the LE is reached, due to favourable pressure gradient experienced by the flow field in most of wall surface. On this side of the blade the more relevant loss seems to be represented by the mixing process between coolant injection and the main flow downstream the TE, responsible for the second high loss stripe of the wake. The shape of the wake from the NGV is almost independent from the relative position between the two rows while losses in the main core of the flow are not evident. When the wake moves toward the rotor blade the effect on the flow can be different depending on the relative position of the two rows. For instance in figure 12.e the wake impinges on the LE of the blade and is split in two different branches, the first one on the PS and the second on the SS. After a half period the wake impinges directly on the blade PS effecting primarily the SS flow on the LE.

In figure 12.d the entropy carpet plot is shown for reference plane 3, located downstream the rotor blade TE for tangential position corresponding to that of fig 12.e. In this plane high loss regions can be clearly identified corresponding to the rotor blade wake. Near the tip entropy production bubbles can be detected according to the combined effect of the tip leakage vortex and shroud boundary layer that are both contributing to the secondary flows in this region.

The ad hoc grid refinement performed for viscous computations in this area were necessary for the more accurate description of the viscous boundary layer profile and the velocity distribution. The shape and the distribution of the high loss region appears to be quite dependent on the relative row positions of the stator/rotor rows. Deep discussion of the results could be possible but is out of the scope of this paper intended to report mainly the challenge and the effort required in solving the unsteady flow field in real stage configuration.

6. CONCLUSIONS

A 3D unsteady solver has been discussed in the viscous and in-viscid assumption through the comparison against experiments. The peculiar aspect of the present application, compared to documented works, is given by the completely hybrid-unstructured nature of the approach. This

feature allows an easy and flexible representation of the stage in view of future more detailed flow investigations, as required by viscous simulations or shock interactions, and of more complex geometry as required by cooling systems or by row leakages.

The use of unstructured grids posed new difficulties for the matching of the stator/rotor rows, which have been here overcome by a crude but general and automatic linear interpolation strategy, but on the other hand offers a great flexibility in the grid generation and modelling with substantial reduction in the grid points demand. The potential stator rotor interaction has been reproduced with a satisfactory accuracy demonstrating that the unsteady Euler approach allows a more realistic description in comparison to steady state computations of the flow pattern, especially in the presence of physical phenomena such unsteady shock interaction which can not be accounted by in a steady assumption.

In order to have a deeper insight of phenomena concerning the periodic evolution of the NGV wakes, tip vortex structures and the effect of unsteadiness on the global stage efficiency, a more accurate analysis , based on full viscous, calculation was required. Viscous calculation on the other hand posed serious problems for the management of the data file and the CPU usage. To accurately reproduce those viscous effects more stringent requirements were imposed on the grid cell dimension especially near boundary layers in the solid surfaces at hub tip and blade profile. The grid dimensions typical of a realistic viscous computations (about 1.8 ML node elements) created difficulties for the management and storage of the input and output data required or produced during the processing of the solution and compelled the complete reconsideration of all the phases involved in the CFD solution and the optimisation of all the pre and post processing routines. The most advanced programming tools such Fortran 90 dynamic memory allocation and de-allocation of unused matrices were necessary for the full storage of geometry, exceeding the capacity of local workstation. Efficient interpolation techniques and a rationale use of the I/O management were necessary to reduce the length of the grid sequencing technique and all the post processing phases of the results management. In conclusion great effort have been successfully carried out on the different aspects of the calculation to face correctly and profitable the challenge to compute and investigate unsteady flow in a full turbine stage.

REFERENCES

Adami P., Martelli F. and Michelassi V., 2000, "Three-Dimensional Investigations for Axial Turbines by an Implicit Unstructured Multi-block Flow Solver", ASME, IGTI TurboExpo 2000, Munich.

Adami P., Michelassi, V., Martelli, F., 1998 "Performances of a Newton-Krylov scheme against implicit and multi-grid solvers for inviscid flows" AIAA paper 98-2429.

Adami, P., 1999 "Computations for internal flows with a low-mach preconditioned Newton-Krylov scheme", 3rd European Conference on Turbomachinery. London.

Barth, T.J.,1991 "Numerical Aspects of Computing Viscous High-Reynolds Number Flows on Unstructured Meshes", AIAA Paper 91-0721, Jan.

Belardini E., Adami P., Martelli F. *"Development of an Unsteady Parallel Approach for 3D Stator-Rotor Interaction"* 4th European Conference on Turbomachinery, Fluid Dynamics and Thermodynamics- Firenze 20-23 March 2001, IMechE Journal of Power and Energy2001- Vol.215. n.A6.

Dawes, W.N., 1992, "The Simulation of Three-Dimensional Viscous Flow in Turbomachinery Geometries Using a Solution-Adaptive Unstructured Mesh Methodology" Transaction of ASME Vol. 114, July.

Dawes, W.N., 1994, "A Numerical Study of the Interaction of a Transonic Compressor Rotor Overtip Leakage Vortex with the Following Stator Blade Row", ASME Paper 94-GT-156.

Dénos R., Sieverding C.H., Arts T., Brouckaert J.F. and Paniagua G., 1999, "Experimental Investigation of the Unsteady Rotor Aerodynamics of a Transonic Turbine Stage", 3rd European Conference on Turbomachinery. London.

Denos, R., Arts, T., Paniagua G., Michelassi, V. and Martelli, F., 2000, "Investigation of the unsteady Rotor Aerodinamics in a Transonic Turbine Stage" 2000-GT-435.

Dorney D.J. and Sharma O.P., 1997, "Evaluation of Flow Field Approximations for Transonic Compressor Stages", J of Turbomeachinery, Vol. 119.

Gallus H.E., Zeschky J. and Hah C., 1994, "Endwall and Unsteady Flow Phenomena in an Axial Turbine Stage" ASME 94-GT-143.

Giles, M. B., 1990, "Stator/Rotor Interaction in a Transonic Turbine" AIAA J. of Propulsion, Vol. 6, No. 5.

Hah C., Copenhaver W.W. and Puterbaugh S.L., 1993, "Unsteady Aerodynamic Flow Phenomena in a Transonic Compressor Stage", AIAA-93-1868.

Haselbacher, A., McGuirk, J.J., Page, G.J., 1999, "Finite Volume Discretization Aspects for Viscous Flows on Mixed Unstructured Grids" AIAA J., Vol. 37, No. 2.

He L.,1996,"Time Marching Calculations of Unsteady Flows, Blade Row Interaction and Flutter", VKI-LS 1996-05.

Kwon, O.J. and Hah, C., 1995, "Simulation of Three-Dimensional Turbulent Flows on Unstructured Meshes" AIAA J. Vol.33, No. 6, June.

M. Von Hoyningen-Huene, A. R. Jung, 2000, "Comparison of Different Acceleration techniques and methods for Periodic Boundary Treatment in Unsteady Turbine Stage Flow Simulations" J. of Turbomachinery, Vol. 122.

Mavriplis D.J. 1995, "Three-Dimensional Multigrid Reynolds Averaged Navier Stokes Solver for Unstructured Meshes" AIAA J., Vol.33, No. 3.

Martelli, F. Adami, P. Belardini, E, "Unsteady Rotor/Stator Interaction : An Improved Unstructured Approach" 46th ASME International Gas Turbine & Aeroengine Technical Congress June 4-7, 2001, N.Orleans, Louisiana, USA

Michelassi, V, Martelli, Denos, R., Arts, T., Sieverding, C.H. 1999 "Unsteady Heat Transfer in Stator-Rotor Interaction by Two-Equations Turbulence Model" J. Turbomachinery,July.

Michelassi, V., Giangiacomo, P., Martelli, F., Dénos, R., Paniagua, G., "Steady three-dimensional simulation of transonic axial turbine stage", offered for IGTI-2001.

Pulliam T.,H., Rogers, S., Barth, T., 1996, "Practical Aspects of Krylov Subspace Iterative Methods in CFD", *Prog. and Challenges in CFD Methods and Algorithms*, Seville, AGARD CP-578.

Rai, M., M., 1989, "Three-Dimensional navier-Stokes Simulations of Turbine Rotor-Stator Interaction; Part I-Methodology" AIAA J. of Propulsion, Vol. 5, No. 3 May-June.

Roe P.L., 1986 "Characteristic based scheme for Euler equations" , Ann. Rev. Fluid Mech., 18.

Saad, Y., 1994 "Krylov Subspace Thechniques, Coniugate Gradients, Preconditioning and Sparse Matrix Solvers", CFD VKI LS 1994-05 VonKarman Institute for Fluid Dynamics.

Saad, Y., 1994, "Krylov Subspace Techniques, Coniugate Gradients, Preconditioning and Sparse Matrix Solvers", CFD VKI LS 1994-05 VonKarman Institute for Fluid Dynamics.

Sayma A. I., Vahdati M., Sbardella L., and M. Imregun, 2000, "Modeling of the Three-Dimensional Viscous Compressible Turbomachinery Flows Using Unstructured Hybrid Grids" AIAA J. Vol. 38, No. 6.

Sharma O.P., Pickett G.F. and Ni R.H., 1992, "Assessment of Unsteady Flows in Turbines", J. of Turbom. Vol. 114.

Slack, D.,C., Whitaker, D.,L., Walters, R.,W., 1994, "Time Integration Algorithms for the Two-Dimensional Euler Equations on Unstructured Meshes", AIAA J. Vol. 32, No. 6.

Venkatakrishnan, V., 1995, "A Perspective on Unstructured Grid flow Solvers", Technical report AIAA Paper 95-0667, AIAA 33rd Aerospace Sciences Conference, Reno.

Walraevens R.E., Gallus H.E., Jung A.R., Mayer F.J. and Stetter H., 1998, "Experimental and Computational Study of the Unsteady Flow in a 1.5 Stage Axial Turbine with Emphasis on the Secondary Flows in the Second Stator" ASME Paper 98-GT-254.

Centaur^{TM} -Grid Generation Software Package Distributed by CentaurSoft (web site www.centaursoft.com)

Paper #37
Discussor's name A. Soulaimani
Author F. Martelli

Q: 1) Since the precondition and its factorization take most of the CPU time, do you compute it at every time step?
2) You can save a substantial amount of computing time if you freeze it for a few time steps (2-5) steps). I am sure of the result!

A: 1) Yes
    2) Okay

This page has been deliberately left blank

_____

Page intentionnellement blanche

Validation of Plasma Injection for
Hypersonic Blunt-Body Drag Reduction

J.S. Shang
Center of Excellence for Computing Simulation
Air Vehicles Directorate
Air Force Research Laboratory
2210 Eighth Street
Wright-Patterson Air Force Base
OH 45433-7512, USA

Summary

The optimum blend of numerical and physical fluid experiment for risk and cost reduction is an actual reflection of the stage of maturation for individual technology development. As an illustration, the detailed validation of drag reduction technique using plasma injection was investigated using a side-by-side experimental and computational approach. The major portion of the reduced drag is found from the favorable counter-flow jet shock interaction and thermal deposition.

Introduction

Improving aerodynamic performance of air vehicles via drag reduction has been steadily pursued since the days of the Wright brothers. In high-speed flight, the need of significant drag and heat load reduction for a better performance becomes even more critical. In an assessment of aeronautical science for the future, one realizes that the air vehicle design has fallen into an evolutional process because the technical innovation is limited to aerodynamics [1]. However, Sear et al pointed out as early as the later 50's, an added new physical dimension of magneto-aerodynamic interaction would revolutionize the performance of high-speed flight [2-5]. Collectively, they demonstrated that electromagnetic force could significantly alter the aerodynamic behavior in plasma media. Therefore, the large volume of magneto-aerodynamic research from Russia in the 80's has stirred a great amount of interests [5-8]. In this interdisciplinary endeavor, at least three independent science disciplines; aerodynamics, quantum chemical kinetics, and electromagnetics are interwoven. In addition, the air plasma (more precisely the weakly ionized air) always associated with an extremely high temperature state, which is a common occurrence in hypersonic flow. This flight environment is not always duplicable in a ground testing facility [9]. Therefore it is essential that the physical-based computing simulation capability be developed if the advantage of a favorable magneto-aerodynamic interaction is to be harnessed for hypersonic flight.

The possible contributors to drag reduction via plasma injection are widely speculated. It is commonly accepted that the counter-flow jet–shock interaction, non-equilibrium thermodynamic state of highly excited international degrees of freedom, and the electromagnetic force could play significant roles. The interdisciplinary phenomenon is extremely difficult to investigate alone by either experimental or computational simulation because each can yield only a partial answer. Also not all observations can be verified independently. Thus, the present investigation resorts to a combination approach.

Optimum blends of numerical and physical fluid experiments span a very wide range of variations for the purposes of validation and calibration of modeling and simulation capabilities. For an interdisciplinary technology development where the aerodynamics, electromagnetics, and quantum chemical physics are integrated both physical and numerical experiments are facing challenges. The synergetic effects to minimize risk therefore are uncertain. In the present effort, a computational and experimental side-by-side investigation on plasma injection for hypersonic blunt-body drag reduction is presented.

Systematic pursuit is guided by hypotheses on physical mechanisms that can generate a favorable magneto-aerodynamic interaction - the counter flow jet shock aerodynamic interaction, the non-equilibrium thermodynamic and chemical phenomenon, and the electromagnetic-aerodynamic interaction. Three-dimensional and axisymmetric, mass-averaged Navier-Stokes equations were solved for counter-flow jet shock interaction. The experimental investigation of the plasma injection was conducted in a nominal Mach 6 open jet, blow-down tunnel. The weakly ionized, counter-flow jet generated by a plasma torch has an electron temperature around 20,000 k, and electron number density greater than 3 x 10^{12}/ cm^3.

Experimental Facility

The counter-flow plasma jet and shock interaction is investigated in a blow-down, open-jet, high Reynolds number wind tunnel. At the stagnation temperature of 610 K and a range of stagnation pressures from 3.44 10^2 to 1.40 10^4 kPa, the air stream sustains a uniform test section from the nozzle exit plane and a diameter of 203 mm at the Mach number of 5.8. The mass flow rate of the tunnel spans a range from 0.77 to 4.63 kg/s. For the present investigation, the tunnel is operated at the lowest density of 0.012 kg/m^3 at the free stream pressure of 2 Torr and static temperature of 79 K. Under this operational condition, the Reynolds number is 45,200 per meter.

The force-measuring model is a hemispherical cylinder, which has a nose radius and a total length of 38.1 and 203.2 mm respectively. The model was fitted with three nozzles (D_t = 2.44, 1.5, and 1.27 mm) to accommodate the plasma torch. However, the drag data is collected only from the nozzle with the throat diameter of 1.27 mm. At the stagnation pressure and temperature of 344.7 kPa and 294 K, respectively, the exit Mach number is 3.63 and yields a mass flow rate of 0.001 kg/s. The nozzle flow changes from over- to under-expanded condition at the stagnation pressure of 1,077 kPa.

The aerodynamic force is measured by a set of 3 piezoelectric force sensors or load cells. The model is isolated from the support strut by these load cells to receive the total axial aerodynamic force exerted on the model. In this arrangement, the wave drag, skin friction drag, and the base drag are not separable but measured together [14,19].

A plasma cutting torch with the PAK Master 50XL power supply and the PCH/M-28 torch supplies the ionized air the counter-flow jet. The maximum power output from this plasma torch is rated at 35 Amp by an AC input single-phase voltage 208. However in the present application, this unit is strictly operated in the starting mode. Therefore, the power output is far below the rated value. The arc starting circuit has a high frequency generator that produces an AC voltage from the 5 to 10 kV at a frequency of approximately 2 MHz. This frequency is far beyond the spectra range of oscillatory drag measurement (up to 5 kHz) for interference. In fact, the basic oscillatory behavior of both air and air plasma is similar, and the predominant oscillatory mode occurs around 100Hz.

The properties of air plasma, such as the electron density and temperature of the air plasma, were measured by a double Langmuir probe. The probe is constructed from a 0.5 mm platinum wire with a double-hole ceramic sleeve and a wire separation distance of 1.0 mm. The sensing area of each probe tip is limited to 2.1 mm^2. A 100 V Keppco bipolar power supply provides the applied electric potential. Meanwhile, a variable resistor in the circuit has an operable range from 75 to 1,000 Ohms to enable the electric current measurement in microampere range.

Counter-Flow Jet

There is a great deal of literature on the jet-spike or counter-flow jet [10-14]. A number of investigations focused on the aspect of thermal protection. The rest concentrated on the understanding of this intricate flow field structure [10-12]. The counter-flow jet issued from a blunt body in supersonic regime has two distinct states. At the lower injecting pressure, the jet displaces the bow shock upstream. The displaced shock envelope is generally conical and the flow field is unsteady [12,13]. At higher injecting pressures, the

displaced shock actually retracts back from the conical to a blunter configuration and the oscillatory motion ceases. The basic flow field structure is depicted in Figure 1.

The driving force of this interaction mechanism is the expanding jet into a low stagnation pressure shock layer, and then the jet is stagnated by a Mach disk. The jet reverses its direction downstream as a free shear layer. A part of the jet stream is also entrained to form a toroidal recirculating zone beneath the free shear layer. At the reattachment point of the free shear layer to the blunt body, it induces a series of compression waves coalescing into a reattachment ring shock. The counter-flow jet interaction with the bow shock replaces the single wave to a triple shock structure [14]. This multiple shock structure degeneration is the major contributor of wave drag reduction for the plasma injection.
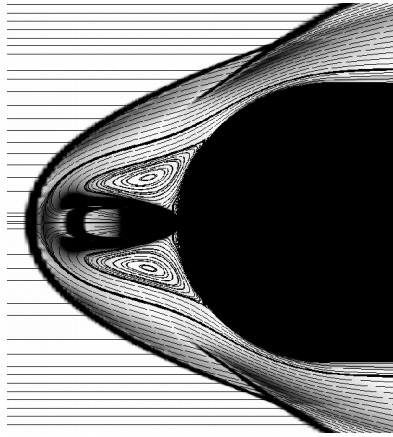
Figure 1. The streamline trace of the jet spike flow field

The shock bifurcation was also discovered by the side-by-side computational and experimental study of the jet spike [14]. At the bifurcation point between the steady and unsteady states, the drag reduction also attains the maximum value. The bifurcation is the consequence of breakdown of the subsonic upstream feedback loop between the Mach disk and the unsteady free shear layer [15]. As the jet injecting pressure increases, the subsonic region connecting the Mach disk and the free shear layer diminishes in size. At the bifurcation point, a part of the supersonic jet actually diverts from the Mach disk and effectively cuts off the feedback loop from the free shear layer and the oscillatory fluid motion ceases. The Mach number contours of the distinct dynamic states astride the bifurcation point are given in Figure 2.
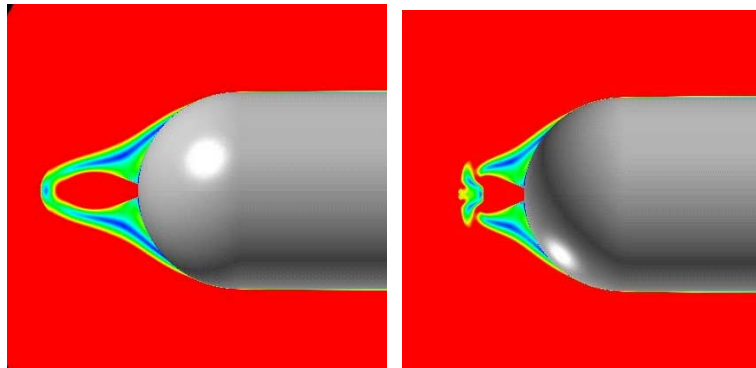
Figure 2, Subsonic Mach number contours of the steady and oscillatory states

An implicit, unstructured Navier-Stokes equations solver, Cobalt [16] was used exclusively to obtain all numerical results. The basic algorithm is that of the Godunov's Riemann formulation coupled with implicit time stepping to yield a second-order spatial and temporal accuracy. The cell-centered, finite-volume

approach can accommodate either the tetrahedron or the hexahedron in three-dimensional space. The governing equations are discretized by the implicit approximation as;

$$[3(\mathbf{U}^{n+1}\text{-}\mathbf{U}^n) - (\mathbf{U}^n - \mathbf{U}^{n-1})] / 2 \, \Delta t + \check{\nabla} \cdot \mathbf{F} = 0$$

Where the U's are the conservative dependent variables $\mathbf{U}(\rho, \rho u, \rho v, \rho w, \rho e)$ and $\mathbf{F}$'s are the flux vectors of the Navier-Stokes equations. The reconstruction of the flux vectors at the cell faces is by a least-square approximation.

$$\mathbf{q}_{i \pm 1/2} = \mathbf{q}_i \pm \mathbf{r} \cdot \check{\nabla} \mathbf{q}_I$$

Where $\mathbf{q}$ is the vector of primitive variables $\mathbf{q}$ (ρ, u, v, w, p) at the centroid of cell i, $\check{\nabla}\mathbf{q}_i$ is the gradient vector and $\mathbf{r}$ is position vector from the centroid to the cell faces.

An outstanding feature of the unstructured grid approach is also derived from the neighbor-cell connectivity of its formulation. The cobalt exhibits an exceptionally scalable, parallel computing performance on all multi-computers using a message passing interface (MPI) library [17]. On an IBM SP3 32-node computation, the data processing rate is 5.28×10^{-6} sec per cell per time step versus a value of 4.22×10^{-5} on a 4-node computation. This parallel efficiency exhibits a nearly linear performance over the range of operations.

In the present application, the no-slip velocity components and adiabatic temperature conditions are imposed on the blunt body surface. For the plasma torch, the sonic throat is prescribed as the entrance boundary for the conical injecting nozzles. The unperturbed free stream condition is specified at the upstream boundary and the no-reflection condition downstream for the far field. The Spalart-Allmaras one-equation model is adopted to achieve the turbulent closure [18].

The computational error is assessed by generating solutions on consecutively refined grid density immediately adjacent to the shock waves. For an embedded conical nozzle in the hemispherical cylinder with a throat diameter of 2.44 mm and exit diameter of 4.70 mm, the exit Mach number is 2.86. Numerical solutions at a free stream Mach number of 5.80 on three grid systems of 185,484, 256,824, and 303,804 were obtained. After the second grid density refinement, the numerical results are essentially grid independent. The identical process was also applied to nozzles of smaller throat diameter ($D_t = 2.5$ and 1.27 mm).

In Figure 3, the first validation of the measured and computed results in the form of schlieren images is presented for the nozzle with a throat diameter of 2.44 mm and the injecting to tunnel stagnation pressure of 0.75 ($P_j/P_o = 0.75$). Under this condition, the blurred schlieren photograph reveals the oscillatory flow field structure. For the long-exposure photograph, the blurred image band actually defined the extremes of shock movements. However, the computed schlieren image is limited to a single event in time, and in general has a shorter penetration length in comparison with experimental observations. The resultant shock wave system exhibits two oscillatory frequencies at 100 and 435 Hz. However, the lower frequency oscillation has a dominant magnitude over the others.
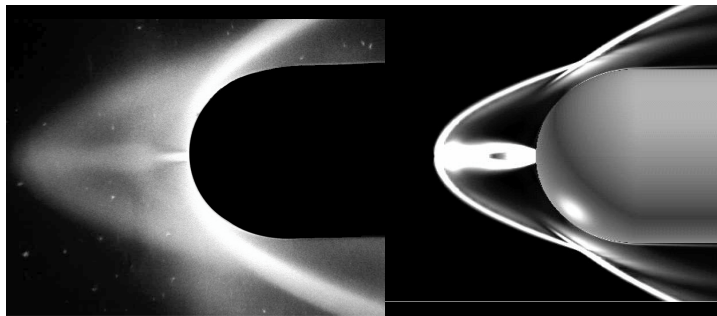
Figure 3. Comparison of Schlieren with computational result at $P_j/P_o = 0.75$

The comparison of schlieren with computed result at an injecting pressure beyond the bifurcation point is depicted in Figure 4. The specific comparison is made for the injecting to the tunnel stagnation pressure of

1.05 (P_j/P_o= 1.05). At this injecting pressure, the shock wave system jumps to a nearly steady state. The schlieren photograph yields a sharper image than the highly unsteady motion at the lower injection pressure domain. In this figure, the Mach disk that terminates the forward motion of the counter-flow jet, the coalesced reattachment ring shock is clearly exhibited. Even the slipstream originating from the intersection of the bow shock and the ring shock is clearly visible. Both the measured and computed standoff distance of the bow shock shows an identical value of Δ /r = 0.744. The agreement of the overall flow filed structure between the experimental and computational results is excellent.
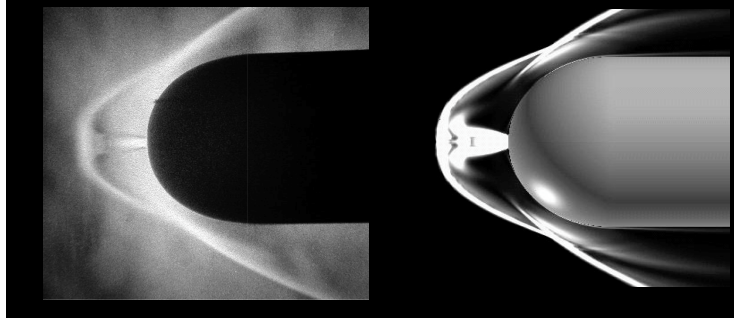
Figure 4. Comparison of Schlieren with computed result at P_j/P_o= 1.05

In Figure 5, the more critical verification of experimental data and the computational result of drag is given. In this graph, the normalized drag coefficient of the blunt body with the counter-flow jet is depicted with respect to the pressure ratio of injection and tunnel stagnation pressure. The drag coefficient is normalized by the drag of the same blunt body at the identical flow condition. Two different wind tunnel stagnation pressure conditions are presented at the tunnel stagnation pressures of 50 and 100 psi (0.344x10^3 and 0.688x 10^3 kPa). The calculated drag includes the base drag correction from experimental measurements. The base drag evaluated from two pressure taps on the model base region yields a nearly constant value over the entire injection pressure range. A reasonable agreement is noted over the entire tested range including the bifurcation. The numerical results also capture the oscillatory force behavior at both tunnel stagnation conditions. However, the numerical results also predicted pressure bifurcation value lower than experimental observation. Nevertheless, the computational error and experimental data scattering band are estimated from 1.7 to 5.1%.
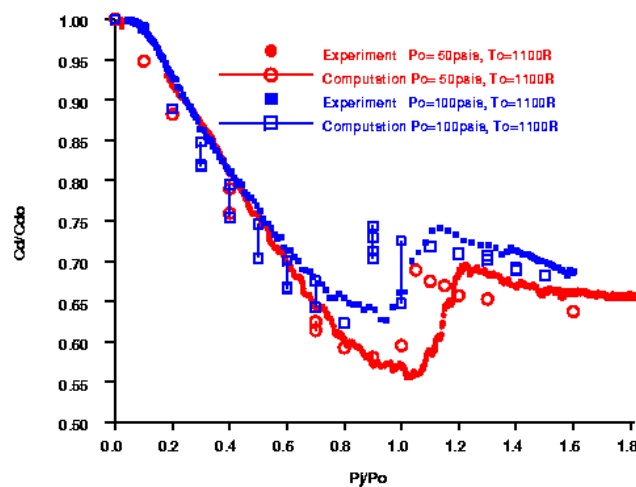
Figure 5. Verified measured and computed drag for blunt body with counter-flow jet

From both experimental observations and computational results, the wave drag reduction for blunt body by a counter-flow jet can be substantial. The reduced drag is mostly derived from the degeneration of a single

bow shock wave to a multiple structure. The amount of drag reduction is strongly dependent on the relative mass flow rate of the oncoming stream versus the injection, the jet exit Mach number, and the specific heat ratio, γ of the injectant (or the chemical composition of the injectant)[12,13]. For the present investigation of the counter-flow jet, the drag reduction increases as the stagnation pressure of the tunnel is decreased to reflected the effect of the higher relative mass flow rate to the drag reduction. This behavior is clearly demonstrated by both computational results (Figure 5) and experimental measurements.

Four sets of normalized drag coefficients with respect to the blunt body data without injection are presented as a function of stagnation pressure ratios of tunnel and the counter-flow jet (P_j/P_o) in Figure 6. The tested wind tunnel stagnation pressures varies from 344.7 10^3 to 2,068.4 10^3 kPa, the maximum drag reduction reaches a value of 40% at the bifurcation point at the lowest wind tunnel stagnation pressure. The drag continuously decreases over the entire tested stagnation pressure range despite the steady rising of the reverse thrust. Associated with the large amount of drag reduction, there is also an abrupt change of dynamic states across a shock bifurcation point. When the injecting pressure or more appropriately the injecting mass flow rate is less than a critical value, the jet-shock interaction will initiate an oscillatory flow motion through the feedback loop of the free shear layer instability [14,15].
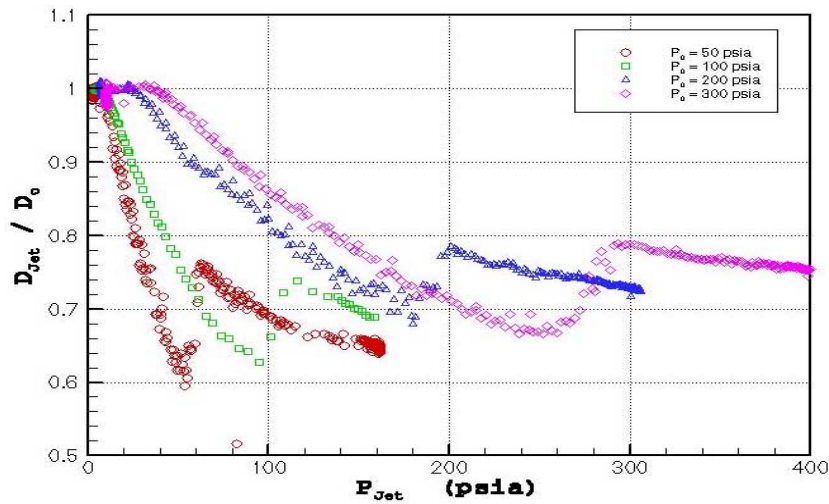
Figure 6. Drag measurements for different wind tunnel stagnation pressures

Non-Equilibrium Phenomenon

The injecting air plasma is generated by a plasma torch embedded within the model and issues from the stagnation point. In Figure 7, a composite picture of the model in the testing condition is depicted. The top half of the figure consists of the video image of the plasma torch in operation; the lower half of the composite is the schlieren of the same test. Overlaid is the sketch of the plasma torch. For the plasma generation in the starting mode of the torch, the power input is relatively low in comparison with the fully rated capacity of 7.28 kW. In order to be compatible with the energy input to the air supply of the torch, the stagnation pressure input to the torch has a limited operation range from 482.6 to 965.2 kPa. At the air supply stagnation temperature of 294 K and the stagnation pressure of 482.6 kPa to the plasma torch, the calculated mass-flow rate is 0.52 gm/sec. This injecting rate is small in comparison with the wind tunnel mass-flow rate of 0.77 kg/sec. Under the testing condition the counter-flow jet and shock interaction is in the subcritical state of shock bifurcation, and the entire flow field is in a self-sustained oscillatory motion. The measurement at a fixed point in space also collected data with wide range of temporal variation. Therefore, the measured data exhibited a large data scattering band.

The temperatures of internal degrees of freedom were determined by the optical emission from the positive electronic transition $C^3\pi_u \Leftrightarrow B^3\pi_g$ of molecular nitrogen N_2, and $C^2\pi_u^+ \Leftrightarrow X^2\pi_g^+$ transition of the ionized

nitrogen N_2^+ [19,20]. A composite spectrum of the plasma torch in the 3400 to 4400 angstrom wavelength range stood out from the obscured by other emission from other species, such as the molecular oxygen, nitric oxide, as well as vapors of copper and iron. Therefore, the spectral match of the positive electronic transition of N_2 for rotational temperature cannot be performed. However, the averaged vibrational temperature, determined from the Boltzmann plot and a blackbody modeling, is 4400±400k. At the relatively high-pressure shock layer region, it would be reasonable to assume that the translational and rotational temperatures are equilibrated to the vibrational excitation. The electron temperature deduced from the langmuir double probe is around 20,000 K. Therefore, the only distinct temperatures are that of electron and the heavy particles [23,24]. The thermodynamic properties are similar to that reported in the works of Ganiev et al [6] and Malmuth et al [7].
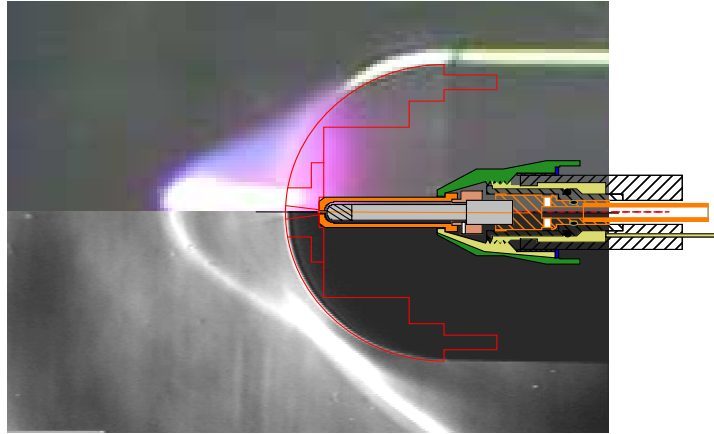
Figure 7. Composite presentation of the air plasma injection

At this temperature and static pressure within the shock layer of 10.5 kPa (78.9 Torr), the air plasma chemical composition in equilibrium condition can be determined from numerical data bases [22]. In term of mass fraction, N_2, O, and NO have the value of 0.69, 0.26, and 0.5 respectively. As one may notice, the molecular oxygen is depleted from the air plasma mixture. The components of NO^+, O^+, N_2^+, and N^+ are in the order of magnitude from 10^{-5} to 10^{-10}.

Figure 8. A typical measured electron number density in the shock envelope

The electron number density and electron temperature of the plasma were measured by a double Langmuir probe. The survey locations of the probe are restricted to the outer envelope of the high temperature jet

plume. The closest survey radial distance from the centerline of the plasma plume is 7.6 mm. In general, the electron number density, electron temperature, electrical conductivity, and field strength attain the maximum value in the plasma plume. This observation can easily be made by examining the electron density and electron temperature distributions along a fixed radial distance from the model's axis of symmetry.

Figure 8 displays the electron number density in the axial coordinate z, from the body surface to the bow shock along a fixed radial distance (r = 7.6 mm). This radial distance is also the minimum separation distance between the probe and the plasma torch so that the plasma plume will not thermally shattered the ceramic sleeve. The highest electron number density is around 5×10^{12} /cm^3. The sharp drop of the measured value indicates the bow shock location. The bow shock exhibits an oscillatory range from 21.2 to 24.6 mm from the blunt body surface. The electron number density upstream of the shock is less than 10^{10}, which is beyond the validated measurement range of the present probe capability.

The electron temperature distribution at corresponding location is presented in Figure 9. Again, the data scattering band is the greatest among all measurements within the entire shock layer envelope. Along the constant radial array, the calculated translational temperature is changing rapidly; the electron temperature is nearly constant to yield a value slightly higher than 20,000 K. Beyond the bow shock envelope, the electron temperature of the oncoming air falls below the value which can be measured with any certainty.

Figure 9. A typical measured electron temperature in the shock envelope

Although the injected air plasma has two distinct temperatures, but the chemical composition of highly excited species only present in trace amount. The plasma counter-flow jet is in a thermodynamically non-equilibrium state, the true species composition and internal energy partition at the present finitely can't be predicted with certainty [24]. Therefore, the detection of the non-equilibrium phenomenon is approached from a calculation based on a locally equilibrium chemical composition. The significance of non-equilibrium phenomenon to drag reduction is assessed through the departure from this state.

The plasma injection is evaluated by the mass-averaged, time-dependent Navier-Stokes equations without the aide of detailed chemical kinetics rates but with equilibrium air plasma composition. In addition, the vibrational temperature (4400 K) is assumed to be equilibrated with the translational and rotational degrees of freedom, but not with the electron temperature (20,000 K). From these stipulated conditions, the specific heat γ, deduced from the chemical equilibrium composition yields a value of 1.281. The comparison of the computed shock structures with the schlieren at an injection pressure of 582 kPa is depicted in Figure 10. It becomes clear that the computed shock structure using the equilibrium air plasma injection captures all essential features of the plasma jet interaction [25,26].
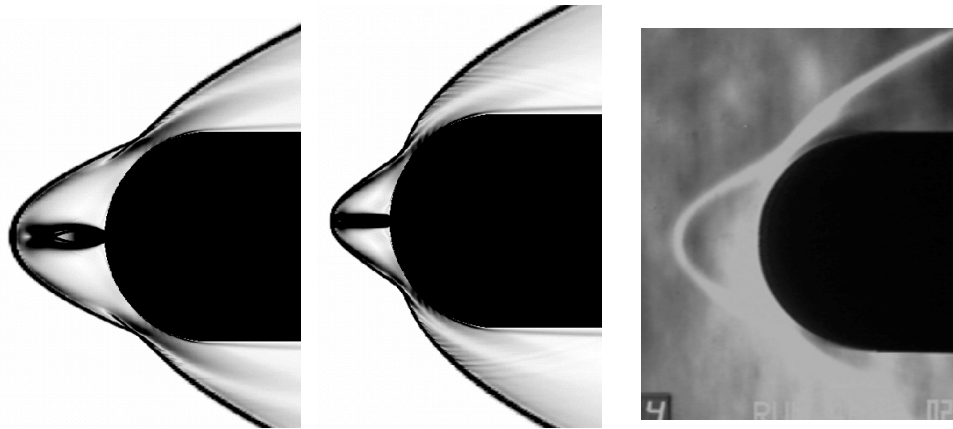
Figure 10. Comparison of schlieren and computation of plasma jet interaction

Figures 10 present two numerical results and a schlieren photograph. The left most image depicts the computed air injection with the perfect gas model at stagnation temperature of 300 K and the stagnation pressure of 582 kPa. The middle image is obtained by solving the Navier-Stokes equations with the equilibrium air plasma composition and at the stagnation temperature of 5280 K. At the numerical boundary of the sonic throat, the temperature then matches the experimental measurement of 4400 K. The computed result using the equilibrium chemical composition exhibits all flow field behaviors as observed in the experiment. When plasma torch is ignited, the overall shock wave system of air plasma injection retracted from the air injection at room temperature. The shock standoff distance of the computation attains a closer value to the experimental observation. Most importantly, the calculated drag agrees with data within a few percents as that of previous counter-flow jet interaction [14].

Analyzing all the computations based on perfect air and equilibrium air plasma composition, the retraction of shock wave system by the air plasma injection is mostly associated with a reduced mass flow rate by the elevated plasma temperature [25,26]. The mass flow rate of a nozzle is linearly proportional to the stagnation pressure, and inverse proportional to the square root of the stagnation temperature $m \sim (P_o/\sqrt{T_o})$. Therefore, at the investigated condition, the mass flow rate of the plasma injection is reduced by a factor of 3.9 from the room-temperature counterpart. For the present experimental process, the record of drag data starts with room temperature air injection. The plasma is then introduced by igniting the plasma torch and is sustained for a duration of 15 seconds. This realization of diminished mass flow rate of plasma injection succinctly explains the contradicting experimental observation that the measured drags actual rise when the plasma is ignited.
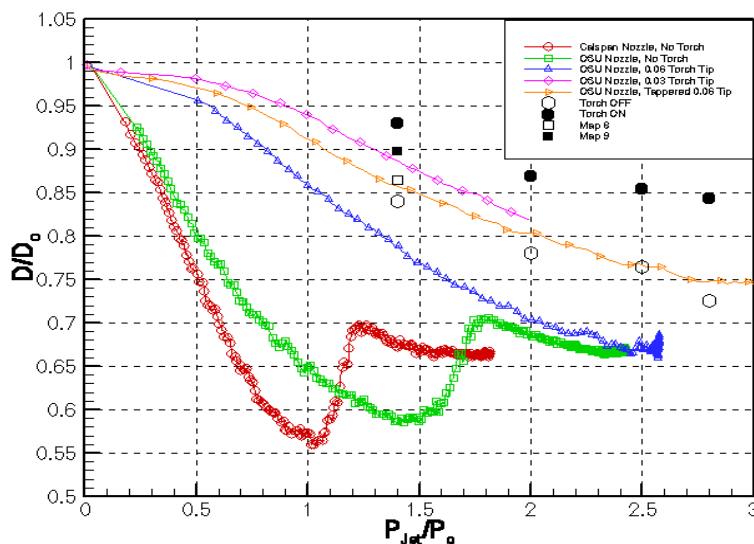
Figure 11. Drag data versus the ratio of plasma injection and tunnel stagnation pressures

In Figure 11, drag data of counter-flow jet from three different nozzles were included. However, the corresponding data of plasma injection is only obtainable at the smallest nozzle throat diameter of 1.27 mm. A single data point at the lowest injecting pressure also contained the effect of an applied magnetic field in the axial direction of the plasma chamber. Its significance will be discussed later.

The data of air injections were collected on different dates and by different procedures. One set of the data was collected by a data sweep for which the data is sampled at 500 points per second. Another set of data was collected in each individual test when plasma injection took place. These data sets indicated the scattering band of measurement about 3.5% over the entire tested range. In this graph, the drag of the blunt body with air plasma injection is reduced from the case when there is no injection, but the drag is greater than the air injection counter part. This erroneous perception is drawn from the incorrect interpretation of data in an inappropriate parametric space of stagnation pressures ratio rather than the mass flow rate.

The drag computations using equilibrium air plasma composition and perfect gas model are presented together with data in mass flow rate in Figure 12. The mass rate is normalized by the maximum air plasma injection rate achievable by the plasma torch. The calculated mass flow rate of 0.13, 0.19, 0.23, and 0.26 corresponds to injecting stagnation pressure ratios, P_j/P_o of 1.4, 2.0, 2.5, and 2.8, respectively. Solutions of Navier-Stokes equations using the perfect gas model over the complete tested range are included as the point of reference. The overall agreement between computations and experiment is reasonable. Numerical results have a maximum discrepancy with the data of about 5% at the low injecting mass flow region. This quantification is believed to be the accuracy bound of the present investigation.
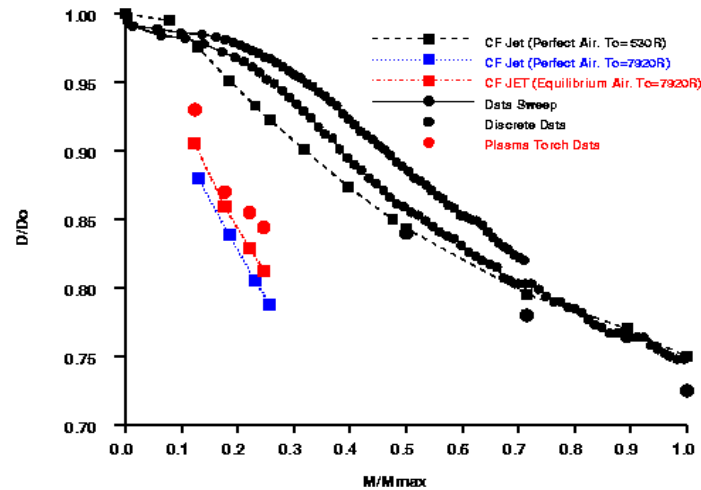
Figure 12. Comparison of computed and measured data of plasma injection

In this physically meaningful parameter of mass flow rate, the drag reduction via air plasma injection can be easily explained. First, at the identical mass flow rate, the air plasma injection indeed produces a greater drag reduction than its room-temperature counter part. The major portion of the reduced drag is derived from the thermal deposition of the air plasma. Based on the computational results using perfect gas and equilibrium air composition of the air plasma at the measured injecting conditions, the drag reduction diminishes for the latter. This observation is understandable in view of the fact that energy is redistributed among different internal degrees of freedom instead of the simple thermal to kinetic energy conversion process by the expansion. Finally, the numerical simulations using the chemical equilibrium composition of the air jet approach that of the data. The difference between computations and experiments is confined within the band of measurement uncertainty.

From the present investigation of air plasma injection from a blunt body, it is clearly demonstrated that the major portion of the drag reduction is derived from the counter-flow jet and shock interaction. The additional advantage of air plasma injection is gained from the thermal deposition. A higher thermal energy

content of the injected plasma leads to a lower required mass injection flow rate. In this sense, the air plasma injection is a more efficient drag reduction system. To achieve the same level of drag reduction, the mass flow rate of plasma injection is less than the air injection counterpart. However, the thermodynamic and chemical non-equilibrium effects in plasma injection are not directly assessable based on the state-of-the-art technique. From the present incremental analyses, these non-equilibrium phenomena under the tested condition are deemed not significant.

Electromagnetic effects

The first significant magneto-aerodynamic interacting phenomenon was demonstrated by the pioneering work of Ziemer [5]. He has shown that the shock standoff distance over a blunt body in a plasma stream increased drastically by an applied magnetic field. His pioneering work indicated that the standoff distance increased by a factor of 7.5 for an electromagnetic interaction parameter ($\sigma B^2 L/\rho u$) of 69. The electromagnetic force has been known to modify the Rankine-Hugoniot jump condition across a shock [2,23]. Taking it one step further, Shang has illustrated that the two additional entropy change mechanisms have been introduced by the electromagnetic field into the second law of thermodynamics across a one-dimensional normal shock [9].

$$\rho u \Delta s = \int(\kappa /T^2)(dT/dx)^2 dx + \int [(2\mu +\lambda)/T](du/dx)^2 dx + \int J^2/(\sigma T)dx - \int u(J\times B)_x/Tdx$$

The above equation clearly shows that the electromagnetic-aerodynamic interaction has the potential to reduce the wave drag for blunt body in supersonic flow. However to obtain the benefit of aerodynamic-electromagnetic interaction, the plasma medium must be introduced upstream of the shock and interacted with an applied electromagnetic field. To obtain the maximum effectiveness, the applied electromagnetic field is preferred in the transverse direction to the charge carrying flowing medium. These conditions were not met in all plasma injection experiments for drag reduction [7-9].

A single data point presented in Figure 11 has recorded a preliminary study of an applied magnetic field to the plasma injection. The applied magnetic field was imposed by a set of Neodymium rare earth (NeFeB) magnets around the plasma torch chamber. The applied field is aligned with the axis of the nozzle to enhance the plasma pinch effect. The magnet has a maximum magnetic flux density of 0.47 Tesla at the pole, but the field strength diminishes rapidly toward the nozzle axis. The estimated value is about 0.17 Tesla locally, the interaction parameter is uncertain far less than unity. This fact is verified by the observation, that the magneto-aerodynamic interaction is negligible. From this experimental setup, one observes that even if the electromagnetic field induced by the injecting plasma would reach the magnitude of the applied magnetic field, the interaction of magneto-aerodynamic interaction is still negligible.

Conclusions

The shock bifurcation phenomenon was discovered by a combined computational and experimental effort in analyzing the injecting plasma phenomenon. The shock structures of the counter-flow jet have two distinct dynamic states. In the sub-critical range, the flow field is in a self-sustained oscillatory motion. In the super-critical range, the entire flow field returns to the steady state. At the bifurcation point, the total aerodynamic force including the wave drag, skin-friction drag, base drag, and the reverse thrust of the counter-flow jet reaches the minimum value.

The present investigation reveals that the major portions of drag reduction by plasma injection are derived from the favorable shock and counter-flow-jet-shock interaction and thermal energy deposition. The non-equilibrium thermodynamics and chemical kinetics has insignificant effect. The contribution from the electromagnetic-aerodynamic interaction is negligible.

It may be interesting to note that an efficient combination of simulation technologies for risk and cost reduction is an actual reflection of the stage of maturation for each individual technology development. The present result also reveals the need for integrating computational fluid dynamics, electromagnetics, chemical kinetics, as well as, quantum chemical physics for future interdisciplinary application.

Acknowledgment

References

1. Shang, J.S., Assessment of Aeronautical Science for the 21st Century, Keynote Speech, Japan Society for Aeronautical and Space Science 37th Air Craft Symposium, Tokyo Japan, Oct 1999, Proceedings of JSASS 13th International Sessions, pp. 571-574.

2. Resler, E.L. and Sears, W.R., The Prospects for Magneto-aerodynamics, JAS Vol. 25, 1958, pp. 235-245 and 258.

3. Bush, W.B., Magnetohydrodynamics-Hypersonic Flow Past a Blunt Body, J. Aero. Sci. Vol. 25, 1958, pp. 685-690 and 728.

4. Meyer, R.C., On Reducing Aerodynamic Heat Transfer Rates by Magneto-hydrodynamic Techniques, J. Aero/Space Sci. Vol. 6, 1958, pp.561-566 and 572.

5. Ziemer, Richard W., Experimental Investigation in Magneto-Aerodynamics, ARC J. Vol. 19, Sept. 1959, pp. 642-646.

6. Klimov A.I., Koblov A.N., Mishin G.I, Serov Yu. L., and Yavor, I.P., Shock Wave Propagation in a Glow Discharge, Sov. Tech. Phys Lett. Vol. 8, No. 4, 1982, pp.192-194.

7. Ganiev, Y.C., Gordeev, V.P., Krasilnikov, A.V., Lagutin, V.I., Otmennikov, V.N., and Panasenko, Aerodynamic Drag Reduction by Plasma and Hot-Gas Injection, J. Thermophysics and Heat Transfer, Vol. 14, No. 1, 2000, pp. 10-17.

8. Malmuth N.D., Fomin, V.M., Maslov, A.A, Formichev, V.P., Shashkin, A.P., Korotaeva, T.A., Shipyuk, A.N., and Pozdnyakov, G.A., Influence of a Counterflow Plasma Jet on Supersonic Blunt Body Pressures, AIAA 99-4883, the Third Weakly Ionized Gases Workshop, Norfolk VA, Nov. 1999.

9. Shang, J.S., Recent Research in Magneto-Aerodynamics, Progress in Aerospace Sciences, Vol. 37, 2001, pp.1-20.

10. Adamson, T.C., and Nicholls, J.A., On the Structure of Jet From Highly Under Expanded Nozzles into Still Air, J. Aero. Science, Vol. 26, 1959, pp. 16-21.

11. Baron, J.R., and Alzner, E., An Experimental Investigation of a Two Layer Invisicid Shock Cap Due to Blunt Body Nose Injection, J. Fluid Mech, Vol. 15, 1963, pp.400-412.

12. Finley, P.J., The Flow of a Jet from a Body Opposing a Supersonic Free Stream, J. Fluid Mech., Vol. 26, Part 2, 1966, pp. 337-368.

13. Barber, E. A. Jr., An Experimental Investigation of Stagnation-Point Injection, J. Spacecraft, 1955, pp.770-774.

14. Shang, J.S., Hayes, J.R., Wurtzler, K., and Strang, W., Jet-Spike Bifurcation in High-Speed Flows, AIAA J., Vol. No.6, June 2001, pp. 1159-1165.

15. Rockwell, D., and Naudascher, E., Self-Sustained Oscillations of Impinging Free Shear Layers, Annual Review of Fluid Dynamics, Vol. 11, Annual Review, Inc., Palo Alto CA, pp. 67-94, 1979

16. Strang, W.Z., Tomaro, R.F., and Grismer, M., The Defining Methods of Cobalt: A Parallel, Implicit, Unstructured Euler /Navier-Stokes Flow Solver, AIAA 99-0786, January 1999.

17. Grismer, M.J., Strang, W.Z., Tomaro, R.F., and Witzeman, F.C., Cobalt: A Parallel, Implicit, Unstructured Euler/Navier-Stokes Solver, Advances in Engineering Software, Vol. 29, 1998, pp.365-373.

18. Sparat, P.R. and Allmaras, S.R., A One-equation Turbulent Model for Aerodynamic Flows, AIAA 92-0439, January 1992.

19. Shang, J.S., Ganguly, B., Umstattd, R., Hayes, J., Arman, M., and Blitzenger, P., Developing a Facility for Magneto-aerodynamic Experiments, J. Aircraft, Vol. 17, No. 6, 2000, pp. 1065-1072.

20. Gilmore, Forrest R., Laher, Russ R., and Espy, Patrick J., Franck-Condon Factors, r-Centroid, Electronic Transition, Moments, and Einstein Coefficients for Many Nitrogen and Oxygen Band Systems, J. Phys. Chem. Rev. Data, Vol. 21, No. 5, 1992, pp.1005-1107.

21. Huber, K.P. and Herzberg, G., Molecular Spectra and Molecular Structure, Vol. IV: Constants of Diatomic Molecules, Van Nostrand Reinhold Co., 1979.
22. McBride, B.J. and Gordon S., Computer Program for Calculation of Complex Chemical Equilibrium Compositions and Applications, II. User Manual and Program Description, NASA Ref. Pub. 1331 June 1996.
23. Mitchner, M. and Kruger, C.H., Partially Ionized Gases, John Wiley and Sons, NY, 1973, pp.163-241.
24. Park, C., Assessment of Two-Temperature Kinetic Model for Ionizing Air, AIAA 87-1574. 1987
25. Shang, J.S., Hayes, J.R., and Menart, J.A., Hypersonic Flow over a Blunt Body with Plasma Injection, AIAA 2001-0344, Reno NV, January 2001.
26. Shang, J.S., Hayes, J.R., Miller, J.H., and Menart, J.A., Blunt body in Hypersonic Electromagnetic Flow Field, AIAA 2001-2803, Anaheim CA, June 2001.

This page has been deliberately left blank

———————————

Page intentionnellement blanche

Experimental Aspects of Code Verification/Validation Application to Internal and Afterbody Aerodynamics

Richard Benay, Bruno Chanetz and Jean Délery
Fundamental/Experimental Aerodynamics Department
Onera-Meudon Centre
92190 Meudon
France

Abstract

The past 40 years have known a spectacular development of CFD capabilities. It is now possible to compute complex three-dimensional unsteady flows even at the design stage by solving the Unsteady Averaged Navier-Stokes Equations (URANS approach) and progress are made every day in still more advanced approaches such as LES and DNS. However, the confidence in CFD methods is still limited because of uncertainties in the numerical accuracy of the codes and of the inadequacy of the turbulence models they use. Thus, there is still a need for well made and well documented experiments to validate the codes and to help in their improvement. Such experiments must also fulfill quality criteria to be considered as safe enough and really useful for code validations. The paper presents a discussion of the strategy to be followed to ensure the reliability and accuracy of a code by placing emphasis on the experimental aspects of code validation. The purpose is illustrated by considering recent examples of CFD validation operations based on basic - or building block - experiments. The first case considers an experiment on a purely laminar shock wave/boundary layer interaction used to assess the numerical accuracy of several codes. Other examples deal with the crucial problem of the validation of turbulence models in strongly interacting flows. The conclusion stresses the importance to constitute high quality data banks on typical flows still difficult to predict. The problem of data dissemination is also briefly addressed.

1. INTRODUCTION

Formerly, validation of predictive methods was made by comparison of the computed results with some measured wall properties, essentially the pressure. In many situations, this kind of comparison was sufficient since "old" predictive methods, which were either fully empirical or based on a multi-component type approach, allowed only the prediction of the wall properties (pressure, skin-friction, heat-transfer) and the global performance of the vehicle. They could also give a gross idea of the flow organization by predicting, for example, the size of a separated region and the location of a separation point, but this information was more or less considered as qualitative. The flow prediction landscape has completely changed with the advent of theoretical models based on the solution of the Navier-Stokes equations. It is clear that this approach is the only suitable to compute complex flows containing shock waves, centered expansion waves, separated regions, shear layers, etc… the dissipative region being turbulent in nearly all the practical situations. Then, not only the wall properties are computed but also field quantities including the mean velocity and the turbulent quantities. However, in its present state the Navier-Stokes approach is still far from being free of critics, difficulties

persisting both on the numerical side and in the physical modeling, in particular of turbulence. There is thus a strong need to validate Navier-Stokes codes before their routine use for design purposes.

Though the prediction of wall properties remains a key target for most predictive methods, since the drag and the thermal loading are the quantities of most practical interest, it rapidly became obvious that a comparison restricted to wall properties was insufficient to properly validate the most advanced predictive methods. In general, Navier-Stokes codes give a faithful and impressive picture of the flow field structure. For example, in propulsion applications, the complex organisation of the jet with its pseudo-periodic pattern of shocks and expansion waves, the separated zone forming inside an overexpanded nozzle or on the afterbody in case of jet pluming are most often well reproduced. However, a more careful analysis of the data shows that the situation is far from being entirely satisfactory.

Firstly, it is observed that a fairly good prediction of the wall pressure can coexist with a poor quantitative prediction of the velocity field. Frequently, the extent of the separated region is underestimated, sometimes considerably. In addition, the turbulent quantities are poorly predicted, especially if the flow is separated. Such discrepancies render suspect the validity of the code since they are indicative of some basic deficiency, either in its numerical scheme or its turbulence model, or both.

Secondly, a rather fair prediction of the flow field can be accompanied by large errors in the calculation of surface properties affecting mainly transfer coefficients such as skin-friction and heat transfer.

Lastly, in certain applications, the knowledge of the outer field itself is of prime interest. This is the case for problems dealing with infrared signature where detailed description of the hot propulsive jet, with an exact localization of the Mach discs, is essential. Pollution studies necessitate a good prediction of the jet properties to allow accurate evaluation of chemical processes and species concentration. A good representation of the flow resulting from interference between the external stream and the propulsive jet(s) also requires a faithful prediction of the flow field. This is also the case of shock intersections which can be of prime importance for the performance of air-intakes at high Mach number.

The problem of code validation is still more stringent in three-dimensional applications where the Navier-Stokes approach becomes mandatory. Due to the complexity of such flows, it is clear that the consideration of the surface pressure alone is completely inadequate because this information gives a very partial view of the flow (in three-dimensional flows, it is no longer possible to infer separation from an inspection of the wall pressure distributions).

In these conditions, the validation of advanced computer codes requires well documented experiments providing detailed and reliable flow field measurements. The progress accomplished in the measurement techniques over the past 40 years, mainly with the advent of laser based optical methods, has operated a true breakthrough in our capacity to investigate complex turbulent flows, containing shock waves, strong expansions, thin shear layers and recirculating regions. We therefore possess now the necessary technical means for performing such investigations.

This paper deals with the global problem of code and models validation by comparison with experiments. After purely numerical tests, this step is essential for determining the degree of reliability of a code using a given model. Two parts can be distinguished:

➢ A first part is devoted to the strategy for code verification and validation with emphasis on the experimental facet of this action. This strategy is presented in the optics of a physical approach of the problem in which one focuses on the prediction of the flow fundamental properties. The performance aspect is not considered, although it is the end product of the validation chain; this ultimate step is more in the hands of engineers than scientists.

➢ In a second part, the verification/validation strategy is illustrated by examining problems met in propulsion aerodynamics. They concern phenomena of internal aerodynamics, affecting supersonic air intakes, base flows and propulsive after-body recently studied at Onera.

2. THE CODE VERIFICATION/VALIDATION PROCESS

2.1 What is required from the code

Before considering a verification/validation action, first of all, the aim of the calculation must be clearly stressed and identified.

➢ If calculation is used to predict the performance of a system or a sub-system, accuracy is mandatory since then the engineer has to rely on the calculation to define the object which must satisfy prescribed specifications or to evaluate the aerodynamic performance achieved by a given object, in terms of drag, thrust, maximum range, stability, fuel consumption, manufacturing and maintenance costs, etc . This consideration applies to an airfoil, a wing, an air-intake, a nozzle, a propelled afterbody, etc. Such aerodynamic calculations are frequently coupled with structural analysis, aeroelasticity, thermal calculations, flight mechanics.

➢ In the design of machines involving complex flows whose experimental simulation is difficult, if not impossible, a calculation showing the flow field organization is of great help for the designer. In this case, accuracy is not essential, but reliability is crucial since one must be confident on the physical features of the computed field. This applies to flow in turbomachines where a detailed experimental description of the flow is still largely out of reach. This is also true for the flow past multi-body space launchers where information on the main flow features can be useful to detect possible hazards and to take precautions to avoid them.

➢ From a fundamental point of view, the physical understanding of complex flows has to be based on a parallel theoretical analysis whose aim is to help in the interpretation of the phenomena and to establish the descriptive approach on firm rational arguments. In this case, accuracy is not needed since, for example, theoretical analyses are nearly always derived from more or less strong simplifying assumptions rendering quantitative results questionable. This is for example the case of stability analyses, perturbation methods or asymptotic expansion techniques. These theories have greatly helped in the understanding of critical phenomena, in spite of a relatively poor quantitative agreement. Numerical calculations are also a precious tool to construct the structure of complex flows by providing information on "hidden" faces of the phenomena which cannot be reached by direct observation. This point concerns for example the topological construction of three-dimensional separated flows. Here accuracy is not essential; even reliability can be limited

since in the process there is a continuous exchange between experiment and calculation - or theory - which allows a cross fertilization of the two approaches.

➢ In the last issue, a code is used as a tool to test a new physical model (or to introduce some improvement in an existing one). Then, numerical accuracy is mandatory since it would be vain to implement a good turbulence model (if there is one) in an inaccurate code in which high gradient regions where turbulent is at work are not correctly captured.

2.2 The different steps of the validation

Considering the above points, it appears that the verification/validation procedure has to be submitted to a four step strategy or tactical actions.

First step : assessment of the code numerical accuracy : Before going into a more involved operation of code validation, encompassing all the aspects of the computing action, it seems obvious to first establish the accuracy and reliability of the code by focusing on its numerical aspects. A clear assessment of this point is not a straightforward issue in the sense that the numerics involves several closely linked aspects. Assessment of the code numerics can be done first from comparison with exact analytical solutions or with well established empirical results. Most often these exact solutions are only available for laminar flows.

In a second phase, verification can be made by confrontation with other codes developed by independent teams. This action implies a close co-operation between the persons involved in the procedure with a complete exchange of information on the calculation methods and a common evaluation of the results. A precaution for this action to be conclusive should be to agree on exactly the same configuration and to insure spatial convergence in all the calculations. If the comparison between the codes exhibits differences which cannot be resolved after a thorough analysis of the results, then one has to refer to the verdict of an independent authority which can be experiment.

A further - and hopefully conclusive - step will be to run the competing codes on a configuration for which good and reliable experimental results exist. This point is far less obvious that it would appear at first sight, since the experimental data should allow to draw clear conclusions. Thus, one should avoid to mix modeling and numerical problems by considering a simple laminar case, in a calorically perfect gas in order that the basic flow physical properties (thermodynamics constants, molecular viscosity) are well known. This point is far from being easy to achieve since it is most often very difficult to maintain an entirely laminar regime in classical aerodynamics.

The geometry of the body should be simple and completely defined to avoid complex meshing problems. From this point of view, a two-dimensional case is preferable but, as it will be seen below, an axisymmetric configuration is preferable. Experimental requirements will be exposed more completely below.

Second step: Validation of the physics implemented in the code on elementary configurations. This is the most important point for the specialist in flow physics, the first step being only a preliminary step simply aiming at verifying the tool. In the second step, the code is used to compute what can be considered as the elementary components of an aerodynamic flow: attached boundary layer, laminar-turbulent transition on a flat plate, separation induced by an obstacle, flow past a base, shock wave/boundary layer interaction, start and development of a vortex structure, vortex breakdown, shock/shock interference or shock crossing, etc. Two-dimensional - preferably axisymmetric - as well as three-dimensional basic situations have to

be considered. For this first validation step, the numerical results are compared with *building block* experiments focusing on a specific elementary phenomenon.

Third step: validation on more complex sub-systems. Once the code and its physical model(s) have been validated on basic cases, a more complete configuration must be considered consisting in a sub-system of a complete vehicle, where several elementary phenomena are combined. This is the case of a profile on which one encounters laminar-turbulent transition, attached boundary layers, transonic shock wave/boundary layer interaction, separation, wake development, etc. The wing constitutes a three-dimensional extension with the additional problems of the vortices emanating from the wing and control surfaces extremities. The supersonic air-intake involves shock/shock interference, shock wave/boundary layer interactions, corner flows with vortex development. After-bodies combine supersonic jets with complex shock patterns (Mach disc formation), shock induced separation, either inside the nozzle (overexpanded nozzle) or on the fuselage (jet pluming at the exit of an underexpanded nozzle). Many other examples can be cited: propulsive nacelle, compressor/turbine cascade, helicopter rotor, etc.

Fourth step: validation on the complete vehicle or object. This is the ultimate target in which the code is applied to a complete airplane, an automobile, a space launcher, a helicopter, etc. This part of the exercise is the domain of engineers and will not be developed here.

2.3 Requirements for good test cases constitution

We are thus naturally led to define what are the requirements for really useful experimental results and ask the question: is the data bank safe? This is a vital issue on which we will concentrate since the points which follow are the every day concern of experimentalists.

Definition of the geometry. A first condition for any experiment aiming at the verification of the numerical accuracy of a code and the validation of its physical models is to focus on a configuration whose geometry must be both representative of a typical situation, precisely defined and as simple as possible. A combination of plane surface (like a two-dimensional ramp) is a good choice but one should carefully avoid special situations, like a sharp leading edge, leading to singularities and to meshing difficulties. When possible, an analytical definition of the contour should be provided. It is preferable to give the dimensions in metric units to avoid risk of confusion in the reference length used to compute a Reynolds number. When possible, a two-dimensional geometry should be adopted - even for three-dimensional problems - since it offers many advantages to visualize the phenomena and to execute measurements, in addition of the lower cost of the test-set up fabrication. Furthermore, the original set-up must frequently be modified before arriving at a fully satisfactory flow; such modifications are far easier on a two-dimensional arrangement.

Boundary conditions. The boundary conditions must be well identified and accurately known. This concerns the upstream flow conditions (Mach number, velocity, pressure, density) when a uniform incoming flow exists. In transonic experiments executed in a channel type arrangement, one often considers phenomena taking place on the channel walls, the test section itself being the model. In this case, a well defined origin with a uniform state at upstream infinity does not exist. Then, the data should provide all the flow conditions in a section located sufficiently far upstream of the region of interest, including the boundary layer properties (mean velocity profile, turbulent quantities).

In all cases the stagnation conditions (pressure, temperature) and the incoming stream thermodynamic properties must be given. Downstream boundary conditions leading to a well

posed problem must be provided. If the flow leaving the zone of interest is supersonic, then no-conditions have to be imposed to perform the calculation. The question of the downstream conditions is more delicate if the configuration is such that the flow leaving the test region is subsonic. When the downstream flow is again uniform, most often a downstream pressure is given, since this quantity is easily obtained. It is far more difficult to provide the pressure field in a complete plane, as some theoreticians sometimes ask for. In transonic channel experiments where a shock is produced by the choking effect of a second throat, the best way is to provide the geometry of the second throat and, in the calculation, to impose downstream conditions insuring the choking of this throat.

Perturbing effects. Side effects or uncontrolled perturbations must be avoided, except if they can be taken into account by the calculation. The side effects due to the finite span of any experimental arrangement strongly affect the flow when separation occurs. Then, the experimented flow can be very different from the assumed ideal two-dimensional flow which would correspond to the infinite span condition. Confrontation of such an experiment with a planar two-dimensional calculation can be deprived of any signification and lead to entirely erroneous conclusions. Much has been said and written about the side effects to arrive at the conclusion that comparison of a two-dimensional calculation with a "pseudo" two-dimensional experiment *should be forbidden*! Even if many experiments show a limited zone in the vicinity of the wind tunnel mid longitudinal plane that can be considered as reasonably two dimensional, this is never a warranty of two dimensionality, at least locally, since the entire phenomenon can be displaced by side effects. This is the case of the separation line on profiles. If one desires to keep the mathematical simplicity of two space dimensions, the best is to compute an axisymmetric flow.

Experimental needs. The description of the flow must be as complete as possible in order to permit a thorough validation of the code and to provide all the information useful to understand the physics of the flow and to help in the elucidation of causes of disagreement. This concerns wall quantities, like pressure, heat transfer, skin-friction, field quantities such as stagnation pressure and temperature, mean velocity, Reynolds tensor components, density, species concentration, etc. Flow visualizations are highly desirable to give a precise idea of the flow field structure: shock waves, location of shear layers, separated region, vortices. A really complete description of the flow is never possible because the experiment cost would become incompatible with the budgets currently allocated to fundamental aerodynamics.

Measurements reliability and accuracy. The experimental data must be reliable. This means that the experiment is not "polluted" by an extraneous phenomenon due to a bad definition of the test arrangement or to a bad functioning of the facility. The general regulation tends now to impose to experimentalists precise information on the uncertainty margins of their measurements. This information, although important for an in depth validation of codes, is not always as essential as claimed if the objective is to test the physical validity of a complex model. The problem is different in the case of performance determination, where quantities like lift, drag, efficiency must be known with high accuracy.

The physical interpretation. Constitution of safe data banks is not restricted to the execution of hopefully good experiments in relation with code development. The experimentalist must also be a physicist able to interpret its findings and to understand the physics of the investigated flow field. This interpretation, which must be based on theoretical arguments, is essential to insure the safety of the results. It must precede any numerical exploitation.

3. APPLICATION OF THE STRATEGY TO INTERNAL AERODYNAMICS AND AFTERBODY FLOWS

3.1 Scope of the action

The propulsion of aerial vehicles, such as military or civil aircraft, missiles, space-launchers, involves parts where aerodynamics plays a major role, both as components participating to the engine functioning and as elements contributing to the thrust of the propulsive unit. These components, or sub-systems, are basically the air-intake, the nozzle and the afterbody. The role of the air-intake is to supply the engine with low Mach number and "good" quality air (i.e., with high stagnation pressure and low distortion). The air-intake contributes also to the thrust and is an important cause of drag (captation and cowl drag). The main roles of the nozzle is to regulate the mass flow traversing the propulsion unit and to insure an optimum expansion of the combustion gas to produce maximum thrust. The afterbody part is most often characterized by recirculating zones situated close to the walls, the pressure level in these zones determining the drag level (base drag). The aerodynamics of propulsion involves interactions between the internal flow and the outer stream which may strongly affect the propulsion efficiency. These phenomena are specially important at the nozzle exit and around the afterbody since they can lead to separation, either inside the nozzle or on the fuselage, according to the nozzle expansion ratio. Internal aerodynamics is probably a domain where major progress can be made in the coming year since it concerns flows involving strong shock waves and stream confluence's which are at the origin of shock/shock interactions, extended separations, shear layer developments, large scale fluctuations, these phenomena taking place in turbulent compressible flows (except in very high altitude flight). In addition, in most applications, the configuration is highly three-dimensional (twin-nozzle of combat aircraft, multi-body space launchers, etc.). All these points make the prediction of such flows difficult since they involve the hardest points met in applied fluid mechanics. The present predictive capacity being still limited there is a strong need to maintain a sustained research effort both on the experimental and theoretical sides for propulsion applications.

These problems are more critical for a hypersonic air-breathing spacecraft which flies in conditions where shock phenomena are much amplified leading to still more severe interactions between the internal and outer flows. Then, integration of the propulsion unit in the vehicle architecture is a vital issue.

The conception of the air-intake must take into account two major aerodynamic interactions. Firstly, compression of the capted high Mach number flow is achieved partly by taking opportunity of the shape of the vehicle front part which allows to realize a nearly isentropic compression, partly by a succession of ramps and/or shock reflections constituting the air-intake itself. The design of the compression ramp system is a complex matter combining the search for maximum efficiency, minimum cowl drag, minimum length or weight of the system, possibility of adaptation, etc. In particular, one is confronted with the risk of separation at a ramp or a shock reflection, with the subsequent loss of efficiency, possible occurrence of instabilities and air-intake unstart. This problem is not restricted to air-intake since separation is likely to occur in several other parts of the vehicle. As it is well known, separation is most often avoided by designers since it leads to a degradation of performance and a rise of the nuisance produced by the vehicle. In addition, at hypersonic velocity the reattaching shear layer of a separation bubble leads to extremely severe high level of heat fluxes. All these reasons make essential an accurate prediction of separated flows.

At the other extremity of the propulsion nacelle, one is faced with another class of phenomena resulting from the confluence between the propulsive jet(s) and the outer flow. In many circumstances, the co-flowing streams are non-adapted, which, in supersonic or hypersonic regimes, generates shock waves interacting with the boundary layers. When the flow issuing from the nozzle is at a pressure well superior to the outer pressure (underexpanded case), the strength of the interaction shock can be so severe as to force the external flow to separate. On the other hand, if the nozzle is overexpanded, the rise in pressure at its exit may cause separation in the nozzle. The non-adaptation phenomena induced by flow confluence have an influence: on the afterbody drag and thrust balance, on the aerodynamic stability and maneuverability of the vehicle, when flow instabilities occur, and on the base heat-flux levels since hot gases are present inside the separated fluid regions.

The examples which follow present typical test cases, constituted at Onera for the majority of them, to help in the development of safer and more accurate codes. These experiments are all (relatively) news, which explain that they have not yet been really exploited, except the first one which is a good example of a nice verification action involving five codes. For the other cases, only one home-made Navier-Stokes code has been run with the main objective to check the completeness and safeness of the test cases.

3.2 The cylinder-flare case for hypersonic laminar separation

Aim of the operation. The aim of the present operation was to assess the ability of numerical codes using various schemes to predict separation on a 30° axisymmetric ramp flow at a Reynolds number sufficiently low to insure laminar flow over the whole interaction domain (Chanetz et al., 1998, 1999). The action consisted in extensive comparisons between measured and calculated wall and flow field properties. Since the calculated wall quantities are particularly sensitive to grid constitution, great attention was paid to the quality of the grids. The results of five codes have been compared in this action:

➢ Two Navier-Stokes codes from Onera using a finite-volume approach. These are the FLU3M code (Borrel et al., 1988) and the Nasca code (Benay and Servel, 1995).
➢ The Navier-Stokes code HIG-2XP from the University of Rome 'La Sapienza' using a finite-volume approach (Grasso and Marini, 1996).
➢ The Navier-Stokes code FLOW from DLR using a finite-element approach (Schulte et al., 1998).
➢ A Direct Simulation Monte-Carlo code (DSMC) from NASA-Langley Research Center (Moss and Olejniczak, 1998).

This operation corresponds to step 1 of the strategy defined in Section 2.3: assessment of the code numerical accuracy.

The experimental part. The experiments have been executed in the low Reynolds number Onera R5Ch wind tunnel. For the nominal stagnation conditions (pressure $p_{st} = 2.5 \times 10^5$ Pa, temperature $T_{st} = 1050$K), the upstream Mach number was equal to $M_0 = 9.91$.

The model (see Fig. 1) is constituted by a hollow cylinder, with a sharp leading edge, followed by a flare terminated by a cylindrical part. The flare angle, $\beta = 30°$, induces a large separated zone. The flare is followed by a cylindrical part in order to facilitate the computations by displacing the base flow sufficiently far downstream of the interesting area, in such a way that the complex phenomena occurring in the base region have no effect on the interaction region. The model has a total length of 170mm, the reference length, based on the distance between the sharp leading edge and the beginning of the flare being equal to $L = 101.7$mm. The Reynolds

number calculated with L is equal to $Re_L = 18{,}375$. The outer diameter of the cylinder is equal to 65m and its inner diameter to 45m.
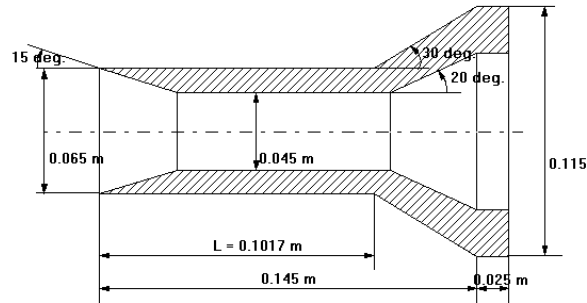
Figure 1: Geometrical definition of the cylinder-flare axisymmetric model

The flow has been qualified by surface flow visualization, wall pressure and heat transfer measurements and probing of the outer field by use of the X-ray electron beam fluorescence technique

CFD codes confrontation. As far as the three finite-volume Navier-Stokes calculations are concerned (FLU3M, Nasca and HIG-2XP), a preliminary grid dependency study by successive dichotomic mesh refinements in both directions was performed with the FLU3M code. As a result, the calculations were performed with the three codes on a (289×97) grid. For the FLOW results, the computational domain is discretized by using a hybrid grid consisting of approximately 61,500 elements (after grid adaptation). The structured subgrid situated on the isothermal model wall is composed of 40 layers, growing with geometric progression.

For the DSMC results, the calculation is made with a four-region computational domain containing 78,100 cells, where each cell is further subdivided into four (2×2 subcells). The collision partners are selected within the subcell; consequently, the flow resolution is much higher than the cell resolution (however, the microscopic properties are extracted from averages within the cell).

A comparison between the three finite-volume Navier-Stokes codes and the FLOW and DSMC codes reveals that the wall pressure distributions plotted in Fig. 2a are in good agreement with experiment in the case of the HIG-2XP and Nasca codes, as far as the prediction of separation extent is concerned. However, the pressure obtained on the flare is higher than that obtained in the experiment. The figure indicates that the HIG-2XP code is in good agreement with experimental values.

In the vicinity of reattachment, the experimental results present a non-smooth behavior. It was not possible to ascertain whether it is due to experimental uncertainties or to a real physical phenomenon (that neither of the codes capture). However, it is interesting to point out that the major discrepancies between codes in the prediction of the wall pressure on the flare start in the reattachment zone.

The examination of the skin friction coefficient distributions (see Fig. 2b) shows a good agreement between the HIG-2XP results and the experimental separation point. The locations of the separation and reattachment points are summarized in Table 1.

Abscissa(*X/L*)	FLU3M	Nasca	HIG-2XP	FLOW	DSMC	Experiment
Separation	0.72	0.74	0.77	0.74	0.75	0.76 ± 0.01
Reattachment	1.33	1.33	1.32	1.33	1.32	1.34 ± 0.015

Table 1 : Separation extent

Concerning the Stanton number distributions (see Fig. 2c), the Nasca and HIG-2XP codes give results on the flare showing the best agreement with experiment.
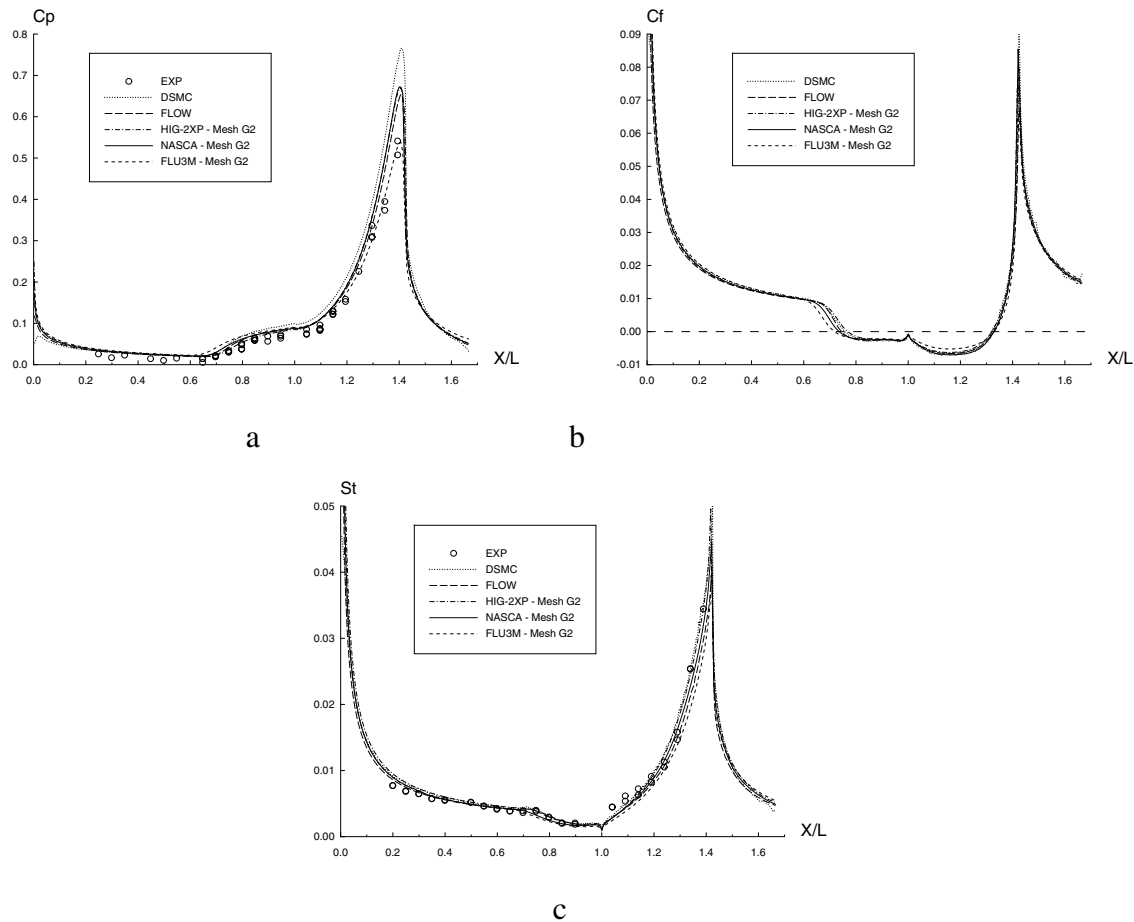
Figure 2: The cylinder flare-model at Mach 9.92 . Comparison of wall quantities
a - Pressure coefficient, b - Skin friction coefficient, c - Stanton number

Since the three finite-volume Navier-Stokes codes (FLU3M, Nasca and HIG-2XP) give nearly the same results, only three codes are considered: the finite-volume Navier-Stokes code Nasca, the finite-element Navier-Stokes code FLOW and the DSMC code.

Three density profiles have been measured by use of X-ray electron beam fluorescence (Chanetz et al.,1999). The profile at *X/L* = 0.3, shown in Fig. 3a, is located upstream of the separation line. At this station, the increase of density is due to the shock generated by the strong viscous interaction at the sharp leading edge. There is a good agreement between numerical and experimental results for the density peak amplitude. However, the calculated radial shock position varies with the simulation used.

At this station (*X/L* = 0.3), leading-edge effects probably subsist, their influence being not accurately represented by the Navier-Stokes codes. This can be due to slip effects that are not

taken into account and the difficulty to keep the correct leading edge location with the mesh in Navier-Stokes approach. The DSMC calculation is in excellent agreement with experiment. For the profiles at $X/L = 0.6$, shown in Fig. 3b, the inverse behavior appears on the radial shock location, the best predictions being furnished by the two Navier-Stokes codes. However, this difference on shock location needs to be confirmed before concluding on this subject. The profiles at $X/L = 0.76$, shown in Fig. 3c, present the same tendencies.
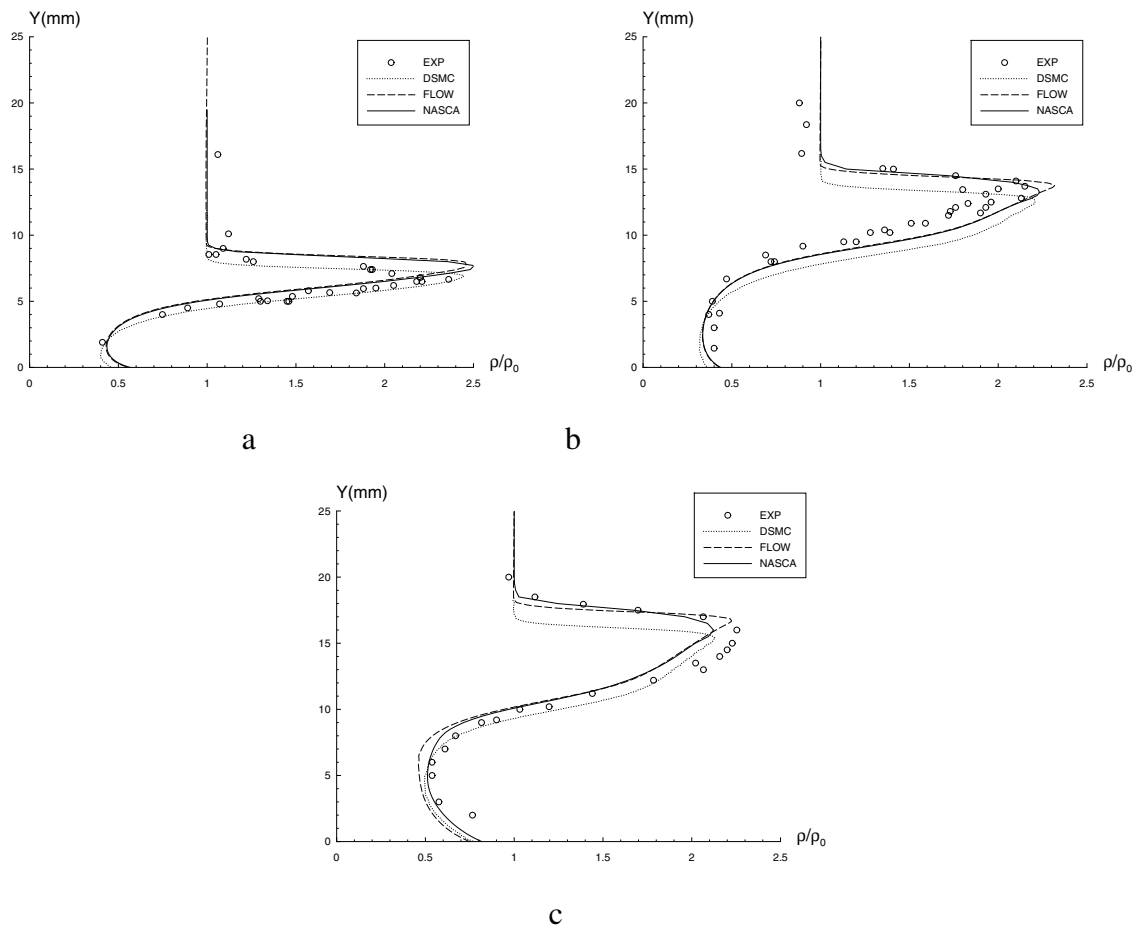
Figure 3: The cylinder flare-model at Mach 9.92 Density profiles in the interaction region. (X-Ray EBF measurements)
a - Station X/L = 0,30, b - Station X/L=0,60, c - Station X/L=076

3.3 Shock wave / boundary layer interaction control in transonic flow

Aim of the operation. Shock-waves and their interaction with the boundary-layer play a major role in determining the performance of propulsion systems such as air-intakes, diffusers, turbomachine cascade, etc. One way to reduce the harmful effects of these shocks is to perform a control action in the interaction region (Délery, 1984, Stanewsky et al., 1997). In the present study, the following techniques have been considered: 1) active control in which a part of the boundary-layer is sucked off through a slot, 2) passive control, 3) hybrid control which is a combination of a passive control cavity and a suction slot (or cavity) located downstream of it. The aim of slot suction is to swallow part of the low energetic flow close to the surface before interaction of the boundary layer with the shock or during the interaction process itself. The principle of passive control consists in establishing a natural circulation between the downstream high pressure face of a shock and its upstream low pressure face. This circulation is achieved through a closed cavity, placed underneath the shock foot region, the face in contact with the outer flow being made of a perforated plate. It has been shown

that, in very limited circumstances, passive control may produce a reduction of an airfoil drag, while postponing to higher incidences the limit of buffet onset. However, the gain being frequently problematic, it has been proposed to combine passive and active control to realize what is called hybrid control. Control methods are more likely to be used in air-intake applications to diminish stagnation pressure losses (improved efficiency) or stabilize a shock-wave.

The experimental part. These experiments were executed in the S8Ch transonic-supersonic basic research wind tunnel of the Onera Meudon Center. This facility is a continuous wind tunnel supplied with desiccated atmospheric air mainly dedicated to LDV measurements. The stagnation conditions were: $p_{st0} = 96{,}000 \pm 800$ Pa and $T_{st0} = 300 \pm 4$ K. A photograph of the test set-up is shown in Fig. 4. It is constituted by a transonic channel having a test section with a maximum height of 100mm and a span of 120mm. The lower wall is rectilinear and equipped to receive the control devices, the upper wall being a contoured profile designed to produce a uniform supersonic flow of nominal Mach number equal to 1.4. A second throat, of adjustable cross section, is placed in the test section outlet to produce by choking effect a shock-wave whose position, and hence intensity, can be adjusted in a continuous and precise manner. It also isolates the flow field from pressure perturbations emanating from downstream ducts, reducing unwanted shock oscillations. The two side walls are equipped with high quality glass windows to allow visualizations and LDV measurements.
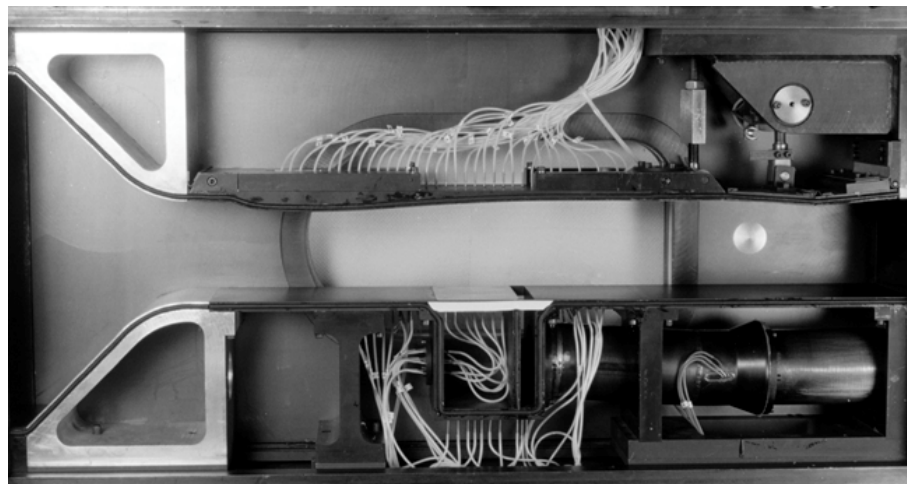
Figure 4: Shock wave/boundary layer interaction control. Test arrangement in the S8Ch wind tunnel.

The type of control taken as example here is passive control. For this device (see Fig. 5), a 70mm-long passive control cavity was used, the shock being centered on it. The cavity, which extends between X = 130mm and X = 200mm, is covered by a perforated plate, with a 5.67%-porosity and 0.3mm-diameter holes.
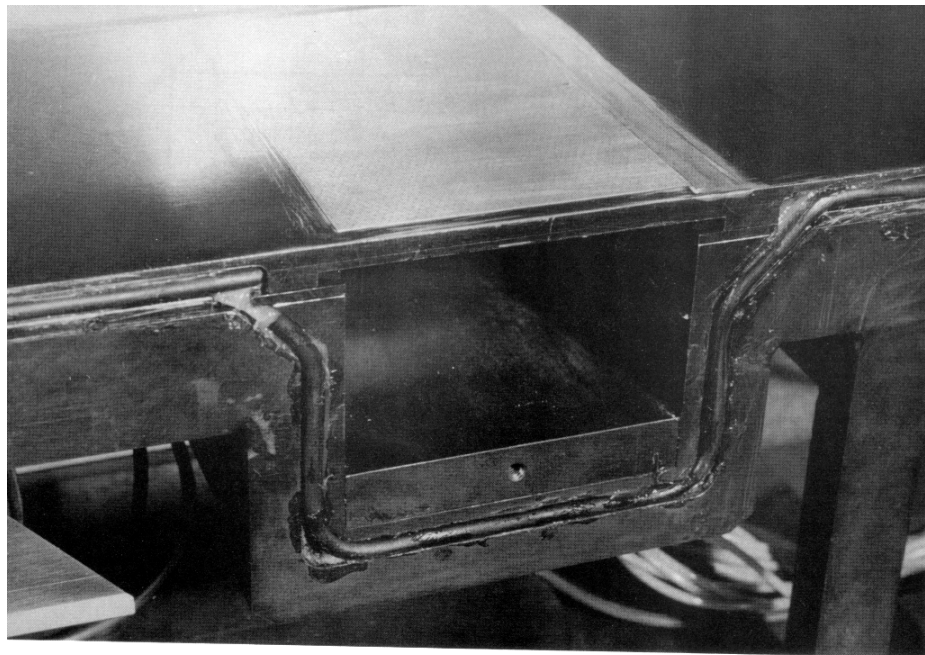
Figure 5: Shock wave/boundary layer interaction control.
Arrangement for passive control

The flows under study were qualified by schlieren visualizations and quantified by measurements of wall pressure distributions (pressure orifices being located in the vertical median plane of the test set-up) and probing of instantaneous velocity with a two-component LDV system (Bur et al., 1998).

A Navier-Stokes code confrontation. The numerical simulations were performed with the Nasca code which solves the classical Reynolds Averaged Navier-Stokes (RANS) equations. Turbulence modelling was first carried out by means of the [k-ε] transport equation models of Chien. (Ch model) (Chien, 1982) and Launder-Sharma (LS model) (Launder and Sharma, 1974). These two models were compared in the reference and passive control case with the new [k-σ] turbulence model, where σ represents a length scale (Benay et al., 2001).

The calculation domain is a part of the experimental channel extending from a well chosen section of the divergent expanding zone, where experimental velocity and turbulent shear stress profiles (obtained by LDV probing) are imposed, to the end of the channel, where the experimental pressure is imposed. Passive control is simulated by prescribing the unit mass flow ρv at the wall, the conditions on the other variables remaining unchanged. The ρv value at the wall is obtained by relations expressing a direct dependence of the wall vertical velocity to the pressure difference between the cavity and the external flow. The cavity pressure is taken as the experimental one. The relations used for the computations are the calibration law of Poll (Poll et al., 1992) and the Bohning-Doerffer law (Bohning and Doerffer, 1997).

Both transpiration/suction laws were implemented in the code and their respective results compared to experiment. The Mach number contours plotted in Fig. 6 are obtained with the [k-σ] model, the three models giving nearly identical pictures at this level. These contours show a good prediction of the large spreading of the shock system, which begins at the origin of the cavity. The difference in the location of the crossing (quasi normal) shock is weak. The thickening of the viscous zone due to the control device is well reproduced by the calculation.

Transonic interaction with boundary layer passive control

Mach number contour lines
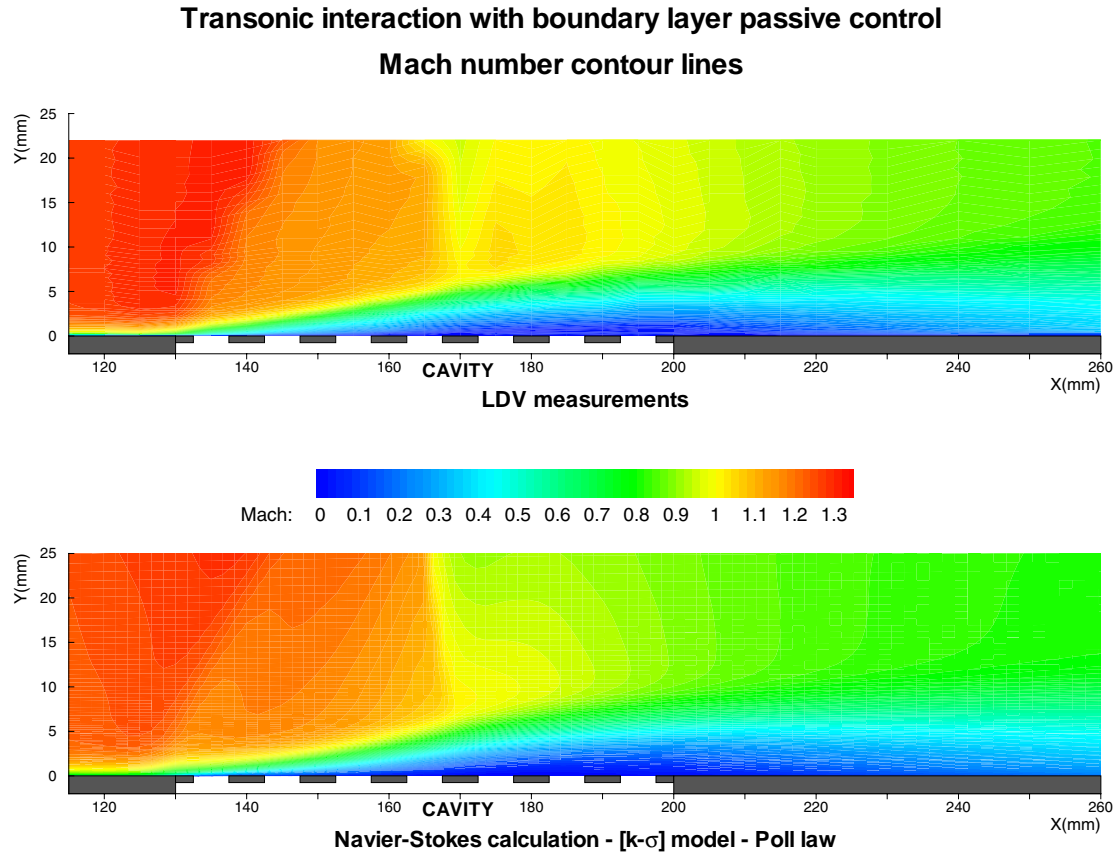
Figure 6: Shock wave/boundary layer interaction with passive control. Mach number contours: confrontation between experiment and Navier-Stokes calculation

The computed wall pressure distributions plotted in Fig. 7 show the difficulty to simulate injection through very small holes by a continuous distribution and a discrete mesh. A rigorous calculation of this problem should have been done by meshing each hole, which is unrealistic with present computing capabilities. We will see in the following results that the apparently rough approximation made to treat the porous wall condition is almost correct. At the beginning of the perforated plate (see Fig. 7), the peak on the computed wall pressure values at X = 130mm is a consequence of the sudden change of boundary condition between the two surrounding mesh points. The numerical approximation and the experimental resolution are not sufficient to give an account of the true physical process. Downstream of the mid cavity, the computed pressure recovers more satisfactory levels. A modification from the imposed experimental pressure levels on downstream boundary was necessary with the [k-ε] calculations in order to adjust the shock to its experimentally observed position. The amplitude of this shifting can be seen on Fig. 7. The agreement with experiment of computed wall pressure from the end of the cavity to the terminal downstream section is satisfactory with the [k-σ] model.
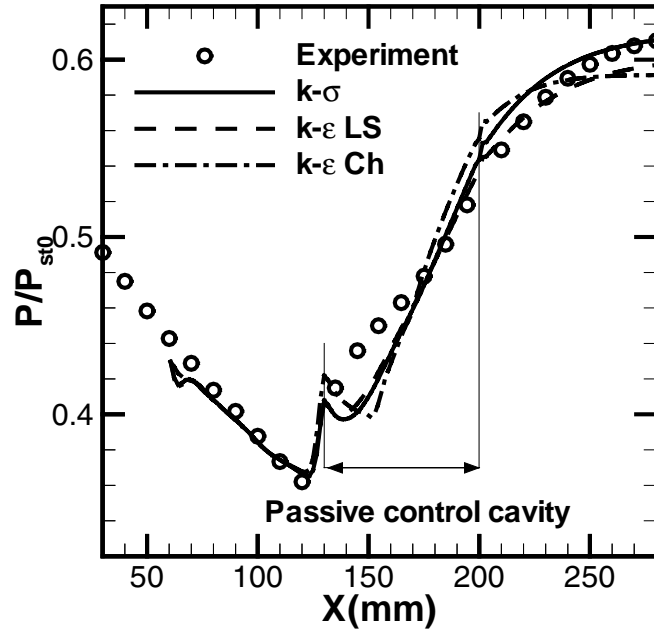
*Figure 7: Shock wave/boundary layer interaction with passive control
Computed and experimental wall pressure distribution*

As shown in Fig. 8, the streamwise velocity profile in the region of maximum wall pressure gradient, at the beginning of the cavity (X = 130mm), is submitted to the effect of the oblique thin compression fan starting from the junction between the solid and porous walls. The evolution of the boundary-layer velocity profiles at the beginning of the interaction is predicted satisfactorily by the models. An effect of passive control on the interaction is the occurrence of a separated flow of small size, above the perforated plate. As a consequence of the poor capture of the reversed flow by the models, the response of the boundary-layer flow to local compressions is too roughly simulated. This fact can be observed in Fig. 8, at X = 180mm and 220mm.
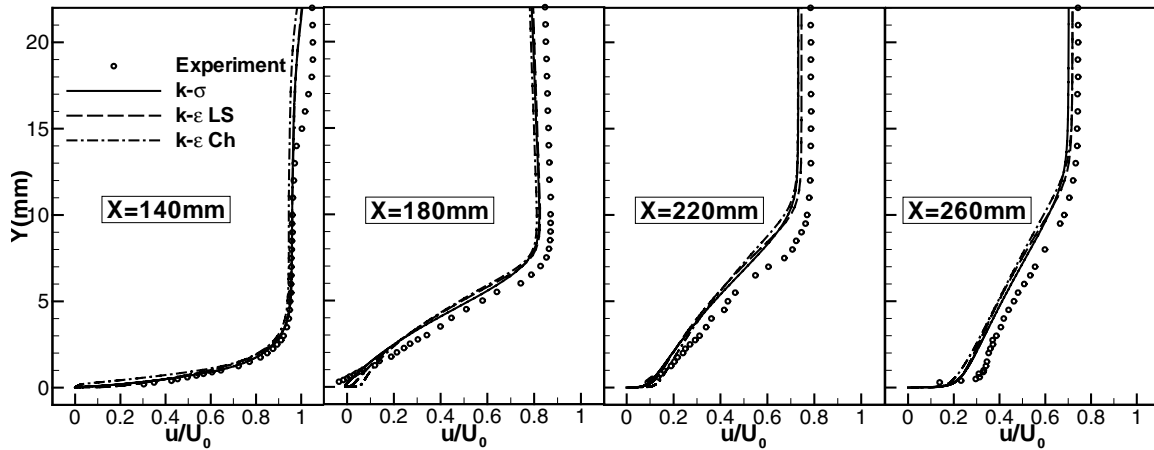
*Figure 8: Shock wave/boundary layer interaction with passive control.
Streamwise velocity profiles in the control region*

An important test for the validity of wall transpiration/suction modeling is the prediction of near-wall vertical velocity profiles. As a preliminary verification, the residual mass flow rate per unit span across the perforated plate, which should be zero, has been computed. In all the cases, the value of the ratio of this mass flow to the mass flow rate deficit $\rho_0 U_0 \delta_0^*$ in the upstream boundary-layer has been found to be lower than 10^{-5}. More detailed information is

presented in Fig. 9. Upstream of the compression system (X = 140mm), wall injection is predicted by all the models, the data at this station being compared to those obtained without control. We verify that the near wall values without injection, which should tend to zero, are affected by an error representing 1% of the upstream external flow velocity. Taking into account this experimental uncertainties, it is seen that the modeling of the passive control gives a fair prediction of the gross tendencies of the field's evolution.
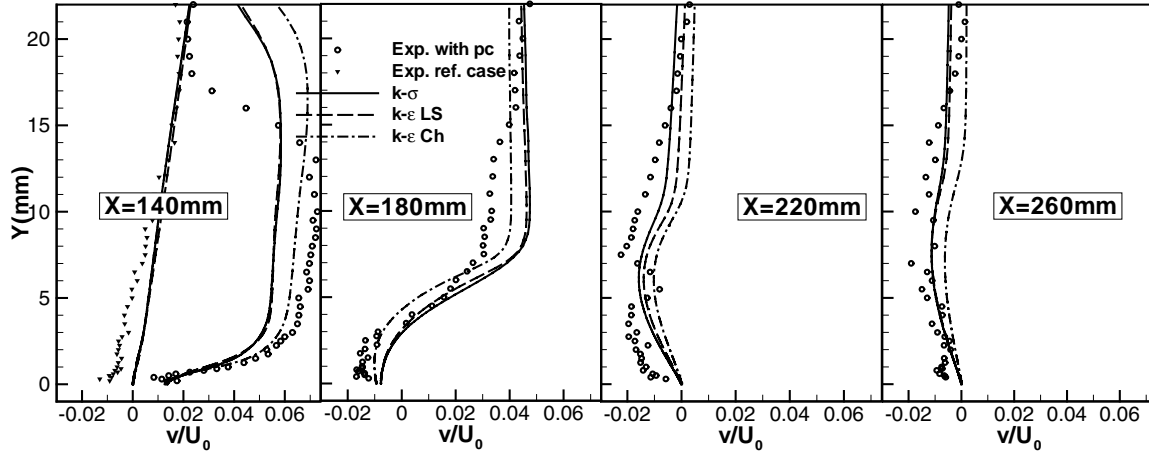
Figure 9: Shock wave/boundary layer interaction with passive control.
Transverse velocity profiles in the control region

At the interaction beginning (X = 140mm), the LS and [k-σ] models anticipate the growth of the maximum $\overline{u'v'}$ level, which is not the case with the Ch model (see Fig. 10). The agreement between the LS and [k-σ] models at X = 180mm is remarkable for this controlled interaction, the Ch model strongly overpredicting the maximum level of $\overline{u'v'}$. Downstream of the interaction region, the agreement between the LS and [k-σ] models is confirmed. The too rapid near-wall variation of the turbulent shear stress level in the downstream boundary-layer characterizes the Ch model.
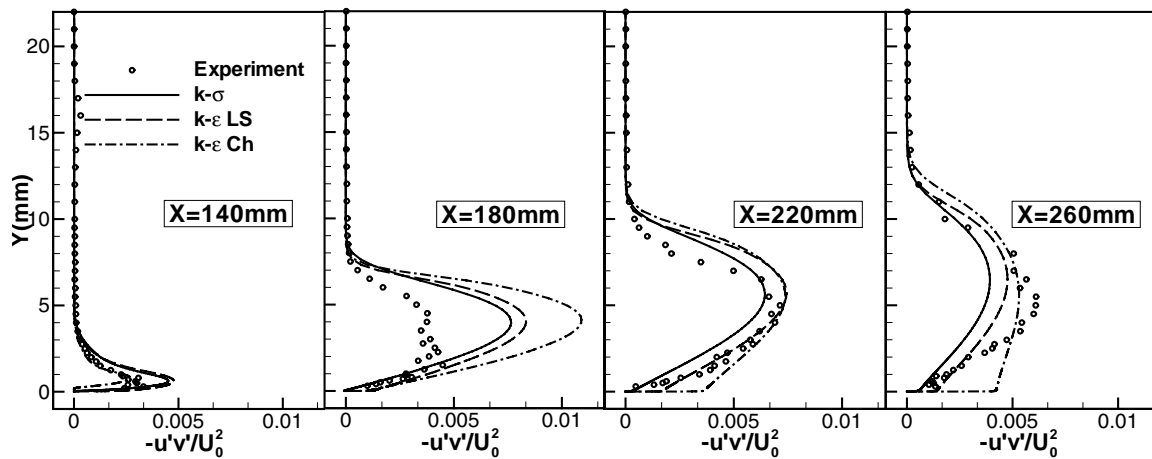
Figure 10: Shock wave/boundary layer interaction with passive control.
Cross-correlation profiles in the control region

3.4 A supersonic base flow

Aim of the operation. Validation of turbulence models requires an important number of calculations to perform the adjustment phase of the constants, which is the indispensable complement of the theoretical development of a turbulence model. Such parametrical studies are still difficult to execute with three-dimensional configurations because of the present technological limitations of the computers. Therefore, two-dimensional tests are still important and, among them, axisymmetric flows are the most appropriate configurations to obtain effective experimental two-dimensionality.

A satisfactory prediction of the turbulence evolution in largely separated flows is still not assumed by any of the presently existing turbulence models. A typical configuration where an extended zone of recirculation exists is the base flow, which constitutes an excellent test case for validating models. Base flows have been the subject of numerous experimental and theoretical studies since the fifties in order to understand the physics of such flows which are of prime importance for projectiles, missiles or space launchers. Due to the complexity of base flows, there is still a need to constitute reliable theoretical tools for predicting the drag of afterbodies and also the aerothermal loads on the base region of propelled afterbodies.

The main goal of the present study was to assess the ability of the [k-σ] two equation turbulence model to predict the mean field and some fluctuating quantities in a supersonic axisymmetric base flow. The chosen test case is an experiment executed by Herrin and Dutton (Herrin and Dutton, 1993) whose results are widely accepted for testing simulations and which has served as data base for previous theoretical studies on the subject (Sahu, 1992; Tucker and Shy, 1993; Espina and Piomelli, 1997; Fureby et al., 1999). Assessment of the model, using the Nasca code, is done by comparisons with these data and with the results given by three other well known models.

The flow field physics. The experiments of Herrin and Dutton were performed in a test facility specially designed to generate axisymmetric flows (Sauter and Dutton, 1989). In particular, profiles of mean and fluctuating velocity fields in the recirculating flow are provided by LDV measurements. The upstream Mach number has been determined from LDV (Herrin and Dutton, 1993) to be 2.46 $\pm$ 1%, while the static wall pressure measured just upstream of the base corner corresponds to a uniform flow with a Mach number of 2.44. During the present calculations we have chosen an upstream Mach number $M_0 = 2.45$.

The rapid variations of the fields and the turbulent mixing in the shear layer forming at the base shoulder are the first challenge for the modeling of the mean and fluctuating fields. Good precision in the prediction of the nearly constant pressure in the recirculating bubble, limited by the mixing layer and the rear stagnation point on the axis, is fundamental for base drag prediction. The recompression subsequent to the flow field realignment at the rear stagnation point is visible in Fig. 11, at the point where the recirculating flow progressively changes into a wake.
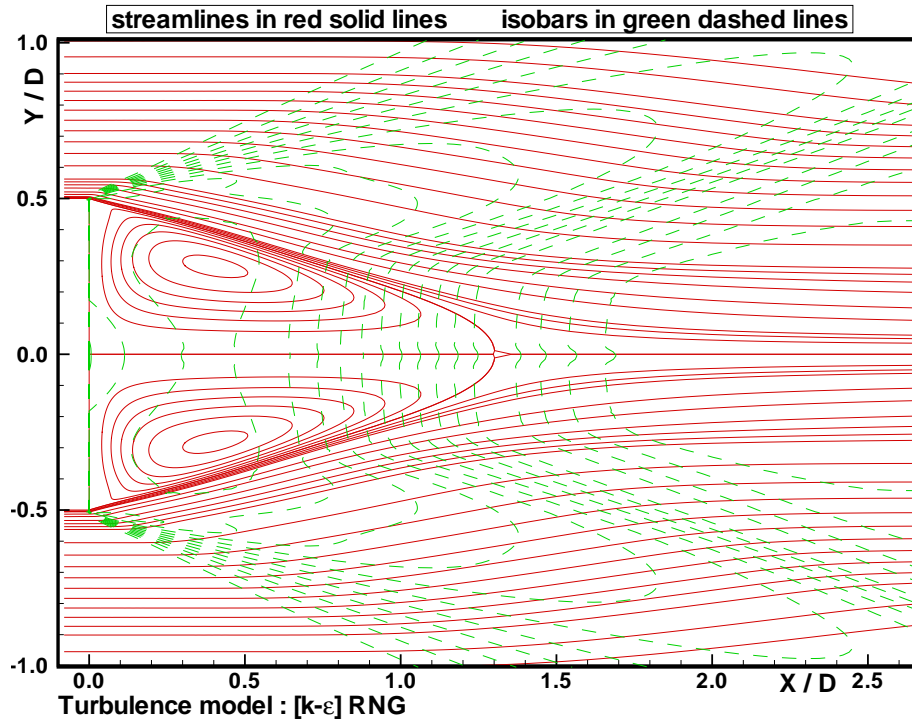
*Figure 11: Base flow in supersonic flow (Mach = 2.45).
Streamlines and pressure levels computed with a [k-ε] model*

The experiment of Herrin and Dutton provides us with data on the evolution of the boundary layer on a restricted part of the body beginning at a distance X = -0.079D from the base (D is the cylindrical body diameter). The experimental profiles at this location must be taken as upstream boundary condition for the computations.

A Navier-Stokes code confrontation. Here, turbulence modeling was carried out by means of a [k-ε] transport equation models whose derivation is based on a renormalisation of the Navier-Stokes equations. (RNG model) (Yakhot and Orszag, 1986), the Launder-Sharma (LS model) and three versions of the [k-σ] turbulence model.

The distributions of the calculated and experimental pressure distributions on the base are shown in Fig. 12. The experimental value of the ratio p_c / p_∞ of the mean base pressure to the uniform upstream pressure is equal to 0.55. This level is 10% higher than data on base flows at the same Mach number extracted from earlier experimental compilations (Délery and Sirieix, 1979). These computed base pressure values are considerably closer to experiment than that obtained with a Baldwin-Lomax calculation (see Fig.12), in agreement with previous studies (Sahu, 1992). However, they contradict overpredictive results obtained with other two equation models (Espina and Piomelli, 1997). In a recent computation using LES (Fureby et al., 1999), a level of 0.52 for the mean base pressure was found.
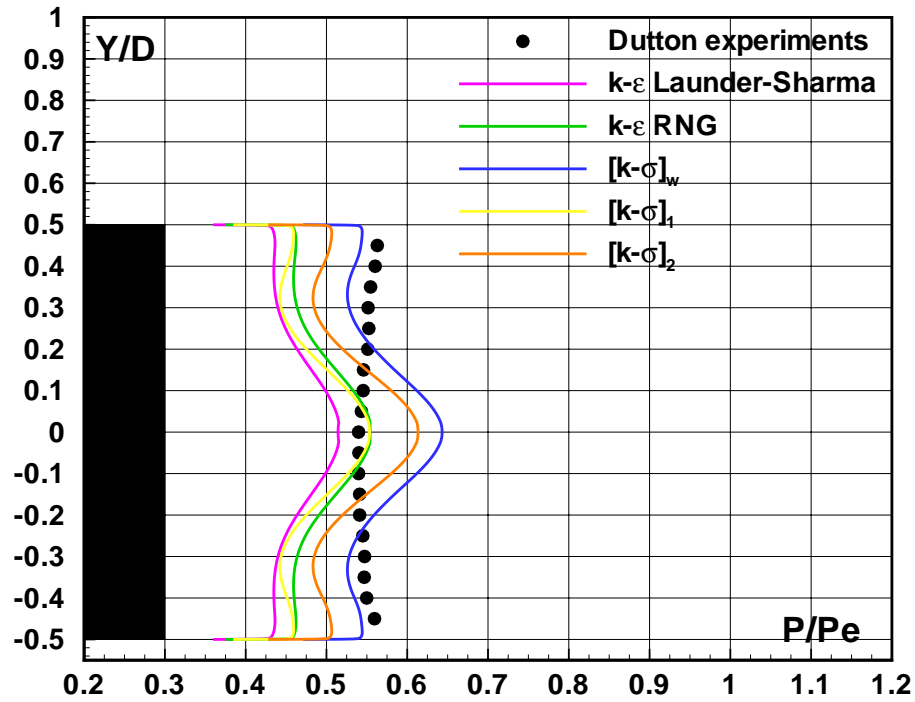
Figure 12: Base flow in supersonic flow (Mach = 2.45).
Base pressure prediction by the models

Profiles obtained in the middle of the bubble, at X = 0.63D downstream of the base, are shown in Fig. 13. A salient fact is the smoothing by the models of the shear stress evolution during the rapid transition between the mixing layer and the reversed flow. This smoothing explains the incapacity of the models to predict the nearly constant reversed flow region in the immediate vicinity of the base, the defect coming from an overprediction of the negative axial velocity on the axis. This too large radial variation of the axial mean velocity is also due to an excessive evaluation of the eddy-viscosity in the part of the bubble situated near the axis.
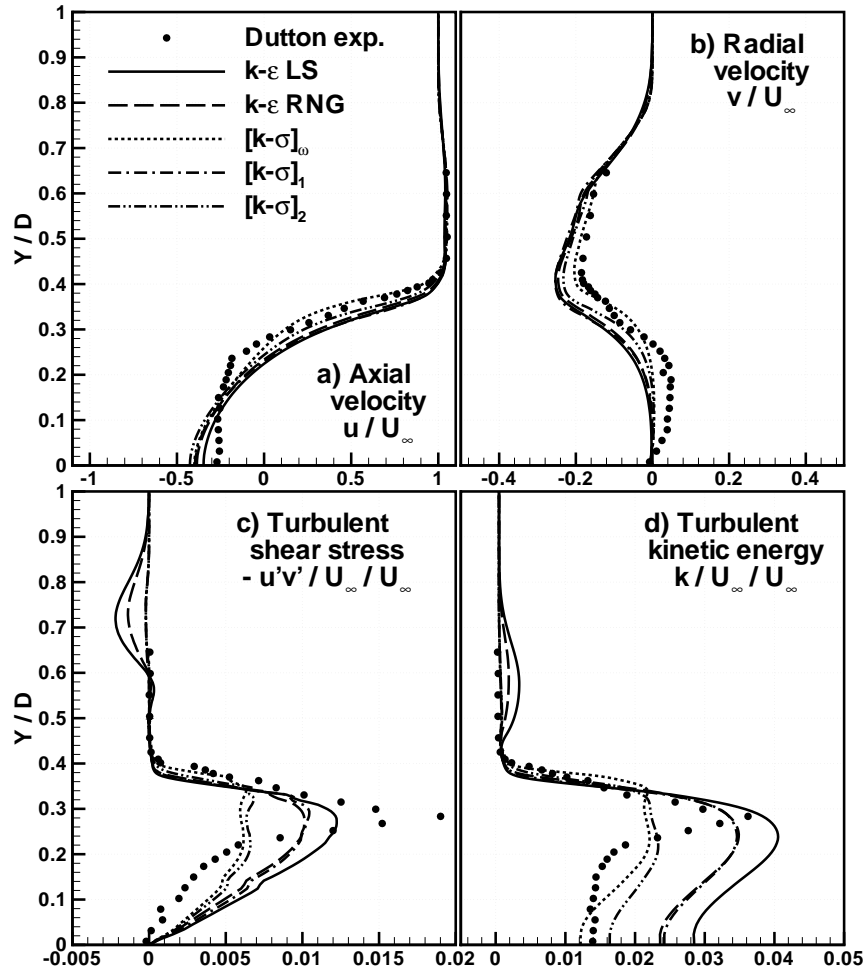
Figure 13: Base flow in supersonic flow (Mach = 2.45)
Profiles at X / D = 0.63

The results obtained by the RNG and $[k-\sigma]_1$ models are satisfactory at the rear stagnation point, located at X = 1.26D (see Fig. 14), except for the k profile. The good agreement of the axial velocity profile with experiment proves that the position of this stagnation point is well predicted by the two models.
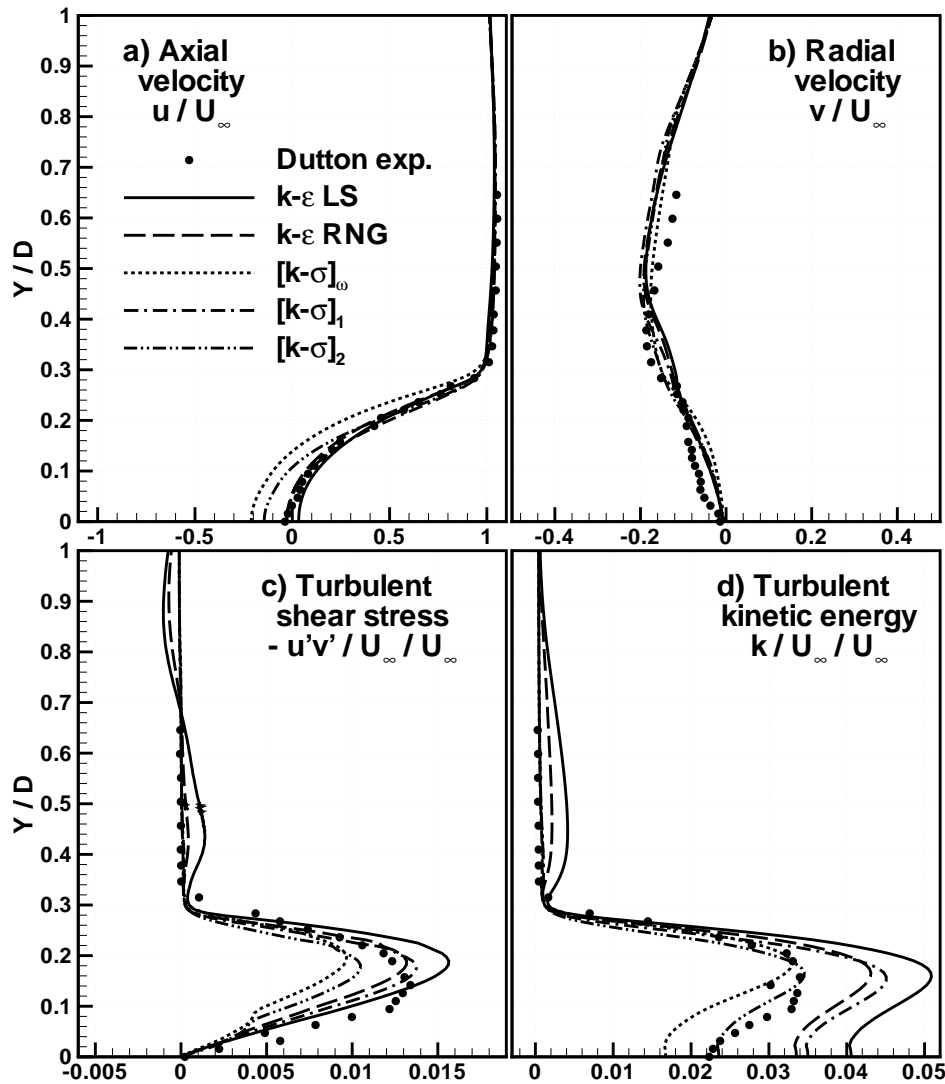
Figure 14 : Base flow in supersonic flow (Mach = 2.45)
Profiles at X / D = 1.26

3.5 Plug nozzle aerodynamics

Aim of the operation. The plug nozzle concept has been proposed in the 60s to limit thrust losses due to jet overexpansion and to confer to the nozzle some self-adaptation capabilities without having to modify its shape. In this arrangement, the supersonic expansion is realized along a center body - or plug - is place of an external contour, as in a classical nozzle. This idea has been reconsidered to equip hypersonic vehicles or space launchers having to fly in conditions strongly out of adaptation. Such nozzles can be linear or axisymmetric. In the later case, the flow coming from the engine can be ejected either through an annular throat or a series of small nozzles surrounding the plug. The present investigation has been focussed on the effects of interactions taking place between the flow produced by the nozzle and an outer supersonic stream (Reijasse and Corbel, 1997).t

The experimental part. This experiment was also executed in the S8Ch wind tunnel. A photograph of the afterbody model in the test section is shown in Fig. 15. The stagnation pressure p_{te} and the stagnation temperature T_{te} were equal to $0.99 \times 10^5 Pa$ and 297K, respectively. The $120 \times 120 mm^2$ test section was equipped with a two dimensional nozzle

designed to give a uniform Mach number equal to 1.95. The axisymmetric afterbody model is mounted at the end of a 40mm diameter central sting fixed upstream of the nozzle throat. The diameter of the model is also equal to 40mm. The model consists of a central annular plug nozzle mounted inside of a hollow cylinder. The cylinder is terminated by a boattail and a small base. The contours of the full-length annular plug nozzle was calculated by the method of characteristics in order to provide, in the case of a perfectly adapted jet, a uniform flow with a Mach number of 3 in the section at the end of the spike. The plug nozzles was fed with desiccated high pressure air at room temperature. The jet stagnation pressure could be varied from 1 to 10×10^5 Pa.
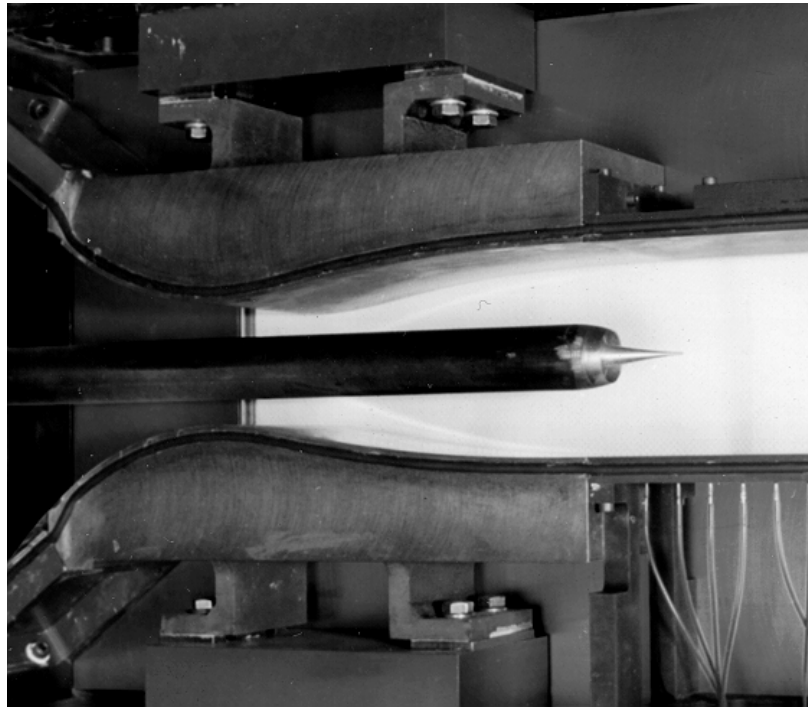
Figure. 15: Plug nozzle aerodynamics. Test set up in the S8Ch wind tunnel

The flow was qualified by means of schlieren visualisations (continuous and short exposure time), surface pressure measurements and probings in the flow vertical meridian plane with the two-component LDV system.

A Navier-Stokes code confrontation. The computed results for an expansion ratio $p_{stj}/p_{ste}=5$, have been obtained with the Nasca code by using the Launder-Sharma [k,ε] turbulence model and the [k,ε] RNG model . The comparison of the iso-Mach contours shown in Fig. 16 for the case of the Launder-Sharma model demonstrates again that a RANS calculation gives a faithful picture of the flow, although a deeper analysis of the results shows that discrepancies exist in the prediction of the strong interaction.
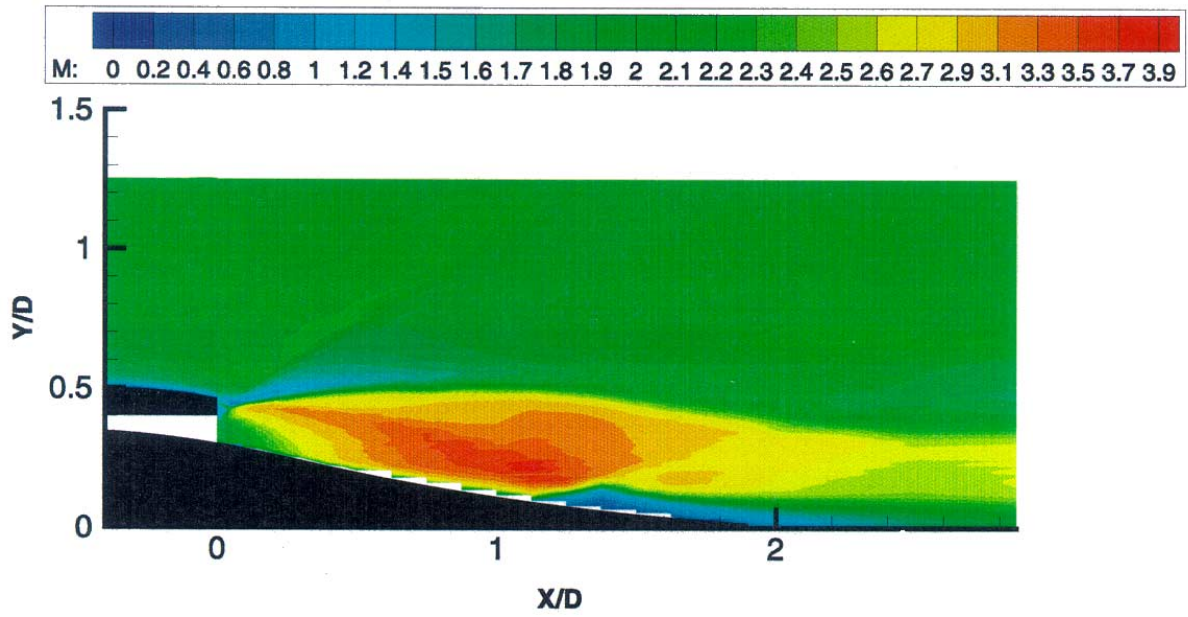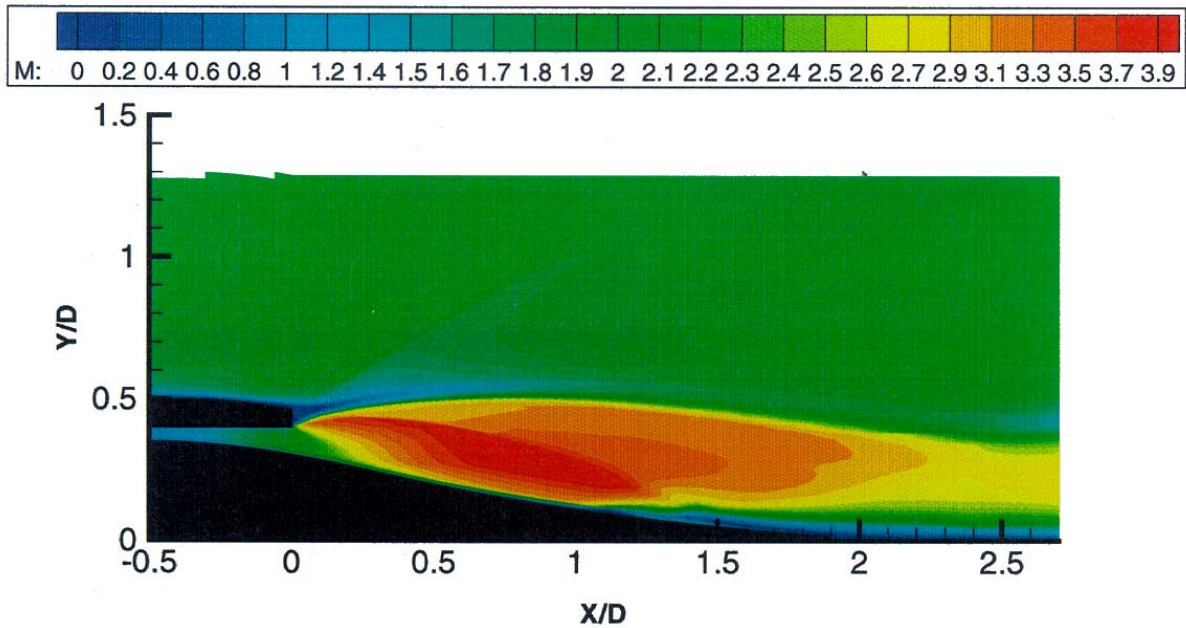
Figure 16: Plug nozzle aerodynamics. Mach number contours for p_{stj}/p_{ste}=5.
a - From LDV measurements, b - Navier-Stokes calculation

The aim of the theoretical exploitation of this experiment is to closely examine the ability of two equation turbulence models to predict mean and fluctuating fields evolutions around the spike. We take as examples, the profiles of the axial velocities, of the estimated turbulent kinetic energy and of the cross correlation u'v' on two stations of the spike situated respectively at 0.1 and 0.75 diameter downstream of the base (see on the preceding figures for these locations). The Launder-Sharma model (in red) is compared with the RNG model (in green) and with the experimental values. We see in Fig. 16, at 0.1 D, that the Launder-Sharma model predicts more satisfactorily the boundary layer developing on the strongly curved wall of the beginning spike. More downstream, at 0.75 D, we observe that the models overpredict the axial velocity (see Fig.17).
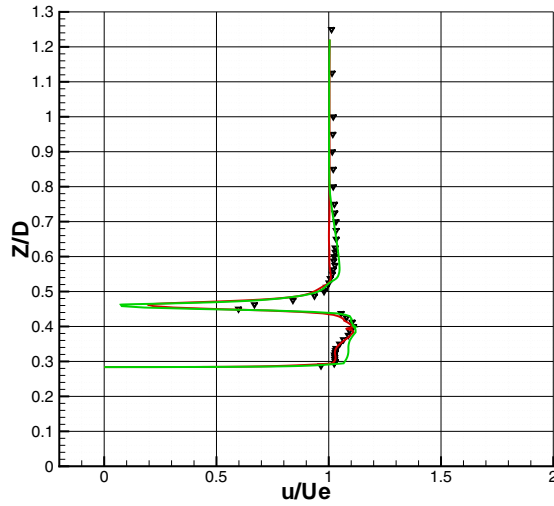
Figure 16: Plug nozzle aerodynamics
Longitudinal velocity profiles at X/D=0.1
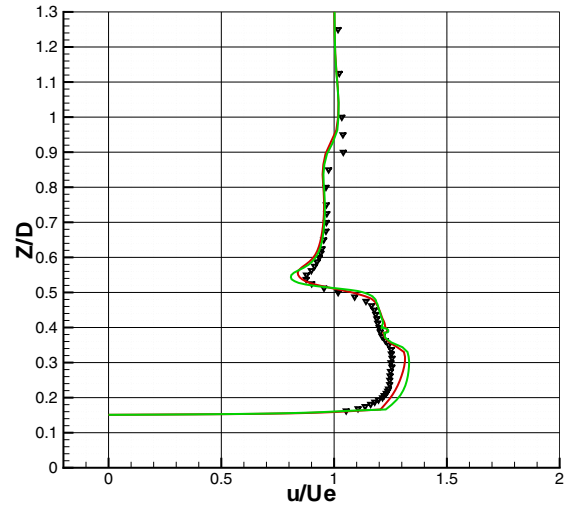
Figure 17: Plug nozzle aerodynamics
Longitudinal velocity profiles at X/D=0.75

The levels of cross-correlation are more satisfactorily predicted by the Launder-Sharma model (see Figs. 18 and 19).
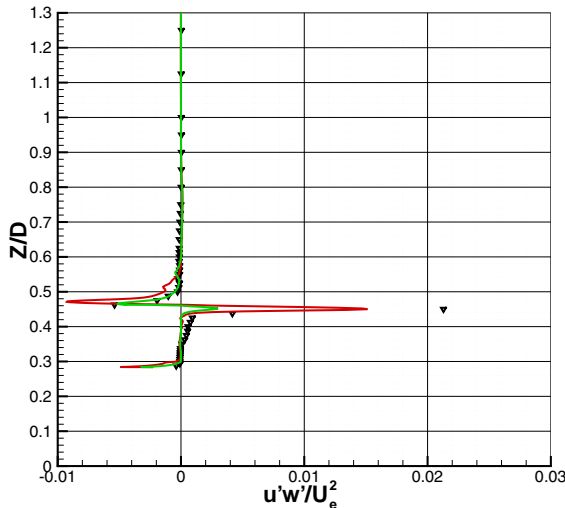
Figure 18: Plug nozzle aerodynamics.
Cross correlation profiles at X/D=0.1
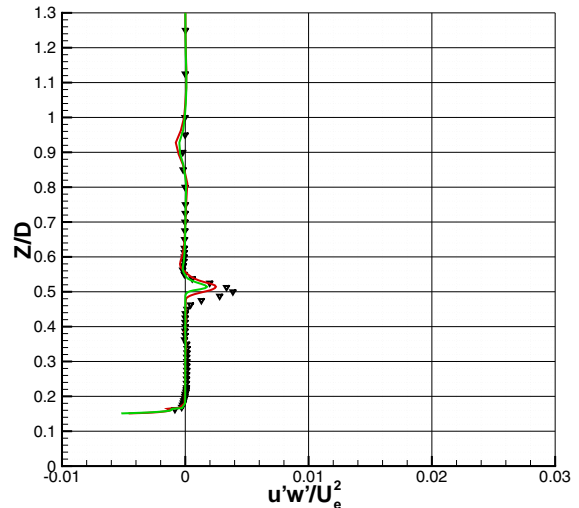
Figure 19: Plug nozzle aerodynamics.
Cross correlation profiles at X/D=0.75

4. CONCLUSION

The spectacular increase in our computing capacity during the past 30 years led to a certain despise of the experimental activity. It was anticipated that "numerical wind tunnels" will soon replace the noisy, difficult to operate, dangerous and costly real wind tunnels. This is not our purpose to enter into this polemics. It would not be wise, by reaction, to despise the computational activity which has taken a considerable place in the design and development of nearly all the industrial products (and in many other sectors too!). Because of the technical and scientific difficulties encountered in the domain and the necessity to rely on safe methods, the aerospace industry has strongly invested in the development of codes since the beginning

of the CFD era. Many of the numerical schemes have been devised to improve calculation methods for fluid mechanics applications, notably in the field of aerodynamics.

However, the development of more and more performant codes has not completely killed the experimental activity. Rather soon, it appeared that the confidence in code predictions was limited, the cause of the shortcomings being due partly to uncertainties in the numerical handling of the equations, partly to the lack of accuracy and representativity of the physical laws - or models - implemented in the codes. This perception of the reality has motivated a renewal of interest for experiments since only the confrontation with experimental data can validate - or invalidate - a code. To validate their codes, numericians need an as complete as possible information on some representative test cases. This information constitutes what is called a data bank which must respect certain rules to be useful. Thus, the data bank must contain a precise description of the configuration, along with all the necessary flow and boundary conditions. The measurements must be considered as safe, and if possible accurate. A great accuracy is not always mandatory (it costs much money), but uncertainty margins must be given.

Constitution of a data bank is not a straightforward operation. In addition of technical skill to fabricate a test set up, to operate the wind tunnel and execute the experiment, to perform the measurements, it requires a solid background in fundamental fluid mechanics. The data bank constitution is not limited to the acquisition of a vast amount of results, but must be accompanied by an in depth analysis of the flow physics. Because of the investment needed by such operations and their strategic importance for the development of predictive methods, the question of the data bank dissemination inevitably arises. It is now realized that a good data bank can be as precious as a code and cannot be freely transmitted. Even basic experiments have now an economic weight and cannot be put on the market without something in exchange. Thus, dissemination rules have to be more precisely defined according to the more or less precious nature of the data bank treasure.

In addition of the permanent scientific concern about more accurate, safer and less expansive predictive methods, the problem of the constitution of valuable, safe, well identified and permanent data banks is now considered as a strategic issue and addressed seriously. In this perspective, the Onera Fluid Mechanics and Energetic Branch has started the constitution of a data bank containing the most prominent experimental results obtained in its research wind tunnels of the Chalais-Meudon Center over the last 30 last years (Benay, 2001). This task will be actively pursued and the data bank contents fed with new experiments satisfying the quality criteria here above defined.

5. ACKNOWLEDGEMENT

6. REFERENCES

Benay, R. (2001) La base de données du DAFE. Mise à jour 2001 (The data bank of the Fundamental/Experimental Aerodynamics Department. Update 2001). Onera Rapport Technique N° RT 3/03589 DAFE, juillet 2001

Benay, R. and Servel, P.(1995) Applications d'un code Navier-Stokes au calcul d'écoulements d'arrière-corps de missiles ou d'avions (Application of a Navier-Stokes code to the calculation of flow past missile and aircraft afterbodies), *La Recherche Aérospatiale*, No. 6, pp. 405-426 (1995)

Benay, R. and Servel, P. (2001) Two-equation [k-σ] turbulence model: Application to a supersonic base flow, *AIAA Journal*, Vol. 39, No. 3, 2001, pp. 407-416

Bohning, R. and Doerffer, P. (1997) Passive control of shock wave/boundary layer interaction. In *Notes on Numerical Fluid Mechanics*, Vol. 56, Vieweg, 1997

Bur, R., Corbel, B., and Délery, J. (1998) Study of passive control in a transonic shock wave/boundary layer interaction. *AIAA Journal*, Vol. 36, No. 3, 1998, pp. 394-400

Borrel, M., Montagne, J.-L., Diet, J., Guillen, Ph. and Lordon J. (1988) Calculs d'écoulements supersoniques autour de missiles tactiques à l'aide d'un schéma décentré (Calculation of the supersonic flows past tactical missiles with a centered scheme). *La Recherche Aérospatiale*, pp. 2-20 (1988)

Chanetz, B., Benay, R., Bousquet, J.-M., Bur, R., Pot, T., Grasso, F. and Moss, J. (1998) Experimental and numerical study of the laminar separation in hypersonic flow, *Aerospace Science and Technology*, No. 3, pp. 205-218 (1998)

Chanetz, B., Bur, R., Pot, T., Pigache, D., Gorchakova, N., Moss, J. and Schulte, D.(1999) Shock wave/boundary layer interactions in low density flow: comparisons between flow field measurements and numerical results, *21st Int. Symposium on Rarefied Gas Dynamics - Vol. 2*, Brun, R., Campargue, R., Gatignol, R., Lengrand J.-C. Editors, Cepadues Eds., Toulouse, France, July 1999, pp. 537-544

Chien, K. Y.(1982) Prediction of channel and boundary-layer flows with a low-Reynolds-number turbulence model. *AIAA Journal*, Vol. 20, No. 1, 1982, pp. 33-38.

Délery, J. (1984) Shock-wave / turbulent boundary-layer interaction and its control. Edited by A.D. Young, *Prog. Aerospace Science*, Vol. 22, No. 4, 1985, pp. 209-280 ; also ONERA TP-1984-27, 1984

Délery, J. and Sirieix, M. (1979) Ecoulements de culot (Base flows). AGARD LS-98 on *Missile aerodynamics*, Ankara, Rome, Bruxelles, 5-16 March 1979, Onera T.P. n° 1979-14F

Espina, P.I. and Piomelli, U. (1997) Validation of the NPARC code in supersonic base flows". AIAA Paper 97-0032, Jan. 1997

Fureby, C., Nilsson, Y. and Andersson, K. (1999) Large eddy simulation of supersonic base flow. AIAA Paper 99-0426

Grasso, F. and Marini, M. (1996) Analysis of hypersonic shock wave / boundary layer interaction phenomena. *Computers and Fluids*, 25, pp. 1-21 (1996)

Herrin, J.L. and Dutton, J.C. (1993) Supersonic base flow experiments in the near-wake of a cylindrical afterbody. AIAA Paper 93-2924

Launder, B. E. and Sharma, B. I. (1974) Application of the energy dissipation model of turbulence to the calculation of flows near a spinning disc. *Heat and Mass Transfer*, Vol. 1, 1974, pp. 131-138

Moss, J. and Olejniczack, J. (1998) Shock wave/boundary layer interactions in hypersonic low density flows. AIAA Paper 98-2668

Moss, J.N., Pot, T., Chanetz, B., and Lefebvre, M. (1999) DSMC Simulation of shock/shock interactions: emphasis on Type IV interactions. *22nd International Symposium on Shock-Waves*, London, UK, July 18-23, 1999, Paper 3570

Poll, D. I. A., Danks, M., and Humphreys, B. E. (1992) The aerodynamic performance of laser drilled sheets. *Proceedings of the First European Forum on Laminar Flow Technology*, Hamburg, Germany, 1992, pp. 274-277

Reijasse, P., and Corbel, B. (1997) Basic experiments on non-adaptation phenomena in aerospike nozzles. AIAA Paper 97-2303, June 1997

Sahu, J. (1992) Numerical computations of supersonic base flow with special emphasis on turbulence modeling. AIAA Paper 92-4352

Sauter, J.M. and Dutton, J.C. (1989) Design of an axisymmetric supersonic wind tunnel and experimental study of supersonic, power-off base flow phenomena. Dept. of Mech. and Ind. Eng., Univ. of Illinois at Urbana-Champaign, UILU ENG 89-4002, Urbana, IL, March 1989

Schulte, D., Henckels, A. and Wepler, U.(1998) Reduction of shock-induced boundary layer separation in hypersonic inlets using bleed. *Aerospace Science and Technology*, 2, No. 4 (1998)

Stanewsky, E., Délery, J., Fulker, J., and Geissler, W. (Eds., 1997) *Euroshock - Drag reduction by passive shock control*. Notes on Numerical Fluid Mechanics, Vol. 56, Vieweg, 1997

Tucker, P.K. and Shyy, W.(1993) A numerical analysis of supersonic flow over an axisymmetric afterbody. AIAA Paper 93-2347

Yakhot, V. and Orszag S.A.(1986) Renormalisation Group Analysis of Turbulence. I. Basic Theory, *Journal of Scientific Computing*, Vol. 1, No. 1, 1986, pp. 3-51

This page has been deliberately left blank

————————————

Page intentionnellement blanche

Fast Aerodynamic Simulation for Military Procurement

M. Khalid, H. Xu, M. Mamou and S. Chen
Institute for Aerospace Research (IAR)
National Research Council
Ottawa, Canada, K1A 0R6

Tel: 613 998 3263
Mahmood.Khalid@nrc.ca

Abstract

Numerical simulation of airborne vehicle performance is of increasing importance to military. Such simulations become integral to procurement strategy when they can provide fast answers to performance related inquiries. Except for being able to identify the more challenging real time turbulence scales and other grid dependent issues related to complex configuration studies, the computational methods have matured to a stage where they are bringing virtues of different disciplines together, to couple efficiently for the best possible design. Increasing computational power has provided modelers the ability to seek more knowledge per design cycle and to increase the actual number of cycles. This article discusses some of the defence related projects in which IAR has used simulation techniques to provide timely answers to such questions as the performance of advanced missile systems, prediction of trajectories of stores released from rotor based and fixed wing aircraft and the use of optimization techniques for aircraft performance. The paper also emphasizes that for most standard performance studies, one may be able to use lower order computational methods to reach satisfactory conclusions.

Keywords: MDO, CF18 store release, Helicopter flow analysis, Missiles, Neural Network

Nomenclature

AR	Aspect ratio
C_f	Skin friction coefficient
D	Drag
ESF	Engine scale factor
h	Altitude
L	Lift
L/D	Lift-to-Drag ratio
M	Mach number
R	Range
SFC	Specific fuel factor
S_{ref}	Wing surface area
T	Throttle
t/c	Thickness/chord
W_E	Engine weight
W_F	Fuel weight
W_T	Total weight
x	Wing box cross section
xs	Horizontal displacement
zs	Vertical displacement

t	time (second)
Λ	Wing sweep angle
λ	Taper ratio
Θ	Wing twist

Introduction

CFD based simulation is beginning to play a very important role in military acquisition of hardware. The old and tried methods of using quick empirical formulation for preliminary estimates are still useful, but the availability of cheaper computer power means that one can, at least in the initial phase, resort to lower order computational tools to obtain better information regarding the performance of the vehicle. These methods provide fast answers to most of the steady state problems encountered under normal operational conditions. Under demanding maneuvers, it is accepted that the lower order computational methods may not be able to meet the complexity of the simulation challenge. For more critical performance regimes one may have to resort to more time consuming rigorous methods to provide the answers. Advances in multi-disciplinary optimization have also provided access to powerful tools for implementing extensive searches of performance parameters across disciplines to obtain optimal combination of characteristics available.

The paper outlines the methods adopted at IAR for conducting simulation studies of military aerospace vehicles to examine their attributes and capabilities both for procurement and in- service performance under a variety of deployment situations. These numerical simulations may range from direct understanding of vehicle performance under standard flight envelope conditions to studies of stores and non-conventional mission kits attached to, and released from airborne military vehicles. For the new procurements, as indeed for the case of the Maritime Helicopter, the Department of National Defence may authorize advanced studies of vehicle performance for a better understanding of the expected service from the anticipated purchase. Very often, the numerical methods of different orders of accuracy as well as optimization techniques may be utilized in conjunction with the wind tunnel measurements to obtain quick and economically efficient answers to some of the more urgent questions.

The Simulation Methods and Discussion

Procurement of fixed wing or rotor-based aircraft, for example, has to go through a very orderly sequence of milestones. In the first stage, it is appropriate to prepare a list of performance requirements expected from the new procurement. The second step would be to identify a short list of the potential contenders, which satisfy all or many of the requirements. Multidisciplinary design optimization (MDO) techniques are advanced at the present time to provide information on the best performance configurations during the program definition phase. Recently, IAR carried out an instructive exercise using the advanced decomposition MDO algorithms, the Bi-Level Integrated System Synthesis (BLISS) [1], the Concurrent Sub-Space Optimization (CSSO) [2] and the Collaborative Optimization (CO) [3] methods to achieve at an optimized configuration designed for a supersonic performance.

The first phase in this procedure is to identify potential configurations in the market, which agree best with this configuration. For an easy management in design, these three methods decompose the complex system design into several subsystems along the line of different expertise, such as the structure, aerodynamics, propulsion and performance in an aircraft design optimization. These subsystems are able to perform optimizations concurrently and then the system gathers information from the subsystems to optimize the maximum range. The coupling information is exchanged between the subsystems and the system through the proper definitions of the objective functions and the constraints (CO), the simulation models (CSSO), and the sensitivity analysis (BLISS). For example, Figure 1 describes the typical steps needed in the BLISS optimization procedure. Table 1 is the optimization results for a supersonic jet design performed by the three methods. The analysis in each subsystem used empirical functions at the current stage. In future studies it

would be appropriate to use more advanced specific CFD techniques to simulate the characteristics of the chosen models. The design time would mostly depend on the CFD analysis for a specific configuration.

Design Variables		R (nm)	λ	x	C_f	T	t/c	h (ft)	M	AR	Λ (deg.)	S_{ref} (ft²)
Initial Value		3378	0.25	1.0	1.0	0.5	0.05	45000	1.6	5.5	55	1000
Optimal Value	CO(S)	3990	0.12	0.99	1.18	0.127	0.08	55442	1.5	5.5	56	1047
	CSSO-RS	3235	0.4	0.84	0.99	0.208	0.081	59154	1.7	3.6	44.7	1208
	BLISS	3235	0.4	0.75	0.75	0.156	0.06	60000	1.4	2.5	70	1500

Coupling Variable		W_T (lb)	W_F (lb)	Θ	L (lb)	D (lb)	L/D	$SFC.$	W_E (lb)	ESF		
Initial Value		41195	11254	1.0285	46231	5264	9.5	0.8818	6550	0.536		
Optimal Value	CO(S)	45207	37708	1.9927	38839	4313	5.8	0.954	7882	0.949		
	CSSO-RS	46828	16241	1.0641	46828	5332	8.783	1.1451	6739	0.530		
	BLISS	51411	7306	1.0002	51411	13478	3.814	1.1075	7058	0.556		

Table 1: Optimization results for a supersonic jet design.

What is most relevant perhaps is that the optimization techniques are being applied to disciplines beyond the traditional line of thinking where one may have considered balancing structural parameters against aerodynamic characteristics. It is providing aerodynamicists a better means to bring the combined benefits of such diverse disciplines as maintainability, variation within the design process as well as design reconfiguring, life cycle costs, fuel economy, maintenance, training, support and a whole new approach to the complete system integration processes. Advanced MDO methods and other numerical modeling techniques have also increased the ability to obtain more knowledge per cycle and the number of design cycles executable in a given time. In a recent neural network study of at IAR [4], optimization based solution were readily used in conjunction with wind tunnel testing to reduce the total number of runs required to clear the store trajectory of a missile released from a CF-18 aircraft. Figure 2 shows the predicted results of the four aerodynamic coefficients by the trained network at M = 0.95, AOA = 0°, and AOA = -3° and -15° respectively. The predictions are in good agreement with the wind tunnel data for all travel paths.

Following the initial phase of shape estimates and performance definitions, the simulation team should produce suitable CFD models of the selected configurations to critically investigate the performance under all operational regimes. For performance investigation under cruise conditions with attached and/or mild separation flows on exposed surfaces, most panel methods are satisfactory. Figure 3 shows a typical example of CFD calculation for a helicopter. With sufficient expertise available in a team it would be possible to produce a good potential method based solution in a couple of days on an SGI Origin 2000 type platform with 8 CPU's. Clearly, panel methods are not expected to cope with flow complexities typically associated with landing and take off maneuvers and more demanding Euler and/or Navier Stokes based computational methods for such studies should be used.

For a more thorough understanding of viscous separating flows, one should to utilize more suitable Navier – Stokes methods. However, there is still an element of uncertainty because of the unsteadiness and interference from the rotor flow. There have been attempts made to acquire a better understanding of the rotor flow using coupling techniques, which treat the rotor as an actuated disk boundary condition in the main flow field [5]. However, this is still an empirical fixing, as the method cannot account for the instantaneous flapping or twisting of the rotor blades. A more advanced simulation would involve treating the rotor blades as separate surfaces represented individually in a Chimera block, which is housed in the outer parent grid. The flow past

each rotational setting of the Chimera block is updated in a quasi-steady fashion to obtain a better understanding of the flow. Results from one such study on ROBIN generic helicopter configuration is shown in Figure 4. A purely unsteady version of this simulation would be addressed when the rotation of the Chimera grid is automatically synchronized with the computational time step of the overall calculation. In terms of turn around times, more complex Navier-Stokes methods for steady solution may require a couple of weeks of meshing and solution. Whereas, quasi-steady or unsteady flow investigation for moving rotor equipped vehicles may require several months to obtain a satisfactory solution. CFD simulations on fixed wing aircraft are comparatively easier to perform. Given that the Navier Stokes method can be considered as most reliable predictive tools next to the actual wind tunnel measurements, panel methods can provide most of the design features during cruise conditions. A comparison of the computational effort required in producing CFD based simulations on an SGI Origin 2000 machine with 8 CPU's for a Bell 412 helicopter using panel methods and more rigorous Euler and Navier-Stokes solutions is shown in Table 2.

Method	Potential based Panel Methods	Euler equations based solution	Navier-Stokes equations based solution
Grid (PY- days)	5	6	7
Steady solution at one rotor setting	Up to 4 hours, depending on the number of panels	5 days	10 days
Complete quasi- steady solution	1 day	10 days	20 days

Table 2: Comparison of turnaround times for CFD based solution on Bell 412 helicopter.

Frequently, equipment vendors have not addressed the extended military implications, which are of primary interest for the procurement. For example, under theatre military situations, the helicopter may be required to perform under conditions for which it was never planned. It was perhaps never designed to carry the type of mission kits and pods that it is subjected to under battle conditions. Computational models do provide the expediency, convenience and accuracy of conducting such studies.

The simulation techniques become increasingly useful when one considers small variation in designs or impact of small protuberances on otherwise smooth aerodynamic designs. In fact one such study was conducted to examine the effect of tiny attachment lugs, which support a missile to a wing surface under carriage conditions. It was learnt through a CFD study that the attachment lugs have strong aerodynamic implications on the performance of the released missile. Figure 5 shows the computed flow past the missile with lugs. The lugs invoke separation effects on C_D and C_N and other aerodynamic interference beyond their size and blockage area.

As mentioned earlier, IAR is also involved with the Canadian Department of National Defence (DND) in studying safe trajectories of weapon systems ejected from a moving platform. Again as the first option one would use the quick and ready potential based methods to carry out the preliminary investigation. However, it would be necessary to carry out a comprehensive validation exercise before applying panel methods for trajectory calculations. The results from one such exercise involving the use of USAERO to calculate the drop of a store from a standard wing are shown in Figure 6. The computed results show encouraging agreement with measurements obtained from literature. The same approach was then adopted to compute the trajectory of the MK82 missile when released from the Bell412 helicopter [6]. The solution is shown in Figures 6 and 7.

For a fixed wing aircraft the approach is very similar. Figure 8 shows a typical CF-18 aircraft configured in a panel grid format. USAERO based computations were carried out to study the path of the stores as they are released from the aircraft. More rigorous studies of this concept have been performed at IAR by Fortin and Benmeddour [7], using more advanced Euler techniques. A typical JDAM store separation from CF-18 is shown in Figure 9 at 0.24s after release. The resources, time and effort required to conduct a panel method based trajectory computation is much smaller than those required for more accurate Euler and Navier-Stokes

investigations. Typically one would require a period of up to one week to construct a satisfactory panel grid followed by a few days of USAERO computations. This would be a fraction of the time, effort and computational resources required to perform a similar Euler or Navier-Stokes equations based study. The first order method may provide a good estimate of a store release trajectory, which has substantial safety margins. In situations where the miss distances are small, one would require more rigorous Navier-Stokes based analysis.

Conclusion

Simulation techniques are beginning to play an increasingly important role in assessing the performance of airborne vehicles procured by DND. Optimization techniques and other CFD methods can be used effectively for evaluating the most appropriate configurations, for given requirements.

Numerical modeling is also extremely useful for studying off-design military applications and other small variations in configuration during the in-service life of a procured vehicle. Fast panel method techniques could be very useful in quick estimates of performance under normal operations. For more challenging maneuvers involving complex surface deployments, one may have to resort to more tedious numerical techniques.

Acknowledgement

References

1. Braun, R. D. and Kroo, I. M. (1995), "Development and Application of the Collaborative Optimization Architecture in a Multidisciplinary Design Environment", SIAM Journal, pp. 98-116.
2. Sell, R. S., Batill, S. M. and Renaud, J. E. (1996), "Response Surface Based Concurrent Subspace Optimization for Multidisciplinary System Design", AIAA Paper 96-0714.
3. Sobieszczanski-Sobieski, J., Agte, J. S. and Sandusky R. R. (1998), "Bi-Level Integrated System Synthesis (BLISS)", NASA /TM-1998-208715.
4. Jiang L. Y and Tang, F. C., (2002) "Application of Neutral Networks of Store Loads Grid-Survey", 40th AIAA Aerospace Science Meeting & Exhibit, Jan. 14-17th, Reno Hilton, NV, AIAA-2002-0281.
5. Xu, H., Khalid M. and He, P. (1999), "Steady/Unsteady Flow Field Calculations on Bell 412 Helicopter using CFD Methods", 7th Annual Conference of the CFD Society of Canada.
6. Khalid, M., and Xu, H., and M. Mamou (2001), "Development of the CFD Capability for Rotor Flowfield Analysis at IAR", CASJ, 47, pp. 139-146.
7. Fortin, F., Benmeddour, A. and Jones D.J. (1999) "Application of the Canadian Code to the F/A-18C JDAM Separation", 37th AIAA Aerospace Sciences Meeting and Exhibit, Jan. 11-14th, Reno NV, AIAA 99-0127.
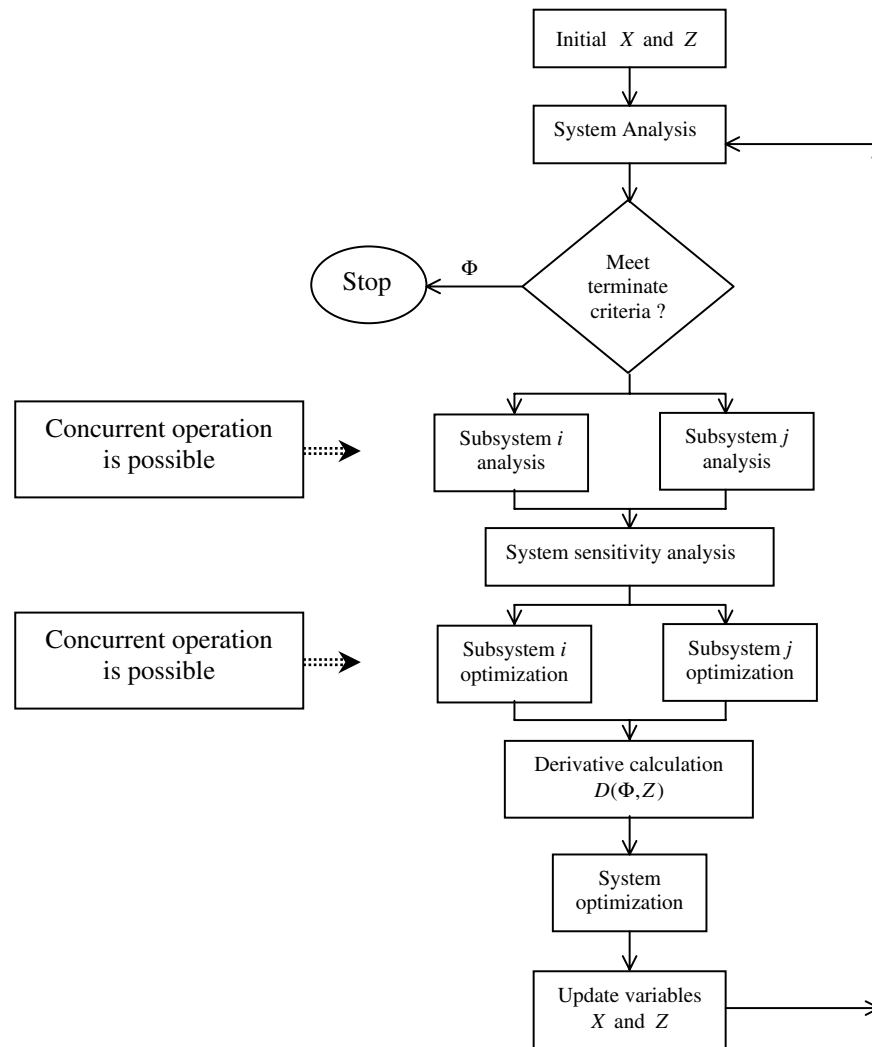
Figure 1: Flowchart of BLISS Algorithm.
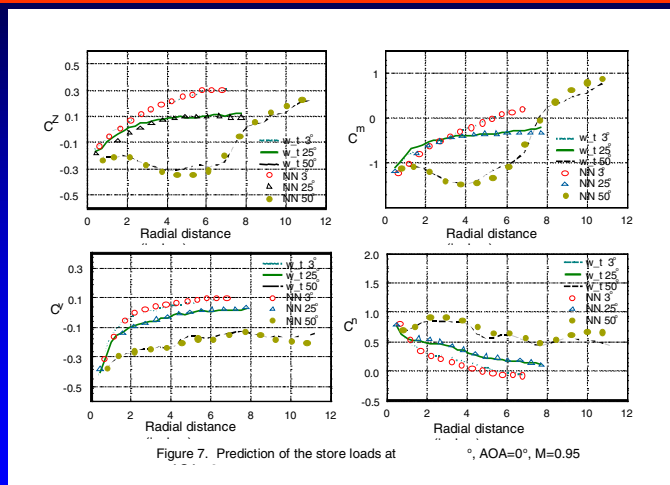
Figure 2: Predicted results of the four major aerodynamic coefficients by the trained network at M = 0.95, AOA = 0°, -3° and -15°, respectively [4].
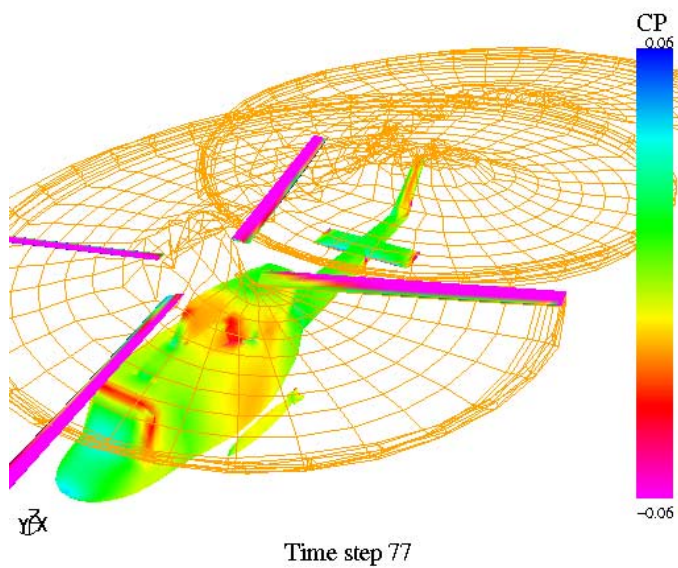
Figure 3: Typical example of CFD prediction of a helicopter flow field.
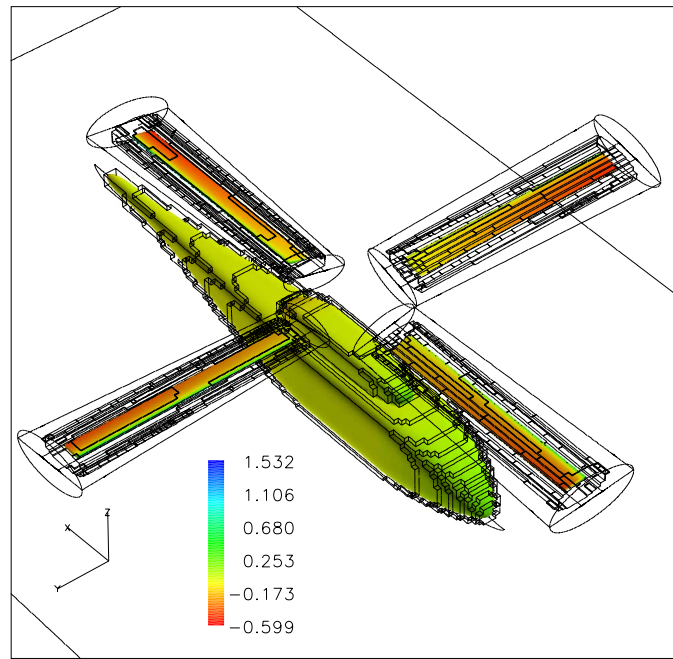
Figure 4: Robin generic helicopter configuration, meshed by Chimera grid technique.
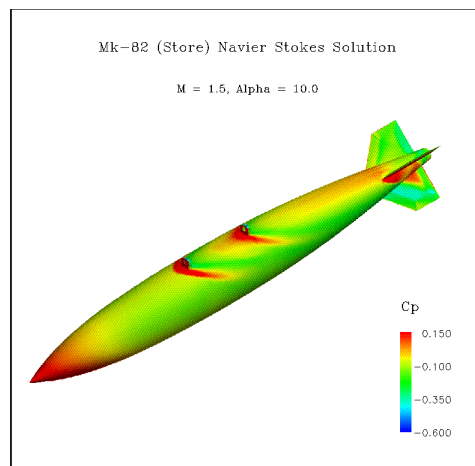
Figure 5: The aerodynamic effect of attached lugs.

Time step 121
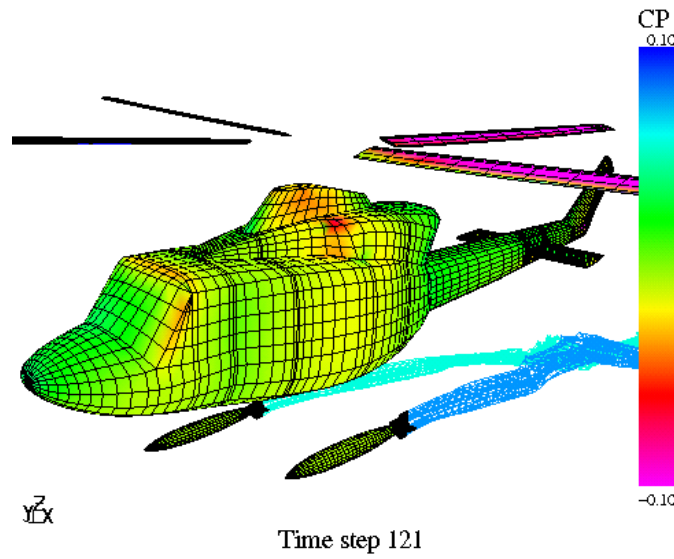
Figure 6: Panel method based modeling of MK82 missile dropped from Bell 412 helicopter.
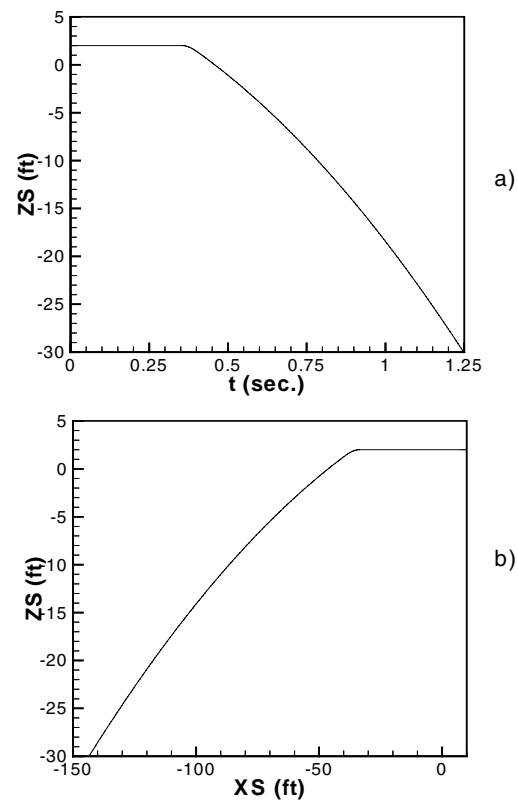
Figure 7: Store release trajectories for a calibration model.
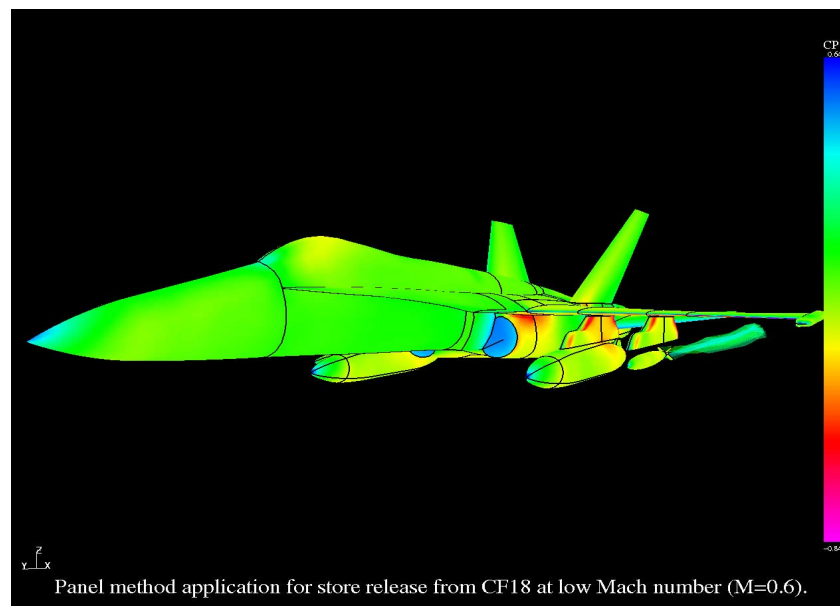
Figure 8: USAERO based computations for the flow around a typical CF-18 aircraft.
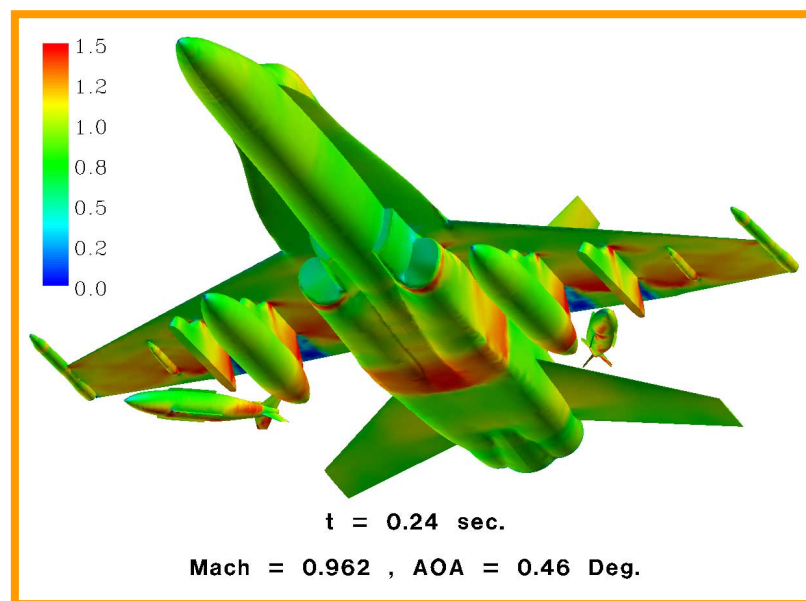
Figure 9: Store release calculations at IAR showing Mach number flow field, M_∞= 0.962, AOA = 0.46° altitude 6332 ft. , dive angle = 43° [7].

Optimesh: Anisotropic Mesh Adaptation with CAD Integrity for Verifiably Accurate CFD Solutions over Complete Aircraft

Wagdi G. Habashi, Claude Y. Lepage, Guido S. Baruzzi and Iyad Akel
Newmerical Technologies International
680 Sherbrooke Street West, 7th Floor
Montreal, QC, Canada H3A 2M7

Introduction

The accuracy of the numerical solution of a Partial Differential Equation (PDE) is a function of the order of the leading terms of the truncation error of the numerical algorithm. These terms in turn depend both on the higher order derivatives of the solution variables and on the local mesh size. In practical applications it is important to guarantee a sufficient level of accuracy, if not mesh independence, of the solution. This condition is normally reached by comparing solutions obtained on successively refined grids, a procedure that is empirical and time-consuming, and further complicated by the fact that mesh generation is conducted heuristically, since the solution is not known in advance.

Given the nature of the truncation error of the numerical algorithms for the solution of PDEs, two basic methods for improving the accuracy of a solution can be readily identified: a) construction of higher-order schemes or, given a fixed numerical scheme, b) to control the numerical error via grid optimization.

In industry, while run-time efficiency is important, access to a code's source may not be guaranteed and it can be impractical to modify existing codes. In addition, commercial code vendors may not be over-enthusiastic about introducing a generic and revolutionary mesh adaptation process, because it may show the shortcomings of the current version of their code. Therefore, a more effective approach consists in adapting the grid to the solution, without access to the source. The process ideally begins with an arbitrary mesh, hopefully coarse and generated by a non-expert, and leads to a highly adapted customized grid, tailor-made to each application. Thus, no expensive algorithm modifications are required and any CFD code can satisfy a predefined level of accuracy, as desired or as required by the problem specifications, without user intervention. This strategy is ideal for parameter sensitivity studies, for example, where all the different solutions could be obtained on automatically adapted grids generated from a single original grid. In such case one becomes sure that the change in performance I sure to the change in parameter and not due to any sensitivity to the grid.

The code discussed here represents an advanced novel anisotropic mesh adaptation approach for unstructured grids that allows the customization of grids based on a specified error level. Equally important, it maintains the CAD integrity of the given geometry. Perhaps the best showcase of the abilities of this software is the adaptation of unstructured tetrahedral meshes over a complete Airbus 320 and a Boeing 747 with flow-through engine nacelles.

Methodology

Any (anisotropic) mesh adaptation algorithm requires two fundamental components: an a-posteriori error estimator and a mechanism to coarsen, refine, swap and stretch the mesh. In general it is impossible to evaluate the exact truncation error of the numerical approximation of a PDE or system of PDEs, since the numerical approximation is only piecewise continuous and in any case the exact solution is unknown. Most of the error estimators in use are based on the first derivative or the residual of a user-specified solution variable. The error estimator proposed here is based on the Hessian (matrix of second derivatives), which is a better representation of the truncation error between the PDEs and the discrete equations actually solved. The Hessian matrix provides not only information on the error density, but also on its directionality, thus making anisotropic mesh adaptation possible.

The edge-based error density γ can be written as:

$$\gamma = \int_0^1 \sqrt{\Delta \mathbf{s}^\mathrm{T} \mathbf{M} \, \Delta \mathbf{s}} \; dt$$

where Δs is the edge length, M is the Hessian matrix and t is the non-dimensional parametrization variable along the edge. Once the error density is determined for every edge in the grid, the user must select the desired error level for the adaptation. Unless dictated by the specific problem, an appropriate error density can be selected visually with any graphic interface.

The Mesh adaptation procedure consists of four main steps: a) edge coarsening, b) edge refinement, c) edge swapping and d) node movement. Steps a) and b) can be deemed binary operations, since two connected edges are combined into one, or one edge is split in two, respectively. These two operations may produce grids that are not optimal, therefore the edge swapping mechanism will correct the orientation of any edge that might not be properly positioned and lead to distorted meshes. Node movement stretches and realigns the edges along the proper direction, and ensures that the error is equi-distributed and the maximum and minimum edge lengths and the minimum aspect ratio are respected. Coarsening, refinement and swapping can be regarded as accelerators for mesh movement.

Node movement is based on a spring analogy, where each element edge in the grid is represented by a spring with a coefficient of elasticity proportional to the error density. The goal in this case is to equi-distribute the error across the computational domain. The original CAD surface definitions are used at each step to ensure that surface nodes are reprojected on the proper surfaces and the original geometry is fully respected. Since the mesh adaptation procedure is a nonlinear process, steps a) to d) are repeated in cycles at every adaptation.

Several control parameters are available to control the quality of the final mesh, among them aspect ratio and a maximum deviation on curvature. High maximum aspect ratio values can lead to extremely stretched grids, and while FENSAP has no difficulties handling highly stretched grids, other flow solvers might. Maximum deviation on curvature allows one to determine the acceptable level of coarseness on curved surfaces that prevents poor surface rendition. This may be noticeable on the lips of the nacelles or on wing tips, where surface curvature is high. In general the meshes adapted show much more faithful renditions of the original CAD than even the finest original meshes.

There is no question that mesh adaptation provides a useful and necessary tool. The expense incurred in adapting the mesh and recomputing the flow solution again and again is not negligible, therefore the focus of our research is to provide some guidelines to facilitate the choice of parameters by illustrating their effect on the mesh quality and overall solution time. The subject of

grid convergence, important from the point of view of computational efficiency, will also be addressed.

Results: Mesh Adaptation on a Boeing 747 and an Airbus 320

Both the Boeing 747 and Airbus 320 feature fuselage-wing-pylon-nacelle geometries, but the Airbus 320 has simple flow-through engine nacelles, while the Boeing 747 has both engine nacelles and fan shrouds and in addition some detail of the cockpit windows. For both geometries, the outer boundary is a hemisphere with a diameter of approximately 40 fuselage lengths. Flight conditions for the Boeing 747 are: Mach number=0.88, altitude of 35,000ft and AoA of 4º. Flight conditions for the Airbus are: Mach number=0.8, altitude of 30,000ft and AoA of 3º. The CFD solutions were obtained with FENSAP (Finite Element Navier-Stokes Analysis Package), also a proprietary technology of Numerical Technologies International.

For the Boeing 747, the initial tetrahedral grid contains 431,181 nodes and 2.3 million linear tetrahedral elements. The error density target value was set y=0.15 and remained constant for all the subsequent adaptations. The minimum and maximum element edge sizes were set at 0.025 in and 25,000 inches. respectively, compared to a fuselage length of approximately 2,700 inches. Eight complete cycles of solution and adaptation were performed. After six adaptations, the final grid size had decreased to 242,310 nodes and 1.3 million tetrahedral elements, an decrease of 43%, for an immense improvement in accuracy.

It should be noted that some intermediate grids, say from iteration 1-3, may become somewhat larger than the original as mesh adaptation begins to cluster the mesh near the salient features (discontinuities and vortices in this case). This phenomenon is related to the density of the original mesh, and how well it captures the initial solution. Initially the discontinuities are smeared and require much refinement, but as they become sharper stretching and coarsening remove some of the grid points and the mesh size begins to decrease. Note that in 3D discontinuities are surfaces and hence it is difficult to estimate the extent of the refinement just by looking at the surface mesh.

The adapted grid shows substantial coarsening on the lower wing surface and refinement on the upper surface. The outboard wing shock is very well captured, and the inboard shock is also beginning to appear. A comparison of the initial and final upper wing grids and corresponding solutions of the Airbus 320 are shown in Figure 1. Figures 2, 3 and 4 show some surface grid details and solutions of the Boeing 747. Note in Figure 5 how adaptation has improved the discretization of the fan cowl lip. Figure 6 shows the Cp distribution at three spanwise locations before and after adaptation. Finally, Figure 7 shows the sequence of error distributions in the computational domain as the adaptation-solution cycles evolve. Note that there is little change from cycle 5 to cycle 6 and the adaptation procedure is converged.

Conclusions

Mesh adaptation is a powerful and cost-effective tool that can be used to increase (or decrease if so desired), to a specified and uniform level, the computational accuracy of any given CFD code without extensive algorithm redesign or initial investment in grid generation. Furthermore the cost of ensuring mesh independence is substantially reduced, and the error level of the results can always be guaranteed.
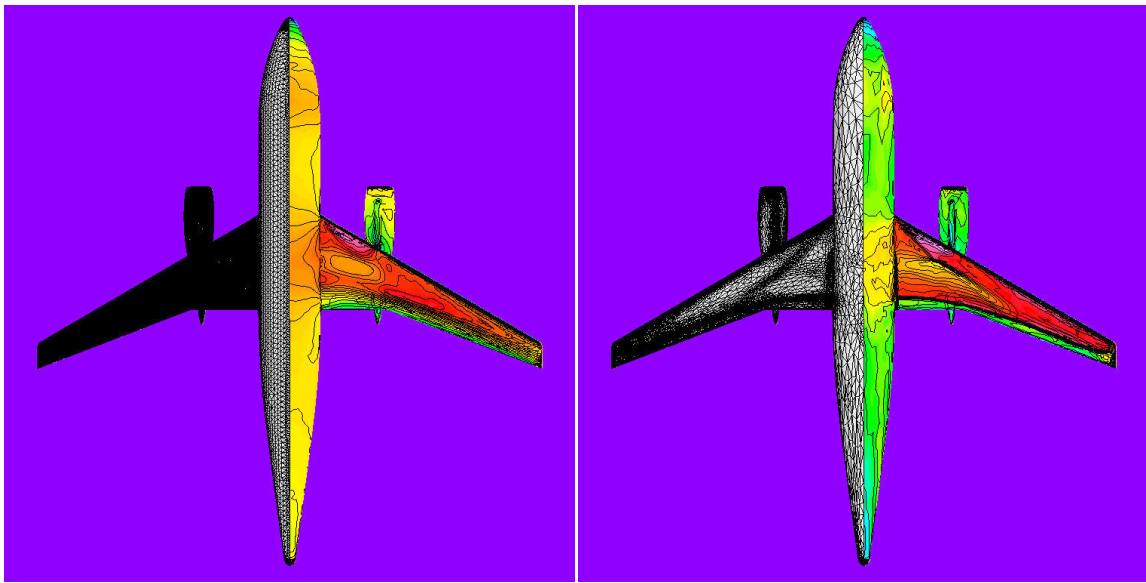
Figure 1. Airbus 320: initial and final grids and solutions

after 6 adaptation cycles
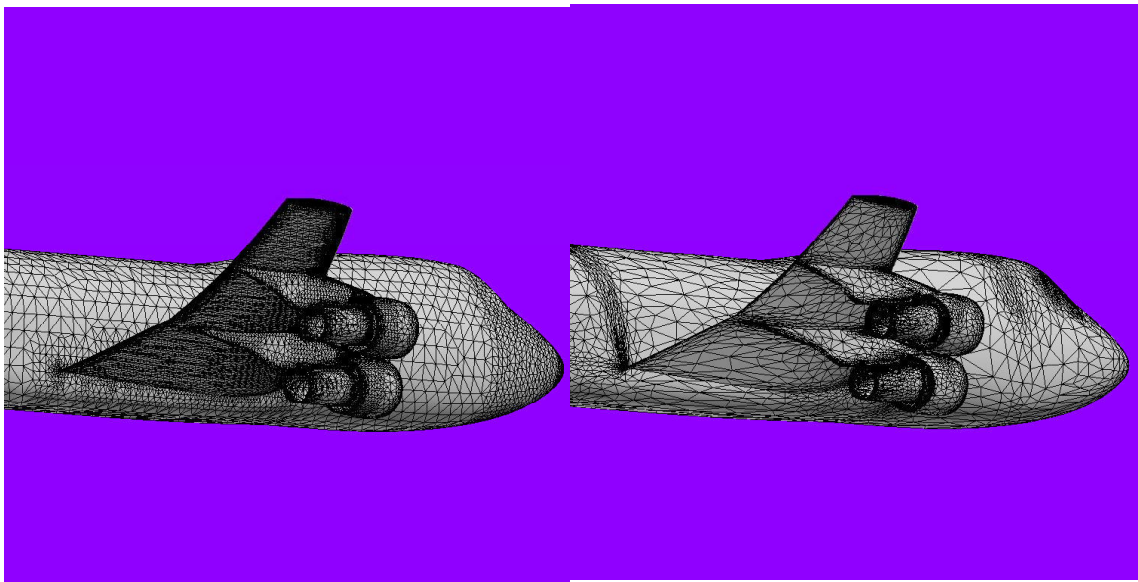
Figure 2. Boeing 747: initial and final grids after 6 adaptation cycles
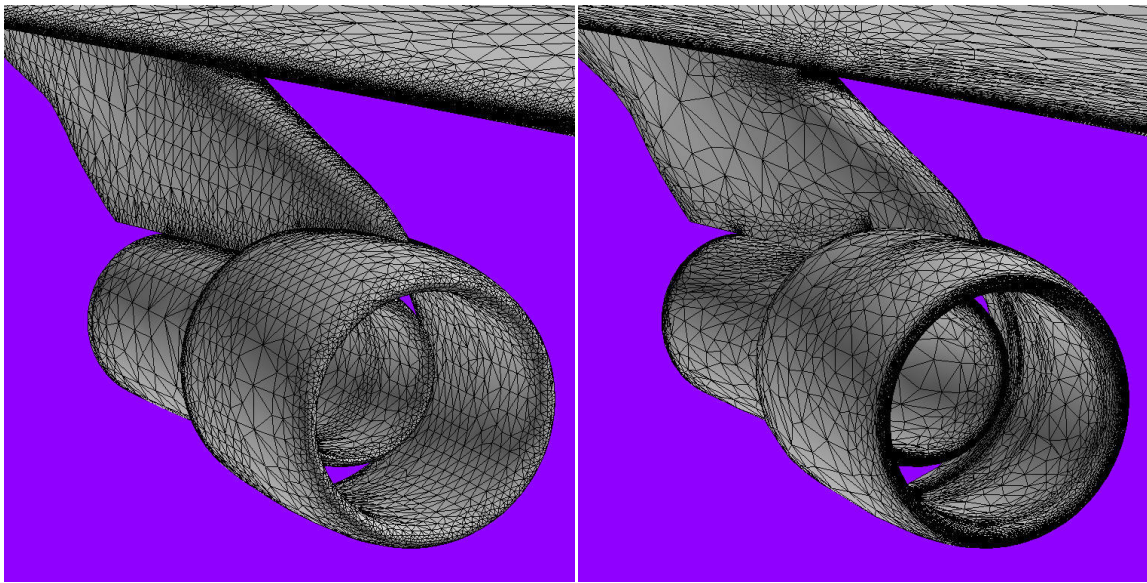
Figure 3. Boeing 747: initial and final grid, pylon-nacelle detail
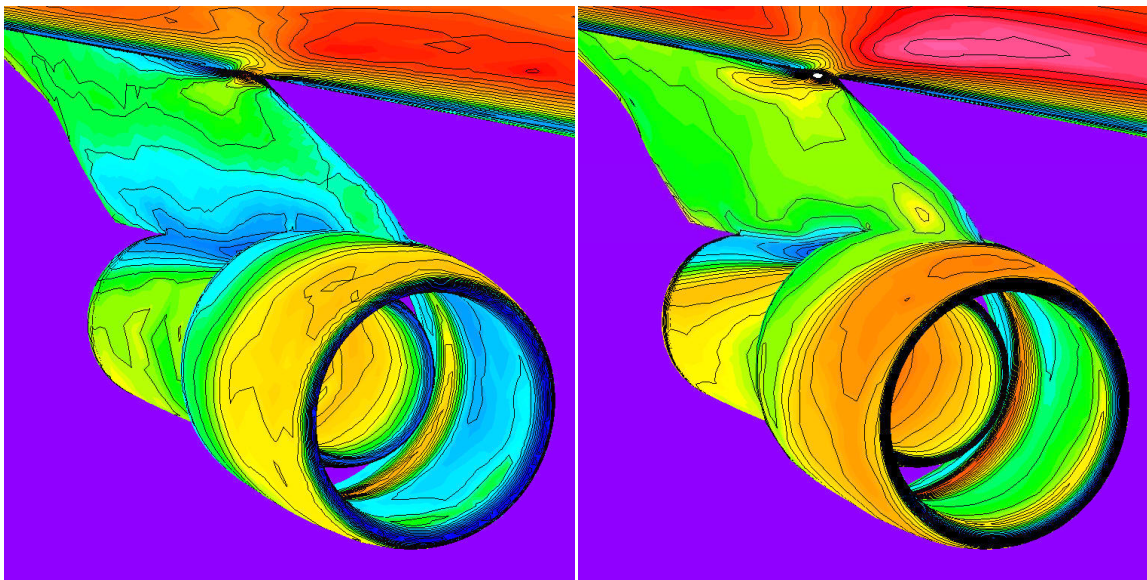
Figure 4. Boeing 747: initial and final grid, pylon-nacelle detail
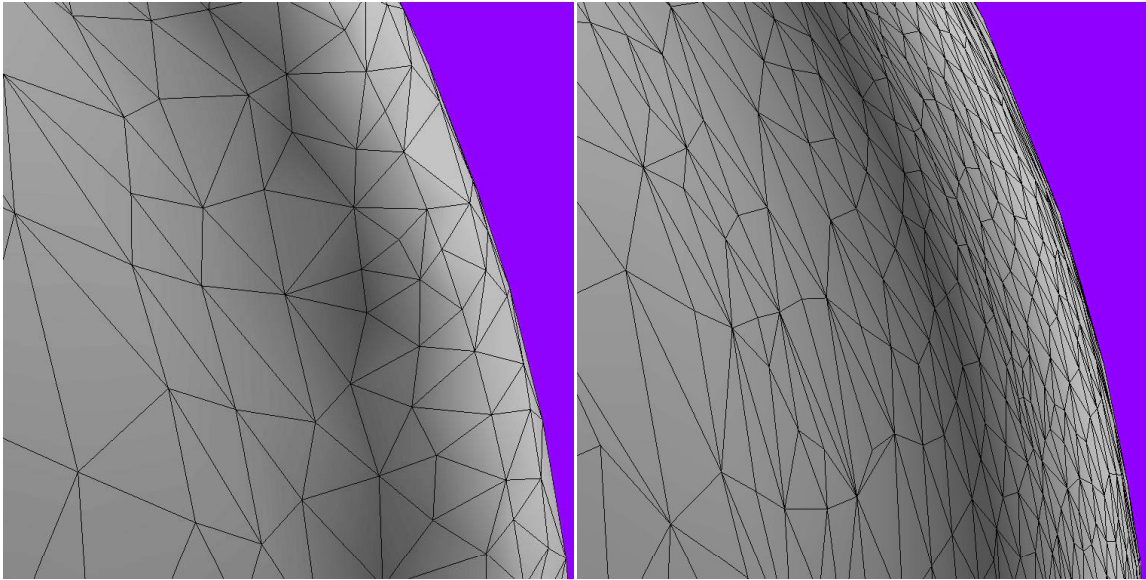
Figure 5. Boeing 747: initial and final grid, fan cowl lip detail
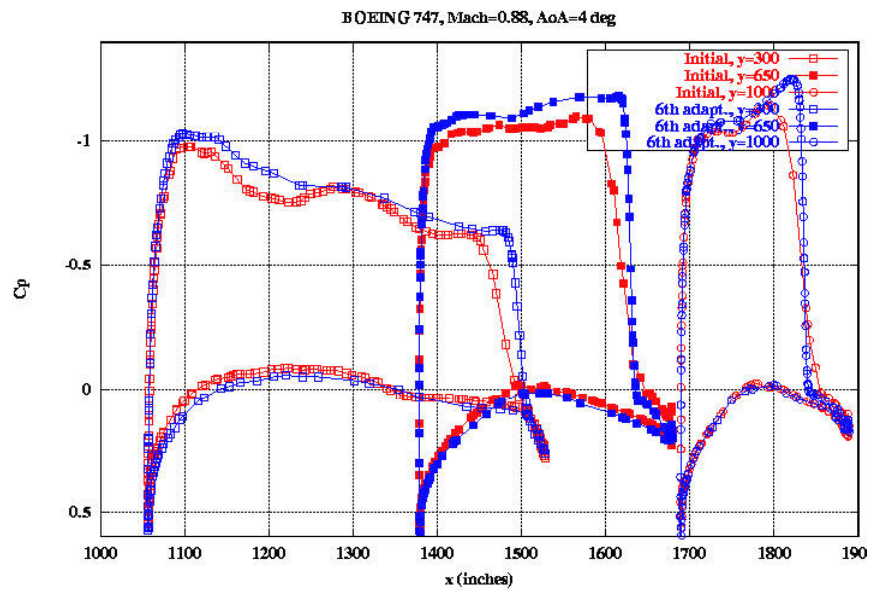
Figure 6. Boeing 747: initial and final Cp distribution at three wingspan stations
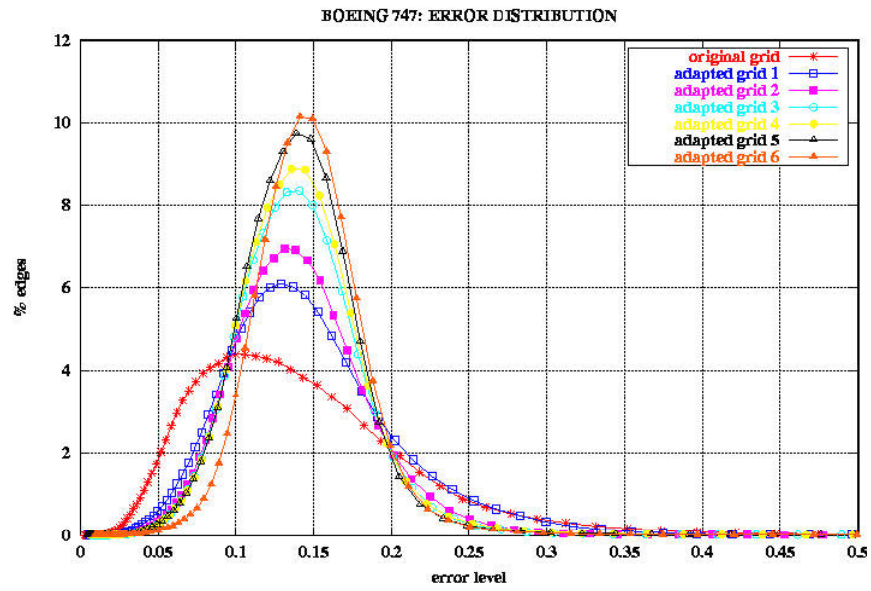
Figure 7. Boeing 747: Error distribution at each adaptation cycle

This page has been deliberately left blank

————————————

Page intentionnellement blanche

From CAD to Adapted Solution for Error Controlled CFD Simulations

M. Delanaye, A. Patel
NUMECA International S.A.
Avenue Franklin Roosevelt, 5
B-1050 Brussels, Belgium

e-mail: michel.delanaye@numeca.be
web page: http://www.numeca.com

K. Kovalev, B. Léonard, Ch. Hirsch
Vrije Universiteit Brussel
Pleinlaan 2
1050 Brussels
Belgium

The aim of this paper is to present an integrated environment (FINE/Hexa™, HEXPRESS™) for the error controlled simulation of industrial flows in complex geometries. The approach uses hexahedral unstructured meshes to ensure accurate solutions and mesh adaptation to optimize mesh resources. Initial hexahedral coarse meshes are automatically generated for complex domains with minor CAD model manipulation thanks to a volume to surface mesh generation approach. A multigrid method tightly coupled with the mesh adaptation history allows the fast resolution of the non-linear discrete flow problem resulting from a second-order cell-centered approximation.

INTRODUCTION

There is still an important effort to make for Computational Fluid Dynamics to become routinely used and trusted in the industrial design environment. Industrials are faced with extremely complex flows within complicated geometries. Besides real physics modeling and turbulence flow aspects, which still remain exploratory domains, it is our duty to provide industry with numerical tools capable of accurately solving the Navier-Stokes equations. The goal is to perform accurate CFD simulations for a new geometry in less than 24 hours with reasonably sized computers, with most of the time being spent for the flow computation. This means that, compared to current CFD tools, it is necessary to reduce the time for importing CAD model in grid generators, limit grid generation time to an hour and minimize computational time by optimizing the grid size for a given flow problem. Error controlling also plays an essential role to gain trust. The present approach accounts for this aspect by emphasizing on mesh adaptation to optimize mesh resources and accuracy in the intricate flow regions.

The first aspect of this quest is the interpretation of CAD models in grid generators. CAD definition of a model is usually poorly defined. Encountered problems are related to overlapping NURBS patches or holes and faults in the geometry definition, etc. Most of them can be attributed to the surface modeling paradigm or to the multiple translations between various formats equipped with different tolerances. A Parasolid™ CAD engine is integrated in the NUMECA generator HEXPRESS™ which allows to automatically import solid models generated with this engine. In case the CAD model is unclean, it is necessary to employ a CAD repair system in order to create a water-tight volume. The computational domain supported by HEXPRESS™ is a triangulated representation of the CAD model. Each surface is supported by a triangulation whose unique purpose is to define the geometry. There is no requirement on its quality except that it has to approximate the geometry sufficiently well. The mesh generation procedure is a top-down approach where the volume mesh is directly created without any reference to a surface mesh. This is an advantage compared to other more common unstructured meshing approaches, which usually require a large human investment in the definition of a surface triangulation compatible with the CFD simulation.

In this work, we choose to exploit the potential of hexahedral unstructured meshes (Schneiders, 1996) although they are much less popular than hybrid tetrahedral prismatic grids because of their inherent topological difficulties to mesh complex geometries. Hexahedral meshes potentially offer higher accurate solutions than tetrahedral meshes when using classical numerical methods. It is the best choice for resolving highly sheared flows such as boundary layers. The computational domain is initially covered with a structured mesh corresponding to the bounding box of the domain. This initial mesh, which does not

conform to the geometry, is successively refined anisotropically in order for the cell sizes to match the geometry length scales. Unlike similar Cartesian based methods (Aftosmis, 1997), we do not cut the cells intersecting the geometry in arbitrary polyhedra since they are impossible to use for high-Reynolds number flow simulations. Those cells are removed from the initial grid. Reconnecting the remaining staircase shape of the volume grid to the geometry is a challenging issue. Several procedures have been proposed such as the creation of hybrid grids intersected with the remaining Cartesian volume grid, or overlaid with the latter by a Chimera procedure, or finally connected to it by a tetrahedralization of the remaining gaps. The present technique differs from the latter by directly fitting the non-body fitted Cartesian grid to the domain boundaries using a snapping method (Taghavi, 1996). Sophisticated algorithms are implemented to recover the geometry features such as corners and ridges not preserved by the surface snapping.

The flow solver is tightly connected to the mesh generator by sharing common C++ classes and can therefore benefit from the mesh generator cell subdivision machinery to perform aggressive adaptation of the mesh to the flow solution. It is based on a finite volume cell centered approach. Space discretization is based on the classical Jameson-type centered scheme augmented by blended second and fourth order scalar dissipation. Fast convergence to steady state solutions is obtained thanks to an explicit Runge-Kutta scheme accelerated by a multigrid strategy. This method is combined with a second-order backward time-integration through a dual time-stepping approach for unsteady computations. The Spalart-Allmaras model and several variants of the k-ε model have been implemented to simulate turbulent flows.

CAD model

The starting point of any simulation is the definition of an appropriate computational domain, which, in most cases, can be interpreted as the complementary of the solid parts present in the model. HEXPRESS[TM] expects a water-tight computational domain. In fact, it is equipped with a topology and a geometry part as presented in Figure 1. The topology describes the skeleton of the model. Basically it allows to define a closed volume. It thus provides information on the connection of the model surfaces (topological faces) trough common curves (topological edges). Similarly, it also connects curves together by common corners (topological vertices). The geometry part defines the actual geometry of the model. Each surface of the model is described by a triangulation; each curve by a list of points connected by segments and the corners eventually are defined by a single point.
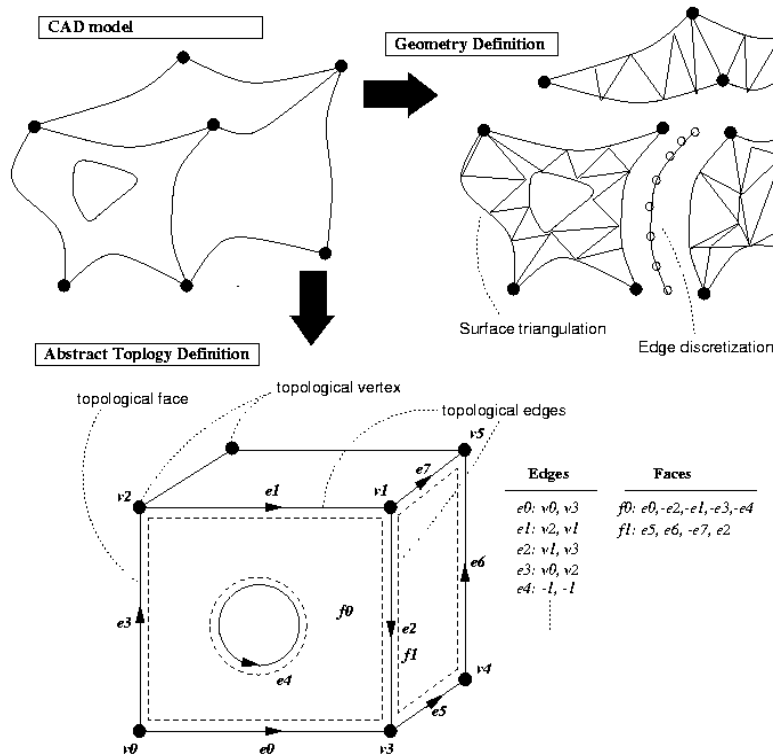
Figure 1: HEXPRESS[TM] computational domain definition.

HEXPRESS^{TM} is equipped with a Parasolid^{TM} CAD engine. Thus, any CAD model native from this engine is transparently loaded by the mesh generator. Other native model must be translated to the Parasolid^{TM} format before being processed.

A CAD model usually exhibits complex features which are useless for the flow simulation. It is therefore wise to remove these geometry details from the model before proceeding to mesh generation. In HEXPRESS^{TM}, such removal is not applied to the model directly but the complexity of the computational domain is simplified by merging some surfaces. The edges in common between the merged surfaces are then removed and are not captured in the mesh. This merge is performed at the topology level, hence no NURBS or surface representation is reconstructed. The solution of HEXPRESS^{TM} to the geometry simplification is therefore simple and fast. Figure 2 presents the computational domain of a draft tube before (left) and after (right) simplification.
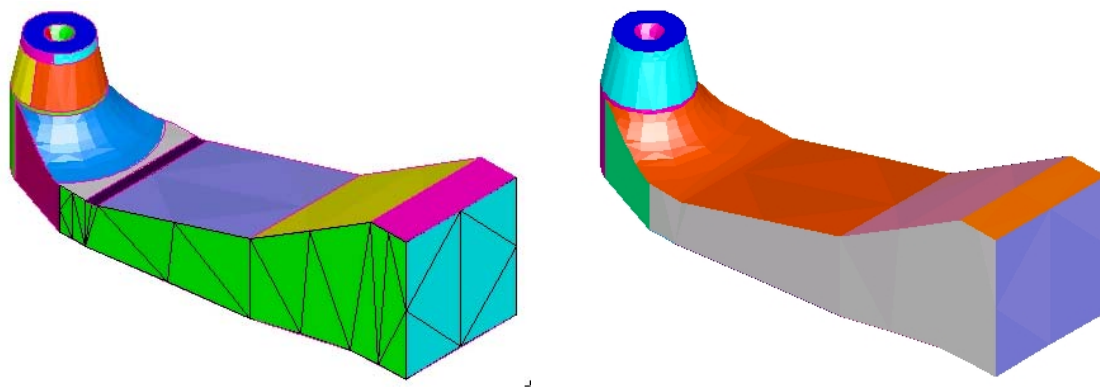
Figure 2 Triangulated Parasolid^{TM} CAD model (left), simplified model (right)

Automatic Hexahedral Mesh Generator

Geometry adaptation

The HEXPRESS^{TM} mesh generator is based on a volume to surface mesh approach. The methodology is described in details in Delanaye *et al* (2000), a short description is presented in the following. An initial mesh surrounding the computational domain is created. This mesh is not conforming to the geometry in most cases. The cell sizes of this initial mesh are most of the time not compatible with the local length scales of the geometry. Mesh adaptation is performed by successive subdivisions of cells in order to achieve clustering of points compatible with geometry length scales typical of high curvature regions, corners, ridges, etc. Further refinements and adaptations of the mesh are subsequently performed during the simulation depending on some indicators measuring the quality of the computed solution.

The local cell subdivision may result in the occurrence of neighboring cells with possibly very different sizes. Since those variations are incompatible with the accuracy of the numerical scheme, the difference of cell refinement levels across a common face is limited to a single level. This criterion advantageously forces the transport of refinement tags to neighboring cells and guarantees some level of smoothness in the mesh. In addition, the propagation of refinement tags from tagged cells to their neighbors and further in the mesh is controlled by a user defined diffusion depth parameter. Anisotropic subdivisions are moreover employed to avoid excessive growth of the number of cells as presented in Figure 3.
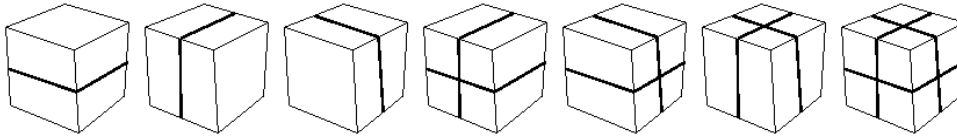
Figure 3 Anisotropic subdivision of hexahedron

At each adaptation iteration, the cells intersecting the geometry are searched. The cell sizes of the latter are compared to target cell sizes, which are defined by the user or automatically by the grid generator itself. Cells are refined if the criteria are not matched.

Geometry Fitting

Once the non body-fitted grid has been sufficiently refined to match the typical length scales of the geometry, we proceed to the recovery of the geometry surface. Cells lying outside the computational domain or intersecting the surface geometry are marked for removal. Starting from a seed cell, a painting algorithm marks all the cells located outside of the computational domain; the latter are removed from the mesh. At this level, the boundary of the volume grid is a staircase surface inappropriate for flow simulations. Hanging nodes which can be present on this boundary due to the cell subdivisions are not removed since finite volume solvers are capable of handling such configurations.

Next, the staircase boundary of the volume mesh is snapped on the geometry surface. A Laplacian-like smoothing procedure is first applied to smooth out the staircase boundary. This smoothed boundary forms a front of quadrilateral facets whose vertices are projected on the geometry by a closest distance criterion. A closest projection point is accepted if the geometry normal computed at that location does not differ too much from the front normal at the corresponding facet vertex.

Important geometry features such as corners and ridges (*e.g.* trailing edges of wings) are not preserved by the snapping procedure. They are actually never present except sometimes if extremely fine grids are employed. For the accuracy of physics simulation, it is important to recover those special features. This step is crucial to produce a final mesh of high quality. Failure to choose the most appropriate vertices to attach to corners and ridges may create a mesh with distorted or even negative cells. The difficulty of associating a vertex to a corner or a curve is to make a choice in a set of several candidates that will eventually lead to the highest quality mesh without actually being able to measure the quality of the final mesh. The reader is referred to Delanaye *et al* (2000) for more details on the procedure. The projection of the smoothed staircase volume mesh boundary and the edge capturing produce angles close to 180 degrees for specific configurations. A layer of cells is extruded off the geometry surfaces and curves to remove these degenerate cells. The procedure is a generalization of the method of Mitchell and Tautges (1995).

Optimization

Some degenerate cells may remain in the mesh after automatic mesh generation. These are due to the high distortion created in the mesh during geometry projection. The presence of those cells may hinder the convergence of the simulation tool or create negative cells during *h*-adaptation. Therefore, a very innovative optimization technique has been developed in HEXPRESS$^{\text{TM}}$. It consists in the successive applications of an algorithm which locally untangles concave cells and transform them in convex ones. The untangling algorithm applies to the set of triangles or tetrahedra which decomposes a quadrilateral or hexahedral cell respectively. An additional optimization algorithm improves the orthogonality of the cells by locally optimizing a functional defined on the convex cells. The reader is referred to Kovalev *et al* (2002) for more details.

High aspect ratio cell layers

High aspect ratio cell layers are subsequently introduced to correctly resolve high shear flow phenomena such as boundary layers. This step can be performed either before any flow computation by the grid generator or during flow computation while adapting the mesh based on flow feature detectors. The user can specify several parameters such as first cell thickness, stretching value and number of layers. They are inserted by successively subdividing the buffer cells closest to the wall. The newly inserted vertices are then redistributed to match the specified distribution requirements. This creates a set of layers which are related to each other through the tree structure produced by the recursive subdivisions. This aspect is important for the performance of the multigrid solver because it allows the easy recovery of coarser cells through parent-child relationship.

Adaptive Flow Solver

Space discretization scheme

The spatial discretization method is based on a cell centered finite volume approach. The advective fluxes across a face are computed by flux averaging with added artificial dissipation (Jameson, 1995). The latter results in a blend of fourth and second order dissipation terms. A pressure switch triggers the second order dissipation factor in discontinuities or in very high gradient flow regions to avoid large amplitude oscillations. The calculation of the artificial dissipation term requires the computation of the solution first differences on the faces and of the second differences in cell centers (Van de velde *et al*, 1998). In a first loop over the cell faces, the variation of the solution vector across each cell face is calculated and stored. In a second loop, these variations across faces are transferred to the cell centers, with a plus sign for the upwind cell center and a minus sign for the downwind cell center. The viscous fluxes require the computation of temperature and velocity gradients on the cell faces. For this purpose, a diamond control volume is created around each face and consists of two pyramid elements. Each of them is formed by the face itself, and the left or right cell center as opposite summit respectively. For this purpose, the solution at the vertices is interpolated from the values stored at the cell.

The two equation k-ε turbulence model (Jones *et al*, 1973) is used to simulate the effect of turbulence on the mean flow. The linear low-Reynolds model implemented in the code is due to Yang and Shih (1992, 1993). The particularity of this model resides in a redefinition of the turbulent time scale which removes the singularity at the solid wall. A wall function variant (Hakimi, 1997) of this model is also available. It dramatically reduces the number of mesh points required to resolve the boundary layer. The first mesh point should reside in the log-law region. The turbulent kinetic energy k and its dissipation rate ε in the cells next to the solid walls are updated according to formula based on DNS data, instead of solving the governing equations. In turbulent calculations, at inlet and outlet boundaries, the turbulent kinetic energy and dissipation rate are extrapolated from interior cells or imposed on the boundaries. On solid walls, the kinetic energy is zero, while the dissipation rate is again extrapolated from interior cells. In addition to the k-ε models, the one-equation turbulence model from Spalart and Allmaras (1992) has also been implemented.

Multigrid acceleration

An explicit Runge-Kutta scheme integrates the discretized set of equations in time to eventually reach the steady state. Convergence acceleration is obtained thanks to local time stepping and multigrid acceleration.

In our multigrid approach, the creation of coarse grid levels is tightly coupled with mesh geometry and flow adaptation. Indeed, the initial mesh is used as the coarsest level, additional levels are created at each mesh

adaptation either during geometry adaptation and/or flow adaptation by using the parent-child connectivity stored in the adaptation module. Since each multigrid level covers the whole computational domain, the final composite grid contains cells at many different refinement levels. The coarse multigrid level generation strategy used in the unstructured solver is derived from Aftosmis *et al* (2000), and consists in replacing all the leaf sibling cells by their parent. If one or more of a set of siblings has children of its own, then coarsening is suspended until those children are removed. In addition, in order to ensure sufficient mesh quality at each grid level, only one hanging node per edge is accepted. Therefore, a balancing function locally suspends the coarsening if a forbidden situation is found on the coarser level.

The grid transfer operators also use the cell parent-child connectivity. The restriction of the residual is simply chosen as the sum of the residual of the children, whereas a weighted averaging is used to restrict the solution. The prolongation operator interpolates the solution correction from a coarse level to a fine level. Basically, the correction is the difference between the new solution on the considered grid level and the restricted solution on the same grid level. A first order prolongation operator is used (Léonard *et al*, 1999). At first, the corrections in the cells of the coarse grid are interpolated in the vertices of the fine grid. In a second step, the corrections in these fine grid vertices are distributed to the cell centers.

Flow adaptation

In the unstructured adaptive solver, mesh adaptation is performed automatically. The basic structure of an adaptive solution procedure consists in:

- Calculation of the solution on the current grid

- Identification of the cells to be refined and the cells to be removed

- Refinement or removal of the flagged cells

The anisotropic refinement functionality allows cells to be split in 2, 4 or 8. In order to ensure mesh quality, refinement flags are propagated to permit only one hanging node per edge. Furthermore, "islands and voids" in the mesh are prevented. A hierarchical mesh coarsening technique has also been integrated. To remove a cell, at least 75% of its siblings have to be flagged for coarsening. Then, the parent cell is recovered by removing all the siblings, including the non-flagged ones. As only one hanging node per edge is accepted, a balancing function is used to locally block the coarsening where forbidden configurations are foreseen.

Mesh adaptation is governed by criteria based on flow physics and geometry particularities. The first ones are flow feature sensors aiming at the detection of regions where significant flow variations exist. The choice of appropriate feature detection parameters is guided by the physical nature of the flow. Various criteria based on the flow physics are used. The undivided difference of pressure gradients is used to detect shock regions. Undivided and divided differences of the velocity magnitude as well as vorticity are used to capture viscous effects. No single sensor can adequately capture all flow features. An ideal sensor is usually defined for each testcase by combining several sensors. Refinement and coarsening threshold values are determined using a statistical formula (Kallinderis *et al*, 1989).

Results

We first considered the simulation of inviscid and viscous flows around the LANN wing (Muller *et al*, 1996). In particular, the CT9 case is characterized by off-design conditions ($M_\infty = 0.82$, $Re_\infty = 7.17 \times 10^6$, angle of attack equal to 2.6 deg.). This test case presents a strong interaction with a separated flow behind the strong shock system. Experimental data (AGARD AR-702, 1982) are provided.

An inviscid computation is carried out starting on an initial all-hexahedra unstructured grid involving 46435 cells (see Figure 4). The geometrical difficulty of this case is the presence of the very thin but blunt trailing edge, which needs to be resolved by the mesh. The mesh is adapted twice using finite differences of the velocity norm as adaptation criterion. After one adaptation, the mesh contains 128819 cells, and after two adaptations, it contains 211119 cells. After each adaptation, the number of grid levels used in the multigrid strategy is increased with a maximum of 3 levels.

Initial mesh, 46435 cells   Adaptation 2: 211189 cells
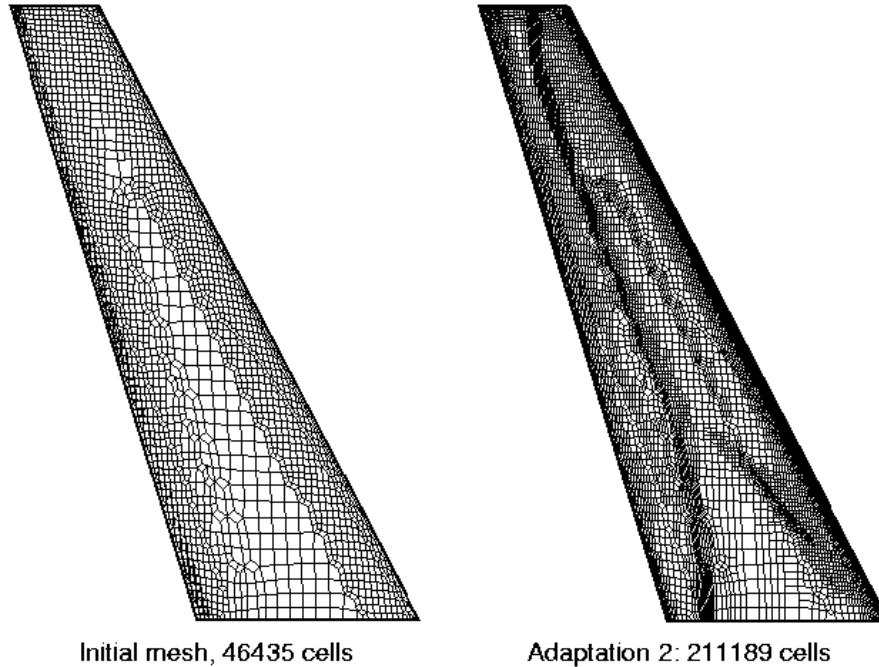
Figure 4 LANN wing, adapted meshes

Figure 5 presents pressure isolines on the surface. The solution actually better and better match the experiments (not shown) after each adaptation in the leading edge area, while the shock position is moved further downstream and the shock becomes crispier. Furthermore, the λ-shock structure becomes wider after each adaptation, *i.e.* the shock junction is moved further in the spanwise direction

The initial mesh is refined close to the wall in order to generate high-aspect ratio cell layers to resolve the boundary layer, 7 layers are added, the total number of cells now reaching 127675 cells. After carrying out one adaptation, the adapted mesh contains 233923 cells. Turbulence is initialized by assuming an initial value of 1% for the turbulent intensity. The pressure distributions computed on the fine mesh match better the experimental data than those computed on the coarser mesh, as shown in Figure 6 for the section located at 20 % and 32.5 % of the span.
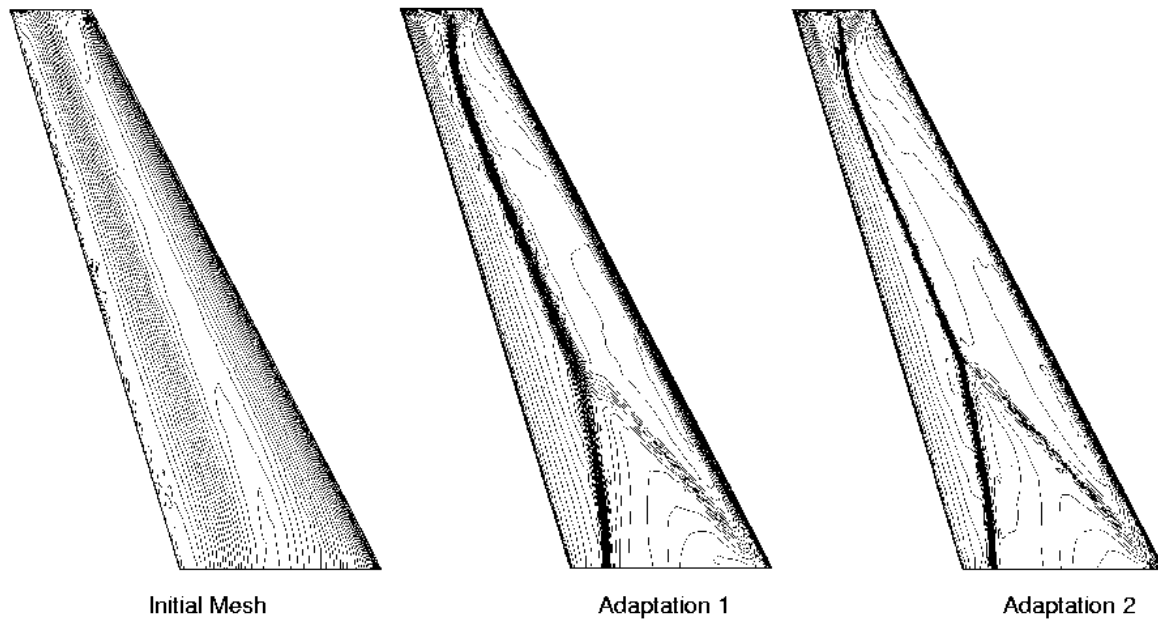
Figure 5 LANN wing, adapted mesh solutions, pressure isolines
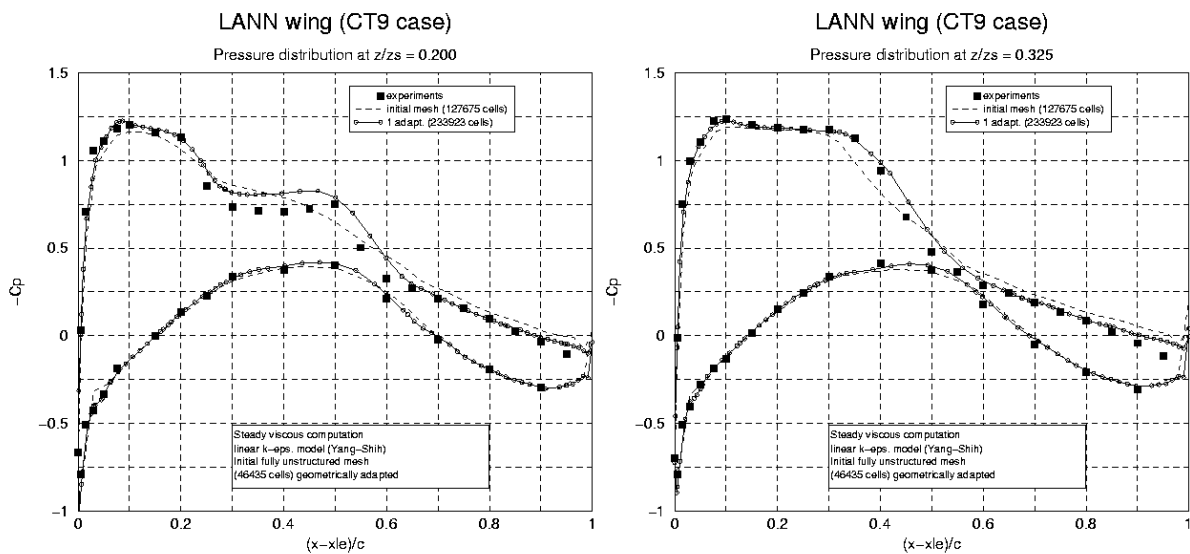
Figure 6 LANN wing, surface pressure distributions, viscous flow simulation

The second case is an aircraft wing-fuselage system referred to as the DLR-F4. This geometry has been recently analyzed in the framework of a CFD drag prediction workshop organized by the American Institute of Aeronautics and Astronautics. The flow is simulated at a Mach number equal to 0.75 and angle of attack equal to 0.93 deg. The unstructured hexahedral mesh contains 1402841 cells, the first cell size is $2.5 \ 10^{-5}$ m and a streching ratio of 1.2 is applied to the 15 layers of high aspect ratio cells used for the boundary layer resolution. The Spalart-Allmaras model is used to simulate turbulence. Figure 7 and Figure 8 represent the mesh and pressure isolines on the aircraft respectively. A converged solution is obtained in 500 cycles, using a full-multigrid approach to initialize the solution (Figure 9). Figure 10 presents the pressure distribution across two sections located at 0.238 and 0.844 fraction of the wing span respectively. They agree well with the results obtained with other codes in the context of the AIAA CFD Drag Prediction workshop.
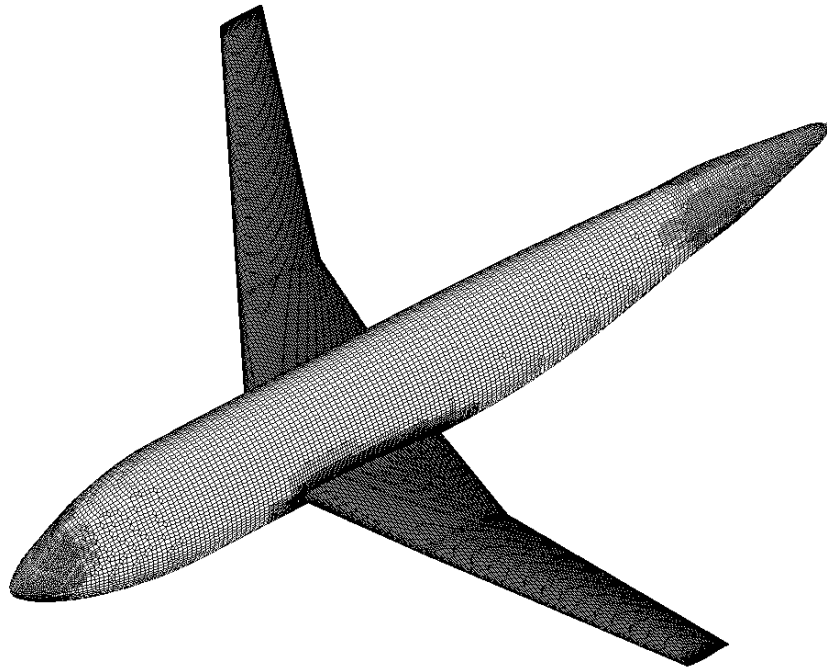
Figure 7 DLR-F4, 1402841 cells
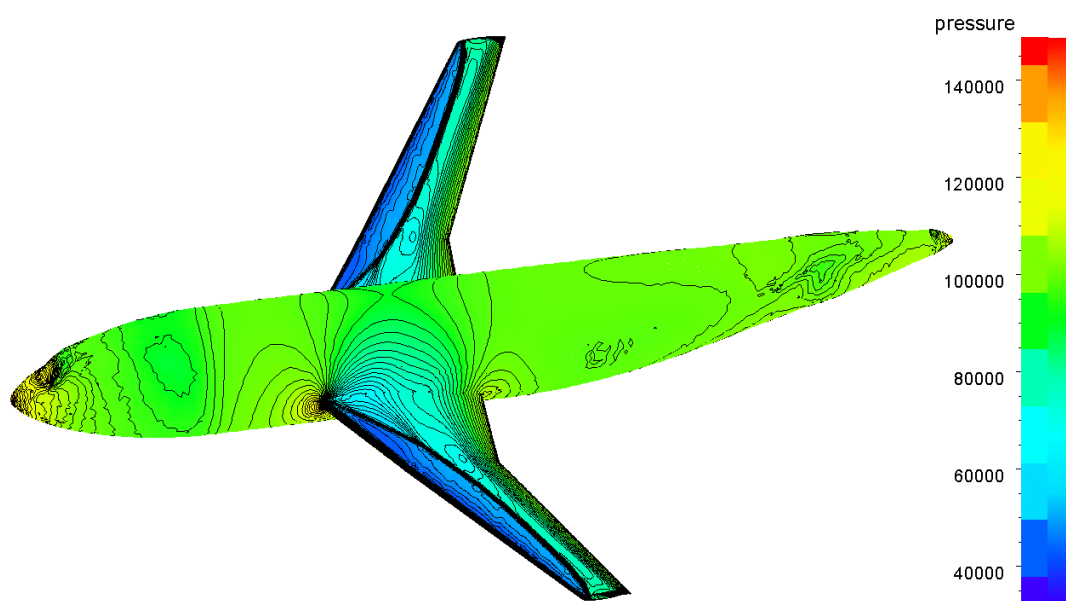
Figure 8 DLR-F4, pressure isolines
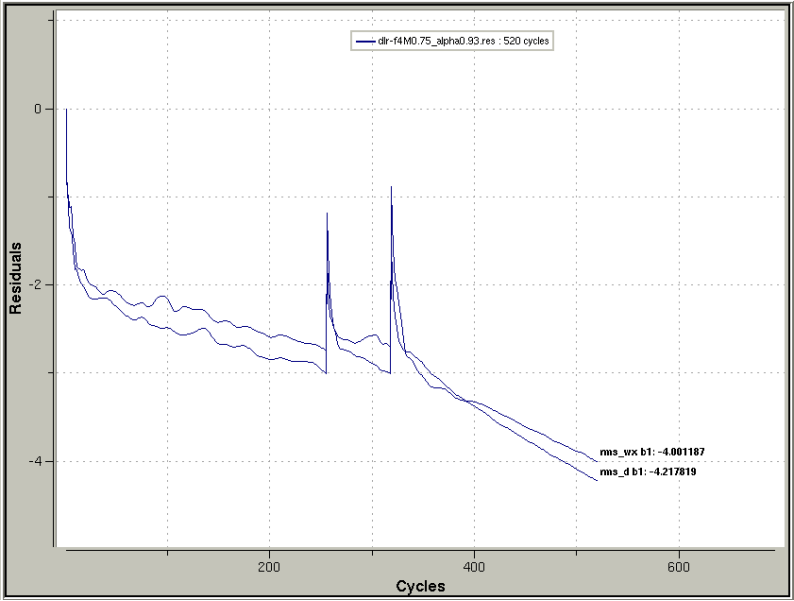
Figure 9 DLR-F4, convergence history
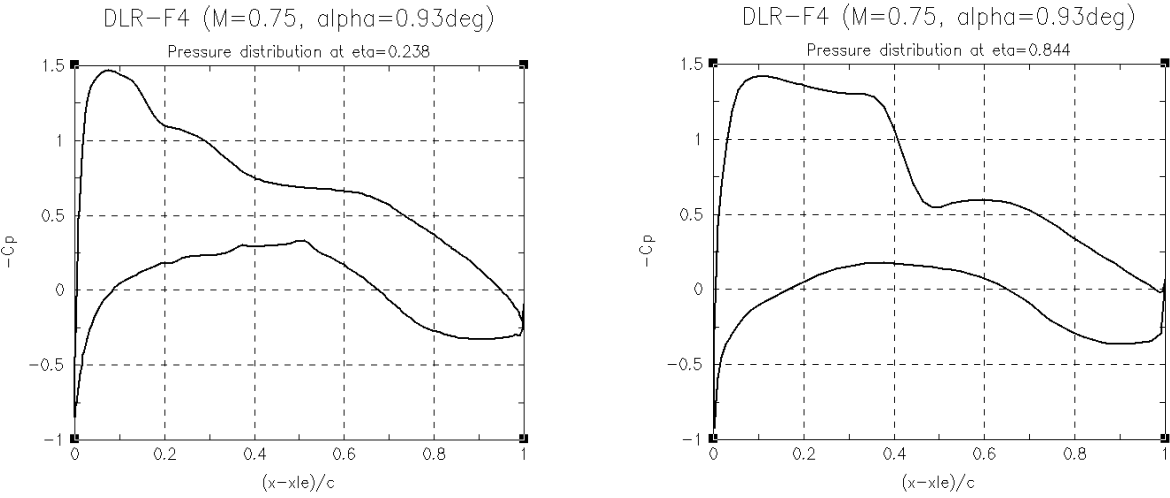
Figure 10 DLR-F4: pressure distribution at two span sections
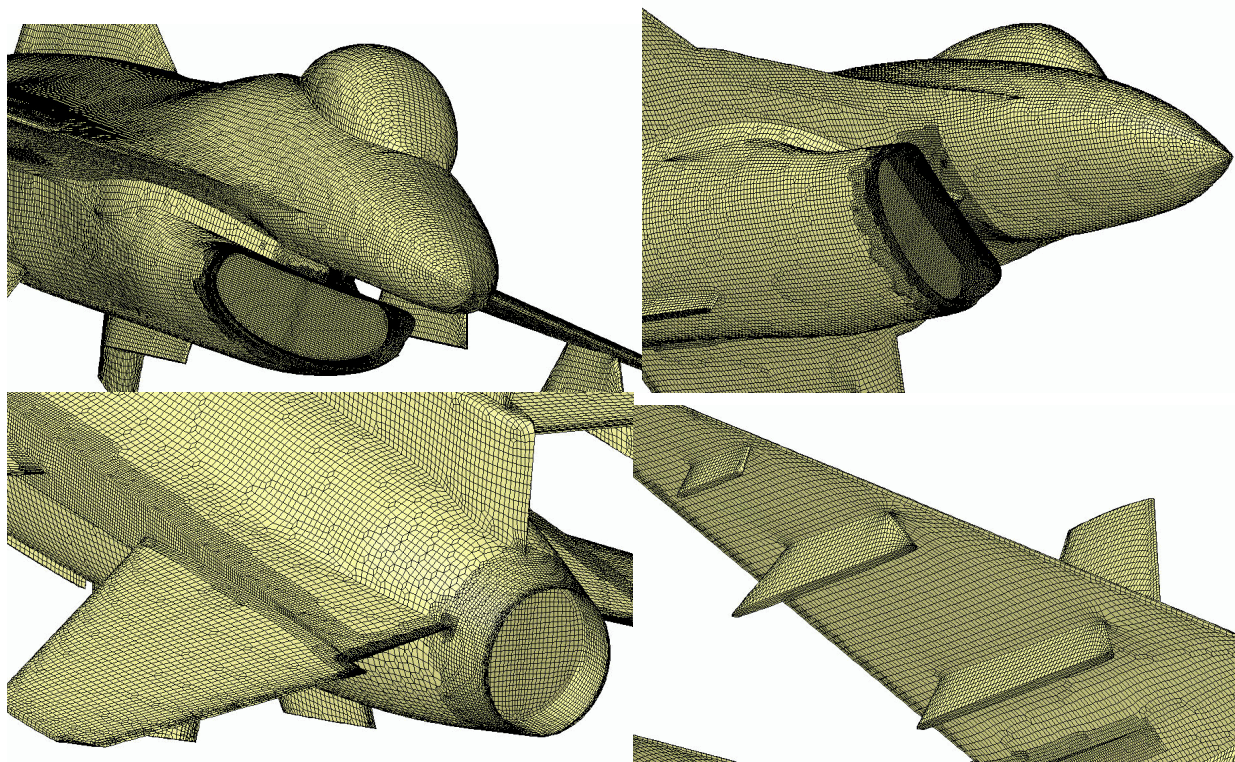
Figure 11 F16 military aircraft. Unstructured hexahedral mesh, 432759 cells (half body)

Figure 11 shows the mesh generated around a F16 military aircraft configuration. An inviscid flow simulation is carried out at a Mach number equal to 2 and no incidence. The mesh involves 432759 cells. The solution presented in Figure 12 and Figure 13 shows strong shock systems on the wings and fuselage. A residual drop of 3 orders of magnitude is obtained in about 200 cycles (Figure 14).
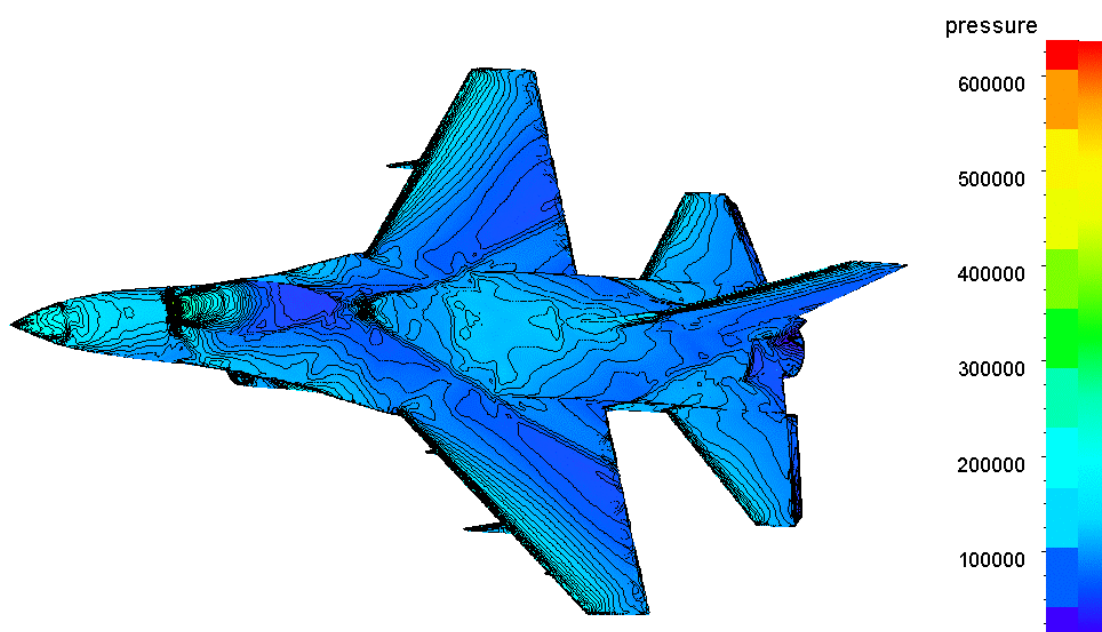
Figure 12 F16 military aircraft at Mach number equal 2, angle of attack 0 deg. Pressure isolines.
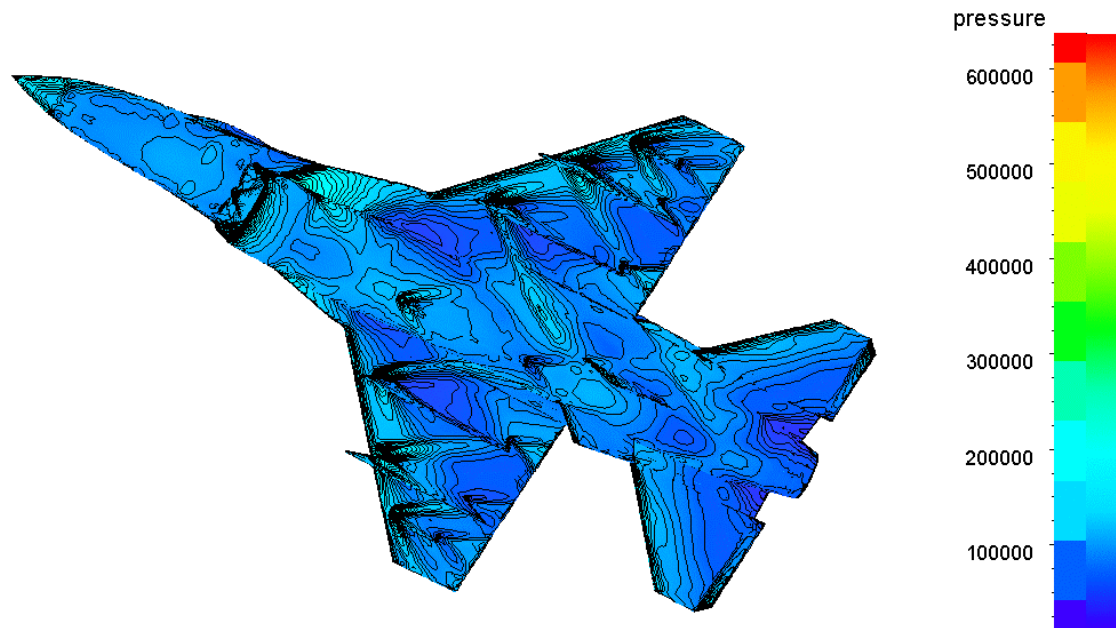
Figure 13 F16 military aircraft at Mach number equal 2, angle of attack 0 deg. Pressure isolines.
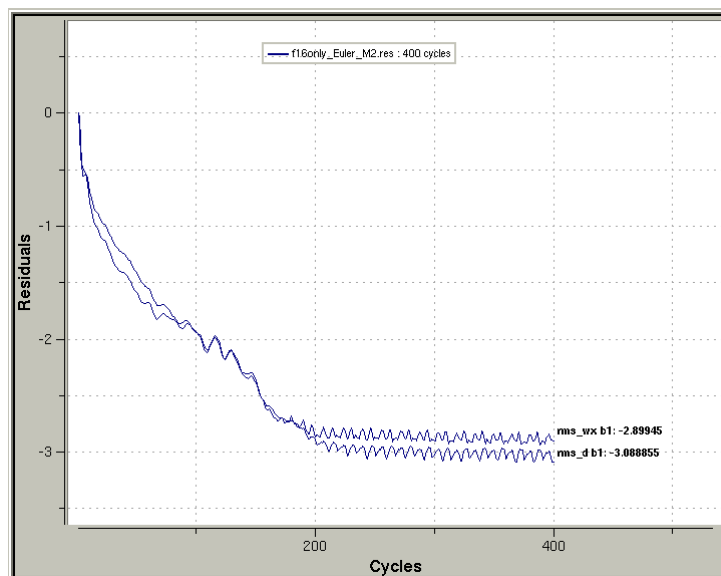
Figure 14 F16 military aircraft at Mach number equal 2, angle of attack 0 deg. Convergence

Conclusion

An error controlled system for flow simulation around complex geometries is presented. The approach is based on automatic hexahedra meshes adaptive flow. Hexahedral meshes present the advantage of preserving the accuracy of well known numerical methods developed for structured meshes, they also minimize the number of cells used to resolve boundary layers for complex geometries. Hexahedra cells can be easily decomposed anisotropically which results in a powerful adaptation technique for flows presenting very different scales. The inherent tree structure resulting from mesh adaptation by successive subdivisions to geometry and further to the flow solution is exploited to devise a fast multigrid convergence acceleration method. These advantages have led to the development of a powerful environment, tightly integrated through

a common object oriented language (C++) capable of solving very complex flows in complex geometries of industrial interest.

Acknowledgements

References

Schneiders, R., A Grid-Based Algorithm for the Generation of Hexahedral Element Meshes, *Engineering With Computers*, 12, 168-177, 1996.

Delanaye, M., Tchon, K.-F., Patel, A. and Hirsch, Ch., All Hexahedra Unstructured Grid Generation, *in Proc. of ECCOMAS 2000*, Barcelona, 2000.

Aftosmis, M.J., Solution Adaptive Cartesian Grid Methods for Aerodynamic Flows with Complex Geometries, *Computational Fluid Dynamics VKI Lectures Series 1997-05*, 1997.

Taghavi, R., Automatic, Parallel and Fault Tolerant Mesh generation from CAD, *Engineering with Computers*, 12, 178-185, 1996.

Mitchell, C.R. and Tautges, T. J., Pillowing doublets: refining a mesh to ensure that faces share at most one edge, *in Proceedings of the 4th International Meshing Roundtable*, 231-242, Albuquerque (NM), 1995.

Jameson, A, Analysis and design of numerical schemes for gas dynamics', *Int. J. Comp. Fluid Dyn.*, 4, No 3-4, 171-217, 1995.

Kovalev, K., Delanaye, M. and Hirsch, Ch., *Untangling and Optimization of Unstructured Hexahedral Meshes*, paper to be presented at the Grid Generation Theory and Applications Workshop, Russian Academy of Sciences, June, 2002.

Van de Velde, O., Lacor, C., Alavilli, P. and Hirsch, Ch, A 3D unstructured Navier-Stokes solver with multigrid on adaptive hexahedral meshes, *in Proc. 4th European CFD Conf.*, 675-680, 1998.

Jones, W.P. and Launders, B.E., The calculation of low-Reynolds number phenomena with a two-equation model of turbulence, *Int. J. of Heat and Mass Transfer*, 106, 119 (1973)

Yang, Z. and Shih, T.H., A k-ε calculation of transitional boundary layers, *NASA Technical Memorandum 105604 ICOMP-92-08*, CMOTT-92-05, 1992.

Yang, Z. and Shih, T.H., A Galilean and tensorial invariant k-ε model for near wall turbulence", *AIAA Paper 93-3105*, 1993.

Spalart, P. and Allamaras, S.R., A One-Equation Turbulence Model for Aerodynamic Flows, *AIAA paper 92-0439*, 1992.

Hakimi, N, Preconditioning methods for time dependent Navier-Stokes equations / Application to environmental and low speed flows, *PhD, Vrije Universiteit Brussel,* 1997.

Aftosmis, M.J., Berger, M.J. and Adomavicius, G., A parallel multilevel method for adaptively refined Cartesian grids with embedded boundaries, *AIAA Paper 2000-0808*, 2000.

Léonard, B., Patel, A. and Hirsch, C., Multigrid acceleration in a 3D Navier-Stokes solver using unstructured hexahedral meshes, *in Proc. 4th Conference on Multigrid*, 1999.

Kallinderis, Y. and Baron, J.R., Adaptation methods for a new Navier-Stokes algorithm, *AIAA Journal*, 27, No 1, 37-43, 1989.

Muller, U.R., Henke, H. and Schulze, B., Computation of Transonic Steady and Unsteady Airfoil and Wing Flow by Inviscid and Viscous-Coupled Solvers", European Computational Aerodynamics Research Project: Validation of CFD Codes and Turbulence Models, Notes on Numerical Fluid Mechanics, *Eds Haase, Chaput, Elshoz, Leschziner, Muller, Vieweg*, 58, pp. 81-88, 1996.

AGARD, Compendium of Unsteady Aerodynamic Measurements, Addendum No.1, *AGARD AR 702*, 1982.

UNSI Brite Euram European Project - Final Report, *Vieweg*, (to be published).

This page has been deliberately left blank

_____

Page intentionnellement blanche

Towards Faster and Safer Flight Flutter Testing

J.E. Cooper
Manchester School of Engineering
University of Manchester
Oxford Road
Manchester, M13 9PL
United Kingdom

Abstract

The current state of the art of flight flutter testing is reviewed, and areas where this part of the certification procedure could be improved are discussed. It is argued that the key towards speeding up the flight flutter test procedure, and also to reduce costs, is to reduce the number of flight test points that are required as part of the test clearance programme. To achieve this aim, the entire modelling and testing procedure needs to be improved, particularly with respect to non-linearities. Non-linear aeroelastic phenomena will then be able to be predicted more accurately. Current work in a number of relevant technologies is considered in relation to flight flutter testing. Suggestions are made as to how these aspects could be improved in order to speed up and reduce the cost of flight flutter testing, while maintaining, if not improving, the levels of safety.

1   Introduction

Flutter is potentially the most disastrous of all aeroelastic phenomena and there have been many instances of structural failure from the resulting unstable oscillations [1,2]. Although the first recorded incident was the Handley Page O/400 bomber in 1916, it was not until the mid 1930s that Von Schlippe introduced the concept of a dedicated flight flutter test. Since then, flight flutter testing [3,4] has matured to become a critical stage in the certification process, see figure 1, providing the final validation of the analytical predictions. All aircraft must be demonstrated to be flutter free throughout the entire flight envelope, plus an additional safety margin. A similar process must also be undertaken for the clearance of new types, or combinations, of stores on military aircraft.

The classical approach to flutter testing has changed little over the past half century and, as can be seen in figure 2, systematically expands the flight envelope for increasing speeds over a range of altitudes. At each flight test point, three separate procedures are performed:

1. The aircraft is excited in some manner and the vibration response measured.
2. The data are curve-fitted using system identification methods and the modal parameters estimated.
3. The decision is made to progress to the next flight test point.

There have been 3 major international meetings held to discuss the progress of flight flutter testing, in 1958[5], 1975[6] and 1995[7]. The major technical developments that have had greatest influence on the test procedure are shown in figure 3. In essence, the basic test philosophy had been developed by the time of the first meeting, the second meeting demonstrated the influence of new computational and other test hardware. The third meeting described advances in analytical methods, new forms of excitation devices and consideration of aeroservoelastic effects. Despite these advances, the basic procedure has remained the same [87,88].

Flight flutter testing is very expensive, time consuming, and often undertaken at a time critical part of an aircraft's development programme. The design flight envelope must be cleared as swiftly as possible so that the rest of the flight testing (systems, etc.) may be completed. However, at no time must safety be compromised. Compared to ground testing, it is often difficult to excite the aircraft with an adequate amount of energy, resulting in data with

poor signal / noise ratios due to atmospheric turbulence corrupting the data. Consequently, the quality of the resulting curve-fits becomes worse, leading to less confidence in the estimated parameters and thus the speed increments between flight test points must be relatively small. The number of flight test points considered is often large. Although the test hardware, computational equipment and analysis techniques used for flight flutter testing have improved with time, aircraft have also become progressively more complex in construction, geometry, flexibility and aerodynamic improvements have led to thinner wings. Also, the influence of non-linear effects is becoming greater although the industry bases most of its analysis on linear aerodynamic and structural models that cannot predict such phenomena as Limit Cycle Oscillations (LCO). Consequently, no reduction in the time required to clear the flight flutter envelope has materialised despite the considerable improvements in technology. Meanwhile, costs have increased dramatically. Henshaw, McKiernon and Mairs [8] state that 75% of effort for flutter clearance is in the modelling and analysis stage, and this results in 25% of the costs. The other 25% of the total effort is devoted to the validation and qualification phases with an associated 75% of the total cost.

In this paper, the current state of the art of the key elements that make up flight flutter testing and also aeroelastic computational modelling and prediction, structural and control modelling, and ground vibration testing, is reviewed. Suggestions are made as to how recent advances in a range of research areas could be used to speed up the whole flight flutter test process and reduce costs whilst still keeping, if not improving, the levels of safety.

2. The Changing Nature of Aircraft Design and Its Effect on Flight Flutter Testing

Recent aircraft designs have tended to differ in a number of significant ways from the designs of, say, 20 years ago. Airframe structures are more flexible with less damping, primarily through the use on modern construction techniques such as use of composites and diffusion bonded structures. The application of structural optimisation methods to optimise the structure with minimum mass has led to designs with far less excess structure than before. The design of aerodynamic surfaces has become more advanced leading to thinner wings and more complex aerodynamic shapes. The complexity of flight control system technology has also developed, leading to a far greater variety and number of aeroservoelastic cases that must be considered [129,132]. Likewise, the use of new technologies such as stealth has led not only to different types of aeroelastic problem, but also a dramatic increase in the number of flutter cases that need to be considered. Further changes in aircraft design will follow, for instance there are a number of research programmes [9-11] world-wide investigating the use of aeroelastic behaviour as a positive benefit rather than as a problem that requires a stiff, heavy structure to reduce its effect.
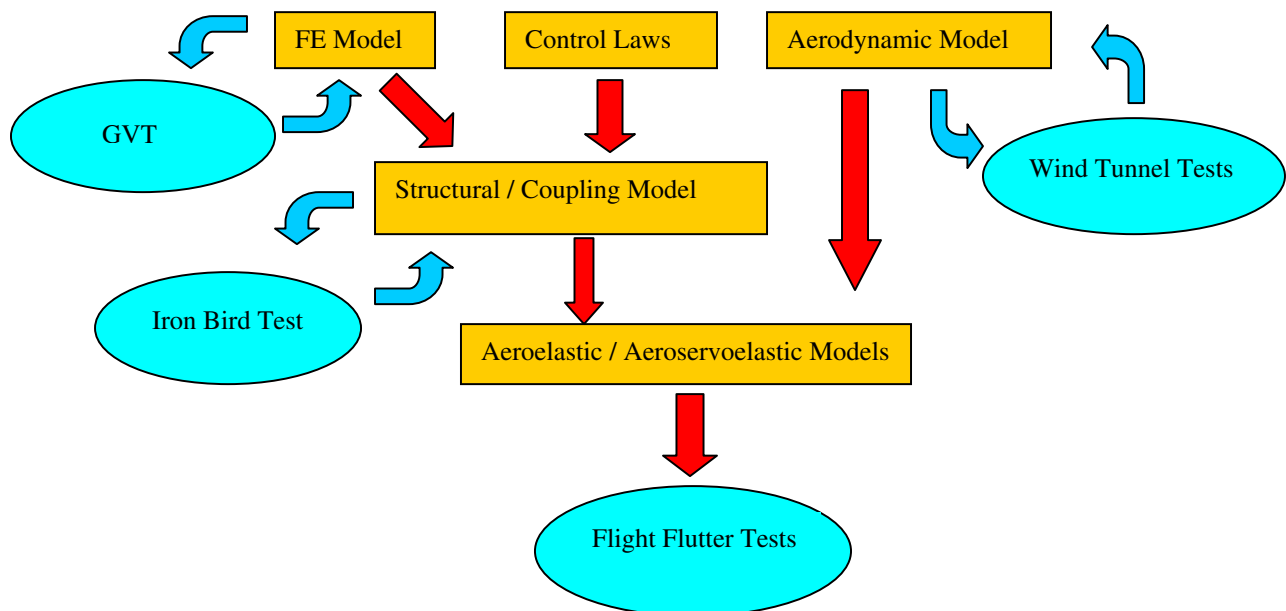
Figure 1. Aircraft Certification Procedure.

These fundamental changes in aircraft design and manufacture have increased the importance of non-linear aeroelastic phenomena [12-14]. The non-linearities manifest themselves via structural (freeplay, stiffening effects, large displacement effects [15]), aerodynamic (transonic effects) and control (time delays, non-linear control laws [16]) mechanisms. One of the key phenomenon that needs to be considered is Limit Cycle Oscillations (LCO). Although not immediately catastrophic, unlike flutter, LCO can be thought of as "only" a fatigue or weapon aiming problem. However, in terms of the prediction of aircraft aeroelastic behaviour, and in particular flight flutter testing, such non-linear phenomena cause significant problems [113]. The vast majority of aeroelastic modelling and flutter clearance is undertaken using linear methods, and these techniques cannot predict the occurrence of non-linear phenomena. Consequently, there is a danger of unforeseen non-linear aeroelastic effects occurring during a flutter test which, at best, cause a significant delay in the flutter clearance and, at worst, can cause an "incident" to occur [114]. A good example of this is the prediction of LCOs occurring when different stores combinations are used on military aircraft; a large amount of flight testing is required to establish the safe flight envelope as there is no efficient predictive alternative. [115,116]
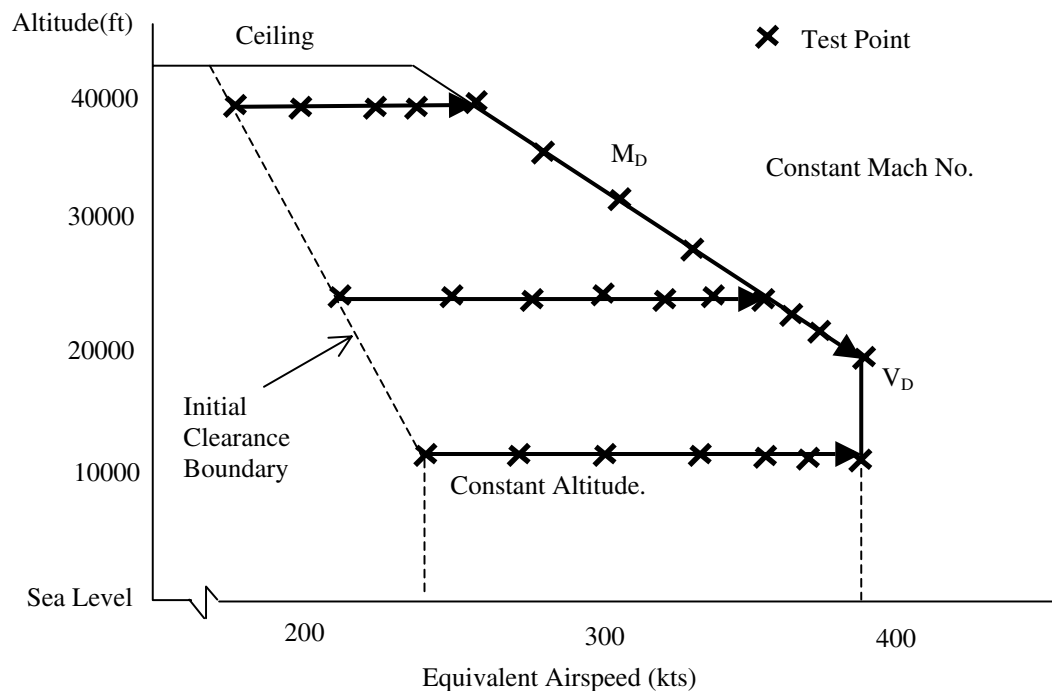
Figure 2. Typical Flight Clearance Envelope

Hardware	Telemetry	Analogue Computer	Digital Computer		
Excitation	Inertial Exciters	Aerodynamic Vanes	FCS		Slotted Rotating Vane
Analysis Methods	Spectral Plotting	Flutter Margin	Fast Fourier Transform	Advanced System Identification Algorithms	μ Method time/frequency methods
Processing of Data	By Hand		Automated Processing	Interactive Processing	
	1950s	1960s	1970s	1980s	1990s

Figure 3. Major Advances in Flight Flutter Testing Methodology

3. Future Developments in Flight Flutter Testing

The last decade has seen a dramatic rise in the interest in modelling and prediction of non-linear aeroelastic effects that can arise due to structural, aerodynamic and control non-linearities. There has also been much interest in identifying non-linear structural models and also predicting flutter boundaries using coupled CFD / structures codes. Other work has considered the analysis of measured flight test data in order to determine flutter boundaries. However, these new developments have not found their way, as yet, to becoming standard use in industry and there is still an overriding reliance upon linear models.

The goal of "Certification by Analysis" has much merit, although this author is horrified at the idea of totally eliminating experimental testing altogether. In respect to flight flutter testing, it is foreseen that a certain amount of testing on the ground and in the air will have to remain. Reductions in both the time and cost of flutter clearance will be achieved by decreasing the number of test flights that are required. This goal can only be achieved by developing more accurate aeroelastic models that can be partially achieved by deducing more information from the data obtained during the ground tests and also during the flight test. The inclusion of more non-linear effects than are currently used will be particularly important along with consideration of the variation in aeroelastic behaviour across aircraft fleets and the effects of ageing. With this in mind, the following sections review the current status of all aspects of the certification process, from aeroelastic modelling through to the flight flutter test itself, in order to examine where possible advances can be made.

3.1   Computational Aeroelasticity

The past decade has seen a significant amount of effort [17-19,83,84] devoted towards the numerical solution of transonic aeroelastic phenomena, not only in the prediction of transonic dip effects but also towards that of LCO. Euler and Navier-Stokes schemes have been both weakly and strongly coupled with structural FE models. Much work has been directed towards the consequences of dealing with two separate meshes, one fluid and the other structural. These approaches are a major advance compared to the linear doublet / vortex lattice types of approach that is still widely used throughout industry and enable non-linear aerodynamic effects to be modelled [82]. Results show that in order to capture all of the physics of non-linear aeroelastic systems in the transonic regime (i.e. the displacements rather than just the frequency of the LCO) very sophisticated models need to be used. The researchers in this field are to be applauded for the development of numerous test cases [20,70] that act as benchmarks used to compare different approaches.

Despite the continual improvements in computational speed and memory, we are still many years, if not decades, from achieving the goal of computing every conceivable case in a practical time scale. Rather than performing a simulation clearance as opposed to flight testing, other techniques should be used to show where in the flight envelope such accurate simulations are needed. Current implementations tend to concentrate upon the non-linear aerodynamic aspects and there is a need to consider the interaction of non-linear structural elements and control systems [85].

3.2   Wind Tunnel Testing

Wind tunnel testing is often used for new configurations in order to obtain aerodynamic data, particularly in the transonic regime [72,79-81,75,76] in support of the CFD calculations [21], particularly in regimes such as buffet where accurate prediction is rather problematic, and also to correct simpler aerodynamic models. There are various areas of uncertainty when performing such tests, for instance: the constraint effects of the tunnel walls and boundary layer, interference effects of the model support, tunnel blockage effects and scaling issues resulting from testing at Reynolds numbers much less than those achieved in real flight. CFD calculations can be used to provide corrections for the wind tunnel effects [74].

Wind tunnel testing is very expensive, both in the construction of scaled models and the use of transonic wind tunnels. Effort is required in order to make the procedure more efficient, through the use of non-contact measurement approaches and simpler models. There is a need to support some of the other technical topics

discussed there through the provision of more benchmark test cases, particularly of aeroelastic models, and also tests where the structure itself is non-linear [73,77,78].

3.3   Structural Modelling

A vast amount of experience has been gained [22] in the use of Finite Element (FE) models for the prediction of structural behaviour although there are still concerns regarding the accuracy of predictions of ultimate loads for static behaviour. As regards dynamic calculations, the FE method has gradually replaced the "stick" models traditionally used by the aerospace industry. A limitation is that the majority of modelling is based upon linear elements, and much work is required to reliably include non-linearities such as joints into structural models. Part of this process will rely on accurate "updating" methods that adjust (i.e. correct) the FE model based upon vibration testing results. Although much work has been devoted to updating methodologies over the past two decades, there are still serious issues in the applicability to real size structures. A recent Garteur exercise [23,24] showed that much progress has been made, although the structures considered are still on a laboratory scale.

A further important issue with structural modelling is that of damping. For many years it has been assumed that it is acceptable to use proportional damping, however, this is not always the case in real structures even if they behave linearly. It can be shown that the proportional damping assumption can cause significant inaccuracies in dynamic response calculations [25], and this will in turn lead to inaccuracies in the aeroelastic calculations where damping is a very important parameter. The damping also has an important contribution to the magnitude and phase of active control feedback [16]. More work is required towards the inclusion of accurate damping models, initially in the measurement and modelling of non-proportional damping, and then non-linear damping.

3.4   Ground Vibration Testing

The standard approach for ground vibration testing in the aerospace industry has not changed a great deal over the past 40 or so years. Traditionally a multi-shaker force appropriation (phase resonance) approach [26,100-102] has been used to excite each mode individually, which enables immediate comparison with the FE model via direct measurement of the natural frequency, mode shape and generalised mass. By exciting around the mode the damping ratio can also be measured. The original manual approach has been replaced with automated procedures. Although most of the modal analysis community tends to use phase separation methods as they are much quicker and easier to implement, these methods are not so commonly used in the aerospace industry as the resulting complex modes are difficult to compare with the FE normal modes.

There is a need to advance the test methodology to gain further information about any structural non-linearities that may be present in the structure. It is required to determine whether non-linearities exist, what type they are, and whereabouts on the structure they can be found. Much work has been devoted [27] to the identification of non-linear structures, but this has resulted in a wide range of different models that have varying degrees of usefulness as regards to the resulting FE models. Also, most experimental validations of these techniques have only been undertaken on laboratory structures containing a few modes. One very promising approach [28,71] is to identify any non-proportional damping and non-linearities as an addition to the usual modal model using the so-called resonant decay method. By using a modal approach it is possible separate modes in terms of whether they have linear or non-linear characteristics and to consider groups of modes that are coupled either due to non-proportional damping or by non-linearities.

3.5   Aeroelastic Modelling

Having established the linear structural and unsteady aerodynamic models, it has been traditional to use one of a number of frequency matching techniques in order to determine the flutter condition, frequency and associated modes. The inclusion of structural and aerodynamic non-linearities does away with the ability to simply predict the flutter point, and there are at present not many techniques that can be used to predict behaviour such as LCO without resorting to numerical simulation of every test point. The harmonic balance method [67] has been used to predict LCO behaviour for non-linear structural cases such as freeplay but there are limits as to the effectiveness

of this approach. There has been much work on characterising non-linear aeroelastic behaviour, and this now needs to be extended to larger systems [118-128].

3.6   Aeroservoelastic Modelling

There are typically many control laws in any flight control system, with the inclusion of notch filters to eliminate any undesirable behaviour. The resulting transfer function contain discrete non-linearities, not only from the different laws, but also from time delays due to signal processing constraints[16, 29-31,37]. It is usual to model these non-linearities with linearised approximations, which enable flutter calculations to be made in a similar manner to a non-FCS aircraft. The number of failure cases that need to be considered also increases dramatically when a FCS is involved [131].

In order to achieve a greater accuracy in aeroservoelastic modelling that will no doubt be needed in the future, the use of non-linear models will have to be employed. As with aeroelastic testing, there is a danger that a large amount of simulation will be required to investigate every case, particularly as the non-linearities will be of a discrete nature and will include switching between a large number of different laws.

3.7   Structural Coupling Tests

For aircraft with active control systems, the coupling of the structure and the flight control must be tested [16,30-36,130] to see how well the linearised laws compare with reality. The procedure consists of frequency sweep excitation of the flight control system, and also the application of loads on the control surfaces with open and closed loop control system. Although there are no airforces present, such tests are extremely important, as this is the only chance to test whether there are coupling problems that could have disastrous consequences. This is one testing element of the certification procedure that is not seen as changing dramatically.

3.8   Reduced Order Modelling

Despite the dramatic increases in computational power, typical aeroelastic models are very large if non-linearities are included, even if considered in a modal sense. Consequently, a number of researchers are investigating means of developing a reduced order modelling capability that will enable predictions to be made using much smaller models. Such approaches will enable a wide range of design cases to be considered efficiently in order to determine the critical cases and also to perform parameter design studies. Outputs from full aeroelastic models are then curve-fitted in order to produce the reduced order model [103,106,107]. Examples include curve fitting impulse responses [38] to produce a linearised model of the aerodynamic state space model [108-112], and fitting of a Volterra series to determine the non-linear effects [39]. Many investigations have considered the POD approach[111].

Other work has examined the use of Normal Form Theory to model aeroelastic systems containing non-linear structural and aerodynamic effects [40,41,104,105]. This approach enables the full non-linear behaviour to be predicted, including the shape of the LCO. There has to be a compromise between including enough non-linear terms to model the behaviour accurately while reducing the model to a small enough size to allow the normal forms to be computed.

3.9   Excitation Signals and Devices.

One of the key difficulties with flight flutter testing is the noisy environment that it is performed in. Although there have been many cases where stick raps or simply turbulence has been used as an excitation signal, some form of excitation device must be used if good quality data is to be obtained. It is very difficult to obtain estimates of the modal properties if the data is poor, and this is ever more the case if non-linear identification is attempted. Since the invention of the slotted rotating cylinder flutter vane [42-44] in the early 1990s, no further advances in excitation technology have been made apart from the suggestion of a contra-rotating propeller driven device for stores[133]. When ground testing an aircraft, it is considered better to use multi-shaker technology in

order to excite close difficult modes, so surely multi-exciter technology should be used in flight. A number of issues are raised as to how to achieve this. One possibility is to use a variety of different exciters (inertial masses, fcs, vanes) placed around the aircraft [45,46], or to use a number of aerodynamic vanes for instance attached to combinations of stores. The positioning of both the exciters and transducers should be optimised using theoretical models before starting the test.

The type of excitation signal should also be considered. When the conventional linear or logarithmic chirp (fast swept-sine) excitation is used, the time data between modes is effectively wasted. Some work has been undertaken to develop both chirp [48] and random signals [49,50] that will give consistently good signal noise ratios with effective crest factors. It would be of interest to implement some of these methods on real aircraft in order to see how well the estimated parameters compare to those obtained using more conventional approaches[86]. There is a need to develop a device for applying random signals in flight apart from the fcs.

3.9   Modal Parameter Identification Methods for Flight Flutter Testing

There is a wide range of different modal parameter identification methods [51] that have been used for flight flutter testing in order to identify natural frequencies and damping ratios from the test data. These techniques have varied in sophistication from a simple half power points analysis [44] to multiple input – multiple output maximum likelihood algorithms [52]. The modal filter approach has been the only recent innovation in this area [69]. All these methods have been used in a form that assumes that the system is at a constant flight condition and is linear. Surprisingly it is unusual to make use of the mode shapes [54] which benefits the mode tracking procedures. Also, there has been little consideration [52,53] of the differences between a conventional modal test on the ground and a test performed in flight. The major difference is the presence of significant process noise acting through the aircraft structure in the form of turbulence. This corruption affects the data in a different way compared to that of the small amounts of measurement noise encountered on a ground test. Further work is required to investigate the reported improvements in using parameter estimation methods that take this into account. The use of techniques such as blind signal processing should be investigated to determine whether this is a suitable means of improving the quality of flight test data. In flight non-linear identification should also be considered.

Recent studies have investigated the use of using some form of on-line estimator [55,58,66,86,97-99] to track changes in the modal parameters as the aircraft changes between flight conditions. The current vogue is for time-frequency methods such as wavelets [56,57,64] or short term Fourier transforms [59], however, an on-line time domain method is just as suitable. If it were possible to track accurately on-line frequency and damping estimates, then this would be a key advance in extending the gap between different flight test points. Taking the view that reaching a test point is a good indication that most (but unfortunately not all) flutters will not occur, then an exciter could be used continuously (the methodology does not work so well for turbulent input [60]) to excite the aircraft as the flight envelope is expanded.

An extension of the multi-shaker test is to apply force appropriation in flight. The burst appropriation approach could also be used to identify non-proportional damping and non-linearities.

3.10   Flutter Prediction Based Upon Flutter Test Data

One of the most critical decisions during any flight test programme is the decision to move onto the next flight test point. Traditionally this has been achieved by tracking and extrapolating the damping values and determining whether stability is maintained. Methods such as the flutter margin and the envelope function [61,93] can be employed to use the estimated frequency and damping values to predict the flutter speed. A notable recent development is the use of the μ robustness methodology [62,89,94] to predict the flutter speed, along with methods based upon neural networks [65,91,95,96,117], time domain methods [63,68] and others [90,92]. These approaches can be combined with the on-line identification methods to produce an on-line estimate of the critical speed that again can aid an increased gap between test points.

The above approaches are suitable for the analysis of linear systems, but cannot be used reliably when there are non-linearities of whatever form. Procedures need to be developed to analyse data from the earliest flight test points in order to establish what non-linearities exist and whereabouts on the structure they occur. These non-linear models could then be used to predict points of instability and also non-linear phenomena such as LCO.

4. Discussion

The above analysis shows that there are a number of improvements that can be made so that the amount of flight flutter test points can be reduced. From the aeroelastic (and aeroservoelastic) point of view, we are well on the way towards improving the modelling capability in terms of non-linearities. However, this is only one step in producing a truly predictive capability and there is a requirement to use the CFD methods in an efficient and intelligent manner. Improvements in reduced order modelling are needed so that prediction of LCO and flutter behaviour can be made efficiently. These efficiency gains will enable parameter studies and consideration of all critical cases to be considered. Having defined the critical flight envelope regimes, the CFD methods can be used to explore them in more detail. These improvements in the modelling capability will provide a greater confidence in the aeroelastic predictions and the number of flight test points can be reduced.

As regards the actual test, further improvements need to be made in the type of excitation signals, along with multiple excitation sources, which will improve the noise signal ratios. The possibilities of using more advanced system identification algorithms that account for process noise should be considered, along with on-line identification schemes with continuous excitation signals throughout the flight envelope to allow for constant monitoring of the stability. Methodologies such as the μ robustness method need further examination for the prediction of the flutter speed, along with consideration of the confidence of the estimated parameters. Such approaches will enable bigger steps to be taken between flight test points. Flight test data should be analysed to determine whether there are non-linearities in the data, and the reduced order modelling approaches adapted to produce in-flight estimates of the characteristics of any non-linear behaviour and its whereabouts in the flight envelope.

In order to achieve the savings in flutter test time, greater effort will have to be placed in the analysis part of the certification process. Ground Testing should not be eliminated but enhanced in order to obtain more information, particularly non-linearities. The 75:25:25:75 distribution of effort/cost for analysis/clearance described by Henshaw, McKiernon and Myers [8] will need to change to become something more along the lines of 90:10:10:90. Also, as the number of flight flutter test programmes decreases, along with the number of experienced practitioners, there is a greater need for more comparative studies using benchmark data and discussions / workshops between interested parties e.g. the recently started TTCP activity in flutter testing. To help maintain the level of expertise, another possibility is the development of a "flight flutter test simulator" where the flutter clearance of an aircraft could be undertaken using predefined sets of data which could contain a variety of different problems (noisy data, non-linearities, etc.) It is dangerous to consider reducing the amount of testing whilst reducing the expertise that could determine whether problems were likely to arise during a test programme.

5. Conclusions

The current status of all elements in aeroelastic / aeroservoelastic modelling and flight flutter testing has been reviewed with the aim of determining how flutter testing can be performed in less time and cost while maintaining, if not improving, safety. Modelling capabilities should be improved to include all forms of non-linearity and Ground Testing improved to aid this. Improvements in reduced order modelling will be required in order to make efficient use of the CFD based simulations. Flutter test procedures and analysis should be extended to allow for on-line updating of the stability and also non-linear identification to predict phenomenon such as LCO from the flight data. The world-wide flutter test community should ensure that expertise is not lost through loss of personnel and should strive towards the development of benchmark flight flutter test data sets.

6.   References   IFASD = International Forum on Aeroelasticity and Structural Dynamics
                              SDM = Structures Structural Dynamics and Materials Conference

1.   Collar A R, "50 Years of Aeroelasticity" Aerospace v5 n2 1978 pp 12 - 20
2.   Garrick IE & Reed W H, "Historical Development of Aircraft Flutter" J.Aircraft v18 n11 1981 pp 897 - 912.
3.   Kehoe M.W., "A Historical Preview of Flight Flutter Testing" AGARD Conf. Proc. 566 Advnanced Aeroservoelastic Testing and Data Analysis. Paper 1. 1995.
4.   Wright J.R., "Flight Flutter Testing" Lecture Series on Flutter of Winged Aircraft. Von Karman Institute 1991.
5.   NASA SP-385 Flight Flutter Testing Symposium. Washington. 1958.
6.   NASA SP-415 Flight Flutter Testing Techniques, Dryden Flight Research Centre. 1975
7.   AGARD CP 566 Advanced Aeroservoelastic Testing and Data Analysis. Rotterdam. 1995.
8.   Henshaw MJ, McKeirnon D & Mairs C, "Flutter Prediction for Complex Configurations" AGARD Conf Proc 507 Numerical Unsteady Aerodynamic and Aeroelastic Simulation Aalborg. 1997 paper 12.
9.   Flick PM & Love MH, "The Impact of Active Aeroelastic Wing Technology on Conceptual Aircraft Design" RTO MP-36 " Structural Aspects of Flexible Aircraft Control" Paper 10. 1999
10. Schweiger J & Krammer J, "Active Aeroelastic Aircraft and its Impact on Structure and Flight Control Systems Design" RTO MP-36 " Structural Aspects of Flexible Aircraft Control" Paper 11. 1999
11. McGowan AM, Horta LG, Harrison JS & Raney DL, "Research Activities within NASA's Morphing Program" RTO MP-36 " Structural Aspects of Flexible Aircraft Control" Paper 13. 1999
12. Dunne S.A., Farell P.A, Budd P.J., Arms, P B, Hardie CA & Rendo CJ., "F/A-18A Flight Flutter Testing – Limit Cycle Oscillation or Flutter ?" IFASD 2001. V3 pp 193-204.
13. Lee BHK, "Recognising Non-Linear Phenomena in Flight Flutter Testing" Canadian Aeronautics and Space Journal v45 n1 1999 pp 17-24.
14. Girard M, "Flutter Testing in the 90's (The GBU-24 Saga)" IEEE Aerospace Conf 1998 pp 39-50.
15. Oliver, M., Climent, H., & Rosich F., " Non Linear Effects of Applied Loads and Large Deformation on Aircraft Normal Modes" RTO MP-36 " Structural Aspects of Flexible Aircraft Control" Paper 21. 1999
16. Koenig K., "Pretension and Reality of Flutter Relevant Tests" AGARD Conf. Proc. 566 Advanced Aeroservoelastic Testing and Data Analysis. Paper 17. 1995.
17. AGARD Conf. Proc. 507. Transonic Unsteady Aerodynamics and Aeroelasticity San Diego 1991.
18. AGARD Report 822. Numerical Unsteady Aerodynamic and Aeroelastic Simulation" Aalborg. 1997.
19. Lacabanne M & Zwaan RJ, "Technical Evaluation Report on Numerical Unsteady Aerodynamic and Aeroelastic Simulation" Aalborg. 1997
20. Ruiz-Calacera et al. "A New Compendium of Unsteady Aerodynamic Test Cases for CFD: Summary of AVT WG003 Activities" IFASD 1999 pp 1 – 12.
21. Cross AGT, " The Use of Computational Fluid Dynamics on Support of Wind Tunnel Testing" I.MechE S555/002/98 Aerospace Application of Computational Methods Versus Testing. pp 7 –20 1998
22. Morris AJ, Dullaway N, Attwall P & Vignjevic R, "Augmenting the Role of Finite Element Structural Analysis in Airworthiness Assessment I.Mech.E S555/004/98. 98 Aerospace Application of Computational Methods Versus Testing. pp 31 – 41 1998
23. Goge D & Link M, " Parametric Updating of Finite Element Models by Minimizing Response Residuals at Resonances" COST Int Conf on Structural System Identification 2001. pp 419 - 430
24. Friswell M I & Mottershead J E, "Physical Understanding of Structures by Model Updating" COST Int Conf on Structural System Identification 2001. pp 81- 98
25. Naylor S, Wright JR & Cooper JE, 'Identification of Non-Proprotionally Damped Structures using a Force Appropriation Technique' 23rd Int Seminar on Modal Analysis 1998
26. Wright JR, Cooper JE & Desforges MJ ,' Normal Mode Force Appropriation – Theory and Application' Mechanical Systems and Signal Processing v31 n2 1999 pp 217-240
27. Worden K & Tomlinson G R, "Non-Linearity in Structural Dynamics" IoP. 2001.
28. Naylor S, Cooper JE & Wright JR, 'Modal Parameter Estimation of Non-Proportionally Damped Systems Using Force Appropriation' 15th International Modal Analysis Conference 1997

29. Becker J & Vaccaro V., "Aeroservoelastic Design, Test Verification and Clearance of an Advanced Flight Control System" AGARD Conf. Proc. 566 Advanced Aeroservoelastic Testing and Data Analysis. Paper 22. 1995.

30. Vaccaro V & Becker J., " Ground Structural Coupling Testing and Model Updating in the Aeroservoelastic Qualification of a Combat Aircraft" AGARD Conf. Proc. 566 Advanced Aeroservoelastic Testing and Data Analysis. Paper 23. 1995.

31. Noll T E, Perry B & Kehoe M W, "A Quarter Century of NASA Wind-Tunnel and Flight Experiments Involving Aeroservoelasticity" AGARD Conf. Proc. 566 Advanced Aeroservoelastic Testing and Data Analysis. Paper 14. 1995

32. Wray WW, "F22 Structural Coupling Lessons Learned" RTO MP-36 " Structural Aspects of Flexible Aircraft Control" Paper 2. 1999

33. Baker, ML, Goggin PJ & Winther BA, " Aeroservoelastic Modeling, Analysis and Design Techniques for Transport Aircraft" RTO MP-36 " Structural Aspects of Flexible Aircraft Control" Paper 3. 1999

34. Becker, J. , Caldwell, B. & Vaccaro V., "The Interaction of Flight Control System and Aircraft Structure" RTO MP-36 " Structural Aspects of Flexible Aircraft Control" Paper 4. 1999

35. Vaccaro V., Caldwell B. & Becker J., "Ground Structural Coupling Testing and Model Updating in the Aeroservoelastic Qualification of a Combat Aircraft" RTO MP-36 " Structural Aspects of Flexible Aircraft Control" Paper 5. 1999

36. Luber W & Becker J., "An Integrated Design Procedure for Aircraft Structure Including the Influence of Flight Control System on Aircraft Flutter" RTO MP-36 " Structural Aspects of Flexible Aircraft Control" Paper 6. 1999

37. Dimitriadis, G. & Cooper J.E., " Characterisation of Nonlinear Aeroserovelastic Behaviour" RTO MP-36 "Structural Aspects of Flexible Aircraft Control" Paper 8. 1999

38. Prudhomme S, Ebdon D & Pacheco T, "On the use of POD and ERA Techniques for Unsteady Aerodynamics Identification" IFASD 2001 pp 249 – 256.

39. Silva WA et al. "Reduced Order Modelling – Cooperative Research and Development at NASA Langley" IFASD 2001 pp 159 – 174.

40. Sedhaghat A, Cooper JE, Wright JR and Leung AYT, "Limit Cycle Oscillation Prediction for Non-linear Aeroelastic Systems", Aeronautical Journal, v106 n 1056 Jan 2002 pp 27 - 32.

41. Sedhaghat A, Cooper JE, Wright JR and Leung AYT, "Limit Cycle Oscillation Prediction for Aeroelastic Systems with Continuous Non-linearities," AIAA-2000-1397, AIAA , Atlanta, 2000.

42. Schippers P & Persoon A J, "Flight Flutter Testing of a Turbo-Prop Aircraft using External Excitation Devices" AGARD Conf. Proc. 566 Advanced Aeroservoelastic Testing and Data Analysis. Paper 3. 1995.

43. Shirley B M & Anderson E L, "US Air Force / DEI Flutter Exciter Test Program" AGARD Conf. Proc. 566 Advanced Aeroservoelastic Testing and Data Analysis. Paper 4. 1995.

44. Dickenson M. "CF-18 Flight Flutter Test Techniques" AGARD Conf. Proc. 566 Advanced Aeroservoelastic Testing and Data Analysis. Paper 11. 1995.

45. Desforges MJ, Cooper JE & Wright JR, "Force Appropriation for Flutter Testing" IFASD1995 Paper 72

46. William C, Cooper JE & Wright JR, "Force Appropriation for Flight Flutter Testing using SMART Devices" SDM 2002.

47. Burrows, AP, Wright JR & Coote JA, "Optimal Excitation for Aircraft Testing" I.MechE J. Aerospace Engineering. 1995

48. Burrows AP, Worden K & Wright J R, "On the use of Rising Falling Chirp Excitation for Vibration Testing" J. Sound and Vibration v192 n2 1996 pp 599 - 604

49. Cooper J.E. & Wright J.R "On the Optimisation of Random Signals with Minimum Rate for Flight Flutter Testing" IFASD. 1997. pp 299-306.

50. De Fonseca. P, Cooper JE & Swivers J, "Optimal Random Excitation" Proc Int Seminar on Modal Analysis 1996 pp 903 – 913.

51. Cooper J E, "Parameter Estimation Methods for Flight Flutter Testing" AGARD Conf. Proc. 566 Advanced Aeroservoelastic Testing and Data Analysis. Paper 10. 1995.

52. Van der Auweraer & Guillaume P, "A Maximum Likelihood Parameter Estimation Technique to Analyse Multiple Input – Multiple Output Flutter Test Data" AGARD Conf. Proc. 566 Advanced Aeroservoelastic Testing and Data Analysis. Paper 12. 1995.

53. Emmett PR, Cooper JE & Wright JR, "Improved Frequency Domain Modal Parameter Identification" IFASD, 1995 paper 55.

54. Cooper J.E, Desforges M.J., Emmett P R & Wright J R, " Advances in the Analysis of Flught Flutter Test Data" AGARD Conf. Proc. 566 Advanced Aeroservoelastic Testing and Data Analysis. Paper 13. 1995.

55. Farhat C, Harris C & Rixwn DJ, "Expanding a Flutter Envelope using Accelerated Flight Data" AIAA Structures, Structural Dynamics and Materials Conf. 2000 .

56. Sahasrabudhe V, Thompson PM, Klyde DH & Mathis S. "Flutter Detection using Wavelet Based Time Varying Transfer Functions" Proc AIAA Atmospheric Flight Mechanics Conf 2000 pp 384-394.

57. Lind R, Brenner M & Freudinger LC, "Wavelet Applications for Flight Flutter Testing" NASA 1999-61885

58. Lo W, Shih C & Yan C, "An On-Line Flutter Analysis System" AIAA Structures, Structural Dynamics and Materials Conf. 2000 .

59. Dimitriadis G & Cooper J E, "On-line Flight Flutter Testing" COST Int Conf on Structural System Identification 2001. pp 583 – 592.

60. Cooper JE, Desforges MJ, & Wright JR, "The On-line Envelope Function – A Guide to Aeroelastic Stability" IFASD 1993 pp 981 - 998

61. Dimitriadis G & Cooper J.E., " Flutter Prediction from Flight Flutter Test Data" AIAA J.Aircraft v38 n2 pp355-367 2001.

62. Lind R, "Flight Testing with the Flutterometer" IFASD 2001 pp 237 – 248.

63. Torii H & Matsuzaki Y, " New Flutter Prediction Method based on ARMA model II Application to Supersonic Wind Tunnel Testing" Japan Soc Aeronautical and Space Sciences J. v38 n7 2000. pp191- 195

64. Lind R, Brenner M & Freudlinger LC., "Wavelet Applications for Flutter Testing" IFASD1999 pp393-402.

65. Cooper J.E & Crowther W J., "Flutter Speed Prediction During Flight Flutter Testing using Neural Networks" IFASD 1999 pp 255-263.

66. Rixen DJ, Farhat C & Peterson LD, "Simulation of the Continuous Parametric Identification of an Accelerating Aeroelastic System" 37th AIAA Aerospace Sciences Meet. 1999.

67. Luber W, "Flutter Prediction on a Combat Aircraft Involving Backlash and Actuator Failures on Control Surfaces" IFASD. 1997. pp 173-182.

68. Torri H & Matsuzaki Y, " Flutter Boundary Prediction Based on Nonstationary Data Measurement" AIAA J.Aircraft 1997 v34 n3 pp 427-432.

69. Shelley SJ & Pickrel CR, "New Concepts in Flight Flutter Parameter Estimation" 15th Int Modal Analysis Conference pp 490-496 1997.

70. Girodroux-Lavigne et al. 'Comparative Study of Advanced Fluid-Structure Interaction Methods in the Case of a Highly Flexible Wing (Results from the UNSI Program)' IFASD 2001 v2 pp 1 – 16.

71. Naylor S, Wright JR & Cooper JE, 'Identification of a Non-Proportionally Damped Truss Structure' Testing' IFASD 1999 pp 847-856.

72. Granasy P, Matsushita M & Saitoh K, 'Non-Linear Aeroelastic Phenomena at Transonic Region' IFASD 1997 v3 pp 379 – 388

73. Lacabanne M & Humbert M, 'An Experimental Analysis of the Aeroelastic Behaviour with a Freeplay in a Control Surface' IFASD 1997 v3 pp 239 – 246.

74. Brink-Spalink J & Bruns JM, 'Correction of Unsteady Aerodynamic Influence Coefficients using Experimental or CFD Data' IFASD 2001 v2 pp 175 – 182.

75. Nakamichi J & Kheirandish HR, 'Nonlinear Flutter Simulation of NAL Non-Powered SST Experimental Airplane and Related Wind Tunnel Tests' IFASD 2001 v3 pp 571-580.

76. Edwards JW, Schuster DM, Spain CV, Keller DF & Moses RW, 'MAVRIC Flutter Model Transonic Limit Cycle Oscillation Test' IFASD 2001 v3 pp 581 – 595.

77. Holden M, Brazier R & Cal A, 'Effects of Structural Non-Linearities on a Tailplane Flutter Model' IFASD 1995 paper 60.

78. Dowell EH, Kholder D & Tang D, 'Non-Linear Aeroelastic Response of a Typical Airfoil Section with Control Surface Freeplay' 41st SDM 2000 AIAA-2000-1621.

79. Cole SR & Garcia JL, 'Past, Current and Future Capabilities of the Transonic Dynamics Tunnel from an Aeroelasticity Perspective' 41st SDM 2000 AIAA-2000-1767.

80. Florance JR & Rivera JA, 'Contributions of Transonic Dynamics Tunnel to Airplane Flutter Clearance' 41st SDM 2000 AIAA-2000-1768.

81. Edwards J, Schuster D, Spain C, Keller D & Moses R, 'MAVRIC Flutter Model Transonic Limit Cycle Oscillation Test' 42nd SDM 2001 AIAA-2001-1291
82. Palacios R, Climent H, Karlsson A & Winzell B, 'Assessment of Strategies for Correcting Linear Unsteady Aerodynamics using CFD or Test Results' IFASD 2001 v2 pp 195-210.
83. Thomas J, Dowell EH & Hall K, 'Nonlinear Inviscid Aerodynamic Effects on Transonic Divergence, Flutter and Limit Cycle Oscillations' 42nd SDM 2001 AIAA-2001-1209.
84. Tang L, Bartels R, Chen P & Liu D, ' Simulation of Transonic Limit Cycle Oscillations Using a CFD Time Marching Method' 42nd SDM 2001 AIAA-2001-1290
85. Schulze S, 'Simulation of Nonlinear Airfoil Control Surface Flutter at Subsonic Speeds using Classical Unsteady Aerodynamics and an Euler Method' IFASD 1999 pp 53-70.
86. Lind RC, Brenner MJ & Freudinger LC, 'Improved Flight Test Procedures for Flutter Clearance 'IFASD 1997 v3 pp 291 – 298.
87. Ramsay RB, 'Flutter Certification and Qualification of Combat Aircraft' IFASD 1995 paper 92.
88. Lo W, Shih C & Yan C, 'An On-line Flutter Analysis System' 41st SDM 2000 AIAA-2000-1830.
89. Lind RC & Brenner MJ, 'A Worst Case Approach for OnLine Flutter Prediction'IFASD1997 v2 pp79-86.
90. Denegri CM, 'Correlation of Classical Flutter Analysis and Nonlinear Flutter Response Characteristics' IFASD 1997 v2 pp 141-148.
91. Denegri CM & Johnson MR, 'Limit Cycle Oscillation Prediction using Artificial Neural Networks' IFASD 1999 pp 71-80.
92. Prudhomme. S, Blondeau C, Humbert M & Bucharles A, 'An Unsteady Aerodynamics Identification Procedure for Flutter Prediction' Testing' IFASD 1999 pp 235-244.
93. Pitt DM,'Flutter Margin Determination for SDOF Aeroelastic Instabilities' IFASD2001v2pp321-332.
94. Lind RC, 'Flight Testing with the Flutterometer' IFASD 2001 v3 pp 237 – 248.
95. Lecce L, Pucci M & Pecora M, 'Flutter Speed Prediction Using the Artificial Neural Network Approach' IFASD 1995 paper 13.
96. Wong YS, Lee BHK & Wong TKS, 'Parameter Estimation in Flutter Analysis by Wavelet and Neural Networks' Testing' IFASD 1999 pp 245-254.
97. Hermans L, Van der Auweraer H & Abdelghani M , 'Identification of Structural Models During System Operation with Application to Flutter Data Analysis' IFASD 1997 v3 pp 323-330.
98. Dimitiadis G & Cooper JE, 'A Time Frequency Stability Analysis of Non-Linear Aeroelastic Systems' IFASD 2001 v2 pp 237-248
99. Brenner M , 'Nonstationary Dynamics Data Analysis with Wavelet SVD Filtering' 42nd SDM 2001 AIAA-2001-1586
100. Sinapius JM & Lake RC, 'Computer Controlled Normal Mode Testing' IFASD 1999 pp 89-100.
101. Degener M, 'Ground Vibration Testing for Validation of Large Aircraft Structural Dynamics' IFASD 1995 paper 70.
102. Gravelle A, Lubrina P & Fargette P, 'Application of Phase Separation Methods to an Actual Airplane GVT' IFASD 1995 paper 71.
103. Silva WA, 'Reduced Order Models Based on Linear and Non-Linear Aerodynamic Impulse Responses' Testing' IFASD 1999 pp 369-380.
104. Grzedzinski J, 'Flutter Calculations of an Aircraft with Non-Linear Structure Based Upon Centre Manifold Reduction' IFASD 1995 paper 61.
105. Sedaghat A, Cooper JE, Leung AYT & Wright JR, 'LCO Prediction for Aeroelastic Systems with Continuous Non-Linearities' 41st SDM 2000 AIAA-2000-1397.
106. Beran PS & Pettit CL, 'Reduced Order Modelling for Flutter Prediction' 41st SDM 2000 AIAA-2000-1446.
107. Dowell EH, Thomas J & Hall K, 'Transonic Limit Cycle Oscillation Analysis Using Reduced Order Aerodynamic Models' 42nd SDM 2001 AIAA-2001-1212
108. Silva W & Ravel D, 'Development of Unsteady Aerodynamic State Space Models from CFD Based Pulse Responses' 42nd SDM 2001 AIAA-2001-1213.
109. Pettit C & Beran P, 'In-Situ Subspace Evaluation in Reduced Order Modelling' 42nd SDM 2001 AIAA-2001-1231

110. Kim T & Bussoletti J, 'An Optimal Reduced Order Aeroelastic Modelling Based on a Response Based Modal Analysis of Unsteady CFD Models' 42nd SDM 2001 AIAA-2001-1525

111. Thomas J, Dowell EH & Hall K, 'Three Dimensional Transonic Aeroelasticity using Proper Orthogonal Decomposition Based Reduced Order Models' 42nd SDM 2001 AIAA-2001-1527

112. Raveh D & Mavris D, ' Reduced Order Model Based Upon CFD Impulse and Step Responses' 42nd SDM 2001 AIAA-2001-1527

113. Dreim DR, Jacobson SB & Britt RT, 'Simulation of Non-Linear Transonic Aeroelastic Behaviour on the B-2' Testing' IFASD 1999 pp 511-522.

114. Dunn SA, Farrell, PA, Budd PJ, Arms PB, Hardie CA & Rendo CJ, 'F/A-18A Flight Flutter Testing – Limit Cycle Oscillation or Flutter ?' IFASD 2001 v3 pp 193 – 204.

115. Alonso A, ' EF-18 BPG-2000 Stores Clearance Program' IFASD 2001 v3 pp 205 – 216.

116. Denegri CM, 'Limit Cycle Oscillation Flight Test Results of a Fighter with External Stores' 41st SDM 2000 AIAA-2000-1394.

117. Denegri CM & Johnson MR, 'Statistical Data Evaluation for Limit Cycle Oscillation Prediction using Artificial Neural Networks' 41st SDM 2000 AIAA-2000-1398.

118. Dessi D, Mastroddi F & Morino L, 'Singular Perturbation Technique for Non-linear Aeroelastic Analysis' Testing' IFASD 1999 pp 523-542.

119. Lui L, Wong YS & Lee BHK, 'Application of the Centre Manifold Theory in Non-Linear Aeroelastic Analysis' Testing' IFASD 1999 pp 533-542.

120. Mastroddi F & Bettoli A. 'Non-Linear Aeroelastic System Identification via Wavelet Analysis in the Neighbourhood of a Limit Cycle' Testing' IFASD 1999 pp 857-866.

121. Dessi L, Mastroddi F & Morino L, 'A Fifth Order No-Reconstruction Multiple Scale Solution for Hopf Bifurcation' IFASD 1997 v3 pp 355 – 362.

122. Matsushita H, Mosehilde E, Christiansen LE, Lehn-Schioler & Granasy P, 'Examination of the Two Degree of Freedom Non-Linear Math Model for Transonic Flutter' IFASD 2001 v2 pp287 – 294

123. Liu L, Lee BHK & Wong YS, 'Dynamical Analysis of Nonlinear Aeroelastic Systems with Hysteresis' IFASD 2001 v2 pp 307 – 320.

124. Angutia L, Maderuelo C, Climent H & Karpel M, 'Efficient Flutter Analysis of Aircraft with Multiple External Stores' IFASD 2001 v2 pp 333 – 346.

125. Dowell EH, Trickey ST & Virgin LN, 'Characterising Stability and Responses in a Non-Linear System' 41st SDM 2000 AIAA-2000-1329.

126. Hodges D & Patil M, 'On the Importance of Aerodynamic and Structural Geometric Non-Linearities on Aeroelastic Behaviour of High Aspect Ratio Wings' Prediction' 41st SDM 2000 AIAA-2000-1448.

127. Wong YS, Lui L & Lee BHK, ' Frequency and Amplitude Prediction of Limit Cycle Oscillations of an Airfoil' Containing Concentrated Structural Non-Linearities' 42nd SDM 2001 AIAA-2001-1293

128. Alighanbari H & Lee BHK, 'Analysis of Non-Linear Aeroelastic Signals' 42nd SDM2001AIAA-2001-1657

129. Britt RT, Jacobson SB & Arthurs TD, 'Aeroservoelastic Analysis of the B-2 Bomber' IFASD 1997 v2 pp 251 – 260.

130. Bonnet JC & Humbert M, 'A Flexible Aircraft Iron Bird for Aeroservoelastic Studies with Hardware in the Loop' IFASD 2001 v3 pp 135 – 144.

131. Becker J, Caldwell B, Vaccaro V & Carano L, 'Procedure for the Selection of Structural Coupling Critical Configuration for Flight Clearance' IFASD 2001 v3 pp 169 – 180.

132. Brenner MJ, 'Aeroservoelastic Uncertainity Model Identification from Flight Data' IFASD 2001 v3 pp 299 – 310.

133. Van Zyl LH, 'A New Concept For a Flight Flutter Excitation System' IFASD 2001 v3 pp 229 – 236.

This page has been deliberately left blank

_____

Page intentionnellement blanche

The Dependence of Store-Induced Limit-Cycle Oscillation Predictions on Modelling Fidelity

P.S. Beran, N.S. Khot, F.E. Eastep, R.D. Snyder, J.V. Zweber, L.J. Huttsell, J.N. Scott
Multidisciplinary Technologies Center
Air Force Research Laboratory (AFRL), Air Vehicles Directorate
AFRL/VASD, 2210 Eighth Street, Building 146
Wright-Patterson AFB, Ohio, 45433
United States

Abstract

Store-induced limit-cycle oscillation of a rectangular wing with tip store in transonic flow is simulated using a variety of mathematical models for the flow field: transonic small-disturbance theory (with and without inclusion of store aerodynamics) and transonic small-disturbance theory with interactive boundary layer (without inclusion of store aerodynamics). For the conditions investigated, limit-cycle oscillations are observed to occur as a result of a subcritical Hopf bifurcation, and are obtained at speeds lower than those predicted (1) nonlinearly for clean-wing flutter, and (2) linearly for wing/store flutter. The ability of transonic small-disturbance theory to predict the occurrence and strength of this type of limit-cycle oscillation is compared for the different models. Solutions computed for the clean rectangular wing are compared to those computed with the Euler equations for a case of static aeroelastic behavior and for a case of forced, rigid-wing oscillation at Mach 0.92.

Nomenclature

α	angle of attack, degrees
c	chord, ft
cg, ea	center of gravity and elastic axis, ft from leading edge
C_L, C_M	lift and moment coefficients (moment about leading edge)
i, j, k	computational index coordinates
l	span, ft
M	Mach number
Re	Reynolds number (based on root chord)
ρ	density, slugs/ft^3
t	time, nondimensional (based on freestream velocity and wing chord)
T	temperature, °R
τ	thickness to chord ratio
U	velocity, ft/sec
x, y, z	physical coordinates (streamwise, spanwise, vertical), feet
ζ	structural damping coefficient, nondimensional

Subscripts

∞	freestream condition
s, w	store or wing property, respectively
o	wing root property

Introduction

High-performance fighter aircraft with external stores are required to operate with high manoeuvrability in the transonic flight regime. In this regime, the potential exists for encountering transonic nonlinear flutter, known as limit-cycle oscillation (LCO). LCO is a limited amplitude, self-sustaining oscillation produced by an aerodynamic-structural interaction, which for the cases of interest, is exasperated by the occurrence of shock waves on the surface of the wing and/or stores. LCO results in an undesirable airframe vibration and limits the performance of the flight vehicle.

The main goal of the current work is to determine the range of applicability of models of varying fidelity to the numerical prediction of store-induced LCO. This form of LCO typically occurs near linear flutter boundaries in the nonlinear, transonic regime (Mach number ranging between 0.8 and 1.1), suggesting that classical flutter predictions using linear aerodynamic theories can be applied to the identification of lightly damped modes that may nonlinearly participate in LCO. Indeed, using traditional approaches, Denegri (2000) had limited success in relating observed store-induced LCO to "hump" (or "soft" crossing) modes found in velocity-damping diagrams. However, in many cases, the linear approach is inadequate in predicting response characteristics of vehicle configurations in the transonic regime.

The transonic regime differs from the linear, subsonic regime by the appearance of shocks. These structures may strongly interact with vehicle boundary layers, with the possible consequences of flow separation or significant shock movement. Following advances in nonlinear modeling and computer hardware, nonlinear aeroelastic predictions, including viscous effects and manoeuvre loads, are tractable for reasonably complex configurations (Melville (2001, 2002), Farhat *et al.* (2000)). Still, the use of modeling techniques that account for viscosity is too computationally demanding for preliminary design. In a coordinated manner, we examine the ability of aeroelastic models of varying fidelity to predict accurately LCO onset and amplitude. Models based on linear analysis, transonic small-disturbance theory (TSDT), and TSDT with interactive boundary layer are considered. Through this approach, we discern: (1) the limitations of linear theory for LCO prediction vis-à-vis the simplest nonlinear theory capable of producing weak shocks; (2) the ability of TSDT to predict store-induced LCO in inviscid flow, and (3) the effects of viscosity on store-induced LCO. This work provides the increased understanding of the LCO phenomenon, while also serving to determine the range of applicability and computational cost of various modeling techniques to the prediction of this phenomenon.

Three computational methodologies are employed in this investigation: the MSC/NASTRAN aeroelastic analysis program, the TSDT-based NASA/LaRC CAPTSDv computational aeroelasticity algorithm for inviscid and viscous flow, and the AFRL ENS3DAE Euler/Navier-Stokes computational aeroelasticity algorithm. MSC/NASTRAN is used in the development and analysis of structural models, the prediction of linear aeroelastic response of selected wing/store configurations, and the search for configurations speculated herein to produce LCO. The CAPTSDv algorithm is used to carry out relatively fast aeroelastic analyses for inviscid flow and viscous flow through interactive boundary layer coupling, starting with cases previously identified by MSC/NASTRAN as LCO-susceptible. ENS3DAE is then applied to validate CAPTSDv predictions for static aeroelastic and dynamic rigid behaviour for a representative set of flow conditions.

Problem Formulation

The wing studied herein is derived from the "heavy" version of the original Goland wing. Like the original, the heavy wing is structurally represented by a beam, but with additional non-structural mass, as defined by Eastep and Olsen (1980). This latest version, referred to as the Goland[+] wing, is a heavy wing modeled with a box structure to enable a variety of store attachment options.

Geometry

The Goland[+] wing is rectangular and cantilevered from an infinite midplane. A planform schematic is given in Figure 1a (including store) and geometric parameters are assigned values in Table 1. The airfoil section is assumed to be constant over the spanwise extent of the wing and is chosen to be that of a symmetric, parabolic-arc airfoil, defined by $z = 2 \ \tau_w \ x \ (1 - x/c_w)$ $(0 \leq x \leq c_w)$. The wing-tip store is

mounted flush to the wing tip (see Figure 1a). The sectional shape of the store is also assumed to be described by a parabolic arc uniform in the spanwise direction. The leading edge of the store is offset (defined positive) upstream of the wing leading edge, thereby providing the shape formula:

$$z = 2 \ \tau_s \ (x + c_{off}) \ [1 - (x + c_{off})/c_s] \qquad (-c_{off} \leq x \leq c_s - c_{off}).$$

Wing Structure and Inertial Properties

The wingbox structure finite element model is built-up from shear panels, modelling the spars and ribs, and membrane elements, modelling the wing skins. In addition, rod elements are included to model spar and rib caps as well as posts that connect the wing skins at every spar/rib intersection. Every element is modelled using the same material properties (shown in Table 1). Notice that the density of this "material" is extremely low. The model was built this way to allow the stiffness and mass properties to be decoupled. This decoupling allows the elements to be sized to tune the model to match the structural dynamic characteristics of the beam model of the heavy Goland wing.

Parameter	Value
c_w, l_w	6, 20
c_s, l_s	10, 1
c_{off}	3
ea	2
τ_w, τ_s	0.04, 0.036
Young's Modulus	1.4976×10^9 slugs/ft^2
Shear Modulus	5.616×10^8 slugs/ft^2
Structural Density	0.0001 slugs/ft^3

Table 1: Selected values of geometric and material parameters.

The geometry of the wing is simple. The origin is at the mid-height of the root of the leading edge spar. The three spars are un-swept and placed at 0, 2 and 4 ft along the positive x-coordinate. The eleven ribs are evenly spaced on 2 ft centres along the positive y-coordinate. The shear elements are defined by the intersections of the spars and ribs, with 10 elements per spar and 2 elements per rib. Next, each spar and rib is 0.33334 ft high and each cell defined by the spars and ribs is capped with a single wing skin membrane element. This results in a total of 40 skin elements. Finally, rods are added on the top and bottom of each shear element and at every spar/rib intersection. The total number of rod elements is 137, consisting of 60 spar caps, 44 rib caps and 33 posts.

The mass properties of this wing are modelled by placing lumped masses with no rotational inertia at each grid point. The lumped masses are sized to match the mass properties (total mass, *cg,* and inertia) of the heavy Goland wing. For the beam model Goland wing, the mass properties are simply modelled as lumped mass with rotational inertia centred at the *cg* of sections placed at 2 ft intervals. For the internal rib locations of the (i.e., 2 ft, 4 ft, 6 ft, etc.) beam model, the lumped mass properties were a mass of 22.496 slugs, with a rotational inertia in pitch of 50.3396 slug-ft^2, centred at $x = 2.6$ ft. For the external rib locations (i.e., 0 ft and 20 ft), the lumped mass properties were halved. In the built-up wing model, the masses used for the internal rib locations are as follows: 1.9650 slugs at each leading edge point, 3.9442 slugs at each point on the centre spar; and 5.3398 slugs for the trailing edge points. Also, similar to the beam model, the masses used at the external spar locations are half of the amount used at the internal locations.

The final step in developing the built-up model is sizing the elements so that its structural dynamic characteristics match those of the beam model Goland wing. For this model development, the elements are sized to minimize the error between the first three frequencies of the built-up and beam models. The boundary condition for each model is cantilevered. To maintain symmetry, the elements are grouped by their component. The thicknesses (in ft) for the 2-D elements are: upper and lower wing skins – 0.0155; leading and trailing edge spar – 0.0006; centre spar – 0.0889, and rib – 0.0347. For the 1-D elements, the areas (in ft^2) are: posts – 0.0008; leading and trailing edge spar caps – 0.0416; centre spar cap – 0.1496, and rib cap – 0.0422.

Store Mass and Linkage

The store configuration examined in this work is that of a tip store. This store structure is modelled as a series of rigid bar elements that result in a 10 ft long rigid bar. The resultant bar is centred 0.5 ft outboard of the wing tip and 2 ft aft of the wing leading edge. The store is then rigidly connected to the six wing tip grid points. This is accomplished by defining a seventh wing tip grid point at the centre of the rib structural model (i.e., $x = 2$ ft, $y = 20$ ft, $z = 0$ ft) and connecting this point to the other six points with a MSC/NASTRAN RBE3 element. This results in the displacement of the seventh grid point being the average of the displacements of the original six points. Finally, an RBAR element is used to connect the seventh wing tip point to the corresponding point (i.e., $x = 2$ ft, $y = 20.5$ ft, $z = 0$ ft) of the tip store model.

The mass properties of the tip store are chosen to match the properties of one section of the wing: a mass of 22.496 slugs and a rotational inertial of 50.3396 slug-ft^2. During this study, the position of the store mass is fixed at the lateral and vertical centres of the store (i.e., $y = 20.5$ ft and $z = 0$ ft) and varied in the streamwise direction.

Computational Aeroelasticity Methods

CAPTSD and CAPTSDv

CAPTSD solves the three-dimensional, transonic, small-disturbance, potential-flow equations for partial and complete aircraft configurations (Batina (1988,1989)). The standard, most widely distributed version of the program computes inviscid, compressible flow for combinations of wings, fuselage, horizontal tail, bodies/stores, and rectangular planform vertical surfaces. CAPTSD solves the aerodynamic equations of motion using a time-accurate algorithm that is capable of simulating both steady and unsteady flow (Batina (1992)). The method is capable of computing aeroelastic interactions by coupling the aerodynamic module with a structural dynamics simulation. The structural dynamics of horizontal surfaces are simulated in CAPTSD by using a modal structural model. The structural analysis is coupled to the aerodynamic analysis by a process that transfers generalized aerodynamic forces and generalized displacements between the aerodynamics and structural dynamics modules. Using this approach, CAPTSD is capable of simulating both static and dynamic aeroelastic phenomena.

A viscous-inviscid interaction version of CAPTSD, known as CAPTSDv, has been developed (Howlett (1987), Edwards (1993)) and applied to a variety of problems involving mildly separated and separation onset flows (Edwards (1998)). The method couples the inviscid CAPTSD algorithm with an inverse integral boundary layer model. The boundary layer equations are solved in a quasi-steady formulation similar to that recommended by Green *et al.* (1977). The outer inviscid solution and the inner viscous solution are computed independently and are coupled using an active control mechanism that minimizes coupling errors for unsteady flows. In this investigation, a single version of the CAPTSDv algorithm is used to perform both inviscid and viscous aeroelastic analysis (execution mode controlled by user).

CAPTSD solves the equations of motion on a sheared Cartesian grid system where lifting surfaces are modeled as thin plates. Thickness and camber information for the upper and lower surfaces of each lifting surface is supplied through a set of surface slopes that are specified as boundary conditions for the algorithm. Similarly, structural mode shapes are supplied as surface slope perturbations. This approach greatly simplifies the modelling task required for an aeroelastic analysis, since the grids are typically simple to generate, and no moving grid algorithm is required for the aeroelastic simulation. CAPTSD is

1-1.5 orders of magnitude more computationally efficient than higher fidelity methods, and offers the potential for nonlinear aerodynamics analysis within a design framework using the CAPTSD methodology.

ENS3DAE

Aeroelastic analysis of the Euler and Navier-Stokes equations is carried out with the Euler/Navier-Stokes 3-Dimensional Aeroelastic (ENS3DAE) method. The Lockheed-Georgia Company, under contract to the Air Force Wright Laboratory, developed ENS3DAE in the late 1980's (Schuster *et al.* (1990)). This program has been used to solve numerous aerodynamic and aeroelastic problems about a wide range of geometries including wings, wing/fuselage, wing/control system, propulsion, and integrated airframe/propulsion configurations (Smith *et al.* (1996), Schuster *et al.* (1998), Lewis and Smith (2000)).

ENS3DAE solves the full three-dimensional compressible Reynolds averaged Navier-Stokes equations, the thin layer approximation to these equations, or the Euler equations using an implicit approximate factorization algorithm. Central finite differences are used for spatial discretization, and a three-dimensional implementation of the Beam-Warming implicit scheme is employed for the temporal integration. Blended second- and fourth-order dissipation is added to the explicit right-hand-side of the equations, and implicit second-order dissipation is added to improve the diagonal dominance of the matrix system. For time-accurate cases, global or local time stepping within an inner sub-iteration loop for each physical time step is employed. The sub-iteration procedure effectively removes the stability limit on the time-step for unsteady flow cases, and improves the temporal accuracy of the method, provided that relevant time-scales within the computed flow field are captured by the selected time step and that a sufficient number of sub-iterates are computed.

The method accepts either single- or multiple-block curvilinear grids. Boundary conditions are imposed explicitly on each computational face of each grid block and the current release of the program requires a one-to-one match of grid points at block interfaces. Turbulence characteristics are predicted using the Baldwin-Lomax algebraic turbulence model or the Johnson-King model (Huttsell *et al.* (2001)). The code is written to take advantage of vectorization; directives for parallel operation on shared memory processors are also included in the programming. The method is regularly executed on eight or more processors.

A linear generalized mode shape structural model is closely coupled with the aerodynamic method to analyse structurally flexible vehicles. ENS3DAE uses a highly efficient, grid-motion algorithm for aeroelastic and control-surface simulations that is based on an algebraic shearing technique. Since dynamic aeroelastic and oscillating control surface simulations require grid models that deform in time, the algorithm now enforces the Geometric Conservation Law (Thomas and Lombard (1979)).

Results

Physical Conditions

The aeroelastic analysis is carried out with enforced consistency between velocity and dynamic pressure, assuming constant density at sea-level conditions. Mach number and Reynolds number are treated as independent variables, such that match-pointed conditions are not achieved. Reynolds number is not varied in this investigation. Structural damping is assumed to vanish for all baseline cases investigated. The selected values of various parameters are summarized in Table 2.

Summary of Grid Construction

Three grids are constructed for the CAPTSDv calculations reported in this paper. Owing to the geometry of the wing/store configuration and the mid-plane formulation of the surface boundary condition used in CAPTSDv, these grids are rectilinear. Clustering of grid points is enforced along the edges of the geometry and normal to the wing and store surfaces. Grids are generated by first computing grid-point distributions in each of the three coordinate directions external to CAPTSDv, subject to the specified clustering conditions, and then using the generator internal to CAPTSDv to obtain the full rectilinear

grid. The first grid (G1) is used for inviscid, clean-wing and wing/store (store mass only) computations; the second grid (G2) is used for inviscid, wing/store computations, and the third grid (G3) is used for viscous clean-wing and wing/store (store mass only) computations. The values of parameters governing grid construction are given in Table 3.

Parameter	Value
ρ_∞	0.0023771
T_∞	518.67
Re_∞	15×10^6
α_o	0
ζ	0

Table 2: Selected values of physical parameters.

Parameter	Grid G1	Grid G2	Grid G3
Domain Size (x,y,z)	(41,13.5,40)	(41,13.5,40)	(41,13.5,40)
Grid Dimensions (i,j,k)	(90,55,60)	(90,55,60)	(150,55,60)
Leading-Edge Spacing	0.01	0.01	0.008
Trailing-Edge Spacing	0.01	0.01	0.008
Normal Spacing (top, bottom)	(0.002,0.002)	(0.002,0.002)	(0.002,0.002)
Wing-Tip Spacing	0.025	0.025	0.025
Wing Index Dimensions (i,j)	(41,32)	(41,32)	(101,32)
Store Index Dimensions (i,j)	N/A	(57,5)	N/A

Table 3: Selected values of CAPTSDv grid parameters (lengths in wing chords, c_w).

A view of grid G2 in the *x-y* plane in the neighborhood of the wing/store configuration is shown in Figure 2a to illustrate the effect of grid clustering along the combined planform.

For the ENS3DAE calculations presented in this paper, only the clean wing (to which the store mass may be added) is considered. A two-block, HH-type grid is used for this configuration and is generated with GRIDGEN V13. The two blocks have equal dimensions and grid spacings, and correspond to the upper and lower halves of the computational space. It should be noted that the wing-tip geometry is slightly modified from the description given above to close the tip and simplify the grid-generation process. Characteristics of the grid are given in Table 4.

Contrary to the convention shown in Figure 1a, in ENS3DAE, the physical coordinates are defined with *x* streamwise, *y* normal, and *z* spanwise. However, consistent with CAPTSDv, the computational coordinates are defined with *i* streamwise, *j* spanwise, and *k* normal. Figure 2b shows a portion of the grid in the root plane. The inset shows a highly magnified view of the leading edge and highlights a gap between the upper and lower blocks equal to 0.053% of the chord. A sharp leading edge is difficult to model using an Euler/Navier-Stokes solver; the gap helps by removing the leading edge from the computational domain. The leading edge is captured numerically through the boundary conditions applied at points around the physical leading edge. In the spanwise direction, the wing tip is modeled by

transitioning the geometry from the full airfoil thickness at the wing tip to zero thickness at the first spanwise station outboard of the wing tip.

Parameter	Value
Domain Size (x,y,z)	(406,400,80)
Block Dimensions (i,j,k)	(161,71,51)
Leading-Edge Spacing	0.02
Trailing-Edge Spacing	0.02
Normal Spacing	0.0006667
Wing-Tip Spacing	0.05
Wing Index Dimensions	(81,41)

Table 4: Selected values of ENS3DAE grid parameters (lengths in feet).

Modal Analysis

Modes of the structural model are computed with MSC/NASTRAN and then splined to aerodynamic surface grids (specified at $z = 0$) with the infinite plate spline, as implemented by Smith *et al.* (1995, 1996). The modes are scaled to yield generalized masses of magnitude 1. Modal amplitudes are computed through time integration of the generalized structural dynamics equations to yield updated approximations of wing/store surface deflections. Unless otherwise stated, results given in this paper are obtained by retaining the 4 modes of lowest frequency in the aeroelastic analysis and by excluding in-plane modes. Sets of retained of modes are shown in Figure 3 for two cases: clean wing with no store and wing with store mass positioned 1.75 feet forward of the wing elastic axis (see discussion below). With the exception of mode 4, the modes in the two sets are quite similar; slightly more torsion is evident at the wing tip in the modes associated with the clean wing.

Linear Analysis

To determine a parameter space (velocity and Mach number for specified altitude) where store-induced LCO possibly exists, a linear flutter analysis of a clear wing and a wing/tip store combination is conducted. The linear flutter speeds (those from linear aerodynamic theories) are determined from data calculated from the *p-k* method of MSC/NASTRAN. The flutter and divergence instabilities can be determined from an inspection of calculated data in graphical form, the so-called *V-g* and *V-ω* diagrams. These diagrams are shown in Figures 4a (clean wing) and 4b (wing with tip store mass) for a selected Mach number of 0.92. From Figure 4a, the flutter speed of a clean wing is determined by the first crossing of one of the modes from negative to positive values of the damping parameter, *g* (i.e., 334 ft/sec), and a corresponding flutter frequency of 2.17 HZ. Additionally, shown in Figures 4a is a divergence instability, whose speed is determined by the simultaneous occurrence of zero damping and zero frequency for another mode (i.e., 630 ft/sec).

The *V-g* diagram of the clean wing is compared to the *V-g* diagram of the wing/store configuration (mass only), shown in Figure 4b, when the store *cg* is located 1.75 ft upstream of the wing *ea* (equivalent to the store pitch axis). By comparing the two diagrams, it is seen that the flutter speed is increased to 559 ft/sec when the store *cg* is placed at this position and that the severity of the flutter instability of the clean wing has been reduced (reflected by less damping). The flutter mode of the wing/store has been converted into a "hump," or lightly damped mode. It is speculated that the initiation of store-induced LCO is associated, in some way, with hump modes, such that the linear flutter investigation defined a beginning region to search for LCO. Of course, since this hump is determined from linear aerodynamics, the region of LCO must be modified by taking into consideration transonic (nonlinear) aerodynamics. This modification is discussed in the following sections for a determination of store-induced LCO.

Linear analysis is carried out for other store mass positions, but not reported herein. These results show the reduction of the peak damping parameter with forward movement of the store mass. The offset position of 1.75 ft (upstream of the wing ea) is selected for use in the CAPTSDv calculations reported below, because of the small peak value of g attained with this parameter value.

Flutter Boundaries

Boundaries of flutter and LCO onset are computed for the clean wing configuration and for the wing with store mass (i.e., store not modeled aerodynamically). The flow is assumed to be inviscid. These results are compared to those obtained with MSC/NASTRAN using linear analysis. LCO solutions are observed at Mach numbers above Mach 0.9 when the store mass is present; these cases will be discussed in greater detail in the next section. Flutter and LCO boundaries are compared in Figure 5a. For the clean wing, CAPTSDv predicts a flutter speed of 433 ft/sec at Mach 0.7, a value 3.5% higher than that predicted by MSC/NASTRAN. With the store mass included, CAPTSDv predicts a flutter speed of 648.5 ft/sec (CAPTSDv), a value 6.8% higher than that provided by MSC/NASTRAN. At Mach 0.7, the aerodynamics are linear and the reasonable comparisons between CAPTSDv and MSC/NASTRAN are to be expected. CAPTSDv clearly confirms that forward movement of the store mass has a stabilizing effect on the aeroelastic system for Mach numbers at or below 0.9.

As Mach number increases beyond 0.7, the clean-wing flutter boundary obtained with CAPTSDv develops a transonic dip with a minimum flutter speed (355 ft/sec) at about Mach 0.88. The boundary is much flatter when the store mass is included; flutter speed averages around 645 ft/sec. Both boundaries show a rapid increase in flutter speed near Mach 0.9. However, at selected Mach numbers between 0.90 and 0.95 (0.91, 0.92, 0.93, and 0.94) with the store mass present, LCO solutions are observed. These nonlinear oscillations are computed at flight speeds much lower than the nominal, wing/store flutter speed, and, for some Mach numbers, lower than the clean-wing flutter speed. Thus, the presence of the store destabilizes the system at higher Mach numbers in an adverse manner, i.e., to lower flight speeds.

On the flutter boundary for the wing/store configuration, two different flutter modes are observed. These are contrasted in terms of the computed lift and moment coefficients (taken about the leading edge) for Mach 0.84 and Mach 0.9, as shown in Figures 5b and 5c. Note that unstable test points are selected above the flutter boundary: U = 750 ft/sec at Mach 0.84 (flutter at 642.5 ft/sec) and U = 850 ft/sec at Mach 0.9 (flutter at about 825 ft/sec). Two different frequencies of divergent oscillation are observed: 1.90 Hz (Mach 0.84) and 9.52 Hz (Mach 0.90). These frequencies are somewhat larger than the natural frequencies corresponding to modes 1 (1.69 Hz) and 3 (9.17 Hz), respectively. For both flutter modes, the phase relationships between peak lift and moment are the same (about 180 degrees out of phase). Differences in frequency correlate well with differences in modal participation between the flutter modes. As shown in Figures 5d and 5e, response is dominated by modes 1 and 2 at Mach 0.84, whereas modes 3 and 4 dominate the response at Mach 0.9. The impact of varying modal participation on wing shape is described in the next section.

A switching of flutter modes is perhaps suggested by the linear MSC/NASTRAN results shown for Mach 0.92 in Figure 4 (the results for Mach 0.9 are not markedly different). The effect of nonlinearity appears to be large in terms of stabilizing the interaction between modes 1 and 2, predicted by MSC/NASTRAN to occur at about 560 ft/sec. At a larger frequency, coalescence of modes 3 and 4 is evident in the MSC/NASTRAN results at a flight speed of about 800 ft/sec, a velocity near the flutter speed predicted by CAPTSDv.

Store-Induced Limit-Cycle Oscillation

In a Mach number range between 0.91 and 0.95, fully developed LCO states are computed with CAPTSDv for the wing/store configuration, excluding store aerodynamics (see Figure 5a). As will be shown later, the effect of including store aerodynamics is not significant, while the effect of viscosity is to reduce LCO amplitude. Two types of LCO are observed: (1) an expected form involving significant time-periodic oscillations of the aeroelastic system that will be described first and referred to as simply LCO, and (2) an unexpected form with very small amplitudes (~3 orders of magnitude less in magnitude) that will be described second and referred to as "embryonic" LCO, or ELCO.

As shown in Figure 5a, LCO is observed over a restricted range of Mach numbers. Generally, LCO amplitudes increase with increasing velocity, and for sufficiently large velocities, computed oscillations become so large that the assumptions of TSDT become invalid. Attention is first given to Mach 0.92, where LCO is first observed at $U = 390$ ft/sec for inviscid flow (onset occurring between 385 and 390 ft/sec) and $U = 410$ ft/sec for viscous flow (onset occurring between 390 and 410 ft/sec). It should be noted that the onset of LCO is computationally expensive to obtain, since very large integration times are necessary for the aeroelastic system to approach time-asymptotic behavior at values of flight speed near critical. In these calculations, the initial state is defined by a flow solution given by a rigid-body calculation, and the modal amplitudes are assumed to vanish, except for the first mode, which is assigned an initial value of 0.01.

The slow growth of lift coefficient to its asymptotic value is shown in Figure 6a for $U = 410$ ft/sec, assuming inviscid flow. LCO frequency is observed to be 2.92 Hz. Time histories of fully developed lift and moment coefficient are shown in Figure 6b; the phase relationship between these quantities is similar to that observed for the two flutter modes previously described. The computed frequency corresponds to the modal content of the aeroelastic response. As seen in Figure 6c, mode 2 (a natural frequency of 3.05 Hz) dominates the response, with strong participation also from mode 1. At this Mach number and flight speed, the first two modes are much more strongly coupled than in the flutter mode found at low transonic Mach numbers (cf. Mach 0.84), with an associated increase in response frequency.

A similar set of plots of LCO response are shown in Figure 7 for the case of viscous flow, assuming an equivalent flight speed of 410 ft/sec at Mach 0.92. Grid G3 is used for viscous calculations, and the aerodynamics of the store are assumed negligible. LCO amplitude is observed to diminish through the effects of viscosity, and frequency slightly increases to 2.99 Hz. Viscous simulations of LCO are somewhat stiffer than inviscid computations, requiring one Newton sub-iterate per time step for stable calculation.

Structural response associated with LCO is contrasted with that of the two flutter modes through visualization of wing-tip motion. Snapshots of instantaneous chordline orientation (lines connecting wing tip leading edge and trailing edge) are shown in Figure 8 for each of the three characteristic aeroelastic responses. The low-speed flutter mode is primarily first bending, which is reflected by a vertical displacement of the wing tip at different times, with introduction of only a slight incidence angle with respect to the freestream. The flutter mode observed at Mach 0.9 is a higher frequency mode involving significant contributions from modes 3 and 4. The response of the wing tip involves both pitch and plunge, with a motion akin to that of a ship moving into ocean waves (a visual rotation about the mid-chord). In the situation of LCO, the response is composed of first bending and first torsion contributions. A pitching motion dominates the resulting movement of the wing tip, with visual rotation about the tip leading edge.

LCO solutions of the type described above are not observed at flight speeds below 390 ft/sec for inviscid flow at Mach 0.92. However, at speeds between 340 and 390 ft/sec, sustained oscillations of very small amplitude and less regular character are computed. In this speed range, the magnitude of system oscillations increases very slowly with increasing U. These ELCO states appear to be physical and not numerical in origin, since ELCO formation is found to be persistent to variation of Mach number and various numerical parameters. However, ELCO amplitude is sensitive to structural damping and the numerical precision of the computation. When ζ is increased from the baseline value of 0 to 0.03, ELCO amplitude is reduced by over a factor of 5 at $U = 385$ ft/sec, and is found to vanish at $U = 350$ ft/sec. Also, increasing the baseline precision of the computation to double, ELCO amplitude is observed to grow considerably (but remaining at levels small compared to LCO).

A time history of lift coefficient is shown in Figure 9 for $U = 385$ ft/sec and assuming baseline values of numerical parameters: the frequency of 2.94 Hz is nearly identical to that found during LCO at $U = 410$ ft/sec, while peak lift coefficient reaches only about 5×10^{-5}.

LCO Sensitivities

The variation of LCO amplitude with respect to changes in flight speed at Mach 0.92 is computed for three categories of analysis: inviscid analysis of wing with store mass (grid G1); inviscid analysis of wing

with store modeled aerodynamically (grid G2), and viscous analysis of wing with store mass (grid G3). Results are compared in Figure 10a to show the effects of varying the level of modeling fidelity within the context of transonic small-disturbance theory. Assuming inviscid flow, it is observed that modelling the store aerodynamically has little impact on the onset or computed amplitude of LCO. However, at speeds exceeding 420 ft/sec, solutions can not be stably computed. In these cases of increased wing-tip twist, numerical destabilization appears to be a result of a very large, localized, pressure spike observed in the region of the juncture between the store and the wing leading edge. This destabilization occurs at about the speed for which LCO amplitude is predicted to grow rapidly when store aerodynamics are ignored; peak lift coefficient begins to take a large jump at $U = 427$ ft/sec with this approximation. At speeds exceeding this value, the validity of the computed inviscid solutions is considered to be diminished, owing to the small-disturbance nature of the methodology. As described above for $U = 410$ ft/sec, the effect of viscosity is to diminish LCO amplitude. When the boundary layer thickness is modelled, no large increase in LCO amplitude is observed, and peak lift coefficient remains bounded by 0.26 over the range of speeds examined, thus reducing the deformation of the wing and extending the speed range over which the assumption of small disturbances is arguably satisfied. Near the bifurcation point, at $U = 388$ ft/sec, non-unique states are observed. One state, obtained with the baseline initial conditions exhibits very small-amplitude ELCO behavior, while the other state, obtained by restarting the aeroelastic solution from $U = 390$ ft/sec, exhibits LCO behavior. However, as velocity is reduced below 388 ft/sec, only ELCO is observed, and as velocity is increased above this same speed, only LCO is observed. These results are indicative of the presence of a subcritical bifurcation just above this speed, causing relatively large jumps in LCO amplitude over a small range of flight speeds. This phenomenon is explored further below for Mach 0.93.

The variation of peak lift coefficient with velocity is found to be more regular at Mach 0.93 than at Mach 0.92. For this higher Mach number, the effects of variation of root angle-of-attack are assessed in Figure 10b using the observed half-differentials between maximum and minimum lift coefficient (to separate the dependence of oscillation amplitude on velocity from the dependence of static aeroelastic response on velocity). When α_0 is increased to 2 degrees, a considerable decrease in LCO amplitude is observed, along with a significant delay in LCO onset to higher velocities.

As stated above for the results computed at Mach 0.92 (cf. Figure 10a), the onset of LCO is subcritical. This is also observed at Mach 0.93, as shown in detail in Figure 11 (for the baseline condition of vanishing root angle-of-attack). For this comparison, aeroelastic solutions are computed using two kinds of initial conditions: the initial conditions described above, and initialisation of the flowfield using a fully developed LCO solution obtained at a higher velocity. It is seen that the latter class of initial condition produces fully developed LCO solutions for a small range of velocities (noted at 386 ft/sec and 388 ft/sec) at which the former class of initial condition does not produce LCO. While the range of hysteresis is slight, the subcritical nature of the bifurcation does explain the rather large jumps in amplitude observed beyond the critical points.

Not surprisingly, over the range of Mach numbers that sustain LCO, amplitude of response is found to be highest over the midsection of the range. This is shown in Figure 12 for a velocity of 410 ft/sec. The response near the low-Mach boundary of the LCO region is characteristic of the subcritical response shown in Figures 10a and 11. However, at the high-Mach boundary of the LCO region, the computed results are not suggestive of non-unique flow responses.

Comparisons with ENS3DAE

To assist in the validation of the transonic aeroelastic modeling employed in CAPTSDv, CAPTSDv solutions (inviscid) are compared to ENS3DAE (Euler) solutions for two clean-wing calculations: prediction of static aeroelastic response for a root angle-of-attack of 2 degrees and dynamic response of a rigid wing undergoing 3-Hz pitch oscillations of ½ degree in amplitude. Both cases show good agreement between the Euler and TSDT results, and are reported here for a transonic condition ($U = 400$ ft/sec and Mach 0.92) in terms of the predicted values of lift and moment coefficients. For the case of static aeroelastic response, C_L predictions agree within 6% (0.126 for ENS3DAE and 0.134 for CAPTSDv) and C_M predictions agree within 15% (-0.0687 for ENS3DAE and –0.0809 for CAPTSDv). In the case of

response to forced pitch oscillations, lift and moment coefficients are compared in Figure 13 as phase portraits, where it is seen that amplitudes and phase relationships are in excellent agreement.

Summary and Conclusions

A class of limit-cycle oscillations was observed for a rectangular wing with tip store. These LCOs occurred at speeds lower than that predicted using linear aerodynamics and at speeds lower than that computed for the clean-wing configuration. The form of the bifurcation was subcritical, such that LCO amplitude jumped abruptly as Mach number increased beyond a critical value. However, it was also found that as Mach number increased to a critical value (~0.94–0.95), LCO states could no longer be sustained. For the configurations examined, the presence of LCO was insensitive to the inclusion of store aerodynamics in the aeroelastic model. Also, the effect of viscosity was to diminish LCO amplitude. A second class of LCO solutions with small amplitude was observed that occurred over a range of speeds below critical, i.e., prior to the initiation of LCOs characterized by large-amplitude aeroelastic response. These states were found to be sensitive to structural damping, such that addition of nominal levels of damping was sufficient to overcome the phenomenon.

The search for LCO states was conducted in two steps. First, linear theory was employed in the identification of "hump" modes, which corresponded to placement of the store mass near the wing leading edge. Such characteristic aeroelastic responses were expected to point to conditions susceptible to LCO. Second, LCO states were computed using the transonic small-disturbance theory algorithm CAPTSDv, assuming both inviscid and viscous flow. This nonlinear mathematical formulation was sufficient to capture properly weak shock formation and movement. The validation of these LCO results using higher fidelity methods (i.e., Euler and Navier-Stokes via ENS3DAE) is currently underway, and preliminary results are encouraging. Also, static aeroelastic and dynamic rigid responses of the clean wing computed with CAPTSDv and ENS3DAE are in close agreement. Additional work is planned for the study of LCO including the presence of underwing stores and for the study of a swept-wing configuration. Further investigation is required to yield a full explanation of LCO development for the wing/store configuration examined herein and to better understand any potential connection between the observed nonlinear LCO phenomenon and the development of hump modes in the reported linear analysis.

Acknowledgements

References

1. Batina, J. T., "Efficient Algorithm for Solution of the Unsteady Transonic Small-Disturbance Equation," *Journal of Aircraft*, Volume 25, July 1988, pp. 598-605.
2. Batina, J. T., "Unsteady Transonic Algorithm Improvements for Realistic Aircraft Applications," *Journal of Aircraft*, Volume 26, February 1989, pp. 131-139.
3. Batina, J. T., "A Finite Difference Approximate-Factorization Algorithm for Solution of the Unsteady Transonic Small-Disturbance Equation," NASA TP 3129, January 1992.
4. Denegri, C. M., "Limit Cycle Oscillation Flight Test Results of a Fighter with External Stores," Journal of Aircraft, Volume 37, Number 5, September-October 2000, pp. 761-769.
5. Edwards, J. W., "Transonic Shock Oscillations Calculated with a New Interactive Boundary Layer Coupling Method," AIAA Paper 93-0777, January 1993.
6. Eastep, F. E., "Transonic Flutter Analysis of a Rectangular Wing with Conventional Airfoil Sections," AIAA Journal, Volume 18, Number 10, October 1980, pp. 1159-1164.

7. Edwards, J. W., "Calculated Viscous and Scale Effects on Transonic Aeroelasticity," AGARD-R-822, Numerical Unsteady Aerodynamic and Aeroelastic Simulation, March 1998, pp. 1-1 – 1-11.

8. Farhat, C., Pierson, K., and Degand, C., "CFD Based Simulation of the Unsteady Aeroelastic Response of a Maneuvering Vehicle," AIAA Paper 2000-0899, January 2000.

9. Green, J. E., Weeks, D. J., and Brooman, J. W. F., "Prediction of Turbulent Boundary Layers and Wakes in Compressible Flow by a Lag-Entrainment Method," R & M No. 3791, British Aeronautical Research Council, 1977.

10. Howlett, J. T., "Efficient Self-Consistent Viscous Inviscid Solution for Unsteady Transonic Flow," *Journal of Aircraft*, Volume 24, November 1987, pp. 737-744.

11. Huttsell, L., Schuster, D., Volk, J., Giesing, J., and Love, M., "Evaluation of Computational Aeroelasticity Codes for Loads and Flutter," AIAA Paper 2001-0569, January 2001.

12. Lewis, A. P. and Smith, M. J., "Euler-Based Aeroelastic Analysis of Shell Structures," *Journal of Aircraft*, Vol. 37, No. 5, September-October 2000, pp. 840 - 845.

13. Melville, R., "Nonlinear Simulation of F-16 Aeroelastic Instability," AIAA Paper 2001-0570, January 2001.

14. Melville, R., "Nonlinear Mechanisms of Aeroelastic Instability for the F-16," AIAA Paper 2002-0871, January 2002.

15. Schuster, D. M., Beran, P. S., and Huttsell, L. J., "Application of the ENS3DAE Euler/Navier-Stokes Aeroelastic Method," AGARD-R-822, Numerical Unsteady Aerodynamic and Aeroelastic Simulation, March 1998, pp. 3-1 – 3-11.

16. Schuster, D. M., J. Vadyak, and E. Atta, "Static Aeroelastic Analysis of Fighter Aircraft Using a Three-Dimensional Navier-Stokes Algorithm," *Journal of Aircraft*, Volume 27, Number 9, September 1990, pp. 820-825.

17. Smith, M. J., Hodges, D. H., and Cesnik, C. E. S., "An Evaluation of Computational Algorithms to Interface between CFD and CSD Methodologies," WL-TR-96-3055, November 1995.

18. Smith, M. J., Schuster, D. M., Huttsell, L. J., and Buxton, B., "Development of and Euler/Navier-Stokes Aeroelastic Method for Three-Dimensional Vehicles with Multiple Flexible Surfaces," AIAA Paper 96-1400, April 1996.

19. Smith, M. J., Hodges, D. H., and Cesnik, C. E. S., "Evaluation of Computational Algorithms Suitable for Fluid-Structure Interactions," *Journal of Aircraft*, Volume 37, Number 2, March-April 2000, pp. 292-294.

20. Thomas, P. D., and Lombard, C. K., "Geometric Conservation Law and Its Application to Flow Computations on Moving Grids," *AIAA Journal*, Volume 17, Number 10, October 1979, pp. 1030 - 1037.

(a) Planform geometry

■ Structural Grid Point

20 ft

4 ft

1/3 ft
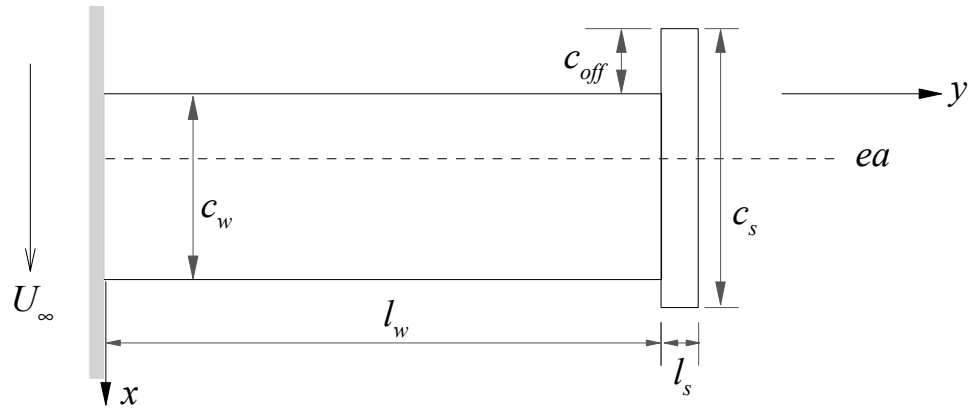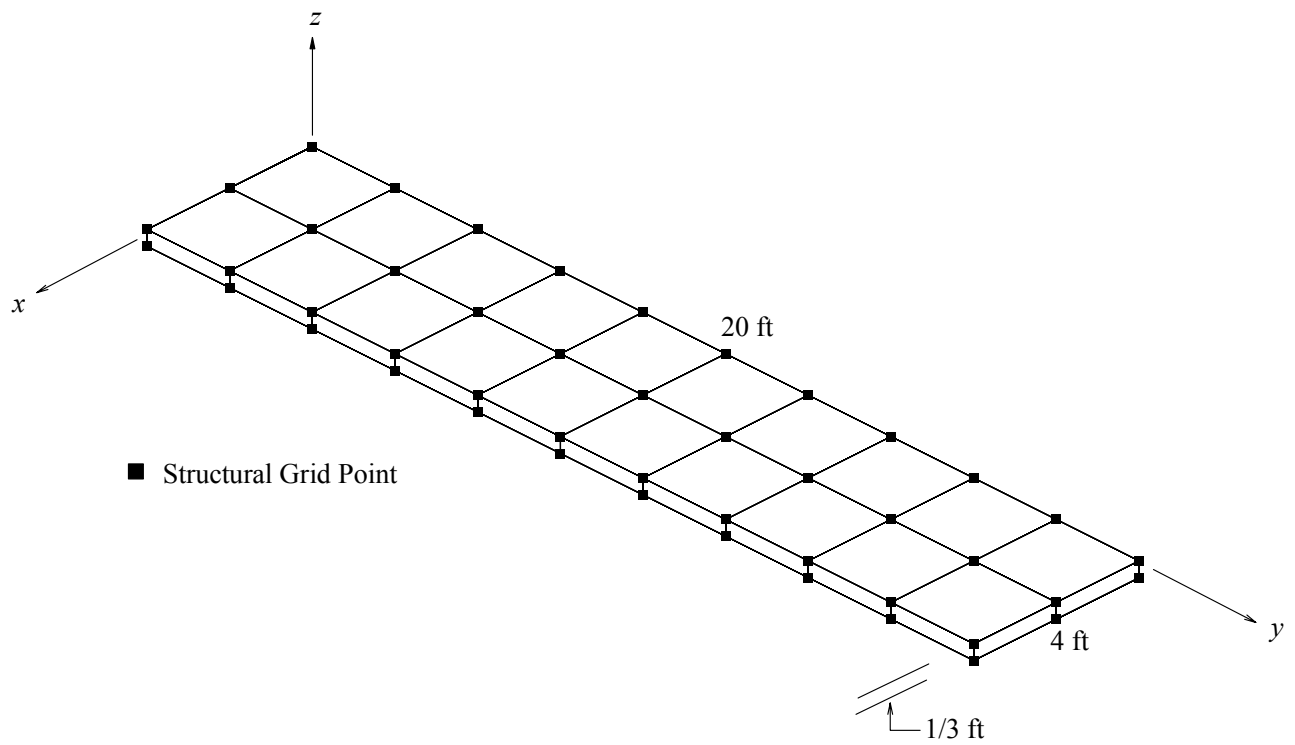
(b) Structural model

Figure 1: Schematics of Goland[+] Wing geometry and structural model.
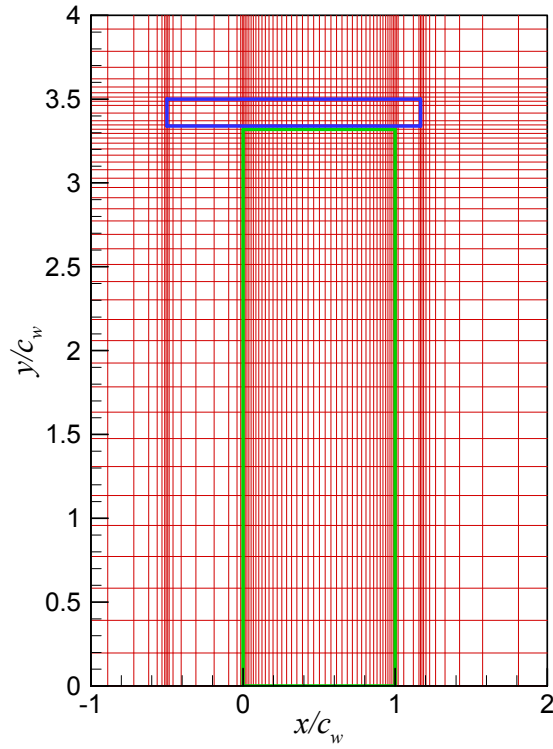
(a) CAPTSDv wing surface grid (G2): grid lines (red); wing boundary (green); store boundary (blue)
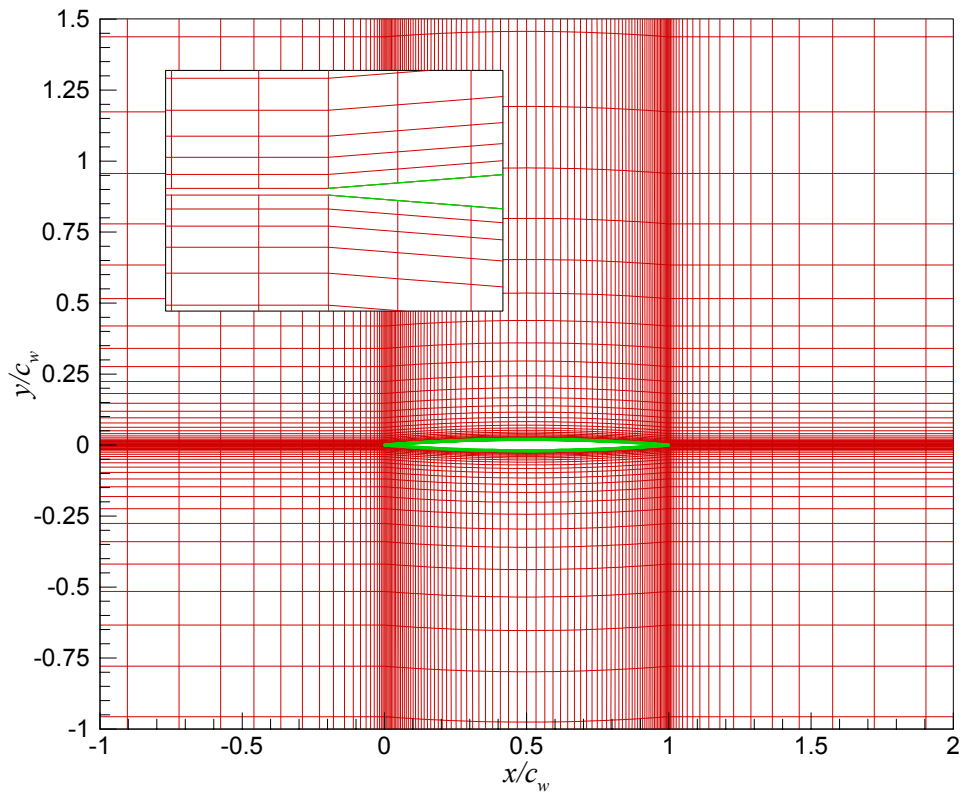
(b) ENS3DAE root-plane grid (inset figure shows leading edge): grid lines (red); wing boundary (green)

Figure 2: CAPTSDv and ENS3DAE computational grids for Goland[+] Wing.

(a) Clean wing

(b) Wing with store mass (offset 1.75 ft forward)
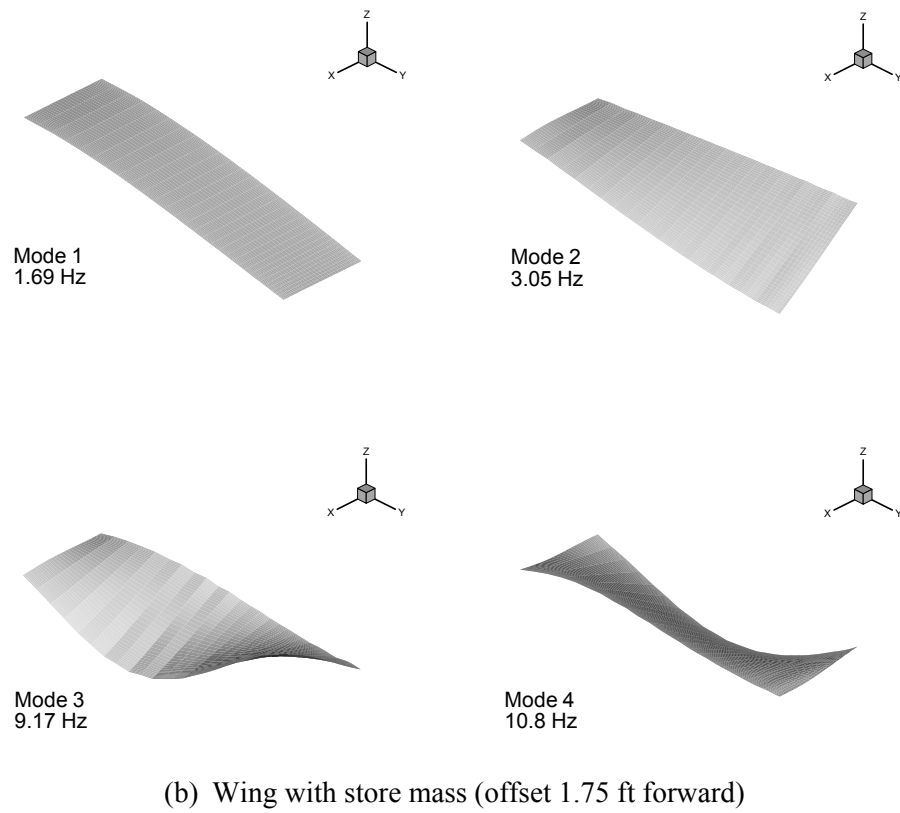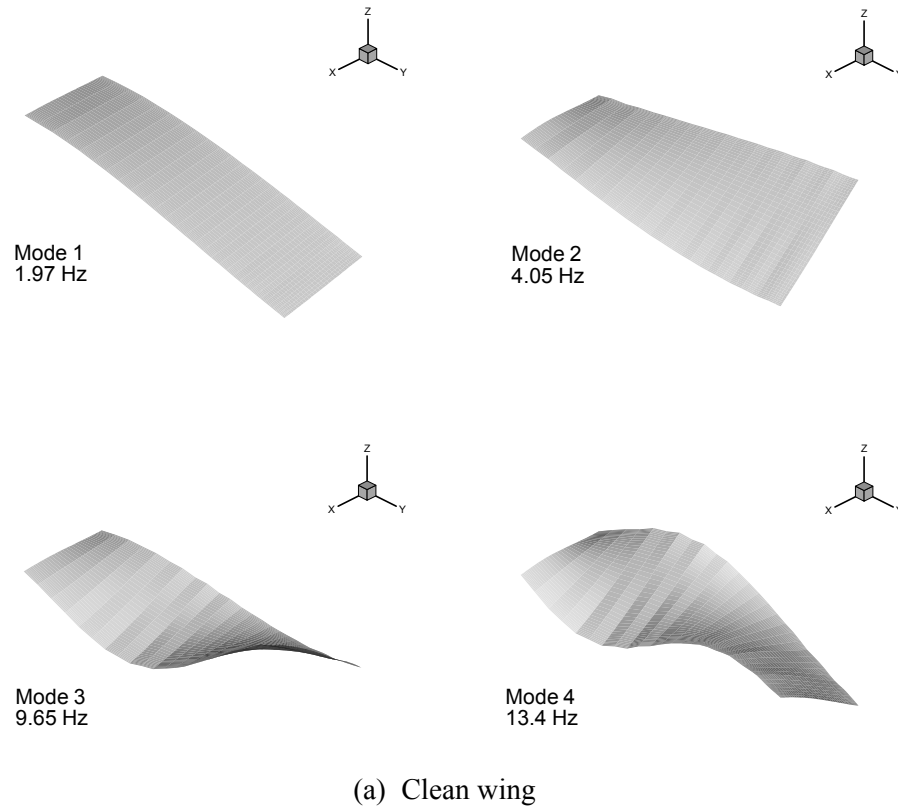
Figure 3: Splined modes retained in aeroelastic analysis of Goland[+] wing with and without store mass.
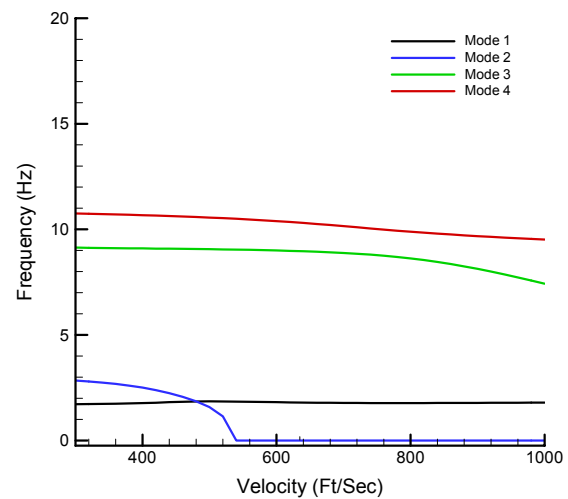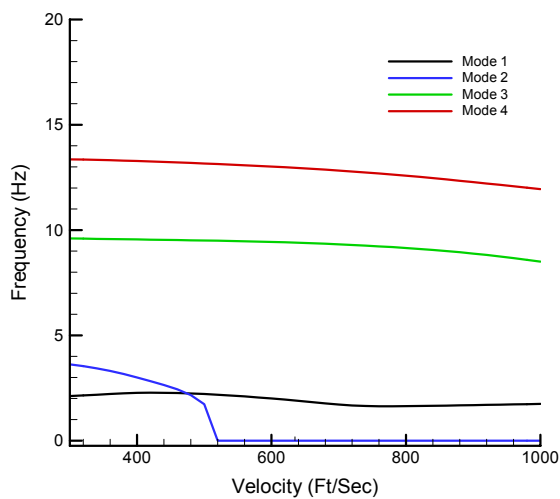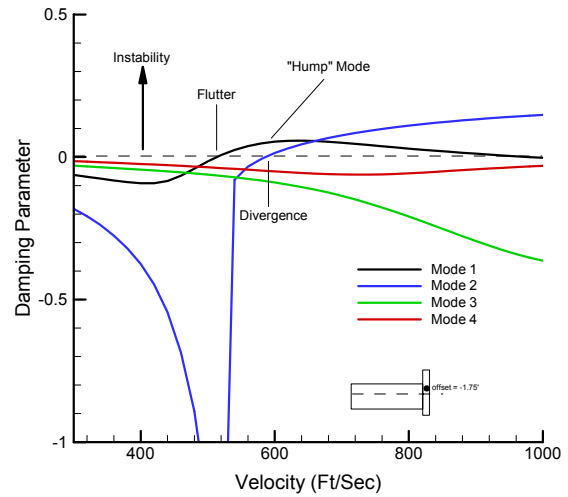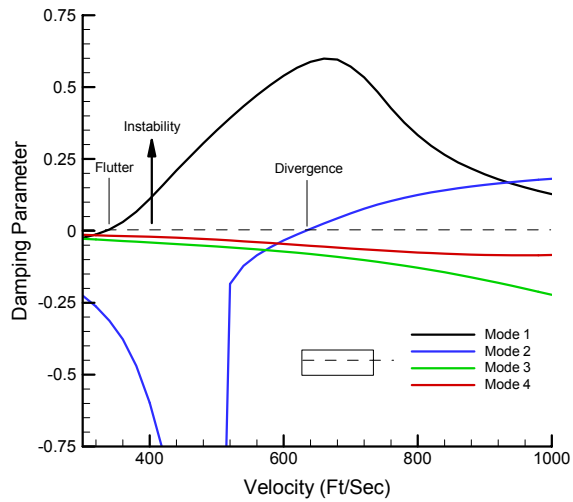
(a) Clean wing damping and frequencies   (b) Wing/store damping and frequencies

Figure 4: Damping and frequency characteristics predicted by linear aeroelastic analysis (MSC/NASTRAN) for the Goland[+] wing with and without store mass at Mach 0.92.
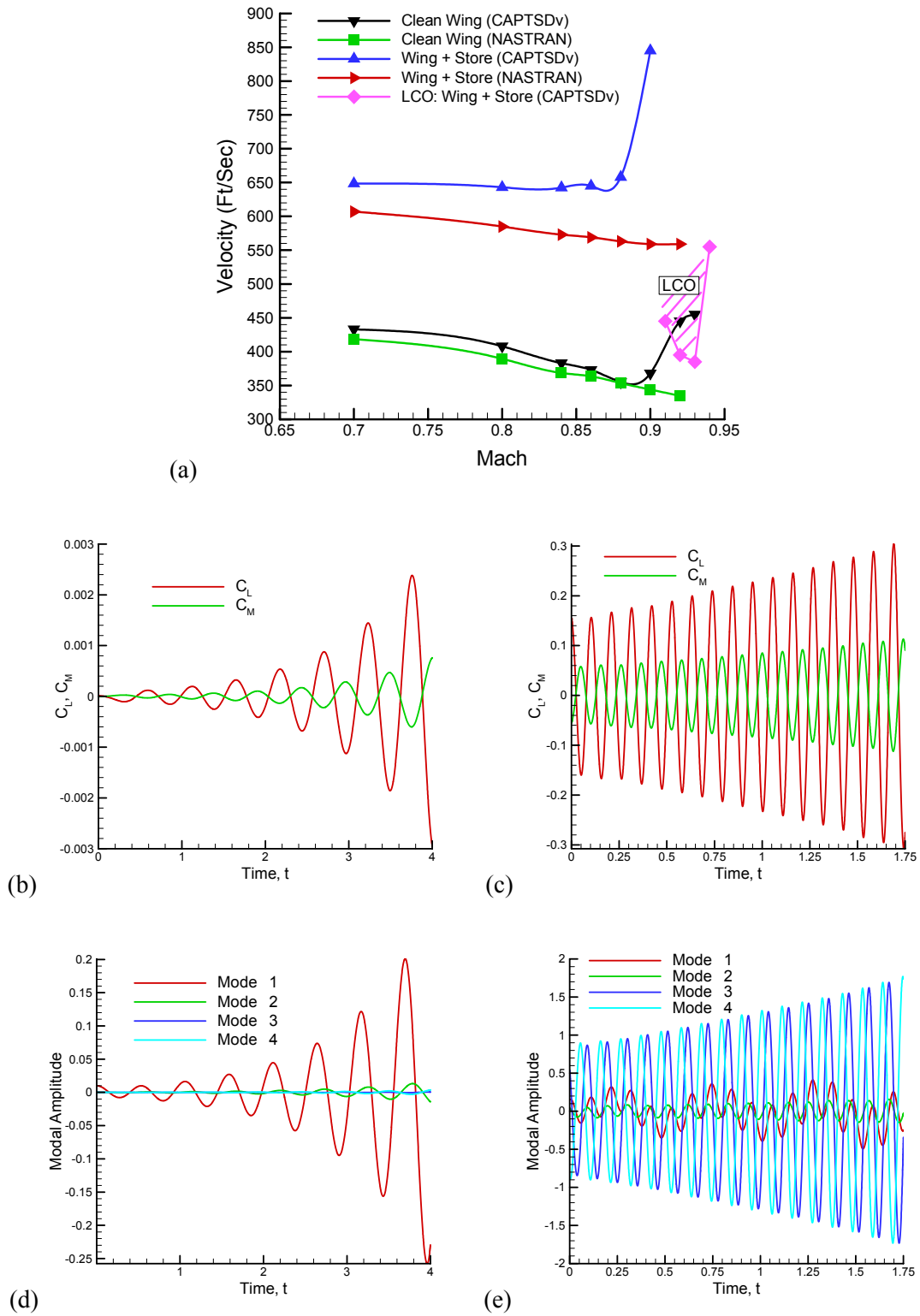
Figure 5: Inviscid CAPTSDv aeroelastic analysis for grid G1 without store aerodynamics: (a) comparison of flutter and LCO boundaries computed with CAPTSDv and MSC/NASTRAN; (b) and (c) force and moment coefficient histories for Mach 0.84 ($U = 750$ ft/sec) and Mach 0.90 ($U = 850$ ft/sec); (d) and (e) modal amplitude histories for Mach 0.84 ($U = 750$ ft/sec) and Mach 0.90 ($U = 850$ ft/sec).
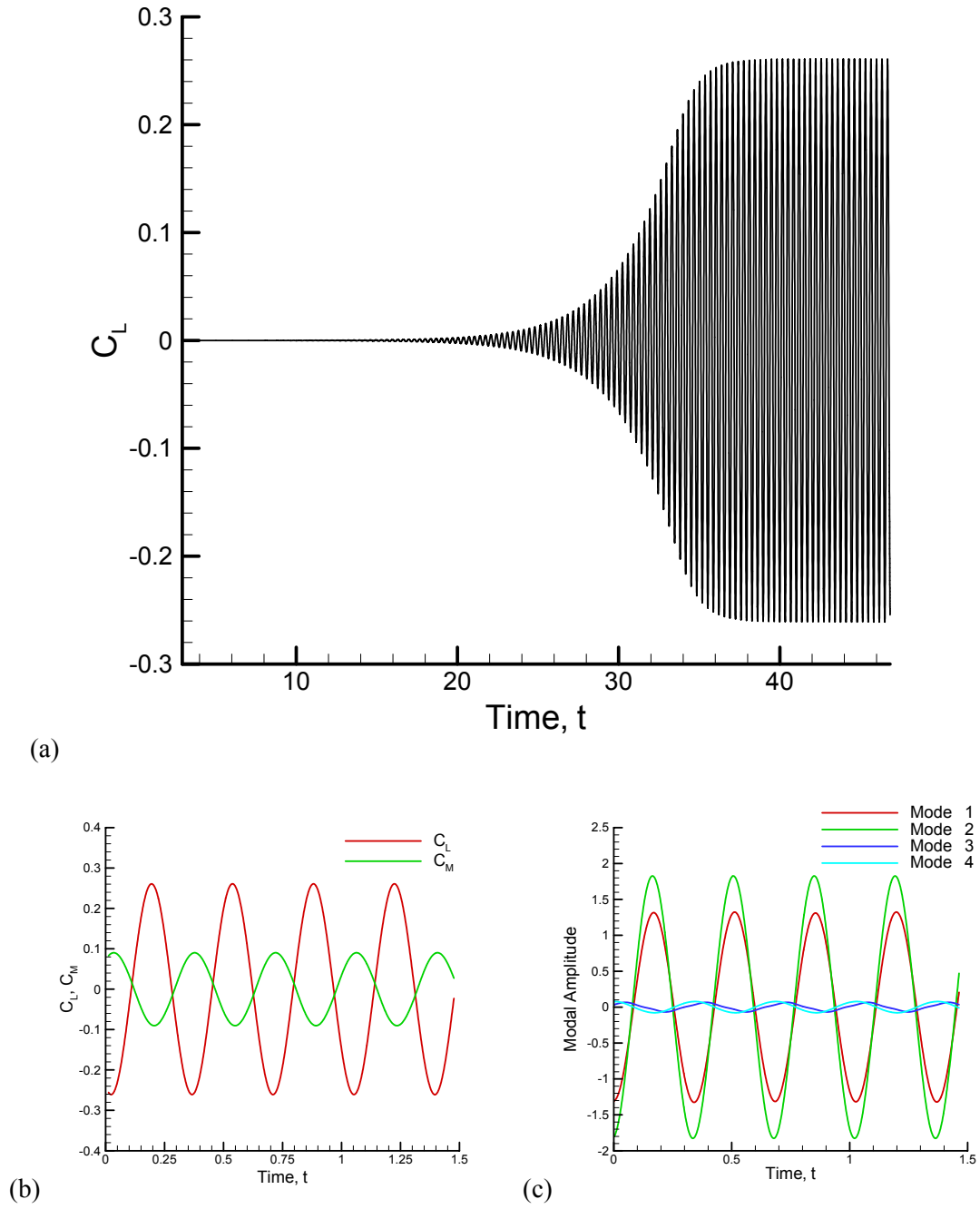
Figure 6: Inviscid CAPTSDv aeroelastic analysis for grid G1 without store aerodynamics at Mach 0.92 and $U = 410$ ft/sec: (a) time history of lift coefficient; (b) lift and moment coefficients at LCO; (c) modal amplitudes at LCO.
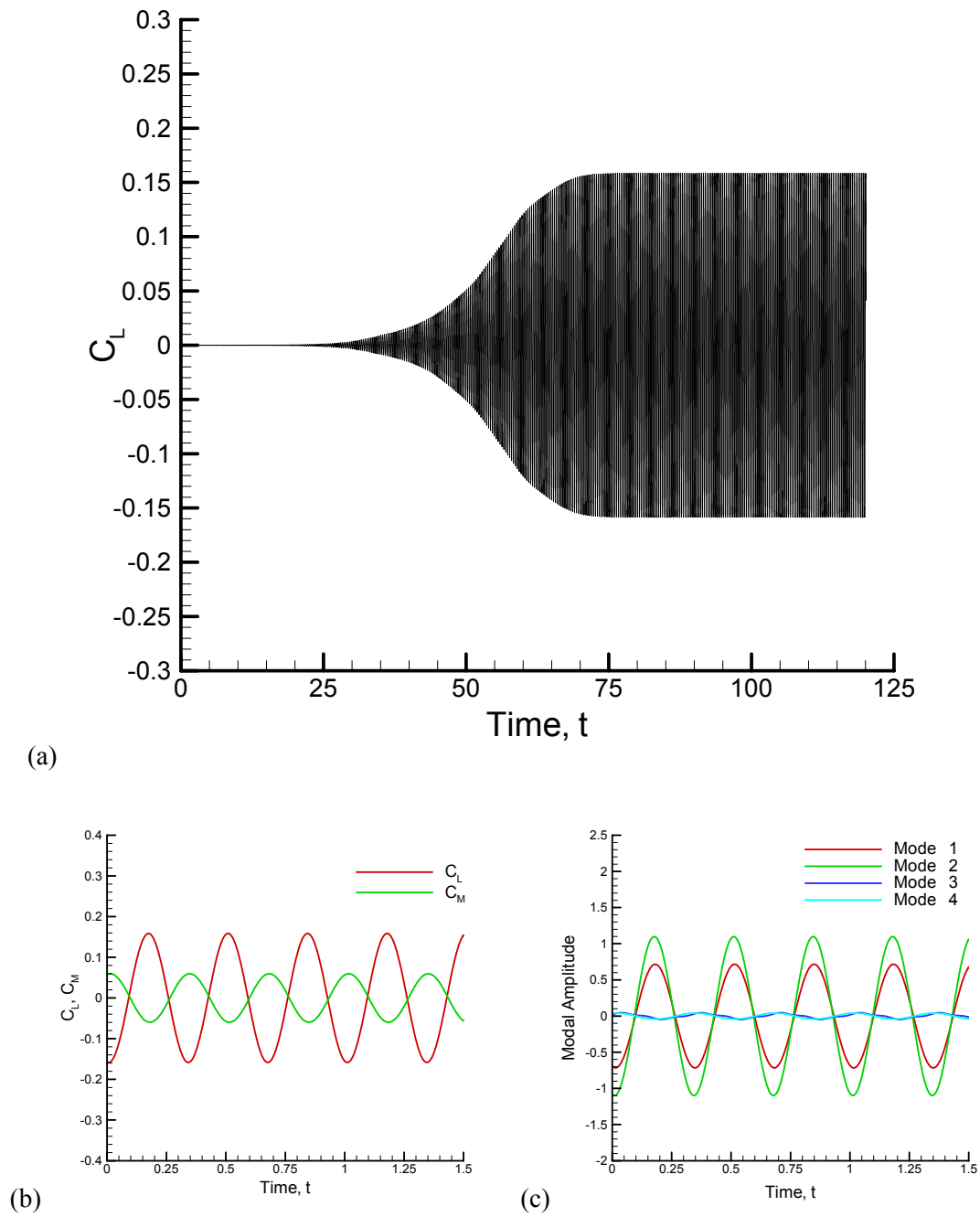
Figure 7: Viscous CAPTSDv aeroelastic analysis for grid G3 without store aerodynamics at Mach 0.92 and $U = 410$ ft/sec: (a) time history of lift coefficient; (b) lift and moment coefficients at LCO; (c) modal amplitudes at LCO.
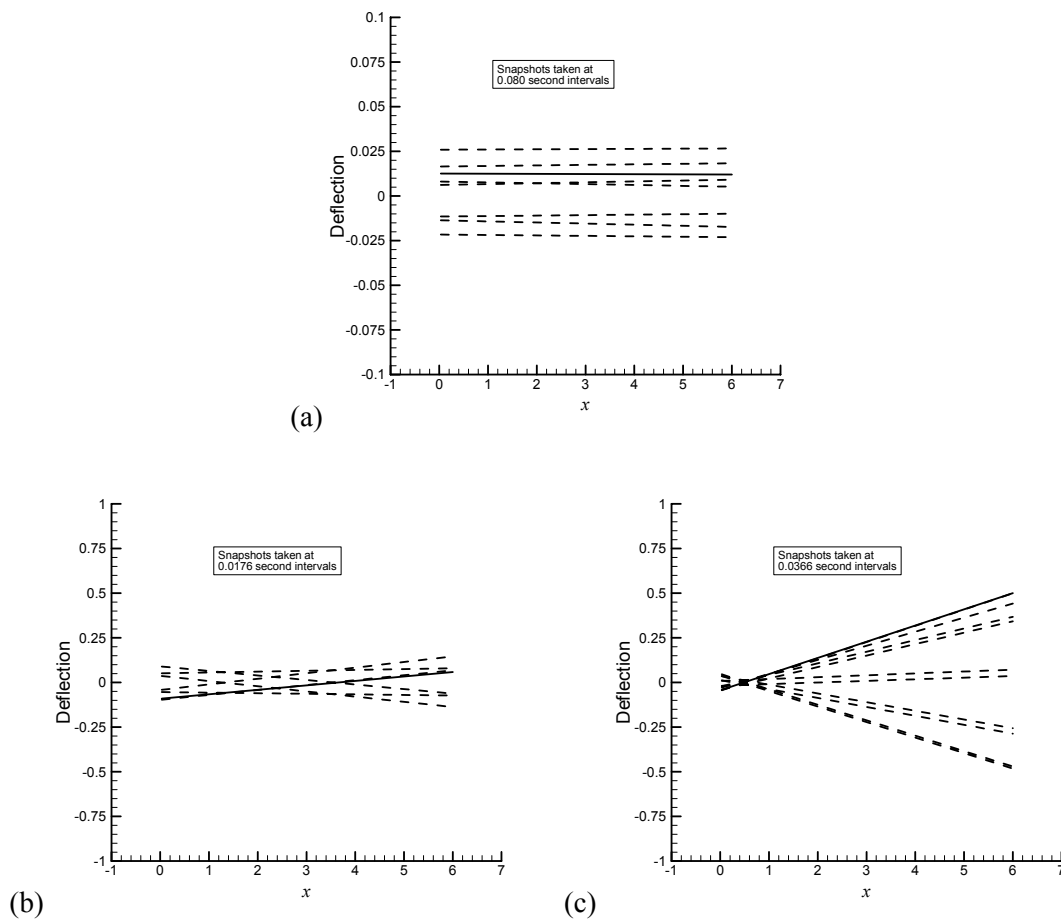
Figure 8: Snapshots of wingtip chordlines (G1) three characteristic aeroelastic responses: (a) flutter at Mach 0.84 ($U = 750$ ft/sec); (b) flutter at Mach 0.90 ($U = 850$ ft/sec); (c) LCO at Mach 0.92 ($U = 410$ ft/sec).
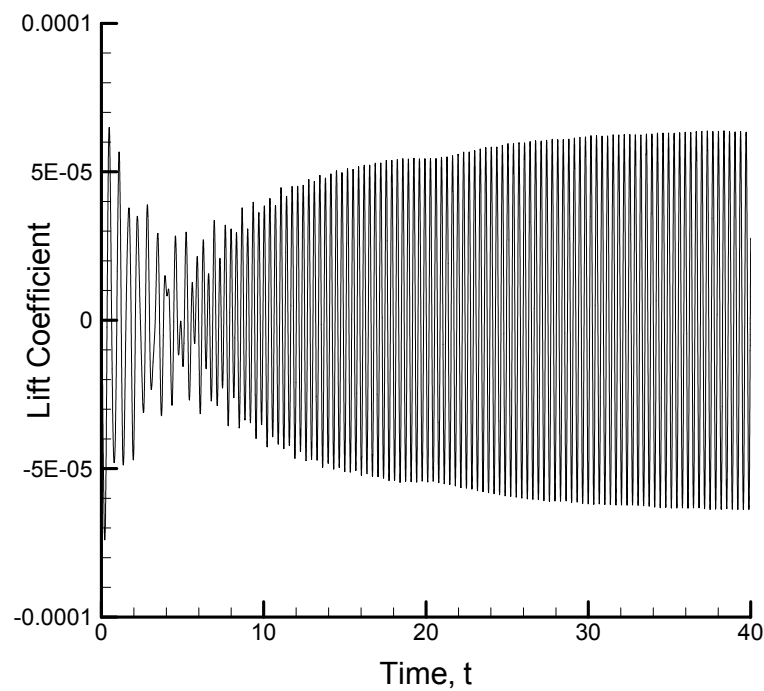
Figure 9: Low-amplitude oscillations at Mach 0.92 and $U = 385$ ft/sec (grid G1).
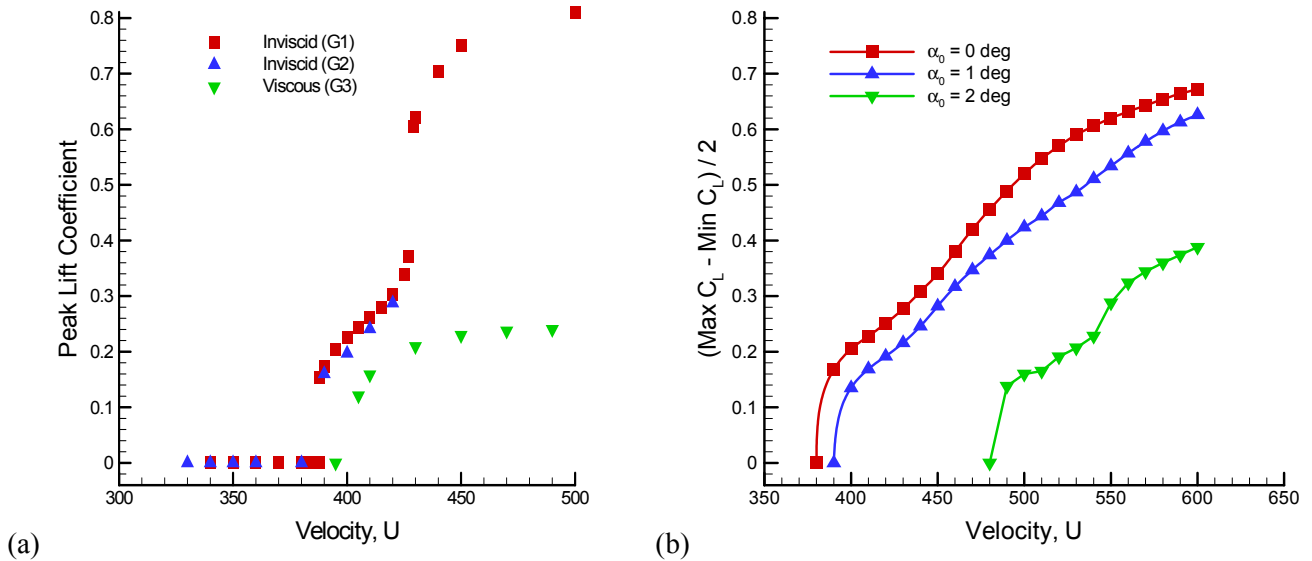
Figure 10: Comparison of LCO response boundaries for different CAPTSDv analyses: (a) inviscid analysis with (G2) and without (G1) inclusion of store aerodynamics, and viscous analysis (G3) for Mach 0.92; (b) inviscid analysis without store aerodynamics at selected angles of attack for Mach 0.93.
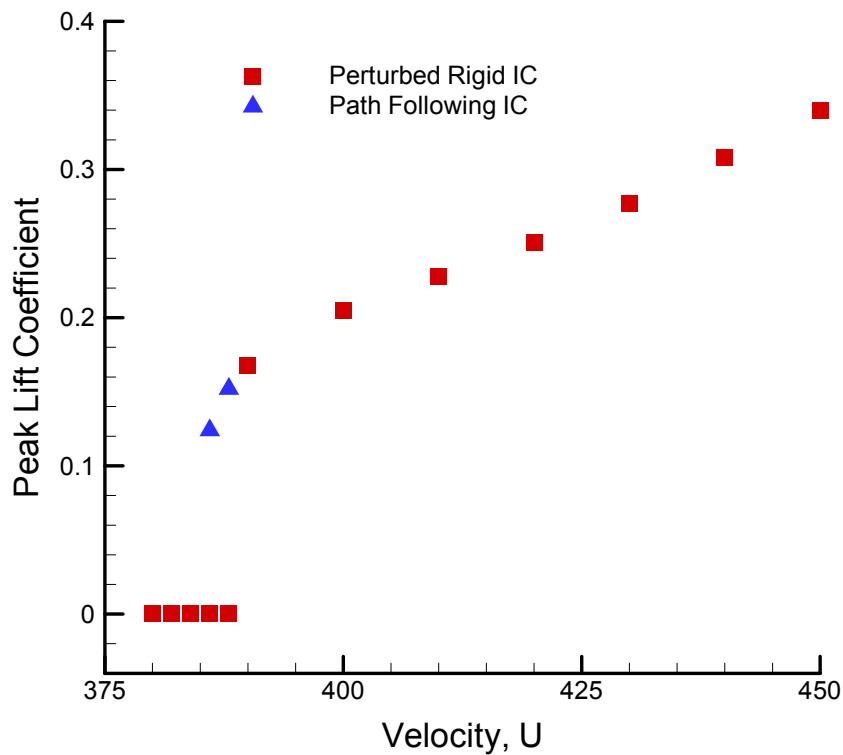
Figure 11: Demonstration of subcritical Hopf bifurcation and non-unique aeroelastic behavior at Mach 0.93 (wing/store model without store aerodynamics). Two initial conditions are employed: baseline initial conditions ("Perturbed Rigid IC") and converged LCO solutions at higher velocities ("Path Following IC").
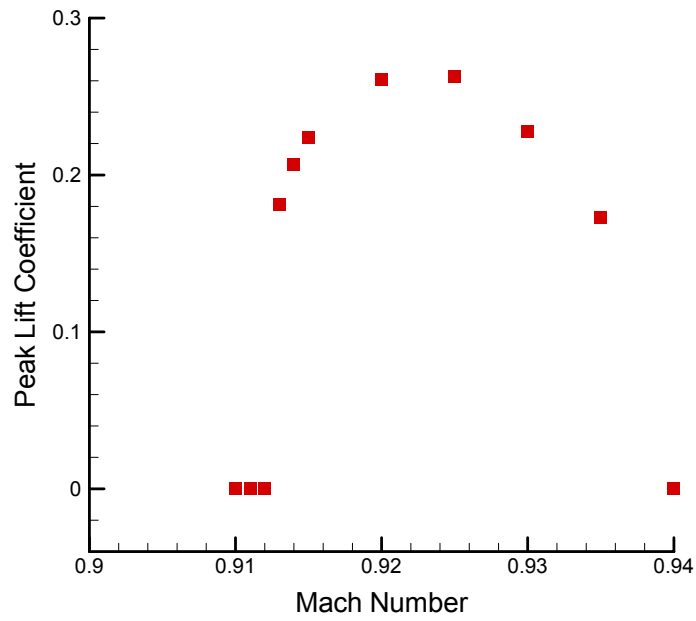
Figure 12: Variation of LCO response for different Mach numbers at U = 410 ft/sec (wing/store model without store aerodynamics).
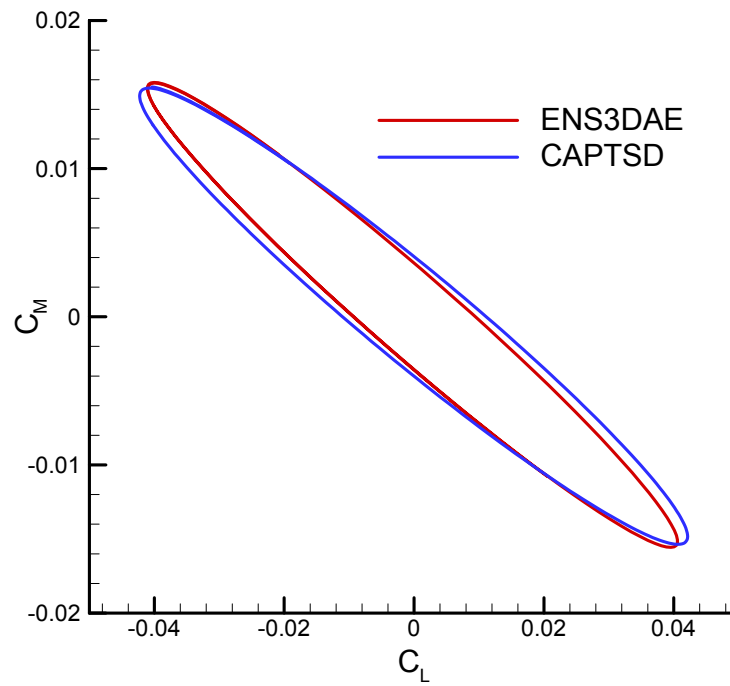
Figure 13: Comparison of C_L–C_M phase portraits predicted by CAPTSDv and ENS3DAE for forced pitch oscillation (amplitude of ½ deg at 3 Hz) of the rigid wing at Mach 0.92 and U = 400 ft/sec.

Nonlinear Computational Aeroelasticity:
Formulations and Solution Algorithms

A. Soulaïmani, A. BenElhajAli and Z. Feng
Département de génie mécanique
École de technologie supérieure
1100 Notre-Dame Ouest
Montréal, Québec
Canada, H3C 1K3

E-mail : asoulaimani@mec.etsmtl.ca

Abstract

This paper highlights some technical features of an analysis methodology being developed for nonlinear computational aeroelasticity. A conservative finite element formulation for the coupled fluid/mesh interaction problem is proposed. Fluid-structure coupling algorithms are then discussed with some emphasis on distributed computing strategies. Numerical results are finally shown for the Agard 445.6 wing.

Introduction

Aeroelasticity is the study of the mutual interactions between aerodynamic, inertial and elastic forces on flexible structures, such as aircraft. The aerodynamic forces induced by the flow on an aircraft depend on the geometric configuration of the structure. On the other hand, the aerodynamic forces cause elastic deformations and displacements of the structure. Accurate prediction of aeroelastic phenomena such as static divergence and flutter is essential to the *design and control* of high performing and *safe* aircraft. Transport aircraft of the future are expected to become much more complex. With the advanced subsonic and the transonic civil aircraft, it is becoming increasingly important to perform static and dynamic aeroelastic analysis using highly accurate fluid and structural computational models. In general, classical aeroelasticity often leads to oversized aircraft design. Thus, more accurate computational capabilities for aeroelascitity analysis are desired. In general, aeroelasticity analysis treats static and dynamic aspects. Static analysis is usually associated with performance. In dynamic analysis, the concern is focused on safety through *stability*, and *dynamic response* studie*s*. Instability problems occur when the structure sustains energy from the fluid that exceeds the capacity of elastic potential energy. Thus, there exists a critical flight speed beyond which instabilities take place that are characterized by high amplitude oscillations. Wing *flutter* is an example of such instabilities. *Buffeting*, which is the unsteady response of a structure caused by the fluctuations in the incoming flow, is another example. In aeroelastic response problems, one looks for the deformation and stress states in the structure as a response to turbulence or any unsteadiness in the flow. When the response of the structure is finite, the structure is stable. The structure flutters when its response to any finite disturbance is highly amplified.

We present an integrated CFD-CSD simulation methodology for flutter calculations based on distributed-parallel finite elements solvers. The main technical features of the proposed approach are:

- **Flow solver:** Stabilized Finite Element Formulations are being used for space discretization of the three-dimensional Euler and Navier-Stokes equations. An implicit parallel solver based on Schwarz Domain Decomposition methods and on the nonlinear version of the GMRES algorithm is developed.

- **Mesh solver:** Arbitrary-Lagrangian-Eulerian kinematics formulation is used in order to adapt the grid motion with the structure displacement. An ALE formulation is developed where, at any instant, the mesh configuration verifies the discrete form of the Geometric Conservation Law (DGCL). Furthermore, the dynamic mesh is modeled as a linear elastic material which undergoes large displacements.
- **Structure solver:** Finite Element commercial models for linear elasticity are used to perform the eigenvalue analysis. The time dependent structural displacement field is then computed using a classical Newmark scheme.
- **Distributed/Parallel computations:** Aeroelastic analyses are computationally intensive. Therefore, they can benefit from parallel processing technology. Intra parallelism (i.e., within each field) and inter parallelism (i.e., to couple the three fields fluid-mesh-structure) is performed using the message-passing paradigm. The computer code developed is designed to run on shared memory machines as well as on distributed machines such as Beowulf clusters. A Beowulf cluster recently developed at ETS containing 24 PCs and 12 GB of RAM is used presently as the distributed computing platform.
- **Fluid-Structure coupling:** Implicit solution algorithms are proposed to solve the CFD-CSD-Mesh coupled problem. It is based on the use of the Newton-GMRES algorithm for the entire problem along with a block preconditioning technique. Each block corresponds to *a functional* domain.
- **Matcher:** A fourth module is built in order to perform the tasks of load transfer from the fluid to the structure and the exchange of structure motion to the fluid.

The computational fluid dynamics code

PFES is our finite element code for the numerical solution of some multi-physics problems. For Euler and Navier-Stokes equations, a new formulation referred to as EBS (Edge Based Stabilized finite element formulation) is developed. This method combines in some way the best features of respectively the Galerkin finite element method (provides high order schemes, easy to implement on unstructured grids, etc.) and the Finite Volume based methods (e.g. ease to construct monotone upwind schemes on unstructured meshes). It was numerically demonstrated [1-3] that EBS can be less diffusive than SUPG [4-6] and the standard Finite Volume schemes. Accuracy is critical for solving shocks and separation regions present in the transonic regime. The implicit solver used is based on the Flexible GMRES algorithm preconditioned by the incomplete factorization ILUT [7]. The parallel version of the code makes use of the domain decomposition approach.

The Euler compressible equations in fixed meshes are written in a compact form and in terms of the conservation variables are written in a vector form as

$$V_{,t} + F_{i,i}^{adv}(V) = F_{i,i}^{diff}(V) + F_s \tag{1}$$

where $\mathbf{V}$ is the vector which components are the specific momentum, density and specific total energy. F_i^{adv} and F_i^{diff} are respectively the convective and diffusive fluxes in the *i*th-space direction, and $\mathbf{F_s}$ is the source vector. Lower commas denote partial differentiation and repeated indices indicate summation. Diagonalizable Jacobian matrices can represent the convective fluxes $A_i = F_i^{adv}{}_{,V}$. Recall that any linear combination of these matrices has real eigenvalues and a complete set of eigenvectors. It is well known that the standard Galerkin finite element formulation often leads to numerical instabilities for convective dominated flows. In the Galerkin-Least-Squares method (or the generalized Streamline Upwind Petrove Galerkin method), the Galerkin variational formulation is modified to include and integral form depending on the local residual $\mathbf{R(V)}$ of equation (1), i.e. $R(V) = V_{,t} + F_{i,i}^{adv}(V) - F_{i,i}^{diff}(V) - F_s$, which is identical to zero for the exact solution. The SUPG formulation reads: find $\mathbf{V}$ such that for all weighting functions $\mathbf{W}$,

$$\sum_e \int_{\Omega_e} \left[W.(V_{,t} + F_{i,i}^{adv} - F_s) + W_{,i} F_i^{diff} \right] d\Omega \tag{2}$$

$$- \int_\Gamma W \cdot F_i^{diff} n_i \, d\Gamma - \int_\Gamma W. A_{\bar{n}} (V - V_\infty) \, d\Gamma + \int_\Omega \mu_c \nabla W. \nabla V d\Omega + \sum_e \int_{\Omega e} A_i^t . W_{,i} \, \tau \cdot R(V) \, d\Omega = 0$$

In this formulation, the matrix τ is referred to as *the matrix of time scales*. The SUPG formulation is built as a combination of the standard Galerkin integral form and a perturbation-like integral form depending on the

local residual vector. The third integral term in (2) takes into account the far field boundary conditions and the forth integral is a stabilizing term for the shocks. Recently, a new method referred to as the Edge-Based-Stabilized finite element method (EBS) was introduced to stabilize the standard Galerkin method while considering the real characteristics of the flow as computed on the normal direction of element edges. This method has been proven to be stable and accurate for solving viscous and inviscid compressible flows, but more time consuming as compared to SUPG. Let us now briefly present the EBS formulation.

Consider the eigen-decomposition of $A_n = \sum A_i n_i, A_n = S_n A_n S_n^{-1}$.

Let $Pe_i = \lambda_i h/2v$ be the local Peclet number for the eigenvalue λ_i, h a measure of the element size on the element boundary, v the physical viscosity and $\beta_i = \min (Pe_i/3, 1.0)$. We define the matrix B_n by

$$B_n = S_n L S_n^{-1} \tag{3}$$

where L is a diagonal matrix whose entries are given by $L_i = (1 + \beta_i)$ if $\lambda_i > 0$; $L_i = - (1 - \beta_i)$ if $\lambda_i < 0$ and $L_i = 0$ if $\lambda_i = 0$. The proposed EBS formulation is similar to (2) but the last integral term is replaced by:

$$+\sum_e \int_{\Gamma_e} W \cdot \tau_n^{ed} \cdot R(V) d\Gamma = 0 \tag{4}$$

with τ_n^{ed} the matrix of *intrinsic length scales* given by $\quad \tau_n^{ed} = \frac{h}{2} \cdot B_n \tag{5}$

Geometrically conservative ALE formulation

One of the considerations in the mathematical formulation of conservation laws is the type of the kinematic description used for the material particles. A Eulerian description is very often used in fluid dynamics, while a Lagrangian is common in solid mechanics. When the material body contains moving boundaries, a mixed description, partially Lagrangian and partially Eulerian (also called Arbitrary Lagrangian-Eulerian), is more convenient [8-9]. This occurs for any flexible structure surrounded by a flow. It therefore becomes necessary to solve the fluid equations on a moving grid in order to match the fluid and the structure boundaries. Thus, besides the fluid and the structure material fields, there is a third field constituted by the moving mesh, which can be viewed as a material body having its own motion and dynamics. The three-field coupled problem is constituted by a set of partial differential equations, which are coupled through boundary conditions. A class of solution procedures called partitioned or segregated has been advocated to solve this coupled problem [10-14]. Given the displacements of the nodes on the wing, i.e. after solving the structure displacement field, a differential elliptic operator is designed to distribute the boundary motion inside the domain in order to avoid nodes collapsing or elements degenerating. After updating the mesh configuration, the flow field is solved on this mesh. It is shown [10] that the algorithm constructed for updating the dynamic mesh must obey a discrete Geometric Conservation Law (DGCL). A physical interpretation of the GCL is that the motion of the nodes must be compatible with the fact that the volume swept by the edges of the control volume or the element should be exactly equal to the variation of its volume (i.e. volume preserving). Our interpretation of the GCL goes as follows. The DGCL is equivalent to satisfying the kinematic Euler equation for the mesh, i.e.

$$\frac{\partial J}{\partial t} = J \, div \, w \tag{6}$$

where J is the determinant of the geometric gradient tensor F from the current mesh configuration to the reference one and w is the velocity of a point of the moving domain. Equation (6) holds for the continuous medium. However, when applying discretization methods in space (FE, FD or FVM) and in time, it is not a priori satisfied due to time and space discretization errors. Those errors should not spoil the accuracy of the coupled problem. In [10,12,13], special time integration schemes satisfying the DGCL for first and second order time accuracy have been proposed in the context of FV methods. Substantial modifications to the original code, which has been developed for fixed meshes, are then required. Given the above interpretation, we propose to investigate the DGCL in another way. The mesh is not updated unless it satisfies equation (6) in a discrete form. Then, a finite element formulation can be easily constructed to solve the operator for distributing the boundary displacement inside the domain constrained to satisfying, in a weak form, the Piola-Kirchoff equation. By doing this, standard time integration procedures usually used for fixed meshes are

accurate and still valid for dynamic meshes. Thus, CFD codes built for rigid meshes could be still valid for dynamic meshes. This idea is detailed in the following.

The conservation equations (1) in moving meshes are rewritten as

$$(JV)_{,t} + J\left(F_i^{adv} - w_i V\right)_{,i} = J\left(F_{i,i}^{diff} + F_s\right) \tag{7}$$

In the above equation, space differentiations are done with respect to the actual coordinates at the current time. Using simple differentiation operations, (7) is transformed into

$$(J_{,t} - J\,div\,w)\,V + J\,(V_{,t} + F_{i,i}^{adv} - w_i V_{,i} - F_{i,i}^{diff} - F_s) = 0 \tag{8}$$

and the corresponding classical Galerkin variational form is :

$$\int_{\Omega_0} W \cdot (J_{,t} - J\,div\,w)\,V\,d\Omega + \int_{\Omega} W \cdot (V_{,t} - F_{i,i}^{adv} - w_i \cdot V_{,i} - F_s)\,d\Omega + \int_{\Omega} W_{,i} F_i^{diff}\,d\Omega - \int_{\Gamma} W \cdot F_i^{diff} n_i d\Gamma = 0 \tag{9}$$

where Ω_0 is the configuration of the mesh at a reference time t_0 and Ω is the current configuration of the mesh at time t. For the continuous solution, Euler identity (6) is satisfied at any instant and for every point of the domain so that the first integral in (9) is identically zero. Thus, the variational formulation of the conversation equations is similar to the case of fixed mesh (up to the additional convective term $-w_i V_{,i}$ or in other words the advective matrices A_i are replaced in the case of moving domains by $A_i - w_i I$ with I the identity matrix):

$$\int_{\Omega} W \cdot (V_{,t} - F_{i,i}^{adv} - w_i \cdot V_{,i} - F_s)\,d\Omega + \int_{\Omega} W_{,i} F_i^{diff}\,d\Omega - \int_{\Gamma} W \cdot F_i^{diff} n_i d\Gamma = 0 \tag{10}$$

For a discrete numerical solution Euler identity is not necessarily satisfied. Thus the first integral term in (9) could not, in principle, be neglected. The usual DGCL condition states that for a dynamic mesh and for any arbitrary constant flow field Vc and for the case of $F_s = 0$, the solution of the discrete problem should be exactly Vc, thus (9) gives

$$\int_{\Omega_0} \phi\,(J_{,t} - J\,div\,w)\,d\Omega = 0 \tag{11}$$

where ϕ is any weighting scalar function. Equation (11) is simply the variational form corresponding to the constraint (6). Note that (10) actually satisfies the usual DGCL condition discussed above. More generally, if it is desired for any purpose to use the non-conservative variational formulation (10) while satisfying explicitly the DGCL condition, the mesh motion could be subjected to the constraint (11). In the finite element methodology one usually interpolates **w** by continuous piece-wise functions, so that the mesh velocity field is continuous in the continuous medium (i.e. the mesh). Then, equation (6) is satisfied for the exact time differentiation of J. However, applying a time discretization scheme, similar to that used for the fluid, to the mesh coordinates to obtain **w** and to $\frac{\partial J}{\partial t}$ yields a truncation error $\frac{\partial J}{\partial t} - J\,div\,w = o(\Delta t^p)$ which is consistent with the truncation error obtained for the discrete (fluid) conservation equations. Thus, one can adopt formulation (10) along with an appropriate time discretization scheme for the evaluation of **w**, and the stability and convergence in time are expected to be obtained. On the other hand, recent theoretical studies by Letallec and his group [15] showed the impact of DGCL on the conservation of energy of the coupled fluid-structure system considered as a unique continuous medium. Energy conservation is a key point in studying fluid-structure interactions. In particular, the evolution of the kinetic energy must be controlled. Most time integration schemes do violate this principle of energy conservation when dealing with deformable domains. More precisely, for fully coupled schemes using conservative formulations and non-volume preserving grid configuration (DGCL), a small pollution term appears in the kinetic energy principle, which may grow exponentially in time. More specifically, it can be shown that using the first order Euler time discretization, the scheme is volume preserving if the fluid equations are integrated over a configuration Ω which is located at the mid distance between two successive configurations of the mesh [10] .

Mesh motion

Many choices can be considered in designing the operator that distributes the fluid-interface motion inside the moving domain. We consider that the mesh motion is defined by the elasto-static equations defined in the mesh configuration at time t :

$$\rho_m \mathbf{x}_{,tt} - div(\mathbf{P}(\mathbf{x})) = b \tag{12}$$

where ρ_m, $\mathbf{P}$ and $\mathbf{b}$ are fictitious density, the PK1 stress tensor and the body force. Equation (12) is solved for the mesh displacements $\mathbf{x}$ with the kinematics condition at the moving boundary $\mathbf{w} \cdot \mathbf{n} = \mathbf{u} \cdot \mathbf{n}$ for inviscid flows, with $\mathbf{u}$ the fluid velocity. The mesh velocity $\mathbf{w}$ is computed using a finite difference scheme (similar to that used for the fluid) to the differential equation $\mathbf{w} = \mathbf{x}_{,t}$. We usually take ρ_m and b equal to zero.

As the mesh moves, it is not always guaranteed that all elements keep an acceptable shape for accurate CFD computations. Especially, small elements are prompt to large distortions. In order to preclude negative volumes or large distortions for small elements, a suitable constitutive law for the mesh medium should be designed.

We consider the mesh as an elastic material undergoing small strains and large rotations. Thus, the PK2 stress tensor $S = P. F^{-t}$, (with $\mathbf{F}$ the deformation tensor) is linear with the Green strain tensor $E = (F^t F - I)/2$, thus:

$$S = C E \tag{13}$$

where C is the fictitious elastic modulo tensor which entries are of order $0(h^{-3})$ with h the element size.

In summary, equations (12) are solved for the finite displacements $\mathbf{x}$ between the mesh configurations at time t and time t+Δt along with the constitutive relation (13) and the boundary conditions. The non-zero boundary conditions for the mesh equations are actually the imposed displacements at the moving boundary which are computed by the CSD module. Note that the mesh motion problem can generate a large system of nonlinear equations. These are solved, at every time step, using a preconditioned Krylov algorithm (CG or even GMRES).

The CSD analysis

The finite element method is well established for solid and structure computations. In industry, commercial codes are very often used for linear structure analysis. In this work, we consider a classical linear model for the structure which can be described by modal equations as

$$\ddot{z}_i(t) + 2\eta_i \omega \dot{z}_i(t) + \omega_i^2 z_i(t) = s_{0i}(t) \tag{14}$$

with z_i the generalized normal mode displacement, η_i and ω_i are respectively the damping and the natural frequency of the ith mode. Newmark's algorithm is used to integrate (14).

Coupling algorithms and distributed computing

In dynamic response problems, one looks for the successive flow and structure behaviours for a given set of initial conditions, such as a perturbation in the flow. In linear theory, the flutter speed of an aircraft can be obtained directly from the solution of an eigenvalue problem. In the nonlinear theory, for a given set of flight conditions, predicting whether an aircraft will flutter or not is much more complex and computationally intensive. There are two possible approaches (a) Starting from a deformed state of the structure the fluid-structure coupled solution is computed in the time domain [10-13], (b) Starting around an initial equilibrium state an eigenvalue problem is established by linearizing the coupled dynamic system [14]. The first approach is simpler to implement and enables to capture all the nonlinearities in the fluid-structure system.

Implicit time marching schemes enable the use of large time steps for the structure as well as for the mesh and the fluid fields. The conventional partitioned procedure commonly used in fluid-structure interactions is illustrated in Figure 1. It is based on the following steps:

1. Update the fluid grid to conform to the structural boundary at time t_n .
2. Advance the flow field using the new boundary conditions.
3. Update the surface load on the structure based on the fluid solution at time t_{n+1}
4. Advance the structure using the new fluid surface load.

For parallel computing, one can use an inter-field partitioned approach as illustrated in Figure 2.
1. The fluid grid is updated to conform to the structural boundary at time t_n and the fluid is advanced using the structural boundary conditions at time t_n
2. The structure is advanced using the fluid surface load at time t_n.

With this procedure, the CFD and CSD solvers can run in parallel during the time interval $[t_n , t_{n+1}]$. Inter-field communication and I/O transfer is needed only at the beginning of each time interval. As time progress, there may be a lag between the fluid and the structure so that a spurious energy exchange at the interface may generates undesirable instabilities.

In the following, an implicit iterative scheme is proposed to enhance the coupling between the mesh, the structure and the flow fields. After time and space discretizations of the fluid, structure and mesh equations, an algebraic system of equations for the unknown variables $\mathbf{S} = (\mathbf{V}, \mathbf{x}, \mathbf{q})^t$ (i.e. flow quantities and structure-mesh displacements) is obtained, which can be formally written as

$$G(S) = 0 \qquad (15)$$

This non-linear system can be solved using Newton's method as follows:

1. Given an initial structure and mesh configurations and a flow field for the current time step t_n;
2. Do n=1, maximum number of time steps;
3. Do i= 1, maximum number of iterations;
4. Find the correction $\Delta\mathbf{S^i}$ solution of :

$$H\,\Delta S^i = -G(S^{i-1})$$

where $\mathbf{H}$ is the Jacobian matrix associated to $\mathbf{G}$;
5. Check the convergence. If satisfied go to 6;
6. EndDo;
7. Update the global solution $\mathbf{S^i} = \mathbf{S^{i-1}} + \Delta\mathbf{S^i}$
8. EndDo.

In this algorithm, the Jacobian matrix $\mathbf{H}$ is needed. While it is difficult to develop its analytical expression, it is possible to compute an approximation. On the other hand, using Krylov-based iterative methods, such as the GMRES algorithm, to solve the linear system in step (4), one actually only need to compute the matrix-vector product of H and a direction vector z. A good approximation can be computed using a finite-difference formula like

$$Hz = \frac{G(V_0 + \sigma z) - G(V_0)}{\sigma} \qquad (16)$$

where σ is a small scalar.

To be efficient, Krylov methods need to be appended by a preconditioned, which is in principle a good approximation of $\mathbf{H}$. A straightforward choice would be to use a *block-diagonal* matrix, which entries are the approximate Jacobians associated with respectively the flow, the structure and the mesh fields. In other words, the coupled problem is seen as a set of non-linear equations obtained by discretizing a continuous medium.

These equations are solved iteratively using preconditioned Newton-GMRES method. While the global residual vector **G(S)** is needed, its main three components are computed by calling the corresponding modules (CFD solver, mesh solver or CSD solver). Obviously, these computations can be performed in parallel and inter-field communications are needed. This decomposition is referred to as the *functional decomposition*. On the other hand, the residuals of the flow field and the mesh motion are computed using a classical *domain decomposition approach*. For CFD, as well as for the mesh motion, we use a robust parallel iterative solver (i.e. intra-parallelism) based on Schwarz-Newton-Krylov techniques. Thus, the available processors are divided into groups of processors; each group is assigned to a specific field. Since CFD computations are more demanding, we assign more processors for the CFD domain than for the mesh solver.

Note that repeated updates of the geometry, for different flow conditions, are needed during the Newton-GMRES iterations. Thus, the flow field continuously drives the geometry so that a better conservation of the energy at the fluid-structure interface can be obtained. Since the main part of the computations is consumed within the CFD solver, the additional communications will not increase the overall simulation cost significantly, provided the number of time steps and non-linear CFD-iterations remains unchanged.

This algorithm is illustrated in Figure 3.
1. Given a geometry and a flow field at time t_n.
2. Compute the initial residual vector **R_0= G(S_0).**
3. Perform Newton–GMRES iterations: Compute the residual for a perturbed solution in a direction **z**: **G(S_0+ σ z)**; this has three major components each one is computed by its corresponding solver.
4. Perform inter-field communications.
5. Test for convergence and update the global solution for time step t_{n+1}.
6. Go to next step.
7.

Note that in the above algorithm one has to perform inter-filed communications in order to compute Krylov-directions for the global problem.

Several variants of this algorithm can be thought of. In its simplest form, one can perform a number of global iterations in which inter-filed communications occur only at the beginning of every iteration (i.e. this is nothing but the fixed-point algorithm). For a reasonable time step, one can observe the convergence for the fluid force transmitted to the structure and for the generalized coordinates after few global iterations.

Inter-field communications

Fluid-structure interactions involve the transfer of loads from the fluid mesh to the structure and the transfer of mesh structure motion to the moving mesh boundary. Since the CFD mesh is much finer than that used by the structure, the traces of these two meshes at the fluid-structure interface do not necessarily match. Then, load and displacements transfer cannot be done in a trivial way. The importance of conservative load transfer in fluid-structure interaction problems has recently been addressed in [16]. We adopt here the algorithm proposed in [16] which main steps consist of:

a) Pairing each fluid grid point S_j on the fluid interface Γ_f with the closet wet structural element $\Omega_S^{(e)} \in \Gamma_S$ (see Figure 4);
b) Determining the natural coordinates χ_j in $\Omega_S^{(e)}$ of the fluid point S_j (or its projection onto $\Omega_S^{(e)}$);
c) Interpolating the displacement of fluid nodes x_f inside $\Omega_S^{(e)}$ using the structure shape functions N_i^s ;
d) Projecting the generalized fluid force to the structure as:

$$f_i = \sum_{j=1}^{j=j_F} \Phi_j N_i^s(\chi_j)$$

with, $\Phi_j = \int_{\Gamma_f} \left(-pn + \sigma_f \cdot n \right) N_j^F d\gamma$

The generalized force associated to the fluid node S_j. It is proved that this algorithm preserves load and energy conservation at the fluid-structure interface. On the other hand, in aeroelasticity, the structure is often represented by plate, shell and beam elements which results in geometric discrepancies between the fluid mesh

skin Γ_F and the structure boundary Γ_S (as illustrated in Figure 4). Thus, the above transfer algorithm is preceded by a projection step of the fluid nodes **M** onto the structure elements to locate the point **P** and to compute the gap vector **PM**. The motion of P is found using the above interpolation procedure and the motion of M is obtained by considering that the vector **PM** rotates with the structural element as it is done in classical plate theory.

Numerical results

Numerical tests have been carried out for the popular AGARD-445.6 [17] wing. The AGARD-445.6 is a thin swept-back and tapered wing with a symmetrical NACA 65A004 airfoil section. The weakened model-3 is considered here. A coarse unstructured grid is employed for Euler computations that has 37965 nodes, 177042 elements and generates 388464 coupled equations. For the structure, a mesh of 1176 quadrilateral shell elements and 1250 nodes. Using the commercial software Ansys, the firs five dry modes have been computed. There respective frequencies are the following: 9.6 Hz, 39.42Hz, 49.60 Hz, 96.095Hz and 126.30 Hz. The shape modes compare well with those of Yates (figure 5). A flow at a free-stream Mach number of 0.96 and zero angle of attack is computed first. At t=0, a Dirac force is imposed on the tip of the wing. The response of the wet structure is computed for different free stream pressures q. We use a second order time differentiation scheme with a non dimensional time step $\Delta t = 0.2$ and three global iterations. The experimental flutter pressure at M= 0.96 is q = 61.3 lb/sq ft [17]. Figure 6 shows that at the computed conditions (M= 0.96 is q = 62.0 lb/sq ft) the structure is neutrally stable and the first two modes are in coalescence. Figure 7 shows a comparison of two models for the mesh motion (with q= 71.3), a nonlinear model as described previously (used the above computations) and a linear one where **F= I** and where the second order terms in **E** are dropped. In the linear model the mesh becomes distorted as the motion amplifies until it collapses at time step 290 (negative jacobians). With the nonlinear model, computations run for 900 time steps. Finally, figure 8 shows a comparison of the flutter boundary obtained with our code with the experimental observations [17] and with some numerical results reported in the literature[18 , 19 and 20].

Conclusion

In this paper we have presented a CFD-based aeroelastic model. A suitable finite element formulation is used for all computational fields (fluid, mesh and structure). A functional decomposition approach is used for the solution of the coupled problem. For every physical field a parallel GMRES algorithm is employed to solve the corresponding discrete system. Inter-filed communications occur during global quasi-Newton coupling iterations. Numerical tests on the Agard 445.6 aeroelastic wing show that the inter-filed communications strongly enhance the numerical stability of the time marching procedure. The flutter dip is well produced when three global coupling iterations are used. On the other hand, a nonlinear model for the moving mesh is proposed. Numerical tests show that this model improves the robustness of the aeroelastic code. Finally, an accurate flutter boundary is obtained for the Agard445.6 wing aeroelastic test case.

Acknowledgments

References

[1]   A. Soulaïmani and A. Rebaine. "An edge based stabilized finite element method for solving compressible flows", the 14th AIAA Computational Fluid Dynamics Conference, paper AIAA-99-3269.
[2]   A. Soulaïmani and C. Farhat. "On a finite element method for solving compressible flows", ICES98, Atlanta, 1998.

[3]   A. Soulaïmani, A. Rebaine and Y. Saad. "An edge based stabilized finite element method for solving compressible flows: formulation and parallel implementation", Comput. Methods Appl. Mech. Engrg, vol. 190, pp.6735-6761 (2001).

[4]   T.J.R. Hughes and Mallet. "A new finite element formulation for computational fluid dynamics III. The generalized streamline operator for multidimensional advective-diffusive systems", Comput. Methods Appl. Mech. Engrg, 58, 305-328, 1986.

[5]   A. Soulaïmani and M. Fortin. "Finite element solution of compressible viscous flows using conservative variables", Comput. Methods Appl. Mech. Engrg., 118, 319-350, 1994.

[6]   N.E. Elkadri, A. Soulaïmani and C. Deschenes. "A finite element formulation of compressible flows using various sets of independent variables", Comput. Methods Appl. Mech. Engrg., 181, 161-189, 2000.

[7]   Y. Saad. "Iterative Methods for Sparse Linear Systems", *Numerical Linear Algebra with Applications*, 1:387-402, 1994.

[8]   J. Donea. "An arbitrary Lagrangian-Eulerian finite element method for transient fluid structure interactions", Comput. Meths. Appl. Mech. Engrg., 33, 689-723, 1982.

[9]   A. Soulaïmani and Y. Saad: "An Arbitrary Lagrangian Eulerian finite element formulation for solving three-dimensional free surface flows", 162, 79-106, 1998.

[10]   C. Farhat and M. Lesoinne. "On the accuracy, stability, and performance of the solution of three-dimensional nonlinear transient aeroelastic problems by partitioned procedures", AIAA-96-1388, 1996.

[11]   R. Löhner et al. "Fluid-Structure Interaction Using a Loose Coupling Algorithm and Adaptive Unstructured Grids", AIAA Paper 95-2259.

[12]   M. Lesoinne and C. Farhat. "Geometric conservation laws for aeroelastic computations using unstructured dynamic meshes", AIAA Paper 95-1709.

[13]   C. Farhat and M. Lesoinne. "Two efficient staggered algorithms for the serial and parallel solution of three-dimensional nonlinear transient aeroelastic problems", Comput. Maths. Appl. Mech. Engrg, 182, 499-515, 2000.

[14]   M. Lesoinne and C. Farhat. "CFD-based aeroelastic eigensolver for the subsonic, transonic and supersonic regimes", Journal of Aircraft, vol 38, no 4, 2001.

[15]   T. Fanion, M. Fernandez and P. LeTallec: "Deriving adequate formulations for fluid-structure interaction problems : from ALE to transpiration". Revue Européenne des éléments finis. Volume 9-6, pp. 681-70, 2000.

[16]   C. Frahat, M. Lesoinne and P. LeTallec . "Load and motion transfer algorithms for fluid/structure interaction problems with non-matching discrete interfaces: Momentum and energy conservation, optimal discretization and application to aeroelasticity". Comput. Maths. Appl. Mech. Engrg, vol. 157, pp. 95-114, 1998.

[17]   E.C. Yates. "AGARD Standard Aeroelastic Configuration for Dynamics Response, Candidat Configuration I.-Wing 445.6", NASA TM 100492, 1987.

[18]   E.M. Lee-Rausch, J.T. Batina. "Wing-flutter boundary prediction using unsteady Euler equations aerodynamic methd". AIAA Paper No. 93-1422, 1993.

[19]   K.K. Gupta. "Development of a finite elemnt aeroelastic analysis capability". J. Aircraft 33 (1996) 995-1002.

[20]   M. Lesoinne, M. Sarkis, U. Hetmaniuk and C. Farhat. "A linearized method for the frequency analysis of three-dimensional fluid/structure interaction problems in all flow regimes". Comput. Maths. Appl. Mech. Engrg. 190 (2001) 3121-3146.
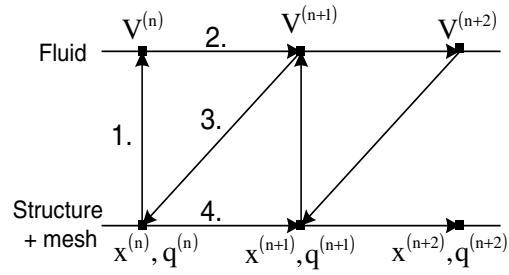
Figure 1. Conventional partitioned procedure
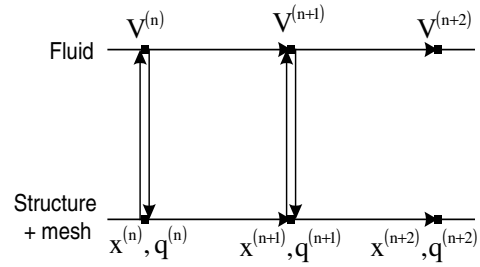
Figure 2. Inter-field partitioned procedure
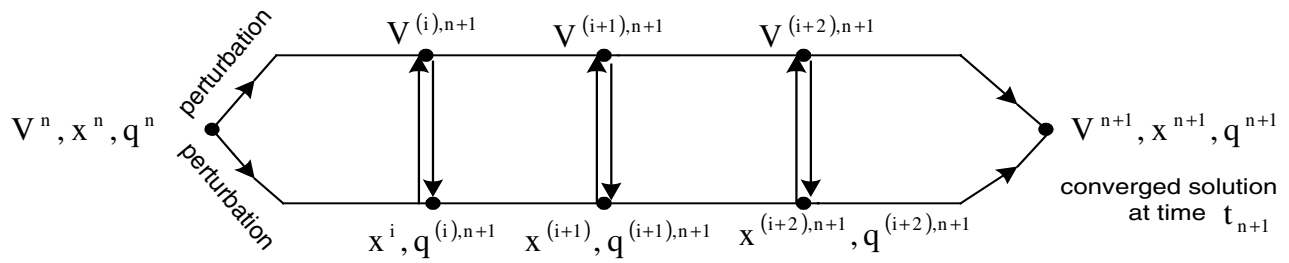
Figure 3. A fully implicit coupled procedure
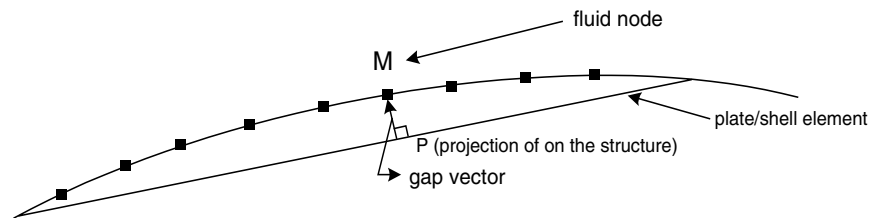
Figure 4. Fluid-solid interface moves according to plate theory
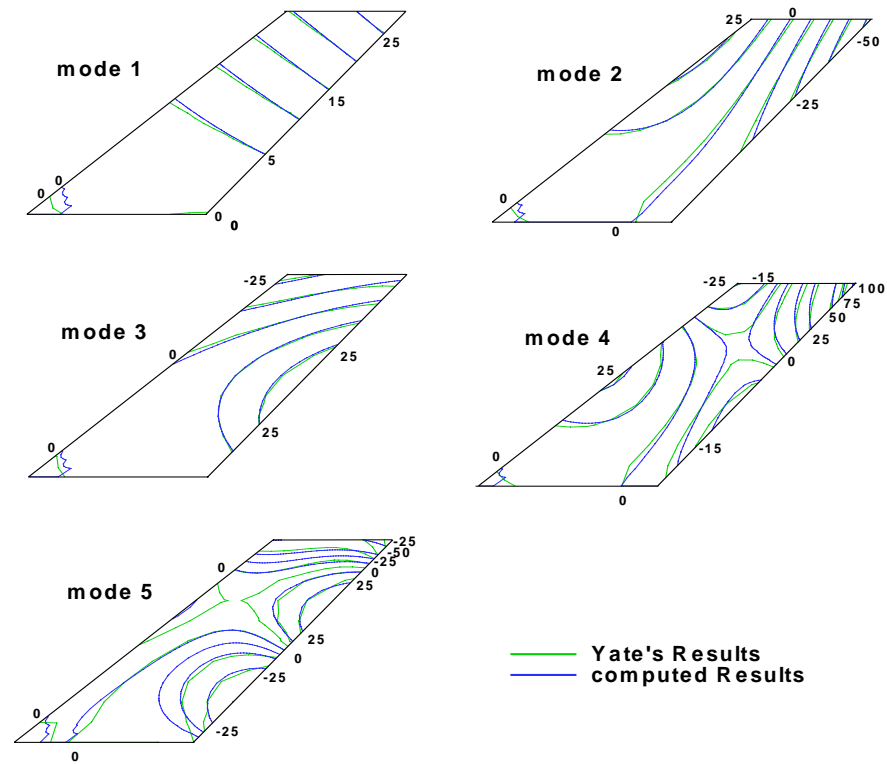
Figure 5. Agard 445.6 structure shape modes
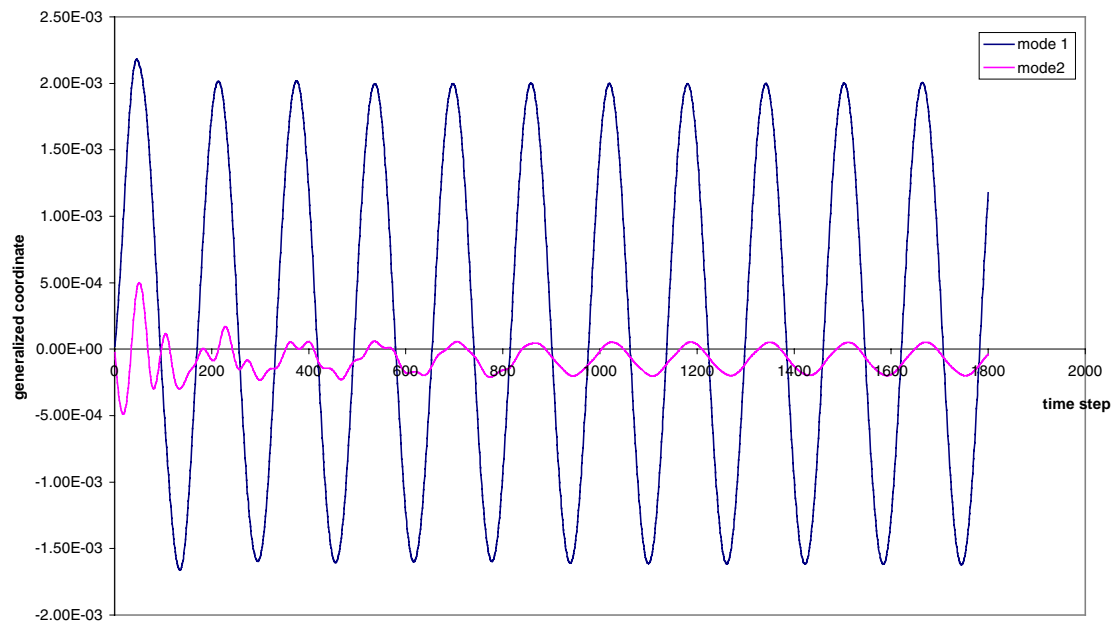
Figure 6. Time history for the first and second modes for Mach= 0.96 and
q= 62 lb /sq ft and using three coupling iterations
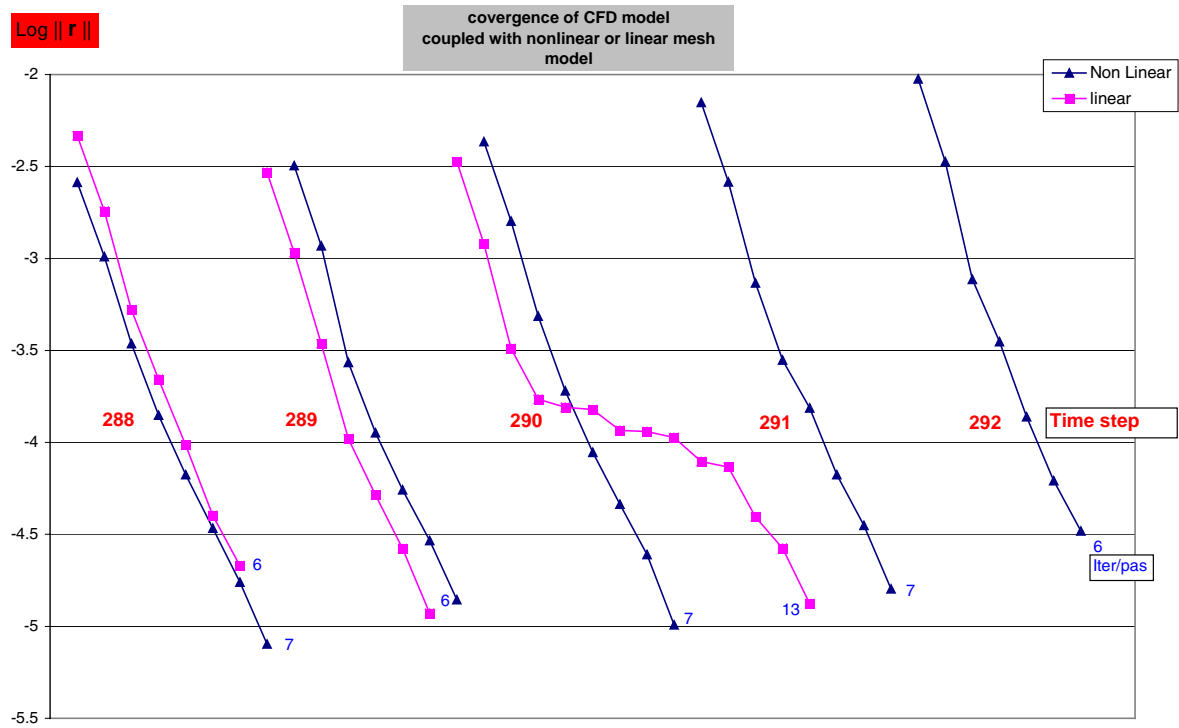
Figure 7. Convergence history for the CFD computations using respectively.
A linear and a nonlinear mesh model
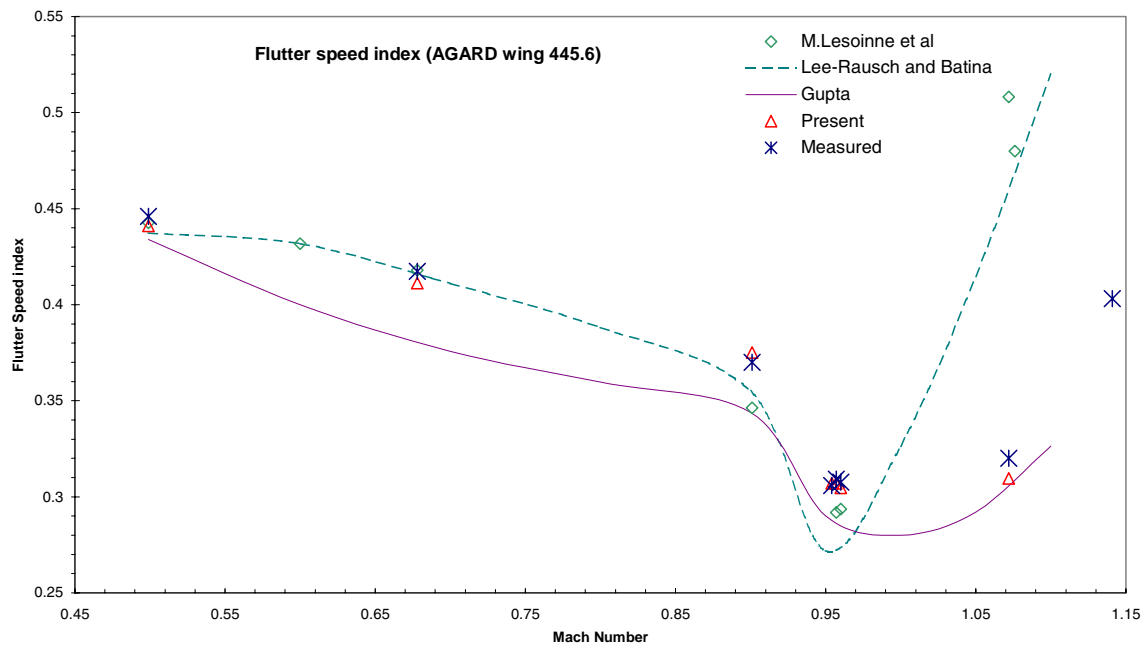
Figure 8. Flutter speed index (AGARD wing 445.6)

Paper #45
Discussor's Name: M. Khalid
Author's Name: A. Soulaimani

Q: When you transfer the aerodynamic loads onto the structural mesh, do you implement any transformation criteria which takes into account the local shear moment and torque equilibrium?

A: Such loads are due to pressure and viscous shear on the skin. In case of a locally attached mass (engine or store), it can be mechanically equivalent to a local force and a torque.

This page has been deliberately left blank

_____

Page intentionnellement blanche

Numerical Simulation of Manoeuvring Aircraft by Aerodynamic and Flight-Mechanic Coupling

A. Schütte, G. Einarsson
A. Madrane, B. Schöning
DLR
Institute of Aerodynamics and Flow Technology
Lilienthalplatz 7
D-38108 Braunschweig
Germany

W. Mönnich
DLR
Institute of Flight Research
Lilienthalplatz 7
D-38108 Braunschweig
Germany

W.-R. Krüger
DLR
Institute for Aeroelasticity
Vehicle System Dynamics
Oberpfaffenhofen
D-82234 Weßling
Germany

Summary

This paper presents results of simulations performed within the scope of the DLR-Project AeroSUM-"**Aero**dynamic **S**imulation of **U**nsteady **M**anoeuvres". The objective of the AeroSUM-Project is to develop a numerical tool to simulate the unsteady aerodynamics of a free flying aircraft, by use of coupled aerodynamic and flight-mechanic computations. To achieve this objective, the unstructured, time accurate CFD flow-solver Tau is coupled with a computational module solving the flight-mechanic equations of motion. By use of an overlapping grid technique (chimera), simulations of a complex configuration with movable control-surfaces is possible.

Results of static calculations are presented to show the basic aerodynamics of the vortex dominated flow-field of the delta wing. The static simulation cases also serve as starting solutions for the unsteady simulations. Results of the unsteady manoeuvre simulations are divided into guided motion and free-flight motion. For the guided motion an oscillating motion with a given frequency and amplitude is presented. For the free-flight motion, the following cases are presented: free-to-roll from a non-zero initial roll-angle (without flap deflection), and free-to-roll initiated by flap deflection from an initial roll-angle of zero. These calculations demonstrate the functionality of the simulation system.

A 65-degree cropped delta wing model, with fuselage and movable trailing edge flaps, is used to gather experimental data. Several forced and free-to-roll experiments around the body fixed axes, both with and without flap deflection, are performed in order to validate the computational results obtained with the simulation tool.

Nomenclature

Θ	Incidence angle, pitch angle at $\phi=0°$	Ma	Mach number
α	Angle of attack	V_∞	On flow velocity
Φ	Roll angle	$Re=V_\infty c_{ref}/\nu$	Reynolds number
$\Delta\Phi$	Roll angle amplitude	T_0	Reference temperature
η	Flap deflection angle	ν	Kinematic viscosity
y	Span-wise coordinate	$c_M=M/(q_\infty Fc_{refM})$	Pitching moment coefficient
s	Half-span	$c_L=L/(q_\infty F)$	Lift coefficient
S	Reference area	$c_P=(p-p_\infty)/q_\infty$	Pressure coefficient
c_{ref}	Chord length of the model	$c_l=l/(q_\infty Fc_{refl})$	Roll moment coefficient
c_{refM}	Reference length pitching moment	f	Frequency
$c_{refl}=s$	Reference length rolling moment	t	time
$c_B=0.676\, c_{ref}$	Balance reference point		

Introduction

The improvement of manoeuvrability and agility is a substantial requirement of modern fighter aircraft. Currently, roll-rates of 200º/s and more can be achieved, especially if the design of the aircraft is inherently unstable. Most of today's and probably future fighter aircraft will be delta wing configurations. The flowfield of such configurations is dominated by vortices developed by flow separation at the wings and the fuselage. The delay in time of vortex position and condition to the on-flow conditions of the manoeuvring aircraft can lead to significant phase shifts in the distribution of loads. In this case, reliable results for the analysis of flight properties can only be achieved by a non-linear integration of the unsteady aerodynamic and real flight movement. Today, these types of data can only be obtained by flight tests, and not during the design period. Flight tests, as well as modifications after the design phase, lead normally to an increase in costs. In order to decrease the costs incurred by extensive flight-tests and the post-design phase modifications, it would be helpful to have a tool which enables aircraft designers to analyse and evaluate the dynamic behaviour during the design phase.

The basic aerodynamic behaviour of a rolling delta wing is described by various authors, e.g. Er-Ei and Weihs [1], Katz and Levin [2], Gordnier[3], Gordnier and Visbal [4], as well as Ericsson [5][6]. Fore the dynamic forced and free-to-roll delta wing there exist several sources by Hanff [7] et al. [8][9][10], Hsia et al. [11], Ericsson [12] et al. [13], Chaderjian [14] and Schiff [15], Stephens [16], Jenkins [17] et al. [18], Jobe et al. [19] and Grismer et al. [20]. All these investigations were done by using structured CFD methods and only the clean delta wing without moveable control devices was considered.

To address the challenge of simulating the dynamic behaviour of fighter aircraft during a flight-manoeuvre, a simulation tool is being designed within the framework of the DLR project AeroSUM. The software package is divided into several independent modules, which can communicate with each other via a computational interface. The computational interface manages the work- and data-flow between the modules, and also serves as the main user interface. By using an unstructured CFD method in connection with an overlapping grid technique, the capability to handle highly complex configurations with components in relative motion is obtained. For the validation of the numerical results, extensive wind tunnel tests are performed, using a generic delta-wing model. **Figure 1** shows schematically the workflow management, data flow and the components of which the simulation tool consists.

1. Solution Algorithm

1.1. CFD Solver Tau

For the simulation of the flow-field around the object of interest the CFD-code Tau, developed by the DLR Institute of Aerodynamics and Flow Technology, is used [21]-[23]. The code solves the compressible, three-dimensional, time accurate Reynolds-Averaged Navier-Stokes equations using a finite volume formulation. The Tau-code is based on an unstructured-grid method. This method makes use of the advantages that hybrid grids offer in the resolution of viscous shear layers near walls, and the flexibility in grid generation offered by unstructured meshes. In order to make the flow-solver independent from the cell types in the initial grid, a dual mesh approach is used. The meshes used in the AeroSUM project are created using the hybrid mesh generator Centaur, developed by CentaurSoft [24]. The unstructured-grid approach is chosen due to its flexibility in creating grids for complex configurations, e.g. a full-configured fighter aircraft with control-surfaces and ordnance.

In the Tau-Code, a central scheme with artificial dissipation, as well as several upwind schemes, are available for spatial discretization. Both Spalart-Allmaras and k-ω turbulence models are implemented. For the results shown in this paper the Spalart-Allmaras turbulence model is used. For steady calculations an explicit multistage Runge-Kutta time stepping scheme is used. For time accurate computations, an implicit dual time stepping approach is used. The Tau-Code is parallelised using grid partitioning, and a multi-grid approach is used in order to increase the performance.

The Tau-Code consists of several different modules: the pre-processor uses the information from the initial grid to create a dual-mesh; the solver performs the flow-calculations using the approaches listed above; the adaptation module is used to refine the mesh to better capture flow phenomena like vortex structures and shear layers near viscous boundaries, among others; the post-processing module is used to create visual representations of the solver output. Furthermore, the overlapping grid technique is used to enable calculations of manoeuvre simulations with movable flaps. The chimera technique is chosen due

to its ability to handle large-amplitude deflections of the control-surfaces, the movement of the model in wind-tunnel surroundings, and the option to extend it in the future to allow for store-release simulations. The chimera mesh for the delta wing with trailing edge flaps is shown in **Figures 2** and **3**. In Figure 2 the surface mesh of the delta wing and the chimera boundaries are shown. On the right side, coloured red, is the boundary of the cut- out background model mesh, and on the left side, coloured green, the boundary of the flap mesh. In Figure 3 the overlapping area of the model and flap mesh is depicted. The flap mesh in this case is created to provide a flap deflection of ±15º. A more detailed description is given in references [25] and [26].

1.2. Tau-Code Extension: Chimera Technique

The chimera technique, as implemented in the Tau-Code, provides the capability to simulate large-amplitude control-surface deflections, as mentioned above. The technique is based on creating overlapping unstructured hybrid grids to handle a time-dependent relative motion of different geometries. The use of the overset concept for unstructured grids was first explored by Nakahashi et al. [27] to solve the Euler equations. The concept has been extended to unstructured hybrid grids for Navier-Stokes equations within the scope of the AeroSUM project.

In the overlapping grids concept, there are two major procedures involved in establishing intergrid communications. The first procedure is hole cutting (automatic or manual). For the cases presented in this paper, manual hole cutting is used. The second procedure is the identification of interpolation stencils, which involves a search of donor cells for all intergrid boundary points. The interpolation is based on the finite element theory, as presented by Ciarlet [28]. Two types of interpolation are implemented. In case the various control volume elements (prisms, hexahedrons, pyramids) are subdivided into tetrahedrons, a linear interpolation is performed. If no subdivision is used a non-linear finite element type interpolation is used. The search algorithm is based on a state-of-the-art alternating digital tree (ADT) data structure [29]. The ADT data structure optimises the search operations to O(logN/log2) as opposed to the total number (N) of elements in the computational domain.

The current implementation of the chimera technique can handle both steady and unsteady simulations for inviscid and viscous flows with multiple moving bodies. The technique currently runs in sequential mode on both workstation and supercomputer (NEC SX5) architectures.

1.3. Tau-Code Extension: Multi-Body Relative Motion

In order to utilise the capabilities offered by the chimera technique, a hierarchy for multi-body relative motion is implemented in the AeroSUM version of the Tau-Code. The current implementation can handle an arbitrary number of moving bodies, as well as an arbitrary depth of branches on the hierarchy list. The motion of each body, and the parent-node it belongs to, are specified in separate files for each body. The available motion types are conventional periodic motion for oscillation, specified with Fourier series and a reduced frequency, and rigid motion for constant rotation, specified with a polynomial series.

For coupled aerodynamic-flight-mechanic simulations, an external module handles the calculations of the motion of the control surfaces relative to the aircraft, while the aircraft motion is handled by the flight-mechanic module. The motions of the control surfaces are specified via a polynomial series, which is based off of the actual motion of the control surfaces during the wind-tunnel experiments.

1.4. Flight Mechanics

For the numerical simulation of the flight mechanics, the multi-body simulation software SIMPACK is used. SIMPACK is developed for the simulation of mechanical systems (automotive, aerospace, etc.) by the DLR Institute for Aeroelasticity in Oberpfaffenhofen. In cooperation with the DLR Institute of Flight Research, the software has been implemented with a module, which solves the flight-mechanic equations of motion. Initially, the numerical integration of the flight-mechanic equations was performed using a first-order Euler explicit scheme. Recently, a second-order Runge-Kutta scheme has been implemented to increase the performance and stability of the integration, thus allowing for increased complexity in the cases to be simulated. See also reference [30].

1.5. Computational Interface – KAPS

For the work- and data-flow management between the several modules that make up the simulation tool, for which the schematic is shown in Figure 1, a computational interface called KAPS [31] has been developed. The interface is based on a socket and thread structure, that allows the different modules to be executed on several different machines, as well as on different architectures, during a single simulation. Currently, the user interface is completely based on text-files, which are used to specify the set-up of a given simulation. In the near future, a graphical user-interface will be developed, based on the TENT [32] simulation environment, developed by DLR. Some initial results of coupled simulations performed by using the KAPS interface are presented in reference [33].

2. Experimental Data

For the validation of the numerical simulation software, various wind-tunnel experiments, designed specifically for the AeroSUM project, are performed. The experiments are done in the Transonic Wind Tunnel Göttingen (TWG). In order to perform these experiments, a wind-tunnel model has been designed and built for the AeroSUM project. The model, shown in **Figure 4**, is a generic cropped delta wing configuration, with fuselage and remote controlled moveable trailing edge flaps. Measurement equipment is installed to determine the aerodynamic forces and moments on the model, as well as the span-wise pressure distribution at two cut-plane locations, at 60% and 80% chord length. For the moveable flaps experiments, a motor is installed in front of the balance support, equipped with sensors to measure the aerodynamic forces and moments acting on the flap. The experiments contained forced and free-to-roll movements around the body-fixed longitudinal axis. For the guided motion, the model is driven by a motor connected to the sting, while for the free-to-roll experiments the motor is uncoupled. The rolling apparatus and the whole testing assembly of the TWG is shown in **Figure 5**. A variety of results are presented and discussed in [34].

3. Results

In this section, recent results obtained within the framework of the DLR Project AeroSUM, are presented. These results provide a verification of the capabilities of the simulation environment.

3.1. Steady Results

The hybrid mesh used for the steady calculations without flaps is shown in **Figure 6**. Due to the lack of an unsteady adaptation within the simulation tool, it is necessary to provide a refinement of the mesh in those areas where the vortices take place over the whole simulation range. Sources implemented within the grid generation provide a fine mesh on the upper and lower side of the wing from the tip beyond the trailing edge of the CFD model. In **Figure 7** a steady solution at Ma = 0.5 and $\alpha = 9°$ calculated using the mesh shown in Figure 6 is presented. The leading edge is adapted once for a better discretisation of the separating vortex sheet.

The results of the static test-cases presented in this section are a good representation of the basic aerodynamics of the delta wing model at different roll angle locations. In **Figure 8** the roll moment is shown over the roll-angle range at a Mach number of 0.5 and a pitch angle of 17.7°. At this pitch angle the roll moment for small roll angles is negative, i.e. the wing is forced to turn back into the trim point of $\phi = 0°$. At a roll angle of $\phi \approx 9°$ the sign of the roll moment changes and the wing is forced to roll in a clockwise direction. This discontinuity in the distribution is caused by a sudden movement of the point of vortex burst upon the luff side of the wing forward in leading edge direction. Finally at a roll angle of $\phi \approx 18°$ the second trim point is reached and the sign of the roll moment changes again. The region of statically unstable behaviour between the point of discontinuity and the second trim point is increased for cases with higher starting pitch angles. At lower pitch angles the delta wing is statically stable in the whole range of roll angles from $\phi = 0° - 90°$. The comparison between the experiments and the Navier-Stokes calculation shows a good fit at $\phi = 0°$ and 9°. For higher roll angles the flow field is completely unsteady, such that finding equivalent conditions is nigh to impossible, and therefore the differences are much more pronounced.

In **Figures 9** to **12** the comparison of the surface pressure between the Navier-Stokes calculation and the experimental data, corresponding to the flow-conditions listed above, is shown at a position of 60% chord length. At $\phi = 0°$ the pressure distribution of the calculation fits well with the experiments. At $\phi = 9°$ it is seen that the primary vortex is a little bit lower than in the experiments because of an over-represented secondary vortex. One reason for this behaviour in the numerical simulation is the usage of a single equation turbulence model, which leads to a higher dissipation in the boundary layer and to a stronger secondary vortex at lower angles of attack.

In **Figures 13** to **15** a static result of the model with trailing edge flaps using the overlapping grid technique is shown. The on-flow Mach number is 0.5, and the pitch angle is 9.3°. In Figure 13 the calculated surface pressure distribution is shown. In comparison to Figures 8 and 10 the effect of the flow through the flap gap is seen to lead to a low pressure area at the flap tip because of the jet trough the gap. The comparison between the calculated and the experimental pressure distribution at 60 and 80% chord length is shown in Figures 14 and 15. The calculated distribution fits well with the experiments at this low pitch angle.

3.2. Forced and Free-to-Roll Results

The results of the dynamic test-cases presented in this section highlight the current capabilities of the simulation tool. In **Figure 16** the integral lift and moment coefficients over roll angle are shown for a simulation of the oscillating delta wing. The pitch angle is constant at 17°, the frequency is 4Hz and the oscillation amplitude is $\Delta\phi = 20°$ around the body-fixed longitudinal axis. The hysteresis of the roll-moment coefficient moves in a counter-clockwise direction, which indicates that the system is highly damped dynamically. In **Figure 17** the hysteresis of the calculated and experimental roll-moment coefficient c_l, over the roll angle ϕ are compared. The hysteresis obtained from the calculation is larger than the experimental values. This indicates that the calculation predicts the system to be more damped than it is according to the experimental results. One of the reasons for this difference is that the calculation does not predict the bursting of the vortex correctly at these flight conditions, which has a major impact on the results in such a vortex dominated flowfield. One of the reasons for this may be a too low grid-resolution of the vortex structure, and affected flow phenomena, due to a lack of an unsteady adaptation being implemented in the simulation environment. Furthermore, as shown in the steady test-cases, the secondary vortex is predicted to be much stronger than in the experiment. A stronger secondary vortex results in higher lift on the luff side of the delta wing and consequently in a higher roll-moment. Furthermore, simulations that investigate the influence of the real-world experimental surroundings need to be done.

For the free-to-roll coupled flight-mechanics/aerodynamics simulations, two different geometries are used for the calculated simulations. The initial geometry is the same as for the forced-to-roll simulations, a clean delta wing without any control surfaces, while for the final geometry trailing-edge flaps are added. The simulations are restricted to a flight-mechanics model with one degree of freedom for motion, in these cases a rotation around the body-fixed longitudinal axis. In **Figures 18** and **19**, a comparison between a coupled flight-mechanics/aerodynamics calculation for the delta wing without flaps and the experimental simulation is shown. The delta wing is released from an initial roll angle of $\phi = 40°$, at a constant pitch angle of 17°, and moves into a trim point due to the effects of the aerodynamic forces. In Figure 18 it is seen that the trim points of the experiment and the calculation are vastly different. In the experiment the trim point is at $\phi \approx -18°$, which corresponds to one of the trim points observed in a static experimental test-case, depicted in Figure 8. The calculated trim point, however, is located at $\phi \approx 12°$. The gradient of ϕ versus time is also much higher for the calculated results, indicating that the calculation predicts a higher rotational velocity than is encountered in the experiment. The roll-moment coefficient over the roll angle, shown in Figure 19, exhibits a similar tendency towards higher than expected values, as previously observed in the forced-to-roll simulations. One reason for the differences between the calculated and experimental behaviour may be the lack of mechanical friction being modelled into the simulation, which results in a higher acceleration of the model after release; also, the effects of the experimental environment are not included in the simulation. Thus, together with the higher damped characteristic of the numerical system as previously mentioned, the numerical calculation predicts a totally different manoeuvre trajectory than the experiment indicates.

In **Figures 20** to **27**, the results of a free-to-roll simulation initiated by a prescribed flap deflection are shown. The delta wing is released from rest at a roll angle of $\phi = 0°$, and a constant pitch angle of 9.3°. The flaps are asymmetrically deflected using the prescribed polynomial shown in Figure 20, which induces a positive roll-moment on the aircraft and forces it to rotate around its longitudinal axis (a clockwise rotation when looking in the direction of the nose of the aircraft). In Figure 21 the roll moment is shown over the roll angle. The states of surface pressure distribution shown in Figures 22 to 27 are specifically marked in Figure 21. It is seen that the wing is accelerating up to a roll angle of $\phi=16°$. Figure 22 shows the surface pressure distribution at the initial state, where the roll moment is zero and the flaps are not deflected. Figure 23 shows the distribution at the first maximum of roll moment, where $\phi=2.2°$, and the flaps are half-way deflected at $\eta=2.5°$. At $\phi=16°$ the roll moment changes sign from positive to negative. The corresponding surface pressure distribution is depicted in Figure 24. At this point the flaps are fully deflected at $\eta=5°$. From here on the system is damped, and the corresponding surface pressure distributions are shown in Figures 24 to 26. As can be seen in these figures, the lower pressure distribution on the luff-side of the wing than on the lee-side causes a negative roll moment and decelerates the wing. At $\phi=50°$ the sign of the roll moment changes again, for which the corresponding pressure distribution is shown in Figure 26. The wing accelerates once again, but at a lower rate than previously, as can be seen by looking at the gradient of the roll moment in Figure 21. The corresponding surface pressure distribution, shown in Figure 27, also indicates a reduced rate of rotation, as the pressure difference between the luff- and lee-side is very slight. It is expected, according to experimental data, that the wing will enter a periodic rotational motion. The calculation would have to be continued to verify that the wing behaves as expected from the experiment.

4. Conclusions

In this paper a simulation tool designed for the simulation of manoeuvring aircraft with moveable control devices has been presented. The simulation tool combines time-accurate aerodynamics and flight mechanics calculations to achieve this objective. Verification of the functionality of the simulation tool has been shown by simulating a delta wing aircraft, with moveable trailing-edge flaps, during a roll manoeuvre.

The validation strategy for the simulation tool consisted of comparisons to experimental data for static, guided motion, and free-to-roll motion simulations. The comparison between the calculations and the experimental data revealed areas for improvement within the simulation tool. One of these required improvements is in the area of turbulence modelling for vortex-dominated flows. Investigations of alternative turbulence models that are currently available in the Tau-Code, but were not used for the cases presented in this paper, need to be done. Also, further investigations into grid adaptation for both steady and unsteady flow conditions need to be done in order to better predict flow phenomena in a vortex-dominated flowfield.

Another area that is currently being improved is the parallelization of the chimera technique inside the Tau-Code, which will result in a more efficient code and a reduction of the simulation time. Furthermore, unsteady adaptation for de-/refining the grid where needed is being implemented, which is expected to reduce the discrepancies owing to the non-dynamic grid-sources not fully capturing the vortex structures affecting the model.

The main objective of this paper is to focus on the necessity for developing an interactive, multidisciplinary engineering tool for predicting the unsteady critical states of complex manoeuvring aircraft. Such a simulation environment has to bring together aerodynamics, aeroelasticity and flight mechanics in a time accurate simulation tool. In order to deliver such a tool in the near future, the DLR Project SikMa-"Simulation of complex Manoeuvres" has been initiated to combine these three disciplines into one simulation environment.

5. References

[1] *Er-Ei, J.; Weihs, D.:* Nonlinear Aerodynamics of a Delta Wing in Combined Pitch and Roll. Journal of aircraft, 1989, vol. 26, no. 3, pp. 254

[2] *Katz, J.; Levin, D.:* Static Measurements of Slender Delta Wing Rolling Moment Hysteresis. Journal of aircraft, 1991, vol. 28, no. 4, pp. 282

[3] *Gordnier, R. E.:* Computation of Delta-Wing Roll Maneuvers.
Journal of aircraft, 1995, vol. 32, no. 3, pp. 486

[4] *Gordnier, R.E.; Visbal, M.R.:* Numerical simulation of delta-wing roll
Aerospace science and technology, 1998, vol. 2, no. 6, pp. 347

[5] *Ericsson, L.E.:* Analysis of the Effect of Sideslip on Delta Wing Roll-Trim Characteristics
Journal of aircraft, 1997, vol. 34, no. 5, pp. 585

[6] *Ericsson, L.E.:* Effect of Angle of Attack on Roll Characteristics of 65-Degree Delta Wing
Journal of aircraft, 1997, vol. 34, no. 4, pp. 573

[8] *Hanff, E.S.; Ericsson, L.E.:* Multiple roll attractors of a delta wing at high incidence
AGARD FDP Symposium on vortex Flow Aerodynamics, AGARD CP 494, Oct. 1990, pp 31-1/10

[9] *Hanff, E.S.; Jenkins, S.B.:* Large-amplitude high-rate roll experiments on a delta an double delta wing
AIAA 28th Aerospace Sciences Meeting, Reno, Jan 1990, AIAA-90-0224

[10] *Hanff, E.S., Huang, X.Z.:* Roll-induced cross-loads on a delta wing at high incidence
AIAA 9th Applied Aerodynamics Conference, Baltimore, MD, September, 1991, AIAA 91-3223

[11] *Hsia, A.H.; Myatt, J.H.; Jenkins, J.E.:* Nonlinear and unsteady aerodynamics responses of a rolling 65-degree delta wing
AIAA Applied Aerodynamics Conference, Monterey, CA, August, 1993, AIAA 93-3682

[12] *Ericsson, L.E.:* Flow Physics of critical states for rolling delta wings
Journal of Aircraft, Vol. 32, No. 3, May-June 1995

[13] *Ericsson, L.E.; Hanff, E.S.:* Unique high-angle roll dynamics of a sharp-edged 65-deg delta wing
Journal of Aircraft, Vol. 31, No. 3, May-June 1994

[14] *Chaderjian, N.M.:* Navier-Stokes Prediction of Large-Amplitude Delta-Wing Roll Oscillations.
Journal of aircraft, 1994, vol. 31, no. 6, pp. 1333

[15] *Chaderjian, N.M; Schiff, L.B.:* Numerical simulation of forced and free-to-roll delta wing motions
Journal of Aircraft, Vol. 33, No. 1, January-February 1996

[16] *Stephens, E.J.:* Analyses of rolled delta wing flows using effective sweep and attack angles
Journal of Aircraft, Vol. 32, No. 5, September-October 1995

[17] *Jenkins, J.E.:* Nonlinear aerodynamic characteristics of a 65 degree delta wing in rolling motion: Implication to testing and flight mechanics analysis (invited)
AIAA 35th Aerospace Sciences Meeting & Exhibit, January 1997, Reno

[18] *Jenkins, J.E.; Myatt, J.H.; Hanff, E.S.:* Body axis rolling motion critical states of a 65-degree delta wing
Journal of Aircraft, Vol. 33, No. 2, March-April 1996

[19] *Jobe, C.E.; Hsia, A.H.; Jenkins, J.E.; Addington, G.A.:* Critical states and flow structure on a 65 deg delta wing
Journal of Aircraft, Vol. 33, No. 2, March-April 1996

[20] *Grismer, D.S.; Jenkins, J.E.:* Critical-state transients for a rolling 65-degree delta wing
Journal of Aircraft, Vol. 34, No. 3, May-June 1997

[21] *Galle, M.:* Ein Verfahren zur numerischen Simulation kompressibler, reibungsbehafteter Strömungen auf hybriden Netzen
DLR-FB 99-04 1999

[22] *Galle, M.; Gerhold, T.; Evans, J.:* Technical Documentation of the DLR Tau-Code
DLR-IB 233-97/A43 1997

[23] *Gerhald, T.; Galle, M.; Friedrich, O.; Evans, J.:* Calculation of Complex Three-Dimensional Configurations employing the DLR Tau-Code
AIAA-97-0167 1997

[24] *Centaur Soft:* http://www.centaursoft.com

[25] *Benek, J.A.; Buning, P.G.; Steger, J.L.:* A 3-D Chimera Grid Embedding Technique
AIAA-85/1523 1985

[26] *Burggraf, U.; Kuntz, M.; Schöning, B.:*
Implementation of the chimera method in the unstructured DLR finite volume code Tau
Notes on Numerical Fluid Mechanics Volume 70 (eds W. Nitsche, H.-J. Heinemann, R. Hilbig) 1999

[27] *Nakahashi,K.; Togashi,F.; Sharov, D.:* An intergrid boundary definition method for overset unstructured Grid
AIAA. Vol 38, No.11, pp. 2077-2084, 2000

[28] *Ciarlet,Ph.:* The finite element method for elliptic problems
530 pp., North-Holland, Amsterdam.1978

[29] *Bonet, J., Peraire, J.:* An alternating digital tree (ADT) algorithm for 3D geometric searching and intersection problems
International Journal for Numerical Methods in Engineering, 31,1-17, 1991

[30] *SIMPAC:* Software distributed by INTEC GmbH
Münchener Straße 20 82234 Wessling, www.simpack.de

[31] *Seidler, G.:* Programmsteuerung für die multidisziplinäre Simulation des manövrierenden Flugzeugs
DGLR, AG STAB, Jahresbericht 1998

[32] *TENT:* http://www.sistec.dlr.de/tent

[33] *Schütte, A.; Einarsson, G.; Schöning, B.; Mönnich, W.:* Numerical Simulation of manoeuvring aircraft by coupling of CFD and computational flight mechanics
CEAS Conference for Multidisciplinary Aircraft Design and Optimisation, Cologne, June 2001

[34] *Psolla-Bress, H.; Haselmeyer, H.; Heddergott, A.; Höhler, G.; Holst, H.:* High-roll rate experiments on a delta wing in transonic flow
ICIASF Record, 2001, pp. 369-377

6. Figures
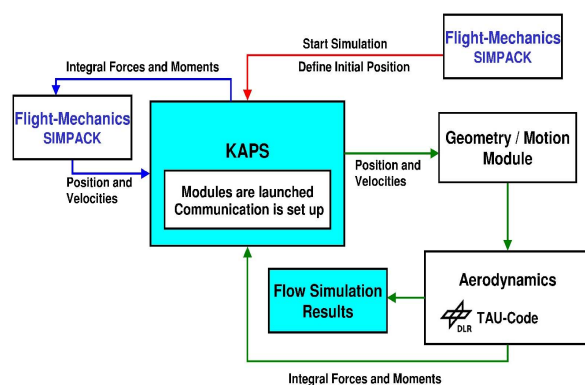
Figure 1:   Work-flow and data management
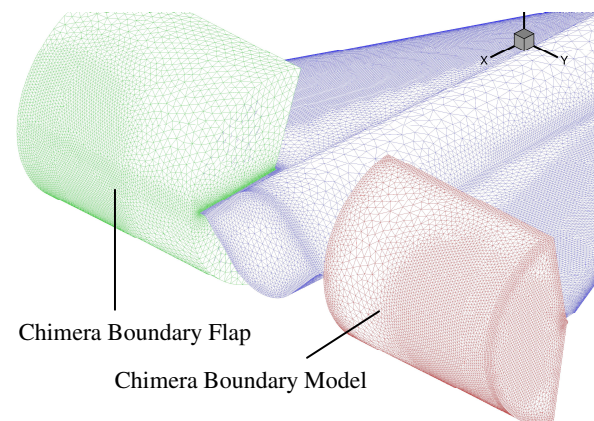
Figure 2:   AeroSUM-Model: Chimera mesh
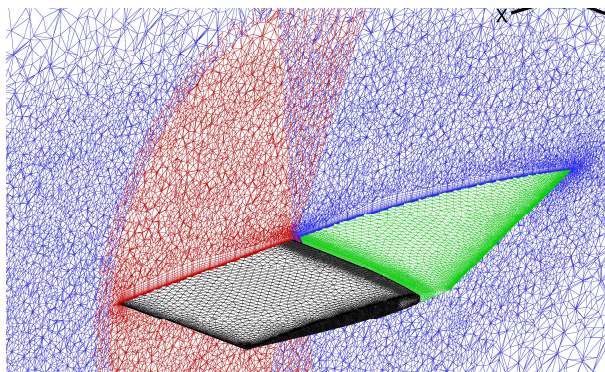
Figure 3:   AeroSUM-Model:
Slice through the overlapping mesh
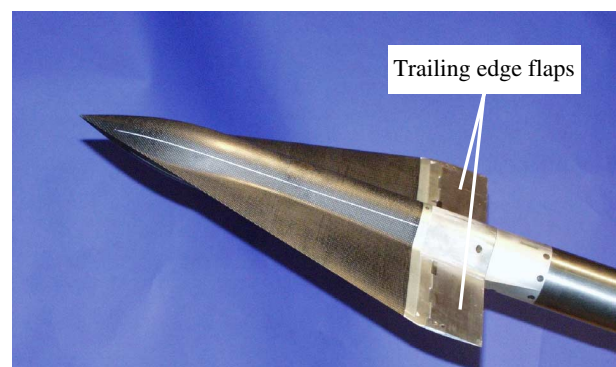
Figure 4:   AeroSUM-Model
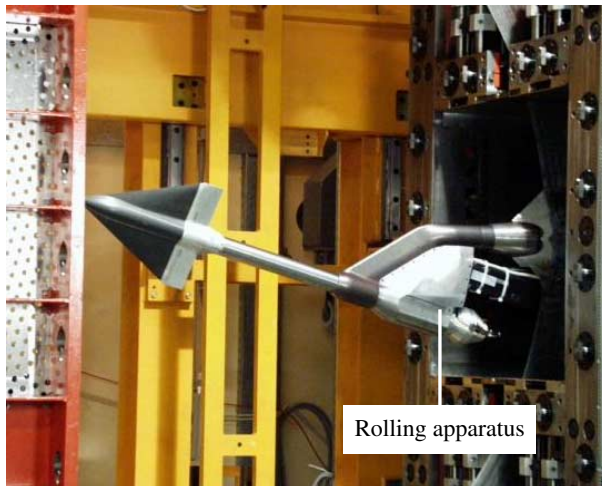
Figure 5:   Test facility surrounding (TWG)
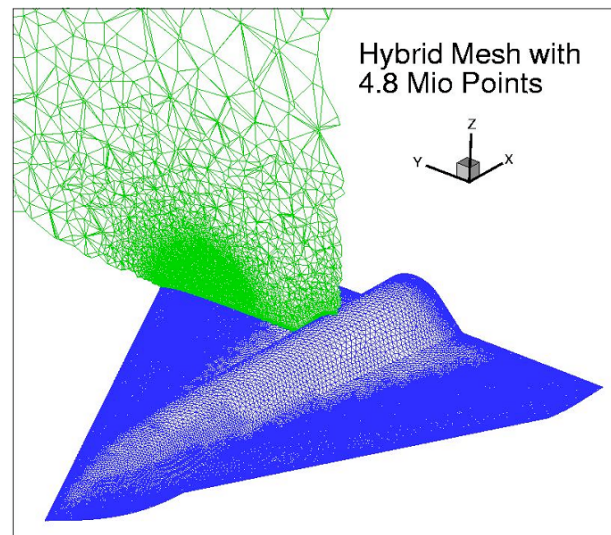
Figure 6:   Unstructured Tau-Code hybrid mesh
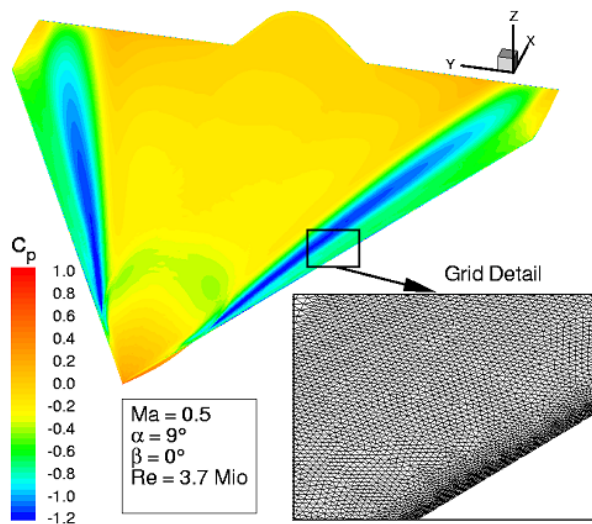
Figure 7:   Tau-Code NS-Solution,
            adapted leading edge
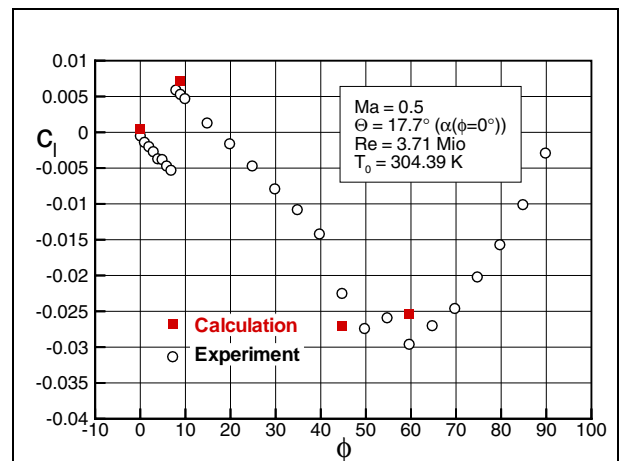
Figure 8:   Integral data of a steady calculation,
            roll moment over roll angle
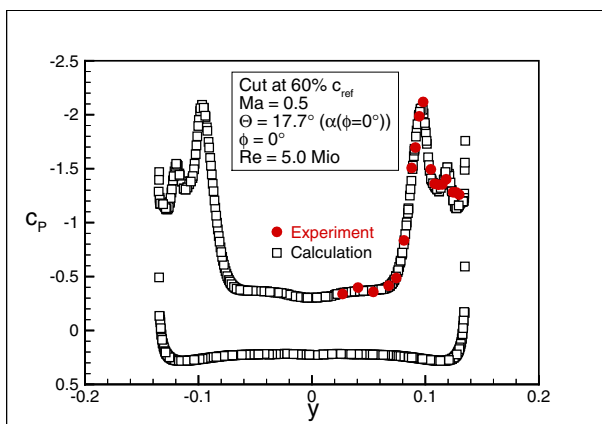
Figure 9:   Pressure distribution at 60% chord
            length (steady case)
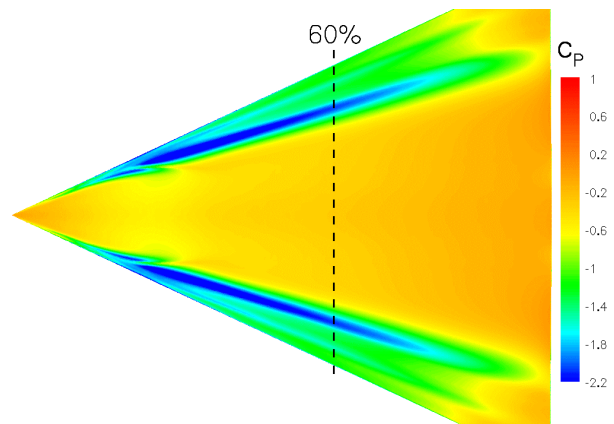
Figure 10:   Surface pressure distribution,
             steady Navier-Stokes calculation
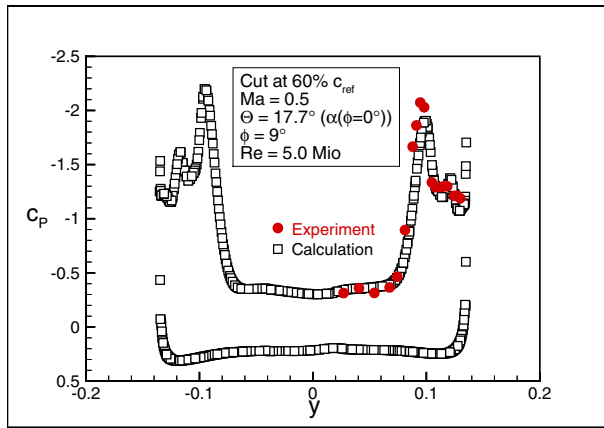
Figure 11: Pressure distribution at 60% chord length (steady case)
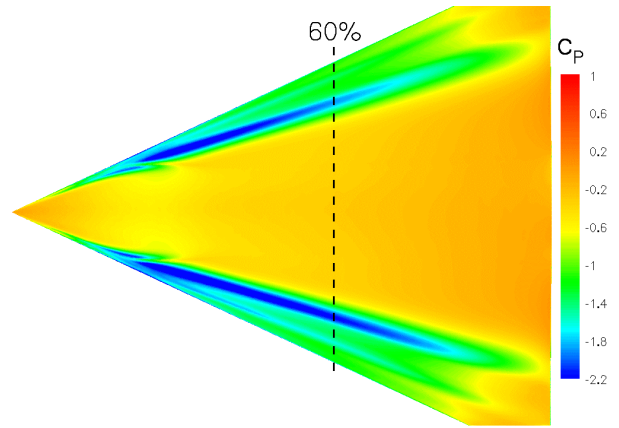
Figure 12: Surface pressure distribution, steady Navier-Stokes calculation
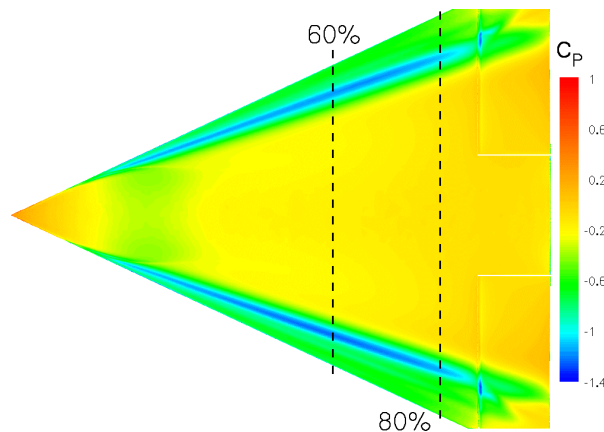
Figure 13: Surface pressure distribution, steady Navier-Stokes calculation (delta wing with flaps)
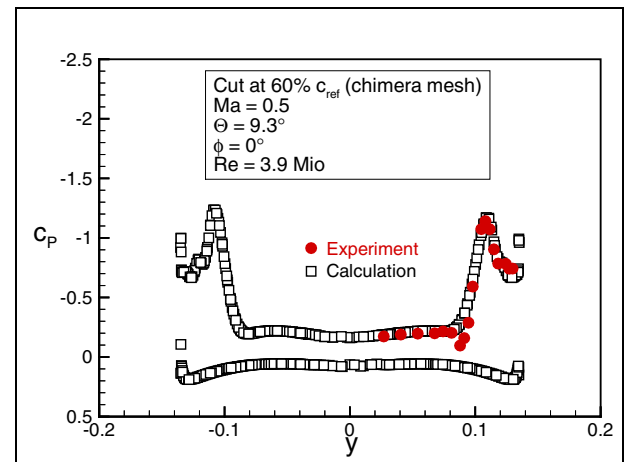
Figure 14: Pressure distribution at 60% chord length (steady case, delta wing with flaps)
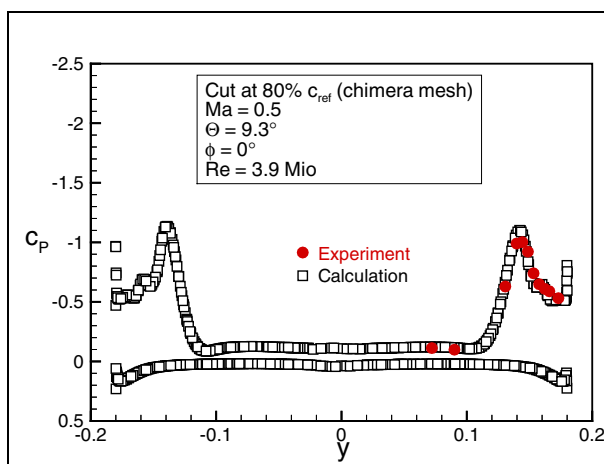
Figure 15: Pressure distribution at 80% chord length (steady case, delta wing with flaps)
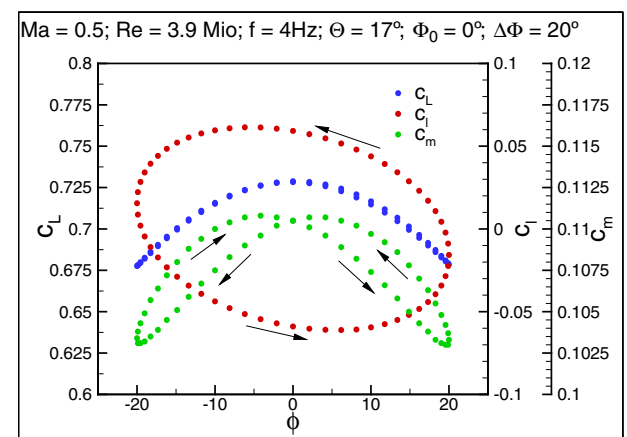
Figure 16: Integral lift, roll and pitching moment of oscillating delta wing
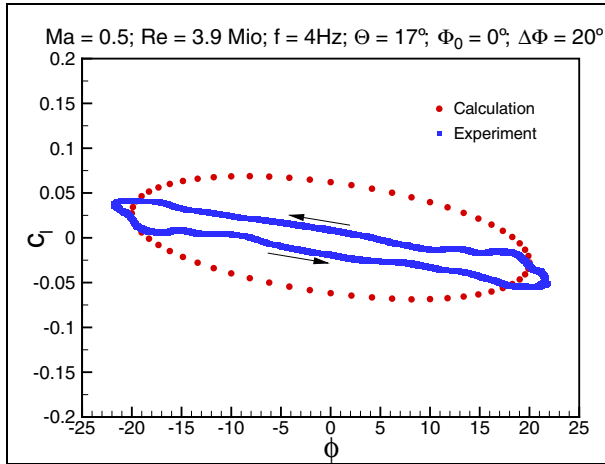
Figure 17: Comparison of experimental and calculated roll-moment for oscillating delta wing
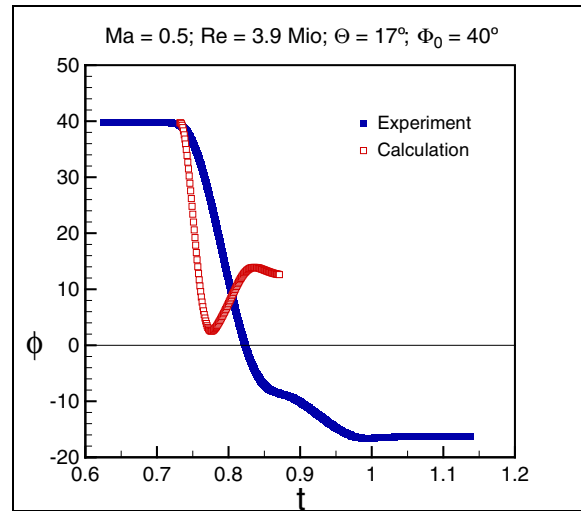
Figure 18: Roll angle ϕ over time t, free-to-roll coupled simulation
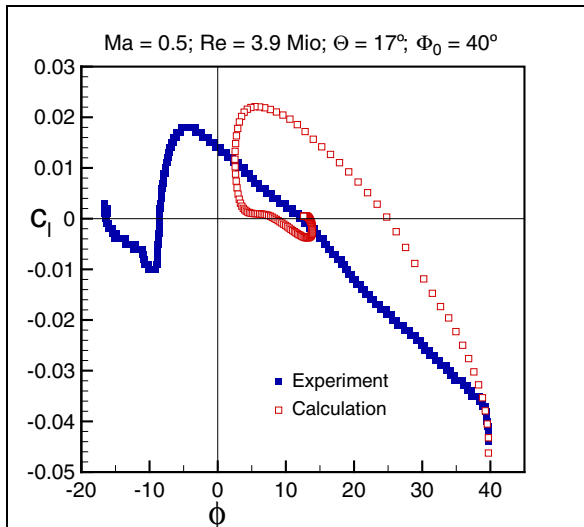
Figure 19: Roll moment c_l over roll angle ϕ, free-to-roll coupled simulation

Figure 20: Flap-deflection angle over time
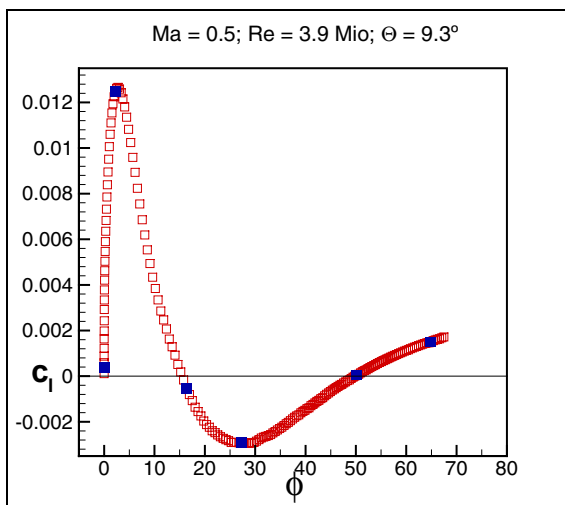
Figure 21: Roll-moment over roll angle, free-to-roll coupled simulation with flap
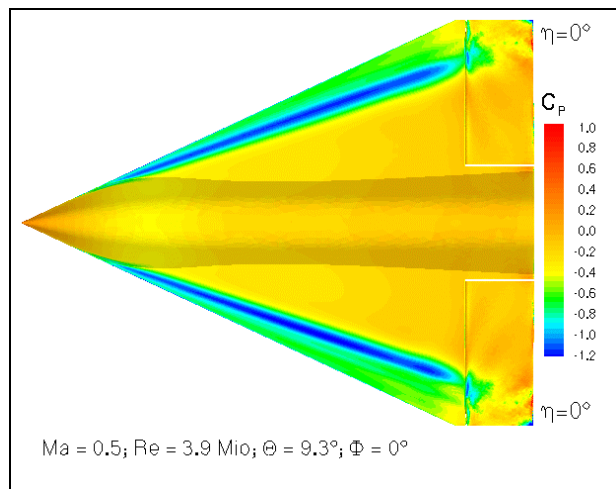
Figure 22: Surface pressure distribution, free-to-roll with flap motion
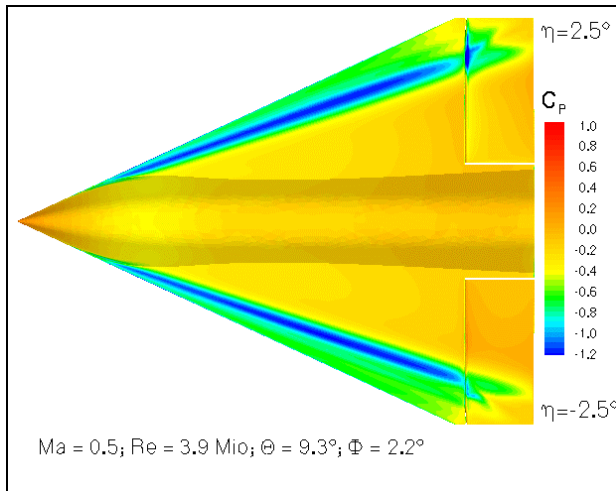
Figure 23: **Surface pressure distribution, free-to-roll with flap motion**
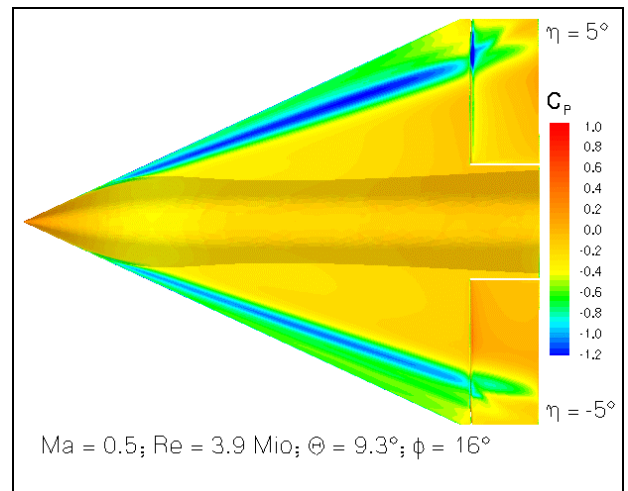
Figure 24: **Surface pressure distribution, free-to-roll with flap motion**
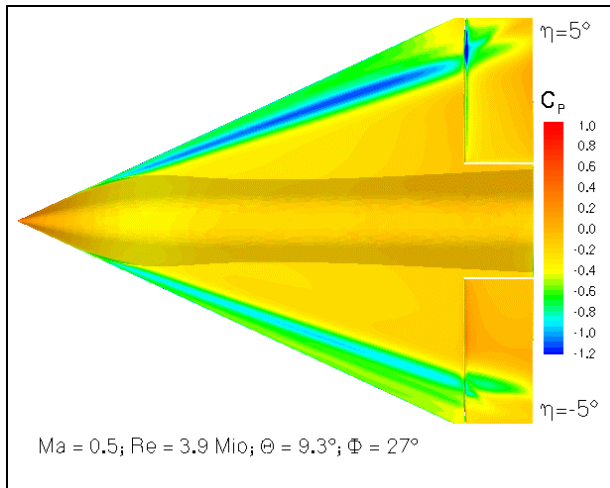
Figure 25: **Surface pressure distribution, free-to-roll with flap motion**
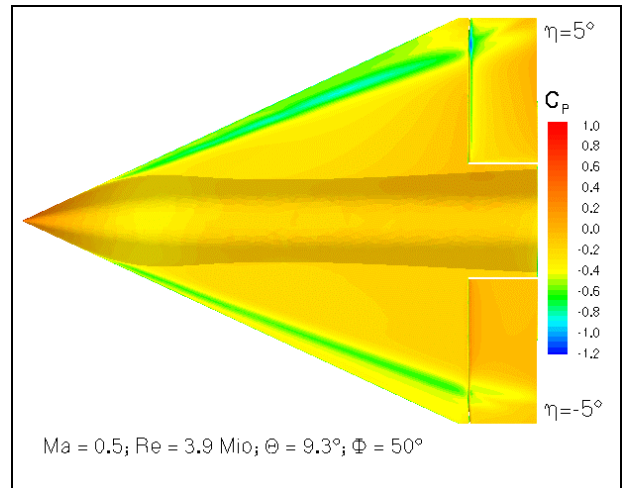
Figure 26: **Surface pressure distribution, free-to-roll with flap motion**
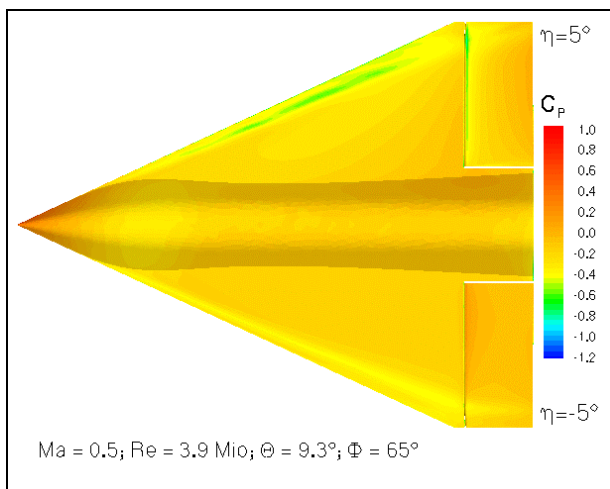
Figure 27: **Surface pressure distribution, free-to-roll with flap motion**

Design of Ice Protection Systems and Icing Certification Through the FENSAP-ICE System

Wagdi G. Habashi, Pascal Tran, Guido Baruzzi
Martin Aubé and Pascal Benquet
Newmerical Technologies International
680 Sherbrooke Street West, 7th Floor
Montreal, QC, Canada, H3A 2M7

Summary

The process of certifying a component or system for operation in an icing environment involves two basic steps, analysis and design, followed by icing tests, both of which can be streamlined by the use of 3-D CFD icing technology. The FENSAP-ICE modular system was conceived to support both design and certification of ice protection systems. The droplet impingement module is used to accurately predict high catch regions, which may require protection. These predictions can be obtained for complex 3-D geometries such as swept wings, air induction systems, radomes and complete aircraft or rotorcraft. The ice accretion module is used to compute ice shapes on unprotected surfaces. The heat load module is used to optimize power output required to protect critical surfaces.

Thus, the judicious use of 3-D CFD technology in the design methodology of ice protection systems yields high-performance configurations for operation in icing conditions and thus reduces or focuses the scope of development testing. In addition, CFD can be used in the certification process to pinpoint the most critical conditions in order to produce a smaller test matrix, but yet ensure adequate coverage of the flight and icing envelopes. The present paper shows validation results of FENSAP-ICE and illustrates examples of the application of 3-D CFD icing technology in support of icing certification.

Introduction

Aircraft icing regulations in the United States have evolved greatly over the years. The federal government started regulating pilots and aircraft in 1928 by the creation of the Civil Aviation Agency, which published the Civil Air Regulations or CARs. Prior to 1945, airplanes were certified to CAR 4. The sole reference to aircraft icing in CAR 4 was in Section 04.5814, which required that if deicer boots were installed, then positive means must be provided for the deflation of all wing boots. In 1945, the CARs were divided into two broad categories: CAR 3 for general aviation airplanes, or Part 23 in the modern Code of Federal Regulations (CFR), and CAR 4 for transport airplanes, or Part 25 in the modern CFR. The requirement of Section 04.5814 was incorporated without change as §3.541, which later was renumbered §3.712 in 1949. In 1953, Section 04.5814 became CAR §4.640 and was modified to include the requirement that for pneumatic deicers, two independent power sources shall be provided. Icing envelopes similar to the current Part 25 Appendix C were introduced in CAR 4 in 1955. There were two significant differences between the icing envelope introduced at that time and the current one: the minimum mean effective droplet diameter for intermittent maximum conditions was 20 microns as compared to the current 15 microns and the LWC/distance factor was 1.5 statute miles versus the current 0.26 nautical miles. The icing envelope was revised in 1957 to the current Appendix C. Ice protection was not addressed in CAR 3 until 1962. During that year, Amendment 3-7 added two articles §3.772 and §3.778, which required that the information provided to the crew specifies the types of operation and the meteorological conditions to which the airplane was limited by the equipment installed. In 1964, CAR 3 became Part 23 when §3.712 was recodified to become §23.1419. §3.772 and §3.778(h) became §23.1559

Paper presented at the RTO AVT Symposium on "Reduction of Military Vehicle
Acquisition Time and Cost through Advanced Modelling and Virtual Simulation",
held in Paris, France, 22-25 April 2002, and published in RTO-MP-089.

and §23.1583(h), respectively. In 1965, CAR 4 was recodified and §4.640 became §25.1419. Since that time the icing regulations have been modified through successive amendments to address propeller, pneumatic deicers, engine installation and several other issues affecting performance of the airplane in icing conditions.[1,2,3]

Currently, demonstration of aircraft compliance to the icing certification requirements is a complex process, which may involve design, analysis and test of several components or systems such as propellers, engines, air induction system, airframe, ice detectors, probes and ice protection systems. The choice of the means of compliance is made through the establishment of a compliance plan, which can include testing, analysis and similarity as means of demonstrating compliance of all systems.

It is believed that design, analysis and testing of an aircraft or rotorcraft for flight in icing conditions can be streamlined by the use of 3-D CFD icing technology. The FENSAP-ICE system originated from an idea enunciated in Ref.[4] took form in successive modules (flow, impingement, accretion, heat loads, performance degradation) described in Refs.[5-9] The FENSAP-ICE system was conceived to support both design and certification of ice protection systems. The droplet impingement module is used to accurately predict high catch regions, which may require protection. These predictions can be obtained for complex 3-D geometries such as swept wings, air induction systems, radomes and complete aircraft or rotorcraft. This type of analysis is sufficient to determine adequate coverage for pneumatic boots or optimal geometry for inertial separation systems. However, for hot air deicing or anti-icing systems, the external wet air calculation is coupled interactively with the internal flow problem and conduction through the solid interface, thereby necessitating a conjugate heat transfer approach. This procedure allows the calculation of minimum anti-icing heat loads required to prevent hazardous ice accretion and water runback. Thus, the judicious use of 3-D CFD technology in the design methodology of ice protection systems yields high-performance configurations for operation in icing conditions and therefore reduces or focuses the scope of development testing. In addition, CFD can be used in the certification process to pinpoint the most critical conditions in order to produce a smaller test matrix, but yet ensure adequate coverage of the flight and icing envelopes. As not all certification conditions can be tunnel-tested, flight-tested, nor encountered in natural icing testing, only analytical methods can make it possible to safely explore, even if only qualitatively, the entire icing envelope.

Advanced notions of using CFD for coupled aerodynamics and icing, using CFD to assess the stability and control of iced aircraft or building a CFD-based in-flight icing simulator, currently absent from the icing community, are within our reach. These state-of-the-art applications of icing CFD technology will ensure vastly improved pilot training and increase our understanding of aircraft flight characteristics in icing conditions, thereby resulting in an increase in flight safety in adverse environmental conditions.

Thus, we advocate that a 3-D Navier-Stokes system is the concurrent engineering tool needed between aerodynamics and icing groups to exchange pre-design information that enhances safety without compromising performance. This is made possible because the icing analytical tools are slowly catching up with the level of sophistication of aerodynamic analyses used to design the aircraft, e.g. 3-D CFD, CAD-based, advanced visualization, multi-disciplinary couplings, inverse design and optimization. Icing can be considered much earlier in the design stages because the incremental cost of the impingement calculation and ice growth prediction is very small compared to the investment required to generate a CAD-based mesh and to solve for the flow at different conditions. Even though 3-D CFD computations may seem intimidating in terms of complexity and CPU time, their cost pales in comparison to a test flight or, worse, an incident or an accident. In addition, any well-written 3-D system like FENSAP-ICE, can be degraded to a 2-D mode, to steady flow, to inviscid flow; simplifications often used in early design stages.

Description of FENSAP-ICE

As shown in Figure 32, FENSAP-ICE is a suite of modules designed for the performance prediction of a system or component in an icing environment. The modularity of FENSAP-ICE is reflected by the fact that each calculation module could be replaced by a commercial package or proprietary code with equivalent functionality.

- FENSAP[5], the Euler/Navier-Stokes solver, can be interchanged with an existing flow solver, which would be coupled to FENSAP-ICE through software interfaces. FENSAP is used for the initial aerodynamic calculation, as well as for the prediction of performance degradation due to the presence of ice[6]. The k-epsilon and k-omega two-equation models are available both as low-Reynolds and high-Reynolds versions. In addition, the Spalart-Allmaras one-equation model is also implemented, with surface roughness and transition.

- DROP3D[7] is an Eulerian particle-tracking module used to compute the catch efficiency distribution on 3-D complex bodies. DROP3D can be used to simulate supercooled water droplets or snow particles. Both FENSAP and DROP3D use a weak-Galerkin finite element method.

- ICE3D[8] is a 3-D ice growth calculation module, or 2.5-D following the surface, and is based on the finite volume method. Surfaces altered by ice accretion are hugged automatically by an Arbitrary Lagrangian-Eulerian (ALE) moving grid method inside the flow solver.

- CHT3D[10] is a conjugate heat transfer interface to couple the convection heat transfer calculations with the conduction through the solid medium. It is crucial for hot air ice protection systems design and analysis.

- Finally, OptiMesh[11] is an anisotropic automatic mesh adaptation module. Starting from a rapidly generated grid, OptiMesh will move grid points, refine edges, coarsen edges and swap edges, to yield a nearly-optimal mesh for the geometry and flow conditions at hand and greatly increase accuracy, besides drastically reducing mesh generation efforts.

All the modules are interlinked seamlessly so as to render possible complex multi-physics calculations such as hot air ice protection with wet air, droplet impingement and runback as illustrated in Ref.[10] Figure 32 illustrates the interaction between all modules.

The last component of the FENSAP-ICE suite is the graphical user interface (GUI), which cements all modules seamlessly. The FENSAP-ICE GUI is quite advanced and comprises file management, window-based inputs, convergence and global values dynamic monitoring, job launch on networks, multi-domain and multi-solver calculations and results archiving. The ease-of-use and complete integration of the icing analysis process reduces engineering time, and therefore costs, ensures traceability and repeatability, and eliminates errors of data transfer between disjoint codes. Figure 33 shows some screen shots of the FENSAP-ICE GUI.

Validation

FENSAP-ICE's flow, impingement, accretion, heat loads and degradation models have been extensively validated against experimental data.[5-8,12,13] FENSAP-ICE's impingement module DROP3D is further validated in the present paper against experimental impingement data gathered by NASA on a 3-D non-axisymmetric Boeing 737 nacelle inlet.[14]

An Euler analysis flow solution was obtained on a tetrahedral mesh. Two cases were analyzed at different incidences of the nacelle, at a true airspeed of 173.33 mph, inlet mass flow of 22.96 lbm/s, droplet Mean Volumetric Diameter of 20.36 μm, and nacelle incidences of 0 (run id 092385-1,2,3-737-0 in Ref.[14]) and

15 deg. (run id 092385-13,14,15-737-15 in Ref.[14]). The comparison of Mach number distributions along circumferential cuts for both incidences is presented in Figures 1 to 10. In order to compute the local catch efficiency β, DROP3D was run for a Langmuir-D droplet distribution. The comparisons of local catch efficiency distribution along the same circumferential cuts are presented in Figures 11 to 20.

The calculated Mach number distributions are in very good agreement with experimental data for all circumferential positions at both incidences.

The comparison between DROP3D and experimental data is very good for most circumferential positions for both incidences. The limits of impingement are correctly predicted and the local catch efficiency peak is also within experimental repeatability estimated in Ref.[14] to vary by 0.20 to 0.25.

The curve for 15 deg. incidence and 135 deg. circumferential position is, however, not in close agreement with the experimental data. Nevertheless, the predictions of LEWICE are even further from the experiments. Since the comparison at zero incidence for the same circumferential position is very good and all the other comparisons at 15 deg. incidence are also quite acceptable for both codes, it is only logical to conclude that the difference for that particular curve may be due to experimental inaccuracies.

Figure 21 illustrates the gain in accuracy that can be achieved by using anisotropic mesh adaptation. The original mesh had 108 000 nodes and 624 000 tetrahedra. After two adaptation cycles, the mesh size increased to 152 000 nodes and 824 000 anisotropic tetrahedral elements. The increased smoothness of the mesh and solution becomes readily apparent when comparing the unadapted mesh and solution shown in Figures 22 and 23 to the adapted mesh and Mach number distribution presented by Figures 24 and 25 respectively.

The ice growth module ICE3D has also been validated against 2-D test cases and 3-D geometries such as a sphere and a helicopter blade.[13]

Numerical Results

Some examples of industrial applications are presented. Because of the proprietary nature of the test cases, only a limited number are shown and the results are only discussed in a qualitative fashion.

Figures 26, 27 and 28 show the structured mesh, streamlines and catch efficiency distribution, respectively, calculated on a helicopter upper cowl with a side-facing inlet. The upper cowl, rotor mast, engine compartment and radial engine intake case down to the first rotor were modeled using a multi-block structured hexahedral mesh. The presence of the inlet screen was neglected. The results shown are for forward flight conditions. Since the engine is installed with the cold end towards the rear, the flow follows the upper cowl skin, turns 90 degrees into the engine plenum and finally turns another 90 degrees into the engine radial intake. The flow field was obtained with a proprietary FENSAP-like viscous flow solver. With the DROP3D Eulerian approach to droplet impingement, the trajectories forming the capture tube of the air induction system were obtained as a post-processing step. For complex geometries, this is vastly more efficient than the hit-and-miss Lagrangian approach to calculate capture tube areas and therefore the ingested water flow rates. This type of capture tube analysis can be used in support of certification to demonstrate that, for side-facing helicopter inlets, forward flight conditions in wet air are very mild in comparison with hover. This is due to the very strong inertial separation effect of the side-facing inlet.

Figures 29, 30 and 31 show the unstructured adapted mesh, Mach number distribution and catch efficiency distribution predicted on a helicopter upper cowl with a forward-facing inlet. The results are shown for a forward flight condition. Several droplet sizes and engine mass flows were simulated in order to understand the effect of engine power on water capture due to the scoop effect of the forward-facing inlet. The analysis was required because an engine growth had to be considered while the geometry of the

air induction system would remain unchanged. In order to determine the necessity of repeating the air induction system icing certification, the potential water ingestion increase had to be quantified. First, a map of mass flow increase as a function of altitude and ambient temperature was constructed for different flight phases such as hover, climb, cruise and descent. Using FENSAP-ICE to calculate droplet impingement, this map was translated to a water capture increase map. Superimposing the Appendix C icing envelope on this map highlighted critical conditions. Decision whether to repeat icing tests is based on such an analysis.

These examples demonstrate the efficiency of the Eulerian particle tracking approach for complex three-dimensional configurations. Because collection efficiency is obtained on all walls and water volume fraction is obtained everywhere in the field, the method yields the particle trajectories of interest as a post-processing step.

Conclusions

FENSAP-ICE, a complete in-flight icing CFD simulation package, was developed to tackle industrial problems involving complex three-dimensional bodies in a timely and cost-effective way. Its accuracy for droplet impingement prediction was demonstrated on a non-axisymmetric nacelle geometry. It can help reduce the amount of testing required by demonstrating the severity, or lack thereof, of certain certification conditions in an accurate, scientific, repeatable and traceable manner. The use of icing CFD in support of aircraft certification offers enormous advantages such as the elimination of the need for scaling or similitude studies, the exploration of the complete icing envelope in a risk-free fashion, the synergy between methods used to design the aircraft and ice protection systems, the elimination of experimental inaccuracies generally associated with icing tests (measurement and control of droplet size, relative humidity, ambient temperature, water flow rate), all of which lead to significant cost reduction.

Although certain phenomena or interaction cannot be simulated at this moment, it is believed that advanced CFD technology, used hand in hand with tunnel or flight tests, can considerably shorten the certification cycle time, reduce the associated costs, reduce post-certification issues and more importantly, increase flight safety in adverse atmospheric conditions.

Future Work

Additions are planned to further increase the range of problems that can be simulated using FENSAP-ICE: SLD models, ice shedding models, ice particle trajectory tracking, one-shot MVD calculations, droplet splashing and breakup, simulation of electro-thermal heater pads, simulation of sand, dust, hail and rain particles, stability and control of iced aircraft, etc.

To further enhance the ease-of-use and integration aspects of FENSAP-ICE, it is planned to very shortly integrate proprietary data post-processing and visualization to the package.

Acknowledgements

NTI would like to thank its industrial partners for permission to present the certification results included in this paper.

References

[1] Chamberlain, H.D., "How Icing Regulations Came to Be", http://www.faa.gov/avr/afs/news/NovemberDecember/IcingReg.htm, Federal Aviation Administration website.

[2]   Federal Aviation Administration, "Certification of Part 23 Airplanes for Flight in Icing Conditions", Advisory Circular AC 23.1419-2A, August 1998.

[3]   Federal Aviation Administration, "Certification of Transport Airplanes for Flight in Icing Conditions", Advisory Circular 25.1419-1, August 1999.

[4]   Habashi, W.G., "Putting Computers on Ice", *ICAO Journal*, Vol. 50, No. 7, October 1995, pp. 14-17.

[5]   Baruzzi, G.S., Habashi, W.G., Guèvremont, G. and Hafez, M.M., "A Second Order Finite Element Method for the Solution of the Transonic Euler and Navier-Stokes Equations", *International Journal of Numerical Methods in Fluids*, Vol. 20, pp. 671-693, 1995.

[6]   Dompierre, J., Cronin, D., Bourgault, Y., Baruzzi, G. and Habashi, W.G., "Numerical Simulation of Performance Degradation of Ice Contaminated Airfoils", AIAA Paper 97-2235, 15th AIAA Applied Aerodynamics Conference, Atlanta, June 1997.

[7]   Bourgault, Y., Habashi, W.G., Dompierre, J. and Baruzzi, G.S., "A Finite Element Method Study of Eulerian Droplets Impingement Models", *International Journal of Numerical Methods in Fluids*, Vol. 29, pp. 429-449, 1999.

[8]   Bourgault, Y., Beaugendre, H. and Habashi, W.G., "Development of a Shallow Water Icing Model in FENSAP-ICE," *AIAA Journal of Aircraft*, Vol. 37, pp. 640-646, 2000.

[9]   Croce, G. and Habashi, W.G. "Thermal Analysis of Wing Anti-Icing Devices", in "Computational Analysis of Convection Heat Transfer", G. Comini and B. Sundén (Eds.), Wessex Institute of Technology Press, 2000, Chapter 10, pp. 409 -432.

[10]   Croce, G., Beaugendre, H. and Habashi, W.G., "CHT3D: FENSAP-ICE Conjugate Heat Transfer Computations with Droplet Impingement and Runback Effects", AIAA Paper 2002-0386, 40th Aerospace Sciences Meeting & Exhibit, Reno, January 2002.

[11]   Habashi, W.G., Dompierre, J., Bourgault, Y., Fortin, M. and Vallet, M.-G., "Certifiable Computational Fluid Dynamics Through Mesh Optimization", Invited Paper in Special Issue on Credible Computational Fluid Dynamics Simulation, *AIAA Journal*, Vol. 36, 1998, No. 5, pp. 703-711.

[12]   Morency, F., Beaugendre, H., Baruzzi, G.S. and Habashi, W.G., "FENSAP-ICE: A Comprehensive 3D Simulation Tool for In-flight Icing", AIAA Paper 2001-2566, 15th AIAA Computational Fluid Dynamics Conference, Anaheim, CA, June 2001.

[13]   Beaugendre, H., Morency, F. and Habashi, W.G., "ICE3D, FENSAP-ICE's 3D In-Flight Ice Accretion Module", AIAA Paper 2002-7134, 40th Aerospace Sciences Meeting & Exhibit, Reno, January 2002.

[14]   Papadakis, M., Elangonan, R., Freund, G.A., Breer Jr., M., Zumwalt, G.W. and Whitmer, L., "An Experimental Method for Measuring Water Droplet Impingement Efficiency on Two- and Three-Dimensional Bodies", NASA CR-4257, DOT/FAA/CT-87/22, November 1989.
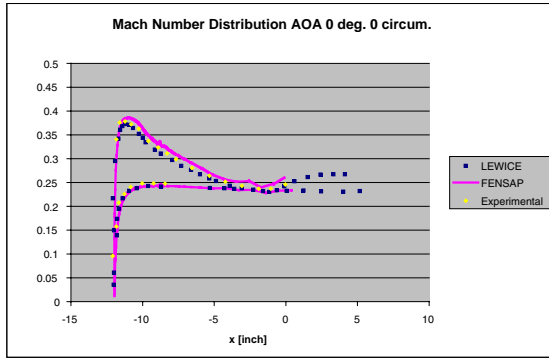
Figure 1: Mach number comparison for zero incidence and 0 deg. circumferential position

Figure 2: Mach number comparison for zero incidence and 45 deg. circumferential position

Figure 3: Mach number comparison for zero incidence and 90 deg. circumferential position

Figure 4: Mach number comparison for zero incidence and 135 deg. circumferential position
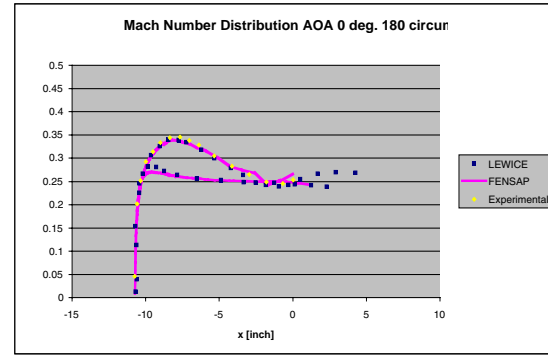
Figure 5: Mach number comparison for zero incidence and 180 deg. circumferential position
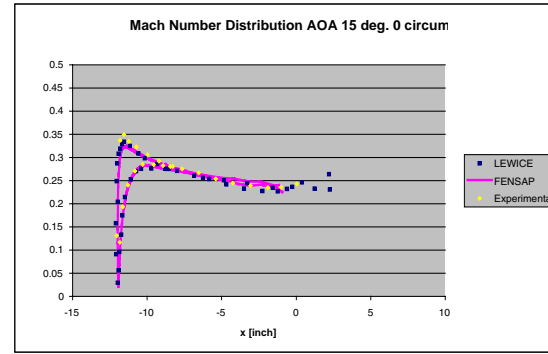
Figure 6: Mach number comparison for 15 deg. incidence and 0 deg. circumferential position
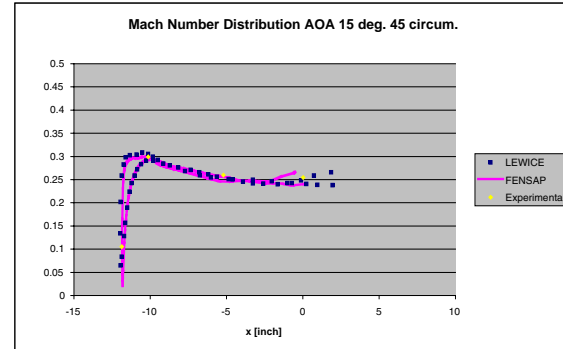
Figure 7: Mach number comparison for 15 deg. incidence and 45 deg. circumferential position
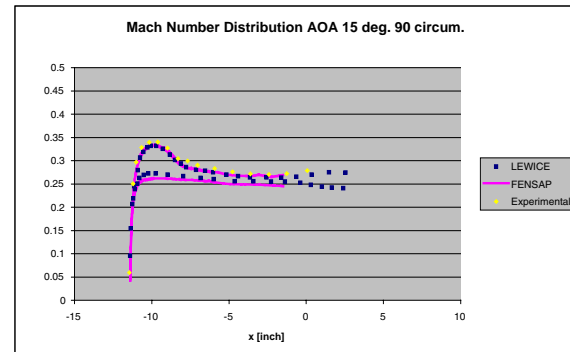
Figure 8: Mach number comparison for 15 deg. incidence and 90 deg. circumferential position
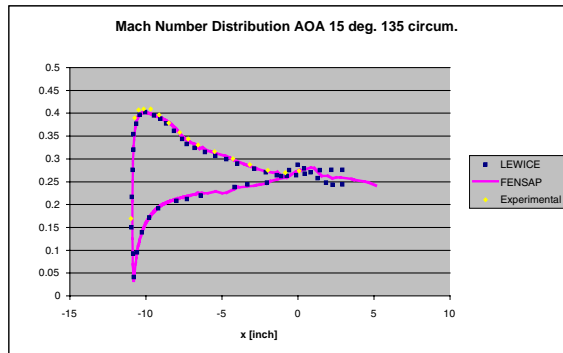
Figure 9: Mach number comparison for 15 deg. incidence and 135 deg. circumferential position

Figure 10: Mach number comparison for 15 deg. incidence and 180 deg. circumferential position

Figure 11: Local catch efficiency comparison for zero incidence and 0 deg. circumferential position
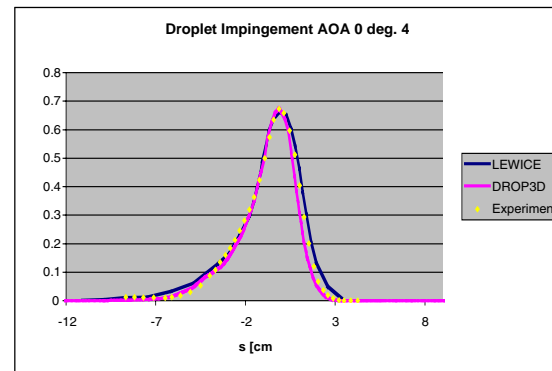
Figure 12: Local catch efficiency comparison for zero incidence and 45 deg. circumferential position
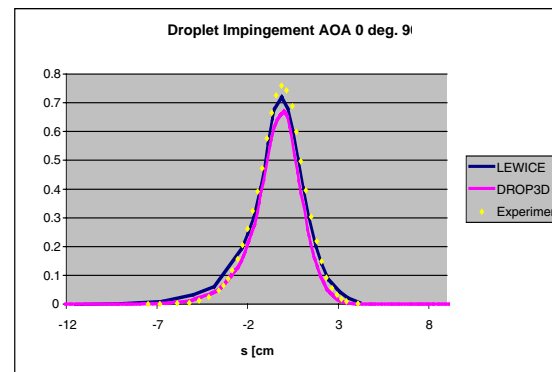
Figure 13: Local catch efficiency comparison for zero incidence and 90 deg. circumferential position
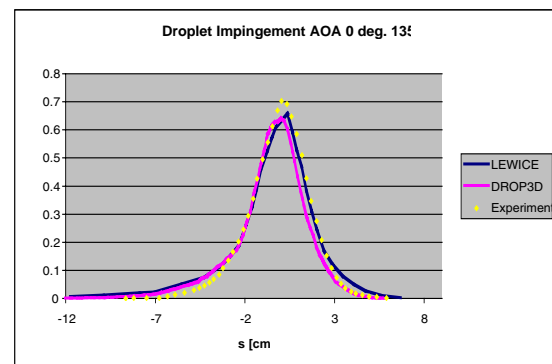
Figure 14: Local catch efficiency comparison for zero incidence and 135 deg. circumferential position
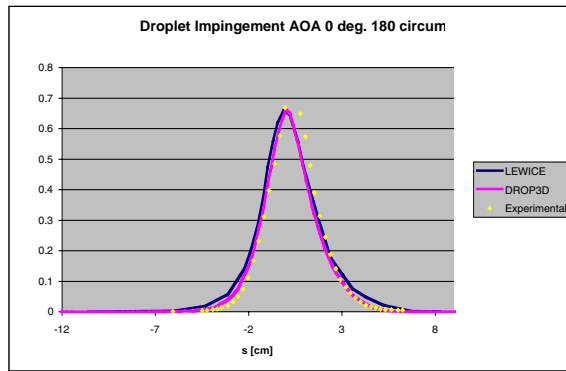
Figure 15: Local catch efficiency comparison for zero incidence and 180 deg. circumferential position
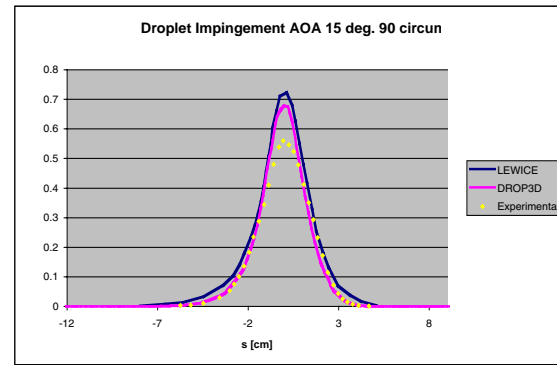
Figure 18: Local catch efficiency comparison for 15 deg. incidence and 90 deg. circumferential position
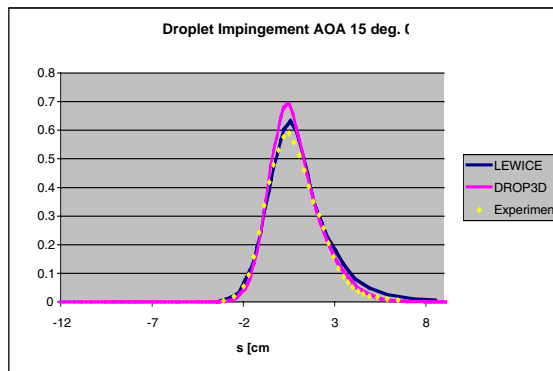
Figure 16: Local catch efficiency comparison for 15 deg. incidence and 0 deg. circumferential position
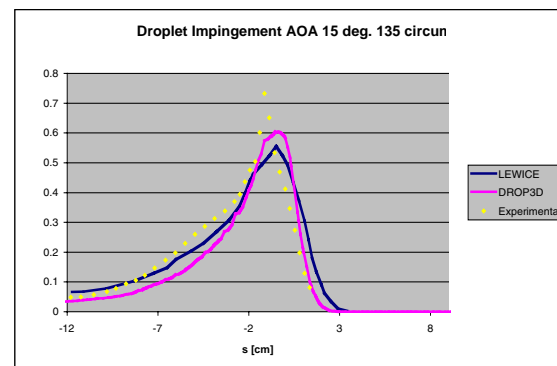
Figure 19: Local catch efficiency comparison for 15 deg. incidence and 135 deg. circumferential position
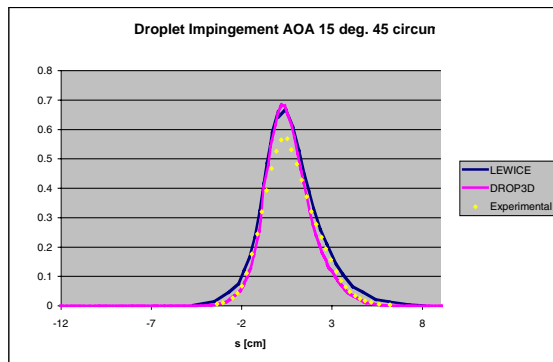
Figure 17: Local catch efficiency comparison for 15 deg. incidence and 45 deg. circumferential position
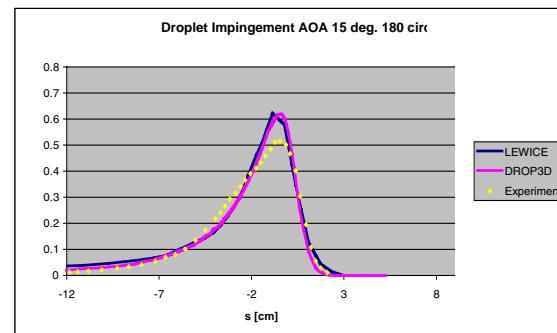
Figure 20: Local catch efficiency comparison for 15 deg. incidence and 180 deg. circumferential position
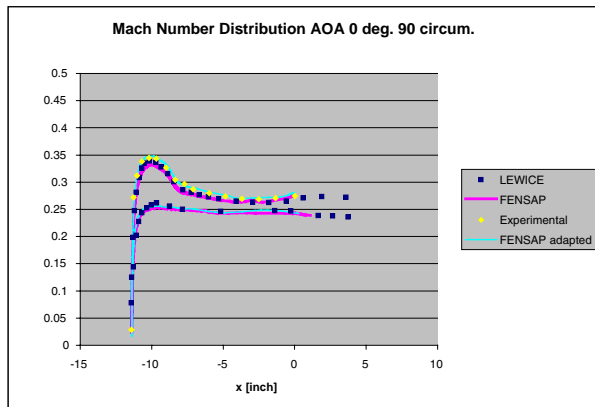
Figure 21: Mach number comparison for 15 deg. incidence and 90 deg. circumferential position, with mesh adaptation
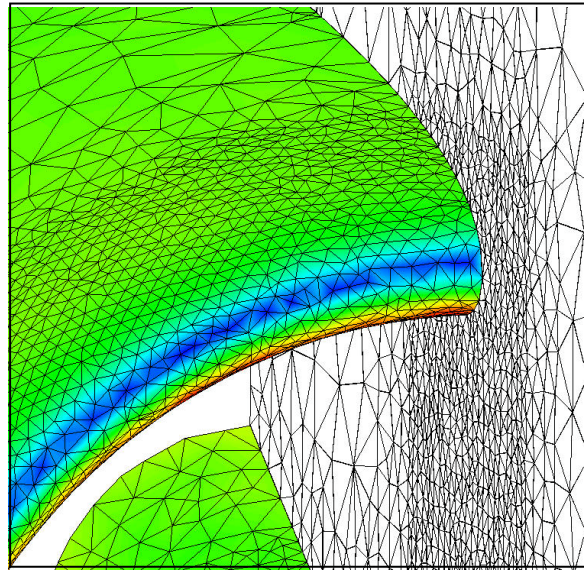
Figure 23: Unadapted mesh and Mach number distribution on nacelle and symmetry plane
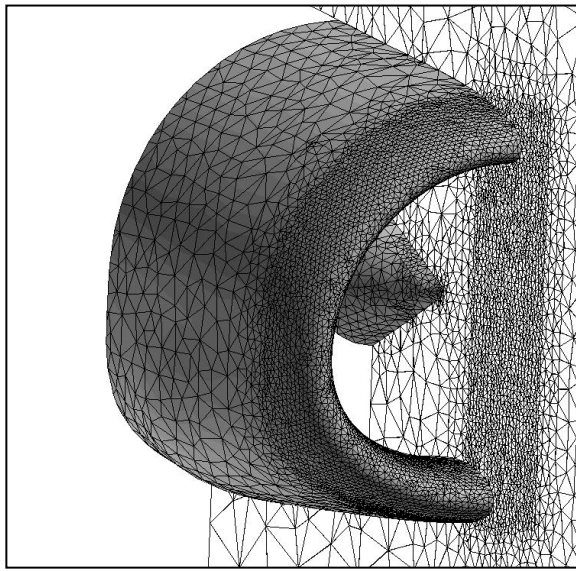
Figure 22: Tetrahedral unadapted mesh on nacelle and symmetry plane
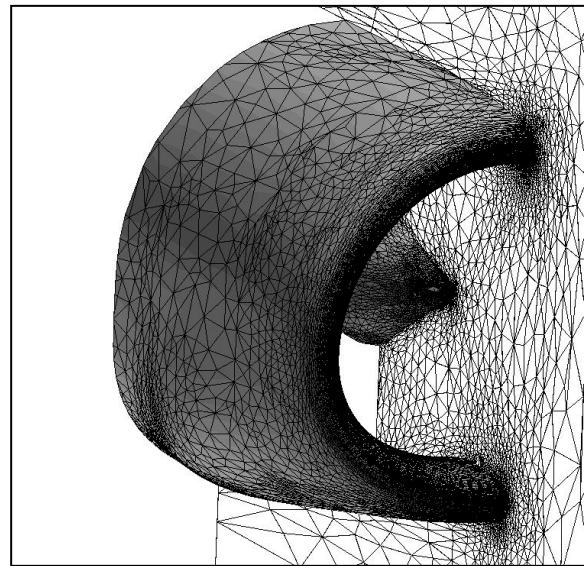
Figure 24: Tetrahedral adapted mesh on nacelle and symmetry plane
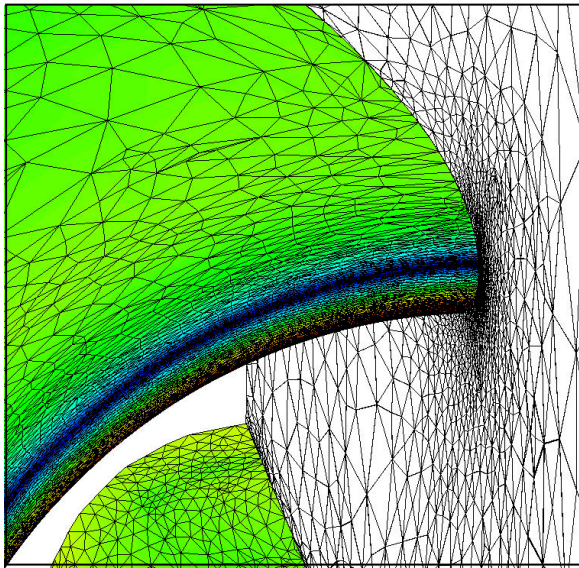
Figure 25: Adapted mesh and Mach number distribution on nacelle and symmetry plane
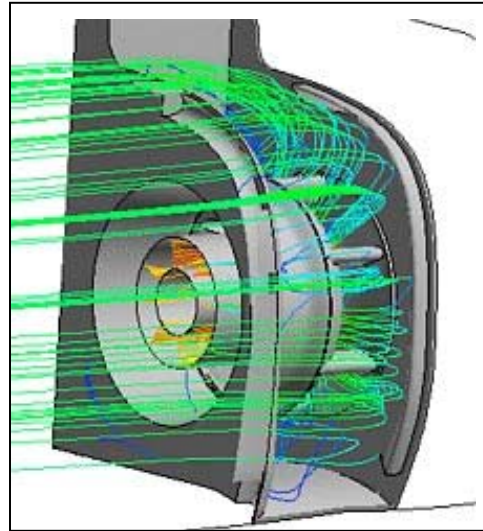
Figure 27: Streamlines on side-facing helicopter inlet
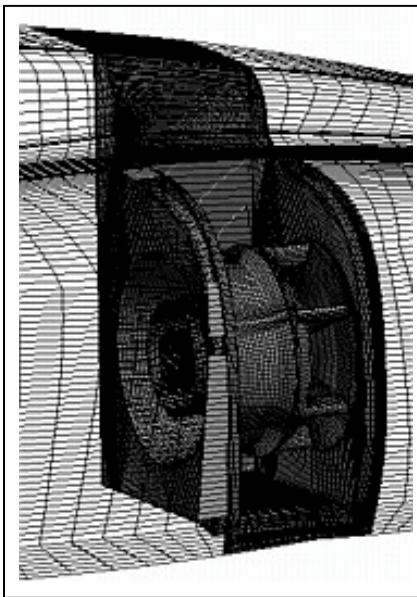
Figure 26: Hexahedral mesh on side-facing helicopter inlet
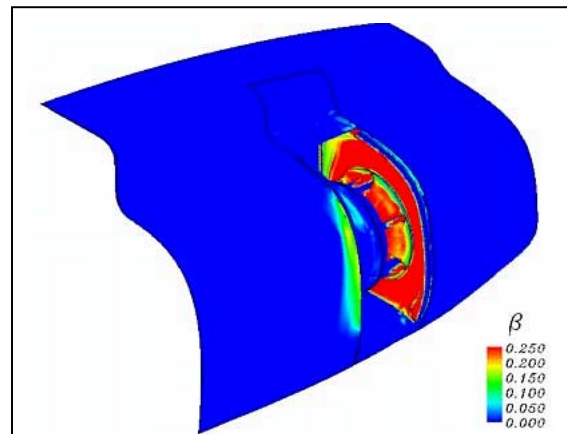
Figure 28: Catch efficiency distribution in helicopter engine compartment
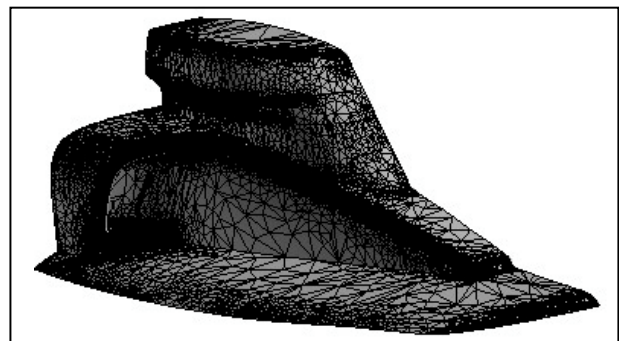
Figure 29: Tetrahedral adapted mesh on forward-facing helicopter inlet and upper cowl
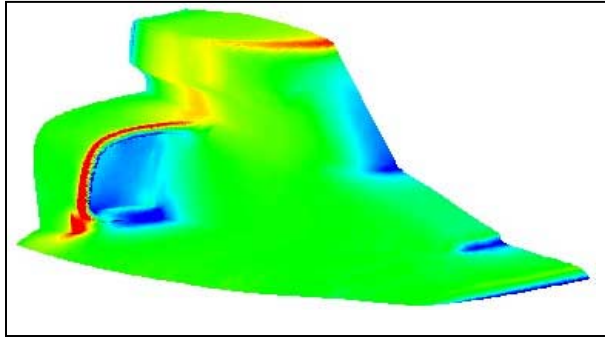
Figure 30: Mach number distribution on helicopter forward-facing inlet and upper cowl
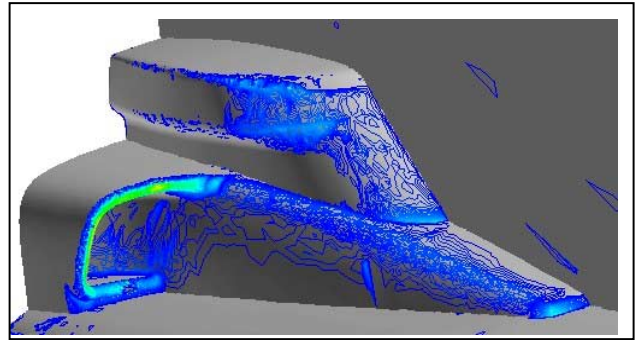
Figure 31: Catch efficiency distribution on helicopter forward-facing inlet and upper cowl

Figure 32: A 3D state-of-the-art Integrated System for Aerodynamics, In-Flight Icing Simulation and Certification
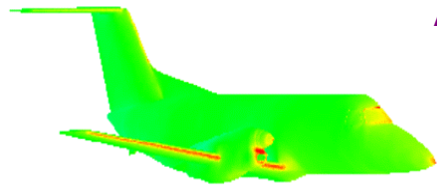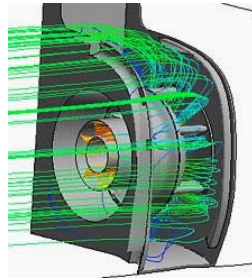
Turboprops   Helicopters   Turbojets   Intakes   Simulators
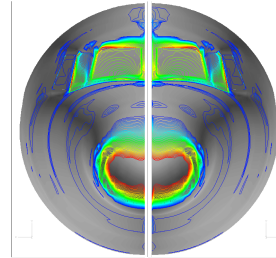
Initial Mesh

FENSAP: 3D Flow Solution

OptiMesh: Mesh Adaptation

FENSAP : Mesh Movement

DROP3D: Droplet Impingement

ICE3D: Ice Accretion

CHT3D: Conjugate Heat Transfer
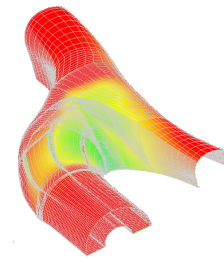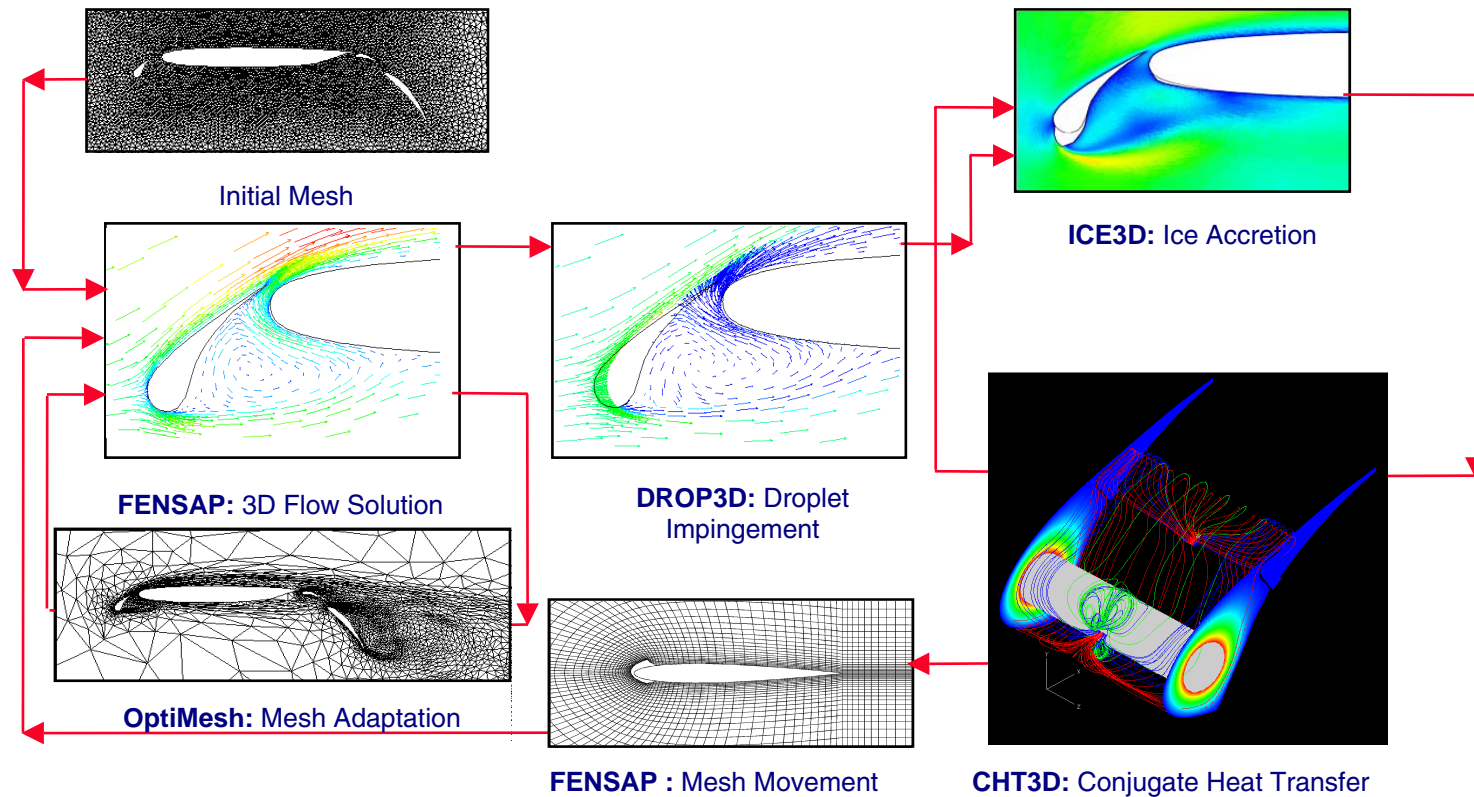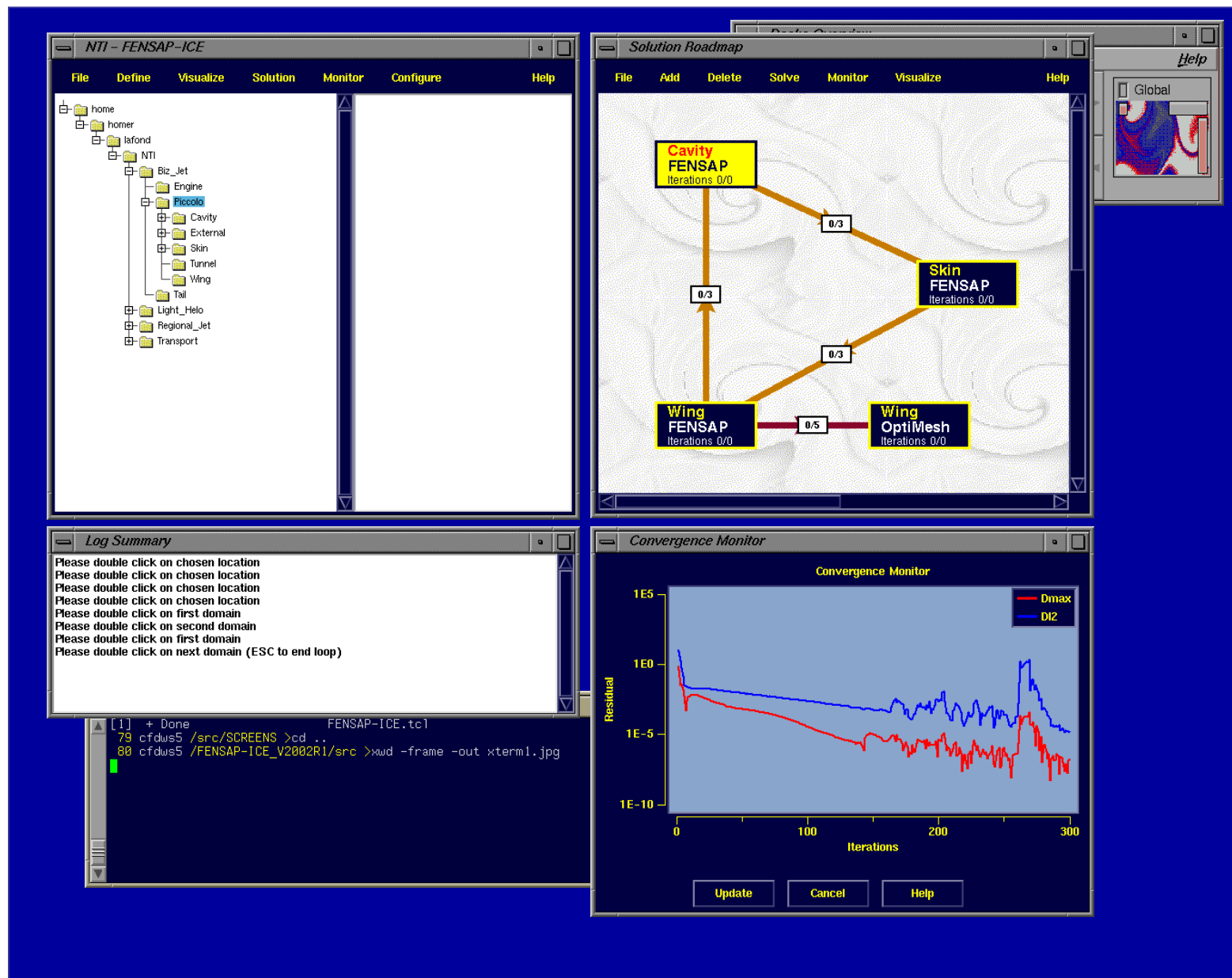
Challenges of Aircraft Design Integration

F. Kafyeke, M. Abdo, F. Pépin, P. Piperni, E. Laurendeau
Advanced Aerodynamics
Bombardier Aerospace
400 Côte Vertu Road
Dorval, Quebec, Canada, H4S 1Y9

Fassi.Kafyeke@notes.canadair.ca
Tel: (514) 855-7186

Abstract

The design of a modern airplane brings together many disciplines: structures, aerodynamics, controls, systems, propulsion with complex interdependencies and many variables. Recent aircraft programs, such as Bombardier's Continental Jet program (Figure 1) use participants located around the world and selected for their cost, quality and delivery capability. These participants share the risk on the program and must therefore be fully implicated in the design. A big challenge is to provide information on current design configuration simultaneously to all disciplines and all participants in the appropriate format. Another challenge of multidisciplinary optimization is to bring together technologies and methodologies of various disciplines in a way that is both practical and inclusive of the expertise that must accompany these individual technologies. This paper discusses progress made to address these challenges, streamline the aircraft design process and implement multidisciplinary optimization in an effective manner [1]. Initiatives include: implementation of the Bombardier Engineering System (BES) and of an MDO software environment (VADOR), linking of aerodynamic and structural design and analysis codes, validation of advanced wing design methods and calibration of viscous flow analysis and drag prediction methods.

Figure 1:Bombardier Continental Business Jet
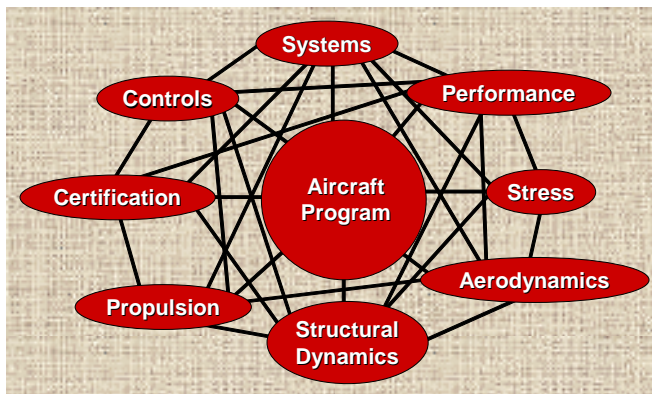
Figure 2: the complex interaction of various disciplines

Bombardier Engineering System (BES©)

The design of a modern airplane brings together many disciplines as illustrated in Figure 2: structures, aerodynamics, controls, systems, propulsion with complex interdependencies. The Bombardier Engineering System (BES©) was introduced to define clearly the phases, milestones and processes of an airplane design cycle and allow each process to be optimized. BES© describes how Bombardier defines, develops, certifies and validates commercial aerospace products. The system was implemented in response to various pressures on the aircraft design and development business. New and derivative aircraft have been launched almost every year in

the past dozen years. Many teams were involved in activities at multiple sites and for multiple programs and there was strong pressure from customers to reduce price, improve quality and deliver on time. On the basis of the company best practices, the roles and responsibilities of each engineering function were clearly defined. The first key elements of BES© are phases and milestones, illustrated in Figure 3. A phase is defined as a significant planned segment of a development project. Each project evolves through seven distinct phases (D1 to D7). A milestone is a planned event at a specific point in the project. It is not necessarily a single point in time. It is an opportunity to check progress and to evaluate plans. Management decision to proceed or not to proceed is determined at each milestone.
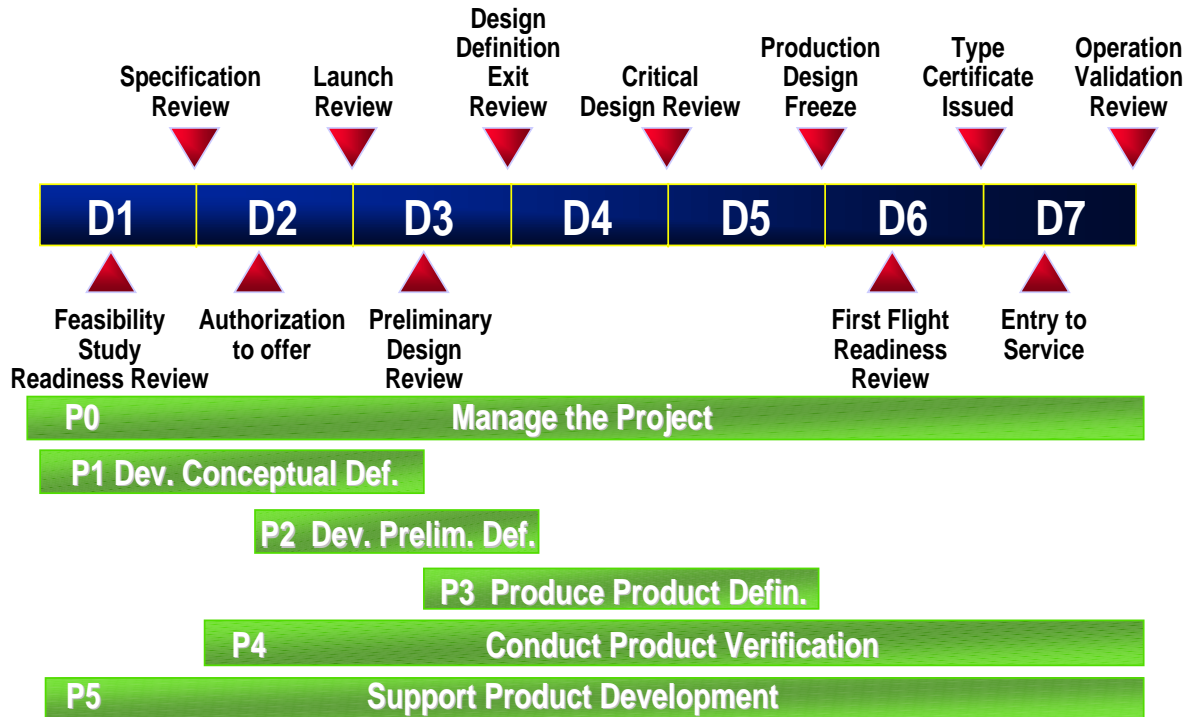
Figure 3: BES Phases, milestones and business processes

An important milestone is the decision to launch a new airplane, which occurs at the end of phase D2. At this point, the aerodynamic configuration must be frozen. This implies that most of the CFD and multidisciplinary design activity must take place in phases D1 and D2. The partners and suppliers of an aircraft program are brought together at two specific occasions. First, during the "Joint Conceptual Definition Phase" (JCDP, occurring in D1) where early configuration trade-offs take place. The second gathering occurs immediately after the aircraft formal launch, during the "Joint Definition Phase" (JDP, in D3).

The next important elements of BES are the product development processes. These are structured in a hierarchy, starting with five top business processes:

- Manage the Program and Project
- Develop the Conceptual Definition
- Develop the Preliminary Definition
- Produce the Product Definition
- Conduct Verification of the Product
- Support Product Development

Each business process is made of "Tier 2" Cross Functional Processes with deliverables associated to each process. A function's deliverable is a tangible data or a document required by an internal or external customer and used to monitor a project's progress. The next level of processes is the "Tier 3" level which describes

functional activities. A Tier 3 process map shows what activities are required to produce BES deliverables, what inputs are required to complete an activity, who supplies these inputs, who the customers for the deliverables are and the interactions with external entities such as vendors, partners or certification authorities. "Tier 4 Functional Tasks" are tasks required for preparing a specific deliverable. They are linked to a function's role and responsibility. Mapping Tier 4 functional tasks is a prerequisite to the wrapping of these tasks in a design automation software environment.

The BD-100 Continental Jet aircraft program is the first one to be developed entirely following BES procedures. The aircraft, shown on Figure 1, is designed to have a true north-American coast-to-coast capability with eight passengers. The overall design is geared towards shared ownership operations, requiring low cost, high utilisation, high dispatch reliability and good maintainability.

The aircraft technical specifications include:

- A maximum take-off weight of 37,500 lbs.;
- A range of 3,100 nautical miles NBAA/IFR with 8 passengers and baggage;
- A normal cruise speed of Mach 0.80 and a high cruise speed of Mach 0.82
- An initial cruise altitude of 41,000 ft and a maximum cruise altitude of 45,000 ft;
- A balanced field length below 5,000 ft;

The BD-100 program completed the Joint Conceptual Definition Phase before the formal program launch. This provided better definition of the aircraft early on. Partners and suppliers joined early. All functional groups participated in the design from the outset and all partners and suppliers used common design technology. Key milestone dates for the program so far are as follows:

- Market Debut   October 18 1998
- Joint Conceptual Definition   Aug 98 - May 99
- Full Program Launch   June 1999
- Joint Definition   June 99- Dec 99
- First Flight   August 14, 2001

Extensive cost trade-off parameters were prepared in all disciplines and all design decisions were subjected to an economic trade-off analysis. Weighing design proposals from vastly different disciplines is a challenging process. Only a fully integrated or collaborative multi-disciplinary optimization approach can guarantee the achievement of a true minimum of an overall aircraft level objective function. In reality, the merit of a design is heavily dependent on the experience and skill of the senior designers called to make the required decisions and on the experience of the design organisation as a whole.

On the multi-site and multi-partner BD-100 project, BES provided an effective method, to monitor and execute projects effectively, determine deliverables of the engineering process by function and harmonize product development processes and practices. BES offers two advantages. First, it helps clarify the company processes and deliverables. An objective analysis of these processes can then be made, possible deficiencies identified and corrected. Wherever possible, improved, more robust processes can be substituted. Secondly, because it requires process flowcharts down to the "Tier 4" functional activities, BES is a natural platform from which to establish integrated design procedures and automate them.

VADOR: an MDO Infrastructure Program

The design of a unique software framework tailored to Bombardier's Engineering System and capable of supporting Multi-Disciplinary Optimization (MDO) was entrusted to CERCA, a research center in numerical methods, located in Montreal. The software CERCA is developing is known as VADOR, for **V**irtual **A**irplane **D**esign and **O**ptimization F**r**amework. [2]. The central contribution of VADOR is the development of a software infrastructure permitting a seamless integration of technical applications and providing a global

perspective of a given design project. The software is capable of representing information, including data and methods, from the BES work flow charts to the detailed engineering tasks. It provides critical information on:

- The location of the data;
- The methods used to produce the data;
- The status of data and tasks;
- The validity of the data;
- The owners of the data and methods

The two main components of VADOR are "Data Components" and "Strategy Components". Data components are objects that encapsulate design and analysis data, usually contained in data files. A data component can encapsulate one or several data files. Strategy components are objects that encapsulate programs or analysis methodologies or processes. A program can be any piece of software that requires an input data and produces output data files. A process is a set of programs that must be executed in a sequence corresponding to a given algorithm. This sequence may include conditional loops. Both components have a set of attributes such as owner information, access permission, history, comments and present status. The framework allows collaboration and sharing of data and enforces proper documentation and promotes standardization of engineering methods. New processes and data are defined in the system during an integration phase. Subsequently, in a typical every day usage, the users simply execute these existing processes to create the required data and inspect the data using appropriate visualization tools provided through the framework. The clear separation between the data and the programs is intended to allow many different programs and processes to produce functionally equivalent data, reinforcing the standardization based on the data. This is crucial because the development and certification of a modern airplane requires extensive and rigorous documentation of all design characteristics.

Figure 4 illustrates the basic architecture of VADOR, composed of five elements, as described in [2]:

The **Graphical User Interface** (GUI) is a Java program running on the user's machine providing an interface between the engineer and the VADOR services.

The **Librarian Server** or Data server is a Java server program responsible for the handling and archiving of components.
The **Executive Server** is a Java server program that manages the execution of "Strategy Components" to create "Data Components". After receiving requests from the GUI to create data, it communicates with the Librarian server to retrieve data components and generates the data creation sequence according to the strategy invoked. The Executive server communicates with the CPU servers to run the required analysis programs and, after execution, notifies the Librarian Server to update the status of the components in the database.

The **CPU servers** are Java programs that wrap programs. They can be installed on any suitable machine. On request from the Executive server, they get the input files required for the execution, run the analysis programs and transfer the output files to the required locations.

The **Database Management System** (DBMS) is used to store, maintain and provide access information for components. The information is stored using a relational model. It should be noted that the framework does not manage detailed engineering data but rather references and information about the detailed data, stored in data files on the network.
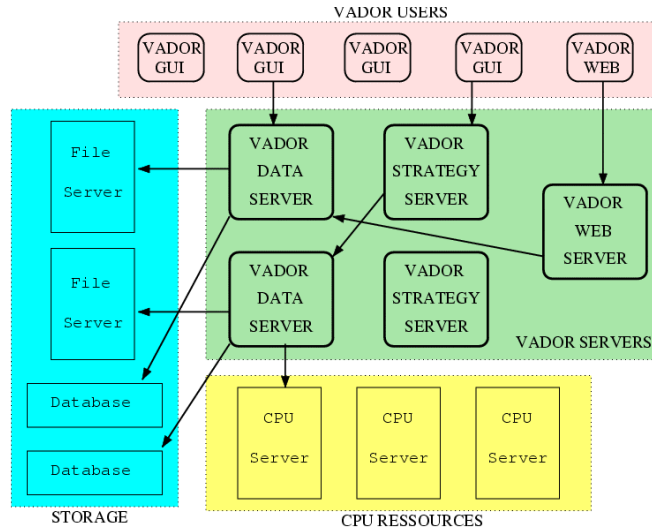
Figure 4: Typical VADOR Architecture

Aerodynamic analysis of transonic flexible wings

One important multi-disciplinary study is fluid-structure interaction. An initial objective was the prediction of wing weight and wing structural deformation (Figure 5) and the influence of this deformation on the aerodynamic load distribution. The prediction of the bending and twisting of wings was achieved by coupling the transonic CFD code KTRAN [3] with a thin-walled structural analysis program (TWSAP). The linear structural capabilities of the NASTRAN structural analysis software are utilized to predict the bending and twisting of a simplified finite element model (stick model) of the actual wing. Deformations predicted using stick models of transonic supercritical wings are in very good agreement with the results of full Finite Element Models (FEM) [4]. Results obtained for the static equilibrium (convergence) state of the Challenger and Global Express wings in 1g flight were found to be in very good agreement with experimental data. This suite of multi-disciplinary programs is wrapped in the VADOR framework.

(a) Rigid wing geometry

(b) Wing geometry under loads
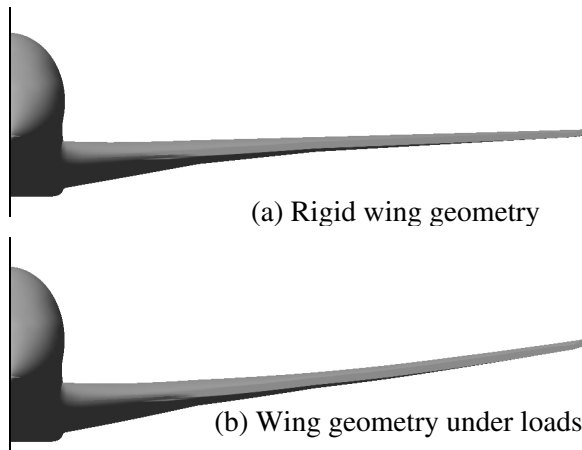
Figure 5: Static aeroelastic deformation of a transonic wing computed by the KTRAN /TWSAP /NASTRAN package at Mach 0.80 and CL=0.5

Wing Structure Conceptual Models

Challenger Wing Structure

Stick Model
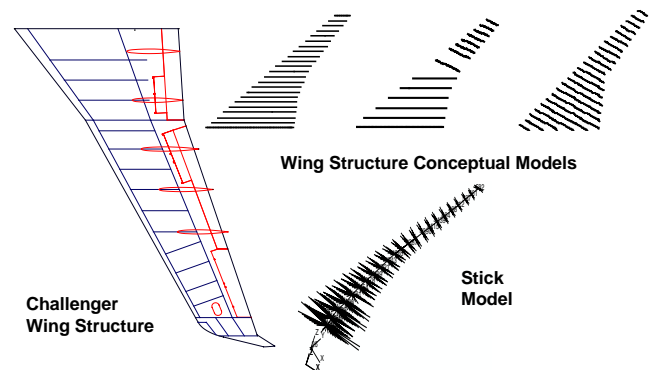
Figure 6: Canadair Challenger wing structure and examples of conceptual structures generated by the TWSAP program

In a following step, the methodology was extended to predict the aeroelastic deformation of wings at the conceptual design stage. The program generates conceptual layouts of wing structural components and creates a beam finite element model of the wing structure (Figure 6). To establish the accuracy of the stick model designed by TWSAP, its prediction of the wing bending and twisting were compared with results obtained with the full finite element model of the real Challenger wing structure, without winglets. Figure 7 shows that the comparison obtained is sufficient for preliminary design purposes
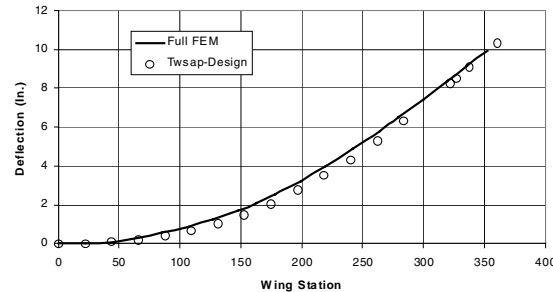
Figure 7: Comparison of wing bending predicted by the conceptual stick model and the full FEM of the Challenger wing without winglets.

Advanced aerodynamic wing design methods

To design wings, several methods are used. The most commonly used at Bombardier is the wing shape optimization program **ALLOP** developed in-house. Using a gradient-based optimizer, it is used to match a user-supplied target pressure distribution. The control points of a NURBS representation of the geometry are used as design variables in order to optimize the pressure distribution locally or globally. The ALLOP optimizer can call a variety of 2D and 3D high speed or low speed aerodynamic analysis codes. These codes return results that are used to calculate the current value of an objective function to minimize. Geometric constraints are imposed using penalty functions. Several developments were made to the representation of wing shape in order to include typical manufacturing constraints on the aerodynamic lines.

A second method, **INDES** [5, 6], an inverse design code originally developed by Tohoku University, in Japan, was linked to two transonic analysis codes. First, INDES was linked to the MGAERO 3D Euler code for complete aircraft configurations of Analytical Methods Inc. The MGAERO version used included a boundary-layer coupling introduced at Bombardier. INDES was also linked to the KTRAN transonic small disturbance code for complete aircraft configurations. This method can also be used to match a given target pressure distribution.

A third method, **AeroPointer** [7], recently licensed from Synaps Inc. of Atlanta, is an optimization environment capable of performing multi-disciplinary optimizations using a global parameter as an objective function, such as the total aircraft drag or weight. AeroPointer was linked to Bombardier's KTRAN transonic analysis code. The different capabilities of these methods are complementary, and each can be used effectively in the overall wing design process.

The main differences between ALLOP and INDES, the two methods for optimizing pressure distributions, is their relative speed of execution and flexibility. Since it is an inverse method, INDES is significantly faster. INDES will converge or achieve its best result in some 20 calls to the analysis code. In comparison, ALLOP requires hundreds of function calls, with the length of the optimization depending on the number of design variables. ALLOP optimizes the location of the control points of a NURBS representation of the geometry, so the more points are used or the greater the number of airfoil sections, the longer the optimization will last. INDES may or may not achieve a given target pressure distribution. If INDES does not converge on the specified target, the best that can be done is to modify the target pressure distribution itself. ALLOP is more

flexible because it can be restarted with a different set of design variables, and will usually continue to converge towards the target. Typically, for a complex design, ALLOP must be restarted a number of times, and the complete process may last in the order of two or three days. Unlike INDES, ALLOP will always produce smooth airfoil sections since it uses NURBS to describe the geometry. Another advantage of ALLOP is that it allows the user to work on a portion of a wing, or on a part of an airfoil section. For instance, the user may optimize only the upper surface of the wing, or only the leading edge, etc. For these reasons, INDES will typically be used to initiate an optimization process, because it does a good part of the work in a short period of time. ALLOP is then used to refine the design.

The major disadvantage of using either ALLOP or INDES is the requirement to define a target pressure distribution. This is not only a time consuming process but it also assumes that the designer has enough experience to "know" what an optimal pressure distribution is for a specific wing. In contrast, no target pressure distribution is required when using the AeroPointer software. The latter is capable of performing a multi-disciplinary optimization by minimizing a global parameter, such as a combination of the total drag and the weight of an aircraft. This capability is very useful since it makes no assumptions about the pressure distribution, and it effectively automates the design process.

Automation in the design process is important not only from the point of view of efficiency, but also because it makes multi-disciplinary optimization possible, since the latter can only be done through the minimization of global parameters. AeroPointer achieves this capability through the use of a hybrid optimizer that combines the capabilities of genetic, gradient, and simplex methods. AeroPointer also allows the user to define any geometric parameter as a design variable or a constraint, and can perform weighted multi-point optimizations. Naturally, the quality of the final design will depend on the fidelity of the analysis code and on the topology of the design space. Typically, a careful selection of design variables and constraints is required to ensure a successful optimization, and the methodology developed for one application may not necessarily be optimal for another. In some cases, AeroPointer will produce a good design but one that can clearly be improved in some areas. In such a case, an AeroPointer optimization would be followed by the further optimization of the pressure distributions using either INDES or ALLOP.

The current best approach therefore is to initiate the design process with AeroPointer to define the general characteristics of the optimal design in an MDO sense (Figure 8). This process would typically be initiated with a low fidelity analysis code and completed with a higher fidelity code whenever practical. Once the general characteristics of the configuration have been defined, any further improvements required in the pressure distributions could then be achieved using INDES if possible or ALLOP when detailed refinements are required (Figure 9).
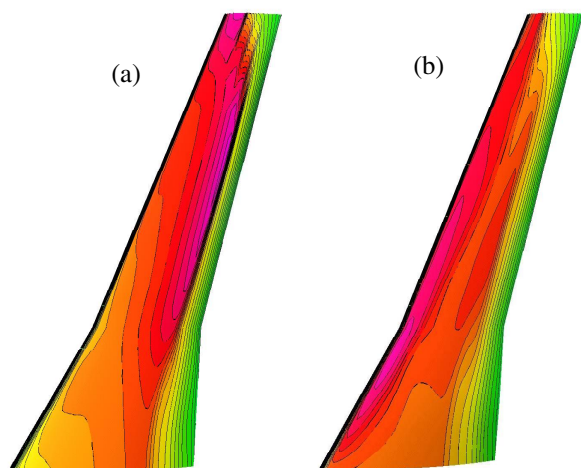
Figure 8: (a) Initial business jet configuration; KTRAN solution; M=0.8 CL=0.5. (b) Configuration optimized with AeroPointer/KTRAN; M=0.8 CL=0.5
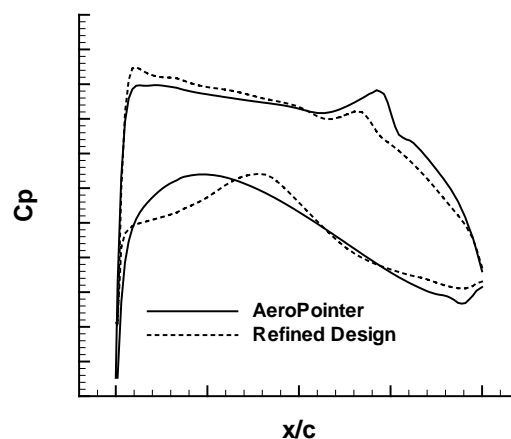
Figure 9: Pressure distribution achieved with an MDO sense optimization compared to a final design including a locally refined pressure distribution.

CFD flow analysis and drag prediction

Bombardier recent CFD development efforts have concentrated on the Full Aircraft Navier-Stokes Code FANSC [8]. The program uses multi-block structured grids, with an unstructured block topology, i.e. it allows any number of blocks to merge at the same location. It uses a cell-centered finite volume approach with a choice of space-discretization schemes and an explicit Runge-Kutta time-marching method. The code can be run in Euler mode, in Euler mode with boundary-layer coupling and in Navier-Stokes mode. The Navier-Stokes code uses the Spalart-Allmaras turbulence model [9].

To be useful in a realistic design environment, the FANSC code was made robust for solutions on complex aircraft geometry. Boundary conditions include no-slip and slip walls, transpiration wall for boundary-layer coupling, symmetry and degenerate lines and points, Riemann and engine inlet/outlet boundary. The code allows also the specification of multiple boundary conditions on each block face. Its run time efficiency was considerably improved by adding coarse grain parallelization on blocks (3.6 out of 4 CPUs) and vectorization (94% efficient).

The large CPU time of Navier-Stokes computations still precludes their inclusion in routine design and optimization loops. Euler/boundary-layer computations are used instead. A boundary-layer code was developed and coupled with FANSC first through the use of a direct Viscous/Inviscid Interaction (VII) scheme [10]. The coupling uses a transpiration velocity approach, with no need to regenerate a new mesh at every VII cycle. Since a direct VII procedure fails when separated flow is encountered, as often found during design iterations, an inverse boundary-layer code was also coupled with FANSC using a quasi-simultaneous VII scheme. The viscous flow is solved with the CIBL3D inverse code, developed by Cebeci et al. at California State University, Long Beach [11]. With this code, separated boundary layers can be computed with accuracy comparing favorably with more time-consuming Navier-Stokes computations for many cases of interest. This is illustrated in Figure 10, showing a pressure distribution computed at mid-span of a Challenger wing-body configuration.
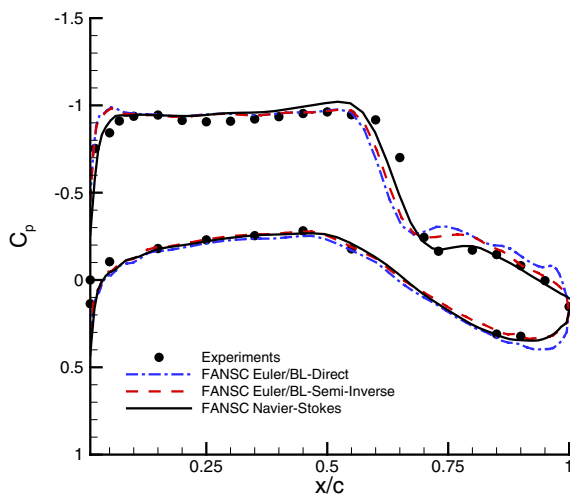
Figure 10: Euler/Boundary layer and Navier-Stokes computations of flow on the Challenger wing/body configuration Mach 0.82, Alpha = 1.5 degrees, Rec = 6 Million, station at 40.5% of the wing semi-span
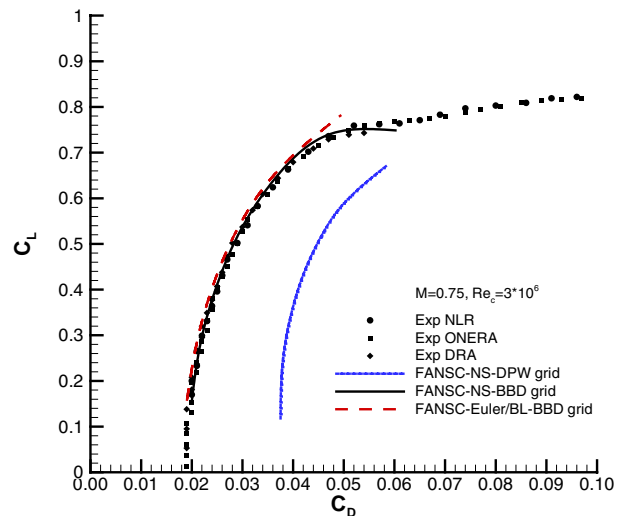
Figure 11: FANSC prediction of drag polar for the DLR-F4 configuration, Mach 0.75, Reynolds number 3 Million.

To be used effectively in aerodynamic design loops, CFD codes must produce accurate, reliable and repeatable drag estimates. Drag modules were constructed as a post-processing step to the Euler/Boundary-layer solutions. They include a semi-empirical module for fuselage and nacelle drag, a Multhopp algorithm for induced drag, Lock's method for computation of wave drag based on shock strength and a Squire-Young

module for the computation of wing and tailplane viscous drag. Far-field methods for the induced drag and the computation of wave drag from the integration of entropy variation across shock waves were also investigated. More recently, investigations were made in the prediction of drag from direct integration of pressures and skin friction obtained with a high-accuracy Navier-Stokes solution.

The difficulties of drag prediction with Navier-Stokes computations were illustrated at an AIAA Drag Prediction Workshop held in June 2001 in Anaheim, California [12]. FANSC was used to predict the drag polar of a DLR-F4 wing-body for which experimental results had been collected in NLR, ONERA and DRA wind tunnels. Drag was obtained from integration of pressure and skin friction coefficients, as specified for the workshop. Initial predictions made by FANSC with the grid supplied by the workshop organizers showed drag levels much higher than experimental values (DPW grid results, in Figure 11). A new mesh of the DLR-F4 configuration generated using Bombardier's MBGRID program was prepared. The mesh had good orthogonality on the solid surfaces, 10^{-6} chord wall spacing, 3.8 Million mesh points, an open wing tip and a blunt trailing edge. Calculations with the same program on this mesh showed excellent correlation with the experimental values (BBD grid results, in Figure 11). The main difference between the two grids was in the orthogonality near solid surfaces (Figure 12). FANSC showed excellent convergence characteristics (density and turbulent viscosity) on the Bombardier generated grid and on the workshop supplied grid, despite its excessive skewness. Integrated lift and pitching moment predictions on the workshop grid were accurate. Mesh skewness introduced discretization errors on the skin-friction evaluations whereas pressure drag was correctly predicted on both grids. This illustrates the great care that must be exercised if drag from Navier-Stokes computations is used as the function to be minimized in a wing design process. One must ensure that mesh modifications do not introduce variations not due to the wing geometry changes. Figure 11 shows that an excellent drag polar was also obtained on the NLR-F4 configuration with FANSC running in Euler/boundary-layer mode with the post-processing drag formulas. The grid required for this calculation was much simpler, with 1.3 million grid points. A solution for one angle of incidence is obtained in 0.45 hours on 8 CPUs of a Cray SV1 computer instead of the 6 hours required by the Navier-Stokes calculation. The Euler solution required 600 Mbytes memory instead of the 2.2 Gbytes required by the Navier-Stokes analysis. There are therefore advantages in using Euler/boundary-layer methods in large parts of the wing design process.

(a)

(b)
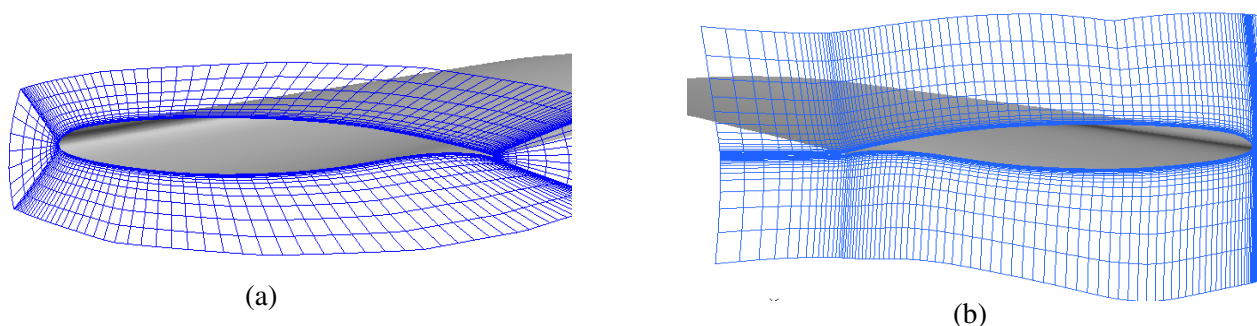
Figure 12: Close-up views of DLR-F4 grids for the AIAA 2001 Drag Prediction Workshop. (a) Initial supplied grid; (b) Bombardier-generated grid.

Despite considerable progress made to date, the use of Navier-Stokes methods in aircraft design integration is still a challenge. The best approach seems to be the use of a full suite of low and high fidelity codes, starting for instance with low fidelity codes and finishing with the more sophisticated methods. The goal is to implement Navier-Stokes codes in design loops in the coming year, following a significant upgrade of the available computing hardware.

Conclusions

The toughest challenge of MDO in the aerospace industry is to bring together technologies and methodologies of various disciplines in a way that is both practical and inclusive of the expertise that must accompany the individual technologies. MDO procedures asking experienced engineers to change completely their methods

have often met with mixed success. Our approach, described here, is to develop this capability in a step-by-step approach that includes either the actual methods in use by the various disciplines, or simplified versions of these methods. Bombardier's approach to automated design integration includes the following steps:

- Understanding, documention and optimization of all engineering procedures required to develop an aircraft (BES)
- Implementation of a software design environment which erases geographical distance and differences in computing platforms and automates BES tier 4 processes (VADOR)
- Implementation and validation of multi-disciplinary analysis and optimization procedures (fluid-structure, aerodynamics and systems simulation, etc.)

Acknowledgments

References

1. W. Elliot and B. Leigh, "Aircraft Loads Methodology For MDO", AIAA-2001-1432.
2. Alzubbi, A. Ndiaye, B. Mahdavi, F. Guibault, B. Ozell and J.-Y. Trépanier, "On the use of JAVA and RMI in the development of a computer framework for MDO, AIAA Paper 2000-4903
3. F. Kafyeke, P. Piperni and S. Robin, "Applications of KTRAN Transonic Small Disturbance code to the Challenger Business Jet Configuration with Winglets", SAE Paper 881483, October 1988.
4. M. Abdo, F. Kafyeke, F. Pépin, Z. Borowiec and A. Marleau, "Transonic Aerodynamics of Flexible Wings", CASI 48th Annual Conference Proceedings, April 2001.
5. Obayashi, S., Takahashi, S. and Fejtek, I., "Transonic Wing Design by Inverse Optimization Using MOGA", CFD98, 6th Annual Conference of the CFD Society of Canada, Quebec City, June 1998.
6. D. Jones, I. Fejtek, and D. Leblond, "Coupling of a Wing Inverse Design Code to a Transonic Small Disturbance Flow Solver", CASI 48th Annual Conference Proceedings, April 2001.
7. Van der Velden, "Aeropointer, a commercial CFD shape optimization tool", CASI 48th Annual Conference Proceedings, April 2001.
8. Zhu, Z., Laurendeau, E. and Mokhtarian, F., "Cell-Centered and Cell-Vertex Algorithm for Complex Flow Configurations", 8th Annual Conference of the CFD Society of Canada, Montreal, June 2000.
9. Spalart, P.R. and Allmaras, S.R., "A One-Equation Turbulence Model for Aerodynamic Flows", AIAA Paper 92-0439, Jan. 1992.
10. E. Laurendeau and F. Mokhtarian, "Coupled Euler/Boundary-Layer Methods with the FANSC Code", CASI 48th Annual Conference Proceedings, April 2001.
11. Cebeci, T., Jau, J. and Vitiello, D. "An Interactive Boundary-Layer Approach to Multi-Element Airfoils at High Lift", AIAA Paper 92-0404, January 1992.
12. AIAA CFD Drag Prediction Workshop Website. http://www.aiaa.org.tc/apa/dragpredworkshop/dpw.html, June 2001

Paper #48
Discussor's Name: D. Lovell
Author's Name: Dr. F. Kafyeke

Q: You have stated that external shape fixed in stages 1 & 2. What do you do about ensuring internal items can be packaged within the external shape?

A: We try and examine structural and systems implications as early as possible in the design stages (D1, D2) hence the value of MDO at conceptual design stage. If this is well done, only <u>minor</u> modifications to the external shapes are needed at D2.

This page has been deliberately left blank

———————————

Page intentionnellement blanche

Undersea Weapon Design and Optimization

Kam W. Ng
Office of Naval Research
800 North Quincy Street
Arlington, VA 22217, USA

ngk@onr.navy.mil

Abstract

This paper provides an overview of the Undersea Weapon Design and Optimization (UWDO) program sponsored by the United States Navy's Office of Naval Research (ONR). Progress, status, and future research directions of the UWDO program are presented. The objective of the UWDO program is to develop computational tools and simulation-based methodology to optimize undersea weaponry system designs with respect to cost and performance. The design tools and environment developed in this program continue to be improved and implemented in the ONR Torpedo Guidance & Control, Undersea Warheads/Explosive, Torpedo Stealth, and High-Speed Supercavitating Undersea Weapons programs. Specifically, the design tools and collaborative design environment are used for the design of torpedo sonar system, new warhead configurations, virtual acoustic design using active control techniques, cost analysis, and simulation of high-speed supercavitating weapons in the virtual environment. Lastly, recommendations and future research directions in UWDO are provided.

Introduction

The objective of the UWDO program is to develop computational tools and simulation-based methodology to optimize undersea weapon system designs with respect to cost and performance. UWDO is the infrastructure that is being developed to support the design of various undersea weapons as shown in Figure 1. The weapons include the High-Speed Quick Reaction, Torpedo Defense, Coordinated Attack, Long Range Stealth, and Advanced Weapons. These undersea weapons cover close-in and extended range scenarios, with affordability as the key requirement.

The UWDO program is based on the Simulation Based Design (SBD) approach. As shown in Figure 2, SBD spans the design, prototyping, acquisition, and operations of undersea weapons. Specifically, it is used in the simulation-based design and engineering, virtual manufacturing, virtual testing [1], training simulations, operations and logistics simulations, and warfare analyses.

The UWDO system architecture (as depicted in Figure 3) consists of four major components-- multi-user access server, design tools, simulation environment, and life cycle factors. The multi-user access server is the project data manager that communicates and interacts with the other three components. The design tool consists of analytical and numerical models, computer codes, and technology object library that supports product design and development. The simulation environment provides performance simulation and virtual training, testing, and tactics evaluation. The life cycle factors component deals with logistics modeling, cost modeling and analyses, and manufacturing process modeling

The ONR UWDO team consists of members from the Naval Undersea Warfare Center- Newport Division, Pennsylvania State University/Applied Research Laboratory, Naval Surface Warfare Center- Indian Head Division, Science Application International Corporation (SAIC), SRI International, Georgia Institute of Technology, and University of Maryland.

Technical Challenges

Affordable Science & Technology (S&T) product development, acquisition, and support for future undersea weaponry requires a software driven simulation based design process that provides:
1) improved (reduced time and cost) product development, 2) a good cost and benefit estimate of new technologies to meet future war-fighting needs, and 3) efficient transition of technology to the end users. The UWDO program develops the infrastructure that supports the development of undersea weapons in torpedo guidance and control, warhead, propulsion, stealth, and torpedo defense technologies, as well as advanced weapons system concepts such as the high-speed supercavitating weapons. This program establishes a modeling and simulation environment that integrates the United States Navy's S&T with Engineering Development efforts in undersea weaponry. The goal of the UWDO project is to develop a system that determines the design that gives optimal performance with a minimal Total Ownership Cost (TOC).

Some of the key technical challenges and S&T issues include:
- Interface of the various design tools and computer codes
- Connectivity of multi-users in a collaborative design environment
- Affordable, optimized designs
- Effective visualization of large amounts of data

Collaborative and Distributive Design Environment

The UWDO program focuses on the development of system architecture and design tools for the collaborative and distributive design environment. Design tools such as a virtual prototype design, Multidisciplinary Optimization (MDO), and cost/performance analyses are emphasized. Cost and performance trade-off studies are conducted by applying the methodology and tools to rapid prototyping of a torpedo upgrade, a new capability, or a new weapon system design. Figure 4 illustrates the virtual prototyping of a torpedo. Given overall system attributes in speed, depth and range, the designers can select the subsystems in power, guidance & control, propulsor, hydrodynamics, shell and structures, and payload. Cost analyses and simulated engagements are then performed to determine the optimal design.

Connectivity needs to be developed for disparate languages, Computer Aided Design (CAD) systems, performance models, external libraries, and users. Boyars et al. [2] identified connectivity among designers and users as one of the key requirements for the collaborative and distributive design environment. The design and optimization process involves building the SBD architecture using physics-based models to provide data for process/mechanical/environmental simulations, which, in turn, forms the basis for the vehicle subsystems, and creates a virtual prototype system design that can be used for performance, cost, and quality assessment. As an example, a web based collaborative and distributive design environment was used to design a torpedo sonar array (Figure 5). Engineering analyses and design were performed by geographically dispersed designers/users.

Multidisciplinary Optimization

Multidisciplinary Optimization (MDO) helps the users and designers to gain the understanding of the interaction among the various components to make effective and efficient tradeoff decisions. Kusmik [3] used MDO, and Belegundu et al. [4] used attributed-based MDO to design undersea vehicles. MDO needs a rapid convergence on optimal system-level design using the various models, simulation tools, and information management systems. Considering the conflicting requirement of the various sub systems and components, such optimization is indeed very complicated. Research efforts in Interval Programming and Probabilistic Methods are underway to develop effective and fast algorithms for optimization.

Multi-objective MDO is being used for a new warhead design (Figure 6). Given the design requirements, and objectives and constraints, the optimizer interacts with the warhead server, torpedo shell analyzer and lethality evaluator to produce the optimal warhead design. In this optimization, warhead lethality, radiated noise, and probability of kill (P_k) are considered simultaneously.

In the electric propulsion design and analysis, thermal and structural analyses are performed simultaneously to optimize motor design. As shown in Figure 7, thermal analysis and finite element analysis are integrated in the motor design.

Cost Analysis

Total Ownership Cost (TOC) has become one of the critical criteria in the weapon system acquisition process. TOC consists of costs from: 1) research and development, 2) production and manufacturing, 3) operation, and 4) maintenance. There are commercial parametric cost estimating software and cost models, e.g., PRICE, CORBA, for cost analyses [5]. Typical cost estimation requires inputs such as design, schedule, and deployment information. The outputs of cost estimation consist of total program cost, cost by phase, cost by type, and cost by category. The cost by category includes drafting, design, system engineering, project management, prototype, production, tooling & test equipment, general & administrative, and overhead. Maintenance cost is one of the most challenging cost estimations, in particular when there is a lack of repair records or cost data.

Virtual Design Environment

Recently, substantial progress has been made in virtual reality and scientific visualization to translate large amounts of data to visual representation. Aukstakalnis and Blatner [6] defined *Virtual Reality* as " a way for humans to visualize, manipulate and interact with computers and extremely complex data." The virtual design environment provides visualization techniques that designers can see design changes and their impact on the overall system.

Virtual reality and collaborative design environment is used for the development of advanced undersea weapons. Specific interests and focus are on torpedo stealth, warhead design, and high-speed supercavitating weapons. For example, the Virtual Reality Laboratory at the University of Maryland is developing the active noise and vibration control techniques [7] for stealth torpedo using this approach (Figure 8). Numerical results from the finite element model of the torpedo shell are displayed in the virtual environment. The animated structural noise radiation can be heard using the sound system and the vibration of the shell can be felt with the touch glove.

With the virtual environment, designers can select a range of subsystem technologies to assemble a conceptual design. This virtual prototyping capability dramatically reduces development time and total ownership cost. The virtual environment provides simulation and modeling capabilities, as well as evaluation of realistic operational scenarios.

The immersive visualization facilities at the Penn State University/Applied Research Laboratory, Virginia Tech, and University of Maryland, are utilized together with basic and applied research related to supercavitation physics, torpedo silencing and warheads to develop a unique integrated design environment. The three virtual reality sites are connected to form a collaborative design cluster among UWDO team members. The capability to visualize real-time simulations of the high-speed supercavitating weapons has been demonstrated at the Penn State University's Applied Research Lab. Modeling and simulation capabilities are augmented with the capability to generate immersive simulations from a synthesis of individual subsystem designs. Collaborative design architecture, multi-disciplinary optimization scheme, cost analysis tools and other relevant subsystem synthesis methods are incorporated into this virtual design environment. The advanced weapon designs are evaluated in operational scenarios modeled using the concept of operations requirements from the operational Naval

community. Standard protocols are utilized so that the conceptual designs can be evaluated in warfare simulation involving real players. This virtual design environment provides a *faster*, *more effective, and affordable* design space to develop undersea weaponry to meet future threats.

Recommendations and Future S&T Directions

Simulation Based Design (SBD) is an effective approach for system design and product development. The UWDO environment provides the foundation for timely, information-based engineering and programmatic decision-making.

Future S&T directions should focus on *Multidisciplinary Optimization, cost analysis, and virtual environment for simulation*. Specifically, the following areas should be of great interests:
- Efficient optimization schemes
- Fast convergence algorithms
- Accurate cost analyses
- Representation and interaction with large amounts of digital data in the virtual environment
- Interfacing design tools and computer codes

References

[1] Hanneman, A. B. and Henderson, R. E., *Visualization, Interrogation, and Interpretation of Computed Flow Field- Numerical Experiments*, AIAA Paper 2000-4089, 2000.
[2] Boyars, A. B., Kusmik, W. A., and Yukish, M., *Collaborative Engineering Across Organizational Boundaries*, ASNE Conference, April 2002.
[3] Kusmik, W. A., *Optimization in the Simulation Based Design Environment*, ASME DETC Paper, Pittsburgh, PA, September 2001.
[4] Belegundu, A. D., Halberg, E., Yukish, M. A. and Simpson, T. W., *Attribute-Based Multidisciplinary Optimization of Undersea Vehicles*, AIAA Paper 2000-4865, 2000.
[5] Yukish, M., *Cost Analysis*, 54th MPFT Meeting, Virginia Beach, VA, April 2000.
[6] Aukstakalnis, S. and Blatner, D., *Silicon Mirage: The Art and Science of Virtual Reality*, Peachpit Press, Berkeley, California, 1992.
[7] Akl, W. and Baz, A., *Design of Quiet Underwater Shells in a Virtual Reality Environment*, AIAA Paper, Atlanta, GA, September 2002.

Paper #49
Discussor's Name: Professor Ramana Grandhi
Author's Name: Dr. Kam W. Ng

Q: You are doing research in multidisciplinary optimization and also in probabilistic mechanics. Are you doing any work where the probabilistics is combined in MDO or reliability optimization or MDO based on stochastic finite element analysis?

A: We do multidisciplinary optimization, and modeling using the various numerical techniques including finite element analysis. We also use probabilistic methods in the undersea weapon design. Our design methodology is based on integrated system approach. Accordingly, we combine the various numerical techniques, computer codes and tools in the multidisciplinary optimization.
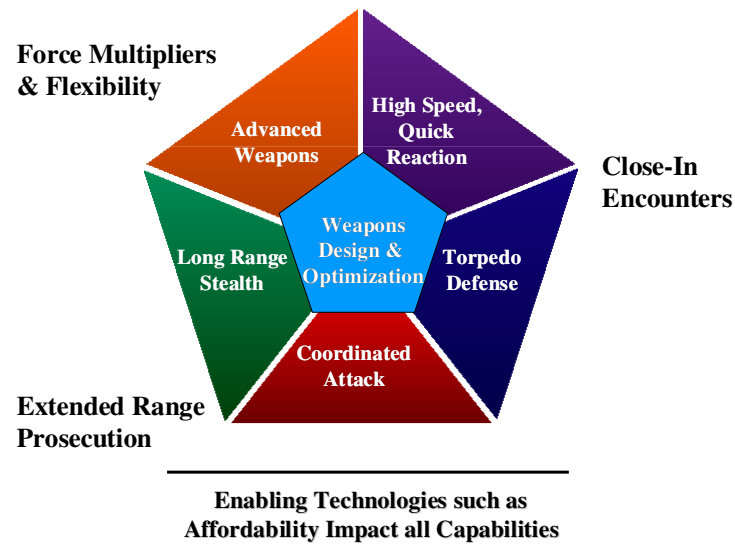
Figure 1. Capabilities of Undersea Weapons
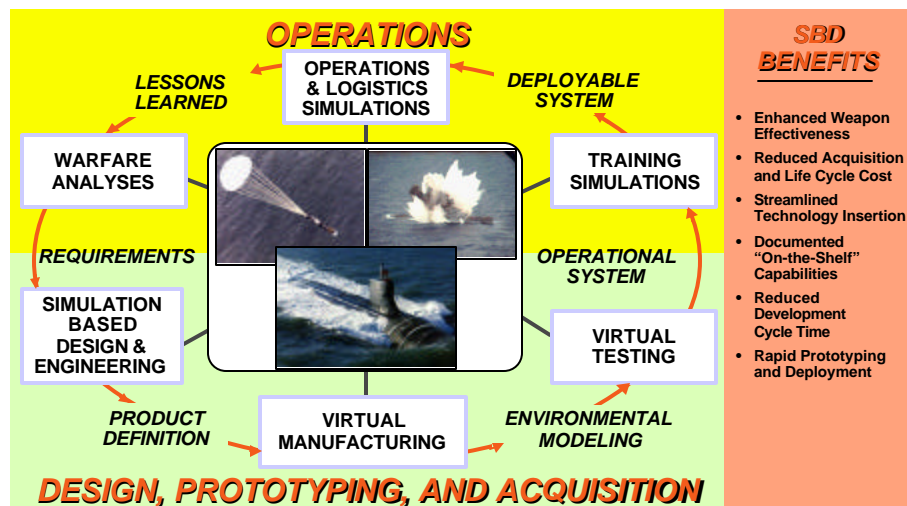
Figure 2. Simulation Based Design (SBD) Vision
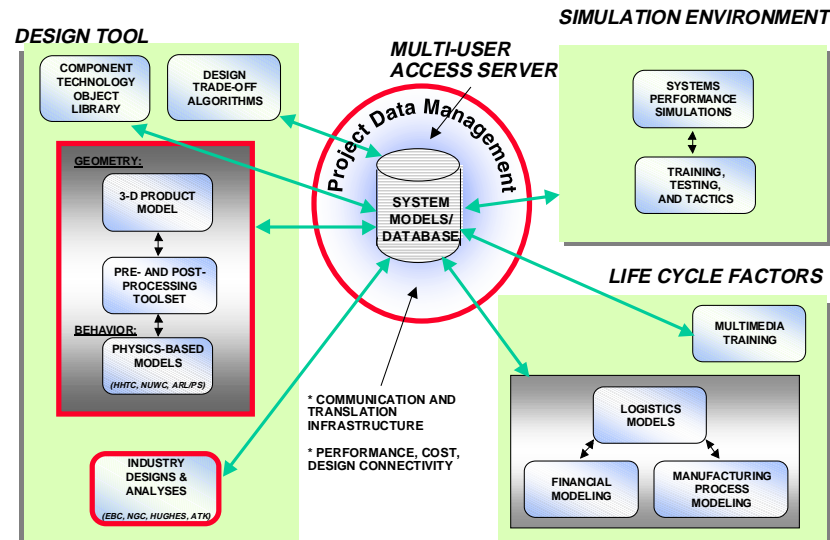
Figure 3. Design System Architecture
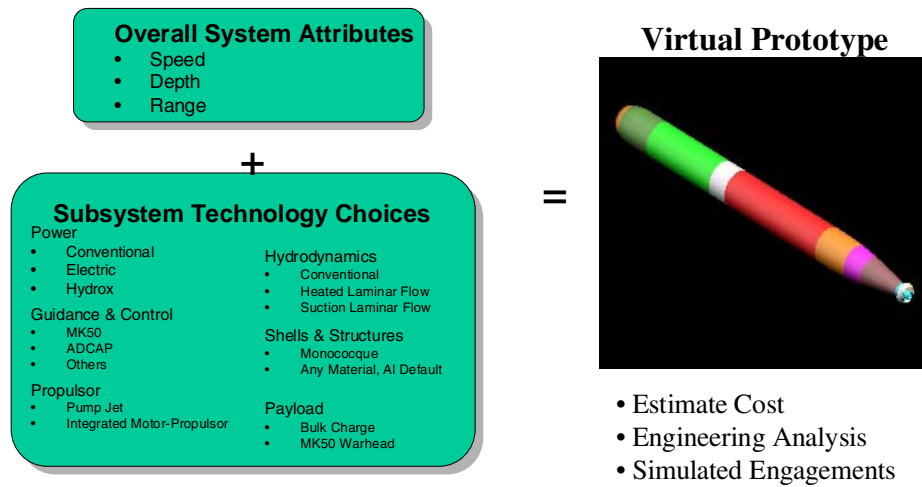
Figure 4. Undersea Weapon Design

- **Establish a web based collaborative environment for distributed team access to program data**
  - — **Design**
  - — **Analysis**
  - — **Technical data**
  - — **Program schedules and correspondence**
- **Modeling services applied for design development**
  - — **Thermal**
  - — **Structural**
  - — **Solids Based Design**
  - — **Shock**
- **Geographically dispersed design reviews**
- **Implement paperless processes**
- **Web based program management and workflow**
- **Model transitions to life cycle support functions**
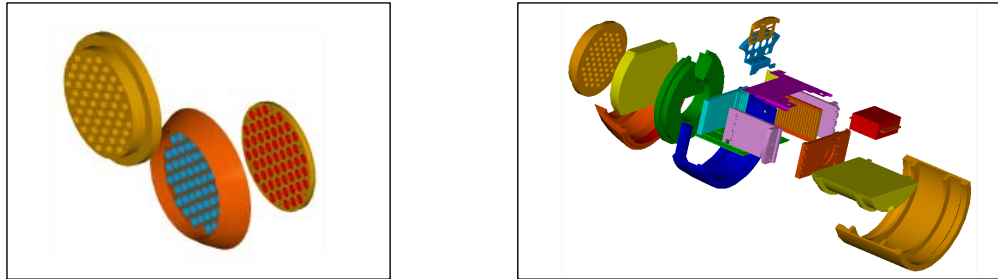
Virtual Reality Modeling Language (VRML) design model with intelligent web based interface

Figure 5. Application to Torpedo Sonar Design
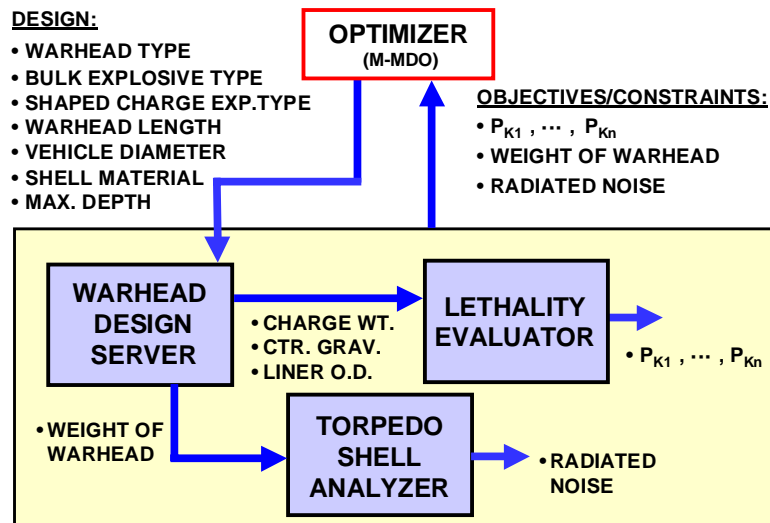
Figure 6. Multi-Objective Multidisciplinary Design Optimization for Warhead
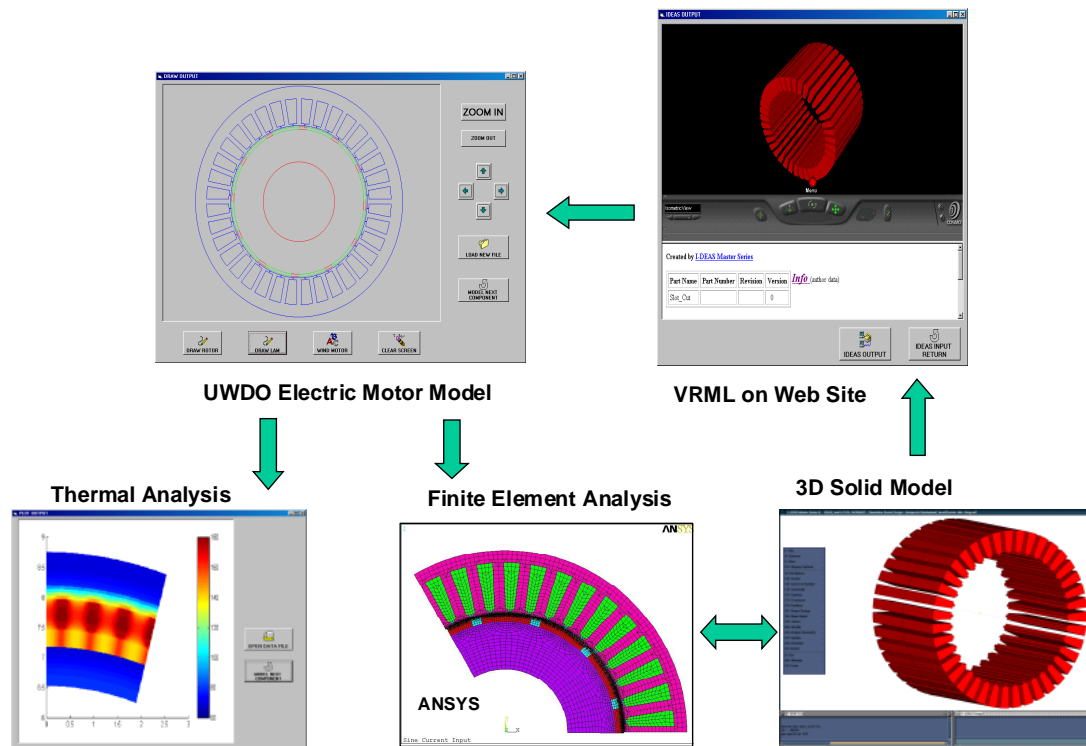
Figure 7. Electric Propulsion Design and Analysis

UWDO Electric Motor Model

VRML on Web Site

Thermal Analysis

Finite Element Analysis

3D Solid Model
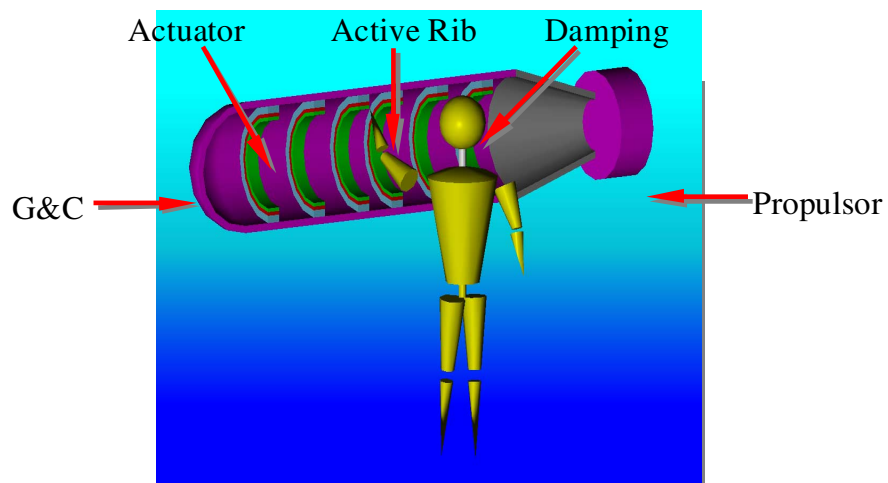
Figure 8. Virtual Acoustic Design of Torpedo Hull

Actuator

Active Rib

Damping

G&C

Propulsor

Collaborative Design Environment for Space Launch Vehicle Design and Optimization

Mark D. Stevenson
2856 G Street, B79
Wright Patterson AFB, OH 45433, USA

Alicia R. Hartong
1970 Monahan Way, B11A R021
Wright Patterson AFB, OH 45433, USA

Jeffrey V. Zweber, Amarshi A. Bhungalia
2210 8th St., B146 R301
Wright Patterson AFB, OH 45433, USA

Ramana V. Grandhi
College of Engineering and Computer Science
Dept. of Mechanical and Materials Engineering
3640 Colonel Glenn Hwy.
Dayton, OH 45435, USA

The design of a hypersonic cruise or space launch vehicle is a large undertaking requiring the team effort of many engineers having expertise in the areas of aerodynamics, propulsion, structures, flight control, performance and mass properties. As the design takes shape, specialists are requested to design such things as the crew station, landing gear, interior layout, weapons location, and equipment installation. The completed vehicle design is a compromise of the best effort of many talented engineers. It should be clear that the design process is a complex integration effort requiring the pulling together and blending of many engineering disciplines.

Figure 1: Trans Atmospheric Vehicles

Like all organizations, the Air Force is interested in conducting its vehicle studies as quickly as possible with as high fidelity an analysis as is feasible and with a proven, repeatable design and analysis process. This research is in support of an approach formulated by engineers at Wright Patterson Air Force Base who seek to integrate design and analysis tools into a collaborative, network-distributed design environment. The benefits of using an integrated design environment to reduce the time and potential errors associated with the transfer of data between design and analysis codes are well documented.[1,2] This research presents the integration of an initial set of space access and future strike vehicle analysis codes designed to improve the entire conceptual-level design process and documents the advantages of using the tools in a collaborative, network-distributed environment. This paper focuses on the design environment including geometry modeling, object design, discipline interactions, and design tools built for this effort including weight, propulsion, and trajectory analysis.

REUSABLE LAUNCH SYSTEMS

Both the US Air Force and NASA have indicated that next-generation reusable launch systems are needed within the next few years. Indications of the area's high importance can be seen through funding of projects like the X-33 and Hyper-X experimental launch concepts. At this stage of the study program, similar technologies and vehicle concepts are being examined to meet both the space access and future strike requirements. Consequently, rapid assessment of a Reusable Military Launch Systems is becoming increasingly important. There is a large array of RMLS options and promising configurations must be selected quickly for higher fidelity analysis. Furthermore all proposals must be analyzed uniformly using the same base-lined analysis tools and objective constraints.

The initial user of the web-based, collaborative application for launch vehicle design is the Air Force's Reusable Military Launch System (RMLS) analysis team. The core of this team has members from five different organizations that are located in four different buildings at two different bases. The team focuses on capability assessment for both future strike and space access vehicles. The goal is to impartially judge RMLS designs without restrictions on mode of operations. These modes include Horizontal Takeoff-Horizontal Landing, Vertical Takeoff-Horizontal Landing, and Vertical Takeoff-Vertical Landing. The team will also judge vehicle configuration options such as air breathing vs. rocket based propulsion and Two Stage to Orbit vs. Single Stage to Orbit.[3,4] A better understanding of the RMLS design space will dictate future areas of research and development needed to increase the viability of promising configurations.

Because of the distributed nature of the team, the initial method used to conduct analyses was to pass files manually via email and a web site bulletin board. This system is sufficient for the relatively small team. However it has obvious areas of inefficiency in communication. Moreover there exists the possibility of errors being introduced due to data translation and loss of configuration control. An improved design and analysis process was needed to prevent these potential errors and to allow the RMLS team to efficiently interact with technology experts from other government agencies, industry and academia.

The current vehicle under study is an in-house design of a fully reusable TSTO. The design (Figure 2) is a departure from the Bimese concept of identical booster and orbiter stages arranged "piggy-back" with an external payload mounted on the orbiter. The in-house concept consists of a booster and orbiter with a similar aeroshape but internal differences. Future vehicles under consideration include a stacked (serial burn) version of the Bimese concept and an air-breathing design.

Figure 2: Reusable Military Launch System

LAUNCH VEHICLE DESIGN ENVIRONMENT

The conceptual-level design process for hypersonic and space access vehicles is dominated by geometric modeling, aerodynamics, aerothermodynamics, engine performance (air-breathing or rocket) analysis, trajectory simulation, mass properties analysis and cost modeling. This process is shown in Figure 3 as a design structure matrix. A design structure matrix is used to graphically display the interactions between the various disciplines in a design process. [5] Each block in Figure 3 represents a different analysis code. These codes could be further associated with different engineers, different computers or even computer platforms.

The process starts with a designer formulating a possible outer moldline of the vehicle. This can be done anywhere from a "back of the envelope" sketch to lofted model in a CAD package. From the geometry, the aerodynamic, propulsion and mass properties analysts generate their models. Using the results of these analyses, a set of trajectories or missions is simulated to determine if the concept vehicle will meet its requirements. Then, from the results of the trajectory simulation, an aerothermoelastic analysis can be performed to determine the heating loads on the vehicle and subsequently
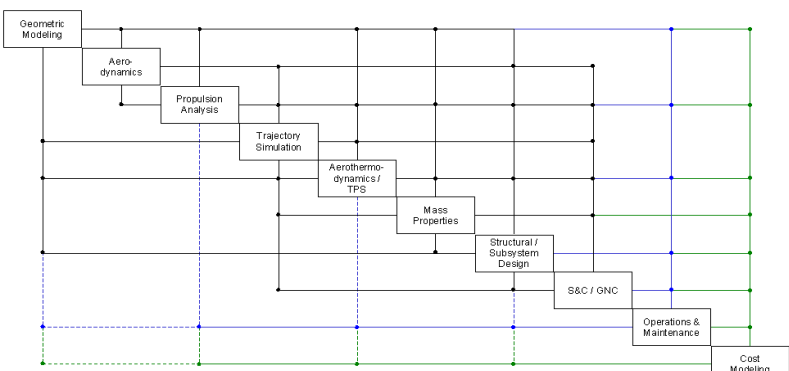
Figure 3: Design Structure Matrix

size the thermal protection system (TPS) and internal structure. The TPS size affects the geometric model by reducing the available internal volume for fuel and payload. Conventionally, this design cycle is repeated, varying geometric parameters, until the size and shape of the vehicle converges to the smallest vehicle that will perform a given set of missions.

One of the well-known shortcomings of this process is that it takes far too long for the design to progress to a point where operations, logistics and life cycle cost analyses are performed.[6] The long-term goal of this research is to demonstrate that, by integrating all the launch vehicle design disciplines into a collaborative design environment, the design data can be fed to the cost and operations disciplines sooner. In addition, by capturing the design process, the results of these analyses can be fed back to the conventional, conceptual design disciplines. By removing the manual data transfer steps, more design iterations can be accomplished in the same amount of engineering time.

The current status of the project is that some tools for the geometric modeling, aerodynamic analysis, propulsion analysis, trajectory simulation and mass properties disciplines have been integrated. Structural weight and aerodynamic results are calculated directly from an initial geometry specification, with the total weight being determined by adding the thermal protection system (TPS), propulsion system, payload and propellant weights. These three disciplines (mass properties, aerodynamics, and propulsion) provide the data that is needed by the trajectory simulation code to determine if the vehicle meets mission requirements (altitude and inclination angle). Finally, an iterative process is employed to vary the vehicle's fuel fraction ratio, and consequently the overall size of the vehicle, to correctly size the vehicle and propulsion system for a specified mission, or to determine that a specific vehicle class will not work for the required payload and orbit.

The Adaptive Modeling Language

For this effort, the Adaptive Modeling Language (AML) developed by Technosoft Inc., was selected as the design-modeling environment. AML is a framework for Knowledge Based Engineering that provides the ability to capture the launch vehicle design and analysis process and manage the data transfer between codes. It is by using the logical functions and calculations in AML, to capture process knowledge and design intent, that the significant timesavings in performing repeated analyses on a family of designs can be achieved. Previous research has demonstrated this knowledge capture in AML models for structural analysis and cost modeling.[7] The current version of AML has a wide variety of features that make it well suited for developing applications to capture a complex, multidisciplinary design process.[8] Perhaps the most important and least unique feature of AML is that it is an object-oriented language. A consensus has been reached in the software industry that object-oriented programming is vital for ease of software development and reuse. By applying the object-oriented paradigm to engineering models, AML allows the reuse of these models (objects). A well-formulated model will represent the component in general, parametric terms. For instance, the 747 and F-16 have very different wing shapes and sizes, but both wings can be represented by the same set of parameters (i.e., aspect ratio, root chord, taper ratio, airfoil section, twist distribution, dihedral and sweep angle). By developing a wing model this way, the same object can be used to model both aircraft.

A second important feature of AML (inherited from its Allegro Common LISP infrastructure) is its hierarchical, dynamic part-model. This feature is what makes AML "adaptive"; that is, models do not need to be recompiled to change the object hierarchy. The subobjects can be added interactively or specified in the definition of the class that was chosen for the top-level model (or in the definition of classes that were added as subobjects). This capability also allows objects and their properties to be added, edited or deleted independent of the order of instantiation. Included in the hierarchical structure is the Unified Part Model paradigm. This paradigm allows the model of a given component, the wing for example, to contain all the data about the wing that will be required by the various analyses. For instance, the wing model could contain a panel aerodynamic model, which would be used for low-speed calculations; a finite-element model of the wing box, which would be used for structural analysis; a second aerodynamic model that includes control surfaces, which would be used for stability analysis; and a thermal model, which would be used to size the wing's thermal protection system.

This modeling paradigm allows the model to grow as the design matures and new parts are created or new analyses are required. By keeping all the design information in a unified model, the "bookkeeping" of the data can be simplified. AML has built-in dependency tracking and demand-driven calculation capabilities to assist in this data management. *Dependency tracking* is important for ensuring that each discipline of the model is working with the current set of design parameters. With a manual design or configuration management system, it is easy for the various discipline specific models to get out of sync. AML automatically builds and maintains a list of dependencies. This list is updated as the objects are instantiated or deleted; or as the formulas associated with a property are changed. AML's dependency tracking also works in the other direction. That is, AML maintains a list of the properties that are affected by each property. The *demand-driven calculation* feature is complimentary to the dependency tracking capability. While the dependency tracking capability notifies all the parts of the model that have been affected by a change in a design parameter, the demand-driven calculation feature ensures that the only calculations to be performed are those needed for the current item of interest.

The last important feature of AML that will be covered here is the Graphical User Interface (GUI) included in AML. AML provides the powerful ability to automatically generate GUI's from an objects coding, eliminating the need for a designer to specifically develop a GUI structure. When writing an object, a developer specifies which parameters should be included in the user interface with only minor modifications in the parameter classes used. AML builds the GUI's during runtime. This eliminates a substantial volume of required coding from an object and reduces object development time. Additionally, when a design is being run over a network, form information does not need to be transmitted because the forms are part of an objects code, and generated on each individual client machine.

Collaborative design requires a distributed set of users running various analyses, possibly hundreds of miles apart. Bringing together a set of analysis tools under a unified environment is only a first step in achieving a fully integrated collaborative environment. Because of the large number of disciplines, an application would be extremely inefficient if limited to a single computer. A new feature being added to AML, under an Air Force Dual Use Science and Technology program termed Web-Based Design Environment (WDE) allows users to be distributed over a wide area network.[9] Users log into a server that contains the vehicle model via a standard WDE browser. Vehicle geometry modification and analysis can then be performed real-time over the network. The browser is platform independent and can access analysis codes on any computer across the entire network. By allowing pieces of the model to reside on different machines, each computer can specialize in a single discipline. This reduces the number of analysis codes needed and can save money by reducing the required software licenses and simplifying the system administration. The tool only passes parameter values of the model, which means that a high-fidelity graphical model requires a very small bandwidth.[10] Security and design configuration control issues are addressed within the modeling environment.

DESIGN DISCIPLINES

Design begins with geometry or an array of geometric considerations. Preferably the geometry object should be fully parametric, allowing the user to change shape into any other shape under consideration. However, the author has found that a single geometric object capable of all design configurations is not desired. The large number of parameters (e.g. number of fuselage cross sections, cross section geometries, cross section positions, wing type, and wing location) for a design forces a user interface to be complicated and unwieldy. There are a number of design possibilities, creating a huge array of very different vehicle designs. A series of parametric models tailored for each vehicle class (e.g. 2-D air-breathing and rocket based lifting body) is being created as part of the ongoing RMLS research. Using only a few parameters these models can be rapidly changed to any vehicle design within a given class. When a desired vehicle falls outside a class, other classes may have to be used or built to accommodate the new vehicle. A new parametric model takes about two weeks to create. The Bimese parametric vehicle class developed in conjunction the RMLS team at WPAFB for the current research with the help of TSI is shown in Figures 2, 8, 10, and 12. The model is able to be non-photographically stretched for vehicle sizing and includes links to previously mentioned analysis tools. The geometry objects developed for this class will also be used for future horizontally stacked configurations.

Rocket Engine Design Code

A focus for any launch vehicle design is centered on the propulsion system. Engine selection impacts several crucial design decisions including fuel type and associated fuel tank selection. Fuel fractions for SA/FS vehicles can be as high as 90% so fuel selection becomes a very important issue. Hydrogen fuels have a higher ISP (a measure of the overall energy contained in a rocket) but are less dense and require cryogenic tanks. Hydrocarbon fuels require smaller fuel pumps that reduce the size and weight of the rocket engine. Trade-offs for both fuel types require detailed analysis to determine the best fuel type for a specific rocket configuration. The importance of the propulsion system requires a rapid rocket design and performance analysis tool for vehicle modeling. The Parametric Rocket Model [11], developed at Wright Patterson AFB, uses a historical data trend approach primarily taken from "Design of Liquid Propellant Rocket Engines".[12]

The author chose to incorporate the simple Parametric Rocket Model into the AML environment because of its simplicity and fast run times. Additionally it provides information required for other analysis codes with a minimal input. The basic procedure for designing the propulsion system using the Parametric Rocket Model is as follows:

1. Select a specific rocket type and fuel, the characteristic velocity and combustor pressure, ratio of specific heat, propellant flow per unit throat area and characteristic combustor length based on previous engine designs are set. This represents the performance level of the engine class.
2. Given the specified nozzle expansion ratio(s) and nozzle type (1 position, 2 position, or dual bell) a nozzle thrust coefficient is calculated as a function of altitude.
3. Thrust at a reference throat area is then calculated as a function of altitude.
4. Given the specified thrust at a specified altitude, a scale factor is calculated that is applied to the reference thrust function to obtain the specified thrust.
5. The scale factor is also applied to the reference throat area to properly scale the geometry.

An example of how engine performance parameters are calculated are the equations used for exit nozzle pressure. The theoretical nozzle expansion ratio is calculation using Equation 1, where γ is the specific heat for a given fuel type, p_e is an assumed exit pressure and p_{cns} is the chamber (nozzle stagnation) pressure for a given fuel. This doesn't include boundary layer displacement correction, heat transfer or shifting γ effects, but it is close to actual values. The exit pressure is then calculated using Equation 2, where ε is the desired expansion ratio. Equations 1 and 2 are related to each other so a Newton-Rhapson iteration method is used for convergence. The iteration is performed on $1/\varepsilon$ because it is more linear than ε.

$$\varepsilon_{th}(p_e, p_{cns}, \gamma) := \frac{\left(\frac{2}{\gamma+1}\right)^{\frac{1}{\gamma-1}}\left(\frac{p_{cns}}{p_e}\right)^{\frac{1}{\gamma}}}{\sqrt{\frac{\gamma+1}{\gamma-1}\left[1 - \left(\frac{p_e}{p_{cns}}\right)^{\frac{\gamma-1}{\gamma}}\right]}}$$

Equation 1: Theoretical Expansion Ratio

$$p_e(\varepsilon, p_{cns}, \gamma) := root\left(\frac{1}{\varepsilon} - \frac{1}{\varepsilon_{th}(p_e, p_{cns}, \gamma)}, p_e\right)$$

Equation 2: Exit Nozzle Pressure

A plot of engine performance (given by thrust coefficient) for several nozzle types vs. altitude is plotted in Figure 4. The plots are characteristic of typical engine performance curves. The discontinuity in the graph for the Space Shuttle Main Engine (SSME) 150 2p (two position) nozzle is a result of moving a secondary nozzle into position at a specific altitude. The method has been correlated with advanced LH-LOX and RP-1-LOX engines. This simple model calculates thrust and Isp as a function of altitude, weight and geometry of the engine based on thrust at a specified altitude, rocket type, nozzle type (1-position, 2-position, or dual bell nozzle), and expansion ratio.
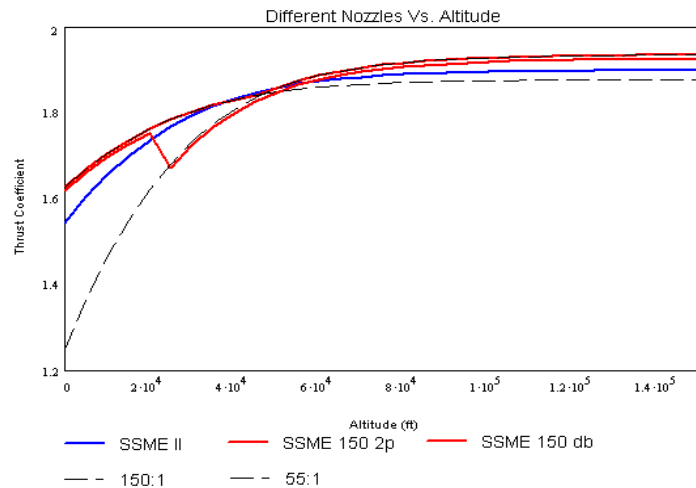
Figure 4: Engine Performance

Simply changing one parameter such as fuel type can radically change the engine geometry; Isp, thrust, and weight are also affected.

Weight Analysis

Figure 5: Engine Geometry

Weight analysis is a crucial aspect of RMLS design. Too much vehicle dry mass and fuel fractions will never be high enough to get a payload to orbit. Additionally, weight and aerodynamic parameters such as G-loading, calculated from trajectory and aerodynamic analysis, drive structural sizing.

Weight analysis equations tend to be strictly proprietary information tightly held by their parent organizations. Consequently no commercial off the shelf weight estimation software was found that suited the RMLS design group. Weight estimation software should be simple, use available information associated with the model and track the physics well. To build weight estimation software, engineers at WPAFB compiled historical trends in launch vehicle design as a way to predict future vehicle designs. Data was compiled from Air Force Flight Dynamics Lab reports produced in the 1970's and 1980's including the Space Shuttle, NASP and BETA vehicle.[13,14,15,16,17,18]

Weight Estimation

The weight analysis software was written directly into the AML environment, and highly coupled with the geometry. Component weights are generally calculated from a vehicle's gross weight, empty weight or geometry (also a function of gross weight). For example, Figure 6 plots the relationship of tail area with tail weight. The relationship is almost linear for a variety of vehicles. The vehicles used for this comparison are the XB-70 Valkyrie (Mach 3 USAF experimental bomber 1964-1969), STS (Space Shuttle), F-106A Delta Dart (supersonic USAF operational interceptor 1956-1960), B-58A Hustler (Supersonic USAF Operational Bomber 1960-1970), F-4 MK-2 Phantom (Supersonic USAF Operational Fighter 1965-1992). The actual relationship used for the weights equation (Equation 3) was chosen to match the Space Shuttle data. Because this weights equation is based on

Figure 6: Historical Weight Trends

$$Weight = 5 * Svt^{1.09} * 0.89$$

Equation 3: Tail Weight Estimation

geometry, which is based on gross vehicle weight, iteration of the overall vehicle is required to close the vehicle size and weight calculations. Component weights can be known values, such as an electrical system power supply that has been set at 770 lbs based on Space Shuttle requirements. Setting a weight to a deterministic value is equivalent to pulling a known power supply off the shelf and adding it to the model. Component weights can also be a simple equation or expanded into geometrical objects depicting sub-system placement. Components can be further broken down into constituent parts for increased model fidelity. The basic procedure for calculating an overall vehicle weight using the system is as follows:

1. Guess the empty weight fraction
2. Calculate component weights based on initial guess
3. Sum the weights and determine difference in empty weight calculations
4. Size the vehicle and adjust the empty weight guess
5. Iterate until vehicle closure

Once the weight estimation and sizing procedure are complete, the model is run through trajectory analysis that is used to update the propellant fraction. The weight estimation procedure is then rerun iteratively with trajectory analysis until overall vehicle closure. This research has discovered that only two to three iterations are required to close the vehicle.

Thermal Protection System Weight Estimation

As part of the weight estimation process, Thermal Protection System (TPS) weight must be addressed. The model uses a simple water-line scheme to estimate what TPS types are needed in what areas. With the knowledge that the vehicle will re-enter the atmosphere at a specified angle (i.e., 30°) surfaces that are in direct line with or at specified increments from the stagnation points are calculated. With the knowledge that surfaces nearest the stagnation points will require the highest temperature TPS, a lookup table of TPS materials (based on Shuttle tiling) is used to place tiles in specific regions. The density and thickness of the tiles is then used to calculate the entire weight of the TPS.

A more physics based approach for predicting TPS design is currently under development through an Air Force Small Business through Innovative Research (SBIR) program. Using high fidelity aerodynamics and heating analysis calculated directly from the geometry of the rocket design and its trajectory profile, the transient heating profile will be coupled with a TPS optimization routine. The thickness of the TPS is varied so that a maximum temperature on the inner rocket structure is not exceeded throughout the trajectory. The heating loads are then applied to the Finite Element model of the inner vehicle structure for sizing. The updated vehicle weight can then be sent back to trajectory analysis in an iterative cycle until vehicle closure. This will not only yield higher fidelity TPS design, but will also include the transient effects in the heating profile. Currently most TPS designs are sized to the point in the trajectory that yields the highest temperature; this overestimates the required TPS and consequently increases the weight of the vehicle.

Weight Estimation Error

There are errors in the weight estimation routines. The vehicles currently being analyzed are roughly five percent under weight, based on historical vehicle designs. The additional weight is accounted for using a weight correction factor, but additional work needs to be done to model vehicle weight better. Five percent under estimation is a considerable factor considering that the RMLS type vehicles may have growth factors of 30 or more. The higher fidelity methods previously discussed could be used to refine the weight synthesis equations for future increased model accuracy. Additionally, members of the RMLS team have modeled aerospace partners design to compare and verify the analysis. Results have shown a good comparison between the reports. Additionally, the comparison found that a few parameters in the model weight were not feeding back into the weight estimation scheme. Future studies will allow higher confidence in the model. Despite these errors, the current weight estimation routines are a good start to capturing vehicle weight, and accurate enough for the level of fidelity desired.

The weight estimation software developed is only for preliminary design. The author knows there are dangers to base weight estimation on historical data trends. This is especially true when the only data point that has been built and flown is the Space Shuttle that was designed for an immense 80,000-pound payload and is an operational nightmare. The Space Shuttle is not a good data point, but it is widely used because it is the only point available. Future work may incorporate higher fidelity tools, which will benefit from the vehicle-sizing starting point this tool gives. Additionally, the physics in the higher fidelity tools could then be captured to increase the accuracy of the preliminary weights equations developed.

Trajectory Analysis

As previously discussed, trajectory analysis is an integral part of RMLS design. The two main trajectory analysis codes used within the industry are OTIS (Optimal Trajectories by Implicit Simulation) and POST (Program to Optimize Simulated Trajectories). Within the aerospace industry, the author has found that new codes are not easily accepted, and various organizations (even within the RMLS team) live and die by their selected code with no thought of change. Consequently both codes have been integrated into the environment using program wrappers. However, the author favors OTIS because its solutions have yielded better results, coupled with the ability to use more parameters and constraints.

OTIS 3.0 is a FORTRAN77 program for simulating and optimizing the point mass trajectories of a wide variety of aerospace vehicles. The version used at Wright Patterson AFB was recently compiled for

use on NT-based windows machines. The most advanced simulation uses implicit integration to generate an open-loop optimal control of a prescribed vehicle.[9] OTIS was designed more like a math program; give it a series of parameters (possibly hundreds), constraints and objectives, and it will solve for the optimal mathematical solution. POST is also a FORTRAN 77 program for a generalized point mass with discrete parameter targeting and optimization.[19] POST behaves more like a traditional trajectory program; give it a series of parameters (under 100), constraints, objectives and a trajectory that the user thinks is good, and it will yield a slightly better trajectory. POST has the benefit of being fast but is hampered by only running in DOS mode on PC-based machines. The POST integration uses a LISP function to traverse the tree to collect data, reformatting it into an input text file required by POST. The text file must then be sent to the trajectory analyst to run POST and send back the updated fuel fractions.

The OTIS 3.0 integration currently only contains the specific information relevant to a particular RMLS class of vehicles. The properties allowed in a specific model are tailored such that a limited set of trajectories can be performed, reducing the incredibly large array of options OTIS 3.0 allows. This reduces the strain on a user of the tool by reducing the number of properties understood and checked during program execution. The few properties relevant to a given design are easily accessible within the design environment. However, the initial trajectory file relevant to a particular vehicle class is required to be generated by an expert user of OTIS 3.0. Trajectory analysis is extremely complicated, and eliminating the expert entirely from the design process would be impossible. Vehicle configuration properties such and aerodynamics, weight, engine propulsion are automatically formatted into the OTIS format, and the updated fuel fractions are automatically read back into the collaborative environment for automated iterative design.

Aerodynamic Analysis

The aerodynamic analysis application used for the Bimese trade studies was Missile DATCOM. DATCOM requires geometry to be broken down into simple known components and then uses empirical equations of the known shapes to calculate the desired aerodynamic coefficients for the overall vehicle. Consequently only simple geometry can be modeled using DATCOM. Multiple bodies also pose a problem becuase they are not handled in DATCOM. The author chose to model the orbiter and the booster separately, with the payload treated as a protuberance on the orbiter. The drag of the orbiter and booster is then summed. The calculated drag using this method ignores whatever interference exists between the wings, which adds to the drag calculation. But this decreases at higher Mach numbers and is not unreasonable to ignore. To check this assumption, a CFD model is being run for the concept. However, the results are not expected soon because of the huge computational expense of CFD analysis.

The analysis shown in Figure 7 demonstrates the expected drag rise going through Mach 1.0; the large increase is a result of the NACA 0012 airfoil chosen for the Bimese concept. The analysis is consistent with predictions on how the model should behave, allowing confidence in the aerodynamic analysis.

For a sanity check a more detailed analysis could be performed using PANAIR, an example of an analysis of the Bimese concept is shown in Figure 8. PANAIR is a linear aerodynamic solver using the technique of boundary elements (commonly referred to as aerodynamic paneling). Surface geometry is "body-fitted" with an array of quadrilateral panels.

Figure 7: Coefficient of Drag Calculation Using DATCOM

Continuous surface singularities (both sources and doublets) are distributed using a number of schemes to meet a number of needs.[20] The program is accurate but requires longer run times, and is not applicable to the quick trade studies desired for the RMLS team. Additionally, PANAIR requires a continuous structured body grid that is difficult to model around protuberances such as wings in an automated fashion. The RMLS Bimese model was not constructed with PANAIR in mind so the wings could not be included in the PANAIR analysis. Consequently, only the body is analyzed in Figure 8 and the analysis cannot be compared with DATCOM. Both aerodynamic analysis objects contain information on how to break the smooth geometry of the model into their respective application inputs. No additional user work is required to run the analysis within the limits of the Bimese concept.

Future work will include adding ZONAIR to the list of aerodynamic analysis tools included in the environment. ZONAIR is a panel method aerodynamic solver based on ASTROS for very accurate results with limited computational time. A benefit of ZONAIR is that meshing can be unstructured, allowing input grids to be automatically generated. Additionally, multiple wingsets will be able to be modeled.
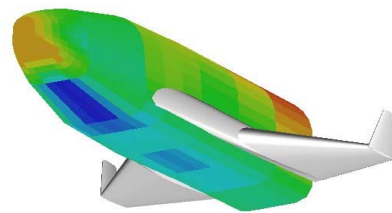
Figure 8: PANAIR Pressure Distribution on RMLS Bimese Vehicle

EXCERSIZING THE MODEL

The majority of the research has focused on the design environment development, and, as a result, the majority of this research is concerned with the environment and associated analysis modules. However the environment is only a foundation for rapid trade studies. Using this tool, the author performed various trade sweeps of the Bimese concept. The vehicle sizing routine incorporating weights and propulsion takes 60-180 seconds (sizing both the orbiter and booster) running on a Pentium III processor with 500 Mbytes RAM. The time difference depends on how many sizing iterations are required (which depends on how close original model sizing guess is to final design). Initial trajectory analysis using POST must be run offline because of the limitations of POST (which must be run in DOS mode), so trajectory and its required aerodynamics analysis are not run in an automated fashion. The input file required for the automated OTIS 3.0 analysis has recently been built and will be used to run through the series of designs the RMLS team wants to look at. With the limited number of analysis tools incorporated (weights, aerodynamics, propulsion, and trajectory) only a few trade study parameters can be considered. But the parameters considered are critical to design formulation. Trade study parameters able to be handled by the model include payload sizing, thrust to weight ratio, fuel selection for both booster and orbiter, wing thickness, rocket nozzle type, and staging velocity. The author will limit discussion to the first three trade studies mentioned.

Payload Sizing

Payload size comes from mission requirements. The payload size trade study performed shows what a top-level mission change will cost in terms of vehicle weight for a given design. In this study, the author changed the payload weight from 4k to 64k pounds, sized both the orbiter and booster vehicles and plotted the
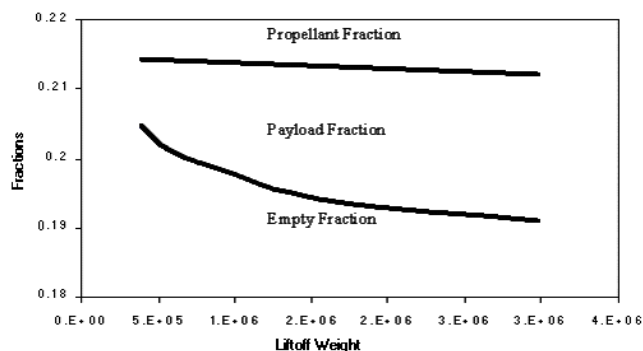
Figure 9: Vehicle Fractions Based on Fuel

resulting overall vehicle fractions in Figure 9. In this plot, the propellant fraction (Pf) plotted is 1-Pf (i.e., about 76% of the vehicle weight). If the ordinate was scaled to one, the entire area between the Pf curve and one would represent the propellant fraction. Payload fraction is the difference between propellant fraction and empty weight. The empty weight plotted is the true empty weight of the vehicle. The increase in the empty weight fraction at the lower vehicle gross weight is largely a result of nearly constant TPS weight, resulting in greater weight fractions. The propellant fraction was held constant at 76% for the payload sweep; the slight decrease seen is a result of

Figure 10: Payload Sizing Comparison

the weight equations not summing the weights properly. Within the range of payloads that were analyzed, greater vehicle efficiency is realized with larger payloads. At a lower liftoff weight, no payload is able to fit within the vehicle.

The vehicles at the extremes of the analysis (4k and 64k pound payloads) are shown in Figure 10. Notice that the sizing is not photographic. The wings grow at a faster rate in comparison with the fuselage. This is a result of the wings depending on the empty weight of the vehicle to maintain an acceptable rate of sink, span loading, and wing loading during landing conditions. The weight mainly depends on the size of the fuel tanks, the engine, and thrust structure, which depend on the fuel volume. Volume is a cubic function, so a small change in the fuselage will lead to a large increase in weight. The planform area only grows by the square of the increase in fuselage size, so if the fuselage grows by a factor of two, the weight increases by a factor of eight, and the wings increase a factor of four.

Thrust-to-Weight Optimization

In the second analysis sweep the thrust-to-weight ratio of the orbiter was varied and plotted as a function of vehicle dry weight (Figure 11). Thrust-to-weight and propellant fractions are closely related; higher thrust to weight ratios require less vehicle fuel fractions. Iteration was required with the trajectory analysis to solve for the fuel fraction. The results ranged from 77.5% at a thrust to weight ratio of 1.0 to 74.5% at a thrust to weight ratio of 1.8. Because the orbiter operates at high altitudes, the thrust to weight effect on vehicle weight is mostly a result of gravity losses (a

Figure 11: Thrust to Weight Optimization

factor of ΔV). Consequently there is only a small shift in dry weight and slight differences in vehicle design. The increase in dry weight at higher thrust to weight ratios results from limiting the G-loading on the vehicle. Additional increases in thrust only add additional engine weight to the vehicle. An optimum thrust-to-weight ratio is found to be between 1.3 and 1.7.
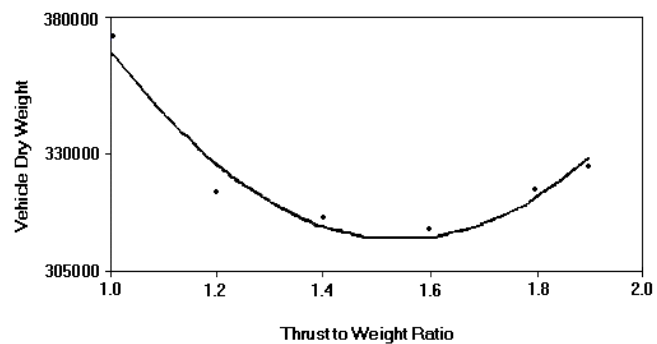
Fuel Selection

In this study, the fuel of both the orbiter and booster where set to either a hydrocarbon (kerosene) or hydrogen based fuel with a LOX (liquid oxygen) for the oxidizer. The vehicles in Figure 12 show that the hydrogen-fueled concept is much larger than the hydrocarbon design. This is a result of the very low density of hydrogen, which requires a larger volume for the same propellant mass, increasing the volume required to store it. However, the vehicle dry weight is still roughly the
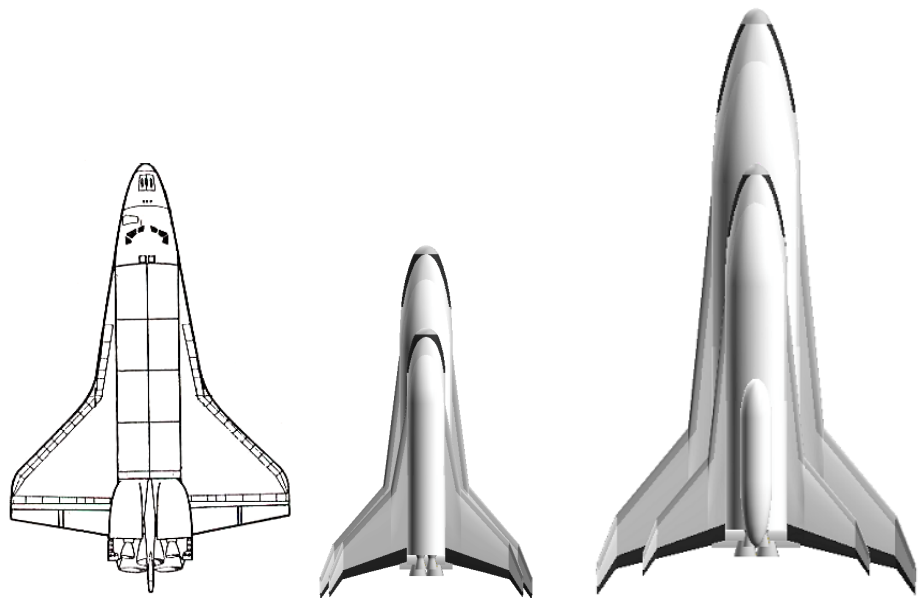
Figure 12: Fuel Selection Vehicle Comparison

same for both concepts. In fact, further studies have shown that the hydrocarbon design could be made lighter than the hydrogen concept by increasing the staging Mach number. The non-photographic scaling in the vehicle concepts results from the same sizing constraints of the payload trade study. Further analysis is required, particularly in the operations area, to determine the optimal staging mach number. The scaled picture of the Space Shuttle is included only as a yardstick as to the size of these concepts.

SUMMARY

The Reusable Military Launch System design environment under development at WPAFB has demonstrated dramatic design and analysis timesavings. The collaborative design environment currently incorporates parametric geometry, aerodynamics, mass properties, aeroheating, rocket propulsion, and trajectory analysis disciplines for the Bimese rocket configuration currently under study by the RMLS team. Continuing Research will incorporate additional analysis tools and optimization techniques for complete vehicle formulation. As the number of analysis objects grows, the usefulness and efficiency of the tool will increase. Further trade study analysis will define optimal vehicle design. These trade studies include:

- o Load-factor
- o Allowable wing loading
- o Number of engines (engine out capability)
- o Engine type
- o Fuel selection
- o Parallel vs. serial burn
- o Staging Mach number

However, performing various single degree of freedom trade studies does not necessarily produce optimal results. The interconnectivity of the various disciplines found in the design structure matrix almost guarantees non-linear results that must be analyzed as a whole. Future work will include optimization across the disciplines to produce optimal vehicles for particular mission categories. The research reported here has created a design environment for rapid design analysis at a conceptual level. This work will be useful for assessing optimal design solutions and will dictate future air force requirements and direction for building RMLS vehicles. This is only the beginning of a much larger process. With additional object creation, higher fidelity analysis will be achieved.

BIBLIOGRAPHY

1. Bhungalia, A. A., Zweber, J. V. and Stevenson, M. D., "Integrated Aerodynamic and Geometric Modeling for Hypersonic Vehicle Design", ASME paper DETC/DAC-14267, presented at the 26th ASME Design Automation Conference, Baltimore, MD, September 10-13, 2000.

2. Stevenson, M. D., Bhungalia, A. A. and Zweber, J. V., "Integrated Trajectory Analysis for Transatmospheric Vehicle Design", AIAA paper 2000-4817, presented at the 8th AIAA/USAF/NASA/ISSMO Symposium on Multidisciplinary Analysis and Optimization, Long Beach, CA, September 6-8, 2000.

3. Stanley, D., *et al.,* "Rocket Powered Single Stage Vehicle Configuration Selection and Design", AIAA 93-1053, Feb. 1993.

4. Freeman, D., Stanley, D., Camarda, C., Lepsch, R., Cook, S., "Single Stage to Orbit: A Step Closer", AIF 94-V3.534, Oct 1994.

5. Olds, J., Bradford, J., Charania, A., Ledsinger, L., McCormick, D., and Sorensen, K., "*Hyperion*: An SSTO Vision Vehicle Concept Utilizing Rocket-Based Combined Cycle Propulsion", AIAA paper 99-4944, presented at the 9th International Space Planes and Hypersonic Systems and Technology Conference, Norfolk, VA, November 1-5, 1999.

6. Prasad, B., *Concurrent Engineering Fundamentals: Integrated Product and Process Organization,* Volume I, Prentice-Hall, Upper Saddle River, NJ, 1996.

7. Zweber, J. V., Blair, M., Kamhawi, H., Bharatram, G. and Hartong, A., "Structural and Manufacturing Analysis of a Wing Using the Adaptive Modeling Language", AIAA paper 98-1758, presented at the 39th AIAA/ASME/ASCE/AHS/ASC Structures, Structural Dynamics and Materials Conference, Long Beach, CA, April 20-23, 1998.

8. *Adaptive Modeling Language Reference Manual: Version 3.0*, TechnoSoft Inc., Cincinnati, OH, 1999.

9. "Web-based Design Environment", DUS&T Program Report to Congress, Air Force Projects for Fiscal Year 1999, http://www.dtic.mil/dust/cgr/af00cgr.htm#airforce19

10. Meltzer, Pete, "Web-based tool speeds up weapon system design", Skywrighter, WPAFB, OH, 26 May, 2000.

11. Livingston, John, "A Parametric Rocket Model", USAF, WPAFB, OH, 2000.

12. Huzel D., Huang D., Rocketdyne Div, N. America Aviation Inc., "Design of Liquid Propellant Rocket Engines", NASA SP-125, 1967.

13. Klich, P., MacConochie, I., NASA Langley, "Mass Estimating Techniques for Earth-To-Orbit Transports with Various Configuration Factors and Technologies Applied", SAWE Paper No. 1315, 38th Annual Conf. Of SAWE, NY, NY 7-9 May 1979.

14. MacConochie I., Klich P., NASA Langley, "Techniques for the Determination of Mass Properties of Earth to Orbit Transportation Systems", NASA TM-78661, June 1978.

15. NASA Johnson Space Center, System Definition Branch: Technology and Project Implementation Office, "Design Mass Properties II: Mass Estimating and Forecasting for Aerospace Vehicles Based on Historical Data", JSC-26098, November 1994.

16. HYCAD – Equations developed by ASC/XR 1985 and 1988.

17. Olds, John, Dissertation NC State 1993, Appendices A and B.

18. Forbis, J., Woodhead, G., Boeing Military Airplanes, "Conceptual Design and Analysis of Hypervelocity Aerospace Vehicles: Vol 1. Mass Properties, Part 1 Transatmospheric Vehicle Weights (TAVWTS)", WL-TR-91-6003, July 1991.

19. Powell, R. and Braun, R., "Program to Optimize Simulated Trajectories (POST)", NASA Langley Research Center, Hampton VA, Oct. 1997.

20. Blair, M., Moorhouse, D., Weisshaar, T., "System Design Innovation Using Multidisciplinary Optimization and Simulation", AIAA 2000-4705

Modelling and Simulation in the Design Process of Armored Vehicles

M. Hönlinger, U. Glauch, G. Steger
Krauss-Maffei Wegmann GmbH & Co.KG
Krauss-Maffei-Str. 11
80997 Munich, Germany

michael.hoenlinger@kmweg.de

Abstract

The use of modern simulation tools in the development of new armoured vehicles permits shorter development times and a reduction in the number of prototypes. This paper shows the importance of virtual prototypes in the development process. Owing to more stringent protection requirements, the design layout of new vehicle concepts is possible only with the help of a complete vehicle simulation. Modelling techniques and simulation methods are presented by the example of mobility and mine protection analyses.

1 Introduction

The requirement for lightweight, armoured vehicles with a high level of protection and good mobility presents a major challenge to development engineers. Based on successes achieved over the past several years in the area of mobility and protection improvements, the focus is now on a drastic reduction in vehicle weight. For instance, unrestricted transport by C130 aircraft requires a transport weight of less than 17 tons, which is no longer practicable with today's vehicle platforms in light of increased protection and mobility requirements.

Today, new drive concepts, such as hybrid drives, and protection concepts, such as modular mine protection, are being developed for future lightweight armoured vehicle platforms. In the overall vehicle concept, suspension and mine protection are of key importance. The suspension is a determining factor for mobility and payload volume, the level of mine protection largely defines the vehicle structure and configuration of the crew compartment.

In developing mine protection characteristics, the design and tuning of the dynamic behaviour of the vehicle structure, along with occupant protection systems, are a demanding task which can be solved only in the context of the complete vehicle. The required test series and qualification trials, some of which are conducted with fully equipped vehicles, are very time-consuming and costly. Apart from the high cost pressure, the short procurement times sought by the customer for new vehicle systems call for a significant reduction in development times.

In order to meet these challenges, modern CAE methods must be consistently applied throughout the development process. Numerical simulation in this process is an important tool for the design layout as well as to substantiate vehicle development data. Generating virtual prototypes in an early phase of the process is an indispensable requirement, as the design and optimization of subsystems is possible only within the complete vehicle system.

The following paper describes the use of simulation in the development process with the emphasis on mine protection and mobility analyses.

2 Virtual Prototype

The concept and layout phase for new vehicles today includes systematic studies of the capabilities, performance potential and technical limitations through simulation. This makes it possible to identify the key system components and to assess them in terms of cost and risk. Simulation techniques are primarily used in the following areas:

- Mobility (longitudinal, transverse and vertical dynamics)

- Structural design (stiffness)

- Mine protection (short-time dynamics)

- Ballistic protection (short-time dynamics)

A virtual prototype of the vehicle is generated from computation and CAD models as early as during the concept phase. Figure 1 and Table 1 gives an overview of the computation models and simulation tools used for this purpose.
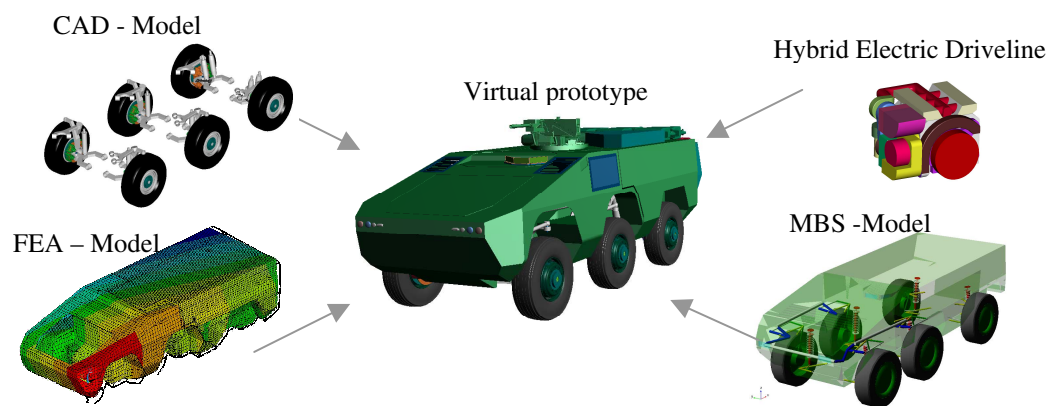
Figure 1: Virtual Prototype

Simulation	Model	Design Tool	
Mobility Analysis	Multi Body System (MBS)	ADAMS/Car	/1/
Power/Energy Management	Longitudinal Dynamic	Matlab	/2/
Structural Analysis	Finite Elements Model	ANSYS	/3/
Geometry/Assembly	CAD Model	Pro/Engineer	/4/
Mine Protection	Finite Elements Model	LS/DYNA	/5/
Human Dummy	Finite Elements Model	LS/DYNA	
Ballistic Protection	Finite Elements Model	LS/DYNA	

Table 1: Computation models and simulation tools

During the concept phase, the virtual prototype primarily consists of physical functions. As the development process progresses, geometries and components are increasingly added and detailed. The virtual prototype then describes the complete vehicle in geometrical, technical and functional terms. The geometrical CAD data, computation and simulation data of the virtual prototype are stored in a common product database (PDM) which serves as a work platform for the various development teams.

The digital mock-up (DMU) of the vehicle can be generated with the CAD models contained in the virtual prototype and the document structure (PDM). The DMU models describes the vehicle topologically and technically and serves the entire product development and design process as a database, e.g. to conduct installation, ergonomics and crash studies. Concurrently with the development activities, the virtual prototype may be integrated into tactical and operation simulations conducted by the contracting authority in order to verify vehicle requirements and, if necessary, adjust these requirements. Figure 2 and 3 show possible uses of virtual prototypes within the development process.
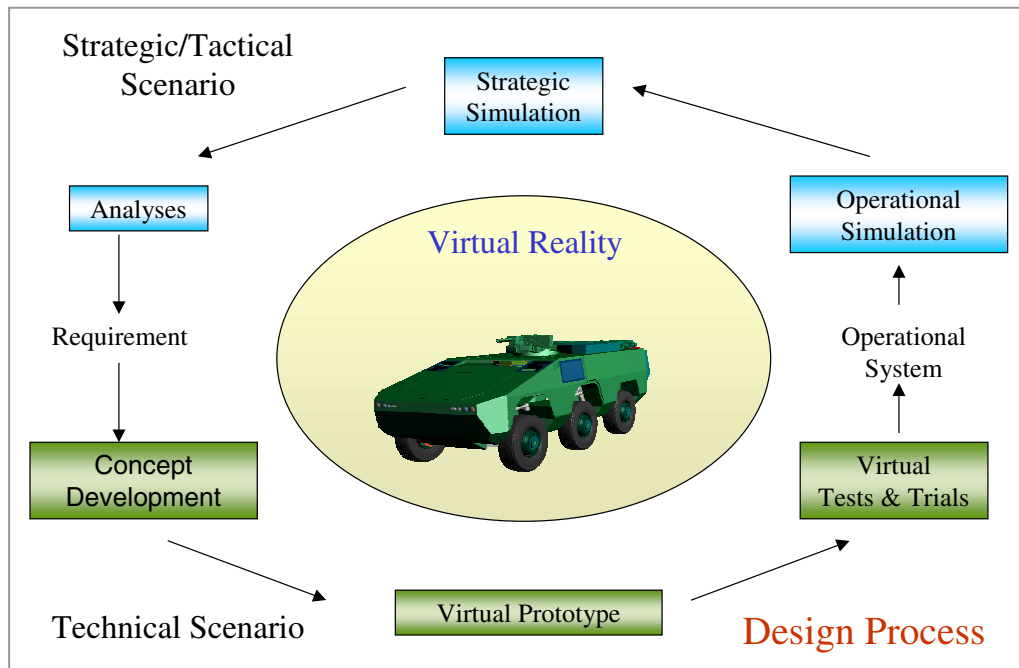
Figure 2: Use of virtual prototypes in the development process
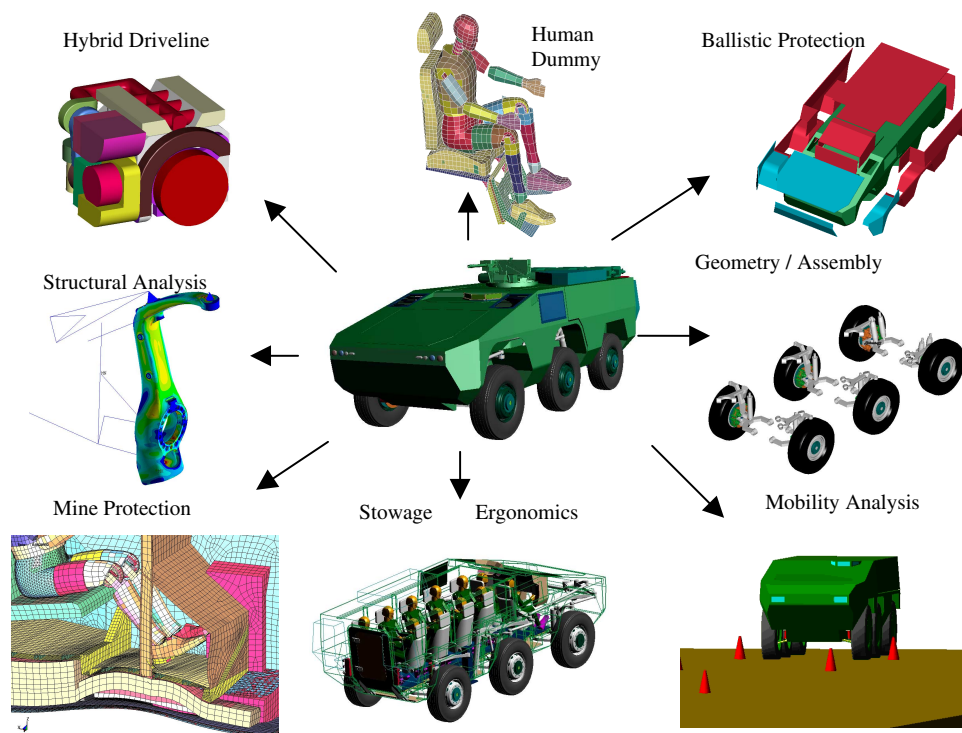
Figure 3: Use of virtual prototypes in analyses and design

3 Modelling and Simulation Tools

3.1 Structural Analysis and Design

Finite element models linked to the CAD model are used to design the vehicle structure. The meshing of the intermediate surfaces with shell elements is most conveniently carried out with the assistance of the mesh generator of the Pro/Mesh CAD software. For linear structural analyses and modal analyses with ANSYS, this mesh quality will normally be sufficient. For explicit non-linear FE analyses, the models are meshed in the FE pre-processor in order to obtain a better mesh quality. The global design of the structure is initially based on standard load cases which are derived from measured data. For the local design of load introduction points, e.g. the suspension, load data are used from mobility analyses conducted with the MBS model. To optimize the structure in terms of stiffness and weight, topology and parameter optimizers provided by the ANSYS/OPT simulation tool are increasingly used.

3.2 Suspension Analysis and Design

The multi-body simulation tool ADAMS/CAR developed specifically for the automotive industry is used for the preliminary layout of the suspension concept. The MBS tools provides a library of suspension concepts and evaluation functions which permit the efficient analysis of various concepts. Initially, a simple MBS sub-model of the suspension is generated to analyse and design the axle kinematics and spring/damper system. The design and tuning of the spring/damper system to match a variety of operational environments and trackway conditions is a demanding optimization task. Basically, a high level of ride comfort requires soft suspension tuning, whereas driving safety relies on a stiff suspension setting. In order to resolve this discrepancy, simulations increasingly use active suspension elements /6/.

The design layout of the suspension components is performed with the assistance of CAD and FE models. The CAD model reproduces the axle kinematics in order to carry out crash studies and to generate the envelope curve for all wheel positions. The envelope curve describes the wheel arch contour and thus defines the interior payload area of the vehicle. The FE model equally reproduces the axle kinematics in order to take account of the influence of elasticities and to optimize the component parts. Experimentally defined standard load situations are normally used to verify the strength of suspension components.
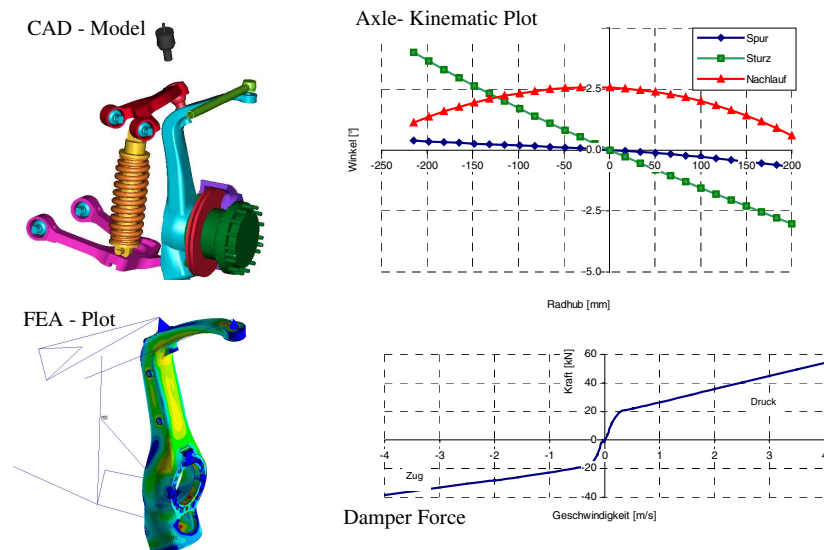
Figure 4: Modelling and Simulation in suspension design

A complete MBS vehicle model is generated to analyse the dynamic vehicle behaviour. The required data, unless already available, are derived from target value functions or measured data.

4 Simulation Techniques Used for the Development of Mine Protection

The design of mine-protected vehicles places high demands on the development. In case of a mine detonating under the vehicle, the floor structure must have a high level of stiffness in order to absorb as much energy as possible and at the same time ensure a low level of deformation of the floor into the crew compartment. On the other hand, the stiffness of the structure must not be such high that the floor structure breaks up and collapses due to material failure. The seat system itself and its connection to the vehicle structure must be of a certain compliance in order to keep the loads imparted to the occupants by forces and shocks as low as possible. All measures taken to protect the occupants must be highly responsive. After 0.3 milliseconds of a mine blast, the floor structure will already show local deformation. After 10 milliseconds, initial movements of the dummy caused by the introduction of forces and shocks can be observed. Initial vehicle movements occur after appr. 30 milliseconds.

In the area of vehicle development activities, mine protection measures generally relate to the following areas:

- Structural measures (floor deformation, introduction of forces and shocks, penetration behaviour)
- Occupant protection systems (seats, footrests, airbag, energy-absorbing elements)
- Interior equipment (padding, mounting of personal equipment, spall liner)
- Measures to preserve residual mobility

In designing mine protection systems, all measures must be well balanced. Computer simulation has proved to be an effective tool in developing mine-proof vehicles. The numerical simulation of the dynamic effects of a mine blast on the vehicle structure makes it possible as early as during the concept phase to predict the structural behaviour and to assess the effectiveness of different design approaches and their effects on the occupants.

4.1 Assessment Criteria

A key objective in vehicle development is the fulfilment of the occupant protection requirements in mine blasts. Generally, the following criteria are used to assess the mine protection level of a vehicle:

- Probability of occupant injury (DRI, dummy values, g loads, forces)
- Hazards caused by local failures (e.g. fuel leakage)
- Hazards caused by flying debris (secondary projectiles)
- Residual mobility

The probability of occupant injury is determined from stress values calculated in simulations with the assistance of dummies or in mine blast tests. The dummies used during these tests included the Hybrid III 50th dummies, which were developed and validated for the motor industry. Figure 5 shows the stress values of a dummy which are today evaluated with respect to the probability of injury.

hip + pelvis F_{max}

head HIC_{max} a_{max}

chest SI_{max} F_{max} a_{max}

spinal column DRI

upper leg F_{max}

knee F_{max}

lower leg F_{max}
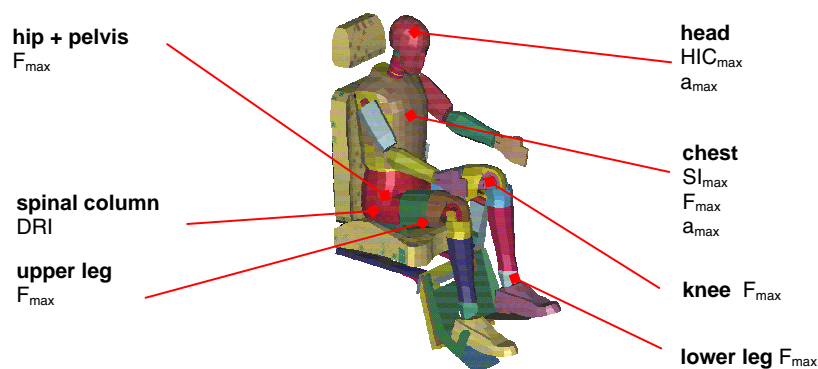
Figure 5: Stress values used to assess the probability of occupant injury

4.2   Model Harmonization With Blast Tests

Mine protection development activities include numerous blast tests conducted to verify and harmonize the simulation models. Experimentally determined are specifically data for material models, e.g. foam materials or welding seams and for pressure curves. The data and models obtained can be used to perform complete vehicle simulations for the purpose of verifying and optimizing mine protection. A comparison of the dummy stress values obtained with complete vehicle simulations with the values measured during qualification tests shows a high level of agreement. Figure 6 shows a comparison of the calculated and measured vertical g loads acting on the pelvic area of a Hybrid III dummy during a mine blast under a vehicle.
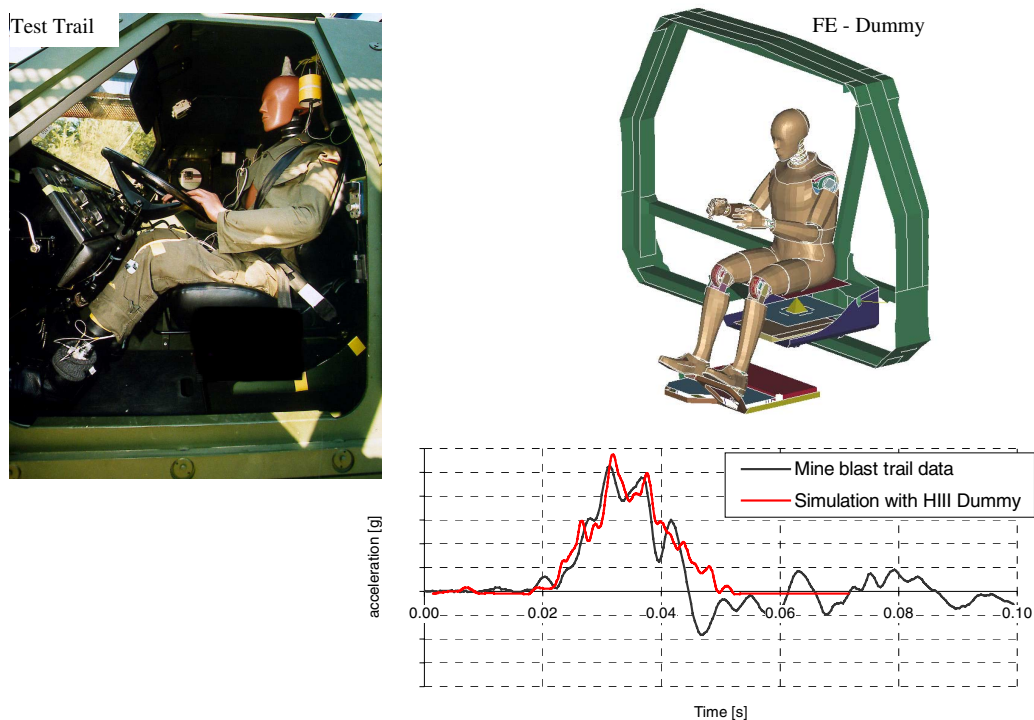
Figure 6:   Comparison of calculated and measured vertical g loads in the pelvic area of a Hybrid III dummy

4.3   Mine Simulation

An FE computation model is based on a CAD model of the vehicle structure. During the development phase, the calculation engineer and design engineer consult each other to make sure that the CAD model of the vehicle stucture can be meshed easily. In this way, it is possible to avoid the frequently considerable effort required to generate a intermediate surface model capable of being meshed. The generation of intermediate surfaces from the ProE data is possible with the assistance of the ProENGINEER module ProMECHANICA. For meshing and the further set-up of the computation model, the FE program ANSYS is used under the ANSYS/LS-DYNA user interface. This is where the vehicle equipment relative to mine protection (e.g. floor liner, stiffening profiles, tank, transfer boxes, etc.) are added, the contacts of the component parts among one another are defined as well as loads are applied and further boundary conditions defined. Also carried out as part of ANSYS is the installation of the dummy in the model as well as the correct orientation of the limbs.

A great deal of attention must be given to those components that are located between the inner and the outer vehicle floor. These components, such as the transfer box, tank or floor liner, reduce the load on the mine protection floor by their very mass (shock absorption) when they are hit and accelerated by a dynamically denting floor structure.

These components must therefore be included in a simulation. However, in conjunction with the simulation, they also represent a good opportunity for design and optimization.

For the actual calculation of the model, the explicit, non-linear equation solver LS-DYNA is used. For the usual model sizes of 100,000 – 300,000 elements, LS-DYNA requires approximately 20-30 hours on a workstation (SGI OCTAINE2) for a computation period of 20 milliseconds, depending on mesh refinement and model structure. Owing to the relatively small storage capacity requirement of LS-DYNA, such an analysis can also easily be performed on a well-equipped PC.

The evaluation of the computation results is subsequently carried out in the LS-POST processor. LS-POST also includes the output and evaluation of the dummy stress values.

The FE model for the explicit dynamic analysis shows a very high level of detail and a high mesh quality. This FE model can therefore also be used without any major effort to conduct implicit static structural analyses or modal analyses.

4.4 Load Introduction

The level of protection of the vehicle is normally specified by the contracting authority. It can be used to calculate the effective energy, the local and time-related impulse of the mine and to derive load conditions for the simulation. Loads created by a mine blast are introduced into the vehicle structure in the form of a pressure distribution on the vehicle floor variable in terms of time and location. In this case, time-variable pressure loads are applied to the vehicle underfloor in a radial pattern starting from the centre of the blast, Figure 7.
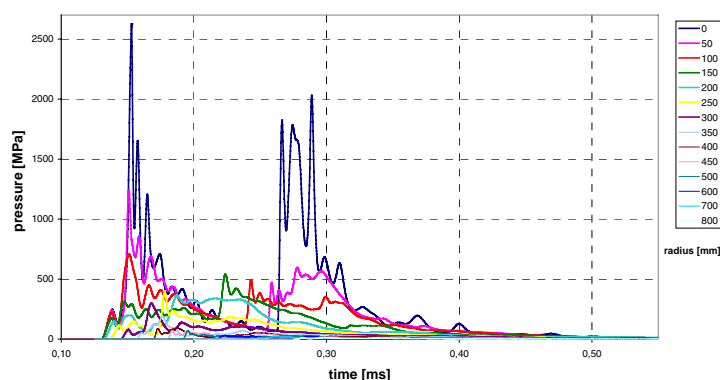
Figure 7: Pressure distribution of a mine blast at 500 mm distance from the floor (freely positioned in a steel collar)

The time-variable pressure distribution is determined as a function of type of mine, type of emplacement, soil condition, underbody ground clearance, shape of the underbody and radial distance from the centre of the blast. The pressure distribution is calculated by means of the SHAMRC program, an explicit simulation program (2D-Euler Code) /7/ operating with higher-order finite differences. The calculated mine load cases have been validated through simulated blast tests with steel plates and vehicle structures.

In the complete vehicle simulation, the decoupling between the load simulation and then structural response analysis is possible, in those cases where loads occur instantaneously as in the case of mine blasts, when boundary conditions (ambient geometry) vary only slightly during the period of load introduction. While the dynamic vehicle floor deformation takes on the maximum value after appr. 1.5 to 3 ms, the pulse load of a mine laid on the surface will have reached almost its final value after 1 ms. The peak pressure at the centre of the blast even has only an effective period of up to 0.3 ms after the start of the blast.

The interaction between the propagation of the detonation fumes and underfloor deformation can therefore be neglected in a first approximation. This permits the separation between load simulation and simulation of the structural response.

4.5   Example: Mine Blast Under Driver's Station

In a mine blast, the vehicle outer floor is dented instantaneously. Components (e.g. propeller shafts, transfer boxes) located directly above the vehicle outer floor are thus subjected to g loads and partly impart the deformation to the inner floor (Figure 8). Depending on the position and orientation of the feet or lower legs, injuries to occupants may result if the necessary safety distance from the inner floor is not sufficient or if the contacting structure is too stiff.
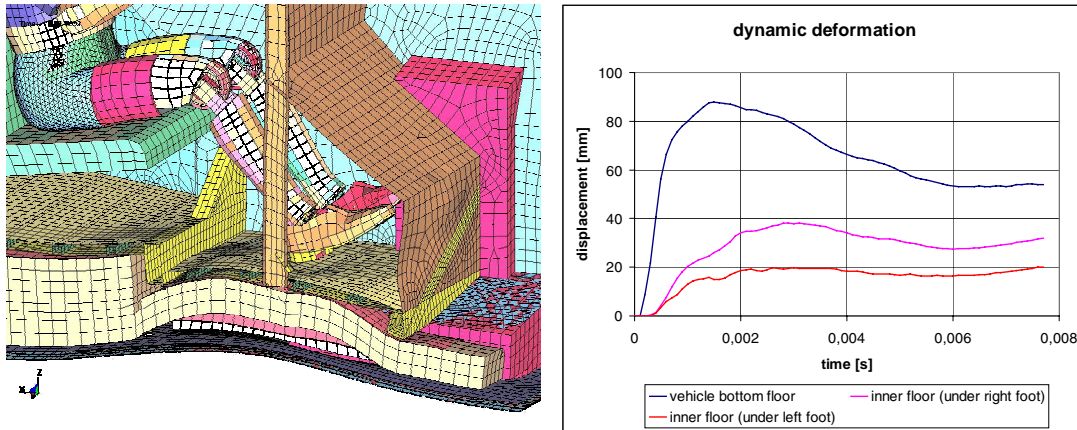
Figure 8,9: Deformation condition after a mine blast in the driver's foot area

Figure 9, the structural response of the vehicle outer floor and inner floor to a pulse-like mine blast. As can be seen, the inner floor of the vehicle is still heavily deformed owing to the coupling effects in the intermediate floor area. Figure 10 shows the effects on the driver's feet resulting from the deformation of the inner floor with the assumed safety distance and the assessment criteria. While the left foot of the driver is not notably stressed, the right foot is exposed to distinct but still negligible loads. Based on such considerations, the blast simulations make it possible to largely analyse the interaction between the vehicle outer floor, intermediate floor components and inner floor in order to be able to take suitable measures for structural optimization. The dummies are used to define the necessary safety distance (footrests) between feet and inner floor or to determine non-critical crew stations.
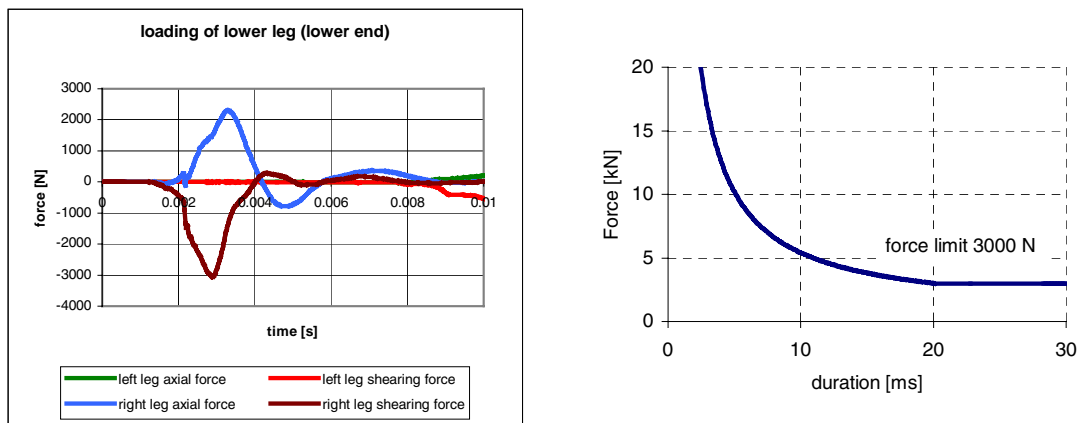
Figure 10: Forces acting in the lower area of the driver's lower leg in a mine blast underneath the driver's feet and assessment criteria

5   Simulation and Analysis of Vehicle Dynamics and Mobility

In the concept phase of vehicle development, driving dynamics and mobility analyses are of special importance in order to determine the loads, required spring travel and steering angles. The space claim of suspension and steering in turn determines the payload area in the vehicle interior and thus the total vehicle concept.

Real test tracks are modelled to simulate and assess the mobility of the vehicle. The geometrical description and discretization of the virtual road and terrain profiles as well as single obstacles are performed with FEM. The surface characteristics, such as coefficient of friction and compliance, are allocated to the individual elements.

In future, load cycles will also be determined on virtual test tracks in addition to mobility assessments. During the development, the calculated load cycles are to be used for structural analyses, computational component part life assessments to activate test stands.

5.1   MBS - Model

The fully parametric MBS complete vehicle model, Figure 11, is composed of the following sub-models and functions, using ADAMS/CAR:

- Chassis and suspension components
- Axle and steering kinematics
- Drive model (torque control); with differentials
- Tyre model
- Spring/damper elements
- Active suspension elements with controllers
- Driver model (steering and speed controller)
- Trackway profiles (terrain courses, bad roads, single obstacles)
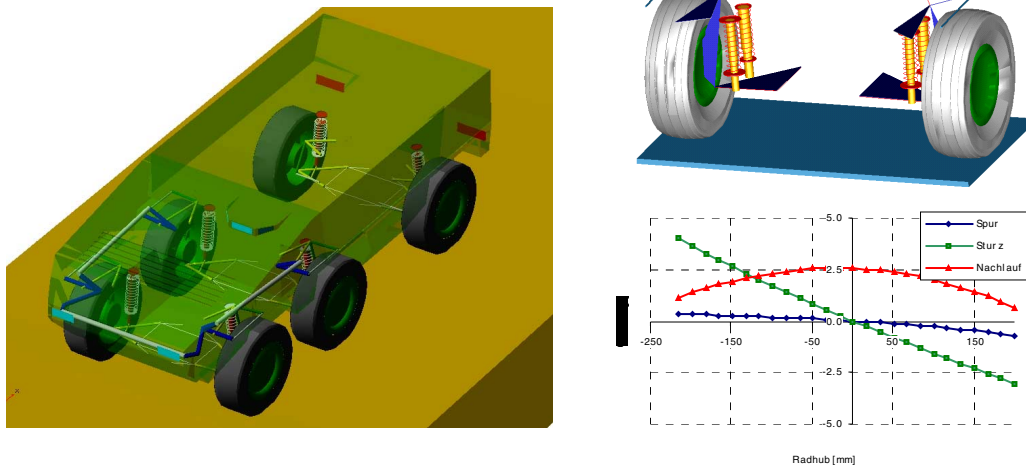
Fig. 11: MBS-Model 6x6 Off-Road Vehicle

The individual axle systems are built up from the kinematic points, the structures, joints and force elements. The spring/damper system can be replaced with active elements using control algorithms.
In the case of the tyre model, the measured data of the tyre manufacturers are used in the Pacejka 89 format. It is possible to provide a 3D contact between the contact patch and road profile. The various 3D trackways are reproduced with triangular elements.
The driveline is reproduced from the wheels to the transmission output shaft. Lockable transverse and longitudinal differentials are used. The torque acting on the transmission output shaft is controlled by the driver model.
The driver model is an intelligent model and controls the steering angle, input torque and brake forces.
The individual systems are easy to replace and modify. During the concept phase, it is possible for example to assess and select centre-of-gravity positions, wheelbases, different axle concepts and suspension systems.

5.2   Assessment Criteria

The mobility of a vehicle is generally assessed at the maximum possible average speed on specified terrain courses. The maximum off-road speed is generally limited by traction, input torque, driving safety and ride comfort.

When obstacles are to be negotiated, the speed at which a maximum driver's station vertical acceleration of 2.5 g occurs, the pitch behaviour and vibrations under bad-road conditions are the subject of the assessment. The reference criteria are data obtained from similar off-road vehicles.

In terms of handling, the objective is neutral or a slight understeer behaviour. The roll reactions are to be minimized. Also desirable is a broad and easily controllable handling limit. This assessment is based on the methods used by the commercial vehicle and car industry.

5.3   Simulations

The following capabilities are verified through mobility analyses:

- Negotiation of single obstacles (step, ditch, ridge)
- Movement on rolling terrain (sinusoidal, offset sinusoidal)
- Bad-road conditions (Belgian block, washboard surface)
- Movement on soil with limited load-bearing capacity

The dynamic driving behaviour in double lane changes, fast cornering, braking in bends, is simulated on different coefficients of adhesion.

5.4   Results – Mobility analyses

Figure 12 shows a comparison of the calculated and measured vertical g loads acting on the driver's station of a 6x6 vehicle when crossing a single obstacle at 60 kph. The use of highly effective bump stops keeps the vertical acceleration below the allowable value of 2.5 g.

Figure 13 shows the cornering behaviour of a 6x6 off-road vehicle for different speeds on dry and wet pavements. Following optimization of the axle kinematics, slight understeering was achieved for all required load conditions. The vehicle remains safely controllable at the handling limits.
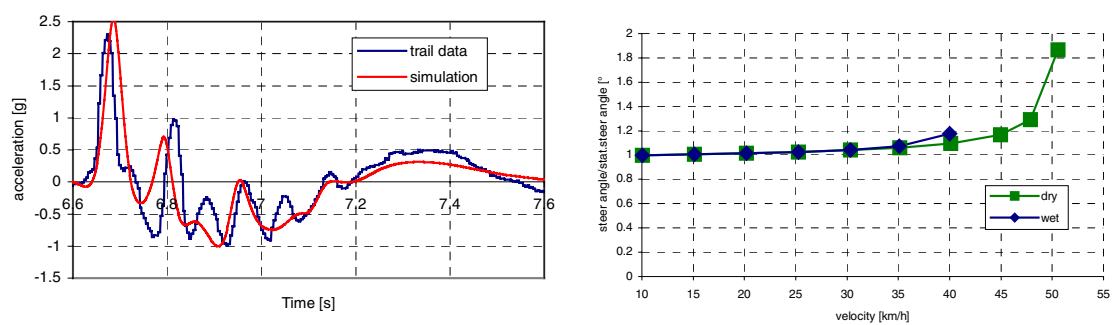
Fig. 12,13: Harmonisation simulation-measurement Single obstacle at 60 kph , Steering behaviour

Figure 14 shows the mobility required for off-road vehicles with the vehicle moving on a ramp at 40 kph. The virtual tuning of the spring/damper system (including the hydraulic bump stops) and the required wheel travel was defined during the mobility simulation runs.

Figure 14: Ramp 1.5m at 40 kph; virtual and physical prototype

Driving safety and ride comfort of a vehicle are essentially influenced by the spring/damper system. Figure 15 shows the effect of a passive and partially active spring/damper system on bad roads and on a sinusoidal course. The simulation shows that the use of active spring elements can significantly reduce the level of vibration and pitch movements of the vehicle. On terrain courses, this helps achieve a greater average speed.
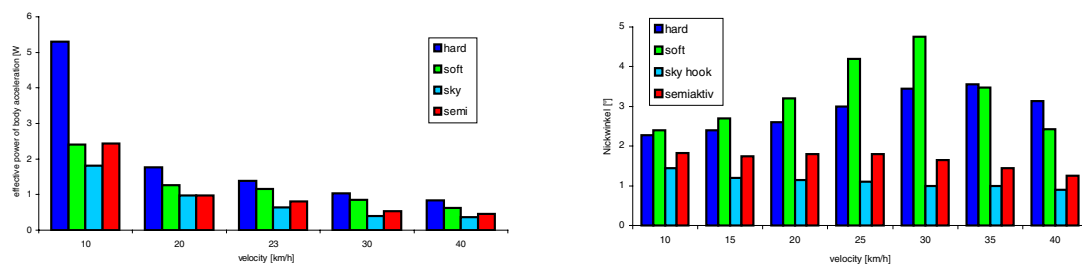
Fig. 15: Comparison of the effect of an aktive (sky hook controlled) and passive spring/damper systems on bad roads

6   Summary and Outlook

Simulation today is an integral part in the development process for new armoured vehicles. The use of simulation tools makes the result of a development predictable and design solutions can be verified or changed or optimized early on in the program. The identification and quantification of discrepancies permit fast decisions and trade-offs between different approaches.

This paper shows the importance of virtual prototypes in the development process to reduce development cost and times. Owing to more stringent protection requirements, the design and optimization of new light armoured vehicles is possible only with the assistance of complete vehicle simulations. To design the suspension and assess vehicle mobility, simulation runs are conducted with verified vehicle models and virtual test tracks. Mine protection is designed and assessed with the assistance of complete vehicle simulations using FE dummies.

The plans for the future are to replace partial qualifications of vehicle variants with simulations in order to further reduce the number of required prototypes. At this time, it is not yet foreseeable that prototypes will become totally unnecessary, as numerical simulations can only answer questions that are explicitly factored into the model. No direct statements can be made on manufacturing influences, spreads in material characteristics and test conditions. The reliability of the solutions calculated can however be assessed with stochastic simulations, e.g. based on the Monte-Carlo Method /8/.

Literature

/1/ Using ADAMS / CAR
Mechanical Dynamics, Inc., Ann Arbour, Michigan; 2001

/2/ MATLAB Relase Guide 12.1
The Mathworks,Inc., Natick, MA; 2002

/3/ Users Manual ANSYS Version 6.0
ANSYS,Inc., Canonsbourg, PA; 2002

/4/ Users Manual Pro/Engineer 2000i2
Parametric Technologie Corporation, Needham, MA; 2001

/5/ Users Manual for LS/DYNA3D
Livermore Software Technologie Corporation, Livermore, CA;2001

/6/ Hönlinger,M.; Glauch U.:
Mobility Analysis of a Heavy Off-road Vehicle Using a Controlled Suspension.
RTO AVT Specialists' Meeting on "Structural Aspects of Flexible Aircraft Control".
Ottawa, Canada; October 1999

/7/ Shamrc
Applied Research Associates, Inc, Albuquerque NM

/8/ Reuter,R.; Hoffmann R.:
Assessment of Analysis Results Using Stochastic Simulation Methods.
In VDI Berichte 1559, Numerical Analysis and Simulation in Vehicle Engineering,
VDI Verlag, 2000.

A Preliminary Engine Design Process for an Affordable Capability

M.J. Jones, S.J. Bradbrook and K. Nurney
New Projects Engineering, Rolls-Royce plc
Bristol, PO Box 3, BS34 7QE
United Kingdom

Abstract

This paper will examine the military engine preliminary design process used by Rolls-Royce to support 'capability vs. cost' trades conducted at the weapon system level.

The engine is a major sub-system of all air vehicle assets making up a force mix. Changes in the engine capability, e.g. thrust/weight and specific fuel consumption, can be tracked through to air-vehicle performance and ultimately to the force mix capability. In the same manner these changes will impact on the engine and air-vehicle life cycle costs and hence the total system costs.

These trades are vitally important in establishing the optimum affordable system solution early in the design and development cycle thereby preventing the need for expensive changes during full-scale development.

Rolls-Royce has developed a preliminary design process to quickly assess engine capability incurred costs. The process has evolved to enable the rapid definition of an engine including performance attributes and Through Life Costs (TLC's).

1.0 Introduction

Military engine designs are no longer focused solely on achieving performance targets, the cost of achieving that performance must be understood. This cost is incurred on several levels, those being unit, development, in service and disposal costs the summation being referred to as through life costs (TLC's). Modern military equipment procurement policies are now more dedicated to providing affordable capability. It is important that this trend is reflected in the design practices within the industries that support the armed forces. Rolls-Royce has recognised this and has developed preliminary design (PD) tools to enable affordability to be assessed at the concept stage of an engine design. This paper will give a brief description of these tools and will also present an example of a study carried out on the engine options for an unmanned combat aircraft (UCAV).

The Rolls-Royce design process is separated in six distinct groupings that take the engine from its early beginnings to retirement. This process is referred to as the "Create Customer Solutions Cycle" (formally Derwent) and is depicted in figure 1 below.

Preliminary Design - where and why

Product Life Cycle - Rolls-Royce Create Customer Solutions Cycle
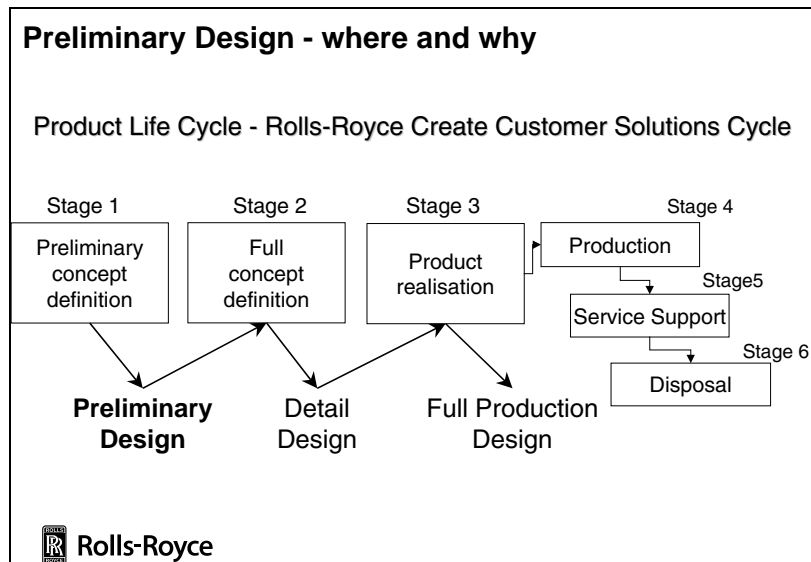
Figure 1. Rolls-Royce development cycle

The preliminary concept definition phase, stage 1, outputs a preliminary design and describes the functional attributes, including cost, that the engine or power system will exhibit.

Preliminary design is a key stage in the design process especially with respect to cost. The basic definition of the engine's thermodynamic cycle defines the fuel burn, the definition of the architecture and hardware defines the weight and so on, all of which have a direct impact on the in service costs.

However, during the preliminary design phase there is a paradox presented: there is little product knowledge but there is a powerful impact on the final design.

The aim therefore of any preliminary design tool set or process is to eliminate as much uncertainty as possible, to increase product knowledge and enable design trades and options to be understood.

The impact of design knowledge vs. determined product cost is depicted in figure 2 which shows that by the end of stage 1, using traditional theory, 70% of the cost is determined but only 5% of the product is defined. The bold line indicates the desire of the Rolls-Royce preliminary design teams, to increase product knowledge in the early stages, to reduce risk for the company and importantly for the customer.
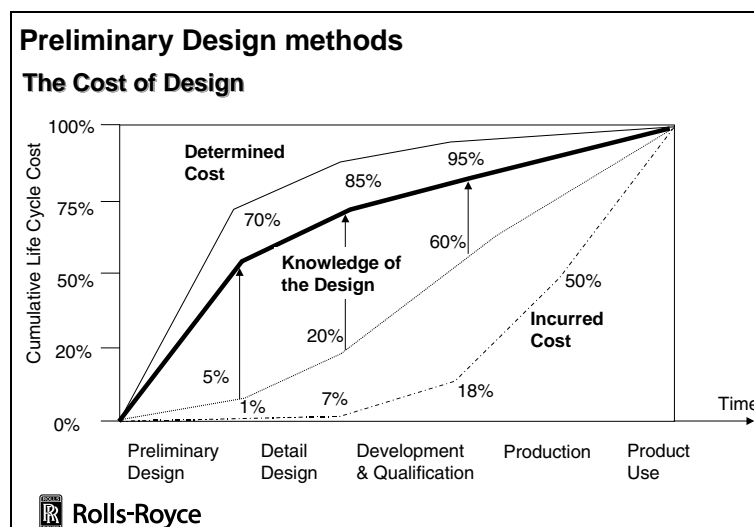
Figure 2. The cost of design vs. knowledge

In order to reliably understand the effects of design decisions in stage 1, it is necessary to have a reliable design tool, one that is also able to produce solutions quickly and enable the whole of the design space to be explored.

Rolls-Royce has developed several design tools to enable this design space exploration to be carried out in stage 1. The tools, which will be described in the first chapter of this paper, cover all the major data groupings:

1. Performance
2. Mechanical design
3. Unit cost
4. Aircraft performance
5. Development cost / inc. production investment
6. In Service and disposal costs

With the outputs from these tools the preliminary design teams within Rolls-Royce are able to assess the affordability vs. the capability of a new or derivative engine. A later chapter in this paper will present an example of a study carried out using these tools.

This paper will conclude by looking at the future of preliminary design within Rolls-Royce. This review will also consider the issues of data integrity and source.

2.0 Preliminary Design methods

The preliminary design process is started with a set of customer requirements that traditionally define the capability requirements of the airframe and power system. A typical requirement will specify the thrust (Fn) and specific fuel consumption (sfc) values around the flight envelope. From this limited data the definition of a possible engine solution can be started. The design iteration loop that is involved is shown in figure 3. This is of course a simplistic representation of the PD process, the iteration often being an order of magnitude more complicated.
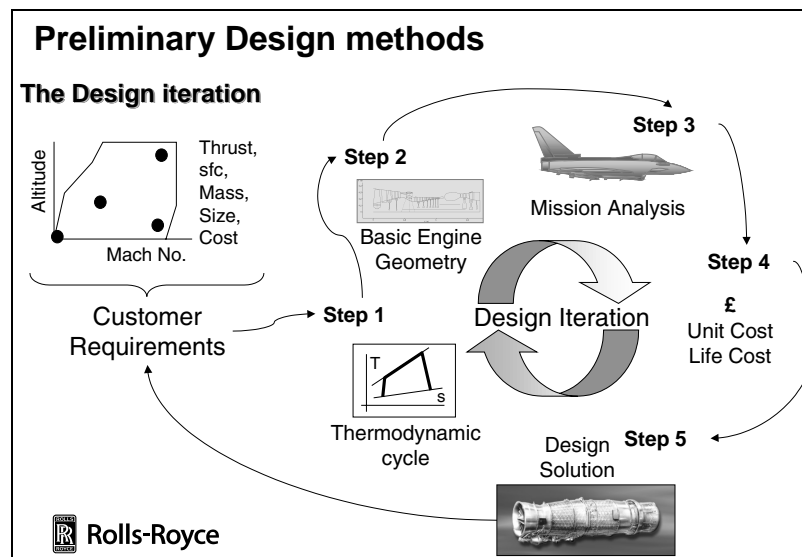
Figure 3. The PD design iteration

2.1 Thermodynamic cycle creation

The first step in the process is to create a basic thermodynamic cycle. This is where the first design choices are made, e.g. pressure ratio, bypass ratio, cycle temperatures etc. Using the Rolls-Royce tools, called RRAP (Rolls-Royce Analysis Programme) it is possible to generate station vectors or thermodynamic data at key stations throughout the engine. The programme makes basic assumptions about engine component characteristics.

2.2 Geometry creation

The second step in the process is definition of the basic engine geometry. This can be a more complex step than that taken by RRAP with the number of variables and the complexity of the calculation being much greater.

The software that is used to calculate these parameters is called Genesis. This programme has been developed by Rolls-Royce over the last 30. The programme is able to make basic assumptions about key aerodynamic and mechanical parameters to enable the calculations to be started. An automatic iteration process is then employed to find a solution.

A feature of the programme is the use of correlations based on a database of Rolls-Royce engines. These correlations are used by the programme to allow for real features and correct geometry for Rolls-Royce design practices and rules. This is done because the level of detail is insufficient at this stage in the design to define features such as seals, bolts, drive arms etc. The correlations allow these features to be accounted for in the mass results as appropriate. An example of this process is shown in figure 4 which describes pictorially how the corrections effect the shape of a high pressure turbine (HPT) disc.
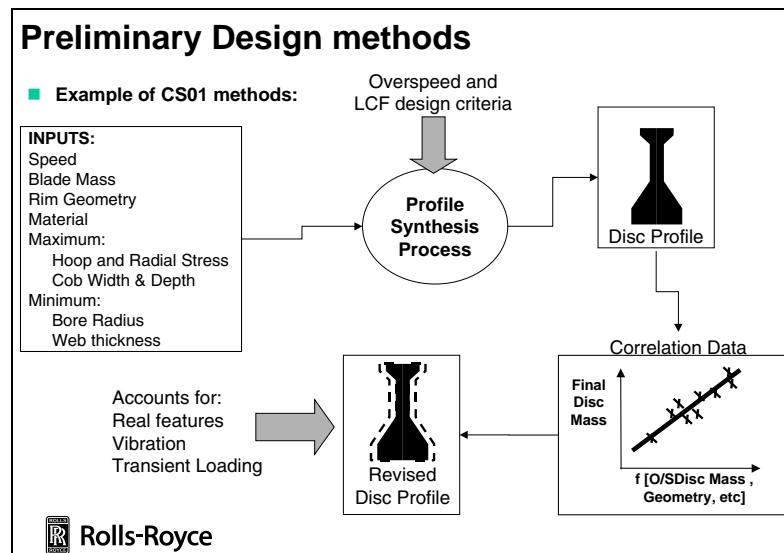
Figure 4. Genesis correlation effect

The main outputs from this element of the Genesis programme are the geometry and mass breakdown. The mass is defined for the whole engine (along with a centre of gravity) and also down to a reasonable level detail e.g. blades and discs.

Once these component attributes have been defined within Genesis this is passed downstream to the aircraft performance and cost analysis phases of the iteration.

2.3 Aircraft performance modelling

Aircraft performance modelling is generally the third step in the iteration problem and Rolls-Royce uses several codes to understand the effect of an engine design on the total weapons system. The most important to this phase in the design process is the scaling capability. This enable the engine to be scaled with the aircraft to understand how the size of the engine improves overall mission capability, e.g. larger engine, larger aircraft, more fuel = longer range. This information is critical to understanding the relationship between the customer requirements and exploring the trade between affordability and capability and its use will be shown later in the UCAV case study.

2.4 Cost calculation methods

The engine unit costing methods are again part of the Genesis package. They rely on geometric and mass data to define simple parameters such as features and numbers, e.g. compressor blades, discs etc. Correlations are applied to once again account for real world features.

The unit costs are calculated using a series of correlations and current cost rate information (manning and material data). The correlations account for scrap rates, casting features (e.g. runners, risers, inserts), machining times and assembly/test times, see figure 5 below.

Preliminary Design methods

Geometry & Mass
Numbers off

Correlation

Machining costs
£/hr

Correlation

Correlation

Whole engine assembly costs
- more parts more cost

→measure of complexity
+ Test costs

Cast shape = total mass used
Scrap rate + foundry labour costs
£/kg, £/hr

Engine
Unit Cost

Rolls-Royce
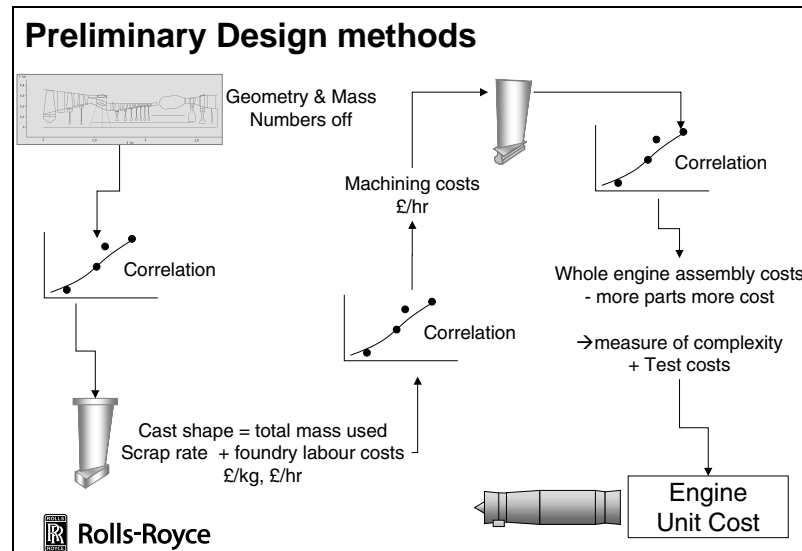
Figure 5. Genesis cost calculation

The development costs are traditionally calculated using correlations based on historical development programme costs. Recently methods have been developed to move away from this arguably pessimistic view. The new methods are risk based and allow the engineer to decide the level of "right-first-time" that will be achieved. This revision has been used to great effect when considering the development costs

The new methods provide the facility to vary the number of assets used during the bench and flight development programmes. Combined with a statistical analysis approach this method will output the least-likely or most-likely non-recurring costs.

The in service costs are calculated using information from the unit cost outputs with the addition of the following:
- Production investment
- Initial support, e.g. support equipment
- Maintenance material, e.g. engine spare parts
- Maintenance labour
- Sustained support, e.g. replacement support equipment
- Fuel and oil

The costs of the above service operations are calculated using a separate programme. This is an engine fleet maintenance simulation model that relies on statistical distributions to predict engine parts failure and rejection. This information is used to calculate investment spares and maintenance labour and material costs. The method takes account of; routine maintenance and inspection, probability of parts rejection due to primary failure, secondary damage or secondary inspection, and probability of repair or replacement.

Fuel and oil costs are approximated by using a mean mission fuel burn per hour, based on an historically derived % of the uninstalled engine max fuel flow. Oil is assumed to be a fixed factor of the fuel usage. The total cost per flying hour is then multiplied by the total fleet flying hours. Alternatively a more rigorous approach can be adopted whereby the engine capability is installed into an aircraft definition and then flown

around a defined mission to calculate total mission fuel usage. Codes for this process are available within Rolls-Royce and airframe manufacturers.

The individual cost elements are combined in the 'Engine TLC' routines together with fleet assumptions to calculate the total engine fleet TLC. These routines also calculate Production Investment, Initial Support and Sustained Support costs based on historical data and the fleet assumptions. In addition, the routines take into account other factors such as learner rates associated with large production runs.

3.0 Example of Trade Study

The following is an example of how the tools described in the previous chapter have been used for a recent engine study.

The aim of the study was to examine the options for a new UCAV due to enter service in the latter part of the next decade. The airframe requirements were received from the aircraft manufacturer and the study team chose to consider five different engine types:
  A. Off the shelf (available)
  B. Off the shelf derivative with additional current technology
  C. Off the shelf derivative with additional new technology
  D. All new engine at current technology levels
  E. All new engine with new technology

The examples of the engine architectures created in Genesis are displayed in the figure 6. The off-the-shelf engine (option A) is representative of a current military turbofan which is then modified (with a fixed core size) to give option B. Option C is derived directly from B with the addition of new LP spool technology. The new engines are D and E. Engine D is all new at current technology levels from and E is derived with the addition of new technology. The study team worked closely with the team from aircraft supplier to derive the scale and size of the engines.
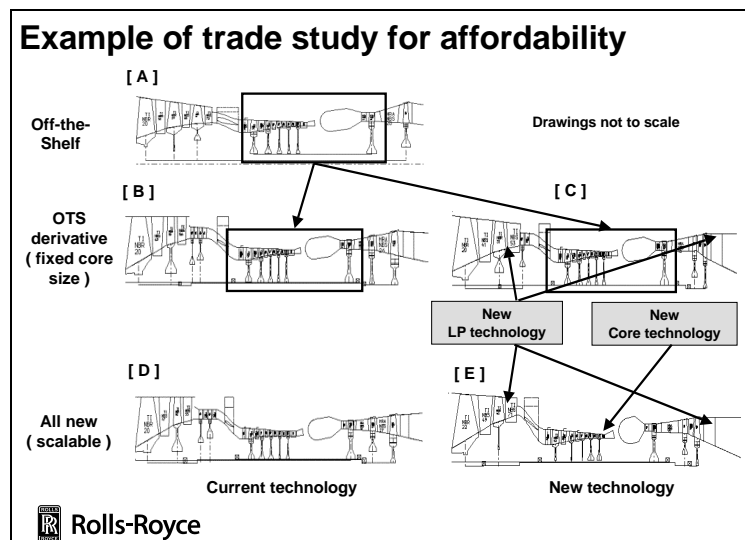
Figure 6. Engine architectures for trade study

The team took all of the engine options and created a series of cost models. The costs (unit, development and ultimately TLC) were calculated to permit a trade of capability vs. affordability.

The results of this study are plotted in figure 7. The engines are plotted against a datum requirement with the y-axis describing the relative TLC, the x-axis radius of action (a measure of capability), both as a % of a datum.
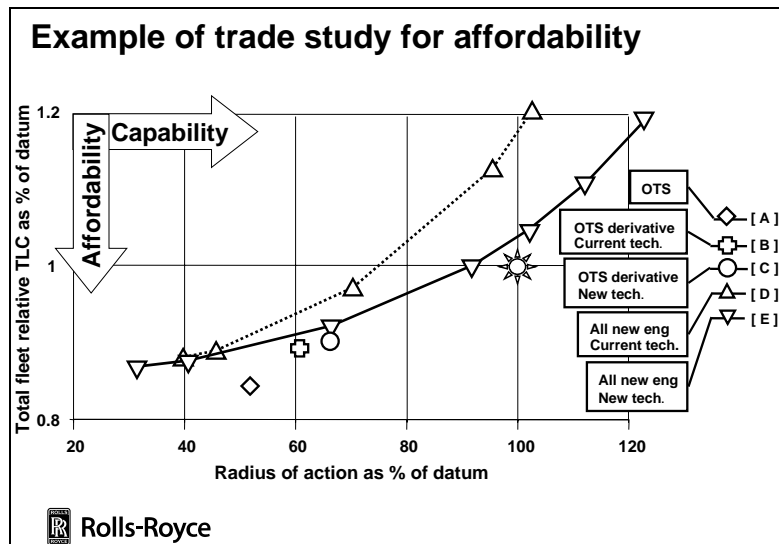
Figure 7. Capability vs. Affordability

The off-the-shelf engines are plotted as single points as they are of a fixed size whereas the all new engine have been scaled to permit a range of sizes. All engines have been modelled in a UCAV with a constant payload and in-flight performance.

From figure 9 it can be seen that the OTS engine achieves approximately 50% of the datum radius-of-action but for 16% lower TLC. A derivative engine, with current technology, will increase the radius-of-action to 60% of datum for an 11% saving in TLC relative to the datum. This is due to the better SFC of this engine and the higher thrust enabling a larger fuel fraction. Technology insertion into the LP system of the derivative engine increases the radius-of-action by a further 6%, relative to the datum, for virtually no increase in TLC. This TLC is approximately 6% less than an equivalent current technology all-new engine. For increases in range greater than this it is necessary to use an all-new engine where the scale of the engine can be increased to match the increase in vehicle size. There is a steady increase in LCC with radius-of-action as vehicle and engine size increases. At all but the lowest levels of radius-of-action the new technology all-new engine achieves a given radius-of-action for a lower LCC. This is due to the better SFC and the higher Thrust/weight ratios, both of which enable smaller and lower cost air-vehicles.

This study is an example of how affordability can be traded against capability and the next chapter will go on to discuss the future of the tools used to calculate this type of data.

4.0 Improving the solution

The dilemma faced by any preliminary design team is the need for accurate and comprehensive data and the obvious lack of any data at all. The following chapter will look at the relative accuracy of the Rolls-Royce PD tools and also review studies for future improvements.

4.1 Accuracy of the solution

The Genesis tools described in the previous chapters use a set of basic correlations against existing engine designs to provide the start point and enable the calculated data to be corrected for the real World. The accuracy of this method is relatively good as depicted in figure 8 below. The accuracy of the solution depends on the nature of the engine, e.g. mixed turbofans are generally very well modelled in Genesis, however, significantly different architectures are less well modelled.
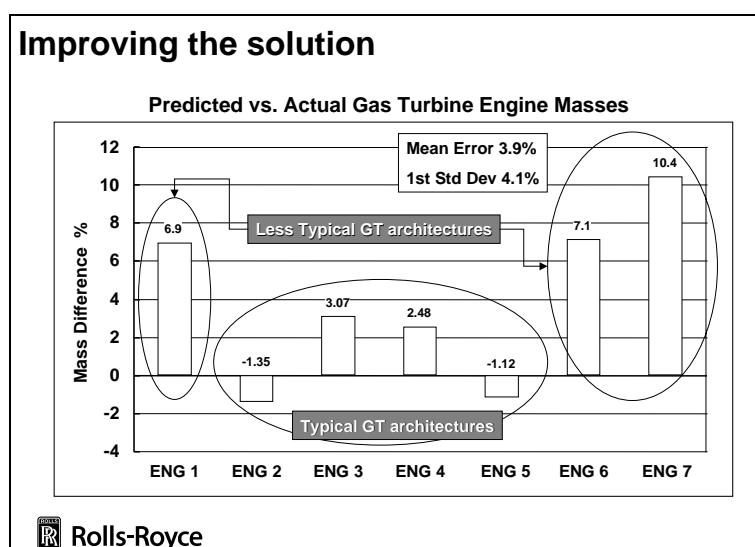
Figure 8. Accuracy of Genesis models

The differing levels of accuracy are due to the database being more populated with data from some types of powerplant, an obvious drawback with the correlation based methods employed. However, the mean error is only in the order of 4%, an accuracy level that is acceptable for this type of stage 1 tool

4.2 The design space

The example study that was carried out and described in the previous chapter highlighted the need for a comprehensive survey of the available design options. By completing a full survey, the proper choice between a new or derivative engine can be made and the proper compromise between capability and affordability chosen.

The next question asked of the preliminary design tools and methods is how to improve the coverage of the design space especially where a solution is more likely to develop. This improvement can be achieved through reduced computation times or use of computer driven intelligent optimisation techniques.

The computation time varies depending on the tool that is being employed. The definition of computation time can be simply defined as the time taken for the computer to execute a series of commands and achieve an answer. With today's computer systems this is less of an issue, the computation time for these relatively simple codes is small. The definition of computation time must therefore be broadened to include the time taken to first generate and subsequently modify the model.

The computation time for a full Genesis geometry model, using the above definition, is in the order of 25 hours for a new model, falling to approximately 10 minutes for a derivative model. This can be compared to the time taken to produce a full TLC model, a more complex and more stage 3-biased tool. On average a new TLC model can take over 80hrs falling to 25 hrs for a derivative model.

It is clear from the above comparison of computation time that a bottleneck downstream of the basic product data creation occurs. Methods development should be directed into this field especially if affordability is to be better understood and for it to emerge as a primary design driver.

Intelligent optimisation is the next step, providing that the time taken for each leg of the calculation is reduced to a more realistic time frame. There are many software codes available in the marketplace that are capable of multi-attribute optimisation (MAO). However, the real difficulty lies in defining how to move the gas turbine engine in a computer based optimisation environment and still use existing "tried-and-tested" modelling codes.

The intelligence in today's optimisation activities are driven by engineers with experience and a great understanding of the nature, form and being of a gas turbine engine. For true MAO to occur using this human interface will be extremely time consuming even if computation times are reduced. The computer offers the better solution but in order to achieve this transition, the computer will have to learn how the gas turbine

works, learn how the armed forces operate engines and learn boundaries and limits to the mechanical machine. Research is underway in one of Rolls-Royce's groups within the USA in partnership with a technology University but the results are unfortunately not yet available.

A feature of computer driven optimisation is the need for the limits of design and the range of customer requirements to be defined simply and in such a way as to be understood by an computer. The next few paragraphs will describe one possible method of improving the understanding of customer requirements.

4.3 Understanding the Customers Requirements

The design limits are relatively easy to define, and indeed they can be bracketed to allow for new technology to be input into the process. However, customer requirements are not as easily understood or refined.

The solution to this is still being debated, however, a possible remedy has been developed and reviewed by the preliminary design team in Rolls-Royce. The solution is based on an analysis method developed by Japanese industry in the post-war period called Quality Function Deployment (QFD). QFD enables the engineering teams to take a set of customer requirements, weight them and turn them into a set of engineering attributes. An example of the customer requirements being used in current QFD analysis is shown in figure 9 below.
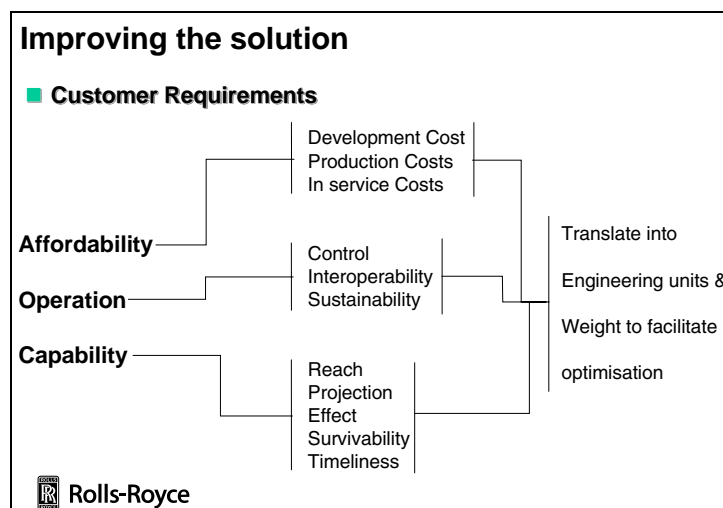
Figure 9. QFD customer requirements input

QFD enables the customer requirements, or WHATS, to be scored against the design criteria or HOWS. An example of the type of output being generated by the Rolls-Royce process is displayed in figure 10 below.
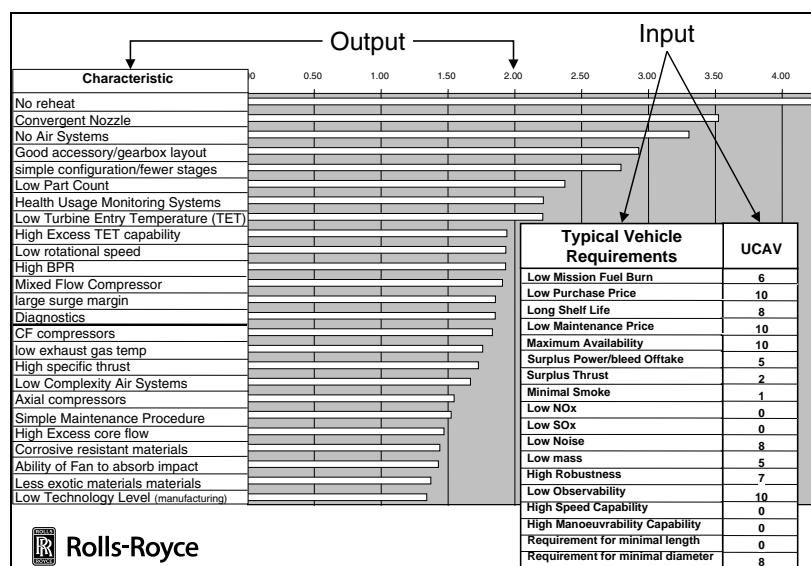
Figure 10. QFD example outputs

In the example above, the customer requirements are predominately focused on low cost and as a consequence the outputs focus on items like no re-heat, low parts count and simple configuration. Using data of the type produced by this example would eliminate some of the options available in the process, e.g. re-heat, and using the basic high level scoring of the customer requirements the optimisation could goal seek more effectively.

5.0 Learning from the past

Looking across the CCS life-cycle there is engine data available in all stages, the accuracy of the data improving as full maturity is reached. Returning to figure 3, the opportunity to increase the design knowledge and therefore reduce risk in stage 1 for derivative or growth engines is great.

A good example of where this opportunity will have greatest effect on affordability is reliability data. The reliability of engine hardware in service is extremely difficult to calculate let alone predict. However, it has a significant effect on maintenance requirements hence LCC and affordability. Therefore, if stage 4 data from fleet engines is imported into models used in stage 1 the accuracy of the solution will only be enhanced.

This future desire for data compatibility throughout the whole life-cycle of the gas turbine engine is currently being designed and worked by teams within Rolls-Royce. The systems design challenges are significant, however, they are perhaps less significant than those of getting the data from in service engines. Co-operation between manufacturers, suppliers and operators will be essential to achievement of this vision through the use of e-enabled environments.

The benefits to the Customer and manufacturers will be reduced risk, the opportunity for more right-first-time programmes and the reduction of overall TLC's. Of course, having more accurate stage 1 data does not lead automatically to this conclusion and it must be complemented by continued capability acquisition through rig or engine test data. However, it will mean that cost will be determined on the basis of robust data early in the design process where the level of design freedom is highest.

6.0 Summary

Rolls-Royce has developed a series of tools that enable is to quickly and reliably define gas turbine engines for the purposes of preliminary design. These tools define cycle data, geometry, mass, unit cost, development cost and finally through life costs. They have been developed to bridge the gap between the knowledge of a design and the determined cost of that design, the aim being to better predict the total impact of design decision as early as possible in the process.

The majority of the tools are at a level of maturity that would make further development a classic case of diminishing returns. However, some of the tools, especially those that have a significant impact on the ability to fully explore affordability aspects of a design are in need of development.

This paper has presented an example of the output from these tools and demonstrated an ability to assess the trade between capability and affordability. The intention behind this is to enable the customers of the future to define the acquisition in terms of capability but also in terms of affordability. To aid this process, Rolls-Royce is developing processes and tools that will enable customer requirements, specified in general terms, to be turned into engineering specifications and weighted to account for their relative importance.

The future of preliminary design tools described in this paper may be somewhat more complex. There is work ongoing within Rolls-Royce to enable more comprehensive surveys of the design space, to further bridge the gap between determined cost and knowledge. This future may include more automated optimisation and more sharing of data across the engine life-cycle. However, the challenges that these futures present are not to be underestimated and will require a great deal of co-operation between all levels of the manufacturing chain and the customer alike.

7.0 Acknowledgements

This page has been deliberately left blank

_____

Page intentionnellement blanche

Scenario-Based Affordability Assessment Tool

Max Blair
Air Force Research Laboratory
Wright-Patterson AFB, OH 45433-7542
USA

Mike Love
Lockheed Martin Aeronautics Company
Mail Zone 2824, PO Box 748
Ft. Worth, TX 76101
USA

Introduction:

Conceptual design in a technology-driven environment happens when reliable and rapid analysis procedures respond to creative design ideas. The value of a design depends on a number of factors. These factors include accurate weight and cost estimates. The Scenario-Based Affordability Assessment Tool (SBAAT) concept addresses these factors with a new approach toward product development and technology investment planning. The resulting design environment (code named MISTC) is currently in the earliest stages of commercial development.

Product development derives benefit from high fidelity data early in the design process. Design intelligence is developed and decisions become responsive to high-level changes. The output of this high fidelity design process allows a system definition with a lower development risk. The authors believe these assumptions are commonly held among the majority of designers.

The improved design activity described in this paper has been called "concept refinement" (CR). CR is appropriate after mission requirements and configuration concepts have been established. These starting concept designs are based on historical regressions and intuition for weight and cost. The CR phase adds significant knowledge where the concept design deviates from historical precedent. The proposed CR process involves the integration of geometric design tools (for vehicle level innovation), knowledge based modeling tools (for rapid product description and modeling), high fidelity modeling tools (for physics-based data generation including manufacturing cost) and operations modeling tools (for system effectiveness studies such as engagement modeling done for the military). Through a philosophy of smart product modeling, the CR process is facilitated. To prove the utility of these assumptions, the Scenario-Based Affordability Assessment Tool (SBAAT) is a design-modeling product, which draws from several commercial sources including MSC.Software and TechnoSoft Inc.

The Air Force Research Laboratory (AFRL) and Lockheed Martin Aeronautics Company (LM Aero) have joined in the cost-shared development of a dual-use product-modeling environment for guiding a concept refinement process in terms of affordability. The target customers will include vehicle manufacturing industries (aerospace and automotive) where early decisions in product development have large consequences in subsequent production. AFRL interests lie in the development of a modeling environment for technology assessment, which anticipates (by necessity) military system product development. The target military application is the Simulation-Based Research and Development (SBR&D) initiative at AFRL Air Vehicles Directorate. At the heart of SBAAT is AFRL's role in identifying technology needs and prioritizing technology solutions with unprecedented attention to affordability issues.

The objective of this paper is to describe and document the practicality, usefulness and payoff in the proposed CR process for meeting affordability interests related to new product design and vehicle technology development.

Simulation-Based Research and Development:

SBR&D provides a common, affordable and flexible environment to improve all phases of a technology's or weapon system's life cycle. In Figure 1, the components of SBR&D are depticted. These are (1) the design analysis process (2) the weapon system analysis and (3) the cost analysis. These three components are all required to generate a meaningful Distributed Product Description. A number of new software developments are required before this process will respond at the envisioned high rate and with the required fidelity. The SBAAT initiative described in this paper will support the rapid Design Analysis component.

The rapid response of the CR models is dictated by the needs of the SBR&D process. SBR&D operates at the engagement level with different mixes of mission objectives, blue and red team assets, and proposed technologies (either individually or integrated as a package). CR models must be rapidly synthesized to set up the SBR&D experiment and capable of overnight reconfiguration with new datasets reflecting new concept capabilities afforded by technology variants.
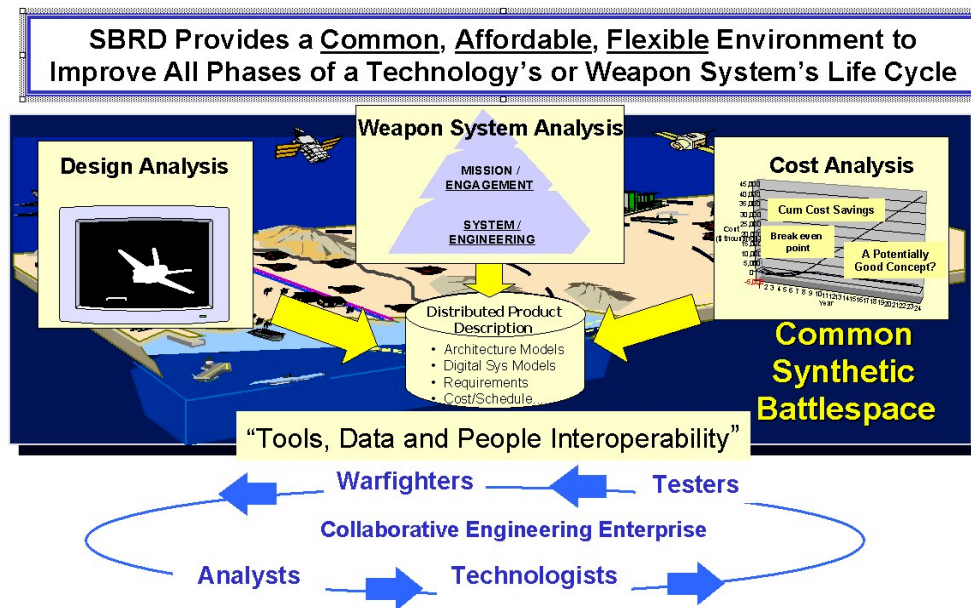
Figure 1: Elements of Simulation-Based Research and Development Initiative

Candidate SBR&D scenario scripts:

The recent proliferation of UAV concepts requires the military to take a fresh look at technology investment. For instance, with the pilot safely out of the cockpit, the relationship of vulnerability and cost can be revisited. For instance, SBAAT will help technology planners identify the best investments for maneuverability and stealth technologies.

The military focus on hypersonic systems also requires a fresh look at technology investment. The cost of sustained hypersonic system operations is heavily influenced by maintenance costs associated with thermal systems. SBAAT will help technology planners identify the best technology investments for affordable operations. For instance, research and development for reducing the cost of hot structures products may be given higher priority over extending hot structures performance.

Background:

Adaptive Modeling Language (a product of TechnoSoft Inc known as AML) has evolved from an in-house (Materials Directorate of AFRL) feature-based design project to a commercial product in use by a number of industries. AML is an object-oriented environment with built-in dependency-tracking and demand-driven calculations that facilitate the integration and control of all aspects of the design process. With dependency tracking, AML facilitates the control of a large number of design alternatives with a single set of driving requirements. Dependency tracking can also be used to facilitate design parameterization and rapid product description through associative properties. With demand-driven calculations, the designer can readily control when and how design information flows.

A significant number of design process innovations have arisen from the AML and it's Web-enabled Design Environment initiative (ref 9 - 11). They cover a number of topics including concept modeling, manufacturing, cost and optimization. Boeing Co developed the PACKS code (ref 5) for composite laminate process modeling. Currently, PACKS is under commercial development. LM Aero internally developed CAD-C in the AML environment for vehicle assembly planning. AFRL entered into a contract with LMAC, which led to the development of Scenario Based Synthesis (SBS), a pilot code for SBAAT development (ref 3). Foster-Miller was funded by AFRL to explore the potential for AML to model their processes with a view toward Web-enabled Design Environment. This proprietary work is documented in reference 12. SBAAT team member, MSC.Software, has developed MSC.FLD (Flight Loads and Dynamics) environment (ref. 13) to work seamlessly with their flagship products, MSC.Nastran and MSC.Patran. In addition, AFRL has invested in a number of other structures modeling innovations such as Interface Elements with Applied Research Associates (ref 6) and MSC.ASTROS for preliminary level multidisciplinary structural optimization (ref 7).

Past and ongoing in-house research in the application of AML in AFRL is documented in references 1, 2, 4 and 8. An early vision for the current development arose from references 1 and 2. An in-house cost-modeling endeavor was covered in reference 4. An example of ongoing in-house effort with joined-wing modeling is addressed in reference 8.
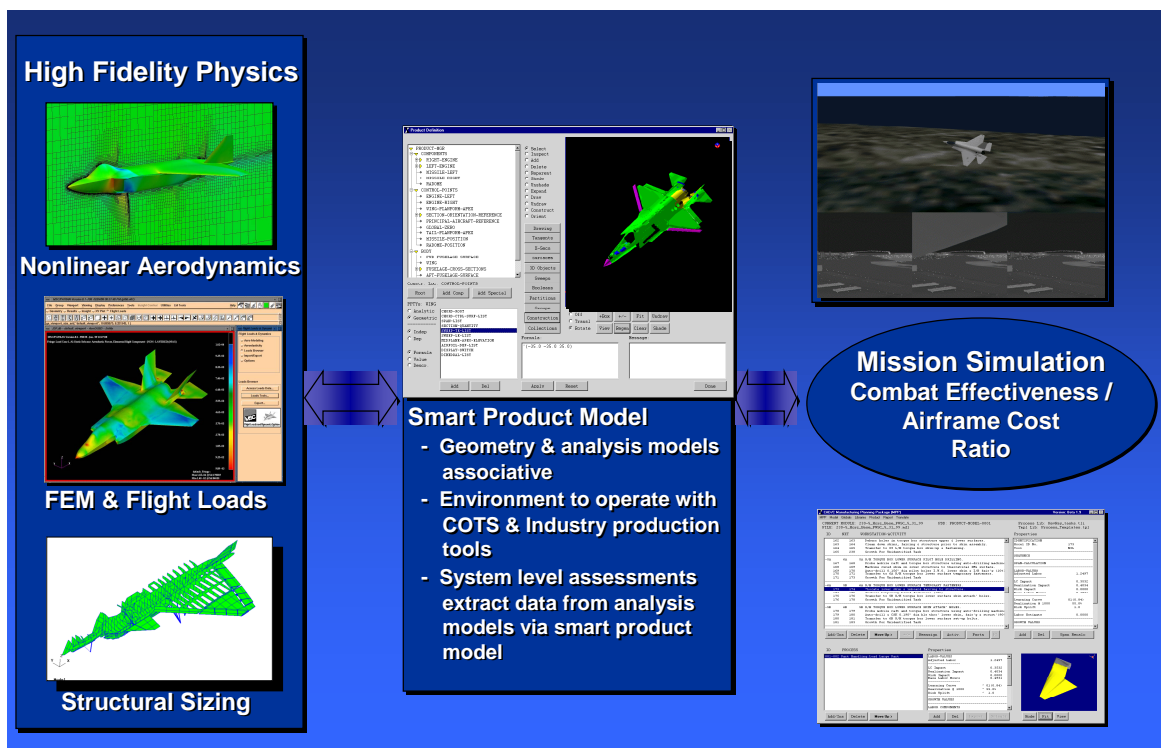
Figure 2: SBAAT Technical Vision is to Implement Smart Product Modeling for Rapid Assessment of Structural Integrity and Costs

Technical Goals:

The technical goals for this program range from successfully implementing the SBAAT conceptual approach to validating concept payoffs. Specifically, the SBAAT program will

- Create a streamlined software environment for integrating high-fidelity physics-based simulation tools with mission simulation tools
- Reduce cycle time for mechanical-structures concept definition, integrity analysis, and manufacturing cost assessment by 75%
- Integrate a process-based affordability assessment into technology development
- Demonstrate our proposed system in a USAF technology planning exercise and a commercial technology planning exercise.

These goals will be accomplished with available commercially based software products that are currently being used to model many products. The SBAAT team will provide integration of structural analysis tools such as MSC.Nastran, MSC.Patran, and MSC.FLDS (Flight Loads and Dynamics System). Through TechnoSoft's AML smart product model concepts will be implemented. Smart product modeling is modeling that builds automatic associativity between product description and product behavior. Smart product model requirements establish context of product development that facilitate layout, sizing, and producibility assessments of structure. Aircraft and automotive applications will be developed.

The technical vision for the SBAAT program is depicted in Figure 2. In the middle of the figure and the process is the development of product data and an associative smart product model. At the left side of the figure are the models that are required to evaluate the structural integrity of a product. At the right hand side of the figure are the system level metrics of the product. The desire is to expedite product behavior analysis such that the product user may understand the benefits of the product concepts and technologies in terms of system performance and cost.

Functional Description:

A primary objective in the SBAAT program is to define and develop smart product modeling relationships in a modeling and simulation environment that facilitates the types of studies performed in the concept development and technology assessment phase of product development. These studies are performed on configuration variants and historically, are known as trade studies. The process of evaluation includes definition of variants to be studied, development of product geometry and associated product data, assessment of product behavior and cost, and finally, a roll-up of behavior and cost into a system level scenario. The variants are evaluated across the range through established performance metrics. Metrics such as weight and cost roll-up into scenario based assessments such as life cycle costs and mission performance. The SBAAT program is focused on the structural integrity and costs aspects of the overall system.
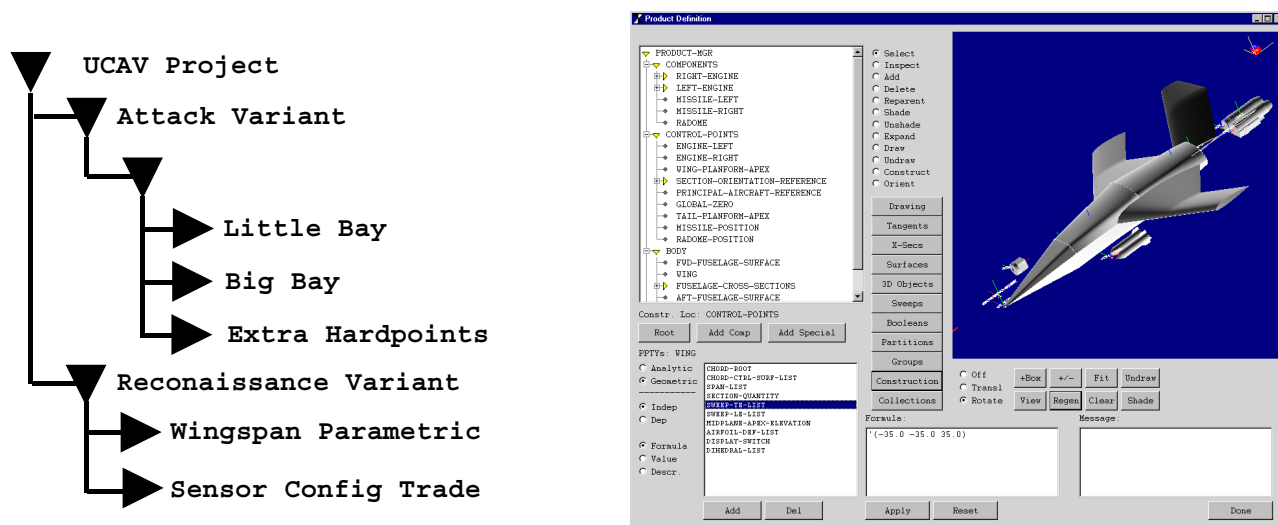
Figure 3: Conceptual Workbench for Product Definition

Configuration Trade Studies: The SBAAT environment will allow a geographically distributed team of engineers to create, maintain, store and retrieve configuration variants in the most efficient approach. While AML does provide a powerful demand-driven environment with run-time object creation, the volumes of data which result from such data operations (finite-element models, aerodynamic models, costing etc) demand the use of efficient database operations for configuration studies and reviews. With SBAAT, configuration changes can branch off at any level of the product description. Objects are not copied. Instead the use of AML's dependency tracking allows rapid propagation through all dependent configuration variants. Data dependencies then are tracked through the user workbench as illustrated in Figure 3.

From the workbench depicted in Figure 3, the user may define multiple weapons carriage concepts that are tracked as configuration trade variants. Another example (not shown) would depict a family of spar spacing concepts that are stored as well, as configuration variants, while maintaining dependency on wing geometry. Of course, changes in geometry may result in large number of calculations for each analysis model in the configuration study. With the demand-driven feature of AML, calculations are performed only when the user demands the output. New configurations are developed by editing the current model and saving the results along with the other configuration variants. Configuration options are callable from an automatically generated tree structure using the efficient filtering operations made possible through the AML environment. Time intensive calculations may be saved for batch processes that are scheduled at convenience.

Geometric Modeling: AML has been successfully deployed with a number of geometry engines. While supporting standard interface for geometry, initial SBAAT development emphasizes ParaSolids with its open environment and existing links to MSC.Software products. Using AML to drive ParaSolids, a number of geometric modeling innovations are being considered for rapid generation of conceptual design studies. One such innovation, Morphing-object, was developed under an SBIR contract with TechnoSoft. This is a procedure for developing a refined geometry transition between controlling sections along a prescribed trajectory. Polygon sections can be morphed into curved sections. Another geometric modeling innovation is the seamless link between AML geometry models and Patran meshes. With this capability, mesh refinement can be controlled at the object level with user-specified dependency on a number of geometric parameters. Control at the object level is key to the smart product modeling concepts because it propagates associativity. Resulting meshes will be used as input to MSC.Software products such as MSC.FLD and MSC.Nastran.

Analysis Tools: Within the SBAAT approach, a product concept is defined, modeled, analyzed and iterated. In defining the product the user emphasis is in describing; geometry, material properties, wing attachment concepts, control surface hinge and actuation concepts, manufacturing processes. The product description acquires modeling information for associated analysis. Regions of the structure are tagged for meshing by the user within the AML workbench. This is done through the use of rules applicable based on historical needs and then is meshed within MSC.Patran. Rules for mesh density are provided in the interface for the user to

select as the model is developed. Within a menu driven system, the user may define product functionality, and the analysis models will derive associated attributes.

A variety of emerging technologies are being considered within the SBAAT environment. One such technology is interface element technology in which parts may be meshed independent of assembly. Geometric compatibility may be provided through the AML environment. The interface element then provides the integration of subassemblies.

MSC.Software products will allow structural integrity assessment within the SBAAT environment. MSC.Nastran provides industry with the standard finite element analysis capabilities merged with a multidisciplinary suite of tools for aeroelasticity and structural optimization. This tool suite is well advertised http://www.mscsoftware.com/. Functional analyses such as static, modal, and aeroelastic analyses are performed within MSC.Nastran. An example of such associative modeling and analysis is provided at the end of the paper.

Cost Synthesis: From a design perspective cost at the early stages of technology development is relative as well as absolute. Compared costs and cost consequences are used in trade studies to prioritize technology implementation and thus, technology maturation. There are many ways to account for cost at the conceptual level. There are simplified weight-based parametric cost models based on historical regression. These are useful for projecting cost with old technology - but potentially misleading where new technology is considered. For instance, technology development in composite materials and manufacturing is focused on reduced labor and processing time. Weight based approaches have no parameter to capture such attributes. Integration issues in technology or concept development are evaluated with respect to cost consequences, and cost is one of those areas where "the devil is in the details."

An alternative to weight-based parametrics is process-based cost models. These models are readily developed with currently available software tools as will be shown in this paper. We expect they can be usefully formulated in terms of confidence intervals for identifying cost risk. Process based models decompose the cost down to whatever level of detail is required to make a judgement. However, decomposing the cost in terms of materials, labor, assembly, outsourcing, capital investment and any other overhead is not the whole story. This capability has to be put into the hands of the lead designer who is making rapid decisions, which have a strong influence on the cost. This capability is addressed in reference 4.

Figure 4: Proposed Edit Manufacturing Operation Form

Manufacturing operations are gathered from various sources for the purpose of synthesizing a cost strategy and identify opportunities for affordability. With SBAAT, the concept designer will have easy access to the operation's time estimates through a graphical user interface. Likewise, other properties and relationships, such as labor rate ($/hr – which is unique within each company), will be customized by the user within an Edit Operation form as depicted in Figure 4.

In general terms, the manufacture of a component occurs by a single operation or by an ordered sequence of operations. The user can browse through the Operation Catalog by utilizing the quick view capability. This allows the user to get a top-level view of any selected operation's properties and children (operation sequences). In order to assign an operation or predefined operation sequence, the user must select it from the Operation Catalog, and then transfer it to the Operation Sequence list. This notifies CAPTURE (ref 4) that the selected process is required to define the component's fabrication. For a multi-step manufacturing procedure the user continues to select and transfer operations to the Operation Sequence list in a user-prescribed order. The form that drives a carbon-carbon woven beam is depicted in Figure 5.

Once the components have been created, the user begins the second task of creating subassemblies. Two-part in nature, this task requires the user to group any number of components and/or subassemblies together, and apply manufacturing assembly techniques to join the components into a unified assemblage.
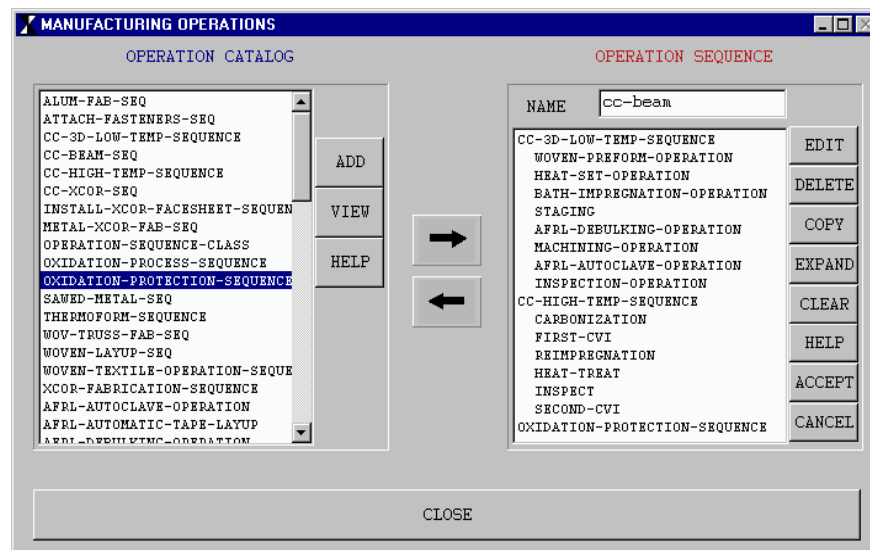
Figure 5: Proposed Manufacturing Operation Catalog

The CR process needs to be responsive to SBR&D data needs at the engagement level. The SBAAT cost models must anticipate the SBR&D needs with prior synthesis, which can be rapidly recalled during the exercise. While the exact cost will never be achieved, specific affordability issues can be addressed. For instance, the projected consequence with respect to a limited set of technologies will be anticipated in SBAAT models.

Smart Product Modeling:

The most time consuming paths in CR is the creation of product analysis models from product description and the update of product description from design changes based on product analyses. Our philosophy of smart product modeling (SPM) is to facilitate the modeling functions needed as depicted in the illustration shown in Figure 6. SPM enables user-defined automated operations that tightly integrate geometric and nongeometric product description data with product behavior data.
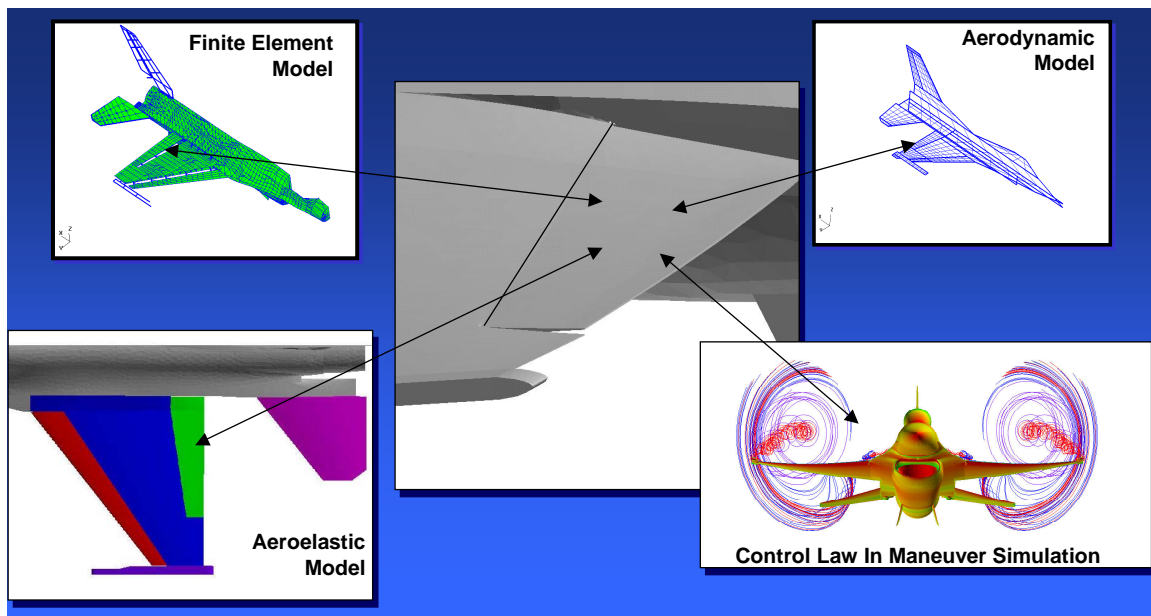
Figure 6: Smart Product Model Role in SBAAT

For example, an aircraft control surface is defined through geometric representation, and it behaves by rotating about a hingeline. The intelligence related to rotation about a hingeline delineates an aircraft maneuver and control mechanism. These attributes are required in the development and use of aerodynamic, structural, and loads models for structural integrity and weight analyses. In another example, an automobile door panel may be defined with a resin-transfer mold process that thus, determines design allowables for structural sizing. Applying smart product modeling provides building blocks for automated modeling and thus, rapid modeling for rapid development of product behavior data. This philosophy will decrease modeling time and enhance trade study capacity in lieu of time and manpower constraints.

The SPM operations encapsulate engineering analysis processes including data flow and translation and thus, enhance multidisciplinary design. Extensive detail of engineering processes are mapped through an object-oriented approach from the creation of a product data description through the development of analytic models and the ensuing high fidelity computational analysis. SPM then provides traceability from the derived design back to the product description. Thus, in the end of trade studies, design decisions are traceable directly to design requirements.

Technology trades and configuration trades will be worked together. With rapid-response product behavior data, scenario based mission performance and cost may be evaluated rapidly as well.

The evaluation process may provide either (1) a sound suite of technologies optimal for a given scenario or (2) to assess technology maturation requirements for a given scenario. The parametric based smart product model lends to design of experiments, probabilistic design, and genetic based algorithms.

Design Model

Finite Element Model

Aerodynamic Model

Aeroelastic Spline

Modal Analysis

Aeroelastic Analysis
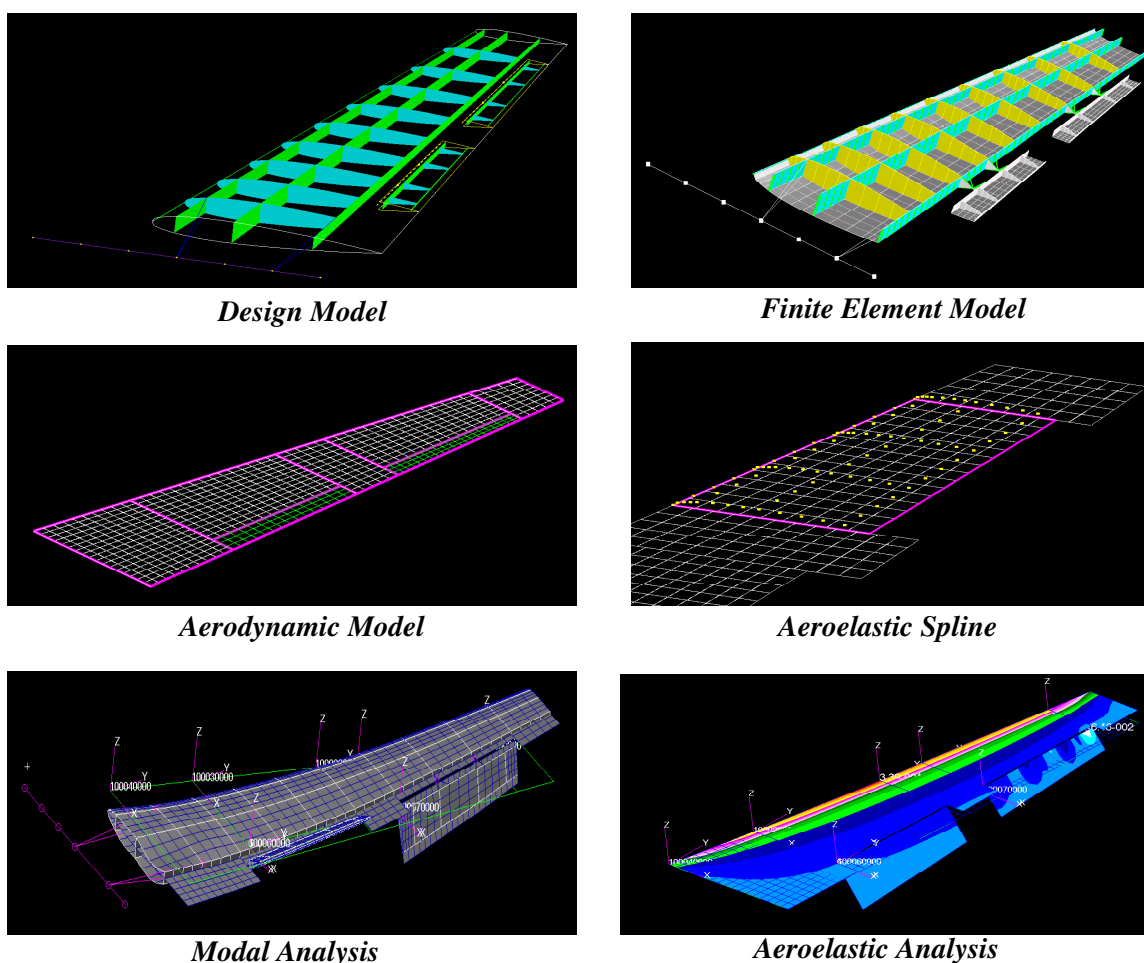
Figure 7: Stages of Product Description and Evaluation

Concept Pilot - Wing Design Example:

A concept pilot environment was developed to initiate the integration of AML, MSC.Nastran, MSC.Patran, and MSC.FLDS and demonstrate key features of smart product modeling. A wing design concept was defined and analyzed. Within the environment, structural arrangement variations are analyzed rapidly including modal and static aeroelastic disciplines. Weight approximation, flight control flex-to-rigid ratios and structural load paths will be available for future refinements in the context of smart product modeling. Figure 7 illustrates various stages of product definition and assessment.

The wing aspect ratio, span, taper, leading edge sweep and airfoil definition are specified. The trailing edge control surfaces and hinge lines are specified. The front spar of the control surfaces and the rear spar of the wing box are set by spacing criteria from the hingeline. Since there is no leading edge flap, the front spar is set by spacing criteria from the leading edge. The wing box spars and rib locations are specified in case parametrically, but may be quite arbitrary.

From the product definition, the structural finite element model is developed automatically. For a wing of this description, the solution is easy within a tightly integrated computer aided design system. The point of this demonstration however is in the concurrent tasking in server/client relationship; in this case, AML and MSC.Patran. In addition to the discrete components that are modeled (i.e., wing box and control surfaces) is the automated linkage through hinges and actuators. The user specifies hinge and actuator locations and types in AML, and the system creates the attachments.

The second row of pictures in Figure 7 illustrates the concurrent tasking between AML and MSC.FLDS (Flight Loads). A doublet lattice aerodynamic model is created through a user defined model that extracts key features from the product description (e.g., planform, control surface definition). Then from user parameters that drive the mesh density, MSC.FLDS automatically creates the aerodynamic model. To link this model to the structural FEM, a spline definition must be created. Historically, a user must perform the tedious task of creating spline boundaries and selecting structural grid points suitable for the spline. This is performed automatically with the aid of predetermined standards in the structural finite element and aerodynamic panel models as well as the selection of grid points only along defined structure (as depicted in Figure 7 for the Aeroelastic Spline).

The third row of pictures in this figure depicts results from a modal analysis and a static aeroelastic analysis. A key feature also explored in the pilot concept is the spline verify feature in MSC.FLDS. This feature uses the mode shapes to graphically verify the spline. The deformation shape for each structural mode is superimposed on the aerodynamic model through the spline. The Modal Analysis picture is captured from this analysis with the structural finite element model and the aerodynamic model shown together. Once assured a valid spline, the user may confidently proceed with the aeroelastic analysis.

The second point of the pilot was to initiate definition of the smart product modeling scheme for SBAAT. In so doing the utility of the pilot should demonstrate rapid response in the definition of a configuration variant. In Figure 7, the concept has four spars and nine ribs. Note that there is no root rib. In the Modal Analysis, the root is cambering as the wing deflects. A second concept and associated results are shown in Figure 8. This concept includes five spars and eleven ribs. A root rib has been defined in this concept. Note the modal results. There is no cambering in this concept. The point, here, is not that cambering is a feature of interest, but rather the behavior of the structure may be rapidly assessed for configuration variants.

Figure 8 repeats the sequence of operations depicted in Figure 7 for a four-spar configuration. While one might not expect a large weight difference and subsequence performance improvement, questions still remain as to the most effective structural layout in terms of weight and cost. This simple design trade example is appropriate for the SBAAT team to get started. More complicated design trades will be encountered during the course of the program.

Summary and Conclusions:

It goes without question; vehicle systems in the next generation will grow more complex. Complexity tends to favor conservative design evolution. Design revolution requires a design modeling environment that can reduce design complexity into metrics that a single designer can understand. For instance, multifunctional structures promise drastic performance improvements and reduced maintenance cost. However, the vehicle designer still needs to capture the fundamental metrics of weight, drag and cost before technology benefits can be understood rationally. Instead of prescribing miracles based on historical guesswork, MISTC software enables a designer to clearly demonstrate how and why new ideas will work and where to place one's developmental focus.

There is little doubt the ongoing developments are setting the stage for designing innovative vehicle systems for the next generation. SBAAT software developments will decrease the time for a team to synthesize a technology-laden design. Subsequently, a single lead concept designer will further explore design space with rapid reacting physics-based models. The customer will communicate needs more clearly with technology development placed in a vehicle and mission context, the raison d'etre for Simulation-Based R&D. Ultimately, this environment will replace risk aversion with excitement for sound technology development.

SBAAT represents a bold step by MSC.Software with aggressive software innovation made possible in this collaboration with TechnoSoft. There is every reason to believe this approach will grow and succeed for future generations with their commercially supported open software approach.

Design Model

Finite Element Model

Modal Analysis

Aeroelastic Analysis
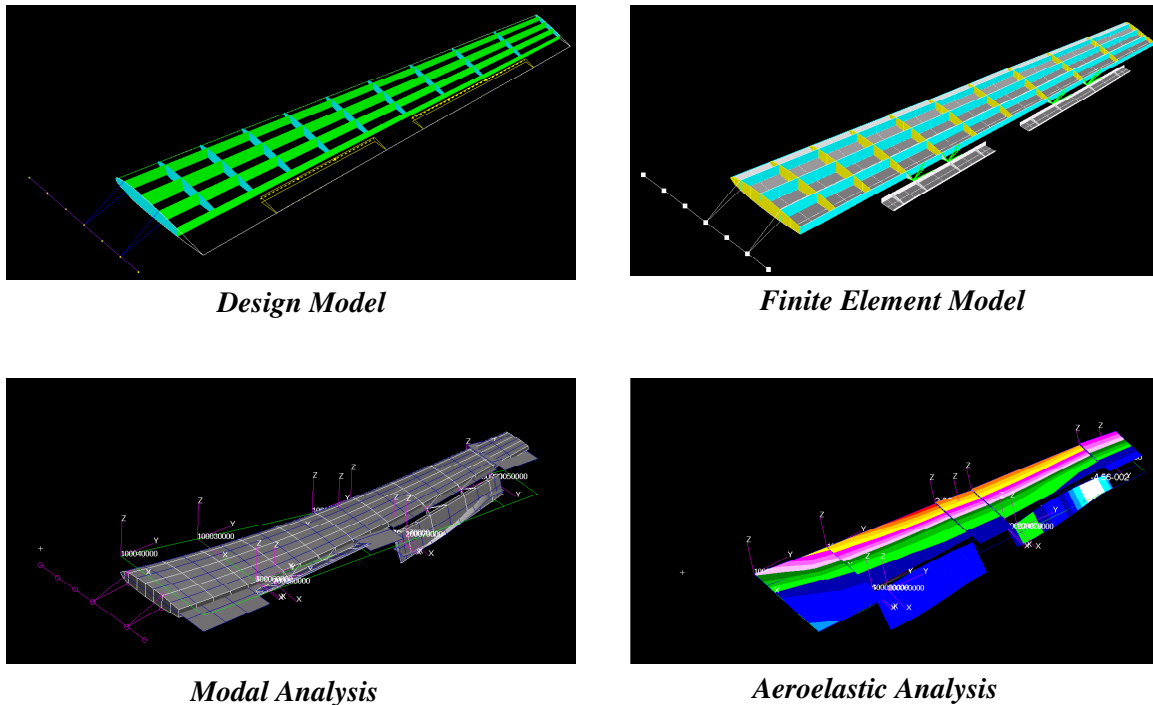
Figure 8: Configuration Variant Rapidly Defined and Reanalyzed

References:

1) Max Blair, Steven R. LeClair, Jeffrey V. Zweber and Adel Chemaly, "MultiDisciplinary Design for Uninhabited Air Vehicles", IEEE Sixth Workshop on Enabling Technologies: Infrastructure for Collaborative Enterprises, Cambridge MA, 18-20 June 1997.
2) Duane E. Veley, Jeffrey V. Zweber, Max Blair, "Aerospace Technology Assessment System", AIAA-98-4825, 7th Symposium on MultiDisciplinary Analysis and Optimization at St. Louis MO 02-04 September 1998.
3) M. H. Love and C. M. McCulley, "MultiDisciplinary Design in a Collaborative Object-Oriented Environment", Final Report, AFRL-VA-WP-TR-2000-3003, October 1999.
4) Max Blair and Alicia Hartong, "MultiDisciplinary Design Tools for Affordability", AIAA-2000-1378, 41st Structures, Structural Dynamics and Materials Conference at Atlanta GA 3 April 2000.
5) V. M. Vasey-Glandon and R. D. Hale, "PACKS (Parametric Composite Knowledge System): An Affordable Structural Definition Process for Composites", AIAA-2000-1478, 41st AIAA/ASME/ASCE/AHS/ASC Structures, Structural Dynamics, and Materials Conference in Atlanta Georgia 3-6 April 2000.
6) Graham Rhodes and Stephane Pageau, "Interface-Driven Design Manager, AFRL-VA-WP-TR-2000-3038, May 2000.

7) D. J. Neill, D. L. Herendeen and V. B. Venkayya, "ASTROS Enhancements", WL-TR-96-3006, May 1995.

8) Maxwell Blair and Robert A. Canfield, "A Joined-Wing Structural Weight Modeling Study", AIAA-2002-1337, 43rd AIAA/ASME/ASCE/AHS/ASC Structures, Structural Dynamics, and Materials Conference in Denver, Colorado 22-25 April 2002.

9) Adel Chemaly, "Using the Adaptive Modeling Language for Web-based Multi-User Collaborative Engineering Design", Third International Conference on Intelligent Processing and Manufacturing of Materials in Richmond, British Columbia, Canada 29 July – 02 August 2001.

10) Dean Kowal, P. Richard Zarda and Fred Baum "Web-based Design and its Impact on the Engineer", Third International Conference on Intelligent Processing and Manufacturing of Materials in Richmond, British Columbia, Canada 29 July – 02 August 2001.

11) Jeffrey V. Zweber, Mark D. Stevenson, Amarshi A. Bhungalia, Steven J. Catron, Alicia R. Hartong, Ramana V. Grandhi, "A Web-based Design Collaborative Application for Aerospace Vehicle Design and Analysis", Third International Conference on Intelligent Processing and Manufacturing of Materials in Richmond, British Columbia, Canada 29 July – 02 August 2001.

12) S. Rosenberg, "Innovative Composite Process Modeling Using Adaptive Modeling Language", Foster-Miller Report No: AFW-00204-1406, February 2001.

13) http://www.mscsoftware.com/products/

Impact Flows and Loads on Ship-Deck Structures

M. Greco and M. Landrini
INSEAN
The Italian Ship Model Basin
Via di Vallerano 139
00128 Roma, Italy

O.M. Faltinsen
Department of Marine Hydrodynamics
NTNU
Otto Nielsens rd. 10
N-7491 Trondheim, Norway

Abstract

The shipping of water on the deck of a vessel in head-sea conditions and zero-forward speed is investigated by experimental and numerical means. The main stages of the fluid-dynamic phenomenon are identified and the related structural loading conditions are studied. It is shown that potential-flow modeling suffices to give a robust estimate of green-water loads until large breaking phenomena, usually following impact events, are observed.

Introduction

The practical prediction of wave-induced ship motions and loads has reached a reliable degree of maturity since the 70's, when the strip-theory codes became available, Salvesen *et al.* (1970). The need to estimate occurrence and severity of dangerous events, such as the shipping of water on the deck of vessels, is not of minor importance but rational prediction tools are not yet available. A fuller understanding of the fluid dynamics involved in, and the ability to predict and control water-shipping events are the general goals of an ongoing research activity, Greco *et al.* (2000a) - Greco *et al.* (2002b), which will be partly recalled in the following.

Here, we consider a synergic investigation where experimental studies are combined with numerical modeling to identify the relevant parameters and to define possible simplified approaches of practical value. In particular, we focus our attention on the structural consequences of the water invading and flowing along the deck, and finally impacting against the deck house in the bow region of a Floating Production Storage and Offloading ship (FPSO) with zero forward speed in head-sea conditions.

FPSO units represent a relatively new concept of oil platform, where a ship moored in open sea is used for production, storage and offloading operations. Generally, FPSOs are cheap to build. However, the lower price is balanced by narrower limits of operation conditions because of the larger motion amplitudes with respect to those of other platforms types. Further, the construction of dedicated equipment (for instance the turret) can be expensive. Unlike semi-submersible and TLP structures, an important feature of FPSOs is represented by the possibility of providing storage capacity for the crude oil. Further, FPSOs can work in a wide range of water depths, and have a larger deck space for operation and equipment. Finally, in hurricane or iceberg areas FPSOs can disconnect and move away from the danger. On the downside, FPSOs can suffer relatively large vessel motions, since natural periods in heave, pitch and roll lie within the wave frequency range. FPSOs are supposed to be weather-vaning, that is head-sea condition is the most-occurring operation condition, and water on deck in the bow region is considered an important risk be taken into account to define operational strategies and ship design. Green-water accidents documented both deck wetness in the bow region and from the ship sides, with damages for deck house and equipment. The location of the deck house can vary: usually FPSOs working in the North Sea have the deck house in the bow region, while units operating in South America have the deck house near the stern.

In this paper, a first global understanding of the phenomenon is gained through experimental investigations. In particular, these allow for identifying the main stages of the flow-field evolution. Each of these is of concern from a structural point of view, and will be further investigated in the second part of the paper. Upon assuming realistic parameters for the ship structure, we define the criticality of the different flow stages and the reliability of the

mathematical model to deal with. Finally, the role of hydroelasticity in deck-house impacts after water shipping is addressed.

Experimental investigation of water shipping

Three-dimensional model experiments
Three-dimensional experiments have been performed to study water-on-deck phenomena on the Esso-Osaka tanker, restrained to move, in head-sea conditions and without forward speed. The model has draft D=0.284m, length between the perpendiculars L=4.44m and beam B=0.74m. The tests have been carried out at INSEAN facilities, in the Towing Tank 2 (length 220m, breadth 9m and depth 3.6 m). By considering FPSO ships and their usual operation conditions, we have determined the main incident wave parameters. In particular, the FPSO water-on-deck accidents in the North Sea documented that the most interesting wavelengths are of the order of the ship length. Further, several casualties occurred during full-loaded conditions, when the effective freeboard is smaller than the nominal value, see Ersdal and Kvitrud (2000). To have realistic heights of water relative to the deck for representative design conditions, the upper portion of the bow has been modified by reducing the freeboard to f=0.064 m, resulting in the non-dimensional parameters $D/L \approx 0.064$, $B/L \approx 0.166$ and $f/L \approx 0.015$.

The analysis has been carried out by combining flow visualizations, image analysis and wave elevation measurements around the bow region. In particular, the uppermost portion of the hull and the bow region of the deck have been made by transparent material to permit visualizations of the water running up along the bow, entering the deck and flowing against a vertical Plexiglas plate to mimic a deck-house wall. To the purpose, a video camera has been used in combination with a mirror placed under the ship deck. The flow evolution was recorded through a black/white video camera with a frame rate of 30Hz.

In real cases, water shipping may be due either to a single large wave, or to the cumulative effect of a small number of events associated with wave groups approaching the ship. In the latter case, the first event is not necessarily the most severe one. In the present tests, the water on deck is caused by a single event due to a wave packet. In this way, we also avoid effects due to wave reflections from the tank walls. The incident wave packet results from the focusing of several wave components generated with suitable phase relationship, Rapp and Melville (1990). The wave spectrum and the focusing point along the tank represent the input data. In the present case, each component has the same amplitude a. A characteristic steepness $k_c a$ of the wave packet can be defined by the wavenumber k_c associated with the mean frequency f_c of the spectrum. In tests here reported, we have chosen f_c=0.6 Hz and the frequency bandwidth Δf=0.4 Hz, respectively. This gives a characteristic wavelength $\lambda_c = 2\pi k_c$ =4.33m≈0.98L. The shortest and the longest wave components correspond to about 0.5L and to about 2.6L, respectively. The wave steepness $k_c a$ has been varied between 0.125 and 0.25. A fuller presentation and an in-depth discussion of the experimental results is reported in Greco *et al*. (2002b), here we summarize the main physical findings.

The sequence of pictures in Fig.1 shows the interaction of the wave packet approaching the ship bow from left to right. After the water exceeds the freeboard, it enters the deck in a non-uniform manner because of the three-dimensionality of the hull form. At the beginning, the water plunges onto the deck at the fore portion of the bow, as indicated by the white arrows in the pictures. As time passes, the shipped water starts to flow along the deck, while the freeboard is exceeded along the ship sides. Later on, the water impacts against the vertical wall in a complex fashion, starting from the lateral sides.

The bottom view in Fig.2 highlights the formation of air entrapment during the early stages of the water shipping. In particular, the right picture shows two cavities developing along the bow edges, with varying cross section and maximum area near the ship centerline.
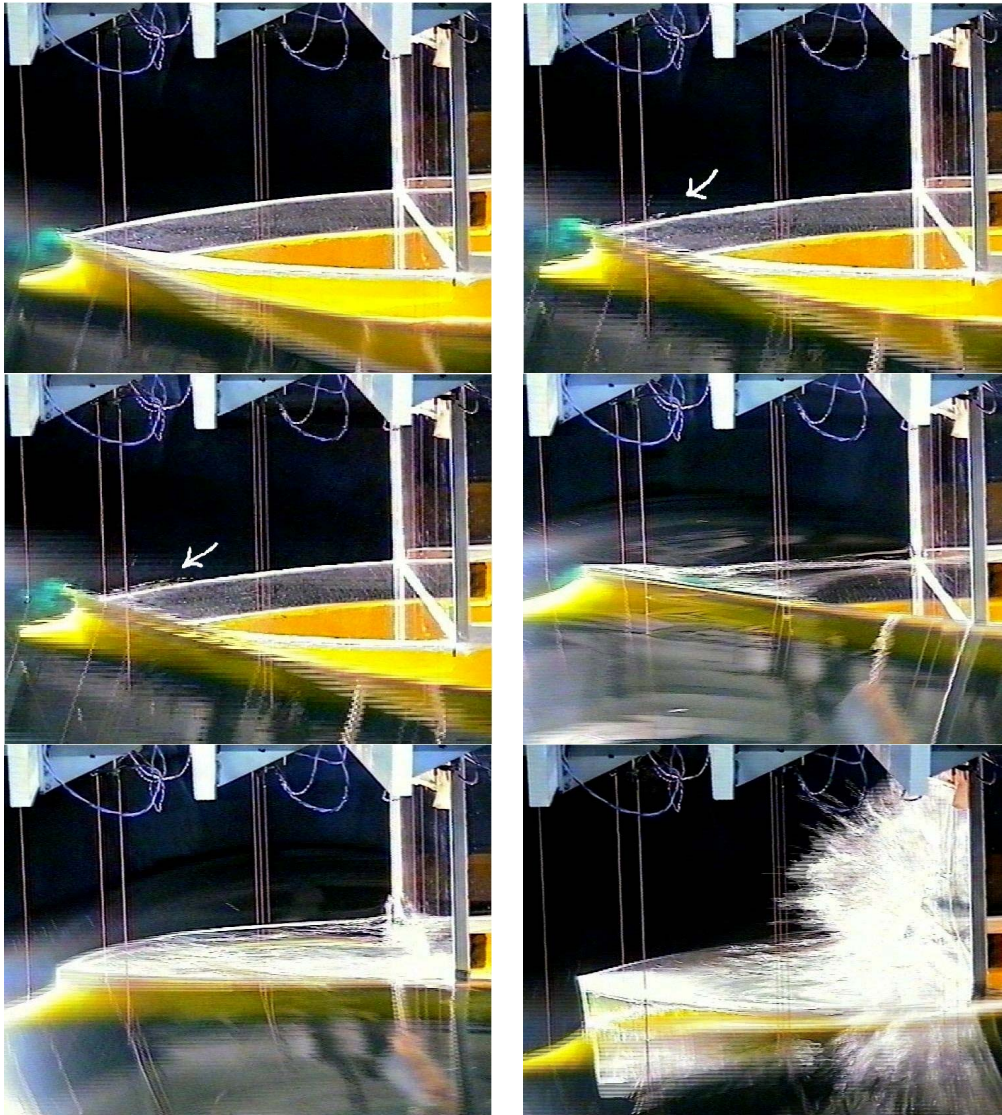
Figure 1. Side view of the water shipping on an ESSO-Osaka model induced by a wave packet, propagating from left to right. The white arrows indicate the region where the water front plunges onto the deck. Time increases from left to right and from top to bottom. The two bottom pictures show the interaction with the vertical wall.
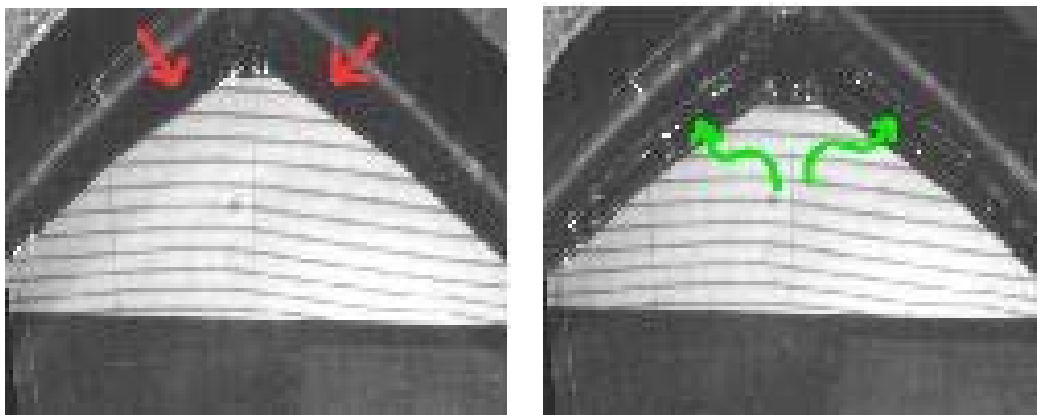
Figure 2. Initial stages of the water shipping. Left: the red arrows show the direction of the water flow entering the deck. Right: the green arrows indicate the location of the cavity structures along the bow sides.

A more complete analysis of the taken flow visualizations led to the interpretation of the fluid-flow evolution during the initial stage of the water shipping, as explained in Fig.3. When the water exceeds the freeboard, the fluid front plunges onto the deck, forming the already mentioned air cavity (sketch 1). As the wave packet propagates downstream the hull, "fresh" water enters the deck along the bow sides, and moves initially inwards. Because of the symmetry of the phenomenon, the lateral water fronts approach each other in proximity of the ship centerline and are diverted outwards by the mutual interaction (sketch 2). An inner blunt fluid structure results from this interaction. As time passes, this structure is fed by the water shipped laterally and moves along the deck towards the deck house (sketch 3). The fourth sketch shows the structure of the water front before the impact against the vertical wall. It is worth stressing the non-uniform distribution of water height, with a maximum value occurring around the ship centerline.
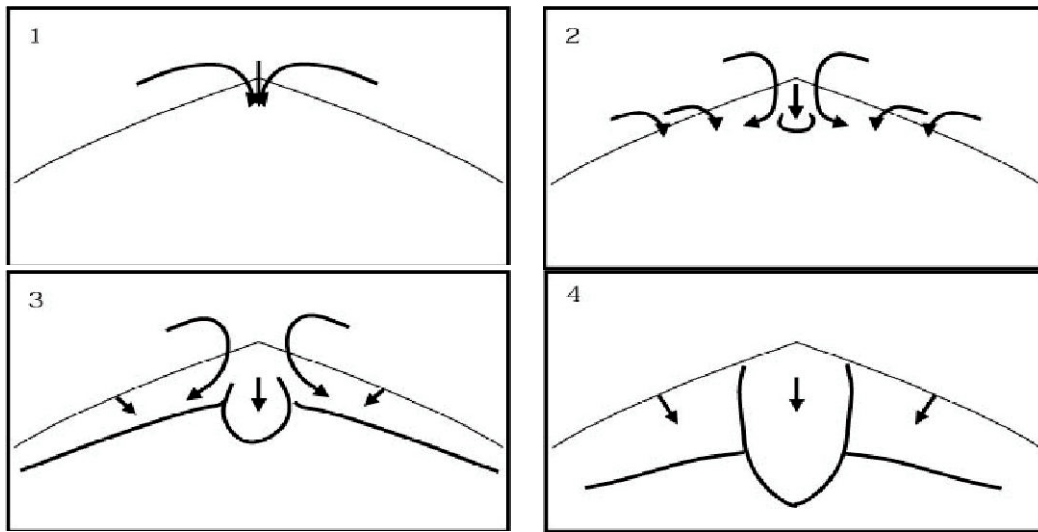
Figure 3. Interpretation of the fluid-flow evolution during the initial stage of the water shipping. 1: The water exceeds the freeboard and plunges onto the deck; 2: The fluid flowing from the lateral sides is diverted outwards along the centerline, and a central blunt water front appears; 3: Intensification of the fluid motion transverse to the dam break-type front and growth of the inner water tongue propagating along the ship centerline; 4: Gross structure of the water front before the impact against the vertical wall.

Two-dimensional laboratory tests

For a clearer understanding of the water shipping dynamics, and to guide the developing of numerical methods, two-dimensional water-on-deck laboratory tests have been performed in the narrow wave flume (length 13 m, depth 1 m and width 0.6 m) at the Department of Marine Hydrodynamics of NTNU. Incoming waves are generated by a flap wavemaker. The body-parameters here considered are: draft $D = 0.2$ m, length $L = 1.5$ m, freeboard $f = 0.05$ m. The bottom corner at the model was rounded with a radius of curvature 0.08 m to avoid significant vortex shedding. Body motions are restrained. Since the generated wave system is highly transient, with the first crest generally steeper than the following ones, we decided to focus our study on the first water-shipping event.

The fundamental stages of the water shipping and the interaction with the deck first, and later with the superstructure are described through the pictures in Figs. 4-6. In particular, Fig. 4 reports the enlarged view of the water front entering the deck. The shipping of the fluid initiates with water plunging directly onto the deck, *cf.* the top-left frame. At this stage, high impact pressures are expected. However, the very high pressures last too short and are too concentrated in space to be dangerous for the structure. After the impact, a cavity entrapping air is formed, as shown in the top-right and following frames. The changes of the cavity volume due to the motion of the surrounding fluid determine time-varying loads on the deck. This phase of the fluid-structure interaction may damage the deck at least if the air in the cavity cannot escape. The latter occurs more easily in three- dimensional conditions rather than in the two-dimensional flow field here considered.
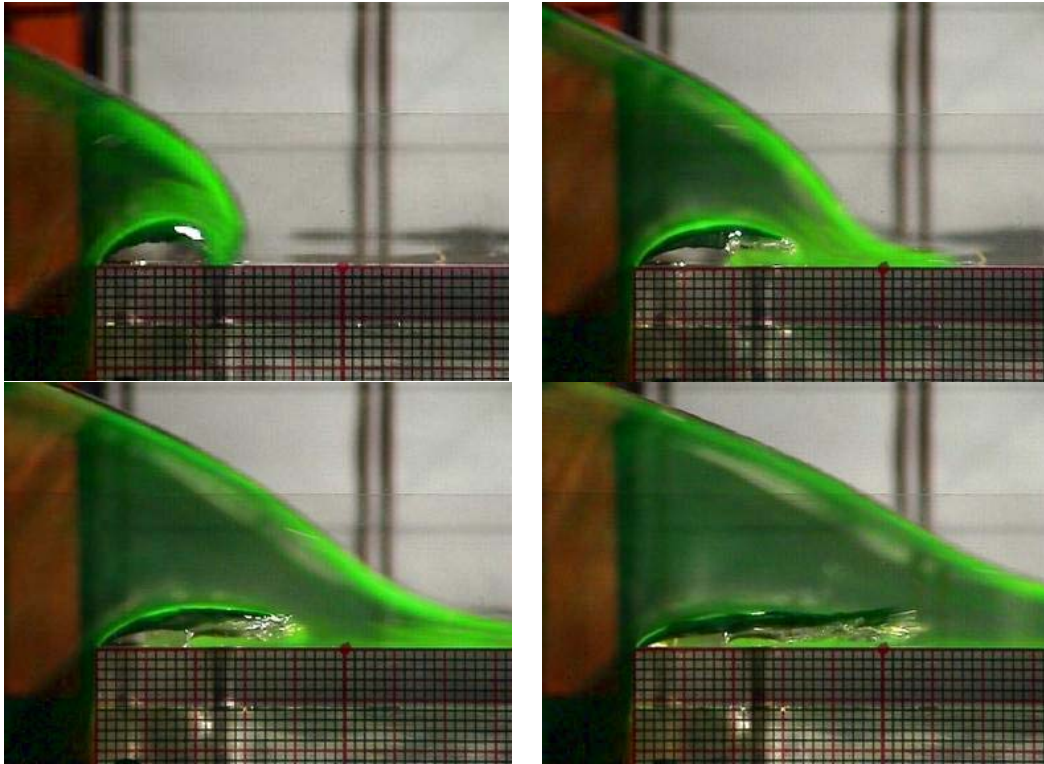
Figure 4. Initial stages of the water shipping: the water front plunges onto the deck forming an air pocket, which is squeezed and stretched downstream by the main flow. Time increases from left to right and from top to bottom.
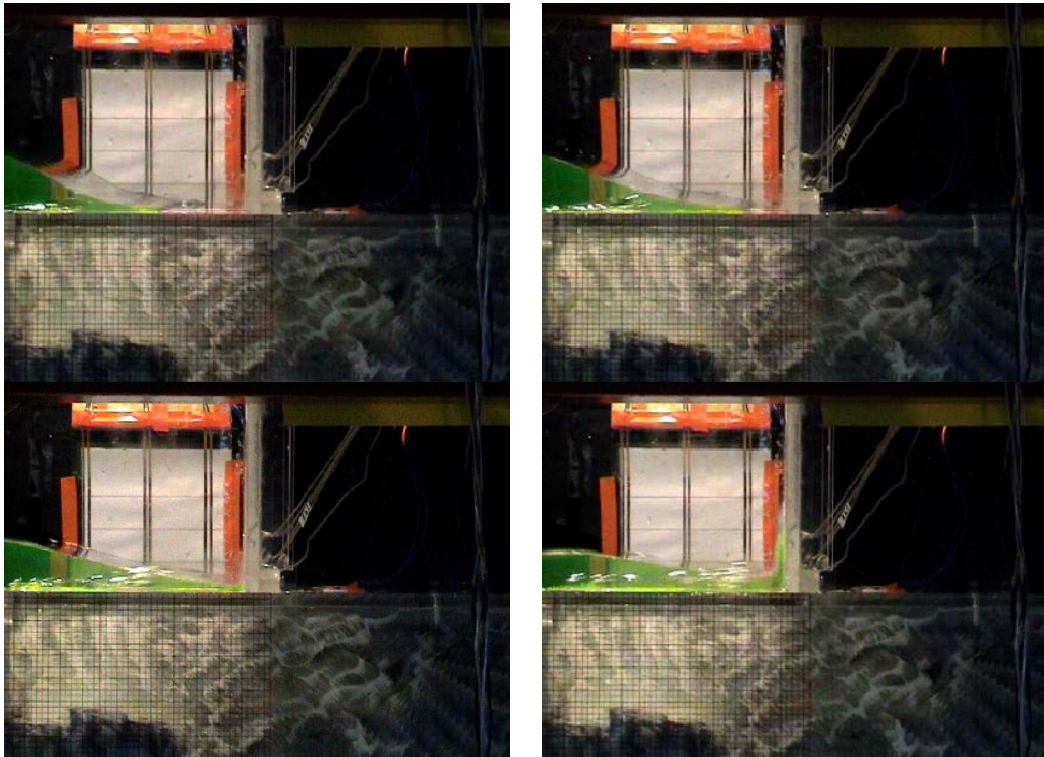
Figure 5. Dam break-type flow developing along the deck and eventually hitting the vertical superstructure. Time increases from left to right and from top to bottom.

Figure 6. Late evolution of the impact against the vertical superstructure: after the maximum run-up the water plunges backwards onto the deck.

After a time short with respect to the duration of the entire water-shipping, the gross features of the flow field resemble those originated after the breaking of a dam, as shown in Fig. 5. Namely, a tongue of fluid develops along the deck, without observation of free-surface breaking. Therefore, the gross fluid dynamics is rather simple, with practically hydrostatic loads in proximity of the water front. In this context, an additional important contribution to local loads would be given by ship motions, though not allowed in our experiments. Actually, numerical results show that there are important interactions between the flow on the deck and the flow field exterior to the vessel. This limits the similarity with dam-break flows and the practical possibility of using shallow-water models (see Greco *et al.* (2000c)).

Finally, the impact against the vertical structure is observed (bottom frames in Fig. 5). In the following evolution, *cf.* Fig. 6, the fluid rises rapidly along the vertical wall. The fluid run up is slowed down by the action of the gravity, and the water front thickens. After the maximum run up has been reached, the water collapses downwards, and a backward overturning is observed.

Analysis of the fluid-structure interaction

In the following, the structural implications of the fluid-structure interaction associated with the shipping of water are investigated. To the purpose, both numerical and experimental data will be used in a combined fashion. According to the previous discussion, three different stages of the water shipping will be considered.

Initial plunging phase and deck impact The first three plots of Fig. 7 show the initial plunging phase observed in the two-dimensional experimental investigation, and the comparison with the numerical prediction obtained by a potential-flow model. The statement of the mathematical problem and the details of the Boundary Element Method developed for its solution are discussed in Greco *et al.* (2000b). In the figure, the waves ($\lambda/D = 10.1$, $H/D = 0.808$) approach the obstacle from left to right and the numerical results are in rather good agreement with the experimental visualization. In the simulation, surface-tension effects have not been modeled, which suggests a limited role of surface tension in determining the initial volume of the entrapped cavity, at least for the wave parameters here considered. Upon this validation, we can use the numerical tool to investigate in more detail the local features of the phenomenon. In the right plot of the same figure, the numerical free-surface configuration (solid line) at the impact is given. It is also shown that close to the separation point at the bow, the cavity profile is well fitted by the local solution $z_1 = C(t)x_1^{2/3}$ (line with circles, *cf.* Zhao *et al.* (1997)) around the fixed separation point. This approximation is obtained by assuming a potential flow and neglecting the gravity effects. In this local solution, the origin of the local coordinate system (x_1, z_1) is at the edge of the deck, the x_1-axis is along the deck and the z_1 axis is vertically upwards. The coefficient $C(t)$ is a time dependent parameter which depends on the complete flow, and therefore cannot be determined by a local flow analysis. The part of the water front impacting on the deck agrees well with a parabolic contour (line with black squares), which would be the path of a free-falling fluid particle. Therefore, at the beginning of the water shipping, the fluid undergoes three stages of evolution: (i) the fluid is diverted vertically upwards, with negligible effects of the gravity; (ii)

an intermediate phase with almost horizontal motion where gravity and pressure gradients are comparable, and (iii) a free-falling evolution up to the impact point.
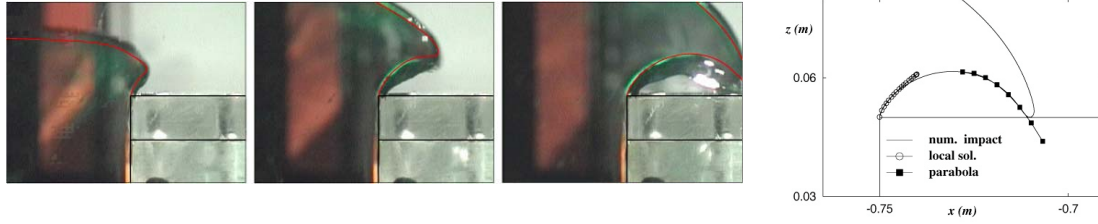
Figure 7. Initial stages of water shipping. Left: the numerical results (red lines) are compared with the experiments. Time increases from left to right. Right: the numerical solution (solid line) is compared with a local solution (line with circles) and with a free-fall trajectory (line with squares).

From a structural perspective, the plunging phase is characterized by the water impact against the deck and the air-cushion phenomenon. In the following, the related effects on the deck of a real FPSO unit have been investigated. In the considered ship, the steel stiffeners along the deck are sketched in the left diagram of Fig. 8. The deck is designed to stand against a maximum spatially uniform pressure of 60 KPa and has been modeled as an equivalent beam (*cf.* the left sketch in Fig. 8) along a longitudinal stiffener.
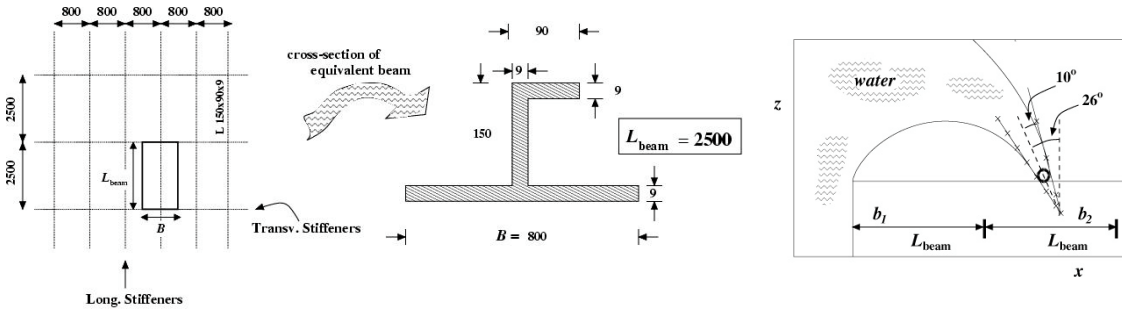
Figure 8. Left: example of stiffeners on the deck of a FPSO, top view and cross-section of the equivalent beam to model the deck in the longitudinal direction. Dimensions are in millimeters. Right: numerical solution at the impact. Close to the impact position, the free surface (solid line) is approximated by a circle with radius $r \approx 0.1$ m. The free surface resembles a fluid wedge of about 20°, inclined of approximately 26° with respect to the vertical direction. The two horizontal arrows (b_1 and b_2) indicate the length of the first and second equivalent beams along the deck.

At full scale, we consider the water impact following the shipping of water caused by incident waves with length 182 m, and height 14.55 m (corresponding to the wave parameters mentioned above, with the FPSO draft equal to 18 m). The free-surface configuration as obtained by the numerical simulation is given in the right plot of Fig. 8. The two horizontal arrows indicate the length of the first two equivalent beams along the deck. The impact starts close to the middle of the second one. From the numerical simulation, an impact velocity of 4.3 m/s is estimated. This value is not large, and in particular is close to the orbital velocity in free-wave conditions (4.4 m/s). The free-surface shape near the initial impact position is rather blunt, with radius of curvature $r \approx 0.1$ m.

The portion of flow field on the deck and closer to the bow is characterized by the cavity originated at the impact instant. During the evolution, the air cavity is stretched by the flow entering the deck and above it. As a consequence, the beam b_1, initially under the action of the atmospheric pressure, suffers loads due to the compressibility of the air entrapped in the cavity. If we assume a uniform pressure in the cavity, and we model the air evolution as an adiabatic process of an ideal gas, the pressure *p(t)* in the cavity can be obtained by $p(t)/p_0 = \left(V(t)/V_0\right)^{\gamma}$. Here, *p(t)* and *V(t)* are the pressure and the volume at time *t* and p_0 and V_0 are the corresponding reference values, *e.g.* the atmospheric pressure ($p_0 = 1$ Atm $\approx 10^5$ Pa) and the air volume in the cavity at the impact instant. The usual value $\gamma = 1.4$ is used for the ratio of the specific heats.
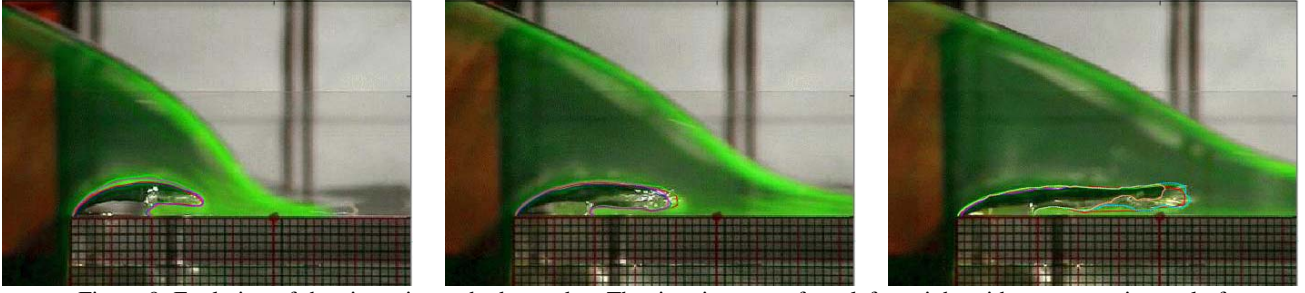
Figure 9. Evolution of the air cavity at the bow edge. The time increases from left to right with a constant interval of 0.38 s (at full scale, D = 18 m). The digitized cavity profiles (colored lines) are superimposed to the video images.

By using the above model and the pictures taken from the experiments, we have carried out a simplified analysis to evaluate the pressure acting on the first beam. In the sequence of Fig. 9, the post-impact evolution is shown with snapshots separated in time by an interval of 0.38 s. Because of the relatively poor resolution of the images, at least for the present purpose, the cavity profile is not sharply detectable from the pictures, and for each snapshot several different curves are candidates as cavity boundary. Therefore, all of them have been considered and are reported, superimposed to the corresponding video images. For each instant of time, the cavity volume has been evaluated and used to estimate the pressure inside the cavity. Because of the uncertainty in the determination of the cavity boundary, for each time step several scattered results will be obtained. Actually, even this simplified analysis requires some extra data, which have been deduced from the numerical simulations. In particular, the cavity volume V_0 at the impact instant t_{imp} is computed numerically. The circles in the left plot of Fig. 10 represent the pressure computed according to the above procedure. As anticipated, different pressure values at the same time instant are obtained, corresponding to different digitized cavity boundaries. The pressure envelope (dashed lines) gives an indication of the order of magnitude of the uncertainty involved in. In the plot, the horizontal solid line is the design pressure for the deck. According to the present analysis, this value can be exceeded during the cavity evolution, and likely this occurs for a time interval not small compared with the first natural dry-beam period $T_{\mathrm{dry}\ 1}$. Therefore, the collapse of the cavity can be critical for the strength of the deck structure and hydroelastic effects may be also relevant.
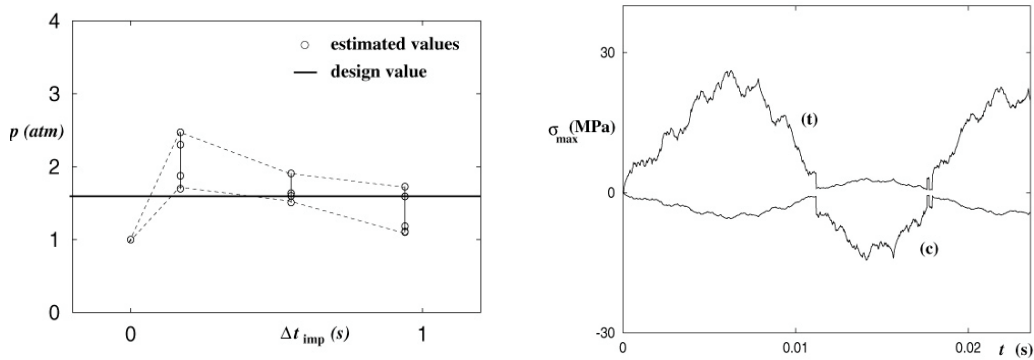
Figure 10. Left: estimated pressure evolution along beam b_1. Right: evolution of the maximum tension (*t*) and compression (*c*) stresses along beam b_2 by assuming a Dirac's delta load. All the quantities are given in full scale (D = 18 m).

The evolution of the loads on the second beam b_2 is roughly characterized by (i) an acoustic phase, (ii) a blunt-impact phase and (iii) a wedge-impact phase. The pressures associated with the initial phase are high but too localized in time and space to give any problem for the structure, *cf.* Greco *et al*. (2001b). The time duration of the second impact phase is larger than the first one, and of the same order of magnitude as the highest natural dry period of the beam, thus the elastic response of the beam could be relevant and should be further investigated. The region of the beam loaded during this blunt-impact phase is small relative to the beam length. Therefore, the evolution of beam stresses can be estimated by considering the beam subjected to a spatial Dirac-delta load, $f(t)\delta(x - x_{imp})$, located at the initial impact position. The amplitude $f(t)$ can be

estimated as the vertical force on a rigid circle penetrating a flat free surface, Faltinsen (1990), and expressed as $\rho C_s(t) r V^2$. The time dependent coefficient $C_s(t)$ has been derived experimentally by Campbell and Weynberg (1980) and is represented by the formula $C_s = 5.15/(1 + 8.5h/r) + 0.275h/r$. Here, $h = Vt$ is the instantaneous submergence of the circle and is equal to the radius r when half-circle penetrated the free surface. From this analysis, right plot of Fig. 10, the resulting maximum stresses on the beam are safely below the yield stress (about 220 MPa). The last wedge-impact phase is more complicated and would require a more direct analysis, investigating also the possible excitation of hydroelastic effects.

Dam-break stage On a longer time scale, the observed water shipping resembles a dam-break type phenomenon. In our experiments, during this stage, the loading is mostly determined by the 'hydrostatic' pressure, since ship motions have been restrained. In reality, additional contributions are due to three-dimensional effects and deck accelerations. This phase is not expected to be dangerous for the deck structure although, depending on the amount of shipped water, it can be relevant for the dynamic behavior of the ship. This issue is not addressed here.

Deck-house impact The water front approaching the vertical superstructure resembles a thin half-wedge, and, at the beginning of the impact with the wall, only small amount of the fluid sharply deviated upwards by the obstacle is affected by the phenomenon. A jet originates vertically upwards, and spray formation is observed. Though without the modeling of the initial plunging phase, the BEM method captures well both the flow evolution on the deck and the water run-up along the vertical wall, as shown in Fig. 11 where the red lines represent numerical results. On this ground, the initial plunging phase appears not relevant for the gross features of the deck flow, as well as for impact loading on the superstructure.
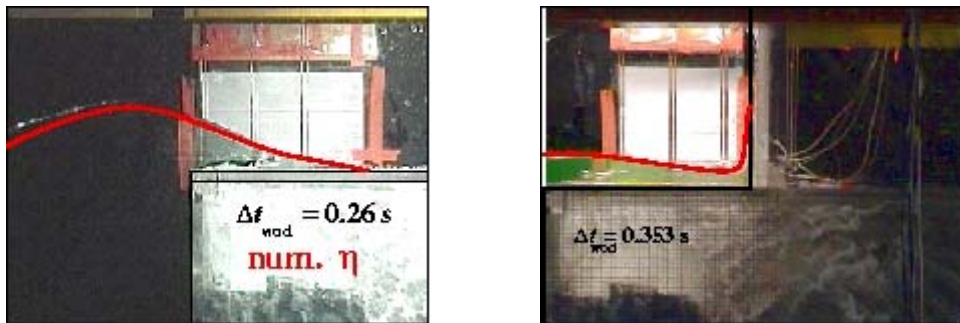
Figure 11. Left: dam break-type flow after the initial impact. Right: impact of the shipped water against the vertical wall of the deck house. The red lines are the present numerical simulations.

The pressure evolutions on the wall, measured at 0.012 m and at 0.032 m above the deck (model scale), are reported in the left and right plots of Fig. 12, respectively. Along the horizontal axis, $t = 0$ s corresponds to the time instant when the numerical pressure (thick line in each plot) at the lowest gauge location attains a non-zero value. Two test results are shown for each pressure gauge (full and empty symbols), showing a not-perfect repeatability and suggesting more careful measurements of local loads.

The experimental data show two pressure peaks of the same order of magnitude. The first peak is associated with the initial water impact against the superstructure. By combining the pressure measurements with the video images, we found that the second pressure peak is related to the backward water overturning, shown in Fig. 6, and appears equally important for the structural safety as the initial impact load.
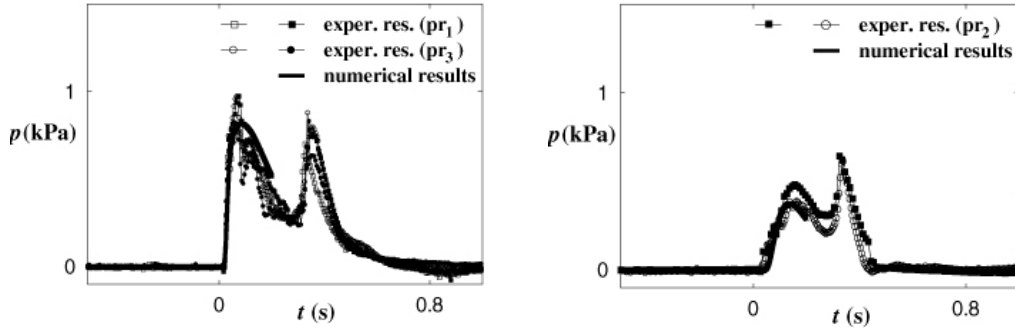
Figure 12. Pressure evolution measured on the vertical wall under impacting conditions, at 0.012 m and 0.032 m above the deck (left and right plots, respectively). Two test results are given for each gauge location. The solid lines give the numerical results, before breaking occurs and computations stopped.

The numerical prediction is rather satisfactory and recovers correctly the first pressure peak. Though the computations have been stopped as soon as the water flux entering the deck attains a zero value, the second pressure peak would not be captured anyway numerically because the boundary element method cannot handle free-surface breaking. In this respect, Level Set, Colicchio *et al.* (2002), SPH, Tulin and Landrini (2000), and VOF techniques, Greco *et al.* (2002b), have been recently proposed to handle the post-breaking evolution but they require further development and validation for extensive and practical use in this context.

Simplified tools for loading estimates

From a pre-design perspective, it is very important to develop simplified tools to quantify green-water loads. Here, we discuss a few of them by using the dam-break problem as a test case. In this framework, the BEM method has been adopted to provide reference data.
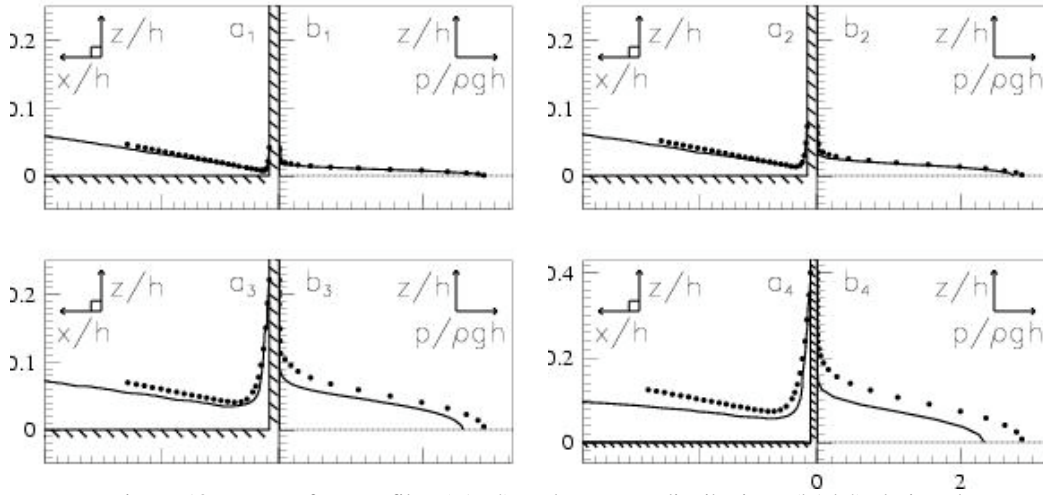
Figure 13. Free-surface profiles (a1-a4) and pressure distributions (b1-b4) during the initial stage of the impact against the vertical wall. Solid lines: present numerical simulations; •: similarity solution from Zhang *et al.* (1996). The plots are progressively enumerated as the time increases. $\Delta\tau_{imp} = \tau - \tau_{imp} = 0.0138, 0.0243, 0.0738, 0.1338$.

τ_{imp} is the initial non-dimensional impact time.

During the initial phase of the impact, the gravity plays a minor role and the phenomenon is governed by the local-flow accelerations. Hence, the gravity-less similarity solution of a fluid wedge hitting a rigid wall, Zhang et al. (1996), describes correctly the flow field and can be used to evaluate the pressure evolution along the structure. Figure 13 shows the actual comparison between the similarity and the *exact* solution: as it can be expected, the two results start to diverge as time increases, with the approximate method over-predicting the pressure along the wall.

Within this simplified analysis, the parameters defining the impact conditions are represented by (i) the velocity V and (ii) the slope β of the water front. By using the similarity solution, Greco (2001b) has shown that $d\left(p_{max}/\rho V^2\right)/d\beta$ is large only for β larger than, say, 60 degrees and is small for β smaller than about 40 degrees. Therefore, for small enough front slopes, the impact velocity V is the most important factor influencing the maximum pressure p_{max}.
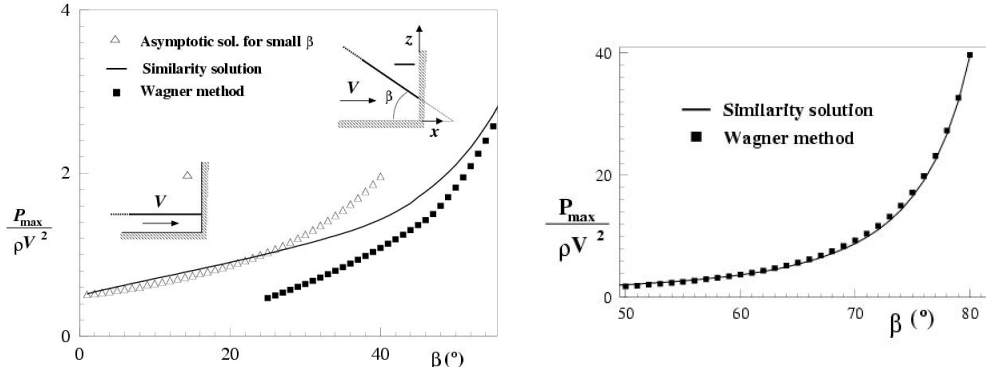
Figure 14. Maximum pressure along the wall. Left plot: the asymptotic solution for small water-front slopes β is compared with the similarity and the Wagner solutions. Right plot: for larger β, only the Wagner and the similarity solutions are shown. V: impact velocity, β: angle of the (half) wedge.

On this ground, the maximum pressure can be evaluated by even simpler methods. Figure 14 gives p_{max} onto the wall associated with the initial impact by using two different approximations valid for small and large values of the water front slope β, respectively. The first one is given in Faltinsen *et al.* (2002a), while the latter is a Wagner-type solution, Wagner (1932). The former appears suitable for $\beta \leq 30°$, while the latter is efficient for $45° \leq \beta \leq 90°$.

Hydroelastic effects

During the most impulsive stages, if the loading time is comparable with the structural natural wet period, hydroelastic effects are excited, and for a correct structural design the hydroelastic effects should be assessed. The influence of hydroelasticity during the water impact with the vertical wall has been investigated in Greco *et al.* (2001a) by using the dam-break problem to model the water flow along the deck and by modeling the wall structure as an Euler beam, simply supported at the ends. The structural properties are chosen by using data from typical steel stiffeners of the deck house of an actual FPSO (see sketch Fig. 15). The fluid-structure interaction is studied by coupling the nonlinear potential-flow model with the linearized beam dynamics.
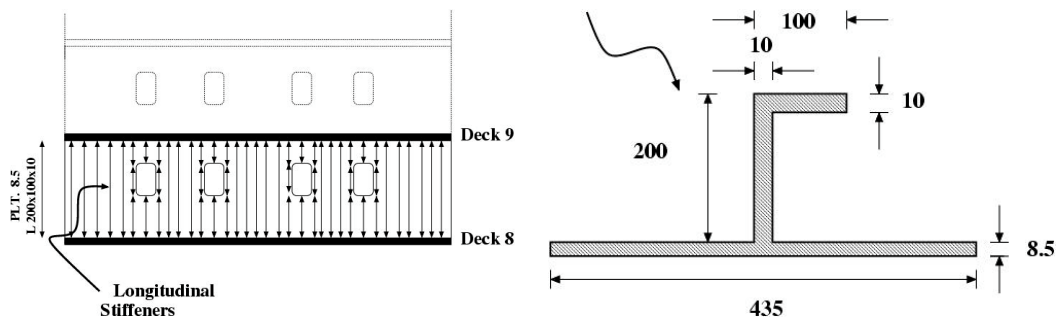
Figure 15. Example of stiffeners of a deck house (front view on the left) and cross-section of equivalent beam (on the right). Lengths are in millimeters.

The results of this analysis are summarized in Fig. 16, through the free-surface evolution during the water run-up along the structure (left) and of the maximum stresses (right) on the wall, always occurring at the lower edge of the beam. The hydroelastic results are compared with the solution obtained by assuming the structure perfectly rigid in the hydrodynamic solution and by evaluating *a posteriori* the structural deformation in a quasi-steady fashion. It is found that the free-surface configurations agree well and the magnitude of the hydroelastic stresses weakly

oscillates around a mean value slightly different than the quasi-steady solution. These observations document the limited role of hydroelasticity during the water impact with the superstructure, at least for the case here considered.
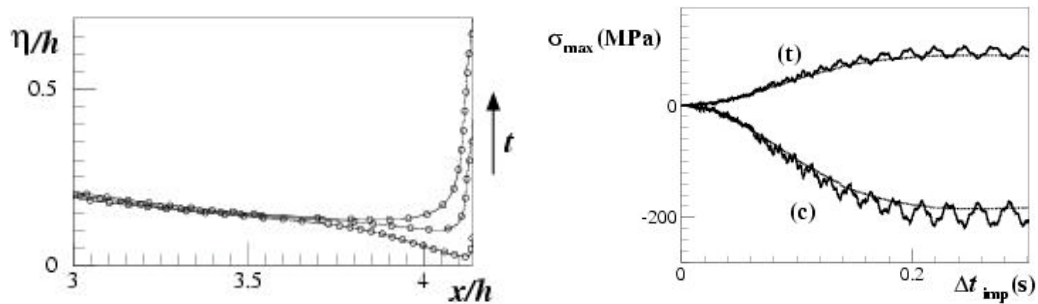
Figure 16. Impact of water with a vertical wall, the incident wave is generated by the break of a dam with initial height of the water reservoir $h = 10$ m. Left: free surface for three different instants after the impact for the case with rigid wall (solid lines) and hydroelastic solution (o). Right: Maximum tension (t) and compression (c) stresses as a function of time as obtained by the quasi-steady analysis (dashed lines) and by the hydroelastic analysis (solid lines).

Conclusions

The shipping of green water on a FPSO ship in head-sea has been studied by experimental and numerical means. The main stages of the flow-field evolution have been highlighted and the related loading regimes have been addressed.

It is shown that water shipping starts always with the fluid front plunging onto the deck and entrapping air in cavities of complex shape and evolution. A simplified analysis of two-dimensional experimental data shows that this air-cushion stage can lead to high pressure (very localized in space and time), and therefore to possible structural damages.

After the cavity disintegration, the following dam break-like evolution is grossly unaffected by the presence of the air bubbles dispersed within the main bulk of water. Numerical simulations, where the presence of the air-phase has been neglected, reproduce well the overall flow scenario and can be used to compute the initial conditions to study the impact against deck structures. In this context, shallow-water models may be useful although the need of boundary data may pose severe limitations to their actual applicability, see the discussion in Greco *et al.* (2000c). This stage is probably more relevant to the dynamics of the vessel rather than to the strength of the deck.

The impact against vertical deck structures is finally addressed. Although the impact loads are of main importance, laboratory measurements have shown that pressure peaks arising during the gravity driven evolution can be of the same magnitude and, therefore, of concern for design purposes.

In this framework, the potential-flow modeling has been proved reliable to simulate the flow and to predict the hydrodynamic loads at least up to breaking and fragmentation of the free surface occurs. Within this regime, even more simplified tools have been proposed which can be easily used for design and certification purposes. In the breaking regime, new strategies of numerical simulations are under development, *e.g.* Greco *et al.* (2002b).

References

Campbell I. M. C., Weynberg P. A. (1980*). Measurement of parameters affecting slamming. Final report*, Technology Reports Centre No. OT-R-8042, 440, Southampton University: Wolfson unit for marine technology.

Colicchio G., Colagrossi A., Greco M., Landrini M. (2002). *Free-surface Flow After a Dam break: A Comparative Study.* Ship Tech. Res. 49/3.

Ersdal G., Kvitrud A. (2000). *Green water on Norwegian production ships*. In 10th Int. Conf. Offshore and Polar Engng, ISOPE'2000, Seattle.

Faltinsen O. M. (1990). *Sea loads on ships and offshore structures*, Cambridge University Press, Cambridge, England.

Greco M., Faltinsen O.M., Landrini M. (2000a). *An investigation of water on deck phenomena*. In Proc. 15th Int. Workshop on Water Waves and Floating Bodies, 55-58, Eds. T. Miloh and G. Zilman, Caesarea, Israel.

Greco M., Faltinsen O.M., Landrini M. (2000b). *Basic studies of water on deck*. In Proc. 23rd Symp. on Naval Hydrod., Val de Reuil, France. National Academy Press, Washington DC.

Greco M., Faltinsen O.M., Landrini M. (2000c). *A parametric study of water on deck phenomena*. In Proc. NAV 2000, Int. Conf. on Ship and Shipping Research, Venice, Italy.

Greco M., Faltinsen O.M., Landrini M. (2001a). *Green Water Loading on a Deck Structure.* In Proc. 16th Int. Workshop on Water Waves and Floating Bodies, Hiroshima, Japan.

Greco M. (2001b). *A Two-dimensional Study of Green-Water Loading*. Ph. D. Thesis, Dept. Marine Hydrodynamics, NTNU, Norway.

Faltinsen O.M., Greco M., Landrini M. (2002a). *Green-water loading on a FPSO*. J. Off. Mech Arc. Engng. (ASME), 124.

Greco M., Faltinsen O.M., Landrini M. (2002b). *Water Shipping on a Vessel in Head Waves*. In Proc. of 24th Symp. on Naval Hydrodynamics, Kyushu (Japan).

Rapp R.J., Melville W.K. (1990). *Laboratory Measurement of Deep-Water Breaking Waves*. Phil. Trans. of the Royal Soc. of London, Series A, 331, pp.735-800.

Salvesen N., Tuck E.O., Faltinsen O.M. (1970). *Ships motions and Sea Loads*. SNAME Trans. 78. 250-287.

Tulin M.P., Landrini M. (2000). *Breaking waves in the ocean and around ships.* In Proc. 23rd Symp. on Naval Hydrodynamics, Val de Reuil, France. National Academy Press, Washington DC.

Wagner H. (1932). *Uber stoss- und gleitvorgange an der oberflache von flussigkeiten*. ZAMM, 12, No. 4, pp. 192-235.

Zhang S., Yue D. K. P., Tanizawa K. (1996). *Simulation of plunging wave impact on a vertical wall.* J. Fluid Mech., 327, pp. 221-254.

Zhao R., Faltinsen O.M., Aarnes J. (1997). *Water entry of arbitrary two-dimensional sections with and without flow separation*. In Proc. of 21st Symp. on Naval Hydrod., National Academy Press, Trondheim, Norway. Val de Reuil, France. National Academy Press, Washington DC.

This page has been deliberately left blank

_____

Page intentionnellement blanche

Optimal Shape Design of a Surface Combatant with Reduced Wave Pattern

Emilio F. Campana, Daniele Peri, Ulderico P. Bulgarelli
INSEAN, The Italian Ship Model Basin
Via di Vallerano 139, 00128, Roma, Italy

Optimal design techniques have received considerable attention in many industrial contests: on contrast, the application of automatic optimization to the hydrodynamic ship design has not yet reached the same maturity. Nevertheless, numerical tools, combining together modern computational fluid dynamics and optimization methods, can aid the ship designer, enhancing the operational performances and reducing development and construction costs. Moreover, specific problems that arise during the design phase could be corrected with the aid of a properly defined optimization problem solution.
In this paper, a new approach to the design methodology, involving together designer experience and optimization strategies, is presented. The forebody geometry of a frigate ship, whose original design produced steep bow wave and consequently hydrodynamic noise near the sonar dome due to breaking, has been modified to reduce wave height and suppress the breaking. The numerical optimised geometry has been produced and tested against the original design to experimentally assess the validity of the procedure.

Ship Design methodology

In common practice, the design of a ship involves several cycles, in which desk studies and model basin experiments are coordinated: solutions coming from the design department are tested in the model basin, and than the experimental results drive the new solution to be produced, as soon as the designer's requirements are fulfilled. A fully automatic and non-interactive alternative approach may be based on a use of optimal design methodology. This choice may lead to a sensible cost reduction in the design phase, since effort in the experimental testing is drastically decreased. A trade-off between these two proposals may be the best choice: an initial solution, to be tested, is proposed by the design team, and than further improved by the CFD group. A final test will verify the so obtained results.
In this paper this strategy is depicted. An alternative solution for the bulbous bow of an already operating frigate ship was tested in the basin. This proposal becomes the parent hull form for an *ad hoc* optimization problem performed by the CFD group. The solution of the optimization problem has been experimentally tested, and the results compared against the performances of the alternative solution.

Problem description

A naval combatant, with a bulbous bow including the sonar dome, is usually applied in anti-submarine (ASW) activity. During these types of missions, a hydrodynamic noise problem was encountered. Due to the presence of the large sonar dome, a high and steep bow wave was observed at the speed on 10-12 knots. As a consequence, depending also on the sea condition, wave breaking may be cyclically produced and, because of the hydrodynamic noise, the effectiveness of the sonar may be greatly reduced.

In figure 1, a picture taken during the towing tank tests (in calm water) of the original unit, is reported. The wave pattern produced by a 6.5 m model at the critical speed (12 knots in full scale) shows a deep hollow in the nearby of station 19. For the wave lengths produced at model scale, the action of the surface tension tends to reduce and postpone the incipience of the breaking, preventing air bubble entrainment in water and hence reducing both noise and post breaking phenomena with respect to the behaviour at full scale. Nevertheless, it is evident that the crest between stations 19 and 18 shows the insurgence of breaking phenomena.

Fig. 1 A view of the experimental tests on the original bow.

In order to resolve this problem, the design team has produced an alternative bulbous bow, moving down the sonar dome location. As a consequence, the interference between the dome and the free surface has been decreased, and the wave elevation has been lowered. In general, the benefits of this choice are questionable, since the bulb is pushed outside the projection of the ship hull on the front plane, hence increasing the frontal area of the ship and augmenting the ship's drag. Moreover, as the depth of the ship increase, a possible reduction of the operability of the ship in shallow water is also encountered. Anyway, the alternative solution proposed by the shipyard was accepted by the purchaser and tested in the INSEAN model basin.

Fig. 2 Numerical verification on the PHF in the same conditions of fig. 1.

The tests confirmed the goodness of this choice, since the bow wave at the critical velocity was greatly reduced and the incipient breaking was suppressed, as reported in fig. 3.

However, the suppression of the breaking wave near the bow did not mean that a
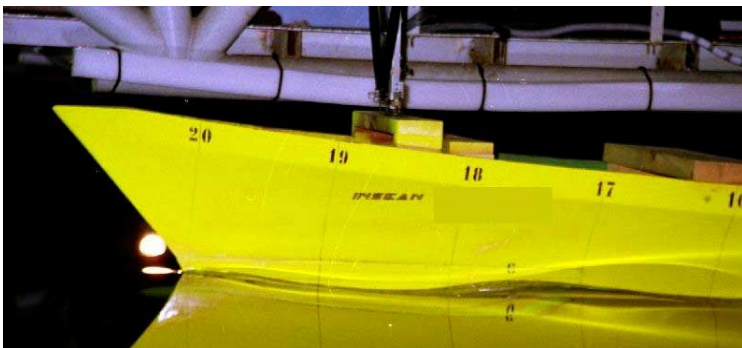
Fig. 3 A view of the experimental tests on the modified bow in the same conditions and viewpoint of fig. 1.

truly optimal solution for the problem was found and a better design may be able to produce even a lower wave pattern. For this reason, starting from the alternative solution (from now on referred as Parent Hull Form - PHF), a numerical optimization cycle has been performed, searching for a better design.

The optimization problem

The numerical prediction of the hydrodynamic noise is quite a difficult task, the accuracy required on the pressure value being too high for available computational tools. Beside that, the numerical prediction of the incipient breaking is another complicated problem, mainly due to the difficulties
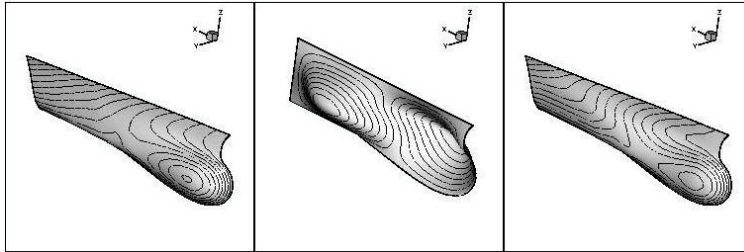
Fig. 4 An example of hull surface modification by superimposition of a Bezier patch. A Bezier surface (middle) is summed to the original hull surface (left), obtaining a modified geometry (right).

encountered in the free surface treatment. To solve the problem, the wave pattern has been estimated by using a steady free surface potential flow model, previously developed and currently applied at INSEAN for the wave resistance computations [2]. This solver is able to compute the wave pattern around a ship with good accuracy. As a consequence, the slope of the wave profile along the hull has been adopted as objective function inside the optimization cycle. The lower the wave slope, the less the probability of breaking waves occurrence near the hull.

As to the geometrical constraints, small variations of the PHF are allowed, the maximum displacement of each grid point being of 1 meter (ship scale). The keel line of the PHF is not modifiable, and the region of the hull to be varied is the same as the one used by the design team in producing the

Fig. 5 An example of Bezier patch.

alternative design. The volume of the bulb is constrained, and cannot vary of more then the 2.5% of its initial value. These limitations are necessary because the sonar must fit in the new bulb too.

The adopted optimiser is described in [5], [6]: it is a derivative-based optimiser, whose main algorithm is a Conjugate-Gradient (Polak-Ribiere). Geometry handling is performed by superimposing of a Bezier surface to the original one, as reported in fig. 4. A Bezier surface is controlled by a fixed number of control points, much less of the number of points of the computational grid. By using this approach, the control points of the Bezier surface are assumed as design variables of the optimization problem, and the shape of the PHF can easily be varied. In figure 5, a detail of a Bezier patch is reported. Control points (the black dots) at the external boundaries of the surface patch are fixed at zero in order to allow a smooth connection between the unmodified hull portion and the modified part. Indeed, if one row (or column) of

control points is fixed at zero on the boundary, the Bezier patch starts from zero, and the position of the grid points at that boundary is not modified. In the same way, if two rows of control points are fixed to zero, the Bezier surface starts from zero with zero tangent, and the modified shape is perfectly faired with the unmodified hull. As a consequence, a careful choice of the control points placement is necessary, in order to obtain a new producible geometry.

Gradient computation: RSM methodology

As stated before, the adopted optimiser is a derivative-based one: in this class of optimiser, a descent direction in the space of the design variables is searched using information derived from the local gradient of the objective function. After a descent direction is fixed, the optimal steplength along this direction is selected, looking at the obtained improvements on the objective function. After that, a new descent direction is searched again, as soon as an optimal condition (zero gradient of the objective function, very small improvement, maximum number of allowed iteration reached, etc.) is found.

The gradient of the objective function is usually computed by a central difference scheme: each design variable is varied, one at time, from the actual value by +/- $\Delta\xi$, the objective functions F^+ and F^- in correspondence of $(\xi_i + \Delta\xi)$ and $(\xi_i - \Delta\xi)$ are computed, finally obtaining the gradient as $g_i = (F^+ - F^-)/(2\Delta\xi)$.
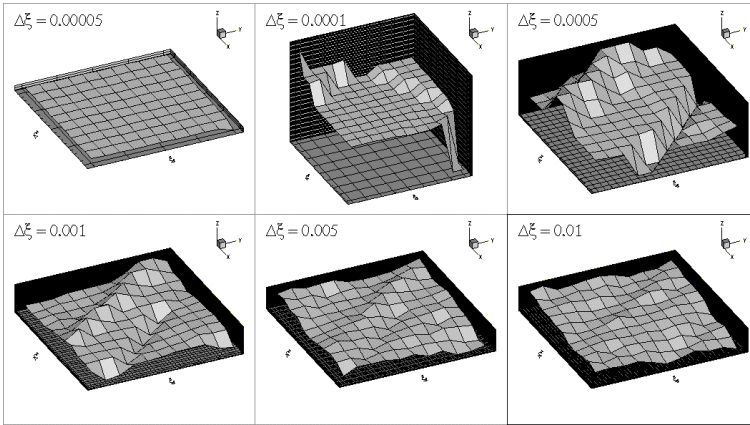
Fig. 6 Pitch motion as function of two design variables: effect of different step of investigation

An alternative approach to this strategy is to use a local approximation of the objective function with an analytical function. To construct this approximation model, some trial values of the objective function are computed (using the potential flow solver describe before) for geometries close to the PHF. The careful choice of this trial points, together with the construction of the approximating model, is performed by applying the Response Surface Methodology (RSM), described in [4]: it is based on the Design Of Experiments (DOE) theory.

The position of the training points is crucial for the correct approximation of the objective function. Usually the training points are placed on the vertex of a hypercube centred on the actual solution. The length of the edge is connected with the portion of the design variable space we are interested to investigate: since we are looking at the local behaviour of the objective function, the length of the edge should be very small, as well as the step $\Delta\xi$ adopted in the central differences scheme.

This method has the great advantage of applying an implicit smoothing of the noise usually introduced by the numerical computation of the objective function for small perturbations of the shape. These inaccuracies have strong effect on the optimization process, since wrong information on the local behaviour of the objective function cause a wrong descent direction: for this reason, often a premature stop of the optimization process is reported. Noise effects on the objective function are clearly reported in figs. 6, 7.
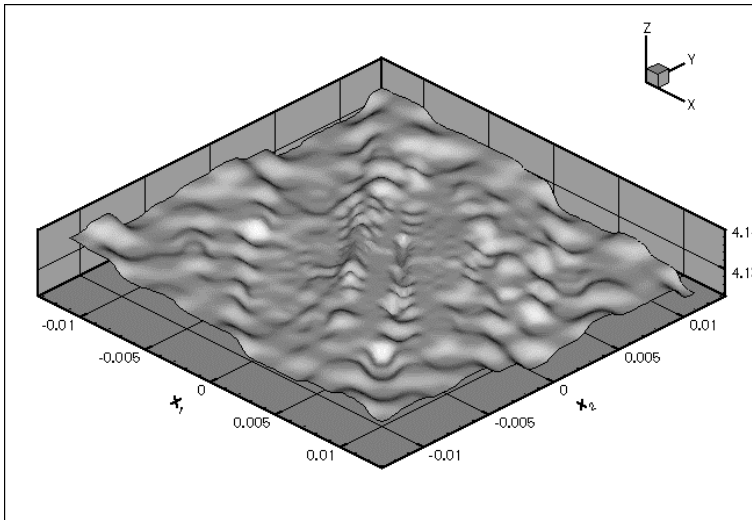
Fig. 7 Global rebuilding of the pitch motion as a function of two design variables.

In the case reported in figure 6 the peak of the pitch response of the ship in head seas is computed. The shape of the combatant has been parameterised by means of two design variables. The function has been computed on a 10 x 10 regular mesh, increasing the wideness of the investigated design variable area, each picture representing a different grid density, i.e. from top to bottom, the amplitude of the interval is increasing. If the mesh is too small (small investigated area), no variation at all is detected for the computed function, while sudden change in the objective functions are detected for some intermediate values of $\Delta\xi$. As a consequence, the step $\Delta\xi$ must be selected carefully: if it is too small, spikes should contribute to an erroneous gradient computation, while the local behaviour is loosed if a too large value is adopted.

In fig. 7, the complete reconstruction of the objective function is reported: here all the previously computed values are plotted together on a single surface. Numerical noise is here evident, and the investigated function suddenly changes his value. As a consequence, local gradient is very unstable, depending on the entity of the selected step $\Delta\xi$, and a smoothing strategy become essential if we need correct information on the local gradient without applying higher order methods for the gradient computation.

A comparison of the gradient components computed with the RSM technique and via a finite differences approach is reported on the following table. The bulb of the PHF was parameterised by using a Bezier patch with 4 design variables, and each gradient component is here presented, as from the two different methods. The high similarity of the exposed values confirms the goodness of the RSM implementation. As a consequence, the following optimization process will be performed by applying this last technique.

Design variable	Finite differences	RSM technique
1	0,791	0,792
2	0,523	0,519
3	0,281	0,282
4	0,149	0,156

Numerical results and experimental verification

Before start the optimization process, a verification of the capability of the adopted numerical solver have been verified on the original geometry: results are reported in fig. 2, that is comparable with the picture of experimental relief, reported in fig. 1. After this first verification, the previously defined optimization problem has been faced and solved, starting from the PHF.

In fig. 8, the numerical results are reported: blue line represents the wave profile along the hull, while the black lines on the models are the buttock lines, that is, the lines at constant y. Bold black lines are the block subdivisions for the numerical grid defining the model. The optimised model has a narrowed leading edge. Also the sonar dome is much narrow than the PHF, and it is curved in the upper part.

Numerical results are reported in fig. 9. The wave profile along the hull is reported for the original model, the PHF and the optimised model. In abscissa the longitudinal coordinate along the model is reported, non-dimensionalized by the model length, while in the abscissa the wave height (ship scale) is reported. Model is cantered on the 0 value, lying in the interval [-0.5 / 0.5]. A strong reduction in the wave profile is predicted, and advantages are also reported in fig. 9.

After that, experimental tests have been conducted on the two new geometries. A quantitative estimatation of the obtained results is deducible by the pictures in figs. 1, 3 and 10. Looking at the horizontal lines traced on the hull, for the original model the wave profile touch the line traced on the model numbered by 6, that means 6 meters from the keel line. Since the draught of the model is 4.6 meters, a wave of 1.4 meters is generated by the original hull. Looking at the PHF (fig. 3), the wave is placed in the nearby of the line at 5.5 meters, so the produced wave is 0.9 meters high, with a reduction of 0.5 meters on a wave of 1.4 meters, that means a gain of about 36%. Finally, the wave produced by the optimized model (fig. 10) touch the line placed at 5 meters on the model: a wave of 0.4 meters is produced by this geometry, and the corresponding gain is of 71% if computed with respect to the original model and of 56% with respect to the PHF. These results are exposed also in the following table.

Fig. 8 Geometrical differences between the optimal hull shape and the alternative design. Contour lines of the lateral coordinate (y) are reported on the hull. Blue line is the wave profile along the hull.
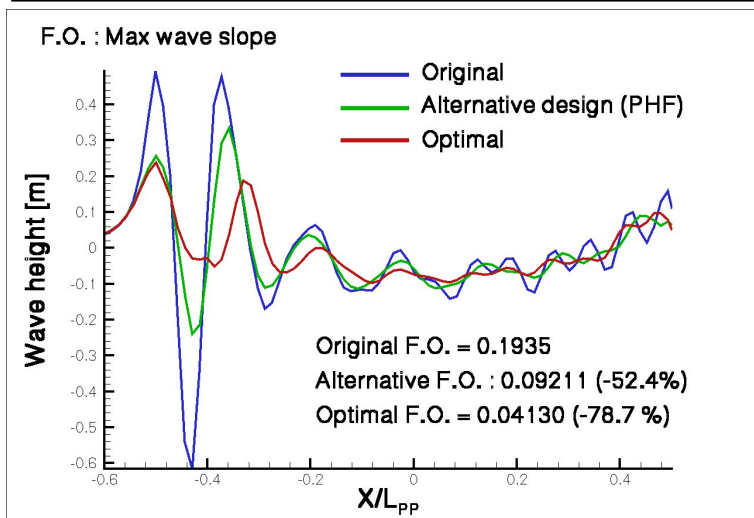
Fig. 9 Comparison of the wave elevation along the hull as computed by the numerical solver for the three hulls.

Bulb	Wave height	% gain (experimental)	% gain (numerical)
Original	1,400	0,000	0,000
PHF	0,900	35,714	52,400
Optimized	0,400	71,429	78,800

Fig. 10 Experimental verification on the optimal hull shape in the same conditions and viewpoint of fig. 1

On constrast, while the total resistance at 12 knots is reduced, a small increase on the total resistance at the other speeds is obtained for the optimized model, as reported in fig. 11, because the flow characteristics are not controlled at the other speeds: as a consequence, the total resistance value at higher speeds is not guaranteed.

The gain on total resistance is very low at 12 knots (of about 1%) if compared with the strong reduction of the wave pattern: this could be addressed to the strong limitations in shape modification toghether with the low optimizing speed. In fact, the form factor of the optimised hullform is very similar to the one of the PHF, due to the small allowed changes in shape: as a consequence, all the differences are addressed to the wave resistance, that is the lower part of total resistance at low speed, being the viscous and frictional part the greater ones: for this reason, a strong reduction on wave resistance component becomes a small variation on total resistance.

Conclusions
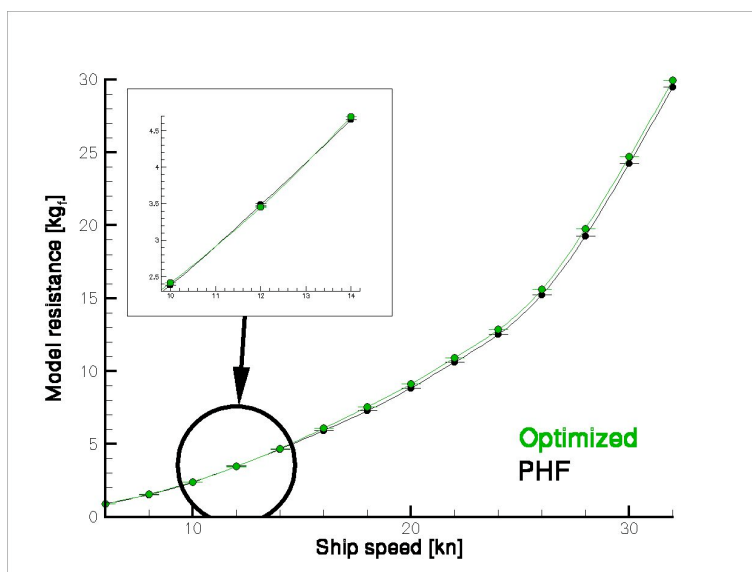
Fig. 11 Experimental value of the total resistance (model scale) for the optimised hull and the alternative design. Optimised hull reduce the total resistance only at the optimising speed.

The experimental results here exposed indicate how the numerical optimization techniques are useful in the design cycle. A further reduction of the objective functions has been achieved, even thought starting from an improved hull form. Drawbacks could be avoided by defining a multidisciplinary (or multiobjective) optimization problem, in which more than a single objective function are considered together, trying to find a solution that is able to enhance the ship under more than a single standpoint: attempts in this application field are presently obtained [7].

Bibliography

[1] Arora JS, 1989,Introduction to optimum design, *McGraw Hill*, Singapore.

[2] Bassanini P, Bulgarelli U, Campana EF, Lalli F, 1994, The Wave Resistance Problem in a Boundary Integral Formulation, *Surveys on Mathematics for Industry*, n.4,pp 151-194.

[3] Gill PE, Murray W, Wright MH, 1981, Practical optimization, *Academic Press*, USA.

[4] Myers RH, Montgomery DC, 1997, Response Surface Methodology, *J. Wyley and sons*, USA.

[5] Peri D, Rossetti M, Campana EF, 2000, Improving the hydrodynamic characteristics of a ship hull via numerical optimization techniques, *9th congress of the International Maritime Association of Mediterranean* - IMAM 2000, Ischia, Italy.

[6] Peri D, Rossetti M, Campana EF, 2001, Design optimization of ship hulls via CFD techniques. J*ournal of Ship Research*, **45**, 2, 140-149.

[7] Peri D, Campana EF, 2002, Multidisciplinary design optimization of surface ships. Submitted to J*ournal of Ship Research.*

Paper #56

Discussor's Name: Professor Ramana Grandhi
Author's Name: D. Peri

Q: 1) Is the sensitivity analysis completely analytical within the CFD code? What is the cost of CFD simulation alone compared to sensitivity analysis? Did you use adjount variade method?
   2) Did you try to build RSM in the feasible set and then build Pareto curve on RSM?

A: 1) Yes, SA is fully integrated in the CFD code. The cost of SA is about 25% of the glow solution, but it depends from the number of design variables, becoming lower when the number of design variables increase. We use both direct and adjoint methods.
2) Yes. It is what we are used to do.

Preliminary Multi-Disciplinary Optimization in Turbomachinery Design

Y. Panchenko, H. Moustapha, S. Mah
Pratt & Whitney Canada Corp.
1000 Blvd Marie-Victorin, MS 01RA4
Longueuil, Quebec J4G 1A1
Canada

K. Patel, M.J. Dowhan, D. Hall
Pratt & Whitney Canada Corp.
1801 Courtney Park Drive, MS 22MC1
Mississauga, Ontario L5T 1J3
Canada

Abstract: The gas turbine engine is a complex aerodynamic machine with performance, structural and manufacturability challenges. This paper gives an overview of a multidisciplinary optimization approach applied to the conceptual design of small aircraft engines. A description of major turbomachinery disciplines and the numerous interactions between disciplines is given followed by a discussion of the need for preliminary design optimization. The approach to development of such a system undertaken at Pratt & Whitney Canada is described including identification of appropriate design tools and their influence on the geometrical definition of an engine cross-section. Finally, preliminary optimization results are presented.

1 INTRODUCTION

Over the past five decades, the gas turbine engine has evolved rapidly to provide a reliable and efficient business solution for global transportation. The engine design process is clearly a large contributor to this evolution. This process is highly iterative, multidisciplinary in nature and complex. The success of an engine depends on a carefully balanced design that best exploits and considers the interactions among the numerous traditional engineering disciplines such as aerodynamics and structures, as well as the life cycle disciplines of cost, manufacturability, serviceability and supportability. A crucial task in the engine design process is to define a concept because "the best engineering effort cannot totally right a poor concept selection" [Ref.1]. Employing multidisciplinary optimization (MDO) at the conceptual phase of design is important, since it is at that stage that the largest influence on the final product is realized. In this paper, the application of MDO methodology to the conceptual stage of the design cycle will be referred to as Preliminary Multi-Disciplinary Design Optimization (PMDO).

Over the last few years, the increasing complexity of engineering systems has stimulated progress towards developing an MDO capability and implementing it into the design process. The concept of MDO can be interpreted as a formal methodology that facilitates exploration and exploitation of interdisciplinary interactions to achieve a better overall system. The earliest MDO developments occurred in the 1970s and have been progressing ever since, revealing great potential to improve product quality and significantly reduce development time, thus, helping the product to remain competitive in a global market.

Current industry applications of MDO include biomechanics, automotive, electromagnetics, nuclear, electronics and, also, aerospace where the interest in MDO has been particularly intense. An extensive survey of MDO applications in aerospace design has recently been presented by Sobieszczanski-Sobieski and Haftka [Ref.2]. This paper identifies the main challenges of MDO implementation as being computational cost and organisational challenges which are being

addressed by developing various approximation and decomposition strategies. Another paper by Sobieszczanski-Sobieski [Ref 3] describes five MDO conceptual components: Mathematical Modelling, Design-Oriented Analysis, Approximation Concepts, Optimization Procedures, System Sensitivity, and Human Interface.

In an effort to solve engineering optimization problems, a number of promising MDO methods have been developed. These include the All-in-One (A-i-O), Individual Discipline Feasible (IDF), Multidisciplinary Feasible (MDF) [Ref. 4], Collaborative Optimization (CO) [Ref. 5], Concurrent Sub-Space Optimization (CSSO) [Ref. 6], and Bi-Level Integrated System Synthesis (BLISS) [Ref. 7] methods. To address the problems of limited computational resources and to analytically substantiate the practical applicability of MDO methods, a two-phase study has been conducted on the performance of a selected set of MDO methods that included MDF, CO, IDF, and BLISS methods at the NASA Langley Research Center. A comparison of the performance, classification of the methods, guidelines for using specific methods and systematic method testing procedures are presented in Refs. 8 and 9.

In any type of MDO applications, the efficient solution of the problem depends greatly on the proper selection of a practical approach to MDO formulation. Six fundamental approaches are identified and compared by Balling and Sobieszczanski-Sobieski [Ref.10]: single-level vs. multi-level optimization, system-level simultaneous analysis and design vs. analysis nested in optimization, and discipline-level simultaneous analysis and design vs. analysis nested in optimization. From the results presented therein, two conclusions are apparent: 1) no single approach is fastest for all implementation cases, and 2) no single approach can be identified as being always the slowest. Therefore, the choice of approach should be made only after careful consideration of all the factors pertaining to the problem at hand.

With the increasing acceptance and utilization of MDO in industry, a number of software frameworks have been created to facilitate integration of application software, manage data, and provide a user interface with various MDO-related problem-solving functionalities. A list of frameworks that specialize in integration and/or optimization of engineering processes includes: iSIGHT (developed by Engineous Software), ModelCenter (developed by Phoenix Integration), Epogy (developed by Synaps), Infospheres Infrastructure (developed at the California Institute of Technology), DAKOTA (developed at Sandia National Laboratories) and many others. An extensive evaluation of select frameworks has been performed at NASA Langley Research Center. The report by R. Krishnan [Ref. 11] presents a number of primary requirements for the "ideal" framework, describes the positive and negative aspects of each of the evaluated frameworks with respect to those requirements, and recommend frameworks that deserve a closer look. Additional detailed descriptions of MDO framework requirements are provided in Salas and Townsend [Ref. 12].

A significant amount of MDO research has been conducted in the field of turbomachinery design. A number of reports have been published presenting the development of optimization environments [Refs. 13 and 14], optimization methods, and procedures for turbine engine design. Particular aspects of multidisciplinary optimization for different turbomachinery design stages are investigated by Dornberger et al. [Ref. 15]. The differences in the optimization approaches and methods used in preliminary and final design steps are also shown. The present paper describes the ongoing work related to the development and implementation of a MDO environment with a focus on its application to the conceptual design of the gas turbine engine.

2   TURBOMACHINERY DISCIPLINES

Overall Design Process

The process of engine design starts at the aircraft level. As depicted in Figure 2.1, an engine is a system that seamlessly integrates into the larger system of an aircraft. Engine design is a top-down procedure in which two processes, design and manufacturing, start and proceed from opposite ends of the system configuration. The design process starts at the overall system level and gradually moves down to the component level. The manufacturing process proceeds in the opposite direction.
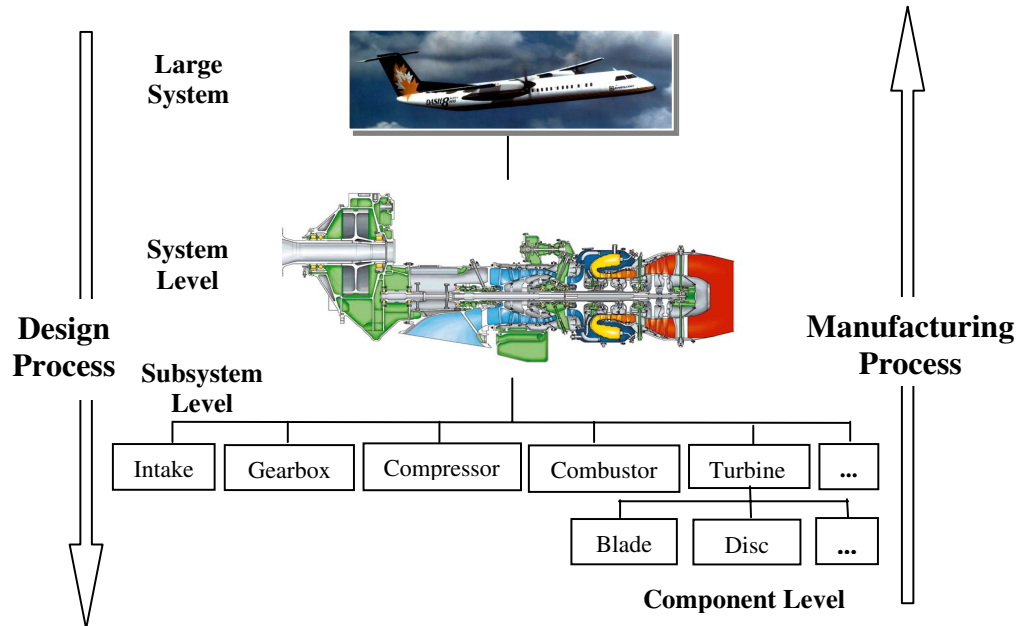
Figure 2.1: Design and manufacturing processes [Ref.16]

The efficient and reliable integration of design and manufacturability aspects of a project has been the focus of Concurrent Engineering (CE). Concurrent Engineering can be defined as a systematic approach to concurrent design of products in which all disciplines, including manufacturability and supportability, are addressed simultaneously. A comprehensive definition of the CE concept is provided in Ref. 17. An example of the implementation of the CE approach for turbomachinery applications is the Agile Engineering Design System developed by Concepts ETI, Inc. The potential benefits of the Agile system for the turbomachinery design process and the latest developments in the field are presented by Japikse in Ref. 18.

Traditionally, the design of the gas turbine engine follows three major phases: Conceptual Design, Preliminary Design, and Detailed Design that involves designing for manufacturing and assembly. As was stated in the introduction, the scope of this paper is the conceptual phase of the design process which involves the exploration of different concepts that satisfy engine design specifications and requirements.

The gas turbine design is a sequential and highly iterative process that is represented by a net of tightly coupled engineering disciplines. The interaction that takes place among the disciplines is a series of feedback loops and trades between conflicting requirements imposed on the system. The complexity of the process is depicted in Figure 2.2. A close-up view of the process that takes place within the discipline of aerodynamics is shown in Figure 2.3.
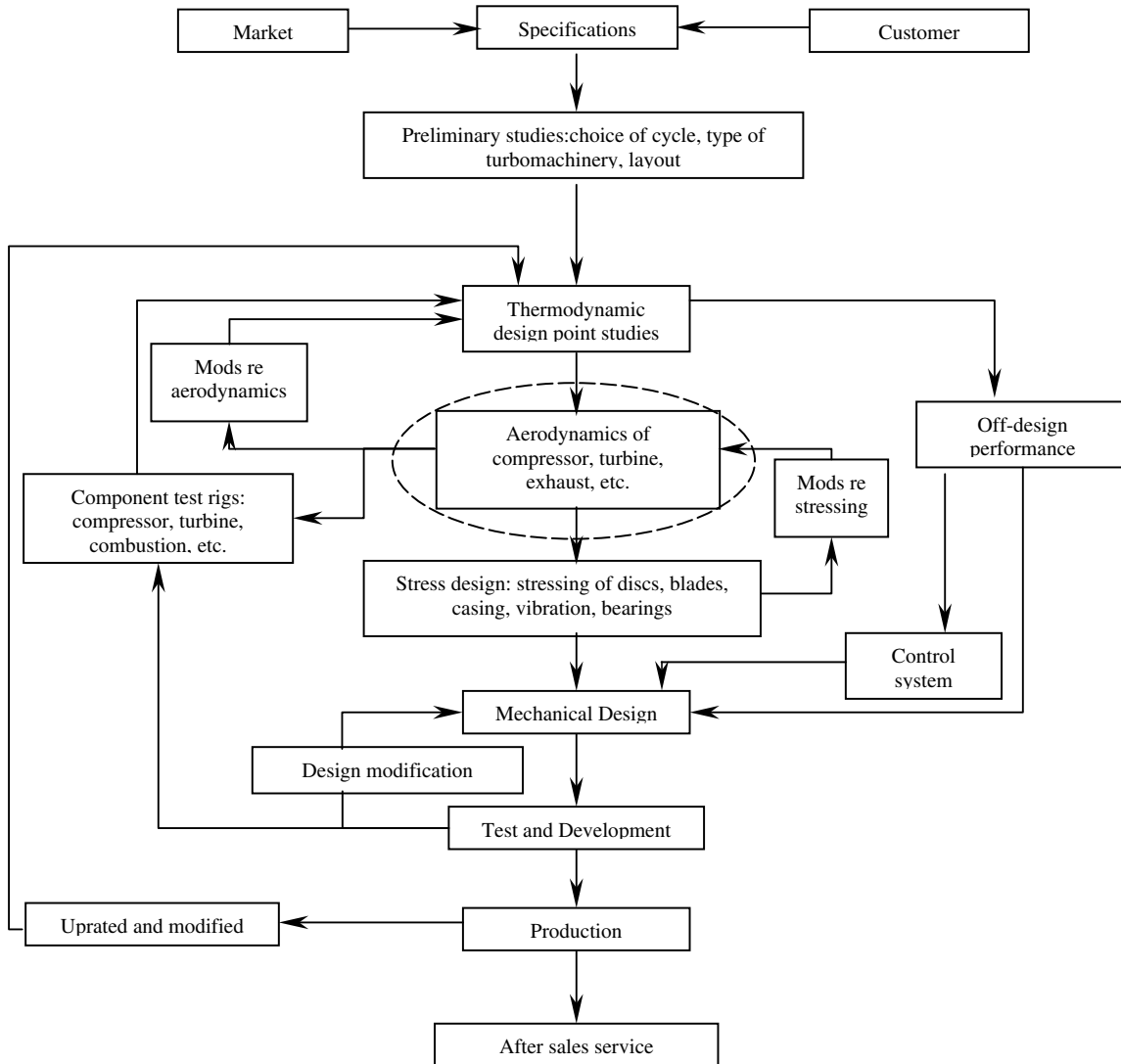
Figure 2.2: Gas turbine design steps [Ref. 19]
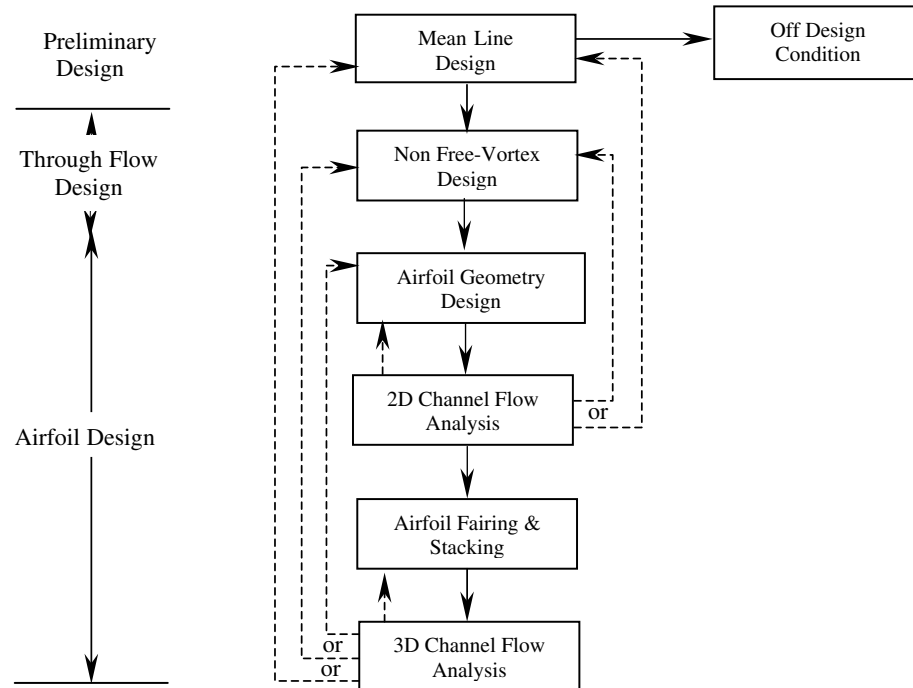
Figure 2.3: Aerodynamic design process

Every design must be grounded in sound physical principles that are grouped into categories named disciplines [Ref. 1]. Figure 2.4 illustrates the hierarchical breakdown of an engine into different engineering disciplines that govern the design of major engine components that, in turn, combine to make the final product.
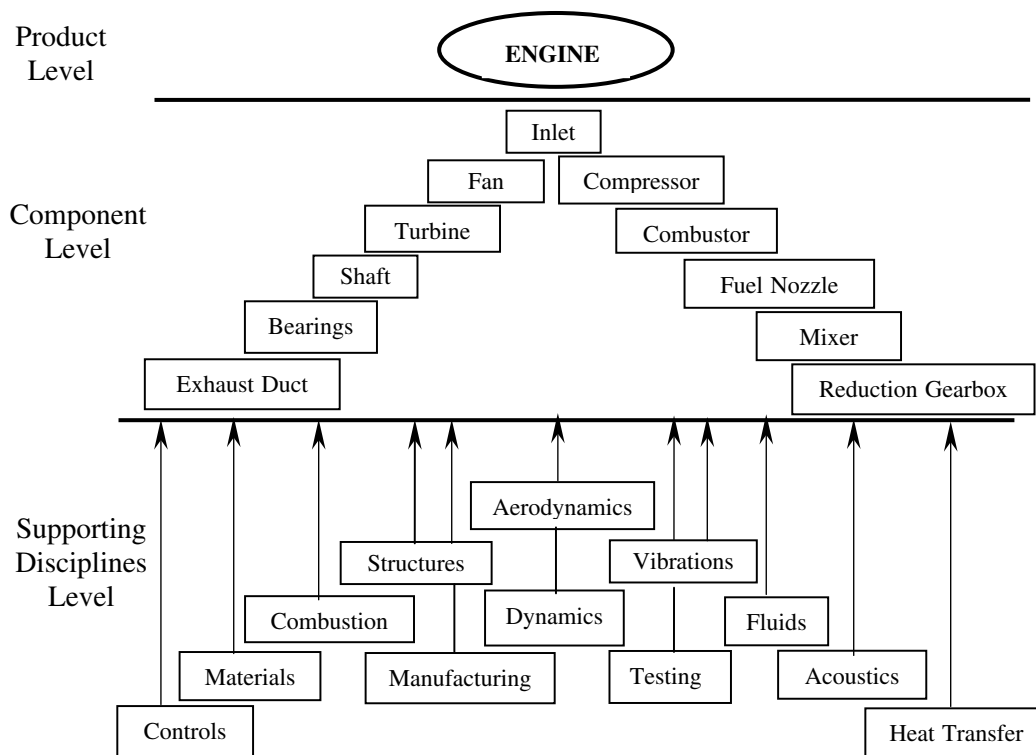
Figure 2.4: Product, components and the supporting disciplines

Interactions Between Disciplines

At the Concept Design stage of an engine, the aim is to develop a concept far enough to be able to estimate with reasonable accuracy the feasibility, weight and the potential production and development cost. This information is used directly in formulating a proposal to the Aircraft manufacturer. In such an advanced system as an engine, the couplings among disciplines are numerous and strong, requiring a multidisciplinary approach to design. The performance of the system depends on harmonious interaction of these disciplines and components that must meet a large set of strict operational requirements and standards. A typical list of parameters usually addressed in the Concept Design Study, and the supporting groups involved, include the following:

1. Basic requirements – Marketing and Customer
2. Thermodynamic cycle – thrust, specific fuel consumption, maximum temperature, pressure, etc. - Advanced Performance Group
3. Installation requirements - Fluid Systems Group
4. Compressor and Turbine definition - Compressor and Turbine Module Centres
5. Materials available and their allowable limits such as temperature, creep, oxidation, strength, low cycle fatigue life capability, and buckling limits - Materials Engineering Group
6. Weight - Product Definition and Weight Groups
7. Air and Oil systems - Fluid Systems Group
8. Manufacturing cost targets and factory standard cost - Product Cost Group
9. Envelope requirements - Design Groups, Customer and/or Nacelle Engineering Group
10. Direct operating costs - Customer Support
11. Manufacturing limitations - Manufacturing Engineering Group

A perfectly balanced design requires all of the above factors to be considered and selected appropriately. There are inherent contradictions between some of the disciplines that make this task difficult. The thermodynamics dictate that parameters that make an engine more efficient (e.g. higher operating temperature) are exactly the opposite of what is required for low cost. Materials capable of operating at high temperatures imply higher development costs as well as use of more advanced manufacturing processes which are, therefore, more expensive. Alternatively, introducing turbine cooling also increases the cost due to manufacturing complexity. The same applies to weight. Lower weight for a given performance requires stronger or advanced light alloy materials, which in general are more expensive. One should not be surprised that current solutions may not be optimum because there is insufficient time to carefully study the interactions between the variables which, generally, are the responsibility of numerous disciplines.

Issues with the technical interaction between disciplines

Over time, the way Concept Design studies are conducted has changed significantly. For many years, a single department (Advanced Engineering) was involved in defining the concept using established rules of thumb, simple 1-Dimensional analysis and past experience. This was followed by the involvement of the groups responsible in the end for bringing the concept to production. In this manner, there was little interaction between Advanced Engineering and the downstream disciplines. Engine concepts were therefore proposed with relatively low effort up front and resources were added as the development program proceeded. This process resulted in end-loaded engine development, where changes to the design in the detail design and development phases were time consuming and expensive.

The model of product development in use at present in P&WC is somewhat different to this.

A larger portion of the work is expected to be done up front, in the Advanced Design/Concept stage, with a smaller increase in resource usage during the detail design and development. Figure 2.5 illustrates the old procedure for engine development versus the current system.
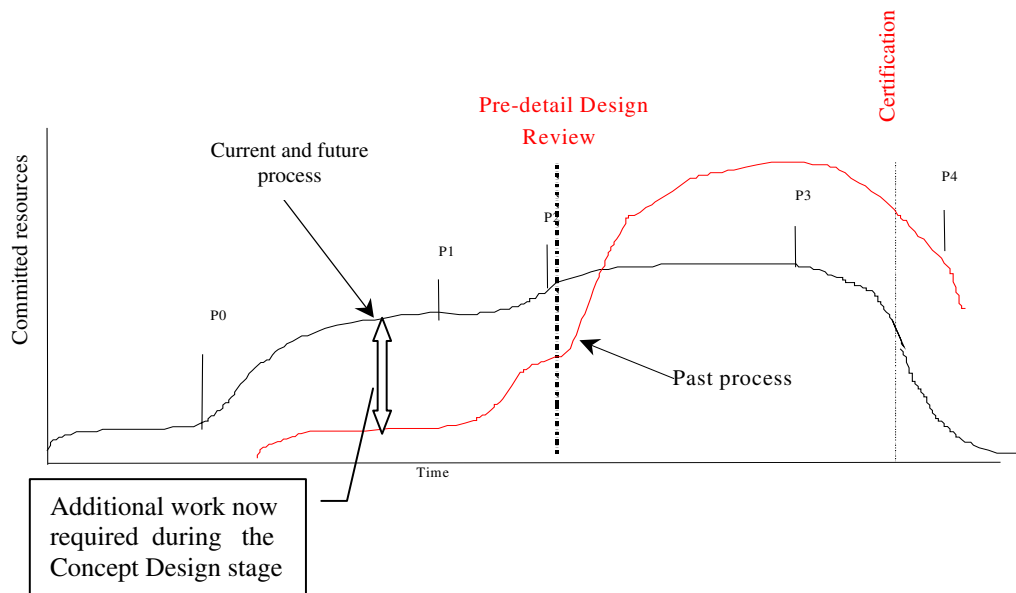
Figure 2.5: Resource usage in a typical engine development program

Since the amount of effort at the Concept Design stage is now much greater than before, the burden could not be carried entirely by the Advanced Design group. A process, which evolved therefore, was to involve the specialist groups directly in the Advanced Concept work. This would potentially avoid downstream redesign. However, it results in significant delay of the concept evolution. The Advanced Design group was expected to deal independently with each of the specialist disciplines, obtain the required input and re-assemble the data into the study and make the required association between the individual inputs in terms of effect on the overall performance, installation envelope and design features. Because the specialist disciplines work with more detailed, such as 2-D and 3-D methods, the results were obtained in a time-scale not commensurate with the time for the concept study and have to be re-inserted into the study manually. A good design is optimized considering all of the parameters above, it is quite clear that interaction between the disciplines must be highly ordered and highly efficient to produce answers in the required time. Many of the parameters or groups are bypassed in the decision-making by resorting to rules of thumb and past experience. Conversely, the decision making may be delayed to the point that competitions are missed.

Some of the common problems with interactions of the disciplines are as follows:

1. Tools of the different disciplines, usually, do not have a common file structure
2. No automated system for transferring data
3. Problems with manually transposing data – typos, etc.
4. Traditional exchange of data is by tables and spreadsheets or graphical.
5. Inefficient and unreliable tools.
6. Time consuming. (Other discipline not available for consultation when needed)
7. Only small areas of the problem are explored because of the time constraint.
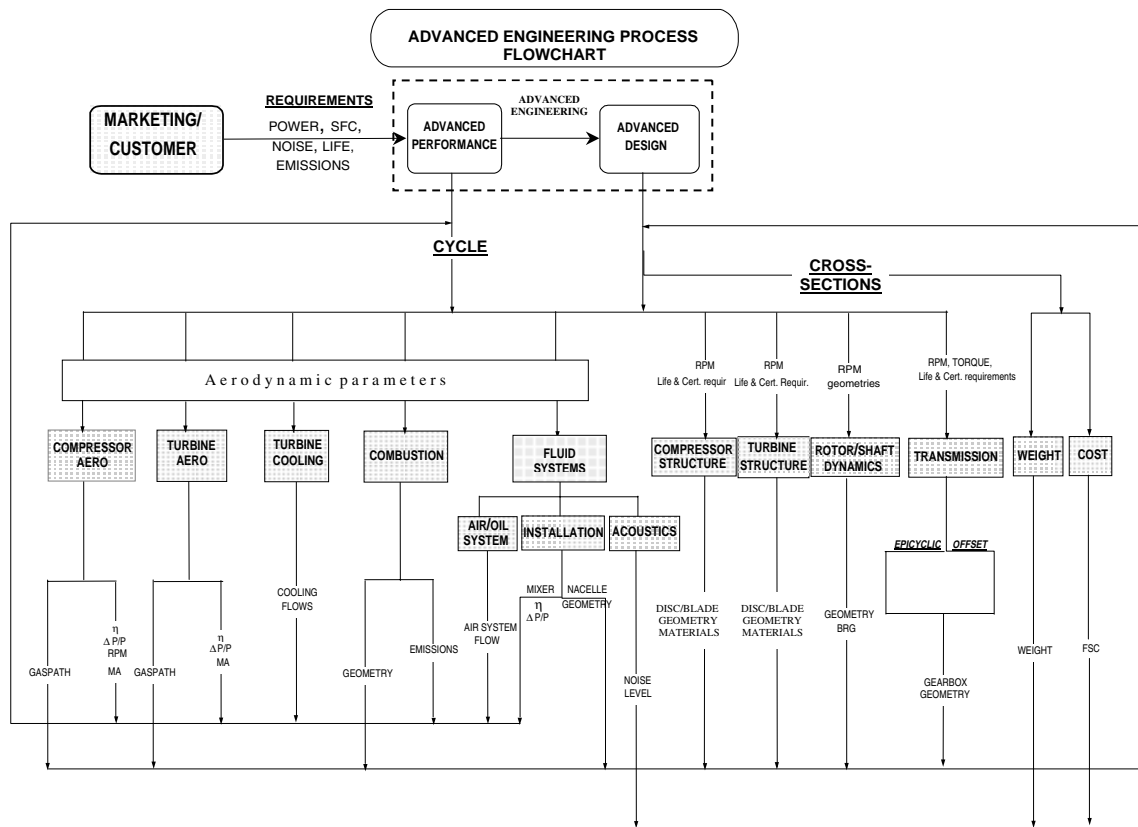
Figure 2.6: Disciplines infrastructure

Figure 2.6 depicts a schematic representation of the infrastructure of the multi-discipline interactions required for a proper preliminary product definition phase in the Advanced Engineering group. This is a simplified chart, whereby data flow between the supporting component groups have not been included to avoid a diagram that is visually unreadable.

3 PRELIMINARY PRODUCT DEFINITION PROCESS

To fully understand the challenges associated with the definition of a preliminary engine configuration, an overview of steps and activities to be performed is required. The design of a new gas turbine engine begins in the New Products Definition group, or "Advanced Engineering" department. It is here that a new powerplant (or a major derivative engine modification) is conceptualized for further follow-on detailed engine definition and hardware materialization. The engine definition in the Advanced Engineering phase normally begins with one of the following circumstances:

- Direct request from a customer (Original Equipment Manufacturer (OEM)) for a new engine to cater to a specific vehicle propulsion need or power generation application.

- Internal company strategic investigation on potential market niche for a suitable powerplant that will fill this gap.

It is from there that the Advanced Engineer will commence a product definition study to conceptualize a new engine to address the request. As will be described, this phase of study

applies all the disciplines needed for proper product definition. Each of the disciplines involved has its own domain of design parameters. Moreover, there is no one unique parameter to optimize, but numerous variables and criteria to consider when optimizing an overall combined vehicle/ engine system. Designing a powerplant to best cater to the overall aircraft requirements in itself encompasses a whole realm of engine design parameters that need to be carefully selected and optimized. A classic example of a gas turbine design optimization is the Overall Pressure Ratio (OPR) and cycle temperature selection. The Figure 3.1 illustrates cycle pressure ratio and temperature influence on basic engine characteristics, such as Specific Fuel Consumption (SFC) and Specific Power. OPR and Temperature in itself are linked to other inter-dependent parameters such as component efficiencies, air-system flows, engine weight, durability, cost, etc., all having an impact on the optimum OPR-Temperature selection.
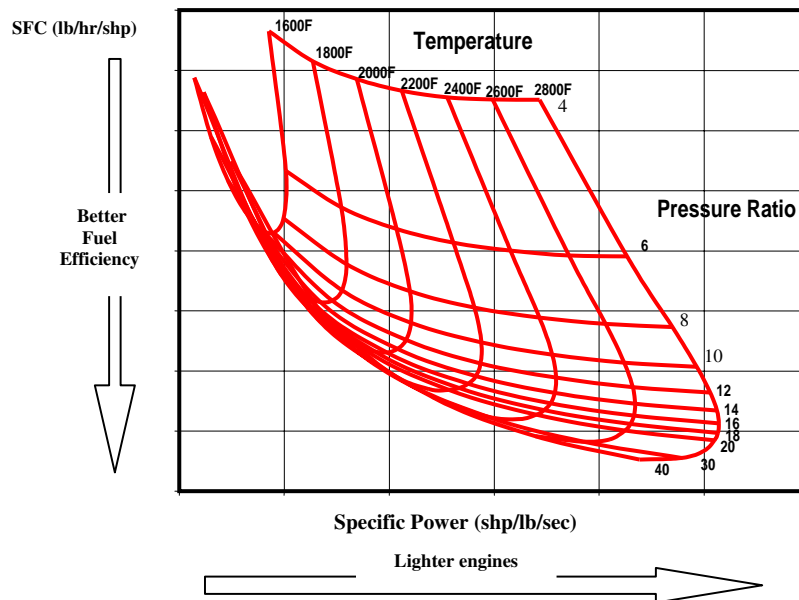
Figure 3.1: Cycle pressure ratio and temperature influence

Other examples of parametric optimization in gas turbine design is the core size optimization as illustrated in Figure 3.2. Maximum power (typically hot day take-off) influences the core size needed to respect the turbine operating temperature limit. Again, a parametric study of this nature will encompass many other inter-dependent parameters influencing the optimum; i.e. air-system flows, component size effects, engine weight, durability, cost, etc. Choosing the right size of the core will need to take all the parameters into consideration.
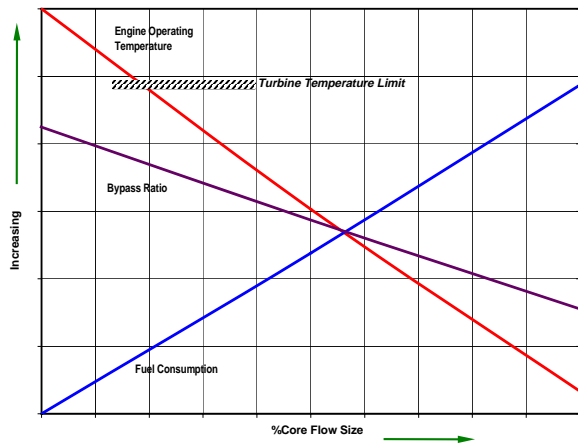
Figure 3.2: Turbofan core size sensitivity
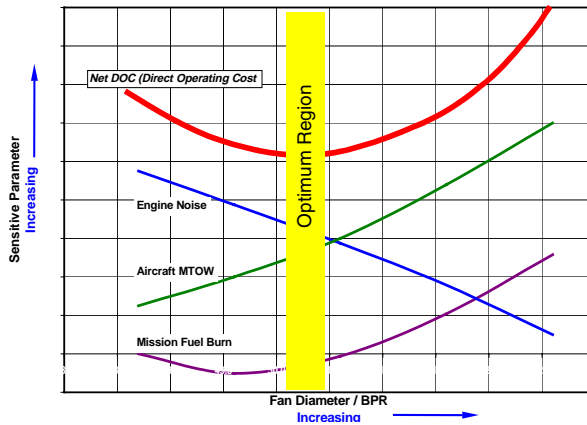
Figure 3.3: Fan diameter/BPR parametric

A good example of a multi-parametric optimization is the bypass ratio (BPR) / fan diameter sensitivity study. An optimization study of this nature typically has many influences on the overall aircraft performance and its associated operating cost (Figure 3.3). Here, increasing the engine fan diameter (higher BPR) will typically improve the engine Specific Fuel Consumption. However, associated with increasing fan diameter is a higher powerplant weight and increased nacelle drag that will inversely impact the overall mission fuel burn. Moreover, the mission fuel burn must also be weighed with the impact of aircraft maximum take-off weight (MTOW), noise levels and ultimately its global impact on the aircraft direct operating cost. As can be seen, optimizing solely on the basis of best engine SFC may not necessarily provide the best for the overall aircraft point of view. Only after considering all the pertinent metrics will the proper optimum be found.

These examples of cycle optimization only touch a few of the many parametric studies necessary to design the best powerplant for a vehicle. Each of the studies will typically involve many disciplines and a multitude of design parameters. There is obviously great potential for process improvement through the creation of an automated multi-disciplinary design system.

Upon receipt of the powerplant requirements, the first technical study involves a parametric "thermodynamic cycle" investigation to establish a viable engine configuration and performance attributes that satisfy the needs of the customer. The cycle investigation, or Advanced Performance study, already encompasses several disciplines. Typically, the following key disciplines will be dealt with during the Advanced Performance activity:

- Compressor aerodynamics (fan, low and high pressure compressors…)
- Turbine aerodynamics (low and high pressure turbines…)
- Air system (particularly hot end cooling)
- Compressor/Turbine structures
- Combustion aerodynamics
- Dynamics
- Weights,
- Cost, etc.

Figure 3.4 illustrates the disciplines involved in an Advanced Performance design study. Numerous variables come into play in the Advanced Performance study that typically include (to name a few):

- Flows
- Temperatures (and work)
- Pressures (and pressure ratio)
- Efficiencies
- Duct losses
- Spool speeds
- Air system...
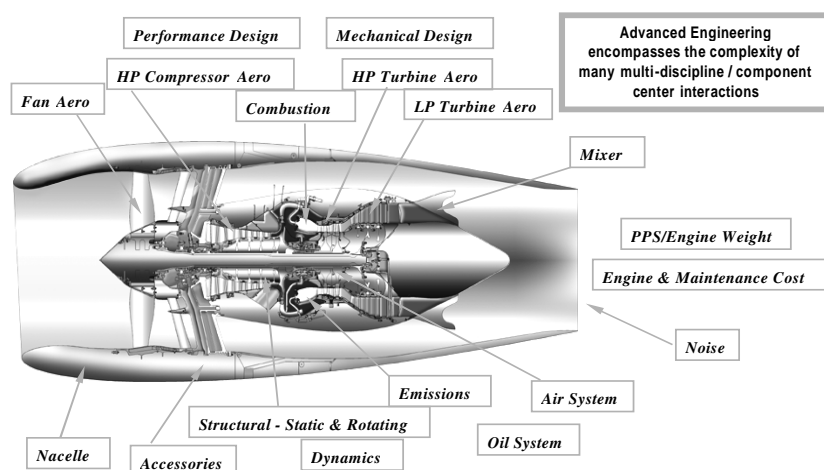
Figure 3.4: Disciplines and components encompassed by Advanced Engineering

An Advanced Performance study requires the analysis and evaluation of individual component performance levels, be it through empirical means or where more critical, a full interactive work process with the corresponding specialist group. With the later, a specialist will analyse/design the component typically using 1-D meanline design tools. When the initial thermodynamic cycle assessment has proven feasible (with the addition of an acceptable business case), a further follow-up Advanced Engineering study is conducted on a more detailed level.

One of the key attributes to be evaluated in an Advanced Engineering study, which follows an Advanced Performance study, is the geometry associated with aerodynamic flowpaths and rotating component discs corresponding to the selected engine configuration (Figure 3.5).
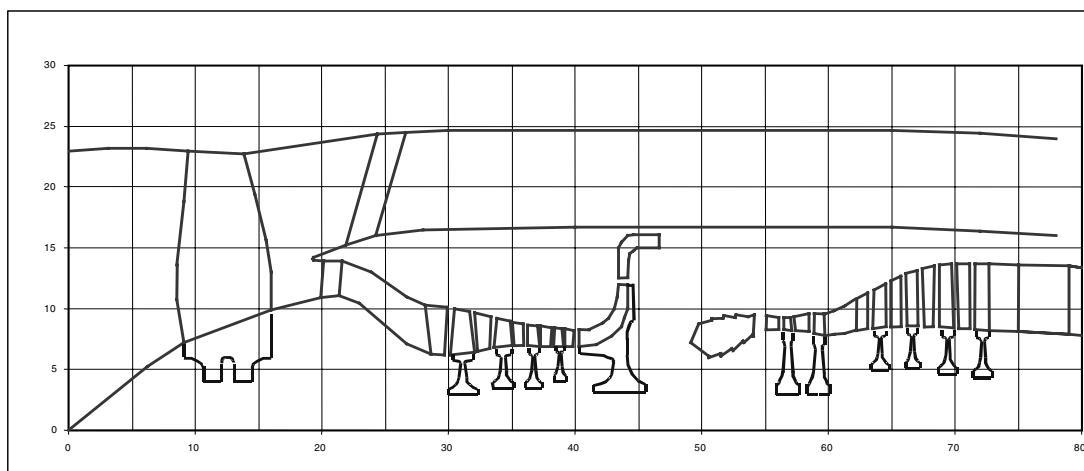
Figure 3.5: Example of geometry assessment

As mentioned in the previous section, the design of an engine starts at the aircraft level. In the aircraft regime, for example, several key criteria that are critical to the optimization and definition of the product include:

- MTOW (maximum take-off weight)
- TOBFL (take-off balanced field length)
- Time to climb
- Mission fuel burn
- Environmental criteria (noise, emission)
- Maintenance cost …

The application, market driving force, vehicle selling attributes, etc. drive the weighting of each of the parameters. Examples of various interactions between the engine design parameters and the aircraft attributes are illustrated in Figure 3.6.
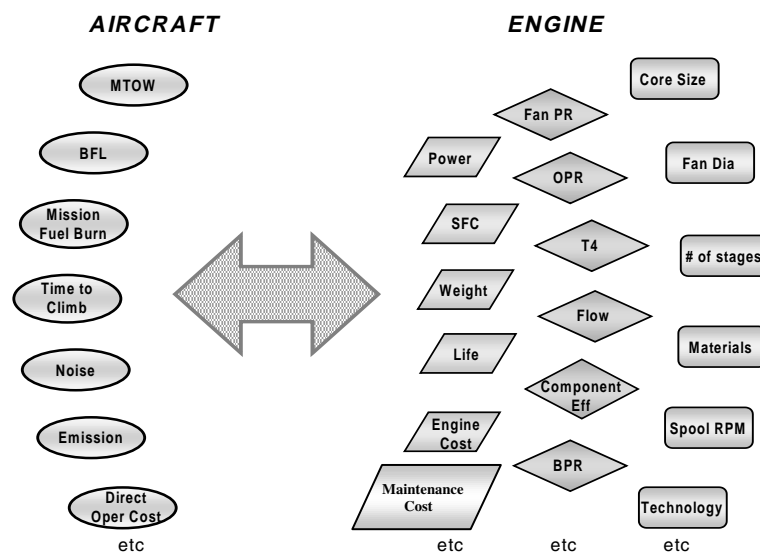
Figure 3.6: Design dependencies between aircraft and engine parameters

Several process levels are evident, each with its own design optimization and all interdependent:

Aircraft

Engine Thermodynamics

Engine components: Aerodynamics / Stress / Dynamics…

Engine Nacelle: Aerodynamics/Mechanical...

Manufacturing

Key deliverables of an Advanced Engineering study include the following:

- Performance
    - Power
    - Fuel consumption
- Emissions and Noise
- Preliminary engine layout/cross-section
- Propulsion system (engine/nacelle) weight

- Factory standard cost
- Estimated aircraft performance:

  - MTOW (maximum take-off weight)
  - TOBFL (take-off balanced field length)
  - Time to climb
  - Mission fuel burn

To fully exploit the best system design, the mentioned parameters require the aircraft/engine design optimization to be conducted in unison and not in isolation. Of course, this can only be most effective with quick data exchange, commonality of tools and fast response rate.

4   THE NEED FOR PRELIMINARY MULTIDISCIPLINARY DESIGN OPTIMIZATION (PMDO)

From the previous sections, it is evident that Advanced Engineering conceptual and preliminary designs encompass a wide field of engineering disciplines and make the largest influence on the final product configuration. Although knowledge increases as the design process goes forward, the freedom to make major design changes decays or causes major delays in the schedule and increased design cost. Therefore, it is of a primary importance that more knowledge is captured in the conceptual phase of the design process in order to avoid problems occurring later in the cycle which require costly efforts to correct.

In general, the concept/preliminary design of gas turbines requires a wide range of factors to be considered and weighed against each other to achieve a viable and competitive gas turbine engine solution. This must usually be achieved in a time scale that is not commensurate with the importance of the task. Thus, decisions are often made with incomplete data and, hence, an increased risk of not meeting all of the design requirements. In the past, it was possible to obtain quick solutions using correlations based on previous engine designs and experience but this will not usually result in an answer of sufficient fidelity for current designs. This method may also lead to data which is conservative by virtue of the fact that the data used is a product of *the way things were* and not the *way things could be*. This can lead to sub-optimal designs and uncompetitive bids in engine competitions. Furthermore, designing in isolation is not viable for a good system design but requires a constant data exchange between the customer and supplier with each expecting fast response to allow immediate reaction for proper design changes to ensure a true optimum system. Another obvious problem with the traditional sequential design approach is the short conceptual phase with unequal distribution of disciplines which does not allow the designer any freedom to improve quality and integrate disciplines for optimization [Ref.20].

Considering the challenges and complex discipline interactions described in previous sections, significant potential benefits can be gained through the incorporation of an automated integration and optimization system. This was the goal of Pratt & Whitney Canada when it initiated the development of an integration/optimization system tool named *PMDO (Preliminary Multi-Disciplinary Design Optimization)* specifically for use in the Advanced Engineering community.

It is the intent at P&WC that Phase I of the PMDO project addresses integration and automation with an optimizer that will quickly generate "Aerodynamic flowpath" results (whole engine) with a follow-up Phase II project to include all basic rotating disc geometry auto-generation. PMDO will be constantly developed and expanded to include additional disciplines (air-system, dynamics, weight, cost, noise, emissions), ultimately leading to the full generation of the engine cross-section (Figure 4.1).
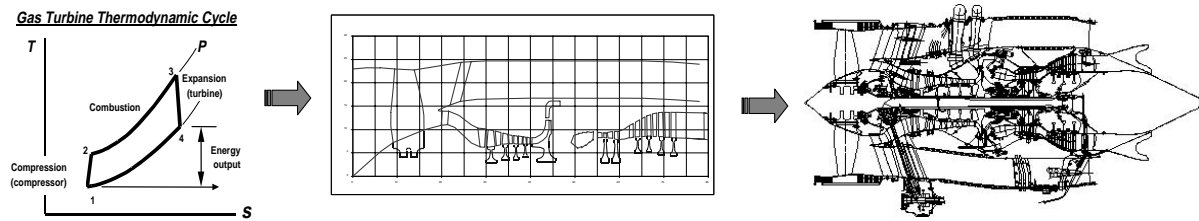
Figure 4.1: PMDO system deliverables

The expected benefits of PMDO include:

- The automated linking of component specialist tools with the thermodynamic cycle program to provide a seamless data transfer with minimal manual intervention
- With the automated link, lead-time for preliminary engine design is significantly reduced
- Reduce the possibility of human error with the elimination of manual data manipulation.
- A more thorough analysis with increased iterations is possible with improved fidelity in design results
- Improved confidence/success level of finding the correct optimum engine design choice

Figure 4.2 illustrates additional goals and improvements in the design process that will be made possible by the PMDO system. The steeper slope of the solid curve reflects that more knowledge will be brought forward to the conceptual and preliminary design phases ensuring that the target engine deliverables are met. Although the time spent in the conceptual phase will increase to capture more knowledge and explore alternative configurations, the time spent in the detailed design will be reduced. The development and implementation of such system is the key to reaping the benefits of improved turnover time and quality of first design during concept study. Thus, the PMDO system will effectively simulate increased resources that are available for the Concept Design stage (Figure 2.5).
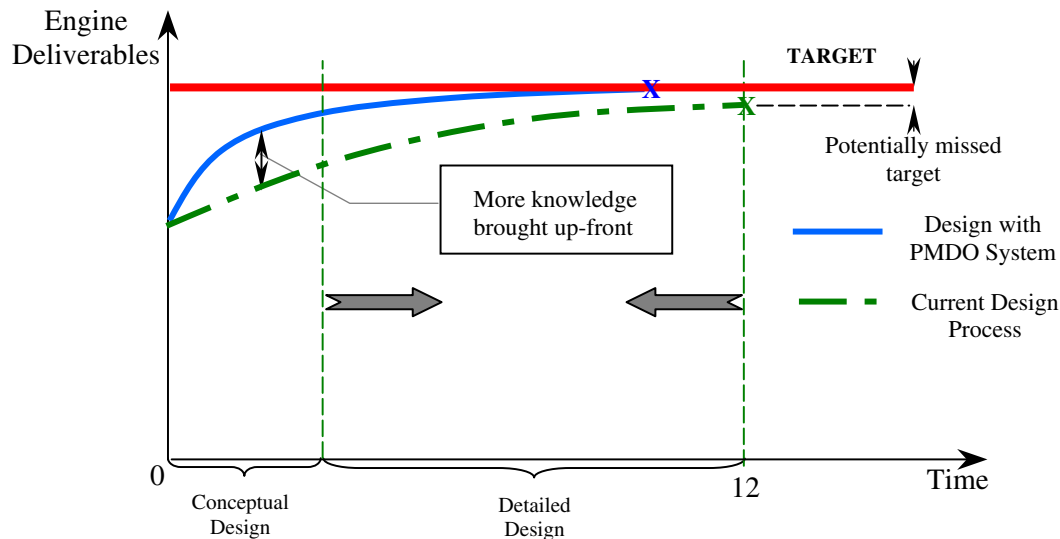
Figure 4.2: Shorten overall design cycle with the PMDO system

5   APPROACH TO PRELIMINARY MULTIDISCIPLINARY DESIGN OPTIMIZATION

The effective introduction of MDO at the conceptual and preliminary design stage depends on adopting the appropriate strategy.   Other requirements include adequate information infrastructure and robust design-oriented analysis tools. The use of high fidelity analyses has always been part of the detailed levels of design.   The benefits of effective inclusion of high fidelity data into the design optimization process at the conceptual stage have been investigated in the Numerical Propulsion System Simulation (NPSS) project [Ref.21]. This multidisciplinary system of analysis tools enables accurate prediction of propulsion system parameters such as performance and life to be determined in the early stages of the design process. One of the aspects NPSS focuses on is the numerical zooming between 0-dimensional and 1-, 2-, 3- dimensional component engine codes. A detailed description of the development of the NPSS environment and results of a successful zooming of 1-dimensional high pressure compressor results to a 0-dimensional simulation are presented by Lytle [Ref.21] and Follen [Ref. 22]. The approach taken by PMDO is to integrate 0- and 1-dimensional analytical tools of various disciplines. A visual illustration of the location of the PMDO system in terms of the three major elements of complex system simulation is depicted in Figure 5.1.
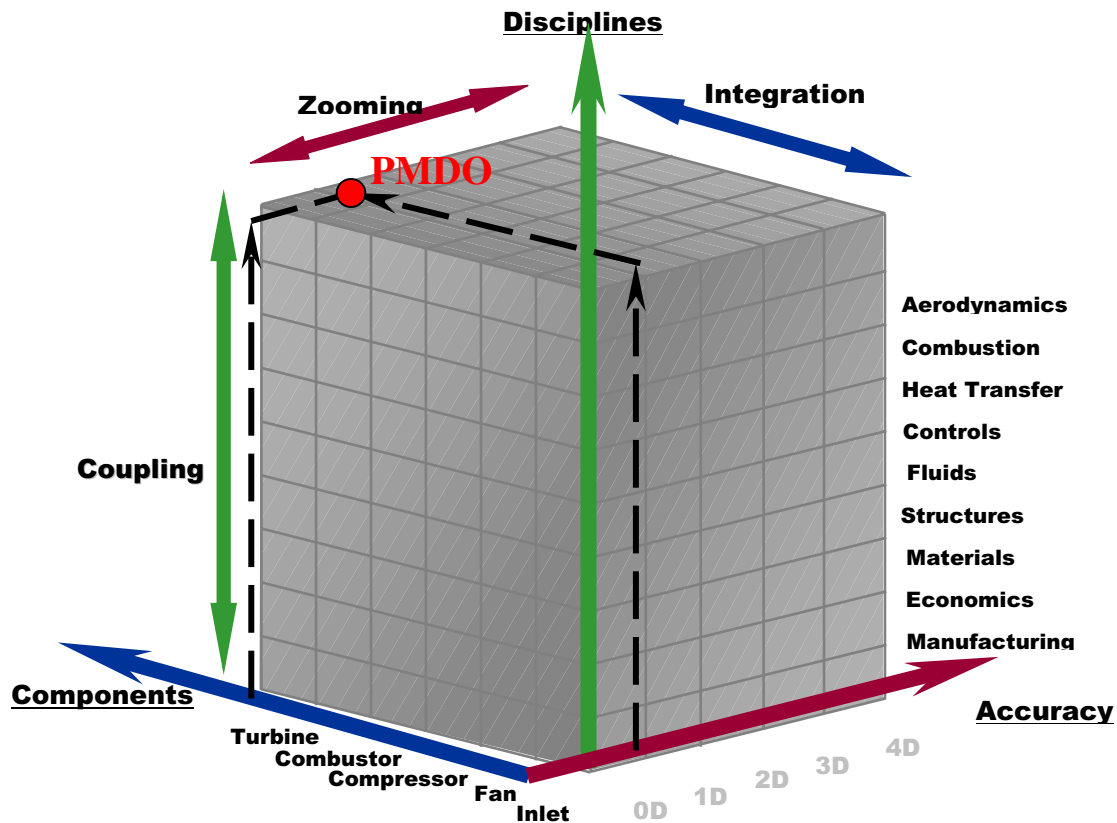
Figure 5.1: Three main elements of complex system simulation [Ref. 21]

The development of an integrated, multidisciplinary optimization tool for the Phase I/II PMDO project is progressing in four steps:

1. Develop a robust tool base
2. Apply single discipline optimization to individual analytical tools
3. Create an integration framework
4. Implement multidisciplinary optimization

The first two steps are well underway and are described with preliminary results. The second two steps are currently being investigated and discussion will be limited to an examination of requirements.

Robust Tool Base

The Phase I/II PMDO project seeks to obtain an optimal engine cross-section (compressor and turbine gaspath and disc shapes) that meets thermodynamic cycle and other constraints at a given design point. Low-fidelity aerodynamic and structural tools (0-D and 1-D) are appropriate for the PMDO project since these tools are robust, execute quickly, and provide sufficient accuracy for the purpose of an advanced engineering study. It is essential that the tools used in optimization are well validated. The optimizer must be constrained to use the tools within their validated ranges so as not to exploit unreliable tool outputs. Higher-fidelity tools (2-D and 3-D) will be incorporated into PMDO in the future to provide additional information to guide configuration decisions.

The aerodynamic characteristics of multi-stage axial compressors and turbines are predicted using 1-D meanline programs in PMDO. Flow prediction in a meanline program is based on the calculation of velocity triangles at the mid-span of the gaspath with empirical models to account for losses. Further information on P&WC meanline programs and loss models is available in Refs. 23 - 25. Typical input to a meanline program includes geometric parameters and engine operating conditions. The output from a meanline program includes a prediction of Mach numbers, pressure ratio and efficiency.

Simple "layout" programs are used to predict the aerodynamic characteristics and geometric cross-sections of fans and centrifugal compressors in PMDO. These programs are based on simple physics, design rules, and audits of previous engines. Losses in ducts such as the engine inlet, bypass duct, and inter-compressor ducts are modeled using either (i) simple correlations with geometric parameters and basic engine operating conditions as input, or (ii) the numerical solution of one-dimensional flow equations with calibrated source terms for blockages such as struts. In the traditional design process, these empirical correlations, "rules of thumb", and calibrated models have been applied manually. As part of the PMDO project, the rules and correlations are captured in computer programs for inclusion in the automated optimization procedure.

Simple 2-D structural tools are used to size rotating compressor discs and predict the stress and life of discs with minimum weight. Cross-sectional geometric disk parameters, standard fixings, and gaspath shape are combined to define the disc shape. A 2-D analysis predicts stress levels, burst speed estimated on the basis of material utilization factor (MUF), average disc hoop stress, and life based on the stresses at critical areas shape. Airfoil weight, which is used as a boundary condition for the analysis, is estimated based on airfoil cross-section and flow parameters from an aerodynamic meanline analysis combined with empirical data.

Rotating turbine discs are sized using a P&WC program that employs empirical equations that simplify the physical modeling of a rotor from the shroud to the disc. The program includes an

airfoil cross-section generator, a fixing designer, and links to a finite element code for disc hub stress evaluation.

Single Discipline Optimization

Optimization with a single tool has been investigated for three cases: axial compressor gaspaths, turbine gaspaths, and turbine discs. In each of these cases, the tool has been linked with an optimizer and successful optimization runs have been accomplished. The purpose of the single-discipline investigations was to:

- Become familiar with the characteristics of various optimization methods
- Determine the best optimization methods for each tool
- Ensure that the selected tools are robust enough for use in optimization
- Explore the effect of alternate sets of optimization variables on convergence and robustness of the solution

The optimizer used for the PMDO project is iSIGHT, developed by Engineous Software Inc. [Ref. 26]. The iSIGHT software is a generic shell environment that supports multidisciplinary optimization. The shell represents and manages multiple elements of a particular design problem in conjunction with the integration of one or more simulation programs. In essence, iSIGHT automates the execution of the different codes (in-house or commercial), data exchange and iterative adjustment of the design parameters based on the problem formulation and a specified optimization plan.

Axial Compressor Gaspath Optimization

A three-stage axial compressor optimization case was run at design point using a P&WC meanline program with the following optimization variables:

- shape of the hub and shroud
- location and corner points of each rotor and stator
- number of airfoils per blade row
- airfoil angles

Constraints were imposed on the following variables:

- diffusion factor
- swirl angle at stator trailing edges
- exit Mach number
- ratio of hub to tip radius
- blade angles
- pressure ratio
- choked flow

The objective of the optimization was to maximize efficiency. The optimization was run for approximately 1000 iterations which took about 1 hour on an HP C-class workstation using a Genetic Algorithm followed by a Direct Heuristic Search. The number of iterations required to achieve an optimum seems excessive and several opportunities are being explored to reduce the iteration count: (i) alternate optimization strategies, and (ii) alternate sets of optimization variables based on "physical" quantities.

The iSIGHT optimizer has a suite of explorative and gradient-based optimization methods that can be applied in any sequence. Different combinations of optimization methods will be investigated in an attempt to improve the efficiency of the optimization process.

The design variables used by the optimizer are expected to have a significant influence on the robustness and speed of optimization. In the current axial compressor meanline application, the optimizer alters the gaspath shape by varying the coefficients of splines representing the hub and shroud curves. The dependence of the compressor pressure ratio and efficiency on the spline coefficients is not direct. An improved set of "physical" optimization variables has been suggested in which the optimizer varies axial distributions of mean radius and area. The advantage of this formulation is that area and radius are "physical" variables that have a direct link to the pressure ratio and efficiency predicted by the meanline program. This direct link should result in a "cleaner" design space, a reduced number of iterations to converge to an optimal solution, and improved robustness of the optimization procedure.

Turbine Gaspath Optimization

A three-stage turbine optimization case was run with a P&WC meanline program in which the optimization variables included the number of airfoils per blade row, the location and cross-sectional shape of each blade and vane, and the shape of the hub and shroud. The only constraint on the output parameters was to keep the Zweifel Coefficient, which is a measure of airfoil loading, constant. The objective of the optimization was to maximize efficiency and minimize the Degree of Reaction which represents the proportion of the static temperature drop occurring in the rotor and, also, reduction in total relative temperature which results in a lower metal temperature for the airfoil. The optimization plan involved three optimization techniques available in the iSIGHT software: Genetic Algorithm followed by Hooke-Jeeves Direct Search Method followed by Exterior Penalty technique.

The results of the optimization run were compared with "baseline" results, as shown in Fig. 5.2. The baseline results were obtained by a turbine design expert in ¾ of a day of dedicated time. In contrast, the optimizer took twenty minutes to set up and two hours and twenty minutes to run on an HP C-class workstation. The baseline solutions are shown as dotted lines in the figure and the optimizer solutions as solid lines. The gaspath shape and number of airfoils per blade row obtained by the optimizer were close to the baseline results. The efficiencies were almost identical with slightly higher efficiencies obtained by the optimizer. Of most significance is order of magnitude reduction in human time required to obtain the solution.
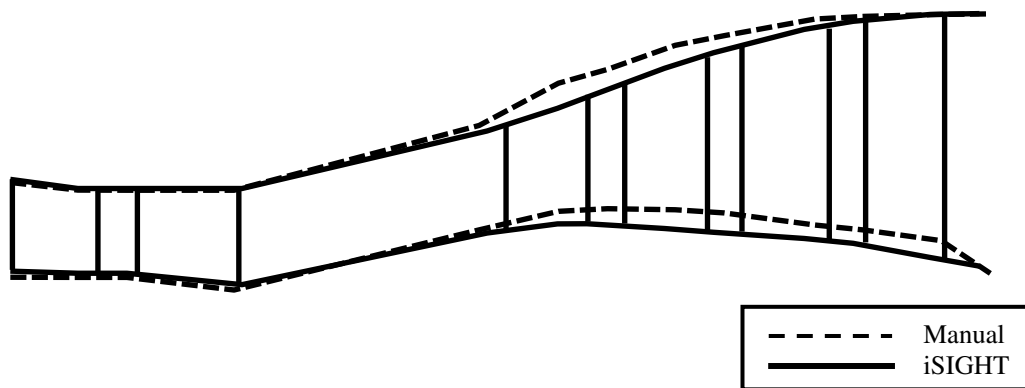
Figure 5.2: Comparison of "baseline" and "optimized" turbine meanline results

Turbine Disc Optimization

The iSIGHT optimizer was linked with a P&WC program used for preliminary 1-D/2-D design and analysis of the turbine rotor discs, as described above. The main objective of the test was to optimize the turbine disc while keeping the airfoil, platform and fixing geometries constant. The problem variables for this particular case included a number of disc shape parameters based on a simplified disc parameterization (Figure 5.3).

The objective of the optimization was to minimize disc weight and maximize burst speed margin. The optimization plan contained three sequential optimization techniques: Genetic Algorithm followed by Sequential Quadratic Programming (NLPQL) followed by Mixed Integer Optimization (MOST). As a starting design point, the optimizer was deliberately given a set of input parameters that generated an unacceptable solution for the disc. The goal of this case was to see how quickly the optimizer could learn about the given design space and obtain a viable design configuration. The first feasible solution satisfying all of the output constraints and objectives was obtained in approximately half an hour on an HP C-class workstation. Relative to a manual design, there was a significant reduction in time required to obtain a feasible solution, the weight of the disc was slightly reduced, and a higher burst speed margin was obtained. Future investigation of optimization strategies will include the use of the Design of Experiments (DOE) to reduce the number of design variables and shorten the time required to converge to a solution.

Integration Framework

In order to automate the design process, an integration framework is required to link the tools in the PMDO project. The requirements for an integration framework are being finalized and several integration frameworks, including commercial products and solutions in development by research groups, are being investigated. A description of framework requirements is given in Ref. 12. The integration framework must satisfy the following requirements:

- automate the transfer of data between tools
- model the links and interactions between all tools and disciplines
- enable concurrent analysis
- allow linking with multiple optimizers
- manage data
- allow automatic execution of optimization involving multiple, user-selected tools
- support task decomposition for multidisciplinary optimization
- have an intuitive Graphical User Interface (GUI)
- be platform independent

Furthermore, the integration framework must be extendable and flexible to meet the requirements of a growing number of tools and disciplines. Future phases of PMDO will encompass additional engineering and economic disciplines and the incorporation of these tools into the PMDO framework in a straightforward manner with minimal effort is necessary. Although PMDO is initially to be used exclusively by P&WC, other UTC divisions such as the Small Military Engine (SME) division will use later versions and the tools of the other divisions will be integrated into the PMDO framework.

Later versions of PMDO will include higher-fidelity tools. The framework must also permit "zooming" [Refs. 21 and 22] to facilitate the selection of a tool with a given level of fidelity for each discipline and include capabilities for transferring data between analyses of different fidelities. As an example of data transfer between data sets of varying fidelity, a feedback mechanism will be included in later versions to allow performance data predicted by the 1-D

aerodynamic meanline tools to effect the data in the thermodynamic cycle analysis. The integration framework must allow zooming, feedback mechanisms, and inclusion of high-fidelity tools.

The integration framework must also be compatible with several large development projects that are underway at P&WC in parallel with the PMDO project. These projects include the integration of parametric CATIA V5 geometry and analysis data, as managed by a Product Data Manager (PDM), to form the basis of a Digital Engine. The PMDO system will be integrated into the Digital Engine which will be seamlessly integrated into the P&WC Digital Enterprise. PMDO will both draw data from and contribute data to the Digital Enterprise database. The Digital Enterprise will manage data and make PMDO data available to the rest of the enterprise to be used, for example, as initial geometry and boundary conditions for detailed engineering design.

Multidisciplinary Optimization

Multidisciplinary optimization (MDO) involves the simultaneous optimization of multiple coupled disciplines and includes the frequently conflicting requirements of each discipline. MDO is an active field of research and several methods have been proposed to handle the complexities inherent in systems with a large number of disciplines and design variables [Ref. 2]. MDO can be described as an environment for the design of complex, coupled engineering systems, such as a gas turbine engine, the behavior of which is determined by interacting subsystems. It attempts to make the life cycle of a product and the design process less expensive and more reliable.

The optimization problem is often divided into separate sub-optimizations managed by an overall optimizer that strives to minimize the global objective. Examples of these techniques are Concurrent Sub-Space Optimization [Ref. 6], Collaborative Optimization [Refs. 5 and 28], and Bi-Level System Synthesis [Ref. 7]. Simpler optimization techniques, such as All-In-One optimization (in which all design variables are varied simultaneously) and sequential disciplinary optimization (in which each discipline is optimized sequentially) can lead to sub-optimal design and lack of robustness [Ref. 28].

Various MDO methods are being investigated to determine the most promising methods to be implemented in PMDO. The selected MDO method must achieve the following goals:

- quick turnaround time
- robust convergence of optimization
- convergence to a robust optimum solution

MDO eases the process of design and improves system performance by ensuring that the latest advances in each of the contributing disciplines are used to the fullest, taking advantage of the interactions between the subsystems. Although the potential of MDO for improving the design process and reducing the manufacturing cost of complex systems is widely recognized by the engineering community, the extent of its practical application is not as great as it should be due to the shortage of easily applied MDO tools.

6   CONCLUSION

In the gas turbine engine design process, the multitude of requirements, criteria and competing objectives can be effectively managed with a system that supports process integration and multidisciplinary optimization. An integrated MDO system will be of most benefit at the conceptual design stage since it is at this stage that the greatest impact on the final engine

configuration is made. The approach to the development and implementation of such a system at Pratt & Whitney Canada is described in this paper.

The goal of the initial phase of PMDO is to create a system that uses 0-D and 1-D tools to automatically generate compressor and turbine gaspath/disc cross-sections that are optimal with respect to given objectives and constraints. The expected benefits of the initial phase of PMDO include automated data transfer between analytical tools, improved turnaround time, reduced design costs, and improved designs.

The development of a robust tool base is the essential first step in the development of a multidisciplinary optimization system and this first step is well underway at P&WC. An understanding of optimization characteristics and requirements is being attained through investigation of optimization on individual discipline tools and this understanding will be applied to multidisciplinary problems. Further work is underway to examine the effect of alternate optimization variables and algorithms on the convergence and robustness of optimization. Investigations into integration infrastructures and various aspects of multidisciplinary optimization such as decomposition have also been initiated.

Future phases of PMDO will include additional disciplines and higher-fidelity tools. The effective inclusion of high fidelity data into the optimization process at the preliminary design level using numerical zooming will be investigated in future phases. An additional area of future research is the use of approximation techniques to accelerate optimization.

Acknowledgments

References

1. Ryan, R., Blair, J., Townsend, J. and Verderaime, V., "Working on the Boundaries: Philosophies And Practices of the Design Process", NASA Technical Paper 3642, July 1996.
2. Sobieszczanski-Sobieski, J. and Haftka, R. T., "Multidisciplinary Aerospace Design Optimization: Survey Of Recent Developments, Structural Optimization", AIAA Paper 96-0711, Jan. 1996.
3. Sobieszczanski-Sobieski, J., "Multi-disciplinary Design Optimization: An Emerging, New Engineering Discipline". In *Advances in Structural Optimization*, Herskovits, J., pp. 483-496, Kluwer Academic, 1995.
4. Cramer, E. J., Dennis, Jr., J. E., Frank, P.D., Lewis, R.M. and Shubin, G.R., "Problem Formulation for Multi-disciplinary Design Optimization". SIAM Journal on Optimization, 4(4), pp. 754-776, November 1994.
5. Braun, R.D., "Collaborative Optimization: An Architecture for Large-Scale Distributed Design", Ph.D. thesis, Stanford University, May 1996.
6. Sobieszczanski-Sobieski, J., "Optimization by Decomposition: A Step from Hierarchic to Non-hierarchic Systems", Proceedings, 2nd NASA/USAF Symposium on Recent Advances in Multidisciplinary Analysis and Optimization, Hampton, Virginia, 1988.

7. Sobieszczanski-Sobieski, J., Agte, J. and Sandusly, Jr., R., "Bi-Level Integrated System Synthesis (BLISS)", NASA/TM-1998-208715, NASA Langley Research Center, Hampton, Virginia, August 1998.

8. Kodiyalam, S., "Evaluation of Methods for Multidisciplinary Design Optimization (MDO)", Phase I, NASA/CR-1998-208716, NASA Langley Research Center, Hampton, Virginia, September 1998.

9. Kodiyalam, S. and Yuan, C., "Evaluation of Methods for Multi-disciplinary Design Optimization (MDO)", Part II, NASA/CR-2000-210313, NASA Langley Research Center, Hampton, Virginia, November 1998.

10. Balling, R.J. and Sobieszczanski-Sobieski, J., "Optimization of Coupled Systems: A Critical Overview of Approaches", AIAA Journal, Vol. 34, No. 1, pp. 6-17, January 1996.

11. Krishnan, R., "Evaluation of Frameworks for HSCT Design Optimization", NASA/CR-1998-208731, Computer Science Corporation, Hampton, Virginia, October 1998.

12. Salas, A.O. and Townsend, J., "Framework Requirements for MDO Application Development", AIAA Paper No. AIAA-98-4740, 7th AIAA/USAF/ NASA/ISSMO Symposium on Multi-disciplinary Analysis and Optimization, St. Louis, MO, September 2-4, 1998.

13. Rohl, P.J., He, B. and Finnigan, P.M., "A Collaborative Optimization Environment For Turbine Engine Development", AIAA Paper No. AIAA-98-4734.

14. Madavan, N.K., Rai, M.M. and Huber, F.W., "Neural Net-Based Redesign of Transonic Turbines for Improved Unsteady Aerodynamic Performance", Presented at the 35th AIAA/ASME/ SAE/ASEE Joint Propulsion Conference and Exhibit, June 20-24, 1999, Los Angeles.

15. Dornberger, R., Buch, D. and Stoll, P., "Multidisciplinary in Turbomachinery Design", Presented at the European Congress on Computational Methods in Applied Sciences and Engineering, September 11-14, 2000, Barcelona.

16. Bailey, M.W., "Integrated Multi-disciplinary Design", ISABE paper No. 99-7174, 1999.

17. CALS Technical Rep 002: "Application of Concurrent Engineering to Mechanical Systems Design", Final Report of RM Mechanical Design Study, June 16, 1989.

18. Japikse, D., "Developments in Agile Engineering For Turbomachinery", Presented at the 9th International Symposium on Transport Phenomena and Dynamics of Rotating Machinery, February 10 - 14, 2002, Honolulu, Hawaii.

19. Cohen, H., Rogers, G.F.C. and Saravanamuttoo, H.I.H., "Gas Turbine Theory", 4th edition.

20. AIAA, "White Paper on Current State of the Art", prepared by AIAA MDO Technical Committee, January 1991.

21. Lytle, J.K., "The Numerical Propulsion System Simulation: A Multidisciplinary Design System for Aerospace Vehicles", ISABE paper No. ISABE 99-7111, 1999.

22. Follen, J.," Numerical Zooming Between the NPSS Version 1 and a 1-Dimensional Meanline Design Analysis Code", ISABE paper No. ISABE 99-7196, 1999.

23. Raw, J. A. and Weir, G. C., " The Prediction of Off - Design Characteristics of Axial and Axial / Centrifugal Compressors ", SAE Technical Paper Series 800628, April, 1980.

24. Kacker, S.C. and Okapuu, U., A Mean Line Prediction Method for Axial Flow Turbine Efficiency; Journal of Engineering for Power; Vol. 104, Jan. 1982.

25. Moustapha, S.H., Kacker, S.C. and Tremblay, B., "An Improved Incidence Losses Prediction Method for Turbine Airfoils; Journal of Turbomachinery", Vol. 112, April, 1990.

26. iSIGHT V5.5 User's Guide, Engineous Software, Inc.

27. Kroo, I. and Manning V., "Collaborative Optimization: Status and Directions", AIAA Symposium on Multidisciplinary Analysis and Optimization, Paper AIAA-2000-4721, September, 2000.

Improved Structural Design Using Evolutionary Finite Element Modeling

Robert M. Taylor and Terrence A. Weisshaar
School of Aeronautics and Astronautics
Purdue University, 1282 Grisson Hall
West Lafayette, Indiana 47907-1282, USA

Abstract

A wing structural layout design experiment conducted with a commercial aircraft manufacturer indicates that a systematic, evolutionary structural design process helps to focus integrated discussion, analysis, and decision-making efforts. The process systematically incorporates optimized structural information into the design process. The technical complexity of aircraft design requires technically skilled individuals to communicate disciplinary needs to people outside of their own disciplines. Tools and methods that help interdisciplinary information transfer and can evolve with the fidelity required by the design process will improve a design organization's capability to produce an integrated aircraft that meets all of design requirements. This paper shows that advanced structural design tools, used in a multidisciplinary team setting, will improve structural information generation and communication. This will enable a design team to better identify and meet structural design requirements. A realistic example demonstrates how high fidelity computational structural tools can generate and communicate structural information appropriate to the process needs. This means that the information is actually used to make decisions.

Introduction

Improving the aircraft development process will produce higher quality, innovative designs faster and at lower cost.

In this paper we examine structural design process needs and tool requirements and then explore a wing structural design problem. For design we define a systematic process for evolving structural detail that integrates physics-based structural analysis and optimization with experience to support higher-quality fact-based design decisions. Finally, we present the results of this approach applied to the design of a wing structural layout for a business jet. This work augments earlier work by Taylor and Weisshaar[1].

Aircraft Structural Design Process

As an aircraft structural design evolves, the need for structural definition and loads definition increases. As a result, design freedom is reduced as it is traded for design fidelity. In early design phases, designers can make decisions and changes relatively easily, but the design lacks fidelity so the team cannot
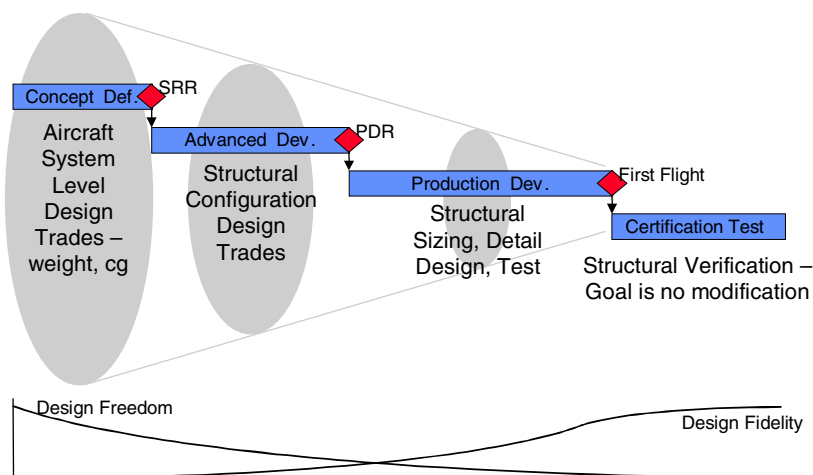
Figure 1—Design process structural needs

fully evaluate the impact of these decisions on product cost, manufacturing details and quality. When design fidelity finally appears later it may conflict with earlier assumptions; the cost of design changes to bring these objectives back into alignment is large.

Whitney[2] observes that design is both an organizational and a technical activity; successful design processes must integrate tools and information from both aspects of design. Process definition provides the foundation for successful integration and application of technical and organizational tools and methods. In a well-designed process, core knowledge - in the form of people and tools - exists at the appropriate places to meet process information needs and dependencies. The customer ultimately defines product quality. The design process, through customer-oriented requirements and design traceability, must reflect this definition.

As shown in Figure 1, system design evolution places requirements on the structural design process, from early design trades to detail design and verification later in the process.

These process needs place requirements on structural tools and models. As shown in Figure 2, structural models reflect systems engineering process needs by evolving from broad conceptualizations that enable exploration of the design space. The systems engineering process[3] establishes a formal evolution of detail and flow of information, promoting design activities that provide the level of detail and fidelity specified by requirements. Information quantity and quality will increase and evolve as the design moves through the funnel.
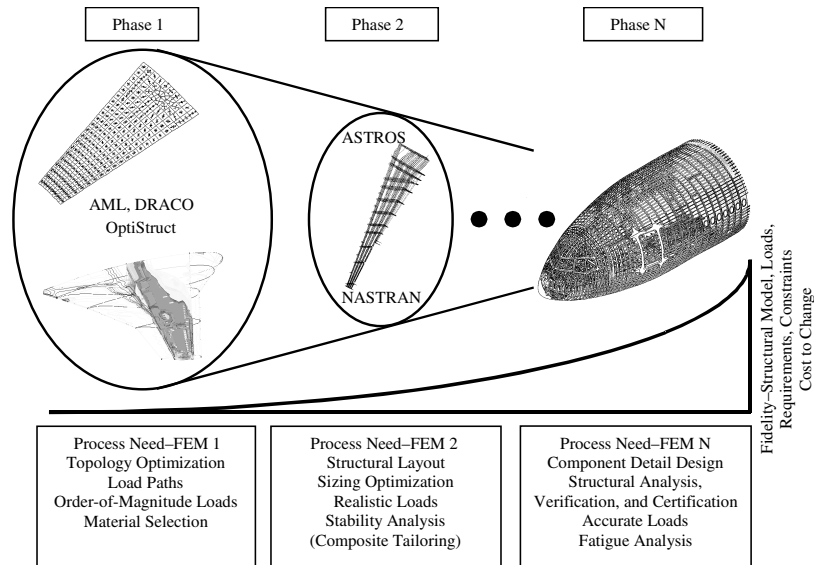
Figure 2—Structural design funnel

At the beginning of the structural design process (Phase 1) structural designers need information, either from tools or experience, to guide configuration and topology decisions to determine the number of ribs and spars and their locations and orientations. This phase is marked by conceptualization and creativity. The latter part of the process (Phases 2 through N) involves structural member sizing, optimization and analysis. Information for later activities requires increasingly greater model fidelity and detail

Effective, appropriate tools to meet the specific needs of each phase will improve the structural design process. Identification of what questions structural design tools answer, what level of structural detail must be input, and what level of structural fidelity results leads to an understanding of the specific value added by each tool set and areas for improvement.

Tools and models that generate and communicate physics-based structural information early in the process elevate the level of the structural design task so that structural issues, and therefore manufacturing and cost issues, can impact top-level aircraft configuration and design. Phase 1 tools must provide quick, communicable, modifiable, and deployable structural information given low-fidelity geometric and loading input. To lay out structural members effectively, structural designers need load path information. Moreover, to interact with non-structural design team members and requirements, structural designers need to be able to present this load path information in a clear, graphical form. Furthermore, to be useful in the early conceptual phase, structural models must become the equivalent of the "back of the envelope" calculation, providing results to evaluate feasibility in real time. Finally, when the time for conceptualization is over, the models must be seamlessly deployable, evolving directly into the models necessary for the remainder of the structural development process.

Background

Multidisciplinary teams drive projects through aircraft development because of the complexity of product and process and the need for technical specialization. However, such teams face tremendous challenges that accentuate the need to integrate organizational and technical activities

Waszak, *et al.*[4] use a systems thinking approach[5] to model multidisciplinary team dynamics and then identify six key determinants of team effectiveness. The present paper addresses methods for improving two of these determinants: effectiveness of team processes; and, balanced levels of technology.

A systematic design process using *structured* design methods (as opposed to *structural* design methods) improves the 'effectiveness of team processes' determinant by formalizing and managing information flow throughout the team, providing insight into design problem structure and a baseline for understanding and improving the design process. Systematic approaches formalize information flow, promoting communication so team members share mental models and learning. In addition, systematic approaches are self-documenting, preserving learning at each stage of design progression.

Systematic approaches clarify the customer's "voice" to team members so they can identify how their function traces back to and adds value to the customer. This clarification pushes the issue of quality upstream into the design process itself, which is much more effective than fixing the design product after the fact[6].

Research in structured design methods is very active; the design and engineering management literature contains many references which provide a scientific foundation to design, for example: Ulrich and Eppinger[7], Eppinger[8], Pugh[9], Dym[10], Cross[11], and many others. Alexander[12] and Simon[13] discuss the nature of design problems.

A Structural Design Process Model

Traditionally, the aircraft preliminary design phase lays out structural configurations based on the insight of experienced designers. Analytical structural design tools enter the process only when system-level design is concluded or near conclusion, so their impact on the aircraft outer mold-line configuration is minimal.

Conventional use of finite element methods depends on detailed models that require large time investments and depend on detailed geometric models. By the time finite element results are available the design team has already committed to a structural configuration. Engineers can use these results to perform sizing optimization, subsystem-level design, and analysis, but the opportunity for configuration design trade studies based on theory has passed.

Weisshaar and Komarov[14] advocate modification of the traditional aircraft design process to include structural theory early by generating load path information in a preliminary finite element optimization model (FEM I). Structural designers then use this load path information as the basis for structural configuration and a more detailed, traditional finite element model (FEM II) of the load carrying structure for shape and sizing optimization.

Structural detail evolves through a series of finite element analysis and optimization activities (FEM 1-FEM N) alternating with team-based design activities (Design 1-Design N). This is opposed to the traditional method of specifying full detail and constraints in the first structural model, locking in details before design trades can be made and neglecting nonstructural requirements in the analysis. At the end of the process, the documented evolution of concepts and evaluation enables traceability of design decisions.

Wing Structural Layout Design Process Experiment

A design experiment was performed at Raytheon Aircraft in Wichita, Kansas to test the validity of a new structural design process that incorporates early-on use of finite element models. Technical team supporting this process included personnel from loads, structural integrity, producibility engineering, and geometric configuration. Our process is described in the ensuing sections.

Wing Structural Design—Problem Definition

The wing structure has weight and cost objectives but must meet requirements and constraints consistent with the aircraft mission and FAA certification. To begin our process, a document was drafted to communicate wing structural requirements to project participants. This document provides the foundation for design and analysis activities, establishing metrics, target values, and scope of the project. The requirements established by this document also flow to lower-level design activities as part of the systems engineering process.

This project focused on primary wing structure and considered additional structure only as it influenced wing structure through interfaces or constraints. For example, flap and aileron structure was not considered. Loads from flap and aileron attachments, however, were applied through flap tracks, hinges, and actuators as appropriate.

Requirements for the wing structural design include the 7 categories shown in the panel below:

Because loads and constraints drive the structural configuration design, choosing the correct, representative set of load cases is critical to designing structure that can evolve into an optimal system whose form fits its function. Too many loads with too much fidelity restrict the design freedom needed to satisfactorily explore the design space during conceptual design. Conversely, insufficient fidelity in load number or distribution leads to missed or misplaced structural connections. Load fidelity must match requirement and design levels of detail within the systems engineering process.

The 5 load cases applied in our experiment were:

1. *Static landing with flaps, maximum positive torque and shear*
2. *Head on gust, landing with flaps, maximum negative torque*
3. *Dynamic gust at cruise, maximum negative bending moment*
4. *Dynamic gust at cruise, maximum positive bending moment*
5. *Static Maneuver, maximum positive torque and shear*

Concept selection without structural analysis

Our design team came from two different experience areas. Part of the team came from a culture that favored multi-spar design, preferring a many spar concept, while others came from a different culture that favored two-spar wings. In the beginning, a design decision based solely on experiential input would have been contentious.

The Weighted Objectives Method is a useful structured design technique. The table in Figure 3 shows a hypothetical weighted objectives scoring

Requirements list
1. Structural Performance
1.1. Stiffness
1.2. Deflection
1.3. Strength
1.4. Durability
1.5. Structural Stability
1.6. Geometric Interface
2. Environmental
2.1. Loads
2.2. Ground Wind Gust Durability and Protection
2.3. Lightning Strike Protection
2.4. Ice Protection
2.5. Fuel Slosh and Vibration
3. Size
3.1. Dimensions
3.2. Weight
3.3. Fuel Volume
4. Costs
4.1. Recurring Costs
4.2. Direct Operating Costs
4.3. Producibility and Process Characteristics
5. Support
5.1. Service Life
5.2. Structural Inspection
5.3. Towing, Jacking, and Hoisting
5.4. Reliability
5.5. Maintainability
6. Safety
6.1. System Safety
6.2. Fire Safety
6.3. Crash Safety
6.4. Bird Strike
6.5. Emergency Egress
7. Certification

matrix that might have resulted if the inputs to this method were based solely on experience. Inputs into this matrix based solely on previous experience lead to little differentiation among the concepts and consequently no basis for a design decision. Inserting finite element "physics-based" information will change this, as we shall see.

Wing Structural Design—Solution Synthesis

Figure 4 depicts the cycle of design and analysis activities used by our process. This section will describe each phase of the process and present results from each phase.

Structural finite element analysis and optimization models address configuration layout with stress constraints. Presentation of these results to project participants generates knowledge feedback to modify the models, generate new practical structural concepts, and evaluate these concepts for manufacturing. This iteration between analysis and design activities is repeated through a series of models and evolves into models with greater configuration detail and additional analytical constraints. The first level of detail develops structural members driven by stress, such as

spar webs and skin thicknesses. The next level of detail adds buckling and deflection constraints, defining ribs and stiffener design.

	weight factor	2 Spar raw	2 Spar wtd	3 Spar raw	3 Spar wtd	4 Spar raw	4 Spar wtd	7 Spar raw	7 Spar wtd
Weight	0.30	0	-	0	-	0	-	0	-
Stiffness		0	-	0	-	0	-	0	-
Fuel Volume		4	-	3	-	2	-	1	-
Cost	0.30	3	0.90	2	0.60	2	0.60	3	0.90
Fabrication		4	-	3	-	2	-	1	-
Assembly		1	-	2	-	3	-	4	-
Accessibility	0.05	4	0.20	3	0.15	2.5	0.13	1	0.05
Inspection		4	-	4	-	2	-	1	-
Maintenance		4	-	2	-	3	-	1	-
Fuel Considerations	0.05	2	0.10	4	0.20	3	0.15	1	0.05
Certification Issues			-		-		-		-
fail safe	0.25	1	0.25	4	1.00	4	1.00	4	1.00
verification	0.05	4	0.20	3	0.15	2	0.10	1	0.05
Weighted Sum	1.00		1.65		2.10		1.98		2.05

Figure 3—Scoring matrix with low quality information input
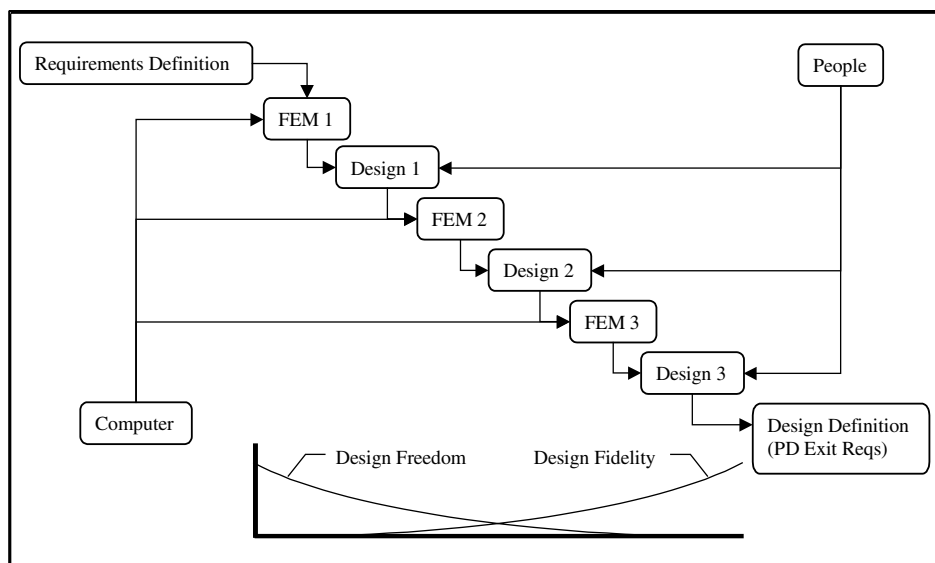
Figure 4—Alternating evolutionary finite element models and design activities for design process experiment

Phase 1

The goal of Phase 1 activities is to provide high quality structural feedback during aircraft system-level design activities; traditionally this phase has only historical weight and center-of-gravity structural input. Phase 1 models provide meaningful structural feedback as early as possible with as little internal geometric definition as possible.

The purpose of the first finite element model, FEM 1, is to generate information about load paths in a hypothetical monocoque structural domain enclosed by the outer mold lines to determine preferred regions for primary structural members. These load paths indicate preferred regions for stress-driven members: spar webs and skin thickness buildup. Following FEM 1, Design 1 activities use the FEM 1 information to generate spar web and rib structural concepts. Structured methods for concept generation, evaluation, and selection communicate and leverage this information for effective design decisions.

Finite Element 1

The FEM 1 model is a very general shell skin with in-plane normal and shear stiffness and a core with out-of-plane normal and shear stiffness, as shown in Figure 5. Output from this model will be load path plots in the form of principal shell forces in the skins, skin thickness distribution plots, and the structural weight of the optimized skin. The analytical structural information that results from the FEM 1 model forms the basis for Level 2 concept generation.

The FEM 1 model generates optimized skin thicknesses based on strength constraints alone and provides a theoretical weight estimate. This weight estimate serves as a reference point to track the effect of each constraint set as it is added and additional model fidelity is developed, and to serve as an early predictor of true wing weight.
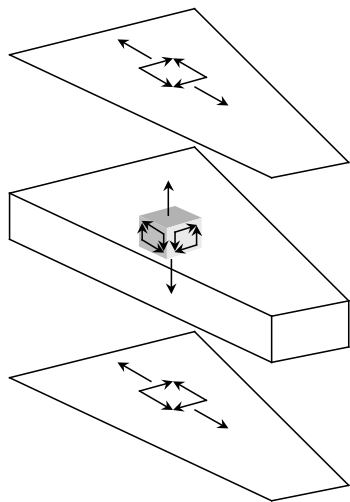
Figure 5 — Initial FEM 1 model showing upper and lower skin with in-plane normal and shear stiffness and core with out-of-plane normal and shear stiffness
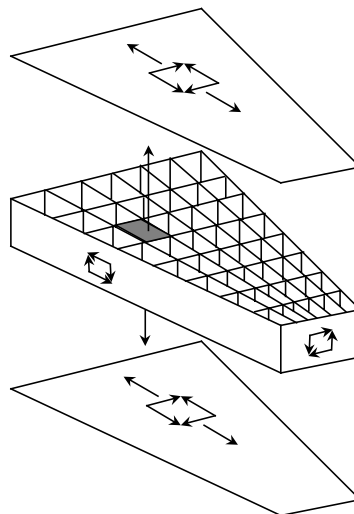
Figure 6—Final FEM 1 model showing upper and lower skin with in-plane normal and shear stiffness and lattice core with out-of-plane normal and controlled directional shear stiffness
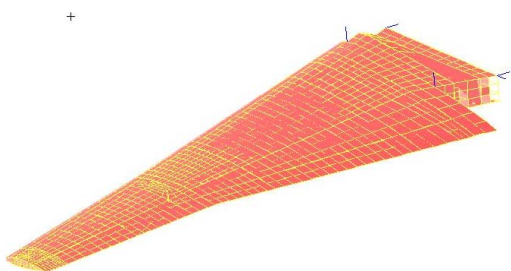
Figure 7—FEM 1 wing structural model-skin
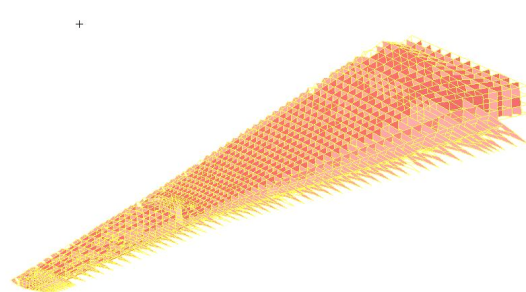
Figure 8—FEM 1 wing structural model—internal lattice structure

Structural modeling for the FEM 1 attempted to allocate bending and in-plane shear carrying capability to the wing skins and out-of-plane normal and shear carrying capability to a core filler material as shown in Figure 5. The initial FEM 1 model used shell elements for the skins and orthotropic brick elements for the core. However, in this model shear stiffness in the core changed direction with element skew and orientation.

To circumvent this problem, a modification of this FEM 1 model used a lattice of chordwise and spanwise shell elements between each brick element in the core as shown in Figure 6. These shell elements have controllable directional shear stiffness properties, while the brick elements have out-of-plane normal stiffness. Figures 7 and 8 show the wing finite element models chosen to represent the structure.

Results from the FEM 1 models indicate optimized skin weight and patterns of force flows through the structural continuum. The force flows are displayed through plots of maximum and minimum shell forces in the skins. As an example, Figure 9 shows these shell force plots for the positive dynamic gust load case applied to the FEM 1 model. Figure 10 shows the skin thickness distribution optimized over all four load cases.

The optimized skin weight for this model allows us to estimate the overall wing structural weight. Subtracting the weight of the elements representing flap and aileron sections of the wing allows estimation of structural box weight.
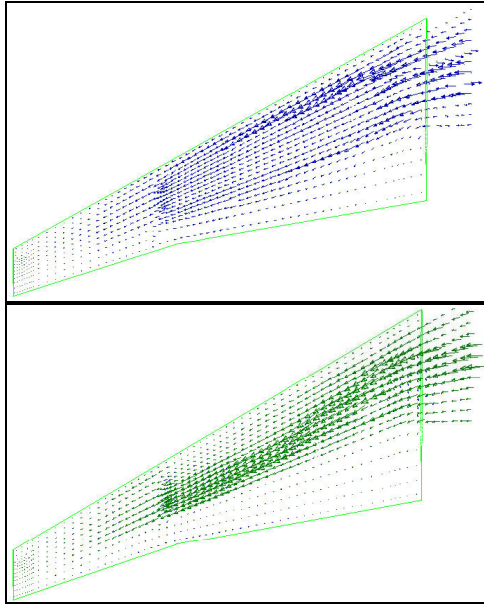
Figure 9 — Maximum/minimum principal shell forces for Critical Load Case 4, Positive Dynamic Gust at V_c-M_c Knee – upper figure—lower skin, lower figure —upper skin
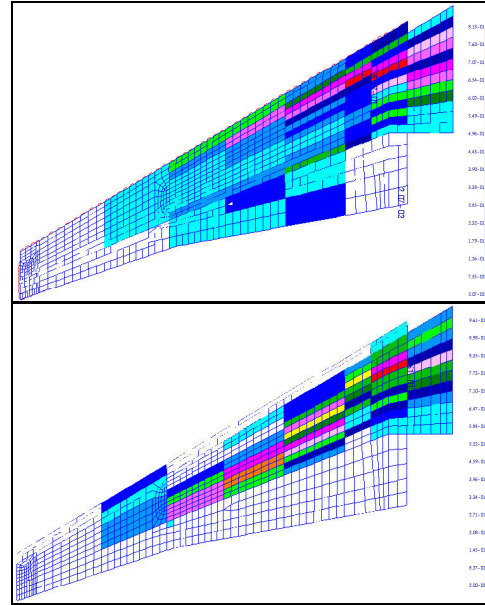
Figure 10 — Skin thicknesses optimized over all load cases. Left—Lower Skin, Right—Upper skin

The wing structural box weight was somewhat higher than expected. The primary reason for this is probably insufficient fidelity in the optimization model, causing high skin thickness over large regions because of local stress concentrations, both computational and real.

The structural information generated during FEM 1 flows into the team-based design activities of Design 1.

Design 1

Design 1 is a series of meetings that bring together the people in the organization capable of applying experience to satisfy requirements. This phase of the structural design process uses the FEM 1 results in a structured organizational process, bringing together people and technical information to evolve structural detail to the next level. Spar web concept generation takes here.

The structural designer presents to the design team the load path results of the FEM 1 model, which identify structural needs and preferences for the design based on strength. Presentation of these results graphically communicates structural needs in a format understandable by non-structural team members so they can provide critical feedback from their area of expertise. The FEM 1 model provides a scientific basis for generating structural concepts. The output of Design 1 is a manageable set of structural concepts that address spar web layout.

The Design 1 activities for the model wing structure yielded four structural concepts that were carried into Level 2. These activities included presentation of the FEM 1 models and generation of FEM 2 concepts. The structural designer presented load path results to the team in the form of principal shell force vector plots, explaining the meaning and purpose of the plots. The design team discussed spar web concept possibilities and settled on a concept pool comprised of 2, 3, 4, and 7 spar web concepts with rib design moved to the FEM 2/Design 2 phase. Design 1 meetings also established manufacturing constraints on rib design, specifying that ribs must be oriented normal to spars.

The FEM 1 models from this experiment were unable to significantly guide design activities due to at least four factors. First, the accuracy of the FEM 1 model formulation was not established, resulting in low confidence levels for the results by the structural designer and other team members. Furthermore, because the design problem was not novel (a high aspect ratio wing is a beam), the structural designer knew from experience what the force flows should be and did not gain new information from the FEM 1 model. In addition, the FEM 1 models may have been more useful had they been present to interact at an earlier stage before aerodynamic and performance design maturity when outer mold line definition could still be influenced. Finally, because there was no established relationship between the FEM 1 weight and the final wing box weight, FEM 1 model utility as feed forward devices was reduced.

Phase 2

The goal of Phase 2 activities is to integrate medium fidelity analysis and optimization results with an organizational design process to promote higher quality design decisions supported by both analysis and experience.

The purpose of the FEM 2 model is to generate useable analytical and optimization information sufficient to evaluate the spar web concepts generated during Design 1. The Design 2 activities that follow then juxtapose the structural evaluation with nonstructural evaluations (e.g., manufacturing cost estimates) to select a spar web/rib concept through structured selection methods. Additionally, Design 2 activities generate structural concepts at the next level of structural detail, stiffeners and fasteners.

Finite Element 2 (FEM 2) model

Figure 11 shows the FEM 2 finite element model for the 2-spar concept generated during Design 1. The FEM 2 finite element model adds new details to the FEM 1 model. Ideally, this would be a seamless evolutionary process with only some parts of the finite element model being replaced (in this case the shear core replaced by rib/spar web layout). The reality of current tools, however, dictated significant rework for the FEM 2 model
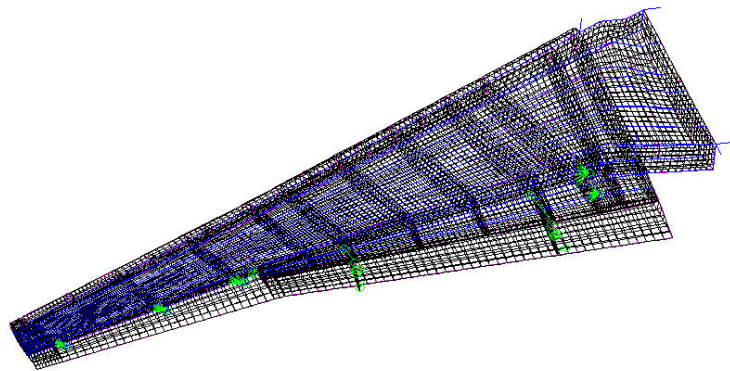
Figure 11- FEM 2 model for 2-spar concept

The FEM 2 model adds buckling, deflection, and manufacturing (minimum gage) constraints to the stress constraints considered in FEM 1. The FEM 2 model includes shell elements for skin, ribs, and spar webs and the same representative set of loads from FEM 1. To effectively design for buckling, the structural designer included circular cross-sectional area rod elements as low-fidelity stringers.

FEM 2 used NASTRAN-based optimization. In addition to skin thicknesses used by FEM 1, FEM 2 models also include spar web, rib thicknesses, and stringer cross-sectional areas as design variables. The design process experiment produced FEM 2 output for each FEM 2 concept as follows:

- A stress map for each load case
- A buckling eigenvalues and mode shape plot for the maximum bending load case
- Optimized thickness distribution for skin, spar webs, and ribs
- Optimized weight (normalized to FEM 1 weight)
- First order cost evaluation (relative ranking)

The addition of buckling constraints required high mesh density for accuracy. These finite element models included about 90,000 degrees of freedom. This caused technical difficulties because the optimization solutions with models of this size consumed large amounts of time and memory. Computer memory limitations caused significant delays and problem reformulation. These design tool limitations impacted the process and the resulting product quality.

Rib design began with the minimum number of ribs for structural connectivity for flap, aileron, systems, and landing gear. The activity then proceeded to iterate with FEM 2 model creation and solution. The structural designer placed ribs, solved the optimization model to determine buckling margin, and experientially placed or moved ribs to bring this margin to the level dictated by defined requirements.
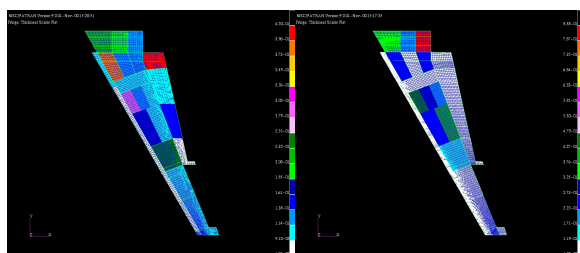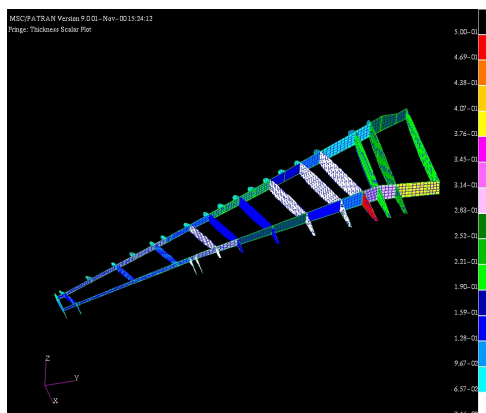
Figure 12 - FEM 2 thickness distribution results for 2 spar concept (lower skin, upper skin, rib/spar web)

Once the structural designer obtained acceptable rib layouts and buckling margins, he then optimized skin and web thicknesses using stress and buckling constraints to determine minimum weight distributions. This procedure was followed to optimize rib number and placement for each of the four concepts.

Each structural concept model contained 7 stringers, whose locations corresponded with possible spar locations. On the 7-spar model, each stringer represented a spar cap. On the 2-spar model, 2 of the stringers represented spar caps and 5 represented actual stringers.

Structural results for the FEM 2 models include stress, buckling, thickness and wing structure weight. Figure 12 shows typical optimized thickness distribution results from the FEM 2 process for the 2-spar concept.

Figure 13 shows optimized weight results for the FEM 2 models normalized to the optimized FEM 1 weight. This figure shows weight results under stress constraints alone and under stress and buckling constraints together. This plot provides a structural basis for a design decision and demonstrates the shift in structural preference depending on what constraints are considered.

The FEM 2-level structural definition enabled generation of geometric layouts to address cost, certification, accessibility, and fuel considerations (slosh, volume, and vibration). These layouts defined concepts for stiffeners, access panels, joints, fasteners, and part counts, providing information for manufacturing cost estimates. All of this information flowed into Design 2 activities to support decision-making.

Figure 13 - Weight as a function of spar count for stress only constraint and with buckling constraint

Design 2

The FEM 2 results were presented to the full design team during the Design 2 effort; the team evaluated rib/spar web layout concepts against a manageable set of differentiating requirements, distilled from the full set of wing structural requirements. These differentiating requirements are not the typical constraints a structural designer would expect to see because all of the concepts meet key analytical constraints such as buckling, stress, and deflection.

These were built into the optimization model. Differentiating requirements are objectives such as optimized weight, estimated cost (producibility), maintainability, and other objectives that are not analytical in nature but determine the viability of each concept.

Table 1- Design 2 concept scoring matrix

	weight factor	2 Spar		3 Spar		4 Spar		7 Spar	
		raw	wtd	raw	wtd	raw	wtd	raw	wtd
Weight	0.30	1	0.30	4	1.20	3	0.90	3	0.90
Stiffness		1	-	2	-	3	-	4	-
Fuel Volume		4	-	3	-	2	-	1	-
Cost	0.30	2	0.60	4	1.20	3	0.90	1	0.30
Fabrication		4	-	3	-	2	-	1	-
Assembly		1	-	2	-	3	-	4	-
Accessibility	0.05	4	0.20	3	0.15	2.5	0.13	1	0.05
Inspection		4	-	4	-	2	-	1	-
Maintenance		4	-	2	-	3	-	1	-
Fuel Considerations	0.05	2	0.10	4	0.20	3	0.15	1	0.05
Certification Issues			-		-		-		-
fail safe	0.25	1	0.25	4	1.00	4	1.00	4	1.00
substantiation	0.05	4	0.20	3	0.15	2	0.10	1	0.05
Weighted Sum	1.00		1.65		3.90		3.18		2.35

Requirements reduction does not eliminate unstated requirements from consideration. Those requirements that are analytical in nature must be included in the analytical models at the appropriate level of modeling. Qualitatively evaluated requirements must likewise be evaluated at the appropriate level of modeling. The key to this process is documentation of assumptions about how each requirement will be dealt with in each modeling and design phase. The set of differentiating requirements for the model wing includes weight, cost, accessibility, fuel considerations, and certification issues.

The set of differentiating requirements goes into the concept selection matrix in Table 1 where the rows represent requirements and the columns concepts.

In the team meeting held to populate this matrix, the team scored each concept on a scale of 1 to 4, where 4 is best. These raw scores were then multiplied by weighting factors, determined by the strategic objectives for the aircraft product in the marketplace. This project team placed greatest importance on weight, cost, and certification. Each concept received a weighted sum score that represents the team's evaluation.

The results clearly show the 3-spar and 4-spar structural concepts as preferred choices. The relative difference between the 3 and 4-spar scores is insignificant compared to the scores of the 2 and 7-spar concepts. Furthermore, these choices are insensitive to adjustments to weighting factors. Even 25% changes in weighting factors yields 3 and 4-spar as clear winners. The quality of the numbers that go into the matrix is extremely important.

The Table 1 scoring matrix represents the results of extensive discussion and team learning. It brings the team to consensus and provides a more solid foundation for design decisions than mandate or vote. The numbers themselves mean very little except that they help to direct the team toward clear design decisions that balance alternatives and maintain or improve the level of team members' commitment.

FEM 2 models in the design process experiment significantly improved the quality of not only the structural weight inputs into the matrix, but also all of the other objectives. The FEM 2 models provided concrete evidence of the effects of stress, buckling, and deflection constraints on the end weight, enabling rational concept evaluation.

The other matrix inputs improved with increased structural input quality because the FEM 2 model provided the specific structural details to enable meaningful discussion and evaluation. The structural definition provided by FEM 2 models enabled preliminary design for access panels, stiffeners, and joints. This geometric configuration then allowed for evaluation of manufacturing cost, accessibility, certification, and fuel considerations (volume, slosh, and vibration).

Unlike Design 1, Design 2 took several meetings. The level of detail included in the FEM 2 models and Design 2 requirements required iteration between FEM 2 modeling and Design 2 assessment. The team refined initial FEM 2 concepts produced by the structural designer through experiential evaluation in preliminary meetings. The final FEM 2 structural models shown earlier in Figure 11 represent significant input from the design team.

Design 2/Fem 2 model and team interaction led to an evolution of detail throughout the level 2 process. Stiffener concepts emerged as part of the FEM 2 model to be carried forward into FEM 3.

The Design 2 process systematically narrowed the wing structural concept pool to the 3 and 4-spar structural concepts with buy-in from all team members. These concepts will be carried forward into FEM 3 and Design 3 for the next level of structural detail to evolve.

Phase 3

Phase 3 activities leverage the remaining design freedom to optimize and validate the final structural design against all constraints and requirements.

The purpose of the final finite element model, FEM 3, is to add structural fidelity sufficient to convey stress and optimized weight information to be able to evaluate stiffener concepts and select a full wing structural concept. The final structural design activity, Design 3, develops the structural concept with full detail.

Finite Element 3

The last stage of structural modeling, or FEM 3, addresses the final level of structural detail considered, as defined by the phase exit requirements for preliminary design. This detail includes stiffener definition and analytical cost and producibility models in addition to the FEM 1 and FEM 2 detail and constraints.

Output of the FEM 3 exercise includes analytical structural results that will then be fed into the Design 3 evaluation and selection process for the final structural concept. Objectives for FEM 3 are to generate useable information sufficient to evaluate stiffener layout concepts from Design 2 and to determine fastener requirements.
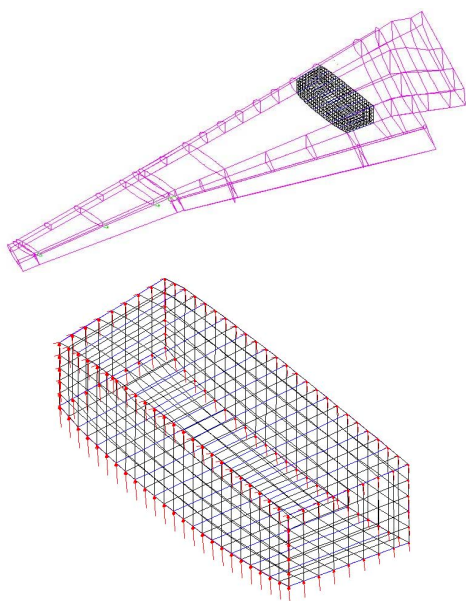
Figure 14—Example of FEM 3 model

The FEM 3 structural model, a portion of which is shown in Figure 14, consists of a master finite element model and several sub-models. The master model determines global behavior of the structure. Solution of the master model, essentially the FEM 2 solution, establishes constraints and boundary conditions for each of the sub-models. The master model contains detail similar to the FEM 2 model, including shell elements for skins, ribs and spar webs and rod elements for stiffeners.

Dividing the master model into sub-models allows for detailed design and analysis. Sub-modeling enables finer finite element meshing, improved definition of design variables, and distributed work. Boundary conditions for these models come from the master model deflection solution at the FEM 2 level. These models use NASTRAN-based optimization with constraints on stress, buckling, and deflection. Design variables for the sub-models include the number and dimensions of stringers and caps and the thicknesses of the skin, ribs, and webs. The increase in detail at this level justifies improved loads definition, incorporating design definition from previous structural design activities and perhaps expanding the load set to include additional conditions.

Design 3

The Design 3 process evaluates the structural concepts that address all of the structural and non-structural requirements. The Design 3 evaluation matrix will contain the same 5 distinguishing requirements as the Design 2 evaluation matrix. The difference between these matrices lies in the fidelity and quality of the information that goes into them and the nature of the concepts being selected. The FEM 3 models not only generate improved structural information, but also enable improved geometric definition. This improved geometric definition enables improved cost, certification, fuel, and accessibility evaluations. These evaluations must be of sufficient quality and fidelity to

select and define a structural concept that meets the preliminary design phase exit requirements. Structural items for this concept include

- skin thickness distribution
- spar and rib locations
- spar cap and stiffener geometry, size and location
- fastener selection and spacing

Observations and Conclusion

This structural design process experiment provided insights into the evolutionary structural design process model and the nature of the interactions between the technical and organizational design processes. Feedback from project participants suggested the following:

- Interactions between the technical and organizational design processes exist and should be addressed through process definition and design
- An evolutionary structural design process helps to integrate design tasks
- The proposed evolutionary structural design process must adapt to organizational needs and should be refined for a specific organizational culture. The organizational processes that occur during design activities influence the design team's effectiveness in making informed design decisions that lead to a quality design.
- The design framework comprised of systematic problem definition (i.e., systems engineering requirements management and process definition) and structured solution synthesis (i.e., matrix-based scoring) improves team processes through more effective communication, problem awareness, and team member commitment. These structured design activities bring the design team to consensus, strengthening team member commitment more than decision by vote.

The evolutionary structural models reduced the technical deficiency of the structural discipline. The structural designer was an important contributor in the design process (not just an analyst) and improved his ability to communicate his needs. However, an undesirable level of technical deficiency was apparent during several attempts to assess producibility and rank concepts for cost. Producibility experts were reluctant to commit opinions until sufficient detail existed to support their opinions. This understandable reluctance reduced the effectiveness of the team.

This tendency to want to delay decisions until sufficient detail exists persisted throughout the design experiment in all disciplines. All participants wanted technical risk reduced to acceptable levels before committing their expert opinions to support design decisions. The longer the process goes without decisions, however, the more unwittingly committed the team becomes to the details being cemented into evaluation models.

The tremendous force for decision postponement must be countered by process definition that promotes decision at appropriate levels of detail and no greater. Quality designs will not result unless design freedom is exploited when it exists. To fully explore the structural design space, structural models must have complexity only as required to support informed decisions at the current level of detail. Additional detail must be withheld to prevent the process from stalling or the design from becoming committed to that detail.

The particular evolution of detail (FEM N and Design N) must be refined to meet organizational needs. When these definitions of the different finite element models and their purpose are understood, activities and decisions are traceable. There will be little need to revisit preliminary design-level activities after preliminary design review, due to requirements creep or other problems.

References

[1] Taylor, R.M., and Weisshaar, T.A., "Merging Computational Structural Tools into Multidisciplinary Team-Based Design," AIAA-2000-4820, *to be presented at the 8th AIAA/USAF/NASA/ISSMO Symposium on Multidisciplinary Analysis and Optimization*, Long Beach, CA, Sept 6-8, 2000.

[2] Whitney, Daniel E., "Designing the Design Process," *Research in Engineering Design*, Vol. 2, 1990, pp. 3-13.

[3] Jackson, S., *Systems Engineering for Commercial Aircraft*, Ashgate Publishing, Brookfield, VT, 1997.

[4] Waszak, M.R., Barthelemy, J.-F., Jones, K.M., Silcox, R.J., Silva, W.A., Nowaczyk, R.H., "Modeling and Analysis of Multidiscipline Research Teams at NASA Langley Research Center: A systems Thinking Approach," *Proceedings of the 7th AIAA/USAF/NASA/ISSMO Symposium on Multidisciplinary Analysis and Optimization*, St. Louis, MO, Sept. 2-4, 1998.

[5] Senge, P. M., *The Fifth Discipline–The Art and Practice of the Learning Organization*, Currency Doubleday, New York, 1990.

[6] Deming, W. E., *Out of the Crisis*, MIT CAES, Cambridge, MA, 1993.

[7] Ulrich, K.T. and Eppinger, S.D., *Product Design and Development*, McGraw-Hill, New York, 2000.

[8] Eppinger, S.D., "Model-Based Approaches to Managing Concurrent Engineering," *Journal of Engineering Design*, vol. 2, 1991, pp. 283-290.

[9] Pugh, S., *Total Design: Integrated Methods for Successful Product Engineering*, Addison-Wesley, 1991.

[10] Dym, C.L. and Little, P., *Engineering Design: A Project Based Introduction*, John Wiley & Sons, Inc., 2000

[11] Cross, N., *Engineering Design Methods*, John Wiley & Sons, New York, 1989.

[12] Alexander, Christopher, *Notes on the Synthesis of Form*, Harvard University Press, Cambridge, 1964.

[13] Simon, Herbert A., *The Sciences of the Artificial*, MIT Press, Cambridge, 1996.

[14] Weisshaar, T. A., and Komarov, V., "Aircraft Structural Design–Improving Preliminary Design Fidelity," *Proceedings of the 7th AIAA/USAF/NASA/ISSMO Symposium on Multidisciplinary Analysis and Optimization*, St. Louis, MO, Sept. 2-4, 1998.

This page has been deliberately left blank

Page intentionnellement blanche

Reduction of Time and Costs for Antennas Integration Through Computational Electromagnetism

Gérard Leflour, Christophe Calnibalosky, Hervé Jaquet
DASSAULT AVIATION
Direction Générale Technique Défense
78, quai Marcel Dassault – Cedex
300 92552 St Cloud Cedex
France

1. INTRODUCTION

Modern combat aircraft increasingly incorporate more and more operational functions.

These functions use a wide range of frequencies over the entire electromagnetic spectrum.

They are essentially related to three functions areas, which are :
- Radar function
- Electromagnetic Countermeasures (ECM)
- Communication - Navigation - Identification (CNI).

Each of these functions calls upon a whole suite of equipment units, to ensure the necessary processing, and of antennas, to ensure the associated radio-electric coverage. Each function has its own antenna, or set of antennas, which, more particularly in the case of the ECM and CNI functions, makes it obvious that :
- such antennas form protuberances, becoming less and less compatible with the aircraft's global performance characteristics (drag, RCS,...)
- the great number of them makes installation, more and more costly.

Also, in the case of the Radar function, the antenna, whether of parabolic, mechanical scan or of active, electronic scan type, is generally positioned on the aircraft forebody, with the consequence that the restricts the obtained coverage and furthermore, wastes a "precious" location which could be profitably used for other functions.

To handle this increasing complexity, new technologies and tools are required which reduce time and cost of the system integration on aircrafts

2. WHAT NEW GENERATION ANTENNAS SHOULD BE

When seeking to remedy these impediments on the performance capabilities of the aircraft and its systems (optronics, air data system,...) by use of new solutions, it becomes obvious that our efforts should be directed towards :

- <u>FEWER ANTENNAS</u>, by use of compatible radioelectric grouping methods, so as to satisfy the needs of the growing number of operational functions, whilst maintaining the number of antennas to be fitted within reasonable limits
    - ⇒ this corresponds to concept of multi-function antennas.

To be noted in this context is - taking the example of CNI functions - that if previous generation aircraft (rougly 20 years ago) often followed the "1 function = 1 antenna" principle, nowadays some degree of function grouping, such as in VHF/UHF/MIDS/TACAN antennas has already been achieved, although the involved dimensions of such blade antennas sometimes prove penalizing for their integration with the aircraft (Fig. 2.1).

- <u>ANTENNAS THAT BETTER CONFORM TO THE STRUCTURE</u>, so as to overcome the drawbacks of the protuberances caused by present-day antennas
    - ⇒ this corresponds to concept of <u>conformal antennas,</u> antennas that fit the aerodynamic shape.
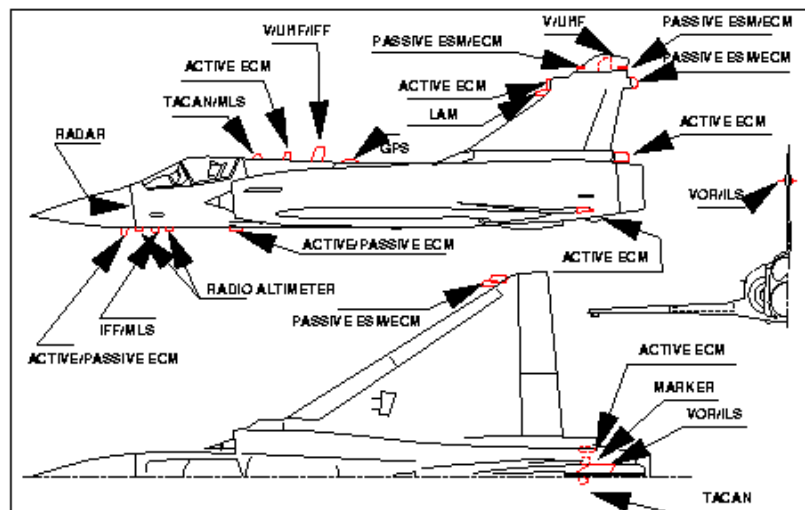
Figure 21: Military antennas proliferation

3. OPERATIONAL INTERESTS

Use of such conformal multi-function antennas should contribute towards improving :
- the performance characteristics of the operational functions making use of such antennas
- the global performance capabilities of the aircraft and their systems
- the maintainability/ reliability aspects.

3.1   Operational function-related aspect

Radio-Electric Coverage

Radio-electric coverage improvements may arise from a better distribution of such antennas. The latter are aircraft structure members and, as such, must be able to be fitted to the spine as well as to the leading edge of the wing, to the lower surface of the forward fuselage...

Three aspects amongst these needs for improvement are currently clearly identified :
- coverage of the radar surveillance and IFF interrogation function, to provide for surveillance of an area of a surface larger than what is currently possible
- possibility to ensure, for firing control purposes, radar target tracking and aircraft/ missile links over larger sectors and not, as currently feasible, exclusively limited to the aircraft front sector
- possibility to have larger antenna bases so as to increase the ESM functions accuracy.

Emission control

For most operational functions, it is furthermore desirable to endow such antenna types with a <u>coverage</u>, and hence, scanning <u>adaptativity</u> function which will provide for improvement of discretion during transmission (via direction, beam provision), or even, for protection against jamming during reception (implying, in this case, via antenna milling provision).

Inter-function compatibility

The problems relative to the compatibility between the different operational functions have to be resolved by use of communal, elementary antennas in conjunction with the necessary components, whether radio-electric (multiplexers, filters,... or processing) sequencing (temporal comparability) units.

Here again, two examples may be given ; the compatibilities between radar/ ECM-jammer and IFF interrogator - responder/ MIDS Data Link.

3.2   Aircraft and Systems Global Performance Characteristic Aspect

Aerodynamic Characteristics

Elimination of the current antenna-generated protuberances (essentially in the ECM and CNI function case) will result in less aircraft drag.

Electromagnetic Signature

Use of conformal, multi-function elements, since this would mean fewer antennas, is expected to result in less global aircraft RCS. This will however, require particular care with such new antenna installations. The apparent RCS reduction that would result from the absence of protuberances, must not be cancelled out by new problems which are bound to arise : gaps, impedance disruption at the aircraft/ antenna interface,...

Global Aircraft System Aspect Integration Constraints

Use of conformal antennas spread over the whole aircraft surface is expected to contribute to global improvement of the airborne system.

As an example and as already mentioned, the benefits of replacing the current antennas ensuring the radar function on the aircraft forebody by conformal antennas spread over the aircraft surface would be :
- liberation of installation areas, thus making them available for accommodation of other sensors (optronics, for example)
- new possibilities to improve the aircraft's air data system performance capabilities (today we remove the pitot tube so as not to interfere with the radar performance capabilities).

Maintainability/ Reliability Aspects

Potential benefits for these aspects would be :
- the need of fewer antennae to be integrated with the aircraft and hence, ultimately, of fewer associated maintenance action. To be noted also is that the conformal antenna aspect will also improve their erosion resistance, which again concurs towards reducing maintenance
- to offer the possibility of using the operational functions in degraded modes without, however, in the case of active antennas, complete loss of the involved function. This would arise from the adaptativity notion which would imply the use of a great number of active modules. Failure of the modules may tolerate progressive, although not necessarily total, function degradation.

4.   ROLE OF MODELLING TOOLS

Significant progress has been yielded over recent years by both the processors and the software used for electromagnetism modeling numerical simulation plays an increasingly important role which is complementary to that of test means. Measurements are a pre-requisite for identification of the elementary constituents' characteristics, for analyses and for validation of electromagnetic systems. Computations offer essential additional functionality for designing antennas that fit the aircraft.

4.1   Hybrid Methods

The DASSAULT AVIATION developed computation code SPECTRE gathers numerical and asymptotical electromagnetic computation methods. The numerical methods use finite-element field modeling. The latter offer great accuracy and robustness for computations on complex structures composed of different dielectric materials which may be prone to attenuation losses. These methods are, however, limited by the size of the matrix problems that can be handled by the processors. On current computers, it is challenging to conduct numerical method computations on the whole aircraft that exceed the Giga Hertz range.

Asymptotical methods are the numerical methods' natural complement to conduct higher frequency computations. These methods describe the electromagnetic field propagation along the ray traces, by use of analytical reference solutions Fig. 4.1 shows the ray tracing taken into account for the computation of a fraction of the antenna pattern. As asymptotical formulations show serial $1/K^{\alpha+N}$ developments, their validity rather applies to the higher frequencies, but is not suited for geometrical parts which are of small-size, compared to the wavelength.

Such methods require continuous validation efforts. The used validation cases are generic cases.

In order to associate the different methods' respective contributions, the SPECTRE code uses hybrid methods. By combining numerical methods, by means of which are computed the fields in small-size complex areas, with asymptotical methods, which take into account larger areas, a great variety of problems can be solved. An example of the use of these methods is given in Fig 4.2. The computation of a blade antenna placed on a circular plate breaks down into 2 parts :

1. Numerical method modeling of a blade antenna placed on a plane gives the field in even point of its surface of allows definition of electric and magnetic currents equivalent to those of an antenna with respect to electromagnetic emission,
2. Asymptotical method modeling of the equivalent current distribution radiation gives the reflections on the plate ant the scattering by the circular rim, to determine the far field pattern.

These methods although very attractive by their potential capabilities require fully mastery in their employment. The choice of how a problem is to be broken down into different sub-domains according to the different associated computation methods calls upon a physical sense of apprehension of the encountered phenomena.
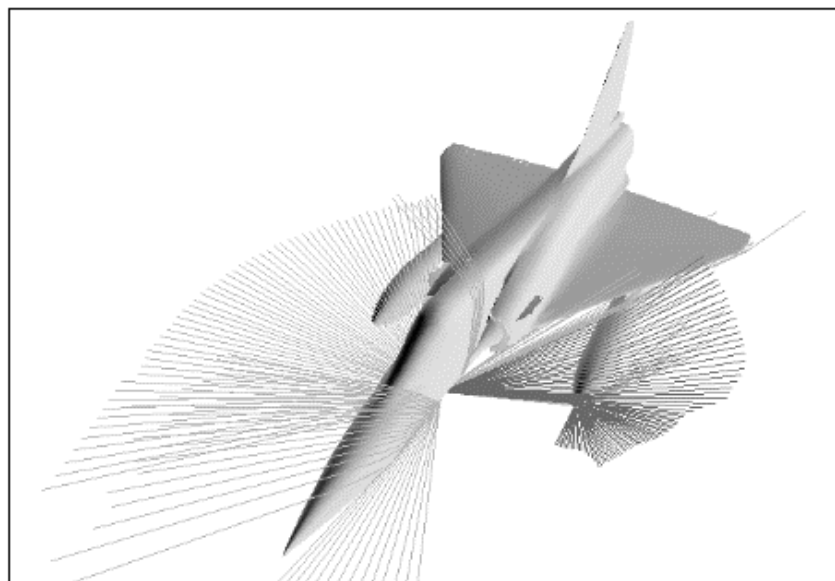
Figure 4.1: Ray Tracing for antenna pattern computation
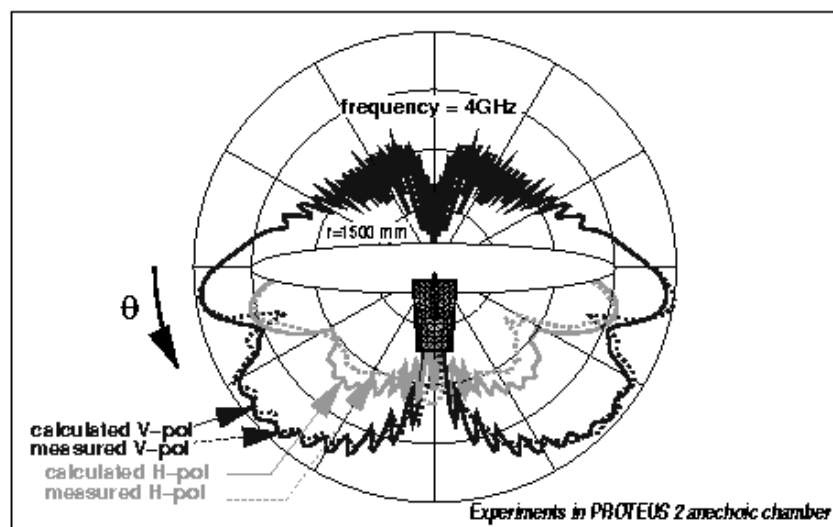
Figure 4.2: Blade antenna on a circular plate, comparison of numerical and experimental patterns,

4.2   Optimization of Antenna Locations

Determining preferred antenna locations is a task becoming increasingly complex on account of the number of antennas and the number of constraints that come into play. From the radioelectrical point of view, such optimization must take into account the sought coverage pattern, as well as the compatibility between the different equipment such optimization must also account for the thermal and chemical aeromechanical environment constraints, notably with respect to structure deflections liable to reach amplitudes that risk jeopardizing the systems' performance capabilities.

Figure 4.3 : Falcon model for comparison of antenna locations
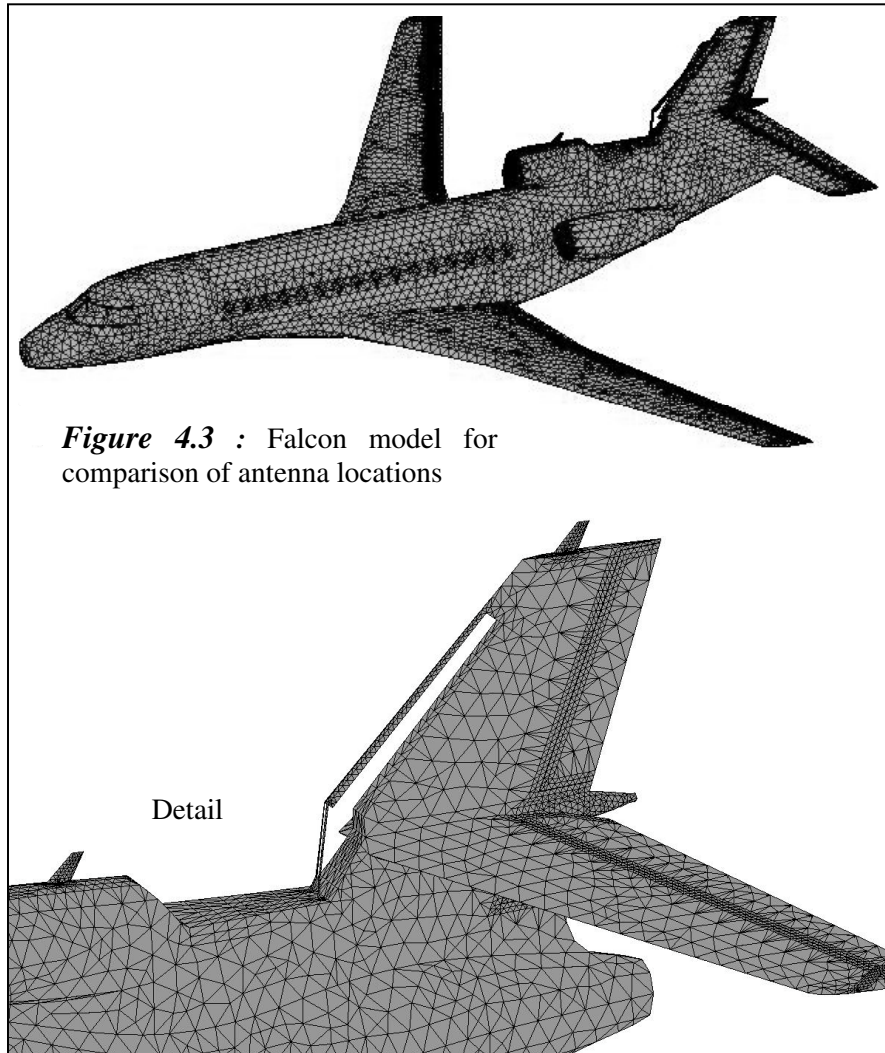
Detail

4.3   Antenna Field Isolation

With the near field computations can be obtained the impedance inputs and the mutual impedance between antennas. The computations require detailed modeling of the geometry around the excitation accesses, together with a precise description of the dielectric materials.

The elementary result leads to the coupling power between 2 antennas. For more global analysis can be represented in each point of the surface, the coupling level vis-à-vis one antenna of a given type. A presentation example is given in Fig. 4.4, showing the coupling vis-à-vis an antenna fitted to the fuselage upper surface.
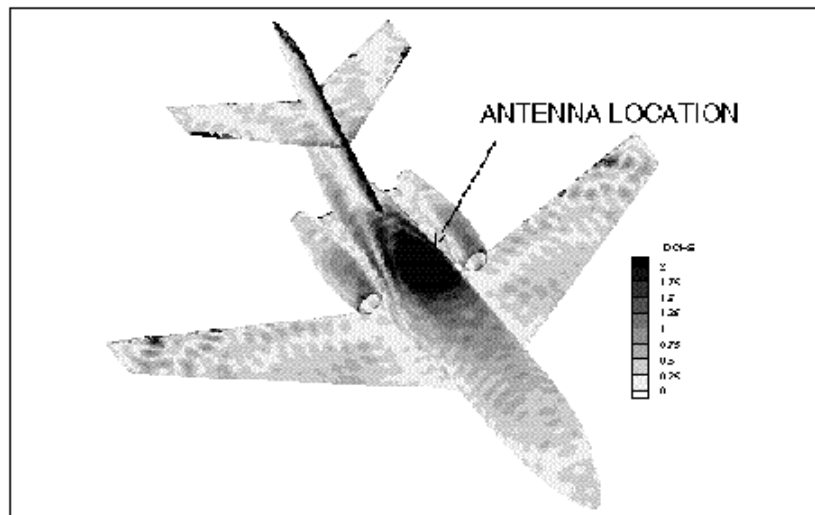
Figure 4.4: Mutual coupling with an antenna in a dorsal location

4.4   Designing Electromagnetic Windows

Radome designing has to take into account a great number of constraints :
- aeromechanical environment (vibrations, deflections)
- thermal and chemical environment
- low observability (radar and improved)
- radioelectric transparency in the used frequency bandwidths.

Electromagnetic computations are used to determine the geometry and materials that offer on acceptable compromise. Fig. 4.5 shows an S-band transparent leading edge structure that allows integration of radiating elements.
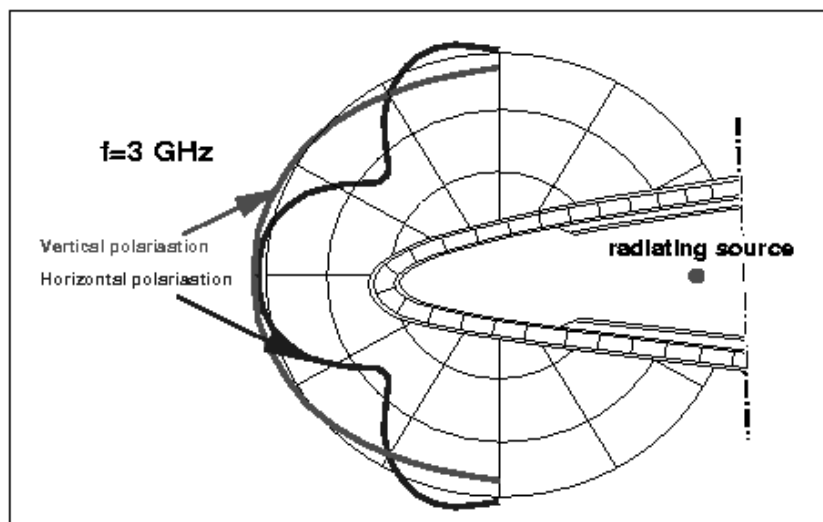
Figure 4.5: Radiation pattern across a leading edge radome

On account of the discretion related constraints, the radom transmission bandwidths have to be limited to those of the used frequencies V/UHF antennas, for example, have RCS of considerable levels. One solution consists in using a radome whose transmission bandwidth is limited to frequencies of less than 1 GHz, with low transmission above such levels.

This characteristic property can be achieved by certain frequency-selective surfaces (FSS) Fig. 4.6 shows the transmission factor, via FSS composed of 3, very dense, cross dipole or tripole type layers. This allows to achieve low transmission factors between 5 and 20 GHz.
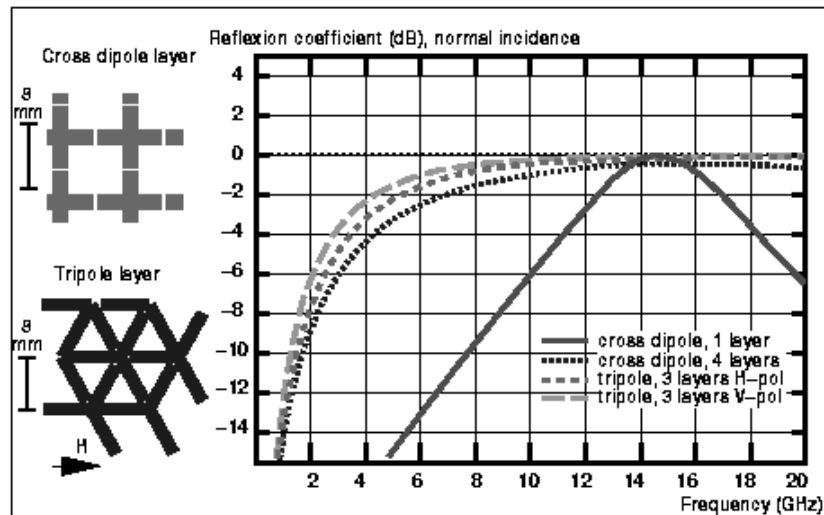
Figure 4.6: Reflectivity of frequency selective surfaces, normal incidence comparison of three different configurations.

5. AEROELASTICITY

Some sensor which are sensitive to phase shift are affected by deflections of the aircraft structure. The analysis of this aerodynamic – structure – electromagnetism coupling is not tractable by ground tests. Multi physics simulations are used to rank the main parameters affecting the system performance, and to develop sensor algorithms robust to these deflections. Fig 5.1 shows the synoptic of such a coupled simulation

Such simulation requires a electromagnetic computation at each time step, on the deflected geometry of the aircraft. Asymptotical methods are well suited because they model accurately the main electromagnetic effects, and their computational time is not affected by the geometrical deflections.
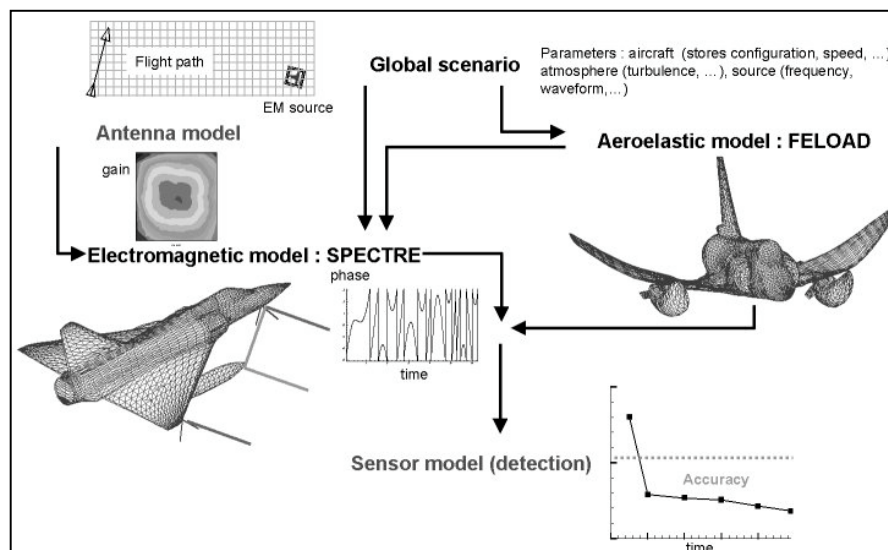
Figure 5.1 : Multi-physics simulation for a wing mounted antenna

6. NEW TRENDS (1) : COLLABORATIVE SIMULATIONS

The before mentioned modeling tools provide for the use of new methodologies to determine the locations of antennas aboard the aircraft the object is to bring into play an equipment model and an aircraft model so as to derive, as early as possible, the behavior of antennas that are to be integrated with the aircraft.

The **equipment model** accurately represents the antenna (power supply, shapes, material...) and gives the radiated fields on a fictitious surface area around the antenna, the lather being fitted to a locally representative surface of the aircraft shape (typically, over a few tens of centimeters).

The aircraft model gives a fine-grid representation of what is fictitious interface surface-external and indicates the electric currents on this electrically bonded surface for each incidence direction.

The reciprocity principle, the date of the two models (fields and currents) can be simply connected on the interface surface and thus give the radiated far field, where :
- $E^{\alpha}(x)$ is the equipment model's electric fields on the interface surface, antenna emitting
- $J^s(x)$ is the aircraft model's electric courant on the bonded interface surface, the aircraft being exposed to a unitary plat wave in î-direction
- $G(\hat{i})$ is the antenna gain in î-direction.

$$\sqrt{G}(\hat{i}) \; = \; \frac{j\omega\mu}{4\pi} \int_{Sint} E^{\alpha}(x) . \, J^s(x)dS(x)$$

This principle is classically used for the hybridization methods presented hereabove. There are several variants to this principle, which, allow adaptations to the cases under study in accordance with the used computation methods.

A validation of a simple case consisting in a monopole antenna mounted on a parallelepiped box is shown in Fig. 6.1, 6.2 and 6.3. The validity of the approach is demonstrated by the compared results of the models coupled with direct computations and a measurement.
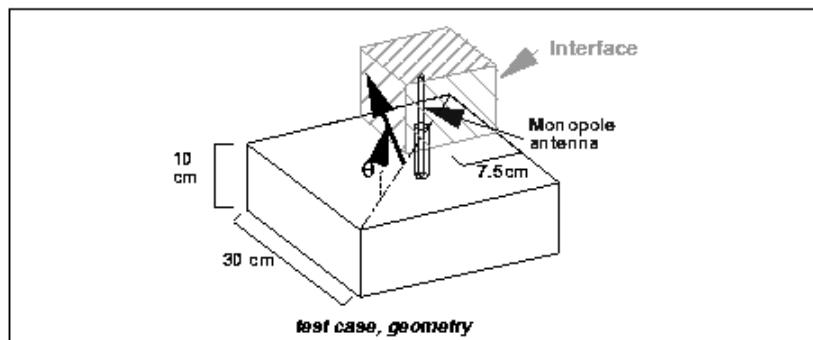
Figure 6 1: Monopole mounted on a box
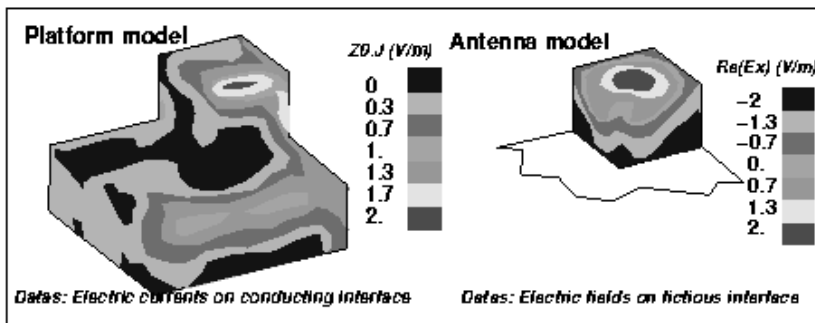
Figure 6 2: Illustration of the platform and antenna models
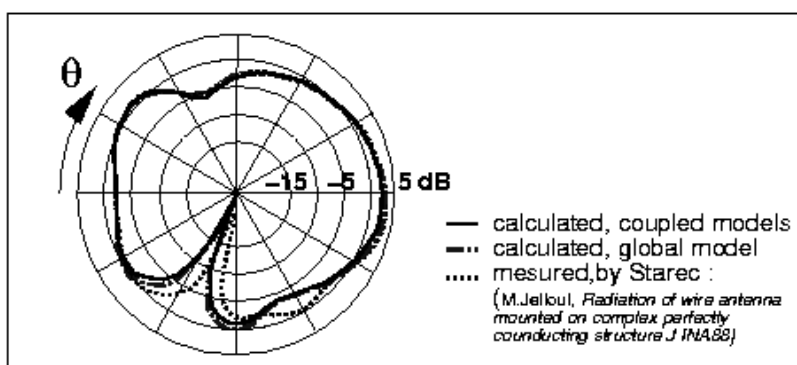
Figure 6 3: Radiation pattern

7.   NEW TRENDS (2) : SHARING APERTURES

- It is at present obviously not conceivable to have, for the envisaged applications, wide band antennas that can globally cover the entire electromagnetic spectrum used on combat aircraft. This hence means that choices have to be made.
- Also, given that, for certain functions, radiation pattern adaptativity is wanted (the lather, here again, depending on the covered spectrum), the possibilities for achieving such adaptativity within one single unique radiation element must not result in elementary antenna sizes that are too big and hence, difficult to integrate.
- Lastly, the functions to be integrated in these new multi-function antennas must be compatible amongst themselves, as regards the performance characteristics to be ensured.

A first line of thought thus could lead to :

7.1   Grouping of the CNI functions, from the IFF to the GPS band within one and the same elementary antenna

A first analysis, essentially focused on printed circuit or wave guide-type antennas, has, indeed, shown that the required sizes of a radiating surface covering the considered bandwidth (200 to 1500 MHz) and providing a potential antenna pattern modulation minimum are in the order of the 700 mm diameter and 100 mm depth.

Given such sizes and the difficulty to integrate them with the aircraft, designing conformal antennas of lower bandwidth (for a civil non-crypted voice transmission VHF function, for example) and of the same performance level as current solutions (faired printed circuit-type antenna in fin tip) cannot be envisaged.

Also, the vast majority of CNI functions require omnidirectional coverage types (voice, IFF response, date transmission... which must be compatible amongst themselves.

7.2   Grouping the Radar/ESM/ECM/IFF Interrogation functions, in conjunction with using a lower radar band

These three functions must, indeed, have common coverage areas and common scanning domains, especially if the lather are to be more extensive than in current practice.

Furthermore, the use of common radioelectric scanning axes (in surveillance areas will, operationally, lead to a better association of the tracks provided by these different sensors.

Also, in the case of the radar function, the fact of distributing several (conformal) antennas over a greater aircraft surface than in current practice, will provide for lowering the working frequency ($> = $ L band) and thus, improve the detection of stealthy targets and enhance anti-jammer protection, both currently inexistant in such frequency domains.

As a conclusion, for future aircraft which should be endowed with conformal multi-function antennas, there are two such-type equipment families that appear to emerge :
- one "low band" family (essentially grouping the CNI functions)
- one "high band" family (countermeasures and radar, amongst others).

An industrial example of a coupled simulation illustrates those recommended solutions. The previously described methodology was successfully applied between DASSAULT AVIATION and THALES Airborne Systems during a feasibility study to install CNI conformal and multi-function antennas on Rafale.

The GPS, IFF, MIDS and TACAN functions were grouped within the same antennas block, located on the Rafale spine behind the canopy. This development was performed to achieve the following specifications :
- conformal antennas
- adaptative patterns for MIDS and GPS to ensure resistance to jamming.

Fig. 7.1 shows the magnetic currents, induced by the radiation of a MIDS element, on the fictitious interface, computed by THALES AS.
Fig 7.2 shows the Rafale fine grid mesh used by DASSAULT AVIATION to compute the radiated pattern of this element, installed on the aircraft.
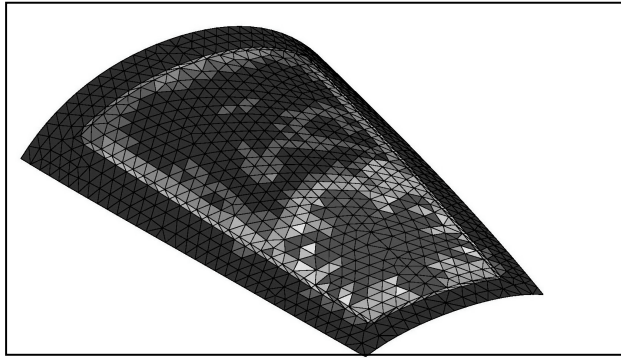
Figure 7.1 : magnetic field on fictitious interface
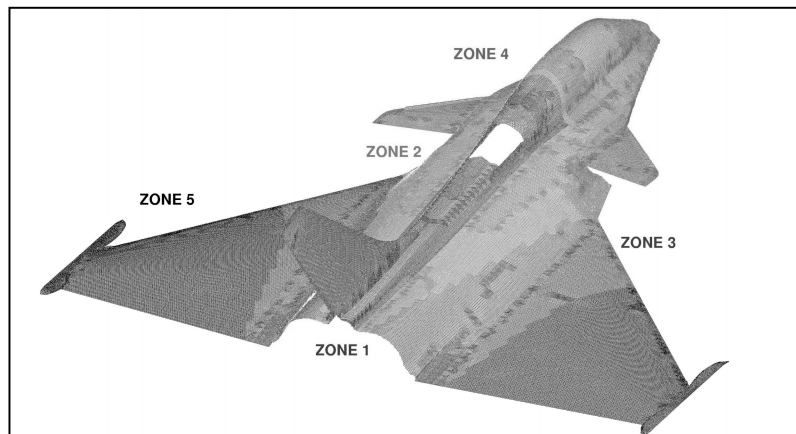
Figure 7.2 : Rafale fine-grid mesh

Improved antenna integration with the aircraft may furthermore arise from exchanges with partner contractors involved in such new design methodologies.

Paper #59
Discussor's Name: David McInroy
Author's Name: Gerard LeFlour

Q: Do you use spectre code for analysis on interference between the radar and an on-board jammer?

A: This will be more easily achieved in the next 5 years or so with modeling. Sodelobe predictions are currently difficult.

Développements numériques récents réalisés en aéroélasticité chez Dassault Aviation pour la conception des avions de combat modernes et des avions d'affaires

E. Garrigues, Th. Percheron
DASSAULT AVIATION
DGT/DTA/IAP
F-92214, Saint-Cloud Cedex
France

1. Introduction :

Il y a encore quelques années, le développement des méthodes et des outils de calcul en aéroélasticité constituait chez Dassault aviation un challenge important. L'outil de calcul CATIA-ELFINI-AEROELASTICITY connaissait à cette époque un essor important, soutenu par des budgets et des équipes de développement conséquents, ainsi que par des besoins grandissants dans le domaine du design et de la justification d'avions modernes tels que RAFALE ou FALCON 2000.

Aujourd'hui, les priorités changent et visent principalement à parvenir à maitriser complètement les outils complexes disponibles, plutôt que de rechercher de nouvelles méthodes. Des stratégies industrielles de calculs et d'essais sont mises au point autours des outils existants. Elles ont pour but de permettre à des ingénieurs de calculs spécialisés, mais aussi à des ingénieurs de conception dans les bureaux de dessin ou à des ingénieurs d'essais en vol, de disposer de modèles fiables au plus tôt dans le cours du projet et à réduire le nombre de configurations à tester, ainsi que le nombre d'essais en vol. L'objectif clairement affiché est la maitrise des risques et des coûts en aéroélasticité dans le cadre du projet avion.

Dans les sections qui suivent, nous illustrons les points les plus importants de ces travaux chez Dassault Aviation. Nous mettons ainsi en relief :

* L'ensemble des méthodes de calcul aujourd'hui disponibles en aéroélasticité.
* La mise ne œuvre de ces techniques dans le cadre de la maitrise des risques et de la réduction des couts.
* A plus long terme, les techniques d'optimisation indispensable pour permettre à l'avionneur de prendre en compte rationnellement dans ces plans de qualification et dans ses dossiers de justification les problèmes liés à la multiplicité et à la variabilité des configurations.
* L'utilisation systématique de méthodes de calibration des procédures de calculs et des modèles numériques sur des résultats d'essais réels.

Plus concrètement, nous donnons des éléments sur la qualité que l'on peut attendre aujourd'hui des prévisions, ainsi que les gains espérés en matière de réduction du nombre d'essais en vol.

2. Outils et méthodes disponibles en Aéroélasticité

2.1 Etat de l'art en aéroéalsticité linéaire

Sur le plan théorique, l'état de l'art en aéroélasticité linéaire est encore globalement fondé sur la méthodologie linéaire classique, dont les principes étaient déjà bien établis dans les années 60. Le détail des méthodes, les stratégies de calcul et les techniques de calibration associées

ont été largement décrits dans la Réf [1]. Nous en résumons les principales caractéristiques dans cette section.

Les modèles mathématiques intervenant dans la chaine de calcul aéroélastique sont décrits ci-dessous :
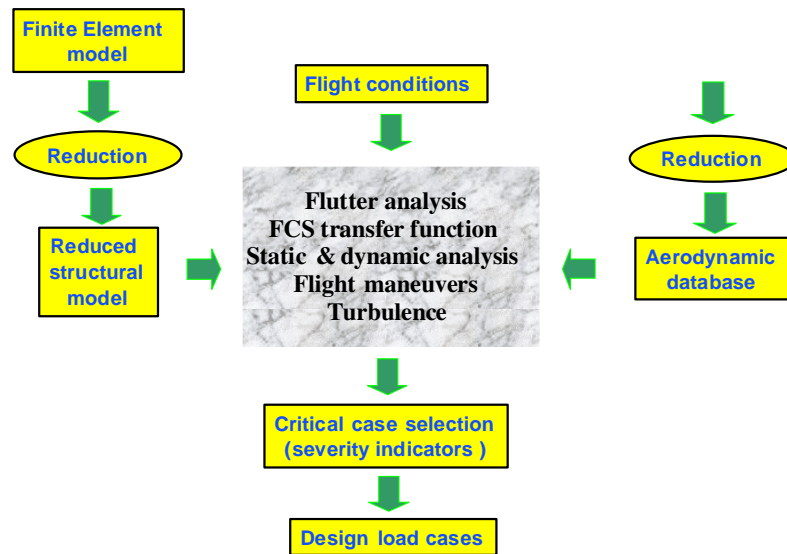
Figure 1:Aeroelastic analys process

On utilise un modèle élastique éléments finis (FEM) de l'avion complet comprenant de l'ordre de 10000 à 100000 degrés de liberté. Pour la modélisation aérodynamique une modélisation en potentiel linéaire par la méthode des singularités est établie dans le domaine fréquence. On pallie les imprécisions de ce modèle en recalant certains termes par des résultats de calculs CFD ou en les recalant sur des résultats d'essais en soufflerie ou d'essais en vol.

Le principe est alors d'effectuer les opérations lourdes sur le modèle éléments finis et sur le modèle aérodynamique indépendamment de toutes les configurations de vol et de toutes les répartitions de masses à considérer. Ces opérations lourdes sont les suivantes :

- Le calcul des déplacements du modèle éléments finis pour quelques centaines de chargements de base. Ces chargements de base correspondent à des charges unitaires de pression ou d'inertie par zones. Tout chargement statique ou dynamique peut être représenté par combinaison linéaire des chargements de base.
- La construction du modèle aérodynamique exprimant les charges aérodynamiques stationnaires et instationnaires dans la base de charges précédentes, en fonction du mouvement de l'avion. Ce mouvement est défini par une combinaison de formes de base aérodynamiques indépendantes des degrés de liberté du modèle élastique.
- L'extraction, à partir de ces modèles élastiques et aérodynamiques encombrants des 'opérateurs de base condensés' contenant les seules données intervenant dans le couplage aéroélastique : matrices de rigidité et de masses réduites dans la base de charge, opérateurs de lissage des déformées éléments finis de base par les forces aérodynamiques de base, 'indicateurs de sévérité' des charges de base.

A partir de ces opérateurs de base, les calculs qui suivent sont très rapides :

- L'élaboration des coefficients des équations de l'aéroélasticité pour les configurations de vol et de masse considérées.
- Les analyses de stabilité (divergence et flutter).
- Le calcul du mouvement souple de l'avion en quasi-statique, ou en dynamique (incluant la prévision des fonctions de transfert pour les études de stabilité CDVE) avec le suivi des indicateurs de sévérité.
- La sélection des cas de charges dimensionnants.
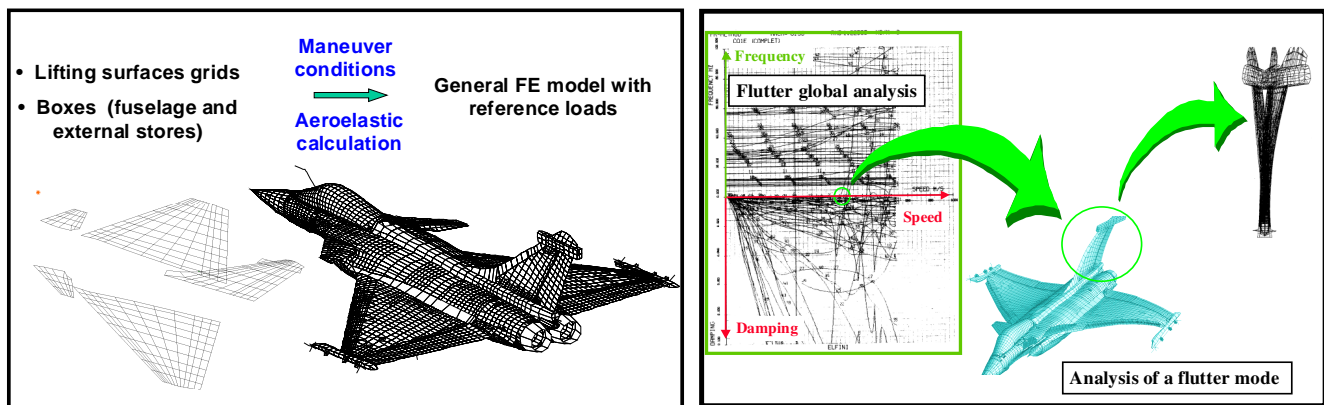
Figure 2: Linear aeroelasticity typical outputs

2.2 Prise en compte des non-linéarités

Afin d'illustrer les méthodes aujourd'hui disponibles et industrielles dans ce domaine, nous ne donnons ici que quelques exemples typiques de traitement des non-linéarités aéroélastique.

- **Non-linéarités aérodynamiques :**

En pratique, que ce soit en stationnaire ou en instationnaire, la méthode lourde consiste aujourd'hui à itérer avec une analyse d'aéroélasticité linéaire recalée à chaque itération sur des calculs CFD (full-potentiel, Euler, …). Les efforts aérodynamiques provoqués par les déformations souples sont alors calculés par la méthode classique des singularités linéaires et servent de pré-conditionneur. La convergence est alors acquise en quelques itérations comme le montre la figure 3 (calcul du Cz d'un avion FALCON équilibré à 1g – M=0.85 – Couplage CATIA/ELFINI/AEROELASTICITY – EULER/EUGENIE) :
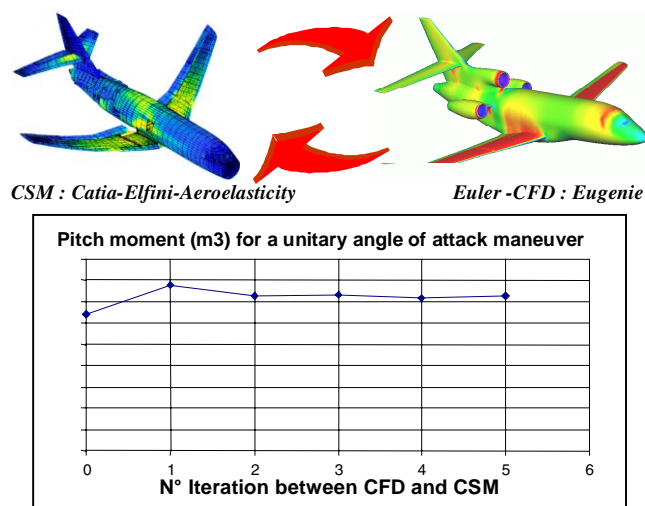
Figure 3: Example of iterative CSM-CFD coupling process

Même si l'augmentation des performances des moyens de simulation numériques permet d'envisager dans l'avenir l'utilisation plus courante d'outils CFD en aéroélasticité, le nombre de cas de calculs à balayer pour couvrir l'ensemble du domaine de vol et l'ensemble des configurations structurales restent trop importants pour pouvoir envisager l'utilisation massive de ces outils à moyen terme. On utilise donc plutôt, lorsque cela est possible, les outils de CFD linéarisés qui permettent d'intégrer les résultats de calcul CFD dans la structure de la base de données aéroélastique linéaire classique (Cf. § 2.1), ce qui permet d'en conserver les performances (coût, stabilité, précision). A titre d'illustration, la planche suivante donne l'exemple de forces généralisées instationnaires calculées sur les premiers modes de flexion/torsion voilure d'un FALCON 2000, par couplage de l'outil CATIA-ELFINI avec

l'outil EUGELIN (outil CFD Euler linéarisé – Cf. Réf [2]). Elles sont comparées aux mêmes forces généralisées calculées par la méthode linéaire classique des singularités.

**Generalized unsteady aerodynamic forces
CSM (*ELFINI*) / Linearized CFD (*EUGENIE*)**

Classical flutter analysis (PK method)
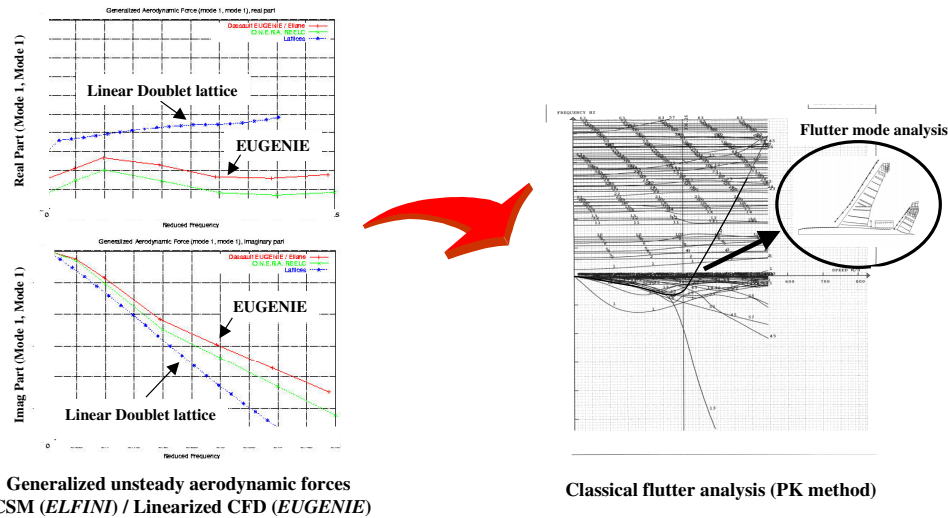
<u>Figure 4</u>: Example of generalized unsteady aerodynamic forces computed using linearized CDD

- **Non-linéarités mécaniques :**

Dans ce domaine, les types de non-linéarités les plus souvent rencontrées sur avion sont principalement dues :

➢ Aux effets des grandes rotations de l'avion (mécanique du vol),
➢ aux non-linéarités de contact liées à la présence de jeux mécaniques (rails, systèmes Fail-Safe, timonerie de servo-commandes, …),
➢ aux couplages de l'avion avec des systèmes mécaniques à comportement non-linéaires (train d'atterrissage, servo-commandes, ejecteurs d'emports, …).

Sur avion militaire, l'exemple typique illustrant la prise en compte de ces phénomènes est la modélisation des phases d'éjection en vol de bidons sous voilure de RAFALE (Cf. figure 5) ou la modélisation des phases de tirs de missiles sur rail au point extrême de voilure du RAFALE, pendant des manœuvres complexes de l'avion (Cf. figure 6).
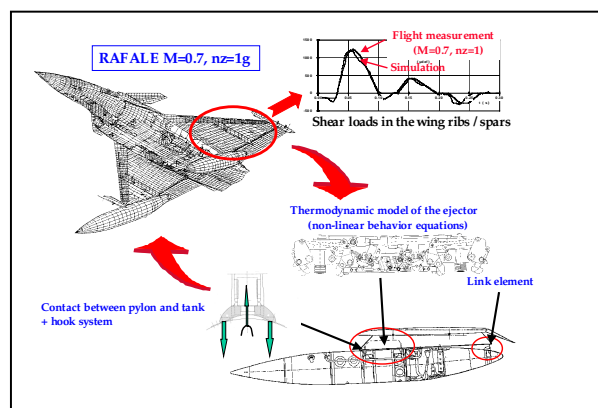
<u>Figure 5</u>: In-flight tank ejection simulation using CATIA-ELFINI-AEROELASTICITY
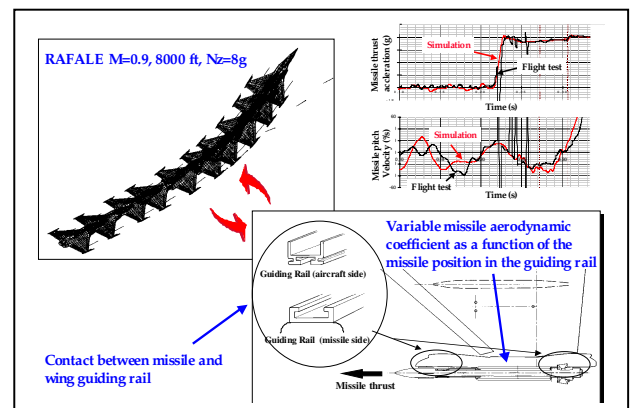
<u>Figure 6</u>: In-flight wing-tip missile launch simulation using CATIA-ELFINI-AEROELASTICITY

Dans ces deux cas, l'outil de calcul doit pouvoir rendre compte avec une bonne précision du couplage simultané des 3 types de non-linéarités précédentes dans la simulation.

Il est à noter que ces analyses non-linéaires nécessitent des intégrations dans le domaine temporel avec formulation préalable des forces aérodynamiques instationnaires dans ce domaine. Les techniques utilisées pour cela sont issues des travaux de Karpel (Cf. Réf. [3]) sur la rationalisation des forces aérodynamiques instationnaires (Cf. figure 7).
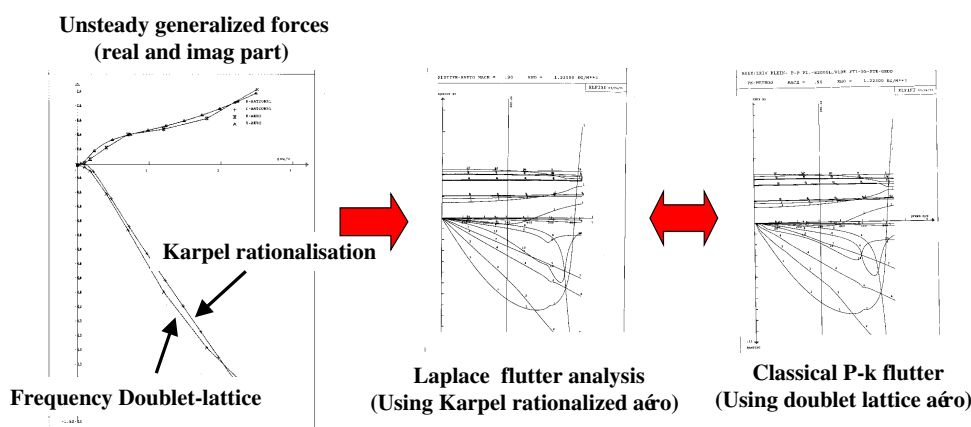
Figure 7: Rationalization of unsteady aerodynamic forces using Karpel method

2.3 Recherche des configurations les plus critiques

Les moyens d'analyse de l'aéroélasticité que nous venons de présenter dans les sections précédentes sont extrêmement utiles pour le calcul d'une configuration particulière de l'avion. Cependant, l'activité de calcul aéroélastique se traduit par un nombre important (voire infini) de configurations structurales et massiques à étudier.

En général, le balayage des cas de calcul s'effectue sur un choix a priori des configurations les plus critiques. La pertinence de ce choix repose sur l'expérience du calculateur et sur sa compréhension des phénomènes physiques.

Dans le cas des calculs de flutter, nous avons été amené à développer un outil d'optimisation pour la recherche des configurations les plus critiques (configurations dites 'les pires'), afin de guider le raisonnement du calculateur, limiter les risques d'oublis et appuyer la démonstration qui conduit au choix de ces configurations. Cet outil est également utilisé pour permettre de tester la sensibilité des analyses de flutter vis à vis des paramètres incertains des modélisations (paramètres 'flous' des modélisations : position du réservoir dans les réservoirs, rigidité des interfaces, interactions aérodynamiques complexes, …).

Les principes théoriques de cet outil ont été abondamment décrits dans la référence [4].

3. Exemple de retombées des études aéroélastiques sur la maitrise des risques et des coûts : études dites 'de transposition'

Les études dites 'de transposition', mises en place chez Dassault Aviation ces dernières années sur les programmes MIRAGE 2000 et RAFALE, concernent la stabilité aéroélastique (flutter) et aéroservoélastique (accrochage du système de commande de vol sur la structure) de l'avion. Elles ont pour objectifs :

- De prédire par calcul, avec un niveau de précision suffisant, le flutter et les fonctions de transfert souples CDVE[1], pour les configurations de base de l'avion.
- De vérifier et de recaler éventuellement ces prévisions sur la base d'essais de vibrations au sol et/ou en vol.

---

[1] On appelle fonction de transfert CDVE les fonctions de transfert des déformations souples au niveau des capteurs gyromètre et accéléromètre du système de commande de vol sur les braquages de gouvernes.

- De **transposer** ces résultats sans essais supplémentaires, pour toutes les versions d'avions (proto <-> série, monoplace <-> biplace, Air version <-> Marine version),dans tout le domaine de vol et pour toutes les sous-configurations.

Ceci suppose de disposer de modèles capables de prédire les instabilités aéroélastiques et les fonctions de transfert souples CDVE, dans tout le domaine de vol, quelque soit la complexité de la configuration et **avec un niveau de confiance maximal**. Ceci suppose également d'avoir maitrisé, intégré et validé des méthodes de recalage expérimentales de modèle efficaces (Cf. §4).

Les retombées importantes attendues de ces études concernent :

- La vérification avant vol des marges de stabilité de l'avion : retombées **sur la maitrise des risques**
- La définition des ouvertures de domaine de vol au 'juste assez' (définition des progressions des vols d'ouverture suivant les marges aux calculs) : retombées **sur la maitrise des couts**.

Le chemin critique de cet organigramme est constitué par les délais (souvent trop courts) entre la fin des essais au sol (dont le T0 est soumis à l'approvisionnement des maquettes d'emports) et le début des essais en vol d'ouverture de domaine. Opérationellement, les plannings d'essais en vol doivent donc être organisés pour laisser suffisamment de temps à l'aéroélasticien pour calibrer les modèles élastiques sur la base des essais de vibrations au sol de l'avion. L'exploitation des vols d'ouverture de domaine donnera lieu, après coup, à un recalage de la partie aérodynamique instationnaire du modèle aéroélastique. Ce modèle sera alors utilisé pour transposer les résultats d'essais à tout le domaine de vol, aux sous-configurations et aux autres types d'avions (proto <-> série, monoplace <-> biplace, Air version <-> Marine version), ce qui permettra d'écrire les dossiers de justification de la définition de l'avion.

Afin d'illustrer la précision que l'on peut attendre aujourd'hui des modèles dans ce domaine, la figure ci-dessous donne les prédictions de la fonction de transfert 'Pitch/symmetric control surface deflection' du RAFALE au sol en présence de missiles aux points externes et médians de voilure et de 3 bidons lourds sous voilure et fuselage. Ces calculs sont comparés à des résultats d'essais de vibrations au sol dans 2 configurations : bidons pleins et bidons vides.
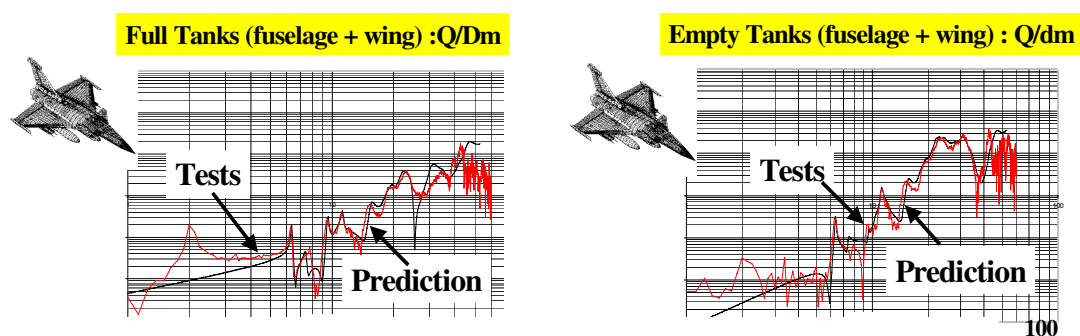
Figure 8: FCS transfer function prediction (on the ground)

Comme le montrent ces comparaisons, la précision du calcul est très bonne. Le modèle prédit bien en particulier le couplage des modes '2 nœuds fuselage' et 'tangage missile au point extrême de voilure', à 9.5 Hz et 11.5 Hz lorsque les bidons sont pleins, en un seul et même pic de fréquence 11 hz, lorsque les bidons se vident. Comme le montrent le modèle et les essais, ce couplage conduit à une augmentation de la fonction de transfert de nature à diminuer la marge de stabilité des commandes de vol. Dans cette affaire, la bonne prévision des modèles

nous a permis, sur la base des calculs, de réduire le nombre de vols d'ouverture de domaine initialement prévus d'environs 50 % (6 vols réalisés au lieu des 12 initialement prévus).

Autre exemple d'illustration : la prédiction de l'influence d'un lest augmenté en pointe avant, sur la fonction de transfert en vol (Mach=0.6) 'Pitch/symmetric control surface deflection' du RAFALE en configuration Air/Air :
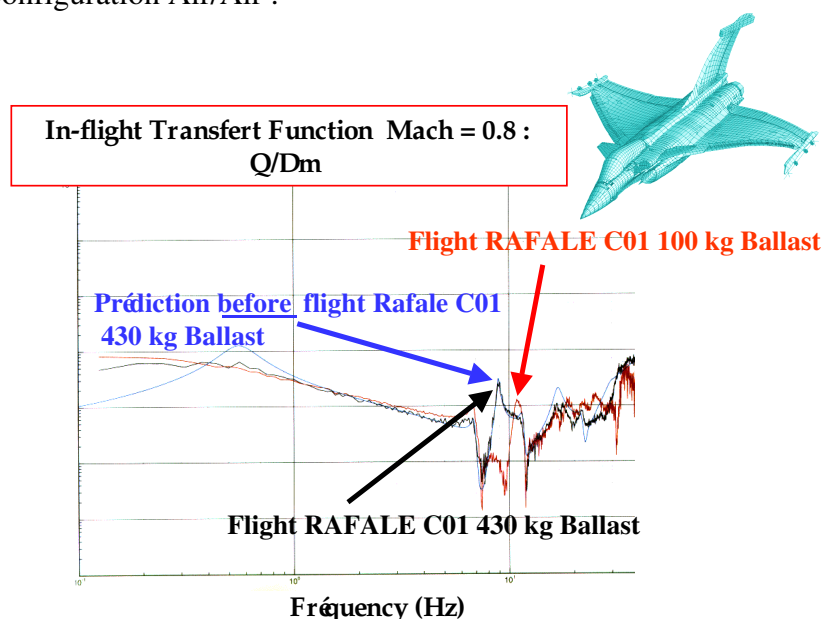
Figure 9: FCS transfer function prediction (on the ground)

Comme le montre ces courbes, le modèle aéroélastique prédit bien la diminution en fréquence du mode '2 nœuds fuselage' due à l'augmentation du lest. Cette diminution en fréquence se traduit a contrario par une augmentation de l'amplitude de ce pic en vol, qui peut être source d'accrochage des commandes de vol sur la structure si ce phénomène n'est pas correctement maitrisé.

4. Validations expérimentales des procédures de calculs et des modèles

Comme il a été vu dans les sections précédentes, l'utilisation des outils de prédictions aéroélastiques dans le cadre de la maîtrise des risques et des coûts suppose que l'on progresse en parallèle sur les techniques expérimentales pour la validation des procédures de calcul et des modèles. Ceci suppose également un niveau de maîtrise comparable des méthodes expérimentales au sol et en vol.

La stratégie aujourd'hui retenue en la matière chez Dassault Aviation est globalement la suivante :

- Utilisation de maquettes souples en soufflerie pour la mise au point des outils, leurs validations et la formulation des procédures d'emplois. Cette tâche supporte également le choix des méthodes et des procédures d'analyse.
- Utilisation d'essais 'grandeur nature' sur avions au sol et en vol pour le recalage des modèles aéroélastiques qui serviront dans le cadre des programmes avions.

4.2 Maquettes souples en soufflerie

Le recours a des essais en soufflerie sur maquettes souples nous paraît capital. Il permet de mettre en correspondance mesures et modélisations, afin de valider les procédures et les méthodes de calculs en aéroélasticité. Il nous est en effet apparu très clairement dans le passé que l'utilisation de résultats d'essais réels permet de faire progresser et de valider les

techniques de calcul, en dévoilant des difficultés non décelables dans le cas de validations purement numériques.

Dans la mesure du possible, on s'arrange pour que l'organisation de ces essais suive une trame semblable à celle de l'enchainement conception/calculs/essais d'un projet avion :
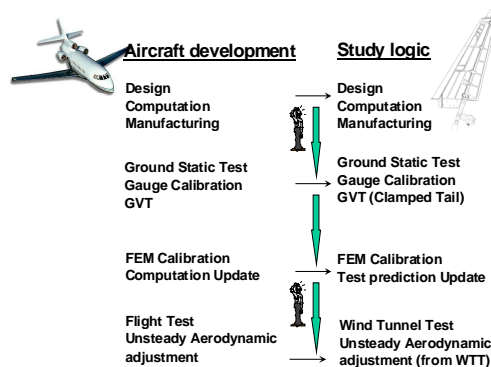
Figure 10: Flexible Wind Tunnel mock-up study logic

Un exemple typique d'étude expérimentale menée dans ce cadre a été réalisée en coopération avec l'ONERA, EADS et DASSAULT dans une étude financée par le MOD Français. Il s'agissait de l'étude en soufflerie (S2 – Modane) d'une maquette souple d'empennage horizontal d'avion de type AIRBUS dotée d'une gouverne de bord de fuite, en présence de jeux mécaniques. Cette étude avait pour but de valider notre méthodologie complète de calcul de flutter en présence de jeu mécanique intervenant pour la certification des timoneries Fail-Safe des empennages de nos avions FALCON. La figure 15 donne un extrait des résultats principaux de ces travaux. Le détail complet de la méthodologie, du montage et des résultats d'essais/calculs peut être trouvé dans la référence [5].
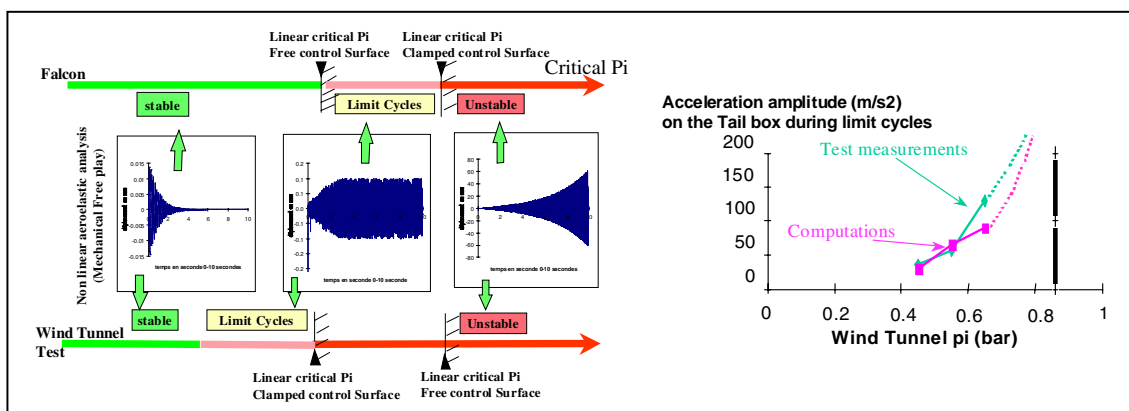
Figure 11: Flexible horizontal tail mock-up in WT : main results

Nous avons montré dans cette étude qu'en procédant à partir des modèles structuraux et aérodynamiques recalés classiquement, la simulation restituait les résultats d'essais à la fois qualitativement (comportement amorti, cycles limites et divergences) et quantitativement (niveaux d'accélération des cycles limites provoqués par les phénomènes de contact de l'axe de rotation de la gouverne sur les butées élastiques).

4.3 Essais réels sol et vol sur avion

Ces essais sont utilisés pour calibrer et valider les modèles aéroélastiques avions dans le cadre des études programmes. Ils sont effectués pour une configuration de base et quelques configurations identifiés comme les plus sensibles : on admet alors qu'après calibration sur ces essais, le modèle aéroélastique puisse représenter les autres configurations.

Les essais au sol sur avion (statiques ou vibrations sol) ont pour objectif de calibrer le modèle élastique de l'avion. Les caractéristiques modales identifiées lors de ces essais peuvent être utilisées pour remplacer le modèle dynamique théorique dans les calculs de flutter et ainsi évaluer les différences de vitesses critiques obtenues par rapport au calcul utilisant le modèle éléments finis. Les essais en vol (manœuvres, vibrations par les gouvernes) serviront eux à calibrer le modèle aérodynamique à travers la mesure des paramètres de vol, des accélérations rigides et des réponses de la structure (jauges et accélérations).
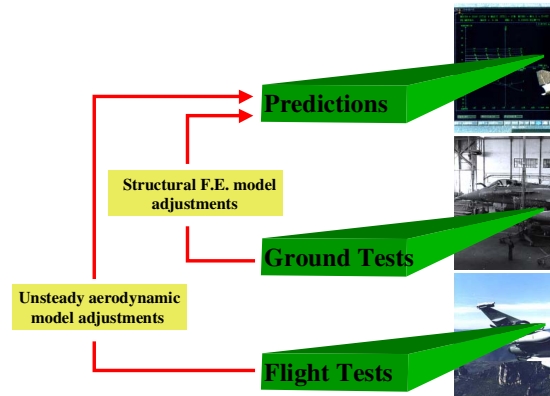
Figure 12: Test versus model calibration strategy

Les techniques associées de recalage des modèles élastiques sur les 'modes mesurés' et de la partie stationnaire des charges aérodynamiques ont été développées et intégrées dans notre code CATIA-ELFINI-AEROELASTICITY dans les années 80. Elles sont aujourd'hui utilisées industriellement dans le cadre des programmes avions et ont fait l'objet de nombreux articles de notre part qui les détaillent (Cf. Réf. [6] et [7] par exemple). Ces outils sont fondés sur une technique mathématique originale d'identification de modèles.

Ces dernières années, notre effort a essentiellement porté sur les outils de recalage des charges aérodynamiques instationnaires, sur la base des essais de vibrations en vol (Cf. figure 16). Dans ces méthodes, nous utilisons toujours la même approche mathématique (Cf. Réf. [8]) :

- Les paramètres d'ajustement λ, inconnues du problème, sont soit les forces généralisées instationnaires, soit directement les composantes des champs de pression sur la grille aérodynamique.
- La fonction de coût à minimiser est l'écart entre les valeurs λ recherchées et leurs valeurs théorique λ_{th} dans le modèle.
- Les contraintes à respecter sont les équations de restitution, par le modèle, des fréquences et des amortissements des modes aéroélastiques mesurés à une précision ε donnée.

Afin d'illustrer le fonctionnement de cette méthode dans le cadre du recalage des champs de pressions sur la grille aérodynamique, nous l'appliquons au cas du calcul en flutter de la maquette en soufflerie souple décrite en Réf. [5]. Le diagramme à gauche de la figure 18 donne la prévision de calcul comparée aux mesures en soufflerie. On constate que la vitesse de flutter est surestimée par le calcul par rapport à la mesure. Le diagramme de droite de la figure 18 donne la courbe de flutter après recalage des champs de pressions instationnaires à partir des deux premiers points de fréquences et amortissements mesurés à 37800 Pa et 60000 Pa (**points nettement inférieurs à la vitesse critique**). Comme le montre ce diagramme, le calcul, recalé à l'aide de points de mesures nettement inférieurs à la vitesse de flutter, prédit désormais la bonne vitesse critique à 84500 Pa.
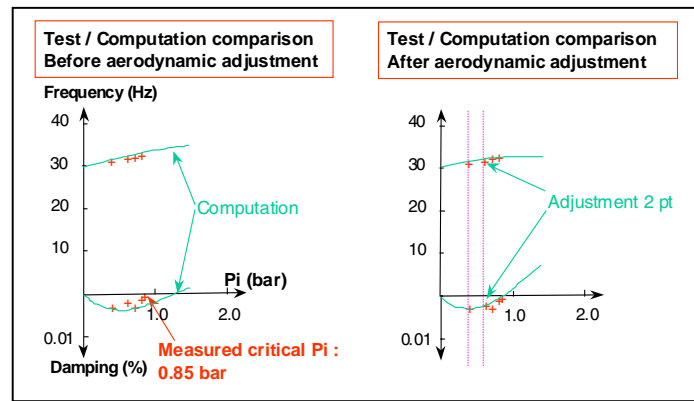
Figure 13: Example of unsteady aerodynamic adjustment on WT tests

Un autre exemple de résultat de cette méthode a été obtenu lors du recalage des forces généralisées instationnaires du MIRAGE F1. La configuration d'étude est représentée sur la figure suivante :
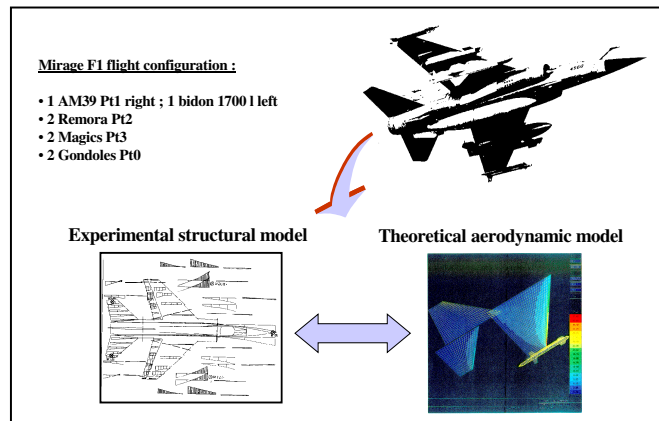
Figure 14: Mirage F1 : configuration studied

A partir de cette configuration, un calcul couplant les modes mesurés au sol de cette configuration à un modèle théorique de forces aérodynamiques instationnaires par la méthode des doublets a été réalisé. La comparaison essais/calculs en flutter est présenté sur la figure suivante. Comme le montre la planche précédente, le calcul de flutter présente une vitesse critique nettement supérieure à celle des essais.
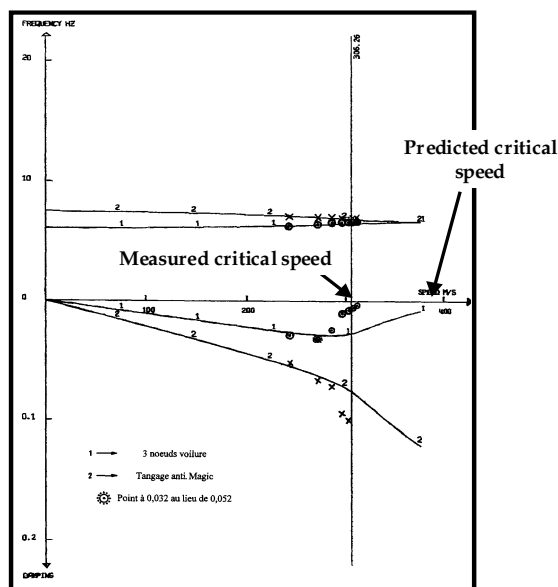
Figure 15: Mirage F1 : comparison test/prediction before adjustement
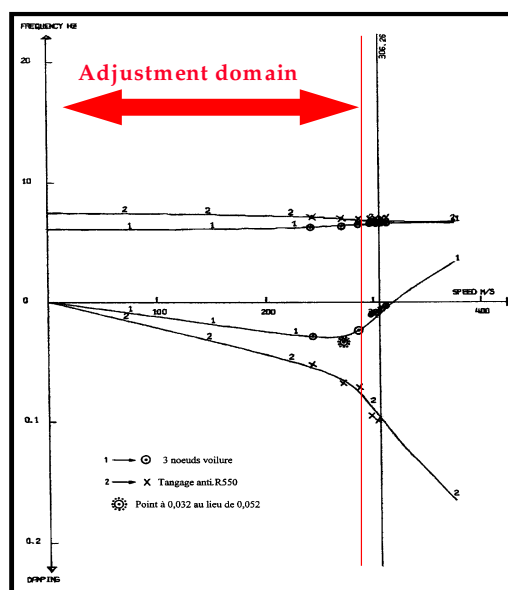
Figure 16: Mirage F1 : comparison test/prediction after adjustement

Pour améliorer les prédictions, ce calcul a donné lieu à un recalage des forces généralisées aérodynamiques instationnaires du modèle, suivant la méthode que nous venons de décrire. Pour cela, les mesures des fréquences et des amortissements des trois premiers points de vol (200 m/s, 300 m/s, 400 m/s, **de vitesses nettement inférieures à la vitesse critique**) sont utilisées. Le calcul de flutter à l'aide de ce modèle recalé est présenté ci-dessous. On constate que la vitesse critique calculée à l'aide du modèle recalé se superpose maintenant à celle issue des essais en vol.

5. Références

[1] : 'Aeroelastic and structural vibrations – state of the art and trends'. C. Petiau. European forum on aeroelasticity and structural dynamics. Strasbourg 1993.

[2] : 'EUGELIN'. G. ROGER.

[3] : 'Time-domain aeroservoelastic modeling using weighted unsteady aerodynamic forces'. M. KARPEL. J. GUIDANCE, Vol 13, N°1, Jan-Feb 1990, p. 30-37.

[4] : 'Recherche automatique de la configuration de flottement la plus critique pour des modèles à données incertaines'. AMD-BA NS N° 26309. Marché SPAé N° 84.95.019 lot 3 bon 13.

[5] : 'Flutter analysis method in presence of mechanical play and experimental verification'. C. PETIAU, B. JOURNEE, E. GARRIGUES. R.T.O Specialist Meeting on Structural Aspects of Flexible Aircraft, OTTAWA 1999.

[6] : 'Analyse Aéroélastique et Identification des Charges en vol'. C. PETIAU, M. DE LAVIGNE, AGARD Conferences proceeding n°375 – 'Operational Loads Data'- Sienne 1984.

[7] : 'A general method for mathematical model identification in aeroelasticity'. C. PETIAU, Ph. NICOT. International forum on Aeroelasticity and Structural Dynamics, Royal Aeronautical Society – Manchester 1995.

[8] : 'Method of mathematical identification of unsteady airloads from flight measurements, experimental validation'. C. PETIAU, E. GARRIGUES, Ph. NICOT. R.T.O Specialist Meeting on Structural Aspects of Flexible Aircraft, OTTAWA 1999.

REPORT DOCUMENTATION PAGE

1. Recipient's Reference	2. Originator's References	3. Further Reference	4. Security Classification of Document
	RTO-MP-089 AC/323(AVT-090)TP/64	ISBN 92-837-0027-9	UNCLASSIFIED/ UNLIMITED

5. Originator	Research and Technology Organisation North Atlantic Treaty Organisation BP 25, F-92201 Neuilly-sur-Seine Cedex, France

6. Title	Reduction of Military Vehicle Acquisition Time and Cost through Advanced Modelling and Virtual Simulation

7. Presented at/sponsored by	the RTO Applied Vehicle Technology Panel (AVT) Symposium held in Paris, France, 22-25 April 2002.

8. Author(s)/Editor(s)	9. Date
Multiple	March 2003

10. Author's/Editor's Address	11. Pages
Multiple	730 (text) 380 (slides)

12. Distribution Statement	There are no restrictions on the distribution of this document. Information about the availability of this and other RTO unclassified publications is given on the back cover.

13. Keywords/Descriptors

Acquisition	Models
Armed forces procurement	Project management
CFD (Computational Fluid Dynamics)	Quality assurance
Computer applications	Requirements
Cost analysis	Research management
Cost control	Resources
Cost effectiveness	Simulation
Defense economics	Standardization
Design	Verification Validation and Accreditation (VV&A)
Government procurement	Virtual Reality
Integrated systems	Weapon systems

14. Abstract

Integrated weapon systems modelling and simulation from concept to operation were treated as essential tool for achieving cost and time reductions which are needed to field new systems. Such tools are being applied to lower the cost and design cycle times from both a design/development and recurring manufacturing perspective. Early identification of problems dramatically reduces costs and improves procurement as well as operations, increasing performance as well as cost effectiveness. The maturing of virtual manufacturing tools led to the review of the various approaches in the NATO framework.

Advanced simulation in design, manufacture, and support were treated in four sessions on:
– Virtual Prototyping and Simulation
– Tool Integration
– Qualification by Analysis
– Design Synthesis

Avoiding cost overruns and schedule delays connected to aerodynamic or hydrodynamic performance was treated in three sessions:
– Cfd Modelling Of Non-Linear Phenomena
– Cfd Validation Procedures And Error Evaluation
– Dynamically Coupled Cfd

This page has been deliberately left blank

_____

Page intentionnellement blanche

NATO's Research and Technology Organisation (RTO) holds limited quantities of some of its recent publications and those of the former AGARD (Advisory Group for Aerospace Research & Development of NATO), and these may be available for purchase in hard copy form. For more information, write or send a telefax to the address given above. **Please do not telephone**.

Further copies are sometimes available from the National Distribution Centres listed below. If you wish to receive all RTO publications, or just those relating to one or more specific RTO Panels, they may be willing to include you (or your organisation) in their distribution.

RTO and AGARD publications may be purchased from the Sales Agencies listed below, in photocopy or microfiche form. Original copies of some publications may be available from CASI.

NATIONAL DISTRIBUTION CENTRES

BELGIUM
Etat-Major de la Défense
Département d'Etat-Major Stratégie
ACOS-STRAT-STE – Coord. RTO
Quartier Reine Elisabeth
Rue d'Evère, B-1140 Bruxelles

CANADA
DRDKIM2
Knowledge Resources Librarian
Defence R&D Canada
Department of National Defence
305 Rideau Street, 9th Floor
Ottawa, Ontario K1A 0K2

CZECH REPUBLIC
DIC Czech Republic-NATO RTO
VTÚL a PVO Praha
Mladoboleslavská ul.
Praha 9, 197 06, Česká republika

DENMARK
Danish Defence Research
 Establishment
Ryvangs Allé 1, P.O. Box 2715
DK-2100 Copenhagen Ø

FRANCE
O.N.E.R.A. (ISP)
29 Avenue de la Division Leclerc
BP 72, 92322 Châtillon Cedex

GERMANY
Streitkräfteamt / Abteilung III
Fachinformationszentrum der
 Bundeswehr, (FIZBw)
Friedrich-Ebert-Allee 34
D-53113 Bonn

GREECE (Point of Contact)
Defence Industry & Research
 General Directorate
Research Directorate
Fakinos Base Camp
S.T.G. 1020
Holargos, Athens

HUNGARY
Department for Scientific
 Analysis
Institute of Military Technology
Ministry of Defence
H-1525 Budapest P O Box 26

ICELAND
Director of Aviation
c/o Flugrad
Reykjavik

ITALY
Centro di Documentazione
 Tecnico-Scientifica della Difesa
Via XX Settembre 123a
00187 Roma

LUXEMBOURG
See Belgium

NETHERLANDS
Royal Netherlands Military
 Academy Library
P.O. Box 90.002
4800 PA Breda

NORWAY
Norwegian Defence Research
 Establishment
Attn: Biblioteket
P.O. Box 25, NO-2007 Kjeller

POLAND
Armament Policy Department
218 Niepodleglosci Av.
00-911 Warsaw

PORTUGAL
Estado Maior da Força Aérea
SDFA - Centro de Documentação
Alfragide
P-2720 Amadora

SPAIN
INTA (RTO/AGARD Publications)
Carretera de Torrejón a Ajalvir, Pk.4
28850 Torrejón de Ardoz - Madrid

TURKEY
Millî Savunma Başkanliği (MSB)
ARGE Dairesi Başkanliği (MSB)
06650 Bakanliklar - Ankara

UNITED KINGDOM
Dstl Knowledge Services
Kentigern House, Room 2246
65 Brown Street
Glasgow G2 8EX

UNITED STATES
NASA Center for AeroSpace
 Information (CASI)
Parkway Center
7121 Standard Drive
Hanover, MD 21076-1320

SALES AGENCIES

**NASA Center for AeroSpace
 Information (CASI)**
Parkway Center
7121 Standard Drive
Hanover, MD 21076-1320
United States

**The British Library Document
 Supply Centre**
Boston Spa, Wetherby
West Yorkshire LS23 7BQ
United Kingdom

**Canada Institute for Scientific and
 Technical Information (CISTI)**
National Research Council
Acquisitions
Montreal Road, Building M-55
Ottawa K1A 0S2, Canada

Requests for RTO or AGARD documents should include the word 'RTO' or 'AGARD', as appropriate, followed by the serial number (for example AGARD-AG-315). Collateral information such as title and publication date is desirable. Full bibliographical references and abstracts of RTO and AGARD publications are given in the following journals:

Scientific and Technical Aerospace Reports (STAR)
STAR is available on-line at the following uniform
resource locator:
 http://www.sti.nasa.gov/Pubs/star/Star.html
STAR is published by CASI for the NASA Scientific
and Technical Information (STI) Program
STI Program Office, MS 157A
NASA Langley Research Center
Hampton, Virginia 23681-0001
United States

Government Reports Announcements & Index (GRA&I)
published by the National Technical Information Service
Springfield
Virginia 22161
United States
(also available online in the NTIS Bibliographic
Database or on CD-ROM)